Akbar Bonakdarpour
William R. Reinus
Jasvir S. Khurana
Editors

Diagnostic Imaging of Musculoskeletal Diseases

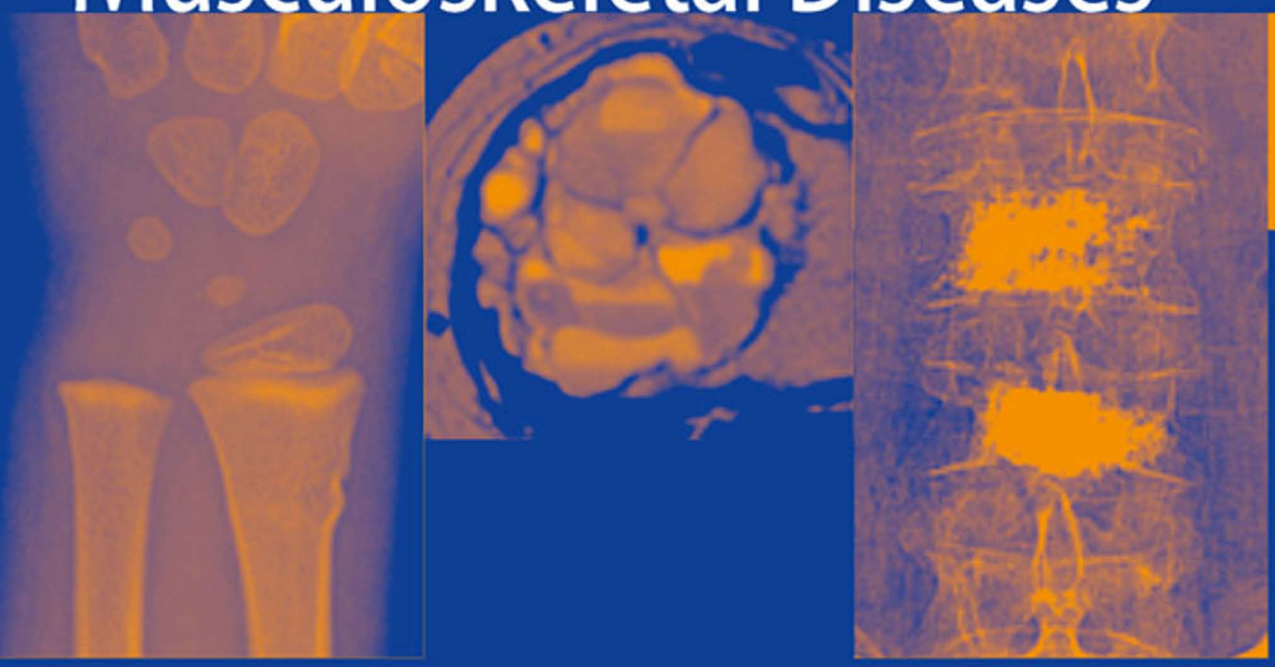

A Systematic Approach

Springer

Diagnostic Imaging of Musculoskeletal Diseases: A Systematic Approach

Akbar Bonakdarpour, MD · William R. Reinus, MD · Jasvir S. Khurana, MD
Editors

Diagnostic Imaging of Musculoskeletal Diseases

A Systematic Approach

Springer

Editors
Akbar Bonakdarpour
Department of Radiology
Temple University Hospital
3401 N. Broad Street
Philadelphia, PA 19140-5189
USA
akbarbonakdarpour@yahoo.com

Jasvir S. Khurana, MD
Department of Pathology
Temple University Hospital
3401 N. Broad St.
Philadelphia, PA 19140-5189
USA
jasvir.khurana@tuhs.temple.edu

William R. Reinus
Department of Radiology
Temple University Hospital
3401 N. Broad Street
Philadelphia, PA 19140-5189
USA
reinusw@tuhs.temple.edu

ISBN 978-1-58829-947-5 e-ISBN 978-1-59745-355-4
DOI 10.1007/978-1-59745-355-4
Springer New York Dordrecht Heidelberg London

Library of Congress Control Number: 2009935060

Preface

We dedicate this text to Drs. Ernest E. Aegerter, a pathologist, and John A. Kirkpatrick Jr., a radiologist. They were among the principal founders of the field of skeletal pathology and radiology. During their time, their residents and colleagues knew them as great educators with a dedication and a passion for their work. Their textbook, *Orthopedic Diseases*, published initially in 1958 was among the first interdisciplinary works devoted to this field. Dr. Aegerter and Dr. Kirkpatrick illuminated many aspects of the field of radiology. Today, with the advent of new technologies, this field has grown to include not only diseases that affect the skeleton but also those that affect muscles, ligaments, tendons, and also the cartilaginous structures within joints.

With this text we intend to carry on Dr. Aegerter and Dr. Kirkpatrick's tradition. We have recruited only well-known musculoskeletal radiologists and pathologists to participate in the writing of this book. Each author has been carefully selected for his expertise on the topic about which he's been asked to contribute. Each author is known as an experienced and seasoned teacher. Each author has made a mark on the field.

With this talent we aim to lay the foundation of a useful and worthy teaching text. Our goal is to create a textbook that is at once readable by the radiology resident experiencing musculoskeletal radiology for the first time and thorough enough to be used by the practicing radiologist. We do not intend, however, to present an exhaustive reference work. We leave that task to other authors.

Instead we aim to provide a text that not only conveys important information about common and some less common musculoskeletal diseases, but more importantly provides a practical and systematic approach to analyzing diseases of bones, muscles, tendons, ligaments, and joints. We will provide with each category a means by which to conceptualize and analyze how pathology changes their appearance on medical images.

To meet these goals we have organized this text according to major categories of disease: trauma, infection, tumors and tumor-like conditions, metabolic diseases, endocrine disorders, dysplastic diseases, and arthritis. Where disease categories overlap, e.g., intraosseous tophus or brown tumor of bone, we discuss those points under each appropriate heading. Where there is debate as to the etiology of a disease, we also discuss these issues guiding the reader, to the best of our ability, to what current thinking has to say about that disease.

We also include a chapter that examines basic interventional techniques that apply to musculoskeletal imaging. Again, the idea is not to provide an exhaustive reference on any one technique, but instead to give the reader a primer on these techniques and their indications with guidance for finding further information.

Finally, in recognition of the importance of orthopedic procedures, we include information on the use, imaging appearance, and pathology affecting prostheses and fixation devices. This information is essential to the practice of modern radiology.

We hope that the reader will both enjoy reading this text and find the experience profitable to their knowledge base, both in fact and in concept. We look forward to receiving readers' impressions, criticisms, and suggestions to improve this text in future editions.

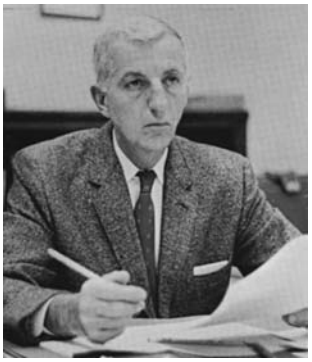

Ernest E. Aegerter

John A. Kirkpatrick

Philadelphia, PA

Akbar Bonakdarpour
William R. Reinus
Jasvir S. Khurana

Contents

Contributors

Sayed Ali, MD Assistant Professor, Department of Radiology, Temple University School of Medicine, Philadelphia, PA, USA, saychink@yahoo.com

Akbar Bonakdarpour, MD, MS (Radiology), FACR* W. Edward Chamberlain Professor of Radiology, Emeritus Professor of Radiology and Former Chief of Musculoskeletal Radiology, Former Professor of Orthopedic Surgery, Temple University School of Medicine, Philadelphia, PA, USA, akbarbonakdarpour@yahoo.com

Avneesh Chhabra, MD Assistant Professor, Department of Radiology, Johns Hopkins School of Medicine, Baltimore, MD, USA, avneesh28@yahoo.com

Shigeru Ehara, MD* Professor and Chair, Department of Radiology Iwate Medical University School of Medicine, Morioka, Japan, ehara@iwate-med.ac.jp

Afshin Gangi, MD, PhD Professor of Radiology, University Hospital of Strasbourg, Strasbourg, France

Jasvir S. Khurana, MD* Associate Professor, Department of Pathology, Temple University School of Medicine, Philadelphia, PA, USA, jasvir.khurana@tuhs.temple.edu

Theodore T. Miller, MD, FACR* Professor of Radiology, Weill Medical College of Cornell University, New York; Attending Radiologist, Department of Radiology and Imaging, Hospital for Special Surgery, New York, USA, millertt@hss.edu

Wilfred C.G. Peh, MBBS, MHSM, MD, FRCPG, FRCPE, FRCR* Clinical Professor, National University of Singapore, Singapore, Republic of Singapore; Senior Consultant Radiologist, Alexandra Hospital, Singapore, Republic of Singapore, wilfred.peh@gmail.com; wilfred@pehfamily.per.sg

Bahman Rafiee, MD Assistant Professor, Musculoskeletal Division, Department of Radiology, University of Pittsburgh, Pittsburgh, PA, USA, rafieeb@upmc.edu; rafieeb@hotmail.com

William R. Reinus, MD MBA FACR* Vice Chairman and Professor, Department of Radiology; Chief, Musculoskeletal Radiology Temple University, Temple University School of Medicine, Philadelphia, PA, USA, reinusw@tuhs.temple.edu

Fayez F. Safadi, PhD Associate Professor, Department of Anatomy and Cell Biology, Temple University School of Medicine, Philadelphia, PA; Adjunct Associate Professor, Department of Cell and Developmental Biology, Weill Cornell Medical College in Qatar, Education City, Doha, Qatar, fayezsafadi@gmail.com

Scott Seibert, MD St. Mary's Medical Center, San Francisco Orthopaedic Residency Program, San Francisco, CA, scottyfifteen@hotmail.com

Carolyn M. Sofka, MD* Associate Professor of Radiology, Weill Medical College of Cornell University, New York; Associate Attending Radiologist, Department of Radiology and Imaging, Hospital for Special Surgery, New York, USA

Jamshid Tehranzadeh, MD* VA Long Beach Health Care System, DMM Health Care Group # 05/114, 5901 E. 7th Street Long Beach, CA 90822 USA, jamshid.tehranzadeh@va.gov

Colleen Veloski, MD Assistant Professor, Department of Endocrinology and Metabolism, Temple University School of Medicine, Philadelphia, PA, USA, cveloski@temple.edu

Seoung-Oh Yang, MD, PhD Professor, Department of Radiology, Eulji University School of Medicine, Daejeon, South Korea, soyang@eulji.ac.kr

Paul Zhang, MD Associate Professor of Pathology, Hospital of the University of Pennsylvania, Philadelphia, PA, USA

* Denotes member of the International Skeletal Society

Chapter 1

Bone Structure and Function

Fayez F. Safadi and Jasvir S. Khurana

Abstract This chapter discusses the normal structure and function of the skeleton and the various ways it is regulated. The skeleton is both an organ and a type of connective tissue. Knowledge of its various identifiable parts greatly facilitates an understanding of skeletal function and also the disease processes that can occur. Normally, the major skeletal processes of resorption and formation are tightly coupled. This feature plays a role in the normal function of skeletal renewal. Disturbances of the remodeling cycle can be seen in a number of generalized skeletal disorders including metabolic bone disease and conditions such as Paget disease. This chapter discusses the macroscopic and microscopic anatomy of the skeleton as well as its biochemical makeup. It introduces the emerging information about the molecular control of bone cells and the skeletal processes.

Keywords Remodeling • Coupling • Formation • Resorption • Mineralization • Cortical • Trabecular • Epiphysis • Metaphysis • Diaphysis • Periosteum • Endosteum • Woven • Lamellar • Osteoblasts • Osteoclasts • Receptor activator of nuclear factor kappa B (RANK) • Transforming growth factor-beta (TGF-β) • Bone morphogenetic proteins (BMPs) • Platelet-derived growth factors (PDGFs) • Insulin-like growth factors (IGFs) • Calcium hydroxyapatite • Collagen • Alkaline phosphatase • Glycosaminoglycans • Proteoglycans • Non-collagenous proteins • Osteopontin • Osteocalcin • Vitamin D • Vitamin A • Estrogen • Androgen • Parathyroid hormone • Wolff's law

F.F. Safadi (✉)
Department of Anatomy and Cell Biology, Temple University School of Medicine, Philadelphia, PA 19140, USA
e-mail: fsafadi@temple.edu; fayezsafadi@gmail.com

Introduction

The Skeleton

Apart from functioning as a major endocrine, hematopoietic, and reticuloendothelial organ, the skeleton serves as the body's structural support and locomotion system. It has mechanisms to grow and change in shape and size to suit varying stressors including the ability to resist mechanical forces. It is also a major organ in the homeostasis of calcium/phosphate balance and in the detoxification of heavy metals.

Bone tissue is continuously formed and remodeled throughout life. This is necessary since otherwise it would fatigue with the daily repetitive stress and torsion of motion and weight bearing.

Initially, the bone achieves its increase in size and shape through *growth* (increase in size) and *modeling*. In late childhood and adulthood there is continuous renewal of the skeleton, by a process termed *remodeling.* Both modeling and remodeling *require* two separate processes, namely bone resorption and bone formation, to *occur in coordination and simultaneously* to be effective. This phenomenon is known as "coupling."

Bone Formation and Degradation

The major functions of bone cells include matrix *formation (osteogenesis)*, *mineralization*, and *degradation (resorption)*. Because formation and resorption are antagonistic processes that proceed simultaneously, bone metabolism must be tightly regulated at all times. During the first two decades of life when the skeleton is growing, there is a net increase in bone mass such that bone formation exceeds its degradation. Once the skeleton has reached maturity, the skeleton maintains a constant balance between formation and resorption to ensure that there is no net gain or loss of bone; this regulated balance is called *coupling*. Uncoupling

A. Bonakdarpour et al. (eds.), *Diagnostic Imaging of Musculoskeletal Diseases: A Systematic Approach*,
DOI 10.1007/978-1-59745-355-4_1, © Springer Science+Business Media, LLC 2010

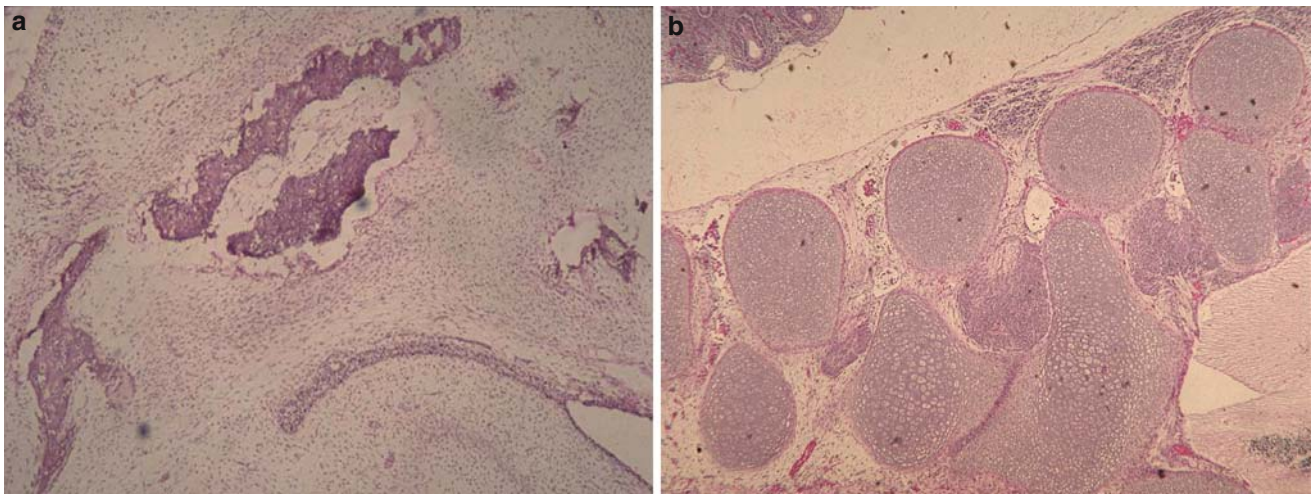

Fig. 1.1 (**a** and **b**) Bone is calcified. The crystal structure of calcium hydroxyapatite makes bone growth more difficult as compared to other organs. Large volumetric growth of bone is achieved by having an intermediate non-mineralized structure (or model) which can grow and then later mineralize. This model can be of either fibrous tissue or cartilage – bone developing on fibrous tissue is called intramembranous ossification and that on cartilage is enchondral (or endochondral) ossification. (**a**) shows vertebrae of an embryo that are still cartilage. They will eventually be replaced by bone (endochondral ossification). (**b**) shows the mandible forming from fibrous tissue (intramembranous ossification)

of formation and resorption is a common feature of most metabolic bone diseases. Among the many effects of aging, the rate of bone formation declines to a greater extent than the rate of resorption, resulting in progressive bone loss as bone remodels.

Bone Architecture

Bone is a composite tissue consisting of mineral, matrix, cells, and water. The mineral is an analog of the naturally occurring crystalline calcium phosphate, hydroxyapatite. The outer cortices of various bones are fashioned in the form of a hollow tube or a bilaminar plate. The architecture is strengthened by internal "struts" of trabecular bone that are oriented either along or perpendicular to the lines of stress. This kind of design is known in engineering terms as "composite" and allows bone to take advantage of the strength of components. Thus, bone resists mechanical compression and can deform a great deal before failing. Indeed, it is this ability to deform that allows the skeleton to absorb the forces of movement.

Gross Morphology

There are four kinds of bones: long bones (femur, tibia, ulna, and radius), short bones (carpal and tarsal bones), flat bones (skull, sternum, and scapula), and irregular shaped bones (vertebra and ethmoid). These bones form through different mechanisms during embryonic development. The majority of long bones and flat bones form by endochondral and intramembranous bone formation, respectively (Fig. 1.1a, b). Some bones, like the clavicle have both kinds of bone formation. Both long and flat bones are organized with a hard, but relatively thin, outer region composed of dense, *compact* bone called the *cortex or cortical bone*. Inside the cortex is the marrow cavity containing hematopoietic elements, fat, and spongy spicules of bone. The bone spicules are also referred to as *trabecular* or *cancellous* bone (Fig. 1.2).

Parts of a Long Bone

Epiphysis

This term refers to the end of a tubular bone, located between the physeal plate (in developing bone) and the articular cartilage. In adults, the physeal plate is absent. The portion of the bone that the epiphysis would have occupied in the growing skeleton is arbitrarily referred to by the same name (Fig. 1.3).

Physis or Epiphyseal Plate

The physis (growth plate) is the region of bone elongation in children. Injuries or other disruptions such as infections can seriously affect the subsequent size and shape of the bone. Abnormally increased vascularity around the epiphysis in certain inflammatory conditions, e.g., juvenile chronic arthritis and hemophilia, can cause elongation of the bone leading

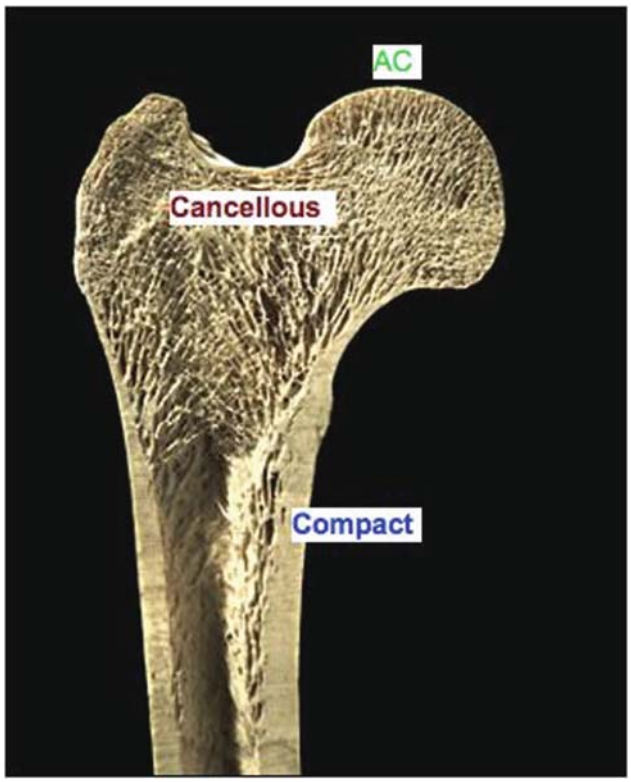

Fig. 1.2 Adult long bone. Sagittal section through the proximal femur showing the internal structure of the bone. The outer dense compact bone (cortical bone) and the inner cancellous (trabecular or spongy) bone are filled with spicules or trabeculae

to limb length discrepancies. Premature closure of the physis may cause shortening and partial closure may cause an angular deformity of the bone. Fractures of the physeal plate are classified using the Salter–Harris classification which is based on the amount and kind of physeal disruption caused by the fracture.

Metaphysis

This refers to the widened portion of bone occupying the area between the cylindrical diaphysis and the physis/epiphysis. This portion of long bones is rich in trabeculae that transfer load from the articular plates into the bone's cylindrical cortex. Remodeling and modeling defects in this region are frequent in conditions such as multiple hereditary osteochondromatosis. Several tumors have an epicenter in the metaphysis.

Diaphysis (Shaft)

This refers to the middle, cylindrical portion of a tubular bone. There is a thick cortex surrounding a marrow space

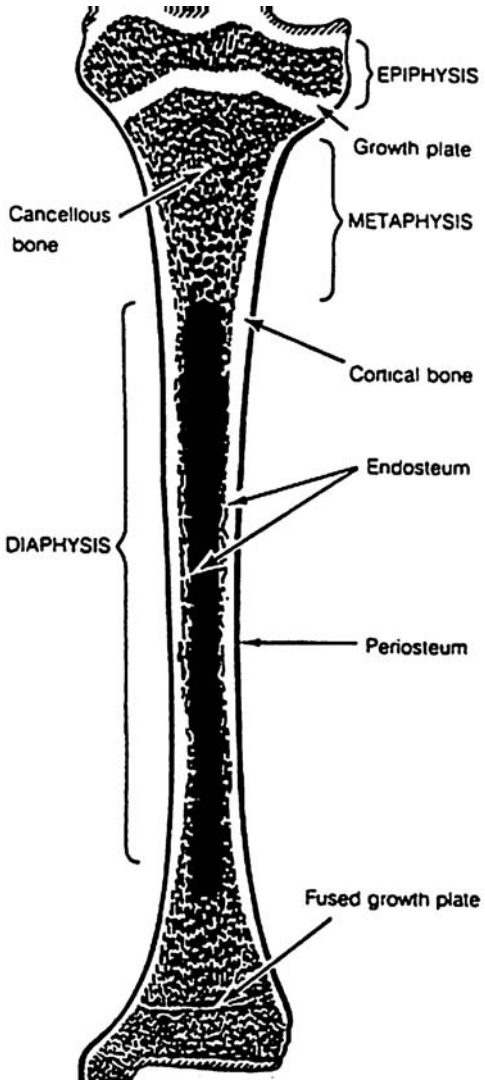

Fig. 1.3 Schematic of a tibia. The interior of a typical long bone showing middle diaphysis, a growing proximal end (epiphysis) with a still active epiphyseal growth plate, and a distal end with the epiphysis fused to the metaphysic. The diaphysis (shaft) of a long bone contains a large marrow cavity surrounded by thick-walled tube of compact bone. A small amount of spongy bone lines the inner surface of the compact bone. The proximal and distal ends, or epiphyses, of the long bone consist of spongy bone with a thin outer shell of compact bone. The outer surface of the bone is covered by a fibrous layer of connective tissue called the periosteum

with few trabeculae. The marrow space also contains reticuloendothelial and hematopoietic elements and fat in varying proportions that change with age.

Bone Marrow

The medullary cavity is filled with varying proportions of hematopoietic marrow (red marrow) and fat (yellow marrow). Red marrow is most prevalent in younger age groups

and in the metaphyseal region of long bones. The diaphyses mainly contain yellow marrow in adults. In comparison to the appendicular (limb) skeleton, the axial skeleton has a greater proportion of red marrow throughout life.

Periosteum

The periosteum is composed of an *outer fibrous* layer and an *inner cambium* (cellular) layer. The cambium layer contains osteoprogenitor cells and fibroblasts. When tendons insert into bone, the collagen fibers (Sharpey's fibers) pass through the periosteum and then into the bone lamellae (see below). Sharpey's fibers contribute to the appositional growth of bone (see intramembranous bone formation).

Endosteum

The endosteum is composed of a resting layer of marrow at its interface with bone. This is not a morphologically recognizable layer of tissue at the light or electron microscopic level. It is, however, a convenient concept that explains the functional changes seen in physiologic and pathologic alterations in bone at the bone medullary cavity interface.

Microscopic Features of Bone

Microscopically too, bone tissue can be either compact (cortical) or spongy (trabecular or cancellous) and can be classified based on collagen fibers arrangements into two different types: woven bone and lamellar bone.

Woven (streamer/immature) bone. This form of bone consists of randomly oriented collagen fibers alongside which reside large numbers of osteoblasts (osteoprogenitor cells). Under polarized light woven bone can be recognized as having a haphazard structure. It contains relatively more cells per unit area than mature bone. It occurs in regions of rapid growth, such as in the immature skeleton (especially in the embryo), fracture callus, fibrous dysplasia, osteosarcoma, and several other tumors.

Lamellar bone. Lamellar bone is the mature form of adult bone. It is readily identified on polarized light microscopy by parallel lines of mineralized bone (Fig. 1.4). Studies have shown that lamellar bone has well-organized collagen fibers. Lamellar bone forms when the rate of deposition is slow and generally it forms only on pre-existing bone.

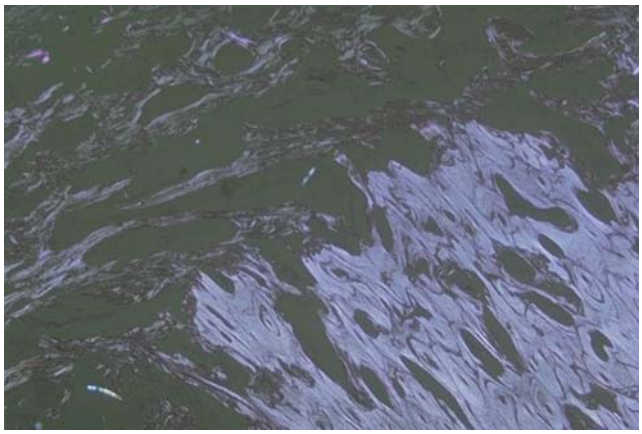

Fig. 1.4 Section from a fracture site. There is lamellar bone seen in the *bottom right* of the picture from which streams of woven bone are emanating toward the *top left*. Note the organized pattern of lamellae seen in the compact, mature lamellar portion under polarized light and contrast with the woven bone

Secondary organization is a hallmark of lamellar bone. In the cortex, the lamellae are arranged in circumferential as well as tubular arrangements. The tubular arrangement is called an osteon. Under the microscope, these tubes can look like circles or parallel sheets depending on how they are cut to make histologic sections. The central part of the tube is the Haversian canal, which contains blood and lymphatic vessels and nerves. Bone cells called osteocytes are located between lamellae (see below). The osteons play an important role in the mechanical properties of cortical bone, since the long axis of an osteon is parallel to the long axis of a long bone. Each osteon acts as a fiber that resists failure (fracture) with deformation (stretch). The surrounding lamellae (circumferential) bone resists compressive forces.

Blood Supply of Bone

Bone has a rich vascular supply. It receives 10–20% of the cardiac output. Blood supply varies with different types of bones. Blood vessels are especially rich in areas containing red bone marrow. The diaphyseal nutrient artery is the most important supply of arterial blood to a long bone. This divides into ascending and descending branches that supply the inner two-thirds of the cortex and medullary cavity. Numerous metaphyseal and epiphyseal arteries that arise mainly from arteries that supply adjacent joints supply the ends of bones. These arteries anastomose with the diaphyseal capillaries and terminate in bone marrow, cortical bone, trabecular bone, and articular cartilage. In growing bones, the epiphyseal arteries are separated from the diaphyseal arteries by the physeal cartilaginous plate. Finally, periosteal arterioles are vessels that supply the outer layer of cortical bone.

Blood is drained from bone through veins that accompany the arteries and frequently leave through foramina near the articular ends of the bones. Lymph vessels are abundant in the periosteum.

Nerve Supply of Bones

Periosteal nerves are sensory nerves, some of which are pain fibers. Therefore, the periosteum is especially sensitive to tearing or tension. Accompanying the arteries inside the Haversian canals are vasomotor nerves that control vascular constriction and dilation. Bone is also innervated by sympathetic fibers. There is a possibility that a neurotransmitter (such as dopamine and serotonin) may play a role in bone metabolism [1]. There is also a possibility that cannabanoids may play a role in bone integrity, since mutations of a cannabanoid receptor produces osteopenia in experimental animals [2, 3].

Bone Cells

The cells important in bone biology are osteoprogenitor cells, osteoblasts, osteocytes, and osteoclasts. Osteoblasts and osteocytes are thought to be derived from primitive mesenchymal cells (the osteoprogenitor cells). Osteoclasts are thought to owe their lineage to cells of the hematopoietic bone marrow related to macrophages/monocytes.

Osteoprogenitor Cells

These are undifferentiated mesenchymal cells and have the properties of stem cells, that is, the potential for proliferation and a capacity to differentiate. These cells can differentiate into osteoblasts, chondroblasts, bone marrow stromal cells, or fibroblasts depending on the nature of the stimulus, and perhaps the local microenvironment. They are present in the inner layer of the periosteum and the endosteum lining marrow cavities, osteonal (Haversian) canals, and the perforating (Volkmann's) canals. Osteoprogenitor cells persist throughout postnatal life as bone-lining cells; they are reactivated in adults during the repair of bone fractures and other injuries.

Osteoblasts

Osteoblasts are derived from the osteoprogenitor cells. Osteoblasts have a cuboidal or columnar shape and vary in size from barely detectable by light microscopy to up to 50 μm when activated (Fig. 1.5). Osteoblasts are responsible

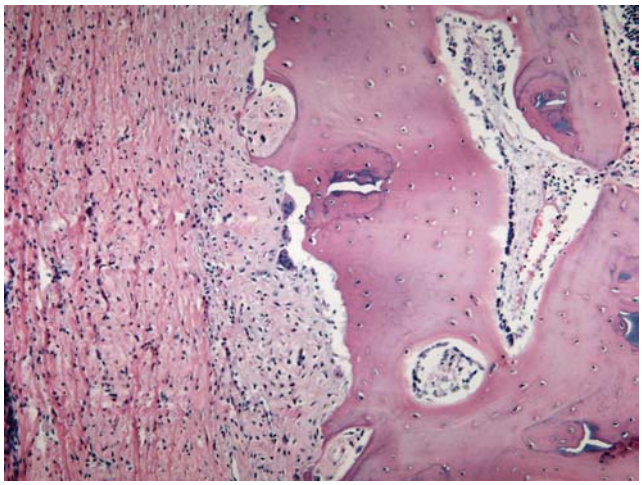

Fig. 1.5 The picture shows a trabeculum of bone centrally with two smaller interconnecting trabeculae above and below it on the *right hand side*. *The left-hand side* of the picture shows fibrous tissue. On the *left* of the main trabeculum are three activated osteoclasts. Note the eroded bone adjacent to them. This erosive pit is called a Howship lacuna. On the *right-hand side* of the trabeculum are a few active osteoblasts rimming the bone. Within the trabeculum are tiny clear spaces containing osteocytes

for the production of collagen type I and glycosoaminoglycan that comprise the osteoid, the non-mineralized organic matrix of bone. Osteoblasts and osteocytes are the principal cells involved in mineralization of bone. They are thought to aid mineral deposition by increasing the local concentration of calcium and phosphate in a complicated process using "matrix vesicles" [4, 5]. Both alkaline phosphatase and parathyroid hormone (PTH) receptor have been discovered on these cells. The phenotype and morphology of osteoblasts depend on their stage of development and differentiation. Osteoblasts secrete the receptor activator of nuclear factor kappa B (RANK) ligand. This ligand plays an important role in the differentiation of osteoclasts (see below). Osteoblasts also secrete variety of collagenous and non-collagenous proteins such as osteocalcin, osteopontin, bone sialoprotein, and osteonectin, as well as a variety of cytokines and colony-stimulating factors (CSF), such as interleukin-6, interleukin-11, granulocyte-macrophage colony-stimulating factor (GM-CSF), and macrophage colony-stimulating factor, and thus have a role in myelopoesis. Other substances secreted by osteoblasts include transforming growth factor-beta (TGF-β), bone morphogenetic proteins (BMPs), platelet-derived growth factors (PDGFs), insulin-like growth factors (IGFs).

Constant mechanical stress is essential for the maintenance of bone mass and strength. Osteoblasts increase their activity in response to mechanical stimuli and so mediate changes in bone size and shape. Perhaps this osteoblastic response is modulated by the piezoelectric properties of the calcium hydroxyapatite crystal.

Molecular Regulation of Osteoblast Differentiation: Osteoblast differentiation is regulated by many secreted growth factors, including transforming growth factor-beta (TGF-β), bone morphogenetic proteins (BMPs), and fibroblast growth factors (FGFs) [6, 7]. Furthermore, transcription factors play fundamental roles in osteoblast differentiation. Runx-2 (runt-related transcription factor 2)/cbfa-1 (core-binding factor a1) and osterix are essential transcription factors for osteoblast differentiation [8, 9]. Also involved with osteoblast regulation is leptin, a peptide synthesized by adipocytes with binding affinity to its receptor in the hypothalamus. This protein regulates bone formation by a central mechanism [10].

Osteocytes

Osteocytes are cells within the substance of bone and are derived from osteoblasts (Fig. 1.5). They are said to be involved in cell signaling and maintaining the viability of the bone matrix. It is possible that these cells are important in the translation of mechanical loads to cellular events such as bone formation.

Osteoclasts

These are multinucleated cells with 2–100 nuclei per cell. Most osteoclasts are closely related to the monocyte/macrophage hematopoietic progenitor cells. Their genesis requires the presence of osteoprogenitor cells along with a variety of hematopoietic cytokines, such as interleukins 1, 3, 6, and 11, tumor necrosis factor (TNF), M-CSF, and stem cell factor. Parathyroid hormone (PTH), 1,25-dihydroxyvitamin D_3, transforming growth factor-alpha (TGF-α), and epidermal growth factor (EGF) act permissively in their formation, whereas calcitonin inhibits the formation of osteoclasts [11].

Osteoclasts Are the Primary Bone Resorbing Cells

Osteoclasts are mostly found at sites where resorption is taking place, within "eaten out" cavities in the surface of bone known as *Howship's lacunae* (Fig. 1.5). The cells can also tunnel through cortical bone creating channels. Osteoclasts are polarized (the nuclei congregate away from the resorbing bone surface), and the cytoplasm of the cell between the nuclei and the ruffled border is rich in carbonic anhydrase and in tartrate-resistant alkaline phosphatase (TRAP) [12]. By electron microscopy, there is an abundance of mitochondria, lysozomes, and free ribosomes in the cytoplasm. Activated osteoclasts show an infolding of the plasma membrane (ruffled border). At the point where the cell membrane is close to the bone, there is a ring-like perimeter called clear zone or sealing zone. This zone contains abundant microfilaments (actin filaments) but lacks other organelles. The formation of the sealing zone is a participation of actin filaments together with $\alpha_v\beta_3$ integrin. Into the space bounded by the ruffled border and bone, resorptive substances can be secreted [13, 14].

Mechanism of Osteoclast-Mediated Bone Resorption

Bone resorption involves protons (hydrogen ions) secreted by an ATP-driven proton pump in the ruffled border of osteoclasts. The enzyme carbonic anhydrase II is essential in the generation of hydrogen ions. Simultaneously, acid hydrolases are released from lysosomes. This combination of the acid created by the hydrogen ions and proteolytic enzymes provides optimal conditions for the resorption of bone and degradation of collagen. Osteoclasts can move over the bone surface creating many such resorptive pits. These pits are well visualized by scanning electron microscopy and correspond to the Howship's lacunae in routine sections.

Osteoclasts have calcitonin (but not PTH or vitamin D) receptors. They are stimulated by IL-6 (perhaps in combination with IL-1, IL-3, and IL-11) and RANK ligand. These cytokines are produced locally by cells of the osteoblast lineage under the influence of PTH, vitamin D_3, TGF-β, IL-1, and TNF. [11, 15–17]. The regulation of osteoclast differentiation is a subject of intense ongoing study with implications for the treatment of a variety of diseases ranging from osteoporosis to skeletal dysplasias such as osteopetrosis. It involves numerous cytokines including macrophages colony-stimulating factor (M-CSF), RANK ligand (present on osteoblasts), RANK receptor (present on osteoclast precursors), and osteoprotegerin (OPG), a decoy protein [18–26].

Bone Matrix

Bone matrix, consists of an organic and an inorganic or mineral component. Forty percentage of the dry weight is composed of the organic component, called osteoid. This includes collagen, proteoglycans, glycoproteins, phospholipids, and non-collagenous proteins (see Table 1.1). The inorganic component makes up the remaining 60% of the dry weight of bone and is composed primarily of calcium hydroxyapatite $Ca_{10}(PO_4)_6(OH)_2$. At an ultrastructural level, bone is once again organized to maximally resist mechanical forces. Calcium hydroxyapatite crystals are arranged parallel to collagen fibers [27]. The orientation maximizes the collagen's resistance to tensile (stretch) forces and the calcium hydroxyapatite's resistance to compressive forces.

Table 1.1 Components of bone matrix

Bone proteins
Collagens
Type I collagen – woven and lamellar bone
Type II collagen – cartilage
Type III collagen found in certain pathologic conditions
Non-collagenous proteins (synthesized mainly from osteoblasts)
Calcium binding – osteonectin, bone sialoprotein
Adhesion proteins – osteopontin, fibronectin, thrombospondin
Mineralization proteins – osteocalcin
Enzymes – collagenase, alkaline phosphatase, metalloproteinases
Cytokines – PG, IL-1, and 6
Growth factors – IGF-1, TGF-β, PDGF
The hydrated (muco)polysaccharide gels

Diseases which result in abnormal collagen disrupt the normal mechanical function of bone. Osteogenesis imperfecta, which is caused by abnormal collagen, results in an abnormal collagen–calcium hydroxyapatite structure and a weak bone matrix.

Classification of Collagens

Connective tissues contain varying amounts of collagen, elastin (a related fibrous protein), glycosaminoglycans, and proteoglycans. Of these, collagen is the most abundant.

Several different types of *fibrillar, basement membrane, and short chain* collagens are recognized. These are the types I–XIII collagens. Each of these differs from each other in their biochemical structure. Of the *fibrillar* collagens, type I collagen is found in bone, skin, meniscus, tendon, ligament, annulus fibrosis, and joint capsules. About 90% of bone matrix is composed of type I collagen. Bone is also the primary organ in which type I collagen is located. There are several subtypes of type I collagens. Hydroxylation and glycosylation are post-translational modifications of collagen and are specific to bone. These differences or modifications explain why mineralization only occurs in bone and not in other sites [28]. Type II collagen is located mainly in hyaline cartilage, the vitreous humor of the eye, and the nucleus pulposus of the intervertebral disk. The other fibrillar collagens are the "minor" collagens, type III occurs in association with type I and also in tissue undergoing repair. Types V and XI occur in association with types I and II, respectively. Type IV collagen is the prototype and major component of the *basement membrane.* Type VII forms the anchoring filament in epithelial basement membranes, while type VIII is localized to endothelial basement membranes. The least understood class of collagens is the *short chain* collagens and are comprised of the types VI, IX, and X. Short chain collagens may function in association with other collagens and have a role in cartilage physiology.

Urinary excretion of hydroxyproline (found exclusively in collagen) and other products of collagen degradation (cross-linked products such as pyridinoline and deoxypyridinoline) act as markers for collagen breakdown. These measurements reflect the amounts of bone turnover.

Enzymes

Alkaline Phosphatase

Although not generally thought of as a matrix component, alkaline phosphatase is an osteoblast product (such as osteocalcin and osteonectin). There are three related isozymes that are tissue related and are associated with three separate genes. These are the *placental, intestinal, and tissue-nonspecific* forms. The last is seen in high levels in a variety of tissues such as bone, liver, kidney and skin. The role on alkaline phosphatase in biomineralization is still speculative. It has been found in matrix vesicles, but its exact role is unclear. Serum alkaline phosphatase activity is increased in growing children, pregnancy, healing fractures, Paget disease, rickets, osteomalacia, hyperparathyroidism, bone-forming tumors, and certain skeletal metastases. It is reduced in hypophosphatasia.

The Hydrated (Muco)Polysaccharide Gels

The functional units of bone extracellular matrix "gels" are the glycosaminoglycans (GAGs). Of the several GAGs, four main groups are present. Hyaluronic acid, chondroitin and dermatan sulfates, heparan sulfate and heparin, and keratan sulfate. The majority are aggregated to a protein core to form a *proteoglycan*. Prior to release from the synthesizing cell, GAGs (except hyaluronic acid) are sulfated. This step allows a net negative charge on these molecules. In turn, this charge serves two functions. First, it keeps the molecules extended, increasing the volume to weight ratio. Second, by attracting osmotically charged cations, it attracts water. This mechanism creates a gel with very high swelling pressures and tremendous resistance to compression.

Highly viscous hyaluronic acid is a major constituent of synovial fluid, where it helps in lubrication and reduces friction. Additionally, it may impede bacteria by its physical and chemical properties. Its synthesis is thought to be by a pathway located in the cell membrane. The remainder of the GAGs mentioned are biosynthesized within Golgi apparatus within the cell cytoplasm.

Mineralization

Calcium hydroxyapatite is the main form of mineral in the human. Calcification in the body occurs in several different

situations. First, there is the physiologic process of cartilage and osteoid mineralization. Second, there is the pathologic extracellular or intracellular "dystrophic" calcification, which occurs in association with inflammation and tissue damage. Third, there is a "metastatic" calcification, which occurs in association with altered serum levels of calcium and phosphate, and finally, calcium can be deposited as a component of crystal forming molecules within the joints in certain disease states.

Most cases of calcium deposition within the soft tissues are caused by local inflammation, trauma, fat necrosis, scleroderma, hyperparathryroidism, familial hyperphosphatemia, sarcoidosis, myeloma, metastases, etc. These encompass both dystrophic and metastatic calcifications and are typically calcium hydroxyapatite.

Punctate or linear calcification seen radiographically, seen along menisci, articular cartilage, or intervertebral disks, is generally due to calcium pyrophosphate deposition (CPPD disease). This deposition can very rarely be massive and simulate tophaceous deposits. In such cases the term tophaceous pseudogout may be appropriate [29].

Calcification of osteoid (bone mineralization) differs from soft tissue calcification in being an orderly process. It is distributed within the hole zones of collagen molecules. This method does not disrupt the spatial organization of collagen. The process is tightly regulated, but poorly understood. The mineral is initially deposited as amorphous calcium phosphate. The initial solid phase is formed at neutral pH. This phase is randomly and poorly oriented. Subsequently a series of solid phase transformations occur that lead to poorly crystalline hydroxyapatite as the final stable solid phase. The initiation of mineralization is probably caused by heterogeneous nucleation, the active binding of calcium, phosphate, and calcium phosphate complexes at the nucleation site in the matrix rather than by simple precipitation. In mature bone, it is possible that poorly crystalline calcium carbonate containing hydroxyapatite is deposited rather than an amorphous calcium phosphate or hydroxyapatite.

The Process of Mineralization

The process of mineralization is complicated and has not been satisfactorily elucidated. It is probably under genetic control, and since the physiologic state of extracellular fluids is supersaturated with respect to octacalcium phosphate, there are probably crystal inhibitors present. These include substances such as pyrophosphate and serum proteins. Matrix vesicles within bone and cartilage cells are thought to be helpful in this process.

It must be emphasized that mineralization is also under hormonal control. Vitamin D plays an important role. Other exogenous factors that affect mineralization include aluminum intoxication, fluoride intoxication (osteofluorosis), and phosphate deficiency. The mechanisms of action of aluminum and fluoride are as yet unclear. Mineralization is thus more than just a straightforward physicochemical process.

Mineral Deposits

Pathologic mineralization can be of several different types (dystrophic, metastatic, or crystal deposition). Calcification deposited in metastatic calcification (associated with increased serum calcium) is often intracellular. There are several factors that are important in mineralization (Table 1.2).

Remodeling of Bone

Bone undergoes "remodeling" throughout life. This involves the *coupling* of "old bone" resorption and "new" bone formation. Thus all skeletal bone is "renewed" on a continuous basis. This mechanism is important, because of the cyclical loading and torsional stresses that the skeleton undergoes. In the absence of renewal, the skeletal bone would fatigue from repetitive loads within a short period of time.

Bone turnover or remodeling is thought to occur in discrete foci or packets scattered throughout the skeleton. Each packet takes 3–4 months to complete. Such foci have been termed bone remodeling units or BRUs by Frost, who described the process in 1964.

About 25% of the metabolically active trabecular and about 3% of the cortical bone completely renews itself each year [15, 30]. The amount of bone added in each remodeling cycle, however, reduces slightly with age. This is probably due to a decreased number of osteoblasts and has been suggested as a possible mechanism for age related (but not post-menopausal) osteoporosis.

In the adult remodeling takes place by three mechanisms:

- Apposition and resorption at the endosteal surface
- Apposition and resorption at the periosteal surface
- Activation, resorption, and formation at the Haversian system

As can be visualized, the first two processes would result in alterations in the thickness and width of tubular bones. Conditions such as acromegaly (increased apposition), osteopetrosis, and hypothyroidism (decreased resorption) as well as hyperthyroidism (increased resorption) are particularly prone to alter the bones by these mechanisms.

Bone formation during the remodeling process requires prior resorption. Resorption takes approximately 10–15 days. The resorption is carried out by a "cutting cone"

Table 1.2 Factors important in mineralization

Collagen	Collagen provides oriented support for the newly formed crystals. The post-translational changes in collagen type I make it possible for diffusion of large hydrated ions such as calcium phosphate into the fibril
Calcium-binding proteins	Phosphoproteins and sialoproteins in the bone matrix may bind calcium to promote crystal deposition and growth, thus acting as nucleators. Crystal growth could then depend on the conformational change in these proteins after deposition. The initiation of mineralization is coincident with the depolymerization of proteoglycan molecules.
	Proteoglycans may inhibit calcification by a number of mechanisms including shielding of collagen, chemical interaction with collagen side chains, sequestering calcium or phosphate ions or occupying critical space in the molecule. Different phosphoproteins have varying importance in mineralization
Pyrophosphate	This is a naturally occurring inhibitor of calcification. It has a short half-life due to its rapid degradation by pyrophosphatases. Pyrophosphates are present in body fluids and increase the stability of the solution phase of calcium phosphate. Diphosphonates are pyrophosphate analogs and are powerful inhibitors of calcification in large doses
Bone Gla proteins	Osteocalcin is a highly conserved protein which is abundant in bone matrix. Because of its Gla residues, it is able to bind calcium, but its role in mineralization is controversial
Lipids and proteolipids	Within bone there are acid phospholipids that form complexes with calcium phosphate and could, thereby, influence mineralization. These substances have the capacity to bind to calcium
Alkaline phosphatase	This is an ectoenzyme produced by osteoblasts and is likely to be involved with the mineralization process. Patients with decreased amounts of enzyme (hypophosphatasia) have impaired mineralization (see osteomalacic syndromes in metabolic bone disease). Alkaline phosphatase may be involved in the degradation of inorganic pyrophosphate, thus providing a sufficient level of organic phosphate for mineralization to proceed

of osteoclasts. The trigger for resorption includes the stimulatory cytokines IL-1 and IL-6 produced by osteoblasts, as well as perhaps, the integrin–RGD sequence interaction as well as multiple factors such as transcription factors and membrane proteins.

The osseous defect created by osteoclastic resorption is filled in by fibrovascular tissue. The fibrovascular core contains pericytes, loose connective tissue, macrophages, mesenchymal stem cells, and undifferentiated osteoprogenitor cells. The outer edge of the osteon (where resorption ends and bone formation first starts) is marked by an intensely basophilic line – the "cement" or the "reversal" line. This area is poor in collagen and mineral and has a high content of sulfur.

Bone formation is carried out by osteoblasts. The process takes approximately 3 months. Osteocytes in small areas of bone that get cut off by newly forming osteons remain as "interstitial" lamellae. Osteoblastogenesis has *identifiable processes of chemotaxis, proliferation, and differentiation of osteoblasts*. This is then followed by mineralization and the cessation of osteoblast activity.

Mediators of osteoblastic activity and bone formation include transforming growth factor-beta (TGF-β), bone GLA protein fragments, platelet-derived growth factors A and B (PDGF A and B) all of which are chemotactic for osteoblasts. Proliferation of osteoblasts is thought to be mediated by TGF-β, PDGF, IGF I and II, and fibroblast growth factors (FGFs). Cytokines that may play a role in the differentiation of osteoblasts and the production of alkaline phosphatase activity within these cells include IGF-I and bone morphogenetic protein-2 (BMP-2).

"Coupling" or bone *formation* and bone *resorption* is unexplained. There is emerging evidence that suggests that "osteoclastogenic" cytokines such as IL-6, IL-1, and IL-11 as well as "osteoblastogenic" cytokines such as leukemia inhibitory factor may be stimulated together by the same signal transduction pathway. Glycoprotein 130 is a molecule present in this pathway and is involved in the transduction of the signal delivered by each of these cytokines. Sex steroids inhibit, whereas parathyroid hormone and vitamin D_3 increase glycoprotein 130 in experimental models [15, 30]. This model, if validated further, would conveniently explain bone formation–resorption coupling as well as coincide with the various acknowledged facts about the role of these hormones in bone turnover.

Another mechanism that may explain "coupling," is the release of osteoblast-stimulating factors such as IGF I and II and TGF-β during the osteoclastic process. Coupling is the rationale for the counterintuitive, but clinically validated method of treating osteoporosis by giving parathyroid hormone.

Several diseases of bone are superimposed on this normal cellular remodeling sequence. In diseases, such as primary hyperparathyroidism, hyperthyroidism, and Paget disease, there is osteoclast activation. There is also a compensatory and relatively balanced increase in bone formation, because of coupling.

Other conditions are due to abnormal coupling. Decreased bone formation after resorption is seen in the osteolytic lesions of myeloma, where there may be a defect in osteoblast maturation. In solid tumors and in elderly patients with age-related osteoporosis there may be similar mechanisms at work. Osteoblastic activity in the absence of prior osteoclastic activation is thought to occur in some special

situations such as osteoblastic metastases, e.g., prostate carcinoma metastases, and in bones' response to fluoride therapy.

The Regulation of Bone and Cartilage

Endocrine

- Parathyroid hormone (PTH) and PTHrP
- Calcitonin
- Vitamin D
- Vitamin A
- Estrogens
- Androgens
- Growth hormone (GH)

Paracrine/Autocrine

- Proteoglycans
- Glyco- and phosphoproteins
- Gamma-carboxyglutamic acid proteins
- Proteolipids
- Growth factors
  - Transforming growth factor-beta (TGF-β)
  - Bone morphogenetic protein (BMP)
  - Insulin-like growth factors (IGF I and II)
  - Epithelial growth factor
  - Fibroblast growth factor
  - Platelet-derived growth factor (PDGF A and B)
- Other cytokines (interleukins IL)

Parathyroid Hormone

Parathyroid hormone (PTH) is an 84-amino acid, single-chain polypeptide (called PTH 1-84). It is synthesized in the parathyroid gland from a biosynthetic precursor pro-PTH. PTH acts on bone, intestine, and kidney. In the latter two, it enhances calcium resorption. It is also involved in the metabolism of phosphate, bicarbonate, ammonium, magnesium and in the regulation of acid–base homeostasis in the body. The actions of PTH are influenced by several factors such as 1,25-dihydroxyvitamin D_3, IL-1, TGF-α, EGF. The production of several of these substances is in turn under the control of PTH in a complicated interrelated web.

The best known effect of PTH is osteoclast activation and subsequent bone resorption. Receptors for PTH are found on pre-osteoblasts, osteoblasts, and chondrocytes. They are not, however, present on osteoclasts. This supports the notion, that the action of PTH on the latter is dependent on the osteoblasts for the production of other cytokines, for example, IL-1, IL-6, and E-series prostaglandins. The net result of exposure to PTH is osteoclast activation and the initiation of bone resorption leading to calcium release from bone.

Additionally, there is evidence to suggest, that in certain situations PTH stimulates bone formation. When administered continuously, it increases osteoclastic resorption and suppresses bone formation. When administered in low doses, intermittently, it stimulates bone formation without resorption. This bone-forming effect of PTH has been termed the anabolic effect. This anabolic effect too (like the resorptive effect) is probably indirect and mediated via substances such as IGF-1, TGF-β. Although the anabolic effect of PTH is dependent on intermittent administration, when serum level of PTH is maintained high even for a few hours it initiates processes leading to new osteoclast formation, and the consequent bone resorption that overrides the effects of activating genes that direct bone formation. Identification of PTH-related protein (PTHrP) expression by cells early in the osteoblast progenitor cells, and its action through the PTH-1 receptor (PTH1R) upon mature osteoblastic cells, together with the observation that PTHrP+/– mice are osteoporotic, raise the possibility that PTHrP is a crucial paracrine regulator of bone formation.

Calcitonin

Calcitonin is a peptide hormone produced by the thyroid parafollicular C cells. Its synthesis and secretion is under the influence of extracellular calcium levels and certain gastrointestinal hormones such as gastrin. It is encoded by a complex gene that undergoes alternate splicing. This gene is responsible for several other peptides such as a calcitonin gene-related peptide.

Calcitonin causes a short lived fall in plasma calcium. It acts via a receptor to stop the resorption of bone. These receptors are present on osteoclasts, preosteoclasts, monocytes, and certain tumor cells. The major effect on blocking of bone resorption, however, is probably via the mature osteoclast. The mechanism of action is via enhancement of adenylate cyclase and stimulating cAMP accumulation. In addition, calcitonin may have mitogenic effect on bone cells. Calcitonin also promotes renal calcium excretion. Its effects on calcium homeostasis are lost after 24–48 h. This loss of effectiveness can be reduced by simultaneous administration of corticosteroids. A possible role of calcitonin in calcium homeostasis is to maintain normocalcemia after a large calcium-containing meal.

The absence of significant changes in bone mineral density caused by decline or overproduction of calcitonin in humans has raised the question, whether the pharmacological action of calcitonin as an inhibitor of bone resorption is

also of physiological relevance. New data suggest that calcitonin has a dual action as an inhibitor of bone remodeling, which may explain, at least in part, why alterations of calcitonin serum levels in humans do not result in major changes of bone mineral density [31].

Calcitonin has a role in the therapy of hypercalcemia of malignancy, in Paget disease, and in osteoporosis. In this context, it should be mentioned that there is evidence to suggest that the osteoclasts of Paget patients are hyperresponsive to calcitonin, and remain so for longer periods of time than do control cells. The molecular mechanisms for this hyperresponsivity is unknown [32].

Vitamin D

Ergosterol and 7-dehydrocholesterol are the precursors for this hormone/vitamin. These compounds are stored in the skin, transported in the body via an alpha-globulin-binding protein or vitamin D-binding protein (DBP) and become activated by ultraviolet light with a wavelength of 315 nm. This activation generates calciferol and cholecalciferol, respectively. These substances are hydroxylated in the liver in the presence of magnesium to yield 25-hydroxyvitamin D and then converted further in the proximal tubule of the kidney to its active form: 1,25-dihydroxyvitamin D. This hormone/vitamin is one of the prime controllers of calcium metabolism in the gut, proximal tubule, and bone. Reduced calcium and increased PTH are the kidneys to increase 1,25-dihydroxyvitamin D production.

The actions of 1,25-dihydroxyvitamin D include stimulation of calcium-binding proteins, increased osteocalcin production, increased osteoclastic activation and bone resorption, monocytic maturation, myelocytic differentiation, skin growth, and insulin secretion. Lack of vitamin D results in impaired mineralization of newly formed bone – the clinical disease resulting from this is known as rickets in children, and osteomalacia in adults. In both of these conditions, osteoid, the proteinaceous bone matrix, accumulates, but does not mineralize. Excessive vitamin D leads to increases in bone resorption and hypercalcemia.

Vitamin D works through specific vitamin D receptors. Receptor sites for 1,25-dihydroxyvitamin D have been identified on several cells. Gene errors in several forms of rickets have been found to occur within these nuclear receptors. There is also a suggestion that post-menopausal osteoporosis may be genetically predetermined by the polymorphisms present in the vitamin D receptor gene [33].

Vitamin A

Retinoids, in excess, decrease the formation of bone and cartilage matrix. A deficiency of vitamin A has the opposite effect. Several years ago, it was discovered that an imbalance of vitamin A during embryonic development has dramatic teratogenic effects. These effects have since been attributed to vitamin A's most active metabolite, retinoic acid (RA), which itself profoundly influences the development of multiple organs including the skeleton. Retinoid signaling involves several components, including the skeletogenic master regulatory factors, Sox9, and Cbfa1.

Estrogens

In experimental situations, reduced estrogen leads to bone loss. This may be a direct effect on osteoblasts and possibly osteoclasts, although it could be mediated via PTH and calcitonin.

Androgens

These act to maintain bone mass through action via receptors on osteoblasts. There is an inhibition of the action of PTH and calcitonin.

Growth Hormone

The effect of growth hormone on bone is mostly mediated via insulin-like growth hormone (IGF). There may, however, be a direct effect through growth hormone receptors on osteoblasts and chondrocytes.

Proteolipids

These are membrane proteins complexed with acidic phospholipids. They cause hydroxyapatite deposition. They have a high concentration in the matrix vesicles, where they are thought to have a role in the export of protons and the import of calcium and phosphate across the cell membrane.

Growth Factors

Transforming Growth Factor-Beta: TGF-β

TGF-β was initially isolated from "transformed" neoplastic cells in tissue culture studies. Two "factors" were isolated and named TGF-α and -β. TGF-α is not found in bone and is now called epidermal growth factor. There are three human isoforms of TGF-β. The largest store of TGF-β in the body is the bone matrix. The current hypothesis is that TGF-β induces bone formation during remodeling. The action of TGF-β in bone induction, however, may be only in conjunction with other factors such as the bone morphogenetic proteins (BMPs).

Bone Morphogenetic Proteins (BMP)

A bone-inducing substance was first postulated in 1952 by Marshall Urist et al. [34]. Since then, at least 10 proteins with this property have been extracted from *demineralized bone* and named bone morphogenetic proteins 1–10. Their amino acid sequences have been characterized and synthesized using recombinant DNA technology [35–40]. Purified BMPs have been used to promote bone repair. Several trials have shown their efficacy in experimental models [41–43].

Insulin-Like Growth Factors: IGF (I and II)

Insulin-like growth factors are produced by many kinds of cells including osteoblasts and chondrocytes. They act via receptors to promote proliferation, differentiation, and matrix production of bone and cartilage. The action of growth hormone is closely linked with the IGFs.

Other Growth Factors

These include epithelial growth factor, acid and basic fibroblast growth factors, and platelet-derived growth factors (A and B). They are thought to be particularly important in bone remodeling. PDGFs are heterodimers of A and B chains and function via specific receptors. Mutations in the fibroblast growth factors have been thought to play a role in certain kinds of skeletal deformities, including achondroplasia, Apert syndrome, Cruzon syndrome, Pfeiffer syndrome, and Jackson–Weiss syndrome.

Cytokines: Prostaglandins and Interleukins

Prostaglandins: Prostaglandins have been shown to have multiple effects on bone cells and sometimes contradictory effects in different species. They are powerful bone resorbers in certain culture studies (especially true of the E series). Prostaglandins are produced by monocytes under appropriate stimuli. It is possible that some of the effects of interleukins are mediated by prostaglandins.

IL-6: This is produced by osteoblasts and bone marrow stromal cells in response to PTH, vitamin D_3, TGF-β, IL-1, and TNF. Human osteoclastoma cells respond to this cytokine. It is still unclear, whether normal mature osteoclasts respond to IL-6. It has a pathogenetic role in diseases such as multiple myeloma, Paget disease, rheumatoid arthritis, and Gorham disease (vanishing bone disease). Experimentally, estrogens and androgens inhibit the production of IL-6 by osteoblasts, and additionally, there is evidence to suggest that osteoclastic activity may be inhibited by anti-IL-6 antibodies [15].

Mechanosensory Systems and Stretch Studies (Wolff Law)

Wolff law – Every change in *form and function* of bones is followed by changes in *the internal architecture and external conformation*, in strict accordance with mathematical laws (Julius Wolff, 1882).

Wolff law has been confirmed by experimental studies, but only recently there have been studies to investigate the basis of the law at *a molecular level*. It is clear that mechanical forces have definite effects on the skeleton. For example, individuals who lift weights tend not only to develop bigger and stronger muscles but also bones. On the other hand, weightlessness associated with decreased gravity causes rapid decrease in bone mass reflecting the need for constant force in maintaining skeletal bone. Further, an inability to use a limb causes it to undergo "disuse" osteoporosis. Children with malunited limb fractures frequently remodel into almost normal bones. If, on the other hand, they are unable to bear weight, or use the limb owing to a disease such as poliomyelitis, then the fractures stay malunited. Paraplegics or quadriplegics with a spastic form of paresis have exuberant callus; if, however, they have a flaccid paresis they fail to develop such an exaggerated response.

These examples illustrate the close linkage of mechanical forces with skeletal response and bone formation. What is poorly understood, however, is how forces get translated into cellular events. It is likely that signaling mechanisms such as electrical or chemical messengers, such as certain cytokines, mediate these responses. Investigations into the mechanisms have suggested the presence of stretch-sensitive ion channels and stretch-dependent DNA synthesis in certain cells. In addition, when fluid flows through bone matrix carrying along a species of ion, it creates a stream-generated potential. Currents are also generated by a "piezoelectric" effect as a result of compression of the hydroxyapatite crystal. These are various methods by which Wolff law might operate to control osseous homeostasis.

References

1. Bliziotes M, Gunness M, Eshleman A, Wiren K. The role of dopamine and serotonin in regulating bone mass and strength: studies on dopamine and serotonin transporter null mice. J Musculoskelet Neuronal Interact 2002; 2(3):291–295.
2. Idris AI, van't Hof RJ, Greig IR, et al. Regulation of bone mass, bone loss and osteoclast activity by cannabinoid receptors. Nat Med 2005; 11(7):774–779.
3. Tam J, Ofek O, Fride E, et al. Involvement of neuronal cannabinoid receptor CB1 in regulation of bone mass and bone remodeling. Mol Pharmacol 2006; 70(3):786–792.

4. Hohling HJ, Barckhaus RH, Drefting ER, Quint P, Athoff J. Quantitative electron microscopy of the early stages of cartilage mineralization. Metab Bone Dis Relat Res 1978; 1:109–114.
5. Landis WJ, Song MJ, Leith A, McEwen L, McEwen BF. Mineral and organic matrix interaction in normally calcifying tendon visualized in three dimensions by high-voltage electron microscopic tomography and graphic image reconstruction. J Struct Biol 1993; 110(1):39–54.
6. Khan SN, Bostrom MP, Lane JM. Bone growth factors. Orthop Clin North Am 2000; 31(3):375–388.
7. Rodan GA. Control of bone formation and resorption: biological and clinical perspective. J Cell Biochem Suppl 1998; 30–31:55–61.
8. Komori T, Yagi H, Nomura S, et al. Targeted disruption of Cbfa1 results in a complete lack of bone formation owing to maturational arrest of osteoblasts. Cell 1997; 89(5):755–764.
9. Otto F, Thornell AP, Crompton T, et al. Cbfa1, a candidate gene for cleidocranial dysplasia syndrome, is essential for osteoblast differentiation and bone development. Cell 1997; 89(5):765–771.
10. Ducy P, Amling M, Takeda S, et al. Leptin inhibits bone formation through a hypothalamic relay: a central control of bone mass. Cell 2000; 100(2):197–207.
11. Takahashi N, Yamana H, Yoshiki S, et al. Osteoclast-like cell formation and its regulation by osteotropic hormones in mouse bone marrow cultures. Endocrinology 1988; 122(4):1373–1382.
12. Watanabe H, Yanagisawa T, Sasaki J. Cytoskeletal architecture of rat calvarial osteoclasts: microfilaments, and intermediate filaments, and nuclear matrix as demonstrated by detergent perfusion. Anat Rec 1995; 243(2):165–174.
13. Horne WC. Toward a more complete molecular description of the osteoclast. Bone 1995; 17(2):107–109.
14. Sakai D, Tong HS, Minkin C. Osteoclast molecular phenotyping by random cDNA sequencing. Bone 1995; 17(2):111–119.
15. Manolagas SC, Jilka RL. Bone marrow, cytokines, and bone remodeling. Emerging insights into the pathophysiology of osteoporosis. N Engl J Med 1995; 332(5):305–311.
16. Ohsaki Y, Takahashi S, Scarcez T, et al. Evidence for an autocrine/paracrine role for interleukin-6 in bone resorption by giant cells from giant cell tumors of bone. Endocrinology 1992; 131(5):2229–2234.
17. Roodman GD, Kurihara N, Ohsaki Y, et al. Interleukin 6. A potential autocrine/paracrine factor in Paget's disease of bone. J Clin Invest 1992; 89(1):46–52.
18. Bucay N, Sarosi I, Dunstan CR, et al. Osteoprotegerin-deficient mice develop early onset osteoporosis and arterial calcification. Genes Dev 1998; 12(9):1260–1268.
19. Dougall WC, Glaccum M, Charrier K, et al. RANK is essential for osteoclast and lymph node development. Genes Dev 1999; 13(18):2412–2424.
20. Hughes AE, Ralston SH, Marken J, et al. Mutations in TNFRSF11A, affecting the signal peptide of RANK, cause familial expansile osteolysis. Nat Genet 2000; 24(1):45–48.
21. Kong YY, Feige U, Sarosi I, et al. Activated T cells regulate bone loss and joint destruction in adjuvant arthritis through osteoprotegerin ligand. Nature 1999; 402(6759):304–309.
22. Kong YY, Yoshida H, Sarosi I, et al. OPGL is a key regulator of osteoclastogenesis, lymphocyte development and lymph-node organogenesis. Nature 1999; 397(6717):315–323.
23. Lacey DL, Timms E, Tan HL, et al. Osteoprotegerin ligand is a cytokine that regulates osteoclast differentiation and activation. Cell 1998; 93(2):165–176.
24. Wong BR, Rho J, Arron J, et al. TRANCE is a novel ligand of the tumor necrosis factor receptor family that activates c-Jun N-terminal kinase in T cells. J Biol Chem 1997; 272(40): 25190–25194.
25. Yasuda H, Shima N, Nakagawa N, et al. Identity of osteoclastogenesis inhibitory factor (OCIF) and osteoprotegerin (OPG): a mechanism by which OPG/OCIF inhibits osteoclastogenesis in vitro. Endocrinology 1998; 139(3):1329–1337.
26. Yasuda H, Shima N, Nakagawa N, et al. Osteoclast differentiation factor is a ligand for osteoprotegerin/osteoclastogenesis-inhibitory factor and is identical to TRANCE/RANKL. Proc Natl Acad Sci USA 1998; 95(7):3597–3602.
27. Sela J, Amir D, Schwartz Z, Weinberg H. Ultrastructural tissue morphometry of the distribution of extracellular matrix vesicles in remodeling rat tibial bone six days after injury. Acta Anat (Basel) 1987; 128(4):295–300.
28. Ressoret J, De Crombrugghe B. Type I collagen. In: JP Bilezikian LGR, GA Rodan (Eds.), Principels of Bone Biology, 2nd ed. San Diego: Academic Press, 2002; 189–210.
29. Ishida T, Machinami R. Reactive bone and cartilage forming processes of the hands and feet. Pathol Int 1995; 45(12):975–976.
30. Manolagas SC, Bellido T, Jilka RL. New insights into the cellular, biochemical, and molecular basis of postmenopausal and senile osteoporosis: roles of IL-6 and gp130. Int J Immunopharmacol 1995; 17(2):109–116.
31. Huebner AK, Schinke T, Priemel M, et al. Calcitonin deficiency in mice progressively results in high bone turnover. J Bone Miner Res 2006; 21(12):1924–1934.
32. Mundy GR, Boyce B, Hughes D, et al. The effects of cytokines and growth factors on osteoblastic cells. Bone 1995; 17(2 Suppl):71S–75S.
33. Morrison NA, Qi JC, Tokita A, et al. Prediction of bone density from vitamin D receptor alleles. Nature 1994; 367(6460):284–287.
34. Urist MR, Mc LF. Osteogenetic potency and new-bone formation by induction in transplants to the anterior chamber of the eye. J Bone Joint Surg Am 1952; 34-A(2):443–476.
35. Kessler E, Takahara K, Biniaminov L, Brusel M, Greenspan DS. Bone morphogenetic protein-1: the type I procollagen C-proteinase. Science (New York) 1996; 271(5247):360–362.
36. Reddi AH. BMP-1: resurrection as procollagen C-proteinase. Science (New York) 1996; 271(5248):463.
37. Urist MR, DeLange RJ, Finerman GA. Bone cell differentiation and growth factors. Science (New York) 1983; 220(4598):680–686.
38. Urist MR, Sato K, Brownell AG, et al. Human bone morphogenetic protein (hBMP). Proc Soc Exp Biol Med (New York) 1983; 173(2):194–199.
39. Urist MR, Wallace TH, Adams T. The function of fibrocartilaginous fracture callus. Observations on transplants labelled with tritiated thymidine. J Bone Joint Surg 1965; 47:304–318.
40. Wozney JM, Rosen V, Celeste AJ, et al. Novel regulators of bone formation: molecular clones and activities. Science (New York) 1988; 242(4885):1528–1534.
41. Cook SD, Salkeld SL, Rueger DC. Evaluation of recombinant human osteogenic protein-1 (rhOP-1) placed with dental implants in fresh extraction sites. J Oral Implantol 1995; 21(4):281–289.
42. Cook SD, Wolfe MW, Salkeld SL, Rueger DC. Effect of recombinant human osteogenic protein-1 on healing of segmental defects in non-human primates. J Bone Joint Surg Am 1995; 77(5):734–750.
43. Shimizu T, Okayama A, Inoue T, Takeda K. Analysis of gene expression during staurosporine-induced neuronal differentiation of human prostate cancer cells. Oncol Rep 2005; 14(2):441–448.

Chapter 2

Systematic Approach to Metabolic Diseases of Bone

Akbar Bonakdarpour

Abstract This chapter begins with a brief introduction to bone metabolism. The main focus is discussing generalized diminished bone density (GDBD), but examples of generalized increased bone density are also briefly presented. Since various causes of GDBD are not considered in the WHO definitions, a radiologic classification based on pathophysiology of GDBD will follow, complementing the WHO definitions and distinguishing osteoporosis from osteomalacia, osteolysis, and marrow proliferative disorders. The primary and secondary osteoporoses are discussed. Diagnostic imaging of osteoporosis by radiography, dual X-ray absorptiometry (DXA), quantitative CT analysis, microcomputerized tomography, quantitative ultrasonography, and MRI is briefly reported. The major risk of advanced osteoporosis is fracture of the spine, hip, and less frequently other bones. A summarized treatment of osteoporosis is followed by discussion of osteomalacia, rickets, hypervitaminoses D and A, as well as fluorosis.

Keywords Metabolic bone disease • Osteoporosis • Osteomalacia • Rickets • Marrow packing disorders • WHO definitions of osteoporosis • Dual X-ray absorptiometry • Quantitative CT analysis • MRI BMD measurement • Scurvy • Reflex sympathetic dystrophy • Osteogenesis imperfecta • Homocystinuria • Osteomalacia • Rickets • Hypophosphatasia • Hypervitaminosis D • Hypervitaminosis A • Fluorosis

Introduction

Metabolic diseases of bone, strictly defined, are those disorders of the skeletal system related to abnormalities of all synthetic (anabolic) and degradative (catabolic) biochemical reactions in the body. With this definition, most skeletal diseases can be considered metabolic in nature. Narrower definitions of the so-called "metabolic diseases of bone" are almost as numerous as the number of authors who write about them. Endocrine dysfunctions, Paget disease, various nutritional problems, some hereditary diseases of bone, and even other categories of disorders have been included under this heading. In this chapter we will limit discussion to diseases that cause generalized reduction in bone mineral and regional osteoporosis.

Metabolic causes of increased bone density such as hypervitaminosis D and fluorosis will be very briefly mentioned as prototypes.

An attempt will be made to correlate the 1994 World Health Organization (WHO) definitions of osteoporosis with radiopathophysiological classification of "generalized diminished bone density" (GDBD). The main purpose is to make the two systems complementary. The WHO "definitions" are basically concerned with various stages of osteoporosis. *Admittedly most, but not all cases of "generalized diminished bone density" (GDBD) are due to osteoporosis.* Our approach will give a road map to distinguish osteoporotic cases from nonosteoporotic entities, such as various forms of osteomalacia, hyperparathyroidism, multiple myeloma, Gaucher disease, and other forms of GDBD.

Bone Metabolism

A brief discussion of metabolism of calcium, phosphorus, parathyroid hormone (PTH), and vitamin D will help to better understand metabolic bone disease, its diagnosis, and treatment.

Calcium Metabolism

There are between 1,000 and 2,000 g of calcium in the average adult human body, 98% of which is in the skeleton. In

Akbar Bonakdarpour (✉)
Department of Radiology, Temple University School of Medicine, Philadelphia, PA 19140, USA
e-mail: akbarbonakdarpour@yahoo.com

A. Bonakdarpour et al. (eds.), *Diagnostic Imaging of Musculoskeletal Diseases: A Systematic Approach*,
DOI 10.1007/978-1-59745-355-4_2, © Springer Science+Business Media, LLC 2010

adults, 80% of calcium is in cortical bone and 20% in trabecular bone. Calcium exists in three forms in plasma: as ions, bound to proteins, and as diffusible complexes. The normal range of calcium in serum is between 9 and 11 mg per 100 cm^3 (US Food and Drug Administration, Investigators Manual 2001). At homeostasis, urinary excretion of calcium typically equals net dietary intake. Serum calcium is increased by PTH and vitamin D and is decreased by acute hypercalcemia and calcitonin.

Three organ systems have roles in calcium (Ca^{2+}) metabolism:

1. GI tract: calcium is absorbed primarily in the proximal small bowel (both vitamin D and PTH influence calcium absorption).
2. Kidneys: control calcium excretion by glomerular filtration and tubular reabsorption. PTH and vitamin D control the latter process. The most active form of vitamin D is [1,25$(OH)^2$ cholecalciferol]. Cholecalciferol is vitamin D3. Its first hydroxylation occurs in the liver and the second one occurs in the kidney to produce the most active form of vitamin D.
3. Bones: PTH and vitamin D cause resorption of calcium from mineralized matrix. *Calcitonin* is produced by the parafollicular cells of the thyroid glands and opposes the actions of PTH, thus decreasing the resorption of calcium from bone. Calcitonin is secreted in response to an increase in serum calcium but does not play an important role in normal calcium homeostasis.

Phosphorus Metabolism

There are about 1,000 g of phosphorus in the average human adult body, 85% of which is in the skeleton. The normal range of phosphorus in the serum is 3–4.5 mg per 100 cm^3, according to the US Food and Drug Administration, Investigators Manual 2001. Phosphorus is filtered through the glomerulus and largely reabsorbed in the proximal tubule. Hypophosphatemia increases tubular reabsorption of phosphorus. Hyperphosphatemia decreases tubular reabsorption of phosphorus. Parathyroid hormone inhibits tubular reabsorption of phosphorus.

Parathyroid Hormone

Parathyroid hormone works at multiple levels. Its effects on the intestinal tract, bones, and kidneys maintain serum calcium levels:

In the presence of vitamin D, PTH stimulates intestinal calcium absorption.

PTH promotes calcium resorption from bone.

In the kidneys, PTH inhibits reabsorption of sodium, calcium, phosphate, and bicarbonate ions in the proximal tubule of the nephron. It stimulates calcium reabsorption in the distal tubule. PTH also stimulates renal synthesis of 1,25$(OH)^2$ D3 (1,25-dihydroxycholecalciferol) from hepatically formed 25 hydroxycholecalciferol.

PTH also maintains serum magnesium level. (The normal range of magnesium in the blood is 1.8–3.6 mg per 100 cm^3 (US Food and Drug Administration, Investigators Manual 2001).) Magnesium influences secretion of PTH but is much less active than calcium.

Vitamin D Metabolism

Vitamin D leads to an increase in serum calcium and phosphate, and can be derived from two main sources. Vitamin D3 is produced as a result of ultraviolet light exposure to the skin, whereas vitamin D2 is obtained from dietary sources.

The primary active form of vitamin D is [1,25$(OH)^2$ cholecalciferol or dihydroxycholecalciferol], made in the kidneys. Cholecalciferol is vitamin D3, which in the liver modifies to 25-hydroxycholecalciferol and in the kidney transforms to the most active form. This form of vitamin D elevates plasma calcium and phosphate levels through several actions.

1. Promotes calcium absorption by the intestines.
2. Promotes phosphorus absorption by the intestines.
3. Potentiates bone resorption induced by PTH.
4. Possibly has a direct effect on bone mineralization.
5. Promotes calcium reabsorption by the kidney.
6. Promotes phosphorus reabsorption by the kidney.

Biochemical Markers of Bone Turnover

Biochemical markers of bone turnover provide an indirect method of evaluating bone metabolism. These markers fall into two groups, those signaling bone formation and those signaling bone resorption. The former are proteins that are secreted by active osteoblasts and include osteocalcin, bone alkaline phosphatase, procollagen type I N-propeptide and C-propeptide. Biochemical markers of bone resorption are mainly products of catabolism from resorbed type I collagen: C-terminal and N-terminal cross-linking telopeptides of type I collagen, cross-linking molecule deoxypyridinoline, and certain amino acids such as hydroxyproline or galactosyl hydroxylysine. Some of these are measured easily and

thus routinely used in the clinical evaluation of patients. In particular, they may be useful for monitoring osteoporosis therapy.

Bone Density

Maintenance of bone mineral depends upon a balance between bone synthesis by osteoblasts and bone resorption by osteoclasts. Normal bone density is related to a balance among the elaboration of osteoid, the mineralization of the osteoid, and the physiologic bone lysis. These functions are controlled directly or indirectly by hormonal and biochemical factors beyond and within the bone. A change in the rate of any of these functions, without a corresponding adjustment in the rate of the others, causes an imbalance that either increases or decreases bone density. Clinically, decreased bone density is more important, because it is much more common than increased bone density.

The healthy human accumulates bone mass from birth until young adulthood. Peak bone mass and consequently peak bone density are achieved around the age of 30 years. This peak is influenced by a number of factors, including diet, sun exposure, race, and sex. In general, blacks attain higher bone mass than do Caucasians and Asians. Peak bone density is higher in men.

Normally, once peak bone mass is achieved, there is almost a decade of stability where bone density remains unchanged. During this stable period, there is normal bone turn over (remodeling or coupling), which means bone resorption and bone production are balanced. Bone remodeling continues during the entire life and it occurs in compact or cortical bone as well as trabecular or medullary bone. At maturity, 80% of bone is cortical and 20% is trabecular. Normal bone remodeling (coupling) affects 2–3% of the whole skeletal mass per year.

Generalized Diminished Bone Density

In young adults, bone resorption and bone formation are in equilibrium and bone density remains stable. When bone loss outweighs bone gain, bone density decreases. In both genders, around 40 years of age the process of involutional osteoporosis (bone loss) starts and bone density begins to gradually decrease. Involutional osteoporosis has an initial rate of 0.3–0.5% of bone loss per year. This process continues throughout life and accelerates with age. Women experience a superimposed, transient period of postmenopausal, accelerated bone loss. Women lose about 35% of their cortical and 50% of their trabecular bone over their lifetime. Peak BMD is higher and bone loss is of smaller magnitude (20–30%) in men. The rate at which this occurs is under the influence of several factors, including activity, diet, tobacco use, and the presence of estrogen.

Postmenopausal women tend to lose bone mineral more rapidly than do the premenopausal women. The accelerated postmenopausal bone loss may cause an additional 2–3% decline in bone mineral content per year. It occurs initially in the trabecular and then in the cortical compartment. This phase of rapid bone loss eventually decreases and gradually reaches a plateau after 8–10 years. In post-oophorectomy cases, bone loss has been reported to be as high as 12% over a 2-year period.

In men and women, the process of protracted bone loss (involutional osteoporosis) accelerates after the age of 70 years. Hormonal imbalances have different effects on the development of osteoporosis in men. Testicular secretory function declines slowly. Even in very old men, the average level of total testosterone is only 20% lower than in young men. In contrast, concentrations of bioavailable testosterone are 50–60% lower than those found in young men. This leads to bone mineral loss, higher levels of biochemical markers of bone turnover, and higher prevalence of fractures.

At the tissue level, increased bone resorption results in the perforation and disappearance of trabeculae (Fig. 2.1). When the trabeculae disappear, the metabolically active surface available for osteoclasts decreases and bone loss tends to slow down.

There are three distinct types of generalized diminished bone density: osteoporosis, osteomalacia, and osteolysis. Each entity has different causes and will be described in more detail in this chapter. Here we introduce them briefly and they will be discussed in more detail later.

In osteoporosis and some cases of generalized osteolysis, such as primary hyperparathyroidism, there is diffuse bone loss, but there is no chemical abnormality in the composition of bone. In other words, one gram of normal bone has an identical chemical composition to one gram of osteoporotic or bone from a patient with hyperparathyroidism. On the other hand, in osteomalacia, where there is diminished mineralization of the osteoid, the chemical composition of bone is abnormal.

Osteoporosis is defined as a *nonfocal* reduction of bone mass per unit volume (cubic centimeter) without change in chemical composition of bone. Osteoporosis can also be defined as a chronic, progressive disease characterized by low bone mass, microarchitectural bone deterioration (Fig. 2.1), and decreased bone strength leading to bone fragility and increased fracture risk.

Regional osteoporosis occurs in cases of disuse osteoporosis (such as immobilization), reflex sympathetic dystrophy,

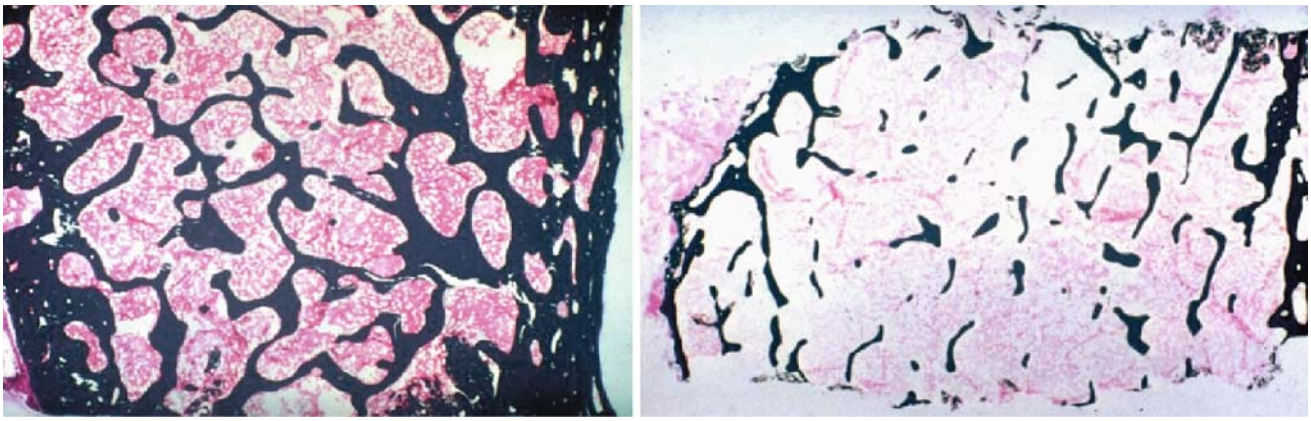

A B

Fig. 2.1 Osteoporosis. **a** – Low power microscopic section of normal bone in an iliac crest biopsy. **b** – Microscopic section of osteoporotic bone in an iliac crest biopsy. Note thinning and discontinuity of bone trabeculae. Coarsening of the trabecular pattern on radiographs and CT images is a reflection of these histological aberrations. **a** and **b** are courtesy of Dr. Peter Bullough, Hospital for Special Surgery, New York and Dr. Vincent Vigorita, State University of New York, Health Sciences Center, Brooklyn, NY

regional migratory osteoporosis, and several other entities that will be discussed later in the appropriate sections of this chapter.

Osteomalacia arises when there is diminished mineralization of osteoid. There may be normal or excessive production of osteoid. The result is an alteration in the chemical composition of the bone with greater elasticity but lower tensile strength. Osteomalacia is diagnosed histologically by the presence of enlarged osteoid seams observed in decalcified sections of the bone.

Osteolysis is generally considered to be a focal loss of bone in direct response to a pathologic process such as infection, neoplasm, other focal processes such as post-traumatic clavicular osteolysis, a local manifestation of a systemic disease such as distal clavicular osteolysis that occurs in hyperparathyroidism and rheumatoid arthritis, or acroosteolysis of the digital tufts as observed in polyvinyl chloride workers, scleroderma, epidermolysis bullosa, hyperparathyroidism, frostbite, and thermal injury. The various forms of regional or focal osteolysis are covered in the appropriate chapters of this book. Here we confine our discussion to comparing osteoporosis with generalized osteolysis. This may be caused by an osteoclast-activating hormone (OAH) (such as parathormone) or osteoclast-activating factors (OAFs) such as the OAFs excreted by myeloma cells or in other types of cancer cells. Generalized osteolysis may also be seen in marrow packing disorders such as Gaucher disease. In this group of patients, generalized diminished bone density (GDBD) is neither due to osteoporosis nor due to osteomalacia.

We will use the general term of osteopenia to include the three distinct forms of generalized diminished bone density (GDBD), which are radiologically documented accurately by DXA, QCT, and quantitative ultrasonography (Table 2.1). *Most but not all cases of diminished bone density result from osteoporosis*.

In the following radiological classification (Table 2.1), we consider other causes of diminished bone density in addition to osteoporosis. This classification is complementary and not contradictory to WHO definitions of diminished bone density, introduced in 1994.

Admittedly, this radiological classification is an oversimplification of a very complicated problem. For

Table 2.1 Radiological classification of generalized diminished bone density (osteopenia)*

Osteopenia
Osteopenia is generalized diminished bone density (*GDBD*) of any cause or if the etiology is unknown. Osteopenia includes osteoporosis, osteomalacia, and osteolysis
Osteoporosis
Osteoporosis is defined as a reduction of bone mass per unit volume (cubic centimeter). The chemical composition of bone is normal. Histologically, it is diminished osteoid** formation
Osteomalacia
Osteomalacia is inadequate osteoid mineralization and chemical composition of bone is changed
Osteolysis
Osteolysis is increased rate of bone resorption by osteoclasts or it is caused by marrow proliferative and/or marrow packing disorders. The chemical composition of bone may or may not be changed. This cause of diminished bone density may be generalized or focal. In this classification we are interested in generalized form of this third group

*This classification takes into consideration pathophysiology of diminished bone density.

**Osteoid is bone matrix before calcification.

example, aging osteoporotic patients also tend to have increased levels of plasma PTH. Age-related secondary hyperparathyroidism is a significant cause of diminished bone density in elderly men and women due to calcium and vitamin D deficiency. Intestinal absorption of calcium decreases with age. Synthesis of endogenous vitamin D decreases from aging of the skin and lower sunlight exposure. Furthermore, synthesis of [1,25(OH)^2 D3] is also diminished from age-related reduction in the activity of renal enzyme (1 α-hydroxylase). Consequently, calcium and vitamin D deficiency causes secondary age-related hyperparathyroidism.

On the other hand, patients with hyperparathyroidism, myeloma, or osteomalacia may also have secondary disuse osteoporosis. Therefore, the distinction among these three types of GDBD is not always clear-cut. Nonetheless, this classification provides a practical systematic approach to differentiate the main causes of generalized diminished bone density GDBD and every type of generalized decreased bone density will not be considered osteoporosis as it is done in WHO definitions.

These three processes may appear similar on radiographs and DXA. Hence, the general term osteopenia is used when the etiology of GDBD is not known. It is important to remember that definition of osteopenia in this classification is quite different from its definition in WHO definitions of diminished bone density.

Osteoporosis

Osteoporosis is the most common bone disease in humans and affects both sexes. By definition, osteoporosis is nonfocal diminished bone mass per unit volume of bone (cubic centimeter).

Normal adults lose bone mass beyond the age of 40 years by the process of involutional osteoporosis, which was described previously. This loss of bone begs the question as to when the loss is pathologic and when it is physiological. The practical answer to this question is that osteoporosis becomes pathologic when the patient is at risk for fracture without major trauma. This risk will depend not only on the bone mass of the individual and the microarchitecture of the bone but also upon several other factors as follows:

- Women at greatest risk for osteoporosis are Caucasian ectomorphs with low calcium intake, sedentary lifestyles, little sun exposure, and early menopause. On the other hand, those individuals who are more active or who take more physical risks are clearly at greater risk for fracture than those who do not. Thus, prediction of osteoporotic fractures cannot been easily and accurately estimated.
- The role of genetic factors in the pathogenesis of osteoporosis is confirmed by epidemiological studies.
- Lifestyle risk factors for osteoporosis include alcohol abuse, smoking, low calcium intake, and lack of physical activity.
- Chronic conditions such as Cushing disease, hemochromatosis, hypogonadism, gastrointestinal abnormalities such as Crohn disease, and chronic pancreatitis predispose the patients to osteoporosis.
- Some drugs such as corticosteroids, thyroid hormone, antiandrogen treatment, and to a lesser extent heparin and loop diuretics cause osteoporosis.
- The risk of developing fractures increases in conditions that increase the possibility of fall such as neurologic disorders, heart conditions leading to orthostatic hypotension, and in patients who are treated with neuroleptics, antidepressants, and antihypertensive medications.

Much research has gone into measuring bone mineral content in order to determine on average when an individual is at risk for fracture. While many of these tests give local measurements of BMD, no clinically practical available test gives information regarding the microarchitecture of the bone. The architecture of bone is likely to be as important in predicting fractures as is the absolute amount of bone since the organization of the material will affect its overall strength. Recently, microcomputed tomography and high-resolution MRI using SNR-efficient sequences, high magnetic field (3 Tesla), and phased array coils have been used for the in vivo study of the trabecular microarchitecture of bone, but these techniques at present are not clinically available. Others have used susceptibility effects to evaluate the overall directional components of bone.

Osteoporosis may be divided into primary or secondary forms. Primary osteoporosis is age related and can be seen in both men and women. In secondary form of osteoporosis, bone loss is precipitated by a variety of chronic medical conditions, medications, nutritional deficiencies, and other causes.

There are multiple pathophysiological mechanisms that lead to secondary osteoporosis. For example, certain amino acids and vitamin C are necessary for osteoid synthesis. A deficiency in these causes dietary osteoporosis. If the necessary amino acids are depleted in the synthesis of sugars (glycogenesis), as probably occurs in diabetes mellitus and Cushing disease, or if the catabolic destruction is greater than the supply, as in thyrotoxicosis, we might

Table 2.2 Etiological classification of osteoporosis

Osteoporosis may be primary or secondary. About 40% of cases are secondary osteoporosis

A. Primary osteoporosis

Primary osteoporosis has 2 types:

1. Type 1 – Postmenopausal osteoporosis
2. Type 2 – Age-related (senile) osteoporosis

B. Secondary osteoporosis

1. Dietary deficiency:
   a. Scurvy – vitamin C
   b. Copper
   c. Protein malnutrition
   d. Calcium malnutrition
2. Endocrine:
   a. Hypogonadism – Primary or secondary
   b. Ovarian agenesis (Turner syndrome) and testicular dysgenesis (Klinefelter syndrome)
   c. Adrenal cortex:
      i. Cushing syndrome – adrenal neoplasm
      ii. Addison disease
   d. Pituitary:
      i. Cushing disease – pituitary adenoma with cortical hyperplasia
      ii. Acromegaly
   e. Hyperthyroidism
   f. Diabetes mellitus (pancreas)
   g. Nonendocrine tumors that secrete ACTH-like polypeptides (such as small cell carcinoma of the lungs)
3. Disuse atrophy or stress shielding – osteoporosis due to lack of stress stimulus, prolonged immobilization, weightlessness in space flights, advanced arthritides, and paralysis*
4. Chronic liver disease and alcoholism
5. Idiopathic juvenile osteoporosis
6. Iatrogenic (excessive steroids, heparin, and vitamin A)
7. Congenital/Genetic:
   a. Osteogenesis imperfecta
   b. Homocystinuria
   c. Neuromuscular disease and dystrophies
   d. Trisomy 18
   e. Trisomy 13–15
   f. Progeria
   g. Ehlers-Danlos syndrome
   h. Menke syndrome (the congenital copper deficiency)

* See discussion of Wolff law in the discussion of fracture healing in Chapter 5 trauma and in Chapter 1.

designate the resulting osteoporosis as endocrine. Cells may inherit genes that code for a deficient or defective set of enzymes, resulting in a congenital inability to differentiate into osteoblasts, a condition we recognize as osteogenesis imperfecta. Thus we may set up a classification of osteoporosis in two primary and seven secondary groups (Table 2.2).

Two forms of osteoporosis are recognized: high turnover osteoporosis where the bone can be shown to be actively remodeling using double labeling with tetracycline and low turnover osteoporosis where the bone shows little or no remodeling activity with tetracycline labeling.

WHO Definitions of Osteoporosis

In 1994, the WHO established definitions for diagnosis of osteoporosis based on the results of quantitative BMD measurements using dual-energy X-ray absorptiometry (DXA). The results of DXA are commonly expressed in terms of *T* scores (standard deviations from young gender-associated normal peak bone mass) or *Z* scores (standard deviations from mean sex and age-matched control bone mass): These definitions divide BMD measurements into four groups (Table 2.3).

Table 2.3 WHO definitions of bone density

- *Normal*: *T* score not more than one standard deviation below the young adult female reference mean
- *Osteopenia (low bone mass)*: *T* score between 1 and 2.5 standard deviations below the young adult female reference mean peak bone mass
- *Osteoporosis*: *T* score more than 2.5 standard deviations below the young female reference mean
- *Severe osteoporosis (established osteoporosis)*: *T* score more than 2.5 standard deviations below the young adult female mean in the presence of one or more osteoporosis fragility fractures

The young adult female reference mean is determined with the use of the mean hip BMD from the National Health and Nutrition Examination Survey reference database of women aged 20–29 years.

If DXA measurements at different sites are considerably disparate, most clinicians use the lowest BMD measurement. The lowest *T* score of the distal third of the nondominant radius may also be used. This approach has been recommended by most experts including the International Society for Clinical Dosimetry. The results are reported as a density measurement in gram per square centimeter in addition to *T* and *Z* scores.

The WHO definitions tell the truth but not the whole truth. There are several problems with these definitions:

- It makes no distinction between various causes of decreased bone density (DBD). Certainly, not all patients with decreased bone density are osteoporotic. Nevertheless, since the majority of cases with diminished bone density, in older age, are due to osteoporosis, the WHO classifications are the best practical approach currently available.
- It is neither a sensitive nor a specific predictor of fracture. This is because it is based on a relatively inaccurate test of projectional BMD determination.
- It makes no attempt to adjust the measurement for bone microarchitecture.
- The definition makes no adjustment for individual lifestyle.

- In the WHO system, *T* scores are based on standard deviations from young female normal peak bone mass. Peak bone mass is different in male and female.

Diagnostic Imaging of Osteoporosis

Radiographic evaluation

Radiographs show generalized and uniform decreased density of the skeleton, with coarse trabeculae, and thinning of the cortices. Trabecular coarsening (Figs. 2.1, 2.2, and 2.3) occurs because initial trabecular loss occurs in the secondary trabeculae. These trabeculae are oriented perpendicular to the loading force on the bone. Their loss effectively increases the length of the primary trabeculae that are oriented along lines of the loading force. As these trabeculae become longer, they have to increase their diameters substantially to mitigate the effects of the increased length and bear the same load.

In the spine, prominent trabeculae sometimes show vertical striations, mimicking the corduroy pattern seen in hemangiomas (Fig. 2.3). Confusing these two entities is unlikely, however, since osteoporosis is a systemic disease with systemic changes while hemangiomas are typically focal lesions. In severe osteoporosis, there is increased lucency of the medullary portion of vertebral bodies and accentuation as well as thinning of cortices, producing an appearance similar to an "empty box" (Fig. 2.3). This appearance has been said to be particularly prominent in steroid-induced osteoporosis.

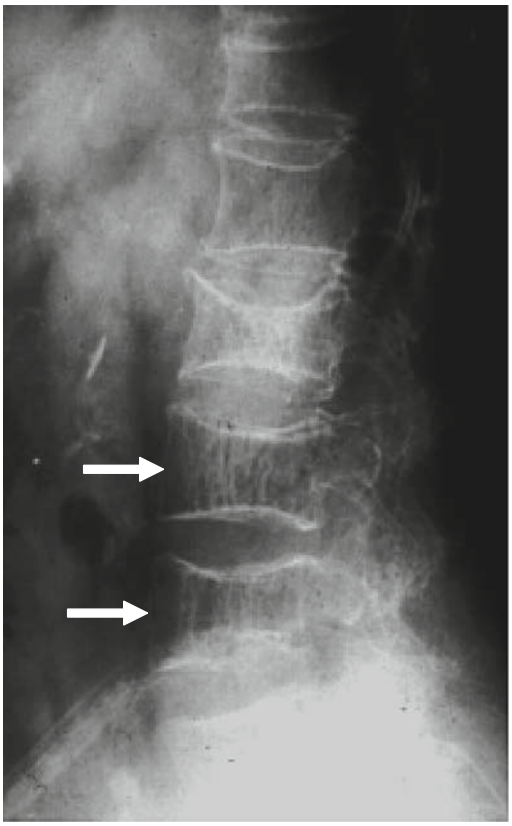

Fig. 2.3 Osteoporosis of the lumbar spine. Lateral radiograph showing diminished bone density, thinning, and accentuation of cortical density compared with the medullary portion of vertebrae, giving the impression of an "empty box." There are various degrees of biconcave deformity of several vertebral bodies related to microscopic insufficiency fractures (see Fig. 2.4c). Note significant coarsening of trabecular markings in the form of vertical striations due to osteoporotic loss of secondary trabeculae (*arrows*). This appearance should not be confused with hemangiomas

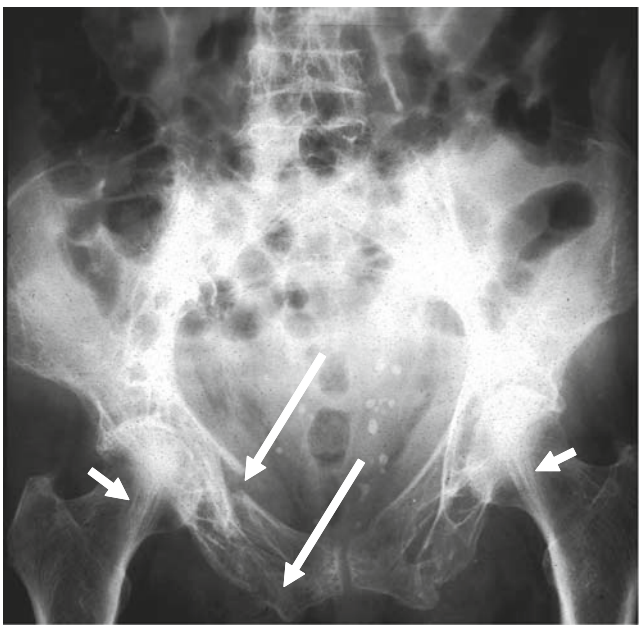

Fig. 2.2 Osteoporosis. There is diminished bone density, coarsening of trabecular pattern (*short arrows*), cortical thinning, and pelvic fractures (*long arrows*)

Fractures of vertebral bodies are the most common insufficiency fractures in osteoporosis. Sometimes the osteoporotic vertebral body "microfractures" cause biconcave deformities that simulate "fish vertebrae" (Figs. 2.3, 2.4, and 2.5). The vertebral bodies may collapse anteriorly, causing wedge deformity (Figs. 2.5 and 2.6) and kyphosis. These patterns of vertebral body deformity also may be seen in other types of osteopenic states (osteolysis and osteomalacia). At times, severe osteoporotic fractures cause significant deformity causing a "crush appearance" (Figs. 2.5 and 2.12). Insufficiency fractures of the skeleton usually can be diagnosed on radiographs, but sometimes they may be subtle and bone scan or preferably MRI is required to make the diagnosis (Figs. 2.7 and 2.8).

Multiple myeloma may present with an appearance that is identical to age-related osteoporosis. About 25%

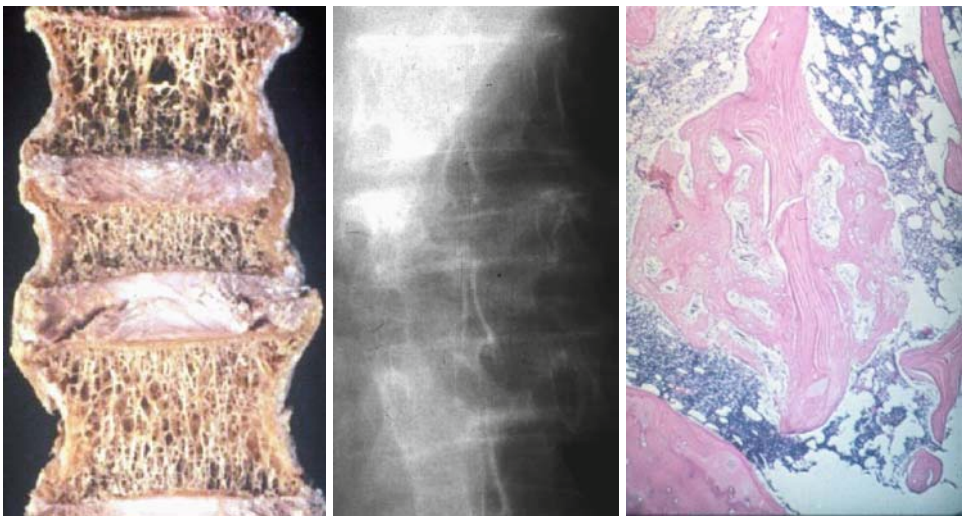

Fig. 2.4 Osteoporosis. **a** is gross specimen of an osteoporotic spine with compression fracture and **b** is a radiograph of an osteoporotic spine, with severe fracture and "fish vertebrae" in a different patient. **c** is a low power magnification revealing a healing microfracture with callus formation in the spine. These microfractures create gross radiological vertebral body deformities. **a** and **c** are courtesy of Dr. Peter Bullough, Hospital for Special Surgery, New York, and Dr. Vincent Vigorita, State University of New York, Health Sciences Center, Brooklyn, NY

of patients with multiple myeloma have marked diffuse and uniform diminished bone density without focal osteolytic lesions. This is related both to excretion of an osteoclastic-activating factor by myeloma cells and to marrow proliferation and packing by the tumor cells (Figs. 2.9 and 2.10). Metastatic disease, osteomalacia, primary and secondary hyperparathyroidism, marrow packing disorders (such as Gaucher disease), hyperthyroidism, chronic immobilization, hepatic insufficiency, diabetes mellitus, drug-induced osteoporosis from corticosteroids and heparin, drug-induced osteomalacia caused by anticonvulsant therapy, Cushing disease/syndrome, and rheumatoid arthritis also cause decreased bone density and are in the differential diagnosis of osteoporosis.

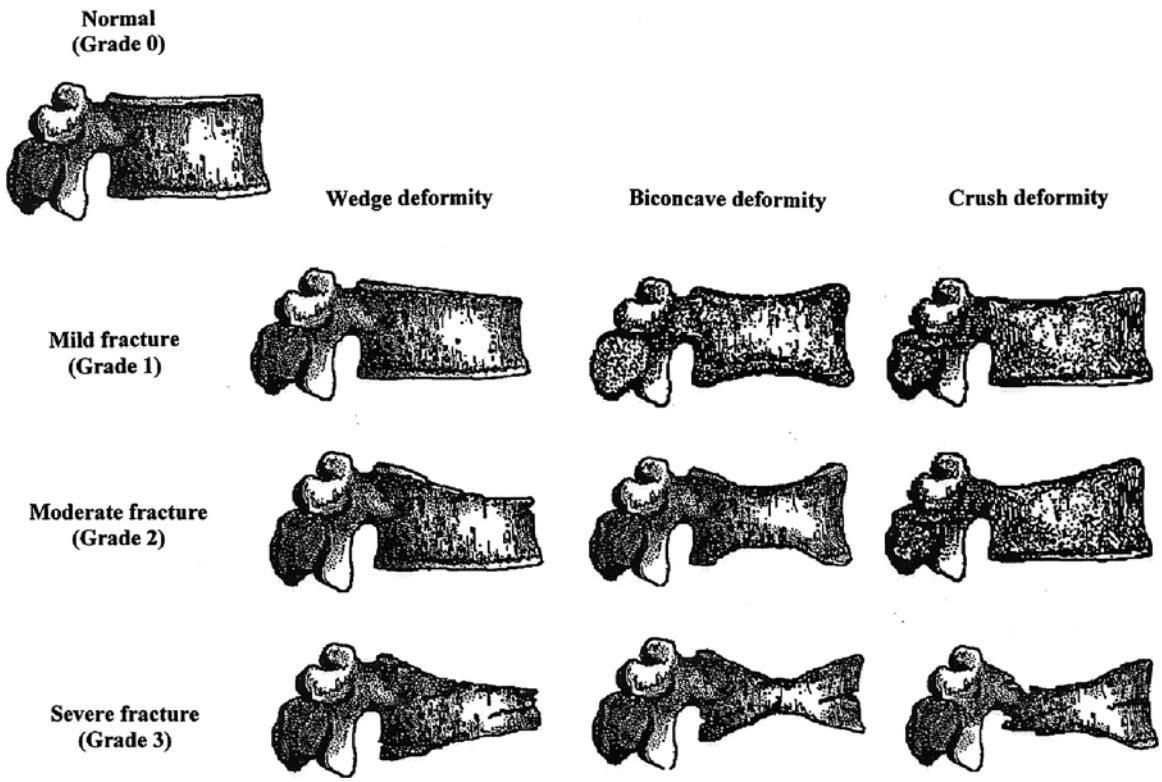

Fig. 2.5 Genants semiquantitative method for reading osteoporotic vertebral fractures. Vertebral body fractures are graded from 0 to 3 in the assessment of osteoporotic fractures in lateral radiographs of the spine. From *left to right*: Wedge, biconcave, and crush deformities are demonstrated in normal and Grades 1–3 fractures

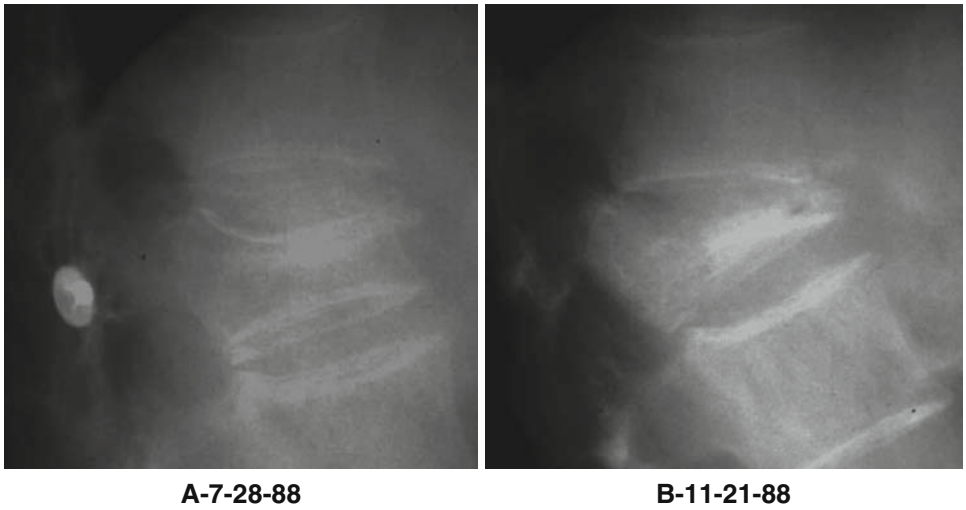

Fig. 2.6 Progress of osteoporotic fracture in lateral spine radiographs. **a** shows compression fracture of the superior vertebral body and anterior decreased height of L1 on July 28, 1988 (Grade 2 fracture). **b** shows increased compression (wedge deformity) after 4 months. Therefore, fracture grading has increased from Grade 2 to 3 in this interval according to Genants semiquantitative criteria

Bone density must diminish by 30–40% before it is recognizable radiographically. For this reason, radiographs are not sensitive to early loss of bone density. Radiographic appearance of congenital forms of osteoporosis such as osteogenesis imperfecta (Fig. 2.11) are more or less similar to the acquired forms. This entity is discussed in more detail in Chapter 13.

Dual X-ray absorptiometry (DXA), quantitative CT analysis (QCT) and quantitative ultrasonography, though imperfect, detect diminished bone density at a much earlier stage of development than do radiographs. At present, DXA is the most commonly used procedure for early detection of osteoporosis (Figs. 2.13, 2.14, 2.15, and 2.16), primarily because its results are easily reproducible from one examination to another.

Even so, radiographs still have a major role in the management of osteoporotic fractures and in the differential diagnosis of causes of decreased bone density. QCT is also more accurate than both radiographs and DXA, but it is more difficult to perform, less precise, and give the patient more radiation than DXA (Fig. 2.17).

The precision error of DXA (1–2%) is relatively high compared with patients' annual rate of bone loss or gain. Thus, a 2-year interval between measurements is necessary for meaningful monitoring using this technique, in monitoring therapeutic efficacy. In the interval, follow-up of osteoporotic patients may be done using standardized visual (or semiquantitative) assessments of vertebral deformities. In standardized assessment radiographs of the spine, numerical scores are assigned to vertebral deformities, and distinct categories are assigned to the shape or the type or the severity of vertebral fractures in a definable and reproducible manner. No measurements of vertebral dimensions are made. This semiquantitative radiographic approach not only helps the clinical research of osteoporosis but also provides more practical accurate follow-up during treatment of this

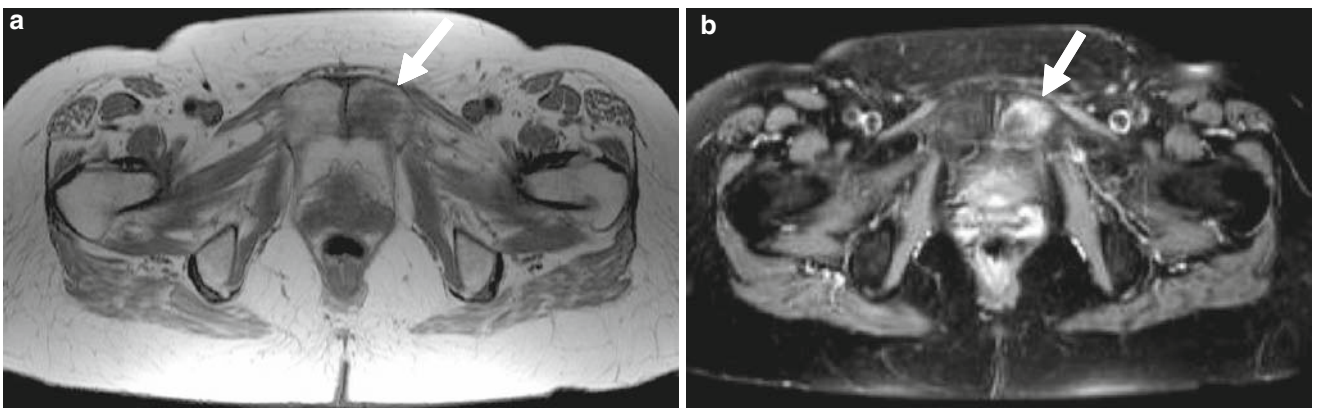

Fig. 2.7 Insufficiency fractures in a 78-year osteoporotic female. **a** is a T1-weighted axial MR image of the pelvis showing an insufficiency fracture with decreased signal intensity of the left pubic bone (*Arrow*). **b** is a T2-weighted axial MR image of the pelvis showing the same fracture with increased signal intensity consistent with acuity (*arrow*). Courtesy of Dr. Murali Sundaram, Cleveland Clinic, Cleveland, Ohio

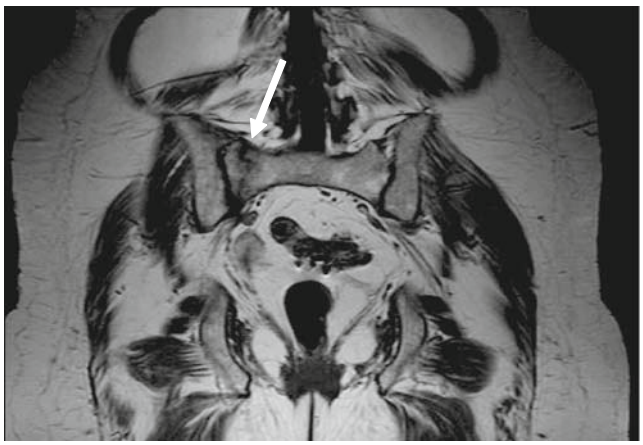

Fig. 2.8 Insufficiency fracture. Same patient. Coronal T1-weighted MR image of the pelvis showing a longitudinal decreased signal intensity in the right sacral wing (*arrow*) consistent with right sacral wing insufficiency fracture. Courtesy of Dr. Murali Sundaram, Cleveland Clinic, Cleveland, Ohio

condition. Several such methods have been introduced by Smith et al., Meunier, Kleerekoper et al., and Genant.

The semiquantitative visual grading introduced by Genant has proven to be most practical and has been widely applied in epidemiological studies and clinical trials (Fig. 2.5). In this approach, the T4 to L4 vertebral bodies are evaluated on lateral radiographs of the spine. Each of these vertebrae is given a grade related to severity of fracture and averaged to create a "spinal fracture index" (SFI: Grade 0, normal; Grade 1, mild fracture; Grade 2, moderate fracture; and Grade 3, severe fracture). In each grade, wedge, biconcave, and crush deformities are evaluated (Fig. 2.5). In Genants method the authors give a "Grade 0.5" also for borderline cases that reveal minimal changes but cannot be called Grade 1 fracture. This system has faults but is practical and reproducible among institutions if used by experienced readers.

Quantitative Evaluation of Osteoporosis

Dual-Energy X-ray Absorptiometry (DXA)

Dual X-ray absorptiometry (DXA) employs an X-ray source that emits two beams of different energy. BMD is calculated based on measuring the differential tissue absorption of energy from these two X-ray beams. DXA measures the projectional or area BMD expressed in gram per square centimeter, which depends on both the volumetric BMD (vBMD, expressed in g/cm^3) and bones dimensions, specifically the thickness of the bone measured. Thus, area BMD does not distinguish higher BMD recordings of a larger amount of bone mineral from bones that are merely bigger. Even so, fracture risk is determined by both the degree of bone mineralization and the bone size, and so area BMD is a good predictor of fracture risk. The accuracy and the precision of DXA are better than those of older, single-energy densitometric methods.

Clinically, DXA (Figs. 2.13, 2.14, 2.15, and 2.16) is used to measure the bone mineral density (BMD) of the lumbar spine, the hip, the distal forarrm [142], the calcaneus, and the whole body. DXA is reliable in diagnosing osteoporosis and to some extent for evaluating fracture risk. Quantitative computerized tomography is superior to DXA, but neither test is

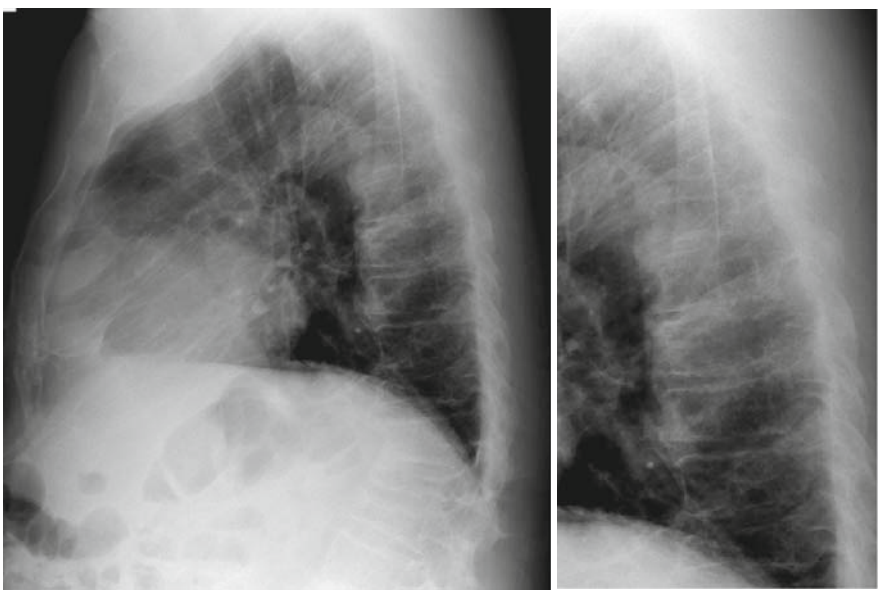

Fig. 2.9 Multiple myeloma. **a** – Myeloma in a 40-year-old man revealing only diminished bone density (osteopenia) without osteolytic lesions in skeletal survey. Note cortical thinning of the sternum and the spine with Grade 1 wedging of the vertebral bodies. **b** – Close-up view of the spine reveals the spinal changes more clearly. The vertebral bodies have the so-called "empty box" appearance, demonstrating changes similar to osteoporosis, best seen in the lower thoracic segments. Courtesy of Dr. Murali Sundaram, Cleveland Clinic, Cleveland, Ohio

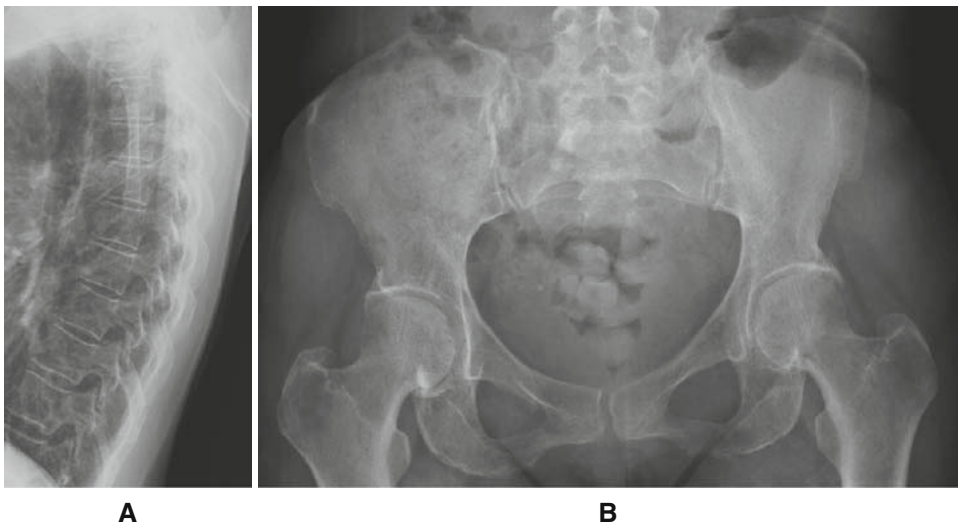

Fig. 2.10 Myeloma. This is a 54-year-old female with myeloma. The skeletal survey reveals no discrete lesions. There is mild osteoporosis. **a** – Lateral thoracic spine shows thinning and disproportionate density of the cortex compared to the trabecular bone, giving an empty box appearance to vertebral bodies. There is Grade 1 biconcave deformity of the lower thoracic segments. **b** – AP view of the pelvis shows cortical thinning and minimal coarsening of the trabecular markings of the hips. Courtesy of Dr. Michael Bromberg, Temple University Hospital, Philadelphia, PA

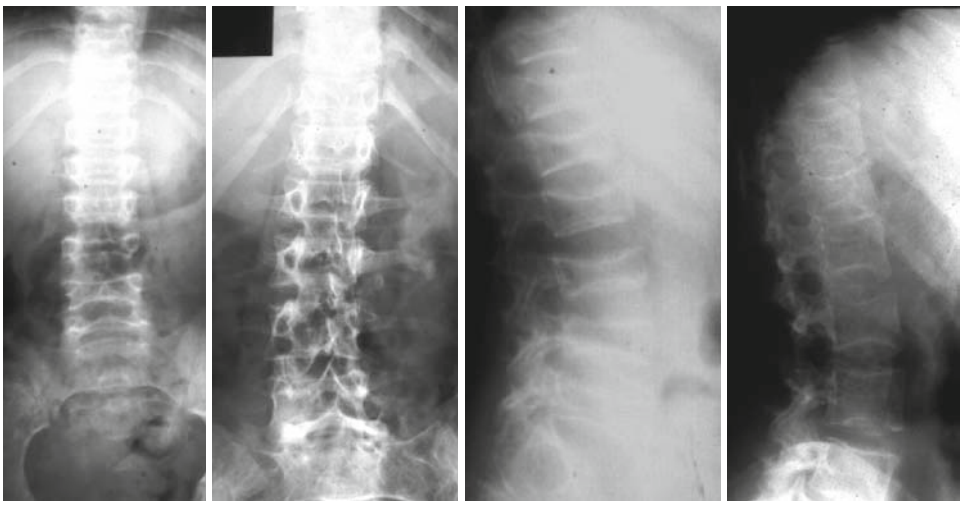

Fig. 2.11 Osteogenesis imperfecta. Lateral and AP lumbar spine radiographs showing progression of osteoporosis in a case of Type 1 osteogenesis imperfecta over a 10-year period. This woman was 11 years old in 1955. The biconcave deformities improve between the two studies, the radiographic findings are more or less similar to the acquired forms of osteoporosis

a good predictor of fracture. There is a fair correlation among BMD measured at different sites in an individual, but the best predictor of risk of fracture at a given site in an individual is BMD measured at that site.

The lumbar spine is a common site for bone densitometry. However, the presence of osteophytes causes spuriously high BMD measurements in patients with spondylosis, especially in men. The most reliable sites of BMD measurement using DXA are the femoral neck and the total hip. Both predict fracture risk equally, but the total hip measurement is more suitable for monitoring treatment as it contains a larger volume of bone comprising both cortical and trabecular bone.

Quantitative Computerized Tomography (QCT)

The advantage of quantitative computerized tomography is that it allows selective measurements of the trabecular bone without cortical bone. This is valuable because trabecular bone has 8–10 times the surface area of cortical bone and is therefore more affected by osteoclastic activity than is cortical bone. QCT is most practical when applied to the spine. It is not as widely used as DXA because of limited availability, relatively high radiation, and a higher precision error (Fig. 2.17).

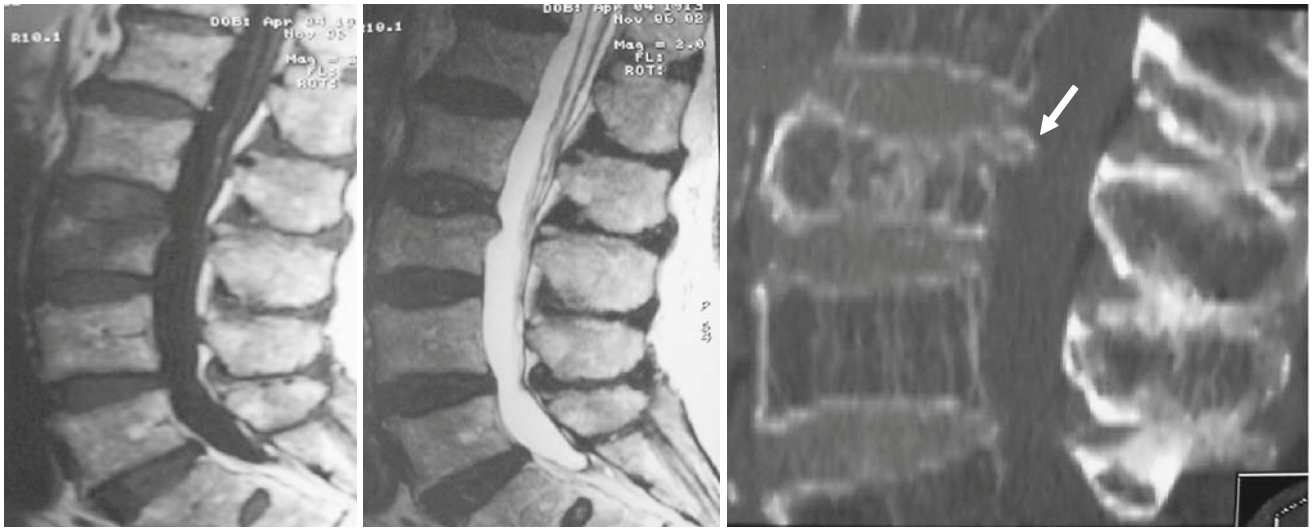

Fig. 2.12 Osteoporosis. MR **a** and **b** and CT **c** sagittal images in a 93-year-old osteoporotic man with compression fracture of the L3 vertebral body. Sagittal T1 MRI **a** shows deformity and decreased signal intensity of the body of L3. Note enlarged spinous processes and decreased intraspinous distances of Baastrup phenomena, which contributed in part to the patients pain. T2 sagittal MRI **b** lack of T2 signal abnormality suggests a nonacute fracture. Sagittal reconstructed CT **c** performed at a later date showing diminished bone density, coarse vertical trabeculae, severe progressive crush deformity, decreased height of central vertebral body, and a retropulsed fragment (*arrow*) into the spinal canal due to the progression of the Grade 3 fracture. Courtesy of Jeffrey P Kochan MD, Temple University Hospital, Philadelphia, PA

Microcomputerized Tomography

Microcomputerized tomography has been developed during the last few years. This technique provides high-resolution images of trabecular architecture. It may be used for specimen evaluation. Its applications have been extended to in vivo animal and human imaging. This technique is still an investigative tool and at present, it is not widely used.

Quantitative Ultrasonography

Quantitative ultrasonography (QUS) measures bone density using changes in two parameters of ultrasound transmission: speed of sound (SOS) and broadband ultrasound attenuation (BUA). The highest BUA and SOS values are observed in young people with high bone mass; these values decrease with age. QUS can be applied where a bone is close to the skin surface, at the calcaneus, phalanges of the fingers, the patella, and the tibia.

The calcaneus is sensitive to disturbances of bone turnover because it contains 90% trabecular bone that is metabolically active. QUS claims to reflect not only bone quantity but also its trabecular microarchitecture, elasticity, and stiffness, an advantage over DXA and QCT, but this claim is weak. Correlation between QUS and BMD measured at different sites is modest. Furthermore, the clinical predictive value of QUS for osteoporotic fractures is slightly lower than DXA. Despite several advantages of QUS (noninvasive, free of ionizing radiation, small and inexpensive equipment), QUS has not yet acquired a place in clinical practice. The long-term stability of these devices is poor. Values of QUS parameters measured in vivo depend on temperature of water bath and skin, positioning of foot, concentration and type of detergent in the water bath, as well as thickness of soft tissues. Few studies have examined the potential utility for evaluation of bone loss and monitoring of treatment. Currently, there are no diagnostic thresholds of osteoporosis for QUS.

Magnetic Resonance Imaging (MRI)

MRI, though currently impractical as a clinical test, shows some remarkable promise as a more accurate predictor of osteoporotic fracture. Two methods of MRI BMD measurement have been developed: one that uses ultrahigh-resolution MRI to evaluate trabecular mass and another that uses susceptibility effects to determine mineral content. The former, though accurate, samples too small a portion of the skeleton to be representative. The second method is based upon the observation that susceptibility effects are directly related to trabecular bone mass. Not only is this the case, but the measurements show anisotropy with respect to the main

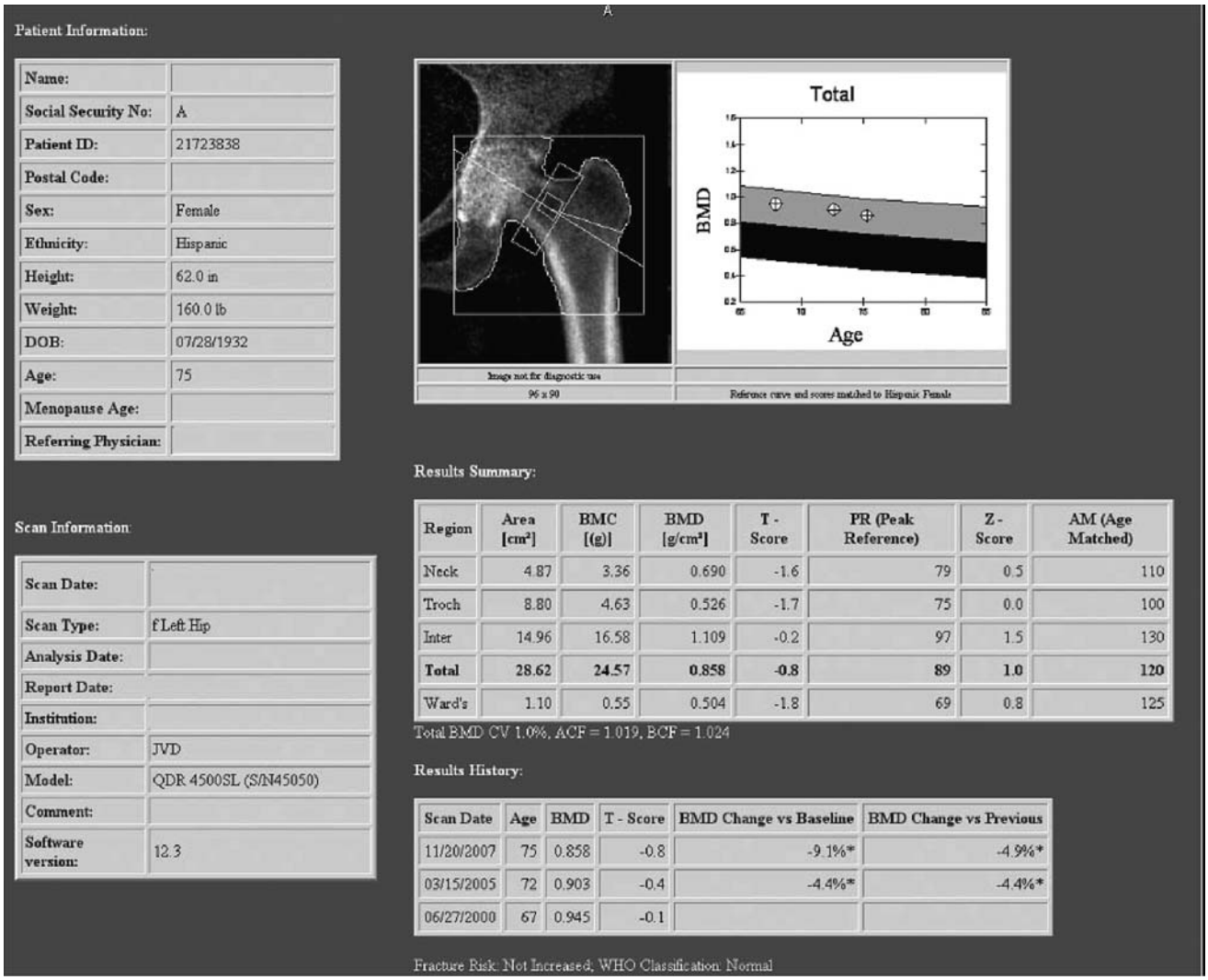

Fig. 2.13 Normal DXA followed for 6.5 years. A 75-year-old woman in 2007, normal follow-up DXA over 6.5 years. The patient had three studies on 6/27/2000, 3/15/2005, and 11/20/2007. Lowest *T* scores: –0.1, –0.4, and –0.8, all within normal limits according to WHO definitions. Courtesy of Dr. Alan Maurer, Temple University Hospital, Philadelphia, PA

magnetic field, suggesting that MR measurements using this technique might also provide some information about bone microarchitecture. Unfortunately, this technique is currently impractical for a number of reasons, including the size of the scanner bore, the time it takes to complete the study, the availability of the equipment, and the cost of MRI compared with DXA.

Osteoporosis Is a Major Public Health Problem

The prevalence of osteoporosis increases with age. One out of three women between ages of 60 and 70 is osteoporotic. Two out of three women at age 80 are osteoporotic. In 1995, 9.4 million American women suffered from osteoporosis. It is estimated that osteoporosis currently "affects 200 million women worldwide". This makes osteoporosis one of the most common diseases of the elderly. In 1988, the direct cost of osteoporotic fractures was estimated at 35 billion dollars in the United States. In Europe the current total direct cost is estimated to be over 31 billion Euros and may rise to a yearly cost of about 76 billion Euros by the year 2050.

Low BMD, due to osteoporosis, is mainly age associated, but other factors such as low BMI, weight loss after the age of 25 years, lack of physical activity, poor nutrition, tobacco smoking, chronic alcoholism, gastrectomy, certain drugs (mainly corticosteroids, loop diuretics, thyroid hormones) also contribute to declining bone mass. Postmenopausal osteoporosis develops prematurely in young individuals who undergo oophorectomy (Fig. 2.18). Patients

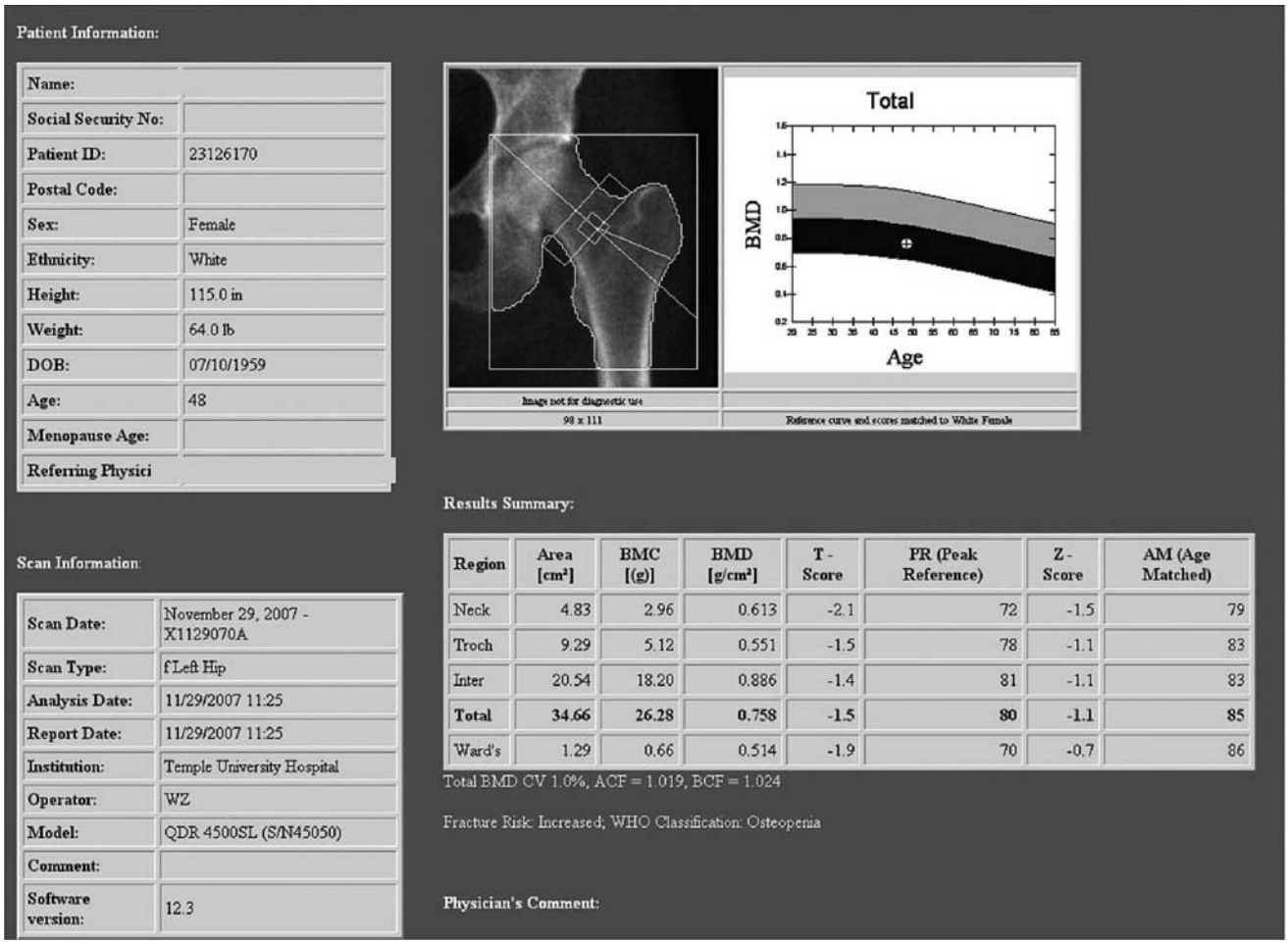

Fig. 2.14 Osteopenia DXA hip. Woman 48, lowest *T* score –2.1 consistent with osteopenia. Courtesy of Dr. Alan Maurer, Temple University Hospital, Philadelphia, PA

may show as much as 12% bone loss in the 2 years following oophorectomy.

About 1.5 million fractures in the United States are attributed to osteoporosis annually. They occur primarily in the spine, the hip, and the distal forearm. Approximately 50% are vertebral, 20% in the hip, 20% in the wrist. At age 60, women suffer osteoporosis-related fractures at a rate that is six times that of age-matched men. By 70 years of age, osteoporosis is present in both genders, and the ratio of osteoporosis-related fractures declines to 2:1. The estimated lifetime risk of sustaining an osteoporotic fracture is 40% for women and 13% for men at age 50 years. The risk for hip fracture is 17.5% for women and 6% for men.

The most common complaint from osteoporosis is back pain. The onset may be insidious or sudden following injury. There is a definite relationship between osteoporosis and spinal compression fractures that occur spontaneously or with minimal trauma. Vertebral fractures are the most common type of osteoporotic fractures [1] (Figs. 2.3, 2.4, 2.5, 2.6, and 2.7).

Hip fracture (Fig. 2.19a) is the most disastrous consequence of osteoporosis. Its incidence increases exponentially with age in both men and women. The risk of hip fracture is increased in people with other common osteoporotic fractures, mainly vertebral and distal radius fractures. There are two main determinants of the risk of hip fracture: low BMD and falls. Unfortunately, balance worsens as people age and so falls become more likely.

Fracture of the distal radius (Fig. 2.19b) is the third most frequent osteoporotic fracture in women at age 80. It is also often one of the earliest manifestations of osteoporosis. In men over 65 years of age, the incidence of distal radius fracture is four times lower compared with women of the same age.

Fracture of the proximal third of the humerus, particularly its surgical neck, is another common fracture in osteoporotic patients.

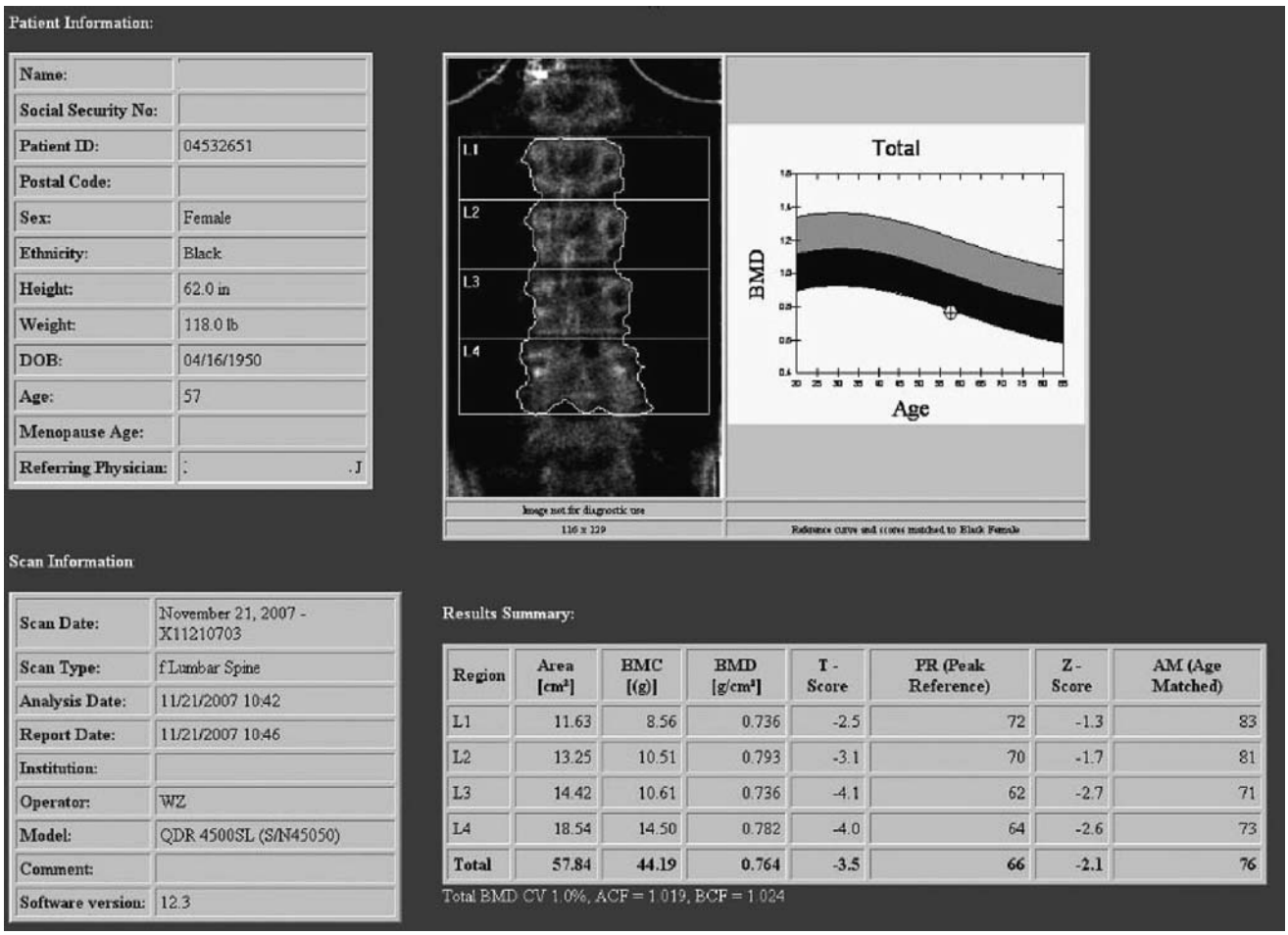

Fig. 2.15 Osteoporosis DXA. Black woman 57, osteoporotic spine, the lowest spinal *T* score –3.5 and *Z* score –2.1. Courtesy of Dr. Alan Maurer, Temple University Hospital, Philadelphia, PA

Prevention and Treatment of Osteoporosis

Prevention

Prevention of osteoporosis is based on nutritional factors and exercise. Dietary calcium should be about 800 mg per day for adults and 1,500 mg per day for adolescents. Recommended calcium intake for postmenopausal women is 1,000–1,500 mg per day.

Treatment

Currently, prevention of bone loss is much more effective than treatment of established osteoporosis. Nonetheless, if detected at an early stage, osteoporosis is a potentially treatable disease. During recent years, several effective new drugs have been approved for the prevention and treatment of osteoporosis. Most of these agents are in the bisphosphonate class of drugs and act by decreasing bone turnover.

Bisphosphonates (BP) – Bisphosphonates (BP) are potent inhibitors of bone resorption that inhibit the activity of osteoclasts. These are commonly used in the treatment of postmenopausal osteoporosis.

Hormone replacement therapy (HRT) – Hormone replacement therapy (HRT), either estrogen alone or in combination with progesterone, increases BMD at all skeletal sites in early and late postmenopausal women. It is associated, however, with an increased incidence of endometrial cancer (about 1% per year) and other complications such as deep venous thrombosis (DVT), pulmonary embolism, hypertension, and gallstones. Therefore, it is indicated only in high-risk patients with evidence of rapid bone loss.

Selective estrogen receptor modulators (SERM) – Selective estrogen receptor modulators (SERM) are synthetic molecules that have the ability to bind to estrogen

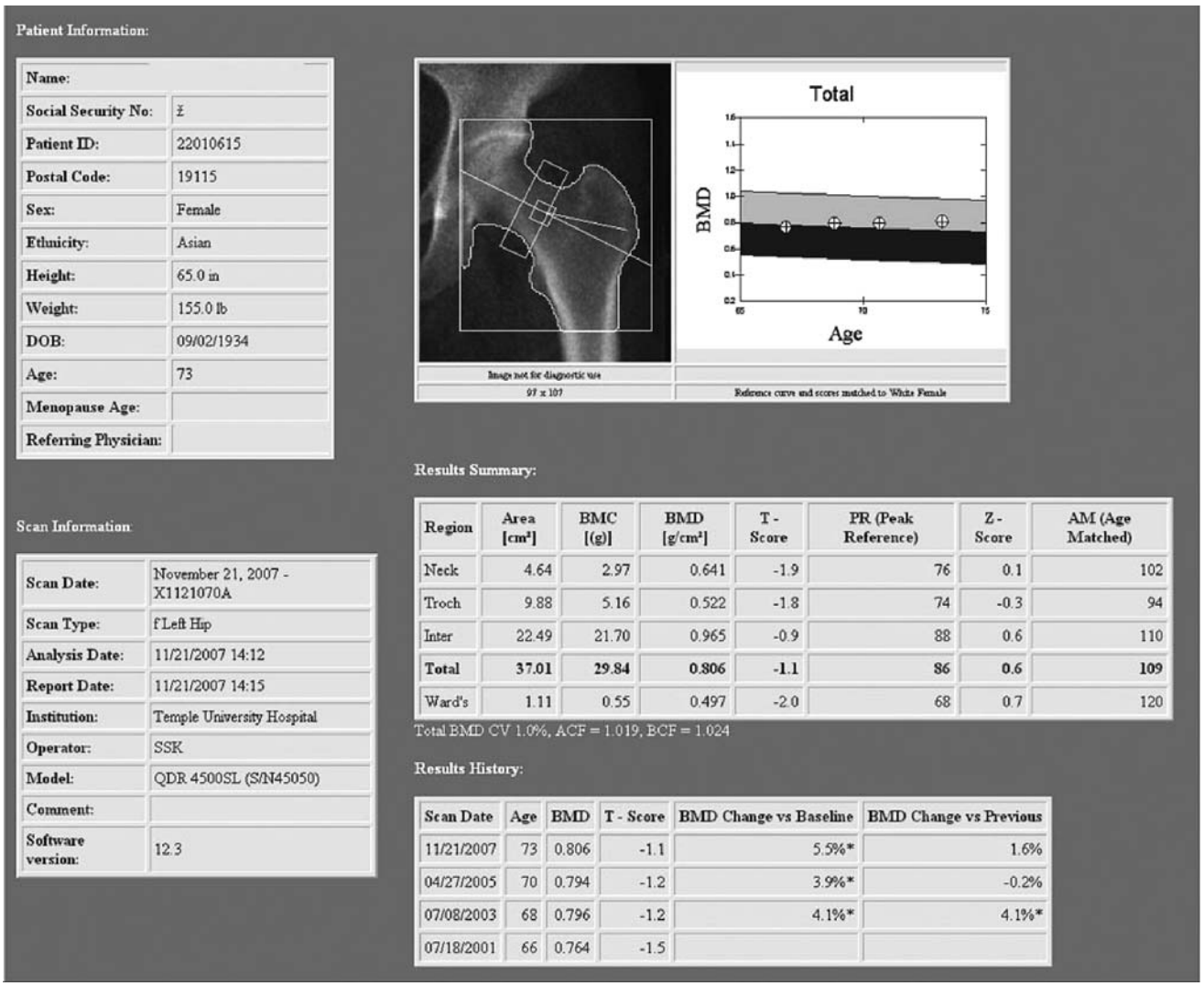

Patient Information:

Name:	
Social Security No:	ž
Patient ID:	22010615
Postal Code:	19115
Sex:	Female
Ethnicity:	Asian
Height:	65.0 in
Weight:	155.0 lb
DOB:	09/02/1934
Age:	73
Menopause Age:	
Referring Physician:	

Scan Information:

Scan Date:	November 21, 2007 - X1121070A
Scan Type:	f Left Hip
Analysis Date:	11/21/2007 14:12
Report Date:	11/21/2007 14:15
Institution:	Temple University Hospital
Operator:	SSK
Model:	QDR 4500SL (S/N45050)
Comment:	
Software version:	12.3

Results Summary:

Region	Area [cm²]	BMC [(g)]	BMD [g/cm²]	T - Score	PR (Peak Reference)	Z - Score	AM (Age Matched)
Neck	4.64	2.97	0.641	-1.9	76	0.1	102
Troch	9.88	5.16	0.522	-1.8	74	-0.3	94
Inter	22.49	21.70	0.965	-0.9	88	0.6	110
Total	**37.01**	**29.84**	**0.806**	**-1.1**	**86**	**0.6**	**109**
Ward's	1.11	0.55	0.497	-2.0	68	0.7	120

Total BMD CV 1.0%, ACF = 1.019, BCF = 1.024

Results History:

Scan Date	Age	BMD	T - Score	BMD Change vs Baseline	BMD Change vs Previous
11/21/2007	73	0.806	-1.1	5.5%*	1.6%
04/27/2005	70	0.794	-1.2	3.9%*	-0.2%
07/08/2003	68	0.796	-1.2	4.1%*	4.1%*
07/18/2001	66	0.764	-1.5		

Fig. 2.16 Treated osteoporosis showing improvement. The patient was a white woman, treated with Fosamax (alendronate sodium) from July 2001 to November 2007. *T* score increased from –1.5 in 2001 at the age of 66 to –1.1 in 2007 at the age of 73. Four DXA studies were performed. Courtesy of Dr. Alan Maurer, Temple University Hospital, Philadelphia, PA

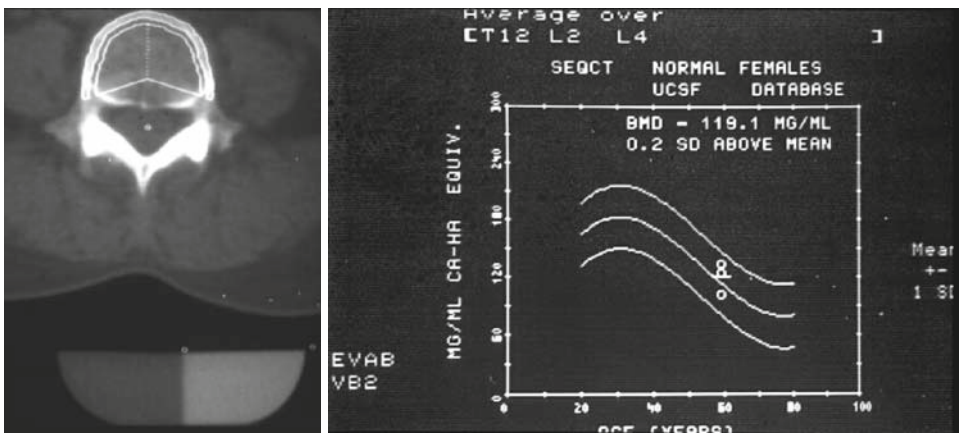

A B

Fig. 2.17 Normal single-energy QCT. **a** is axial CT image of L4 of a 59-year-old female. **b** reveals that the study is normal and BMD is 0.2 SD above mean

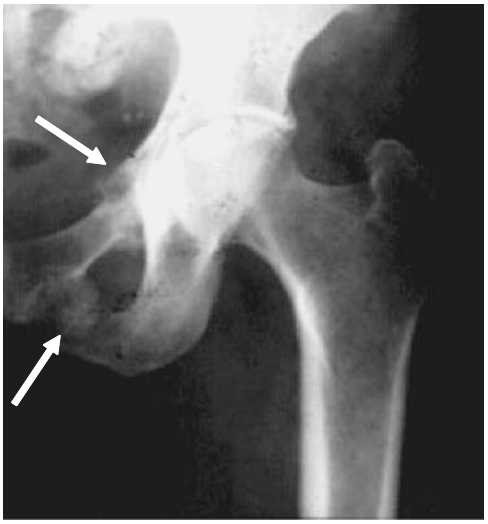

Fig. 2.18 Post-oophorectomy osteoporosis. There are healing fractures of the *left* superior and inferior pubic rami in a 31-year-old female, after oophorectomy (*arrows*)

receptors throughout the body and act as estrogen agonists or antagonists depending upon the target organ. Raloxifene is the only SERM currently on the market for osteoporosis.

Calcium and vitamin D – Calcium and vitamin D are indicated mainly for the prevention of bone loss in the elderly and are a useful adjunct therapy in osteoporosis.

Teriparatide rhPTH – The first effective stimulator of bone formation, the recombinant 1–34 fragment of human parathyroid hormone [rhPTH(1–34)], has recently been approved.

Vertebroplasty and Kyphoplasty

Vertebroplasty, discussed in more detail in Chapter 14, is an injection of methyl methacrylate into a compressed vertebral body. This technique yields excellent relief of spinal pain. It is an outpatient procedure performed under local anesthesia and sedation and consequently has become very popular (Fig. 2.20).

Kyphoplasty, similar to vertebroplasty, is the injection of cement into a compressed vertebral body with the intent of reducing the kyphotic deformity. First, a high-pressure balloon is inserted into the vertebral body in an attempt to elevate the depressed endplate and to create a cavity. The balloon is withdrawn and a high-viscosity preparation of acrylic cement is injected to fill the cavity. Unlike vertebroplasty, this is a surgical procedure that typically requires a hospital admission and general anesthesia.

Scurvy

Scurvy is caused by a deficiency in vitamin C (ascorbic acid) and is rarely encountered in the western hemisphere. Vitamin C deficiency results in an inability on the part of the finer ramifications of the vascular tree to contain blood, resulting in a bleeding diathesis. Vitamin C is also essential in the production of adequate normal intercellular collagen and organic bone matrix. Thus, its absence leads to osteoporosis.

The radiographic manifestations of infantile scurvy (Figs. 2.21 and 2.22) reflect osteoporosis and hemorrhage. Alterations are first apparent and are most marked in areas in

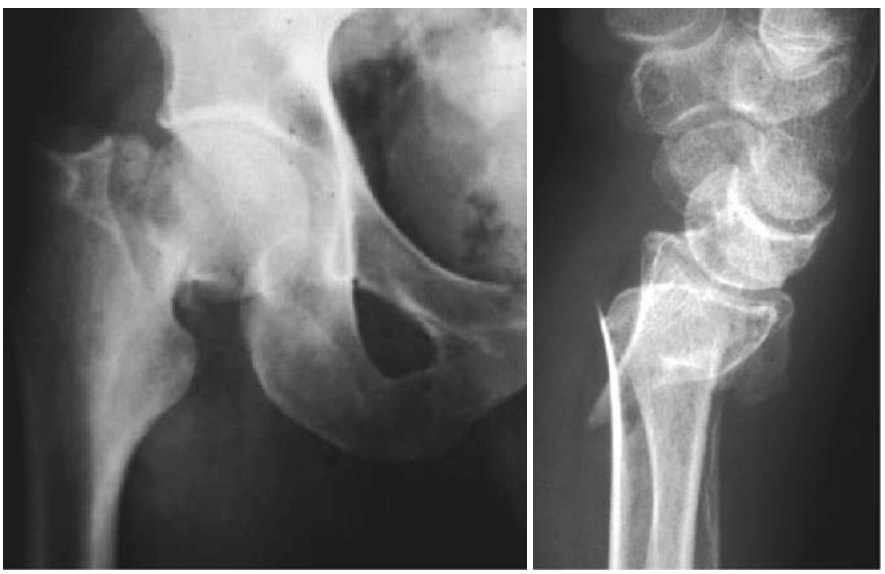

Fig. 2.19 AP right hip radiograph. **a** shows a femoral neck fracture and lateral wrist radiograph. **b** shows a radial fracture, which are the second and the third most common osteoporotic insufficiency fractures, respectively. Vertebral body fractures are the most common osteoporotic fractures

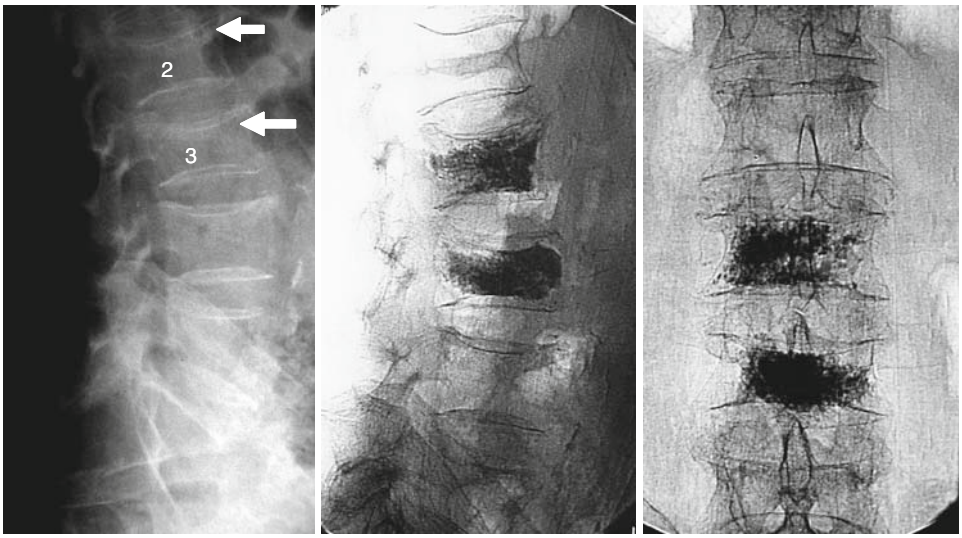

Fig. 2.20 Vertebroplasty in a 93-year-old osteoporotic man. The patient was bedridden for 8 months due to severe pain secondary to compression fractures of L2 and L3 vertebral bodies (*arrows*). A remarkable recovery was noted immediately following vertebroplasty reconstruction of the L3 vertebral body and after subsequent vertebroplasty of the L2 vertebral compression fracture several months later. The patient was able to ambulate within days of each procedure. Courtesy of Jeffrey P Kochan MD, Temple University Hospital, Philadelphia, PA

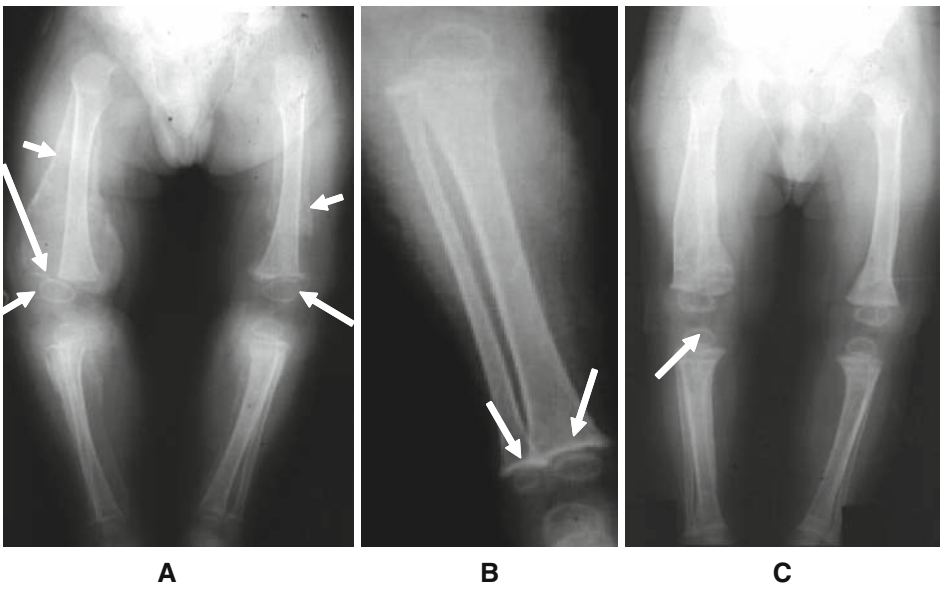

Fig. 2.21 Scurvy. **a** shows diminished bone density, thinning of cortices, ring epiphyses of distal femurs (*arrows*), and subperiosteal calcifying hematomas (*short arrows*). Note fracture of the R distal femur through scorbutic zone, causing lateral slipped distal femoral epiphysis (*long arrow*). **b** reveals increased density of the zone of provisional calcification in distal tibia and fibula (*arrows*). **c** demonstrates that the fracture has healed without shortening of the femur. The epiphysis is centrally located (*arrow*). Distal femur is undergoing remodeling and will be similar to the left femur after completion of the remodeling process

which the enchondral growth of bone is most rapid, e.g., the wrists, knees, and costochondral junctions.

The zone of provisional calcification in the physeal plate forms normally, but it shows increased density (Fig. 2.21b). This is known as the white line of Frankel. There is a radiolucent band adjacent to the zone of provisional calcification, the so-called Trummerfeld zone or the "scorbutic zone." This band may be evident first at the periphery of the metaphysis and present as a notch at the metaphyseal margin, the corner sign. Fractures through this zone superficially suggest epiphyseal separations but are really subepiphyseal; hence, healing occurs without disturbing the bone growth. These fractures are responsible for lateral spurring at the end of the shaft, the so-called Pelkin spur (Fig. 2.21a).

Epiphyseal centers are affected in the same way as is the metaphysis. The zone of provisional calcification around the centers becomes thicker than normal and, combined with the thin, sparse trabeculae of the center, results in a radiographic appearance described as "ring epiphysis" or Wimberger ring (Fig. 2.21a).

The bone cortex becomes thin as a consequence of bone resorption and deficient periosteal new bone production. The trabeculae become small as a result of continued resorption of bone combined with defective formation of new bone. Many of the finer trabeculae completely disappear.

In untreated scurvy, subperiosteal hemorrhage appears on radiographs only as a vague, irregular shadow of soft tissue density adjacent to the cortex of the bone. Once the scurvy is treated and healing begins, the subperiosteal hematomas calcify peripherally and appear as large juxtacortical densities. This is probably one of the earlier radiographic signs of healing.

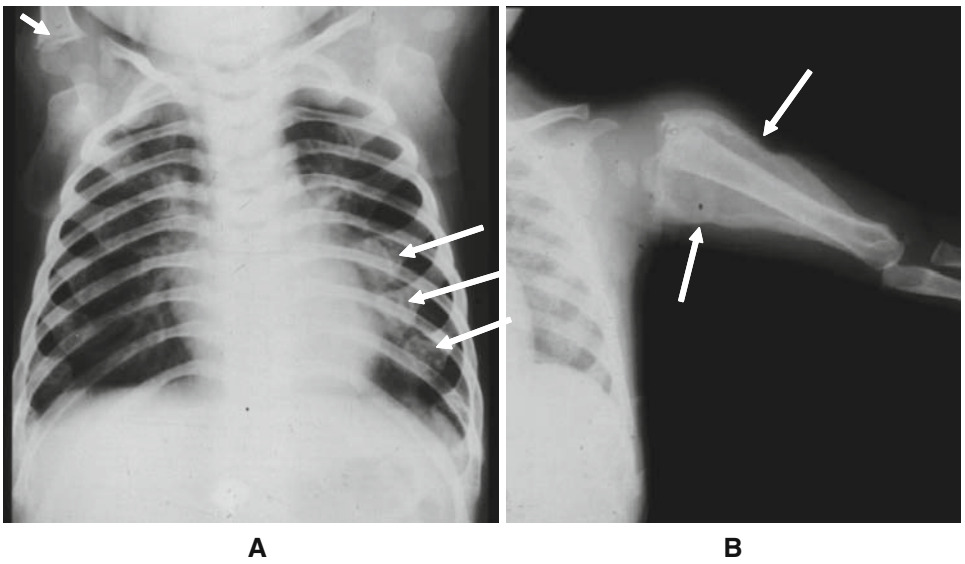

Fig. 2.22 Scurvy. **a** shows enlargement of several of the left costochondral junctions (*arrows*), the so-called scorbutic rosary. Note the lucency, the scorbutic zone, adjacent and proximal to dense epiphyseal zone of calcification of the right upper humerus (*short arrow*). **b** shows extensive calcified subperiosteal hematoma that should not be mistaken for periosteal reaction or myositis ossificans. Given the required time calcified hematoma will be absorbed

Prognosis

Scurvy is a preventable disease and one that is readily amenable to dietary adjustment. Moreover, massive doses of vitamin C do not produce toxicity. Unless scurvy has been present for a long time, all signs of its presence are reversed by adequate therapy.

Copper Deficiency

Although rare, both congenital and acquired deficiencies of copper have been described. The congenital form is Menke kinky hair syndrome, and the acquired type results from nutritional deficiency of copper. The radiological manifestations of copper deficiency resemble those of scurvy because in both, collagen is deficient and improperly constituted causing poor bone formation and osteoporosis. As opposed to scurvy where ascorbic acid itself is lacking, in acquired copper deficiency the pathology relates to copper requirements of ascorbic acid oxidase.

When copper is deficient, many systems are affected: red blood cells, leukocytes, hair, bones, and blood vessels – from impaired formation of collagen and elastin; and in the brain, copper deficiency results in a failure of myelinization.

Menke syndrome is a sex-linked recessive disorder that results in a defect in the intestinal absorption of copper. Parenteral administration of copper may be therapeutic. In patients with this disease, levels of serum copper and ceruloplasmin are low. Infants with this disease are susceptible to infection, have convulsions, mental retardation, unstable temperature regulation with hypothermia, nodular twisted hair, tortuous vessels, and osseous alterations. The last are characterized by metaphyseal spurs, flaring of the anterior end of the ribs, periosteal new bone and in the skull, Wormian bones (sutural bones). Within months of birth, osteoporosis becomes apparent. Patients frequently die early in life because of sepsis.

Nutritional copper deficiency may be encountered in malnourished infants who have been rehabilitated on a high-calorie, low-copper diet (milk). These patients develop osseous alterations similar to those found in Menke syndrome. Similar alterations in bones can also be seen in small infants receiving total parenteral alimentation (Fig. 2.23). In infants with chronic intestinal malabsorption and in premature infants, anemia and neutropenia develop in addition to

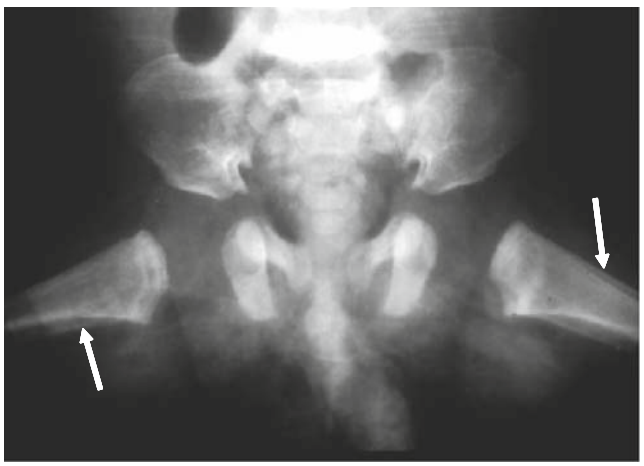

Fig. 2.23 Copper deficiency. The patient is a premature hyperalimented infant. Note periosteal reaction in both femurs (*arrows*) and the presence of osteopenia

osseous abnormalities. Osteoporosis is noted early and is associated with retardation of bone development, resulting in a retarded bone age. Periosteal new bone may also develop.

Endocrine Osteoporosis

Estrogen, androgens, or a combination of the two is necessary for normal osteoblastic activity. Hypogonadism related to ovarian agenesis (Turner syndrome) and testicular dysgenesis (Klinefelter syndrome) may be associated with osteoporosis.

Excess cortisol (the major adrenocorticoid) producing Cushing syndrome/disease may also lead to osteoporosis. Iatrogenic Cushing syndrome is caused by long-standing use of corticosteroids in systemic diseases such as systemic lupus erythematosus or rheumatoid arthritis. Besides osteoporosis, steroids may also cause ischemic necrosis of the bones, especially femoral heads, humeral heads, and femoral condyles.

The osteoporosis that results from thyrotoxicosis is believed to be caused by the high rate of catabolism of proteins that it induces and hence a lack of substrate to form osteoid. Osteoporosis in diabetes mellitus occurs from diversion of substrate proteins into much needed glycogen.

Stress Deficiency Osteoporosis (Disuse Atrophy)

The physiology of stress remodeling of bone is discussed in Chapter 5. According to Wolff Law, dynamic loading of a bone induces remodeling and bone formation; the absence of load causes bone to reabsorb. Thus, immobilization of a limb will cause bone reabsorption with consequent osteoporosis. Signs of disuse osteoporosis may be noted after only a few weeks of complete bed rest. If a limb is immobilized in plaster, the osteopenia is more dramatic. Space flights likewise cause osteoporosis due to weightlessness.

Reflex Sympathetic Dystrophy

Reflex sympathetic dystrophy (RSD), also known as causalgia, Sudeck atrophy, algoneurodystrophy, and several other names, is a syndrome of pain, hyperesthesia, vasomotor disturbances, and dystrophic changes that may improve with sympathetic denervation. RSD usually develops following an injury, even one that is deemed insignificant. Pain swelling and a dramatic patchy decrease in bone substance develop (Fig. 2.24). Although not proven, it is believed that increased blood flow from a neurogenic loss of vasomotor control induced by the inciting event leads to osteoporosis. Precipitating factors are numerous and include soft tissue injury, arthritides, infection, fractures, sprains, dislocations, and operative procedures. RSD has been reported in association with central nervous lesions such as brain tumors and severe head injury as well as myocardial infarction, cervical osteoarthritis, and other causes. These changes usually affect an entire extremity or the distal portion of an extremity such as hand or foot. It may occur along the distribution of a single nerve involving a portion of a hand.

Radiological Findings: Early on radiographs of patients with RSD show only soft tissue swelling that corresponds to the clinical findings of swelling, vasomotor tissue discoloration, and hyperesthesia. Later the swelling decreases and patients' radiographs appear normal, or they show osteopenia. Eventually, if not treated, the musculature of the affected part atrophies and patients develop osteoporosis.

Osteogenesis Imperfecta

Osteogenesis imperfecta is discussed in Chapter 13. Please see also (Fig. 2.11)of this chapter.

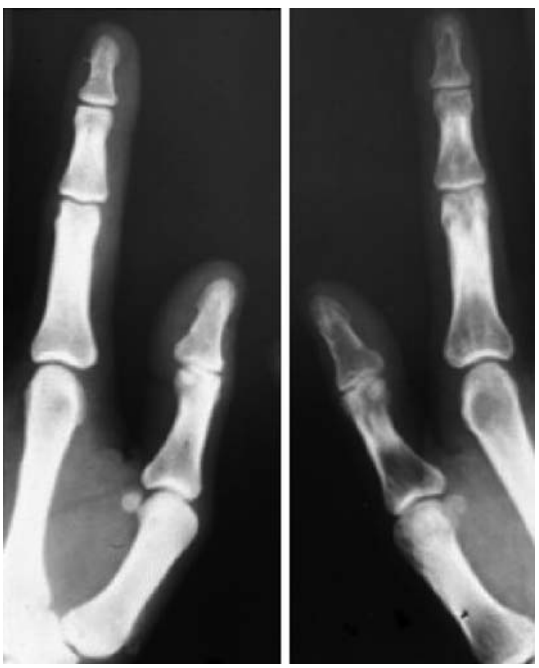

Fig. 2.24 RSD. Coned down radiographs of the first and second digits of both hands show reflex sympathetic dystrophy (RSD) of the right hand, compared to the normal on the left. There is diminished bone density of the right hand

Idiopathic Juvenile Osteoporosis

Idiopathic juvenile osteoporosis is a rare disease that clinically begins about 2 years before puberty in otherwise healthy children who complain of back pain or ankle or knee pain from metaphyseal infractions. Although diaphyseal fractures may occur, metaphyseal injuries are typical of this entity. There is no sex predilection. Serum calcium, phosphorus, and alkaline phosphatase are normal. The only consistent finding is a low positive to markedly negative calcium balance, usually correlating with clinical and radiological findings. Mild, moderate, and severe forms of the disease have been described. Idiopathic juvenile osteoporosis is self-limiting, but if significant trabecular bone is lost, the bone mass and hence its radiological appearance do not return to normal.

Radiological Manifestations: Patients have generalized osteoporosis, vertebral body deformities in the form of fish vertebrae or compression fractures. They also develop metaphyseal and occasionally diaphyseal fractures in the long bones.

Homocystinuria

Homocystinuria is an autosomal recessive disease caused by an inborn error of methionine metabolism. Clinically, patients have mental retardation, dislocation of the optic lens (typically into the anterior chamber of the globe), thromboembolic disease, and osteoporosis. They may have a Marfan-like appearance and seizures. Some cases respond to pharmacologic doses of vitamin B6. Homocystine is found in the urine.

In early life, usually no radiological changes are visible in the skeleton. In the growing skeleton, patients may develop accelerated formation of the hamate and capitate in the wrist and the cuboid and lateral cuneiform in the foot. Arachnodactyly may be present, but it is not as marked as in Marfan syndrome.

Osteoporosis with vertebral flattening, biconcavity (Fig. 2.25), anterior wedging, kyphosis, and scoliosis may be seen. Elongation of the long bones, metaphyseal flaring, and joint deformity may be present. Sometimes prominent growth arrest lines are observed.

Idiopathic Regional Migratory Osteoporosis

This is a disorder of unknown etiology with multiple episodes of articular pain and regional osteoporosis. Once considered a disease state of the third trimester of pregnancy, it is now known to be more common in men around the third decade of life.

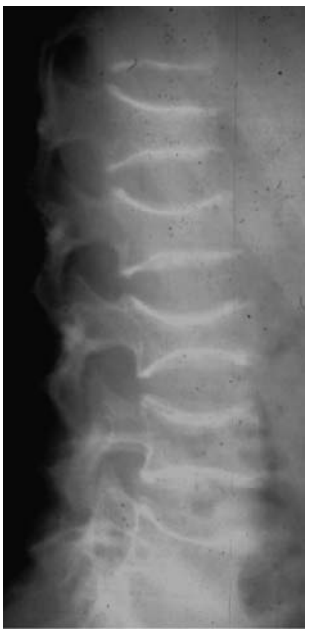

Fig. 2.25 Homocystinuria. Lateral lumbar radiographs showing spinal changes in a 15-year-old patient with homocystinuria. Radiologic changes are very similar to those of osteogenesis imperfecta and other types of childhood osteoporosis. Note severe fish vertebrae and thickening of the vertebral endplates

The demineralization is transitory and typically occurs in the lower extremity, particularly the proximal femur. Regional migratory osteoporosis and transient osteoporosis may be examples of the same spectrum of disease with migration being a relatively uncommon manifestation. Rarely, it may be associated with spinal osteoporosis. The diagnosis is now made accurately on MR imaging of the

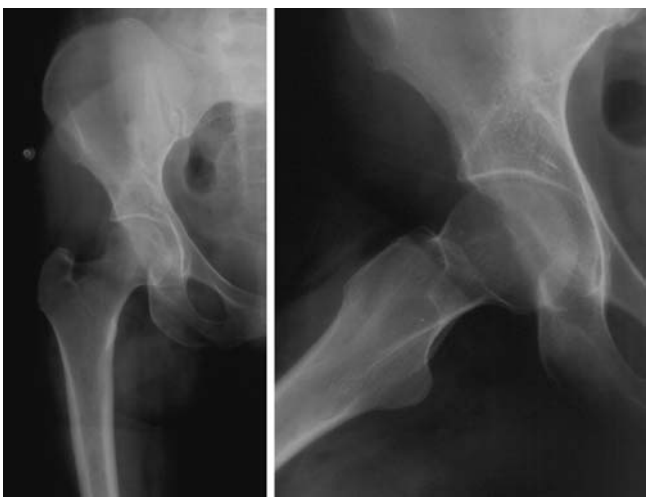

Fig. 2.26 Transient osteoporosis. In May 2007, this 34-year-old female physician presented with right hip pain in immediate postpartum period. AP and frog-leg radiographs of the right hip show mild osteopenia of the proximal right femur, more pronounced in the frog-leg view. Courtesy of Dr. Mahvash Rafii, New York

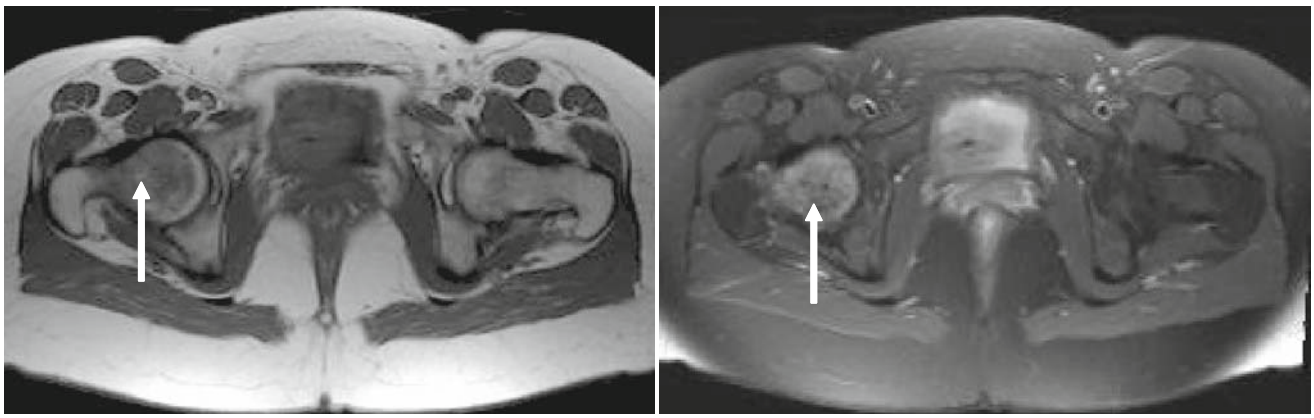

A B

Fig. 2.27 Transient osteoporosis. Same patient as in Fig. 2.26. **a** is the axial T1-weighted MR image of the hips revealing decreased signal intensity of the right femoral neck, extending to the femoral head, and sparing the subchondral region. **b** is the axial T2-weighted, fat-suppressed MR image showing increased signal intensity consistent with bone marrow edema (*arrows*). Courtesy of Dr. Mahvash Rafii, New York

hip with normal or equivocal findings on radiographs (Figs. 2.26, 2.27, 2.28, and 2.29). For further information, refer to Chapter 5.

Inadequate Osteoid Mineralization

A variety of skeletal diseases have normal or near-normal osteoid production but mineralization is defective. More than 30 different etiologies cause clinical syndromes related to disturbances of matrix mineralization. In the majority of these diseases, the pathology lies in an inadequate amount of available calcium, phosphorus, or both in the fluid that permeates osteoid. A number of mechanisms lead to this deficiency including inadequate dietary intake, defective absorption through the gut wall, and failure of the kidneys to conserve the mineral supply. During pregnancy and during the periods of accelerated growth, there is increased demand for mineral and this may outstrip a tenuous level of intake. In other diseases such as hypophosphatasia and vitamin D-dependent rickets, mineral supply may be normal but the formed osteoid may not accept it.

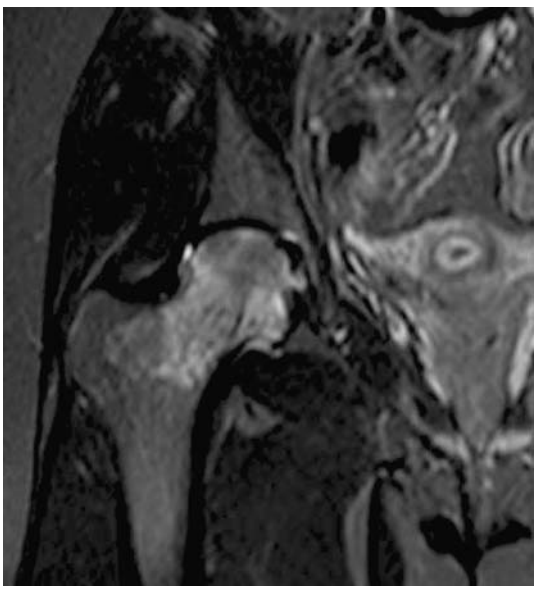

Fig. 2.28 Transient osteoporosis. The same case as Fig. 2.27. Coronal STIR MR image also shows increased signal intensity consistent with bone marrow edema of the right femoral head and neck. Courtesy of Dr. Mahvash Rafii, New York

The common denominator in all these conditions is a lack of osseous rigidity (increased elasticity) in the immature skeleton at sites of growth and in mature bones at points of stress where turnover (physiologic lysis plus replacement) is most rapid. Defective mineralization becomes apparent first at sites of rapid growth because of the high rate of bone production.

Several approaches have been used to classify the diseases associated with osteomalacia. An etiologic approach is probably most practical. In a comprehensive review of the subject, Mankin classified rickets and osteomalacia on a pathophysiological basis. Table 2.4 represents a modified classification of the most important of these diseases.

All these conditions are called *rickets* when they occur in growing bone and *osteomalacia* if they involve the mature skeleton. We discuss nutritional rickets and osteomalacia as the archetype of most of these diseases, followed by discussion of some of the more important specific diseases (Table 2.4).

Rickets

Rickets is a disturbance in the formation of bone in the growing skeleton caused by a failure of deposition of mineral

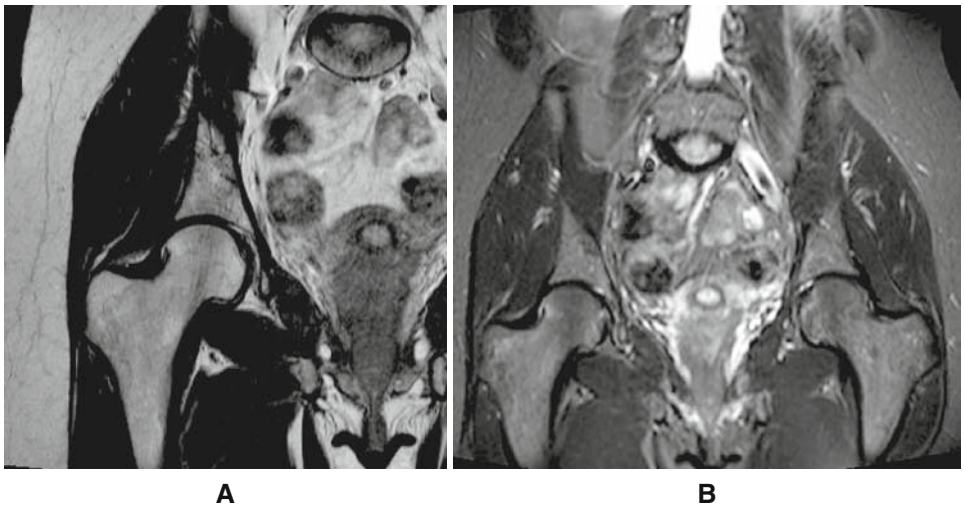

Fig. 2.29 The same case as Fig. 2.28. Transient osteoporosis follow-up MRI in October 2007. **a** is the T1-weighted coronal image of the right hip and **b** is the coronal STIR image of the pelvis including both hips. Both images show resolution of bone marrow edema and normal signal intensity of the right proximal femur. The patient was asymptomatic at this time. Courtesy of Dr. Mahvash Rafii, New York

Table 2.4 Etiological classification of rickets and osteomalacia

1. Deficiency states
   a. Vitamin D deficiency
   b. Calcium deficiency
   c. Phosphorus deficiency
   d. Solar irradiation deficiency
   e. Rickets of prematurity
2. Absorptive
   a. Gastrointestinal abnormalities
   b. Hepatobiliary disease
   c. Pancreatic abnormalities
3. Hereditary renal tubular diseases (renal rickets)
   a. Vitamin D-dependent rickets (VDDR)
      i. Autosomal recessive
   b. Vitamin D refractory rickets (VDRR)
      i. X-linked dominant
      ii. Autosomal dominant, recessive or sporadic (Rare)
   c. Vitamin D refractory rickets with glycosuria
   d. Fanconi syndromes
      i. Autosomal recessive form
      ii. Lowe syndrome
      iii. Wilson disease
      iv. Tyrosinemia
      v. Lignac-Fanconi syndrome
   a. Renal tubular acidosis (distal tubular)
   b. Autosomal dominant with variable penetrance
4. Renal osteodystrophy (uremic osteopathy)
5. Iatrogenic
   a. Anticonvulsant therapy
   b. Intravenous hyperalimentation
   c. Nonabsorbable antacids
   d. Peritoneal dialysis
   e. Hemodialysis (amyloidosis – B2 microglobulin – 100% involvement in adults following 15 years of dialysis)
6. Tumor related
7. Miscellaneous
   a. Hypophosphatasia
   b. Vitamin D refractory rickets, type II
   c. Atypical axial osteomalacia

within the organic matrix of cartilage and bone at the growth plate. The failure may result from a deficiency in the dietary intake of calcium or phosphorus to a failure of adequate absorption through the gut wall or other causes presented in Table 2.4.

Because active rickets is manifested only in the growing skeleton, its expression is seen in the first period of rapid growth, between 6 months and 3 years, though its effect may be encountered earlier. Less severe form rickets may not manifest themselves until the prepubertal years.

Economically advanced nations have learned that it is possible to prevent nutritional rickets even among its less advantaged citizens. Both calcium and phosphorus are ubiquitous in milk and other dairy products. Today, an inadequate intake of vitamin D in infancy and early childhood is the most common cause of nutritional rickets. In lieu of sun exposure as a means to vitamin D formation, synthetic preparations of vitamin D, also in milk, have all but eliminated this form of rickets. Only in underdeveloped nations with low sun exposure, populations suffering from famine and cults with dietary eccentricities does advanced rickets occur in numbers.

Rarely severe fibrocystic disease of the pancreas or more often celiac disease may interfere with calcium absorption to an extent that insufficient calcium is absorbed through the gut. In these diseases, calcium binds to fats and passes in the stool.

Rickets has been reported in premature infants of very low birth weight with increasing frequency. The pathogenesis is probably metabolic, nutritional, and in some cases iatrogenic.

Radiological Manifestations

Radiographic changes of rickets are best illustrated in the long bones (Fig. 2.30). Although generalized osseous alter-

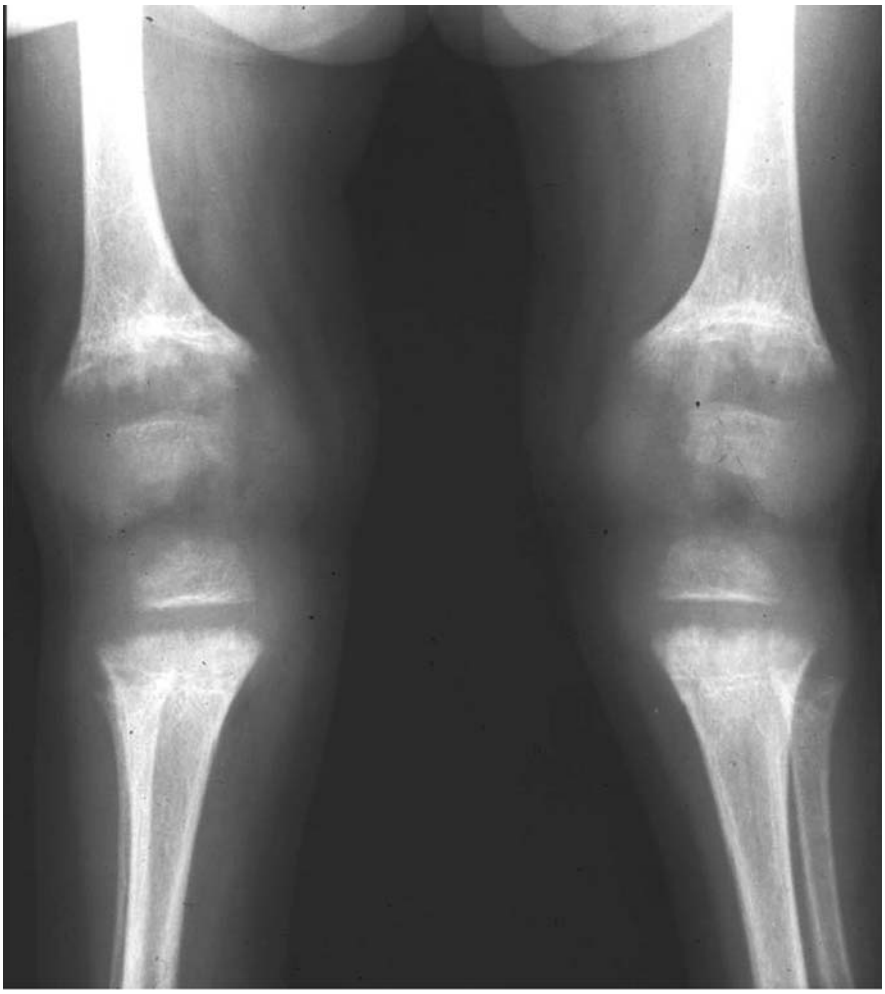

Fig. 2.30 Nutritional rickets. AP radiograph of the knees demonstrates diminished bone density, haziness of epiphyseal contour, paint brush appearance of metaphysis and decreased density of the zone of provisional calcification of the femur and tibia on both sides

ations occur, the first and most apparent are found at sites where the growth of bone is most rapid, e.g., the wrist, knees, and costochondral junctions (Fig. 2.31).

The earliest radiographic sign of rickets is haziness, followed by disappearance, of the zone of provisional calcification. Radiographic findings in the metaphysis are more apparent because bone growth is most rapid in this portion of long bones. Radiographically, the width and depth of the radiolucent physeal cartilaginous matrix interposed between the epiphyseal center and the metaphysis increases. Attempts at ossification of the irregularly deposited osteoid enhance the irregularity of the metaphyseal region, resulting in a radiographic appearance that has been compared to the bristles of a paintbrush. Cupping of the ends of diaphyses of the bones probably results from mechanical factors acting upon the soft, unmineralized osteoid at the metaphysis.

The smaller trabeculae may undergo complete resorption so that the bones have nearly similar radiodensity as the soft tissue marrow. For the same biomechanical reasons as in osteoporosis, the trabeculae oriented along the lines of stress accrue mineral and appear prominent. Defective mineralization leads to deceptively thick cortices, but they are made up

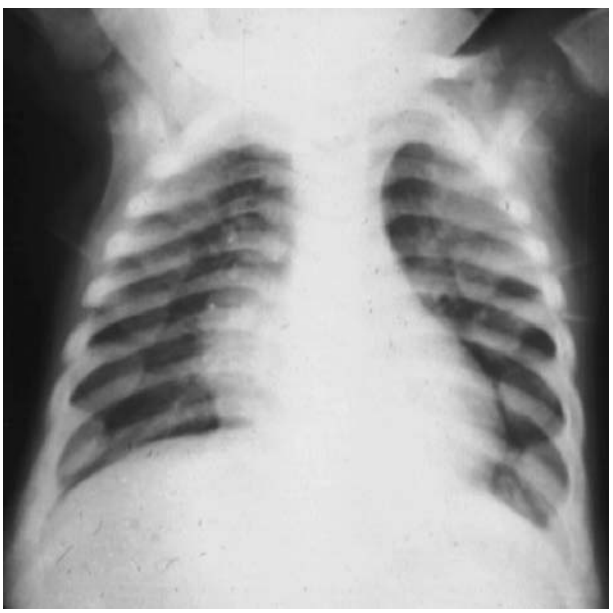

Fig. 2.31 Nutritional rickets. This is a different patient. AP radiograph of the chest demonstrating rachitic rosary more obviously on the left

of poorly ossified osteoid that may show cortical radiolucent streaks. In the infant, failure of mineralization at the margins of the cranial sutures creates an appearance of increased width of the sutures. In the chest, rachitic rosary may be seen at the costochondral junctions.

Greenstick fractures are common in patients with rickets. The soft osteoid predisposes to bowing in weight-bearing bones. Sharply defined, focal areas of decreased density (Looser zones) may be seen perpendicular to the cortex and traversing incompletely the shaft of the long bones. These are rare in childhood rickets but are common in adult osteomalacia.

When rickets begins to heal, the zone of the provisional calcification appears at the site it would normally occupy if there had been no interference with mineralization and the bone had grown normally. Later the radiolucent metaphysis fills in with new bone. At this time, the radiographic appearance of concavity at the diaphyseal ends of the long bones may be most marked. The epiphyseal centers reconstitute hemispherically since the base of the center grows at a slower rate than the periphery. The epiphyseal centers failed to ossify because rickets reappear falsely, suggesting a rapid increase in the patients bone age (Fig. 2.32). Bowing of the weight-bearing long bones persist after completion of treatment of nutritional rickets (Fig. 2.33), but they eventually will remodel and disappear as normal growth continues.

Regardless of cause, the radiological changes of rickets, whether caused by failure of calcium absorption in biliary atresia (Fig. 2.34) or in nutritional rickets, are similar. Scurvy and rickets may occur simultaneously, in economically deprived regions of the world, where starvation is often rampant (Figs. 2.35 and 2.36).

Summary of Radiological Manifestations of Rickets:

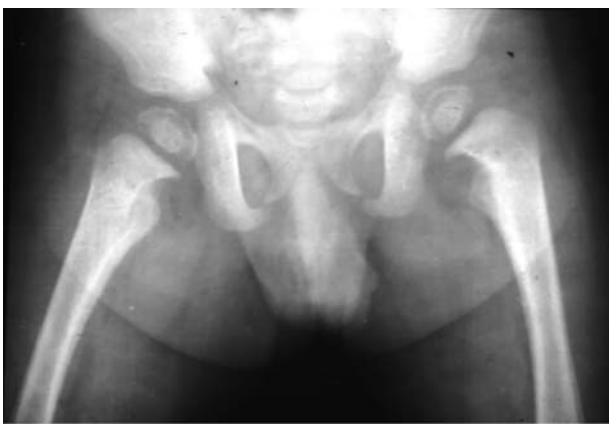

Fig. 2.32 Nutritional rickets. AP pelvis of another patient with nutritional rickets after treatment. The proximal femoral epiphyses show remineralization. This phenomenon is not related to the growth of the epiphyses, but it is demonstrating the result of treatment and partial recalcification of the epiphyseal cartilage

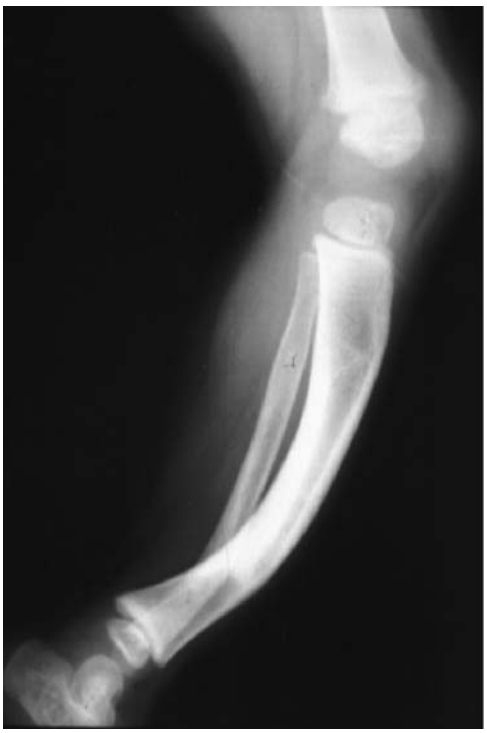

Fig. 2.33 This is a case of treated rickets with residual bowing deformity. The deformity will improve with remodeling during growth of the patient. This is in contrast to osteomalacia where deformities do not improve but remain as sequelae of the disorder

1. Haziness and later disappearance of the zone of provisional calcification.
2. Diminished bone density.
3. Widening of the physeal plate.
4. Irregularity of the metaphysis.
5. Concavity of metaphysis and later cupping.
6. Coarsening of the trabecular pattern.
7. Cortex deceptively thick initially and later thin.
8. Greenstick fractures.
9. Deformity (bowing of weight-bearing long bones).
10. Looser zones (rare).
11. Blurring of the contour of epiphyseal centers.
12. Rachitic rosary – physeal enlargement and irregularity at the anterior ends of the ribs.
13. Delayed growth.
14. False widening of cranial sutures.

Prognosis

Ordinarily, the assurance of adequate intake of calcium and phosphorus and the addition of vitamin D to the diet are all that is required to treat nutritional rickets. If the disease

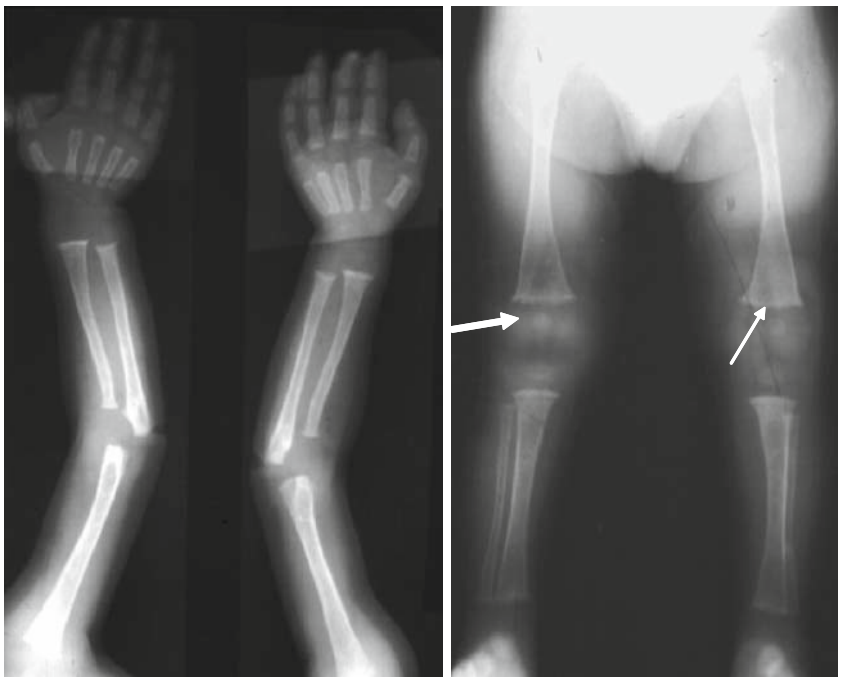

Fig. 2.34 Biliary rickets. AP radiographs of the upper (**a**) and lower extremities (**b**) of a $5\frac{1}{2}$-month-old girl with biliary atresia showing mild ricketic changes. Metaphyseal irregularity (*thin arrow*) and loss of cortex of the distal femoral epiphyses (*arrow*) are present

does not respond to dietary measures, then other confounding causes of the rickets should be sought.

Osteomalacia

Osteomalacia is a disease of mature remodeling bone. The pathogenesis of osteomalacia is exactly the same as that of rickets. The differences between the two conditions result only from differences in the response of growing and mature bone to a deficiency of calcium, phosphorus, or vitamin D. Full-blown osteomalacia rarely occurs in the western hemisphere.

The causes of the inadequate mineral supplies for skeletal maintenance are listed in Table 2.4. Dietary deficiencies severe enough to cause osteomalacia are rare in industrial countries. Nevertheless, there are reports of osteomalacia among vegetarians and diet faddists. There are also reports of

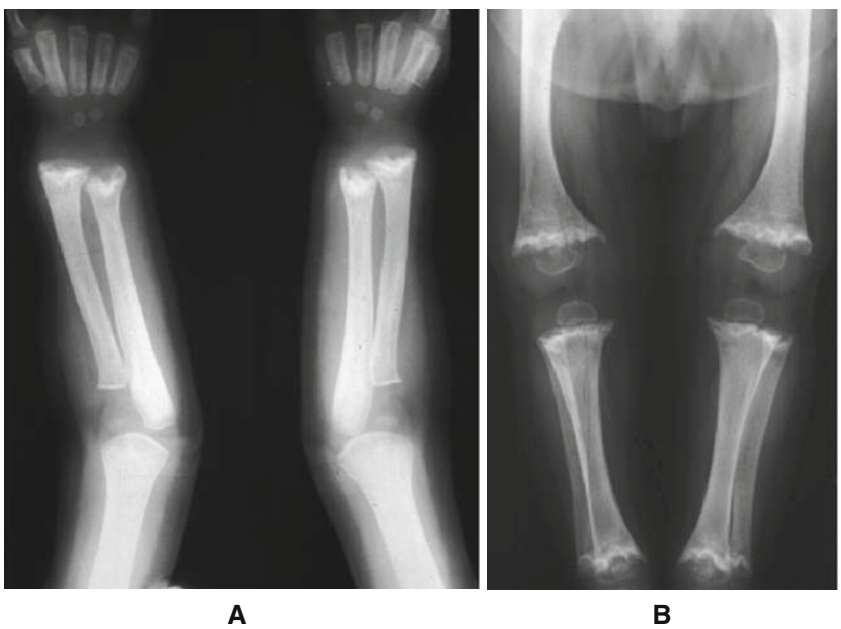

Fig. 2.35 Combined rickets and scurvy. AP radiographs of the upper (**a**) and lower extremities (**b**) of a patient with rickets and scurvy. Bowing and fraying of the metaphyses are manifestations of rickets and ring epiphyses as well as dense provisional zone of calcification are manifestations of scurvy

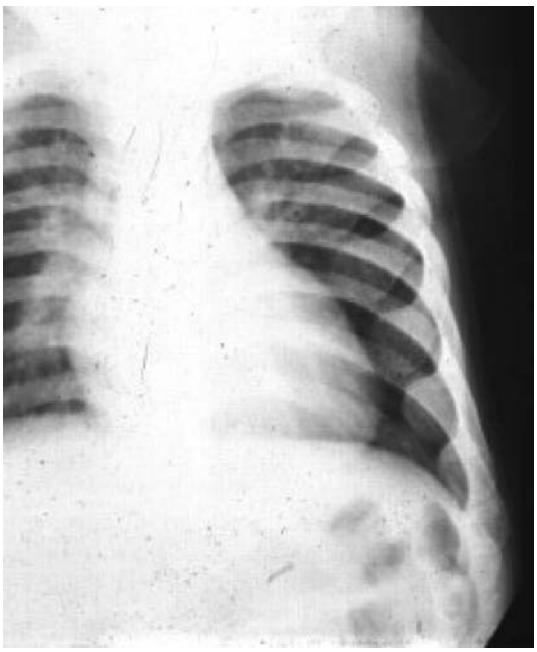

Fig. 2.36 Combined rickets and scurvy. AP radiograph of the left ribs of the same patient as in Fig. 2.34 with combined rickets and scurvy. Rosary of the costochondral junctions is a manifestation of both disorders, but it is dense related to scurvy

osteomalacia in elderly people who eat poorly, the so-called "tea and toast" diet.

Dietary deficiencies are more common in economically underdeveloped countries, among those who live on inadequate rations and those denied sunlight. Social practices such as completely covering clothing in women in some cultures in India and parts of Asia have been reported to cause osteomalacia from lack of vitamin D as a result of actinic rays deprivation.

Fat absorption disturbances that result from chronic disease of the bowel and pancreas may also result in osteomalacia. Chronic steatorrhea, sprue, fibrosing pancreatic disease, disturbances in the biliary duct system, and long-standing ulcerative colitis may result in conditions that inhibit the absorption of fat-soluble vitamin D. Unabsorbed fatty acids may form insoluble soaps with the available calcium in the bowel. This in turn stimulates bowel motility, causes diarrhea, and moves the intestinal contents through the gut too fast for efficient absorption. The net result is poor absorption of vitamin D, calcium, and phosphorus from the bowel lumen to the blood.

A rare type of osteomalacia, known as puerperal or multiple pregnancy osteomalacia, occurs in young women who bear several children in rapid succession and nurse them between confinements. This practice depletes the skeletal calcium and phosphorus stores in order to meet the demand of the growing fetus and the nursing infant.

As with patients suffering from rickets, patients with latent or early symptomatic osteomalacia, Milkman syndrome, may also develop Looser zones or Milkman pseudofractures. These occur more often in the diaphyses of large cylindrical bones but flat bones, particularly those of the pelvis, may also be involved. Looser zones may also be seen in the femoral necks, inferior pubic rami, and medial borders of the scapulae. They are usually multiple, often symmetrical. They have the appearance that resembles stress fractures although usually there is no history of trauma.

Some authors have reported an association between osteomalacia and femoral neck fractures. Some have postulated that osteoporotic patients who develop hip fracture may have subclinical osteomalacia.

As the skeleton softens, weight bearing causes bowing of the long bones of the lower extremity. The pelvis becomes flattened laterally causing the pubic bones to protrude anteriorly.

Radiological Manifestations

Early in the course of osteomalacia, a coarse trabecular pattern may be the only evidence of pathology. The coarse trabecular pattern is a consequence of inadequate mineralization of secondary trabeculae; the larger primary trabeculae are well seen in contrast with the unossified osteoid and soft tissues of the marrow (Fig. 2.37). The weight-bearing

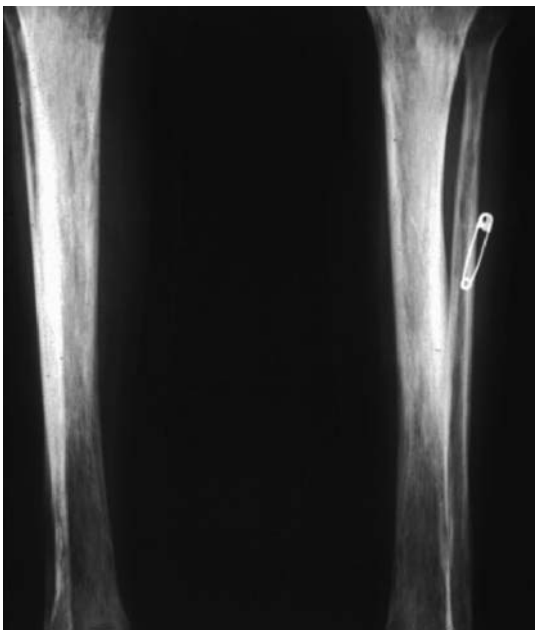

Fig. 2.37 Osteomalacia. There is diminished bone density, coarsening of the trabecular pattern of bones, and cortical thinning. In the absence of Looser zones and deformity, these findings alone do not establish diagnosis of osteomalacia

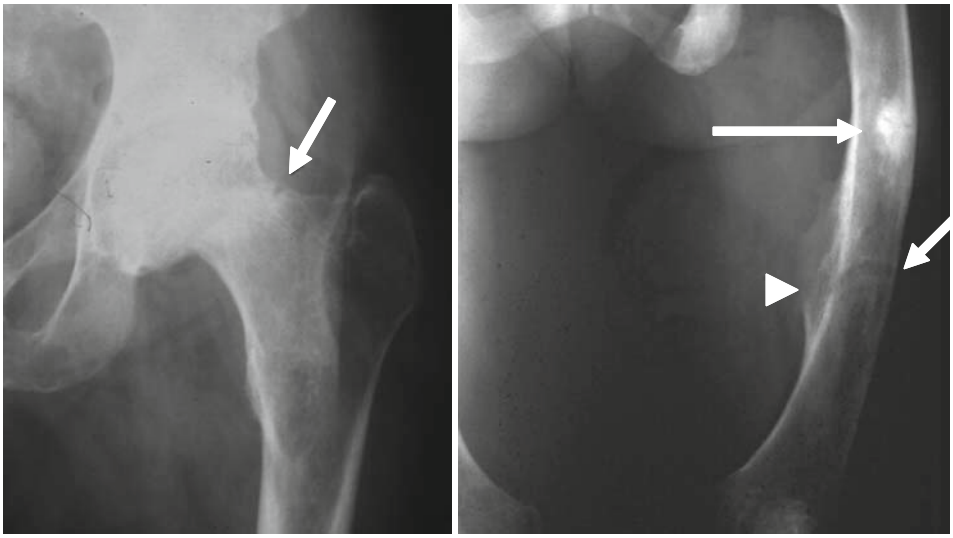

Fig. 2.38 Osteomalacia. **a** – AP radiograph of the hip shows diminished bone density, cortical thinning, a Looser zone in the superior border of the femoral neck (*white arrow*), and mild coxa vara. **b** – AP radiograph of the femur shows healing Looser zone on the convex border of the femur (long arrow). There is a broad-base osteochondroma-like bony protuberance at the site of a healed fracture and/or a Looser zone along the medial border of the body of the femur (*arrow head*). The short arrow points at a previous fracture or Looser zone (osteoid seam). Note lateral bowing of the femur. Looser zones and deformities establish the diagnosis of osteomalacia

long bones, especially femur deform and bow (Fig. 2.38). In anteroposterior projection the angle between the femoral neck and the shaft may become more acute, causing coxa vara deformity (Figs. 2.38 and 2.39). The pelvis and the spine deform as the result of bone softening (Fig. 2.40). In the final stages, disuse osteoporosis complicates the picture so that the bones show severe and marked trabecular loss and cortical thinning. Looser zones are more commonly seen.

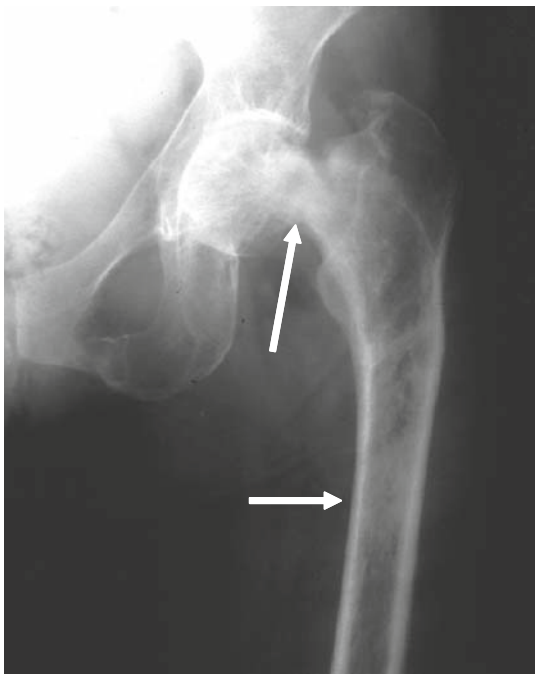

Fig. 2.39 Osteomalacia. There is diminished bone density shown by thinning of the cortices (*arrow*). A healing Looser zones (osteoid seam) is present in the left femoral neck (*long arrow*). Note the presence of moderate coxa vara

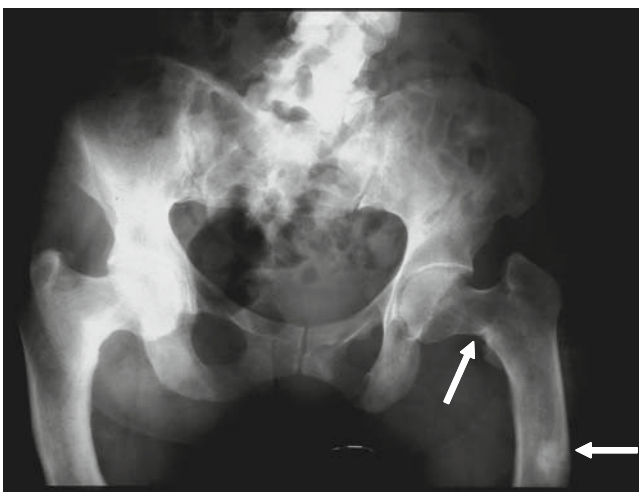

Fig. 2.40 Osteomalacia. There is diminished bone density demonstrated by cortical thinning, bilateral coxa vara, Looser zones of the left femoral neck, and body of the left femur (*arrows*), as well as levoscoliosis of the lower lumbar spine. Note deformity of the pelvis and lateral bowing of both femurs. Looser zones and deformities establish the diagnosis of osteomalacia. There is bilateral coxa vara

As already mentioned, Looser zones or pseudofractures are transverse lucencies traversing the diameter of bone incompletely. They are radiolucent by virtue of their composition of osteoid and fibrous tissue (Figs. 2.38, 2.39, and 2.40). Pseudofractures may be seen in other conditions such as Paget disease and fibrous dysplasia. When they occur in bones that otherwise have a normal appearance, Looser zones strongly suggest the presence of osteomalacia. Looser zones are more commonly seen in the pubic

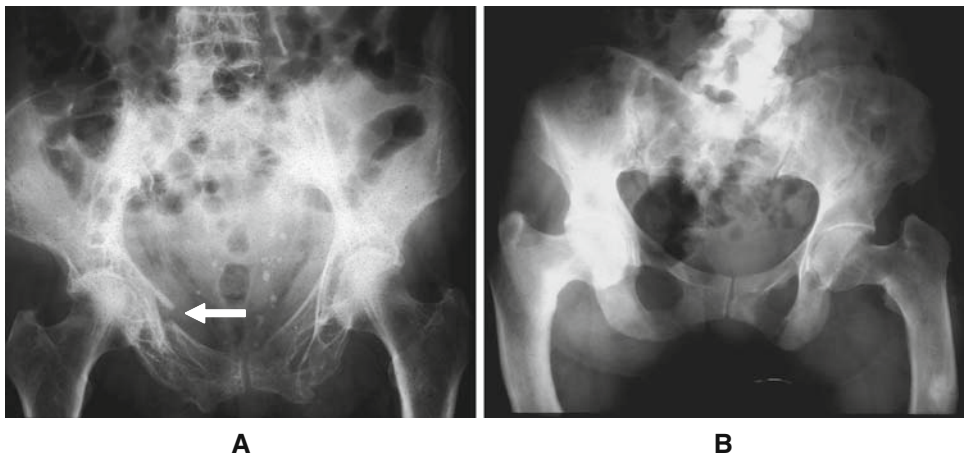

Fig. 2.41 Simulation of osteomalacia and osteoporosis to "cheese and crackers." AP pelvic radiograph in a case of osteoporosis (**a**) with pelvic fracture (arrow) *simulates cracker* and AP view of the pelvis of osteomalacia (**b**) showing deformities of the pelvis, the lumbar spine, femoral necks, and body of both femurs *simulates cheese*

bones, the medial aspect of the femoral neck, the diaphysis of the femur, the axillary border of the scapula, and the bones of the forearms. Healing Looser zones show heavy calcification (Figs. 2.38 and 2.40). Rarely, there may be a broad-base osteochondroma-like bony protuberance at the site of a healed pseudofracture or Looser zone (Fig. 2.38b).

The unossified osteoid in osteomalacia permits deformities such as extensive bowing and bending of bones. In contrast, osteoporotic bones are brittle and fracture easily. Bowing and deformity in osteomalacia permits radiographic differential diagnosis between osteomalacia and osteoporosis in pure cases. By analogy, osteomalacia resembles soft cheese, while osteoporotic bones resemble brittle crackers. This difference can be appreciated by comparing Fig. 2.41a showing the brittle bones of osteoporosis with pelvic fracture and Fig. 2.41b showing elasticity of bones causing deformity without fracture in osteomalacia.

Summary of Radiological Manifestation of Osteomalacia:

1. Decreased bone density.
2. Coarse trabecular patter (early).
3. Cortical striations and later cortical thinning.
4. Softening causes various forms of deformity:
   - Pelvis: Triradiate
   - Spine: Kyphosis
   - Legs: Bowing
   - Chest: Bell shaped
   - Skull: Basilar invagination
5. Looser zones (Milkman syndrome) probably related to stress on abnormal bone.
   - Uncommon in renal osteodystrophy (1%)
   - Common sites of Looser zones:
   - Obturator rings of the pelvis
   - Lower ribs
   - Inferior angles of the scapula
   - Long bones (femoral necks and convex borders)
   - Metatarsal shafts

Renal Osteodystrophy

Chronic renal failure causes many physiologic changes that affect bone. Concomitant with the progress of renal failure, renal tubular management of electrolytes, including calcium and phosphorous, also fails. Renal tubular calcium wasting leads to secondary hyperparathyroidism. The elevated parathormone levels lead to mineral resorption from bone. Simultaneously, renal conversion of 25(OH) vitamin D3 to $1,25(OH)_2$ vitamin D3 [$1,25(OH)_2$ cholecalciferol] diminishes. As the latter is the most active form of vitamin D and the mineral is being mobilized from bone, instead of moved into it, patients develop osteomalacia. Untreated patients will advance further pathologically and develop fibrosis within their marrow space, a form of the disease known as osteitis fibrosa cystica.

Widespread availability of renal dialysis and kidney transplant has meant longer survival for patients with renal failure. Although dialysis performs many of the functions of the failing kidneys, it does not prevent the secondary hyperparathyroidism of renal failure and it does not address the loss of vitamin D conversion. Hence as patients with renal failure survive longer, the skeletal system has enough time to develop renal osteodystrophy. As a result, this disease has become more common. Awareness of this problem has led to improved monitoring and therapy of renal dialysis patients. Usually, secondary hyperparathyroidism is the dominant feature of renal osteodystrophy. For further discussion, please refer to Chapter 3 on skeletal manifestations of endocrine disorders.

Hereditary Renal Tubular Diseases

In 1937 and again in 1946, Albright and coworkers reported a type of rickets that is resistant to vitamin D therapy and responding only to massive doses of this vitamin. In 1933 and 1956, de Toni published papers describing cases of dwarfism accompanied by marked renal dysfunction. Since these original publications, it has been recognized that this type of rickets results from an inability of the renal proximal tubules to reabsorb certain substances, particularly glucose, amino acids, phosphate, and bicarbonate, from the glomerular filtrate.

These cases were classified under the general heading of "de Toni–Debre–Fanconi syndrome" and in the United States they are called the "Fanconi syndrome."

There are a variety of conditions in which the proximal tubules are congenitally unable to reabsorb a number of substances or in which a number of toxic agents may induce this inability. When phosphorus, or less frequently calcium, is lost by renal tubular dysfunction, rickets develops because of inadequate mineral for normal ossification.

Dent et al. did much of the early work that resulted in better understanding of these conditions. Several other investigators have made major contributions by reporting various forms of osteomalacic syndromes (rickets and osteomalacia) that result from congenital abnormalities of the renal tubules. A number of workers have tried to classify these hypophosphatemic rachitic and osteomalacic states. Abnormalities may occur in the proximal renal tubules, the best example of which is X-linked hypophosphatemic rickets. Tubular dysfunction may be associated with renal tubular acidosis, several types of which have been reported. About 70% of patients with chronic renal tubular acidosis (Table 2.4) develop nephrocalcinosis. For further details on renal osteodystrophy refer to Chapter 3.

X-Linked Hypophosphatemic Vitamin D Refractory Rickets (Familial Vitamin D-Resistant Rickets) (MIM 307800)

X-Linked hypophosphatemic vitamin D refractory rickets is in group 25 of the International "Nosology and Classification of Genetic Skeletal Disorders 2006 Revision" (Table 13.1).

This is the most common type of rickets caused by renal tubular dysfunction. It is transmitted as an X-linked dominant and mutation is in *PHEX* gene (Table 13.1).

It occurs in both men and women but men are more severely affected. As the name implies, patients have low serum phosphate levels. Clinically, they resemble nutritional rickets, but their disease is refractory to treatment with vitamin D.

Manifestations of dwarfing and bone deformity usually become apparent at the commencement of weight bearing.

Radiological Manifestations

The radiographic manifestations of hypophosphatemic vitamin D refractory rickets are those of advanced rickets of any etiology because the underlying osseous disturbance is that of inadequate mineralization of osteoid (Fig. 2.42). In hypophosphatemic VDRR, the patient is apt to be older than the patient with vitamin D deprivation rickets and in most cases the osseous alterations at the end of the bone tend to be somewhat less severe (Figs. 2.43 and 2.44). Because of the chronicity of the process, bowing and shortening of the long bones may be prominent features.

The long bones have a coarse trabecular pattern superimposed on moderate but generalized diminished density. At the ends of the long bones the trabeculae assume a longitudinal direction. Bowing of the bones of the lower extremities laterally may be marked and associated with Looser zones. As a result of the bowing, the medial cortex thickens due to the compressive forces on the concavity of the

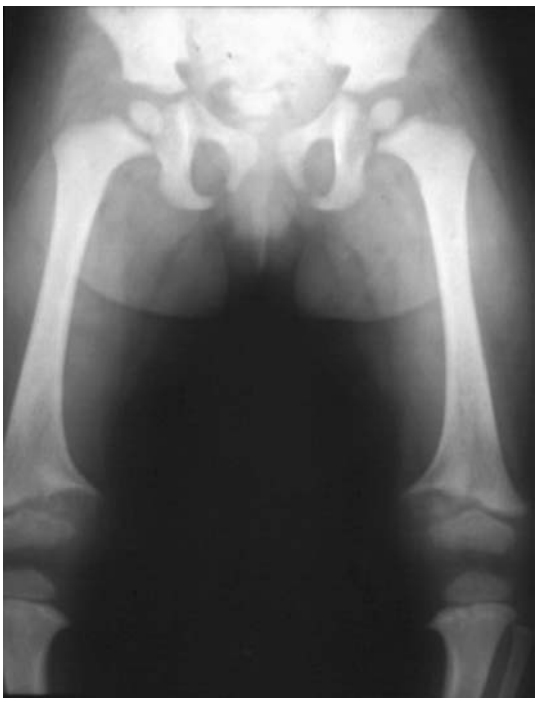

Fig. 2.42 Vitamin D refractory rickets. AP radiograph of a 2-year-old girl with refractory rickets showing widening of the epiphyseal plates in distal femurs and both proximal tibia. There is fraying of the metaphyses

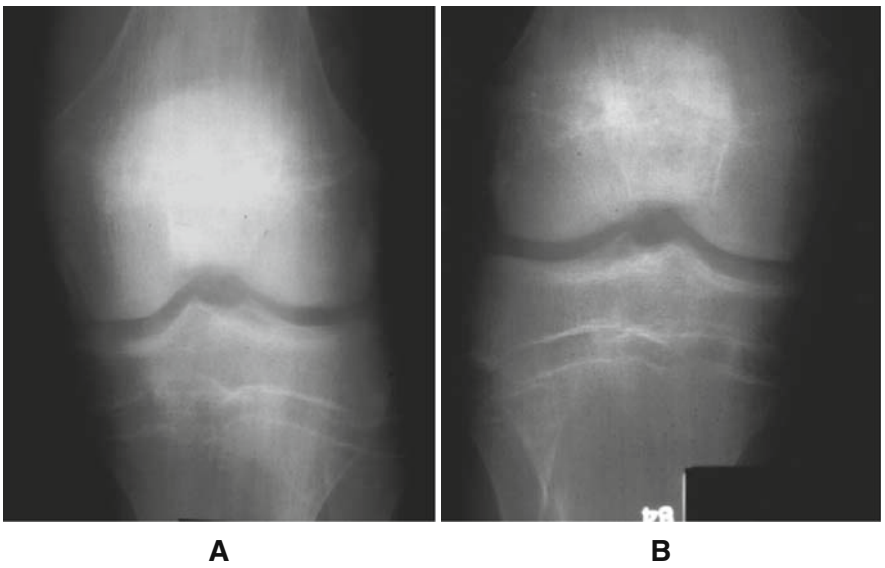

Fig. 2.43 Vitamin D refractory rickets. AP radiographs of the knees (**a)** and (**b**) of a 16-year-old boy with late onset of refractory rickets. Note widening of the epiphyseal plates and diminished bone density manifested by marked cortical thinning

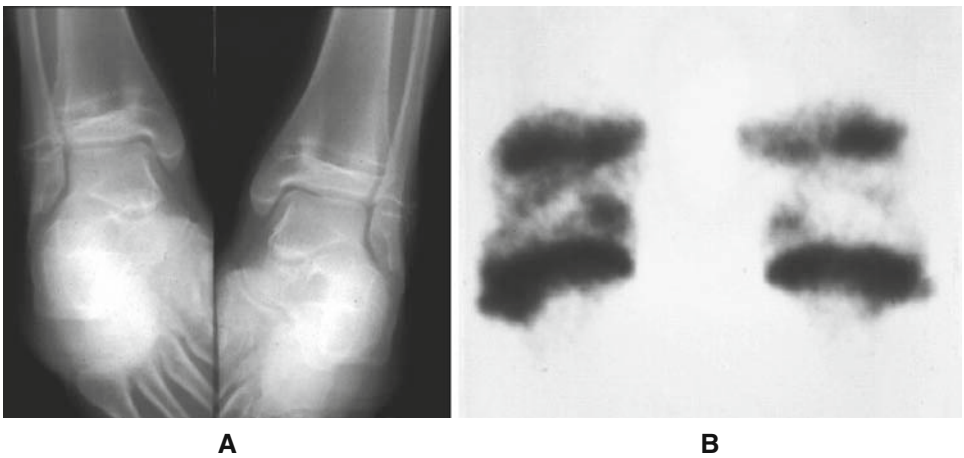

Fig. 2.44 Refractory rickets. AP view of both ankles (**a**) from the same 16-year-old boy as in Fig. 2.43 with late onset of refractory rickets. Note widening of the epiphyseal plates. Anterior projection of a bone scintigram of the same patients knees revealing increased metaphyseal uptake (**b**)

bone. Metaphyseal changes may not be florid, but the medial aspects of the femoral and tibial metaphyses about the knee are widened. Unlike most types of osteomalacia, Looser zones tend to occur on the convexity of the bone in this disease.

Vitamin D-Dependent Rickets

This type of rickets results from an autosomal recessive inborn error of vitamin D metabolism. Hypophosphatemia is present in this disease, but the underlying cause is diminished intestinal calcium absorption. The cause may be related to deficiency of the renal enzyme 25-OH-D-α-hydroxylase causing impairment of calcitriol [$1,25(OH)_2$ D3] production. This form of vitamin D is essential for efficient calcium absorption by the gut. Clinical and biochemical abnormalities resemble advanced nutritional rickets but they may be present as early as 3 months of age. The patients do not respond to 25(OH) vitamin D but are responsive to $1,25(OH)_2$ vitamin D (calcitriol).

Iatrogenic Osteomalacic Syndromes

Anticonvulsant Drug-Induced Rickets and Osteomalacia

Diphenylhydantoin alone or in combination therapy with phenobarbital and other drugs may cause rickets and osteomalacia caused by anticonvulsant drugs are similar to nutritional forms.

Aluminum Intoxication

A special form of osseous abnormality has been reported in patients with chronic renal failure undergoing dialysis.

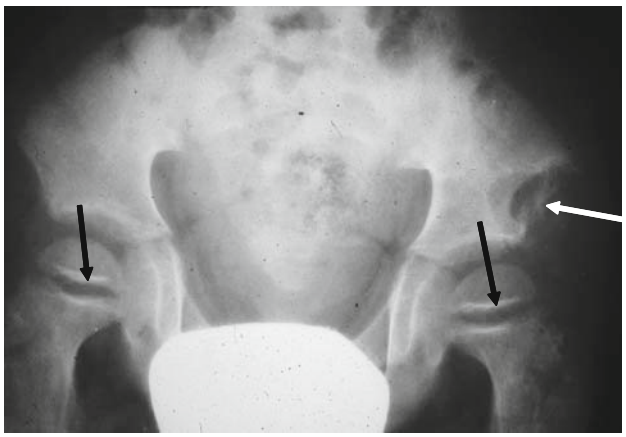

Fig. 2.45 Tumor-induced osteomalacia. This patient developed tumor-induced rickets secondary to osteosarcoma of the left iliac bone (*white arrow*). AP radiograph of the pelvis shows widening of the proximal femoral epiphyseal plates due to rickets (*black arrows*). Figures 2.45, 2.46, and 2.47 belong to the same case. Courtesy of Dr Murray K Dalinka, University of Pennsylvania

Histologically, these patients have osteomalacia and deposition of aluminum in the bone. The aluminum comes from the dialysate used during dialysis. The patients may also develop progressive encephalopathy and dementia which are probably associated with the accumulation of aluminum in the brain.

This form of low turnover osteomalacia should not be confused with typical renal osteodystrophy caused by renal failure. In low turnover osteomalacia, parathyroidectomy should not be performed. Since the identification of aluminum in dialysate as the cause of this disease, purified water has been substituted in dialysis, and the disease has been virtually eliminated. For further discussion, review Chapter 3.

Tumor-Related Rickets and Osteomalacia

Osteomalacia may occur in association with some soft tissues or osseous tumors. Most commonly, oncogenic osteomalacia arises with mesenchymal phosphatonin-excreting tumors, such as hemangiopericytomas. These cause phosphaturia and result in osteomalacia. Other tumors and tumor-like lesions such as giant cell tumor, fibrous dysplasia, neurofibromatosis, giant cell reparative granuloma, nonossifying fibroma, and osteosarcoma may also cause oncogenic osteomalacia (Figs. 2.45, 2.46, and 2.47). Identification and removal of the tumor cures the osteomalacia, but these tumors can be small and difficult to localize. Partial improvement has been reported from vitamin D and phosphate therapy, until the tumor is discovered.

Hypophosphatasia

Please refer to Chapter 13 on bone dysplasias for discussion of this disease entity.

Atypical Axial Osteomalacia

This is an entity that was described in 1961. The patients are adults with minimal symptoms and normal biochemical studies. Only the axial skeleton is involved, showing decreased bone density and coarsening trabecular pattern that primarily involves the cervical spine, the lumbar spine, the pelvis, and the ribs. Biopsy shows histological evidence of osteomalacia. Sometimes the patients have features of ankylosing spondylitis.

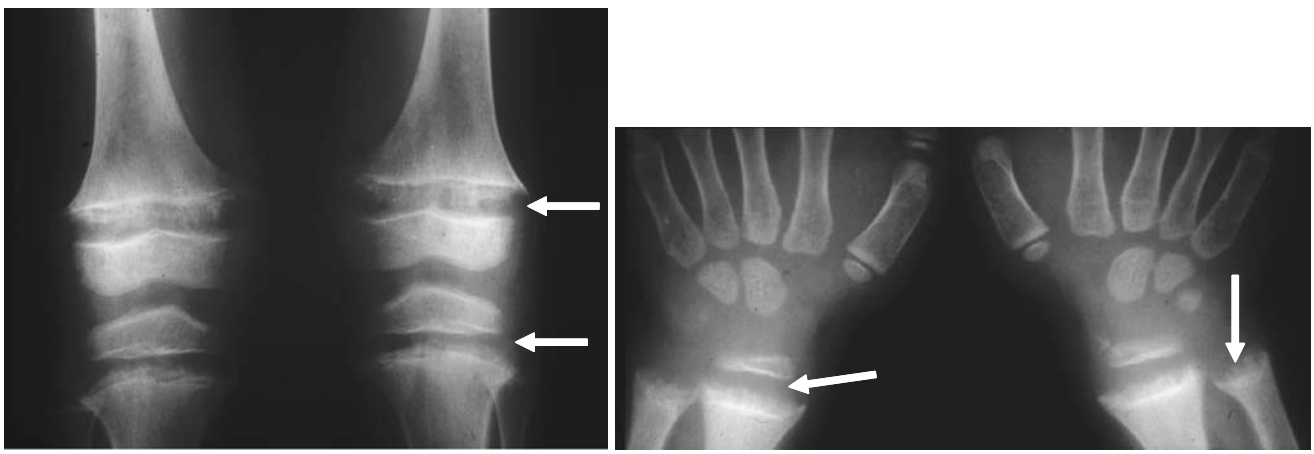

Fig. 2.46 Tumor-induced rickets. The patient developed tumor-induced rickets secondary to osteosarcoma. AP radiographs of the wrists and knees show widening of the epiphyseal plates and metaphyseal fraying due to rickets (*arrows*). Courtesy of Dr. Murray K Dalinka, University of Pennsylvania

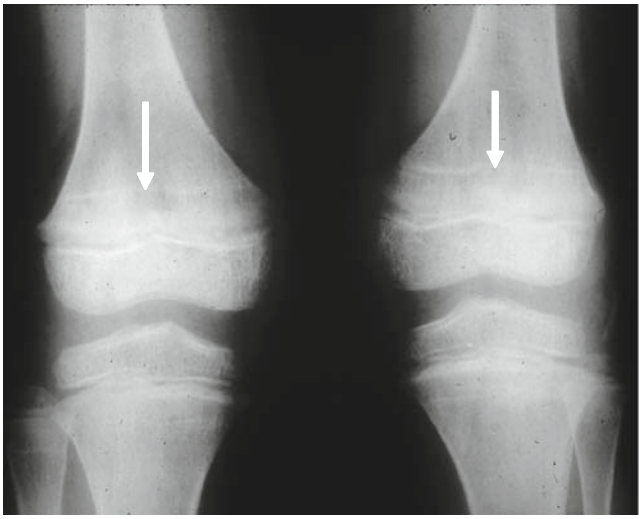

Fig. 2.47 Tumor-induced rickets. This is a follow-up of the patient in Figs. 2.45 and 2.46 with oncogenic osteomalacia secondary to osteosarcoma. AP radiographs of the knees show improvement of the rickets after treatment of osteogenic sarcoma of the left iliac bone. The epiphyseal plates have a normal appearance. Growth arrest lines are also present (*arrows*). Courtesy of Dr. Murray K Dalinka, University of Pennsylvania

Hereditary Hyperphosphatasemia (Juvenile Paget Disease)

Hereditary hyperphosphatasemia (osteoectasia with hyperphosphatasemia) is discussed in the Chapter 13 on bone dysplasias.

Hypervitaminosis D

Radiographic manifestations of hypervitaminosis D in the adults are demineralization of skeletal structures that may be focal or diffuse. Amorphous calcified masses may be present in periarticular regions. These periarticular soft tissue calcifications must be differentiated from cases of renal osteodystrophy, milk-alkali syndrome, scleroderma, and idiopathic tumoral calcinosis. Joint capsules or vessels may be visible by virtue of calcification. Sometimes renal stones may occur.

In contrast to adults, the radiographic manifestations of excessive vitamin D intake during childhood consist of an increase in density of skeletal structures, but symmetrical areas of radiolucency adjacent to the zone of provisional calcification may be seen. The epiphyseal centers could be ringed by a dense opaque band. In the spine and skull (Fig. 2.48), increased density produces an appearance similar to osteopetrosis. Calcification of soft tissues, such as the kidneys, falx cerebri, and tentorium may be present. In cases in which renal damage occurs, renal osteodystrophy may complicate the picture.

Hypervitaminosis A

Hypervitaminosis A is manifested by changes in the skin, mucous membranes, the skeleton, and the central nervous system. Acute and chronic forms have been reported in both children and adults. Skeletal changes are similar to those of Caffey disease. In fact, Caffey mistakenly included two cases of hypervitaminosis A in his early series reporting infantile cortical hyperostosis.

Acute hypervitaminosis A may occur at any age from digestion of excessive amounts of vitamin A. Frontal headaches, bulging fontanelles in infants, and drowsiness indicate the sudden increase in intracranial pressure. Desquamation of the skin and mucous membranes may begin within 36 hours and becomes severe. There are no skeletal changes.

Chronic hypervitaminosis A begins with anorexia, weight loss, and finally causes nausea and vomiting. There are signs and symptoms of increased intracranial pressure.

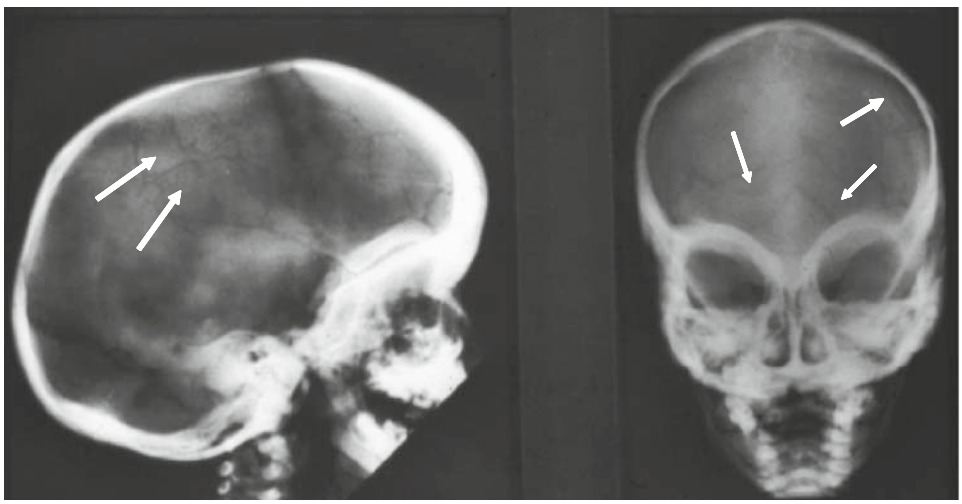

Fig. 2.48 Hypervitaminosis D. AP and lateral radiographs of the skull in a child reveal increased density of cranial bones. Note the presence of Wormian bones (*arrows*). The skull mimics the radiographic appearance of osteopetrosis

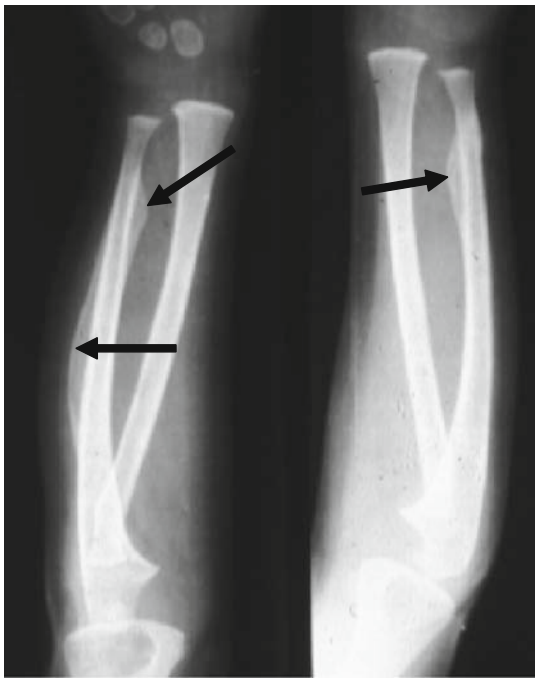

Fig. 2.49 Hypervitaminosis A. AP radiograph of the forearms showing asymmetrical periosteal reaction of both ulna. Periosteal reaction is more prominent on the *left* (*arrows*) than the *right* (*short arrow*). Ulnar and metatarsal periosteal reactions are more common than other sites

Headaches, irritability, and insomnia have been reported. The skin becomes dry and pruritis may develop. Radiographs reveal periosteal reaction, which is more prominent in mid-diaphysis. The ulna (Fig. 2.49), the metatarsals, and the metacarpals (Figs. 2.50 and 2.51) are the bones most commonly affected. Epimetaphyseal abnormalities may be observed in chronic hypervitaminosis A, including invagination of the epiphysis into the metaphysis and thinning of the physeal plate. In the distal femur, in particular, the epiphysis may take on a conical shape, invaginated into the metaphysis. The distal articular surface of the femur loses its curvature in advanced cases.

Fluorosis

Fluorosis is an endemic problem in parts of China, India, and Africa and affects millions of people in the world, but it is uncommon in the United States and other industrial countries. The intoxication may be caused by chronic ingestion or inhalation of fluoride. Endemic fluoride poisoning exists where the fluoride content of natural water is higher than four parts per million and more than 10 mg fluoride is consumed daily for at least 10 years. It also develops when there is industrial exposure to fluoride in fumes or dust. Less common causes are fluoride supplements, certain teas and wines, and some toothpastes.

Radiographic abnormalities may be seen in the teeth and the skeletal system. Mottled enamel develops early and later on dental discoloration and depressions manifest. There is periapical sclerosis and resorptive changes in dental roots.

Skeletal fluorosis is more prominent in the axial than the peripheral skeleton. The axial skeleton reveals severe increased bone density (Fig. 2.52a–c). There may be calcification of various spinal and the sacrospinous ligaments. Osteophytosis, narrowing of the spinal canal, and the inter-

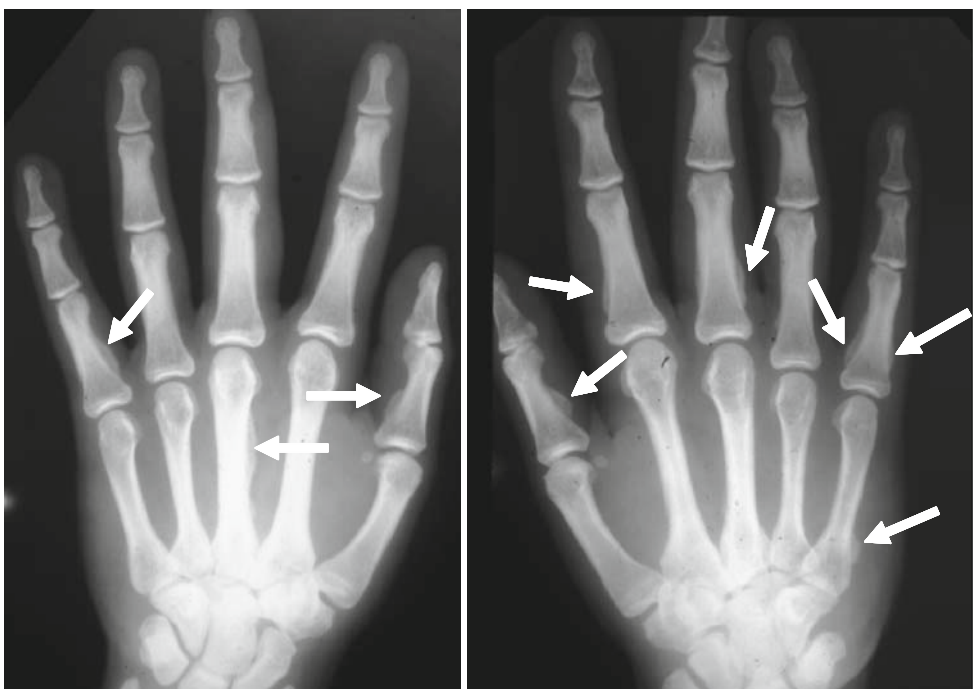

Fig. 2.50 Hypervitaminosis A. Radiographs of the hands showing asymmetrical periosteal reaction associated with soft tissue swelling in the fingers and metacarpals of both hands (*arrows*). Courtesy of Dr. Paul Radecke, formerly of Temple University Hospital Philadelphia, PA

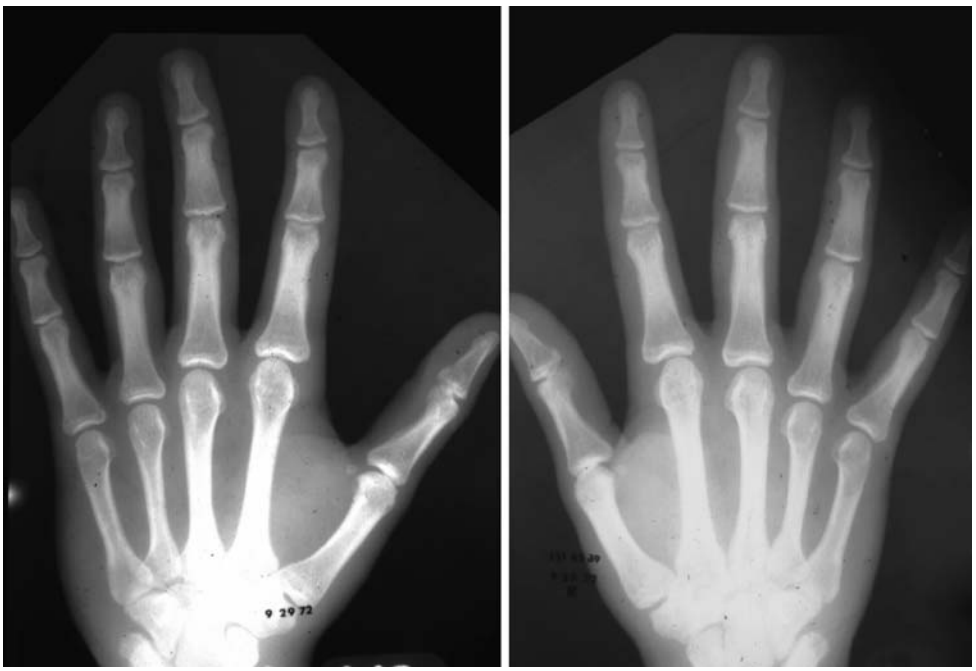

Fig. 2.51 Hypervitaminosis A. Radiographs of both hands from the same patient as in Fig. 2.50 after discontinuation of vitamin A show complete resolution of periosteal reaction. Courtesy of Dr. Paul Radecke, formerly of Temple University Hospital Philadelphia, PA

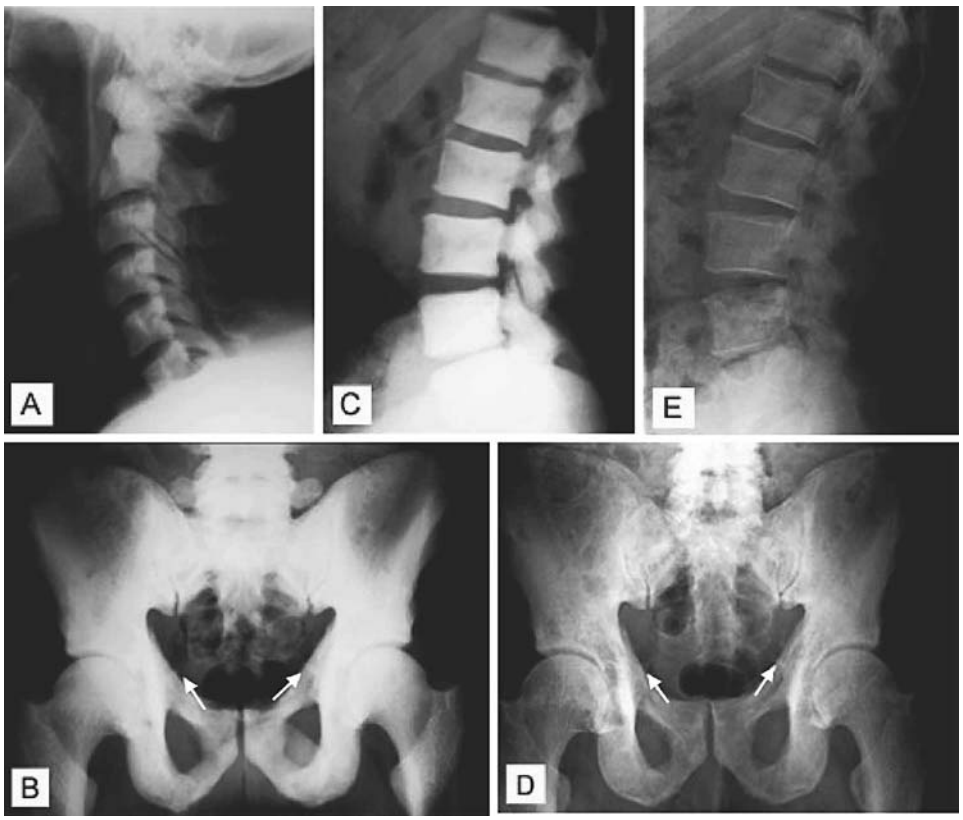

Fig. 2.52 Fluorosis. **a** – Lateral radiograph of the cervical spine at referral in 1996 shows sclerosis of the spine but sparing of the mandible. Pelvis (**b**) and lateral lumbar spine from 1996 reveal marked sclerosis. There is cortical thickening of the pelvic inlet (*arrows* **b**). Repeat radiographs of the pelvis (**d**) and the lumbar spine (**e**) about 9 years after diagnosis show significant improvement of osteosclerosis with minimal residual sclerosis and remaining cortical thickening of the pelvis (*arrows* **d**). Courtesy of Dr. William R Reinus, currently Temple University Hospital. See also (Figs. 5.10 and 5.11) in Chapter 5 for further details

vertebral foramina are common findings. Cortical thickening may be present (Fig. 2.52b, d). Enthesopathy is also noted in advanced cases.

An interesting American case of fluorosis has been reported in a 52-year-old man from ingestion of fluoride-containing toothpaste (Fig. 2.52). He presented clinically with severe cervical immobility and worsening of joint pain in the past 7 years. Radiographs showed marked increased density of the spine and the pelvis as well as cortical thickening in the pelvis (Fig. 2.52a–c). The patient also had cal-

cification of the sacrospinous ligaments. No dental abnormalities were detected. Serum and urine fluoride levels were elevated and the iliac crest biopsy revealed fluorosis. Bone markers were distinctly elevated. DXA of lumbar spine, femoral neck, and distal third of the radius revealed *Z* scores of +14.3, +6.6, and –0.6. Diffuse tetracycline uptake revealed osteomalacia.

Follow-up radiographs 9 years after the cessation of fluoride-containing toothpaste demonstrated significant improvement of increased bone density.

Clinically, the patient demonstrated significant correction of his disorder for a decade after the removal of toothpaste containing fluoride. However, new onset of nephrolithiasis developed within 9 months and became a chronic problem. The authors conclude that, with the removal of the source of fluoride exposure, skeletal fluorosis is reversible but likely impacts the skeleton for decades. During the recovery, the patient should be monitored for nephrolithiasis.

Further Readings

Bone Metabolism

1. Aegerter E, Kirkpatrick JA. Orthopedic Diseases (Physiology, Pathology, and Radiology), 4th ed., Philadelphia: WB Saunders, 1975.
2. Garimella R, Tag SE, Zhang J, et al. Expression and synthesis of bone morphogenetic proteins by osteoclasts: a possible path to anabolic bone remodeling. J Histochem Cytochem 2008; 56:569–577.
3. Kemi VE, Karkkainen MUM, Lamberg-Allardt CJE. High phosphorus intakes acutely and negatively affect Ca and bone metabolism in a dose-dependent manner in healthy young females. Br J Nutr 2006; 96:454–452.
4. Neer RM, Arnaud CD, Zanchetta JR, et al. Effect of parathyroid hormone (1–34) on fractures and bone mineral density in menopausal women with osteoporosis. New Engl J Med 2001; 344:1434–1441.
5. Orwell ES and Meier DE. Alterations in calcium, vitamin D, and parathyroid hormone physiology in normal men with aging: relations to the development of senile osteopenia. Endocrin Metab 1986; 63:1262.
6. Polekhani G, Diefenbach-Jagger H, HO PWM, Sato K, et al. Structural basis for antibody discrimination between two hormones that recognize the parathyroid hormonemone receptor. J Biol Chem. 2009; 284:15557–15563.
7. Whyte MP, Obrecht SE, Finnegan PM, et al. Osteoprotegerin deficiency and juvenile Paget's disease. New Engl J Med 2002; 347:175–184.

Bone Density

1. Centrella M, Canalis E. Local regulators of skeletal growth: a perspective. Endoc Rev 1985; 6:544
2. Cummings SR, Black DM, Nevitt MC. Bone density at various sites for prediction of hip fracture. Lancet, 1993; 341:72–75.
3. Heaney RP, Recker RR. Effects of nitrogen, phosphorus, and caffeine on calcium balance in women. J Lab Clin Med 1982; 99:46.
4. Hofeldt F. Proximal femoral fractures. Clin Orthop Relat Res 1987; 218:12.
5. Jones G, Nguyen T, Sambrook PN, Kelly PJ, Gilbert C, Eisman JA. A longitudinal study of spinal degenerative disease on bone density in the elderly. J Rhumatol 1995; 22:932–936.
6. Licata A. Bone density versus bone quality: what's a clinician to do? Clev Clin J Med 2009; 76:331–336.
7. Lonial S. Myeloma Bone Disease. MMRF (Multiple Myeloma Research Foundation). September 2005, Available at: www.Multiplemyeloma.org/about_myeloma/2.08 php. Accessed December 39, 2007.
8. Parsons TJ, Prentice A, Smith EA, Cole TJ, Compston JE. Bone mineral mass consolidation in young British adults. J Bone Miner Res 1996; 11:264–274.
9. Riggs BL, Melton LJ. Involutional osteoporosis. New Engl J Med 1986; 314:1676
10. Roodman GD. Biology of osteoclast activation in cancer. Journal of Clinical Oncology 2001; 19(15):3562–3571
11. Shipman AJ, Guy GWG, Smith I, Ostlere S, Greer W, Smith R. Vertebral bone mineral density, content and area in 8789 normal women aged 33–73 years who have never had hormone replacement therapy. Osteoporos Int 1999; 9:420–426.

Generalized Diminished Bone Density

1. Aaron JE, Makins NB, Sagreiya K. The microanatomy of trabecular bone loss in normal aging in men and women. Clin Orthop Rel Res 1987; 215:260–271.
2. Assessment of fracture risk and its applications to screening for postmenopausal osteoporosis: Geneva: World Health Organization; 1994. Technical Report Series, No. 843.
3. Baron R, Gertner JM, Lang R, Vignery A. Increased bone turnover with decreased bone formation by osteoblast in children with osteogenesis imperfecta tarda. Pediatr Res 1983; 17:204.

4. Bélanger A, Candas B, Dupont A, Cusan L, Diamond P, Gomez JL, Labrie F. Changes in serum concentrations of conjugated and unconjugated steroids in 40- to 80-year old men. J Clin Endocrinol Metab, 1994; 79:1086–1090.
5. Blunt BA, Klauber MR, Barrett-Connor EL, Edelstein SL. Sex differences in bone mineral density in 1653 men and women in the sixth through tenth decades of life: the Rancho Bernardo study. J Bone Miner Res, 1994; 9:1333–1338.
6. Burger H, de Laet CEDH, van Daele PLA, Weel AEAM, Witterman JCM, Hofman A, Pols HAP. Risk factors for increased bone loss in an elderly population. The Rotterdam study. Am J Epidemiol 1998; 147:871–879.
7. Centrella M, Canalis E. Local regulators of skeletal growth: a perspective. Endoc Rev 1985; 6:544
8. Dent CE, Stamp TCB. Vitamin D, rickets and osteomalacia. In: L Avioli, S Krane (Eds.), Metabolic Bone Disease. New York: Academic Press, 1977; 237.
9. Dunmill MSA, Anderson JA, Whitehead R. Quantitative histological studies on age changes in bone. J Pathol Bacteriol 1967; 94:275.
10. Duursma SA, Raymakers JA, Van Beresteyn ECH, Schaafsma G. Clinical aspects of osteoporosis. World Rev Nutr Diet 1987; 50:92.
11. Firooznia H, Golimbu C, Rafii M, Schwartz MS. Rate of spinal trabecular bone loss in normal perimenopausal women: CT measurement. Radiology 1987; 167:735.
12. Genant HK, Cann CE, Ettinger B, Gordon GS. Quantitative computed tomography of vertebral spongiosa: a sensitive method for detecting early bone loss after oophorectomy. Ann Intern Med 1982; 97:699.
13. Glynn NW, Meilahn EN, Charron M, Anderson SJ, Kuller LH, Cauley JA. Determinants of bone mineral density in older men. J Bone Miner Res 1995; 10:1769–1777.
14. Kanis JA, Melton LJ III, Christiansen C, Johnston CC, Khaltaev N. The diagnosis of osteoporosis. J Bone Miner Res, 1994; 9(8):1137–1141.
15. Lane JM, Vigorita VJ. Osteoporosis. J Bone Joint Surg, 1983; 65A:274.
16. Madewell JE. Involutional (Senile)osteoporosis, idiopathic juvenile osteoporosis, and Homacystinurea. RSNA Syllabus Metabolic and endocrine disorders affecting the skeleton. 209A, 1981.
17. Mauck, KF, Clarke, BL. Diagnosis, screening, prevention, and treatment of osteoporosis. Mayo Clin Proc. May 2006; 81(5):662–672.
18. Murray RO, Jacobson HG. The Radiology of Skeletal Disorders. (Vol. 1) 2nd ed. Edinburgh: Churchill-Livingston, 1977; 700.
19. Raisz LG. Osteoporosis. J Am Geriatr Sci 1982; 30:127.
20. Orwell ES, Meier DE. Alterations in calcium, vitamin D, and parathyroid hormone physiology in normal men with aging: relations to the development of senile osteopenia. Endocrin Metab 1986; 63:1262.
21. Raisz LG. Osteoporosis. J Am Geriatr Sci 1982; 30:127.
22. Szulc P, Delmas PD. Vertebral Fracture Resource Document, Part 1: osteoporosis and Related Fractures, IOF and ESSR, revised 2005 Jan; 1–19.

Osteopenia

1. James JR, Congdon PJ, Truscott J, Horsman A, Arthur R. Osteopenia of prematurity. Arch Dis Child 1986; 61:871.
2. Khosla S, Melton III LJ. Osteopenia. N Engl J Med 2007; 356:2293–2300.
3. Pasco JA, Seeman E, Henry MJ, Merriman EL, et al. The population burdon of fractures originates in women with osteopenia, not osteoporosis. Osteoporos Int. 2006; 17:1404–1409.

Osteoporosis

1. Dunmill MSA, Anderson JA, Whitehead R. Quantitative histological studies on age changes in bone. J Pathol Bacteriol 1967; 94:275.
2. Duursma SA, Raymakers JA, Van Beresteyn ECH, Schaafsma G. Clinical aspects of osteoporosis. World Rev Nutr Diet 1987; 50:92.
3. Foresta C, Ruzza G, Miani R, et al. Osteoporosis and decline of gonadal function in the elderly male. Horm Res 1984; 19:18.
4. Glynn NW, Meilahn EN, Charron M, Anderson SJ, Kuller LH, Cauley JA. Determinants of bone mineral density in older men. J Bone Miner Res 1995; 10:1769–1777.
5. Hans D, Baiada A, Dubouef F, Vignot E, Bochu M, Meunier P. Expert-XL: clinical evaluation of a new morphometric technique on 21 patients with vertebral fracture. Osteoporos Int 1996; 6:79.
6. Bjarnasson NH, Hassager C, Christiansen C. Postmenopausal bone remodeling and hormone replacement. Climacteric, 1998; 1:72–79.
7. Kanis JA, Melton LJ III, Christiansen C, Johnston CC, Khaltaev N. The diagnosis of osteoporosis. J Bone Miner Res, 1994; 9(8):1137–1141.
8. Majumdar, S. Magnetic resonance Imaging for osteoporosis. Skeletal Radiol 2008; 37:95–97.
9. Mauck KF, Clarke BL. Diagnosis, screening, prevention, and treatment of osteoporosis. Mayo Clin Proc. May 2006; 81(5):662–672.

10. Melton LJ III, Chrischilles EA, Cooper C, Lane AW, Riggs BL. How many women have osteoporosis? J Bone Miner Res 1992; 7:1005–1010.
11. Mussolino ME, Looker AC, Madans JH, Langlois JA, Orwoll ES. Risk factors for hip fracture in white men: the NHANES I epidemiologic follow-up study. J Bone Miner Res 1998; 13:918–924.
12. Peacock M, Turner CH, Econs MJ, Foroud T. Genetics of osteoporosis. Endocrine Rev 2002; 23:303–326.
13. Raisz LG. Osteoporosis. J Am Geriatr Sci 1982; 30:127.
14. Rianco JA, Valero C, Naranjo A, et al. Identification of an aromatasehaplotype that is associated with gene expression and postmenopausal osteoporosis. J Clin Endocrinol Metab 2007; 92:660–665.
15. Rosen CJ. Postmenopausal osteoporosis. N Engl J Med 2005; 353:594–603.
16. Smith RW, Eyler WR, Mellinger RC. On the incidence of senile osteoporosis. Ann Int Med 1960; 52:773–781.
17. Styrkarsdottir U, Halldorsson BVGretarsdottir DF, et al. Multiple genetic loci for bone mineral density and fractures. New Engl J Med 2008; 93:110–117.
18. Szulc P, Delmas PD. Vertebral Fracture Resource Document, Part 1: osteoporosis and Related Fractures, IOF and ESSR, revised 2005 Jan; 1–19.
19. The American College of Radiology Bulletin. July 1998; 54(7).
20. Wanish RD, Benfante RJ, Yano K, Heiburn L, Vogel JM. Thiazidd effect on the mineral content of bone. N Engl J Med 1983; 309:344.

Radiographic evaluation of osteoporosis

1. Aegerter E, Kirkpatrick, JA. Orthopedic Diseases (Physiology, Pathology and Radiology), 4th ed. Philadelphia: WB Saunders, 1975.
2. Genant HK, Jergas MJ, Kuijk, CV. Vertebral Fracture Resource Document, Part 2: Radiological Assessment of Vertebral Fractures. IOF and ESSR, revised January 2005; 1–40.
3. Hedlund LR, Gallagher JC. Vertebral morphometry in diagnosis of spinal fractures. Bone Miner 1988; 5(1):59–67.
4. Madewell JE. Involutional (Senile) osteoporosis, idiopathic juvenile osteoporosis, and Homacystinurea. RSNA Syllabus Metabolic and endocrine disorders affecting the skeleton. 209A, 1981.
5. Mauck KF, Clarke BL. Diagnosis, screening, prevention, and treatment of osteoporosis. Mayo Clin Proc. May 2006; 81(5):662–672.
6. Kleerekoper M, Parfitt AM, Ellis BI. Measurement of vertebral fracture rates in osteoporosis. In: Christiansen C, Arnaud CD, Nordin BEC, Parfitt AM, Peck WA, Riggs BL (Eds.), Copenhagen International Symposium on Osteoporosis June 3–8, 1984, Vol. 1. Copenhagen: Department of Clinical Chemistry, Glostrup Hospital, 1984; 103–108.
7. Genant HK, Jergas M, Palermo L, Nevitt M, Valentin RS, Black D, Cummings SR. Comparison of semiquantitative visual and quantitative morphometric assessment of prevalent and incident vertebral fractures in osteoporosis. The Study of Osteoporotic Fractures Research Group. J Bone Miner Res 1996; 11(7):984–996.
8. Genant HK, Wu CY, van Kuijk C, Nevitt MC. Vertebral fracture assessment using a semiquantitative technique. J Bone Miner Res 1993; 8(9):1137–1148.
9. McCloskey EV, Spector TD, Eyres KS, Fern ED, O'Rourke N, Vasikaran S, Kanis JA. The assessment of vertebral deformity: a method for use in population studies and clinical trials. Osteoporos Int 1993; 3(3):138–147.
10. Kanis JA, Melton LJ III, Christiansen C, Johnston CC, Khaltaev N. The diagnosis of osteoporosis. J Bone Miner Res 1994; 9(8):1137–1141.

Dual X-ray absorptiometry (DXA)

1. Arlot ME, Sornay-Rendu E, Garnero P, Vey-Mart B, Delmas PD. Apparent pre- and postmenopausal bone loss evaluated by DXA at different skeletal sites in women: the OFELY cohort. J Bone Miner Res 1997; 12:683–690.
2. Dunmill MSA, Anderson JA, Whitehead R. Quantitative histological studies on age changes in bone. J Pathol Bacteriol 1967; 94:275.
3. Faulkner KG, McClung MR, Schmeer MS, Roberts LA, Gaither KW. Densitometry of the radius using single and dual energy absorptiometry. Calcif Tissue Int 1994;54, 208–211.
4. Genant HK, Engelke K, Fuerst T, Glüer CC, Grampp S, Harris ST, Jergas M, Lang T, Lu Y, Majumdar S, Mathur A, Takada M. Noninvasive assessment of bone mineral and structure: state of art. J Bone Miner Res 1996;11, 707–730.
5. Glynn NW, Meilahn EN, Charron M, Anderson SJ, Kuller LH, Cauley JA. Determinants of bone mineral density in older men. J Bone Miner Res 1995;10:1769–1777.
6. Guessous J, Cornuz C, Ruffieux C, Burckhardt P, Krieg MA. Osteoporotic fracture risk in elderly women: estimation with quantitative heel ultrasound and clinical risk factors. Radiology 2008; 246:179–184.

7. Jergas M, Lang TF, Fuerst T. Morphometric X-ray Absorptiometry. In: HK Genant, M Jergas, C van Kuijk (Eds.), Vertebral Fracture in Osteoporosis. San Francisco: Radiology Research and Education Foundation, 1995; 331–348.
8. Kelly TL, Crane G, Baran DT. Single X-ray absorptiometry of the forearm: precision, correlation, and reference data. Calcif Tissue Int 1994; 54:212–218.
9. Lehmann R, Wapniarz M, Randerath O, Kvasnicka HM, John W, Reincke M, Kutnar S, Klein K, Allolio B. Dual-energy X ray absorptiometry at the lumbar spine in German men and women: a cross-sectional study. Calcif Tissue Int 1995; 56:350–354.
10. Lewiecki EM, Laster AJ. Clinical applications of vertebral fracture assessment by X-ray absorptiometry. J Clin Endocrinol Metab 2006; 91:4215–4222.
11. Maghraoui AE, Roux C. DXA scanning in clinical practice. QJM 2008; 101:605–617.
12. Mauck KF, Clarke BL. Diagnosis, screening, prevention, and treatment of osteoporosis. Mayo Clin Proc. May 2006; 81(5):662–672.
13. Steiger P, Cummings SR, Genant HK, Weiss H. Morphometric X-ray absorptiometry of the spine: correlation in vivo with morphometric radiography. Study of Osteoporotic Fractures Research Group. Osteoporos Int 1994; 4(5):238–244.
14. Szulc P, Delmas PD. Vertebral Fracture Resource Document, Part 1: osteoporosis and Related Fractures, IOF and ESSR, revised January 2005; 1–19.
15. Yu W, Qin M, Xu L, van Kujik C, Meng X, Xing X, Cao J, Genant HK. Normal changes in spinal bone mineral density in a Chinese population: assessment by quantitative computed tomography and dual-energy X-ray absorptiometry. Osteoporosis Int 1999:179–187.

Quantitative CT absorptiometry

1. Bauer JS, Henning TD, Mueller D, LU Y, Majumdar S, Link TM. Volumetric quantitative CT of spine and hip derived from contrasr-enhanced MDCT: conversion factors 2007; 188:1249–1301.
2. Genant HK, Cann CE, Ettinger B, Gordon GS. Quantitative computed tomography of vertebral spongiosa: a sensitive method for detecting early bone loss after oophorectomy. Ann Intern Med 1982; 97:699.
3. Genant HK, Engelke K, Fuerst T, Glüer CC, Grampp S, Harris ST, Jergas M, Lang T, Lu Y, Majumdar S, Mathur A, Takada M. Noninvasive assessment of bone mineral and structure: state of art. J Bone Miner Res 1996; 11:707–730.
4. Guglielmi G, Grimston SK, Fischer, KC, Pacifici R. Osteoporosis: diagnosis with lateral and posteroanterior dual x-ray absorptiometry compared with quantitative CT. Radiology 1994; 192:845–850.
5. Lochmuller EM, Burklein D, Khun V, et al. Mechanical strength of the thoracolumbar spine in the elderly: prediction from the in situ dual-energy X-ray absorptiometry, quantitative computed tomography (QCT), upper and lower limb QCT, and quantitative ultrasound. Bone 2002; 31:77–84.

Quantitative ultrasonography for evaluation of osteoporosis

1. Daele PLA van, Burger H, Algra D, Hofman A, Grobbee DE, Birkenhäger JC, Pols HAP. Age-associated changes in ultrasound measurements of the calcaneus in men and women: the Rotterdam study. J Bone Miner Res 1994; 9:1751–1757.
2. Hans D, Glüer CC, Njeh CF. Ultrasonic evaluation of osteoporosis. In: PJ Meunier (Ed.), Osteoporosis: Diagnosis and Management. London UK: Martin Dunitz 1998:59–78.
3. Looker AC, Wahner HW, Dunn WL, Calvo MS, Harris TB, Heyse SP, Johnston CC, Lindsay RL. Updated data on proximalfemur bone mineral levels of US adults. Osteoporos Int 1998; 8:468–489.
4. Montagnani A, Gonnelli S, Cepollaro C, Mangeri M, Monaco R, Bruni D, Gennari C. Quantitative ultrasound at the phalanges in healthy Italian men. Osteoporos Int 1999;11:499–504.
5. Nicholson PHF, Müller R, Cheng XG, Rüegsegger P, van der Perre G, Dequeker J, Boonen S. Quantitative ultrasound and trabecular architecture in the human calcaneus. J Bone Miner Res 2001; 16:1886–1892.

Magnetic resonance Imaging (MRI)

1. Akkaya T, Ersozlu S, Ozgur AF, Karaminogullari O, Akgun RC, Tandogan NR. Early results of Kyphoplasty in osteoporotic vertebral Compression fractures Acta Orthop Traumatol Turc 2007; 41:127–131.
2. Link TM, Majumdar S, Grampp S, et al. Imaging of trabecular bone structure in osteoporosis. Eur Radiol 1999; 9:1781–1788.
3. Link TM, Majumdar S, Grampp S, et al. Osteoporosis imaging. Radiol Cli North Am 2003; 41:813–839.

4. Majumdar S. Magnetic resonance imaging for osteoporosis. Skeletal Radiol 2008; 37:95–97.
5. Smith RW, Eyler WR, Mellinger RC. On the incidence of senile osteoporosis. Ann Int Med 1960; 52: 773–781.

Osteoporosis: A major health problem

1. Baron JA, Karagas M, Barrett J, Kniffin W, Malenka D, Mayor M, Kellet RB. Basic epidemiology of fractures of the upper and lower limb among Americans over 65 years of age. Epidemiology 1996; 7:612–618.
2. Burger H, de Laet CEDH, van Daele PLA, Weel AEAM, Witterman JCM, Hofman A, Pols HAP. Risk factors for increased bone loss in an elderly population. The Rotterdam study. Am J Epidemiol 1998; 147: 871–879.
3. de Laet CEDH, van Hout BA, Burger H, Weel AEA, Hofman A, Pols HAP. Hip fracture prediction in elderly men and women: validation in the Rotterdam study. J Bone Miner Res 1998; 13:1587–1593.
4. Fraser D, Scriver CR. Familial forms of vitamin D-resistant rickets revisited. X-linked hypophosphatemia and autosomal recessive vitamin D dependency. Am J Clin Nutr 1976; 29:1315.
5. Delmas PD, Genant, HK, Adams JE. Vertebral Fracture Resource Document, IOP and ESSR, VFI Course Slide kit CD # 1 (PPT), S1–90, 2007.
6. Hannan MT, Felson DT, Dawson-Hughes B, Tucker KL, Cupples LA, Wilson PWF, Kiel DP. Risk factors for longitudinal bone loss in elderly men and women: the Framingham Osteoporosis Study. J Bone Miner Res 2000; 15:710–720.
7. Hofeldt F. Proximal femoral fractures. Clin Orthop Rel Res 1987; 218:12.
8. Mauck KF, Clarke BL. Diagnosis, screening, prevention, and treatment of osteoporosis. Mayo Clin Proc May 2006; 81(5):662–672.
9. Mallmin H, Ljunghall S, Persson I, Naessén T, Krusemo UB, Bergström R. Fracture of the distal forearm as a forecaster of subsequent hip fracture: a population-based cohort study with 24 years of follow-up. Calcif Tissue Int 1993; 52, 269–272.
10. McCloskey EV, Spector TD, Eyres KS, Fern ED, O'Rourke N, Vasikaran S, Kanis JA. The assessment of vertebral deformity: a method for use in population studies and clinical trials. Osteoporos Int 1993; 3(3):138–147.
11. Hedlund LR, Gallagher JC. Vertebral morphometry in diagnosis of spinal fractures. Bone Miner 1988; 5(1):59–67
12. Nevitt MC, Johnell O, Black DM, Ensrud K, Genant HK, Cummings SR. Bone mineral density predicts non-spine fractures in very elderly women. Osteoporos Int 1994; 4:325–331.
13. Nguyen TV, Center JR, Sambrook PN, Eisman JA. Risk factors for proximal humerus, forearm and wrist fractures in elderly men and women. The Dubbo osteoporosis epidemiology study. Am J Epidemiol 2001; 153:587–595.
14. Orwell ES, Meier DE. Alterations in calcium, vitamin D, and parathyroid hormone physiology in normal men with aging: relations to the development of senile osteopenia. Endocrin Metab 1986; 63:1262.
15. Owen RA, Melton LJ III, Ilstrup DM, Johnson KA, Riggs BL. Colles' fracture and subsequent hip fracture risk. Clin Orthop Rel Res 1982; 171:37–43.
16. Schwartz AV, Kelsey JL, Sidney S, Grisso JA. Characteristics of falls and risk of hip fracture in elderly men. Osteoporos Int 1998; 8:240–246.
17. Smith RW, Eyler WR, Mellinger RC. On the incidence of senile osteoporosis. Ann Int Med 1960; 52:773–781.
18. Seeman E, Metlon LJ, 0'Fallon WM, Riggs BL. Risk factors for spinal osteoporosis in men. Am J Med 1983; 75:977.
19. Tosteson ANA. Economic impact of fractures. in: E Orwoll (Ed.), Osteoporosis in Men. The Effects of Gender on Skeletal Health. San Diego: Academic Press, 1999; 15–27.
20. Tosteson AN, Hammond CS. Quality-of-life assessment in osteoporosis: health-status and preference-based measures. Pharmacoeconomics. 2002; 20(5):289–303

Prevention and treatment of osteoporosis

1. Bélanger A, Candas B, Dupont A, Cusan L, Diamond P, Gomez JL, Labrie F. Changes in serum concentrations of conjugated and unconjugated steroids in 40- to 80-year old men. J Clin Endocrinol Metab, 1994; 79: 1086–1090
2. Kauffman RF, Bryant HU. Selective estrogen receptor modulators. Drug News Perspect 1995; 8:531–539.
3. Riggs BL, Melton LJ. Involutional osteoporosis. New Engl J Med 1986; 314:1676.
4. Seeman E, Metlon LJ, 0'Fallon WM, Riggs BL. Risk factors for spinal osteoporosis in men. Am J Med 1983; 75:977
5. Torgerson DJ, Bell-Syer SEM. Hormone replacement therapy and prevention of non-vertebral fractures. A meta-analysis of randomised trials. JAMA, 2001; 285:2891–2897.

Scurvy

1. Joffe N. Some radiological aspects of scurvy in the adult. Br. J Radiol 1961; 34:429.
2. Karthiga S, Dubey S, garber S, Watts R. Scurvy: MRI appearances. Rheumatology 2008; 47:1109.
3. Smith MS. The diagnosis and treatment of scurvy: an historical perspective. J R Nav Med Ser 1986; 72:104.
4. Sprague PL. Epiphysio-metaphyseal cupping following infantile scurvy. Pediatr Radiol 1976;4: 122.

Copper deficiency

1. Danks DM, Campbell PE, Stevens BJ, Mayne V, Cartwright E. Menkes kinky hair syndrome. An inherited defect in copper absorption with widespread effects. Pediatrics 1972; 50:188.
2. Grunebaum N, Horodniceau C, Steinberg R. The radiographic manifestations of bone changes in copper deficiency. Pediatr Radiol 1980; 9:101.
3. Heller RM, Kirchner SG, O'Neil JA, Haugh AJ, Howard L, Kramer SS, Green HL. Skeletal changes of copper deficiency in infants receiving prolonged total parental nutrition. J Pediatr 1978; 92:947.
4. Kirkpatrick JA. Abnormalities of Copper and Their Differential Diagnosis. The RSNA Syllabus, Metabolic and Endocrine Disorders Affecting the Skeleton. Course 409C, 1981.
5. Siegle RL, Rabinowitz JG. Radiographic findings resembling scurvy and rickets in prematures on hyperalimentation. Mt Sinai J Med 1981; 48:241.

Endocrine osteoporosis

1. Carpenter PC: Cushing's syndrome; update of diagnosis and management. Mayo Clin Proc 1986; 61:49.
2. Dwyer AJ, Frank JA, Doppman JL, Oldfield EH, Hicky AM, Cutler GB, Loriaux DL, Schiable TF. Pituitary adenomas in patients with Cushing disease: initial experience with Gd-DTPA-enhanced MR imaging. Radiology 1987; l63:421.
3. Orwell ES, Meier DE. Alterations in calcium, vitamin D, and parathyroid hormone physiology in normal men with aging: relations to the development of senile osteopenia. Endocrin Metab 1986; 63:1262.
4. Pojunas KW, Daniels DL, Williams AL, Thorsen MK, Haughton VM. Pituitary and adrenal CT of Cushing syndrome. AJ R 1986; 146:1235.

Reflex sympathetic dystrophy

1. Genant HK, Kozin F, Bekerman C, et al. The reflex sympathetic dystrophy syndrome. Radiology 1976; 117:21.
2. Helms CA, O'Brien ET, Katzberg RW. Segmental reflex sympathetic dystrophy syndrome. Radiology 1980; 135:67.
3. Katz MM, Hungerford DS, Krachow KA, Lennox DW. Reflex sympathetic dystrophy as a cause of poor results after total knee arthroplasty. J Arthroplasty 1986; 1:117.
4. Schwartzman RJ, McLellan TL. Reflex sympathetic dystrophy. A review. Arch Neurol 1987 May; 44:555.

Osteogenesis imperfecta

1. Baron R, Gertner JM, Lang R, Vignery A. Increased bone turnover with decreased bone formation by osteoblast in children with osteogenesis imperfecta tarda. Pediatr Res 1983; 17:204.
2. Schwartzman RJ, McLellan TL. Reflex sympathetic dystrophy. A review. Arch Neurol 1987 May; 44:555.
3. Sillence, D. Osteogenesis imperfecta: an expanding panorama of variants. Clin Orthop Rel Res 1981; 159:11.
4. Sillence DO, Barlow KK, Cole WG, Dietrich S, Garber AP, Rimoin DL. Osteogenesis imperfecta type III. Delineation of the phenotype with reference to genetic heterogeneity. Am J Med Genetics 1986; 23:821.
5. Stoddart PGP, Wickremaratchi T, Hoillingworth P, Watt I. Fibrogenesis imperfecta ossium. Br J Radiol 1984; 57:744.

Idiopathic juvenile osteoporosis

1. Clouter MPD, Hayles AB, Riggs, BL, Jowsey J, Bickel WH. Juvenile osteoporosis: report of a case including description of some metabolic and microradiographic studies. Pediatrics 1967; 40:649.
2. Dent CE, Friedman M. Idiopathic juvenile osteoporosis. Quarterly J Med New Series 1965; 34:177.
3. Houang MTW, Brentokn DP, Renton P, Shaw DG. Idiopathic Juvenile osteoporosis. Skel Radiol 1978; 3:17.
4. Madewell JE. Involutional (Senile)osteoporosis, idiopathic juvenile osteoporosis, and Homacystinurea. RSNA Syllabus Metabolic and endocrine disorders affecting the skeleton. 209A, 1981.

Homocystinuria

1. Brill PN, Milty HA, Gaull GF. Homocystinuria due to cystathionine synthase deficiency. Chemical et roent genologic correlation. AJR 1974; 121:45.
2. Madewell JE. Involutional (Senile)osteoporosis, idiopathic juvenile osteoporosis, and Homacystinurea. RSNA Syllabus Metabolic and endocrine disorders affecting the skeleton. 209A, 1981.
3. Ruano MM, Castillo M, Thompson JE. MR imaging in a patient with homocystinuria. Am J Roentenol 1998; 171:1147–1149.

Idiopathic Regional Migratory Osteoporosis

1. Bray S, Partain CL, Treates CD, et al. The value of bone scan in idiopathic regional migratory osteoporosis. Clin Nucl Med 1979; 4:330.
2. Mavichak V, Murray TM, Hodsman AB, Rovert NJ, Sutton RA. Regional migratory osteoporosis of the lower extremities with vertebral ostoeporosis. Bone 1986; 7:343.
3. Naides SJ, Resnick D, Zvaifler NJ. Idiopathic regional osteoporosis: a clinical spectrum. J Rheumatol 1985; 12:763.
4. Rosen RA. Transitory demineralization of the femoral head. Radiology 1970; 94:509.
5. Toms AP, Marshall TJ, Becker E, Doneil ST, et al. Regional migratory osteoporosis: a review illustrated by five cases. Clin Radiol 2005; 60:425–438.

Rickets

1. Dent CE, Stamp TCB. Vitamin D, rickets and osteomalacia. In: L Avioli, S Krane (Eds.), Metabolic Bone Disease. New York: Academic Press, 1977;237.
2. Dent CE. Rickets and osteomalacia from renal tubule defects. J Bone Joint Surg 1952; 34B:266.
3. Dent CE, Harris H. Hereditary forms of rickets and osteomalacia. J Bone Joint Surg 1956; 38B:204–226.
4. Dent CE, Richens AT, Rowe DJF, Stamp TCB. Osteomalacia with long-term anticonvulsant therapy in epilepsy. Br Med J 1970; 4:69.
5. Doppelt SH. Vitamin D, rickets and osteomalacia. Orthop Clin N Am 1984; 15:671.
6. Laing IA, Glass EJ, Hendry GM, Westwood A, Elton RA, Lang M, Hume R. Rickets of prematurity: calcium and phosphorus supplementation. J Pediatr 1985; 106:265.
7. Lyon AJ, McIntosh N, Wheeler K, William JE. Radiological rickets in extremely low birthweight infants. Pediatr Radiol 1987; 17:56.
8. Wagner CI, Greer FR, and the section on breastfeeding and committee on. Prevention of rickets and vitamin D deficiency in infants, children, and adolescents. Pediatrics 2008; 122:1142–1152.

Osteomalacia

1. Aaron JE, Gallagher JC, Anderson J. Frequency of osteomalacia and osteoporosis in fractures of the proximal femur. Lancet 1974; 1:229.
2. Anderson I, Campbell AER, Dunn A, et al. Osteomalacia in elderly women. Scott Med J 1966; 11:429.
3. Chalmer J, Conacher WDH, Gardner DL, et al. Osteomalacia A common disease in elderly women. J Bone Joint Surg 1967; 49B:403.
4. Holick, MF. Vitamin D deficiency. New Engl J Med 2007; 357:266–281.
5. Kaplan FS, Soriano S, Fallon MD, Haddad JG. Osteomalacia in a night nurse. Clin Orthop Apr 1986; 205:216.
6. Lee DM, Tajar A, Ulubaev A, et al. Association between 25-hydroxy vitamin D levels and cognitive performance in middle-aged and older European men. J Neurol Neurosurg Psychiatry 2009;80:772–779.
7. Mankin HJ. Rickets, osteomalacia and renal osteodystrophy. Part I. JK Bone Joint Surg 1974; 56A:l0l
8. Mankin HJ. Rickets, osteomalacia, and renal osteodystrophy. Part II. J Bone Joint Surg 1974; 56A:352.
9. Mankin HJ. Rickets, osteomalacia, and renal osteodystrophy, An update. Orthop Clin North Am 1990; 21:81–86
10. Milkman LA. Multiple spontaneous idiopathic symmetrical fractures. Am J Roentgenol 1934; 32:622.
11. Paice EW, Hoffbrand BI. Nutritional osteomalacia presenting with plantar fascitis. J Bone Joint Surg (Br) 1987; 69:38.
12. Pitt MJ In: Resnick D and Kransdorf: Bone and Joint Imaging, 3rd Ed. Elsevier Saunders, 2005, on “Rickets and Osteomalacia”, pp. 563–575.
13. Subbarao K. Osteomalacia, RSNA Syllabus on metabolic and endocrine disorders affecting the skeleton, Course 1981; 509A.
14. Weissman B Y, Hochberg Z. Genetic rickets and osteomalacia. Curr Ther Endocrinol 1994; 492–495.

Hereditary renal tubular diseases

1. Albright F, Butler AM, Bloomberg E. Rickets resistant to vitamin D therapy. Am J Dis Child 1937; 54:529.
2. Albright F, Burnett C, Parson W, Reifenstein EC, Roos A. Osteomalacia and late rickets. The various etiologies met in the United States with emphasis on that resulting from a specific form of renal acidosis, the therapeutic indications for each etiological sub-group and the relationship between osteomalacia and Milkman's syndrome. Medicine, 1946; 25:399–479.
3. Brooks MH, Bell NH, Love L, Stern PH, Orfei E, Queener SF, Hamstra AJ, Deluca HF. Vitamin D-dependent rickets type II: resistance of target organs to 1,25 dihydroxyvitamin D. N Engl J Med 1978; 298:996.
4. Chan JC, Alon U, Hirchman GM. Renal hypophosphatemic rickets. J Pediatr 1985; 106:533.
5. Chan JCM. Renal hypophosphatemic rickets: a review. The Intl J Pediatric Nephrol 1982; 3:305.
6. Dent CE. Rickets and osteomalacia from renal tubule defects. J Bone Joint Surg 1952; 34B:266.
7. de Toni G. Remarks on the relations between renal rickets (renal dwarfism) and renal diabetes. Acta Pediatr 1933; 16:479.
8. de Toni G. Renal rickets with phospho-gluco-amino renal diabetes. Detoni-Debre-Fanconi syndrome. Ann Pediatr 1956; 187:42.
9. Fraser D, Scriver CR. Familial forms of vitamin D-resistant rickets revisited. X-linked hypophosphatemia and autosomal recessive vitamin D dependency. Am J Clin Nutr 1976; 29:1315.
10. Lifshitz F, Maclaren NK. Vitamin D-dependent rickets in institutionalized mentally retarded children receiving long-term anticonvulsant therapy: I.A. survey of 288 patients. J Pediatr 1973; 83:612.
11. McAlister WH, Kim GS, Whyte MP. Tibial bowing exacerbated by partial premature epiphyseal closure in sex-linked hypophosphatemic rickets. Radiol 1987; 162:461.
12. Parfitt AM. Hypophosphatemic vitamin D refractory rickets and osteomalacia. Orthop Clin N Am 1972; 3:653.
13. Schwartz AV, Kelsey JL, Sidney S, Grisso JA. Characteristics of falls and risk of hip fracture in elderly men. Osteoporos Int 1998; 8: 240–246.
14. Wallis LA, Engle RL. The adult Fanconi syndrome. II. Review of eighteen cases. Am J Med 1957; 22:13.

Renal osteodystrophy

1. Bonakdarpour A. Renal osteodystrophy, RSNA Syllabus, Metabolic and endocrine disorders affecting the skeleton. Course 1981; 409B.
2. Bonakdarpour, A. "Renal Osteodystrophy." Radiology Today, 4-A, Multinational Series, 1987; 119–124.
3. Kriegshauser JS, Swee RG, McCarthy JT, Hauser MF. Aluminum toxicity in patients undergoing dialysis: radiographic findings and prediction of bone biopsy results. Radiology 1987; 164:399.
4. Murphy MD, Sartoris DJ, Quale, JL, Pathria MN, Martin NL. Musculoskeletal manifestations of chronic renal insufficiency. Radiographics 1993: 13(2): 357–379.

Iatrogenic Osteomalacia

1. Christiansen C, Rodbro P, Lund M. Incidence of anticonvulsant osteomalacia and effect of vitamin D: controlled therapeutic trial. Br Med J 1973; 4:695.
2. Wolschendorf K, Vanselow K, Moller WD, Schulz H. A quantitative determination of anticonvulsant-induced bone demineralization by an improved x-ray densitometry technique. Neuroradiology 1983; 25(5):315.

Oncogenic Osteomalacia

1. Clunie GPR, Fox PE, Stamp TCB. Four cases of acquired hypophosphatemic (oncogenic) osteomalacia. Problems of diagnosis, treatment and long-term management. Rheumatology 2000; 39:1415–1421.
2. Daniels RA, Weisenfeld I. Tumorous phosphaturic osteomalacia. Am J Med 1979; 67:155.
3. Renton P, Shaw DG. Hypophosphatemic osteomalacia secondary to vascular tumors of bone and soft tissue. Skeletal Radiol 1976; 2:21.
4. Robertson A. Case of the winter season. Hypophosphatemic osteomalacia secondary to hemangiopericytoma of the right femur. Semin Roentgenol 1983; 18:5.
5. Sundaram M, McCarthy EF. Oncogenic osteomalacia. Skeletal Radiol 2000; 29:117–124.
6. van Boekel G, Ruinemans-Koerts J, Joosten F, et al. Tumor producing fibroblast growth factor 23 localized by two staged venous sampling. Eur J Endocrinol 2008; 158:431–437.
7. Warren RC, McKenzie CF, Rodeck CH, Moscoso G, Brock DJ, Barron L. First trimester diagnosis of hypophosphatasia with a monoclonal antibody to the liver/bone/kidney isoenzyme of alkaline phosphatase. Lancet 1985; 2:856.
8. Wladimiroff JW, Niermeijer MF, Van der Harten JJ, Stewart PA, Versteegh FG, Blom W, Huijmans JG. Early prenatal diagnosis of congenital hypophosphatasia: Case Report. Prenat Diagn 1985; 5:47.

Hypophosphatasia

1. Coto H, Douglas JE. Adult Hypophosphatasia. South Med 1983; J76:1570.
2. Baker DH. Hypophosphatasia and osteogenesis imperfecta. Course, RSNA Syllabus on metabolic and endocrine disorders affecting the skeleton. Course 1981; l09C.
3. Fraser D. Hypophosphatasia. A J Med 1957; 22:730.
4. Macfarlane JD, Kroon HM, Cats A. Ectopic calcification in hypophosphatasia. Eur J Radiol 1986; 6:228.
5. Rathburn JC. Hypophosphatasia. Am J Dis Child 1948; 75:822.
6. Yagel S, Milwidsky A, Ornoy A, Palti Z, Gutman A. Imaging case of the month. Hypophosphatasia. Am J Perinatol 1985; 2:261.

Atypical axial osteomalacia

1. Frame B, Frost H, Ormond R, Hunter R. Atypical osteomalacia involving the axial skeleton. Ann Intern Med 1961; 5:632.
2. Nelson AM, Riggs BL, Jowsey JO. Atypical axial osteomalacia, Report of four cases with two having features of ankylosing spondylitis. Arthritis Rheum 1978; 21:715.

Hereditary hyperphosphatasia (Juvenile Paget disease)

1. Bakwin H, Elger MS. Gragile bones with macrocranium. J Pediatr 1956; 49:558.
2. Bonakdarpour A, Maldjian C, Weiss S, Roach N, Stein E. Hyperphosphatasemia: report of three cases. Eur J Radiol 2000; 35:54–58.
3. Caffey J. Familial hyperphosphatasemia with ateliosis and hypermetabolism of growing membranous bone: review of the clinical, radiographic and chemical features. Bull Hosp Jt Dis 1972; 38:81.
4. Garimella R, Tag SE, Zhang J, et al. Expression and synthesis of bone morphogenetic proteins by osteoclasts: a possible path to anabolic bone remodeling. J Histochem Cytochem 2008; 56:569–577.
5. Whalen JP. Familial bone dysplasia with hyperphosphatasemia (FBDH) and allied disorders. RSNA Syllabus on metabolic and endocrine disorders affecting the skeleton. Course 1981; 609B.
6. Woodhouse NJY, Fisher MT, Sigurdsson G, Joplin GE, McIntyre IP. Paget's disease in a 5 year old: acute response to human calcitonin. Brit Med J 1972; 4:267.
7. Whyte MP, Obrecht SE, Finnegan PM, et al. Osteoprotegerin deficiency and juvenile Paget's disease. New Engl J Med 2002; 347:175–184

Hypervitaminosis D

1. Aegerter E, Kirkpatrick, JA. Orthopedic Diseases (Physiology, Pathology and Radiology), 4th ed. Philadelphia: WB Saunders, 1975.
2. Heany RP. Vitamin D in health and disease. CJASN 2008; 3:1535–1541.
3. Holick MF. Sunlight and vitamin D for bone health and prevention of autoimmune disease, cancers and cardiovascular disease. Am J Clin Nutr. 2004; 80: 1678S–1688S.
4. Jacobus CH, Holick MF, Shao Q, et al. Hypervitaminosis D associated with drinking milk. New Engl J Med 2002: 326:1173–1177.
5. Nako Y, Tomomasa T, Morikawa A. Risk of hypervitaminosis D from prolonged feeding of high vitamin D premature infant formula. Pediatr Int 2004; 46:439–443.
6. Resnick D, Kransdorf MJ. Bone and Joint Imaging, 3rd ed. Philadelphia: Elsevier Saunders, 2005, Hypervitaminosis D: p. 1026.

Hypervitaminosis A

1. Aegerter E, Kirkpatrick, JA. Orthopedic Diseases (Physiology, Pathology and Radiology), 4th ed. Philadelphia: WB Saunders, 1975.
2. Chernoff SM. Micronutrient requirements in older women. Am J Clin Nutr 2005; 81:1240s–1245s.
3. Lips P. Hypervitaminosis A and fractures. New Engl J Med 2003; 348:347–349.
4. Resnick D, Kransdorf MJ. Bone and Joint Imaging, 3rd ed. Philadelphia: Elsevier Saunders, 2005, Hypervitaminosis D: p. 1026.

Fluorosis

1. Kurland ES, Schulman RC, Zerwekh JE, Reinus WR, Dempster DW, Whyte MP. Recovery from skeletal fluorosis (an enigmatic, American case). JBMR 2007:153–170.

2. Resnick D, Kransdorf MJ. Bone and Joint Imaging, 3rd ed. Philadelphia: Elsevier Saunders, 2005, Fluorosis, pp. 1016–1017.

Vertebroplasty and Kyphoplasty

1. Deramond H, Depriester C, Galibert P, Le Gars D. Percutaneous vertebroplasty with polymethylmethacrylate. Technique, indications, and results. Radiol Clin N Am 1998; 36:533–546.
2. Fourney DR, Schomer DF, Nader R. Percutaneous vertebroplasty and kyphoplasty for painful vertebral body fractures in cancer patients. J Neurosurg 2003; 98:21–30.

Chapter 3

Systematic Approach to Radiology of Endocrine Disorders Affecting the Musculoskeletal System

Akbar Bonakdarpour and Colleen Veloski

Abstract Diagnostic imaging has two major roles in the management of the patients with endocrine dysfunction:

(1) Localization of the abnormal endocrine gland and demonstration of the nature and extent of abnormality.
(2) Visualizing the radiological musculoskeletal abnormalities in target organs.

Gigantism and acromegaly are caused by excessive secretion of growth hormone. MRI is the best imaging modality for localization of the pituitary adenoma. Endocrine causes of attenuated growth include hormonal deficiencies such as GH deficiency and congenital hypothyroidism. In congenital hypothyroidism the body appears immature for the chronological age. Untreated overt hyperthyroidism is clearly associated with osteoporosis and an increased risk of fracture. The pathognomonic finding in well-established primary or secondary hyperparathyroidism is subperiosteal resorption. Renal osteodystrophy is the most common cause of secondary hyperparathyroidism in the western world. Amyloidosis and destructive spondyloarthropathy are major complications of dialysis. Ischemic necrosis of bone is a major complication of renal transplantation.

Keywords Endocrine glands • Gigantism • Acromegaly • Sotos syndrome • Congenital hypothyroidism • Hyperthyroidism • Thyroid acropachy • Hyperparathyroidism • Secondary hyperparathyroidism • Renal osteodystrophy • Dialysis • Amyloidosis • Destructive spondyloarthropathy • Complications of renal transplantation • Pseudohypoparathyroidism • Brown tumors • Aluminum toxicity

A. Bonakdarpour (✉)
Department of Radiology, Temple University School of Medicine, 3401 North Broad Street, Philadelphia, PA 19140, USA
e-mail: akbarbonakdarpour@yahoo.com

Introduction

The main purpose of this chapter is to present a systematic approach to diagnostic imaging of endocrine abnormalities affecting the musculoskeletal system. Diagnostic imaging has two major roles in the management of the patients with endocrine dysfunction:

(1) Localization of the abnormal endocrine gland and demonstration of the nature and extent of abnormality.
(2) Demonstration of radiological musculoskeletal abnormalities.

Diagnostic imaging is not only important in confirming the diagnosis of a particular endocrinopathy but it records the gross pathology in vivo at various phases of the disease process. Consequently, it will create a baseline to follow during the treatment and also long term follow-up of the patient. There is no doubt that hormone levels and other laboratory and clinical studies are essential in the diagnosis and treatment of endocrine disorders, but imaging modalities permanently demonstrate the gross pathology during the active phase of the disease and the response to treatment.

For example, in acromegaly, the MRI will show the exact location and size of the pituitary tumor and extension of the lesion to the adjacent structures in the brain. After surgical debulking, the MRI shows the extent of reduction in the size of the tumor and is a guide for planning additional treatments such as radiation or further surgery. Furthermore, radiographic imaging of target organs, such as the skull, facial bones, spine, hands, and feet, also demonstrate pathologic effects of excessive growth hormone as well as the effects of treatment.

Similarly, in renal osteodystrophy due to advanced renal failure, skeletal imaging establishes the characteristic pathologic findings that, when compared over time, can show progression or regression in response to therapy. Clearly the basis for the diagnosis of endocrine disorders lies in the realm of the clinical and hormonal evaluation. However, radiologic

A. Bonakdarpour et al. (eds.), *Diagnostic Imaging of Musculoskeletal Diseases: A Systematic Approach*,
DOI 10.1007/978-1-59745-355-4_3, © Springer Science+Business Media, LLC 2010

studies often confirm the pathology of the endocrine gland, record the systemic effects of hormonal imbalance, and demonstrate the response to therapy. In this chapter, only endocrine abnormalities with major musculoskeletal manifestations will be discussed.

Bone Changes of Pituitary Dysfunction

Major periods of growth are intimately related to growth hormone (GH) that is secreted by the pituitary gland. Other hormones such as thyroid and sex hormones as well as genetic, environmental, and nutritional factors also play an important role in human growth and development.

Growth hormone or somatotropin is a 191-amino acid single-chain polypeptide hormone weighing 22 kDa that is synthesized by somatotroph cells in the anterior pituitary. The GH gene family is located on the long arm of chromosome 17 [1]. The growth-promoting actions of GH are mainly mediated by insulin-like growth factors (IGF-1 and IGF-2), but some metabolic actions are direct effects of GH. Growth hormone is secreted in a pulsatile manner under the control of two hypothalamic peptides: growth hormone-releasing hormone (GHRH), which stimulates GH release, and somatostatin, which inhibits GH release [2].

In infancy and childhood, growth hormone and thyroid hormone as well as genetic and environmental factors are responsible for growth. During adolescence, gonadal and adrenal sex steroids stimulate accelerated growth. In girls, the pubertal growth spurt begins early in puberty and is generally completed by menarche. The pubertal growth spurt for boys begins toward the end of puberty and occurs about 2 years later than in girls. In addition to environmental factors, normal growth and development during adolescence is dependent on multiple hormonal factors including growth hormone, IGF-1, and thyroid hormone.

During adulthood, linear growth ceases at the time of epiphyseal fusion. Estrogen is critical for epiphyseal fusion in both males and females [3] as evidenced by the failure of epiphyseal fusion in males with estrogen receptor defects [4] and premature fusion in children with precocious puberty.

Gigantism

Pituitary gigantism is a rare cause of accelerated and excessive linear growth resulting in abnormally tall status. It is caused by the abnormal hypersecretion of GH occurring before fusion of the epiphyseal growth plates in a child or adolescent resulting in abnormal height growth and weight gain. In addition to abnormally tall stature (in excess of 8 feet in some cases), affected patients may have features characteristic of acromegaly, such as large hands and feet, frontal bossing, coarse facial features, and excessive sweating.

Although commonly called "pituitary gigantism," the term is somewhat misleading since the source of GH excess may be a pituitary adenoma [5, 6], hypothalamic GHRH excess [7], inadequate somatostatin secretion [8], or, rarely, ectopic secretion of GH or GHRH [9]. Familial syndromes associated with GH hypersecretion include McCune Albright Syndrome, multiple endocrine neoplasia type 1 (MEN1), and Carney complex. The differential diagnosis of children with abnormally rapid growth also includes conditions unrelated to GH hypersecretion such as hyperthyroidism, precocious puberty, Klinefelter syndrome, sex hormone deficiency or insensitivity, Marfan syndrome, glucocorticoid deficiency or insensitivity, and cerebral gigantism.

Laboratory confirmation of the diagnosis of gigantism is the same as that of acromegaly and is discussed in detail in that section. Once biochemical evidence of growth hormone hypersecretion is confirmed, radiographic imaging should be performed to evaluate the hypothalamus and pituitary. Magnetic resonance imaging is the best radiologic study for examining the hypothalamic–pituitary area.

Transsphenoidal resection is the preferred treatment for pituitary tumors amenable to surgery. Radiation may be used as adjunctive therapy but the effect of therapy is delayed and often results in panhypopituitarism [10]. Pharmacologic therapy with a dopamine antagonist, somatostatin antagonist, or both has been shown to be effective [11–13].

Cerebral Gigantism (Sotos Syndrome)

Cerebral gigantism was first described by Sotos et al. in 1964 [14]. It is an autosomal dominant condition characterized by a distinctive facial appearance, learning disability, overgrowth resulting in tall stature, and macrocephaly present from birth [15]. Affected children are larger than normal at birth and have excessive growth until puberty. Macrocephaly is present in both childhood and adulthood. In 2002, Sotos' syndrome was shown to be caused by mutations and deletions of *NSD1* gene [16]. GH hypersecretion is not the cause of excessive growth in Sotos' syndrome [17].

Acromegaly

Acromegaly is a condition caused by excessive secretion of growth hormone resulting in overgrowth of mesenchymal tissues during adult life [18, 19]. GH hypersecretion stimulates

hepatic IGF-1 which is responsible for most of the clinical manifestations of acromegaly.

In adults, GH hypersecretion affects the soft tissues, cartilage, skin, joints, and viscera. The incidence is estimated to be 3 cases per 1 million persons per year with a prevalence of about 60 per million [20]. Since the clinical manifestations are subtle and develop insidiously, most patients present with severe features after years of GH hypersecretion. The mean age of diagnosis is 40–45 years.

In more than 90% of cases, acromegaly is caused by a benign monoclonal GH-secreting pituitary adenoma [21]. Other rare causes of acromegaly include excess GHRH secretion from the hypothalamus or an ectopic tumor such as bronchial carcinoid, pancreatic islet, adrenal, medullary thyroid carcinoma, or small cell lung cancer [22]. Very rarely, a pancreatic islet cell tumor or lymphoma may secrete GH [23, 24]. Hyperprolactinemia may be present in up to 30% of patients due to the cosecretion of prolactin and GH by the adenoma, or compression of the hypothalamic–pituitary stalk by the tumor may interfere with the dopaminergic inhibition of prolactin secretion (stalk effect).

The features that characterize acromegaly are the result of abnormal growth of cartilage, bone, and fibrous tissues after the normal growth period has ended. In acromegalic adults, the normal sites of enchondral (endochondral) bone growth, the epiphyseal plates, are ossified. GH excess, therefore, causes overgrowth of the articular cartilage. Enchondral bone formation from the deep layers of the articular cartilage is slow and abnormal, leading to skeletal distortions that characterize the disease. Hypertrophic arthropathy of the knees, hips, spine, and other joints may occur [25]. Excessive intramembranous bone formation from the periosteum causes abnormal thickening of the cortices without proportionate longitudinal growth. Also, no growth occurs in areas of bone lacking cartilage; therefore, the overall picture is one of disharmonious skeletal enlargement.

In areas where considerable amounts of fibrous tissue are normally concentrated, growth results in a curious type of enlargement. This accounts for thickening of the lips (Fig. 3.1) and the tufting of the fingers (Fig. 3.2). There is a generalized thickening and sagging of the skin. Where cartilage is not directly associated with bone formation, the chondroblastic hyperplasia increases the cartilage mass but does not go on to enchondral bone formation. This type of growth accounts for the enlargement of the nose.

Once acromegaly is suspected, the diagnosis is established by documenting GH excess. Both serum IGF-1 and GH are elevated in patients with acromegaly. Since IGF-1 levels are more stable than GH, measurement of IGF-1 is the best single diagnostic test. If the IGF-1 level is equivocal or further confirmation is required, a GH suppression test can be performed by measuring GH after a 75-g oral glucose load. The normal response is suppression of GH to less than 1 ng/dL within 2 h of the glucose load [26].

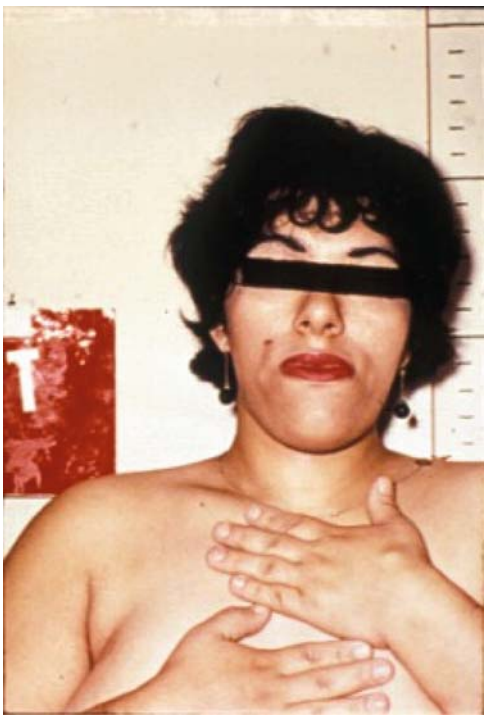

Fig. 3.1 Acromegaly. This patient reveals large nose, prominent maxillary sinuses, thickening of the lips, enlarged mandible causing prognathism, mild disproportionate growth of hands, and mildly enlarged phalanges

Radiological Manifestations

MRI is the best imaging modality for localization of the pituitary adenoma and demonstration of the shape and size of the tumor. Multi-planar, multi-sequence MR imaging, without and with gadolinium contrast injection, delineates the exact dimensions of the tumor, extent of extrasellar extension, compression of the optic chiasm and nerve, and invasion of the brain tissue, neighboring vessels, bones, and sinuses. Most growth hormone secreting adenomas are larger than 10 mm in diameter at the time of diagnosis. Two acromegalic cases with MRI localization of pituitary adenomas will be presented here. The first patient is a 42 year old female (Figs. 3.3, 3.4 and 3.5) and the second one is a 44 year old male (Figs. 3.6, 3.7, 3.8 and 3.9). Osseous changes of the skull and sella turcica are best demonstrated by CT (Figs. 3.8 and 3.9). An important differential diagnosis of pituitary adenoma is the empty sella syndrome. The sella turcica is slightly enlarged, but MRI proves that the cause is an empty sella turcica (Fig. 3.10). In 90% of cases of

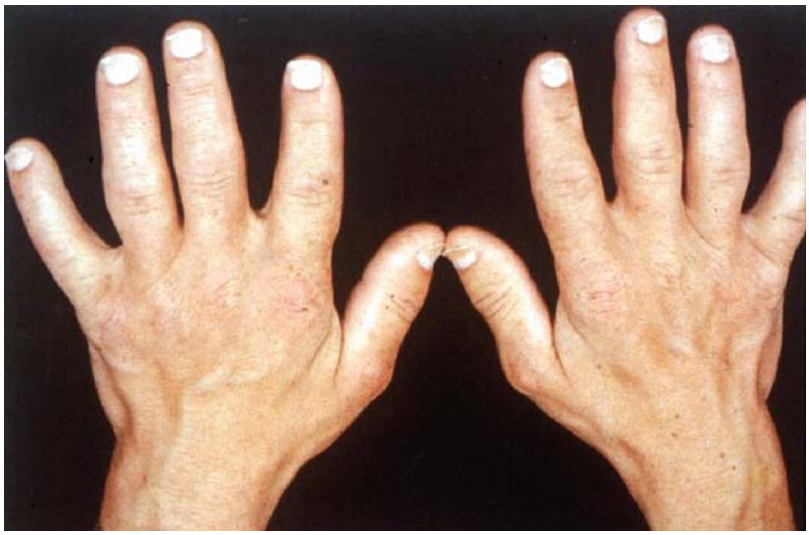

Fig. 3.2 Acromegaly. There is increased girth of fingers related to increased intramembranous bone formation as well as increased soft tissue thickness. There is clubbing of the fingers, without cardiopulmonary disease

well established acromegaly, lateral skull radiographs reveal enlarged sella turcica, thickening of the calvarium, enlarged paranasal sinuses frontal bossing and prominent external occipital protuberance (Fig. 3.11).

Multi-detector computerized tomography with multiplanar reconstruction is also very helpful. It shows the size and extension and/or invasion of tumor, but not as accurately as MR imaging. However, bony details are better demonstrated by CT scans and specifically cortical thickening and hyperostosis frontalis interna are best demonstrated in detail by CT (Figs. 3.8b and 3.9).

The mandible is increased in length by enchondral growth from the cartilage remaining at the condyle, and its length is accentuated by the apposition of bone to the outer lamina of the anterior surface of the mandibular body. The huge jaw producing dental malocclusion and prognathism is one of the most characteristic features of the disease (Figs. 3.1 and 3.8a). The walls of the sinuses and mastoid cells become greatly thickened and the air spaces are enlarged. Despite this growth of bone in the cranial and facial areas, there is no enlargement of the cranial cavity (Figs. 3.8a and 3.11) due to the complete ossification of the centers of cranial growth before the onset of the disease.

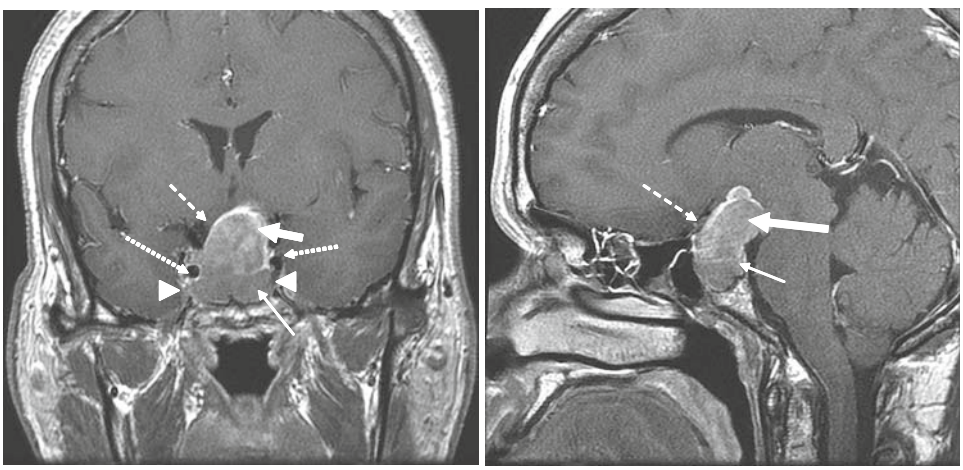

A **B**

Fig. 3.3 Acromegaly. This is a 42-year-old female with growth hormone abnormality (Figs. 3.3, 3.4, and 3.5 are from the same patient). Gadolinium-enhanced T1 coronal (**a**) and sagittal (**b**) MRI images demonstrate a pituitary macroadenoma of sellar origin (*thin arrows*) with suprasellar extension (*thick arrows*) measuring 3.2 × 2.6 × 2.7 cm. There is mass effect on optic chiasm and left optic nerve (*dashed arrow*), and invasion of the cavernous sinuses (*arrow heads*), *right* more so than *left*. Note the normal appearance of the intracavernous segment of both internal carotid arteries in the coronal images (*dotted arrows seen clearly in the original image A are solid in prints*). Courtesy of Dr. Jeffrey P Kochan, Temple University Hospital, Philadelphia, PA

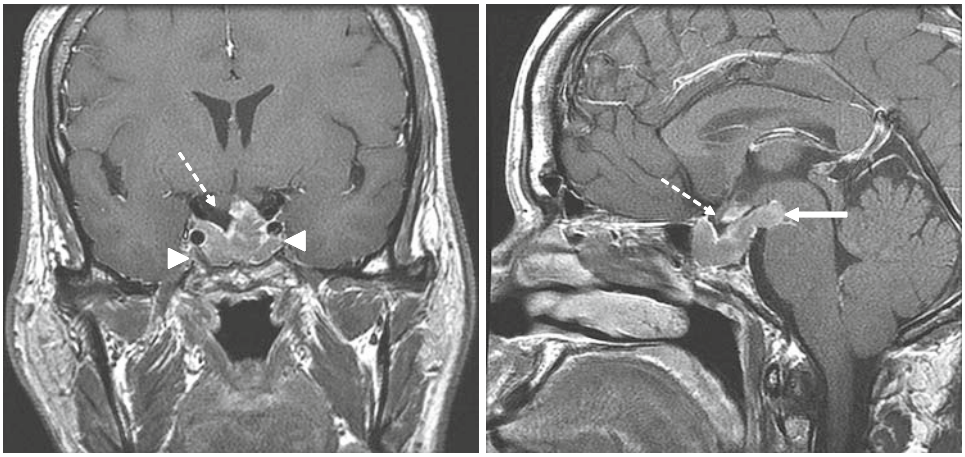

A B

Fig. 3.4 Acromegaly. Gadolinium-enhanced T1 coronal (**a**) and sagittal (**b**) MRI after debulking of the pituitary macroadenoma. There has been significant surgical decompression of the optic chiasm (*dashed arrow*), with overall reduction in size of the suprasellar component. There is now, however, a more pronounced posterior extension into the interpedicular cistern (*arrow*) with possible encasement of the basilar artery and persistent invasion of the cavernous sinuses (*arrowheads*). Courtesy of Dr. Jeffrey P Kochan, Temple University Hospital, Philadelphia, PA

Longitudinal growth of long bones is never proportional to the increase in thickness. Because reactivation of chondroblastic activity takes place at all sites of residual cartilage, the areas with the greatest number of articular cartilages exhibit the greatest increase in length. This is demonstrated in the disproportionate growth of the hands and feet where each digit has four units with six articular cartilages (Figs. 3.2, 3.12, and 3.13). The ungual tufts may show an arrow head appearance (Figs. 3.12 and 3.13).

The ribs are increased in diameter by periosteal apposition of bone and in length by enchondral bone formation at the costochondral junction. This increase in length anteriorly causes the characteristic chest deformity with an increased anteroposterior diameter. Osteoarthritis is a complication of acromegaly and may involve spine, hips (Fig. 3.13), hands and feet (Figs. 3.12 and 3.13). Sometimes hook-like projections of distal metacarpal and metatarsal bones are present (Figs. 3.12 and 3.13).

Lateral radiograph of the foot or ankle may reveal increased thickness of the heel pad exceeding 22 mm which is the upper limit of normal (Figs. 3.5a and 3.14). The vertebrae enlarge by apposition of bone to the lateral and anterior surfaces of the vertebral body. This new bone is intramembranous in origin and forms a collar of cortical bone applied to the vertebra on three sides, anteriorly and to the right and left, causing increased width and AP diameter of the vertebral bodies (Fig. 3.15). The height of intervertebral disc space is increased (Fig. 3.16).

Treatment options for acromegaly include transsphenoidal surgery, radiotherapy, and medications. The goal is to normalize IGF-1 levels and lower the serum GH concentration to <1 ng/mL (1 mcg/L) after a 75-g glucose load. When IGF-1

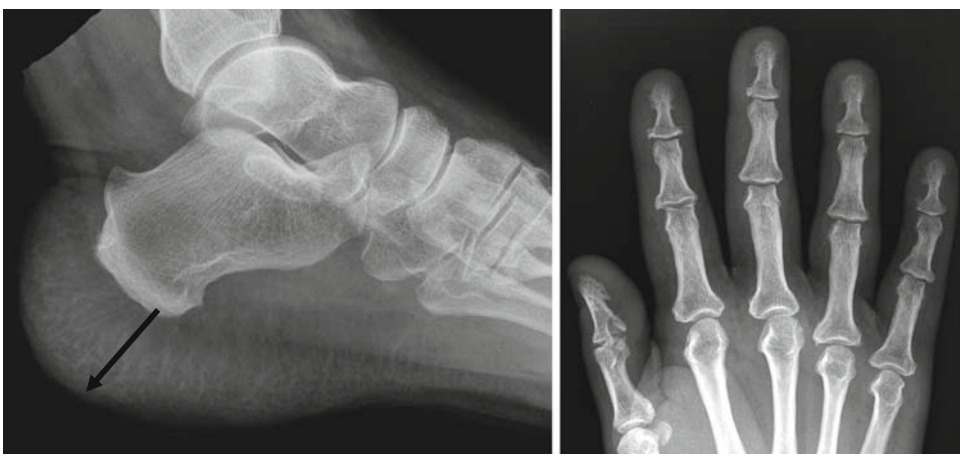

A B

Fig. 3.5 Acromegaly. This is the same 42-year-old female with macroadenoma. **(a)** The heel pad thickness is 29 mm (*arrow*) in this patient. The maximum normal heel pad thickness is 22 mm. (**b**) There is minimal thickening of the fingers and possible arrow head deformity of the ungual tufts

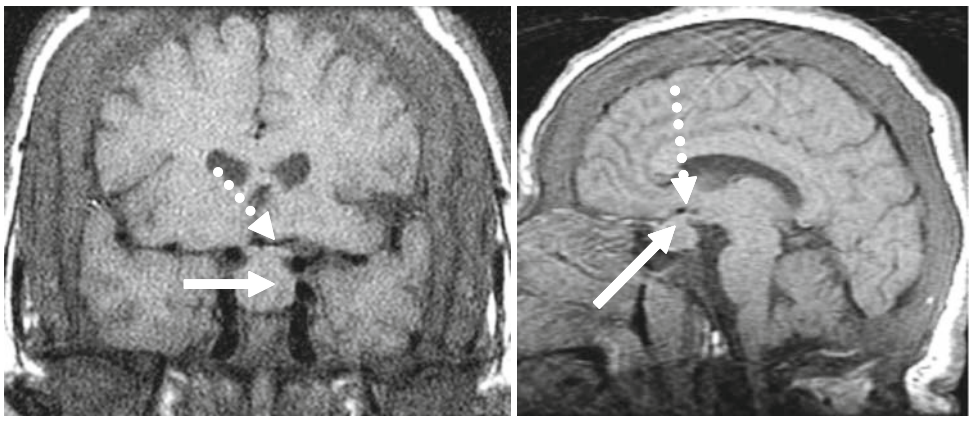

A B

Fig. 3.6 Acromegaly. This is a 44-year-old male with clinical diagnosis of acromegaly (Figs. 3.6, 3.7, 3.8 and 3.9 are from the same patient). Unenhanced coronal (**a**) and sagittal (**b**) T1-weighted MR images demonstrate the presence of a 1.9 × 1.6 cm intrasellar pituitary adenoma (*arrows*) with compression of optic chiasm (*dashed arrows*), but without evidence of parasellar extension. There is diffuse calvarial thickening consistent with the diagnosis of acromegaly. There is no frontal bossing as the frontal sinus is aplastic. Courtesy of Dr. Jeffrey P Kochan and Dr. Uday S Kanamala, Department of Radiology, Temple University Hospital, Philadelphia, PA

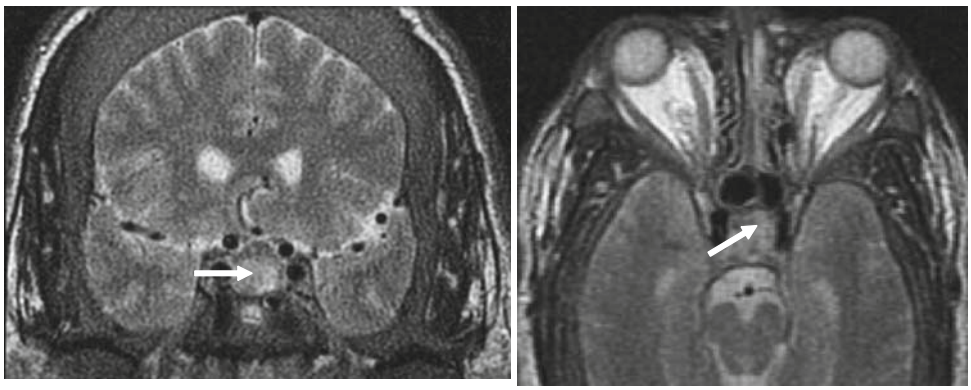

A B

Fig. 3.7 Acromegaly. T2 coronal (**a**) and axial (**b**) images again demonstrate the pituitary macroadenoma (*arrows*) without parasellar invasion. Courtesy of Dr. Jeffrey P Kochan and Dr. Uday S Kanamala, Department of Radiology, Temple University Hospital, Philadelphia, PA

and GH levels approach normal, some of the characteristic somatic changes gradually improve. These somatic changes can be best recorded by radiological modalities, over many years of follow up.

Transsphenoidal surgery debulks or resects the adenoma, normalizes IGF-1, and achieves a GH level less than 2.5 μg/L in more than 80% of patients with microadenomas. However, less than 50% of those with macroadenomas achieve optimal GH and IGF-1 levels with surgery alone. MRI is the best available technique to show the result of surgery and to find out if there is residual tumor. Medical treatment with a somatostatin receptor ligand such as octreotide results in constrained tumor growth or shrinkage in 50%, and approximately 70% achieve normal IGF-1 and GH < 2.5 μg/L. Radiotherapy arrests tumor growth but metabolic results are not realized for years after treatment with less than 35% of patients achieving GH and IGF-1 goals and more than 50% developing hypopituitarism [26].

Pegvisomant is a new GH receptor antagonist used to treat acromegaly that has not responded to other treatments. It does not directly affect tumor size, but has been shown to lower IGF-1 and improve peripheral soft tissue features [27, 28].

Prognosis: Normalization of IGF-1 and GH in acromegalic patients is associated with a normal life span but poorly controlled patients have decreased survival [29].

Endocrine Causes of Short Stature

Failure of the mesenchymal derivatives to attain a size within the limits of the normal variation results in short stature. In children, short stature is defined as more than two standard deviations below the mean height of a child of the same sex and age. Idiopathic short stature is a term applied in cases when no metabolic, endocrine, or other cause of short stature is identified.

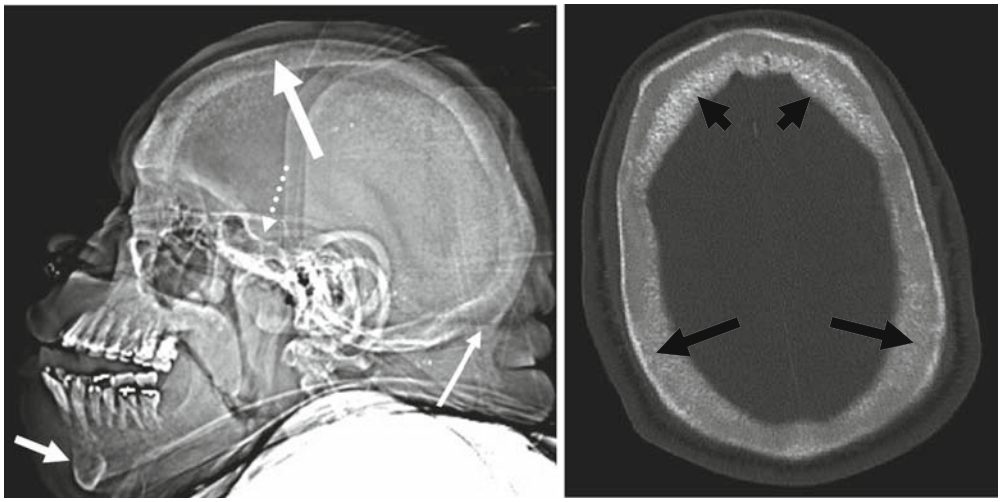

A B

Fig. 3.8 Acromegaly. This is a 44-year-old male with clinical diagnosis of acromegaly. Lateral scout radiograph of CT (**a**) showing moderate enlargement of the sella turcica (*dashed arrow*), increased thickness of the calvarium (*thick arrows*), marked prognathism (*short arrow*), and prominent external occipital protuberance (*thin arrow*). Axial CT in bone algorithm (**b**) shows marked calvarial thickening (*black arrows*). There is no frontal bossing as the frontal sinus is aplastic. Note the presence of hyperostosis frontalis interna (*short black arrows*). Courtesy of Dr. Jeffrey P Kochan and Dr. Uday S Kanamalla, Temple University Hospital, Philadelphia, PA

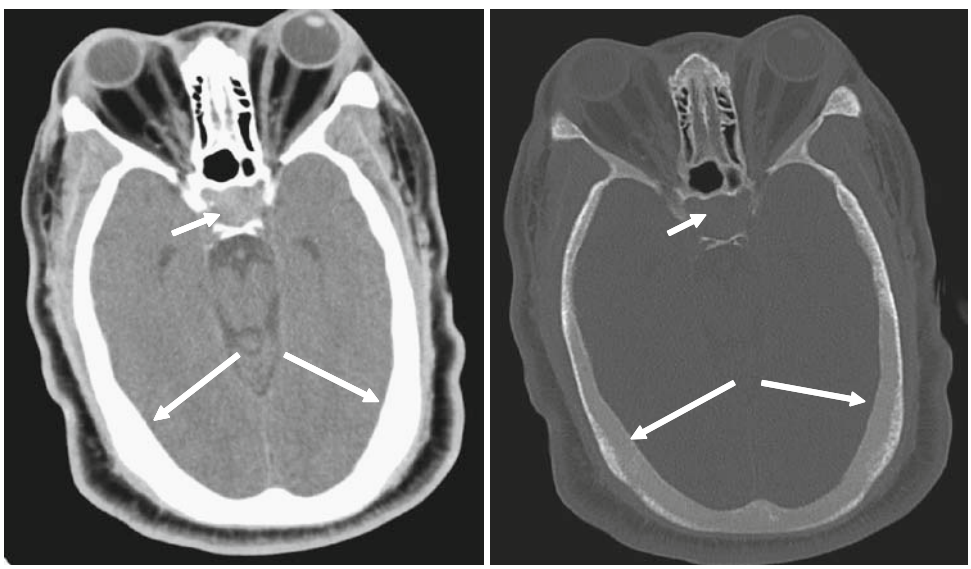

A B

Fig. 3.9 Acromegaly. Non-contrast CT examination of the head in soft tissue (**a**) and bone algorithm (**b**) demonstrating an enlarged sella turcica with an intrasellar mass (*short arrows*) and increased calvarial thickness (*long arrows*) effecting predominantly the inner calvarial table and diploe. Courtesy of Dr. Jeffrey P Kochan and Dr. Uday S Kanamalla, Department of Radiology, Temple University Hospital, Philadelphia, PA

Endocrine causes of attenuated growth include hormonal deficiencies such as GH deficiency and hypothyroidism. Thyroid function should always be thoroughly evaluated in children with suspected growth failure. If hypothyroidism is diagnosed early, treatment with thyroxine will restore normal growth. Children affected with complete GH deficiency have growth failure, delayed bone age, and low GH, IGF-1, and IGF-binding protein-3 levels [30]. Pharmacologic treatment with recombinant growth hormone beginning at an early age can result in normal adult height [31].

Mutations of the GH-binding region for the GH receptor cause complete or partial growth hormone insensitivity syndrome (Laron syndrome) characterized by high GH concentrations with low IGF-1 and IGF-binding protein-3 levels. Treatment with recombinant IGF-1 has been shown to be effective [32].

Hypercortisolism, whether due to Cushing disease or administration of glucocorticoid therapy, interferes with GH secretion and bone formation and may cause attenuated growth [33]. Any cause of abnormally high sex steroids

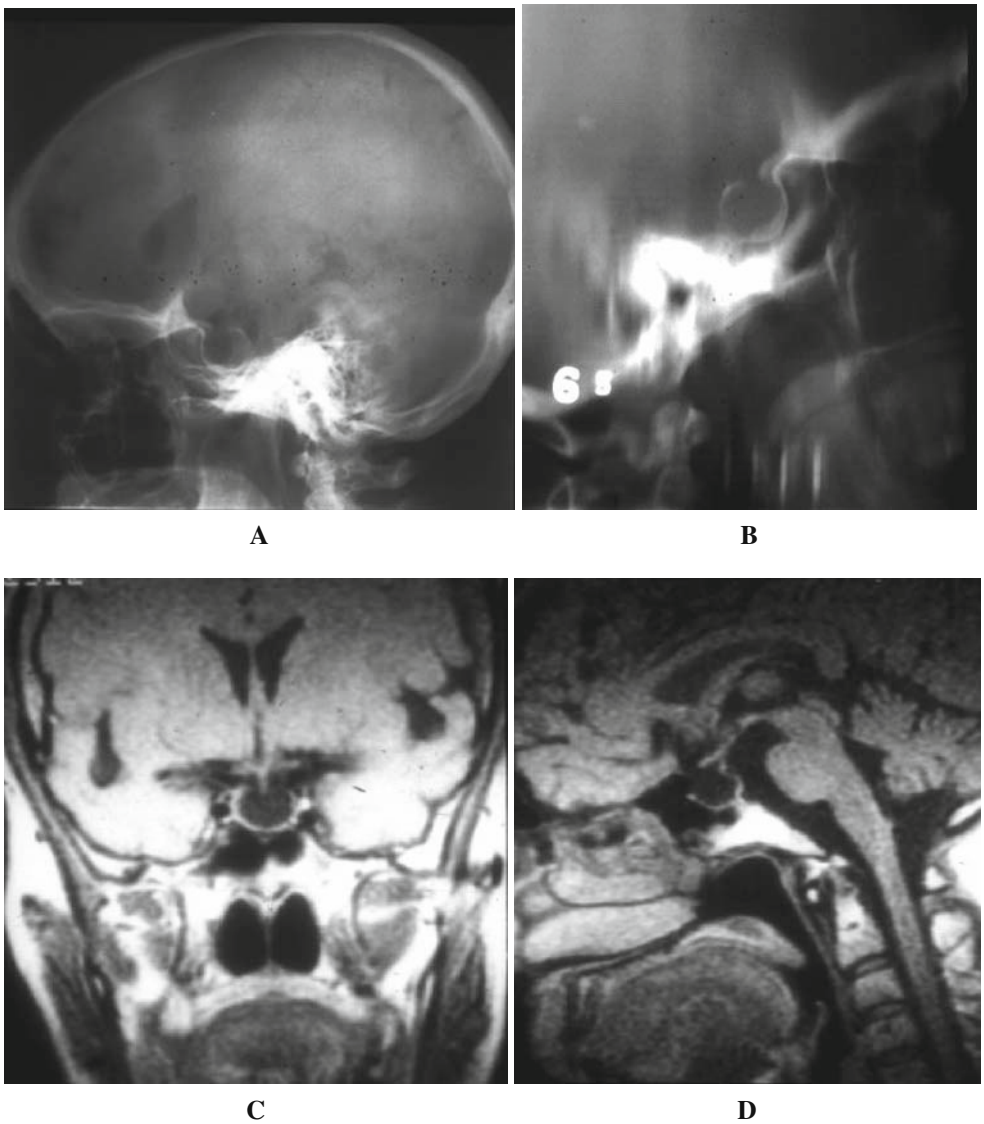

Fig. 3.10 Empty sella turcica should not be confused with pituitary adenoma. The patient is a 58-year-old female. (**a)** radiograph and (**b)** tomogram show mildly enlarged sella turcica. (**c)** coronal T1 MRI, and (**d)** sagittal T1 MRI demonstrating that the changes of sella turcica are related to an empty sella

before the usual chronologic age of puberty, such as precocious puberty or congenital adrenal hyperplasia, can cause rapid childhood growth with advanced bone age. If untreated, the high sex steroids will cause the epiphyseal growth plates to close prematurely. The children, though tall for their age during childhood, are usually short in adulthood.

Bone Changes of Thyroid Dysfunction

Hypothyroidism

Hypothyroidism refers to the clinical syndrome resulting from deficient levels of thyroid hormones. It is a relatively common disorder that is more common in women than men and increases in prevalence with age.

The majority of cases of hypothyroidism are due to a defect of the thyroid gland that impairs synthesis and secretion of thyroid hormones (primary hypothyroidism). Much less commonly, hypothyroidism is caused by defective secretion of thyroid-stimulating hormone (TSH) from the pituitary gland (secondary hypothyroidism) or thyroid-releasing hormone (TRH) from the hypothalamus (tertiary hypothyroidism). Iodine deficiency is the most common cause of primary hypothyroidism throughout the world, but Hashimoto thyroiditis is the leading cause in iodine sufficient areas.

The typical clinical manifestations of adult hypothyroidism include fatigue, cold intolerance, constipation, mental

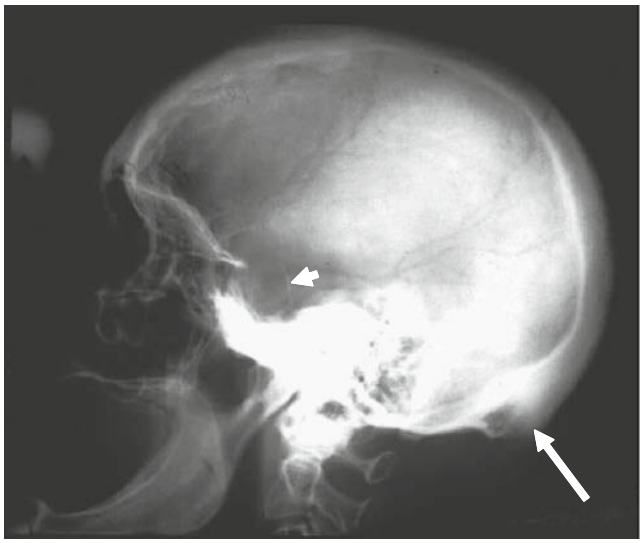

Fig. 3.11 Acromegaly. There is thickening of the calvarium, most pronounced in occipital regions, frontal bossing, and prominence of the occipital protuberance (*long arrow*). The sella turcica is enlarged with thinning of the dorsum sellae (*short arrow*)

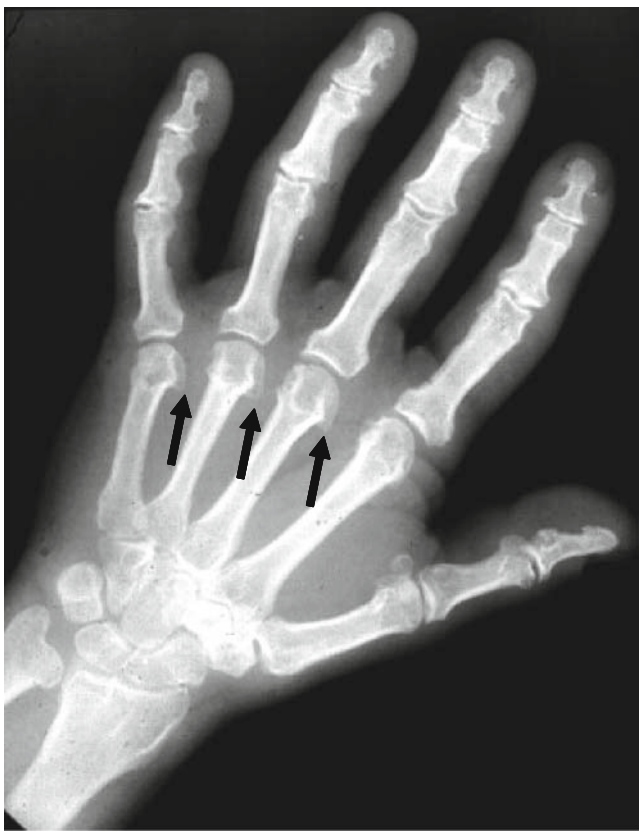

Fig. 3.12 Acromegaly. The hand reveals increased girth of bones and soft tissues of digits and distal metacarpals. There is hook-like projections of distal metacarpals (*arrows*), widening of the metacarpophalangeal, and proximal interphalangeal joints. There is a mild degree of *arrow head* deformity of the ungual tufts. This finding may be seen to some extent in normal individuals

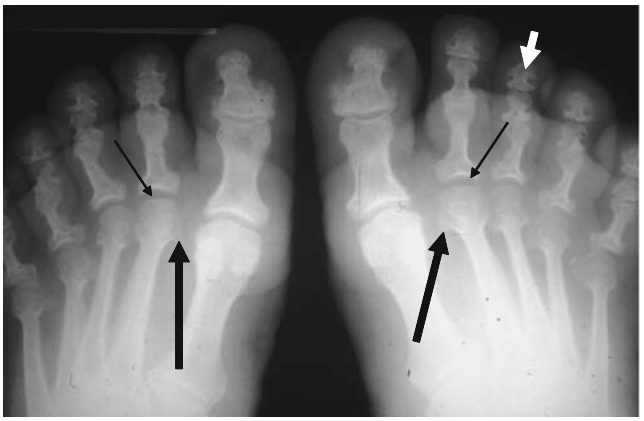

Fig. 3.13 Acromegaly. Changes similar to hands are present in the feet. Arrow head deformity of the ungual tufts (*white arrow*), widened joints (*thin arrows*), and hook-like projections of distal metatarsal (*long arrows*) are noted

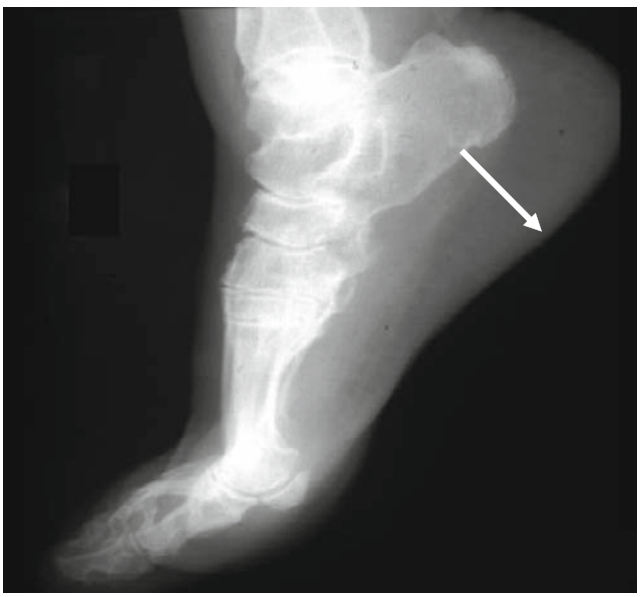

Fig. 3.14 Acromegaly. This is the same case as Fig. 3.13. Heel pad thickness is 35 mm (*arrow*). The normal heel pad thickness is up to 22 mm

slowness, and weight gain. Deposition of glycosaminoglycans in the interstitium can cause non-pitting edema and periorbital puffiness. Myxedema coma, the most severe form of hypothyroidism, is an endocrine emergency with a high mortality rate.

Measurement of TSH is the best screening test for hypothyroidism. However, when hypothyroidism is suspected, both TSH and free thyroxine (either directly or by calculation of the free thyroxine index using T3-resin uptake) levels should be measured. In primary hypothyroidism, the TSH is elevated and the free thyroxine is low. In secondary or tertiary hypothyroidism, the TSH is low or inappropriately

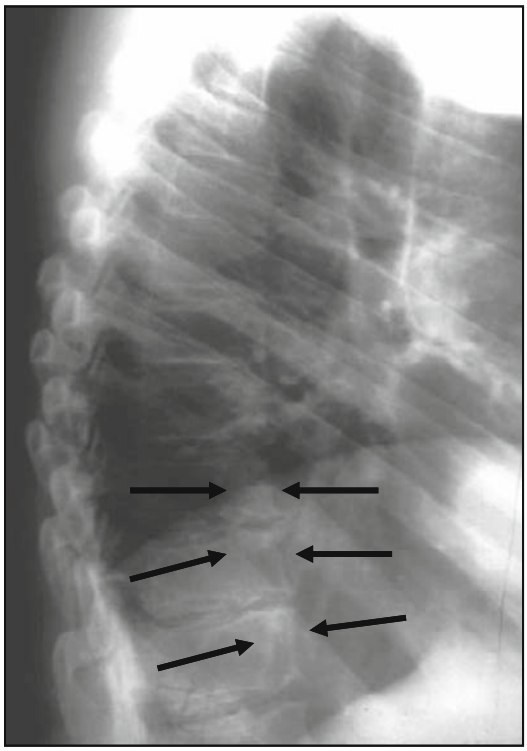

Fig. 3.15 Acromegaly. There is no increase in the height, but a significant increase in the AP diameter of vertebral bodies of the thoracic spine (*arrows*) is seen. The vertebra bodies increase in size on two dimensions (transversely and anteroposteriorly). In this lateral view only increased AP diameter can be evaluated, which is shown by *arrows*

normal, and the free thyroxine is low. Treatment consists of administration of synthetic thyroxine at a dose sufficient to restore euthyroidism.

The effect of hypothyroidism on the newborn can be devastating if not detected soon after birth. Congenital hypothyroidism (previously called cretinism) occurs in about 1:4,000 births and is the leading treatable cause of mental retardation in the world [34].

Causes of congenital hypothyroidism include thyroid dysgenesis, inborn errors of thyroid hormone metabolism, as well as transient forms of hypothyroidism due to maternal iodine deficiency or excess, or transplacental transfer of maternal TSH receptor blocking antibodies or antithyroid medications. Since the majority of newborns with congenital hypothyroidism exhibit few if any symptoms [35] screening of newborns is routine in most developed countries and in various stages of implementation in many developing countries.

If congenital hypothyroidism is undiagnosed and untreated, mental and skeletal growth retardation occur in addition to the typical clinical manifestations seen in adult hypothyroidism.

Radiological Manifestations

The radiologic manifestations of hypothyroidism are related to the severity and duration of the condition and are present only in growing bones.

Since thyroid hormones directly effect bone growth and development, the body appears immature for the chronological age. Skeletal growth does not catch up with fetal cranial growth resulting in the head appearing disproportionately large and the extremities short. Endochondral growth of bone

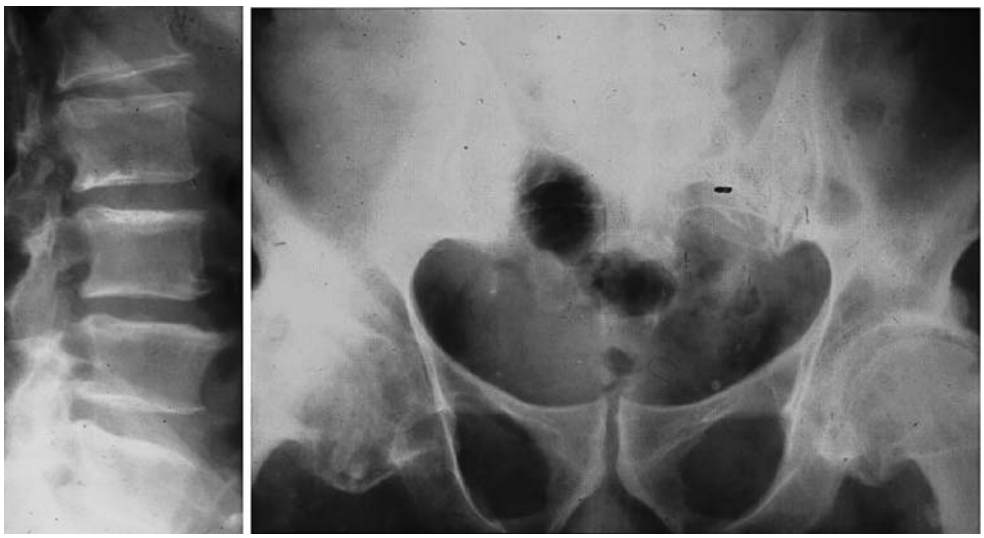

Fig. 3.16 Acromegaly. Osteoarthritis is a complication of acromegaly. In the patient there is osteoarthritis of the lumbar spine, both hips and SI joints. Note posterior scalloping and increased height of intervertebral disc spaces. Courtesy of Dr. M. Dalinka, Hospital of the University of Pennsylvania

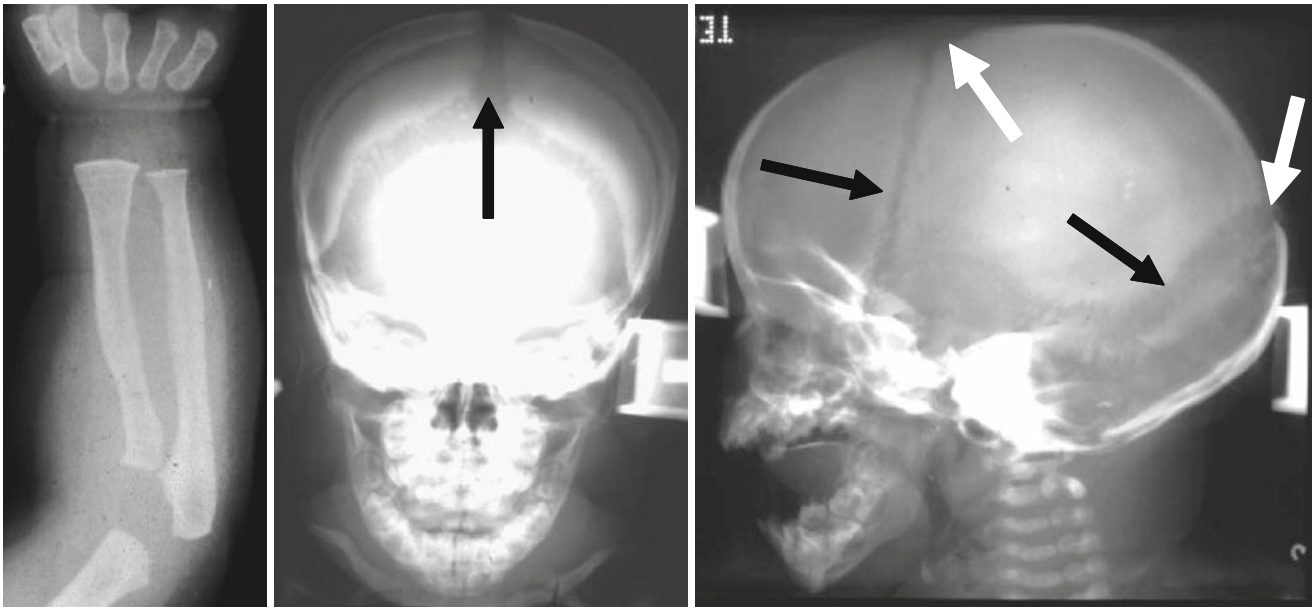

Fig. 3.17 Congenital hypothyroidism in a 22-month-old infant. **(a)** shows marked delayed bone age with no ossification of the carpal bones. The wrist bone age according to the standards of Greulich and Pyle is equal to new born. The radius and ulna are relatively short related to delayed enchondral growth, but they have normal girth, because periosteal (intramembranous) bone growth is normal. (**b** and **c)** are the frontooccipital and lateral radiographs of the skull showing delayed closure of the sutures (*black arrows*) and fontanels (*white arrows*)

is decreased and the appearance of the ossification centers is delayed [36] (Fig. 3.17a).

Skeletal growth is greatly inhibited. The problem appears to be in the conversion of cartilage to bone, i.e., in endochondral bone formation (Fig. 3.17). Intramembranous bone formation progresses at a normal rate so that eventually the cylindrical bones become disproportionately thick for their subnormal length.

The osseous nuclei within the cartilaginous epiphyses are late in appearing, so that the bone age appears to be much younger than the chronologic age (Figs. 3.17 and 3.18). When centers do appear, they tend to be smaller than normal and are often irregular in outline and spotty in their ossification, particularly at the shoulders and hips (Figs. 3.19 and 3.20). There is probably decreased chondroblastic replication in the enchondral plate because the mature cells of the epiphyseal columns are not actively dissipated. The retarded bone age may be ascertained by comparison of the radiographic appearance of the hands, wrists, and knees with available standards.

The child with untreated congenital hypothyroidism fails to grow in height. There is not only delay in appearance of the osseous epiphyseal centers but also delay of ossification of the epiphyseal plate (Figs. 3.21 and 3.22). All enchondral bone growth is inhibited, resulting in dwarfism. The bones that enlarge predominantly by enchondral growth, particularly those of the extremities, are the ones most dramatically affected (Figs. 3.21 and 3.22).

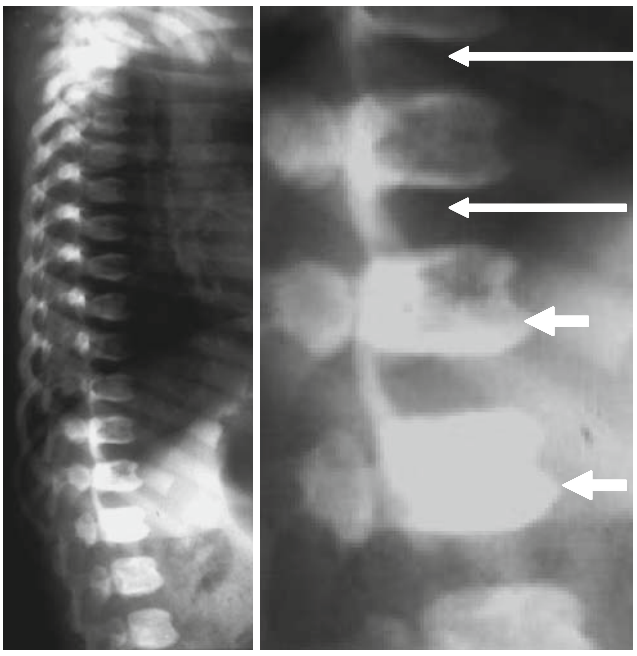

Fig. 3.18 Congenital hypothyroidism. This is the same case as in Fig. 3.17. **(a)** is the lateral view of the spine, revealing delayed bone age, increased height of intervertebral disc spaces and inferior beaking of vertebral bodies of thoracolumbar junction. **(b)** is magnification of the thoracolumbar junction, demonstrating increased height of intervertebral disc spaces (*long arrows*) and inferior beaking of vertebral bodies (*short arrows*)

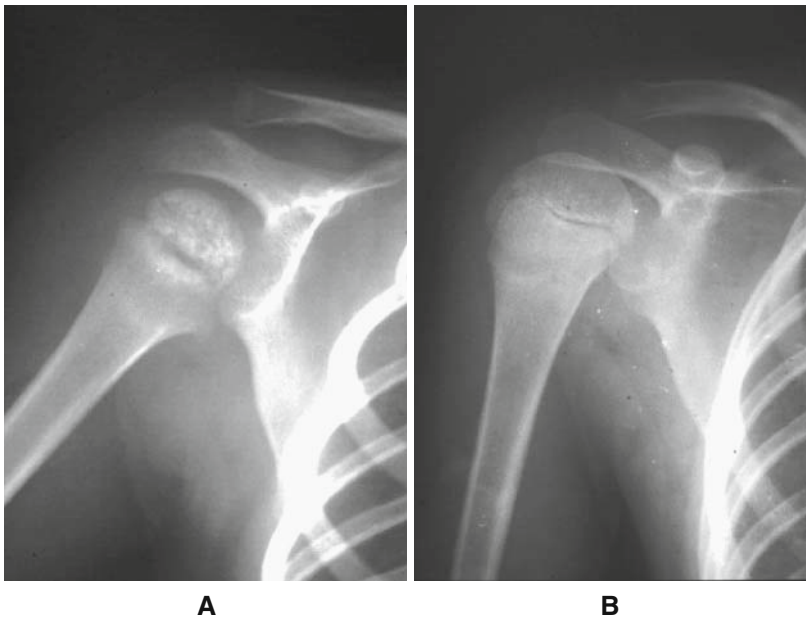

Fig. 3.19 Congenital hypothyroidism. This is a hypothyroid child before **(a)** and after **(b)** treatment showing that the epiphyseal densities have become normal in **(b)**

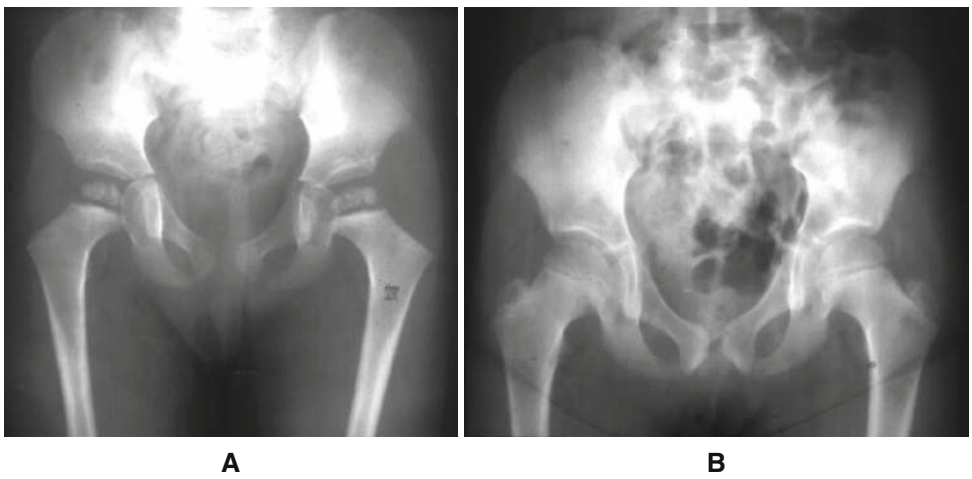

Fig. 3.20 Congenital hypothyroidism. The same patient as Fig. 3.19 of a hypothyroid child (**a**) before and (**b**) after treatment

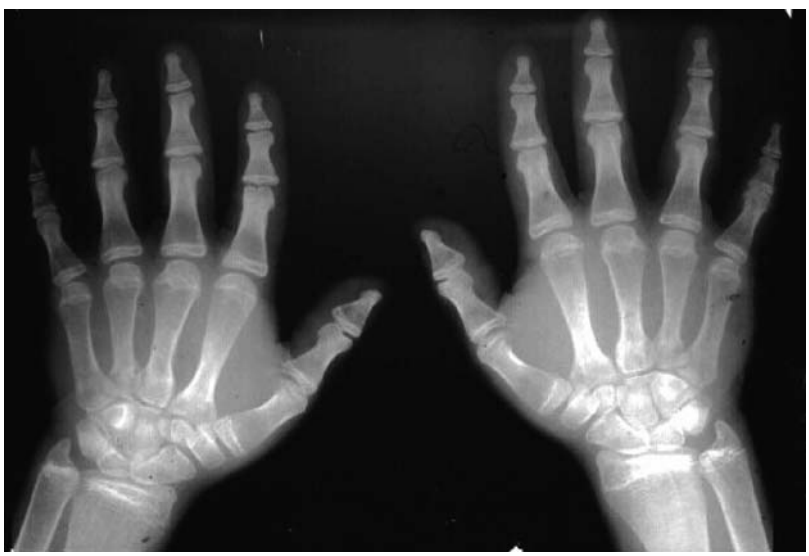

Fig. 3.21 Untreated congenital hypothyroidism (cretinism). Hands and wrists belong to a 34-year-old hypothyroid patient. There is significant delayed bone age. The radial, ulnar, metacarpal, and phalangeal epiphyseal plates are still open, longitudinal growth of bones is delayed, but bone girth is slightly increased

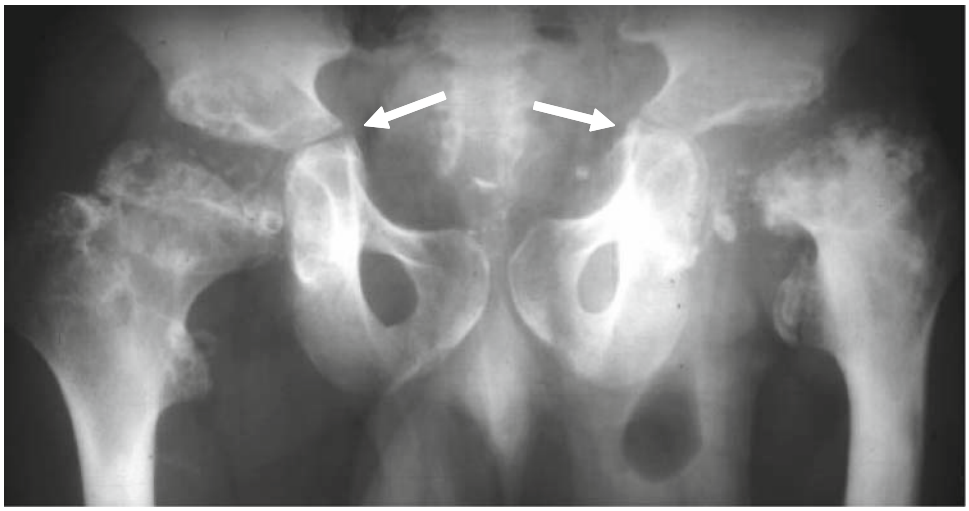

Fig. 3.22 Untreated congenital hypothyroidism. This is the pelvis of the same case as in Fig. 3.21 with congenital hypothyroidism. There is significant delayed bone age. The proximal femoral epiphyses have a fragmented appearance and not completely fused with femoral necks. The trident cartilages are still open and ilium is not fused with the rest of the iliac bone (*arrows*). Longitudinal growth of bones is delayed, but bone girth is slightly increased

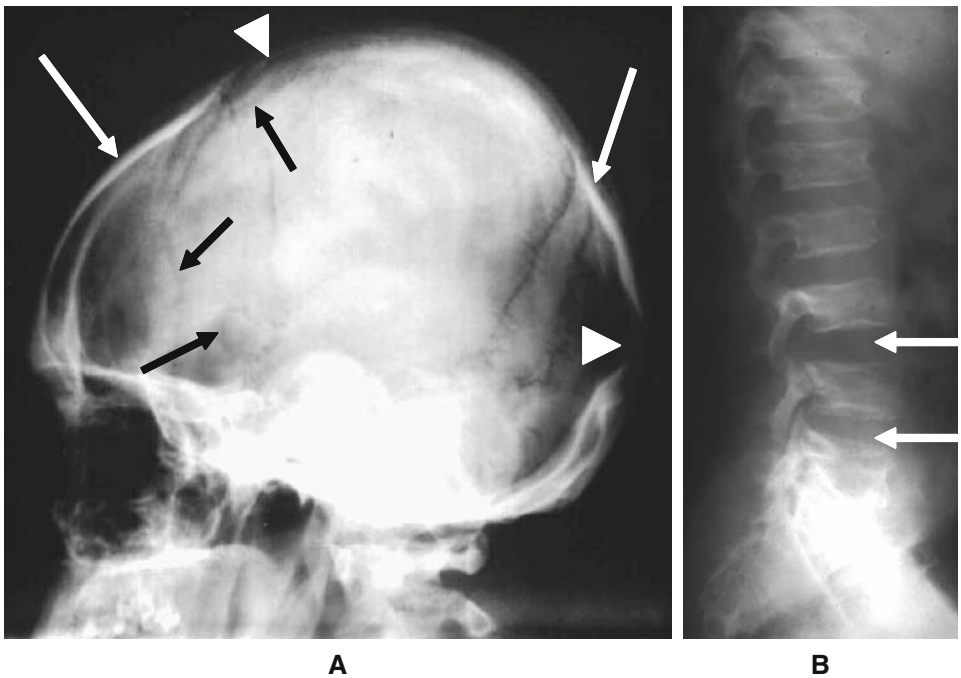

Fig. 3.23 Untreated congenital hypothyroid male at age 34. **(a)** The skull shows the sutures and fontanels are open. Occasional wormian bones (*black arrows*) and underdevelopment of the calvarial thickness (*long arrows*) are seen. Note the anterior and posterior fontanels are open (*arrow heads*). (**b)** The lumbar spine reveals increased height of intervertebral disc spaces due to underdevelopment of vertebral body heights (*arrows*). The vertebral body girth is normal. Courtesy of Dr. Barbara L Carter, New England Medical Center, Boston, Mass

The fontanels, sutures, and synchondroses at the base of the skull remain unossified for prolonged periods (Fig. 3.17 and 3.23a). The radiographic examination of the skull reveals the vault to be normal in size. The sutures are wide as a result of retarded ossification. Intersutural (wormian) bones may be present (Fig. 3.23a). The sella turcica has been found to be larger in congenital hypothyroidism than in normal individuals. The enlargement of the sella turcica in primary hypothyroidism is due to secondary pituitary hypertrophy. Pituitary hypertrophy as a consequence of primary hypothyroidism has been documented by computed tomography and improves after treatment of hypothyroidism [37, 38]. In later life there is poor differentiation of the diploic space and underdevelopment of the paranasal sinuses.

In the spine, growth of the vertebral height is delayed, causing an apparent increased height of intervertebral disc spaces (Figs. 3.18 and 3.23). The first lumbar vertebra is often hypoplastic and beaked anteroinferiorly (Fig. 3.18) and a kyphosis may be present in this area. Alterations in the lower dorsal and upper lumber spine mimic those seen in Hurler disease (mucopolysaccharidosis IH).

There is delay in eruption of the deciduous teeth and irregular delayed shedding, eventually leading to impaction of permanent dentition. The teeth, however, appear to be

normally formed, suggesting that there is no disturbance in normal matrix formation or mineralization. Dental difficulties probably stem from the failure of normal growth of the jaw.

Hyperthyroidism

Hyperthyroidism or thyrotoxicosis is the clinical syndrome that occurs when tissues are exposed to high levels of circulating thyroid hormones resulting in a general acceleration of metabolic processes. Typical clinical manifestations include palpitations, heat intolerance, insomnia, nervousness, increased appetite, and weight loss. Patients with Graves disease may also have exophthalmos or pretibial myxedema in addition to the symptoms of thyrotoxicosis. A small percentage of Graves patients develop a form of osteoarthropathy, called thyroid acropachy (Fig. 3.24) characterized by soft tissue swelling and marked rough and irregular periosteal reaction of the long bones and phalanges.

Since thyroid hormone stimulates bone resorption, chronic hyperthyroidism, whether overt or subclinical, results in reduced bone density. Cortical bone is affected more than trabecular, and postmenopausal women are more at risk than premenopausal women [39]. The increased bone resorption can cause hypercalcemia [40] with suppression of parathyroid hormone (PTH) secretion. The low serum PTH results in decreased conversion of 25-hydroxyvitamin D to the activated 1,25-dihydroxyvitamin D [41], thereby reducing intestinal calcium absorption and increasing renal calcium excretion. The net affect is a state of negative calcium balance.

The effects of thyrotoxicosis on bone are significant and can be long lasting. Untreated overt hyperthyroidism is clearly associated with osteoporosis and an increased risk of fracture. Chronic untreated subclinical hyperthyroidism is associated with an increased risk of osteoporosis [42]. Patients with a history of overt hyperthyroidism remain at increased risk for hip fracture later in life [43].

In neonatal hyperthyroidism, virtually all patients have a maternal history of hyperthyroidism. It is self-limited and clinical symptoms resolve by the age of 3–4 months. The newborn infant shows clinical and radiological evidence of hyperthyroidism. Radiographs reveal markedly advanced bone age to such an extent that a premature infant may reveal a bone age as advanced as 1.5 years (Fig. 3.25). Advanced bone age also normalizes with growth of the infant, but at a slower rate than clinical symptoms [44].

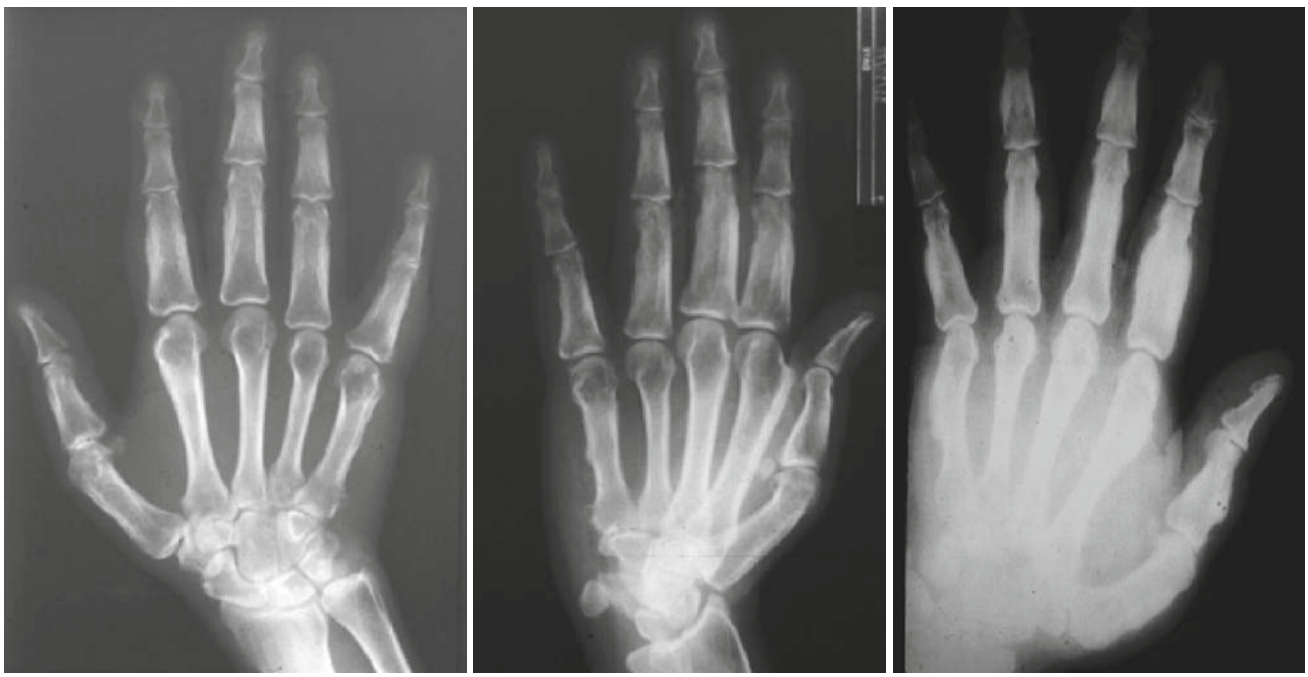

A B C

Fig. 3.24 Thyroid acropachy. **(a)** is a PA radiograph and (**b)** is an AP oblique view of the right hand in a patient with moderate thyroid acropachy revealing moderate solid periosteal reaction of the 2nd and 5th metacarpals as well as 2nd, 3rd, and 4th proximal phalanges. **(c)** is a PA view of the R hand in another patient with advanced disease demonstrating solid periosteal reaction along the metacarpals as well as proximal and some of the middle phalanges. (**a** and **b)** are courtesy of Dr. Murray K Dalinka, Hospital of the University of Pennsylvania. Philadelphia, PA

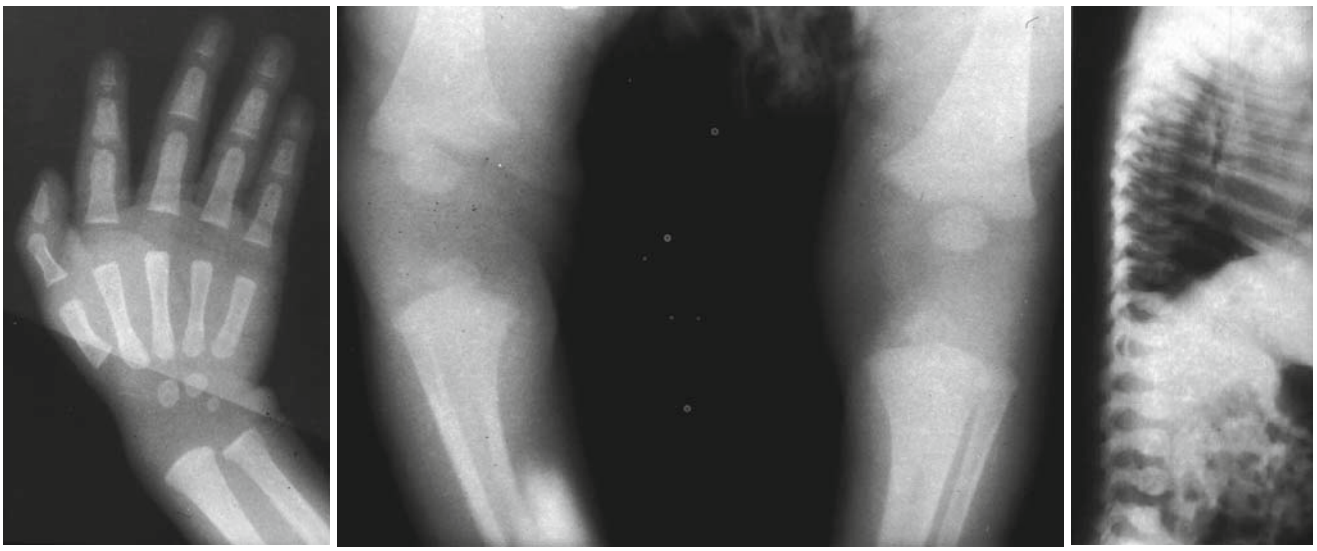

A B C

Fig. 3.25 Infantile hyperthyroidism seen in a premature female infant that was born to a 26-year-old hyperthyroid mother. **(a)** is PA radiograph of the R hand and wrist, **(b)** is AP of the knees, and **(c)** is the lateral radiograph of the thoracolumbar spine. The bones are normal in shape, but the bone age is markedly advanced. The bone age of the hand according to the standards of Greulich and Pyle is about 18 months

Bone Changes of Parathyroid Dysfunction

Hyperparathyroidism

Parathyroid hormone is a peptide hormone that tightly controls the ionized calcium level of the blood and extracellular fluid. It is secreted by four parathyroid glands located behind the upper and lower poles of each of the two thyroid lobes, within the fibrous supportive tissue of the neck. One or more glands may be situated in the thyroid capsule within the substance of the thyroid, or in an ectopic location such as the mediastinum. Up to 13% of normal persons have a fifth parathyroid gland at autopsy [45].

The parathyroid glands are usually moderately flattened anteroposteriorly, light tan in color, and have an average measurement of 5 × 3 × 2 mm. When sectioned and examined through the microscope they are found to consist of epithelial cells and stromal fat. The chief cell is predominant epithelial cell found in fields of polyhedral gland cells with clear cytoplasm and very little tendency to acinus formation. Also present to a lesser degree are larger cells with intensely eosinophilic cytoplasm called oxyphil cells. The oxyphil cells first appear at puberty and increase in number with age. While both cells contain PTH, the chief cells are most sensitive to changes in ionized calcium.

Hyperparathyroidism is a generalized disorder of calcium, phosphate, and bone metabolism that results from an increased secretion of parathyroid hormone. Hyperparathyroidism may be manifested as asymptomatic mild hypercalcemia or if severe can cause symptomatic hypercalcemia with hypophosphatemia, nephrolithiasis, hypertension, constipation, mental changes, and bone resorption. Hyperparathyroidism may be primary, secondary, tertiary, ectopic, or part of multiple endocrine neoplasia syndromes.

Primary Hyperparathyroidism

Primary hyperparathyroidism occurs when one or more of the parathyroid glands secrete PTH autonomously due to tumor or hyperplasia. Single adenomas account for about 89% of cases of primary hyperparathyroidism. Multiple gland hyperplasia is found in 6% of cases and parathyroid carcinoma in 1–2% [46].

Primary hyperparathyroidism (HPT) is a common endocrine problem with a 3:1 female predominance affecting up to 1 in 1,000 postmenopausal women [47]. The incidence is highest in patients over 45 years, but may occur in children and the elderly. There is usually no gross evidence of the offending parathyroid mass.

Prior to the introduction of routine multichannel biochemical screening in the 1970s, primary HPT typically presented clinically with overt complications such as osteitis fibrosa cystica, nephrolithiasis, nausea, vomiting, or in severe hypercalcemia, obtundation and coma. Now, the majority of patients in western countries are asymptomatic at presentation manifesting only mild hypercalcemia discovered on routine biochemical testing [48].

Fig. 3.26 Dual isotope subtraction study for demonstration of a left parathyroid adenoma (*arrow*). Figures 3.26, 3.27, 3.28, and 3.29 demonstrate localization of parathyroid tumors. Fig. 3.26 is courtesy of Dr. Alan Maurer, Temple University Hospital Philadelphia, PA

Primary HPT is characterized by the finding of an elevated or inappropriately high normal intact PTH level (as measured by immunoradiometric assay) in the setting of hypercalcemia. However, measurement of the 24 h urinary calcium excretion is also performed to distinguish primary HPT from familial benign hypocalciuric hypercalcemia (FBHH). The finding of a fractional excretion of calcium less than 1% is found in FBHH, a benign syndrome requiring no intervention.

The signs and symptoms of primary HPT are related to both increased PTH and hypercalcemia. Moderate to severe hypercalcemia is the main cause of the constipation, pancreatitis, peptic ulcer disease, anorexia, muscle weakness, neourocognitive disturbances, and renal insufficiency. Increased PTH secretion is more directly responsible for the skeletal manifestations and nephrolithiasis [49].

PTH increases bone resorption, affecting cortical bone more than trabecular bone. In countries where primary HPT is diagnosed later, the classic manifestations of osteitis fibrosis cystica, subperiosteal resorption of the phalanges, and brown tumors are common findings.

Radiological Imaging of Parathyroid Tumors

The most accurate study for localization of parathyroid tumors is dual isotope subtraction technique (Fig. 3.26). Tc-99m Sestamibi is first injected to visualize both thyroid and parathyroid glands. Then I-123 is injected to show only the thyroid gland, and finally the thyroid image is subtracted from the Sestamibi image to visualize the parathyroid tumor. Other imaging modalities such as ultrasonography (Fig. 3.27), CT, MRI, or combined imaging (Figs. 3.28 and 3.29) may be used to demonstrate the tumor.

Radiological Manifestations of Well-Established Hyperparathyroidism

The renal manifestations of primary HPT include nephrolithiasis (Fig. 3.30a), nephrocalcinosis (Fig. 3.30b), chronic renal insufficiency, and hypercalciuria. Despite early diagnosis by biochemical testing, up to 17% of cases of primary HPT develop nephrolithiasis [50]. As previously discussed, PTH stimulates increased bone resorption leading to hypercalcemia. Although PTH stimulates distal tubular reabsorption of calcium, the increased in filtered calcium due to hypercalcemia can cause increased urinary excretion of calcium, predisposing to stone formation. PTH also stimulates formation of calcitriol from calcidiol resulting in increased absorption of dietary calcium, which may worsen hypercalcemia and hypercalciuria. Eventually hypercalciuria may produce nephrocalcinosis (Fig. 3.30b) and impaired kidney function.

PTH increases bone resorption, affecting cortical bone more than trabecular bone. In western countries, where less than 2% of patients present with overt skeletal manifestations, the only skeletal manifestation may be decreased bone density on dual-energy X-ray absorptiometry examination preferentially affecting areas richest in cortical bone, such as the distal third of the forearm.

In countries where primary HPT is diagnosed later, the classic manifestations of osteitis fibrosis cystica are seen more commonly. In advanced cases, bone resorption is the major radiologic finding. Subperiosteal resorption

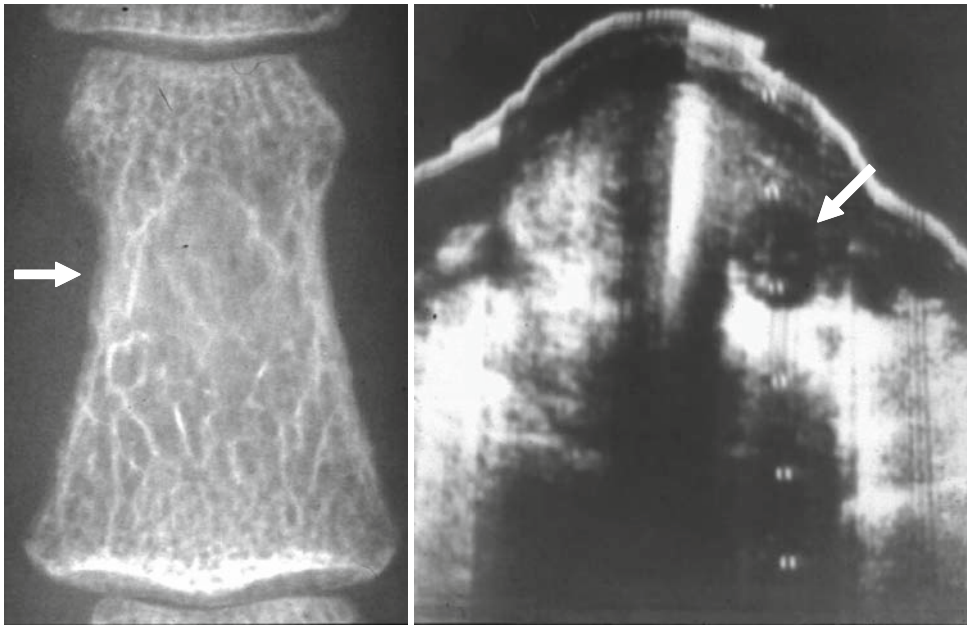

Fig. 3.27 Localization of parathyroid adenoma by ultrasonography. (**a)** shows subperiosteal resorption of the medial border of the middle phalanx of the index of the right hand (*arrow*). (**b)** is ultrasonography demonstrating a parathyroid adenoma in the same patient (*arrow*). Courtesy of Dr. H Amiri

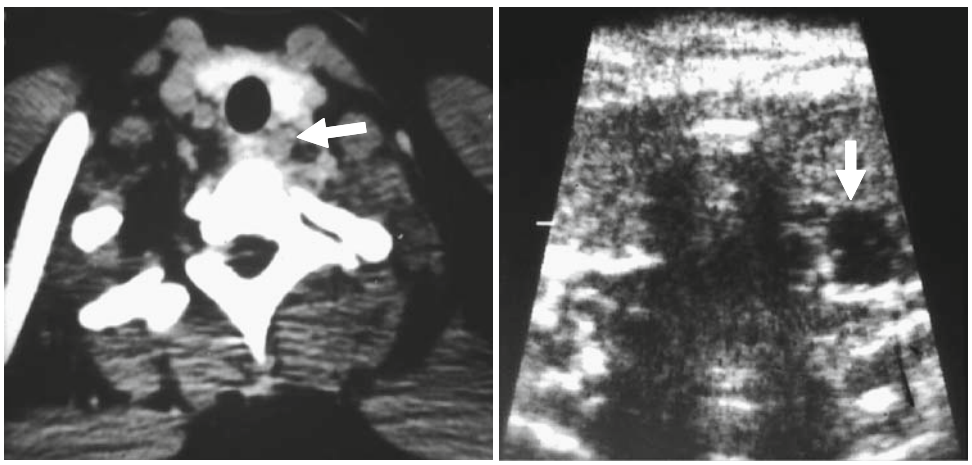

Fig. 3.28 Localization of parathyroid adenoma by CT and US. (**a)** is an axial CT with soft tissue window of the neck showing a left parathyroid adenoma (*arrow*). (**b)** is an ultrasonography of the same patient demonstrating the left parathyroid adenoma (*arrow*)

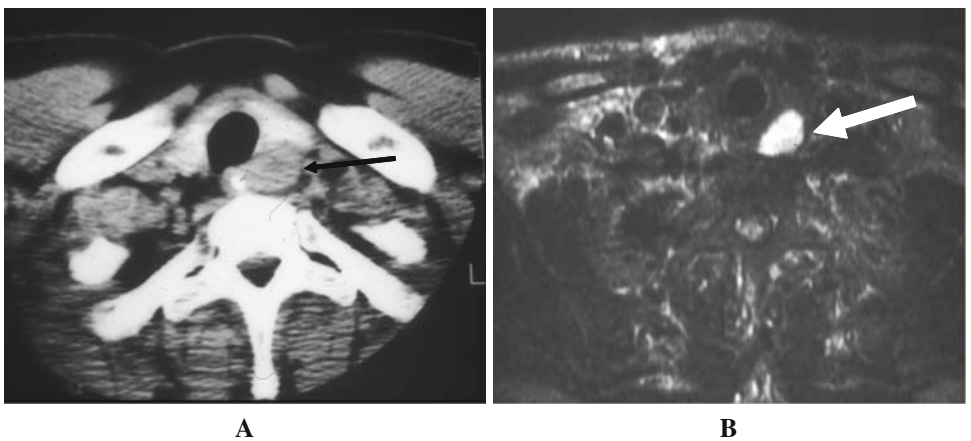

Fig. 3.29 Carcinoma of one of the left parathyroid glands. (**a)** is an axial CT of the neck with soft tissue window and (**b)** is an ultrasonography, both demonstrating a carcinoma of a left parathyroid gland (*arrows*). Courtesy of Dr. Murray K Dalinka, Hospital of the University of Pennsylvania

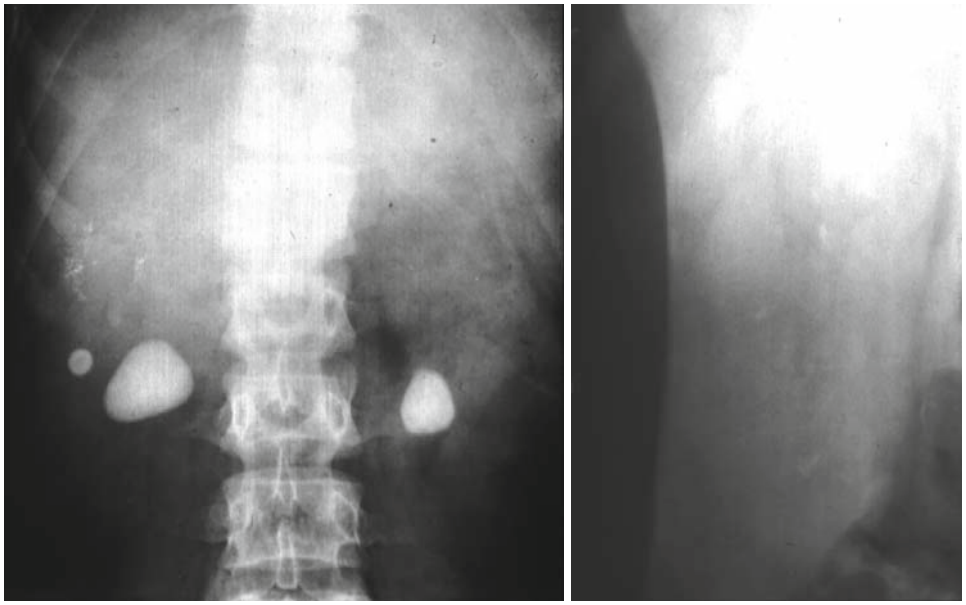

A-kidney stones **B**-Nephrocalcinosis

Fig. 3.30 Hyperparathyroidism. A-H K a 58-year-old female with primary hyperparathyroidism and kidney stones. (**b)** is a different case with hyperparathyroidism and nephrocalcinosis. (**a** and **b)** demonstrate renal complications of hyperparathyroidism

is characteristic of hyperparathyroidism (Figs. 3.31 and 3.32). Furthermore, bone resorption may be intracortical, endosteal (Fig. 3.33, subchondral 3.34 and 3.35), periodontal (Fig. 3.36) or subtendinous.

Osteolytic bone resorption due to PTH-mediated osteoclast activation causes generalized diminished bone density. In the skull, bone resorption produces a "salt-and-pepper appearance" (Fig. 3.37).

Brown tumors may be seen in up to 40% of advanced cases of primary HPT (Fig. 3.38 and 3.39), but are rarely observed in the industrial nations any more. Brown tumors calcify after removal of parathyroid adenoma (Fig. 3.40).

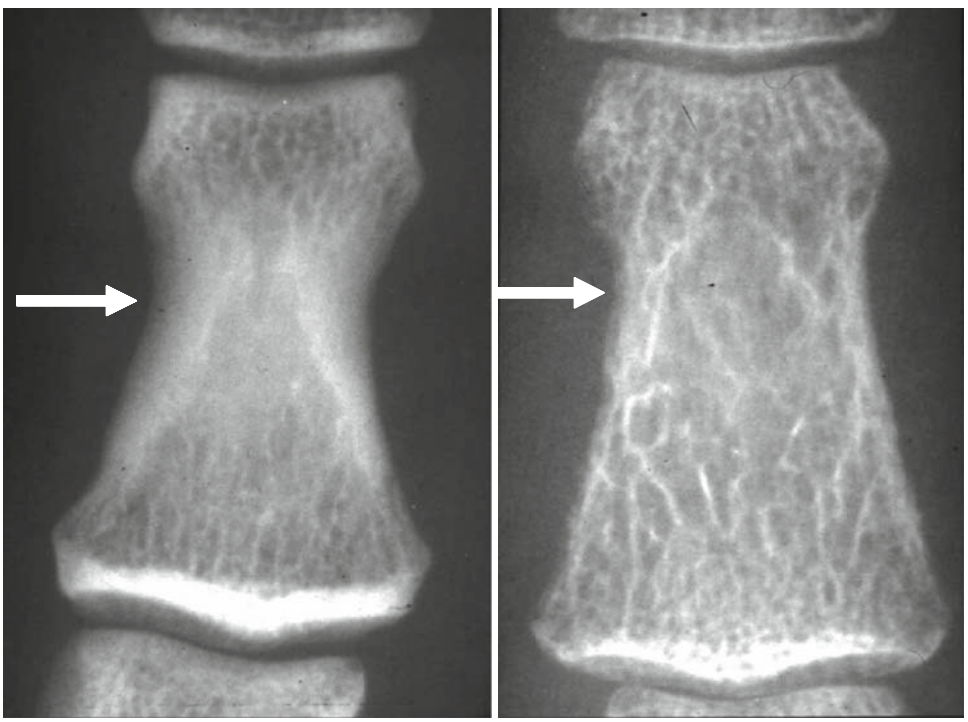

A-Normal cortex **B**-Subperiosteal resorption

Fig. 3.31 Hyperparathyroidism. **(a)** shows the normal appearance of the cortex of the index (*arrow*). **(b)** is demonstrating subperiosteal resorption in hyperparathyroidism (*arrow*)

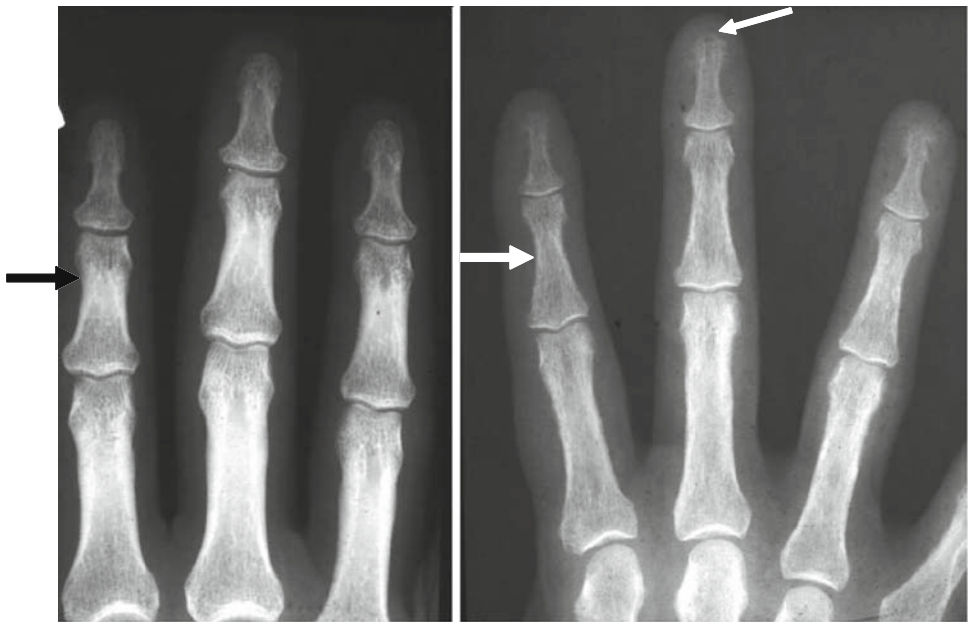

A-Normal **B**-Subperiosteal resorption

Fig. 3.32 Hyperparathyroidism. **(a)** is normal to show the smooth outer border of the normal cortex (*arrow*). (**b**) reveals moderately advanced subperiosteal resorption, most marked in the middle phalanx of the index (*arrow*), but also present to a lesser extent in other fingers. Note also subperiosteal resorption of the ungual tufts (*thin arrow*). Note significant thinning of the cortex which is a non-specific finding in hyperparathyroidism

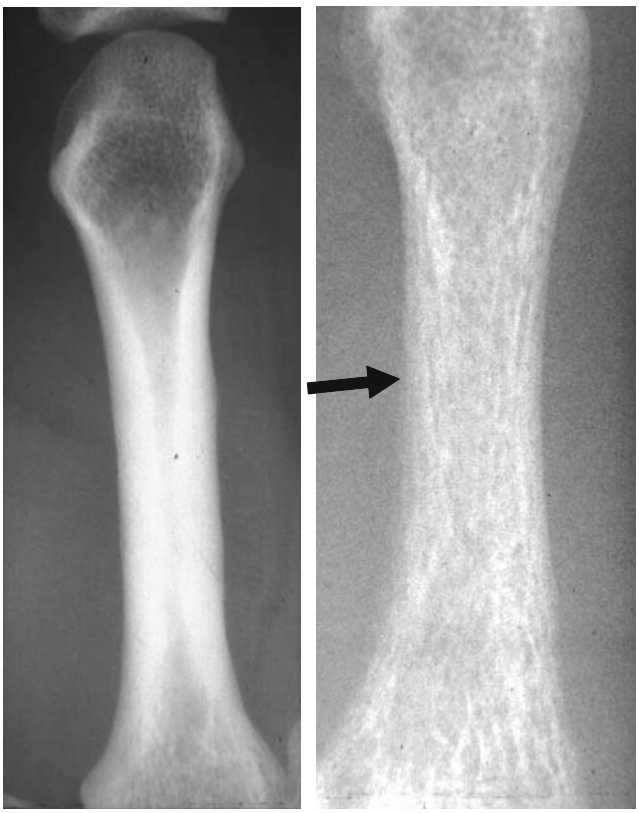

A-Normal cortex **B**-Intracortical resorption (tunneling) and endosteal resorption

Fig. 3.33 Intracortical and endosteal resorption. **(a)** is normal. (**b**) demonstrates intracortical and endosteal resorption. In contrast to subperiosteal resorption, these two types of bone resorption are not specific to hyperparathyroidism

Fractures are also a complication of advanced hyperparathyroidism (Fig. 3.41).

Prognosis: If appropriate criteria for surgical intervention are met, primary hyperparathyroidism may be cured by surgical removal of the hyperfunctioning gland or glands. The standard surgical approach is bilateral neck exploration under general anesthesia [51]. Minimally invasive parathyroidectomy is another approach directed at removing the gland that has been identified as hyperfunctioning on preoperative

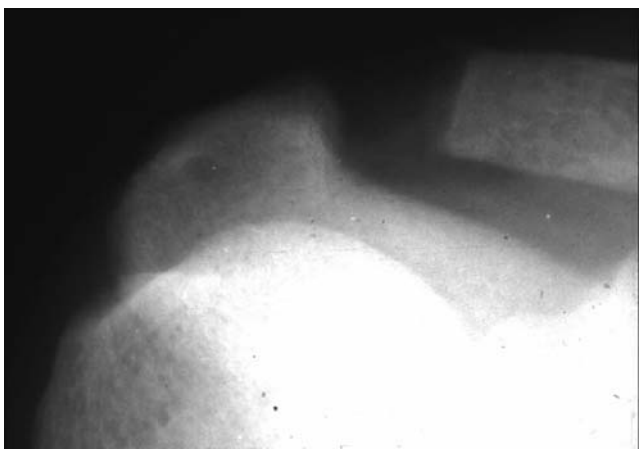

Fig. 3.34 Subchondral resorption of the AC joint. M L, a 27-year-old male with renal osteodystrophy (ROD) due to secondary hyperparathyroidism. Note the presence of osteosclerosis in ROD. We have observed this type of resorption before the appearance of subperiosteal resorption in several cases of ROD. This is also a typical finding in chest radiographs of patients with ROD if associated with bone sclerosis. AC resorption may be seen in other entities, such as RA (bilateral) and gout

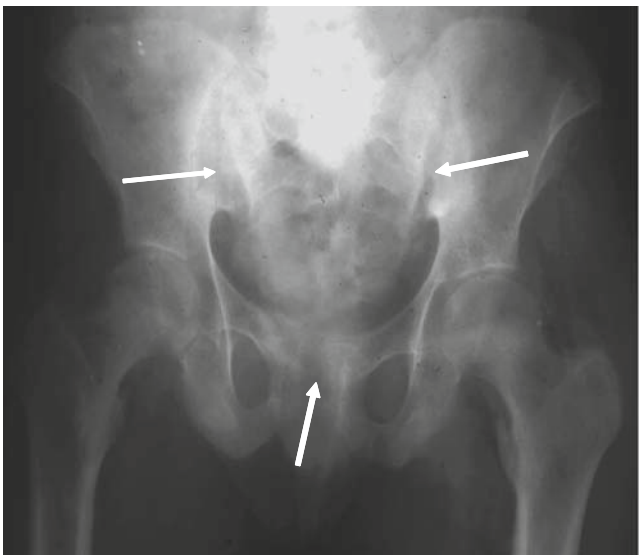

Fig. 3.35 Subchondral resorption SI joints and symphysis pubis. Subchondral resorption is seen in both primary and secondary HPT (*arrows*). It may also develop rarely in advanced RA in 5%.of cases as well as several other entities

parathyroid imaging [52]. Cure rates for both surgical procedures exceed 95% in experienced hands [53–55].

In four-gland hyperplasia, a more aggressive approach is required. Total removal of three glands and removal of ½ of the fourth is recommended. Half of the most normal appearing gland is either left in place marked with a clip or autotransplanted into the forearm.

Secondary Hyperparathyroidism

Secondary HPT is characterized by the persistent elevation of PTH in response to factors extrinsic to the parathyroids. The increased secretion of PTH is an appropriate physiologic response triggered by hypocalcemia in order to maintain normal levels of ionized calcium. Laboratory testing shows low or normal serum calcium and elevated PTH. Depending on the underlying cause, the 25-hydroxyvitamin D level may be low (vitamin D deficiency) or the 1,25-dihydroxyvitamin D level may be low (chronic kidney disease).

The causes of secondary HPT include hypocalcemia, hypovitaminosis D, and chronic renal failure. Chronic renal failure is the most common cause of secondary hyperparathyroidism. The prevalence of chronic renal disease exceeds 13% in US population [56]. Although chronic renal failure is the most common cause of secondary HPT, vitamin D deficiency is a significant worldwide problem that is often unrecognized and underdiagnosed [57].

In the vitamin D deficient state, decreased absorption of dietary calcium and the subsequent fall in ionized calcium stimulates the release of PTH allowing increased resorption of calcium from bone [58]. Chronic vitamin D defi-

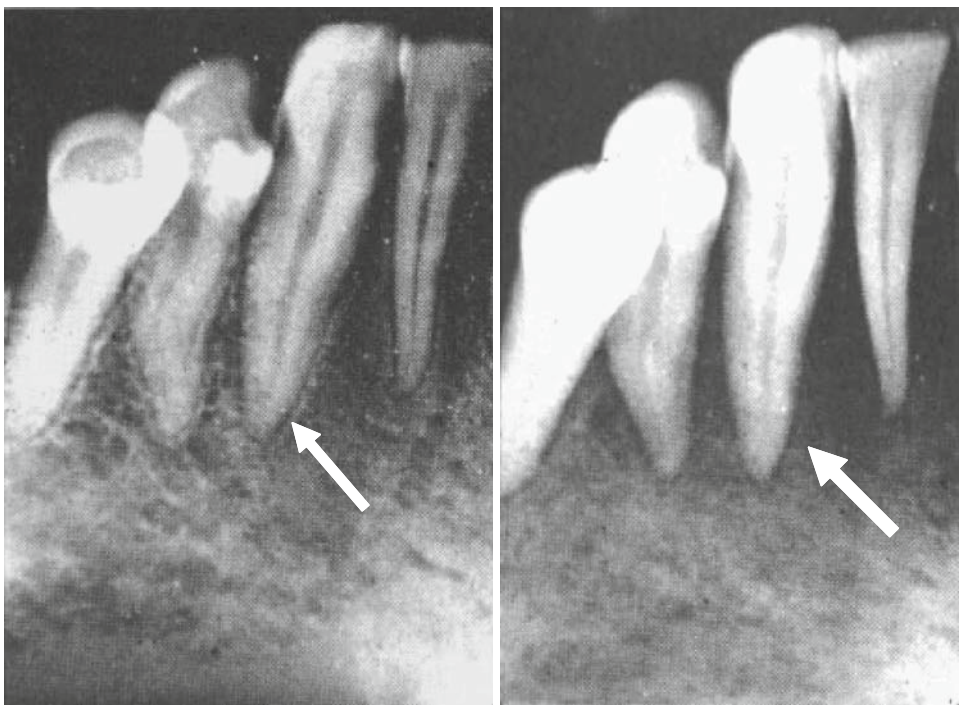

A-Normal lamina dura (arrow)

B-HPT, loss of lamina dura (arrow)

Fig. 3.36 Periodontal resorption. This is a non-specific finding for hyperparathyroidism

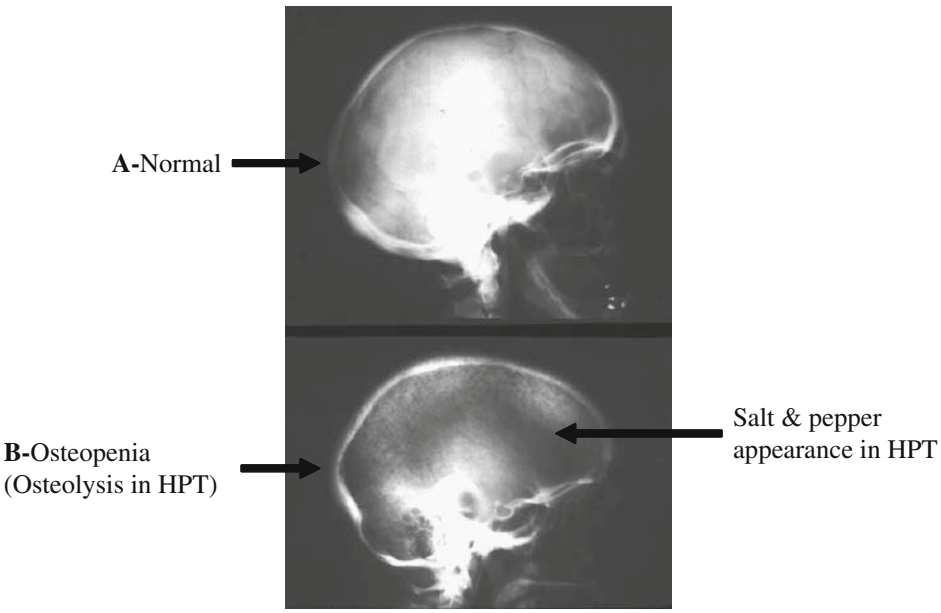

Fig. 3.37 Primary hyperparathyroidism. Salt-and-pepper appearance of the skull. (**a**) normal. (**b**) HPT

ciency causes generalized diminished bone density. Treatment consists of supplementation with vitamin D to achieve an optimal 25-hydroxyvitamin D level of about 30 ng/mL (75 nmol/L) [59, 60].

In renal failure, calcium homeostasis is disrupted by insufficient renal hydroxylation of 25-hydroxyvitamin D to the active form, 1,25-dihydroxyvitamin D. In addition, diminished excretion of phosphorus by the failing kidneys leads to hyperphosphatemia. The calcitriol deficiency and hyperphosphatemia ultimately result in hypocalcemia that directly induces the increased PTH secretion characteristic of secondary hyperparathyroidism due to renal disease [61]. The serum calcium levels are low or normal in secondary HPT due to renal disease in contrast to tertiary hyperparathyroidism described below.

Medical management of the secondary HPT of renal disease consists of phosphate binders to lower serum phosphorous levels, active vitamin D analogs, and/or calcimimetics (agents that increase the sensitivity of the calcium-sensing receptor to calcium and suppress PTH secretion). Left untreated, renal osteodystrophy and/or tertiary hyperparathyroidism may develop. Adynamic bone disease and

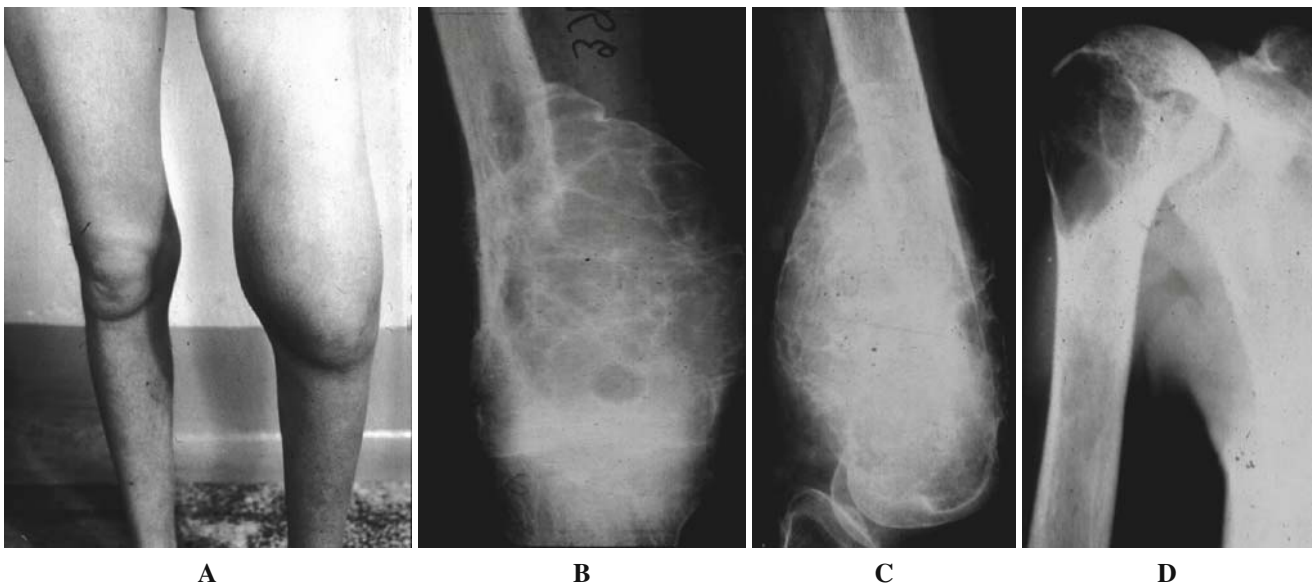

Fig. 3.38 Brown tumors in primary HPT. (**a**) Photograph of a brown tumor above the left knee. (**b** and **c**) AP and lateral radiographs of the brown tumor. (**d**) Radiograph of another brown tumor of the right upper humerus, in the same patient

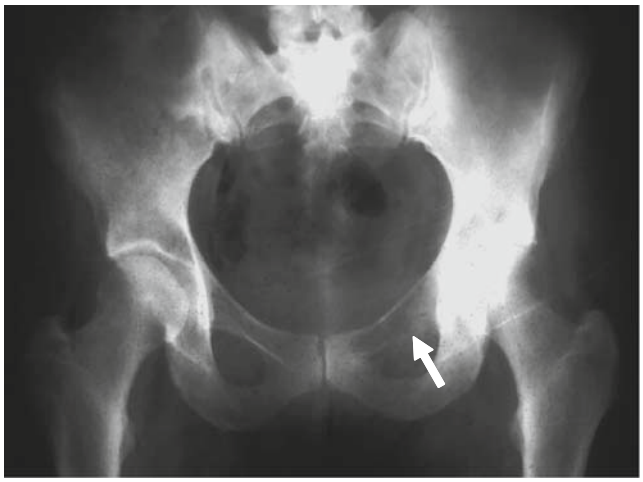

Fig. 3.39 Brown tumor with aggressive appearance. This is a 53-year-old female with brown tumor of the superior ramus of the left pubic bone showing an aggressive appearance (broad zone of transition and cortical erosion of the inferior border of the bone (*arrow*) in a patient with primary HPT)

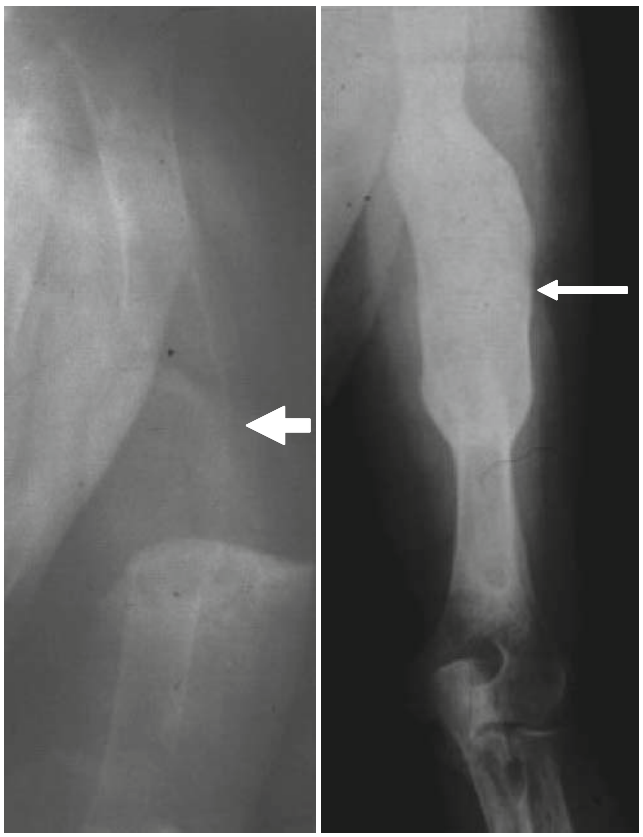

A **B**

Fig. 3.40 Brown tumor of the left humerus. (**a)** is before (*short arrow*) and (**b)** is after removal of a parathyroid adenoma (*long arrow*). Note remarkable regeneration of the bone after surgery. Courtesy of Professor Fridrick Heuck, Stuttgart, Germany

osteomalacia are sequelae of the medical treatment of secondary HPT due to renal disease.

Tertiary Hyperparathyroidism

Tertiary HPT is a state of excessive PTH secretion that results in hypercalcemia. The most common causes of tertiary HPT are secondary HPT of chronic kidney disease that is refractory to treatment, or persistent HPT following renal transplantation [62]. After prolonged periods of secondary HPT, the hypertrophied parathyroid glands may no longer respond appropriately to calcium and calcitriol levels. The excessively high PTH level leads to hypercalcemia and renal osteodystrophy. Treatment requires subtotal parathyroidectomy or total parathyroidectomy with autotransplantation.

Miscellaneous Causes of Hyperparathyroidism

The humoral hypercalcemia of malignancy is caused by the secretion of PTH-related protein (PTH-rP) by malignant neoplasms. PTH-rP has the same systemic effects as PTH and produces a clinical picture of hyperparathyroidism. Ectopic secretion of authentic PTH is a very rare cause of hypercalcemia associated with some malignant tumors causing ectopic or pseudohyperparathyroidism [63] (Figs. 3.42 and 3.43).

Primary Infantile Hyperparathyroidism

This is a rare entity. Without treatment (parathyroidectomy) no survival is reported [64, 65]. After parathyroidectomy the infants reveal a significant improvement in the skeleton (Figs. 3.44, 3.45, and 3.46).

Renal Osteodystrophy

Renal osteodystrophy is the term used to define bone morphology alterations observed in chronic kidney disease including osteitis fibrosa cystica, osteomalacia, and adynamic bone disease. With advances in dialysis and renal transplantation, the longevity of patients with chronic renal failure has increased and renal osteodystrophy is observed more frequently.

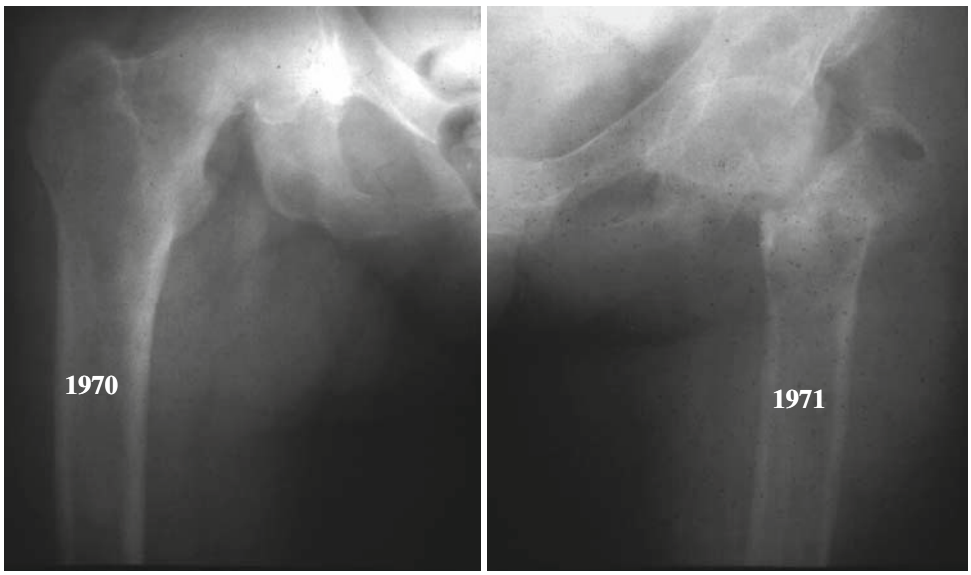

Fig. 3.41 Ectopic mediastinal parathyroid adenoma. R L, a 53-year-old female, follow-up 1970 and 1971 with very high parathormone levels. In second and third exploration of her neck no parathyroid adenoma was found. Blood samples of the peripheral vein, as well as superior and inferior venae cavae, revealed very high parathormone level in the superior vena cava. A mediastinal adenoma was removed. Clinical follow-ups showed a remarkable recovery

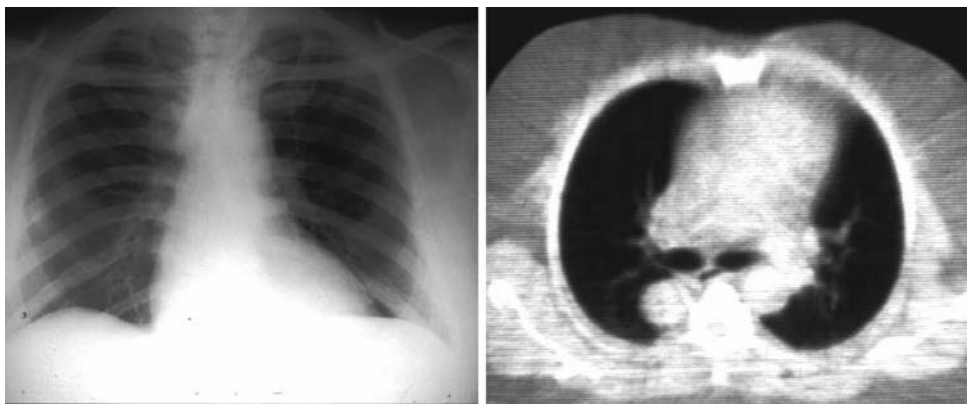

Fig. 3.42 Pseudohyperparathyroidism (ectopic hyperparathyroidism) secondary to pulmonary malignancy. This was a 53-year-old man that revealed clinical and laboratory findings similar to HPT. This was related to a right upper lobe tumor producing parathormone-like peptides

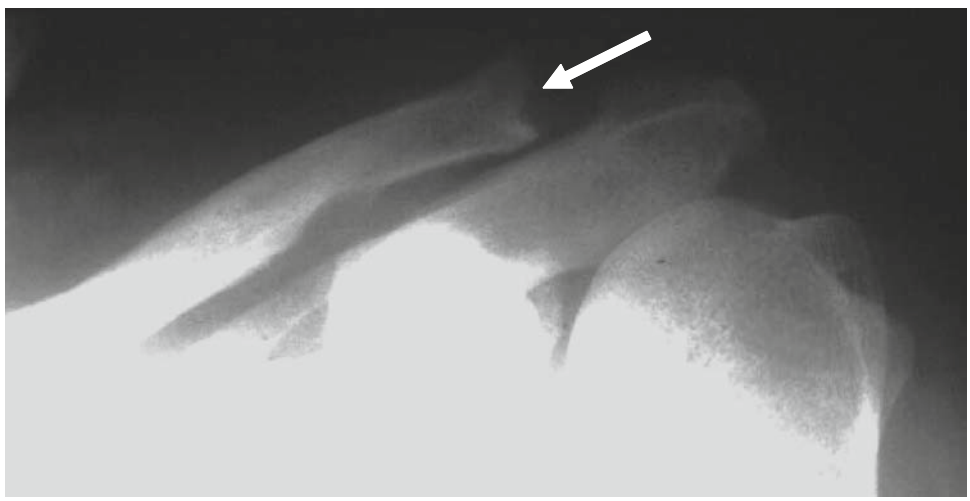

Fig. 3.43 Ectopic or pseudohyperparathyroidism. The same case as before revealing subchondral resorption of the clavicle related to pseudohyperparathyroidism secondary to pulmonary malignancy. Note subchondral resorption of the distal clavicle (*arrow*)

Osteomalacia in Renal Osteodystrophy

Osteomalacia is characterized by low bone turnover and defective mineralization resulting in increased unmineralized bone. The osteomalacia associated with chronic kidney disease differs from that caused by vitamin D deficiency in that most cases are the result of aluminum intoxication associated with the treatment of end-stage renal disease. The incidence

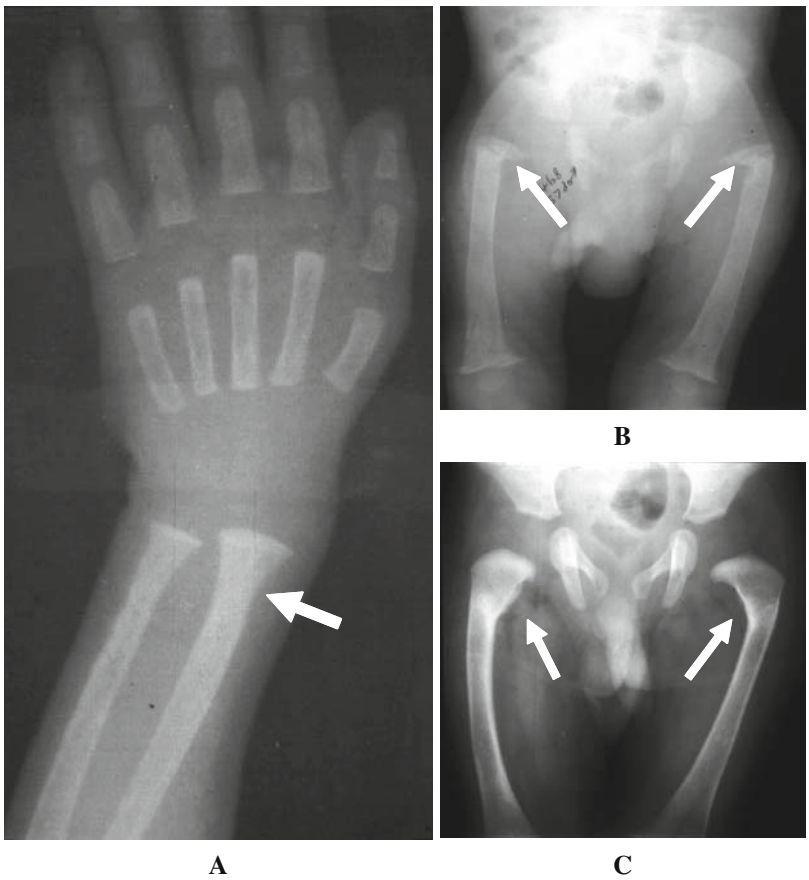

Fig. 3.44 This is a 37-day-old boy with neonatal hyperparathyroidism. **(a)** hand and (**b**) pelvis of this patient with neonatal hyperparathyroidism related to a parathyroid adenoma. Note subperiosteal resorption of radius and medial proximal femurs (*arrows*). **c** shows significant improvement, 4 months after removal of the parathyroid adenoma (*arrow*). Courtesy of Dr. F Eftekhari, MD Anderson Hospital, Houston, Texas

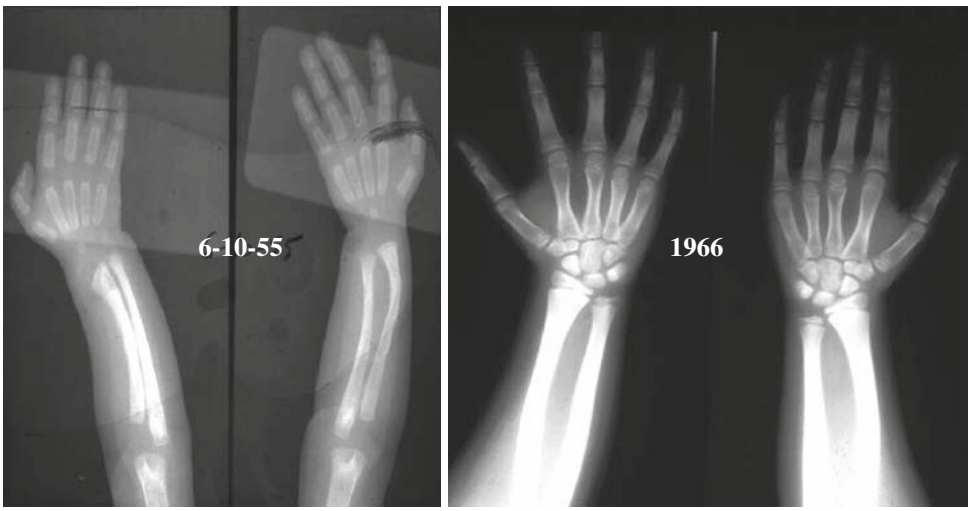

Fig. 3.45 Infantile hyperparathyroidism, **(a)** is in 1955 before parathyroid surgery and (**b**) is in 1966 after surgery. There is a significant improvement. Courtesy of Dr. Farzin Eftekhari, MD, Anderson Hospital, Houston, Texas

of osteomalacia in chronic kidney disease has fallen since aluminum-containing antacids are now rarely used to bind dietary phosphate [66].

Common radiologic findings in osteomalacia are decreased bone density, a coarse trabecular pattern seen early in the disease, cortical striations, and later, cortical thinning. Bone deformities may cause changes in the pelvis, spine, legs, chest, and skull. Looser zones or Milkman syndrome is uncommon in renal osteodystrophy and is seen in less than 1% of cases. Osteomalacia of renal osteodystrophy causes widening of the epiphyseal plate, irregularity and concavity of the metaphyses, and deformity of bones that is similar to nutritional rickets. Delayed growth may also be present. In contrast to nutritional osteomalacia, most patients with renal osteodystrophy have osteosclerosis [67, 68].

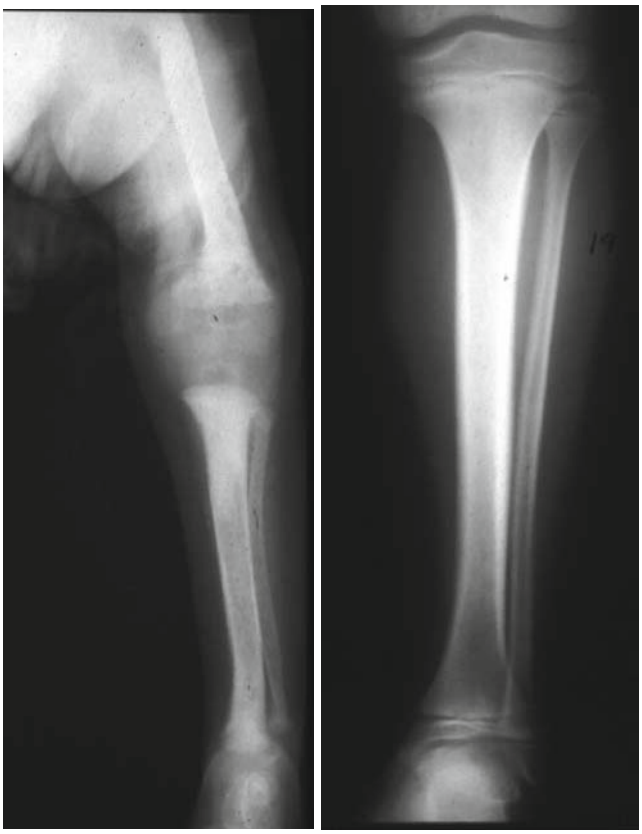

A B

Fig. 3.46 Infantile hyperparathyroidism, same case as in Fig. 3.45. **(a)** is in 1955 before parathyroid surgery and (**b**) is in 1966 after surgery. There is a significant improvement. Courtesy of Dr. Farzin Eftekhari, MD Anderson Hospital, Houston, Texas

Osteitis Fibrosa Cystica

The pathophysiology of secondary HPT in chronic kidney disease is described above. Skeletal changes in secondary HPT are very similar to the primary type but there are some distinguishing differences. Brown tumors are rare in secondary form, but are being reported with increasing frequency. In secondary HPT, soft tissue calcifications are more common than in the primary type. Periosteal reaction and osteosclerosis are seen in secondary HPT [68–71].

Radiological Abnormalities in Secondary Hyperparathyroidism Due to Chronic Renal Failure

Imaging of primary HPT has been described in detail earlier in this chapter. Although several modalities such as scintigraphy, MRI, and quantitative imaging are available, plain digital radiography with magnification available in PACS is still a practical and most widely used examination [71] in the diagnosis and follow-up of renal osteodystrophy.

The radiological findings in secondary HPT are similar to those of primary HPT. The main features will be described briefly as follows:

1. Bone resorption
2. Osteopenia
3. Osteosclerosis
4. Periosteal reaction
5. Joint abnormalities
6. Soft tissue calcifications
7. Brown tumors
8. Fractures and slipped epiphyses

1. *Bone resorption*: Bone resorption may be subperiosteal, intracortical, endosteal, subchondral, periodontal, or subtendinous. Subperiosteal resorption is pathognomonic of HPT, in both the primary and secondary forms. The most common sites of involvement are the middle phalanges of the hands and ungual tufts (Fig. 3.47). The third most common site of subperiosteal resorption is the upper medial border of tibia (Fig. 3.48). It may be seen in the upper femur, upper humerus, distal radius, and upper and lower borders of ribs.

   Subchondral resorption is most commonly seen in the acromioclavicular and sacroiliac joints. It is more prominent in the distal ends of the clavicles (Fig. 3.49) and the iliac bones. Subchondral resorption may be seen in other joints such as the symphysis pubis and sometimes in the synovial joints. Periodontal resorption is manifested by loss of lamina dura and may be seen in a number of other diseases.

   Subtendinous and subligamentous resorption are observed at the sites of tendon and ligament attachments to bone such as the lesser and greater trochanters of the femur, the ischial tuberosities (Fig. 3.50), and the posterior superior calcaneus.
2. *Osteopenia*: Osteopenia (diminished bone density) may be one of the features of ROD. It is probably a combination of osteoporosis, osteomalacia, and osteolysis (secondary HPT). Radiographs reveal decreased density, cortical thinning, and coarsening of the trabecular pattern (Fig. 3.48). The skull may have a salt-and-pepper appearance. Basilar invagination has been reported.
3. *Osteosclerosis*: Osteosclerosis is a common radiologic finding in renal osteodystrophy due to secondary HPT. It may involve the base of the skull, the ribs, and the pelvic bones. In the vertebral bodies, it produces the typical appearance of "rugger jersey" spine (Figs. 3.51 and 3.52). Occasionally osteosclerosis may be focal (Fig. 3.52c). In reporting cases of ROD, osteosclerosis must not be overlooked. With careful examination of bones, even in the distal extremities, osteosclerosis often can be detected.

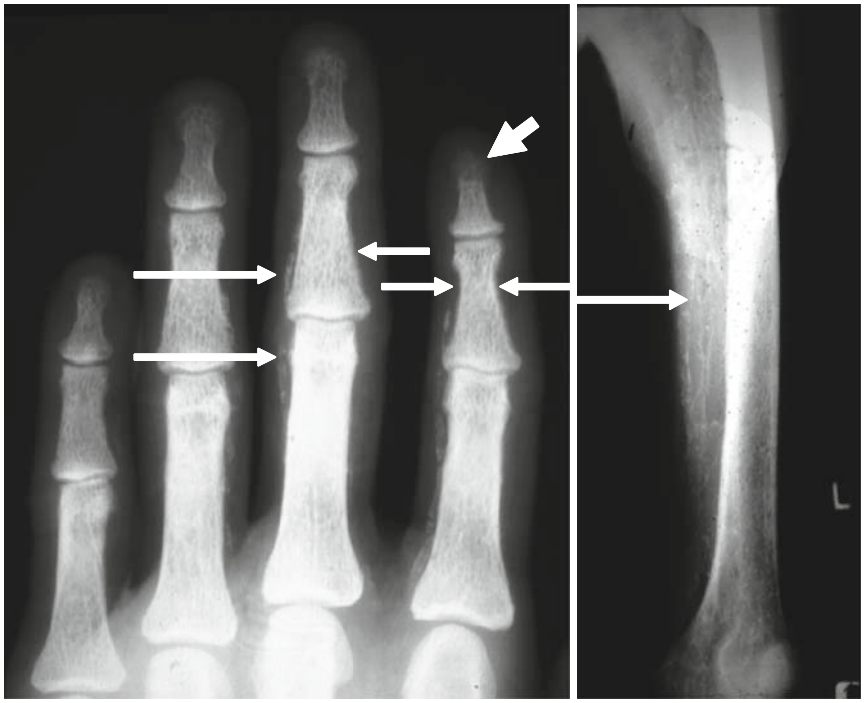

A **B**

Fig. 3.47 Subperiosteal resorption and arterial calcification. **(a)** This patient is a 29-year-old male undergoing hemodialysis for chronic renal disease revealing subperiosteal resorption of the middle phalanges of the second and third digits (*arrows*), as well as the ungual tufts (*short arrow*). (**a** and **b)** demonstrate arterial calcification in these two different cases of ROD due to secondary HPT (*long arrows*)

4. *Periosteal reaction*: Periosteal reaction is most common in the metatarsals, pelvis, femur, and humerus [68–71]. Rarely seen in primary HPT, it simulates changes of hypertrophic osteoarthropathy. It appears solid with a linear lucency between the periosteal reaction and the outer border of the cortex (Fig. 3.53). If associated with joint abnormalities, it may be justified to use the term hypertrophic renal osteoarthropathy. The irregular surface of subperiosteal resorption may simulate periosteal reaction (pseudoperiostitis) [69] and should not be confused with true periosteal reaction.
5. *Joint abnormalities*: Joint abnormalities in secondary HPT may be manifested as periarticular calcification, erosive arthritis, chondrocalcinosis, and crystal deposition disease [69].

   Periarticular calcification (Fig. 3.54c and d) is common in secondary HPT and is related to deposition of hydroxyapatite crystals. Chondrocalcinosis is more often seen in primary HPT because of deposition of calcium pyrophosphate dehydrate (CPPD) crystals. Occasionally monosodium urate deposition may cause secondary gout in ROD (Fig. 3.55).

   Erosive arthritis is similar to rheumatoid arthritis (Fig. 3.54a, b). It may be seen in large joints and should not be mistaken for infection. Amyloidosis (Figs. 3.56 and 3.57) and erosive spondyloarthropathy (Fig. 3.58) will be discussed later as complications of long-standing hemodialysis.
6. *Soft tissue and arterial calcification*: Soft tissue (Fig. 3.55) and arterial calcification (Fig. 47b) occurs when the product of plasma calcium and phosphorus level is persistently higher than 75 mg/dL and is uncommon when it is under 70 mg/dL [69]. Calcifications may occur at various locations including periarticular, arterial (Fig. 3.47b), ocular, cutaneous, subcutaneous, and visceral.

   Soft tissue (Fig. 3.55) and periarticular calcifications (Fig. 3.54c and d) consist of hydroxyapatite crystals with a molar ratio of Ca:Mg:P of 30:1:18. Visceral calcification has a higher magnesium concentration and cannot be detected on radiographic examination. Periarticular calcifications are amorphous and similar to tumoral calcinosis. Fluid–fluid levels may be demonstrated in MRI and CT scan within these multifocal fluffy calcifications. The differential diagnoses of periarticular calcifications are tumoral calcinosis, hypervitaminosis D, scleroderma, CREST, and milk alkali syndrome. Arterial calcification is medial and intimal in location [69].
7. *Brown tumors*: In the past, brown tumors were rare in secondary HPT, but with advancements in treatment and increased longevity of the patients with chronic kidney disease, they are being observed more frequently (Figs. 3.59 and 3.60). Some cases of reported brown tumors (without biopsy) in renal osteodystrophy may be related to amyloidomas.

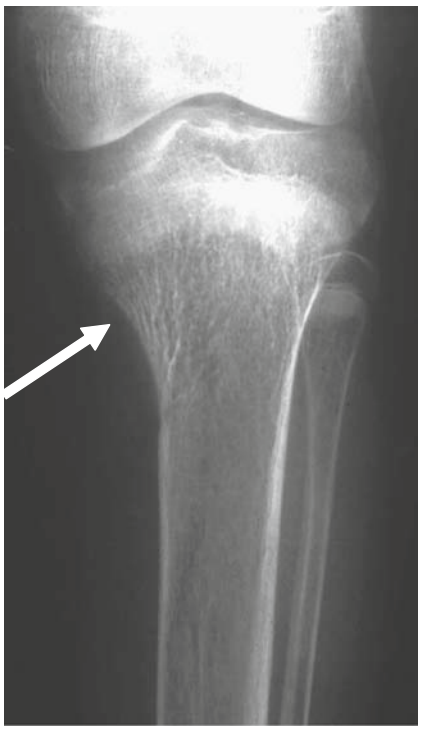

Fig. 3.48 Female 14, with ROD and secondary hyperparathyroidism and osteopenia. There is subperiosteal resorption along the medial border of the upper tibia. This is the third most common site of subperiosteal resorption in both primary and secondary HPT. Note osteopenia (diminished bone density) manifested by cortical thinning and coarsening of the trabecular pattern

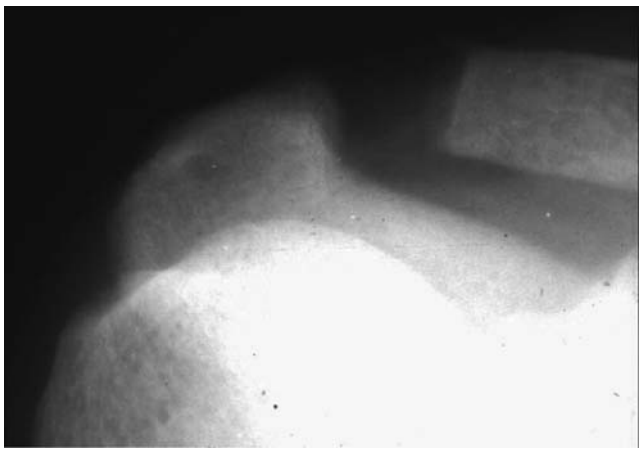

Fig. 3.49 Shows subchondral resorption of the AC joint mainly in distal clavicle, in a 27-year-old male, with ROD and secondary hyperparathyroidism. Note the association of osteosclerosis with bone resorption. Sometimes this type of resorption is manifested before the appearance of subperiosteal resorption in hands. It is also a typical bilateral finding in chest radiographs of patients with ROD. AC resorption may be seen in other entities, such as RA (bilateral) and gout without osteosclerosis

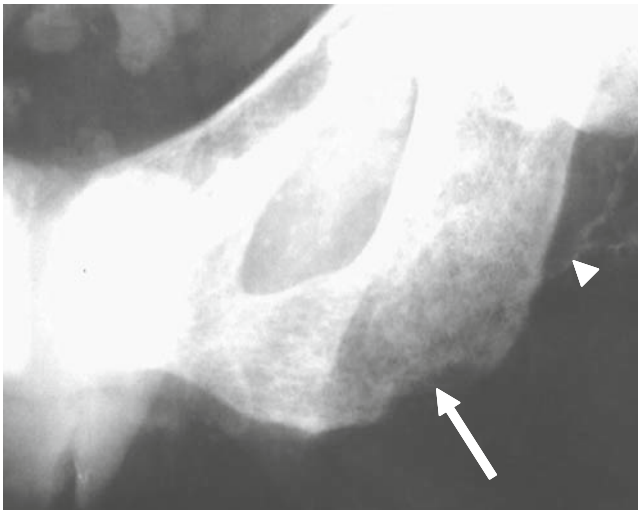

Fig. 3.50 Subtendinous resorption. This is a 55-year-old female with secondary hyperparathyroidism (ROD) revealing subtendinous resorption of ischial tuberosity (*arrow*). Note associated osteosclerosis and arterial calcification (*arrow head*)

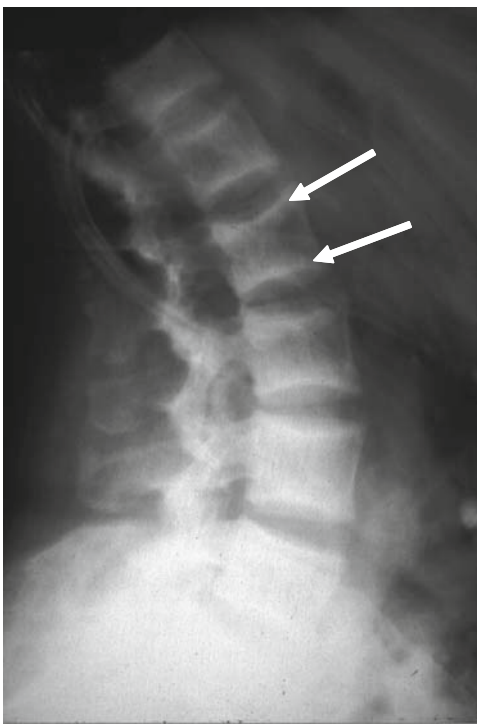

Fig. 3.51 Osteosclerosis. osteosclerosis is a prominent feature of renal osteodystrophy. The best characteristic example of osteosclerosis is the Rugger jersey spine, in which the superior and inferior portions of vertebral bodies reveal increased density (*arrows*)

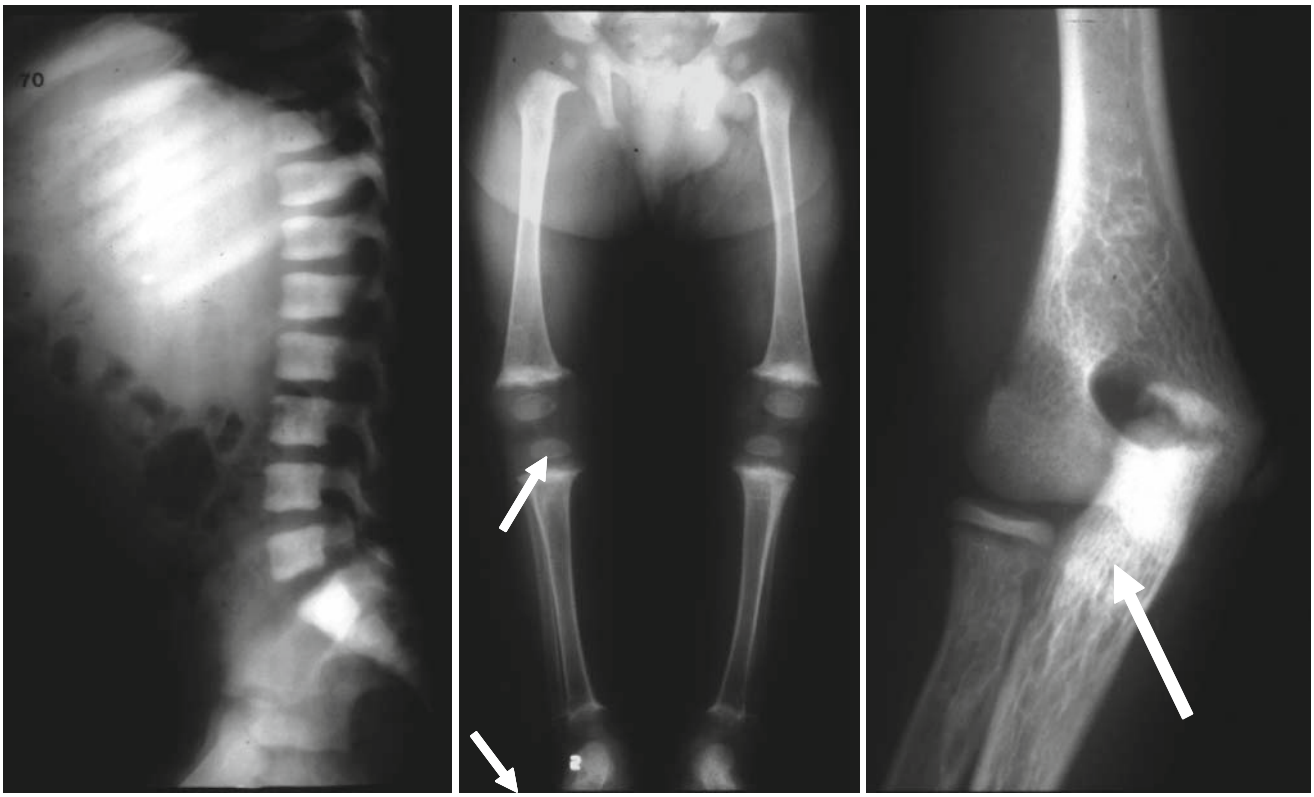

Fig. 3.52 Osteosclerosis. (**a**) is lateral thoracolumbar radiograph in a child with ROD. There is diffuse osteosclerosis which is more prominent in the superior and inferior vertebral bodies (rugger jersey spine). (**b**) is AP radiograph of the lower extremity of the same child revealing marked increased density of metaphyses (*arrows*). (**c**) is a different ROD patient showing focal osteosclerosis of the upper ulna (*long arrow*)

8. *Fractures*: Fractures are most common in the ribs and vertebral bodies [69]. Metaphyseal fractures causing slipped epiphyses are complications of ROD in children (Fig. 3.61). Spontaneous fractures are also more common in dialysis patients.

Benefits and Complications of Treatment of End-Stage Renal Disease

Dialysis and renal transplantation are the major forms of treatment of end-stage chronic renal failure. They both are very beneficial, but both also create their own specific complications. Widespread availability of renal dialysis and renal transplants has meant longer survival for patients with renal failure.

Dialysis

Although dialysis performs many of the functions of the failing kidneys, it does not prevent the secondary hyperparathyroidism of renal failure, or address the loss of the conversion of vitamin D to the active form. Hence, renal osteodystrophy has become more common in the current era, because improved survival subjects the skeletal system to the systemic effects for years to decades. Awareness of this problem has led to improved monitoring and therapy of renal dialysis patients. Medical management of the secondary hyperparathyroidism with phosphate binders to lower serum phosphorous levels, active vitamin D analogs, and/or calcimimetics has improved significantly. Renal osteodystrophy may improve (Fig. 3.62) or advance during dialysis (Fig. 3.63a–c).

Aluminum Toxicity

In the past aluminum toxicity occurred from aluminum in dialysate, causing "dialysis bone disease" that is also called "dialysis osteomalacia" or "aluminum-related osteomalacia." Dialysis bone disease is no longer seen with improved techniques of hemodialysis. However, aluminum toxicity continues to be a problem due to the ingestion of aluminum salts in the form of phosphate-binding antacids used to treat

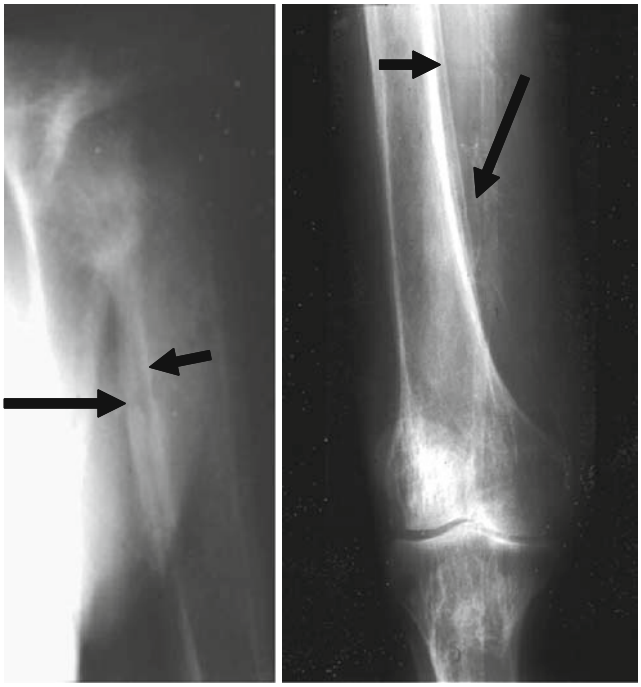

A B

Fig. 3.53 Periosteal reaction**:** Solid periosteal reaction (*arrows*) is more often seen in secondary hyperparathyroidism of ROD than in primary HPT. (**a)** humerus and (**b)** femur (*black arrows*). This is similar to hypertrophic osteoarthropathy. A thin radiolucency is present between the periosteal reaction and the outer border of the cortex (*short arrows*). Note arterial calcification in the lower leg

hyperphosphatemia in chronic renal failure. The incidence of osteomalacia in chronic kidney disease has fallen since aluminum-containing antacids are now rarely used to bind dietary phosphate [66]. Aluminum osteomalacia and rickets may cause rib, vertebral, proximal femoral, and other tubular bone fractures. The occurrence of three or more fractures in the absence of trauma is highly suggestive of aluminum toxicity [70].

Amyloidosis

Another complication of renal dialysis is development of amyloidosis. Dialysis can cause accumulation of beta-2 microglobulin (beta2 M) in the serum that can be deposited in the periarticular soft tissues, joint capsule, cartilage, intervertebral disc, and bones [70, 72]. Deposition in the joints may cause erosive arthritis. Common sites of involvement are shoulder (Fig. 3.56), hip (Fig. 3.57) and wrist as well as the spine. In the wrist it may cause carpal tunnel syndrome and in the spine causing destructive spondyloarthropathy (Fig. 3.58). In majority of patients amyloidosis decreases or even disappears after renal transplantation [72].

Destructive Spondyloarthropathy (DSA)

In long-standing dialysis of more than 10 years, destructive spondyloarthropathy (DSA) may develop. DSA is related to

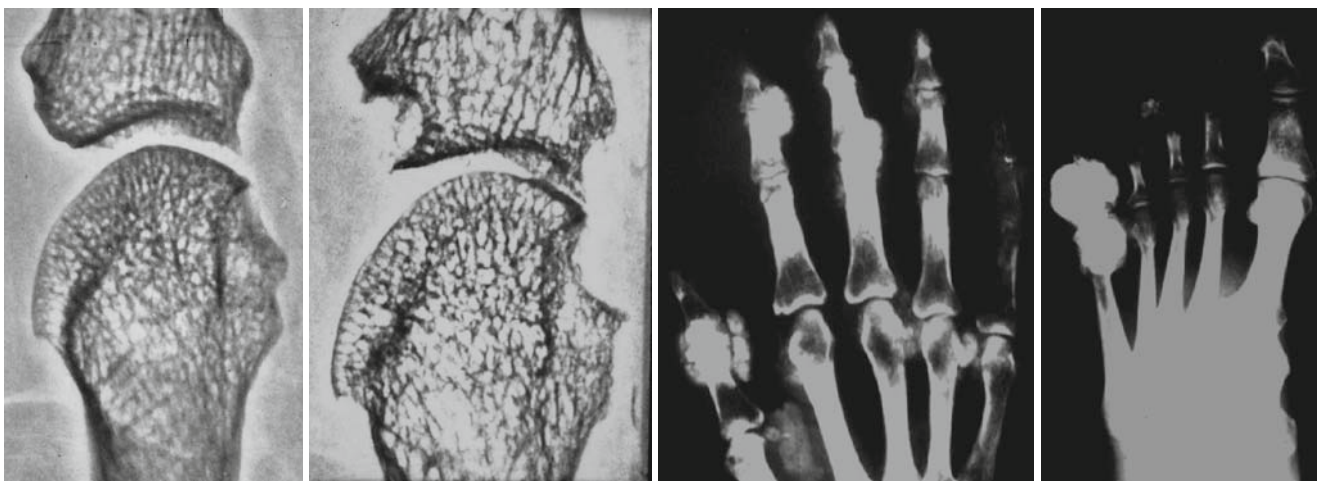

A B C D

Fig. 3.54 Joint abnormalities. **(a)** represents the right second metacarpophalangeal joint of a 61-year-old female with secondary HPT (ROD). There is minimal juxta articular erosion on the ulnar side of the metacarpal. (**b)** is the same joint 2.5 years later, while undergoing hemodialysis with advancement of ROD. Erosion of the metacarpal has increased in size and in addition medial and lateral erosions have developed in proximal phalanx. (**c** and **d)** belong to a different case of secondary HPT due to ROD. Significant Periarticular calcification is present in hand and foot. In primary HPT joint calcification is usually in form of chondrocalcinosis, but in ROD fluffy periarticular calcifications are present which have a similar appearance to idiopathic tumoral calcinosis

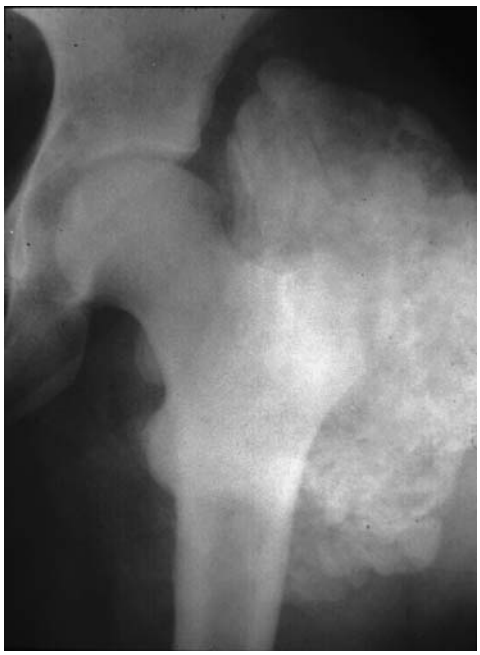

Fig. 3.55 Soft tissue calcification. A large non-uniform soft tissue calcification is present adjacent to the greater trochanter of the left femur in this patient with ROD. There is marked diffuse osteosclerosis. In CT and MRI (not shown here) fluid–fluid levels can be demonstrated in these fluffy calcific densities. Lack of trabeculations and absence of cortical bone, in addition to osteosclerosis exclude the possibility of myositis ossificans

a number of factors including amyloidosis, secondary HPT, and crystal deposition [70].

DSA should be differentiated from infectious spondylitis, which is also a complication of chronic renal disease. Both DSA and infection cause bone destruction of vertebral bodies adjacent to involved disc space. Both reveal sclerotic margins, but in DSA (Fig. 3.58a, b) sclerotic borders have a serrated appearance. In infectious spondylitis the sclerotic margin has a smoother border. In contrast to infection, DSA often has multi-level involvement and bony bridging is absent or minimal (Fig. 3.58a, b). MRI of the spine in DSA reveals low or isointense signal intensity of intervertebral disc spaces, compared to normal disc spaces in both T1 and T2 images (Fig. 3.58c, d), but infection shows increased signal intensity in T2-weighted images.

Renal Transplantation

The progression of renal osteodystrophy following renal transplant is intimately related to the condition of bone at the time of renal transplantation, the success of the transplanted organ and, of course, the age of the patient. Osseous changes due to osteomalacia, and to some extent, those related to secondary HPT may improve after transplantation (Figs. 3.63d and 3.64), but osseous deformities may remain unchanged (Fig. 3.63d).

Persistent secondary HPT, tertiary HPT, post-transplant osteoporosis, pain in the distal extremities known as "symmetric bone pain syndrome," spontaneous femoral head necrosis, and localized osteonecrosis are common complications of renal transplantation.

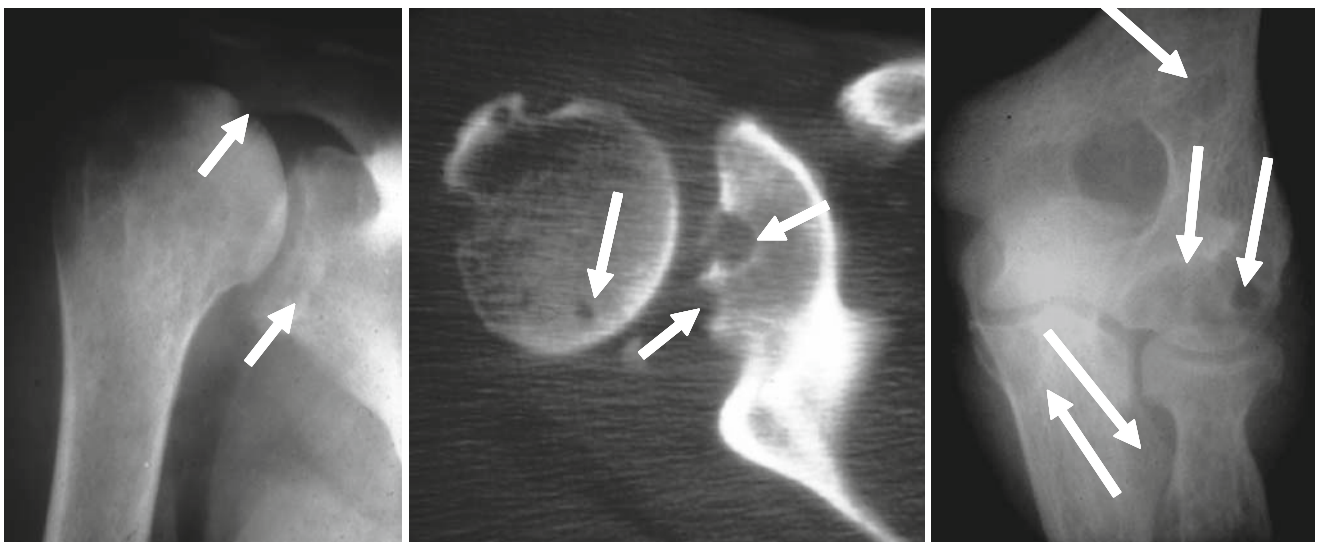

A B C

Fig. 3.56 Amyloidosis. This is a 74-year-old female with a 10-year history of hemodialysis for treatment of CRI. (**a)** is AP radiograph, (**b)** is CT of the right shoulder and **c** is AP radiograph of the right elbow. Note amyloidomas, related to deposition of beta-2 gammaglobulin, that at the articular surface cause erosions (*arrows*) and in the bone cause lucencies which should not be confused with brown tumors (*long arrows*)

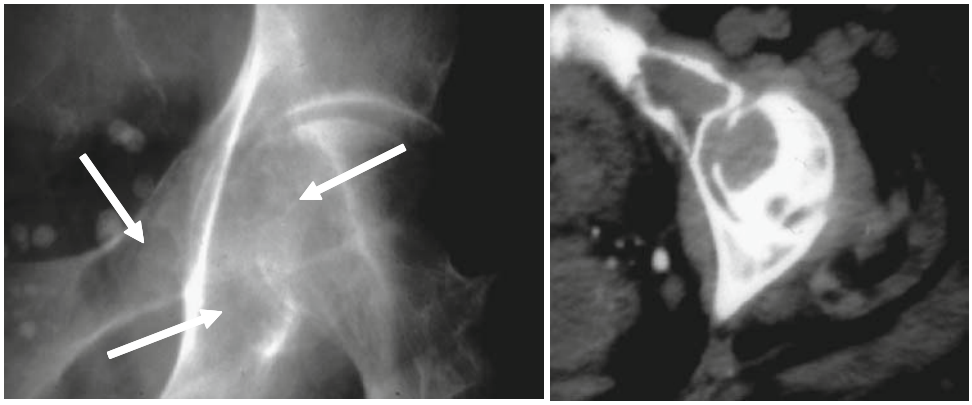

A B

Fig. 3.57 Amyloidomas. **(a)** radiograph and **(b)** CT of the left hip of an 80-year-old female with secondary HPT due to ROD demonstrating biopsy-proven amyloidomas (*arrows*)

Persistent Secondary HPT

After successful renal transplantation, hyperparathyroidism may persist in up to 30–50% of patients [73]. Parathyroid hyperplasia may be so great that it takes months to years for the glands to involute after transplant [74]. In some cases, monoclonal expansion can lead to autonomous PTH secretion and tertiary hyperparathyroidism [75, 76].

Ischemic Necrosis

A common complication of renal transplantation is ischemic necrosis which occurs in 5% of post-transplant patients. The femoral head (Fig. 3.65) is the most commonly affected site [69–72]. The incidence of osteonecrosis of the proximal femur has declined from 15% in the past to 4.8% at present [72]. Although the exact

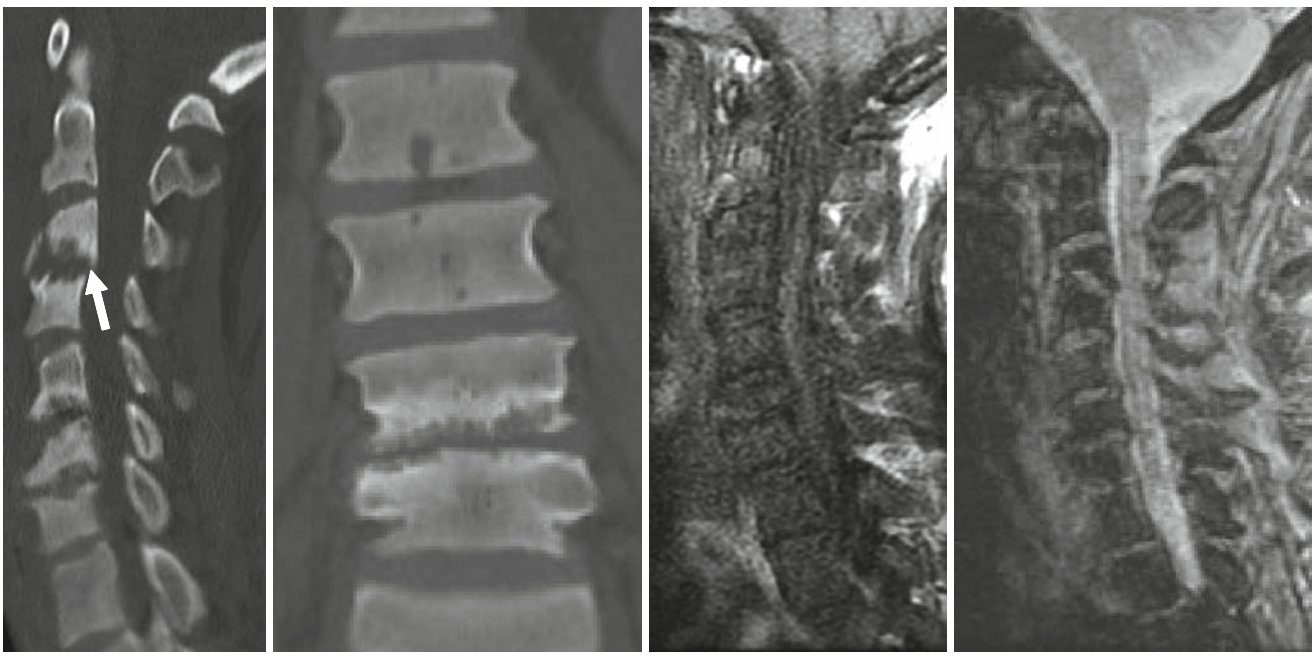

A B C D

Fig. 3.58 Destructive spondyloarthropathy (DSA) in a patient with renal osteodystrophy undergoing long-term dialysis. **(a)** is sagittal reconstruction CT of the cervical spine showing involvement of C3–C4, C5–C6, and C6–C7 intervertebral disc spaces. **(b)** is mainly involving the L3–L4 intervertebral disc space. In both regions there is serrated irregular erosions of the end plates, destruction of adjacent vertebral bodies (causing decreased height), heavy sclerosis next to erosions, and narrowing or widening of the disc spaces. Infections erosions do not reveal serrations seen in amyloidosis. Infections also produce bony bridging in long-standing cases. Note posterior mild subluxation of C3–C4 (*arrow*). The findings are due to both amyloid deposition and secondary HPT. **(c)** is T1- and **(d)** is T2-weighted MR sagittal images of the cervical spine. The involved intervertebral disc spaces are isointense with normal spaces in T1 image, but in T2 image they are isointense or hypointense. Infection in MR is excluded because there is no increased signal intensity of involved disc spaces in T2 image. Furthermore, multi-level involvement and lack of bony bridging, better seen in CT, support the diagnosis of destructive spondyloarthropathy

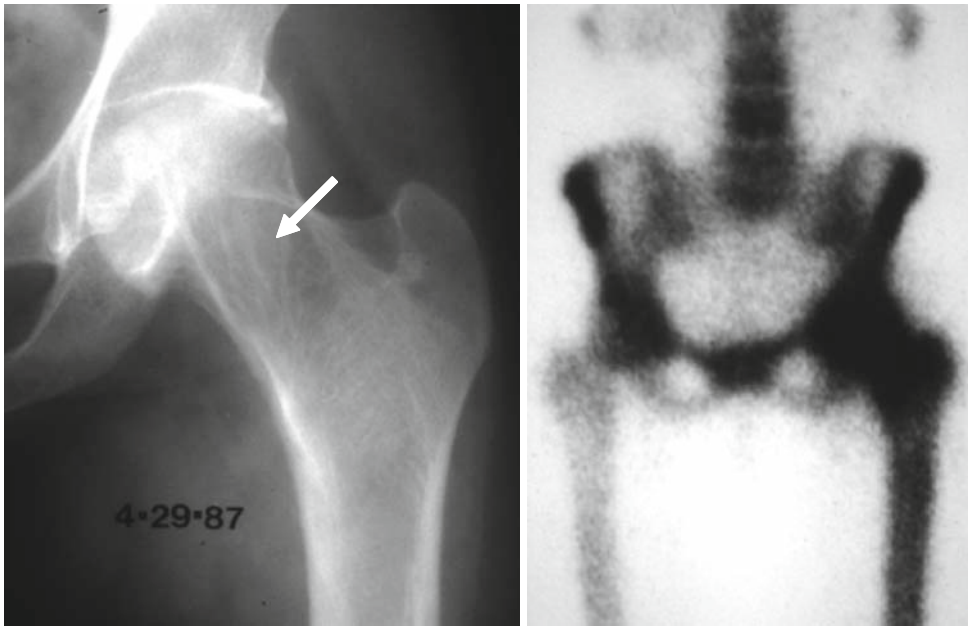

Fig. 3.59 Brown Tumor. (**a)** is radiograph and (**b)** is bone scan of the left hip of a 41-year-old female with secondary HPT due to ROD. There is a biopsy-proven brown tumor of the left femoral neck (*arrow*). (**b)** shows non-specific increased uptake

pathogenesis is not completely understood, glucocorticoids are thought to be the major risk factor.

Post-transplant Osteoporosis

Post-transplant osteoporosis is common and may be extensive during the first year following renal transplantation. Long-term steroid and cyclosporine therapy may chronically activate osteoclasts while inhibiting osteoblastic activity. Up to 4% of renal transplant recipients have osteoporotic pain also called "symmetric bone pain syndrome." There is also a high incidence of osteoporotic fractures 2 years after transplant.

Amyloidosis

Return of normal kidney function in post-renal transplant patients leads to regression of beta-2 microglobulin-related disturbances of bone metabolism. However, articular amyloidosis, if present, may remain detectable 10 years after transplantation. Fortunately, in the majority of patients, amyloidosis decreases or even disappears after renal transplantation [72].

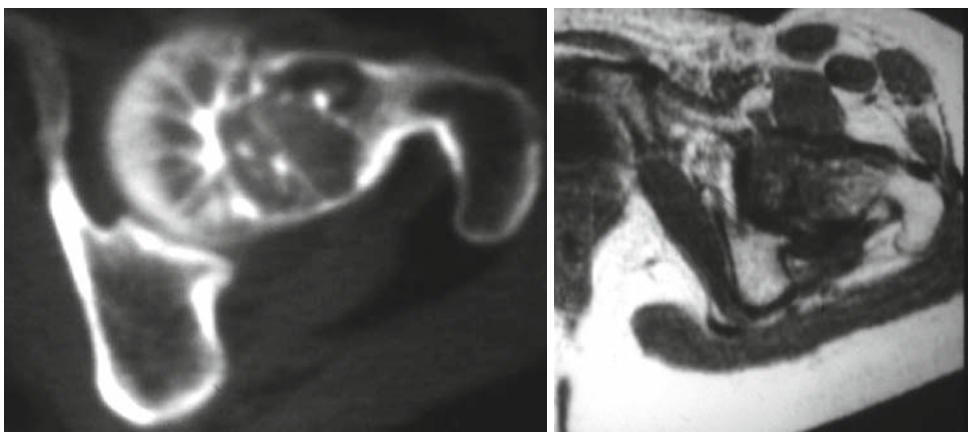

Fig. 3.60 Brown tumor: This is the same patient as in Fig. 3.59. (**a)** CT scan and (**b)** is T1 axial image of the left hip of this 41-year-old female with secondary HPT due to ROD. There is a biopsy-proven brown tumor of the left femoral neck

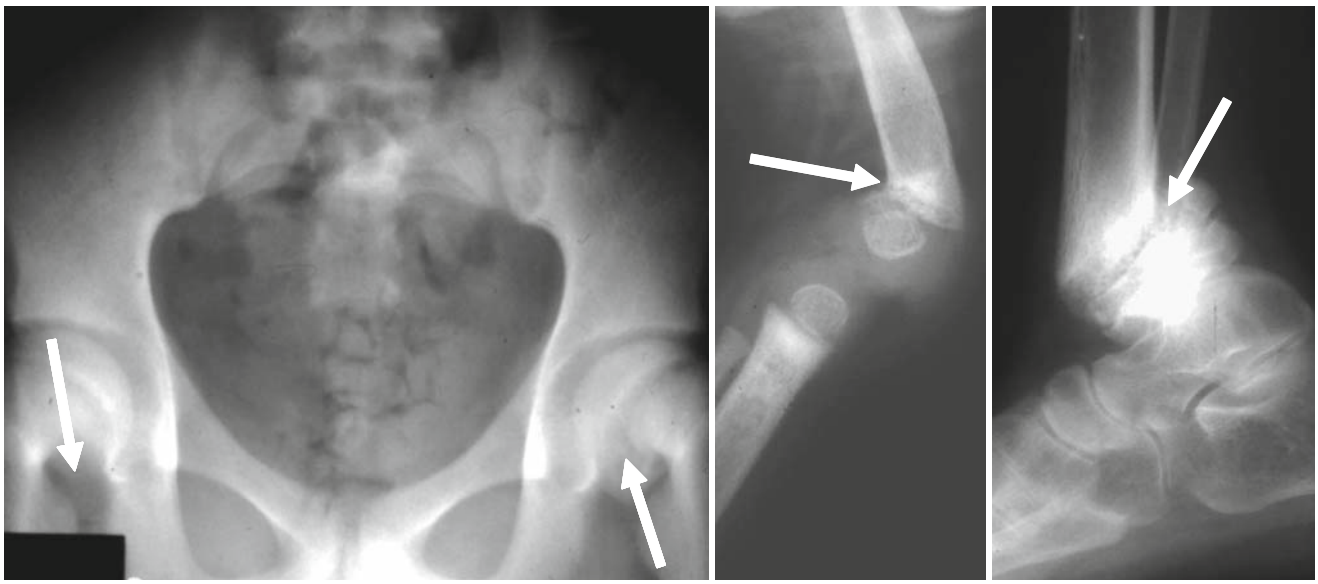

Fig. 3.61 Demonstrates slipped epiphyses, in a child with ROD. (**a**) shows bilateral capital femoral slipped epiphyses (*arrows*). (**b**) demonstrates mild posterior distal femoral slipped epiphysis (*arrow*). (**c**) reveals marked posterior slipped epiphyses of the distal tibia and distal fibula (*arrows*)

Tendonitis and Tendon Rupture

Tendonitis with spontaneous tendon rupture after kidney transplantation is probably the result of corticosteroid therapy. The common sites of involvement are the Achille's, quadriceps (Fig. 3.66), and rotator cuff tendons [71].

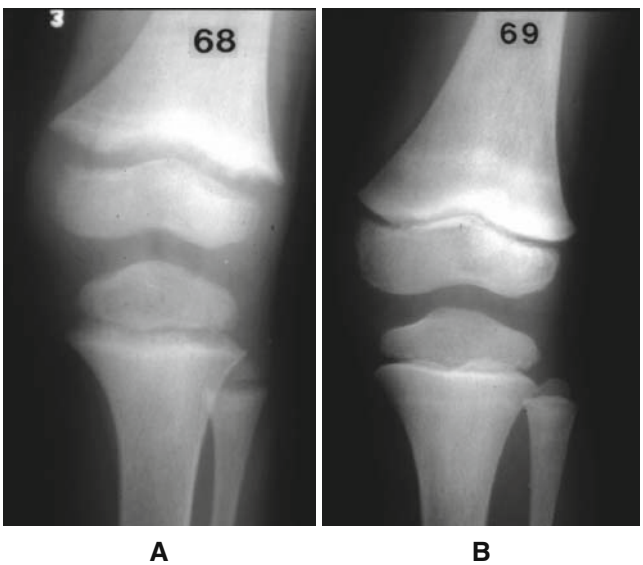

Fig. 3.62 Shows improvement after dialysis. (**a**) is the left knee radiograph of a child with ROD. There is widening of the epiphyseal plates of the distal femur and upper tibia with metaphyseal irregularity (paint brush appearance). There is osteosclerosis that gives a false impression of normal zone of provisional calcification. (**b**) is more than 1 year later, during which time the patient underwent hemodialysis. Note significant improvement of rachitic changes

Hypoparathyroidism

PTH modulates calcium and phosphate homeostasis across bone, kidneys, and intestines. It defends against hypocalcemia by mobilizing calcium (and phosphorous) from skeletal stores to increase the inflow of calcium into the extracellular fluid. PTH also lowers the serum phosphorus level by inhibiting reabsorption of phosphate by the renal tubule cells, thus causing phosphate excretion in the urine. The hypoparathyroid state is characterized by hypocalcemia, hyperphosphatemia, and an inappropriately low or undetectable PTH level except in the setting of PTH resistance, where PTH levels can be high, normal, or elevated. Hypoparathyroidism may be the result of impaired synthesis or secretion of PTH, defects of the calcium-sensing receptor, or end-organ resistance to PTH.

Signs and Symptoms of Hypoparathyroidism

The predominant clinical manifestations of hypoparathyroidism are related to hypocalcemia and vary according to the severity and chronicity of the hypocalcemia state. In patients who develop hypocalcemia acutely, neuromuscular irritability, including perioral paresthesias, tingling of the fingers and toes and spontaneous or latent tetany, grand mal seizures,

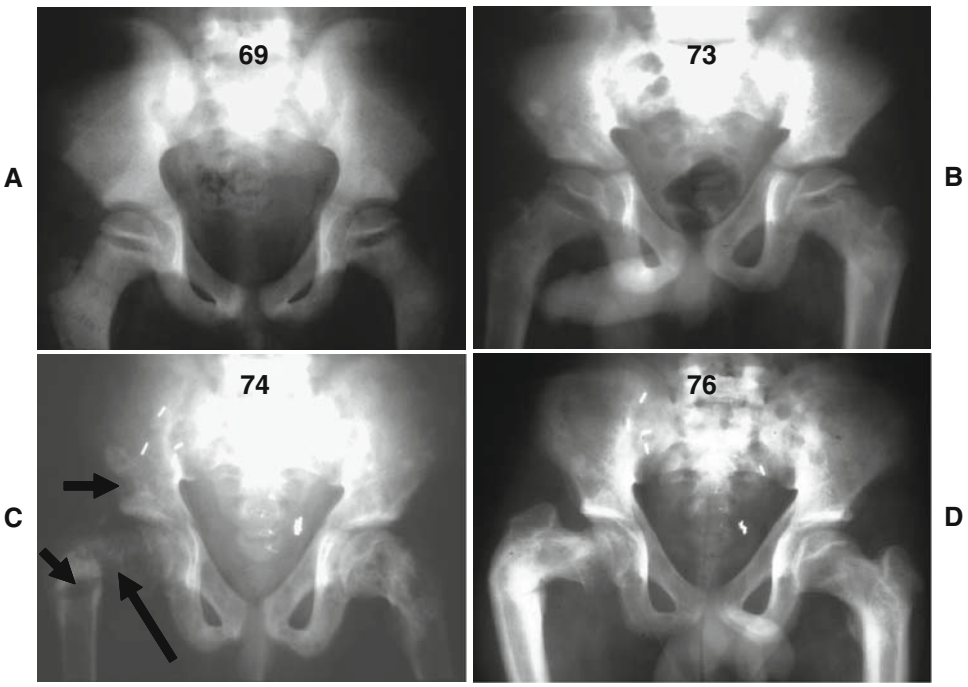

Fig. 3.63 Renal transplantation. **(a**, **b** and **c)** show the progress of ROD while the patient was undergoing hemodialysis. **(c)** shows that, at the time of surgery, there was cortical thinning, amyloidomas and less likely brown tumors. As well as a looser zone in the R femoral neck (*long arrow*), R coxa vara, and bilateral protrusio acetabulae. **(d)** was made 2 years after surgery and reveals significant improvement of rachitic changes and improvement of osseous lucencies, but deformities (R coxa vara and bilateral protrusio acetabulae) persist. Courtesy of Dr. Murray K Dalinka, Hospital of the University of Pennsylvania, Philadelphia, PA

papilledema, and laryngeal spasm, can be present. Chronic hypocalcemia may be asymptomatic, or may manifest with mild neuromuscular irritability, calcification of the basal ganglia (Fig. 3.67), extrapyramidal disorders, cataracts, alopecia, abnormal dentition, coarse brittle hair, mental retardation, or personality disorders.

Impaired Synthesis or Secretion of PTH

The most common cause of hypoparathyroidism is damage to or destruction of the parathyroid glands as a complication of neck surgery. Rarely, destruction of the parathyroid glands

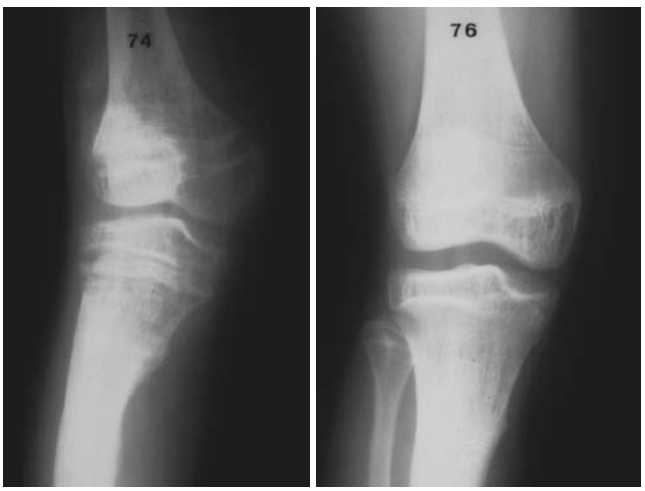

Fig. 3.64 Shows improvement after kidney transplantation. This is the same case as Fig. 3.63. **(a)** is the right knee before and **(b)** is the same knee 2 years after renal transplantation. A reveals widening of epiphyseal plate and metaphyseal irregularity in distal femur and upper tibia as well as minimal lateral bowing of the tibia that show significant improvement in **(b)**

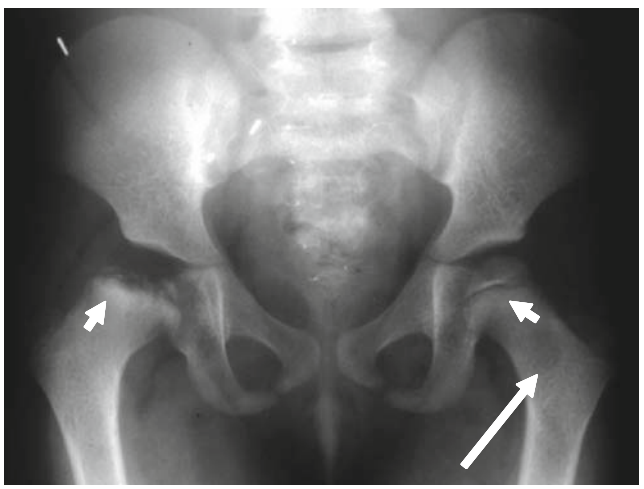

Fig. 3.65 Ischemic necrosis. Development of right proximal femoral epiphyseal osteonecrosis in a 6-year-old female with ROD after kidney transplantation and use of steroids. Surgical clips of the right-sided transplanted kidney are seen in the pelvis. There is deformity and non-uniform density of the right proximal femoral epiphysis, related to ischemic necrosis. A hazy lucency in the left femoral neck may be related to amyloidosis or brown tumor (*long arrow*). Increased bone density is best manifested by prominence and sclerosis of proximal femoral metaphyses (*short arrows*)

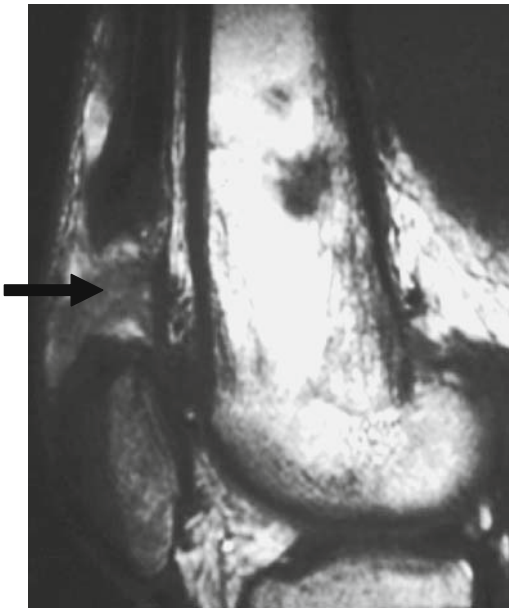

Fig. 3.66 Tendon rupture after renal transplantation: There is **r**upture of the quadriceps tendon in a 28-year-old male with ROD, after renal transplantation, due to steroid therapy (*arrow*). Courtesy of Dr. Murray K Dalinka, Hospital of the University of Pennsylvania, Philadelphia, PA

occurs as a consequence of radioiodine treatment of thyroid disease or external beam radiation. Autoimmune processes and infiltrative diseases such as hemochromatosis, Wilson disease, and granulomatous diseases can affect the parathyroids and cause hypoparathyroidism.

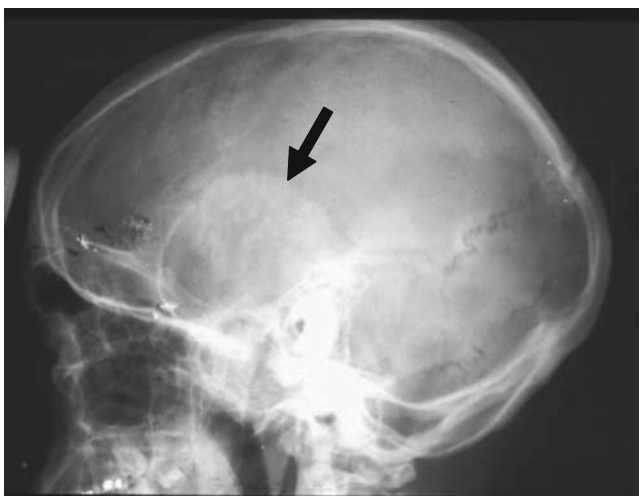

Fig. 3.67 Hypoparathroidism with intracranial calcification. The patient is a 15-year-old female. Calcification of the basal ganglia is evident. The bones of the skull are normal in thickness

Defects of the Calcium-Sensing Receptor

Hypocalcemia with an inappropriately normal PTH and hypocalciuria characterize the autosomal dominant disorder called familial hypocalcemic hypercalciuria [77, 78]. Mutations of the calcium-sensing receptor result in constitutive activation, thereby lowering the set point for serum calcium levels and suppressing PTH.

End-Organ Resistance to PTH (Pseudohypoparathyroidism)

In 1942 Albright, Burnett, Smith, and Parson reported three cases of idiopathic hypoparathyroidism that did not respond to PTH injection and considered them as cases of pseudohypoparathyroidism (PHP) [79] (Fig. 3.68). They believed that in these cases, the parathyroid glands were normal but that the target organs were unresponsive. The patients were hypocalcemic, hyperphosphatemic, and exhibited the features of Albright hereditary osteodystrophy, including round facies, short stature, shortened fourth metacarpal bones, obesity, subcutaneous ossifications, and developmental delay.

It is now well established that the development defects known as Albright hereditary osteodystrophy are different subtypes of PHP caused by mutations in a single gene, Gs alpha gene (GNAS1), which encodes the alpha subunit of the G-protein, coupled to the PTH receptor [80]. These genetic mutations render the G-protein unable to activate adenyl cyclase upon the binding of PTH to its receptor, resulting in unresponsiveness of affected end organs [81]. In PHP, PTH resistance affects the proximal renal tubules, but other target organs such as bone are not affected [82, 83].

PHP is characterized biochemically by hypocalcemia, hyperphosphatemia, and elevated PTH levels. Because of PTH resistance, the serum concentration of 1,25-dihydroxyvitamin D is diminished causing hypocalcemia and hyperphosphatemia [84, 85]. PHP is divided into two main types. In PHP type 1, both renal cAMP and phosphate excretion is diminished in response to exogenous PTH administration as compared to unaffected individuals [72, 86]. In PHP type 2, renal cAMP is normal but the excretion of phosphate is impaired [87]. PHP type 2 is not well characterized.

PHP type 1 is further subdivided into three distinct subtypes. PHP type 1a is characterized by autosomal dominant inheritance, phenotypic features of Albright hereditary dystrophy, and PTH resistance of the proximal renal tubule leading to hyperphosphatemia, hypocalcemia, and ultimately, secondary hyperparathyroidism and hyperparathyroid bone disease (osteitis fibrosa). Maternal transmission

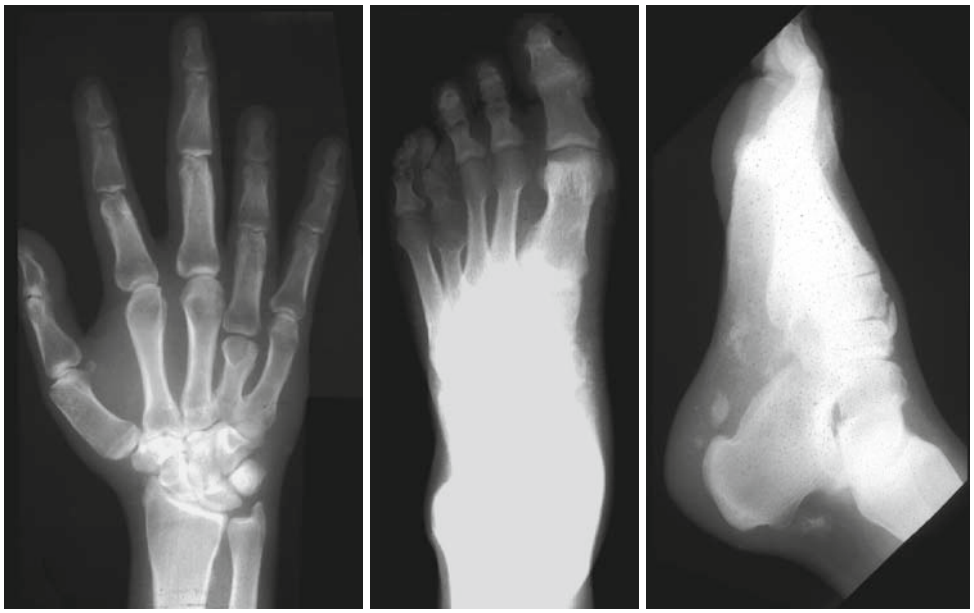

A B C

Fig. 3.68
Pseudohypoparathyroidism. The patient is a 23-year-old male. (**a** and **b)** reveal significant shortening of the 4th metacarpal and 4th metatarsal, characteristic of pseudohypoparathyroidism. In this case, there is also associated relative shortening of the other metacarpals and metatarsals. (**c)** is the lateral radiograph of foot demonstrating calcifications in the sole of the foot and dorsal soft tissues of the ankle.

of the mutation is required for full expression of type 1a PHP [88]. Patients may also exhibit resistance to other G-protein-coupled hormones such as thyrotropin and gonadotropins [89].

Pseudopseudohypoparathyroidism and Progressive Osseous Heteroplasia

Pseudopseudohypoparathyroidism and progressive osseous heteroplasia are related genetically to type 1a PHP despite their distinct phenotypes [90]. Renal expression of GNAS1 is determined only by the maternal allele; therefore, unresponsiveness of the renal tubule to PTH binding will result only when the mutation occurs in the maternal allele [91].

Paternal transmission of a mutated GNAS1 gene causes pseudopseudohyperparathyroidism (PPHP), manifesting only the phenotypic findings of Albright hereditary dystrophy with normal responsiveness of the renal tubules to PTH. Paternal transmission of GNAS1 mutations has also been associated with progressive osseous heteroplasia, a disorder causing severe heterotopic ossification of skeletal muscle without Albright hereditary dystrophy or PTH resistance [92, 93].

PHP type 1b is characterized by PTH resistance without features of Albright hereditary dystrophy. It is also autosomal dominant and requires maternal transmission of the mutated allele [90]. PHP type 1c has clinical and laboratory findings similar to those observed in patients with PHP type 1a.

Treatment

Treatment of hypoparathyroidism varies with the severity of the hypocalcemia and the underlying cause of the hypoparathyroidism. In acute symptomatic cases of hypocalcemia, calcium infusions followed by oral calcium and calcitriol are necessary. In patients with chronic hypocalcemia due to hypoparathyroidism, the goal of therapy is to keep the calcium level in the low normal range, thereby preventing symptomatic hypocalcemia while avoiding hypercalciuria. Without the stimulatory effect of PTH on renal tubular reabsorption of calcium, even normal serum calcium concentrations can lead to hypercalciuria and predispose to nephrolithiasis.

In PHP, the goals of therapy are to maintain ionized calcium levels within the normal range to avoid hypercalciuria, suppress PTH levels to normal, and prevent increased bone remodeling leading to hyperparathyroid bone disease.

References

1. Chen EY, Liao YC, Smith DH, et al. The growth hormone locus: nucleotide sequence, biology, and evolutions. Genomics 1989; 4:479.
2. Hartman ML, Veldhuis JD, Thorner MO. Normal control of growth hormone secretion. Hormones 1993; 40(1–3):37–47.
3. Faustini-Fustini M, Rochira V, Carani C. Eur J Endocrinol 1999; 140:111–129.
4. Smith EP, Boyd J, Frank GR, et al. N Engl J Med 1994; 331: 1056–1061.

5. Gelber SJ, Heffez DS, Donohoue PA. Pituitary gigantism caused by growth hormone excess from infancy. J Pediatric 1992; 120(6):931–934.
6. Blumberg DL, Sklar CA, David R, et al. Acromegaly in an infant. Pediatrics 1989; 83(6):998–1002.
7. Zimmerman D, Young WF, Ebersold MJ, et al. Congenital gigantism due to growth hormone releasing hormone excess and pituitary hyperplasia with adenomatous transformation. J Clin Endocrinol Metab 1993; 76(1):216–222.
8. Manski TJ, Haworth CS, Duval-Arnold BJ, et al. Optic pathway glioma infiltrating into somatostatinergic pathways in a young boy with gigantism. Case report. J Neurosurg 1994; 81(4):595–600.
9. Thorner MO, Perryman RL, Cronin MJ, et al. Somatotroph hyperplasia: successful treatment of acromegaly by removal of a pancreatic tumor secreting a growth hormone releasing factor. J Clin Invest 1982; 70:965.
10. Ludecke DK, Herrmann HD, Schulte FJ. Special problems with neurosurgical treatments of hormone-secreting pituitary adenomas in children. Prog Exp Tumor Res 1987; 30:362.
11. Ritzen EM, Wettrell G, Davies G, Grant DB. Management of pituitary gigantism. The role of bromocriptine and radiotherapy. Acta Paediatr Scand 1985 Sep; 74(5):807–814.
12. Zacharin M. Paediatric management of endocrine complications in McCune-Albright syndrome. J Pediatr Endocrinol Metab. 2005 Jan; 18(1):33–41.
13. Moran A, Pescovitz OH. Long-term treatment of gigantism with combination octreotide and bromocriptine in a child with McCune-Albright syndrome. Endocr J 1994; 2:111.
14. Sotos JF, Dodge PR, Muirhead D, et al. Cerebral gigantism in childhood. N Engl J Med 1964; 271:109–116.
15. Tatton-Brown K, Douglas J, Coleman K, et al. Genotype–phenotype associations in Sotos syndrome: an analysis of 266 individuals with NSD1 aberrations. Am J Hum Genet 2005; 77: 193–204.
16. Kurotaki N, Imaizumi K, Harada N, et al. Haploinsufficiency of NSD1 causes Sotos syndrome. Nat Genet 2002; 30:365–366.
17. Wit JM, Beemer FA, Barth PG, et al. Cerebral gigantism (Sotos' syndrome). Compiled data 22 cases. Analysis of clinical features, growth and plasma somatomedin. Eur J Pediatr 1985; 144: 131.
18. Scheithauer BW, Kovacs K, Randall RV, Horvath E, Laws ER Jr. Pathology of excessive production of growth hormone. Clin Endocrin & Metab 1986; 15:655.
19. Karpf DB, Braunstein GD. Current concepts in acromegaly: etiology, diagnosis and treatment. Compr Ther 1986; 12:22.
20. Holdaway IM, Rajasoorya C. Epidemiology of acromegaly. Pituitary 1999; 2:29–41.
21. Sanno N, Teramoto A, Osamura RY, et al. Pathology of pituitary tumors. Neurosurg Clin N Am 2003; 14:25–39.
22. Melmed S. Acromegaly. N Engl J Med 1990; 322:966–977.
23. Melmed S, Ezrin C, Kovacs K, et al. Acromegaly due to secretion of growth hormone by an ectopic pancreatic islet-cell tumor. N Engl J Med 1985; 312:9.
24. Beuschlein F, Strasburger CJ, Siegerstetter V, et al. Acromegaly caused by secretion of growth hormone by a non-Hodgkin's lymphoma. N Engl J Med 2000; 342:1871.
25. Biermasz NR, Pereira AM, Smit JW, et al. Morbidity after long-term remission for acromegaly: persisting joint-related complaints cause reduced quality of life. J Clin Endocrinol Metab 2005; 90:2731.
26. Melmed S, Jackson I, Kleinberg D, et al. Current treatment guidelines for acromegaly. J Clin Endocrin Metab 1998; 83(8): 2646–2652.
27. Trainer PJ, Drake WM, Katznelson L, et al. Treatment of acromegaly with the growth hormone-receptor antagonist pegvisomant. N Engl J Med 2000; 342:1171–1177.
28. van der Lely AJ, Hutson RK, Trainor PJ et al., Long-term treatment of acromegaly with pegvisomant, a growth hormone-receptor antagonist. Lancet 2001; 358:1754–1759.
29. Kauppinen-Makelin R, Sane T, Reunanen A, Valimaki MJ, Niskanen L, Markkanen H, Loyttyniemi E, Ebeling T, Jaatinen P, Laine H, Nuutila P, Salmela P, Salmi J, Stenman UH, Viikari J, Voutilainen E. A nationwide survey of mortality in acromegaly. J Clin Endocrinol & Metabol 2005 Jul; 90(7):4081–4086.
30. Rosenfeld RG, Albertsson-Wikland K, Cassorla F, et al. Diagnostic controversy: the diagnosis of childhood growth hormone deficiency revisited. J Clin Endocrinol Metab 1995; 80:1532.
31. Root AW, Kemp SF, Rundle AC, et al. Effect of long-term recombinant growth hormone therapy in children – the National Cooperative Growth Study, USA, 1985–1994. J Pediatr Endocrinol Metab 1998; 11:403.
32. Chernausek SD, Backeljauw PF, Frane J, et al. Long-term treatment with recombinant insulin-like growth factor (IGF)-I in children with severe IGF-I deficiency due to growth hormone insensitivity. J Clin Endocrinol Metab 2007; 92:902.
33. Allen DB. Growth suppression by glucocorticoid therapy. Endocrinol Metab Clin North Am 1996; 25:699.
34. Delange F. Neonatal screening for congenital hypothyroidism: results and perspectives. Horm Res 1997; 48:51–61.
35. Alm J, Hagenfeldt LA, et al. Incidence of congenital hypothyroidism: retrospective study of neonatal laboratory screening versus clinical symptoms as indicators leading to diagnosis. BMJ 1984; 289:1171.
36. Harris F. In R Owen, J Goodfellow, P Bullough (Eds.), Hormonal Control of Growth in Scientific Foundations of Orthopedics and Traumatology. Rickets and Osteomalacia. Philadelphia: W.B. Saunders, 1980.
37. Poretsky L, Garber J, Kleefield J. Primary amenorrhea and pseudoprolactinama with primary hypothyroidism. Reversal of clinical, biochemical, and radiologic abnormalities with levothyroxine. Am J Med 1986; 81:180.
38. Katevuo K, Valimaki M, Ketonen L, Lamberg B-A, Pelkonen R. Computed tomography of the pituitary fossa in primary hypothyroidism. Effect of thyroxine treatment. Clin Endocrinol 1985; 2:617.
39. Ross DS. Hyperthyroidism, thyroid hormone therapy and bone. Thyroid 1994; 4:39.
40. Mosekilde L, Eriksen EF, Charles P. Effects of thyroid hormones on bone and mineral metabolism. Endocrinol Metab Clin North Am 1990; 19:35.
41. Jastrup B, Mosekilde L, Melsen F, et al. Serum levels of vitamin D metabolites and bone remodeling in hyperthyroidism. Metabolism 1982; 31:126.
42. Mudde AH, Houben JHM, Kruseman ACN. Bone metabolism during anti-thyroid drug treatment of endogenous subclinical hyperthyroidism. Clin Endocrinol 1994; 41:421.
43. Cummings SR, Nevitt MC, Browner WS, et al. Risk factors for hip fracture in white women. N Engl J Med 1995; 332:767.
44. Bonakdarpour A, Kirkpatrick JA, Renzi A, Kendall N. Skeletal changes in neonatal thyro-toxicosis. Radiol 1971; 102:149–150.
45. Akerstrom G, Malmaeus J, Bergstrom R. Surgical anatomy of human parathyroid glands. Surgery 1984; 95:14.
46. Ruda JM, Hollenbeak CS, Stack BC Jr. A systematic review of the diagnosis and treatment of primary hyperparathyroidism from 1995 to 2003. Otolaryngol Head Neck Surg 2005; 132:359.
47. Silverberg SJ, Bilezikian JP. Clinical presentation of primary hyperparthyroidism in the United States. In JP Bilezikian, et al. (Eds.), The Parathyroids, 2nd ed. New York: Academic Press, 2001; 349–360.
48. Silverberg SJ, Bilezikian JP. Evaluation and management of primary hyperparathyroidism. J Clin Endocrinol Metab 1996; 81:2036.

49. Bilezikian JP, Brandi ML, Rubin M, Silverberg SJ. Primary hyperparathyroidism: new concepts in clinical, densitometric and biochemical features. J Intern Med 2005; 257:6.
50. Silverberg SJ, Bilezikian JP. Nat Clin Pract Endocrinol Metab 2006; 2:494–503.
51 Clark OH. How should patients with primary hyperparathyroidism be treated? J Clin Endocrinol Metab 2003; 88:3011–3014.
52. Udelsman R, Donovan POI, Sokoll LT. One hundred consecutive minimally invasive parathyroid explorations. Ann Surg 2000; 232:331–339.
53. Chen H, Zeiger MA, Gordon TA, et al. Parathyroidectomy in Maryland: effects of an endocrine center. Surgery 1996; 120: 948–952.
54. Chen H, Parkerson S, Udelsman R. Parathyroidectomy in the elderly: do the benefits outweigh the risks? World J Surg 1998; 22:531–535.
55. Bergenfelz A, Lindblom P, Tibblin S, Westerdahl J. Unilateral versus bilateral neck exploration for primary hyperparathyroidism: a prospective randomized controlled trial. Ann Surg 2002; 236: 543–551.
56. Coresh J, Selvin E, Stevens LA, et al. Prevalence of chronic kidney disease in the United States. JAMA 2007; 298(17):2038–2047.
57. Holick MF. Vitamin D deficiency. N Engl J Med 2007; 357: 266–281.
58. Silver J, Russell J, Sherwood LM. Regulation by vitamin D metabolites of messenger ribonucleic acid for preproparathyroid hormone in isolated bovine parathyroid cells. Proc Natl Acad Sci USA 1985; 82:4270–4273.
59. Dawson-Hughes B, Heaney RP, Holick MF, et al. Estimates of optimal vitamin D status. Osteoporos Int 2005; 16:713.
60. Vieth R. What is the optimal vitamin D status for health. Prog Biophys Mol Biol 2006; 92:26.
61. Marx SJ. Hyperparathyroid and hypoparathyroid disorders. N Engl J Med 2000; 343:1863–1875.
62. Ahmad R, Hammond JM. Primary, secondary, and tertiary hyperparathyroidism. Otolaryngol Clin North Am 2004 Aug; 37(4): 701–713, vii–viii.
63. Stewart AF. Hypercalcemia associated with cancer. N Engl J Med 2005; 352:373–379.
64. Eftekhari F, Yousefzadeh DK. Primary infantile hyperparathyroidism: clinical, laboratory, and radiographic features in 21 cases. Skeletal Radiol 1982; 8(3):201–208.
65. Orwoll E, Silbert J, McClung M. Hypercalcemia asymptomatic neonatal familial. Pediatrics 1982; 69(1):109–111.
66. K/DO0I. Clinical practice guidelines for bone metabolism and disease in chronic kidney disease. Am J Kidney Dis 2003; 42(Suppl 3):PS1–201.
67. Bonakdarpour A. Renal osteodystrophy. Radiology Today, 4-A, Multinational Series, 1987; 119–124.
68. Bonakdarpour A. Renal osteodystrophy. RSNA Syllabus on Metabolic and endocrine disorders affecting the skeleton. 1981; Course 409B:1–12.
69. Murphy MD, Sartoris DJ, Quale JL, Pathria MN, Martin NL. Musculoskeletal manifestations of chronic renal insufficiency. Radiographics 1993; 13(2):357–379.
70. Stevens K. Musculoskeletal manifestations of chronic renal disease, 34th International Skeletal Society Refresher course 11B 2007; 1-6 Budapest.
71. Jevtic V. Imaging of renal osteodystrophy. Eur J Radiol 2003; 46(2):85–89.
72. Sperschneider H, Stein G. Bone disease after renal transplantation. Nephrol Dial Transplant 2003; 18:874–877.
73. Heaf J, Tvedegaard E, Kanstrup IL, Fogh-Andersen N. Hyperparathyroidism and long-term bone loss after renal transplantation. Clin Transplant 2003; 17(3):268–274.
74. Julian BA, Quarles LD, Niemann KM. Musculoskeletal complications after renal transplantation: pathogenesis and treatment. Am J Kidney Dis 1992; 19(2):99–120.
75. Arnold A, Brown MF, Urena P, Gaz RD, et al. Monoclonality of parathyroid tumors in chronic renal failure and in primary parathyroid hyperplasia. J Clin Invest 1995; 95(5):2047–2053.
76. Drueke TB. The pathogenesis of parathyroid gland hyperplasia in chronic renal failure. Kidney Int 1995; 48(1):259–272.
77. Pearce SH, Williams C, Kifor O, et al. A familial syndrome of hypocalcemia with hypercalciuria due to mutations in the calcium-sensing receptor. New Engl J Med 1996; 335:1115–1122.
78. Pollak MR, Brown EM, Estep HL, et al. Autosomal dominant hypocalcaemia caused by a Ca2+-sensing receptor gene mutation. Nat Genet 1994; 8:303.
79. Albright F, Burnett CH, Smith PH, Parson W. Pseudohypoparathyroidism: an example of "Seabright-Bantam syndrome." Report of three cases. Endocrinol 1942; 30:922.
80. Bastepe M, Juppner H. GNAS locus and pseudohypoparathyroidism. Horm Res 2005; 63:65.
81. Spiegel AM, Weinstein LS, Shenker A. Abnormalities in G protein-coupled signal transduction pathways in human disease. J Clin Invest 1993; 92:1119.
82. Murray T, Gomez I, Rao E, et al. Pseudohypoparathyroidism with osteitis fibrosa cystica: Direct demonstration of skeletal responsiveness to parathyroid hormone in cells cultured from bone. J Bone Miner Res 1993; 8:83–91.
83. Ish-Shalom S, Rao LG, Levine MA et al., Normal parathyroid hormone responsiveness of bone derived cells from a patient with pseudohypoparthyroidism. J Bone Miner Res 1996; 11:8–14.
84. Breslau NA, Weinstock RS. Regulation of 1,25 (OH) 2D synthesis in hypoparathyroidism and pseudohypoparathyroidism. Am J Physiol 1988; 255:E730–736.
85. Drezner MK, Neelon FA, Haussler M, et al. 1,25-dihydroxycholecalicferol deficiency: the probable cause of hypocalcemia and metabolic bone disease in pseudohypoparathyroidism. J Clin Endocrinol Metab 1976; 42:621–628.
86. Chase LR, Melson GL, Aurbach GD. Pseudohypoparathyroidism: defective excretion of 3'5'-AMP in response to parathyroid hormone. J Clin Invest 1969; 48:1832–1844.
87. Drezner M, Neelon FA, Lebovitz HE. Pseudohypoparathyroidism type II: a possible defect in the reception of the cyclic AMP signal. N Engl J Med 1973; 289:1056.
88. Nakamoto JM, Sandstrom AT, Brickman AS, et al. Pseudohypoparathyroidism type Ia from maternal but not paternal transmission of a Gs alpha gene mutation. Am J Med Genet 1998; 77:261.
89. Levine MA, Downs RW Jr, Moses AM, et al. Resistance to multiple hormones in patients with pseudohypoparathyroidism. Association with deficient activity of guanine nucleotide regulatory protein. Am J Med 1983; 74:545.
90. Bastepe M, Jüppner H. GNAS locus and pseudohypoparathyroidism. Horm Res 2005; 63(2):65–74.
91. Hayward BE, Kamiya M, Strain L, et al. The human GNAS1 gene is imprinted and encodes distinct paternally and biallelically expressed G proteins. Proc Natl Acad Sci USA 1998; 95:10038.
92. Kaplan FS, Shore EM. Progressive osseous heteroplasia. J Bone Miner Res 2000; 15:2084–2094.
93. Shore EM, Ahn J, Jan de Beur S et al., Paternally inactivated mutations of the GNAS1 gene in progressive osseous heteroplasia. N Engl J Med 2002; 346:99–106.

Chapter 4

Circulatory Diseases of Bone and Adjacent Soft Tissues

Wilfred C.G. Peh and Seoung-Oh Yang

Abstract The blood circulation of bone may be affected by a variety of insults, involving the arterial, capillary, sinusoidal or venous networks. Blood flow impedance may be due to mechanisms such as intraluminal obstruction, vascular compression or physical disruption of the vessel. In circulatory diseases of bone, imaging aims to demonstrate the reparative host response. Avascular necrosis (AVN) is a lesion in which an early diagnosis is vital in order that the appropriate management can be undertaken, with the femoral head being the most important affected site. There are numerous predisposing factors for AVN. The radiographic hallmark of femoral AVN is increased femoral head density in an otherwise normal joint. Established AVN is seen as collapse of the articular surface and fragmentation. MR imaging is the most accurate technique for diagnosing early AVN, demonstrating characteristic marrow changes. Trauma-induced AVN may affect specific sites, following injuries such as the scaphoid and lunate fractures, and slipped capital femoral epiphysis. Spontaneous osteonecrosis of the knee (SONK) affects the weight-bearing surface of the medial femoral condyle. AVN precursor syndromes include regional osteoporosis, reflex sympathetic dystrophy, transient osteoporosis and regional migratory osteoporosis. Osteochondroses related to osteonecrosis include Legg-Calve-Perthes disease, Kienbock disease, Freiberg infraction, Kohler disease and osteochondritis dissecans. Miscellaneous vascular disease that affects the musculoskeletal system encompass, frostbite, thermal and electrical injuries, compartment syndrome/myonecrosis, venous insufficiency of soft tissue, and ischemic fasciitis.

Keywords Ischemic necrosis of bone • Avascular necrosis of bone • Medullary bone infarct • AVN of the femoral head • Trauma-induced AVN • SONK • Reflex sympathetic dystrophy • Transient osteoporosis • Regional migratory osteoporosis • Legg–Calve–Perthes disease • Kienbock disease • Freiberg infraction • Kohler disease • Osteochondritis dissecans • Frostbite • Thermal and electrical injuries • Compartment syndrome • Venous insufficiency of soft tissues and ischemic fasciitis

Wilfred C.G. Peh (✉)
Department of Diagnostic Radiology, Alexandra Hospital, Singapore 159964, Republic of Singapore
e-mail: wilfred.peh@gmail.com

Introduction

Bone is a dynamic organ that not only has vital structural, protective, and locomotive roles but also serves important metabolic (calcium and phosphorus homeostasis) and hematopoietic functions. Even in the mature skeleton, bone undergoes constant remodeling with areas of bone formation and resorption, both physiologically and in response to disease. The high metabolic activity of bone requires a sizeable blood supply.

Arterial feeders to bone consist of numerous small periosteal arterioles and capillaries that pierce the cortex and a smaller number of larger nutrient arteries that enter the cortex through nutrient canals. These vessels coalesce within the cortex to form a vascular rete. The cortical bone is composed of units called osteons that have a central haversian canal containing the neurovascular supply. Each haversian canal branches and interconnects with neighboring haversian canals. The cortical vessels re-exit the endosteal cortex to join the sinusoid network of the spongiosa or cancellous bone of the medullary cavity. The sinusoidal vascular network forms an extensive, anastomosing complex among the fat cells of the bone marrow. Blood is drained via a central venous sinus in the medullary cavity that gives veins that exit through nutrient foramina in the cortex.

A large and variable number of insults may affect the blood circulation of bone and may involve the arterial, capillary, sinusoidal, or venous networks. Increased impedance to blood flow may occur from various mechanisms, including intraluminal obstruction, vascular compression, or physical disruption of the vessel. Anoxia causes progressive ischemic injury and ultimately osteocyte cell death. The ability of bone

A. Bonakdarpour et al. (eds.), *Diagnostic Imaging of Musculoskeletal Diseases: A Systematic Approach*,
DOI 10.1007/978-1-59745-355-4_4, © Springer Science+Business Media, LLC 2010

to mount a reparative response after injury depends on local factors, including blood supply, specific local anatomic and mechanical requirements. Imaging shows the host response to circulatory diseases to bone, but does not show cell death per se. This chapter focuses on avascular necrosis (AVN), particularly of the femoral head, and also covers AVN precursor syndromes, AVN-related osteochondroses, and some miscellaneous diseases related to circulatory problems.

Avascular Necrosis

Avascular necrosis (AVN), also known as aseptic necrosis, osteonecrosis, or ischemic necrosis, refers to the death of cellular elements of bone, from interruption of its blood supply. The resultant collapse of osseous structures leads to destruction, pain, and loss of function. AVN is the term usually used when these changes involve the epiphysis or subchondral bone, with the femoral head being the most important affected site. AVN will almost always progress if appropriate treatment is not instituted. It is therefore vital to make an early diagnosis so that appropriate management can be undertaken, thereby delaying or preventing the need for major surgery such as joint replacement. Imaging has an important role in the diagnosis and follow-up of AVN. It is therefore important to be aware of the predisposing factors for AVN.

Pathophysiology and Causes

The pathophysiology of epiphyseal AVN is poorly understood except when it is caused by direct interruption of the blood supply following a femoral neck fracture or hip dislocation. In the majority of cases, AVN results from trauma, typically after a displaced subcapital femoral neck fracture. In other circumstances, impaired vascular perfusion leading to subsequent bone necrosis may result from other mechanisms. Etiologic factors that have been identified include systemic corticosteroid use, alcohol abuse, pancreatic disease, cytotoxic agents, rheumatoid arthritis, systemic lupus erythematosus, sickle cell anemia, and caisson disease. Up to one-third of cases of femoral head AVN may be idiopathic, i.e., may not have an identifiable cause (Table 4.1).

Etiologies of AVN may be divided into intravascular and extravascular. Intravascular mechanisms include blood vessel occlusion (e.g., traumatic mechanical interruption or contusion of arteries, fat embolism, sickle cell crisis) and blood vessel wall injury (e.g., radiation, infection, vasculitis, connective tissue disease). Extravascular mechanisms include increased intraosseous pressure compressing blood vessels (e.g., lipid accumulation in osteocytes from corticosteroids, abnormal cell proliferation within the medullary space as is seen in conditions like Gaucher disease, increased intracapsular pressure from infection and arthritis) and direct toxic effect from cytotoxic factors, e.g., alcoholism.

Except for direct traumatic interruption to the blood supply to bone, the exact cause for AVN may not be readily identifiable and in many cases the etiology is multifactorial. For radiologists, it is more important to be able to recognize the typical features of established AVN on radiographs and in equivocal cases, to recommend magnetic resonance (MR) imaging in order to detect early disease. Knowledge of the clinical background is useful when interpreting the images of a patient with possible AVN.

Table 4.1 Etiological factors causing AVN

A. Toxic
*Systemic corticosteroid use
*Anti-inflammatory drugs
*Immunosuppression, e.g., renal transplant
*Alcohol abuse
Anti-cytotoxic drugs, e.g., vinblastine, vincristine, cisplastin, cyclophosphamide, methotrexate, bleomysin, 5-fluorouracil
B. Traumatic
*Idiopathic, e.g., Legg–Calve–Perthes disease
*Fractures and dislocations
Radiation therapy
Heat, e.g., burns, frostbite, electrical injuries
Fat embolism
Vibration syndrome
C. Inflammatory
*Rheumatoid arthritis
*Systemic lupus erythematosus
Scleroderma
Infection
Pancreatitis
Psoriasis
Polyarteritis nodosa
Giant cell arteritis
D. Metabolic and endocrine
Pregnancy
Diabetes mellitus
*Cushing syndrome
Hyperlipidemia
Gout
Amyloid
E. Hematopoietic diseases
*Hemoglobinopathies, e.g., sickle cell anemia
Polycythemia rubra vera
Gaucher disease
Hemophilia
F. Thrombotic and embolic
Caisson disease
Arteritis

*Indicates the more common and important causes

AVN of the Femoral Head

The femoral head is the most common and important site of AVN. In the United States, the rate of femoral head AVN is 2–4.5 cases per patient-year, with 15,000 new cases reported each year and accounting for more than 10% of total hip replacements. The age of onset depends on the etiology, with the age range for idiopathic AVN being 30–50 years. Involvement of one hip increases risk of contralateral involvement to as high as 70% in some series. Non-traumatic AVN is commonly bilateral. When screening for AVN with MR imaging, it is therefore essential to image both hips (Fig. 4.1). Patients with femoral head AVN may present with non-specific symptoms and signs such as groin, thigh and knee pain, limping, and limitation of hip movement.

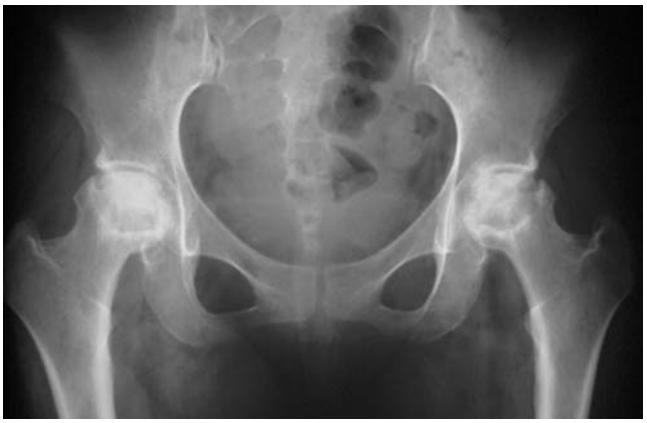

Fig. 4.1 Bilateral femoral head AVN. Frontal pelvic radiograph shows typical changes of established AVN in both femoral heads

A high index of clinical suspicion is required for the diagnosis of AVN, particularly in its early stages. Patients need to be evaluated and managed aggressively with the aim of preventing disease progression. An understanding of the natural progression of femoral head AVN aids in choosing appropriate therapy. In general, symptomatic patients with AVN who are conservatively managed are likely to progress, while most asymptomatic patients remain so. The likelihood and rate of femoral head collapse are also dependent on factors such as etiology, stage of AVN at initial diagnosis, the volume of the infarction, and its location in the femoral head.

Numerous classification systems exist for evaluation of patients with femoral head AVN. The key factor is whether or not there is a subchondral fracture, and if present, whether there is more advanced disease. The most time-honored staging system was developed by Ficat and Arlet, based on clinical findings, radiographic changes, and functional bone investigations (Table 4.2). The Ficat and Arlet staging system has been the foundation for many subsequent classifications that incorporate MR imaging findings, the most widely accepted probably being the ARCO staging system (Table 4.3). Radiologists should be familiar with these systems, so as to be able to incorporate the relevant information into their imaging reports and to facilitate communication with orthopedic surgeons and other clinical colleagues.

Table 4.2 Ficat and Arlet staging system for AVN of the femoral head

Stage	Clinical and radiographic findings
I	Normal radiographs No pain Increased medullary pressure
II	Variable change in trabecular bone appearance (sclerosis, cystic changes) but preserved femoral head shape on radiographs Variable pain
III	Specific changes on radiographs (collapse of subchondral bone and/or crescent sign) due to subchondral bone fracture Pain
IV	Marked collapse of subchondral bone with preserved joint space
V	Secondary osteoarthritis

Conservative management of symptomatic femoral AVN consists of non-steroidal analgesics and avoidance of weight-bearing. For early AVN, core decompression, with or without bone graft, is currently employed and is effective for pain control. In later stage AVN, hemiarthroplasty or total hip replacement, depending on the status of the acetabular articular cartilage, is the most appropriate treatment.

The radiographic hallmark of AVN is increased bone density in the femoral head with an otherwise normal joint. Advanced femoral head AVN appears radiographically as collapse of the entire articular surface and fragmentation (ARCO stage IV) (Fig. 4.2). Unlike joint-centered disorders, i.e., arthropathies, the changes occur only on one – the femoral – side of the joint. Even when secondary osteoarthritis develops causing some decrease or loss of joint space, there is still predominant and typically asymmetric femoral-sided involvement (Fig. 4.3). The earliest radiographic sign of impending collapse is a subchondral fracture, which is seen radiographically as a curvilinear radiolucent line located immediately deep to and parallel to the articular surface (crescent sign), or abrupt disruption or depression of the subchondral bone plate. This is typically present at the weight-bearing portion of the femoral head. The femoral head shape and joint space is preserved (ARCO stage III) (Fig. 4.4).

Radiographs are generally insensitive at detecting early stages of femoral head AVN and may be normal, even when there is histological evidence of osteonecrosis (ARCO stage I). Initial radiographic findings include patchy sclerosis that may be seen throughout the femoral head (ARCO stage II) (Fig. 4.5). Computed tomography (CT) sometimes may show the subchondral sclerosis that delineates

Table 4.3 Staging system based on the consensus of the subcommittee of nomenclature of the International Association on Bone Circulation and Bone Necrosis (ARCO)

Stage	Clinical, laboratory, and imaging findings
0	No symptoms
	Normal radiographs and MR images
	Osteonecrosis at histology
I	Presence or absence of symptoms
	Normal radiographs
	Abnormal MR images
	Osteonecrosis at histology
II	Symptoms
	Trabecular bone changes on radiographs without subchondral bone changes
	Preserved joint space
	Diagnostic MR findings
III	Symptoms
	Variable trabecular bone changes with subchondral bone fracture (crescent sign and/or subchondral bone collapse). Preserved shape of femoral head and preserved joint space
Subclassification based on extent of crescent:	
IIIa	Crescent is less than 15% of the articular surface
IIIb	Crescent is 15–30% of the articular surface
IIIc	Crescent is more than 30% of the articular surface
IV	Symptoms
	Altered shape of femoral head with variable joint space
Subclassification depends on the extent of collapsed surface:	
IVa	Less than 15% of surface is collapsed
IVb	Approximately 15–30% of surface is collapsed
IVc	More than 30% of surface is collapsed

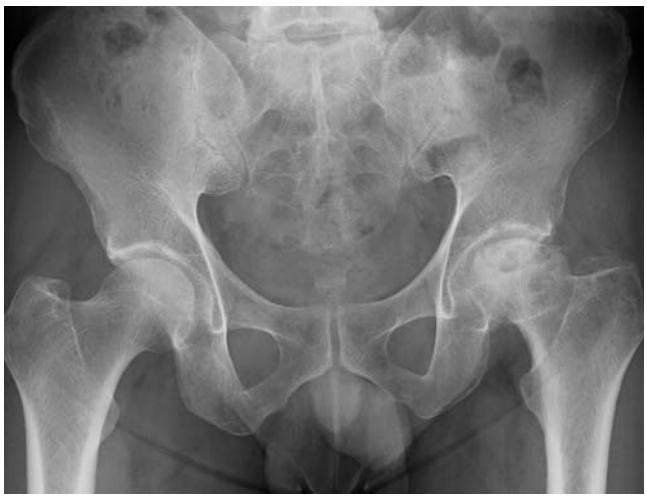

Fig. 4.2 ARCO stage IV femoral head AVN. Frontal pelvic radiograph shows mild flattening of the left femoral head with subchondral collapse. There are patchy areas of subchondral sclerosis and the fracture fragment is clearly seen. The left hip joint space is relatively preserved. Extent of femoral head collapse is consistent with ARCO stage IVc. The right femoral head is normal

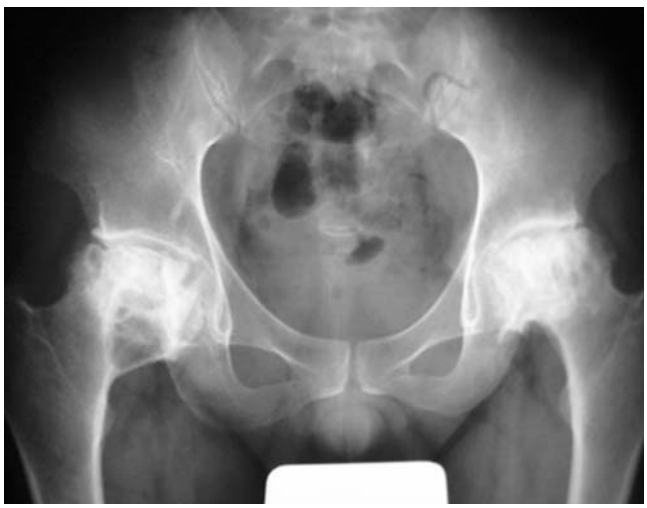

Fig. 4.3 ARCO stage IV femoral head AVN with secondary osteoarthritis. Frontal pelvic radiograph shows severe deformity of both femoral heads with cortical irregularity, fragmentation and prominent subchondral sclerosis. Secondary degenerative changes are seen as bilateral joint space narrowing, marginal osteophytes and subchondral cysts

the infarction better than radiographs (Fig. 4.6a). CT is superior to radiographs for showing subchondral fractures (Fig. 4.6b) and other features of the disease such as secondary osteoarthritis (Fig. 4.7). Except for patients who have radiographic features of established AVN, most will require MR imaging for further evaluation. Technetium-99m methyl diphosphanate bone scintigraphy was used in the past for early detection of AVN. Bone scintigraphy allows earlier detection of changes compared to radiographs, but is not as specific and not quite as sensitive as MR imaging.

MR imaging is currently the most accurate imaging technique for diagnosing AVN. MR imaging changes develop approximately 4 weeks following osteonecrosis. The development of marrow changes at the periphery of the necrotic area enables its detection, since the necrotic yellow marrow retains normal signal on MR imaging. These marrow changes consist of a T1-hypointense curvilinear rim bordering the subchondral area of normal fatty signal, typically involving the anterolateral portion of the femoral head, and in

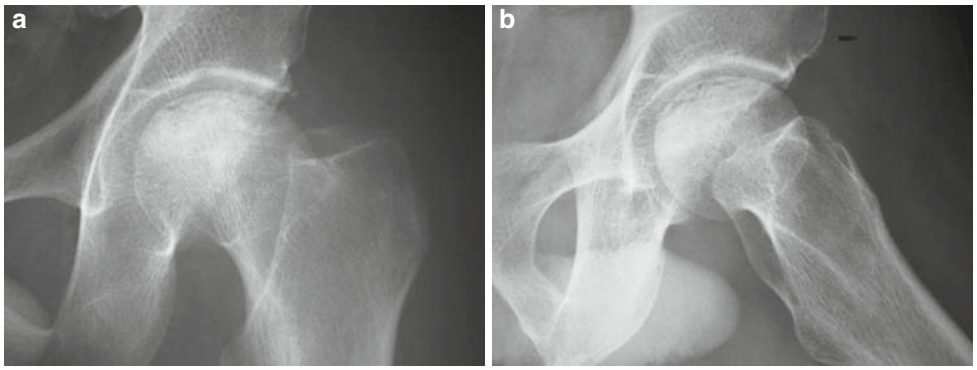

Fig. 4.4 ARCO stage III femoral head AVN. (**a**) Frontal and (**b**) frog-leg radiographs show the typical crescent sign, seen as a curvilinear radiolucency in the subchondral region. The femoral head shape and joint space are still preserved. Extent of femoral head involvement is consistent with ARCO stage IIIc

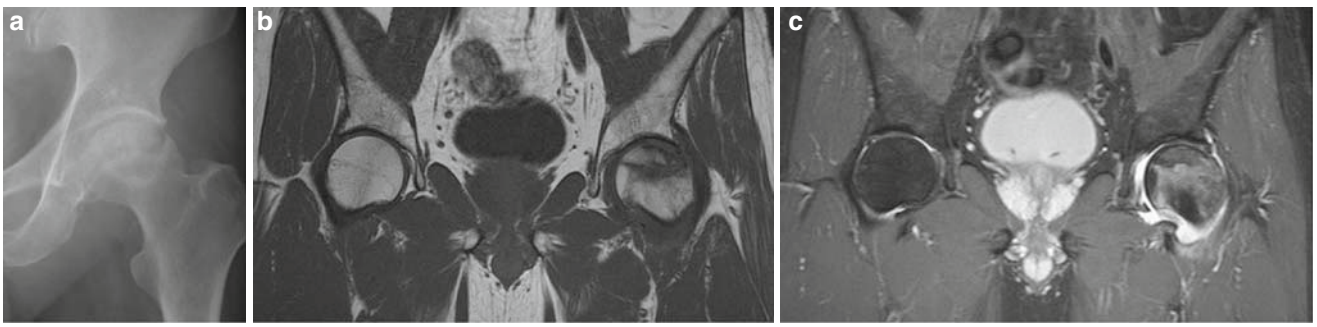

Fig. 4.5 ARCO stage II femoral head AVN. (**a**) Frontal radiograph shows ill-defined patchy sclerosis in the left femoral head. The femoral head shape and joint space are preserved. Coronal (**b**) T1-W and (**c**) TIRM MR images shows the typical changes of left femoral head AVN much better. The right femoral head is normal

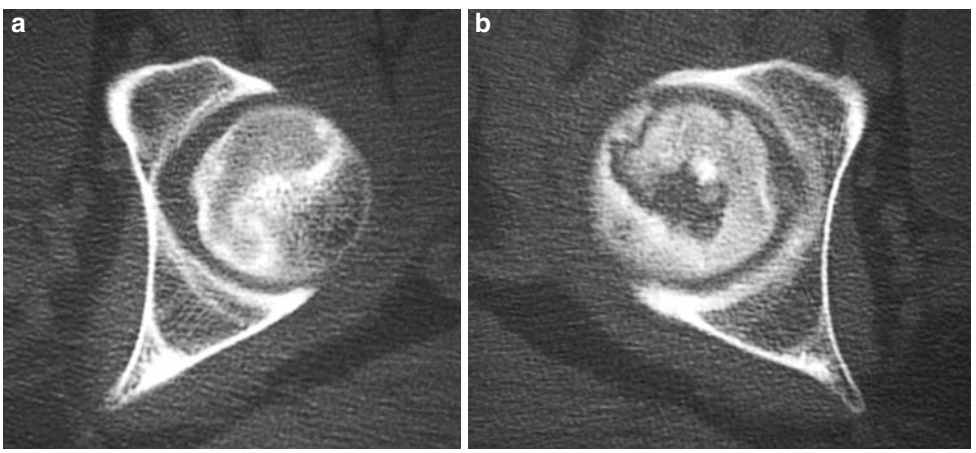

Fig. 4.6 CT changes of bilateral femoral head AVN. (**a**) Axial CT image of the left hip shows curvilinear reactive sclerosis delineating the infarcted area. (**b**) Axial CT image of the right hip shows more advanced changes, with subchondral fragmentation and collapse

a majority of cases, this interface may be seen as a "double-line" (double-line sign) consisting of a hypointense outer and hyperintense inner area of signal change on T2-weighted MR images. These MR imaging findings correspond to ARCO stage II changes (Fig. 4.8).

Subchondral fracture presents as either as a definite and abrupt depression of the subchondral bone plate with loss of femoral head sphericity or a curvilinear area of T2-hyperintensity extending just deep to the subchondral bone plate, representing fluid accumulation in a fracture cleft (ARCO stage III) (Fig. 4.9). The first of these two signs (contour depression) occurs more frequently in the weight-bearing area of the femoral head, while subchondral cleft fractures are more prevalent in non-weight-bearing portions of the head. The local signal changes (seen in ARCO stages II and III) may be blurred by adjacent bone marrow signal alterations from various causes, including reactive edema and fibrovascular repair tissue. These adjacent signal changes

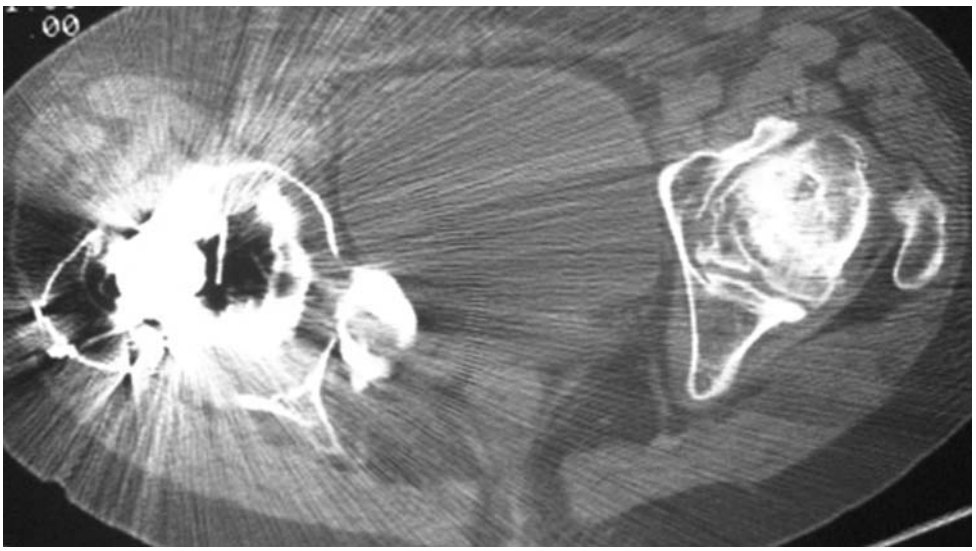

Fig. 4.7 CT changes of bilateral advanced femoral head AVN. Axial CT image shows deformity and prominent subchondral sclerosis of the left femoral head, with associated secondary degenerative changes of joint space narrowing and marginal osteophytes. The patient had a right total hip replacement for right femoral head AVN

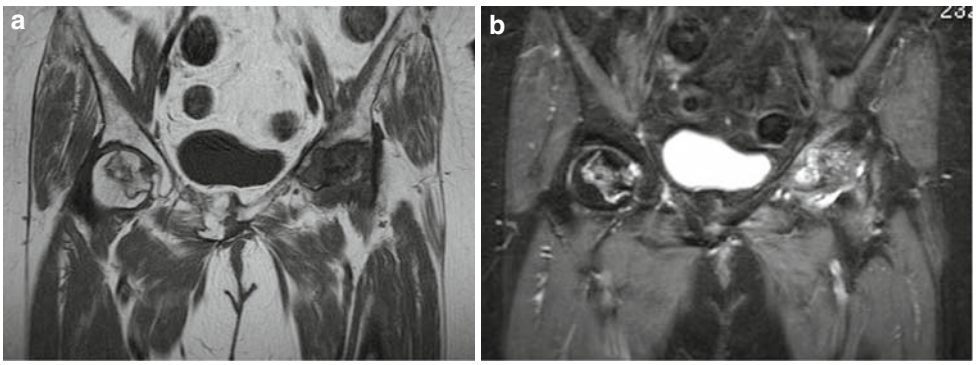

Fig. 4.8 MR imaging changes of ARCO stage II right femoral head AVN. Coronal (**a**) T1-W and (**b**) TIRM MR images show a hypointense curvilinear rim bordering the subchondral femoral head which has largely normal fatty signal, except for small areas of edema. On the TIRM image, double-line sign, consisting of a hypointense outer and hyperintense inner area, is seen at the reactive interface

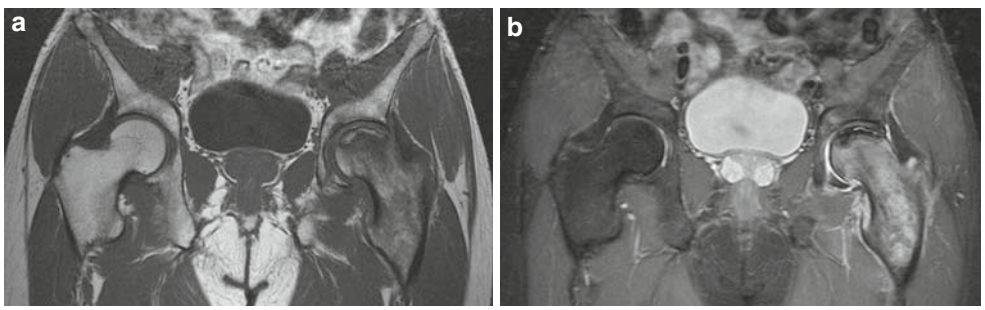

Fig. 4.9 MR imaging changes of ARCO stage III left femoral head AVN. Coronal (**a**) T1-W and (**b**) TIRM MR images show the subchondral cleft fracture in the left femoral head. Intrafracture cleft fluid is seen on the TIRM image. The right femoral head is normal

usually appear T1-hypointense and T2-iso- to hyperintense (Fig. 4.10).

Another MR imaging appearance of femoral head AVN is a diffuse area of signal change. In these cases, no detectable interface is seen and instead, there is diffuse decreased T1 and increased T2 signal intensity in the femoral head that may extend to the femoral neck. These edema-like changes are similar to and should be differentiated from those seen in other lesions, such as transient osteoporosis, bone marrow edema syndrome, subchondral insufficiency fractures, and marrow edema related to synovial disease.

MR images should be carefully evaluated to look for subchondral necrosis indicative of AVN. Subchondral necrotic tissue appears as a well-defined zonal area of hypointensity on all sequences. MR imaging signal changes in patients with normal radiographs may herald ARCO stage I disease (Fig. 4.11). In contrast, the proximal segment of subchondral bone in subchondral insufficiency fracture shows marrow

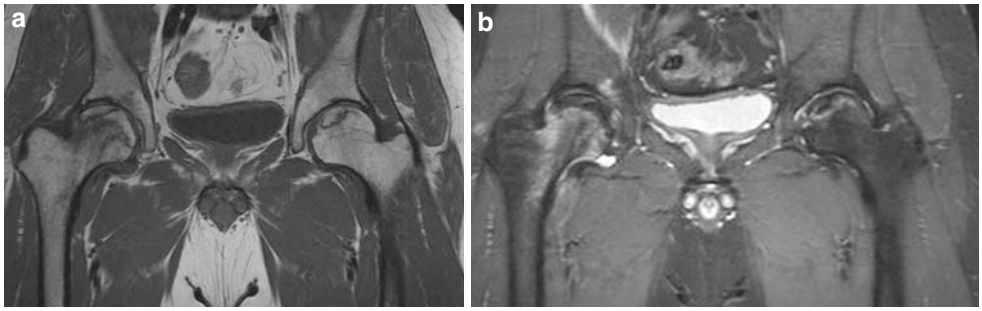

Fig. 4.10 MR imaging of bilateral femoral head AVN with right-sided reactive edema. Coronal (**a**) T1-W and (**b**) TIRM MR images show typical changes of AVN in both femoral heads, with a left-sided double line sign and patchy marrow edema bordering the reactive interface of the right-sided femoral head AVN

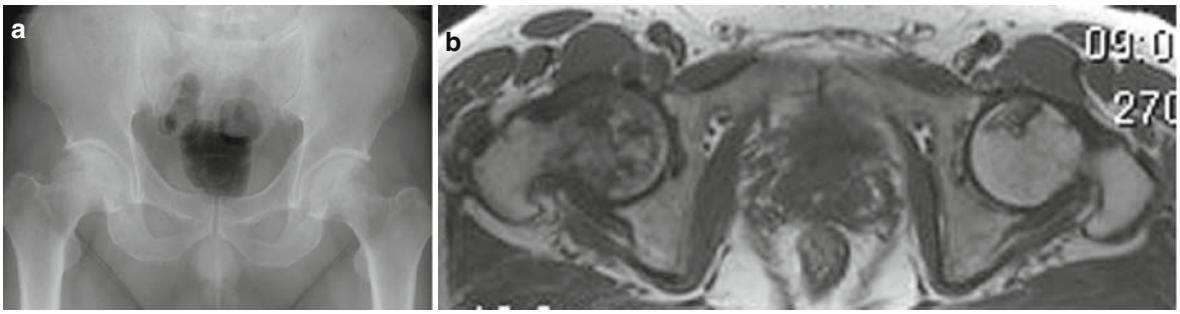

Fig. 4.11 Radiographically occult left femoral head AVN. (**a**) Frontal pelvic radiograph shows patchy sclerosis in the right femoral head (ARCO stage II) and a normal left femoral head (ARCO stage I). (**b**) Axial T1-W MR image shows typical changes of femoral head AVN, more severe on the right side

edema and repair tissue, therefore appearing hyperintense on T2-weighted images.

MR imaging is also useful to assess other abnormalities such as joint effusion (Fig. 4.12), articular cartilage integrity (Fig. 4.13), and the status of the hip after core compression (Fig. 4.14). Without treatment, femoral head AVN causes destruction of the head and secondary osteoarthritis. To prevent progression, early surgical intervention is currently recommended. Core decompression is the most common surgical procedure and aims to reduce the elevated intraosseous venous pressure, as well as to promote revascularization (Fig. 4.15).

Trauma-Induced AVN

Different anatomic sites have different patterns of blood supply. The cartilage-covered rounded surface present in the ends of bone in certain synovial joints, particularly those with a large range of motion, are especially prone to the development of osteonecrosis. The bone deep to this type of convex joint surface receives blood supply from only one direction, and is therefore particularly susceptible to disruption by trauma and other mechanisms. A typical example is the scaphoid bone where a fracture through its waist may result in osteonecrosis of the bone's proximal pole. The fragment of ischemic or dead bone may show considerable sclerosis on radiographs (Fig. 4.16). Osteonecrosis may also occur within segments of subchondral cancellous bone that have broken free from the surrounding bone. Severely comminuted, segmental and open fractures are usually associated with more significant osteonecrosis. Dislocations without fractures may also disrupt the osseous blood supply. Examples include the lunate which may dislocate following severe wrist trauma, and the femoral head, which, as already discussed, is prone to develop AVN. Development of AVN after dislocation appears to be correlated with the length of time the dislocation has remained untreated.

Slipped capital femoral epiphysis (SCFE) in the pediatric population is comparable to femoral neck fractures in adults, in that this injury may cause loss of the blood supply to the femoral epiphysis and cause head AVN. This Salter I fracture usually occurs during the early teenage growth spurt when the physeal plate has widened and so is susceptible to shear injury. The affected young adolescent usually presents with pain and limping and limitation of hip motion, particularly on internal rotation and abduction. In SCFE the femoral epiphysis displaces posteroinferiorly and so the frog-leg lateral radiograph best shows the slipped epiphysis.

Treatment aims at stabilizing the femoral head epiphysis to allow growth plate fusion, with pinning being the most frequent procedure for mild to moderate slips. Severe slips

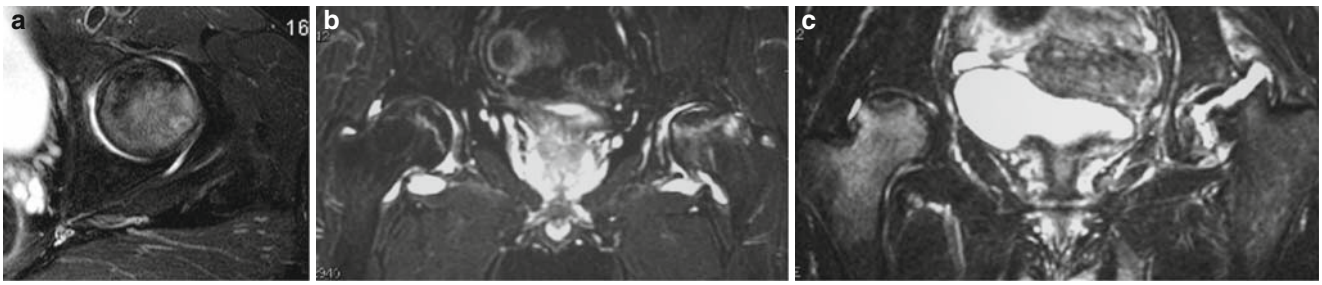

Fig. 4.12 Joint effusions associated with femoral head AVN in three different patients. (**a**) Axial T2-W MR image shows a small joint effusion in early AVN. (**b**) Coronal T2-W MR image shows bilateral hip joint effusions. There is bilateral AVN, worse on the left. (**c**) Coronal T2-W MR image shows a large left effusion that extends into the fragmented and collapsed left femoral head. Early changes are noted in the right femoral head

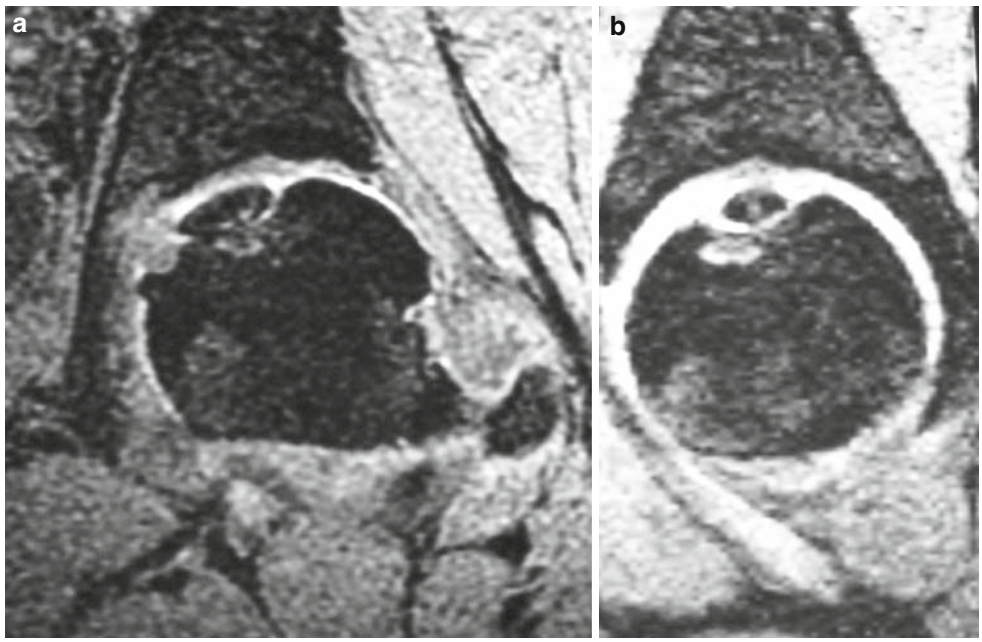

Fig. 4.13 Cartilage involvement in femoral head AVN. (**a**) Coronal and (**b**) reconstructed sagittal 3D SPGR fat-saturated MR images show the subchondral fracture cleft, with breech of the overlying articular cartilage

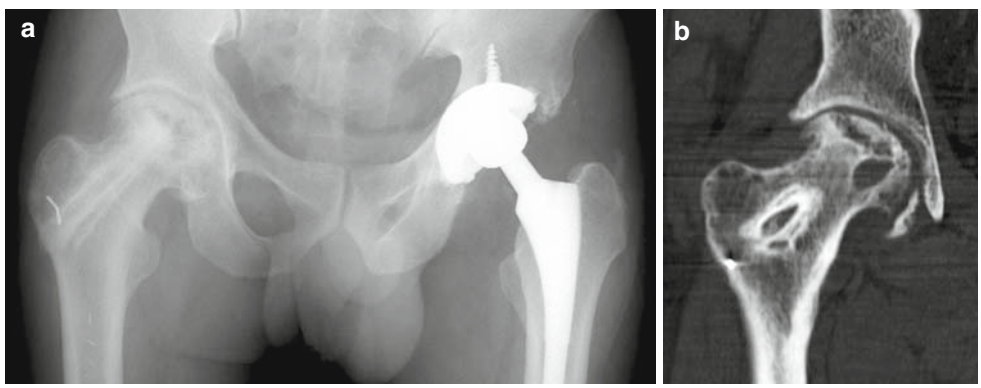

Fig. 4.14 Core decompression in advanced femoral head AVN. (**a**) Frontal pelvic radiograph and (**b**) reconstructed coronal CT image show the core compression track in the right femoral intertrochanteric region, neck, and head. There is advanced right femoral head AVN, with subchondral fragmentation. Total hip replacement had been performed for left femoral head AVN

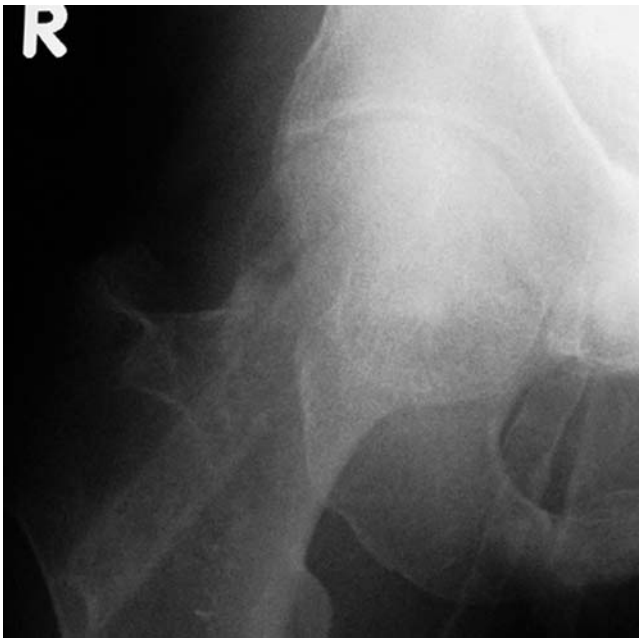

Fig. 4.15 Core decompression in early femoral head AVN. Frontal radiographs shows the core compression track and patchy sclerosis in the left femoral head. The femoral head shape and joint space are preserved (ARCO stage II)

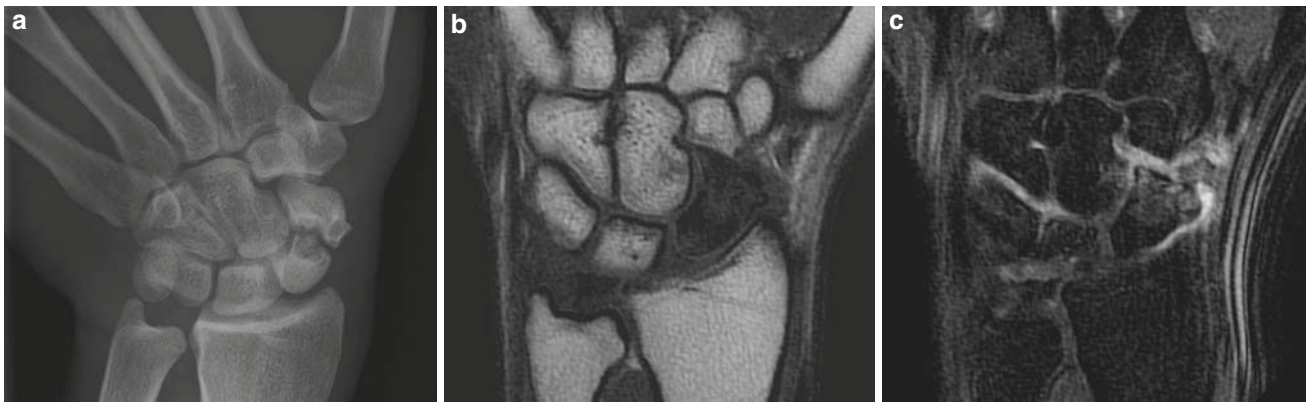

Fig. 4.16 AVN of the proximal scaphoid following a midpole fracture. (**a**) Frontal radiograph shows a wide fracture gap with sclerosis of the proximal scaphoid fragment. Coronal (**b**) T1-W and (**c**) post-Gd fat-saturated T1-W MR images show absence of marrow signal or enhancement in most of the necrotic bone

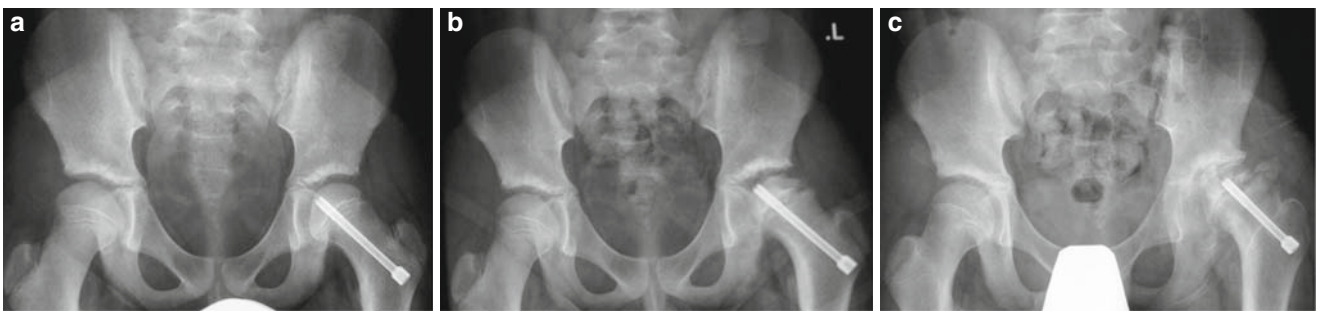

Fig. 4.17 AVN developing following pinning for SCFE. Serial radiographs taken (**a**) initially post-surgery, (**b**) 5 months later, and (**c**) 12 months later show progressive development of left femoral head AVN, with worsening sclerosis, fragmentation and collapse

may be treated by closed or open reduction or osteotomy. The surgical manipulation may cause vascular damage in an already tenuously supplied epiphysis. This may lead to AVN, a known serious iatrogenic complication of therapy (Fig. 4.17).

SONK

Spontaneous osteonecrosis of the knee (SONK) affects the weight-bearing surface of the medial femoral condyle in 95% of cases. The lateral condyle is involved in 5% of cases; rarely the tibial plateau can also be affected. Approximately 80% of SONK cases are associated with a meniscal tear. The true etiology of SONK is uncertain. Possible etiologies include vascular insufficiency and trauma, particularly a form of subchondral insufficiency fracture. The vascular pathogenesis is attributed to interruption of the femoral condylar microcirculation by thrombotic venous occlusion.

Patients with SONK are typically elderly, usually women, and present with an acute onset of knee pain. Radiographs are usually normal initially, followed later by development of flattening of the weight-bearing segment of the medial femoral condyle. Later, there is a radiolucent focus in the subchondral bone, with adjacent zone of osteosclerosis. A horizontal subchondral fracture may occur within 6–9 months, with an osteochondral fragment. In late-stage disease, secondary degenerative changes may occur. Periosteal reaction along the medial femoral shaft may be present in about one-third of cases. On MR imaging, the lesion characteristically shows a T1- and T2-hypointense focus with a convex upper border that is located subchondrally in the weight-bearing medial femoral condyle, with surrounding T1-hypointense and T2-hyperintense changes of marrow edema. Cystic changes may be present in the subchondral infarcted area (Fig. 4.18).

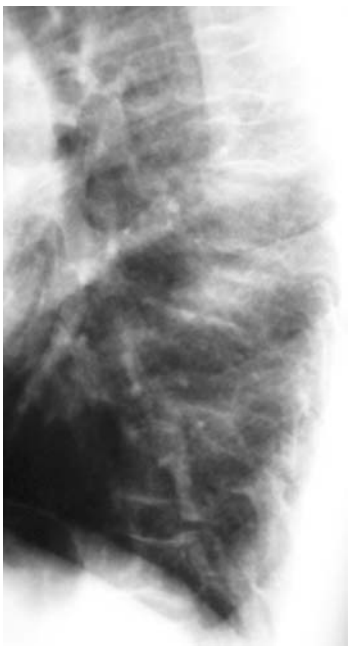

Fig. 4.19 End-plate infarcts of the vertebral bodies in 21-year-old male patient with sickle cell anemia. Lateral radiograph of the thoracic spine shows slight compressions of the midthoracic vertebral bodies with characteristic step-like central end-plate depressions

Medullary Bone Infarcts

Although both entities are virtually identical, the term bone infarct refers to osteonecrosis of the metaphyseal or diaphyseal bone, in contrast to AVN which occurs in the epiphysis

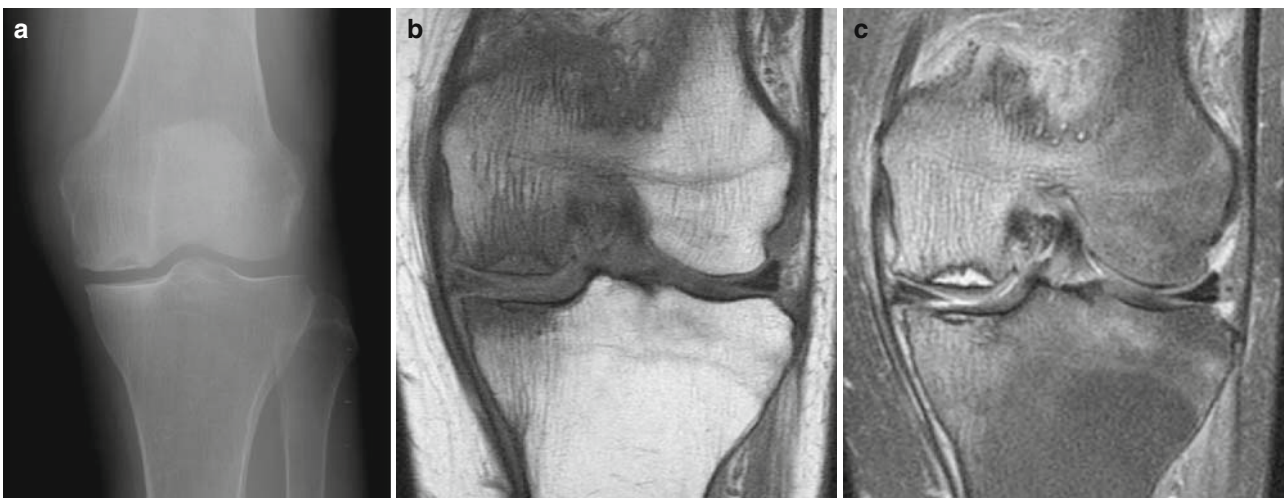

Fig. 4.18 SONK in a 72-year-old female patient. (**a**) Frontal radiograph of the left knee shows slight flattening of the articular surface of the medial femoral condyle, with a small oval radiolucent focus in the subchondral bone, bordered by an osteosclerotic rim. Coronal (**b**) T1-W and (**c**) T2-W MR images show a hypointense focus with a convex upper border that is located subchondrally in the weight-bearing portion of medial femoral condyle, with surrounding T1-hypointense and T2-hyperintense changes of marrow edema. Cystic changes within the infarcted area are appreciated on the T2-weighted image. There is an associated medial meniscus tear

or subchondral bone. The causes of bone infarction are similar to those of subchondral AVN. In patient with conditions that predispose to AVN such as sickle cell anemia (Fig. 4.19), corticosteroid therapy, or connective tissue disease and arteritis, the diagnosis of early bone infarction should be considered, especially if the lesions are multiple and located metadiaphyseally. In long bones, the nutrient artery usually provides the major blood supply to the diaphysis. Typical locations of bone infarcts are the distal femur, proximal tibia, ilium, ribs, and humerus (Fig. 4.20).

Morphologically, the changes seen in bone infarcts differ from those typically seen in AVN. Early in the course of disease, a bone infarct may appear radiographically as an area of rarefaction and, later, may have a patchy or mixed osteolytic–sclerotic pattern. With healing, the lesion becomes well-demarcated, with a serpiginous or linear zone of calcification and ossification. Areas of increased bone density indicate healing. These radiographic features are typical and identify a bone infarct as a "do not touch" lesion, a lesion that requires no further evaluation. The MR imaging appearance of a bone infarct is characteristic and useful when radiographs are equivocal. On T1-weighted images, a chronic bone infarct has a serpiginous hypointense border of reactive bone and a central component of hyperintense fatty marrow. On T2-weighted images, a linear area of signal hyperintensity outlining the infarct border, caused by a chemical shift artifact or reactive tissue, is seen. Areas of calcifications within infarcts are T1- and T2-hypointense (Fig. 4.21).

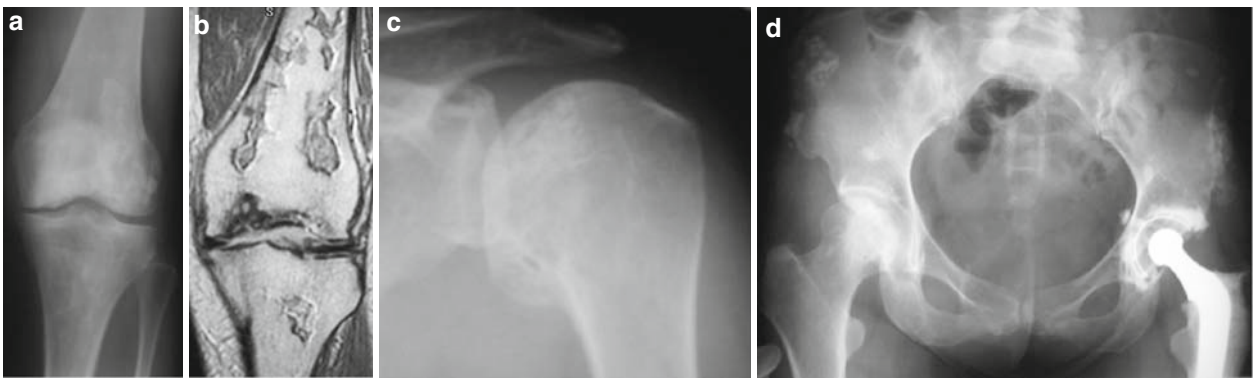

Fig. 4.20 Multiple infarcts in a 38-year-old female patient on long-term corticosteroid therapy for systemic lupus erythematosus. (**a**) Radiograph of the left knee shows dense serpiginous areas in the metadiaphyseal regions of the distal femur and proximal tibia. (**b**) Coronal PD-W MR image shows the typical appearances of multiple medullary infarcts. Frontal radiographs of the (**c**) left shoulder and (**d**) pelvis show classical changes of humeral head and right femoral head AVN, with total hip replacement for left femoral head AVN

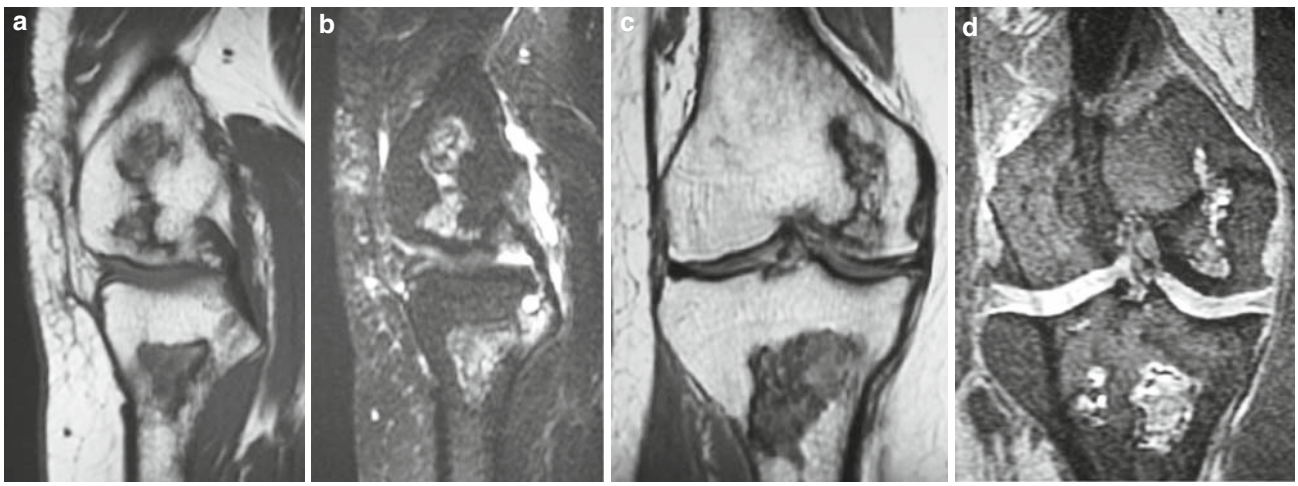

Fig. 4.21 Multiple infarcts in a 39-year-old female patient on long-term corticosteroid therapy for systemic lupus erythematosus. Sagittal (**a**) T1-W and (**b**) T2-W and coronal (**c**) T1-W and (**d**) 3D SPGR fat-saturated MR images show characteristic well-demarcated serpiginous lesions in the distal femur and proximal tibia. The lesions have T1-hypointense borders with a central component of iso- to hyperintense fatty marrow. On T2-weighted images, a linear area of signal hyperintensity outlining the infarct border is seen

AVN Precursor Syndromes

Regional Osteoporosis

There are several localized forms of osteoporosis that are unrelated to any known underlying metabolic process. These differ from generalized osteoporosis because they are reversible once the cause has been identified and treated. The most common form of regional osteoporosis is *disuse osteoporosis*, which occurs in a bone or bones that have been immobilized, most commonly as a result of trauma but from other types of immobilization as well, e.g., stroke, infection, tumor, or post-surgery (Fig. 4.22). The rapid development of osteoporosis results from osteoclastic resorption which is stimulated by local bone hyperemia. *Reflex sympathetic dystrophy* is a condition that is related to disuse osteoporosis. Other forms of regional osteoporosis include *transient osteoporosis* and *regional migratory osteoporosis*. *Periarticular osteoporosis* associated with inflammatory and infective arthropathies are outside the scope of this chapter and will be discussed elsewhere in this book.

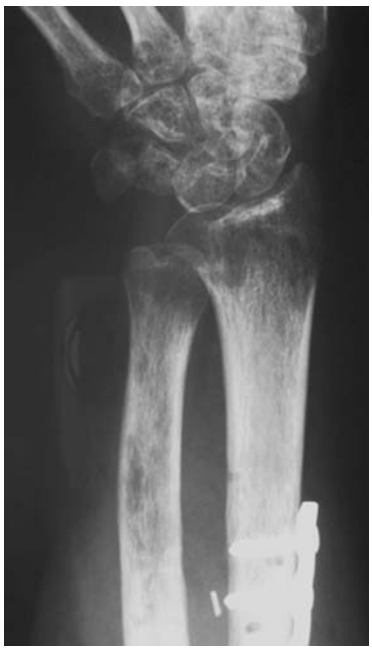

Fig. 4.22 Disuse osteoporosis in a 36-year-old male patient who underwent upper limb reimplantation. Radiograph shows patchy osteoporosis of the distal radius and fibula, carpal bones, and proximal metacarpals

Reflex Sympathetic Dystrophy

Also known as Sudeck atrophy, causalgia, and post-traumatic osteoporosis, reflex sympathetic dystrophy characteristically occurs secondary to minor trauma to a limb or from immobilization. Its etiology is not clearly understood, but it is thought that the initiating stimulus produces abnormal neural reflexes that induce the peripheral nerves to vasodilate the vessels supplying the bone. Patients present with severe pain and tenderness that is disproportionate to the degree of injury. They have local skin changes such as edema early on that progresses to atrophy later in the disease. Patients also may have Raynaud phenomenon, local vasomotor changes, and hyperhydrosis. The entire extremity distal to the injury is typically affected.

Radiographically, the bones show patchy osteoporosis that is indistinguishable from other types of osteoporosis. Bone scintiscans are often highly suggestive of the diagnosis, with increased uptake in the perfusion, blood pool and delayed images, particularly of the periarticular bones (Fig. 4.23). MR imaging may be normal or may show non-specific soft tissue edema, atrophy or marrow edema. This lesion gen-

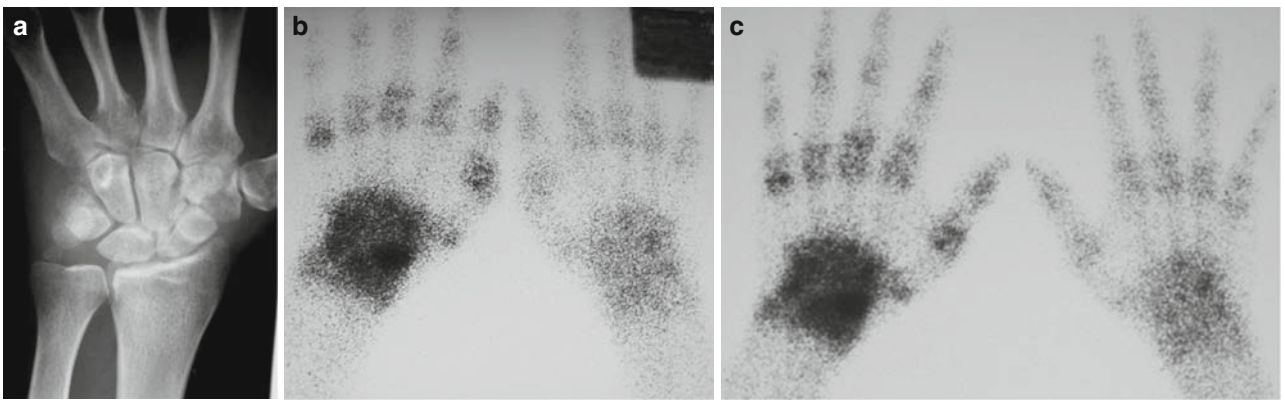

Fig. 4.23 Reflex sympathetic dystrophy in a 29-year-old male patient with minor upper limb trauma. (**a**) Frontal radiograph shows mild patchy osteoporosis in the carpal and pericarpal bones. Tc-99m MDP (**b**) blood pool and (**c**) delayed bone scintiscans show intense tracer uptake in the soft tissues and bones around the wrist

erally resolves within 6–9 months, although some patients develop contractures and have residual soft tissue atrophy.

Transient Osteoporosis

Transient osteoporosis is a poorly understood, self-limiting disorder in which a patient presents with a painful hip and there is no underlying disorder or findings, other than osteoporosis on radiographs. Although this condition was originally described in pregnant women, it most often affects middle aged adults, with a male predominance. Hip pain typically begins spontaneously and is aggravated by weight-bearing. The pain progressively decreases and completely regresses 6–12 months after onset. Although the hip is the most commonly involved, any joint may be affected, usually in the lower extremity, e.g., knee, ankle or foot. Generally, only one joint is affected at a time.

Initially, radiographs are normal, but develop marked osteopenia around the affected joint within weeks after symptom onset. This is followed by an eventual return to a normal radiographic density. There is no joint space narrowing or subchondral bone change. The diagnosis of transient osteoporosis is often a retrospective one, dependent on the temporal development and complete resolution of clinical and radiographical findings. Bone scintigraphy shows intense homogeneous uptake within the femoral head and neck. MR imaging appearances resemble those of early AVN (ARCO stage II), being seen as diffuse areas of T1-hypointensity and T2-hyperintensity in the epiphyseal region (Fig. 4.24). Unlike AVN, MR imaging does not show subchondral or segmental interface signal changes and will spontaneously resolve together with symptomatic improvement. The pathophysiology of transient osteoporosis is unknown, and postulates include an ischemic or traumatic etiology. Others have suggested that the disease is an atypical form of reflex sympathetic dystrophy.

Regional Migratory Osteoporosis

Regional migratory osteoporosis is another variant of transient bone marrow edema. Like transient osteoporosis, middle-aged men are affected and they present with rapid onset of joint pain, which is self-limited, as well as disability due to severe pain on weight-bearing. Radiographs also show severe localized osteopenia. However, unlike transient osteoporosis, there is repetitive occurrence of the same symptoms in other joints. A patient with this disorder is usually otherwise in good health, and no history of significant

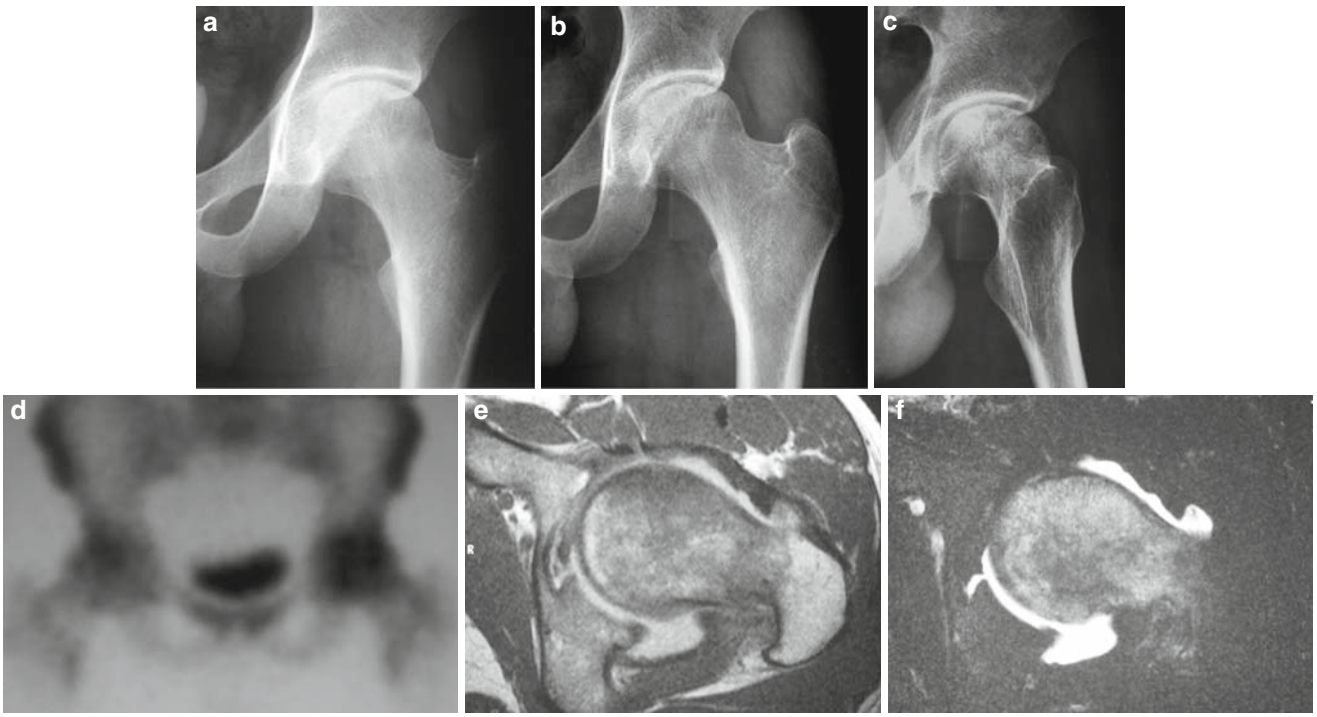

Fig. 4.24 Transient osteoporosis of the hip in a 22-year-old man with progressive left hip pain. (**a**) Initial frontal radiograph is normal. (**b**) Frontal and (**c**) oblique radiographs taken 3 months later show patchy osteoporosis of the left femoral head. (**d**) Tc-99m MDP bone scintiscan (delayed phase) shows intense tracer uptake over the left femoral head. Axial (**e**) T1-W and (**f**) T2-W MR images show T1-hypintense and T2-hyperintense signal changes in the left femoral head and neck. There is an associated hip joint effusion

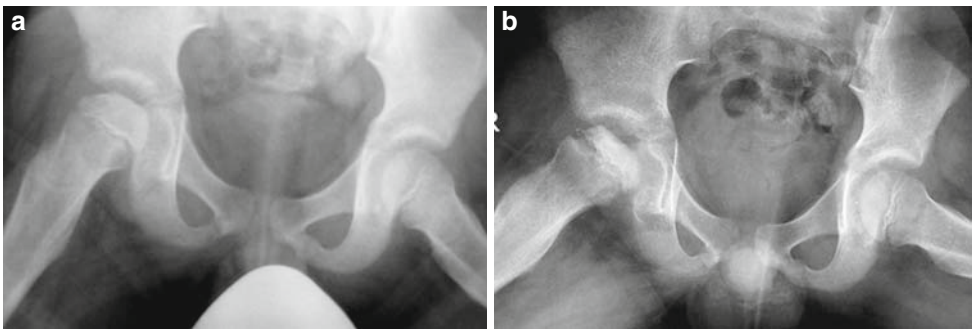

Fig. 4.25 Progression of Legg–Calve–Perthes disease in a 10-year-old boy. (**a**) Initial pelvic frog-leg radiograph shows subtle mixed sclerotic-lytic changes in the right femoral head. (**b**) Frog-leg radiograph taken 4 months later shows flattening and sclerosis of the right femoral head. The left femoral head is normal

trauma can be elicited. The lower extremity (i.e., ankle, knee, and hip) is usually involved. Localized osteoporosis may be detected radiographically within 4–8 weeks after symptom onset. Patients may have linear or wavy periosteal reaction, but the joint space and subchondral bone are preserved. MR imaging shows a bone marrow edema pattern, with diffuse areas of T1-hypointensity and T2-hyperintensity. Regional migratory osteoporosis usually persists for 6–9 months in one area. The whole cycle of symptoms may last for several years as serial joints are affected.

Osteochondroses (Related to Osteonecrosis)

The terms "osteochondritis" and "osteochondroses" are probably misnomers as they are not based on morphological findings. These terms have been used historically, however, to describe a group of disorders that involve an epiphysis or apophysis, affect the immature skeleton, and have radiographic features such as sclerosis, collapse and fragmentation of bone. Many of these conditions have been given eponyms based on varying anatomical sites at which they occur, and are named after the person who was credited for discovering them. It is now recognized that many of these "osteochondroses" are not related at all, have different etiologies, and some are even considered to be normal variants. Only the diseases traditionally classified under "osteochondroses" that are related to osteonecrosis will be described in this section, and include Legg–Calve–Perthes disease, Kienbock disease, Freiberg infraction, Kohler disease and osteochondritis dissecans. Legg–Calve–Perthes disease, or idiopathic osteonecrosis of the juvenile femoral head, is the most important of these diseases.

Legg–Calve–Perthes Disease

Legg–Calve–Perthes disease is the most common cause of AVN of the femoral head in children. There is a higher incidence in Caucasians compared to Asians, with black populations having the lowest incidence. It is occurs more frequently in girls, and the typical age of onset ranges from 3 to 8 years. At this age, the epiphyseal growth plate acts as a barrier to blood supply, with the femoral head blood supply coming from only the medial circumflex and lateral epiphyseal arteries. Insufficient blood supply therefore contributes to development of AVN. Predisposing causes include trauma, particularly posterior hip dislocation, and closed reduction of congential hip dislocation. Bilateral involvement occurs in 10% of cases. The staging systems are similar to those for adult femoral head AVN. The Catterall classification is the most widely used system and is based on radiographic assessment of the extent of epiphyseal abnormalities. Radiographic findings range from sclerosis and cystic changes in early disease (Fig. 4.25); to decreased femoral epiphyseal size (Fig. 4.26), flattening and sclerosis (Fig. 4.27); and late changes such as subchondral fracture, fragmentation, femoral neck cysts, coxa plana, and coxa magna (Fig. 4.28). Similar to adult AVN, MR imaging is useful for evaluation in equivocal radiographic findings. Radiographs are also useful for monitoring the progression of disease (Fig. 4.29).

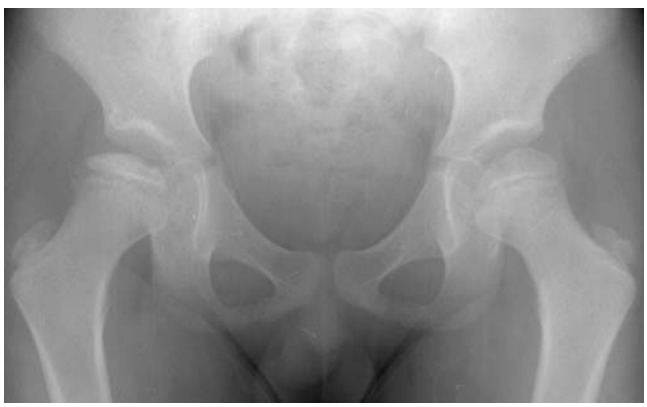

Fig. 4.26 Intermediate Legg–Calve–Perthes disease in an 8-year-old boy. Frontal pelvic radiograph shows decreased right femoral epiphyseal size and sclerosis

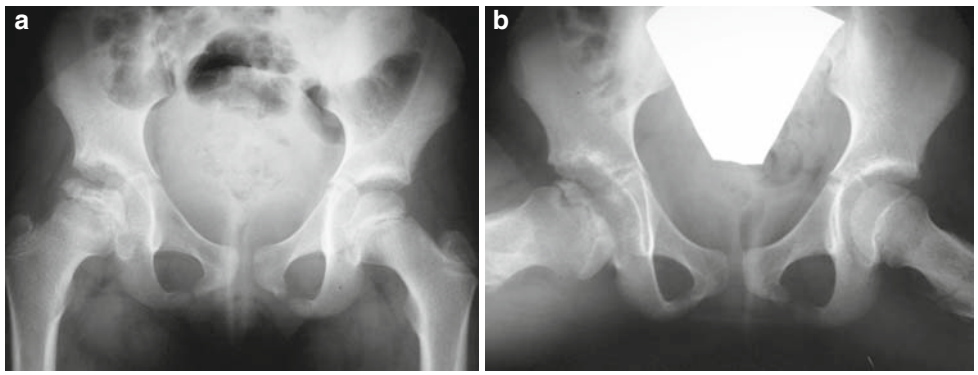

Fig. 4.27 Advanced Legg–Calve–Perthes disease in an 8-year-old girl. (**a**) Frontal and (**b**) frog-leg pelvic radiographs show flattening, sclerosis, and fissuring of the right femoral epiphysis. Frog-leg radiograph shows femoral metaphyseal remodeling deformity

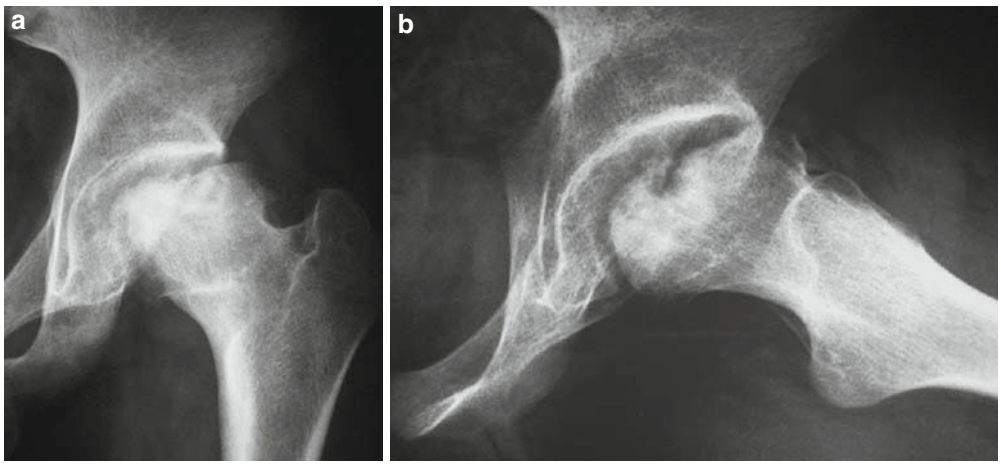

Fig. 4.28 Advanced Legg–Calve–Perthes disease in a 14-year-old boy who was diagnosed late and was hence untreated. (**a**) Frontal and (**b**) frog-leg radiographs show cortical irregularity, sclerosis and fragmentation of the left femoral head

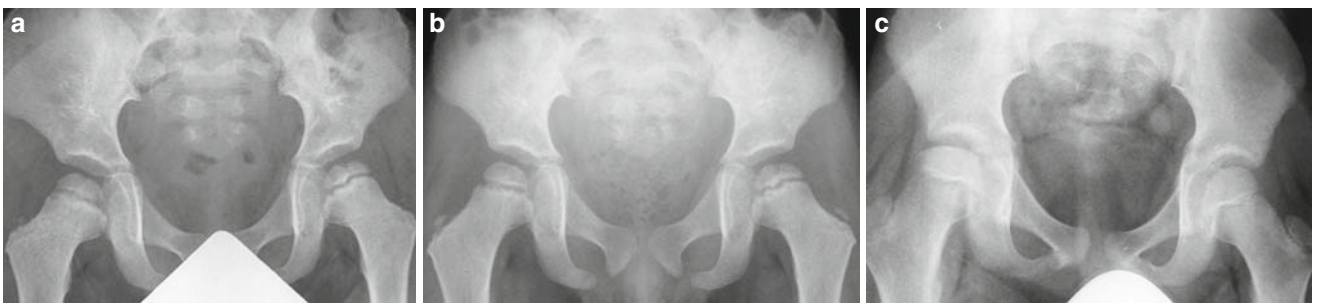

Fig. 4.29 Resolution of Legg–Calve–Perthes disease in a 4-year-old girl. (**a**) Initial frontal pelvic radiograph shows mild irregularity, with small patchy sclerotic and lucent areas, in the left femoral epiphysis. Serial radiographs taken (**b**) 6 months and (**c**) 18 months later show gradual resolution of the disease

Kienbock Disease

Kienbock disease, also known as lunatomalacia, refers to osteonecrosis of the lunate. It may result from a single traumatic episode or from repeated microtrauma in manual workers. Kienbock disease is associated with negative ulnar variance in 75% of cases. Affected patients are typically 20–40 years and present with progressive pain and soft tissue swelling of one wrist, usually the dominant hand. Initially, radiographs may be normal. With disease progression, there is sclerosis, reduction in size and shape alteration, and finally collapse of the lunate (Fig. 4.30). The disease is frequently detected after a fracture has occurred through the necrotic part of the bone. MR imaging is particularly useful for detection of early disease, when the radiographs are negative or equivocal. Bone marrow signal changes that are T1-hypointense and T2-hyperintense are present (Fig. 4.31).

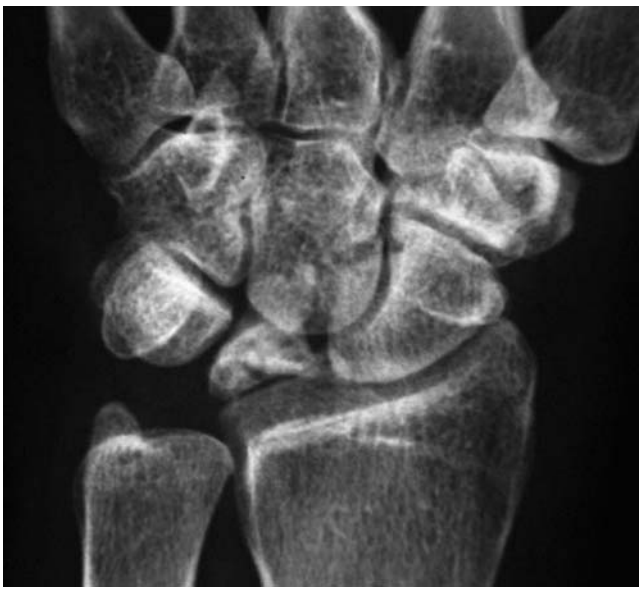

Fig. 4.30 Advanced Kienbock disease of the lunate in a 42-year-old woman. Frontal radiograph shows sclerosis, decreased size, and deformity of a collapsed lunate

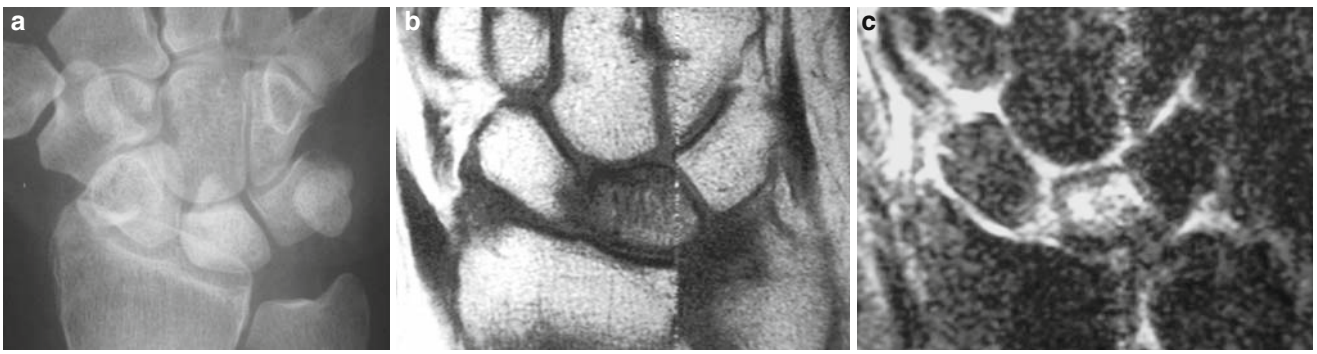

Fig. 4.31 Early Kienbock disease of the lunate in a 33-year-old woman. (**a**) Frontal radiograph shows patchy sclerosis of the lunate. The lunate shape is still preserved. Coronal (**b**) T1-W and (**c**) TIRM MR images show T1-hypointense and T2-hyperintense signal within the marrow of the lunate

Freiberg Infraction

Freiberg infraction of the metatarsal head was originally described as osteonecrosis of the second metatarsal. Any other metatarsal head, most commonly the third, may also be affected. There is a female predominance, with an age of onset of 10–15 years. Although this condition occurs during adolescence, it is usually not recognized until adulthood, when a deformity of the metatarsal head is detected on radiographs, often performed for other reasons. Patients present with pain near the affected bone. Radiographs show typical features of osteonecrotic bone at a metatarsal head, with subchondral sclerosis, cortical irregularity (Fig. 4.32) and sometimes, fragmentation. Patients may develop secondary osteoarthritis.

Kohler Disease

Kohler disease refers to idiopathic osteonecrosis of the tarsal navicular. It is usually found in boys aged 3–10 years, near the time that ossification in the navicular normally appears. The patient may be asymptomatic or have mild aching pain. On radiographs, the navicular is flattened, with an irregular outline and sclerosis. It may be fragmented. The adjacent joint spaces are usually preserved.

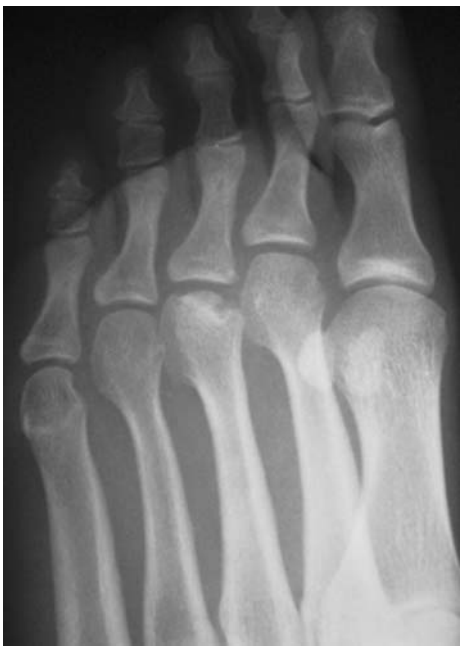

Fig. 4.32 Freiberg infraction in a 15-year-old girl. Radiograph shows cortical irregularity, mild flattening, and subchondral sclerosis of the third metatarsal head

Osteochondritis Dissecans

Ostochondritis dissecans, also known as osteochondral fracture or lesion, is a form of osteochondroses that is characterized by bony osteonecrosis, followed by reossification and healing. Its etiology, similar to SONK, is thought to be ischemia and/or trauma. This lesion is commonly found in the medial femoral condyle of the knee, dome of the talus, and occasionally the capitellum. It usually affects adolescents, with a male predominance. Patients may be asymptomatic or present with clicking, locking, limitation of joint movement, and swelling. In the knee, it may resemble spontaneous osteonecrosis (or SONK) but differs in that it primarily affects boys and young men, typically aged 10–20 years old, and usually involves the lateral aspect of the medial femoral condyle (Fig. 4.33).

Radiographically, a fracture line that parallels the joint surface may be seen. Often, the lesion leads to a small fragment of bone being sloughed, resulting in a free fragment in the joint ("joint mouse") and a defect or crater with sclerotic margins at the donor site ("mouse bed"). CT better defines

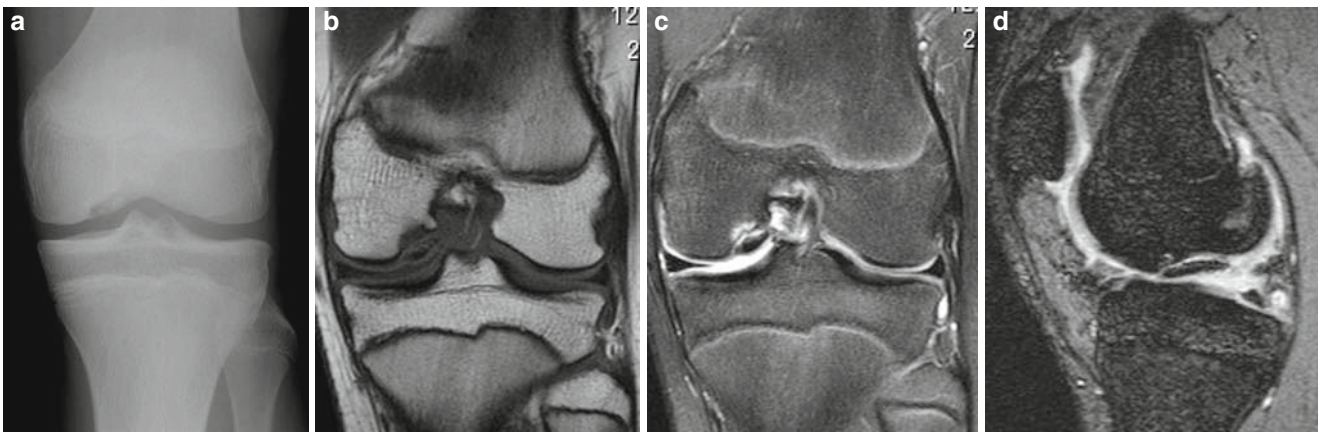

Fig. 4.33 Osteochondritis dissecans in the knee of a 17-year-old boy. (**a**) Anteroposterior radiograph shows an oval loose body (joint mouse) adjacent to a crater (mouse bed) in the lateral aspect of the medial femoral condyle. Coronal (**b**) T1-W, (**b**) T2-W, and (**c**) 3D SPGR fat-saturated MR images show the cleft between the loose body and the adjacent medial condyle

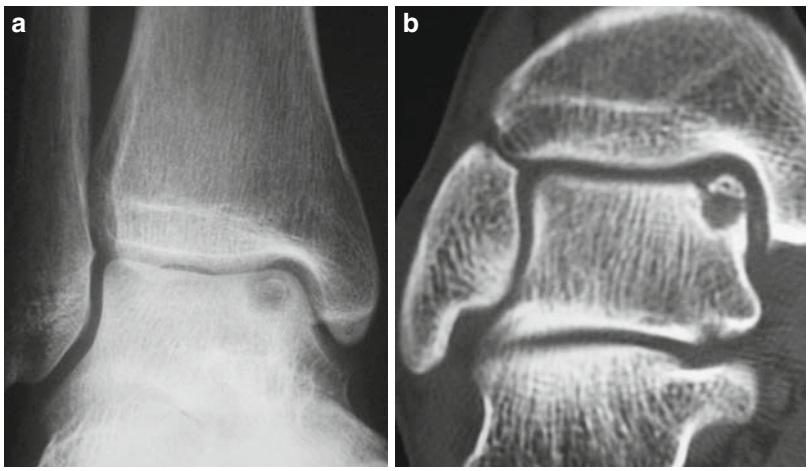

Fig. 4.34 Osteochondritis dissecans in the talar dome of a 34-year-old man. (**a**) Anteroposterior radiograph shows a rounded osteolytic lesion in the medial talar dome, not definitive for the diagnosis of an osteochondral lesion. (**b**) Coronal CT image better shows the small sloughed-off bone fragment within crater with sclerotic margins

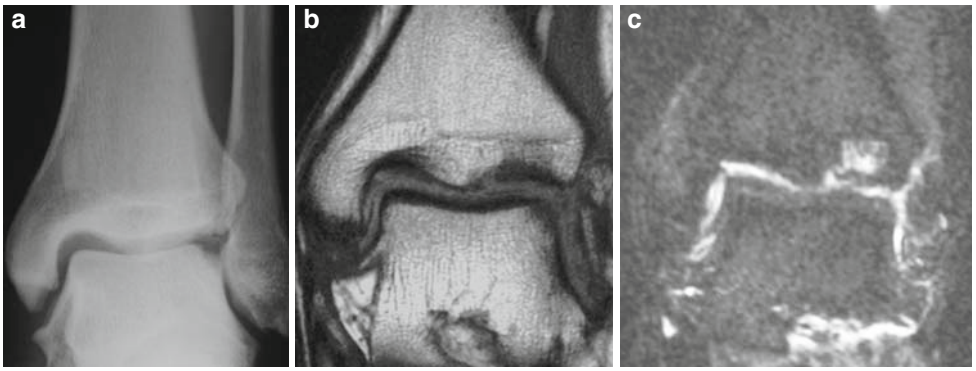

Fig. 4.35 Early osteochondral lesion of the distal tibia of an 18-year-old boy. (**a**) Anteroposterior radiograph shows a normal looking ankle joint. Coronal (**b**) T1-W and (**c**) T2-W MR images shows a small patchy T1-hypointense and a T2-hyperintense area in the lateral aspect of the distal tibia, consistent with subchondral marrow edema

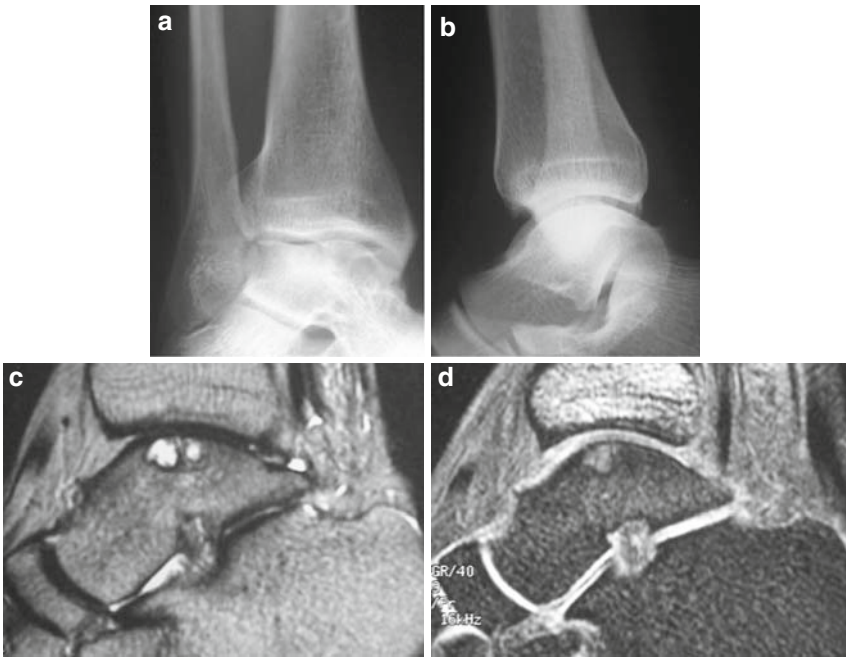

Fig. 4.36 Cystic ostechondral lesion in the talar dome of a 41-year-old man. (**a**) Anterior oblique and (**b**) lateral radiographs show a possible ostechondral lesion in the medial talar dome. Sagittal (**c**) T2-W and (**d**) 3D SPGR fat-saturated MR images show round well-defined cystic areas in the subchondral talar dome. The overlying cartilage is intact

the lesions that are equivocal on radiographs (Fig. 4.34). A pure cartilaginous fragment will usually be unrecognized on radiographs, and MR imaging is most useful for detecting chondral fragments and also early osteochondral lesions.

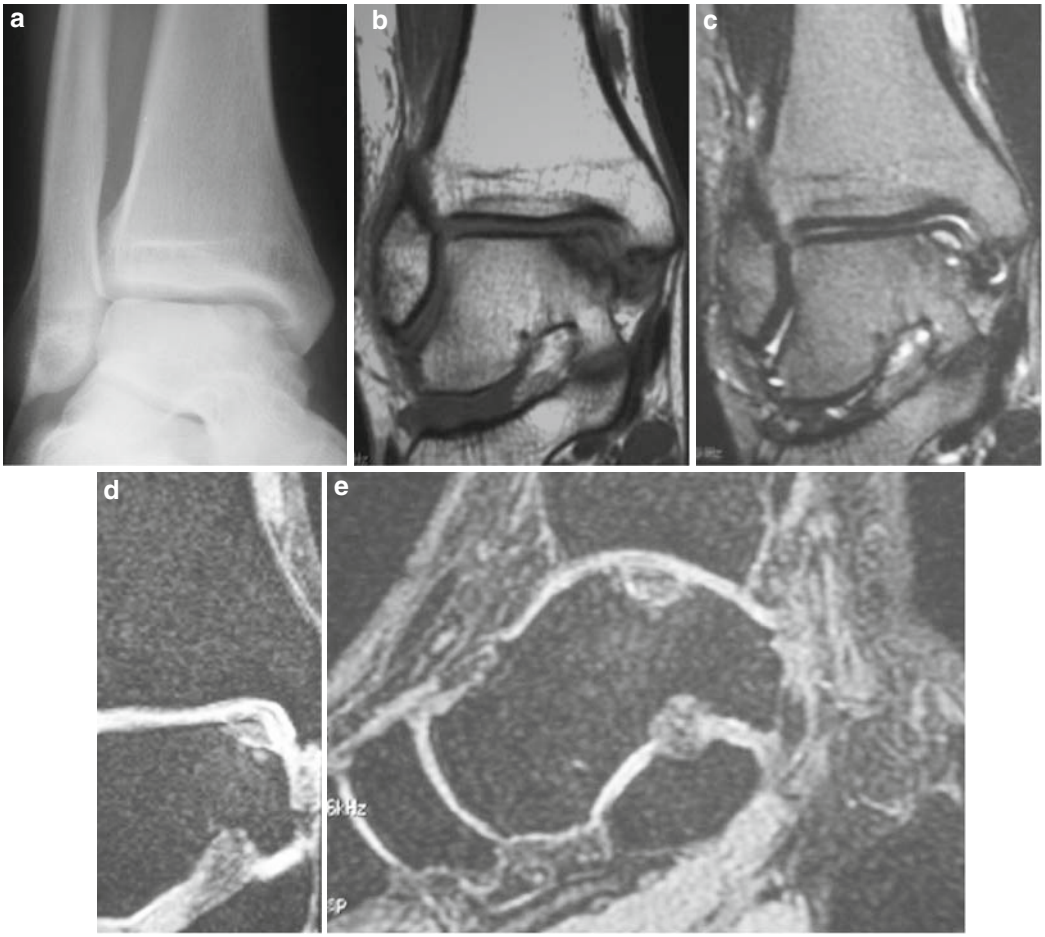

Fig. 4.37 Separated osteochondral lesion in the talar dome of a 17-year-old boy. (**a**) Anteroposterior radiograph shows an osteochondral fragment in the medial aspect of the talar dome. Coronal (**b**) T1-W and (**c**) T2-W MR images show a small subchondral lesion in the medial talar dome. (**d**) Coronal and (**e**) sagittal 3D SPGR fat-saturated MR images show fluid around the undisplaced osteochondral fragment

For the knee and talar dome, the surgical staging systems are based principally on whether or not the overlying articular cartilage is intact; if there is an osteochondral cleft, and whether there is an undisplaced or displaced fragment. The MR imaging protocol should therefore be designed to evaluate these findings, and include cartilage sequences, in additional to the standard T1- and T2-weighted sequences in the appropriate planes. MR imaging findings can be used to guide therapy, both non-surgical and surgical. MR imaging shows an area of subchondral marrow edema in the earliest stage (Fig. 4.35), followed by a subchondral cyst later on (Fig. 4.36), then development of a partially separated subchondral fragment. Fluid may then be seen between an undisplaced fragment and the parent bone (Fig. 4.37), followed in the late stage by displacement of a detached osteochondral fragment.

Miscellaneous Vascular Diseases

Frostbite

Frostbite results from cessation of circulation secondary to accumulation of cellular aggregates and thrombi in vascular beds within frozen tissue. The blood vessels are severely or irreparably damaged, as a result of exposure to low temperatures below –13°C. The more acrally located tissues, such as the digits, are damaged by formation of tiny ice crystals. Immersion foot differs from frostbite in that the foot is exposed to low but not freezing temperatures in combination with persistent dampness. This disease affects all tissues, including bone and surrounding soft tissues. The pathogenic pathway in both variants of injuries resulting from low temperatures is the development and progression of

hypoxic tissue damage directly related to circulatory abnormalities. During the exposure period in patients with frostbite, there is vascular spasm in the involved limb. With thawing, vasodilation leads to vascular wall permeability, fluid transudation, perivascular edema, and intravascular stasis.

In children, the distal phalangeal epiphyses are typically injured, with fragmentation, destruction, and premature fusion. Secondary infection, articular cartilage damage, and shortening and deformity of the fingers may occur. In adults, radiographs show osteoporosis 4–10 weeks post-injury. Periostitis may develop and resorption of the tufts of the phalanges may occur secondary to soft tissue loss. In the hands, the thumbs are typically spared due to the clenching of the fist with the thumb protected within the palm during the exposure to cold. Angiography can be used to identify vasospasm, vascular occlusion and stenosis, as well as collateral vessel formation during the recovery period. Bone scintigraphy can be used to assess tissue viability, with perfusion and blood pool images showing areas of ischemic tissue at risk, and delayed images showing the extent of deep tissue and bone infarction. Patients with scintigraphic abnormalities in all three phases and the absence of radionuclide uptake by bone on delayed images have the worst prognosis. Rhabdomyolysis may also be identified on bone scintigraphy as areas of increased uptake due to hyperperfusion in the damaged muscles (Fig. 4.38).

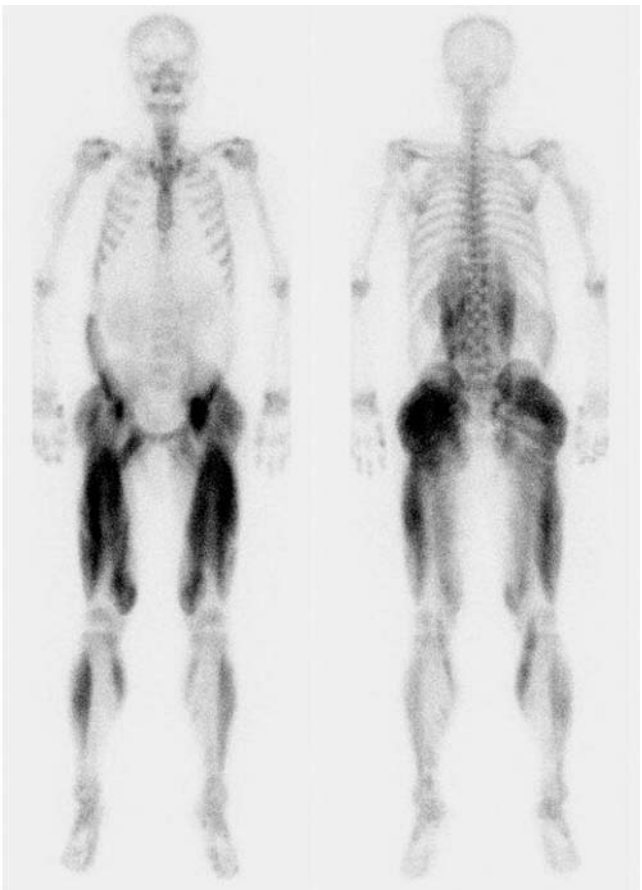

Fig. 4.38 Rhabdomyolysis due to frostbite in a 47-year-old man. Tc-99m MDP bone scintiscans show intense tracer uptake in the damaged muscles (Images courtesy of Dr. MH Sohn)

Thermal and Electrical Injuries

Both thermal and electrical injuries cause musculoskeletal tissue damage through heating of tissues. There is both vascular and lymphatic damage, frequently complicated by secondary infection, leading to tissue necrosis. In electrical injuries, besides the damaging effects of heat, mechanical trauma from uncoordinated muscle spasms, neural and vascular tissue damage, and possible direct effects of electricity also occur. Radiographic findings include osteopenia, periostitis, osteophytosis, various articular abnormalities, acro-osteolysis, pathologic fractures, osteonecrosis, and bony ankylosis. In children, epiphyseal injury and growth disturbances may occur. Initial soft tissue changes include soft tissue loss, while later changes include periarticular calcification and ossification, with eventual development of contractures, particularly around the elbow and hand. Bone scintigraphy is useful in evaluating the extent of tissue damage in burn injuries, with perfusion and blood pool images correlating well with level of amputation required. Delayed images more clearly identify necrotic lesions (Fig. 4.39).

Compartment Syndrome/Myonecrosis

Compartment syndrome results from elevated pressure within an anatomic compartment of a limb, leading to irreversible damage to its contents. The elevation of intracompartmental pressure leads to venous obstruction, then reduction of the arteriovenous gradient leading to reduced perfusion, and subsequent muscle and nerve ischemia. Compartment syndromes have numerous etiologies, including trauma with closed intracompartmental hemorrhage particularly after fractures, postischemic swelling after arterial injury, increased vascular permeability following burns, and even intense physical exertion and iatrogenic causes like application of overly tight casts and dressings. Typical clinical presentations are pain, weakness, hypesthesia, and finding of a tense, swollen muscle compartment in a limb. Untreated compartment syndrome may lead to subsequent myonecrosis and contractures.

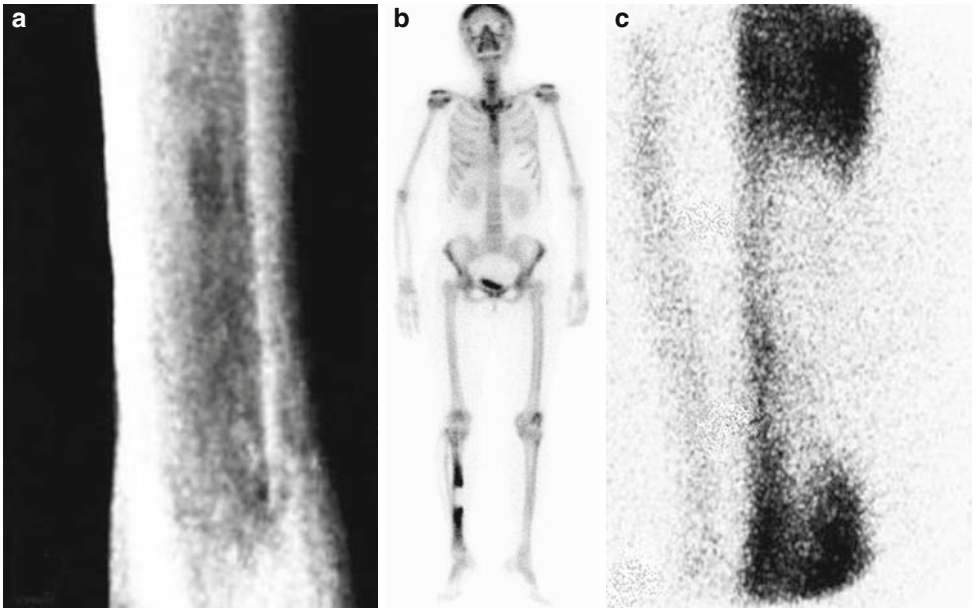

Fig. 4.39 Thermal-induced osteonecrosis of the right tibia in a 49-year-old woman. (**a**) Anteroposterior radiograph shows patchy areas of osteolysis in the tibia, with involvement of the medial cortex. The lateral cortex is preserved. (**b**) Whole-body and (**c**) pinhole Tc-99m bone scintiscans show a well-defined focal segmental defect in the midshaft of the right tibia. (Images courtesy of Dr. YW Bahk. Reproduced with permission from Bahk YW. The value of Tc-99m HDP scan in the diagnosis of tibial avascular necrosis caused by thermal injury. Nucl Med Mol Imaging 2007; 41(5):377–379)

MR imaging is the imaging modality of choice in evaluating patients with acute compartment syndrome. MR imaging features consist of muscle enlargement, loss of the normal muscle architecture, and signal abnormalities of muscles in the involved compartment, typically T1-hypointense and T2-hyperintense signal alterations. Follow-up MR imaging may show fibrosis, cystic changes, and fatty degeneration of the affected compartment. MR imaging is also useful in the assessment of myonecrosis. On T1-weighted images, there is isointense muscle swelling with fascial plane displacement, while T2-weighted images show diffuse heterogeneous hyperintensity of muscle, perifascial fluid collection, and subcutaneous edema. Post-enhancement MR images show a focal area of heterogeneously enhancing mass with peripheral enhancement. Calcific myonecrosis is a rare, late sequela that occurs almost exclusively in the lower limb. It may resemble an aggressive skeletal tumor radiographically, but is characterized by the presence of a typical peripheral and plate-like mineralization pattern.

Venous Insufficiency of Soft Tissue

Chronic venous insufficiency may produce periosteal bone formation. Postulated mechanisms for development of periostitis include hypoxia created by vascular stasis or venous hypertension and increased interstitial fluid pressure upon the periosteum. The frequency of periostitis is proportionate to the severity and duration of venous insufficiency. The distal lower limbs are almost exclusively affected, involving the tibia, fibula, metatarsals, and phalanges. On radiographs, there is soft tissue swelling due to subcutaneous edema, and there may be associated soft tissue calcifications and phleboliths. Periostitis manifests as new bone formation on the outer aspect of the cortex, usually of the diaphysis and metaphysis (Fig. 4.40). The pattern of periostitis can be variable, appearing laminated, undulating, and even irregular. With time, the periosteal layer may merge into the underlying cortex.

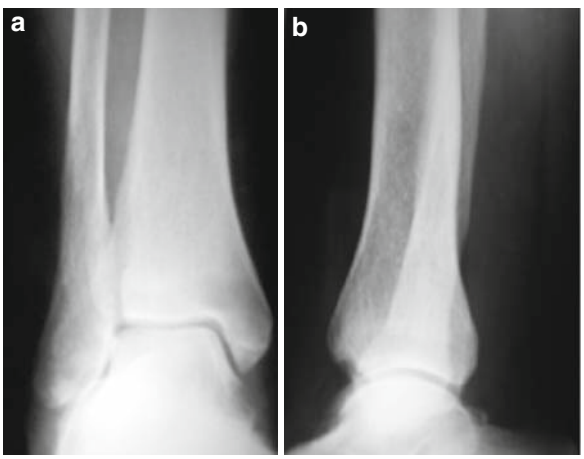

Fig. 4.40 Chronic venous insufficiency in the calf of a 73-year-old woman. (**a**) Anteroposterior and (**b**) lateral radiographs show soft tissue swelling and phleboliths posterior to the distal tibia, with mild undulating periostitis

Ischemic Fasciitis

Ischemic fasciitis, also known as atypical decubital fibroplasia, is a recently reported entity that occurs predominantly at pressure points of elderly, debilitated, and bedridden patients. Although rare, the importance of recognizing this condition is that it can be mistaken clinically, cytologically, and histologically for a soft tissue sarcoma. Ischemic fasciitis is a reactive non-neoplastic lesion that occurs in the deep subcutaneous tissue and is thought to have an ischemic pathogenesis produced by intermittent deep tissue compression. MR imaging shows a mass-like lesion that is T1-isointense, heterogeneously T2-hyperintense, and intensely enhancing except for central necrotic foci. Although these MR imaging features alone are non-specific and resemble those of necrotic sarcomas and abscesses, the distinctive finding is the location of the mass at a pressure point within the subcutaneous tissues in an elderly, chronically immobilized patient.

Further Reading

Avascular Necrosis

1. Bjorkengren AG, AlRowaih A, Lindstrand A, et al. Spontaneous osteonecrosis of the knee: value of MR imaging in determining prognosis. AJR Am J Roentgenol 1990; 154:331–336.
2. Duda SH, Laniado M, Schick F, Claussen CD. The double-line sign of osteonecrosis: evaluation on chemical shift MR images. Eur J Radiol 1993; 16:233–238.
3. Ficat RP. Idiopathic bone necrosis of the femoral head. Early diagnosis and treatment. J Bone Joint Surg 1985; 67B:3–9.
4. Huang GS, Chan WP, Chang YC, et al. MR imaging of bone marrow edema and joint effusion in patients with osteonecrosis of the femoral head: relationship to pain. AJR Am J Roentgenol 2003; 181:545–549.
5. Iida S, Harada Y, Shimizu K, et al. Correlation between bone marrow edema and collapse of the femoral head in steroid-induced osteonecrosis. AJR Am J Roentgenol 2000; 174:735–743.
6. Ito H, Kaneda K, Matsuno T. Osteonecrosis of the femoral head. J Bone Joint Surg 1999; 81B:969–974.
7. Jergesen HE, Lang P, Moseley M, Genant HK. Histologic correlation of magnetic resonance imaging of femoral head osteonecrosis. Clin Orthop 1990; 253:150–163.
8. Koo KH, Ahn IO, Kim R, et al. Bone marrow edema and associated pain in early stage osteonecrosis of the femoral head: prospective study with serial MR images. Radiology 1999; 213:715–722.
9. Kubo T, Yamamoto T, Inoue S, et al. Histological findings of bone marrow edema pattern on MRI in osteonecrosis of the femoral head. J Orthop Sci 2000; 5:520–523.
10. Lafforgue P, Dahan E, Chagnaud C, et al. Early-stage avascular necrosis of the femoral head: MR imaging for prognosis in 31 cases with at least 2 years of follow-up. Radiology 1993; 187:199–204.
11. Lafforgue P. Pathophysiology and natural history of avascular necrosis of bone. Joint Bone Spine 2006; 73:500–507.
12. Lecouvet FE, van de Berg FC, Maldague BE, et al. Early irreversible osteonecrosis versus transient lesions of the femoral condyles: prognostic value of subchondral bone and marrow changes on MR imaging. AJR Am J Roentgenol 1998; 170:71–77.
13. Lieberman JR, Berry DJ, Mont MA, et al. Osteonecrosis of the hip: management in the 21st century. Instr Course Lect 2003; 52:337–355.
14. Lieberman JR. Core decompression for osteonecrosis of the hip. Clin Orthop Rel Res 2004; 418:29–33.
15. Milgram JW. Osteonecrosis due to trauma and idiopathic causes. In: Radiologic and Histologic Pathology of Nontumorous Diseases of Bone and Joints. Northbrook: Northbrook Publishing, 1990; 959–1026.
16. Mitchell D, Kressel H, Arger P, Dalinka M, Spritzer C, Steinberg M. Avascular necrosis of the femoral head: morphologic assessment by MR imaging, with CT correlation. Radiology 1986; 161:739–742.
17. Mitchell DG, Rao VM, Dalinka MK, et al. Femoral head avascular necrosis: correlation of MR imaging, radiographic staging, radionuclide imaging, and clinical findings. Radiology 1987; 162:709–715.
18. Munk PL, Helms CA, Holt RG. Immature bone infarcts: findings on plain radiographs and MR scans. AJR Am J Roentgenol 1989; 152:547–549.
19. Narvaez J, Narvaez JA, Rodriquez-Moreno J, Roig-Ecofet D. Osteonecrosis of the knee: differences among idiopathic and secondary types. Rheumatol 2000; 39:982–989.
20. Sakai T, Sugano N, Nishii T, et al. MR findings of necrotic lesions and the extralesional area of osteonecrosis of the femoral head. Skeletal Radiol 2000; 29:133–141.
21. Sakamoto M, Shimizu K, Iida S, et al. Osteonecrosis of the femoral head: a prospective study with MRI. J Bone Joint Surg 1997; 79B:213–319.
22. Seiler JG III, Kregor PJ, Conrad EU III, Swiontkowski MF. Posttraumatic osteonecrosis in a swine model. Correlation of blood cell flux, MRI and histology. Acta Orthop Scand 1996; 67:249–254.
23. Shimizu K, Moriya H, Akita T, Sakamoto M, Suguro T. Prediction of collapse with magnetic resonance imaging

of avascular necrosis of the femoral head. J Bone Joint Surg 1994; 76A:215–223.
24. Steinberg ME, Hayken GF, Steinberg DR. A quantitative system for staging avascular necrosis. J Bone Joint Surg 1995; 77B:34–41.
25. Stevens K, Tao C, Lee SU, et al. Subchondral fractures in osteonecrosis of the femoral head: comparison of radiography, CT, and MR imaging. AJR Am J Roentgenol 2003; 180:363–368.
26. Vande Berg BC, Malgehm JJ, Labaisse MA, et al. MR imaging of avascular necrosis and transient bone marrow edema of the femoral head. Radiographics 1993; 13:501–520.
27. Vande Berg BC, Lecouvet FE, Maldague B, Malghem J. Osteonecrosis and transient osteoporosis of the femoral head. In: AM Davies, K Johnson, RW Whitehouse (Eds.), Imaging of the Hip and Bony Pelvis. Technique and Applications. Berlin: Springer, 2006; 195–216.
28. Watson RM, Roach NA, Dalinka MK. Avascular necrosis and bone marrow edema syndrome. Radiol Clin North Am 2004; 42:207–219.
29. Yamamoto T, Bullough PG. Spontaneous osteonecrosis of the knee: the result of subchondral insufficiency fracture. J Bone Joint Surg 2000; 82A:858–866.

AVN Precursor Syndromes

1. Borre GE, Borre DG, Hofer B, et al. Sudeck's dystrophy of the hand. MR imaging. Clin Imaging 1995; 19:188–192.
2. Davies M, Cassar-Pullicino VM, Darby AJ. Subchondral insufficiency fractures of the femoral head. Eur Radiol 2004; 14:201–207.
3. Gill HC, Levine SM, Zoga AC. MRI findings in the subchondral bone marrow: a discussion of conditions including transient osteoporosis, transient bone marrow edema syndrome, SONK, and shifting bone marrow edema of the knee. Semin Musculoskeletal Radiol 2006; 10:177–186.
4. Hayes CW, Conway WF, Daniel WW. MR imaging of bone marrow edema pattern: transient osteoporosis, transient bone marrow edema syndrome, or osteonecrosis. Radiographics 1993; 13:1001–1011.
5. Koch E, Hofer HO, Sialer G, et al. Failure of MR imaging to detect reflex sympathetic dystrophy of the extremities. AJR Am J Roentgenol 1991; 156:113–115.
6. Milgram JW. Localized forms of osteoporosis. In: Radiologic and Histologic Pathology of Nontumorous Diseases of Bone and Joints. Northbrook: Northbrook Publishing, 1990; 943–950.
7. Quek ST, Peh WCG. Radiology of osteoporosis. Semin Musculoskeletal Radiol 2002; 6:197–206.
8. Potter H, Moran M, Schneider R, et al. Magnetic resonance imaging in diagnosis of transient osteoporosis of the hip. Clin Orthop 1992; 280:223–229.
9. Schweitzer ME, Mandel S, Schwartzman RJ, et al. Reflex sympathetic dystrophy revisited: MR imaging findings before and after infusion of contrast material. Radiology 1995; 195:211–214.
10. Takatori Y, Kokubo T, Nimomiya S, Nakamura T, Okutsu J, Kamogawa M. Transient osteoporosis of the hip. Magnetic resonance imaging. Clin Orthop 1991; 271:190–194.
11. Vande Berg BC, Malghem JJ, Lecouvet FE, Jamart J, Maldague BE. Idiopathic bone marrow edema lesions of the femoral head: predictive value of MR imaging findings. Radiology 1999; 212:527–535.
12. Wilson AJ, Murphey WA, Hardy DC, Totty WG. Transient osteoporosis: transient bone marrow edema? Radiology 1988; 167:757–760.
13. Wuisman PI, Noorda RJ. Transient osteoporosis of the hip. J Bone Joint Surg 1998; 80B:743.
14. Yamamoto T, Kubo T, Hirasawa Y, et al. A clinicopathological study of transient osteoporosis of the hip. Skeletal Radiol 1999; 28:621–627.
15. Yamamoto T, Schneider R, Bullough PG. Subchondral insufficiency fracture of the femoral head: histopathologic correlation with MRI. Skeletal Radiol 2001; 30:247–254.
16. Zyluk A. The usefulness of quantitative evaluation of three-phase scintigraphy in the diagnosis of posttraumatic reflex sympathetic dystrophy syndrome. J Hand Surg 1999; 24B:16–21.

Osteochondroses Related to AVN

1. Bohndorf K. Osteochondritis (osteochondrosis) dissecans: a review and new MRI classification. Eur Radiol 1998; 8:103–112.
2. Catterall A. The natural history of Perthes' disease. J Bone Joint Surg 1971; 53B:37–53.
3. De Smet AA, Fisher DR, Graf BK, Lange RH. Osteochondritis dissecans of the knee: value of MR imaging in determining lesion stability and the presence of articular cartilage defects. AJR Am J Roentgenol 1990; 155:549–553.
4. De Smet AA, Ilahi OA, Graf BK. Reassessment of the MR criteria for stability of osteochondritis dissecans

in the knee and ankle. Skeletal Radiol 1996; 25: 159–163.
5. Hinshaw MH, Tuite MJ, De Smet AA. "Dem bones": osteochondral injuries of the knee. Magn Resonan Imaging Clin N Am 2000; 8:335–348.
6. Hochbergs P, Eckervall G, Wingstrand H, et al. Epiphyseal bone marrow abnormalities and restitution in Legg-Calve-Perthes disease. Evaluation by MR imaging in 86 cases. Acta Radiol 1997; 38:855–862.
7. Loredo R, Sanders TG. Imaging of osteochondral injuries. Clin Sports Med 2001; 20:249–278.
8. Milgram JW. Osteonecrosis due to trauma and idiopathic causes. In: Radiologic and Histologic Pathology of Nontumorous Diseases of Bone and Joints. Northbrook: Northbrook Publishing, 1990; 959–1026.
9. Purry NA. The incidence of Perthes' disease in three population groups in the Easterrn Cape region of South Africa. J Bone Joint Surg 1982; 64B:286–288.
10. Rowe SM, Jung ST, Lee KB, et al. The incidence of Perthes' disease in Korea: a focus on differences among races. J Bone Joint Surg 2005; 87B:1666–1668.
11. Rubin DA. Magnetic resonance imaging of chondral and osteochondral injuries. Top Magn Resonan Imaging 1998; 9:348–359.
12. Sanders RK, Crim JR. Osteochondral injuries. Semin Ultrasound CT MR 2001; 22:352–370.

Miscellaneous Vascular Diseases of Bone and Soft Tissue

Frostbite

1. Carrera GF, Kozin R, Flaherty L, McCarty DJ. Radiographic changes in the hands following childhood frostbite injury. Skeletal Radiol 1981; 6:33–37.
2. Cauchy E, Chetaille R, Lefevre M, et al. The role of bone scanning in severe frostbite of the extremities: a retrospective study of 88 cases. Eur J Nucl Med 2000; 27: 497–502.
3. Crouch C, Smith WL. Long term sequelae of frostbite. Pediatr Radiol 1990; 20:365–366.
4. Mehta RC, Wilson MA. Frostbite injury: prediction of tissue viability with triple phase bone scanning. Radiology 1989; 170:511–514.
5. Reed MH. Growth disturbances in the hands following thermal injuries in children. 2. Frostbite. Can Assoc Radiol J 1988; 39:95–99.
6. Rosenthal L, Kloiber R, Gagnon R, et al. Frostbite with rhabdomyolysis and renal failure: radionuclide study. AJR Am J Roentgenol 1981; 137:387–390.

Thermal and Electrical Injuries

1. Balen PF, Helms CA. Bony ankylosis following thermal and electrical injury. Skeletal Radiol 2001; 30:393–397.
2. Brinn LB, Moseley JE. Bone changes following electrical injury: case report and review of literature. AJR Am J Roentgenol 1966; 97:682–686.
3. Evans EB. Heterotopic bone formation in thermal burns. Clin Orthop 1991; 263:94–101.
4. Kao PF, Tzen KY, Chang LY, et al. 99Tc-MDP scintigraphy in high-voltage electrical burn patients. Nucl Med Commun 1997; 18:846–852.
5. Kolar J. Locomotor consequences of electrical and radiation injuries, burns and freezings. Ballieres Clin Rheumatol 1989; 3:99–110.
6. Trapnell DH, Jackson D. Bone and joint changes following burns. Clin Radiol 1965; 16:180–186.

Compartment Syndrome/Myonecrosis

1. Dhillon M, Davies AM, Benham J, et al. Calcific myonecrosis: a report of ten new cases with an emphasis on MR imaging. Eur Radiol 2004; 14:1974–1979.
2. Elsayes KM, Lammle M, Shariff A, et al. Value of magnetic resonance imaging in muscle trauma. Curr Probl Diagn Radiol 2006; 35:206–212.
3. Holobinko JN, Damron TA, Scerpella PR, Hojnowski L. Calcific muonecrosis: keys to early recognition. Skeletal Radiol 2003; 32:35–40.
4. Lu CH, Tsang YM, Yu CW, et al. Rhabdomyolysis: magnetic resonance imaging and computed tomography findings. J Comput Assist Tomogr 2007; 31:368–374.
5. Kattapuram TM, Suri R, Rosol ME, et al. Idiopathic and diabetic skeletal muscle necrosis: evaluation by magnetic resonance imaging. Skeletal Radiol 2005; 34:203–209.
6. Rominger MB, Lukosch CJ, Bachmann GF. MR imaging of compartment syndrome of the lower leg: a case control study. Eur Radiol 2004; 14:1432–1439.

Venous Insufficiency

1. Dannels EG, Nashel DJ. Periostitis. A manifestation of venous disease and skeletal hyperostosis. J Am Podiatry Assoc 1983; 73:461–464.
2. Kumar R, Roper PR, Guinto FC Jr. Subcutaneous ossification of the legs in chronic venous stasis. J Comput Assist Tomogr 1983; 7:377–378.
3. Lippmann HI, Goldin RR. Subcutaneous ossification of the legs in chronic venous insufficiency. Radiology 1960; 74:279–288.

4. Wang L, Fritton SP, Weinbaum S, Cowin SC. On bone adaptation due to venous stasis. J Biomech 2003; 36:1439–1451.

Ischemic Fasciitis

1. Ilaslan H, Joyce Bauer T, Sundaram M. Decubital ischemic fasciitis: clinical, pathologic, and MRI features of pseudosarcoma. AJR Am J Roentgenol 2006; 187:1338–1341.
2. Kendall BS, Liang CY, Lancaster KJ, et al. Ischemic fasciitis. Report of a case with fine needle aspiration findings. Acta Cytol 1997; 41:598–602.
3. Montgomery EA, Meis JM, Mitchell MS, Enzinger FM. Atypical decubital fibroplasia. A distinct fibroplastic pseudotumor occurring in debilitated patients. Am J Surg Pathol 1992; 16:708–715.
4. Perosio PM, Weiss SW. Ischemic fasciitis: a juxta-skeletal fibroblastic proliferation with a predilection for elderly patients. Mod Pathol 1993; 6:69–72.

Chapter 5

Imaging Approach to Musculoskeletal Trauma

William R. Reinus

Abstract Trauma is a common and major cause of musculoskeletal pathology. The entire musculoskeletal system is subject to trauma from minor muscle strains to full-scale fractures and dislocations. In this chapter, we present the principles and approach to imaging trauma including fractures; dislocations; ligament, fibrocartilage, hyaline cartilage tears; tendon sprains; and muscle strains. Each topic is discussed with a focus on pathophysiologically correct diagnosis and appropriate imaging technique, including radiographs, computed tomography, ultrasound, and magnetic resonance imaging. The interaction between various parts of the musculoskeletal system in response to a traumatic event is discussed. Types of fractures and their clinical implications will be reviewed. Common dislocations are discussed. Typical cartilage injuries are reviewed. Muscle strains, tendon, and ligament injuries are reviewed.

Keywords Fracture • Dislocation • Sprain • Strain • Wolff law • Insufficiency fracture • Myofascial herniation • Rotator cuff • Meniscus • Ligament • Tendon • Infraction • Osteochondral fracture

Introduction

Diagnosing trauma comprises a major part of musculoskeletal radiology. In fact, since the advent of magnetic resonance imaging, the role of the musculoskeletal radiologist has expanded greatly. Not only is musculoskeletal imaging important in diagnosing fractures and dislocations, but soft tissue injury and internal derangements of joints have become as important, if not more important, as imaging osseous trauma. In addition, MRI has made it possible to diagnose subtle trauma-related inflammatory conditions such as overuse syndromes.

W.R. Reinus (✉)
Department of Radiology, Temple University School of Medicine, Philadelphia, PA 19140, USA
e-mail: reinusw@tuhs.temple.edu

We will leave detailed discussion of individual fractures and soft tissue injuries to other authors as the topic is too vast to be considered in a textbook of this scope. Instead we will address osseous and soft tissue trauma each as a class and discuss the principles that will help the reader to understand, diagnose, and evaluate healing of different types of trauma.

Osseous Trauma

Bones are subject not only to fracture but also to infraction and contusion. There is some confusion among these terms and usage has been somewhat loose, particularly differentiating between contusion and infraction and differentiating between infraction and fracture. For our purposes, fractures violate more than one cortex of the traumatized bone and the fractured fragments are displaced visibly (Fig. 5.1). Infractions generally violate only one cortex at a single region and although the bone may show focal impaction, no fragments

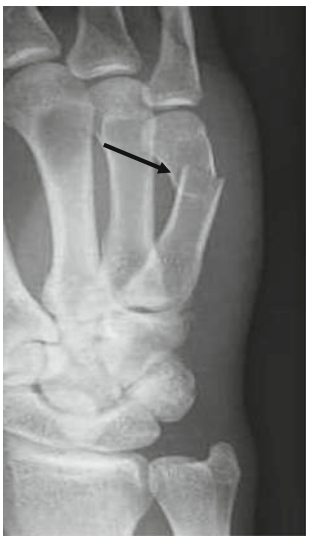

Fig. 5.1 Oblique coned down radiograph showing a fracture of the 5th metacarpal bone (*arrow*)

A. Bonakdarpour et al. (eds.), *Diagnostic Imaging of Musculoskeletal Diseases: A Systematic Approach*,
DOI 10.1007/978-1-59745-355-4_5, © Springer Science+Business Media, LLC 2010

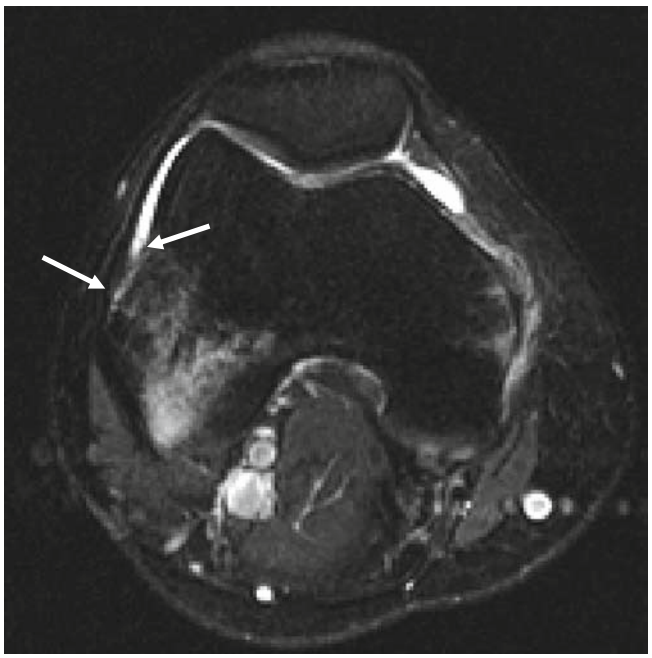

Fig. 5.2 Fast spin-echo, T2-weighted, fat-suppressed (FSE T2W FS) axial MR image showing lateral femoral condylar infraction. Note the small cortical defects (*arrows*) and the adjacent edema consistent with contusion

are displaced visibly on plain radiographic studies. When subtle, infractions may require CT or MRI for accurate depiction (Figs. 5.1, 5.2, and 5.3). Contusions, also called bone bruises, cause only trabecular disruption, but no cortical disruption. As a result, with rare exception, they are visible only on MR imaging (Figs. 5.3 and 5.4). Some radiologists have subclassified contusions and called infractions Type II contusions, but we will adhere to the basic terminology described above.

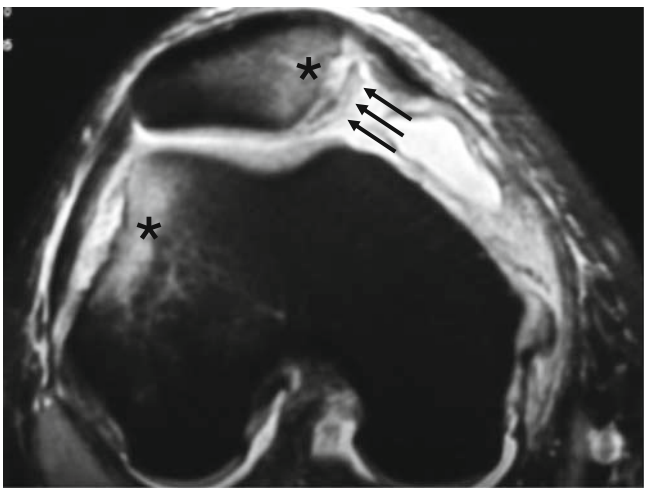

Fig. 5.3 FSE T2W FS axial MRI showing lateral femoral condylar contusion with a cortical infraction (∗). Note the contusion of the medial aspect of the patella (∗) and the avulsion fracture (*arrows*). This pattern of contusions is typical of a recent patellar dislocation

Bones: Fracture

Certain types of trauma are more frequent than others, e.g., falls and motor vehicle accidents. Bones also have areas of relative weakness. As a result, certain types of fractures will also be more common (Table 5.1). The fracture caused by any episode of trauma will vary depending on the age of the patient, the force of the impact, its orientation, the ligamentous integrity of the skeleton, the position of the skeleton at the time of trauma, and the quality of the traumatized bone.

Finally, fractures and infractions that extend to the articular ends of bones and fracture hyaline cartilage have an osteochondral component. That is, they involve the hyaline cartilage surface of the joint. If the fracture is small and localized to the end of the bone (Fig. 5.5), the fracture is called an osteochondral fracture. MR has the ability to depict the hyaline cartilage as well as the marrow space and so may be useful in the evaluation of the hyaline cartilage portion of the fracture.

Osseous Anatomy and Physiology

Understanding fractures and their healing requires a thorough understanding of osseous anatomy, biomechanics, and physiology.

Wolff's Law

Understanding Wolff's law is essential to understanding bones' clinical response to stress and hence fracture. In 1892, Julius Wolff, a surgeon, recognized that bones respond to dynamic mechanical loads. He observed that bones remodel and increase their mass in response to increased dynamic loads and similarly that they lose mass in response to absent or decreased load. Thus, patients who have sudden loss of use of a portion of their skeleton, for example, as the result of a fracture, will lose bone mass in that portion of the skeleton. This phenomenon is known as disuse osteoporosis or, as observed on radiographs, disuse osteopenia (Fig. 5.6). The latter signifies the loss of mineral density without specifying the pathological cause that the first implies.

On the other hand, bones given enough time to remodel under stress will adapt by increasing their mass and strength. This phenomenon occurs routinely in athletes and may be used strategically to increase peak bone mass in younger individuals who will be prone to senile osteoporosis later in life.

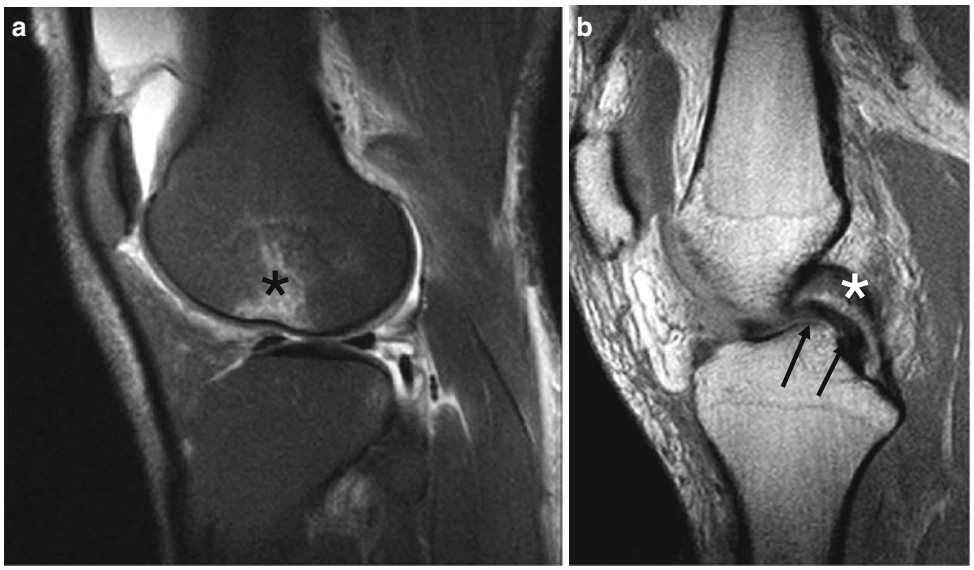

Fig. 5.4 Sagittal FSE T2W FS MR image (**a**) showing a contusion of the lateral femoral condyle. This contusion is typically seen in patients with acutely torn anterior cruciate ligaments as is seen in this sagittal proton density-weighted MR image (**b**). Note the torn ACL creates an appearance of a second PCL (*arrows*) just inferior to the normal PCL (∗). This appearance may also be seen with a bucket handle tear of a meniscus and is known as the Double PCL sign.

Table 5.1 Common fractures

	Child and Adolescent	Young adult	Middle aged	Elderly
Facial bones	Zygomaticomaxillary, nasal bone, LeFort, orbital blow out fracture			
Cervical spine		Jefferson, Hangman's, flexion teardrop, extension teardrop		Compression
Thoracic spine		Flexion compression		Compression
Lumbar spine		Flexion compression, chance		Compression
Pelvis	Ischial and iliac spine apophyseal avulsion (hurdlers' fractures)	Acetabular; anterior, lateral, and shear compression		Pubic straddle fractures
Sacrum				Sacral insufficiency
Shoulder	Surgical neck			
Elbow	Supracondylar	Radial head		
Wrist	Radial buckle	Scaphoid	Colles'	
Hand	Metacarpal, phalangeal			
Hip			Subcapital	Intertrochanteric
Knee	Patella, ACL footprint	Tibial plateau, Patella		
Ankle		Lateral malleolus, bimalleolar, trimalleolar		

Cortical and Trabecular Bone

The second important concept in understanding fractures is understanding the mechanical function of cortical and trabecular bone. Cortical bone serves two major functions. The first, although somewhat mundane, is essential; the cortex serves as an envelope through which the medullary cavity of the bone is isolated from the surrounding tissues. The second function is one of a load bearing both along the long axis of tubular bones and where load is transferred from one bone to another, e.g., the superior cortex of the acetabulum known as the sourcil (Fig. 5.7), or from one part of a bone to another part, e.g., the calcar of the femoral neck (Fig. 5.7). The implication of the last is that cortices will vary in thickness depending on the load experienced at a given location in a bone and as determined by the functional need of the organism. Thus, the medial cortex of the normal femoral neck will be markedly thicker than the lateral cortex because the former is under compression, while the latter is under distraction (Fig. 5.7).

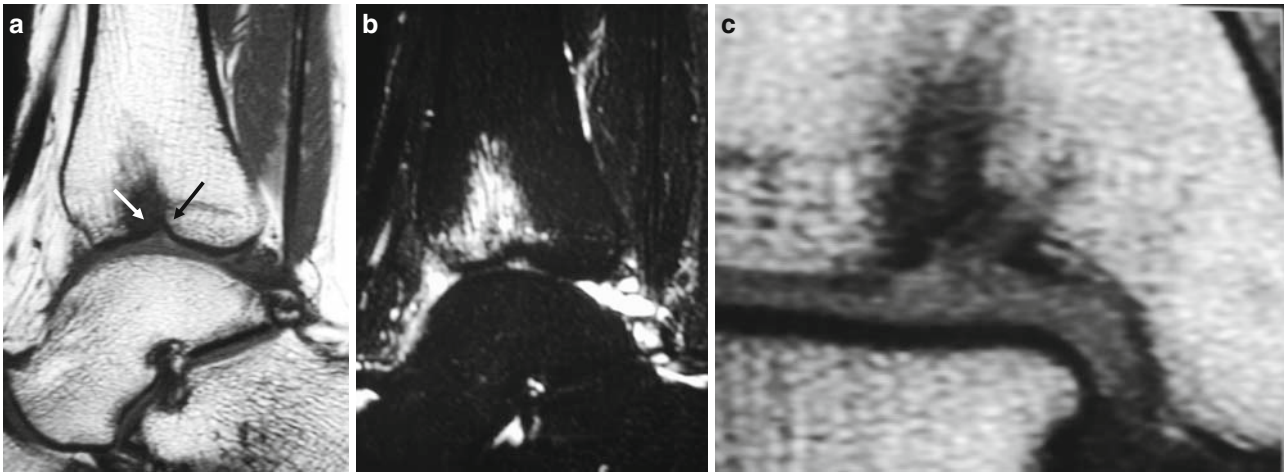

Fig. 5.5 (**a**) Sagittal T1-weighted (T1W), (**b**) FSE T2W FS, and (**c**) detailed coronal T1W MR images showing an osteochondral fracture of the tibia with a subjacent contusion. Note the marked deformity of the cortex along the tibial articular surface

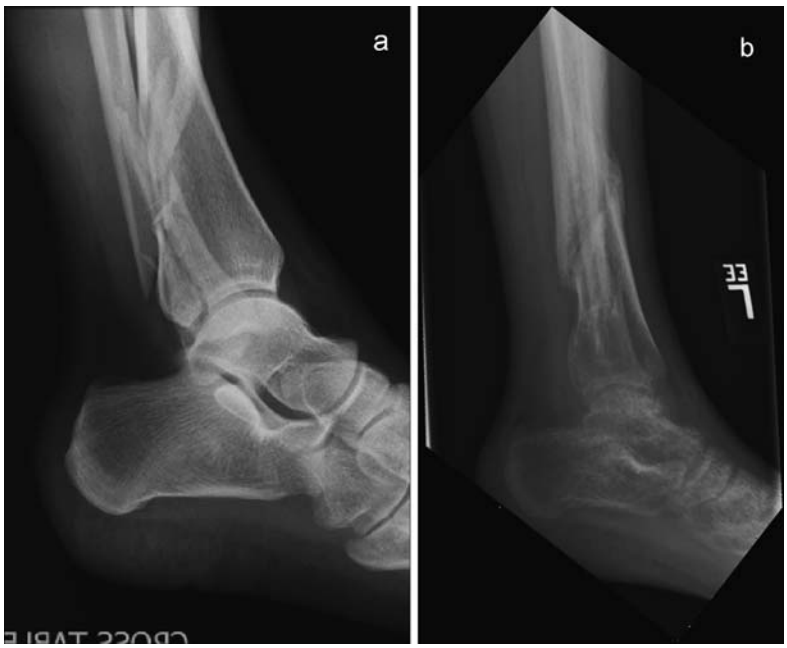

Fig. 5.6 Mortise views (**a**) immediately after fracture and (**b**) 4 months later showing interval loss of density in the distal tibia around the fracture. These findings relate to disuse and the early healing response of the bone to the fracture

The physical design of the bone is such that it maximizes its load-carrying capacity while simultaneously minimizing its weight. This is accomplished through a hollow column design. This principle is well established physically and employed routinely in architecture. It is also easy to visualize intuitively. Consider a solid rod of steel and a hollow steel tube, each containing the same amount of steel (Fig. 5.8). A section of rebar that is used to reinforce concrete is a good example of the former and a bicycle's tubing serves as a good example of the latter. By creating a hollow tube the longitudinal load-carrying capacity of the tube is increased relative to the rebar, which would bend at loads much less than the tube can withstand. This increased load-carrying capacity of the tube comes at a cost, however. That cost is the sacrifice of its capacity to withstand transversely applied forces because of its relatively thin wall. This model applies well to human long tubular bones, such as the femur and even those in the hands and feet. For all intents and purposes, therefore, the diaphyseal portions of long bones need to contain only cortical bone and the medullary space needs to contain only marrow, but no trabeculae in order to carry their long-axis loads. This approximates, in fact, what

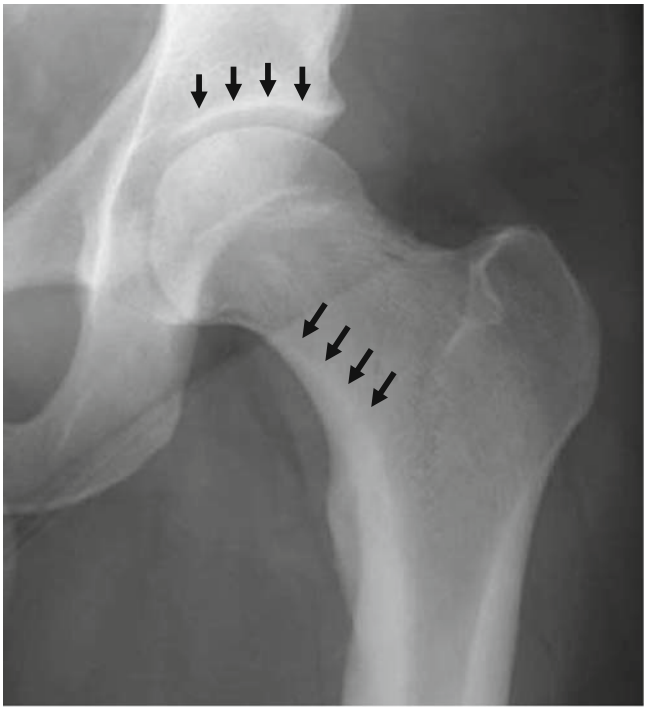

Fig. 5.7 AP Radiographs of the left hip showing normally thickened cortices (*arrows*) where loads are transferred along the superior acetabulum and the medial femoral neck

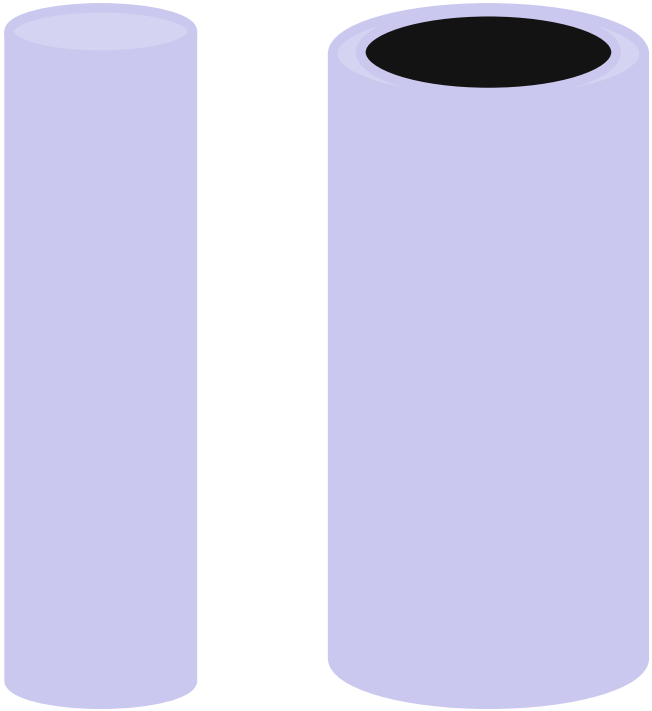

Fig. 5.8 A solid bar and a hollow tube, each containing the same mass, will have different physical load-carrying capacities depending on the diameter of the tube. In general, the greater the diameter of the hollow tube, the greater the longitudinal load it can withstand. Similarly, their ability to resist side impact will vary inversely with the thickness of the wall and, since we have defined constant mass, the diameter of the tube

is found in life, and it means that long bones are highly resistant to longitudinally applied forces but not forces applied out of axis. Forces applied out of axis, if not mitigated by the movement of the bone in the same direction as the force, may result in fracture that applied purely longitudinally otherwise would not. This concept explains why longitudinal fractures are unusual in healthy bones, but do occur in osteopenic bones.

Trabecular bone, like cortical bone, has two essential functions. Trabeculae are not capricious or random in their orientation but are highly organized and form an architectural truss (Fig. 5.9). Trusses, whether in suspension bridges, airplane wings, skyscrapers, or the skeleton, provide efficient load transference through the structure and an ability to withstand dynamic changes in load through temporary deformation.

Thus, the first function of trabeculae is the transfer of load from one point to the next. The major trabeculae, known also as columns, align along the lines of load and stress. The columns transmit the force from a load along their axis. Secondary trabeculae, also known as struts, align perpendicular to lines of stress. These struts serve to reduce the overall length of the columns and to transfer the stress across to adjacent columns, thus minimizing point loads. As a result, trabeculae will be prominent where bones have a complex, nontubular shape or as discussed below experience wide variations in the loads they experience, e.g., vertebral bodies.

Trabeculae are prominently visible on radiographs in the healthy skeleton, for example, the hip (Fig. 5.10) or the vertebral bodies (Fig. 5.11). Complex bones such as the carpal scaphoid bone or the talus rely especially on trabeculae to transfer force from one portion of the bone to another. In long bones, the need for trabeculae is primarily toward the end of long bones where the forces across a broader articular surface at the joint must be transmitted to a narrower cortical tube and vice versa. This means that the epiphyseal and metaphyseal regions of long bones will contain large numbers of the trabeculae (Fig. 5.12), while the diaphyseal regions will be relatively devoid of trabeculae (Fig. 5.13). As will be discussed, this difference in trabecular location has important implications as to where bone mineral loss will be most prominent in the aging skeleton and therefore where fractures occur most often in different aged groups.

The second function of the trabecular truss is to act as a shock absorber for dynamic changes in load. The configuration of the trabeculae as a truss allows trabecular bone to deform in response to short-lived changes in load without suffering a fracture. Of course, this deformation can occur only within certain limitations. Beyond that the trabeculae will suffer microfractures – contusions or fractures (*vide*

Fig. 5.9 Examples of architectural trusses. (**a**) and (**b**) From TotalStructures.com. (**c**) Example of articulated architectural trusses in building. (voestalpine.com)

supra). Unlike an inanimate suspension bridge, however, the living trabeculae will repair themselves over time assuming that the stress abates. Further, if the new stresses deforming the trabecular truss are repetitive and below a threshold that causes fracture, the truss will reinforce itself and become stronger (see discussion of Wolff's law above). Obversely, chronic lack of stress on the trabecular truss will lead to its diminution and weakening.

Osseous Elasticity, Mineralization, Aging Phenomena, and Physeal Growth Plates

The third important concept in the understanding of fractures is how the relative elasticity and mass of the skeleton changes with age. The growing juvenile skeleton has relatively more cartilage than the adult skeleton. Hence, bones are significantly more elastic in children than in adults. This means that immature bone can absorb relatively more energy from trauma without fracturing than mature adult bone. As a result, when impacted, immature bone may behave like a piece of green wood that has not fully dried, giving rise to an irregular fracture (Fig. 5.14) or an impaction "buckle" or torus fracture that buckles the bone's cortex (Fig. 5.15) instead of a through-and-through fracture with sharp margins that is typical of adult fractures (Fig. 5.16). This first type of juvenile fracture is known aptly as a greenstick fracture. Another less common variant of a greenstick fracture, known as a dynamic bowing fracture or plastic fracture, has a similar mechanism. Here, the trauma causes diffuse trabecular injury that results in bowing of the bone without an actual cortical break (Fig. 5.17). These fractures are most often seen in the ulna and the radius. Reducing plastic bowing fractures requires completion of the fracture and reduction.

Normal humans increase their bone mass until the age of 30–35 years. After that age, bone mass declines (Fig. 5.18). The rate of decline is related to the hormonal substrate within the body. Women with their higher premenopausal estrogen levels lose bone mass slowly until menopause. Afterward the rate accelerates rapidly. Men, on the other hand, tend to show a slow relatively linear decline in their bone mass beyond the age of peak mass. These phenomena are discussed further in Chapter 2. With the decline in overall bone mass, bones become less strong and lacking their juvenile elasticity become increasingly brittle.

Furthermore, the rate of bone resorption at any given point in a bone is directly linked to the surface area on which osteoclasts – the cells that mediate bone resorption – have to act. This means the trabecular bone, with its six- to eightfold greater surface area than equivalent masses of cortical bone, will tend to resorb at a much faster rate than cortical bone. Therefore, as individuals age, regions of bone with a greater proportion of trabecular bone compared with cortical bone are particularly prone to mineral loss and hence to fracture.

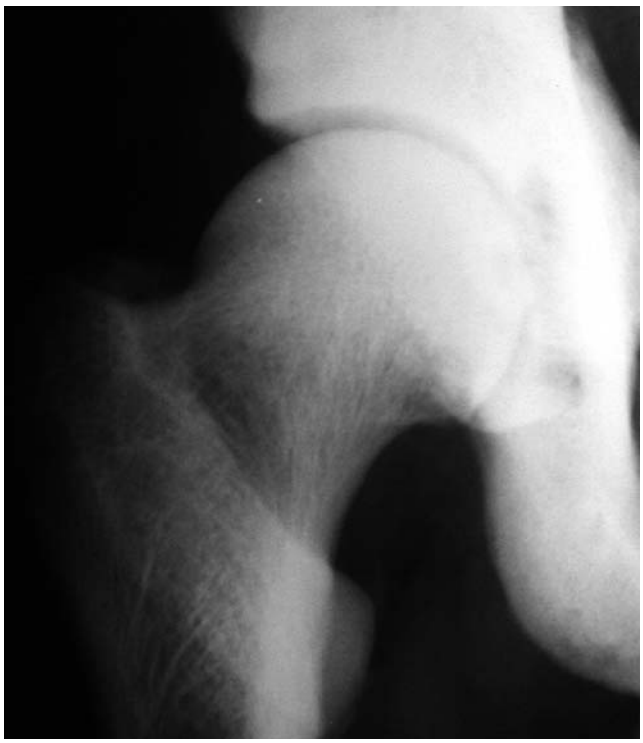

Fig. 5.10 AP radiograph of the right hip from a patient with fluorosis showing accentuated trabecular pattern with major trabeculae oriented along the axis of load into the proximal diaphyseal cortex

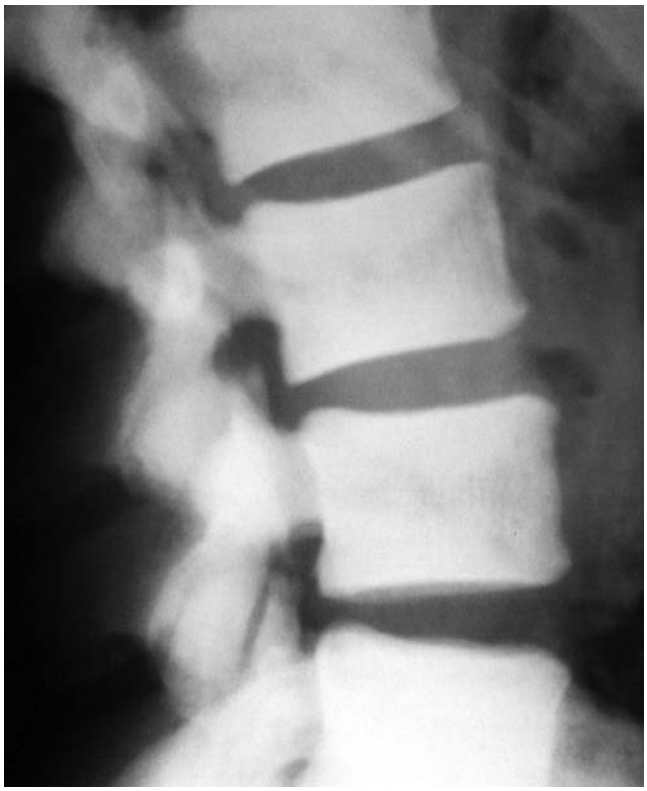

Fig. 5.11 Lateral radiograph of the lumbar spine in a patient with fluorosis showing trabecular orientation along the axis of weight bearing

In particular, this includes vertebral bodies and the metaphyses of long bones where trabeculae predominate and cortices are thin.

Because of these age-related changes in elasticity and local bone mass and architecture, the same force applied to a portion of the skeleton may result in completely different fractures. Consider, for example, a patient who falls on his outstretched hand.

In the young, prepubescent patient, the skeleton is largely unossified and still contains a large amount of the elastic

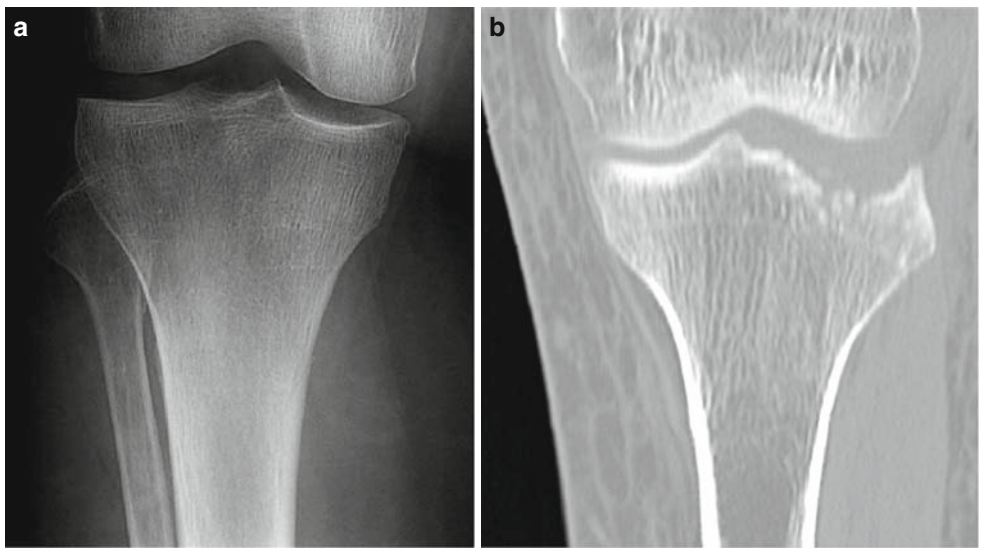

Fig. 5.12 AP radiograph (**a**) in a normal knee and coronal CT reconstruction (**b**) in a patient with a lateral tibial plateau fracture showing the predominantly epiphyseal and metaphyseal distribution of trabeculae

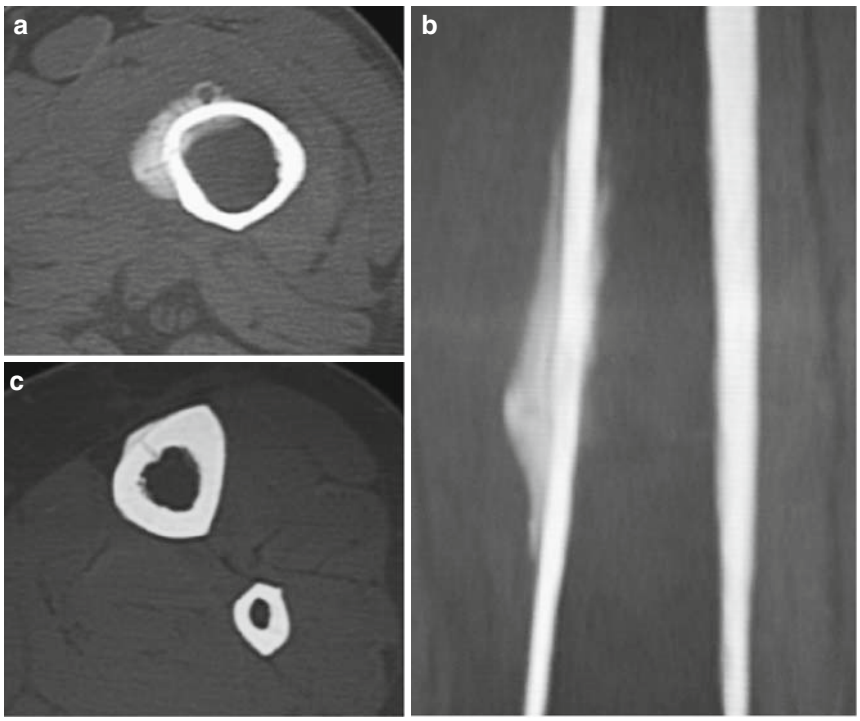

Fig. 5.13 Axial (**a**) and coronal (**b**) CT images from the diaphysis of a femur and (**c**) from the diaphyses of a tibia and a fibula of two different patients showing virtually no trabeculae and only fatty marrow within the medullary space. Note the callus formation along the cortices related to the patients' underlying stress fractures

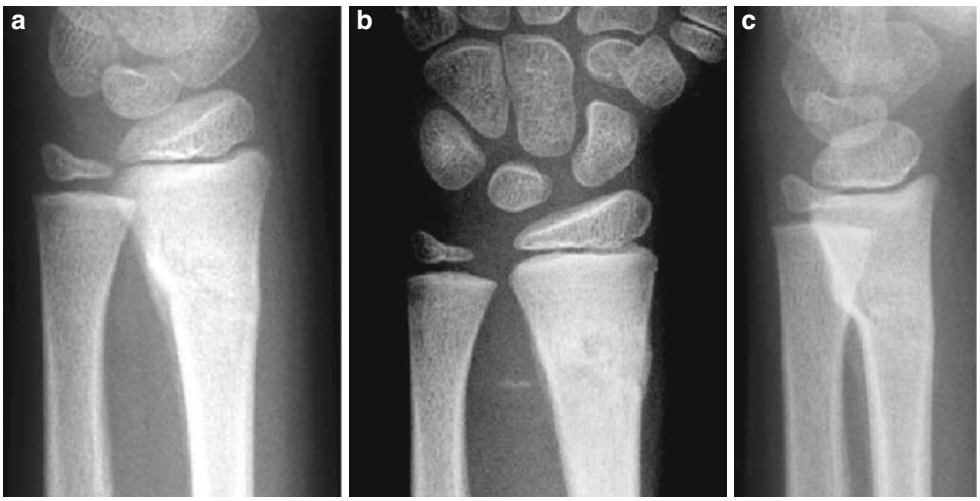

Fig. 5.14 AP (**a**), oblique (**b**), and lateral (**c**) radiographs of the distal forearm in a child showing an irregular greenstick fracture of the radial metadiaphysis. The fracture extends completely through the distal radius though the fracture line is irregular and jagged. (Case courtesy of Dr. John Hunter)

enchondral cartilage model from which the mature bone forms. Thus, as the child impacts the ground, the bones of the forearm, the wrist, and the hand will absorb and store the kinetic energy from impact through compression in the form of potential energy. The elastic portion of the bone will then re-expand once the impact has passed, releasing the potential energy. If the compression of the bone is large enough, not only will the elastic portion of the bone compress but the portion of the bone that is highly ossified – the cortex – will compress as well. The ossified cortex cannot convert the kinetic energy to potential energy and so it will buckle. This causes a "buckle" or torus fracture where the cortex deforms, but the bone is otherwise normal in appearance (Figs. 5.15 and 5.19).

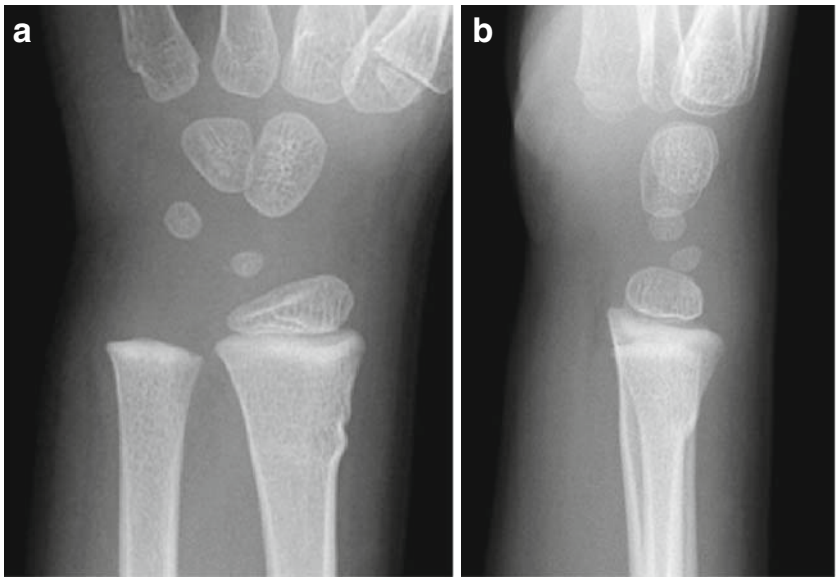

Fig. 5.15 AP (**a**) and lateral (**b**) radiographs of the radius in a 5-year-old child after a fall on an outstretched hand showing a "buckle" fracture of the dorsal and the lateral distal radial cortex. Note the buckling of the dorsal and the lateral radial cortex

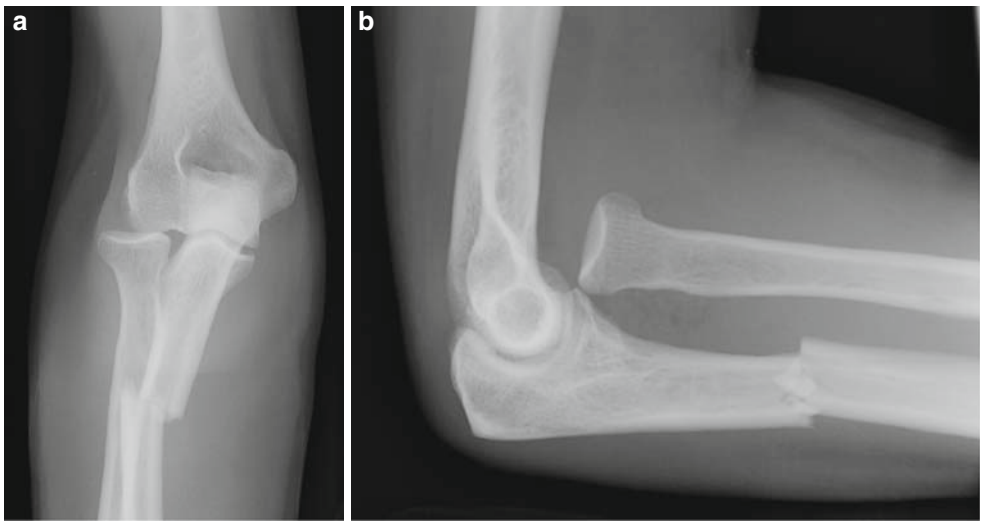

Fig. 5.16 Monteggia fracture dislocation. AP (**a**) and lateral (**b**) radiographs show a fracture of the proximal ulna and a volar dislocation of the radial head. Note that the articular surface of the radial head does not articulate with the capitullum. The dislocation is most apparent on the lateral view but can also be recognized on the AP view by the loss of articular parallelism between the radial head and the capitullum

In a patient who is in the third and early fourth decade of life, bone mass will be maximal and the cartilage model would have disappeared. Now the forces transmitted through the impact of the extended hand against the ground cannot be absorbed through elastic compression. Instead, if the force is greater than the bones are prepared to withstand, the energy will dissipate through fracture. At this age, since all of the bones are at their peak mass and strength, the fracture will tend to occur in the smallest and most vulnerable bone. This means that the fracture will occur in one of the carpal bones.

Analysis of carpal anatomy reveals that the force of the impact will transmit from the hand and across the wrist through one of three carpal columns (Fig. 5.20):

- A medial column consisting of the hamate, the triquetrum, and the triangular fibrocartilage complex (TFCC), an elastic fibro cartilaginous structure.
- A middle column consisting of the capitate and the lunate.
- A lateral column consisting of the trapezoid, the trapezium, and the scaphoid.

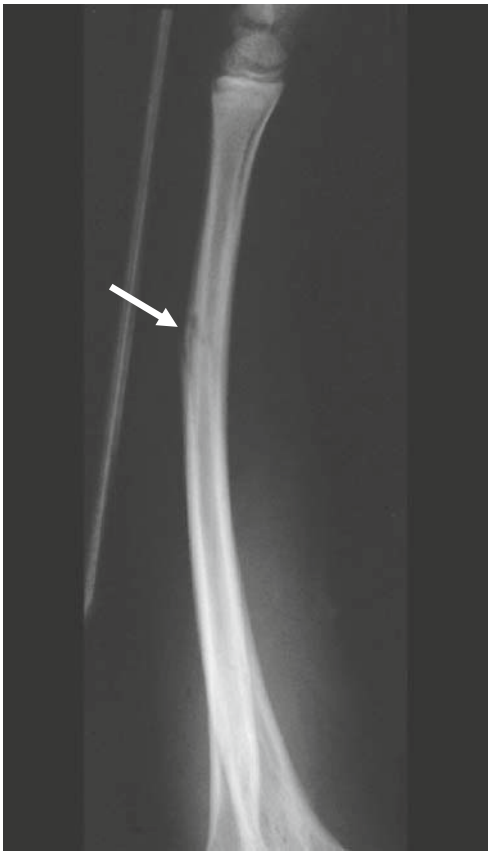

Fig. 5.17 Lateral radiograph of a patient with an ulnar bowing fracture and a minimally displaced fracture of the radius (*arrow*). Note the long curve of the ulna

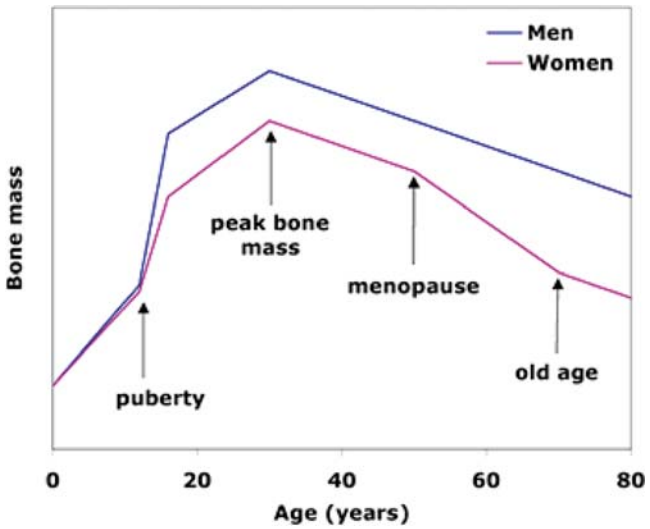

Fig. 5.18 Bone mineral content variation with age. Note the acceleration of bone mass accumulation with the onset of puberty until late teens and the peak bone mass at the age of 30 years. Also note the acceleration of bone mass loss with menopause in women. This phenomenon does not occur in men and along with lower peak masses explains why women are more frequently subject to senile osteoporosis. (Image from http://www.mrchnr.cam.ac.uk/research/bone_health/pbm.html, Accessed January 8, 2007)

In the extended position, the lunate, which has a cup-like shape, will be tilted dorsally allowing some dissipation of force through rotation (Fig. 5.21). The triquetrum will impact on the triangular fibrocartilage again allowing some absorption of the force transmitted through the medial column. The scaphoid, on the other hand, which in neutral is

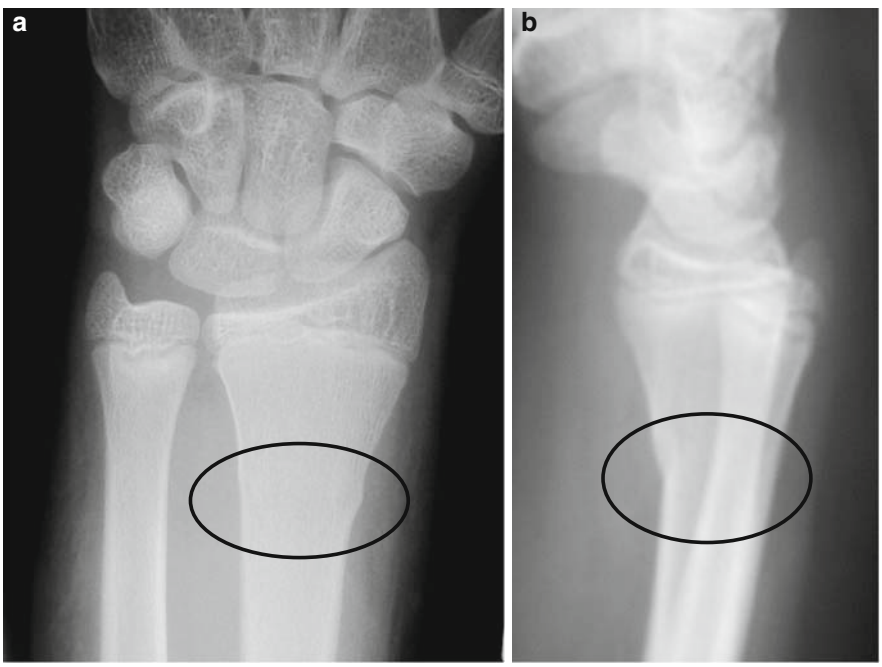

Fig. 5.19 AP (**a**) and lateral (**b**) radiographs of the distal forearm in a 15-year-old boy with a torus fracture of the radius (*ovals*)

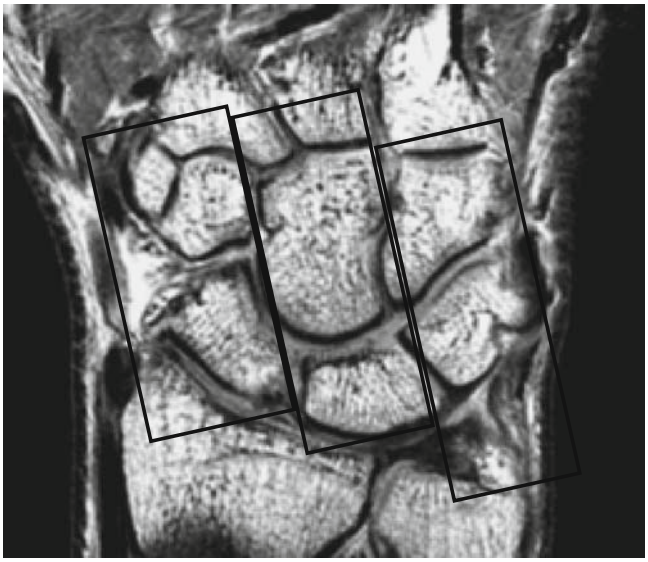

Fig. 5.20 Cross section of the wrist showing the lateral, middle, and medial columns of force transmission

volarly angled, will come into perfect alignment between the metacarpals and the radius in extension. The scaphoid, it should also be remembered, has a curved banana shape in the coronal plane (Fig. 5.22). Thus, the scaphoid will be the bone that will absorb the majority of the force transmitted across the wrist. Thus scaphoid fractures are most common in this age group (Fig. 5.23). Furthermore, since the scaphoid has a curved orientation, it will tend to fracture at the apex of its curve and also its narrowest point, resulting in the commonly observed scaphoid waist fracture.

In an older age group, a fall on an outstretched hand will cause yet a third type of fracture. Once a patient passes their peak in bone mass, bone mineral reabsorbs according to the surface area available to activated osteoclasts. As discussed above, trabecular bone with its greater surface area will be lost much more quickly than cortical bone. Furthermore, the larger the trabecular volume in the bone and the lower the cortical thickness, the more the bone will weaken from the alteration in trabecular architecture. This means that of all the bones in and around the wrist, the distal radial metaphysis will be most weakened. The result is that the scaphoid, now relatively stronger than the radial metaphysis, will act as a hammer against the distal radius and cause a fracture of the latter's metaphysis. In addition, because of the orientation of the hand and the wrist as impact occurs, the distal radius will angle dorsally as it fractures. If the medial column should impact the ulnar styloid instead of the triangular fibrocartilage, as likely occurs when the wrist is inverted or hyperpronated, the ulnar styloid will also fracture. The result is a dorsally angled distal radial fracture with or without an accompanying fracture of the ulnar styloid (Fig. 5.24). This fracture, also known as a Colles' fracture, is one of the most common fractures of the adult population.

Another factor to consider in assessing the likelihood of a fracture is whether the bone is normally formed. Many diseases, whether congenital as with osteopetrosis and osteogenesis imperfecta or acquired as with Paget disease, alter the

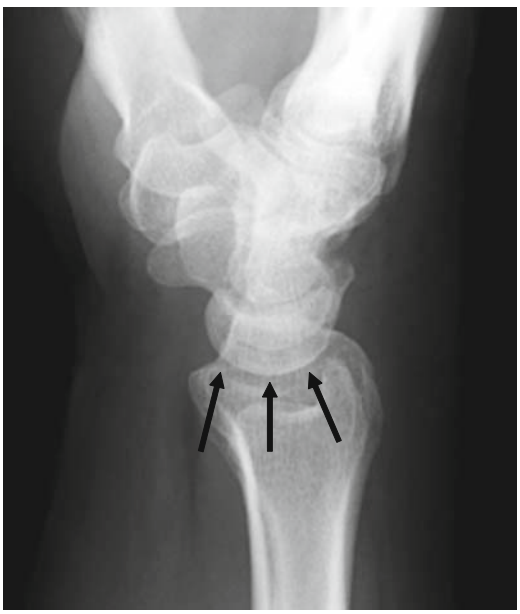

Fig. 5.21 Lateral radiograph of the wrist showing the rounded shape of the lunate as it articulates with the radius (*arrows*)

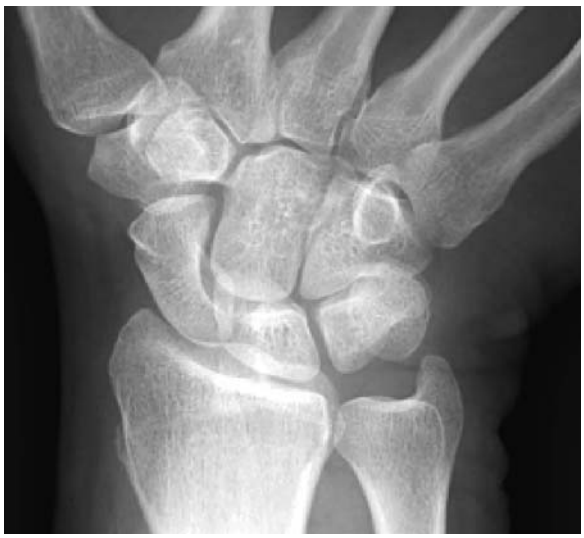

Fig. 5.22 PA radiograph of the wrist in ulnar deviation. In this position the scaphoid comes into the coronal plane and can be seen to be curved along its major axis

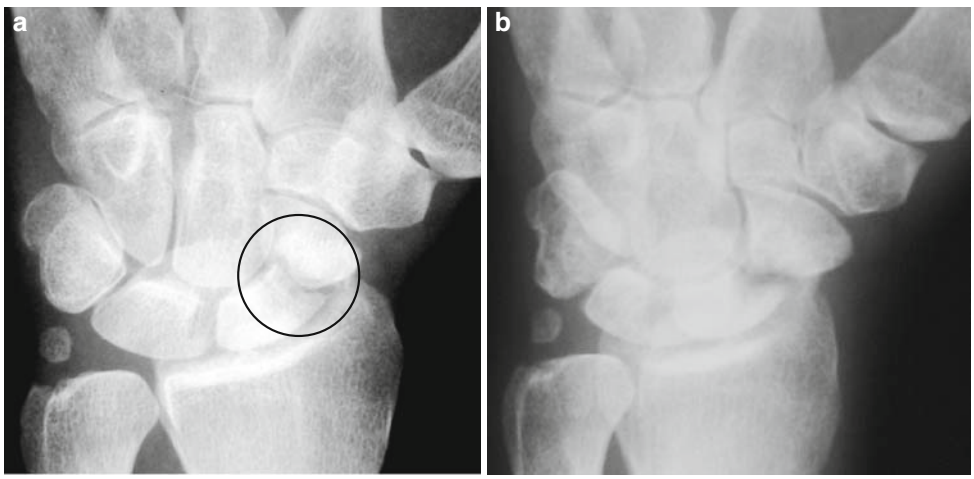

Fig. 5.23 PA (**a**) and oblique (**b**) radiographs of the left wrist of a 23-year-old man after a fall on an outstretched hand showing a mid-waist scaphoid fracture (*circles*). Note the ulnar styloid ossicle

ability of a bone to absorb traumatic impact. If the elasticity of the bone is too little as occurs in osteopetrosis, the bone will be prone to fracture easily. In other situations where the elasticity of the bone is great, the bone may tend to bow as often occurs with chronic rickets, osteomalacia, polyostotic fibrous dysplasia, and Paget disease. In these diseases the bones often develop the so-called pseudofractures, also known as Looser lines or Milkman zones (Fig. 5.25). These represent small areas of cortical and local trabecular infraction along the diaphyses of long bones where the elasticity of the bone is typically normal – a situation that harkens back to the physiology of greenstick and buckle fractures. These Looser zones are most common in weight-bearing bones and may occur on either the compression side or the distraction side of the bone.

Immature skeletons have another feature that requires special attention. This feature is the physeal growth plate that occurs at the ends of growing long bones and at the apophyses of both flat and long bones. These plates, because of their relative absence of ossification, are weaker than the adjacent epiphyses and metaphyses, especially during growth spurts when the plates tend to widen. The result is that these plates represent a path of least resistance to the transmission of traumatic forces and so are involved frequently in pediatric fractures (∼15%). Salter and Harris classified physeal growth plate fractures according to the involvement of the bone adjacent to the growth plate (Table 5.2) (Figs. 5.26, 5.27, 5.28, 5.29, and 5.30). Their classification has been modified and enlarged over the years, but its basic format remains. The major concern with fractures that

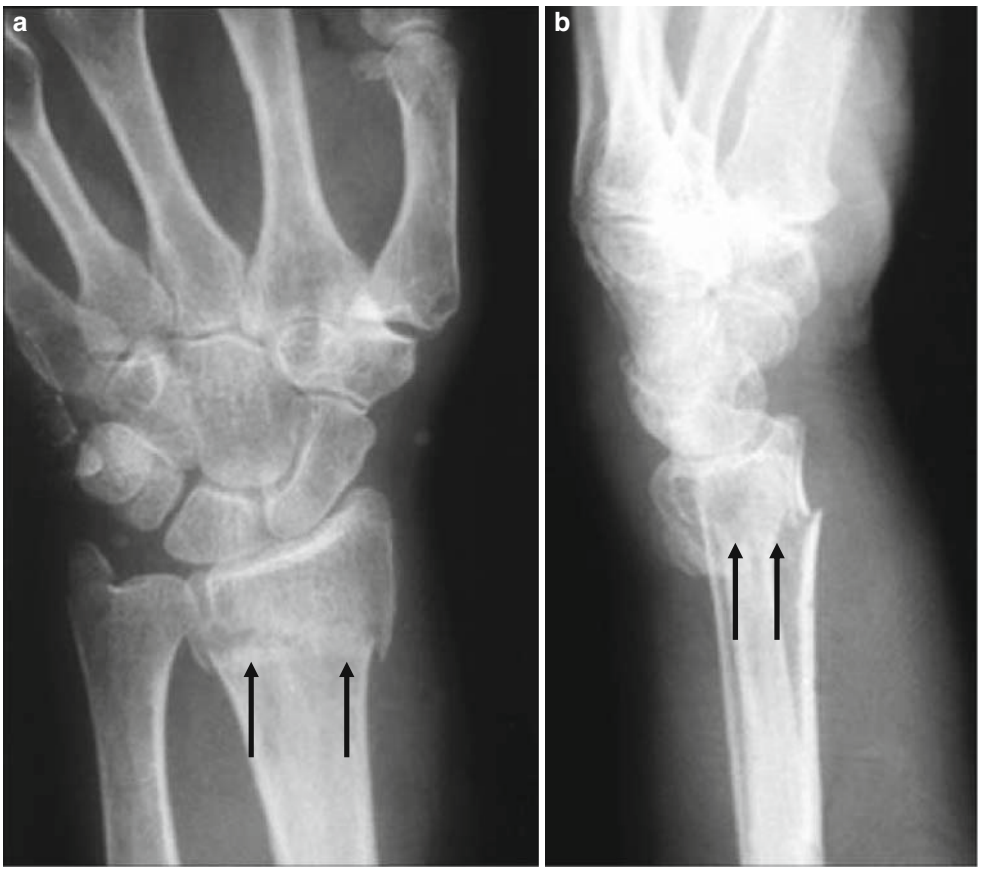

Fig. 5.24 PA (**a**) and lateral (**b**) radiographs of the left wrist of a 74-year-old patient who suffered a fracture of her distal radius (*arrows*) after a fall on an outstretched hand

Table 5.2 Salter–Harris classification of physeal fractures

Classification	Description
I	Fracture through the physeal plate without involvement of adjacent metaphysis or epiphysis
II	Fracture through the physeal plate with involvement of the adjacent metaphysis
III	Fracture through the physeal plate with involvement of the adjacent epiphysis
IV	Fracture through the physeal plate with involvement of both the adjacent metaphysis and the epiphysi.
V	Crush fracture of the physeal plate

involve the growth plate is that they cause premature closure of the plate and result in a shortened limb. In general, the higher the fracture is in the Salter–Harris classification, the greater the chance of premature plate closure.

Even so, Salter I fractures (involving only the physeal plate and no adjacent bone) can be concerning. For example, slipped capital femoral epiphyses (SCFE) typically occur in heavy-set children as they go through their prepubescent growth spurt around the age of 12 years or so (Fig. 5.26). The growth spurt leads to widening and relative weakening of the growth plate, leaving it open to a shear fracture through the plate. Typical ambulatory forces with the angled configuration of the femoral neck normally cause shear across the growth plate. Thus, the expected SCFE injury will be medial displacement of the proximal femoral epiphysis as the shear forces the epiphysis off the femoral neck. If the epiphysis is displaced enough, the mature hip will be deformed with an enlarged head, a laterally displaced femoral neck, and an abnormally shaped acetabulum – a coxa magna deformity (Fig. 5.31). On the other hand, reduction of the fracture may cause enough injury either to induce premature closure of the growth plate and thus a shortened limb or to cause avascular necrosis of the epiphysis. These countervailing problems have made therapy of these fractures difficult.

Another group of growth plate fractures that result from growth spurts occurs at the apophyses around the pelvis. These fractures, know as hurdlers' fractures, involve the apophyses of the ischium at the hamstring origins (Fig. 5.32), the anterior superior iliac spine at the origin of the sartorius, and the anterior inferior iliac spine at the origin of the rectus femoris (Fig. 5.33). Often, when these fractures heal, they may leave behind telltale deformities of the ischia or iliac spines or they may not heal and leave bone fragments in the soft tissues.

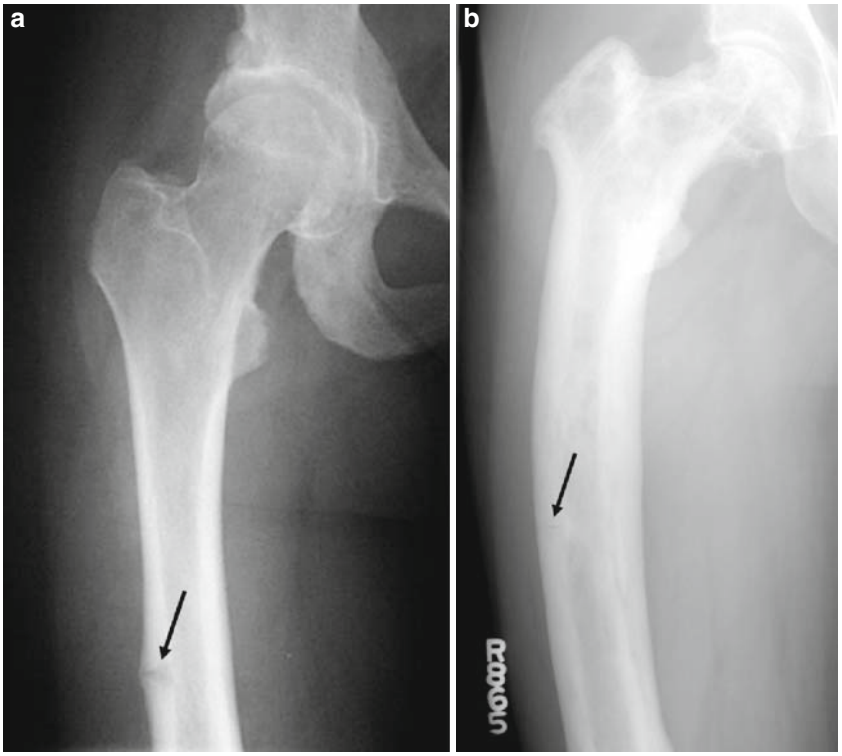

Fig. 5.25 AP femur in a patient with osteomalacia (**a**) and a patient with Paget disease (**b**) each showing a pseudofracture or Looser zones (*arrows*) in the lateral diaphyseal cortex. In (**b**) note the markedly increased cortical thickness and the coarsened trabeculae that are indicative of Paget disease

Force and Environment External to the Skeleton

The fracture a patient experiences will not only be the product of the mineral status of the skeleton and the orientation of the bones with respect to one another but also the magnitude and duration of the force applied to the skeleton and whether both ends of the traumatized bone(s) are fixed in place. For example, a strike against the lateral distal thigh with the foot planted may cause a tibial plateau fracture, but the same force applied without fixing the extremity may result only in a muscular contusion.

The amount of force and the rate at which the force is applied to the skeleton are important. With a small amount of force, the trabecular truss may be able to absorb the force of impact, and so the patient will suffer only a bone bruise instead of a fracture. On the other hand, a higher magnitude of force may exceed the trabecular truss' ability to absorb the impact and result in a fracture. An even greater or more prolonged force may cause other traumatic configurations to occur. For example, a high level of force to the wrist, instead of a scaphoid fracture, may cause accompanying ligamentous disruption around and within the wrist, particularly of the scapholunate and lunotriquetral ligaments. In this case, instead of the scaphoid being compressed between the metacarpals and the radius, the loss of ligamentous integrity frees the mass of the carpus from connection with the lunate. This, along with the dorsal tilt of the lunate, may permit the entire carpus except for the lunate to dislocate dorsally – a perilunate dislocation (Fig. 5.34). If the carpus reduces from its dorsally displaced position back into alignment with the radius, the lunate then may be forced to dislocate volarly (Fig. 5.35).

The chronicity of the forces on the skeleton also plays an important role. An impact, not large enough to cause a fracture with a single blow, if repeated often enough, eventually may result in a fracture. In this event, the repetitive force must be frequent and great enough to outcompete the bone's ability to remodel and so the injury gradually increases in severity. Eventually the bone will fracture – a type of fracture known as a stress fracture. Stress fractures occur in two basic varieties.

The first is a fatigue fracture. These fractures occur with abnormal or excessive repetitive use of a normal bone. Typically these fractures are seen in younger individuals who suddenly place a bone under unusual stress. For example, military recruits who go from a sedentary lifestyle to an active one that includes long marches with a heavy pack on their backs are prone to fatigue-type stress fractures in

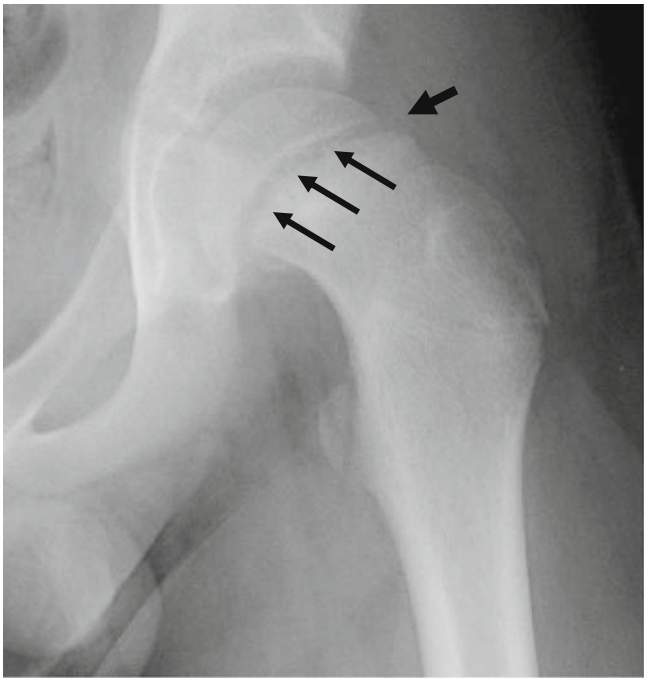

Fig. 5.26 Salter–Harris I fracture through the proximal epiphysis of the femur in a 12-year-old boy. This is common in prepubescent children, particularly boys, and is known as a slipped capital femoral epiphysis (SCFE). Note the medial displacement of the femoral epiphysis with a smooth lateral margin of the femoral neck (*thick arrow*) and widening of the physeal plate (*arrows*)

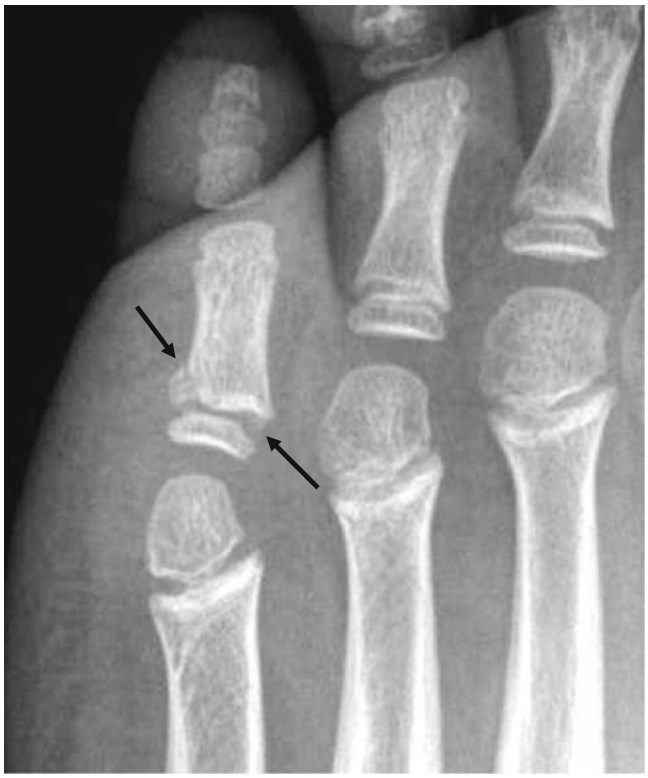

Fig. 5.27 Salter–Harris II fracture through the proximal metaphysis and the physeal plate of the 5th proximal phalanx in a 15-year-old boy after stubbing his toe. Note that the fracture extends through a portion of the lateral metaphysis (*arrow*) and a portion of the physeal plate (*arrow*)

their lower extremities, particularly their femoral necks and tibiae (Fig. 5.36). Often these fractures are radiographically occult early on and require either a bone scan or an MRI to identify (Fig. 5.37). Another example of fatigue fractures occurs in the high-end athlete who precipitously increases their training in preparation for a competitive event. In each of these cases, the bone is placed under unusual and sudden new stress. According to Wolff's law, fatigue fractures can be avoided through gradual increases in the level of exercise to allow the bone to lay down new mineral, reinforce itself, and so adapt to the increased stresses.

The second type of stress fracture is known as an insufficiency fracture. Here, normal activities result in a fracture because the bone has lost its normal mineral mass. This type of fracture typically occurs in an older population where senile osteoporosis is a problem (Fig. 5.38). Of course, it may occur in any patient where the underlying pathological process prevents normal bone formation, e.g., osteogenesis imperfecta, or causes premature marked loss of bone mineral, e.g., Hajdu–Cheney syndrome.

MRI has proven useful for evaluation of osteochondral stress lesions such as osteochondritis dissecans (OCD), where determination of fragment loosening is important to guide therapy. In this condition and in spontaneous osteonecrosis of the elderly (SONK), a small fragment of subchondral bone in the distal femoral condyle becomes isolated and infarcts (Fig. 5.39). In both of these cases, trauma is the likely cause of the small bone infarct. OCD is typically seen in young active teenage patients and is felt to result from a focal osteochondral fracture and is akin to a fatigue fracture. SONK, on the other hand, arises in the subchondral bone of older, osteopenic patients and is felt to be the result of an insufficiency-type stress fracture. Otherwise these two conditions have similar appearances to one another.

As long as the hyaline cartilage overlying the infracted fragment is intact, the infracted bone fragment remains stable. If, however, the cartilage covering the bone fragment is fragmented, then the fragment may migrate into the joint space and become a loose body within the joint. When the hyaline cartilage is disrupted, MRI shows fluid on T2-weighted, fat-suppressed imaging tracking along the margins of the fragment (Fig. 5.40). MR arthrography improves sensitivity for loosening of the fragment as the contrast injected into the knee joint increases the pressure within the joint and so can drive fluid into a small defect in the hyaline cartilage.

It is important to differentiate insufficiency stress fractures from pathologic fractures. The latter results from a focal process, usually a neoplasm (either benign or malignant), replacing and weakening the bone so that it fractures

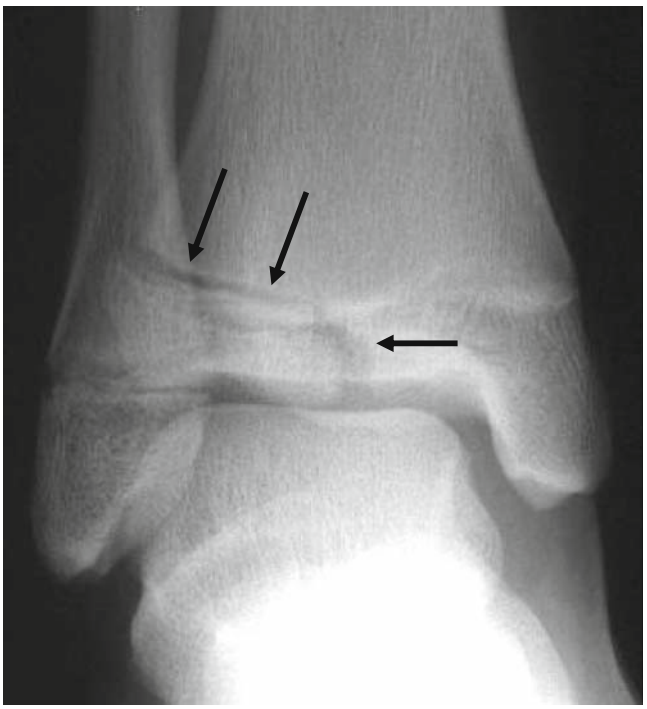

Fig. 5.28 Salter–Harris III fracture through the distal epiphysis and the physeal plate of the tibia in a 12-year-old girl after a fall. Note that the fracture extends through the central epiphysis and laterally through the physeal plate (*arrows*)

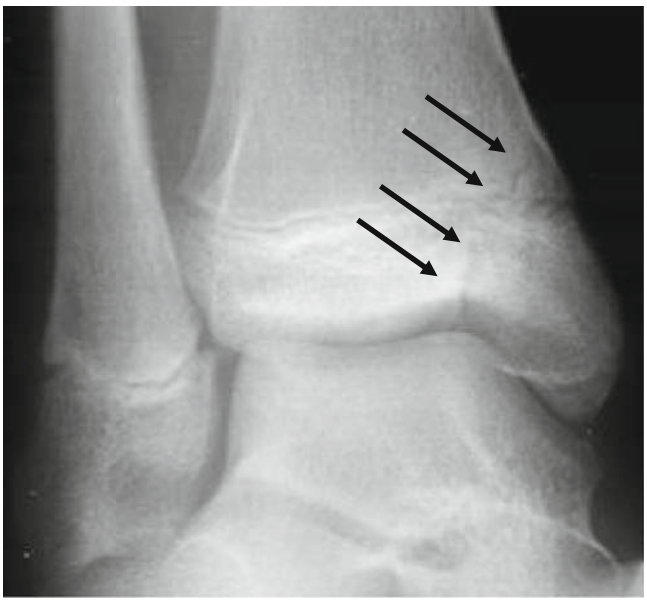

Fig. 5.29 Salter–Harris IV fracture through the distal epiphysis, the physeal plate, and the metaphysis of the tibia in a young boy (*arrows*). Note that the fracture is only minimally displaced in this case

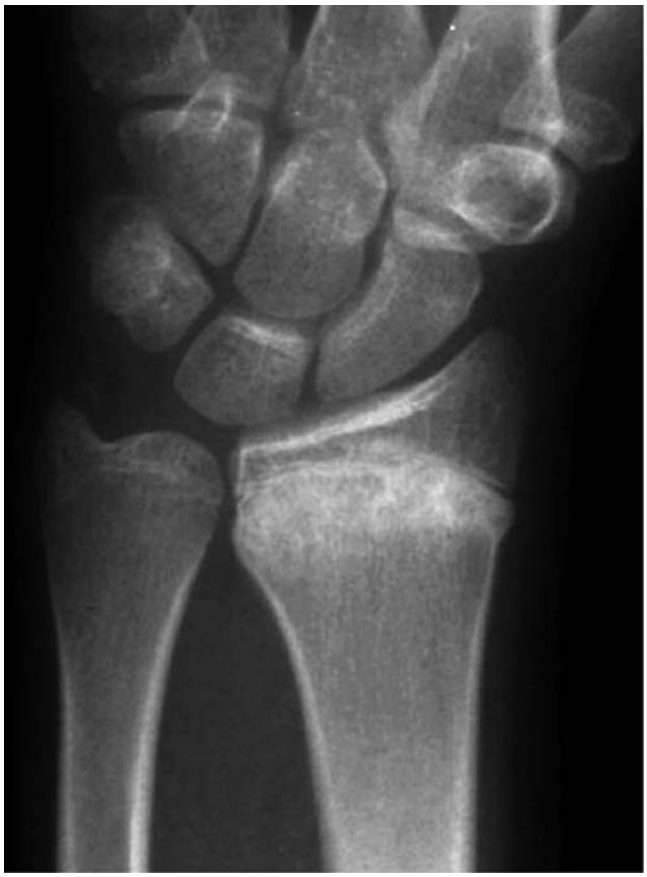

Fig. 5.30 Salter–Harris V fracture of the distal radial physeal plate. Note the sclerosis across the physeal plate from the crush injury. (Case courtesy of Dr. Ken Schreibman)

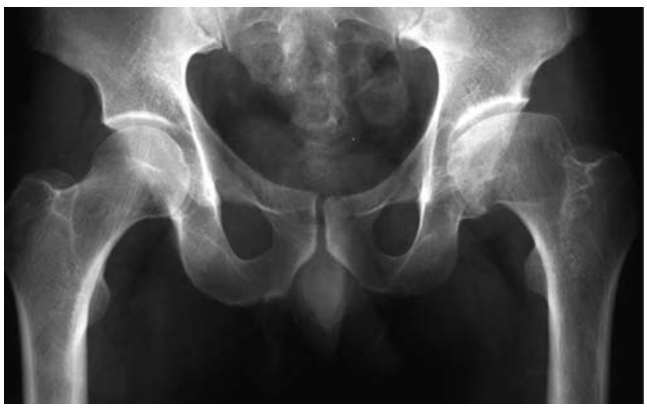

Fig. 5.31 AP radiograph of the pelvis showing coxa magna deformity of the left femoral head

under normal stress (Figs. 5.41 and 5.42). Pathologic fractures will typically show evidence of the underlying lesion and occasionally may be the cause of the initial presentation of patients not only with primary tumors of bone but more commonly with multiple myeloma and epithelial tumors that have asymptomatically metastasized to bone.

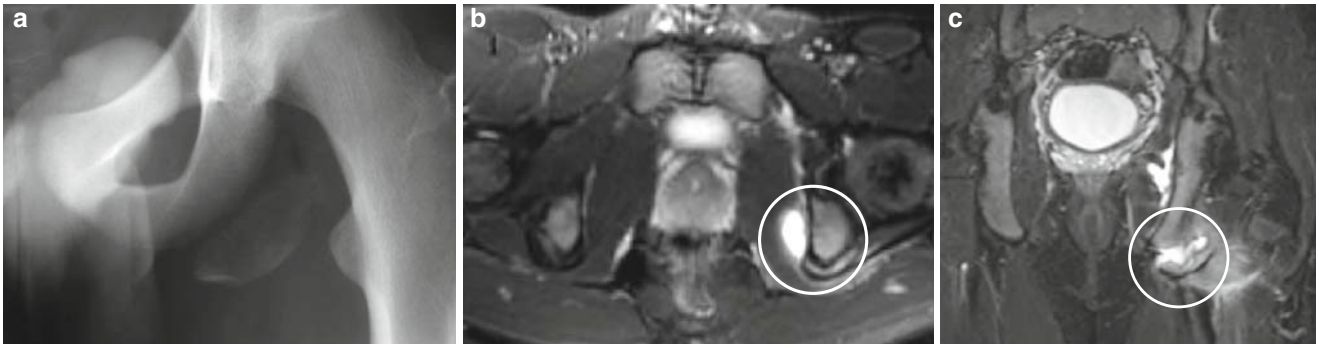

Fig. 5.32 AP coned down radiograph of the left pelvis (**a**), T2-weighted coronal (**b**), and axial (**c**) MR images showing an avulsion fracture from the ischium (*circles*) related to an avulsion of the semimembranosus muscle origin

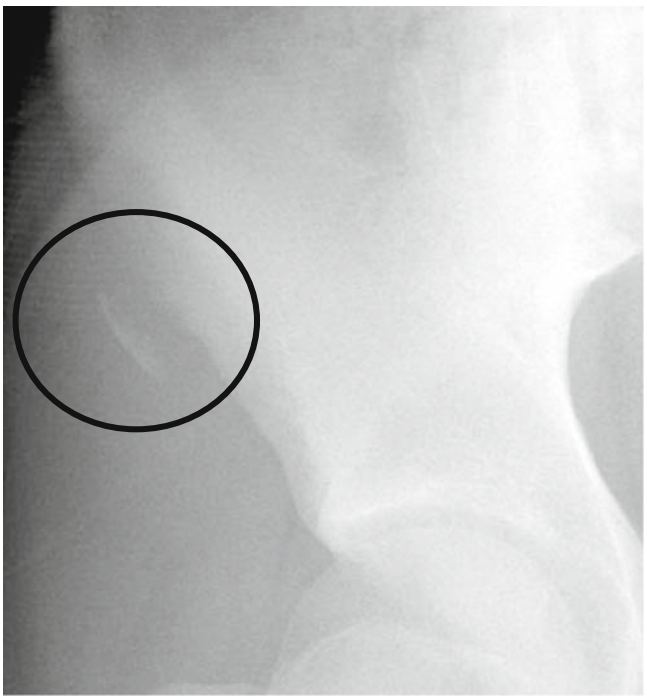

Fig. 5.33 Coned down AP radiograph of the right pelvis showing an avulsion fragment from the anterior inferior iliac spine (AIIS) in a 14-year-old girl (*circle*). This is an avulsion of the origin of the rectus femoris muscle and has been associated with activities that put tension on this muscle such as running hurdles in track and field

Ring Rule

When considering a force applied to a portion of the skeleton, it is important to understand the implications of different geometrical configurations. In particular, bones that either alone or in combination form rings should always be examined for a second fracture once one fracture has been identified (Fig. 5.43). This is because rings generally do not break in a single location increasing the probability of a second fracture. Rings include the obturator rings in the pelvis, the pelvic ring, the mandibulomaxillary ring of the jaw, the radioulnar ring in the forearm, and the tibiofibular ring in the leg. In all, except the obturator rings, the ring is formed by more than one bone joined together by synovial or synchondroidal joints. In the case of the obturator rings, the bones are fused without intervening joints. A separation of one of the joints, either a subluxation or a dislocation, may occur instead of a second fracture (Fig. 5.16).

Many of these combined fractures or fracture dislocations are so typical that they have eponyms, e.g., Monteggia fractures, a fracture of the proximal ulna associated with a radial dislocation (Fig. 5.16); a Galeazzi fracture, a fracture of the distal radius with a distal radioulnar joint dislocation (Fig. 5.44); or an Essex–Lopresti fracture, a proximal radial fracture with a distal radioulnar joint dislocation (Fig. 5.45). Others, though common, do not have eponyms associated with them, e.g., combined tibial and fibular fractures.

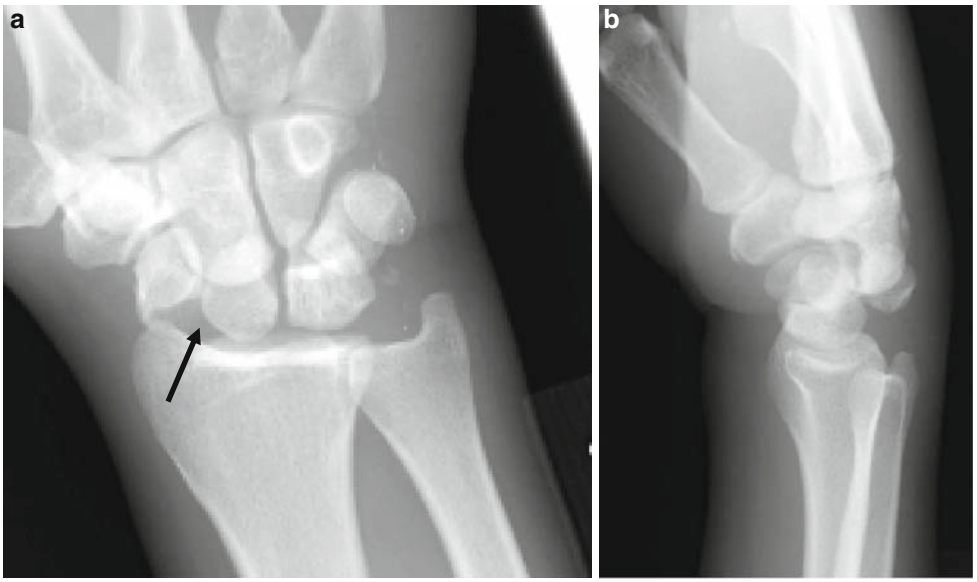

Fig. 5.34 PA (**a**) and lateral (**b**) radiographs of the wrist showing a perilunate dislocation. Note that on the PA radiograph, there is a mid-waist scaphoid fracture (*arrow*). Otherwise, all of the carpal bones except for the lunate appear congruent and normally articulating with one another. On the lateral (**b**) the lunate is articulating normally with the radius. The remaining carpal bones are dislocated dorsally to the carpus but are articulating normally with one another

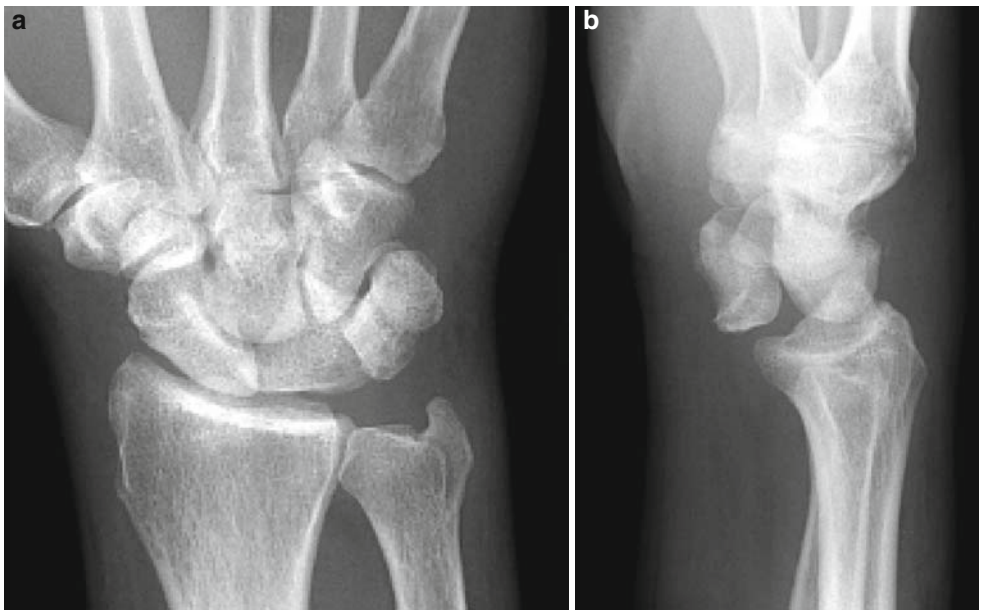

Fig. 5.35 Lunate dislocation. PA (**a**) and later (**b**) radiographs showing volar lunate dislocation. In this case, note that the carpus has returned into alignment with the radius and has displaced the lunate volarly. As a result, the lunate no longer articulates with the radius and has rolled so that its distal surface now faces volarly

Two of these rings, radioulnar and tibiofibular rings, are elongated. As a result a well-placed impact of the correct magnitude along the diaphysis of one of these bones may result in a single fracture. A good example of this phenomenon is the so-called "nightstick" fracture of the ulnar diaphysis (Fig. 5.46). This fracture results from an impact across the ulnar diaphysis, usually when the victim puts an arm up to deflect a facial blow. Another situation where an impact to an elongated ring may not result in a double fracture arises when the impact on the ring occurs along the long axis of one of the bones. Typical examples of this type of fracture are radial head fractures (Fig. 5.47), where the capitellum of the humerus drives into the radial head, and tibial plateau fractures (Fig. 5.12b and 5.48), where the

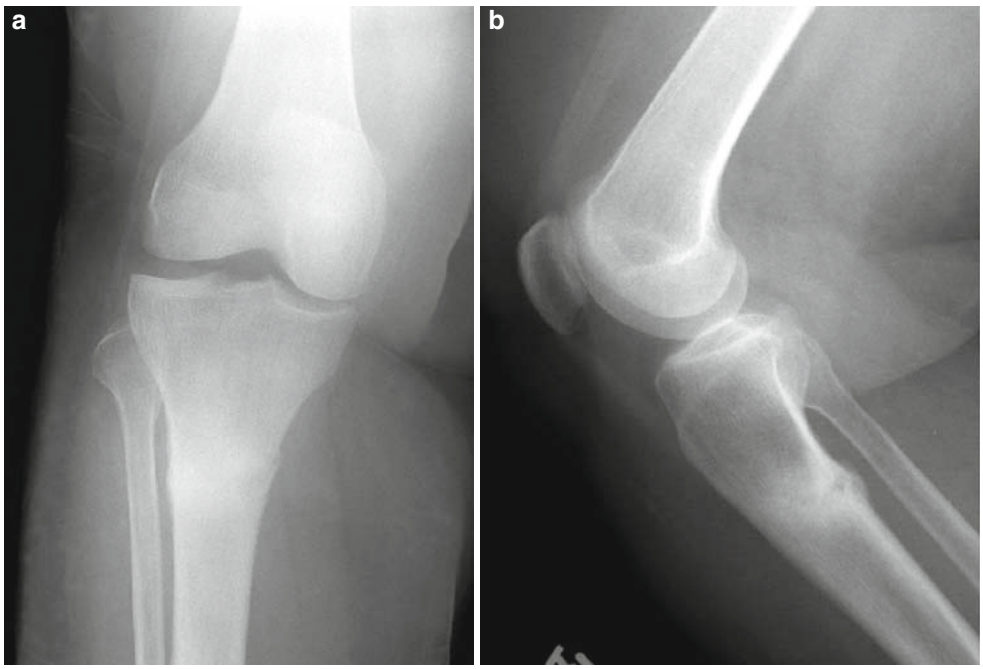

Fig. 5.36 AP (**a**) and lateral (**b**) radiographs of a 35-year-old woman, who recently took up running, showing a proximal tibial stress fracture. The prominent sclerosis shows that the fracture has been present for some time and is now healing

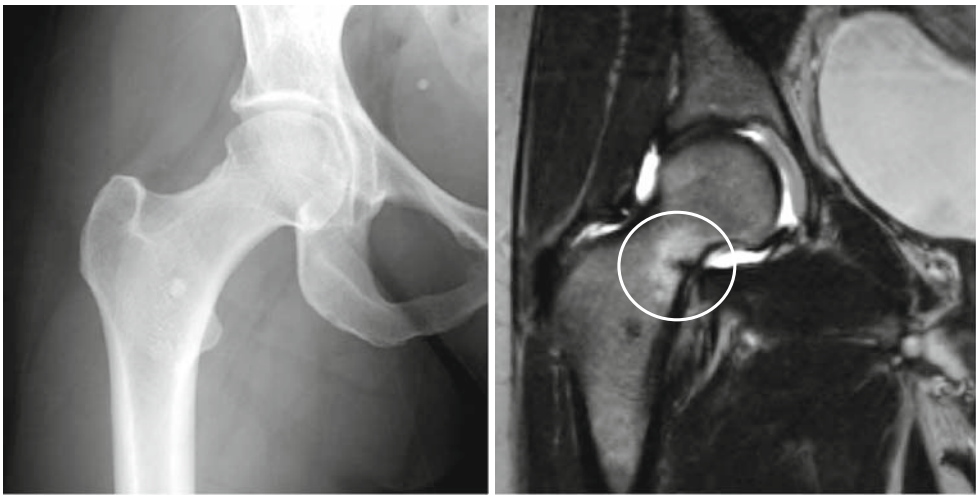

Fig. 5.37 AP (**a**) and coronal T2-weighted MR images (**b**) and (**c**) showing an occult medial femoral neck stress fracture (*circle*). Both the fracture and the joint effusion show high signal on T2-weighted images related to the water content

femoral condyles drive into either the medial or the lateral tibial plateaus.

A final consideration is that the entire bone, though involved in a ring, may not all be entirely within the ring. For example, the medial and the lateral malleoli project inferior to the anterior and posterior distal syndesmotic ligaments where the tibiofibular ring joins inferiorly. Thus, malleolar fractures with a few exceptions as discussed below will not involve the tibiofibular ring (Fig. 5.49). Instead the ligaments around the ankle tend to control the appearance of ankle fractures. The same is true of certain radial and ulnar fractures.

Ligaments: Anatomy and Strength

Not only does the magnitude of the traumatic force and degree of bone mineralization affect the result of trauma, so too does the ligamentous anatomy. As already indicated, carpal fracture versus dislocation will depend on whether or not the ligaments tear at the time of the trauma.

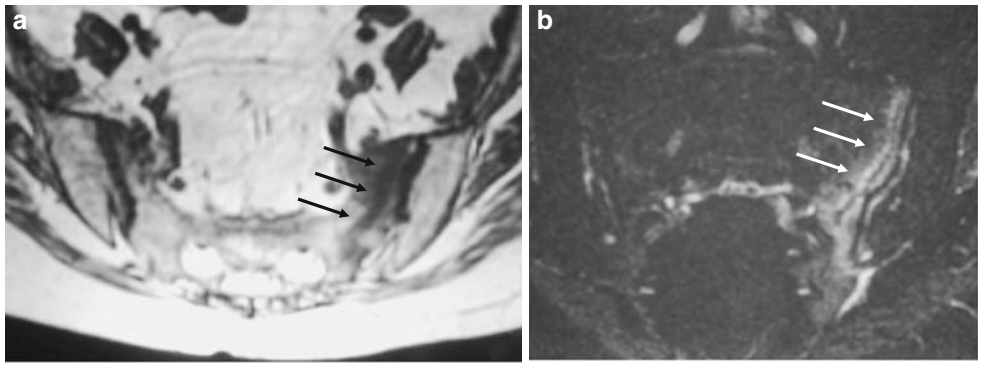

Fig. 5.38 Axial T1-weighted (**a**) and coronal fat–suppressed, T2-weighted (**b**) MR images showing an occult left sacral ala stress fracture (*arrows*) in an 80-year-old woman complaining of pain of several weeks duration. She gave no history of trauma

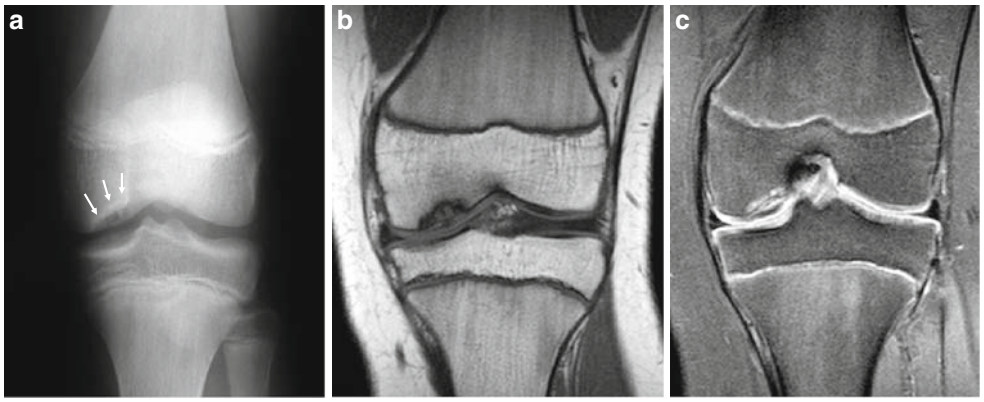

Fig. 5.39 AP knee radiograph (**a**), coronal T1-weighted (**b**), and T2-weighted, fat-suppressed (**c**) MR images showing osteochondritis dissecans. This is an osteochondral fracture of the articular surface of the distal femur (*arrows*). It occurs most typically in younger teenagers and along the lateral aspect of the medial femoral condyle as in this 13-year-old boy

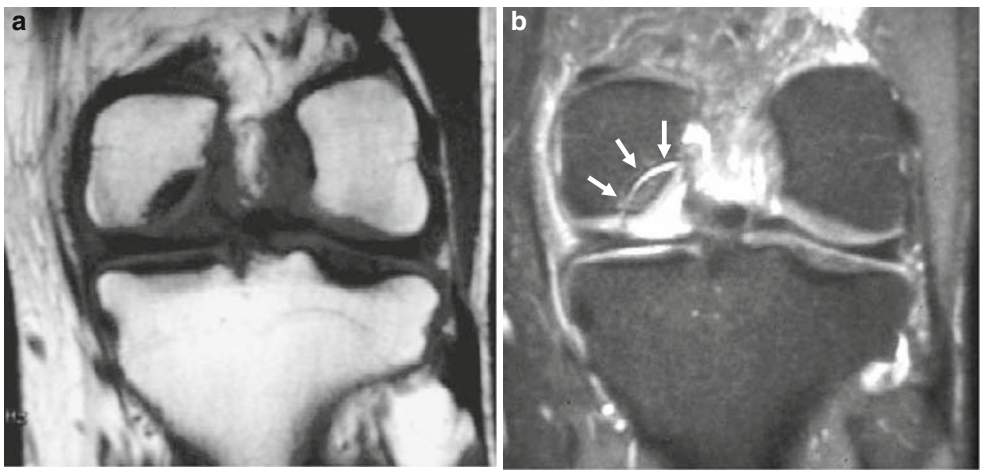

Fig. 5.40 Coronal T1-weighted (**a**) and T2-weighted, fat-suppressed (**b**) MR images showing osteochondritis dissecans with a loosened fragment. Note the high fluid signal on the T2W image (*arrows*) surrounding the fragment, indicating that the fragment is loose and able to become a loose body within the joint

Whether the ligaments tear or the bone fractures often depends not only on the magnitude of the applied force but also on the relative strength of each. In younger skeletons, for example, the anterior cruciate ligament (ACL) may be stronger than the bone to which it attaches. As a result, a force that would typically tear the ACL, e.g.,

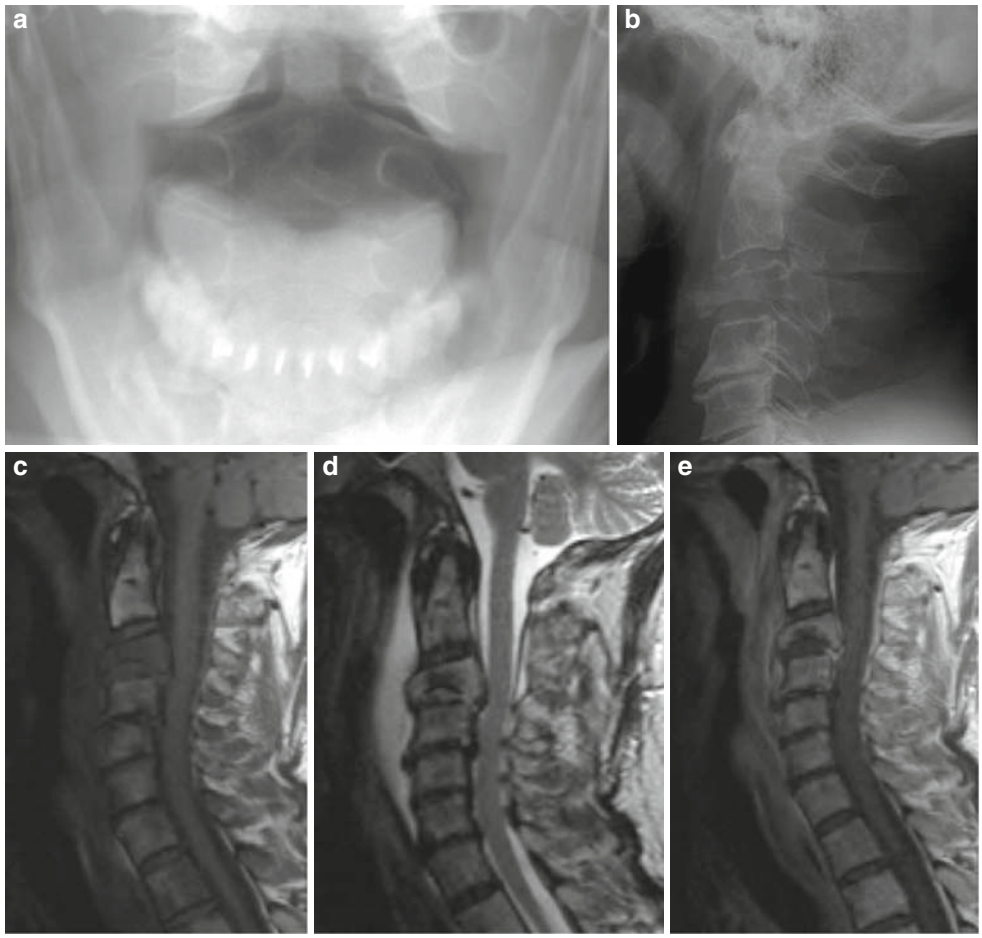

Fig. 5.41 Open mouth (**a**) and lateral (**b**) radiographs and sagittal T2-weighted (**c**), T1-weighted pre (**d**) and post (**e**) administration of intravenous gadolinium MR images showing collapse and destruction of the C3 vertebral body from renal cell carcinoma metastasis. On the MR, note the large, enhancing soft tissue mass anterior to the vertebral column and extending from C2 to C6. There is no involvement of the spinal canal

twisting or anterior subluxation of the tibia relative to the femur, may instead cause an avulsion fracture of the bone at the ACL's footprint on the tibia (Fig. 5.50).

Although it is true that ligaments are commonly stronger than the bone in younger patients, the age of the patient is not always a useful way to determine if the ligament will tear or the bone will fracture. Other variables are important in this prediction, including the size of the ligament, its orientation at the time of the trauma, the relative amount of cortical and trabecular bone at the ligament's insertion, the bone's mineralization, and the morphology of the bone. As a result, ankle trauma may easily cause either a fracture or a sprain depending on any number of variables such as the force applied, the position of the ankle, the direction of the force, and the relative strength of the bone.

Regardless, a thorough understanding of the ligamentous anatomy around joints will help in understanding not only sprains (ligament tears) but also the fractures that result in corresponding locations. Nowhere has this concept been better studied than in the ankle. Here, two fracture classifications are commonly employed. One, the Weber–Danis classification focuses only on lateral malleolar fractures and their position relative to the ankle syndesmosis. The other, the Lauge–Hansen is more comprehensive, classifying fractures of all three ankle malleoli according to the position of foot at the time the fracture is initiated, supination or pronation, and the direction of the force applied to the ankle, i.e. adduction, abduction, and external rotation. While these classifications are useful and help to predict ankle joint stability and therefore therapy, understanding the biomechanics of these fractures is more important from an analytical point of view.

When the ankle is abducted or externally rotated, the talus strikes the lateral malleolus (Fig. 5.49) creating an oblique fracture in this location, either mediolaterally or anteroposteriorly from the point of impact. At the same time the medial ligaments of the ankle (the deltoid ligament complex) are stretched inferiorly. Most often the deltoid ligament is stronger than the bone of the medial malleolus and so a

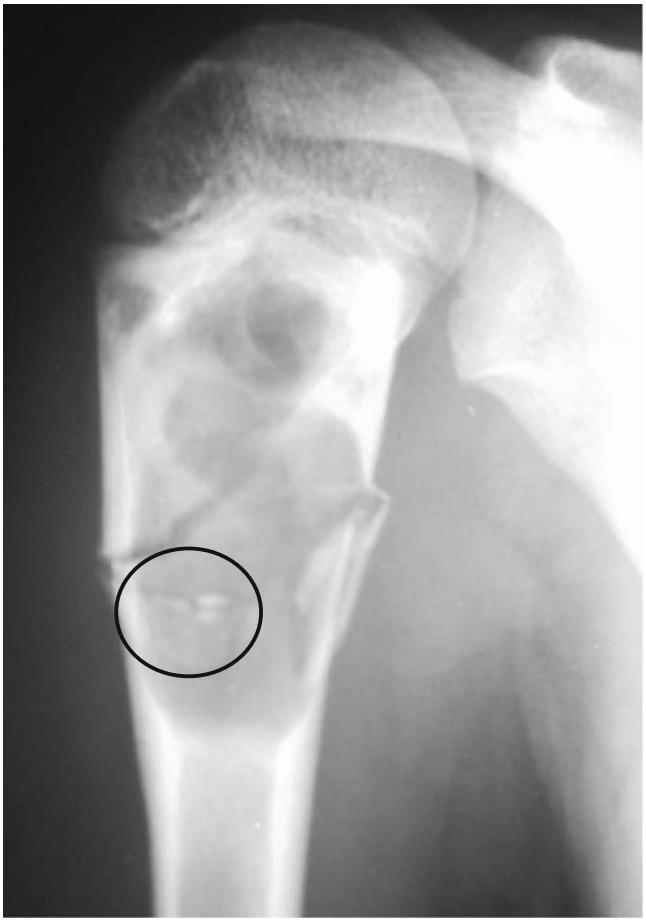

Fig. 5.42 AP radiograph showing a pathological fracture through a unicameral bone cyst in the proximal humerus. Note the small fragment within the lesion (*circle*). This is called a fallen fragment and is pathognomonic of a unicameral bone cyst. It results from a chip of bone falling into the cyst when it fractures

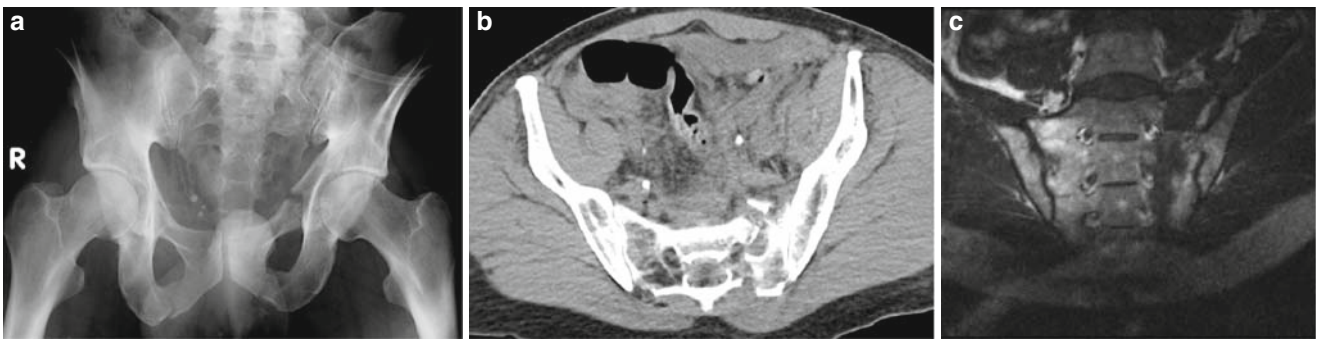

Fig. 5.43 AP pelvic radiograph (**a**), CT image (**b**), and off-axis, coronal T2-weighted MR image (**c**) showing fractures of the superior pubic rami and inferior ischiopubic rami bilaterally (**a**) with a left superoinferior sacral alar fracture. This is a typical example of the ring rule. Both obturator rings are fractured in two locations and the pelvic ring is fractured in three – both pubic rami and the sacrum. Note that the sacral fracture is extremely difficult to see on the radiograph but is quite obvious on the CT and MRI. Note also that the fracture is just lateral to the left anterior neuroforamina of the sacrum. It is clear that these fractures may have neurological complications

transverse medial malleolar fracture results from the downward stretching of the deltoid ligament. Alternatively, one or more of the four major components of the deltoid ligament may be avulsed at their distal insertions, leading to small avulsion fractures from the navicular bone (tibionavicular ligament), the talus (anterior tibiotalar ligament more common than the posterior tibiotalar ligament), and the medial aspect of the calcaneus (tibiocalcaneal ligament). Least

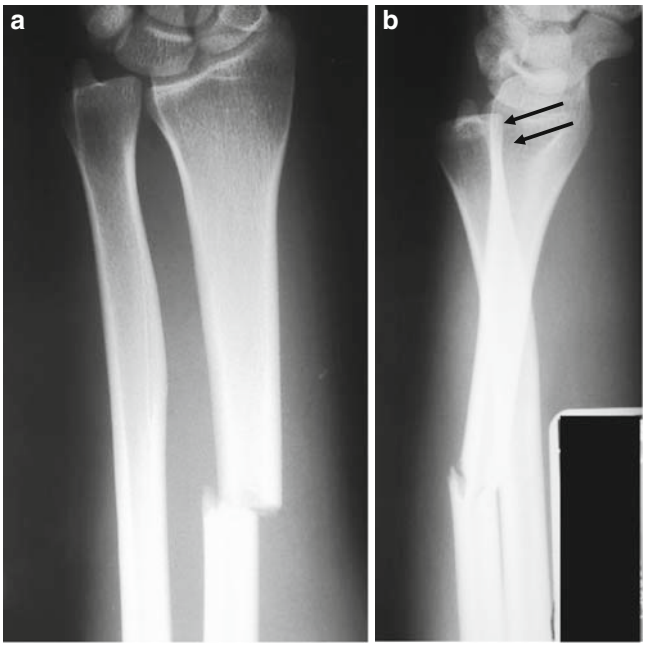

Fig. 5.44 AP (**a**) and lateral (**b**) radiographs of the forearm showing a Galeazzi fracture dislocation. This fracture, similar to the Monteggia fracture shown in Fig. 5.16, also disrupts the radioulnar ring. In this case it is the radius that fractures and the distal radioulnar joint (DRUJ) that dislocates (*arrows*), thereby breaking the ring into two locations

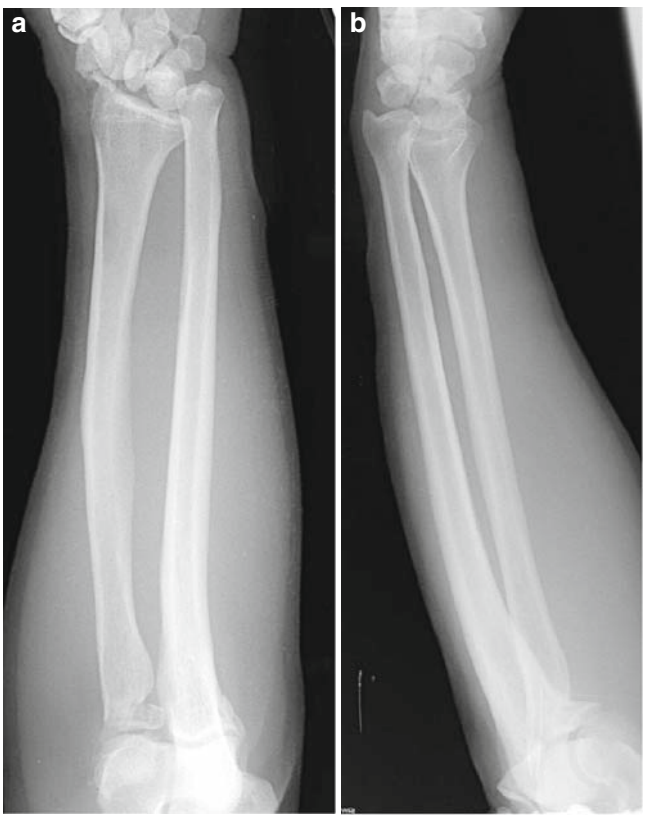

Fig. 5.45 Essex–Lopresti fracture. AP (**a**) and lateral (**b**) radiographs show a fracture of the radial head and the neck with dislocation of the DRUJ. Note that the radius has shortened. This means that the interosseous membrane between the radius and the ulna also has torn. In addition, note the scaphoid fracture in the wrist along with the posterior perilunate dislocation, best seen on the lateral images. (Case courtesy of Dr. D. Dean Thornton)

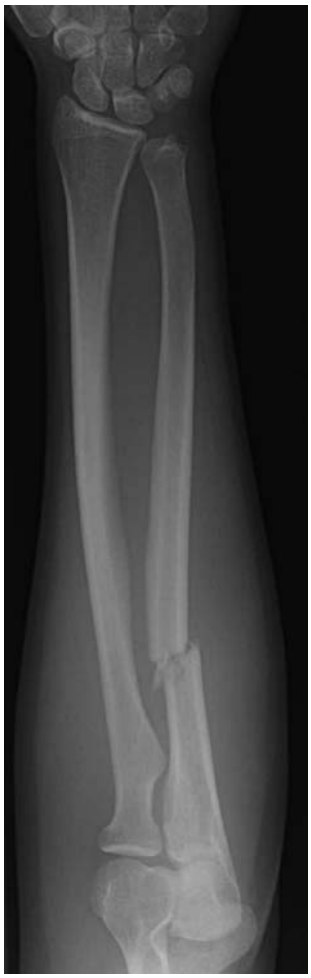

Fig. 5.46 AP radiograph showing a displaced nightstick fracture of the ulnar diaphysis. In this case, the ring is fractured in only one location because the blow impacted the long side of the ring and the joints at either end were able to dissipate the energy imparted to the ring. A nightstick fracture is a classic self-defense type of fracture as the victim raises his arm to ward off a blow to the face

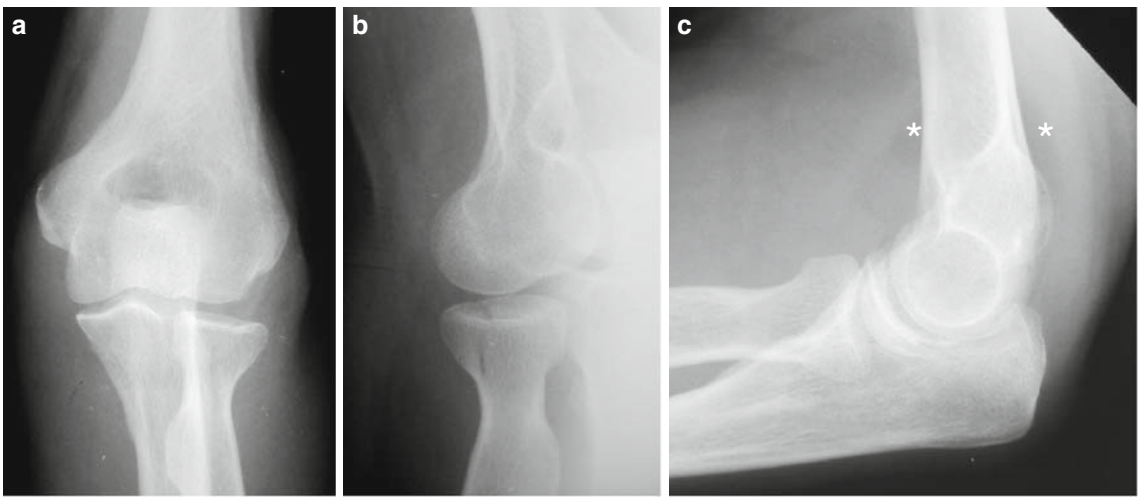

Fig. 5.47 AP (**a**), coned down radial head view (**b**), and lateral elbow (**c**) radiographs showing a joint effusion and a radial head fracture. The AP and coned down views show a minimally displaced fracture of the radial head. The lateral view shows a sailed anterior fat pad and a visible posterior fat pad (∗), indicating an effusion

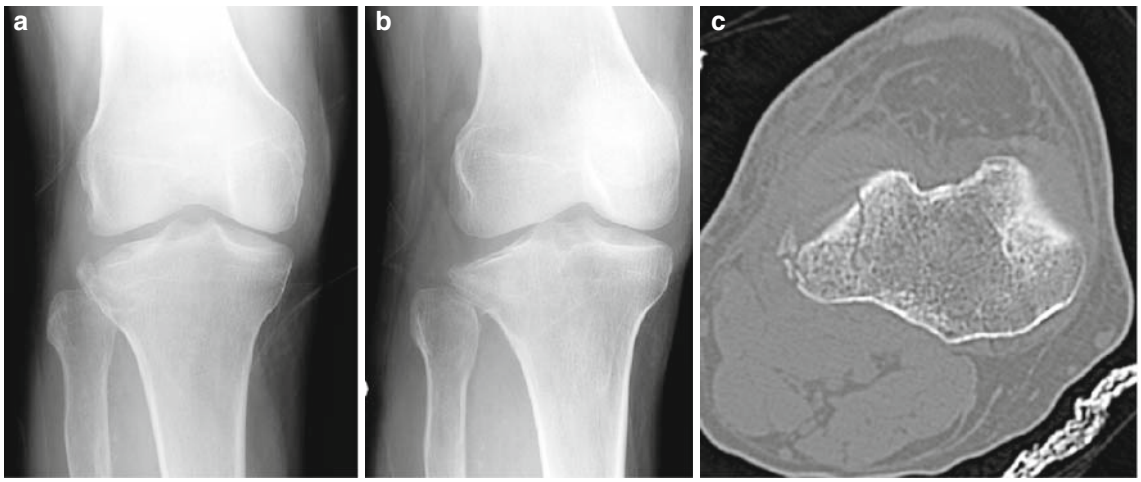

Fig. 5.48 AP (**a**), internal oblique (**b**), and CT (**c**) images showing a lateral tibial plateau fracture

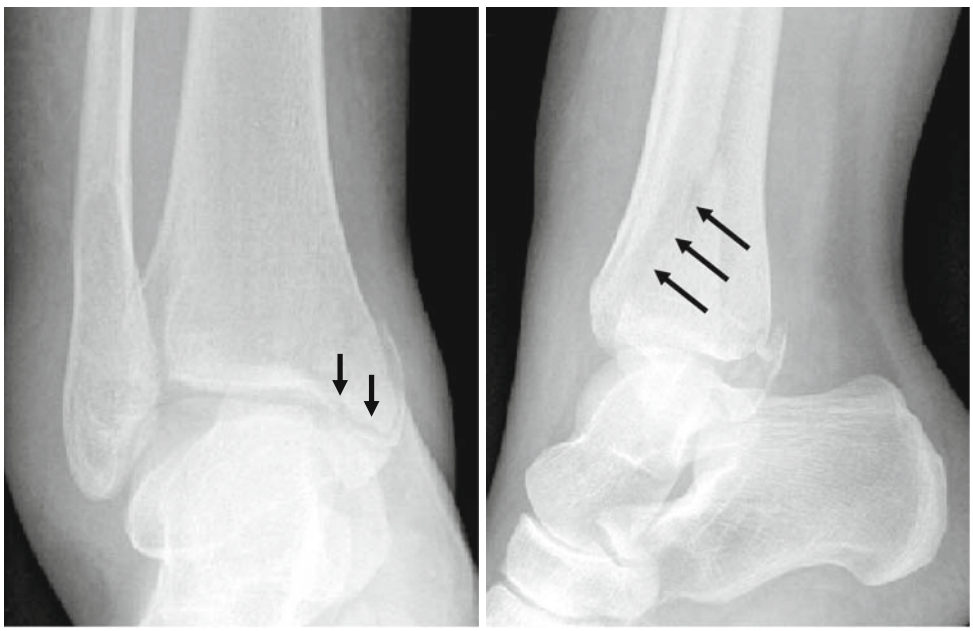

Fig. 5.49 AP radiograph (**a**) and lateral radiograph (**b**) showing an obliquely oriented anteroposterior plane lateral malleolar fracture (*long arrows*) and a transversely oriented medial malleolar fracture (*short arrows*). These are consistent with an external rotation injury

commonly, a sprain (tear) of the superficial fibers (the tibionavicular and/or the tibiocalcaneal ligament) of the deltoid will result. The deep fibers (posterior tibiotalar ligament) are rarely torn. This topic will be addressed more completely in the section "Soft Tissue Trauma and Internal Derangement of Joints".

Furthermore, the fracture location will be determined principally by the orientation of the talus at the initiation of the trauma. The more the pronated the ankle at initiation of the trauma, the more superior the fracture of the lateral malleolus. Indeed, with hyperpronation injuries, radiographs may show only a transverse medial malleolar fracture. The radiologist should be alert for this appearance as it may suggest that the energy from the talar impact against the fibula has migrated up the fibula and interosseous membrane to be released at the proximal fibular neck. In this case the clinician should be alerted to the possibility of a proximal fibular fracture and the superior lateral aspect of the leg should be checked for point tenderness. Radiographs are generally unnecessary. This configuration of a transverse medial malleolar fracture and a proximal fibular fracture is known as a Maisonneuve fracture (Fig. 5.51).

Likewise, adducting the talus will result in the talus impacting the medial malleolus and causing an oblique

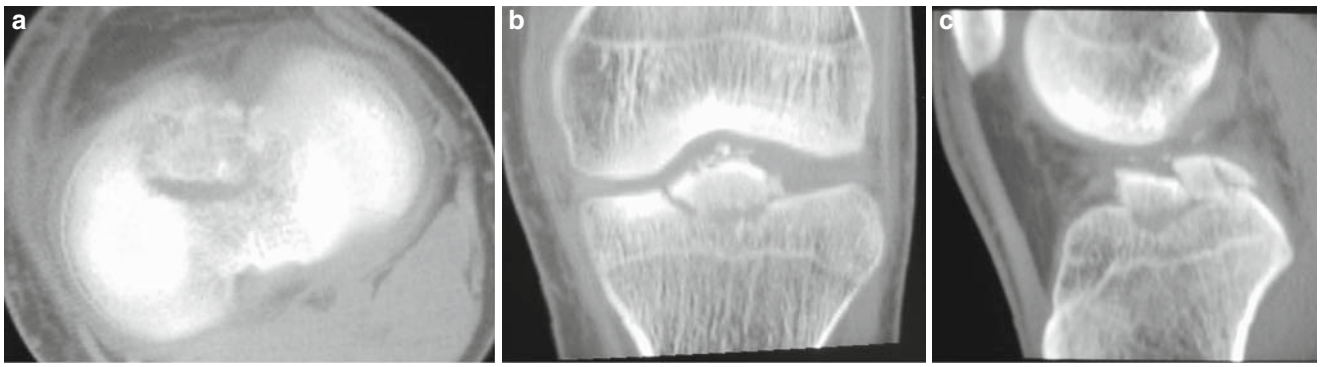

Fig. 5.50 Axial (**a**), coronal (**b**) and sagittal (**c**) CT images in a 16-year-old boy showing an avulsion of the tibial footprint of the anterior cruciate ligament (ACL) with extension into the interspinous region of the tibia

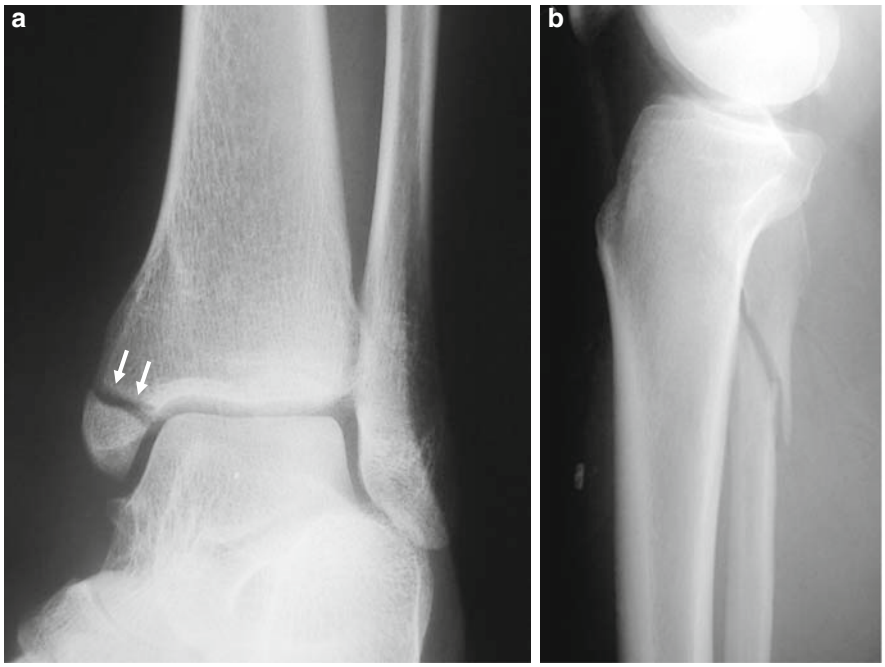

Fig. 5.51 Mortise view ankle radiograph (**a**) and lateral proximal tibial–fibular radiograph (**b**) showing a Maisonneuve fracture. The medial malleolus shows a nearly transverse fracture (*arrows*), while the proximal fibular neck is also fractured from the energy as it moved through the intraosseous membrane

fracture of this malleolus. Stretching of the lateral ligaments – anterior talofibular, calcaneofibular, and posterior talofibular – may result in a transverse avulsion fracture from the lateral malleolus as the force on the malleolus is directly perpendicular to its tip. As with abduction fractures, the ligaments may also avulse from their distal insertions or more commonly one or more of them may tear, resulting in a lateral ankle sprain. The anterior talofibular ligament, in particular, is weak and more often torn (Fig. 5.52) than the calcaneofibular ligament and the rarely torn posterior talofibular ligament. Finally, as with abduction, small distal avulsion fractures from the tarsal bones may result from these forces.

Fracture Features and Terminology

The analysis of acute fractures includes consideration of several features that affect therapy. These include the displacement of the fracture parts, the angulation of the fracture parts, the comminution of the fracture, the intraarticular extension of the fracture, the presence of a wound in the region of the fracture, and a compound fracture where bone is exposed to air directly.

Certain conventions apply to the description of fractures. First, displacement and angulation of the fracture are evaluated in terms of the position of the distal fracture part

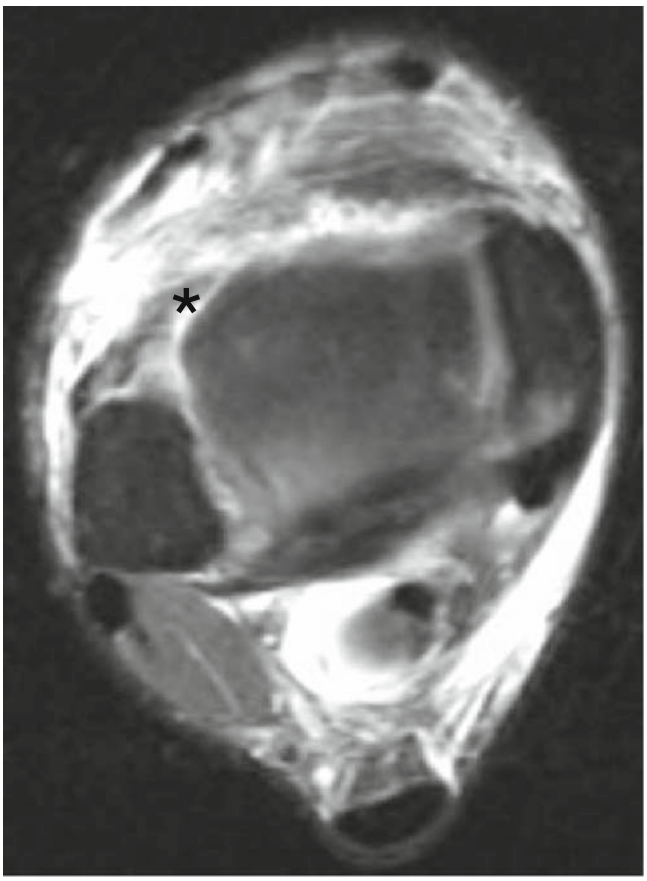

Fig. 5.52 Axial T2-weighted MR image showing an incomplete tear of the anterior talofibular ligament (∗). Note the thickening of the ligament and the surrounding edema. High signal is visible interdigitating with the anterior and posterior insertions of the ligament

relative to the proximal fracture part. For example, if the distal fractured part is displaced laterally relative to the proximal part, the fracture is said to be laterally displaced (Fig. 5.44a). Second, with respect to angulation, there are some discrepancies between the terminology adopted by radiologists and that adopted by orthopedists. While radiologists describe angulation relative to the position of the distal fracture fragment, orthopedists describe angulation of fractures by the vertex of the angle formed by the fracture parts. Thus, radiologists describe the angulation of a long bone fracture where the distal fracture part angles posteriorly as posteriorly angulated. Orthopedists, on the other hand, describe this as anterior angulation since the vertex of the angle points anteriorly. To avoid confusion, therefore, the best practice for describing fracture angulation is to follow both conventions and describe the fracture in reports as "posteriorly angled with vertex anterior", for example.

Comminution is typical of adult fractures and common in pediatric ones. The more comminution that accompanies the fracture, the more difficult will be reduction. A butterfly fragment – a large triangular or trapezoidal fracture fragment that goes cortex to cortex in the diaphyseal fracture of a long bone (Fig. 5.53) – increases the difficulty of anatomic reduction because of the difficulty in reducing the parts to anatomic position. In other fractures, certain types of comminution or accompanying fractures are common. For example, an ulnar styloid fracture often accompanies a distal radial metaphyseal fracture (*vide supra*). Similarly, tuberosity fractures often accompany surgical neck fractures of the humerus and trochanteric avulsions often accompany intertrochanteric fractures of the hip.

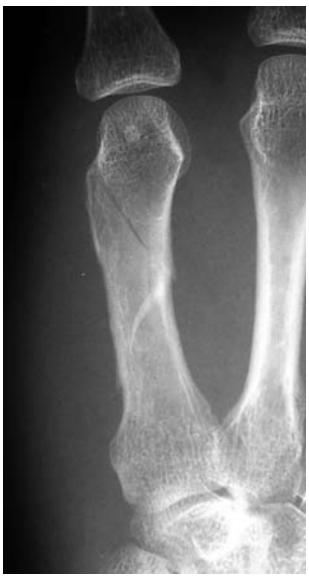

Fig. 5.53 PA coned down radiograph of the 5th metacarpal showing a triangular true butterfly fragment in the mid-diaphyseal fracture. (Case courtesy of Dr. Ken Schreibman)

Evaluation of Fracture Healing

Radiographs are an important tool in the evaluation of fracture healing. As with the cause of fractures, to evaluate fracture healing, certain concepts must be understood. The two most important of these are the granulation response to fracture and the osseous blood supply. The phases of fracture healing are discussed in the chapter on fracture fixation (Chapter 6). Here we discuss general principles of healing.

Osseous Blood Supply

A bone's vascular supply has important implications in terms of fracture healing. In general, the better the blood

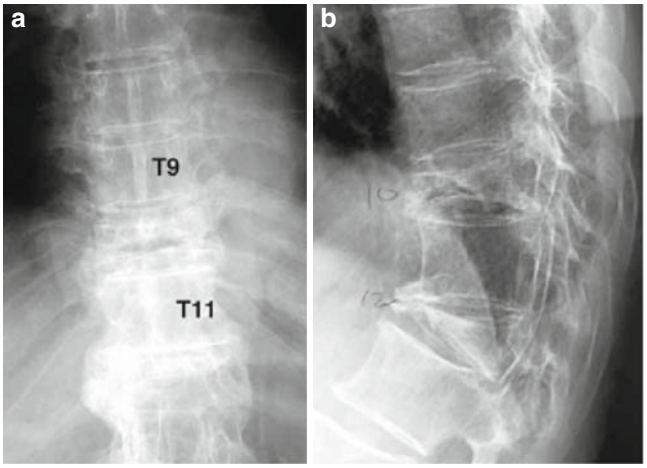

Fig. 5.54 AP (**a**) and lateral (**b**) radiographs showing collapse of T10 with a linear collection of air consistent with Kummel disease. (Case courtesy of Dr. John Hunter)

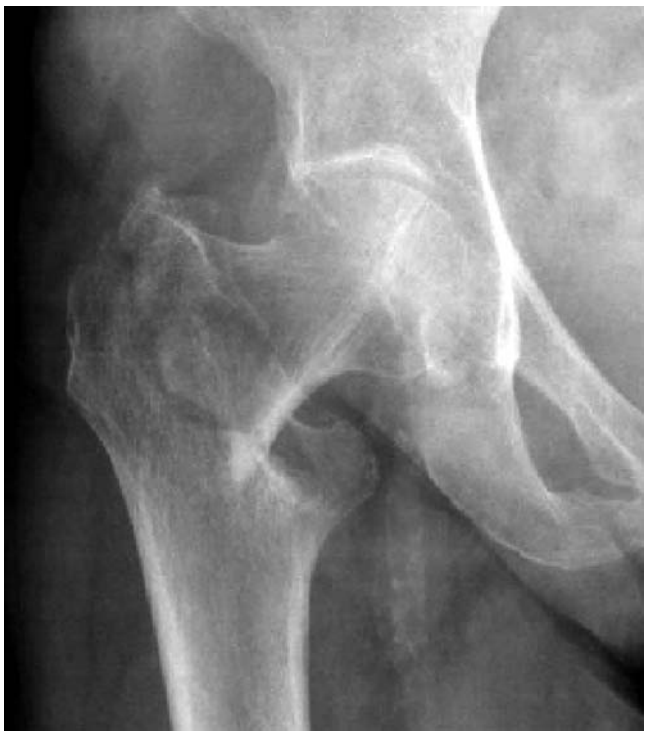

Fig. 5.55 AP right hip radiograph showing a two-part right hip intertrochanteric (IT) fracture with mild varus angulation

supply around the fracture, the faster the fracture healing. This observation has two important implications: one related to bones' response to trauma with age and the other related to where the fracture occurs within the bone.

Pediatric patients heal fractures comparatively rapidly because immature bone is remodeling rapidly as a normal part of growth, but once the growth plates close, much of the rate of healing relates to blood supply. As with other organs, underlying vascular pathology, most commonly atherosclerotic disease, affects the blood supply to the skeleton. As the blood supply to a bone declines, bone remodeling slows. An extreme example of this phenomenon is Kummel disease, seen primarily in elderly patients. In Kummel disease, patients develop chronic, nonhealing vertebral body insufficiency fractures in the thoracolumbar region of the spine, leading to a linear intravertebral vacuum phenomenon (Fig. 5.54). Current thinking is that these fractures fail to heal because of poor blood supply related to atherosclerotic disease that is common in the elderly. In fact, ischemia or infarction of the vertebra may permit the fracture to progress in severity and ultimately give rise to a *vertebra plana* appearance. Thus, as aging progresses the rate at which fractures will heal will slow as well.

Second, different bones have different blood supplies. This means that some bones may heal more easily than others. Further, the blood supply will vary depending on the portion of the bone. For example, the majority of long bones receives their nutrient blood supply diaphyseally and has their endarterial supply toward the ends of the bone. As a rule of thumb, the closer a fracture is to the endarterial distribution of the supplying vessels, the greater will be the likelihood of complications in healing, in particular failure of fracture healing and avascular necrosis (AVN) of the fractured part that is distal to the vascular supply. Thus, knowledge of a bone's blood supply is essential to understanding the location and likelihood of the fracture causing avascular necrosis. For example, the major blood supplies to the carpal scaphoid, the femoral neck, and the tarsal talus are recurrent in nature. This means that the supply enters the bones distally and returns more proximally. From this information, it is possible to predict that avascular necrosis will occur more commonly in the proximal pole of the scaphoid, the subchondral femoral head, and the proximal talus after a fracture of the scaphoid waist, the femoral neck, and the talar neck respectively. In addition, the closer the fractures in these parts are to the endarterial supply, the more likely will be the development of avascular necrosis. For example, the incidence of avascular necrosis will increase as fractures progress from the intertrochanteric region of the femur (Fig. 5.55) to the subcapital region of the femoral neck (Fig. 5.56). In the former, the overall incidence of AVN is about 4% but increases to over 40% in the latter.

Closer analysis shows that the incidence of AVN after fracture depends not only on the location of the fracture line relative to the endarterial supply to the bone but also on the displacement of the fracture parts. Subcapital femoral fractures illustrate this point well. Minimally displaced fractures have a low incidence of AVN, but severely displaced fractures will all develop AVN. Because the likelihood of developing AVN or nonunion varies with displacement of fracture parts, therapy requires

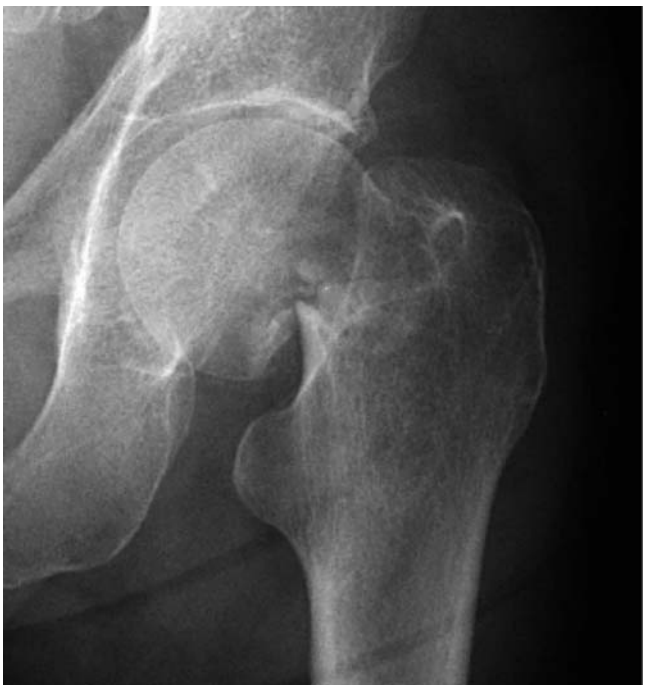

Fig. 5.56 AP radiograph of the left hip showing a displaced supcapital (Garden IV) left hip fracture

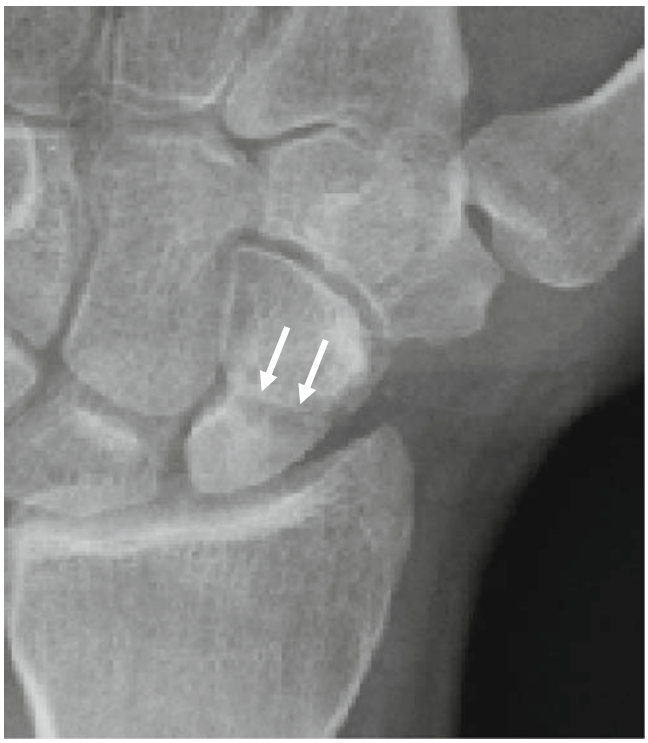

Fig. 5.57 Coned down PA radiograph of a mid-waist scaphoid fracture (*arrows*) showing resorption along the fracture line causing apparent widening. This is consistent with early healing and is expected

subclassification of fractures to improve outcomes, e.g., the Garden classification for subcapital fractures of the hip (Table 5.3).

Table 5.3 Garden classification of subcapital hip fractures

Type	Abnormality
I	Impacted or incomplete with valgus angulation
II	Complete without displacement
III	Partial displacement
IV	Displaced or angulated

Granulation and Periosteal New Bone

When a fracture occurs, the healing response begins almost immediately. The first part of the healing process is an increase in local blood supply and development of granulation tissue. This means that radiographs may show some early bone demineralization around the fracture. As the granulation tissue increases, the cells reabsorb the bone along the fracture. As the margins of the fracture are reabsorbed, the edges become less sharp and distinct. In addition, this process causes an apparent widening of the fracture line on radiographs (Fig. 5.57). Apparent widening of the fracture line may cause the paradoxical impression that the fracture is actually worsening instead of healing. An understanding of this phenomenon will prevent misinterpretation of the early healing process.

The next step in healing is the recruitment of pluripotential stem cells to form new bone. This is most apparent in the form of callus along the fracture margins. Callus is periosteal new bone formation that eventually will bridge the fracture margins. As healing progresses, the callus ossifies and bridges the fracture (Fig. 5.58). The rate at which healing occurs will depend on a number of factors, including the blood supply to the bone around the fracture, the bone involved by the fracture, and the stability of the fixation during the healing process.

As callus bridges the fracture, the trabecular bone undergoes a like process so that eventually the entire fracture is repaired and other than possibly some residual deformity, the fracture line will be inapparent radiographically (Fig. 5.58c). This latter process often takes longer than the time to form bridging callus. This means that the definition of when a fracture has healed is somewhat arbitrary and will depend on the lifestyle of the patient. At a minimum the radiographic definition of healing is some, not circumferential, bridging bone formation, regardless of trabecular healing. While this degree of healing may be sufficient for some level of activity, it would clearly be insufficient for a highly trained athlete to resume stressful work. In fact, clinical healing may not correspond at all with radiographic findings. The reason for this is that routine radiographs do not depict nonmineralized callus. Thus, a patient

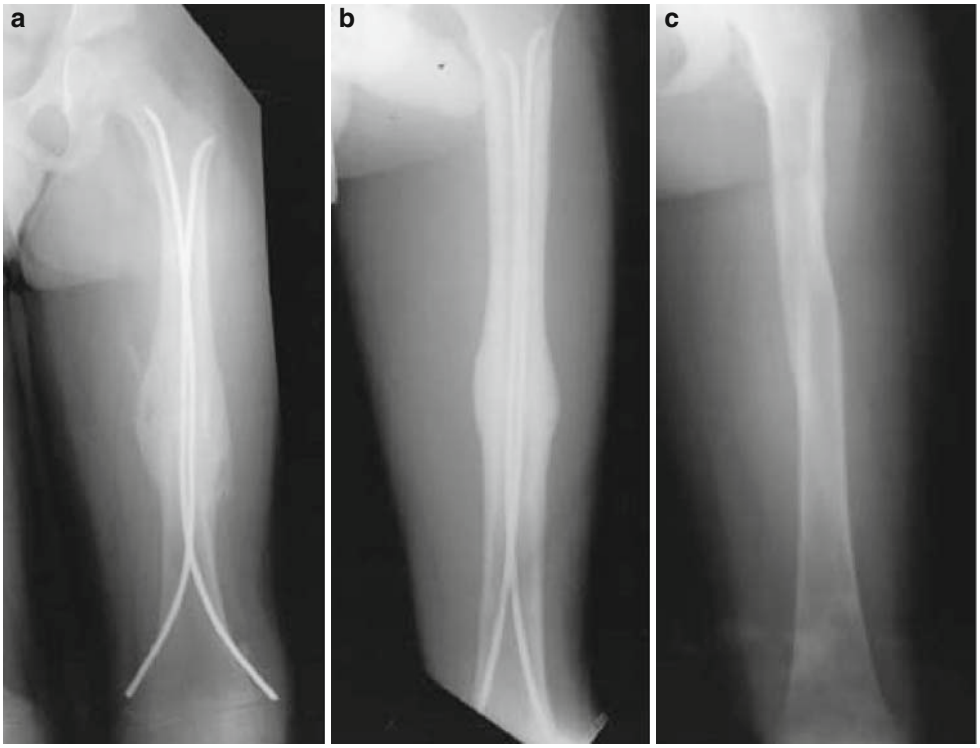

Fig. 5.58 AP radiographs (**a**–**c**) of pediatric midfemoral healed fractures showing mature callus in various stages of remodeling

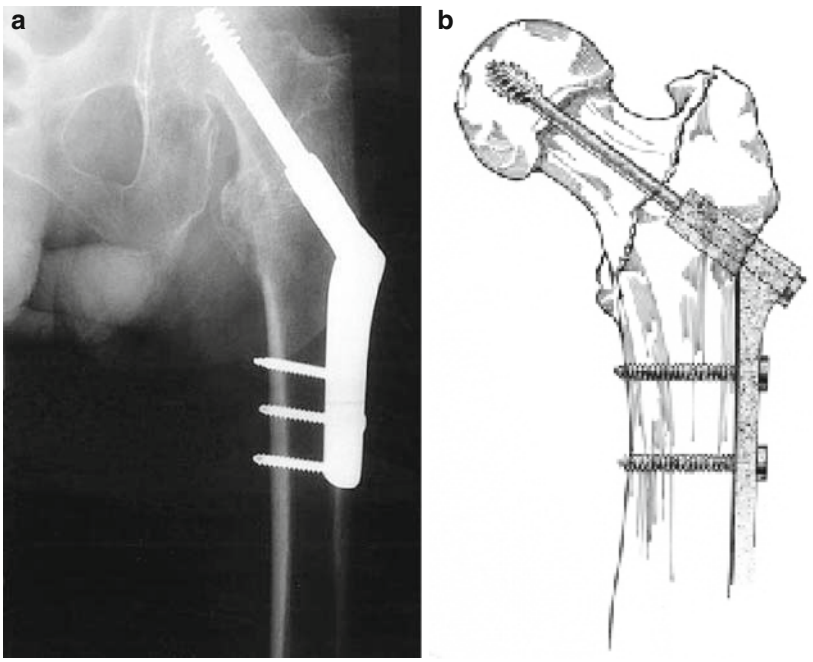

Fig. 5.59 AP radiograph (**a**) and graphic (**b**) showing a dynamic hip screw and fixation device. Note that the angled barrel of the femoral plate compresses along the screw axis with weight bearing, thereby increasing the load across the fracture

whose fracture appears unhealed on radiographs may clinically appear stable and asymptomatic, at least at rest. Ultimately then, the actual decision as to what level of activity a fracture patient may resume is a clinical one that integrates both the clinical evidence and the radiographic data.

Fracture Fixation and Stability

If a fractured bone is not immobilized, the fractured parts will have a tendency to move relative to one another. This will prevent the formation of callus that bridges the fractured parts and as a result either delay healing or prevent it altogether. In fact, paralyzed patients who fracture an affected limb often show markedly delayed healing and very marked callus formation. This results from the absence of proprioception in the fractured limb, preventing the patient from splinting the limb. Thus, as is obvious, a certain degree of immobilization is essential in order to achieve fracture healing. On the other hand, complete immobilization will prevent healing as well. Without a load across the fracture, the bone will tend to reabsorb but not produce callus.

Understanding Wolff's law has enabled orthopedists to invent fracture fixation devices that maximize the chances of fracture healing. For example, many fixation devices today provide an opportunity to "dynamize" a fracture. What this means is that the device either in its native state or after manipulation can be made to provide a dynamic load across the fracture line in the hopes of improving fracture healing. For example, the dynamic hip fixation screw device (Fig. 5.59) is designed such that as the patient ambulates, the sleeve of the distal femoral portion of the device slides over the screw in the neck causing a changing load across the fracture line. Similarly, many intramedullary fixation nails in use today have elongated oval slots as well as round holes through which to place the locking screws. The idea is that if the fracture fails to heal while fixed in static position by the locking screws in the holes, these can be removed leaving the screws through slots that then will permit some motion of the bone along the axis of the rod. These concepts will be covered in more detail in Chapter 6, which discusses orthopedic fixation devices.

Dislocations

Of course, fractures are not the only result of musculoskeletal trauma. Joints are often injured as well. These injuries, as with fractures, depend on a number of factors including the direction of the applied force, the amount of force applied, the chronicity of the applied force, the shape of the joint, the orientation of the articulating bones at the time of impact, the level of mineralization of the articulating bones, and the strength of the ligaments supporting the joint. As with fractures and contusions, these factors integrated together determine the pathological result of the trauma. Thus, as discussed above, numerous factors determine whether wrist trauma causes a carpal bone fracture, a perilunate dislocation, a lunate dislocation, or a distal radial fracture.

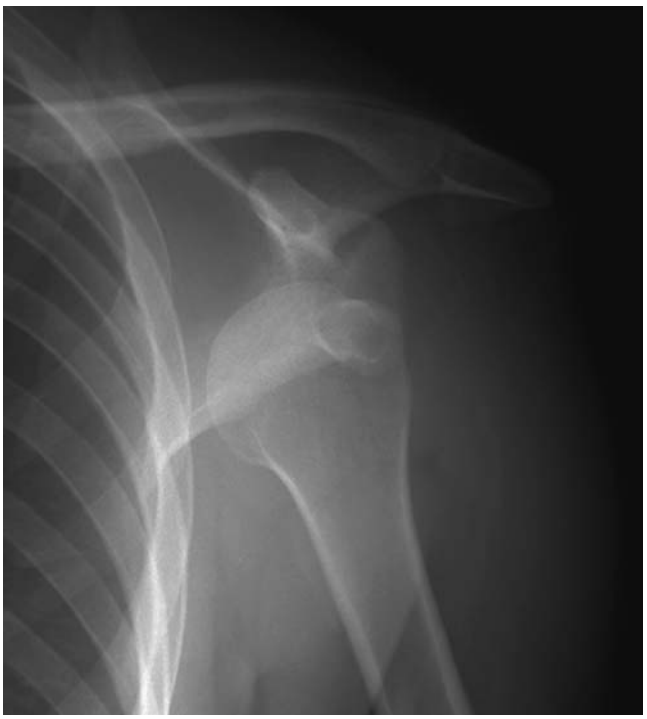

Fig. 5.60 AP radiographs showing an anterior subcoracoid shoulder dislocation with typical inferior and medial displacement of the humeral head. This is the most common type of anterior shoulder dislocation. Subglenoid dislocations are less common

Joint Morphology and Ligaments

Some joints are more prone to dislocation than others because of the morphology of the joint and the ligaments within and around the joint. For example, a shoulder joint with its shallow glenoid fossa, relatively weak glenohumeral ligaments, and redundant capsule dislocates much more easily and commonly than the hip with its deep acetabulum, strong ligamentum teres, and tighter capsule.

The configuration of the joint also contributes to the type of dislocation that it is likely to undergo. Again, the shoulder, primarily as a result of the configuration of its ligaments, its shallow glenoid, and the position of the arm at the time of trauma, is much more likely to undergo anterior dislocation (>85%) than posterior or inferior (Fig. 5.60). The hip, on the other hand, is most likely to dislocate posteriorly (>85%) (Fig. 5.61). Posterior dislocations mainly result from the fact that the majority of hip dislocations occur when the hip is flexed and a strong anteriorly applied force hyperabducts the hip. Patellar dislocations are most frequent laterally as the result of the shallow shape of the lateral side of the patellofemoral joint (Fig. 5.62) and the strength of the medial patellofemoral ligament.

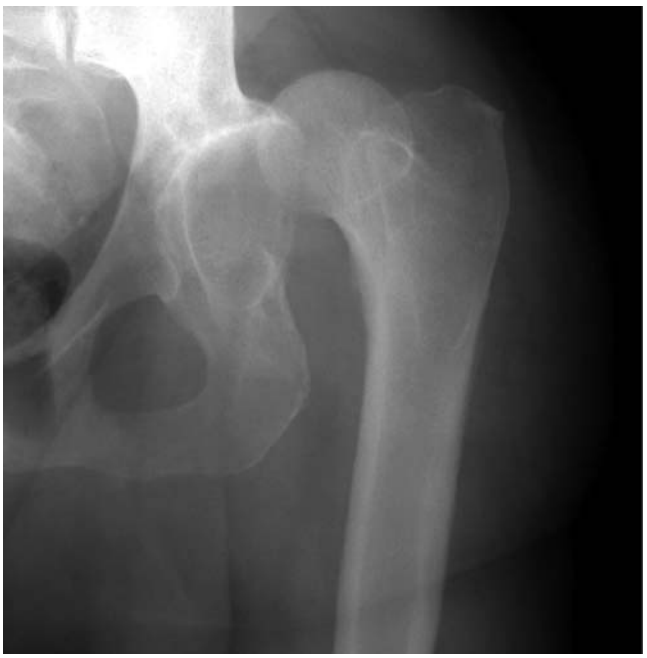

Fig. 5.61 AP hip radiographs showing a posterior hip dislocation with superior displacement of the femur. No posterior acetabular lip fracture, though common, is visible in this case

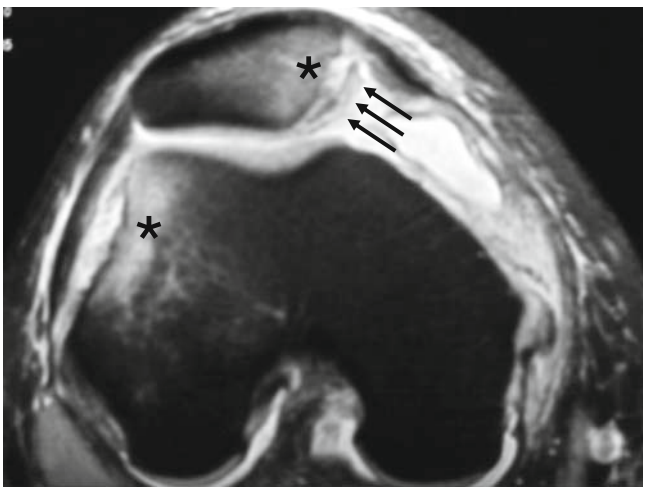

Fig. 5.62 Axial T2-weighted, fat-suppressed MR image showing the shallow trochlear groove on the femur. Note the contusion on the lateral femoral condyle and the small fracture from the medial aspect of the patella. This patient had recently suffered a lateral dislocation of the patella, now reduced. The contusion and the fracture are from the impact of the patella on the lateral condyle

Many dislocations have a tendency to fracture parts of the articulating bones, either from direct impact of the bones as they dislocate, from avulsions at ligament or tendon insertions, or from the body's attempt to reduce the dislocation after it has occurred. Some of these are so typical as to have earned eponyms, e.g., the Hill–Sachs deformity seen in the superior posterior aspect of the humeral head from impaction of this portion of the humeral head on the inferior lip of the glenoid during anterior dislocation of the shoulder. A fracture of the anterior inferior glenoid corresponding to the point of humeral impaction on the glenoid and is known as a Bankart fracture (Fig. 5.63). Common dislocations and their associated fractures are shown in Table 5.4.

Soft Tissue Trauma and Internal Derangement of Joints

The advent of MRI has enabled a detailed anatomic evaluation of the internal structures of joints, their surrounding ligaments, and musculature. This, in turn, has improved our ability to diagnose and understand the pathophysiology of soft tissue and joint-centered trauma. In particular, MRI has enabled direct visualization of muscle, tendon, ligament, and cartilage trauma – both fibrocartilage and hyaline cartilage, not to mention trauma within the marrow space as discussed in fractures.

Muscle Strain

Muscle injury can readily be identified on MRI. These strains, as muscle injuries are termed, may involve both the muscle belly and the tendon. Muscle belly trauma occurs most commonly at the musculotendinous junction where fiber attachments to the tendon tend to be weak, relatively speaking.

Three factors correlate best with the incidence of muscle injury. First, muscles that cross more than one joint, e.g., rectus femoris, sartorius, and hamstring muscles, are more prone to trauma than muscles that cross only one joint. Second, muscles that frequently undergo eccentric contraction, i.e., contraction while being forced to elongate by a resisting force, are more prone to injury than those that usually undergo concentric contraction, i.e., contraction that results in shortening of the muscle length. Third, muscles with a higher proportion of type 2 (fast twitch) fibers are injured more than chronic work horse muscles with a high proportion of type 1 (slow twitch) fibers. Combined, these three factors help to explain clinical observations that muscles in the lower extremity are more likely to be injured than upper extremity muscles.

Most muscle injuries are easily evaluated clinically. Often muscle injuries are identified on imaging in conjunction with other types of trauma, and in some circumstances the clinical situation requires imaging to evaluate the extent of injury. For example, professional athletes may require evaluation of muscle trauma to determine how long they should be excluded from competition or whether they need more aggressive therapy for their injury.

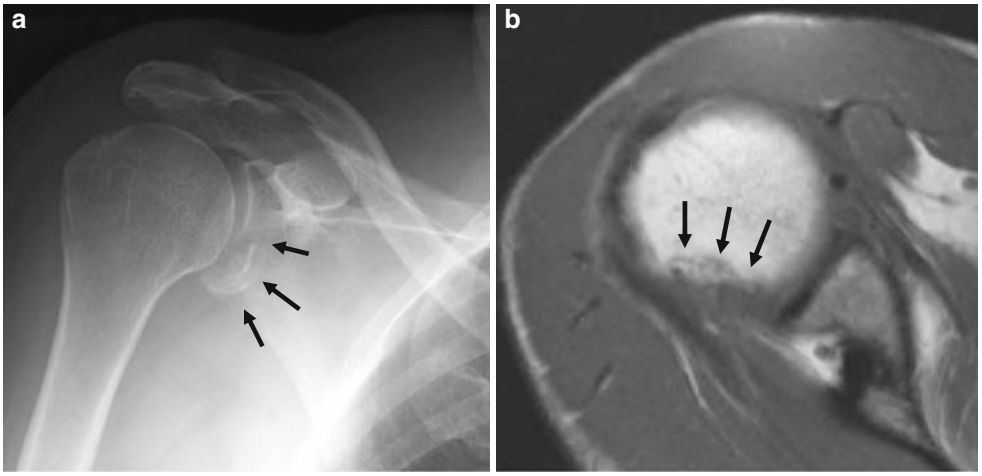

Fig. 5.63 AP radiograph of a shoulder (**a**) showing a fracture of the anterior inferior glenoid (*arrows*) that occurred during a recent dislocation. This fracture is called a Bankart fracture. Axial T1-weighted MR image (**b**) from another patient showing a defect in the posterior superior humeral head (*arrows*) consistent with a Hill–Sachs deformity. This is the corresponding impaction fracture that occurs on the superior posterior aspect of the humeral head as it impacts the glenoid

As with many musculoskeletal injuries, muscle belly injuries are classified on a three-point scale ranging from Type I showing mild hemorrhage and edema, often feathered in with the muscle fibers, related to microscopic fiber injury (Figs. 5.64 and 5.65) to Type III showing complete disruption and retraction of the muscle (Figs. 5.68 and 5.69). Type II injuries represent a midway point with partial muscle disruption (Figs. 5.66 and 5.67). Hematomas may form within and around the area of muscle tear, particularly in Type II and III strains. These will be evident on MRI by their multilayered signal intensity related to hemoglobin at different stages of degradation.

Myofascial herniation is an uncommon form of muscle injury. These hernias result from small tears in the overlying muscular fascia, resulting in bulging of the muscle fibers through the tear during active contraction. While these can also be diagnosed clinically, their presentation may be confusing and MRI may be helpful. In this event the MRI should be carried out using short-duration imaging sequences during muscle contraction and relaxation, respectively. Some authors have suggested that having the patient exercise prior to scanning also helps evoke the abnormality.

Another post-traumatic injury results from sudden overuse of a muscle or a muscle group as might be seen in

Table 5.4 Common dislocations and associated fractures

Joint	Direction	Frequency	Subtype	Associated fracture	Eponym
Shoulder	Anterior	High	Subcoracoid, subglenoid	Superior humeral head	Hill–Sachs
				Anterior inferior glenoid	Bankart
	Posterior	Low		Anterior humeral head	Trough fracture or reverse Hill–Sachs
				Posterior superior glenoid	Reverse Bankart
Inferior	Rare	Luxatio erecta			
Elbow	Posterior	Moderate		Proximal ulna	Monteggia fracture dislocation
Wrist	Posterior	Moderate	Perilunate	Scaphoid	
	Anterior	Uncommon	Lunate	Scaphoid	
Hand	Posterior	Common	MCP or IP joint	Dorsal plate chip fracture	
Hip	Posterior	Common		Posterior acetabular wall fracture	
	Anterior	Rare			
Patella	Lateral	Common		Medial patella Lateral femoral contusion	
Ankle	Lateral	Common		Bimalleolar, trimalleolar	
Subtalar	Lateral	Rare			
Tarsometatarsal	Dorsal	Common	Homolateral Divergent	Base of second metatarsal	Lisfranc fracture dislocation

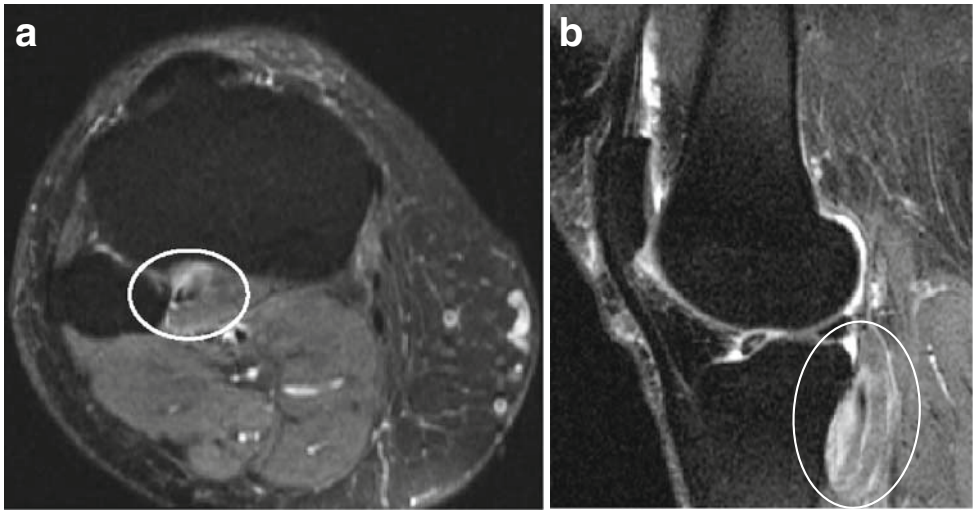

Fig. 5.64 Axial (**a**) and sagittal (**b**) T2-weighted, fat-suppressed MR images showing a mild, grade I, muscle strain of the popliteus muscle (*ovals*). Note the mild edema in the deep portion of the muscle immediately posterior to the tibia

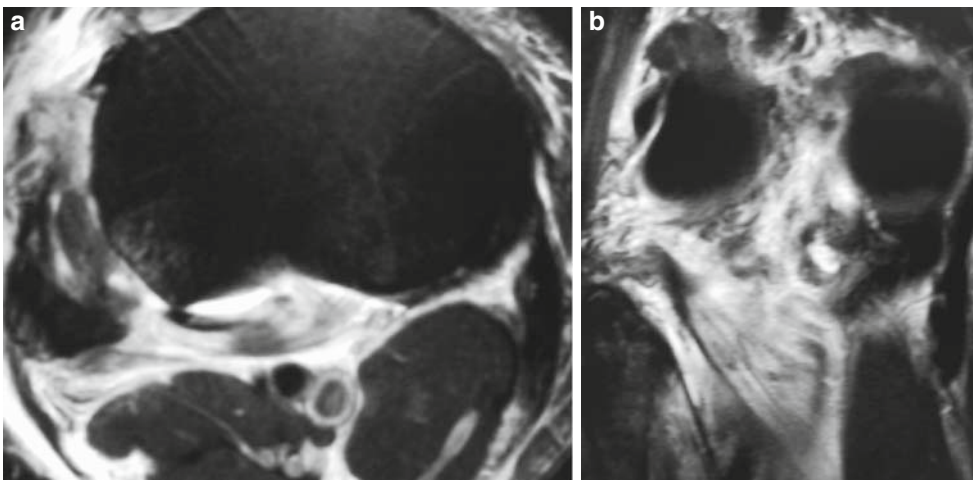

Fig. 5.65 Axial (**a**) and coronal (**b**) fat-suppressed, T2-weighted MR images from a patient with a posterolateral corner tear of the knee showing a severe Grade I strain of the popliteus muscle. The muscle and surrounding tissues show marked edema but no evidence of hematoma deep to the fascia, and the tendon is intact and inserted normal in the popliteus groove on the femur (not shown)

a patient who exercises only occasionally. Known as delayed onset of muscle soreness (DOMS), the muscle belly typically shows some diffuse edema that persists for a few days and then remits. The appearance of DOMS may mimic type I or II tears, but these entities are usually easily distinguished by clinical history.

MRI also permits evaluation of muscle for evidence of atrophy, whether from chronic disuse (Fig. 5.70) or acute denervation. In the former, the muscle will appear small and low in bulk. This may also be detected on radiographic examination in systemic diseases such as poliomyelitis (Fig. 5.71) or long-standing atrophy after a stroke. With severe long-standing atrophy, the fat will infiltrate the central portions of the muscle. Acute denervation usually shows reactive edematous changes within the substance of the muscle related to the decline and resorption of muscle proteins. This acute atrophy occurs during the acute phase of muscle wasting after spinal cord injury, with some acute neuropathies such as Parsonage–Turner syndrome (Fig. 5.72) that cause the nerve to stop functioning, and nerve entrapment syndromes, for example, anterior interosseous nerve syndrome in the volar aspect of the forearm (Fig. 5.73).

Tendon Strain and Traumatic Tendonitis

Trauma may damage tendons instead of or along with their attached muscles. Tendons are readily imaged and evaluated with MRI. Clinical evaluation is often sufficient to make the

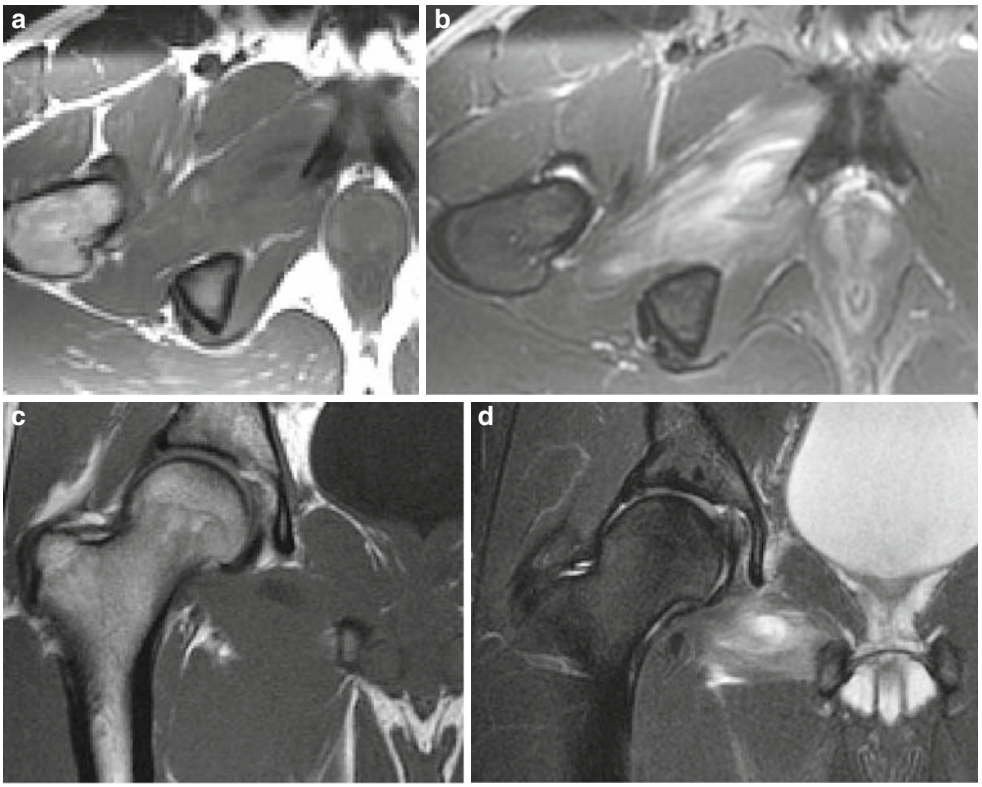

Fig. 5.66 Axial T1-weighted (**a**) and T2-weighted (**b**) and coronal T1-weighted (**c**) and T2-weighted (**d**) MR images of a mild grade II obturator externus muscle strain. Note the rounded area of high signal without traversing fibers consistent with a small hematoma within the muscle

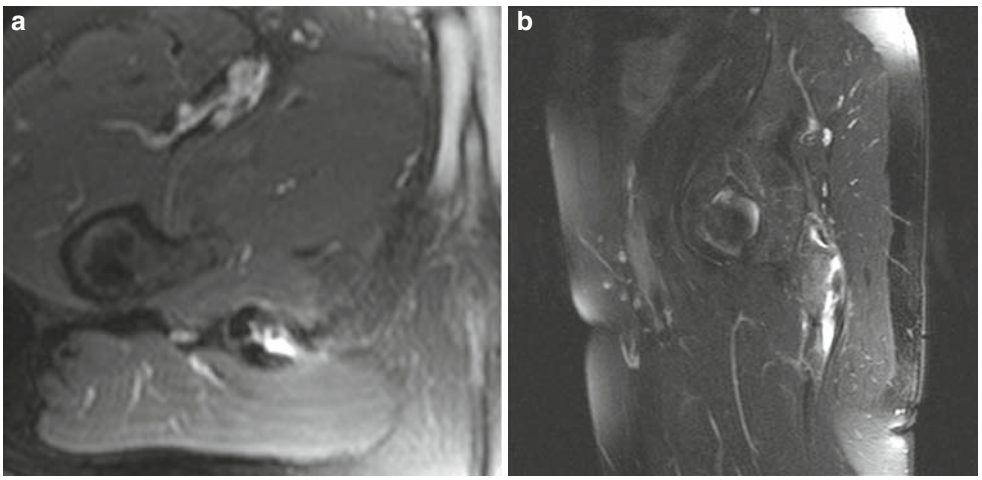

Fig. 5.67 Axial (**a**) and sagittal (**b**) fat-suppressed, T2-weighted MR images showing a severe grade II semimembranosus muscle strain. Note the tendon is nearly completely severed but the axial shows some continuity. The tendon has surrounding fluid, likely hematoma

diagnosis, but MR assessment of the completeness and size of the tear provides important prognostic information.

As with muscle tears, signal changes and morphology help to determine the severity of tendon tears. Tendons may tear acutely or show chronic changes related to overuse. In the former instance, tendon tears resemble muscle tears. With complete tears, the discontinuity of the tendon and the retraction of the attached muscle are readily imaged with MRI (Fig. 5.74). With incomplete tears, tendons show high signal within the substance of the tendon that approximates free water on T2-weighted, fat-saturated imaging but some intact fibers are present (Figs. 5.75 and 5.76). Subacute tears and mild acute trauma may cause reactive tendonitis, evidenced by some increased signal within the tendon that is lower

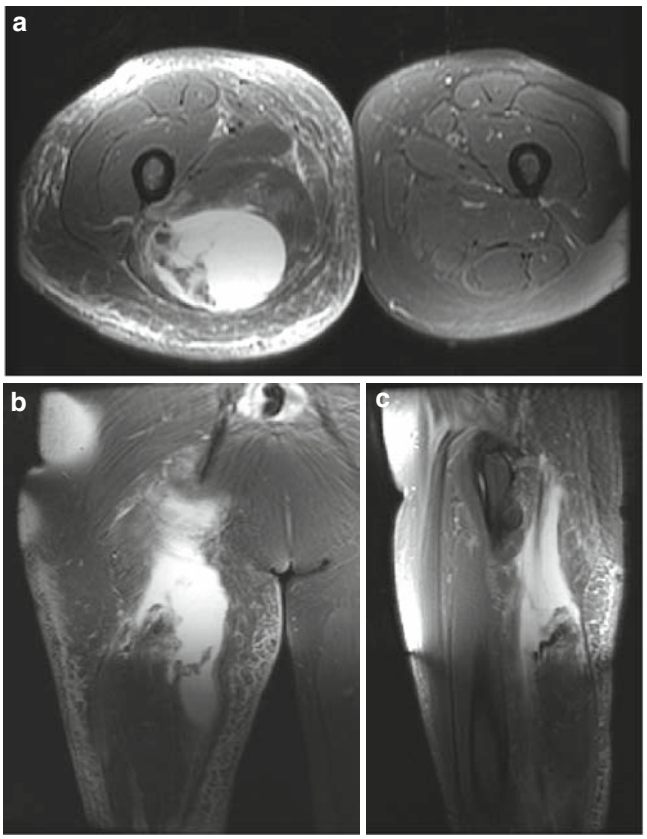

Fig. 5.68 Axial (**a**), coronal (**b**), and sagittal (**c**) T2-weighted, fat-suppressed MR images showing a grade III strain of the biceps femoris. The tendon is severed and there is marked intrafascial hematoma

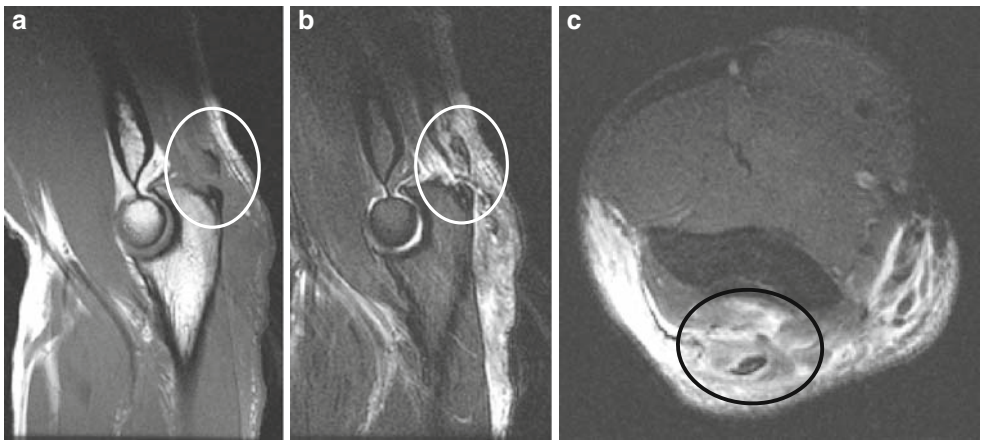

Fig. 5.69 Sagittal T1-weighted (**a**) and fat-suppressed T2-weighted sagittal B0 and axial (**c**) MR images of a grade III tear triceps tendon strain and small avulsion of the olecranon (*ovals*). The triceps tendon is severed from the olecranon right at its insertion

than that of free water on T2-weighted, fat-saturated imaging. If the tendon has a sheath in the region of the trauma, there may be an abnormal amount of fluid within the sheath as well. Caution is advised, however, since all high signal within tendons does not represent inflammation as was once thought. Instead it may represent myxoid changes related to fiber degeneration without accompanying inflammation. The term tendonopathy or tendonosis is used to describe this phenomenon.

Some muscles' tendons are more likely to tear acutely than others. In particular, tears of the insertions of the biceps brachii muscle (Fig. 5.77), the long head of the biceps femoris (Fig. 5.78), quadriceps (Fig. 5.79), and Achilles tendon (Figs. 5.74, 5.75, and 5.76) are very common. The

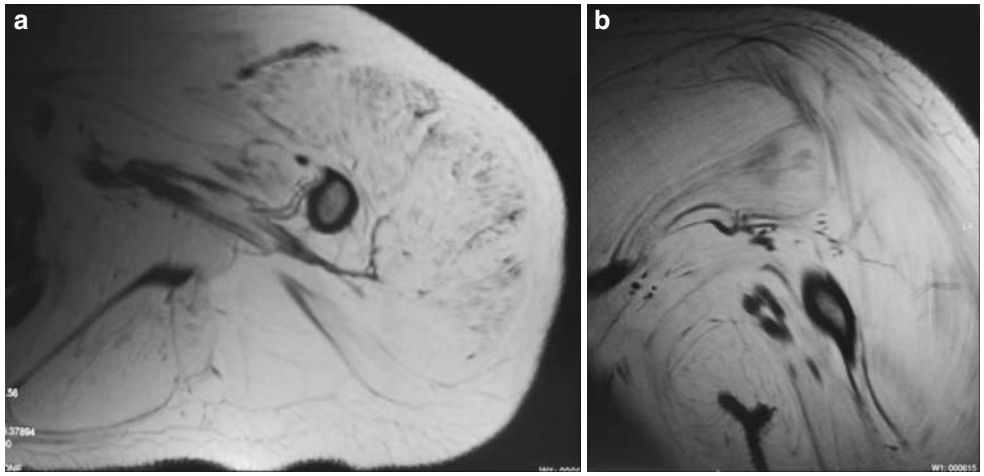

Fig. 5.70 Axial (**a**) and coronal (**b**) T1-weighted MR images showing complete fatty involution of the muscles in a patient with amyotonic muscular dystrophy

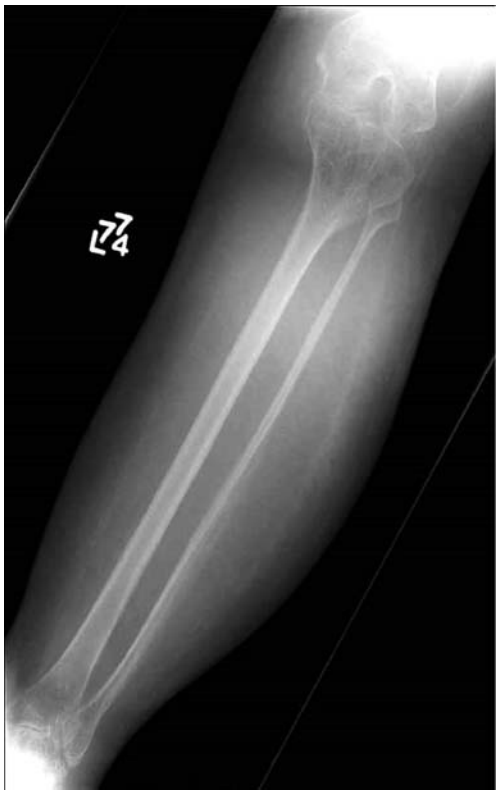

Fig. 5.71 AP calf radiograph in a patient with poliomyelitis. The muscles have atrophied and been completely replaced by fat. The bones are thin and gracile related to the absence of weight bearing

frequency with which these tendons tear relates to factors that are similar to those that predict muscle tears and to the size of the attached muscle and hence the force that it can generate on the tendon's insertion point. Acute tendon tears tend to occur in the early middle-aged patient and in patients who have overexerted themselves for their level of training. For example, the typical clinical setting in which to see an Achilles tendon tear is the weekend warrior athlete in his mid-thirties. Similarly, biceps brachii tendon tears are most common in the dominant extremity of patients in their mid-forties. Quadriceps tears are more commonly seen in older patients who have underlying tendon degeneration but also occur in younger patients who engage in jumping as in basketball players who increase their level of exertion on the court without preparing for it. Patellar tendon tears are more common in younger patients at its insertion into

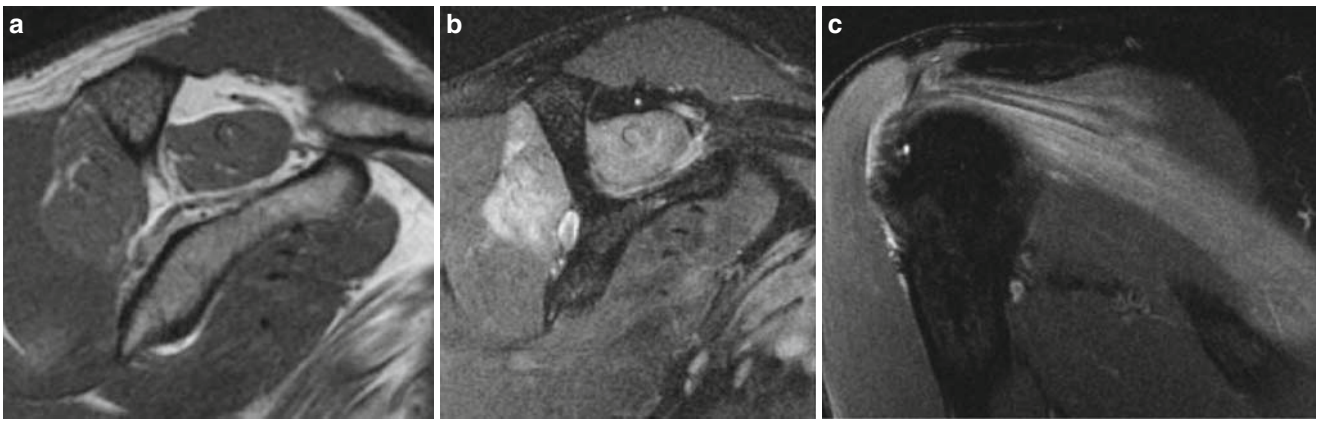

Fig. 5.72 Sagittal T1-weighted (**a**) and T2-weighted, fat-suppressed (**b**) and coronal T2-weighted, fat-suppressed MR images in a patient with post viral rotator cuff neuropathy (Parsonage–Turner syndrome) showing acute muscle atrophy. Note the edema in the supraspinatus and infraspinatus muscles on the T2-weighted images. The T1-weighted image shows minimal fat injection into the muscles

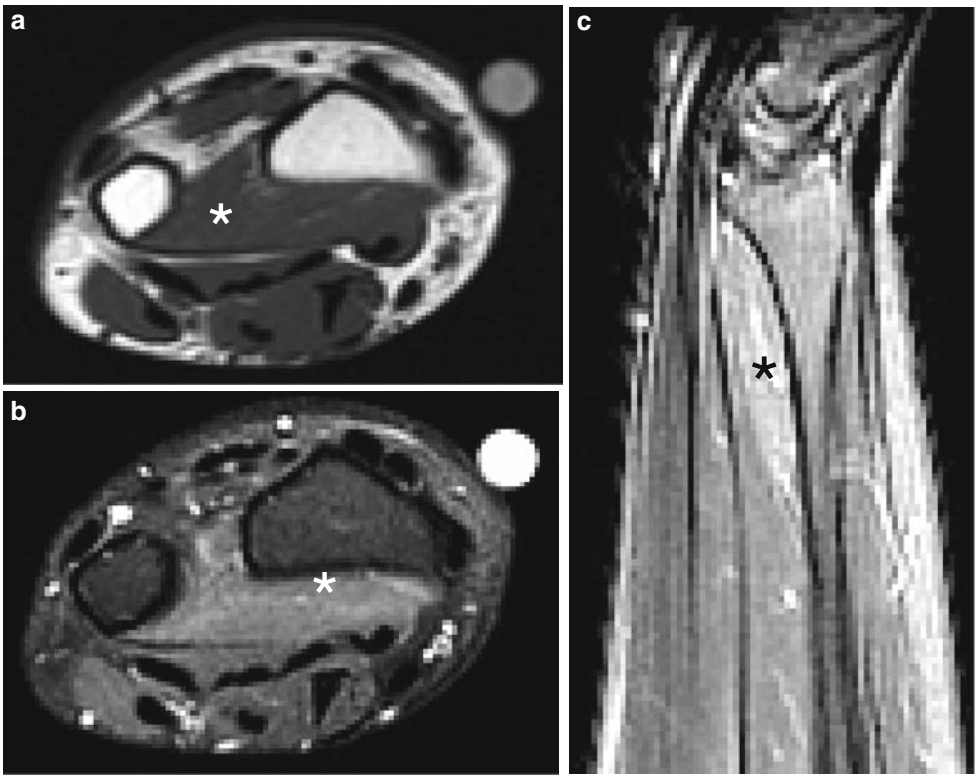

Fig. 5.73 Axial T1-weighted (**a**) and T2-weighted, fat-suppressed axial (**b**) and sagittal (**c**) MR images showing acute pronator quadratus muscle atrophy secondary to intersection syndrome from compression of the anterior interosseous nerve. Compared with the other musculature, note the increased signal in the muscle related to acute denervation

the tibial tubercle. Thus, acute tendon tears can be analogized to fatigue stress fractures of bone, occurring in tendons that are overused for their level of preparedness to the activity.

The second and more common type of tendon tear relates to chronic overuse. As a result these are more common in an older population. In many ways, these tears can be likened to insufficiency stress fractures in that normal use of the tendon in an abnormal anatomic and physiological environment will slowly lead to the formation of a tear. For example, quadriceps tears arise typically in older patients (>40 years) with systemic diseases such as diabetes and atherosclerosis that cause alterations in the small arterial supply to the distal tendon and fibrinoid necrosis within the tendon substance.

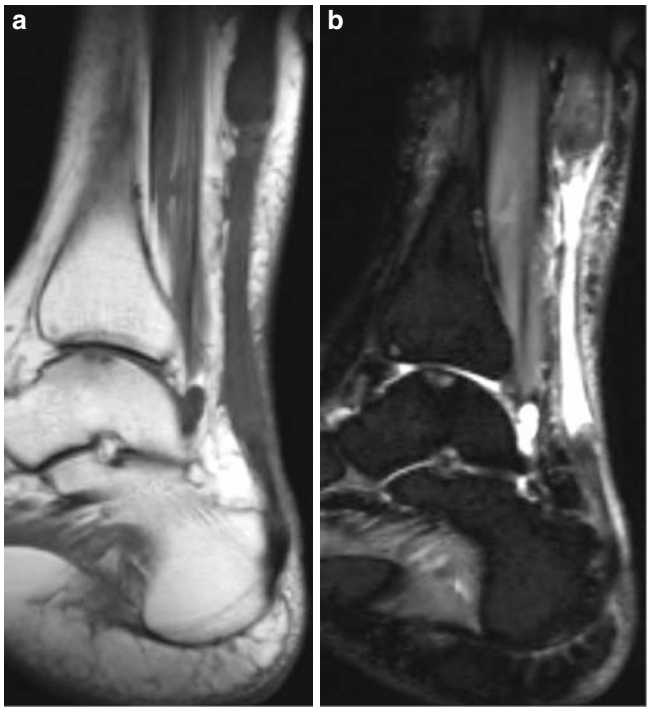

Fig. 5.74 Sagittal T1-weighted (**a**) and T2-weighted, fat-suppressed (**b**) MR images showing a complete tear of the Achilles tendon with hemorrhage and fluid in the intervening gap. No fibers are visible crossing the tear

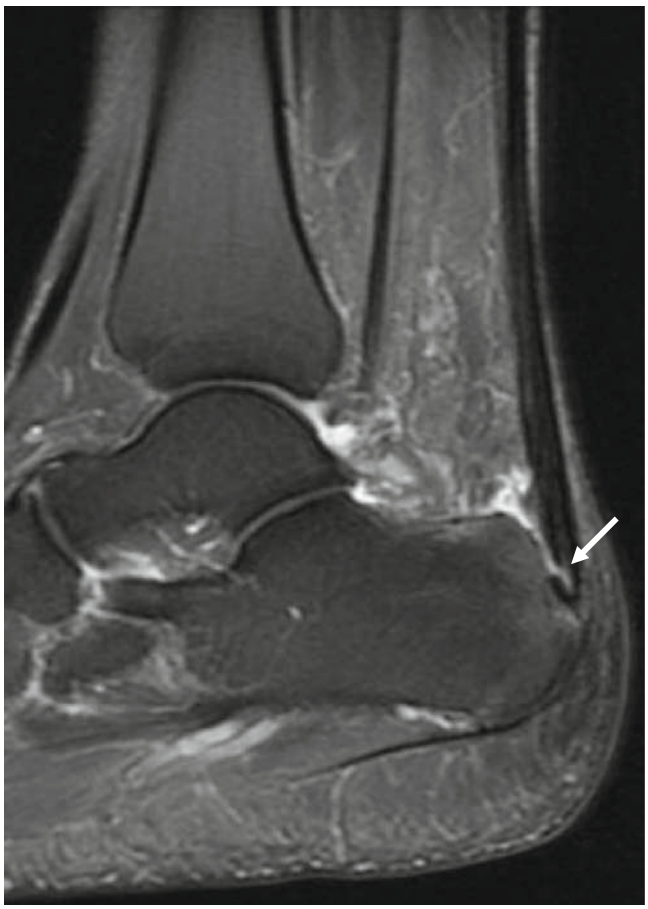

Fig. 5.75 T2-weighted, fat-suppressed sagittal MR image showing an insertional partial Achilles tendon tear (*arrow*). Note that the tear extends approximately through the anterior 75% of the tendon

These changes are often completely asymptomatic prior to tear.

The rotator cuff of the glenohumeral joint in the shoulder is the set of tendons most commonly torn in this manner. As with quadriceps tears, rotator cuff tears are most common in patients over the age of 40 years and increase in prevalence with each decade. The rotator cuff includes four muscle tendons, the subscapularis anteriorly, the supraspinatus superiorly, the infraspinatus posterosuperiorly, and the teres minor posteriorly. Tears of the supraspinatus tendon either alone or with other rotator cuff tendons account for about 90% of rotator cuff tears. Two major factors relate to the increasing prevalence of rotator cuff tears with age. The first relates to hypertrophy of ligaments and bones that form the coracoacromial and coracoclavicular arches under which the supraspinatus passes. Narrowing of these arches inhibits relaxation of the supraspinatus muscle, particularly under eccentric contraction. This impingement on the muscle means that its tendon will be stretched as the humerus adducts toward the side of the body from an abducted position. Since tendons are inelastic, stretching will result in microtears within the substance of the tendon along its entire length. As long as the body is able to repair these microtears faster than they form, no visible or clinically significant tear will occur.

On the other hand, if microtears start to form faster than they can be repaired, they will begin to coalesce and form macrotears. Microtear formation tends to outcompete healing in older patients as a result of not only the above-mentioned impingement but also a worsening blood supply to the tendon related to atherosclerotic vascular disease. This latter phenomenon is most apparent in the watershed zone of the rotator cuff tendons. This zone, known as the critical zone, occurs about 1 or 2 cm proximal to the tendon's insertion into the humerus. The critical zone represents the junctional region of a perforator blood supply to the distalmost tendon arising from the greater tuberosity of the humerus meeting the main arterial supply to the tendon that extends distally from the muscle itself. Thus, it is clear that the majority of rotator cuff tears (~90%) will occur in the critical zone of the cuff tendons. The second most frequently torn portion of the rotator cuff tendons, as might be predicted from the discussion of muscle belly tears, is the musculotendinous junction.

As with acute tendon tears, MRI depicts rotator cuff tears as areas of water intensity signal on T2-weighted,

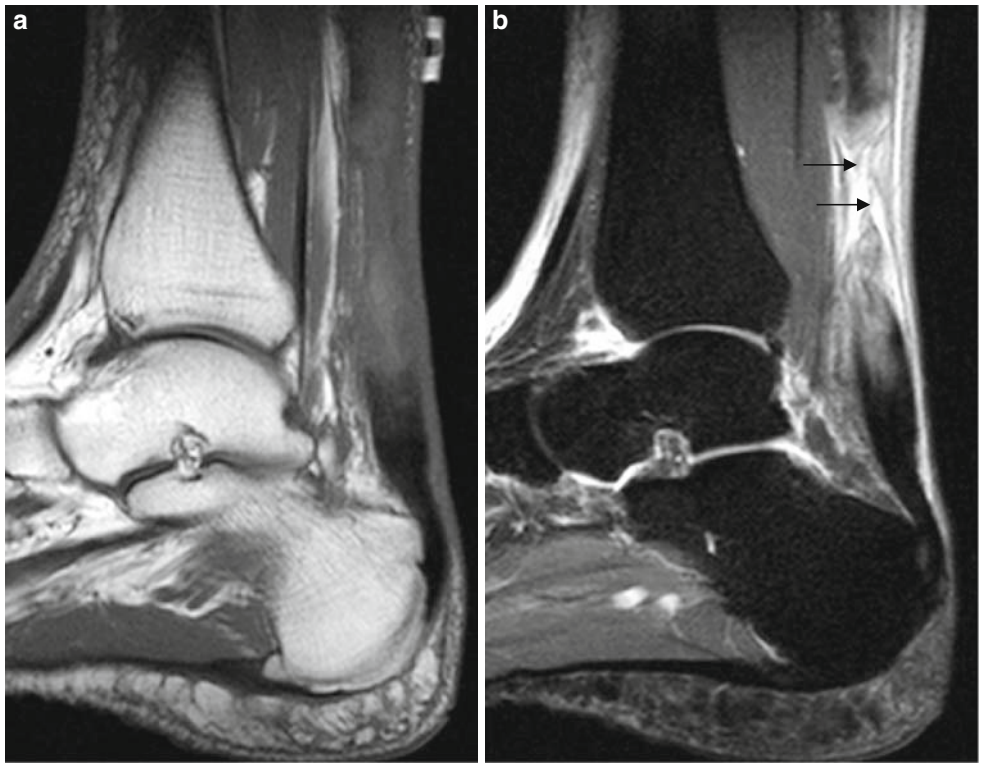

Fig. 5.76 Sagittal T1-weighted (**a**) and T2-weighted, fat-suppressed (**b**) MR images showing a near-complete tear of the Achilles tendon with hemorrhage in the intervening gap. A few fibers are visible on the T2-weighted image crossing the tear

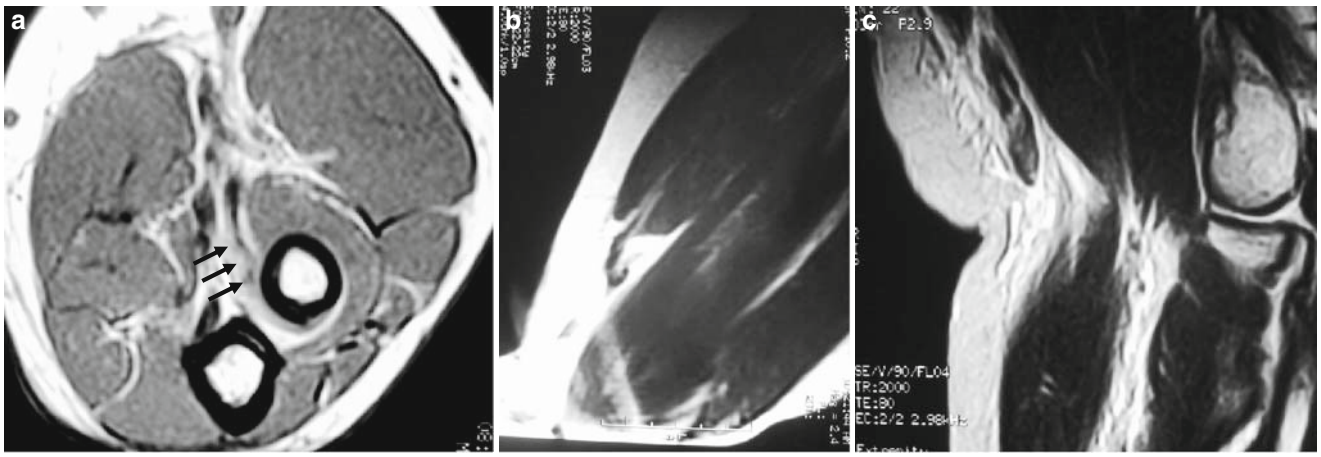

Fig. 5.77 T2-weighted axial (**a**) and sagittal (**b** and **c**) MR images show the biceps brachii tendon torn and retracted into the anterior soft tissues of the arm. The axial image (**a**) shows the residual distal tendon fragment (*arrows*) at its normal insertion point over the radial tubercle. Note the high signal within the fragment consistent with edema from the tear. The sagittal images show the torn retracted tendon

fat-saturated imaging sequences. Partial tears can occur on either the bursal or the joint surface of the rotator cuff (Fig. 5.80), with the latter being slightly more common than the former. Tears may also occur completely within the tendon's substance (Fig. 5.81) in which case they will not be visible on arthroscopy. Any of these partial tears may propagate so that the entire thickness of the tendon is torn in a full-thickness tear (Fig. 5.82). These tears may be focal or may extend across the entire anteroposterior diameter of one or more of the flat, shingle-like rotator cuff tendons (Fig. 5.83). The larger the tear, the greater the retraction of the tendon away from the attachment, making the tear more conspicuous. As a rule of thumb, rotator cuff tears tend to start in the anterior aspect of the supraspinatus critical zone and to propagate posteriorly over time. This natural progression of cuff tears is most likely related to the fact that the anterior aspect

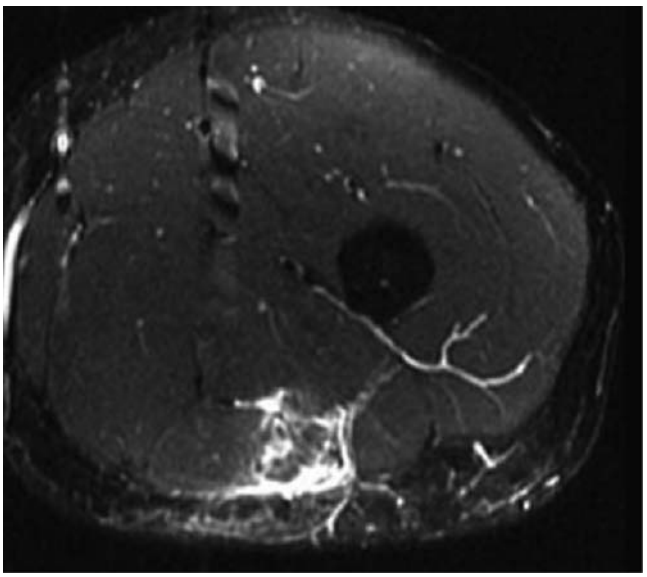

Fig. 5.78 Axial T2-weighted MR image of the distal thigh showing a grade II tear of the biceps femoris muscle and tendon. (Case courtesy of John Hunter, MD)

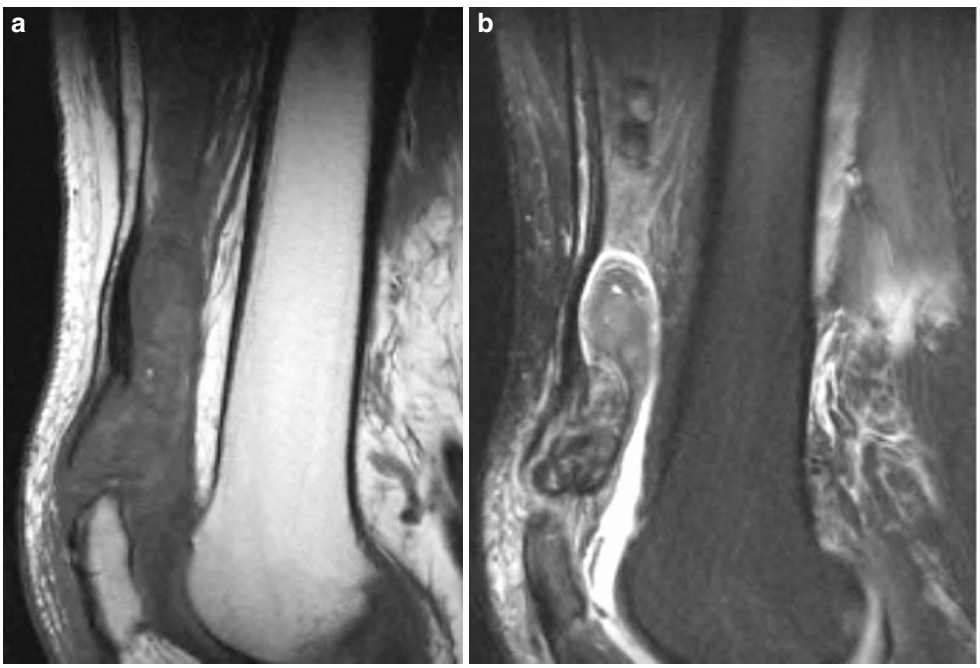

Fig. 5.79 T1-weighted (**a**) and T2-weighted, fat-suppressed (**b**) sagittal MR images show a complete tear of the quadriceps tendon superior to the patella. The frayed end of the tendon is balled up

of the supraspinatus borders the rotator interval (Fig. 5.84) where the long head of the biceps tendon passes into the glenohumeral joint to insert on the anterior superior glenoid. As a result, the anterior margin of the supraspinatus is relatively unprotected.

Not all high signal within the rotator cuff tendon represent tear. Experience has shown that signal that is lower than that of free water denotes tendinopathy (Fig. 5.85). As mentioned above, this signal relates to degeneration of portions of the substance of the tendon, possibly related to myxoid changes or to granulation tissue from the competition between microtear formation and healing. Thus, care must be taken in diagnosing rotator cuff tears. In fact, this same rule applies to all tendons.

Of course, not only the rotator cuff is subject to tearing and traumatic tenosynovitis, but also the tendons about

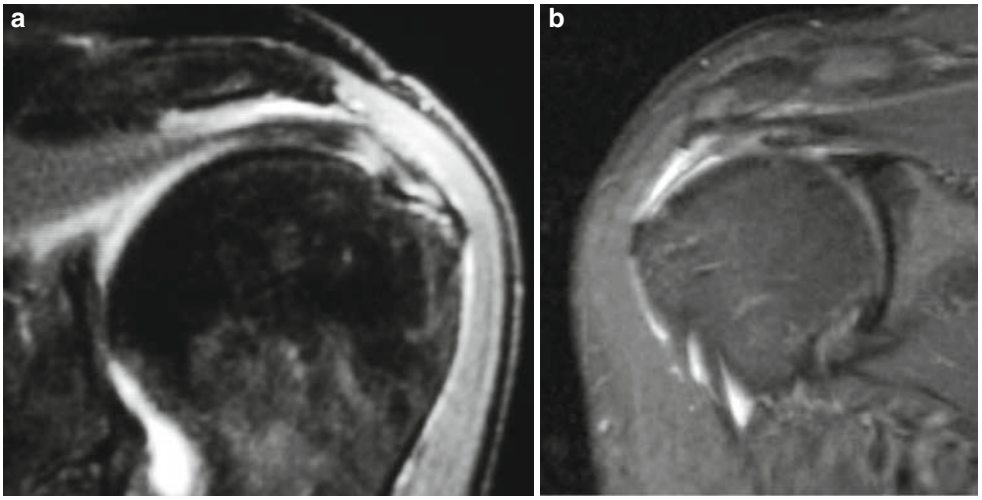

Fig. 5.80 T2-weighted, fat-suppressed images of the left shoulder in one patient (**a**) and the right shoulder in another patient (**b**) showing partial supraspinatus rotator cuff tears. In (**a**) the tear is small and visible along the undersurface of the tendon in the critical zone near its insertion onto the greater tuberosity. Note that to be called a tear, the signal in the tendon must be as bright as water on this sequence. Lower intensity signal corresponds to tendinopathy. In (**b**) the tear is near full thickness and markedly thins the distal supraspinatus tendon

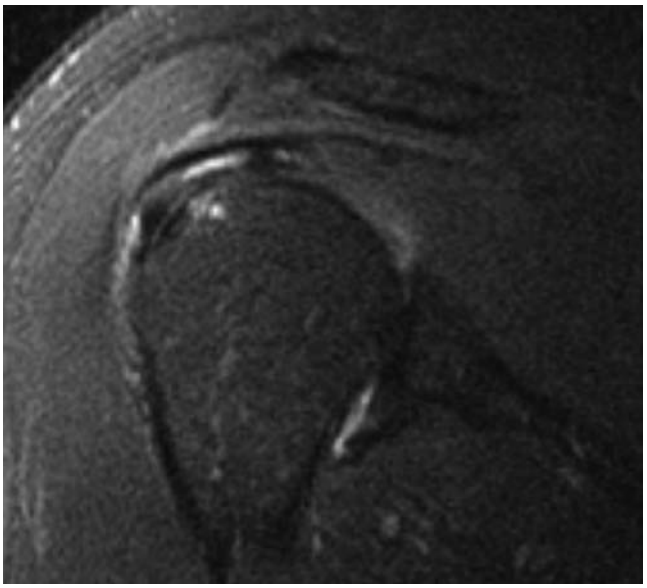

Fig. 5.81 T2-weighted, fat-suppressed coronal MR image showing an infraspinatus intrasubstance tear. As with the partial tears in Fig. 5.80, the tear shows signal as bright as water on the image

the elbow, including the common carpal extensor wad origin (tennis elbow), the common carpal flexor wad origin (golfer elbow), are often injured during sports (Fig. 5.86). Similarly the tendons around the ankle, medially – the posterior tibial, flexor hallucis longus and flexor digitorum longus tendons (Fig. 5.87) – and laterally – the peroneus longus and brevis tendons (Fig. 5.88) – are frequently subject to traumatic tenosynovitis. The anterior ankle tendons are less frequently involved. Tendons at other joints are also subject to traumatic tenosynovitis, but less frequently than the elbow and the ankle. Not only will these tendons show varying degrees of high signal on T2-weighted, fat-suppressed

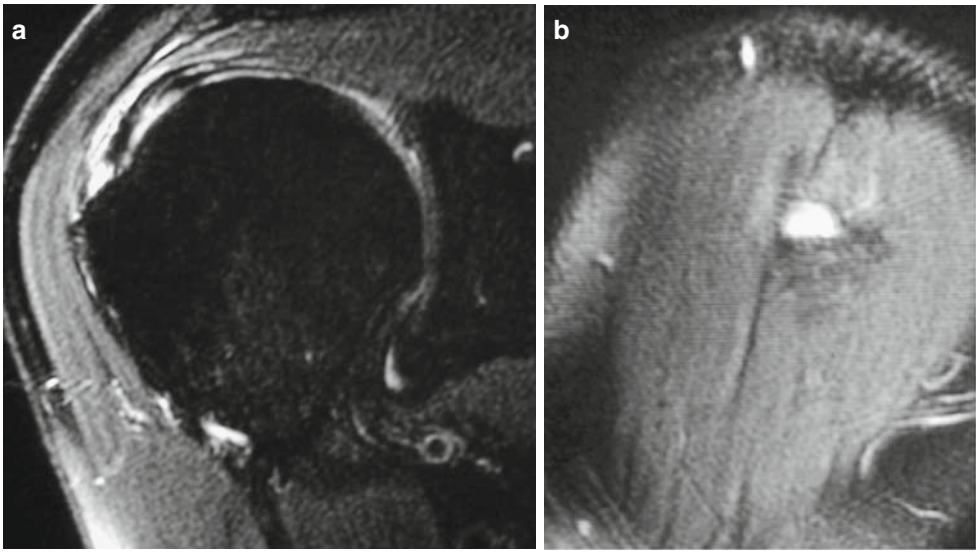

Fig. 5.82 T2-weighted, fat-suppressed coronal (**a**) and sagittal (**b**) MR images of a shoulder show a focal full-thickness tear of the supraspinatus tendon. On the coronal image the tear appears as a discontinuity of the tendon, while on the sagittal image the tear appears as a round fluid-filled (*bright signal*) hole in the tendon

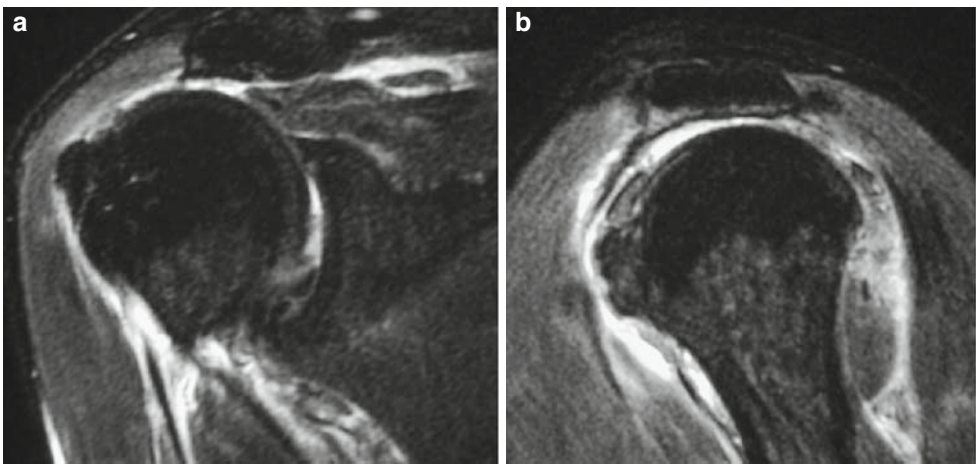

Fig. 5.83 T2-weighted, fat-suppressed coronal (**a**) and sagittal (**b**) MR images of a shoulder show a large full-thickness tear of the supraspinatus tendon. The supraspinatus tendon is retracted and on the sagittal is absent along its entire anteroposterior extent. Note the superior subluxation of the humeral head as it moves to fill in the space once occupied by the supraspinatus tendon

imaging, but also there may be edema in the adjacent tissues. Furthermore, the tendons at the ankle and the wrist have tendon sheaths to facilitate their movement over curved or angled body parts. These sheaths may also become inflamed with post-traumatic tenosynoritis and develop effusions similar to joint effusions (Figs. 5.88 and 5.89). If the inflammation within the sheaths persists long enough, the sheath may become irregular and thickened showing nodules and/or ectatic outpouching (Fig. 5.90). Eventually, the sheath may scar down around the tendon and give rise to stenosing tenosynovitis.

Ligament Sprain

As MRI resolution has improved, the ability to diagnose ligamentous disruption (sprain) has improved significantly and MR is now the imaging test of choice for diagnosis of ligament injuries. In some cases, MR shows the ligaments well without the use of intraarticular contrast augmentation, e.g., in around and within the knee and the ankle (Fig. 5.91). In others, although ligament visualization may be possible without intraarticular contrast, the use of contrast increases diag-

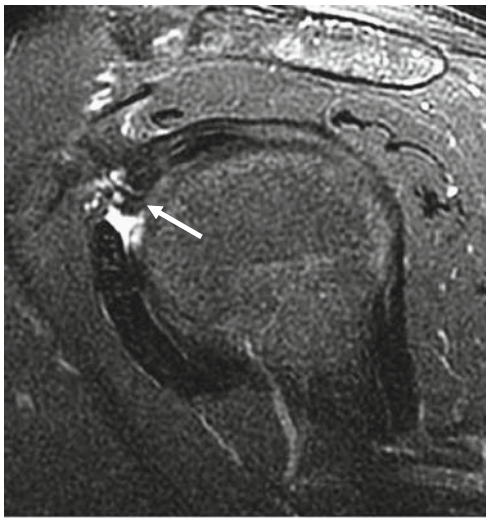

Fig. 5.84 T2-weighted sagittal image of the shoulder showing the long head of the biceps tendon in the rotator interval (*arrow*) between the subscapularis anteriorly and the supraspinatus superiorly. The roof of the rotator interval is formed by the coracohumeral ligament, a relatively thin and weak structure

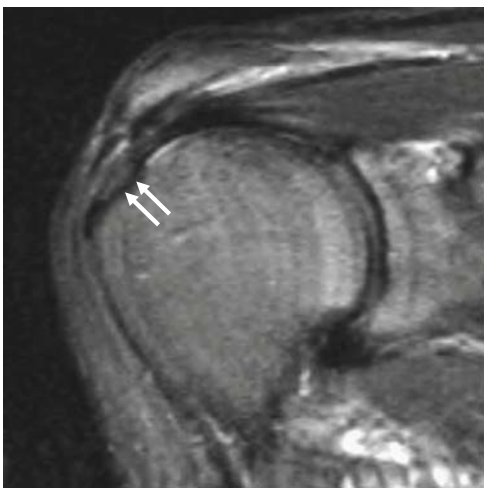

Fig. 5.85 T2-weighted, fat-suppressed coronal MR image showing signal in the supraspinatus tendon (*arrows*) that is lower than pure water but higher than normal tendon signal. Note the small undersurface partial tear at the insertion of the tendon into the greater tuberosity of the humerus and its higher signal comparable with the effusion in the joint space

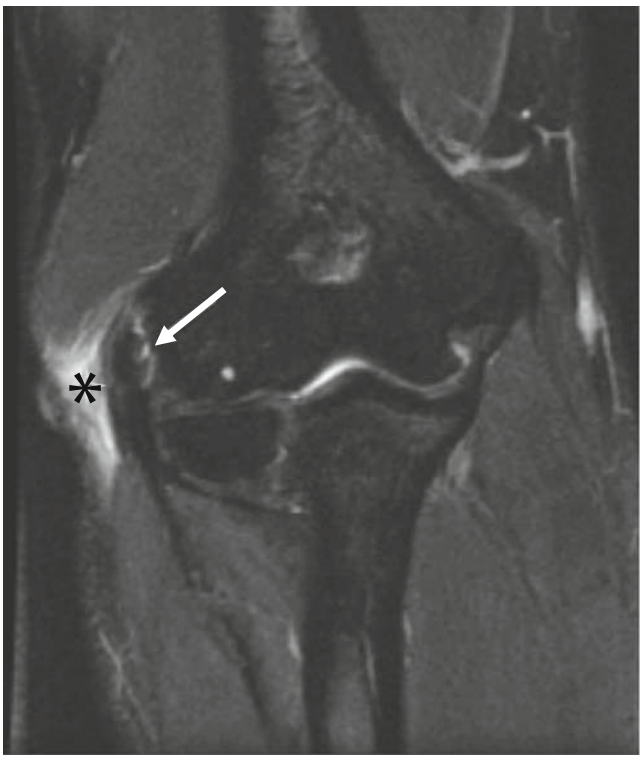

Fig. 5.86 T2-weighted, fat-suppressed coronal MR image showing a partial tear of the common extensor wad at its insertion with the lateral epicondyle (*arrow*) and surrounding edema in the soft tissues (*star*). These findings are consistent with tennis elbow

nostic confidence and accuracy. With gadolinium contrast in the joint (MR arthrography), MR shows the ligaments of the hip, the shoulder, the elbow, and the intrinsic ligaments of the wrist to diagnostic advantage (Fig. 5.92).

While many ligaments are very thin and tend to tear completely, others, e.g., the medical collateral and posterior cruciate ligaments of the knee, are thick enough and have enough component layers that they may show partial tears. If the ligament is torn completely, it will either be absent from view or show frank discontinuity with an abnormal course and bright surrounding T2 signal on MR corresponding to edema and inflammation (Fig. 5.93). On the other hand, partial tears will reveal fibers of the native ligament coursing through the area of edema and inflammation (Figs. 5.94 and 5.95).

As with fractures, certain types of ligamentous injury are more common than others. Again, this relates to a number of factors, including the strength of the ligaments around the joint, the position of the joint at the time of the trauma, and the joint's normal range of motion. Thus, anterior cruciate ligament (ACL) tears (Fig. 5.96) far outnumber posterior cruciate ligament (PCL) tears (Fig. 5.97) in the knee. In some cases, the location of the ligament tear is also typical. For example, ACL tears occur most often at the insertion points of the ligament, particularly at its femoral attachment, while PCL tears tend to occur in the mid body of the ligament.

Lateral ligament sprains account for 85% of ankle ligament sprains and of those the ligament most prone to tear is the anterior tibiofibular ligament (ATFL) (Figs. 5.87 and 5.88). Not only is this ligament the weakest of the three

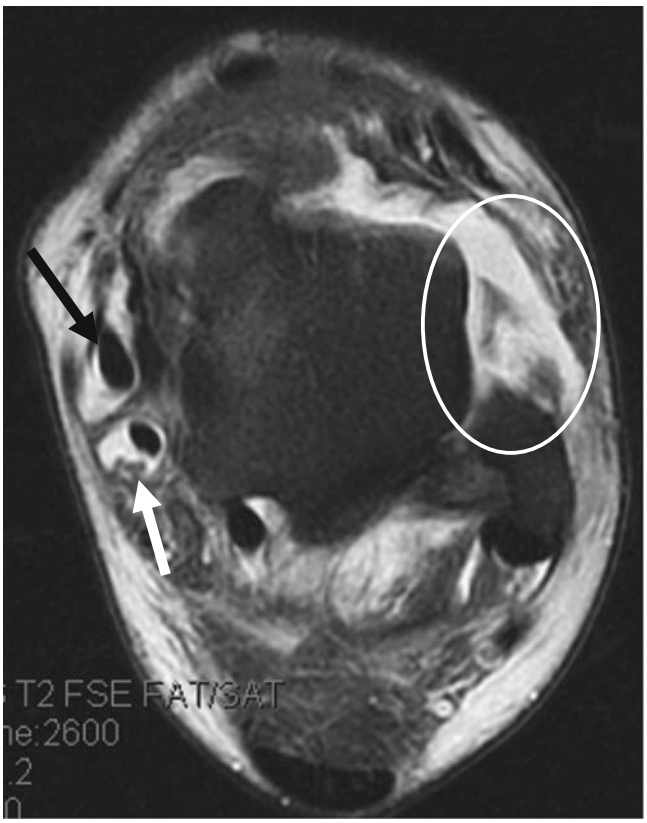

Fig. 5.87 Axial T2-weighted, fat-suppressed MR image showing the absence of the anterior tibiofibular ligament (ATFL) (*oval*), a joint effusion and posterior tibial (*black arrow*), and the flexor digitorum longus tendon (*white arrow*) tenosynovitis

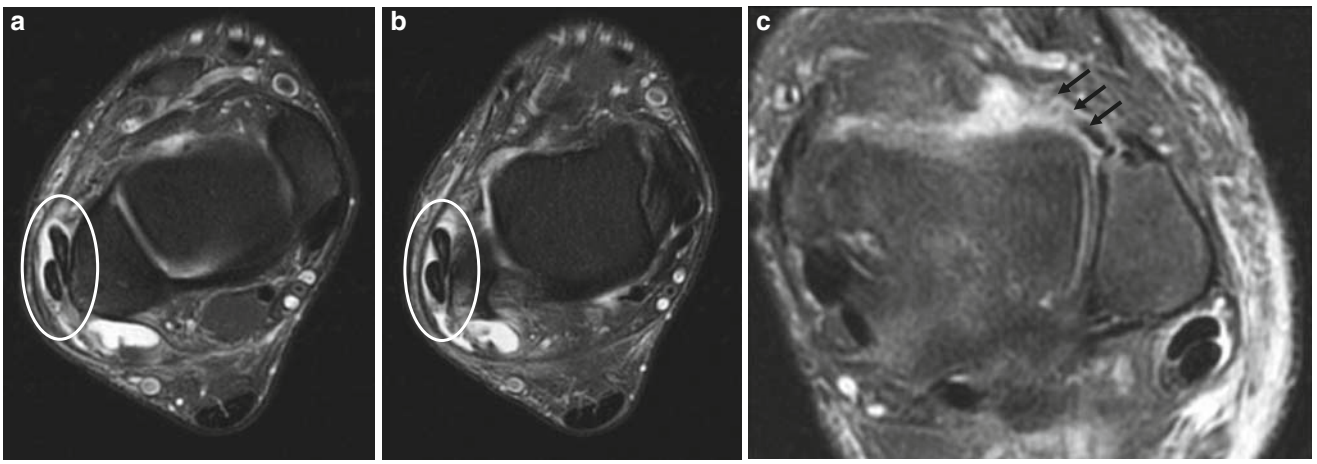

Fig. 5.88 Axial T2-weighted, fat-suppressed MR images (**a**) and (**b**) showing severe peroneal tenosynovitis. Both the peroneus longus and the brevis tendons are dislocated anteriorly and have increased signal and marked abnormal fluid in the surrounding tendon sheath (*ovals*). T2-weighted, fat-suppressed axial MR image (**c**) from another patient showing fluid within the common peroneal tendon sheath indicating tenosynovitis. The ATFL is also torn (*arrows*). The overlying superficial edema is related to recent trauma, possibly the cause of the tenosynovitis and the ligament tear (*ankle sprain*)

major lateral ankle ligaments, but it is also the most prone to stretching by ankle movement. Indeed, if other lateral ankle ligaments are torn, it goes without saying that the ATFL is also torn.

Hyperextension trauma to the elbow, common in baseball pitchers, causes injury to the medial collateral ligament, specifically the anterior band, most often in its midsubstance but also at its insertion onto the coronoid process and at its

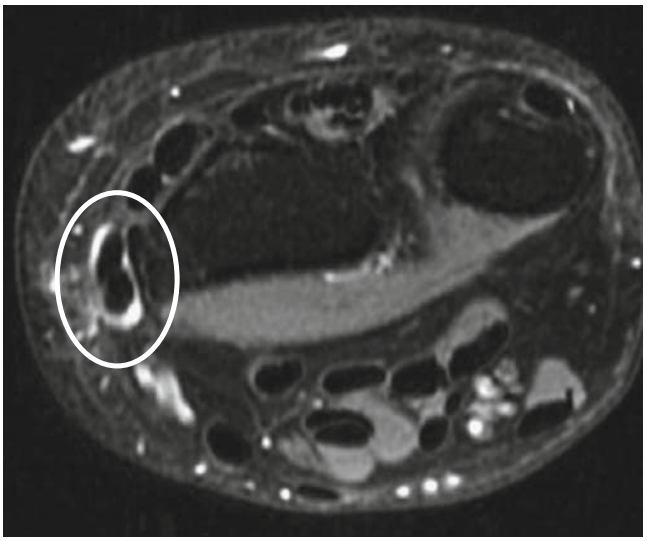

Fig. 5.89 T2-weighted, fat-suppressed axial MR image showing fluid within the first carpal extensor compartment tendon sheath and mild increased signal within the abductor pollicis longus and extensor pollicis brevis tendons (*oval*) consistent with tenosynovitis. These findings are consistent with DeQuervain tenosynovitis

origin from the humerus. While full-thickness tears of this ligament, particularly proximal ones, are identifiable on plain MRI (Fig. 5.93), diagnosis of partial tears, typically at its distal insertion, may require MR arthrography (Fig. 5.98). Lateral collateral ligament injuries of the elbow, on the other hand, are uncommon.

Currently, MR is able to depict the intrinsic ligaments of the wrist, including the scapholunate and lunotriquetral ligaments (Fig. 5.99). It also depicts the triangular fibrocartilage complex (Fig. 5.100). Although debated, these structures and their tears may be better seen with MR arthrography. In particular, small pinhole tears through the membranous portions of the intrinsic ligaments require arthrography. Identification and evaluation of the extrinsic ligaments of the wrist, even on routine 3T MR images, remains problematic.

Hyaline Cartilage

Clinical evaluation of hyaline cartilage is best done with MRI. Today, two sequences are promoted as cartilage

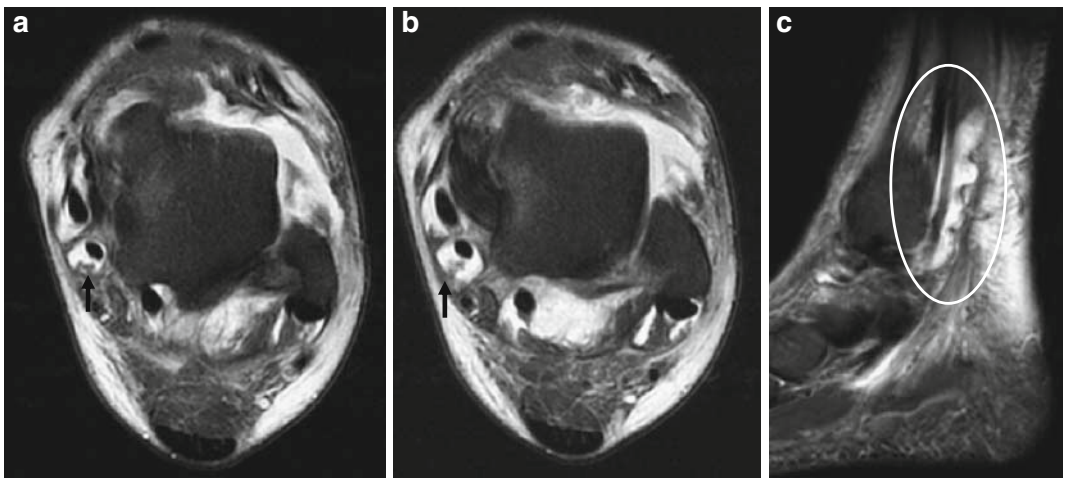

Fig. 5.90 Axial (**a** and **b**) and sagittal (**c**) T2-weighted, fat-suppressed MR images of an ankle showing nodular tenosynovitis. All of the posterior medial and lateral tendon sheaths, including the posterior tibial tendon, the flexor digitorum longus, the flexor hallucis longus, and the peroneal tendon sheaths have abnormal amounts of fluid. In addition, note the abnormal soft tissue along the sheath of the flexor digitorum longus sheath consistent with nodular changes (*arrows*) (**a** and **b**) and the ectasia of the tendon sheath (*oval*) (**c**)

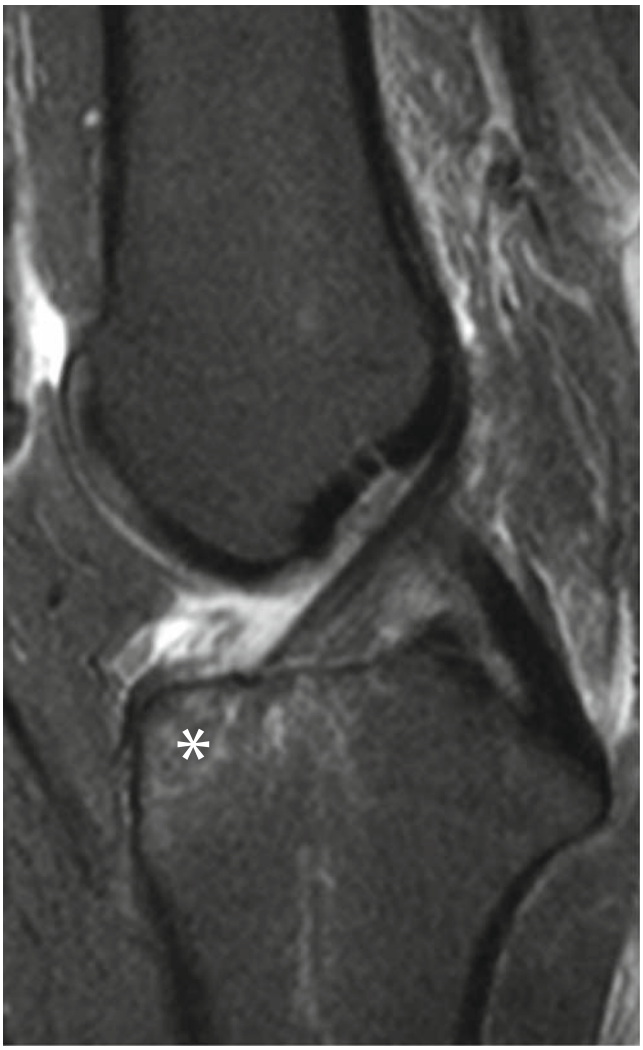

Fig. 5.91 Sagittal T2-weighted, fat-suppressed image of a knee showing a normal and intact anterior cruciate ligament (ACL) and portions of the posterior cruciate ligament (PCL). Edema, representing a mild contusion, is present in the proximal tibia (∗)

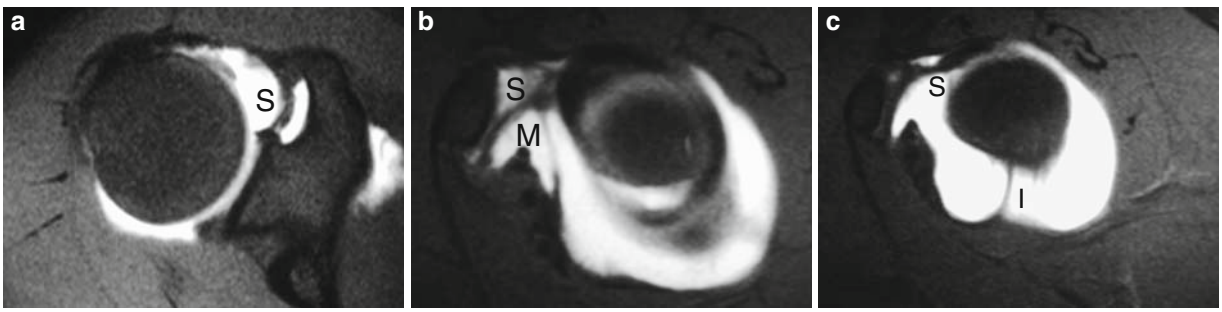

Fig. 5.92 Axial (**a**) and sagittal (**b**) and (**c**) T1-weighted, fat-suppressed MR images from a gadolinium arthrogram of the shoulder showing normal superior (S), middle (M), and the anterior band of the inferior (I) glenohumeral ligaments. These structures are poorly visualized without an arthrogram

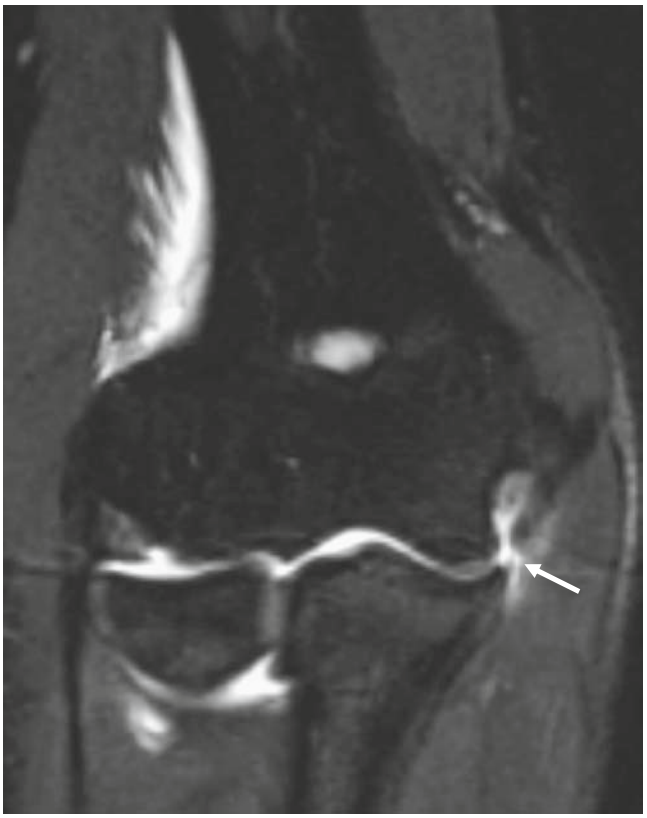

Fig. 5.93 MR arthrogram showing a complete tear of the insertion of the ulnar collateral ligament of the elbow at its insertion onto the coronoid process (*arrow*)

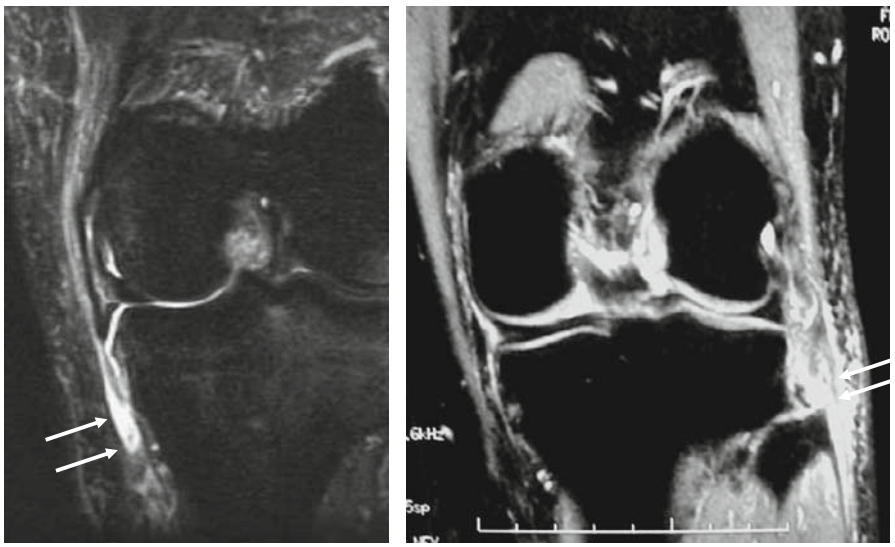

Fig. 5.94 Coronal T2-weighted, fat-suppressed MR images from two separate patients showing complete tears of the inferior insertion of the medial collateral ligament (*arrows*) (**a**) and the fibular insertion of the lateral collateral ligament (*arrows*) (**b**) of the knee

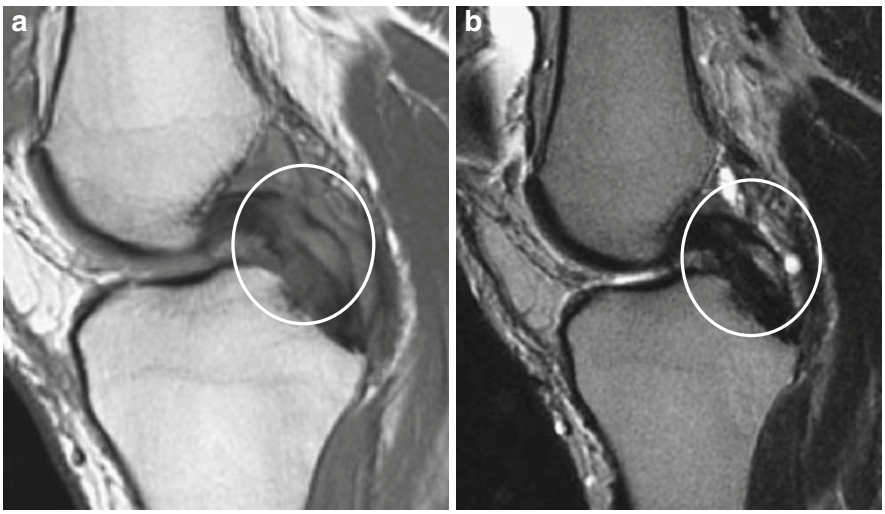

Fig. 5.95 Sagittal proton density (**a**) and fat-suppressed, T2-weighted (**b**) MR images showing a partial tear of the posterior cruciate ligament of the knee (*ovals*)

sensitive, a T2-weighted, fat-suppressed fast spin-echo sequence and a 3D spoiled gradient-echo (SPGR) short TE sequence. Both sequences show the hyaline cartilage as separate signal intensity from that of either fluid or bone and are used in routine imaging. The 3D SPGR sequence shows the hyaline cartilage as very bright compared with all other tissues that appear dark (Fig. 5.101). As a result, its only real utility is looking for defects and thinning in the hyaline cartilage. The FSE T2W sequence, on the other hand, shows hyaline cartilage as moderately bright, but less than fluid (Fig. 5.102). This sequence shows not only hyaline cartilage pathology but also pathology in the marrow space and the soft tissues with high sensitivity. As such, it has proven to be practical as a routine clinical sequence.

Imaging with either of these sequences permits reasonable evaluation of the hyaline cartilage associated with joints. They are sensitive to areas of chondrosis or cartilage softening, shown as moderate increased signal within the cartilage itself on the T2-weighted, fast spin-echo, fat-saturated sequence (Fig. 5.103). The sequences can also show focal or diffuse cartilage thinning (Fig. 5.104). Thus, MR has become a tool for evaluation of early osteoarthritis in patients who may be candidates for cartilage replacement therapy.

Fibrocartilage

Most joints contain some fibrocartilage structures. In some joints, e.g., the hip and the shoulder, the fibrocartilage takes the form of labra, cartilage that rings one side of the joint and deepens the articular fossa. In others, e.g., the knee, the labrum is detached and turned inward creating a meniscus. Menisci, though usually less well developed, can be seen in other joints including the small joints of the hands, feet, the wrist, the temporomandibular joint, and the elbow and may even cause pathology (Fig. 5.105). The wrist also has a fibrocartilage structure that spans the distance between the medial aspect of the distal radius and the ulnar styloid. This cartilage along with its adjacent small meniscus forms the triangular fibrocartilage complex (Fig. 5.106 and 5.100).

All of these structures are subject to tearing and degeneration. MR plays an important prearthroscopic role in determining the degree and type of pathology in these fibrocartilage structures.

Knee

The menisci of the knee tear frequently either secondary to trauma or degeneration with age. These "C"-shaped cartilages (Fig. 5.107), one on either side of the knee joint, provide hoop stress reduction, thereby allowing the knee to withstand high compressive force. Essentially, the menisci act as shock absorbers converting vertical forces across the joint into transverse ones. They can do this by virtue of their shape, being triangular in cross section (Fig. 5.108). When torn, their function is reduced and thus increased force crosses the joint. This, in turn, may lead to the development of secondary osteoarthritis. As a result, meniscal tears are not trivial and require medical attention. In the United States, the medial meniscus and in particular its posterior horn is most commonly torn. In fact, the posterior horn of the medial meniscus is involved in nearly 85% of meniscal tears of the knee.

The peripheral one-third of the meniscus has a blood supply and is innervated, but the central two-thirds has neither. The peripheral portion of the meniscus, referred to as the red

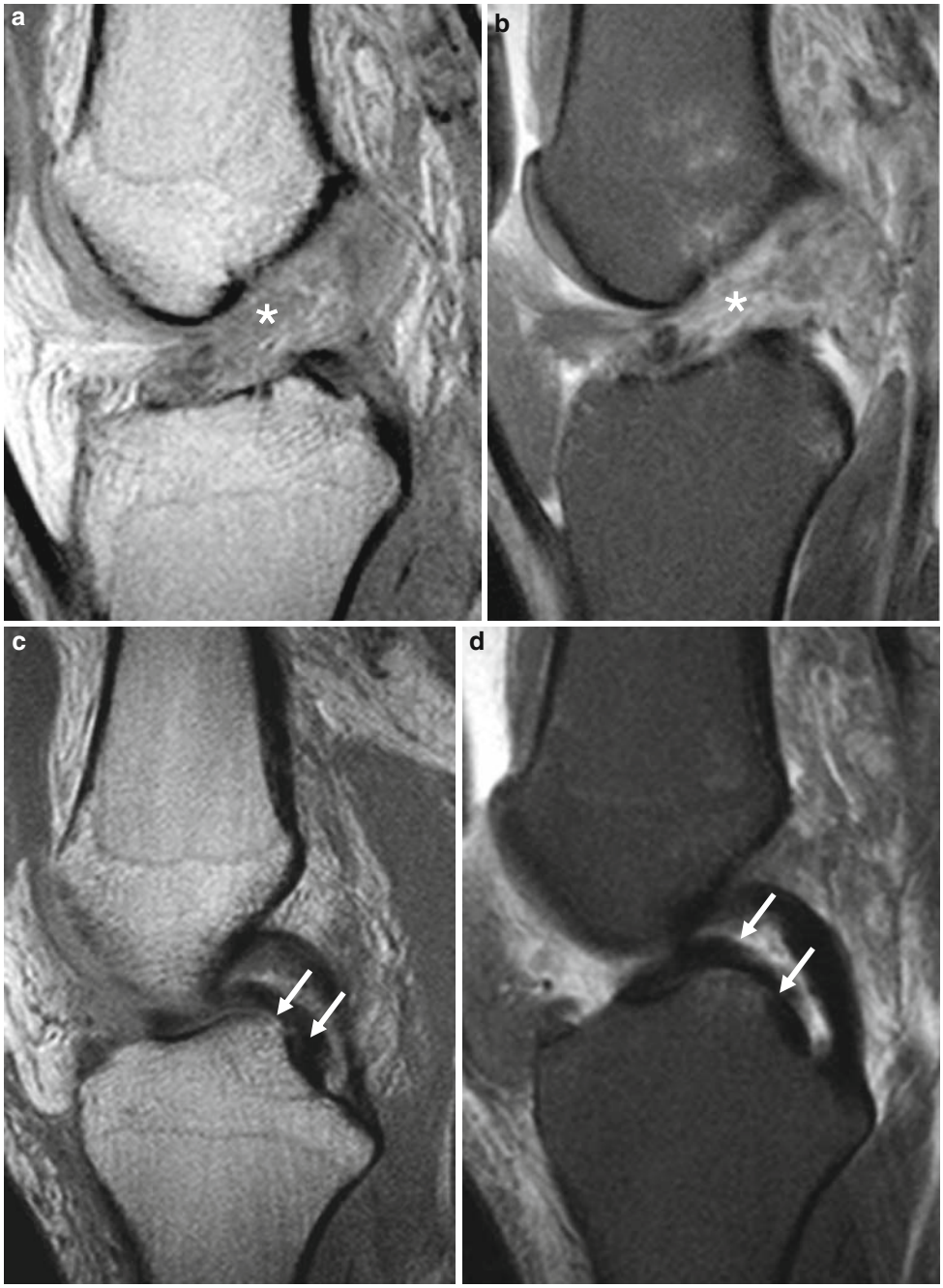

Fig. 5.96 Corresponding sagittal proton density (**a**) and (**b**) and T2-weighted, fat-suppressed (**c**) and (**d**) images of a knee showing a completely torn ACL (∗) and a double PCL sign from the ACL laying on the tibia (*arrows*)

zone because of its vascular supply, may form granulation tissue within a tear and so, in some cases, repair itself. On the other hand, the central portion or the white zone of the meniscus has no blood supply and as a result cannot repair itself.

Meniscal tears may be visualized on T1-weighted, proton density and T2-weighted, fat-suppressed sequences. To date, the proton density sequence has shown the highest accuracy for tear identification, but all sequences should be used lest a subtle tear is missed. Because fibrocartilage is dark on all sequences, meniscal tears will appear as areas of relatively bright signal on any of these sequences (Fig. 5.109). Signal, however, is not the only criterion for diagnosing a meniscal tear. Changes in morphology, e.g., blunting or distortion of the normal triangular morphology of the meniscus, is equally important as a criterion for recognition of meniscal tears.

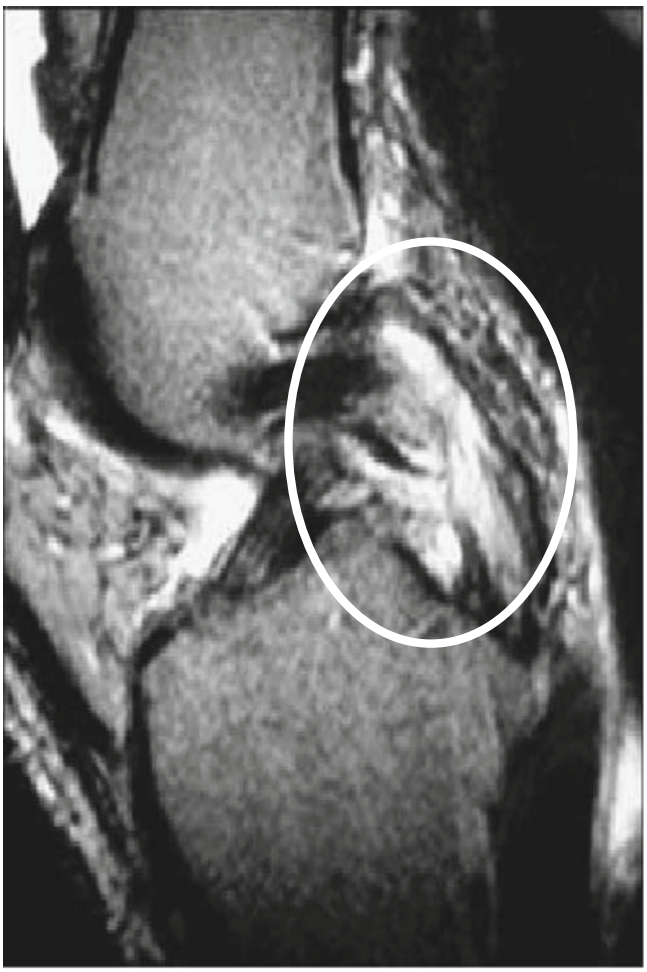

Fig. 5.97 Sagittal T2-weighted, fat-suppressed MR image of a knee showing complete disruption of the PCL (*oval*)

Overall, MRI has an accuracy for meniscal tears that surpasses 95%.

As might be predicted, menisci can tear in any of three basic directions: vertically and longitudinally along their curvature (Fig. 5.110), vertically and radially along across the curvature (Fig. 5.111), and horizontally from the apex of the free edge of the meniscus toward its base (Fig. 5.112). Furthermore, each of these types of tears can propagate into more complex variants. For example, the vertical longitudinal tear may extend along the majority of the circumference of the meniscus, giving rise to a centrally free fragment tethered at either end (Fig. 5.113 and 5.114). This configuration is known as a bucket handle tear and is most common on the medial side of the knee joint. If the longitudinal tear is large enough, not only may it extend into a bucket handle but it may twist on itself, giving rise to a flipped bucket hand with its characteristic MR appearance (Fig. 5.115). Radial and horizontal tears can also propagate into distinct complex configurations. The radial tear may turn to extend longitudinally parallel to the circumference of the meniscus and so gives rise to a partially attached fragment that resembles a parrot's beak (Fig. 5.116). A horizontal tear may fold superiorly or inferiorly on itself creating a flap type of meniscal tear (Fig. 5.117).

Another indicator of a meniscal tear is a meniscal cyst. These may occur either within the meniscus (Fig. 5.118) or in the tissues around the meniscus (Fig. 5.119). Either way the major significance of a meniscal cyst is that it indicates the presence of a meniscal tear, whether directly visualized or not. Earlier literature suggested that meniscal cysts are most common in the region of the body of the lateral meniscus, but current experience suggests that these are equally likely to arise in any portion of the menisci, lateral or medial.

The current standard of therapy for meniscal tears depends on multiple factors. In general, however, vertical tears are treated with meniscectomy. Horizontal tears, on the other hand, tend to be degenerative in etiology and often are associated with osteoarthritis in the knee in the same compartment as the meniscal tear. As a result, these tears may not be candidates for resection. Several

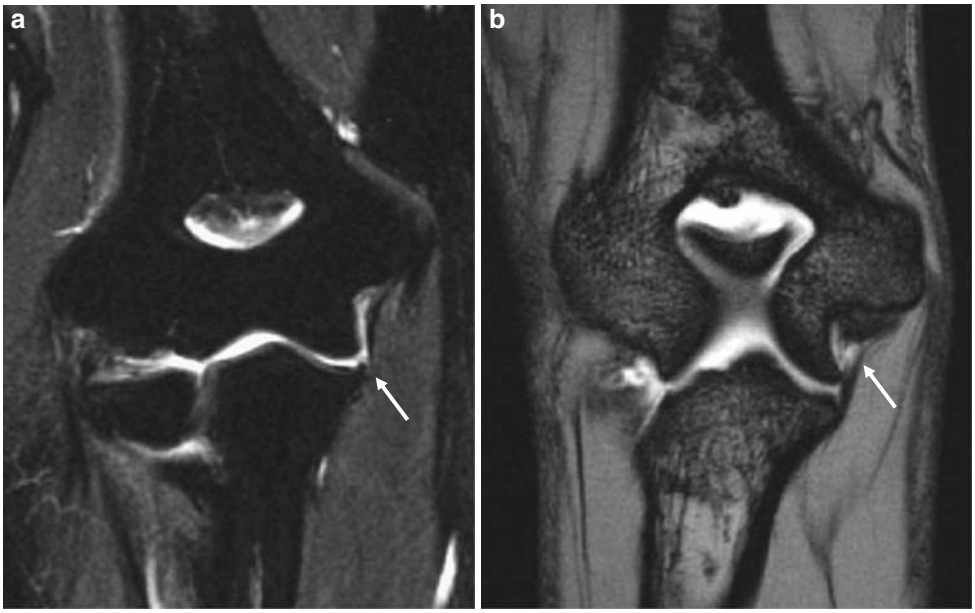

Fig. 5.98 Two patients with elbow MR arthrograms and partial tears of the UCL. The patient in (**a**) has a partial tear at the distal coronoid insertion of the UCL from the sublime tubercle (*arrow*). The patient in (**b**) (case courtesy of D. Dean Thornton, MD) has a partial undersurface tear at the proximal aspect of the UCL (*arrow*)

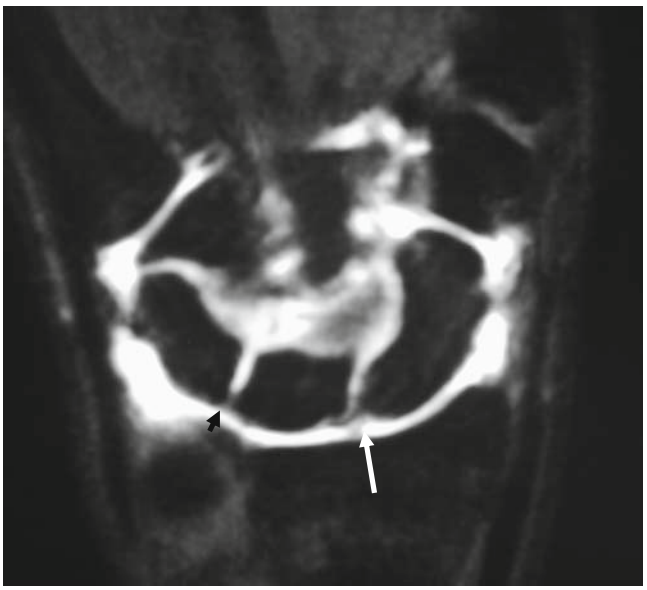

Fig. 5.99 MR arthrogram showing the normal scapholunate (*white arrow*) and lunotriquetral (*black arrowhead*) ligaments. Note that they are thin fibrous bands along the proximal aspect of their respective joints. These ligaments have fibrous portions volarly and dorsally with a membranous central portion. This membranous portion is subject to pinhole tears. Note as well the radial and ulnar attachments of the scaphoid and the triquetrum, respectively

investigators are experimenting with meniscal replacement, but this therapy is not widely accepted yet. Replacement does have a certain theoretical appeal, however, since meniscectomy destroys the hoop stress reduction mechanism of the meniscus and therefore is associated with accelerated development of osteoarthritis secondary to the altered biomechanics.

Shoulder

The labrum of the shoulder is in many ways similar to the menisci within the knee. It is triangular in cross section just as the knee menisci are. The base of the triangle is affixed to the margin of the glenoid, thereby deepening its cup (Fig. 5.120). As with the menisci, it is not a completely

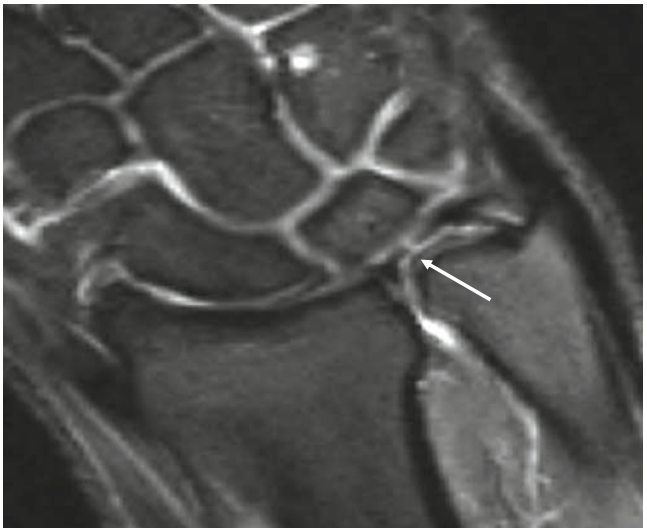

Fig. 5.100 Coronal images from a wrist MR arthrogram showing a tear of the triangular fibrocartilage complex (TFCC) just medial to its insertion onto the radius consistent with a Palmer Ia tear

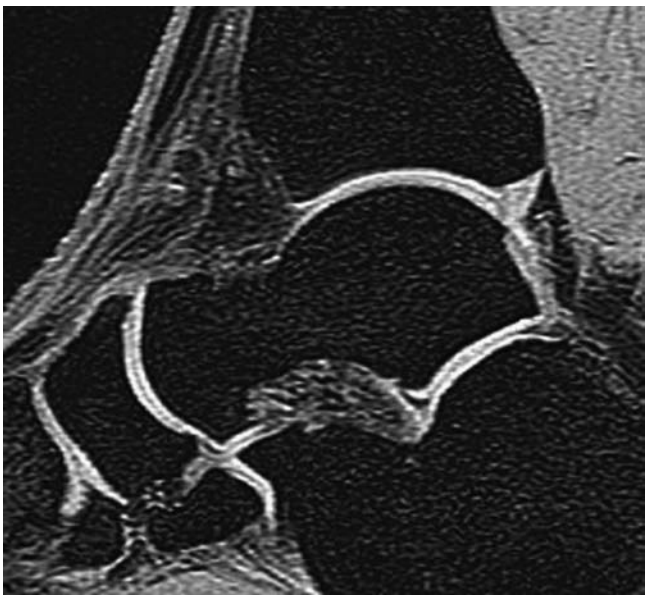

Fig. 5.101 Sagittal 3D SPGR cartilage image of a normal ankle shows bright hyaline cartilage signal while suppressing virtually all other tissue signals

closed figure but instead has a deep "C" shape as it wraps around the glenoid with an atretic inferior portion.

This glenoid labral fibrocartilage is subject to tears as well. The cause and type of the tear is highly dependent on the anatomical region of the labrum. The majority of authors believe that labral tears and SLAP tears are best imaged using MR arthrography. In contrast, the sensitivity of MRI for detection of labral tears is as high as 92%. Its specificity for anterior labral and SLAP tears, is 92 and 84%, respectively.

Most authors divide the labral fibrocartilage into four discrete zones, the posterior labrum, the superior labrum, the superior anterior labrum, and the inferior anterior labrum. The posterior and anterior inferior labral regions are subject to tearing related to instability of the shoulder. The superior labrum usually tears as the result of traction injuries to the long head of the biceps tendon, which inserts on the anterior aspect of the superior labrum with an anteriorly obliquely oriented trajectory. These tears are known as superior labral

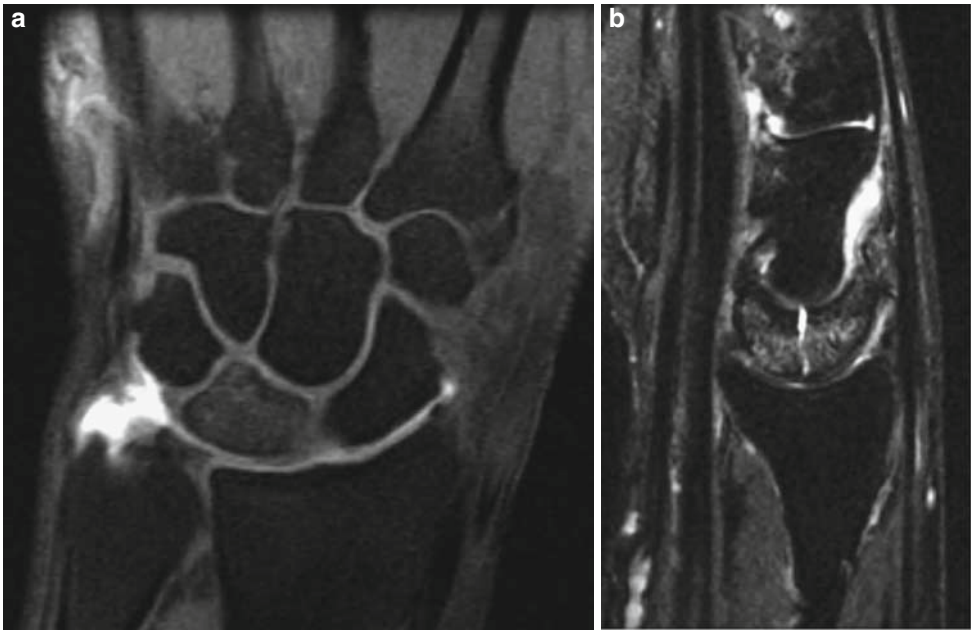

Fig. 5.102 Coronal (**a**) and sagittal (**b**) T2-weighted, fat-suppressed MR images from a wrist with a coronal plane lunate fracture and edema within the lunate. Note that the hyaline articular cartilage around the carpal bones is brighter than the suppressed marrow and darker than the fluid within the joint space

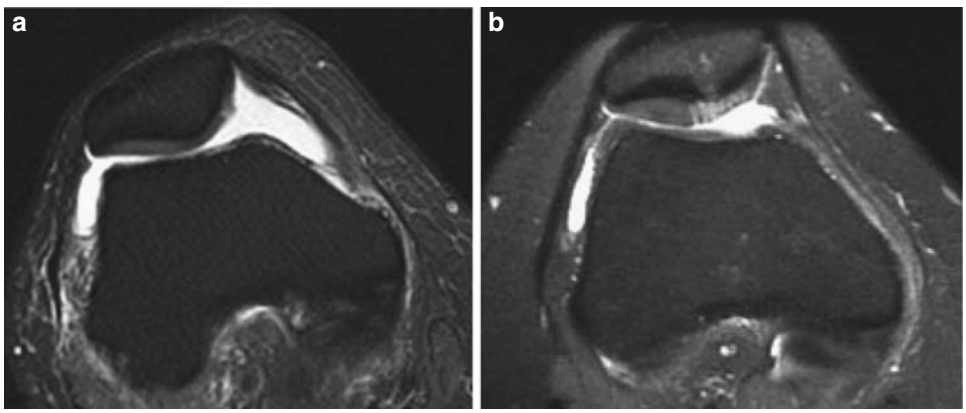

Fig. 5.103 Axial T2-weighted, fat-suppressed MR image of the knee showing early blistering and signal change of the cartilage of the medial patellar facet in one patient (**a**) and fibrillation of the patellar cartilage over the median ridge in another patient (**b**)

anterior to posterior (SLAP) tears because of their general direction of propagation. The remaining zone of the labrum – the anterior superior labrum – tears infrequently but shows a number of congenital variants that may be confused with tears. The two most common of these are an anterior superior labral foramen and a Buford lesion. The former is an area where the labrum is not firmly attached to the bone and as a result fluid may interpose itself between the fibrocartilage and the bone (Fig. 5.121). While this may appear as an avulsion of the labrum, it is usually just an inconsequential variant. In the Buford complex, the anterior superior labrum is absent and the middle glenohumeral ligament (MGHL) is markedly enlarged (Fig. 5.122). Again, the absent labrum may be misinterpreted as at tear, but in this location it is usually a normal variant. Seeing the enlarged MGHL is a cue to the correct diagnosis.

Shoulder instability and dislocations cause the majority of labral tears seen in the labrum. As a consequence of the high incidence of anterior shoulder instability and dislocation – about 80% of shoulder dislocations – the majority of labral tears occur in the anterior inferior zone of the labrum. Posterior dislocations are less common and so correspondingly are posterior labral tears. Anterior labral tears are generally classified as Bankart labral tears (Fig. 5.123). At times, the

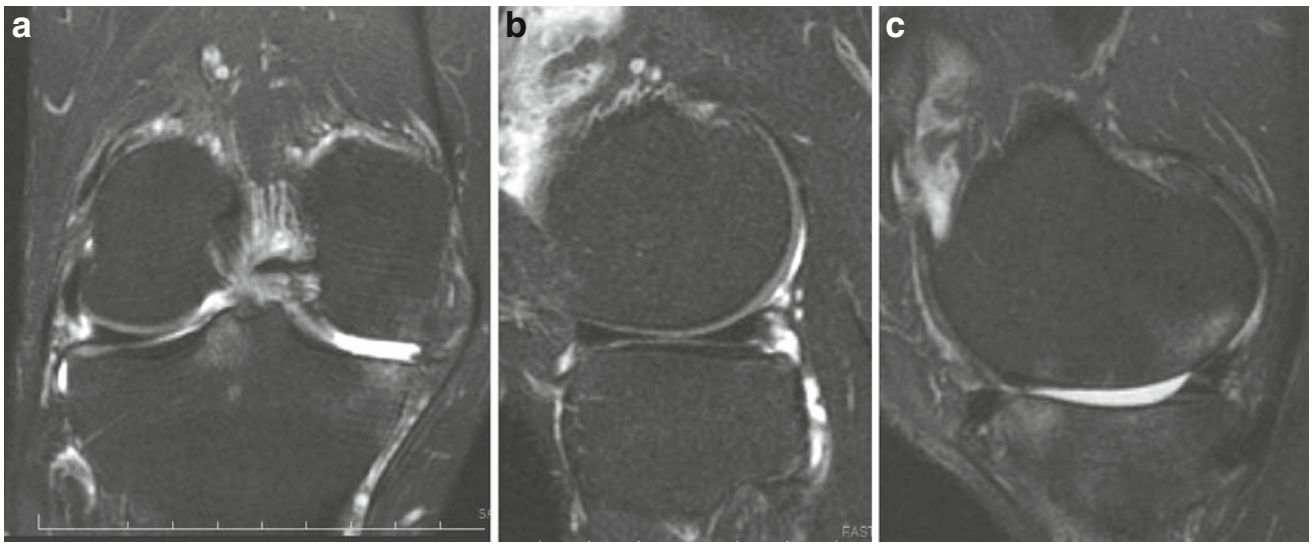

Fig. 5.104 Coronal (**a**) and sagittal lateral (**b**) and medial (**c**) compartment T2-weighted, fat-suppressed MR images showing medial compartment hyaline cartilage loss. Note the normal hyaline cartilage covering in the lateral compartment of the knee (**a** and **b**) and the absence of cartilage in the medial compartment where fluid density goes all the way to the cortex (**a** and **c**)

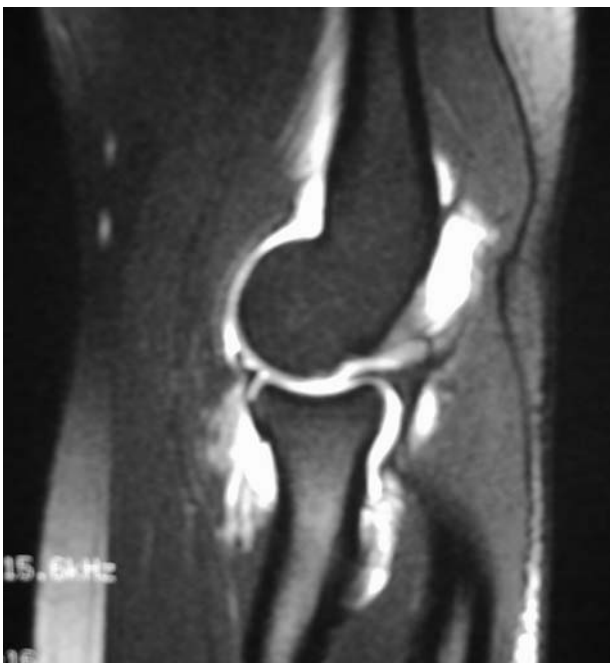

Fig. 5.105 Sagittal MR image from an elbow MR arthrogram showing an enlarged discoid meniscus in the radiohumeral joint. A small meniscus is normally present in this portion of the elbow, much smaller than the large posteriorly projecting meniscus visible in this joint

tear of the anterior labrum may avulse completely, giving rise to a free fragment. This fragment has been termed a glenoid labrum ovoid mass (GLOM) and may be the only MR sign of an anterior labral tear. This fragment should not be confused with the MGHL since it is smaller and not band-like.

When the labrum tears, it may also tear concomitantly the structures to which the fibrocartilaginous labrum attaches. The labral fibrocartilage as it rings the glenoid attaches to the hyaline cartilage on the articular surface of the glenoid centrally and to the periosteum on the glenoid neck peripherally. In addition, the far anterior inferior labrum has an attachment to the anterior band of the inferior glenohumeral ligament (IGHL) whence it extends to attach along the medial aspect of the humerus. A series of subtypes of labral tears have been recognized depending on their configuration and involvement of adjacent structures.

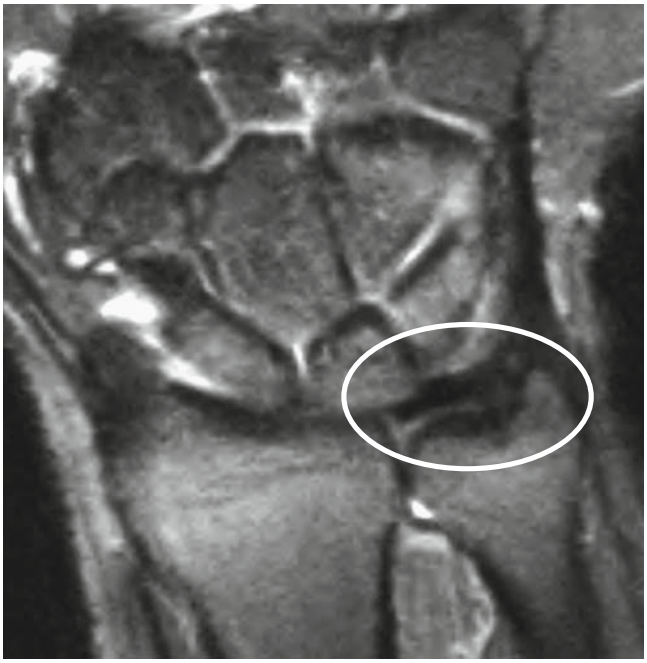

Fig. 5.106 T2-weighted coronal wrist MR image through a normal TFCC (*oval*)

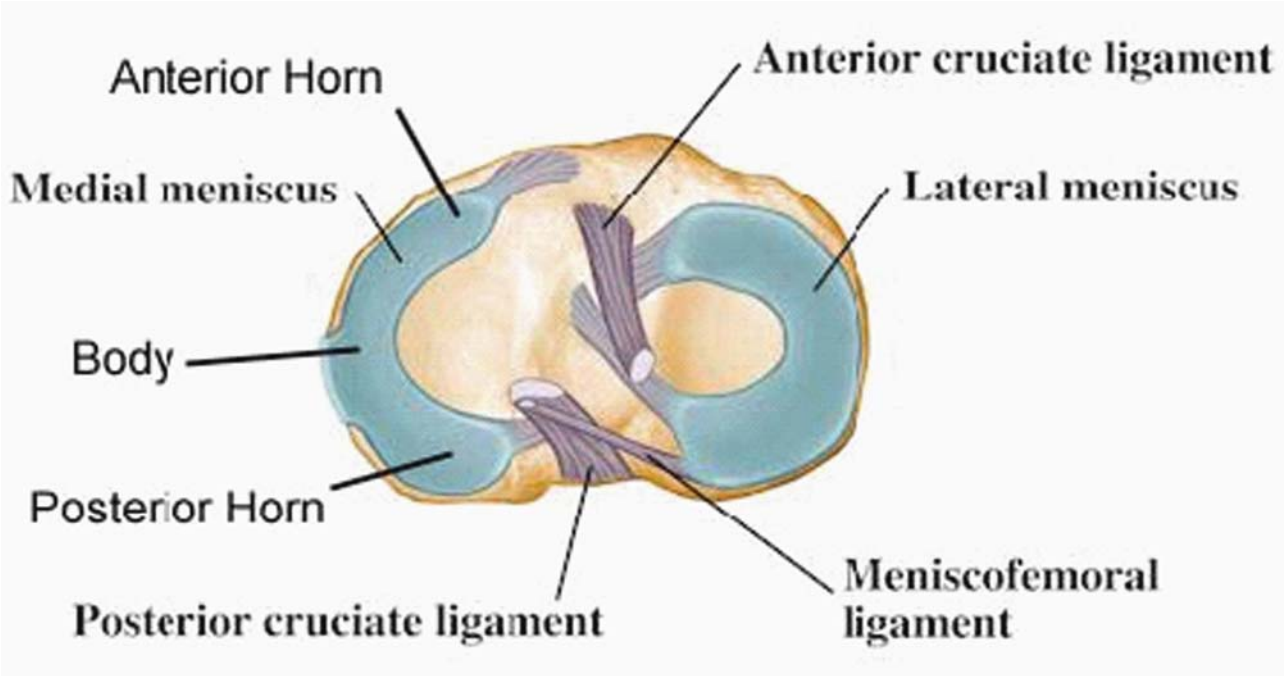

Fig. 5.107 Diagrammatic representation of the menisci and their attachments in the axial plane. Note that the roots of the menisci attach to the tibial spines. The medial meniscus is more elongated than the lateral meniscus. The lateral meniscus transmits the popliteus muscle tendon through its peripheral attachment posteriorly

The most common of these is the glenoid labrum articular disruption (GLAD) tear. Here, the labral tear also affects a portion of the adjacent articular hyaline cartilage (Fig. 5.124). This the most common of the complex anterior inferior labral tears and is easily recognized on MRI anthrography.

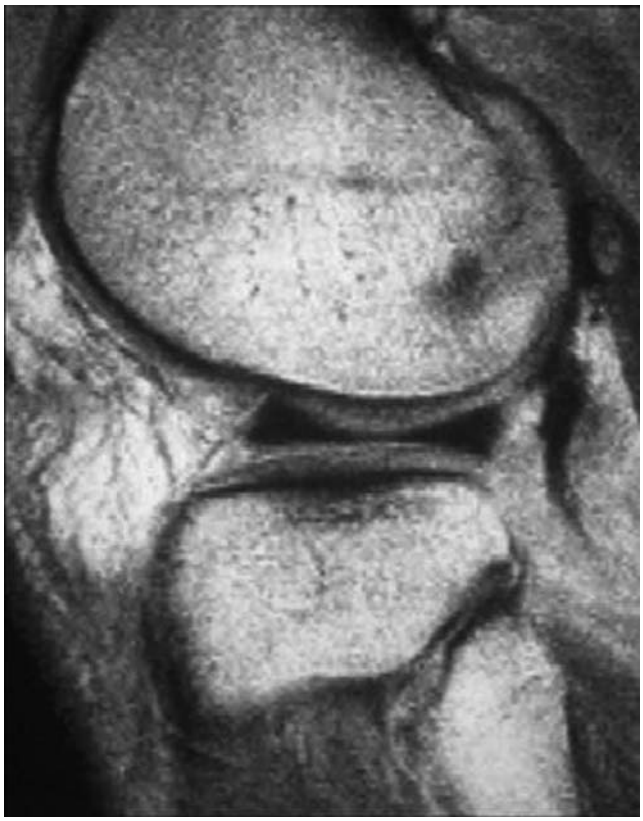

Fig. 5.108 Sagittal proton density MR image through the lateral meniscus showing the triangular shape of the menisci in cross section. As the menisci are "C" shaped, a sagittal image will portray the anterior and posterior horns of the menisci together as a bowtie

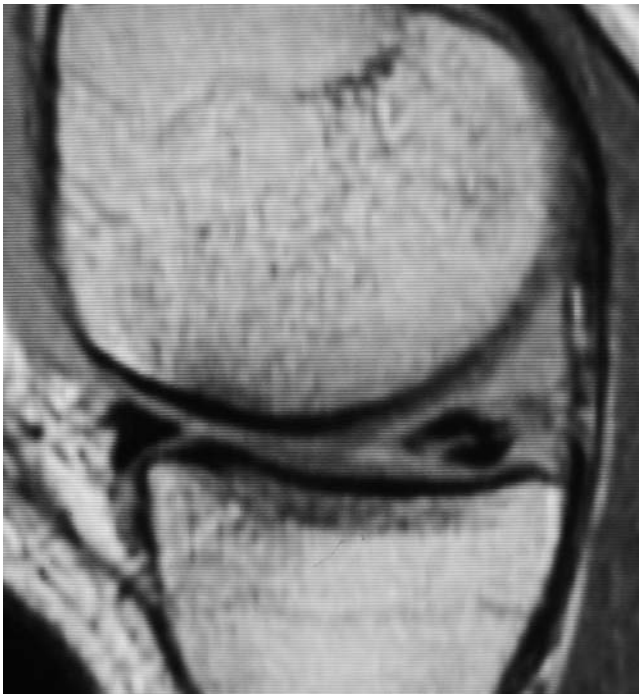

Fig. 5.109 Sagittal proton density MR image through the medial meniscus showing truncation of the posterior horn and an obliquely oriented linear tear of relatively high signal compared with the meniscus itself

Another two of these tears, instead of involving the adjacent hyaline cartilage, strip the periosteum from the anterior glenoid neck along with the labral tear. The first of these, the Perthes lesion, leaves a fragment of labrum floating at the end of a periosteal tether (Fig. 5.125). In the second of these, the anterior labrum periosteal sleeve avulsion (ALPSA), the free labral fragment balls up inferomedially within the periosteal sleeve, giving rise to a rounded fibrocartilage lump anterior to the glenoid neck (Fig. 5.126). If left unresected, the ALPSA lesion may calcify and fuse to the anterior glenoid neck. The Perthes lesion, on the other hand, has been treated nonsurgically in the past, but this may be because it has been difficult to identify at arthroscopy since the fluid injected during the procedure tends to force the periosteal tail back into its normal position.

The last two of these tears involve the labrum and the anterior band of the IGHL. One, a humeral avulsion of the inferior glenohumeral ligament (HAGL) (Fig. 5.127) and the other, a bony avulsion of the inferior glenohumeral ligament (BAGL), each avulse the distal humeral attachment of the anterior band of the anterior band of the IGHL (with or without a bone fragment) with or without

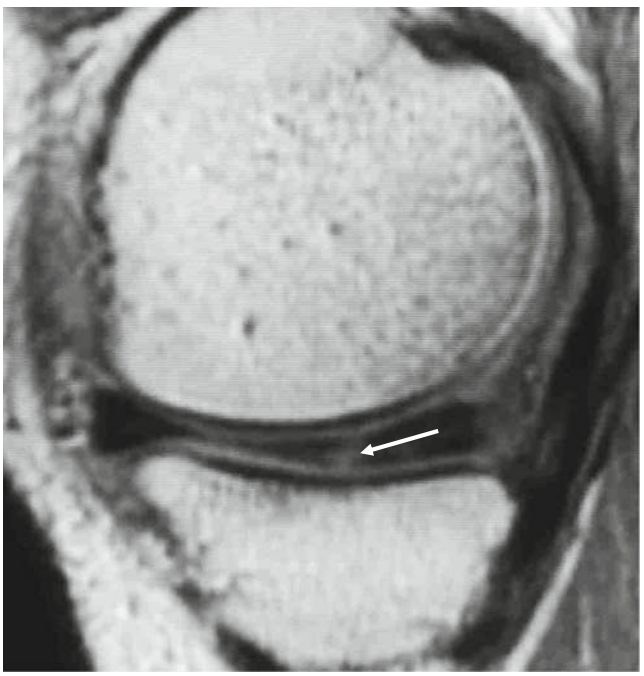

Fig. 5.110 Sagittal proton density MR image through the medial meniscus showing a vertical tear in its posterior horn (*arrow*). This tear extends circumferentially around the meniscus

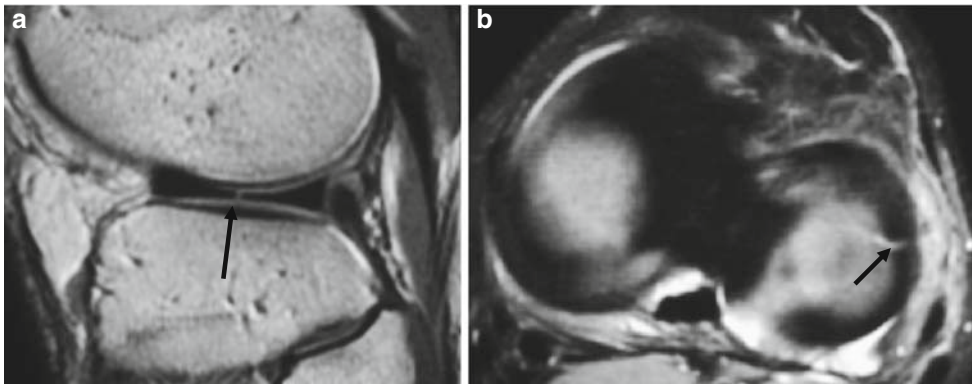

Fig. 5.111 Sagittal proton density (**a**) and axial T2-weighted, fat-suppressed (**b**) MR images through the lateral meniscus showing a radially oriented vertical tear (*arrows*) in its body

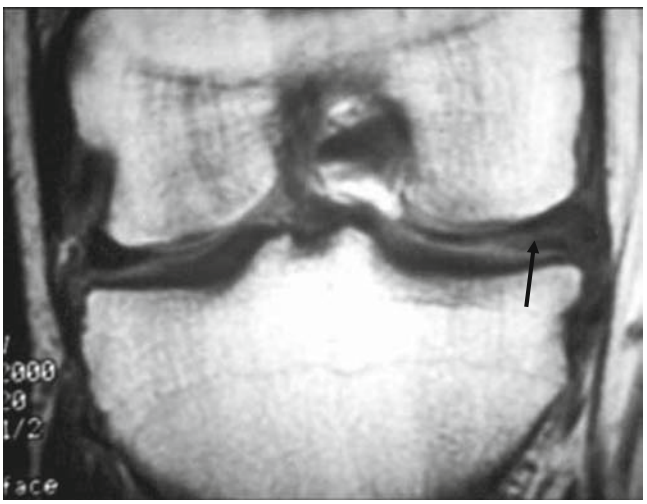

Fig. 5.112 Coronal T1-weighted MR image showing a normal lateral meniscus and a horizontal tear (*arrow*) through the medial meniscus

inferior anterior labrum tears. These lesions are associated with subscapularis tears and occur in about 9% of patients with anterior shoulder instability.

While it stands to reason that typical posterior labral tears (Fig. 5.128) might have similar associated attachment lesions to those seen with inferior anterior labral tears, these are generally not seen. On the other hand, posterior labral tears have been associated with an extracapsular calcified lesion in the soft tissues adjacent to the inferior posterior labrum known as a Bennett lesion (Fig. 5.129). It is most commonly seen in throwing athletes, particularly baseball pitchers, and is believed to represent an avulsion injury to the shoulder capsule or the posterior band of the IGHL. If left untreated, it may result in posterior instability. Clinically, it is associated with posterior labral tears and undersurface rotator cuff tears.

The superior labrum is subject to tears related to traction and/or compression injuries on the long head of the biceps tendon as it inserts on the anterior superior glenoid labrum. Among other things, these tears are thought to be responsible for dead arm syndrome in baseball pitchers. Superior labral tears are relatively uncommon, visible in about 6% of arthroscopies.

The traction type of injury generally results from throwing injuries or sudden loss of control of a heavy object that the patient was carrying. The compression mechanism results from a fall on an outstretched arm that precipitously increases the load on the superior labrum from impact by the humeral head. SLAP tears have been classified into four basic types (Table 5.5). Type II and III tears are most common. Recently, this classification has been expanded, but for clinical purposes the original classification largely

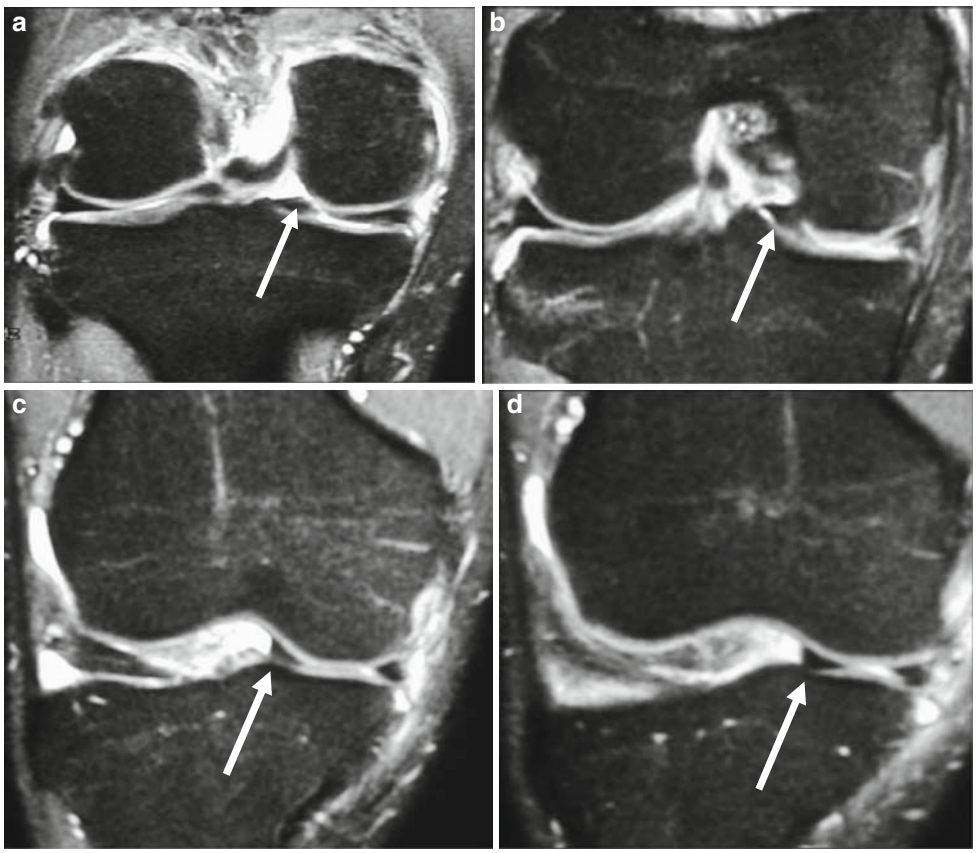

Fig. 5.113 Serial coronal T2-weighted, fat-suppressed MR images from posterior (**a**) through anterior (**d**) showing a bucket handle tear of the medial meniscus. Note the centrally displaced meniscal fragment (*arrows*) that first moves away from the peripheral fragment and then as the anterior portion of the joint is reached starts to move back toward the peripheral fragment

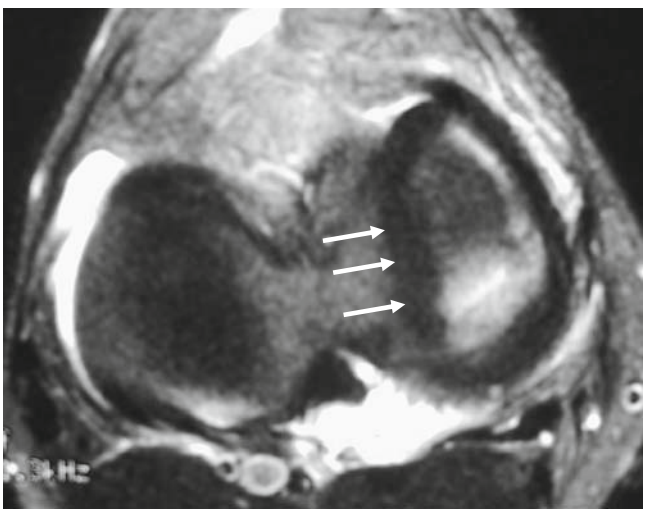

Fig. 5.114 Axial T2-weighted, fat-suppressed MR image in a patient showing the bucket handle fragment of the medial meniscus displaced into the central portion of the joint (*arrows*)

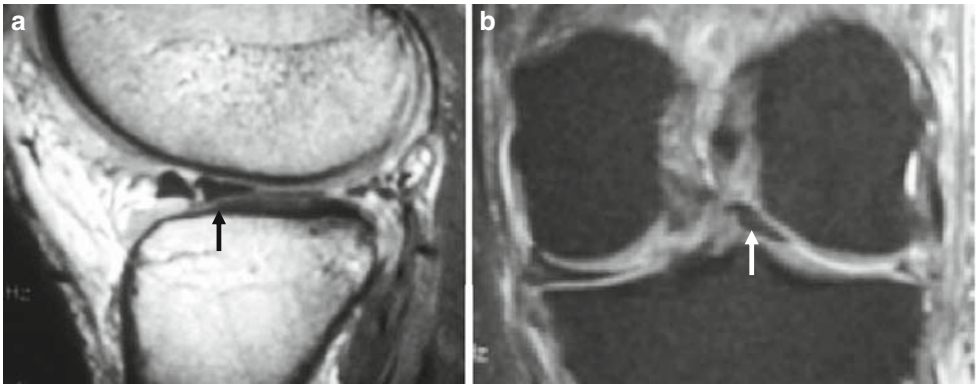

Fig. 5.115 Sagittal proton density (**a**) and coronal T2-weighted, fat-suppressed (**b**) MR image through the medial meniscus showing a flipped posterior horn bucket handle tear with the posterior horn of the meniscus now aligned with the anterior horn (*arrow*). Note the typical centrally displaced free fragment in (**b**) (*arrow*)

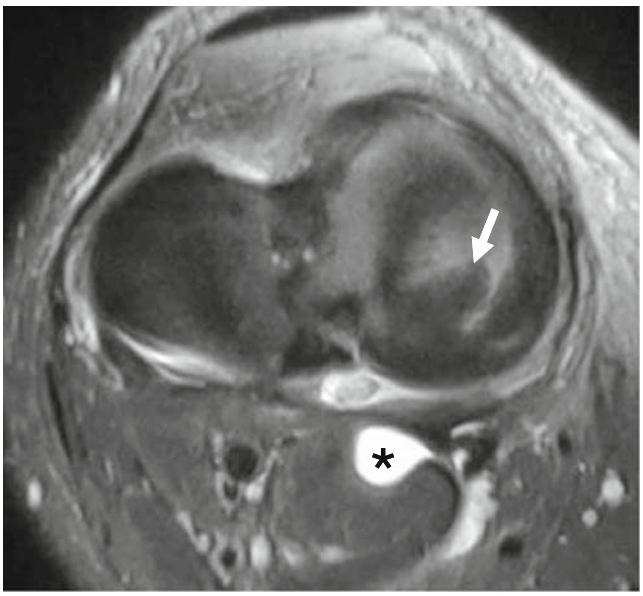

Fig. 5.116 Axial T2-weighted, fat-suppressed axial MR image showing a posterior parrot beak tear of the medial meniscus (*arrow*). Note the medial posterior joint extension extending into the soft tissues between the medial head of the gastrocnemius muscle laterally and the tendon of the semimembranosus muscle medially (∗). This location represents a congenitally weak point in the capsule. As a result, posterior extensions are common. If they enlarge or become symptomatic, they are called Baker cysts. (Image courtesy of Dr. E. Kulenovic)

Table 5.5 Classification of superior labral anterior posterior tears

Type	Abnormality	Tears (%)
I	Fraying of undersurface of biceps tendon anchor	9.5–21
II	Labral tear causing biceps anchor instability	41–55
III	Bucket handle tear of the superior labrum	6–33
IV	Bucket handle tear of the superior labrum extending into the substance of the biceps tendon	3–15

suffices as the other types are distinctly uncommon. These tears are best visualized on MR arthrography where they appear as abnormal signal within the superior labrum posterior to the region of the biceps tendon anchor (Fig. 5.130) or as distortions of the morphology of the superior labrum (Fig. 5.131).

As with the knee, the shoulder too may have cysts formed around the joint arising from the labrocapsular portion of the joint. Until the advent of MRI, these were diagnosed uncommonly. Today they are recognized relatively commonly and are generally called labral cysts, paralabral cysts, or ganglion cysts. They have the same significance as meniscal cysts. That is, the identification of a labral cyst should raise the issue of a cryptogenic labral tear.

Labral cysts most commonly arise from the posterior superior and posterior portions of the labrum where they can track along a number of courses, including into the suprascapular (Fig. 5.132) and spinoglenoid notches (Fig. 5.133), into a rotator cuff muscle belly along the tendon (Fig. 5.134), or along the scapular spine (Fig. 5.135). Alternatively, cysts may project directly through the posterior labrum or the anterior labrum. While meniscal cysts in the knee are usually identified incidentally during scan interpretation, labral cysts may cause other clinical problems that may in fact be the reason for diagnostic imaging. When they move into the suprascapular or the spinoglenoid notch, they may cause nerve compression and resulting weakness of the supraspinatus and/or infraspinatus muscles. The result of this is that the patient presents clinically as though they have a rotator cuff tear. Cysts traversing into the substance of the muscle may present with nonspecific shoulder pain.

Treatment of labral cysts requires both resection of the cyst and repair of any labral tear that might be underlying. Otherwise, the cysts are likely to recur and the shoulder instability associated with the cryptogenic tear will not be cured.

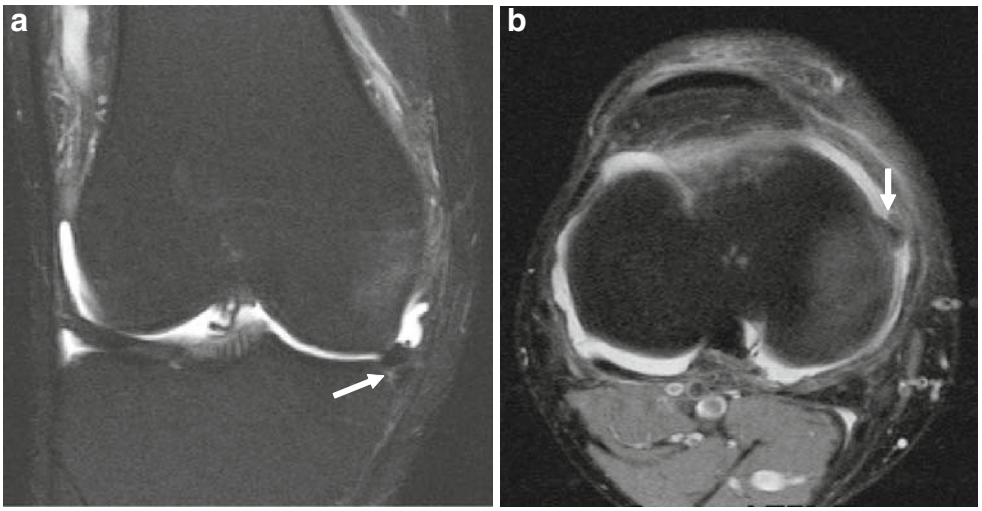

Fig. 5.117 Coronal (**a**) and axial (**b**) T2-weighted, fat-suppressed MR images showing a flap tear of the medial meniscus (*arrows*). This is a horizontal tear where one half folds back on itself either superiorly or inferiorly. In this case, note the flap extending inferiorly into the tibial gutter. This location makes arthroscopic identification difficult and makes MRI important for identification. The flap projects focally beyond the margin of the knee joint on the axial image (**b**). (Case courtesy of Dr. E. Kulenovic)

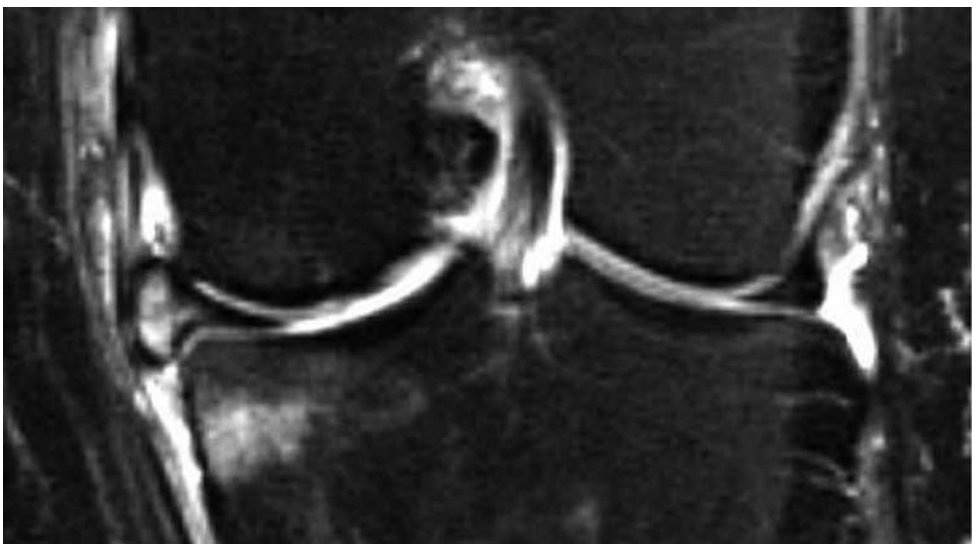

Fig. 5.118 Coronal T2-weighted, fat-suppressed MR images showing an intrameniscal cyst in the body of the medial meniscus. The fluid signal intrameniscal cyst distorts the normal triangular contour of the meniscus

Hip

The fibrocartilage of the acetabular labrum of the hip is very similar to the glenoid labrum of the shoulder. It forms an incomplete ring around the osseous acetabular margins and forms an upside down horseshoe. The free margins of the horseshoe are connected by an inferior transverse acetabular ligament (Fig. 5.136). This ligament, unlike the IGHL of the shoulder, is straight and does not form a hammock beneath the joint. As with the menisci in the knee and the glenoid labrum of the shoulder, the acetabular labrum is mostly triangular in cross section. Like the glenoid labrum, it inserts along the osseous lip of the acetabulum with attachment to the articular hyaline cartilage centrally and the periosteum along the periphery of the acetabulum.

Unlike glenoid labral tears in the shoulder, joint instability and dislocations do not account for a large percentage of acetabular labral tears. The hip joint, with its deep acetabulum, is less prone to instability than the shoulder joint. In fact, most hip dislocations occur only after major trauma such as a motor vehicle collision with the knee striking the dashboard straight on in the sitting (hip flexed) position. The impact will drive the acetabular head directly into the posterior acetabulum.

Many other etiologies have been ascribed to acetabular labral tears, including direct trauma, athletic activities that

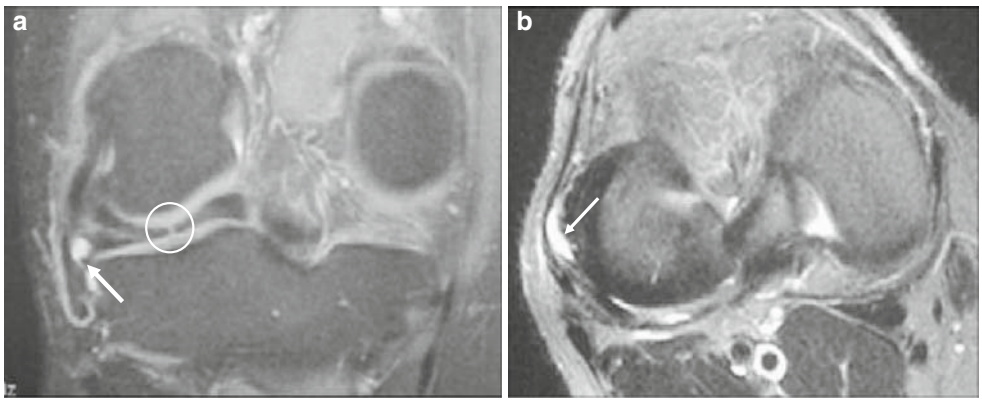

Fig. 5.119 Coronal (**a**) and axial (**b**) T2-weighted, fat-suppressed MR images showing a parameniscal cyst (*arrows*) of the body of the lateral meniscus. This type of meniscal cyst is more common than the intrameniscal type. A posterior meniscal radial tear is also present (*circle*)

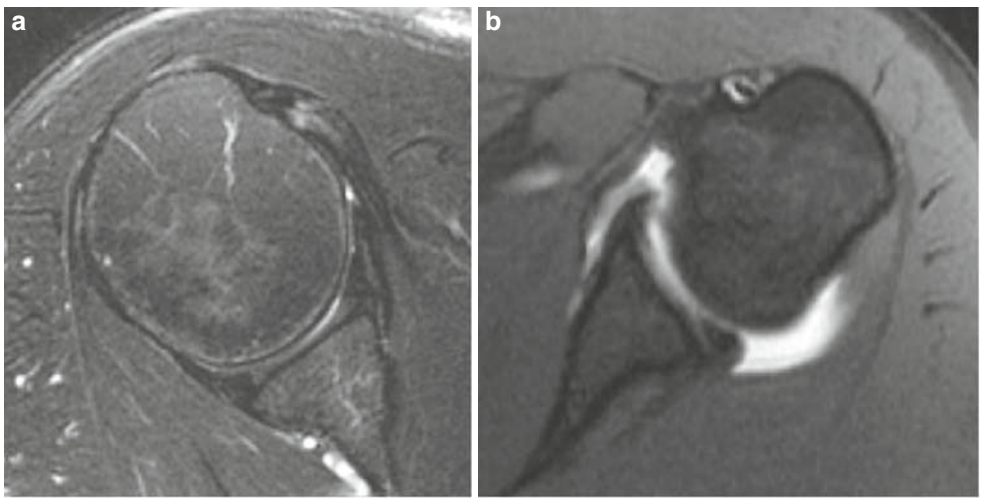

Fig. 5.120 Axial T2W FS MR image (**a**) and T1W FS image from an MR gadolinium arthrogram in a second patient (**b**) showing the normal anterior and posterior labra deepening the osseous shoulder glenoid. Despite the presence of the fibrocartilage labrum, it is clear that the shoulder glenoid is shallow, making the joint very susceptible to dislocations. Note that the labral cartilage is triangular in cross section, very similar to the menisci of the knee

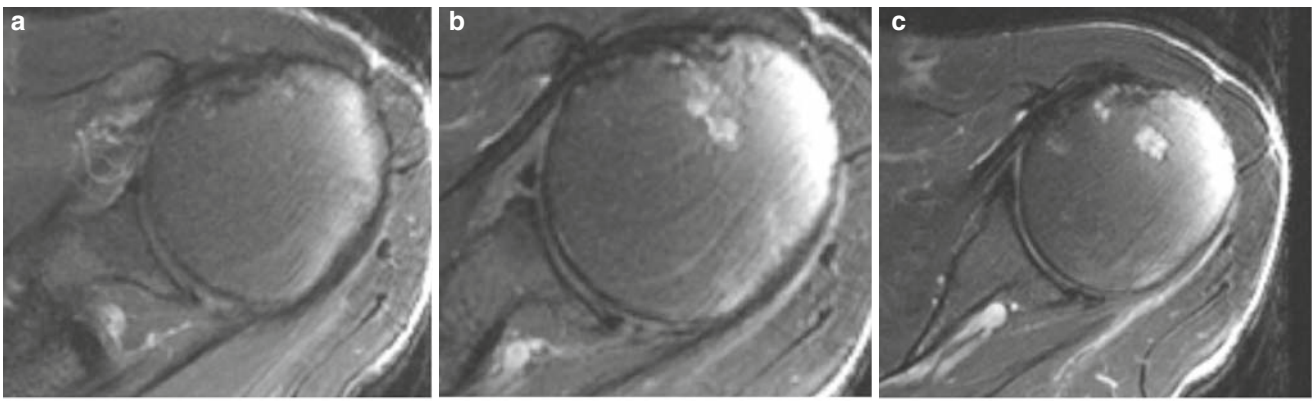

Fig. 5.121 Serial axial T2W FS MR images of a shoulder from superior (**a**) to inferior (**c**) showing a focal separation of the anterior superior labrum (**b**) representing a sublabral foramen in the anterior superior portion of the glenoid

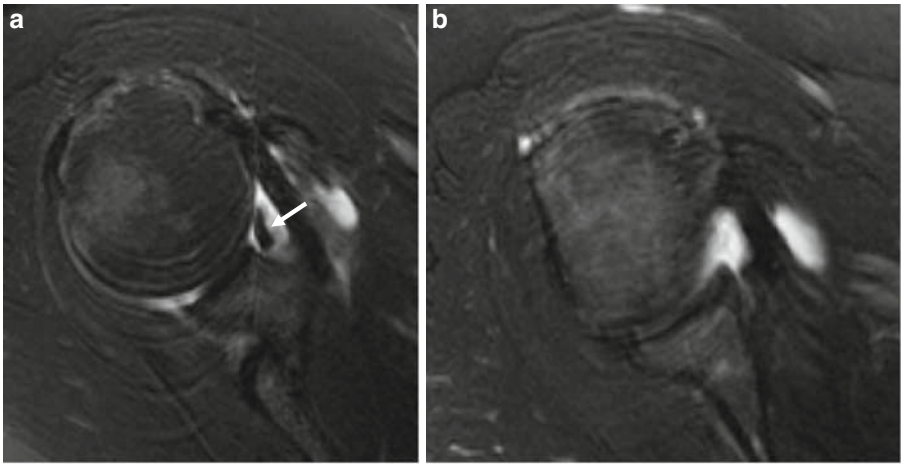

Fig. 5.122 Axial T2W FS MR images of a shoulder superiorly (**a**) and inferiorly (**b**) showing a Buford complex. Note the absent anterior labrum superiorly paired with the cord-like MGHL (**a**) and the normal appearing anterior labrum inferiorly (**b**)

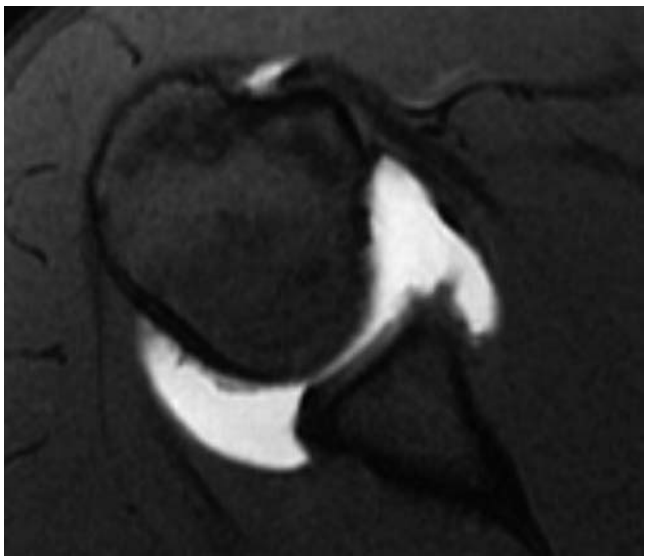

Fig. 5.123 Axial T1W FS image from an MR arthrogram of the shoulder showing distortion of the anterior inferior labrum, a typical anterior inferior glenoid labral tear (Bankart tear)

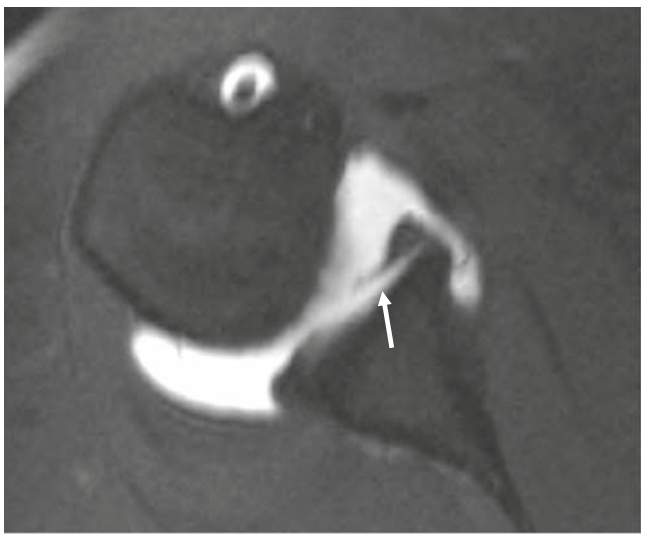

Fig. 5.124 Axial T1W FS image from an MR arthrogram of the shoulder showing a tear of the anterior inferior labrum that is also avulsing a portion of the labral hyaline articular cartilage (*arrow*). This is a glenoid labrum articular disruption or GLAD lesion

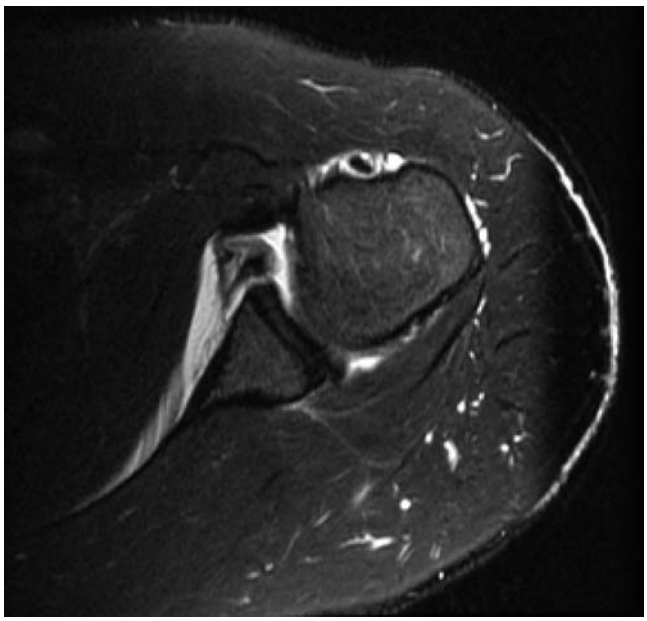

Fig. 5.125 Axial T1W FS image from an MR arthrogram of the shoulder showing a tear of the anterior inferior labrum that is also stripping a portion of the anterior glenoid periosteum creating a labrum on a tether appearance. This is known as a Perthes lesion. (Case courtesy of Dr. John Hunter)

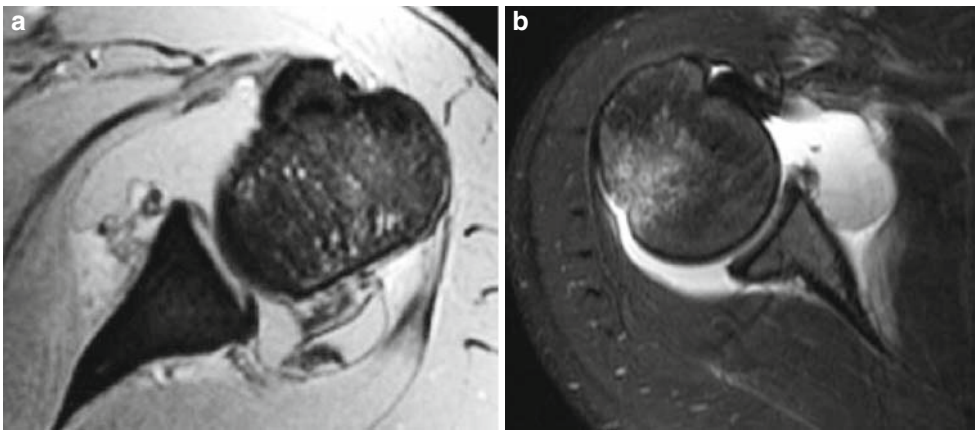

Fig. 5.126 Axial GRE MR arthrographic image in one patient (**a**) and axial T1W FS MR arthrographic image from another patient (**b**) of the shoulder showing an anterior inferior labral tear that has rolled up in the stripped anterior glenoid periosteum creating a sleeve around the fragment. This is known as an anterior labrum periosteal sleeve avulsion or ALPSA lesion. In (**b**) note the small Hill–Sachs deformity and bone edema from a recent anterior dislocation. (Image (**b**) courtesy of Dr. John Hunter)

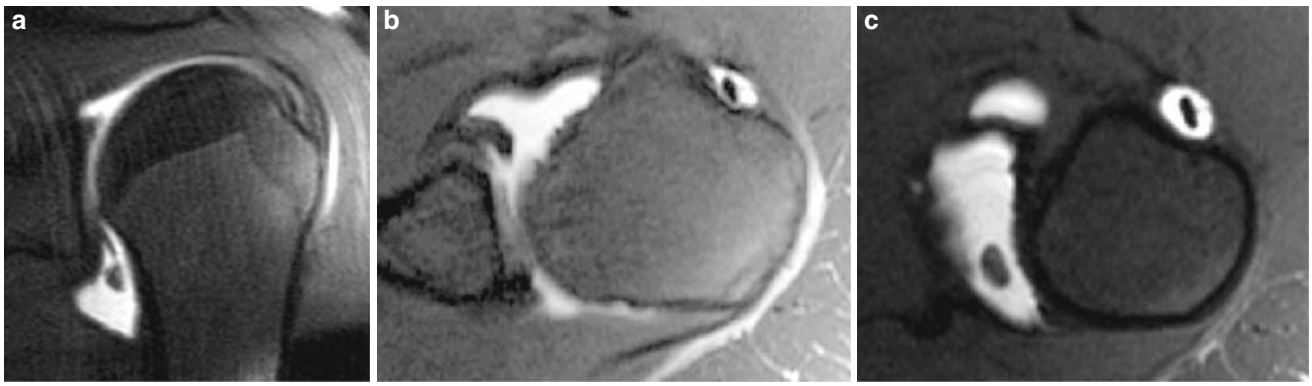

Fig. 5.127 Coronal (**a**) and axial (**b**) and (**c**) T1W FS MR arthrogram images showing an avulsed IGHL within the axillary recess of the joint (**a**) and (**c**) and an anterior inferior labral tear (**b**). Often contrast will be seen extravasating from the joint at the axillary recess with HAGL and BAGL lesions. In this case, the HAGL lesion was chronic and no extravasation was observed

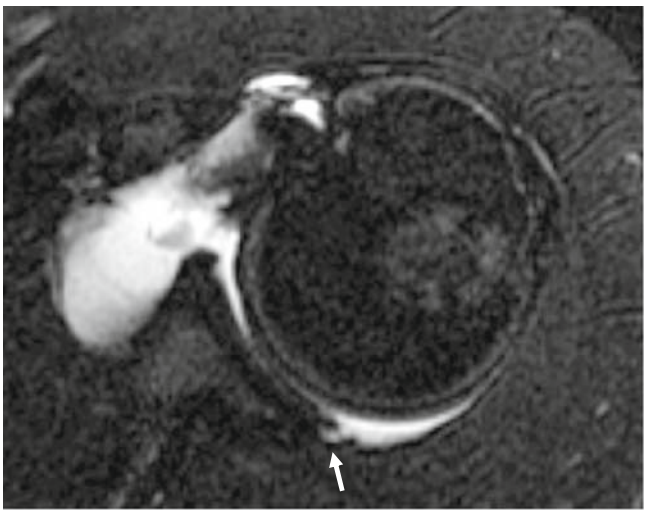

Fig. 5.128 Axial T1W FS image from an MR arthrogram of the shoulder showing a tear of the posterior labrum (*arrow*). This tear resembles the standard Bankart tear but is seen along the posterior margin of the labrum instead of involving the anteroinferior labrum

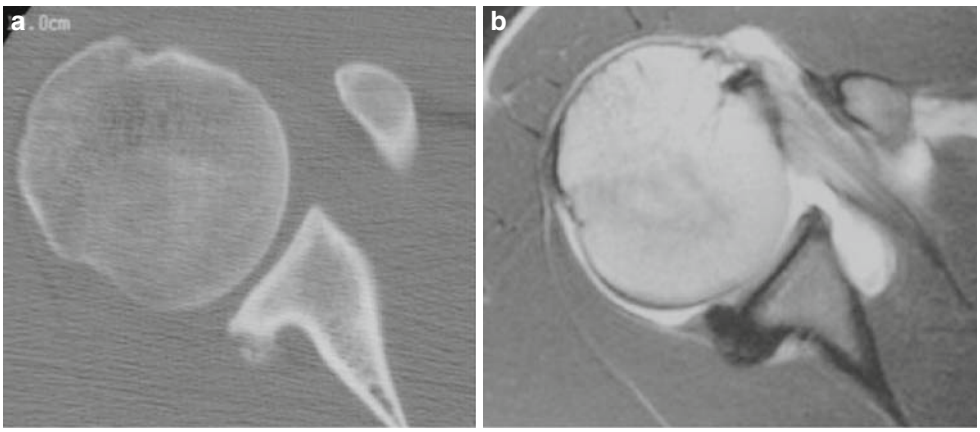

Fig. 5.129 Axial CT image (**a**) and T1W MR arthrogram image (**b**) of the shoulder showing a calcified/ossified lesion at the posterior labrum consistent with a Bennett lesion. (Case courtesy of D. Dean Thornton, MD)

require frequent external rotation, twisting movements, and hyperabduction. Despite studies that show some correlation between these activities and labral tears, nearly 75% of labral tears have no obvious explanation. In fact, the prevalence and clinical significance of labral tears is uncertain. Some studies show that the prevalence of acetabular tears, like intrinsic ligament tears in the wrist, increases with age but is not significantly pathologic. Other studies show a correlation between joint pathology and tears. As with ligament tears of the wrist, acetabular labral tears are not always associated with clinical symptoms. Regardless, acetabular tears are the likely explanation of pain in between 25 and 50% of younger patients with hip pain and popping.

Patients with hip dysplasia have a higher incidence of acetabular tears. In fact, this incidence may be as high as 75%, and these tears are usually in the anterior aspect of the acetabulum (Fig. 5.137). Other structural abnormalities have also been associated with acetabular tears. Hip dysplasia may also account, at least partially, for the increased prevalence of acetabular tears in women compared with men since women have an increased prevalence of hip dysplasia.

Clinically, patients with acetabular tears complain of anterior hip pain that may radiate into the groin. Often they have clicking, popping, or a sensation of catching. These symptoms correlate with the fact that most labral tears, in the Western world at least, occur in the anterior or the anterosuperolateral portion of the labrum (Fig. 5.138). The reason for this has been related to a larger amount of stress to the anterior labrum, a decreased blood supply, and relative weakness of the tissue of the anterior labrum. Oddly, however, in Japan, labral tears more often involve the posterior labrum.

MR arthrography has become the test of choice for diagnosing acetabular labral tears with accuracies as high as

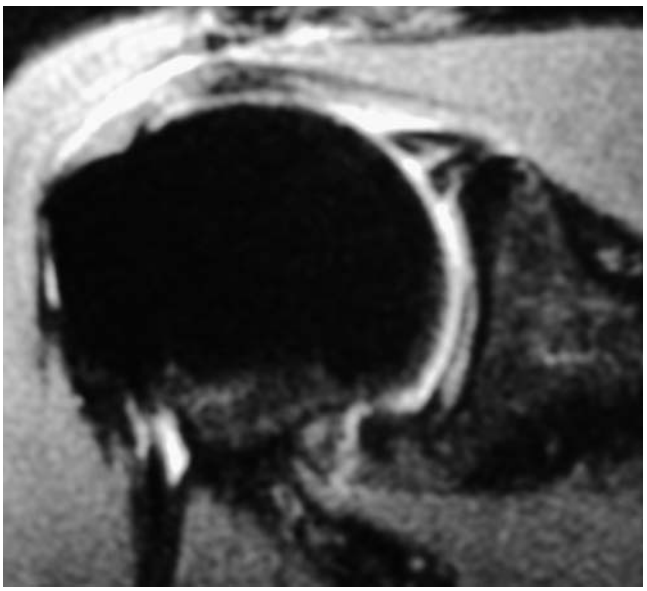

Fig. 5.130 Coronal T2W FS image showing a tear in the superior glenoid labrum, SLAP tear. High signal is present in the superior labrum transecting the labral triangle

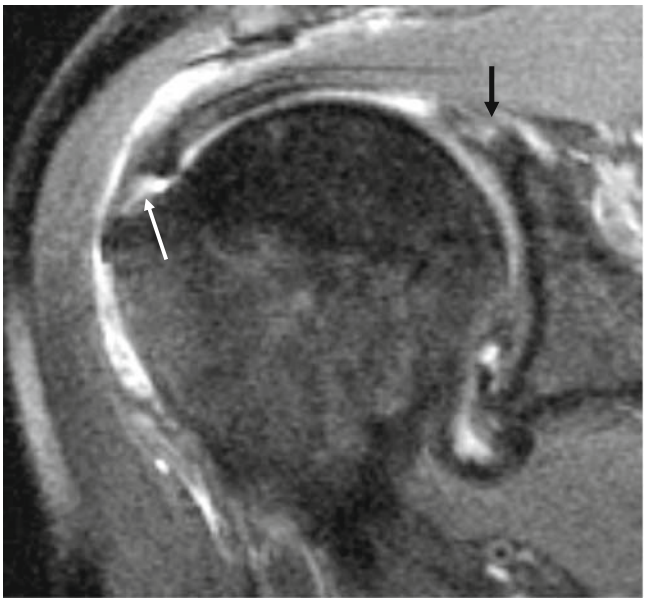

Fig. 5.131 Coronal T2W FS MR image showing distortion of the superior labrum (*black arrow*) proven to be the result of a SLAP tear. Note also the undersurface rotator cuff tear of the supraspinatus tendon (*white arrow*)

90%. Without arthrography, MRI is much less accurate. Normal sulci between the labrum and the hyaline cartilage may at times cause confusion and reduce MR arthrography's specificity for diagnosing tears, but this appears to be less of a problem in the hip than it is in the shoulder. As with meniscal tears and glenoid labral tears, diagnosing acetabular labral tears relies on identification of one of two basic findings: alteration of the basic cross-sectional triangular morphology of the labrum (Fig. 5.136) and the intralabral signal that corresponds to water signal on T2-weighted, fat-suppressed imaging or the gadolinium signal on T1-weighted, fat-suppressed imaging (Fig. 5.138 and 5.139). In the latter case, even if the abnormal signal does not extend to the free edge of the labrum, the presence of intralabral gadolinium indicates a tear that communicates with the surface.

Although thought to be less common, labral cysts may arise around the hip joint both within the labrum (Fig. 5.140) and adjacent to it. As with the menisci in the knee and the glenoid labrum of the shoulder, their presence should be

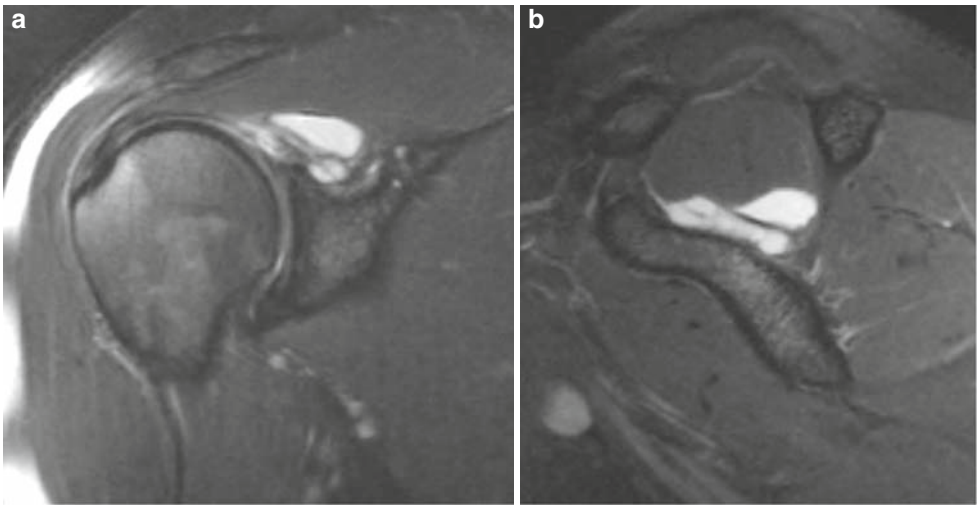

Fig. 5.132 Coronal (**a**) and sagittal (**b**) T2W FS MR images of the shoulder showing a labral cyst occupying the suprascapular notch

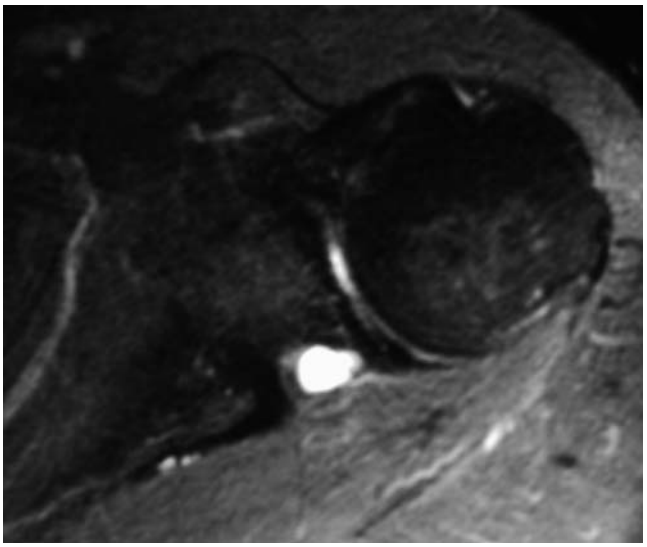

Fig. 5.133 Coronal T2W FS MR image of the shoulder showing a labral cyst occupying the spinoglenoid notch along the posterior neck of the glenoid

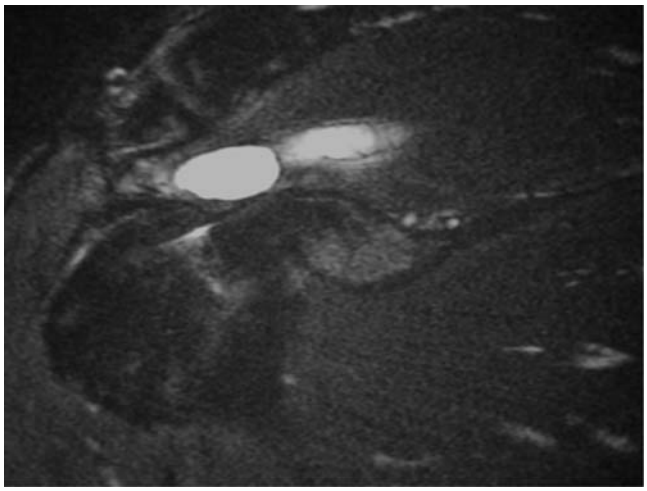

Fig. 5.134 Coronal T2W FS MR image of the shoulder showing a labral cyst coursing along and parallel to the fibers of the supraspinatus tendon

taken as an indicator of an acetabular labral tear. While not well studied, as with shoulder labral cysts, the treatment of hip labral cysts should involve not only aspiration or resection of the cyst but also repair of any coincident tear in order to prevent cyst recurrence.

Wrist

The triangular fibrocartilage complex represents the major fibrocartilage structure in the wrist. This complex consists of the triangular fibrocartilage (TFCC) itself; its attachments to the ulna – the ulnocarpal ligaments; its distal attachments to the triquetrum and the lunate – the ulnocarpal ligaments; and the adjacent meniscal analogue (Fig. 5.106). The TFCC, as its name suggests, is a large triangular fibrocartilage structure with a shape similar to the cross section of a knee meniscus or the glenoid or the acetabular labra. The base of the triangle nestles into the notch formed by the distal articular surface of the ulna and the protruding ulnar styloid to which it is attached. The apex of the triangle attaches to the radius between the lunate and the sigmoid notches of the radius at the medial most aspect of the radius. Here it forms the distal margin of the distal radioulnar joint (DRUJ).

While the meniscal analogue is infrequently the target of trauma, the TFCC and its ligaments are subject to frequent tears. This follows as a result of the complex function that the TFCC plays in the wrist. First, it is the major stabilizer

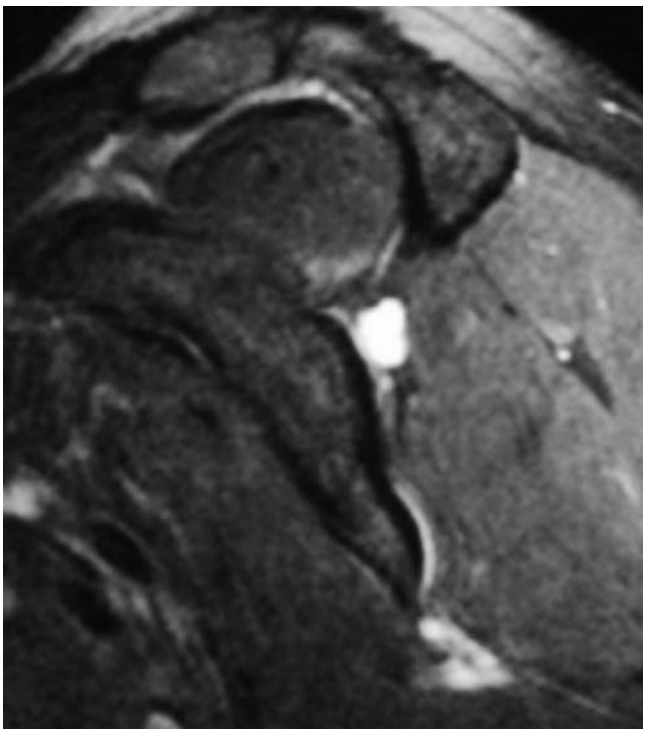

Fig. 5.135 Coronal T2W FS MR image of the shoulder showing a labral cyst coursing along and parallel to the scapular spine deep into the infraspinatus muscle

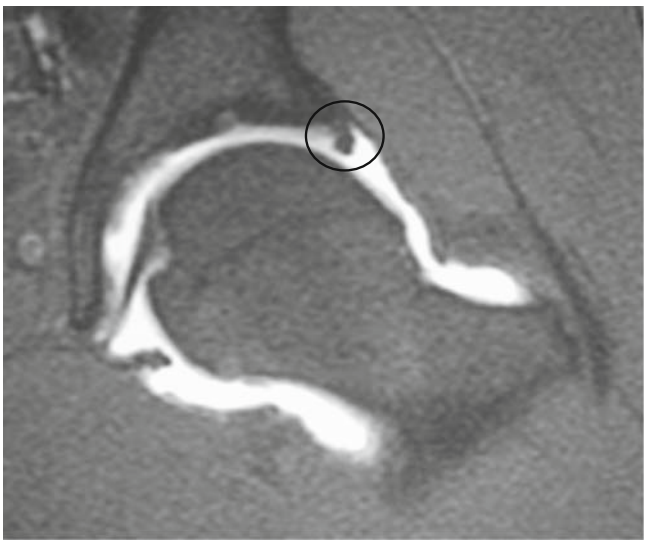

Fig. 5.136 Coronal T1W FS MR hip arthrogram image showing a tear of the superior labrum. Note the truncation of the superior labrum from its normal triangular shape (*circle*). Inferiorly note the transverse acetabular ligament in cross section

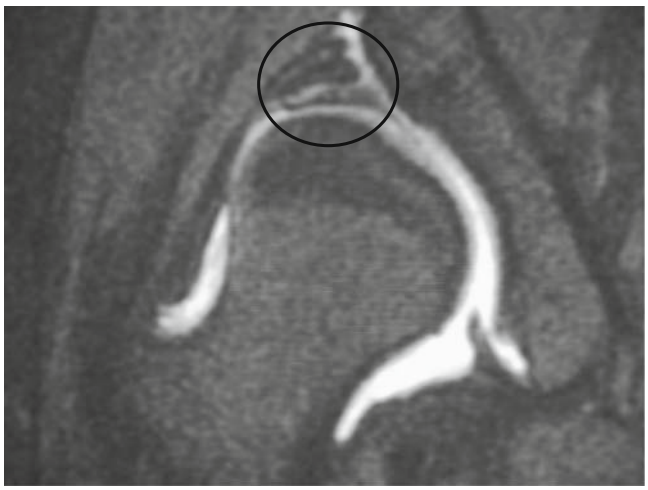

Fig. 5.137 Coronal T1W FS MR hip arthrogram image in a patient with congenital hip dysplasia showing a shallow acetabulum, a deformed femoral head, and a large tear of the labrum (*circle*)

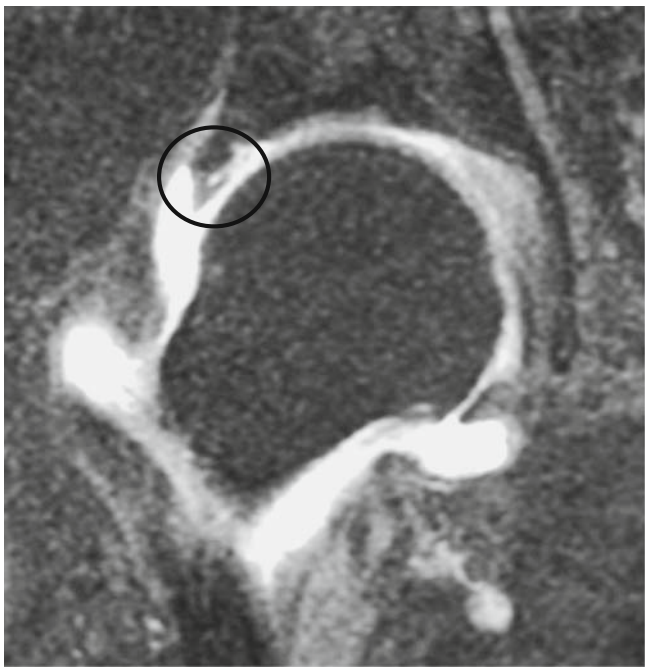

Fig. 5.138 Coronal T1W FS MR hip arthrogram image showing a tear of the superior labrum with high signal within the substance of the labrum and extending to its free edge (*circle*)

of the DRUJ, forming a strong bridge across the distal joint. Second, the TFCC complex is a major stabilizer of the ulnar side of the carpus via the ulnocarpal ligaments. Third, and perhaps most significant, the TFCC acts as a shock absorber for compressive loads placed across the ulnar side of the carpus. These loads are exponentially increased in falls on an outstretched, dorsiflexed hand. Finally, it also plays a role as a pulley for the overlying extensor carpi ulnaris tendon.

Tears of the TFCC may result in carpal instability. Patients may present with pain and clicking in the ulnar side of the wrist, but often tears are detected incidentally at imaging. Here again, the issue of clinical significance of asymptomatic tears arises. To date, their significance remains uncertain.

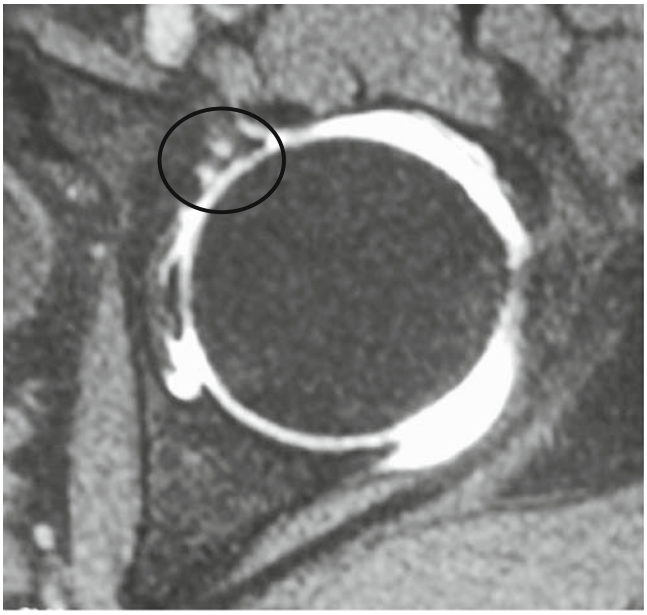

Fig. 5.139 Axial T1W FS MR hip arthrogram image showing a tear of the anterior labrum with high signal within the substance of the labrum extending to its free edge (*circle*)

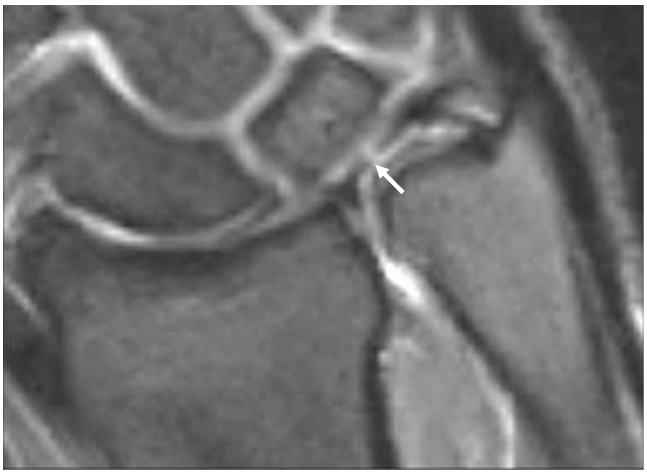

Fig. 5.141 Coronal T1W FS MR wrist arthrogram image showing a defect in the body of the TFCC (*arrow*). This represents a Palmer Ia tear of the TFCC

Some studies have shown that TFCC tears, though symptomatic initially, do not progress over time if the wrist has neutral ulnar variance (the distal ulna is parallel with the distal radius). Furthermore, as many as one-thirds of patients may become asymptomatic over time without therapy.

Palmer classified acute traumatic TFCC tears into four types:

IA – Traumatic perforation;
IB – Ulnar attachments avulsion;
IC – Distal carpal attachment avulsion;
ID – Radial attachment avulsion.

The "I" designates an acute tear. Of these, type A and B tears are most common (Fig. 5.141). Type C is rare. Of all four types, only type B tears occur in a vascularized region of the TFCC. As a result they may heal without therapy; other tears must be debrided and treated surgically. Considering that type C tears occur at the base of the TFCC, the presence of a vascular supply is predictable. The peripheral portion of the knee menisci, known as the red zone, is also vascular and meniscal tears in this region may also heal.

Traditionally, the diagnosis of TFCC tears was made using standard multiple compartment injection arthrography. This technique has largely been supplanted by MRI, particularly MR arthrography. Although it is possible to visualize some tears without intraarticular contrast injection, small and subtle tears require contrast, at least at 1.5 T imaging. Even so, the diagnosis of a large TFCC tear is often made while

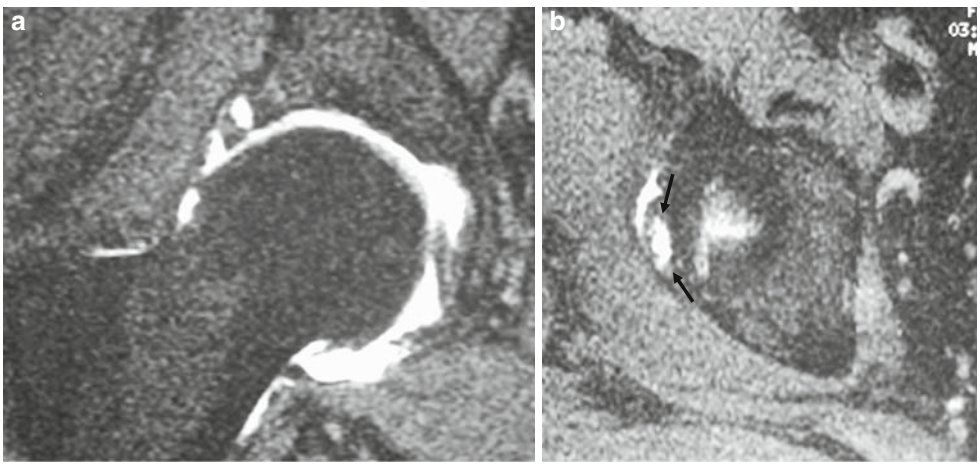

Fig. 5.140 Coronal (**a**) and axial (**b**) T1W FS MR hip arthrogram images showing a tear of the superior labrum with cyst formation within the labrum (**a**) and extending beyond its lateral margin (**b**) (*arrows*)

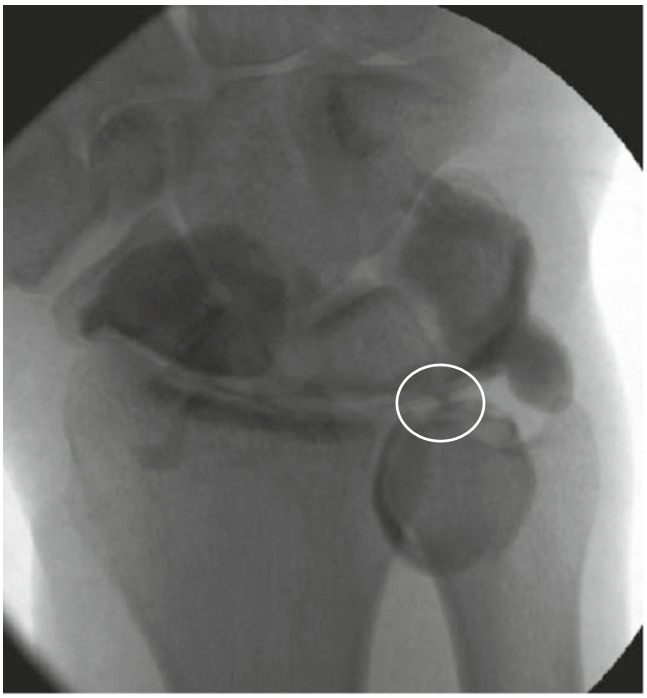

Fig. 5.142 PA wrist spot radiograph from a wrist arthrogram showing a Palmer Ia tear of the TFCC (*circle*)

injecting the patient before the scan (Fig. 5.142). The scan, even in these cases, helps to delineate the size of the tear and accompanying findings. For example, the MRI may give information regarding accompanying hyaline cartilage malacia and thereby suggest that the tear may be of a more chronic variety and so fall into the second portion of the Palmer classification that describes chronic degenerative changes of the TFCC and surrounding structures:

IIA – Irregularity of the TFCC.
IIB – Irregularity of the TFCC associated with adjacent lunate or triquetral malacia.
IIC – TFCC perforation with lunate or triquetral malacia.
IID – TFCC perforation with associated intrinsic lunotriquetral ligament tear.
IIE – TFCC perforation and lunotriquetral ligament tear with developing proximal carpal osteoarthritis.

Imaging may also provide information about other chronic traumatic conditions of the wrist. Primarily, these include impaction syndromes and instability complexes. In the former, differences in the relative length of the ulna and the radius (ulnar variance) or of the ulnar styloid process may result in abnormal carpal bone motion and hence abnormal focal forces on the bones and their hyaline cartilage coating. MRI depicts these syndromes as areas of marrow edema and high signal within the hyaline cartilage. The pattern of involved bones and the osseous anatomy allow diagnosis of the correct impaction syndrome.

In the latter, chronic carpal instability arising from chronic intrinsic and extrinsic carpal ligament tears leads to abnormal motion of the carpal bones relative to one another. These instabilities can be diagnosed on plain radiography, but MRI may give more clues to the underlying etiology of the instability by identifying the torn ligaments conclusively.

Conclusion

The diagnosis of trauma, both osseous and soft tissue, is a vast topic that requires detailed discussion and we encourage the reader to pursue these topics in more detail. The purpose of this chapter has been to serve as an introduction to the topic. We have intended to provide a conceptual framework on which to build. Our goal was to show the underlying biomechanical principles by which trauma can be understood and the resulting commonalities among different types of trauma at all locations throughout the body.

Further Readings

Osseous Trauma and Bone Biomechanics

1. Aaron RK, Ciombor DM, Wang S, Simon B. Clinical biophysics: the promotion of skeletal repair by physical forces. Ann NY Acad Sci 2006 Apr; 1068:513–531.
2. Abraham FF. Very large scale simulations of materials failure. Philos Transact A Math Phys Eng Sci 2002 Mar 15; 360(1792):367–382.
3. Akkus O, Yeni YN, Wasserman N. Fracture mechanics of cortical bone tissue: a hierarchical perspective. Crit Rev Biomed Eng 2004; 32(5–6):379–426.
4. Altizer L. Forearm and humeral fractures. Orthop Nurs 2003 Jul–Aug; 22(4):266–273.
5. Ammann P, Rizzoli R. Bone strength and its determinants. Osteoporos Int 2003; 14(Suppl 3):S13–18. Epub 2003 Mar 19.
6. Augat P, Schorlemmer S. The role of cortical bone and its microstructure in bone strength. Age Ageing 2006 Sep; 35(Suppl 2):227–231.
7. Augat P, Simon U, Liedert A, Claes L. Mechanics and mechano-biology of fracture healing in normal and osteoporotic bone. Osteoporos Int. 2005 Mar; 16(Suppl 2):S36–43. Epub 2004 Sep 15.
8. Babis GC, Soucacos PN. Bone scaffolds: the role of mechanical stability and instrumentation. Injury 2005 Nov; 36(Suppl 4):S38–44.

9. Bano KY, Kahlon RS. Radial head fractures – advanced techniques in surgical management and rehabilitation. J Hand Ther 2006 Apr–Jun; 19(2):114–135.
10. Bolin D, Kemper A, Brolinson PG. Current concepts in the evaluation and management of stress fractures. Curr Sports Med Rep 2005 Dec; 4(6):295–300.
11. Bonnaire F, Zenker H, Lill C, Weber AT, Linke B. Treatment strategies for proximal femur fractures in osteoporotic patients. Osteoporos Int 2005 Mar; 16(Suppl 2):S93–102. Epub 2004 Oct 16.
12. Bouxsein ML, Karasik D. Bone geometry and skeletal fragility. Curr Osteoporos Rep 2006 Jun; 4(2):49–56.
13. Bouxsein ML. Determinants of skeletal fragility. Best Pract Res Clin Rheumatol 2005 Dec; 19(6):897–911.
14. Boyde A. The real response of bone to exercise. J Anat 2003 Aug; 203(2):173–189.
15. Brownbill RA, Ilich JZ. Hip geometry and its role in fracture: what do we know so far? Curr Osteoporos Rep 2003 Jun; 1(1):25–31.
16. Cain EL Jr, Dugas JR, Wolf RS, Andrews JR. Elbow injuries in throwing athletes: a current concepts review. Am J Sports Med 2003 Jul–Aug; 31(4):621–635.
17. Ceder L. Predicting the success of rehabilitation following hip fractures. Disabil Rehabil 2005 Sep 30–Oct 15; 27(18–19):1073–1080.
18. Chao EY, Inoue N. Biophysical stimulation of bone fracture repair, regeneration and remodelling. Eur Cell Mater 2003 Dec 31; 6:72–84; discussion 84–85.
19. Childs SG. Stimulators of bone healing. Biologic and biomechanical. Orthop Nurs 2003 Nov–Dec; 22(6): 421–428.
20. Currey JD. Bone architecture and fracture. Curr Osteoporos Rep 2005 Jun; 3(2):52–56.
21. Currey JD. How well are bones designed to resist fracture? J Bone Miner Res. 2003 Apr; 18(4):591–598.
22. Dalle Carbonare L, Giannini S. Bone microarchitecture as an important determinant of bone strength. J Endocrinol Invest. 2004 Jan; 27(1):99–105.
23. DeGoede KM, Ashton-Miller JA, Schultz AB. Fall-related upper body injuries in the older adult: a review of the biomechanical issues. J Biomech 2003 Jul; 36(7):1043–1053.
24. Doblare M, Garcia JM. On the modelling bone tissue fracture and healing of the bone tissue. Acta Cient Venez 2003; 54(1):58–75.
25. Egol KA, Kubiak EN, Fulkerson E, Kummer FJ, Koval KJ. Biomechanics of locked plates and screws. J Orthop Trauma 2004 Sep; 18(8):488–493.
26. Einhorn TA. The structural properties of normal and osteoporotic bone. Instr Course Lect 2003; 52:533–539.
27. Ferguson SJ, Steffen T. Biomechanics of the aging spine. Eur Spine J 2003 Oct; 12(Suppl 2):S97–103. Epub 2003 Sep 9.
28. Frakes MA, Evans T. Evaluation and management of the patient with LeFort facial fractures. J Trauma Nurs 2004 Jul–Sep; 11(3):95–101.
29. Frost HM. Bone's mechanostat: a 2003 update. Anat Rec A Discov Mol Cell Evol Biol 2003 Dec; 275(2): 1081–1101.
30. Furman BD, Olson SA, Guilak F. The development of posttraumatic arthritis after articular fracture. J Orthop Trauma 2006 Nov–Dec; 20(10):719–725.
31. Fyhrie DP. Summary – Measuring "bone quality". J Musculoskelet Neuronal Interact 2005 Oct–Dec; 5(4):318–320.
32. Guilak F, Fermor B, Keefe FJ, Kraus VB, Olson SA, Pisetsky DS, Setton LA, Weinberg JB. The role of biomechanics and inflammation in cartilage injury and repair. Clin Orthop Relat Res. 2004 Jun; (423):17–26.
33. Hart ES, Albright MB, Rebello GN, Grottkau BE. Broken bones: common pediatric fractures – Part I. Orthop Nurs 2006 Jul–Aug; 25(4):251–256.
34. Helmy N, Hintermann B. New trends in the treatment of proximal humerus fractures. Clin Orthop Relat Res. 2006 Jan; 442:100–108.
35. Hoch AZ, Pepper M, Akuthota V. Stress fractures and knee injuries in runners. Phys Med Rehabil Clin N Am 2005 Aug; 16(3):749–777.
36. Hogan KA, Gross RH. Overuse injuries in pediatric athletes. Orthop Clin North Am. 2003 Jul; 34(3):405–415.
37. Indelli PF, Nisbet JK, Taljanovic MS, Cohen R, Grana WA. Subchondral fracture of the hip caused by axial loading: a case report and review of the literature. Am J Orthop. 2005 Apr; 34(4):198–201.
38. Jacobson JA, Miller BS, Morag Y. Golf and racquet sports injuries. Semin Musculoskelet Radiol. 2005 Dec; 9(4):346–359.
39. Jee WS, Tian XY. The benefit of combining non-mechanical agents with mechanical loading: a perspective based on the Utah paradigm of skeletal physiology. J Musculoskelet Neuronal Interact 2005 Jun; 5(2): 110–118.
40. Kadel NJ. Foot and ankle injuries in dance. Phys Med Rehabil Clin N Am 2006 Nov; 17(4):813–826, vii.
41. Karlsson M. Has exercise an antifracture efficacy in women? Scand J Med Sci Sports 2004 Feb; 14(1):2–15.
42. Kehoe T. Bone quality: a perspective from the Food and Drug Administration. Curr Osteoporos Rep 2006 Jun; 4(2):76–79.
43. Kiuru MJ, Pihlajamaki HK, Ahovuo JA. Bone stress injuries. Acta Radiol 2004 May; 45(3):317–326.
44. Knapik JJ, Reynolds KL, Harman E. Soldier load carriage: historical, physiological, biomechanical, and medical aspects. Mil Med 2004 Jan; 169(1):45–56.
45. Kohrt WM, Bloomfield SA, Little KD, Nelson ME, Yingling VR. American College of Sports Medicine.

American College of Sports Medicine Position Stand: physical activity and bone health. Med Sci Sports Exerc 2004 Nov; 36(11):1985–1996.
46. Lane JM, Gardner MJ, Lin JT, van der Meulen MC, Myers E. The aging spine: new technologies and therapeutics for the osteoporotic spine. Eur Spine J 2003 Oct; 12(Suppl 2):S147–154. Epub 2003 Oct 8.
47. LaStayo PC, Lee MJ. The forearm complex: anatomy, biomechanics and clinical considerations. J Hand Ther 2006 Apr–Jun; 19(2):137–144.
48. Mandi DM, Nickles WA, Mandracchia VJ, Halligan JB, Toney PA. Ankle fractures. Clin Podiatr Med Surg 2006 Apr; 23(2):375–422, vii.
49. May TJ, Judy TA, Conti M, Cowan JE. Current treatment of plantar fasciitis. Curr Sports Med Rep 2002 Oct; 1(5):278–284.
50. McDonough EB, Crosby LA. Periprosthetic fractures of the humerus. Am J Orthop. 2005 Dec; 34(12): 586–591.
51. Megas P. Classification of non-union. Injury 2005 Nov; 36(Suppl 4):S30–37. Erratum in: Injury. 2006 Sep; 37(9):927.
52. Mehta JA, Bain GI. Elbow dislocations in adults and children. Clin Sports Med 2004 Oct; 23(4):609–627, ix.
53. Meyer U, Kruse-Losler B, Wiesmann HP. Principles of bone formation driven by biophysical forces in craniofacial surgery. Br J Oral Maxillofac Surg 2006 Aug; 44(4):289–295. Epub 2005 Sep 12.
54. Muller R, van Lenthe GH. Trabecular bone failure at the microstructural level. Curr Osteoporos Rep 2006 Jun; 4(2):80–86.
55. Murray PM. Diagnosis and treatment of longitudinal instability of the forearm. Tech Hand Up Extrem Surg 2005 Mar; 9(1):29–34.
56. Murray SR, Reeder MT, Udermann BE, Pettitt RW. High-risk stress fractures: pathogenesis, evaluation, and treatment. Compr Ther 2006 Spring; 32(1):20–25.
57. Niemeyer P, Sudkamp NP. Principles and clinical application of the locking compression plate (LCP). Acta Chir Orthop Traumatol Cech 2006 Aug; 73(4):221–228.
58. Nijs S, Broos PL. Fractures of the distal radius: a contemporary approach. Acta Chir Belg 2004 Aug; 104(4):401–412.
59. Nuti R, Martini G, Merlotti D, Valleggi F, De Paola V, Gennari L. Professional sport activity and micronutrients: effects on bone mass. J Endocrinol Invest 2005; 28(Suppl 10):52–60.
60. O'Brien FJ, Brennan O, Kennedy OD, Lee TC. Microcracks in cortical bone: how do they affect bone biology? Curr Osteoporos Rep 2005 Jun; 3(2):39–45.
61. O'Brien MF. Low-grade isthmic/lytic spondylolisthesis in adults. Instr Course Lect 2003; 52:511–524.
62. Pepper M, Akuthota V, McCarty EC. The pathophysiology of stress fractures. Clin Sports Med 2006 Jan; 25(1):1–16, vii.
63. Perren SM. Evolution of the internal fixation of long bone fractures. The scientific basis of biological internal fixation: choosing a new balance between stability and biology. J Bone Joint Surg Br 2002 Nov; 84(8): 1093–1110.
64. Rodeo SA, Maher SA, Hidaka C. What's new in orthopaedic research. J Bone Joint Surg Am 2004 Sep; 86-A(9):2085–2095.
65. Runge M, Schacht E. Multifactorial pathogenesis of falls as a basis for multifactorial interventions. J Musculoskelet Neuronal Interact 2005 Jun; 5(2):127–134.
66. Santavirta S, Bohler M, Harris WH, Konttinen YT, Lappalainen R, Muratoglu O, Rieker C, Salzer M. Alternative materials to improve total hip replacement tribology. Acta Orthop Scand 2003 Aug; 74(4):380–388.
67. Saraph V, Linhart WE. Modern treatment of pathological fractures in children. Injury 2005 Feb; 36(Suppl 1): A64–74.
68. Schonau E. The peak bone mass concept: is it still relevant? Pediatr Nephrol 2004 Aug; 19(8):825–831. Epub 2004 Jun 9.
69. Seeman E, Delmas PD. Bone quality – the material and structural basis of bone strength and fragility. N Engl J Med 2006 May 25; 354(21):2250–2261.
70. Seeman E. The structural and biomechanical basis of the gain and loss of bone strength in women and men. Endocrinol Metab Clin North Am 2003 Mar; 32(1): 25–38.
71. Shugars RA, More RC. Arthroscopic hip surgery. AORN J. 2005 Dec;82(6):976, 978–984, 986–992 passim; quiz 999–1002.
72. Suominen H. Muscle training for bone strength. Aging Clin Exp Res 2006 Apr; 18(2):85–93.
73. Szulc P. Bone density, geometry, and fracture in elderly men. Curr Osteoporos Rep 2006 Jun; 4(2):57–63.
74. Taylor NF, Dodd KJ, Damiano DL. Progressive resistance exercise in physical therapy: a summary of systematic reviews. Phys Ther 2005 Nov; 85(11):1208–1223.
75. Turner CH. Bone strength: current concepts. Ann NY Acad Sci 2006 Apr; 1068:429–446.
76. Vashishth D. Age-dependent biomechanical modifications in bone. Crit Rev Eukaryot Gene Expr 2005; 15(4):343–358.
77. Viguet-Carrin S, Garnero P, Delmas PD. The role of collagen in bone strength. Osteoporos Int. 2006; 17(3): 319–336. Epub 2005 Dec 9.
78. Wang X, Puram S. The toughness of cortical bone and its relationship with age. Ann Biomed Eng 2004 Jan; 32(1):123–135.

79. Wearing SC, Hennig EM, Byrne NM, Steele JR, Hills AP. Musculoskeletal disorders associated with obesity: a biomechanical perspective. Obes Rev 2006 Aug; 7(3):239–250.
80. Zura RD, Browne JA. Current concepts in locked plating. J Surg Orthop Adv 2006 Fall; 15(3):173–176.

Dislocations

1. Bishop JY, Flatow EL. Pediatric shoulder trauma. Clin Orthop Relat Res 2005 Mar; (432):41–48.
2. Bishop JY, Kaeding C. Treatment of the acute traumatic acromioclavicular separation. Sports Med Arthrosc 2006 Dec; 14(4):237–245.
3. Brucker PU, Gruen GS, Kaufmann RA. Scapulothoracic dissociation: evaluation and management. Injury 2005 Oct; 36(10):1147–1155. Epub 2005 Feb 23.
4. Budoff JE, Wolf EM. Arthroscopic treatment of glenohumeral instability. J Hand Surg [Am] 2006 Oct; 31(8):1387–1396.
5. Cheng CY, Hsu KY, Tseng IC, Shih HN. Concurrent scaphoid fracture with scapholunate ligament rupture. Acta Orthop Belg 2004 Oct; 70(5):485–491.
6. Christian SR, Anderson MB, Workman R, Conway WF, Pope TL. Imaging of anterior knee pain. Clin Sports Med 2006 Oct; 25(4):681–702.
7. Chung CB, Stanley AJ, Gentili A. Magnetic resonance imaging of elbow instability. Semin Musculoskelet Radiol. 2005 Mar; 9(1):67–76.
8. Clohisy JC, Keeney JA, Schoenecker PL. Preliminary assessment and treatment guidelines for hip disorders in young adults. Clin Orthop Relat Res. 2005 Dec; 441:168–179.
9. De Baere T, Delloye C. First-time traumatic anterior dislocation of the shoulder in young adults: the position of the arm during immobilisation revisited. Acta Orthop Belg 2005 Oct; 71(5):516–520.
10. Desmond EA, Chou LB. Current concepts review: Lisfranc injuries. Foot Ankle Int 2006 Aug; 27(8): 653–660.
11. Dillon JE, Connolly SA, Connolly LP, Kim YJ, Jaramillo D. MR imaging of congenital/developmental and acquired disorders of the pediatric hip and pelvis. Magn Reson Imaging Clin N Am 2005 Nov; 13(4): 783–797.
12. Elias DA, White LM. Imaging of patellofemoral disorders. Clin Radiol 2004 Jul; 59(7):543–557.
13. Emery KH. Imaging of sports injuries of the upper extremity in children. Clin Sports Med 2006 Jul; 25(3):543–568, viii.
14. Frick MA. Imaging of the elbow: a review of imaging findings in acute and chronic traumatic disorders of the elbow. J Hand Ther 2006 Apr–Jun; 19(2): 98–112.
15. Gove N, Ebraheim NA, Glass E. Posterior sternoclavicular dislocations: a review of management and complications. Am J Orthop 2006 Mar; 35(3):132–136.
16. Grabow RJ, Catalano L III. Carpal dislocations. Hand Clin 2006 Nov; 22(4):485–500; Abstract vi–vii.
17. Handoll HH, Hanchard NC, Goodchild L, Feary J. Conservative management following closed reduction of traumatic anterior dislocation of the shoulder. Cochrane Database Syst Rev 2006 Jan 25; (1):CD004962.
18. Harvey C, Bhakoo P, Allen S, O'Regan D. Interpretation of paediatric trauma. Br J Hosp Med (Lond) 2006 Jul; 67(7):M134–137.
19. Hassett RG. The role of imaging of work-related upper extremity disorders. Clin Occup Environ Med 2006; 5(2):285–298, vii.
20. Hunt SA, Ropiak C, Tejwani NC. Lisfranc joint injuries: diagnosis and treatment. Am J Orthop 2006 Aug; 35(8):376–385.
21. Jenabzadeh AR, Haddad FS. Injuries around the elbow. Br J Hosp Med (Lond) 2005 Oct; 66(10):M54–55
22. Juliano PJ, Dabbah M, Harris TG. Talar neck fractures. Foot Ankle Clin 2004 Dec; 9(4):723–736, vi.
23. Kovacic J, Bergfeld J. Return to play issues in upper extremity injuries. Clin J Sport Med 2005 Nov; 15(6):448–452.
24. Labler L, Eid K, Platz A, Trentz O, Kossmann T. Atlanto-occipital dislocation: four case reports of survival in adults and review of the literature. Eur Spine J 2004 Mar; 13(2):172–180. Epub 2003 Dec 13.
25. Labriola JE, Lee TQ, Debski RE, McMahon PJ. Stability and instability of the glenohumeral joint: the role of shoulder muscles. J Shoulder Elbow Surg 2005 Jan–Feb; 14(Suppl 1):S32–38.
26. Langlais F, Lambotte JC, Lannou R, Gedouin JE, Belot N, Thomazeau H, Frieh, JM, Gouin F, Hulet C, Marin F, Migaud H, Sadri H, Vielpeau C, Richter D. Hip pain from impingement and dysplasia in patients aged 20–50 years. Workup and role for reconstruction. Joint Bone Spine 2006 Dec; 73(6):614–623. Epub 2006 Oct 25.
27. LaStayo PC, Lee MJ. The forearm complex: anatomy, biomechanics and clinical considerations. J Hand Ther 2006 Apr–Jun; 19(2):137–144.
28. Levine WN, Rieger K, McCluskey GM III. Arthroscopic treatment of anterior shoulder instability. Instr Course Lect 2005; 54:87–96.
29. Lindley SG, Rulewicz G. Hand fractures and dislocations in the developing skeleton. Hand Clin 2006 Aug; 22(3):253–268.

30. Manaster BJ, Zakel S. Imaging of femoral acetabular impingement syndrome. Clin Sports Med 2006 Oct; 25(4):635–657.
31. Mangi Q, Ridgway PF, Ibrahim Z, Evoy D. Dislocation of the mandible. Surg Endosc 2004 Mar; 18(3):554–556. Review. Erratum in: Surg Endosc 2004 May; 18(5):874. Ridgway RF.
32. McFarland EG, Gill HS, Laporte DM, Streiff M. Miscellaneous conditions about the elbow in athletes. Clin Sports Med 2004 Oct; 23(4):743–763, xi–xii.
33. Mehta JA, Bain GI. Posterolateral rotatory instability of the elbow. J Am Acad Orthop Surg 2004 Nov–Dec; 12(6):405–415.
34. Morrey BF. Results of reoperation for hip dislocation: the big picture. Clin Orthop Relat Res 2004 Dec; (429):94–101.
35. Pacelli LL, Guzman M, Botte MJ. Elbow instability: the orthopedic approach. Semin Musculoskelet Radiol 2005 Mar; 9(1):56–66.
36. Papatheodorou A, Ellinas P, Takis F, Tsanis A, Maris I, Batakis N. US of the shoulder: rotator cuff and non-rotator cuff disorders. Radiographics 2006 Jan–Feb; 26(1):e23.
37. Quick TJ, Eastwood DM. Pediatric fractures and dislocations of the hip and pelvis. Clin Orthop Relat Res 2005 Mar; (432):87–96.
38. Quillen DM, Wuchner M, Hatch RL. Acute shoulder injuries. Am Fam Physician 2004 Nov 15; 70(10): 1947–1954.
39. Rafii M. Non-contrast MR imaging of the glenohumeral joint. Part II. Glenohumeral instability and labrum tears. Skeletal Radiol 2004 Nov; 33(11):617–626. Epub 2004 Sep 16.
40. Rasool MN. Dislocations of the elbow in children. J Bone Joint Surg Br 2004 Sep; 86(7):1050–1058.
41. Robertson A, Nutton RW, Keating JF. Dislocation of the knee. J Bone Joint Surg Br 2006 Jun; 88(6):706–711.
42. Robinson CM, Dobson RJ. Anterior instability of the shoulder after trauma. J Bone Joint Surg Br 2004 May; 86(4):469–479.
43. Saati AZ, McKee MD. Fracture-dislocation of the elbow: diagnosis, treatment, and prognosis. Hand Clin 2004 Nov; 20(4):405–414.
44. Shindle MK, Ranawat AS, Kelly BT. Diagnosis and management of traumatic and atraumatic hip instability in the athletic patient. Clin Sports Med 2006 Apr; 25(2):309–326, ix–x.
45. Smith TO. Immobilisation following traumatic anterior glenohumeral joint dislocation: a literature review. Injury 2006 Mar; 37(3):228–237. Epub 2005 Aug 24.
46. Soprano JV. Musculoskeletal injuries in the pediatric and adolescent athlete. Curr Sports Med Rep 2005 Dec; 4(6):329–334.
47. Steinbach LS. Magnetic resonance imaging of glenohumeral joint instability. Semin Musculoskelet Radiol 2005 Mar; 9(1):44–55.
48. Tashjian RZ, Katarincic JA. Complex elbow instability. J Am Acad Orthop Surg 2006 May; 14(5):278–286.
49. Ufberg JW, Vilke GM, Chan TC, Harrigan RA. Anterior shoulder dislocations: beyond traction-countertraction. J Emerg Med 2004 Oct; 27(3):301–306.

Muscle and Tendon Strain, Ligament Sprain and Traumatic Tendonitis

1. Armfield DR, Kim DH, Towers JD, Bradley JP, Robertson DD. Sports-related muscle injury in the lower extremity. Clin Sports Med 2006 Oct; 25(4):803–842.
2. Banks KP, Ly JQ, Beall DP, Grayson DE, Bancroft LW, Tall MA. Overuse injuries of the upper extremity in the competitive athlete: magnetic resonance imaging findings associated with repetitive trauma. Curr Probl Diagn Radiol 2005 Jul–Aug; 34(4):127–142.
3. Barr AE, Barbe MF, Clark BD. Work-related musculoskeletal disorders of the hand and wrist: epidemiology, pathophysiology, and sensorimotor changes. J Orthop Sports Phys Ther 2004 Oct; 34(10):610–627.
4. Bencardino JT, Rosenberg ZS. Sports-related injuries of the wrist: an approach to MRI interpretation. Clin Sports Med 2006 Jul; 25(3):409–432, vi.
5. Bencardino JT, Mellado JM. Hamstring injuries of the hip. Magn Reson Imaging Clin N Am 2005 Nov; 13(4):677–690, vi.
6. Bencardino JT, Rosenberg ZS. Entrapment neuropathies of the shoulder and elbow in the athlete. Clin Sports Med 2006 Jul; 25(3):465–487, vi–vii.
7. Bencardino JT, Rosenberg ZS. Sports-related injuries of the wrist: an approach to MRI interpretation. Clin Sports Med 2006 Jul; 25(3):409–432, vi.
8. Benjamin HJ, Briner WW Jr. Little league elbow. Clin J Sport Med 2005 Jan; 15(1):37–40.
9. Bredella MA, Stoller DW. MR imaging of femoroacetabular impingement. Magn Reson Imaging Clin N Am 2005 Nov; 13(4):653–664.
10. Cassas KJ, Cassettari-Wayhs A. Childhood and adolescent sports-related overuse injuries. Am Fam Physician 2006 Mar 15; 73(6):1014–1022.
11. Cerezal L, del Pinal F, Abascal F. MR imaging findings in ulnar-sided wrist impaction syndromes. Magn Reson Imaging Clin N Am 2004 May; 12(2):281–299, vi.
12. De Marchi A, Robba T, Ferrarese E, Faletti C. Imaging in musculoskeletal injuries: state of the art. Radiol Med (Torino) 2005 Jul–Aug; 110(1–2):115–131.

13. Edson CJ. Conservative and postoperative rehabilitation of isolated and combined injuries of the medial collateral ligament. Sports Med Arthrosc 2006 Jun; 14(2): 105–110.
14. Elsayes KM, Lammle M, Shariff A, Totty WG, Habib IF, Rubin DA. Value of magnetic resonance imaging in muscle trauma. Curr Probl Diagn Radiol 2006 Sep–Oct; 35(5):206–212.
15. Emery KH. Imaging of sports injuries of the upper extremity in children. Clin Sports Med 2006 Jul; 25(3):543–568, viii.
16. Ferran NA, Oliva F, Maffulli N. Recurrent subluxation of the peroneal tendons. Sports Med 2006; 36(10): 839–846.
17. Harish S, O'Donnell P, Connell D, Saifuddin A. Imaging of the posterolateral corner of the knee. Clin Radiol 2006 Jun; 61(6):457–466.
18. Hayes CW, Coggins CA. Sports-related injuries of the knee: an approach to MRI interpretation. Clin Sports Med 2006 Oct; 25(4):659–679.
19. Hermann BF. Ligament injuries of the hand and wrist. Clin Occup Environ Med 2006; 5(2):323–331, vii.
20. Hillier JC, Peace K, Hulme A, Healy JC. Pictorial review: MRI features of foot and ankle injuries in ballet dancers. Br J Radiol 2004 Jun; 77(918):532–537.
21. Hreljac A. Impact and overuse injuries in runners. Med Sci Sports Exerc 2004 May; 36(5):845–849.
22. Ivins D. Acute ankle sprain: an update. Am Fam Physician 2006 Nov 15; 74(10):1714–1720.
23. Kadel NJ. Foot and ankle injuries in dance. Phys Med Rehabil Clin N Am 2006 Nov; 17(4):813–826, vii.
24. Kennedy JG, Knowles B, Dolan M, Bohne W. Foot and ankle injuries in the adolescent runner. Curr Opin Pediatr 2005 Feb; 17(1):34–42.
25. Kijowski R, Tuite M, Sanford M. Magnetic resonance imaging of the elbow. Part I: normal anatomy, imaging technique, and osseous abnormalities. Skeletal Radiol 2004 Dec; 33(12):685–697. Epub 2004 Oct 5.
26. Koulouris G, Connell D. Imaging of hamstring injuries: therapeutic implications. Eur Radiol 2006 Jul; 16(7):1478–1487. Epub 2006 Mar 3.
27. Latz K. Overuse injuries in the pediatric and adolescent athlete. Mo Med 2006 Jan–Feb; 103(1):81–85.
28. Lin CF, Gross ML, Weinhold P. Ankle syndesmosis injuries: anatomy, biomechanics, mechanism of injury, and clinical guidelines for diagnosis and intervention. J Orthop Sports Phys Ther 2006 Jun; 36(6):372–384.
29. Linklater J. Ligamentous, chondral, and osteochondral ankle injuries in athletes. Semin Musculoskelet Radiol 2004 Mar; 8(1):81–98.
30. Ly JQ, Sanders TG, Beall DP. MR imaging of the elbow: a spectrum of common pathologic conditions. Clin Imaging 2005 Jul–Aug; 29(4):278–282.
31. Matherne TH, Monu JU, Schruff L, Neitzschman HR. Avulsions around the knee portend instability. Emerg Radiol 2005 Jun; 11(4):213–218.
32. Melloni P, Valls R. The use of MRI scanning for investigating soft-tissue abnormalities in the elbow. Eur J Radiol 2005 May; 54(2):303–313.
33. Miller C. Dance medicine: current concepts. Phys Med Rehabil Clin N Am 2006 Nov; 17(4):803–811, vii.
34. Nassab PF, Schickendantz MS. Evaluation and treatment of medial ulnar collateral ligament injuries in the throwing athlete. Sports Med Arthrosc 2006 Dec; 14(4): 221–231.
35. Nelson EN, Kassarjian A, Palmer WE. MR imaging of sports-related groin pain. Magn Reson Imaging Clin N Am 2005 Nov; 13(4):727–742.
36. Orchard J, Best TM, Verrall GM. Return to play following muscle strains. Clin J Sport Med 2005 Nov; 15(6):436–441.
37. Ouellette H, Kassarjian A, Tretreault P, Palmer W. Imaging of the overhead throwing athlete. Semin Musculoskelet Radiol 2005 Dec; 9(4):316–333.
38. Paavola M, Jarvinen TA. Paratendinopathy. Foot Ankle Clin 2005 Jun; 10(2):279–292.
39. Pena FA, Coetzee JC. Ankle syndesmosis injuries. Foot Ankle Clin 2006 Mar; 11(1):35–50, viii.
40. Pleacher MD, Glazer JL. Lower extremity soft tissue conditions. Curr Sports Med Rep 2005 Oct; 4(5): 255–261.
41. Potter HG, Ho ST, Altchek DW. Magnetic resonance imaging of the elbow. Semin Musculoskelet Radiol 2004 Mar; 8(1):5–16.
42. Quillen DM, Wuchner M, Hatch RL. Acute shoulder injuries. Am Fam Physician 2004 Nov 15; 70(10): 1947–1954.
43. Robinson P, White LM. The biomechanics and imaging of soccer injuries. Semin Musculoskelet Radiol 2005 Dec; 9(4):397–420.
44. Safran M, Ahmad CS, Elattrache NS. Ulnar collateral ligament of the elbow. Arthroscopy 2005 Nov; 21(11):1381–1395.
45. Shah SN, Miller BS, Kuhn JE. Chronic exertional compartment syndrome. Am J Orthop 2004 Jul; 33(7): 335–341.
46. Soprano JV. Musculoskeletal injuries in the pediatric and adolescent athlete. Curr Sports Med Rep 2005 Dec; 4(6):329–334.
47. Ufberg J, Harrigan RA, Cruz T, Perron AD. Orthopedic pitfalls in the ED: Achilles tendon rupture. Am J Emerg Med 2004 Nov; 22(7):596–600.
48. Wainstein JL, Nailor TE. Tendinitis and tendinosis of the elbow, wrist, and hands. Clin Occup Environ Med 2006; 5(2):299–322, vii.

49. Wilson JJ, Best TM. Common overuse tendon problems: a review and recommendations for treatment. Am Fam Physician 2005 Sep 1; 72(5):811–818.
50. Yu JS, Habib PA. Common injuries related to weightlifting: MR imaging perspective. Semin Musculoskelet Radiol 2005 Dec; 9(4):289–301.

Hyaline Cartilage

1. Armfield DR, Towers JD, Robertson DD. Radiographic and MR imaging of the athletic hip. Clin Sports Med 2006 Apr; 25(2):211–239, viii.
2. Bredella MA, Stoller DW. MR imaging of femoroacetabular impingement. Magn Reson Imaging Clin N Am 2005 Nov; 13(4):653–664.
3. Campbell SE. MRI of sports injuries of the ankle. Clin Sports Med 2006 Oct; 25(4):727–762.
4. Cerezal L, Abascal F, Garcia-Valtuille R, Del Pinal F. Wrist MR arthrography: how, why, when. Radiol Clin North Am 2005 Jul; 43(4):709–731, viii.
5. Chung CB, Isaza IL, Angulo M, Boucher R, Hughes T. MR arthrography of the knee: how, why, when. Radiol Clin North Am 2005 Jul; 43(4):733–746, viii–ix.
6. Crawford DC, Safran MR. Osteochondritis dissecans of the knee. J Am Acad Orthop Surg 2006 Feb; 14(2): 90–100.
7. Eckstein F, Hudelmaier M, Putz R. The effects of exercise on human articular cartilage. J Anat 2006 Apr; 208(4):491–512.
8. Gold GE, Hargreaves BA, Reeder SB, Vasanawala SS, Beaulieu CF. Controversies in protocol selection in the imaging of articular cartilage. Semin Musculoskelet Radiol 2005 Jun; 9(2):161–172.
9. Gold GE, Hargreaves BA, Stevens KJ, Beaulieu CF. Advanced magnetic resonance imaging of articular cartilage. Orthop Clin North Am 2006 Jul; 37(3): 331–347, vi.
10. Lang P, Noorbakhsh F, Yoshioka H. MR imaging of articular cartilage: current state and recent developments. Radiol Clin North Am 2005 Jul; 43(4): 629–639, vii.
11. Lotke PA, Nelson CL, Lonner JH. Spontaneous osteonecrosis of the knee: tibial plateaus. Orthop Clin North Am 2004 Jul; 35(3):365–370, x.
12. Manaster BJ, Johnson T, Narahari U. Imaging of cartilage in the athlete. Clin Sports Med 2005 Jan; 24(1): 13–37.
13. Mosher TJ. MRI of osteochondral injuries of the knee and ankle in the athlete. Clin Sports Med 2006 Oct; 25(4):843–866.
14. Polster J, Recht M. Postoperative MR evaluation of chondral repair in the knee. Eur J Radiol 2005 May; 54(2):206–213.
15. Potter HG, Foo LF. Magnetic resonance imaging of articular cartilage: trauma, degeneration, and repair. Am J Sports Med 2006 Apr; 34(4):661–677. Epub 2005 Dec 19.
16. Rafii M. Non-contrast MR imaging of the glenohumeral joint. Part I. Normal anatomy. Skeletal Radiol 2004 Oct; 33(10):551–560. Epub 2004 Aug 27.
17. Recht MP, Goodwin DW, Winalski CS, White LM. MRI of articular cartilage: revisiting current status and future directions. AJR Am J Roentgenol 2005 Oct; 185(4):899–914.
18. Stanton I, White LM, Satchithananda K, Compson J, Elias DA. The postoperative patellofemoral joint: expected radiological appearances and complications. Curr Probl Diagn Radiol 2006 Mar–Apr; 35(2):55–64.
19. Tsou IY, Yegappan M, Ong WS, Goh PO, Tan JL, Chee TS. Cartilage injury and repair: assessment with magnetic resonance imaging. Singapore Med J 2006 Jan; 47(1):80–87.
20. White LM, Kramer J, Recht MP. MR imaging evaluation of the postoperative knee: ligaments, menisci, and articular cartilage. Skeletal Radiol 2005 Aug; 34(8):431–452. Epub 2005 Jun 21.

Fibrocartilage

1. Bencardino JT, Beltran J. MR imaging of the glenohumeral ligaments. Radiol Clin North Am 2006 Jul; 44(4):489–502, vii.
2. Bencardino JT, Rosenberg ZS. Sports-related injuries of the wrist: an approach to MRI interpretation. Clin Sports Med 2006 Jul; 25(3):409–432, vi.
3. Bin SI, Kim JM, Shin SJ. Radial tears of the posterior horn of the medial meniscus. Arthroscopy 2004 Apr; 20(4):373–378.
4. Boks SS, Vroegindeweij D, Koes BW, Hunink MG, Bierma-Zeinstra SM. Follow-up of posttraumatic ligamentous and meniscal knee lesions detected at MR imaging: systematic review. Radiology 2006 Mar; 238(3):863–871. Epub 2006 Feb 1.
5. Chaipat L, Palmer WE. Shoulder magnetic resonance imaging. Clin Sports Med 2006 Jul; 25(3):371–386, v.
6. Coggins CA. Imaging of ulnar-sided wrist pain. Clin Sports Med 2006 Jul; 25(3):505–526, vii.
7. Court-Payen M. Sonography of the knee: intra-articular pathology. J Clin Ultrasound 2004 Nov–Dec; 32(9): 481–490.

8. De Maeseneer M, Van Roy P, Shahabpour M. Normal MR imaging anatomy of the rotator cuff tendons, glenoid fossa, labrum, and ligaments of the shoulder. Radiol Clin North Am 2006 Jul; 44(4): 479–487, vii.
9. De Smet AA. MR imaging and MR arthrography for diagnosis of recurrent tears in the postoperative meniscus. Semin Musculoskelet Radiol 2005 Jun; 9(2): 116–124.
10. Frick MA, Collins MS, Adkins MC. Postoperative imaging of the knee. Radiol Clin North Am 2006 May; 44(3):367–389.
11. Hayes CW, Coggins CA. Sports-related injuries of the knee: an approach to MRI interpretation. Clin Sports Med 2006 Oct; 25(4):659–679.
12. Jones AO, Houang MT, Low RS, Wood DG. Medial meniscus posterior root attachment injury and degeneration: MRI findings. Australas Radiol 2006 Aug; 50(4):306–313.
13. Lippe CN, Suprock MD. Bilateral medial meniscal cysts in a 15-year-old girl. Am J Orthop 2005 Apr; 34(4): 195–197.
14. Manaster BJ, Johnson T, Narahari U. Imaging of cartilage in the athlete. Clin Sports Med 2005 Jan; 24(1): 13–37.
15. Martin RL, Enseki KR, Draovitch P, Trapuzzano T, Pilippon MJ. Acetabular labral tears of the hip: examination and diagnostic challenges. J Orthop Sports Phys Ther 2006 Jul; 36(7):503–515.
16. McCarthy CL, McNally EG. The MRI appearance of cystic lesions around the knee. Skeletal Radiol 2004 Apr; 33(4):187–209. Epub 2004 Feb 27.
17. McCarty LP III, Cole BJ. Nonarthroplasty treatment of glenohumeral cartilage lesions. Arthroscopy 2005 Sep; 21(9):1131–1142.
18. Naraghi A, White L. MRI evaluation of the postoperative knee: special considerations and pitfalls. Clin Sports Med 2006 Oct; 25(4):703–725.
19. Noyes FR, Barber-Westin SD, Rankin M. Meniscal transplantation in symptomatic patients less than fifty years old. J Bone Joint Surg Am 2005 Sep; 87(Suppl 1) (Pt 2):149–165.
20. Osinski T, Malfair D, Steinbach L. Magnetic resonance arthrography. Orthop Clin North Am 2006 Jul; 37(3):299–319, vi.
21. Petersilge C. Imaging of the acetabular labrum. Magn Reson Imaging Clin N Am 2005 Nov; 13(4): 641–652, vi.
22. Rafii M. Non-contrast MR imaging of the glenohumeral joint. Part II. Glenohumeral instability and labrum tears. Skeletal Radiol 2004 Nov; 33(11):617–626. Epub 2004 Sep 16.
23. Ramnath RR. 3T MR imaging of the musculoskeletal system (Part II): clinical applications. Magn Reson Imaging Clin N Am 2006 Feb; 14(1):41–62.
24. Robinson G, Ho Y, Finlay K, Friedman L, Harish S. Normal anatomy and common labral lesions at MR arthrography of the shoulder. Clin Radiol 2006 Oct; 61(10):805–821.
25. Ruzek KA, Bancroft LW, Peterson JJ. Postoperative imaging of the shoulder. Radiol Clin North Am 2006 May; 44(3):331–341.
26. Sahin G, Demirtas M. An overview of MR arthrography with emphasis on the current technique and applicational hints and tips. Eur J Radiol 2006 Jun; 58(3):416–430. Epub 2006 Feb 7.
27. Steinbach LS. Magnetic resonance imaging of glenohumeral joint instability. Semin Musculoskelet Radiol 2005 Mar; 9(1):44–55.
28. Toms AP, White LM, Marshall TJ, Donell ST. Imaging the post-operative meniscus. Eur J Radiol 2005 May; 54(2):189–198.
29. White LM, Kramer J, Recht MP. MR imaging evaluation of the postoperative knee: ligaments, menisci, and articular cartilage. Skeletal Radiol 2005 Aug; 34(8): 431–452. Epub 2005 Jun 21.
30. Youm T, Chen AL. Discoid lateral meniscus: evaluation and treatment. Am J Orthop 2004 May; 33(5):234–238.
31. Zlatkin MB, Rosner J. MR imaging of ligaments and triangular fibrocartilage complex of the wrist. Radiol Clin North Am 2006 Jul; 44(4):595–623, ix.
32. Zlatkin MB, Rosner J. MR imaging of ligaments and triangular fibrocartilage complex of the wrist. Magn Reson Imaging Clin N Am 2004 May; 12(2):301–331, vi–vii.

Chapter 6

Imaging and Understanding Fracture Fixation

Bahman Rafiee

Abstract In this chapter, the radiological aspects of surgical fracture management are discussed in detail. History of fracture fixation and the work of the pioneers of the field in the early and mid-twentieth century are introduced. Biology of bone healing is discussed in detail, with emphasis on the new understanding of the effect of mechanical environment and the concept of direct and indirect. Techniques of absolute stability that result in direct bone healing, such as lag screw fixation and compression plating, are described. Generations of compression plates from the round hole plate of Müller to dynamic compression plate (DCP), limited-contact dynamic compression plate (LC-DCP), and the more recent locking compression plate (LCP) are discussed at length. Tension band principle and its application to fracture fixation is introduced. Techniques of relative stability resulting in indirect or callus healing are discussed, including a discussion of intramedullary nailing and its various modes, bridge plating, and external fixation. Different types of external fixators and the pioneering work of Gavriil Ilizarov are introduced. The new concepts of internal fixator and less invasive stabilization system (LISS) are also described.

Keywords Fixation • Direct bone healing • Indirect bone healing • Arbeitsgemeinschaft für Osteosynthesefragen (AO) • Lag screw fixation • Tension band wiring • Compression plate • Intramedullary nail • External fixator • Internal fixator • Less invasive stabilization system

Introduction

History of Osteosynthesis

In the nineteenth century, the European surgeons were deeply divided between two opposite schools of thought on fracture healing: *immobilizers* and *mobilizers* [1]. In the first group, prominent surgeons such as Hugh Owen Thomas, the father of British Orthopedic surgery, believed in *total immobilization* (prolonged and uninterrupted) to manage fractures. The second group, including Sir James Paget and Seutin, appreciated the importance of *ambulation* and joint motion during the course of fracture treatment to prevent complications such as joint stiffness, muscle wasting, and osteopenia.

Surgical fracture treatment dates back to the eighteenth century, with wire ligature of the fracture ends by French surgeons. Later in the nineteenth century, early plate and screw fixation techniques were developed. The Belgian surgeon *Albin Lambotte* (1866–1955) is considered the father of *osteosynthesis* [2] and was probably the first to use this term. He manufactured many early surgical instruments and implants, such as plates, screws, and an external fixation device in his workshop.

Most of the screws used at that time had a close resemblance to the traditional wood screw, with its tapered threads and low holding power (Fig. 6.1). Surgeons such as Lambotte, Lane, and Sherman improved upon early screw designs with introduction of parallel-thread screws with improved holding (purchase) power [1].

Despite these early surgical experiences, by the mid-twentieth century fracture treatment methods mainly consisted of plaster immobilization and traction, which had the effect of inhibiting limb and body function during the lengthy healing process. Ultimately, this prompted development of modern open reduction techniques in the latter part of the century. Today, open fixation techniques are the accepted standard practice.

B. Rafiee (✉)
Department of Radiology, Division of Musculoskeletal Imaging, University of Pittsburgh, Pittsburgh, PA 15213, USA
e-mail: rafieeb@upmc.edu; rafieeb@hotmail.com

A. Bonakdarpour et al. (eds.), *Diagnostic Imaging of Musculoskeletal Diseases: A Systematic Approach*,
DOI 10.1007/978-1-59745-355-4_6,

Fig. 6.1 Silicon Bronze wood screws. Courtesy of Merton's fiberglass and marine supply, East Longmeadow, MA

Biology of Bone Healing: The Traditional Concept of Callus Healing

Hunter divided fracture healing into four stages [3, 4] (Fig. 6.2):

1. Stage of hematoma and inflammation (1–7 days).
2. Stage of soft callus (2–3 weeks).
3. Stage of hard callus (2–4 months).
4. Stage of remodeling (several months to several years).

1. *Stage of inflammation and hematoma (1–7 days)*: Immediately following fracture, tissue necrosis occurs at the two ends of fracture. Bleeding from the disrupted vessels causes hematoma formation. An inflammatory response is also initiated with recruitment of inflammatory cells and non-cellular inflammatory elements such as cytokines. Osteoclasts remove the necrotic ends of the bone. Granulation tissue eventually develops and replaces the hematoma.

2. *Stage of soft callus*: During the first 2–3 weeks following the fracture, the osteoprogenitor cells are progressively recruited from the periosteum and endosteum and differentiate into chondroblasts and osteoblasts that replace the granulation tissue. There is also vascular ingrowth reestablishing the blood supply. At the end of this stage, the two ends of fracture are linked with soft callus composed of osteoid, cartilage, and collagen.

3. *Stage of hard callus (2–4 months)*: In the next 2–4 months, progressive osteoid calcification occurs through intramembranous ossification and formation of woven bone. The cartilage at the fracture margins also calcifies through endochondral ossification. At the end of this stage, the fracture has solid hard callus and no motion at the fracture ends. At this point, the patient is clinically pain-free. Radiographically, solid bridging callus is present (Fig. 6.3a).

4. *Stage of Remodeling (several months–years)*: In this stage, the woven bone is gradually converted to lamellar bone. Under the physiologic stresses applied to the bone, continuous bone resorption and apposition occur, and the osteons – the functional units of lamellar or cortical bone – will eventually realign along the longitudinal axis of the bone.

With complete remodeling, more typical in the pediatric age group, the normal architecture and morphology of the bone is restored without any residual deformity and scarring. Radiographically, the areas of prominent callus are remodeled and the medullary canal is restored. Remodeling is usually less than complete in the adult skeleton (Fig. 6.3b).

Robert Danis and the Concept of Callus-Free Bone Healing

Robert Danis (1880–1962) (Fig. 6.4) is regarded as one of the pioneers of modern *osteosynthesis* [1]. He was a professor of surgery at the University of Brussels with great interest in surgical treatment of fractures. Under the influence of the mobilizers' school of thought, he developed his noble concept of *stable internal fixation* to permit functional rehabilitation. He observed that if he applied enough compression to a diaphyseal fracture to create absolute stability and prevent motion between the fracture fragments, healing would take place without callus formation. At the same time, the adjacent joints and muscles could be safely mobilized. He called this process *soudure autogène*, or self-welding. To achieve stability, Danis designed an early compression plate which he called the "Coapteur" [1, 5] (Fig. 6.5).

This was a revolutionary step heralding the modern era of internal fixation. Healing without callus meant significantly reduced healing time that avoids the lengthy remodeling stage.

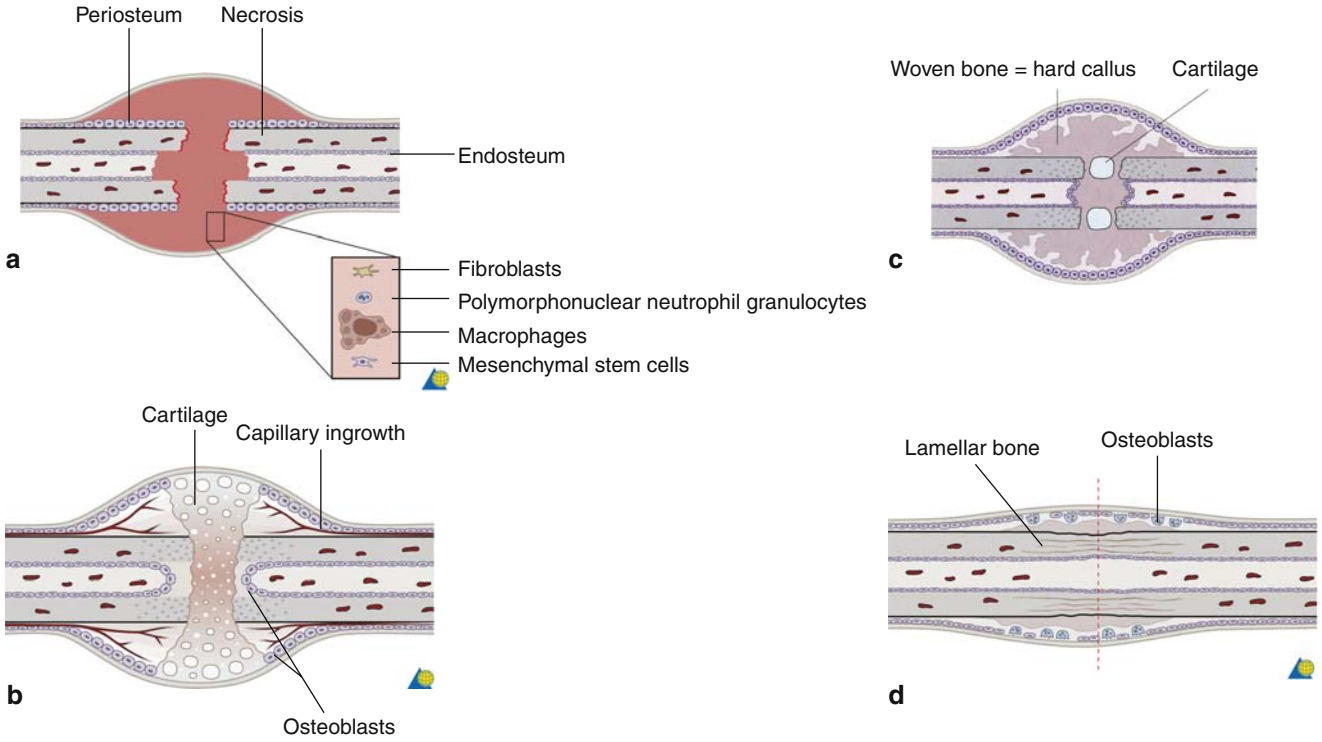

Fig. 6.2 Four stages of callus bone healing. (**a**) *Stage of Inflammation*. Fracture hematoma resolves into granulation tissue with the typical inflammatory cascade. (**b**) *Stage of soft callus*. Recruited chondroblasts and osteoblasts replace the granulation tissue. Vascular ingrowth into the calcified callus re-establishes the blood supply. (**c**) *Stage of hard callus*. Complete calcification of callus through intramembranous and endochondral ossification. (**d**) *Stage of remodeling*. Conversion of woven bone into lamellar bone through surface erosion and osteonal remodeling (With permission from [13])

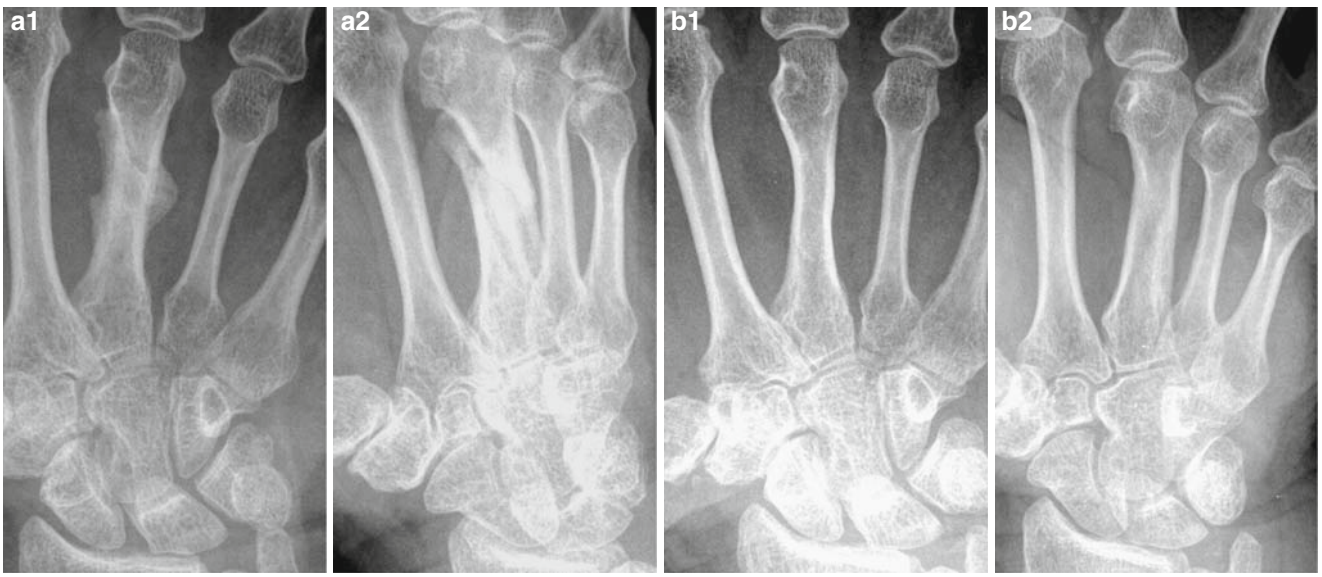

Fig. 6.3 Callus bone healing: (**a**) Stage of hard callus. Coned down PA (**a**1) and oblique (**a**2) radiographs of the hand show hard callus bridging a mildly displaced 3rd metacarpal fracture. (**b**) Stage of remodeling. Coned down PA (**b**1) and oblique (**b**2) radiographs of the hand obtained 18 months after fracture show the stage of remodeling. The excess callus has resorbed. The normal bone morphology is near completely restored and the medullary cavity is reestablished

Fig. 6.4 Robert Danis (1880–1962). (With permission from [24])

Maurice Müller and Development of the AO Group

The next major step was made when a young Swiss surgeon, Maurice Müller, visited Danis in Brussels in 1950 [1, 2]. He returned to Switzerland with an autographed copy of Danis' Book entitled "et Pratique de l'Ostéosynthèse," committed to scientifically investigate the basis of Danis' observations [2, 6]. He inspired a number of close colleagues, including Hans Willenegger, Robert Schneider, and Martin Allgöwer, and in 1958 they developed a study group in Switzerland named *Arbeitsgemeinschaft für Osteosynthesefragen* or *AO*, which in later years became known as the *Association for the Study of Internal Fixation* or *ASIF* in the English-speaking countries.

The AO's activities were focused on three crucial areas: basic research, surgical technical development, and documentation of clinical experience [1].

1. A laboratory of experimental surgery was developed in Davos, Switzerland, which at its early stages was able to clearly define the revolutionary concept of *direct bone healing,* first observed by Robert Danis, and the influence of *skeletal stability* on the pattern of bone union. This became the foundation for our current understanding of bone healing in various mechanical environments [1, 12].
2. Using the basic knowledge obtained from the experimental studies, collaborative work was initiated with metallurgists and engineers in Switzerland to develop systems of implants and instruments. Even today, AO remains in the forefront of the cutting-edge technology in implant design and manufacture.
3. A center for documentation of clinical experiences was developed in Bern, which continues to the present day with documentation of internal fixations performed throughout the world.

Since its development, the AO's scientific activities have been steadily expanding and have gained worldwide influence, with development of the AO Foundation, AO-sponsored courses in many parts of the world, and provision of hundreds of annual AO-sponsored fellowships, grants, and publications.

Biology of Bone Healing in Various Mechanical Environments: *The Concepts of Direct and Indirect Bone Healing*

Thanks to the observations of Robert Danis and the early work of the AO group described below, it is now a common knowledge that the four Hunterian stages of bone healing occur only under unstable mechanical conditions or with relative stability, such as in cast immobilization. This pro-

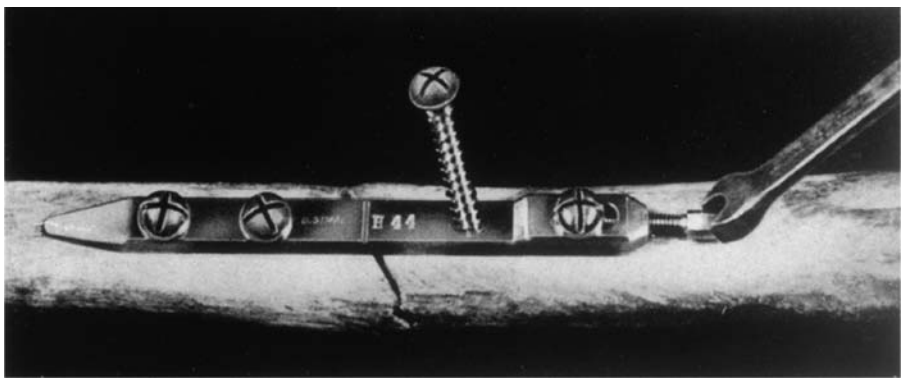

Fig. 6.5 Coapteur de Danis. To create compression between the fracture fragments, the plate was first fixed to the far fragment using the two round screw holes, and subsequently to the near fragment through the oval-shaped screw hole. The far fragment was then pulled toward the near fragment by tightening the bolt at the end of the plate. When enough compression was created, the last screw was inserted in the round hole in the near fragment, to maintain compression (With permission from [14])

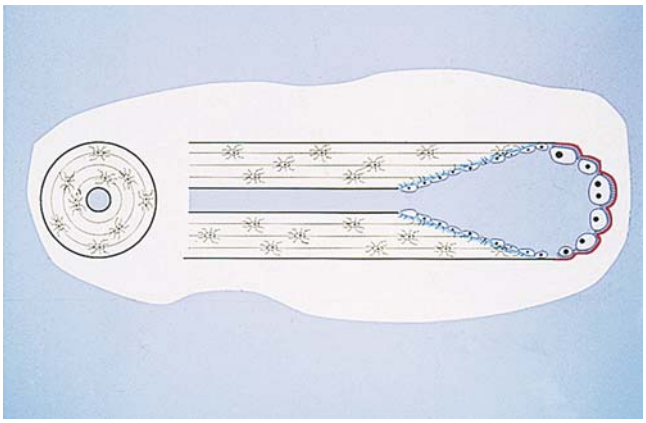

Fig. 6.6 Haversian remodeling. The osteon carries a layer of osteoclasts at its tip that act as a cutting head and drill a tunnel through the necrotic ends of the fracture. Behind the cutting tip, osteoblasts form new bone with living cells and connection to the capillaries (With permission from [13])

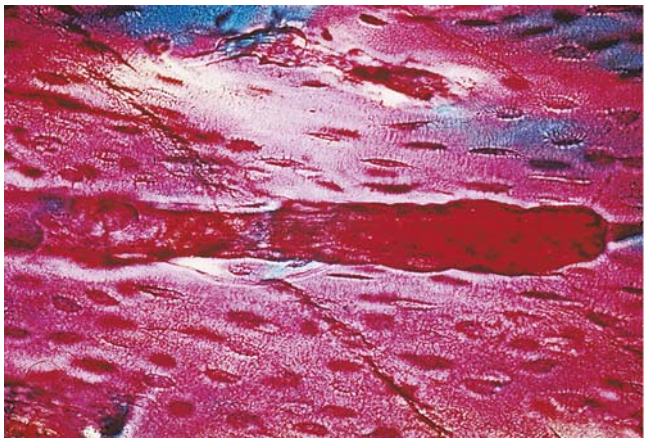

Fig. 6.7 Histological appearance of direct bone healing. The areas of dead bone are replaced by internal Haversian remodeling (With permission from [13])

cess, known as *indirect bone healing*, is characterized by callus bridging of the fracture with woven bone, callus solidification, and eventually a lengthy period of remodeling into lamellar cortical bone.

On the other hand, when a diaphyseal fracture is anatomically reduced and rigidly fixed by a plate or other interfragmentary fixation technique, little or no external callus forms. Only a very small gap is present between the two fracture

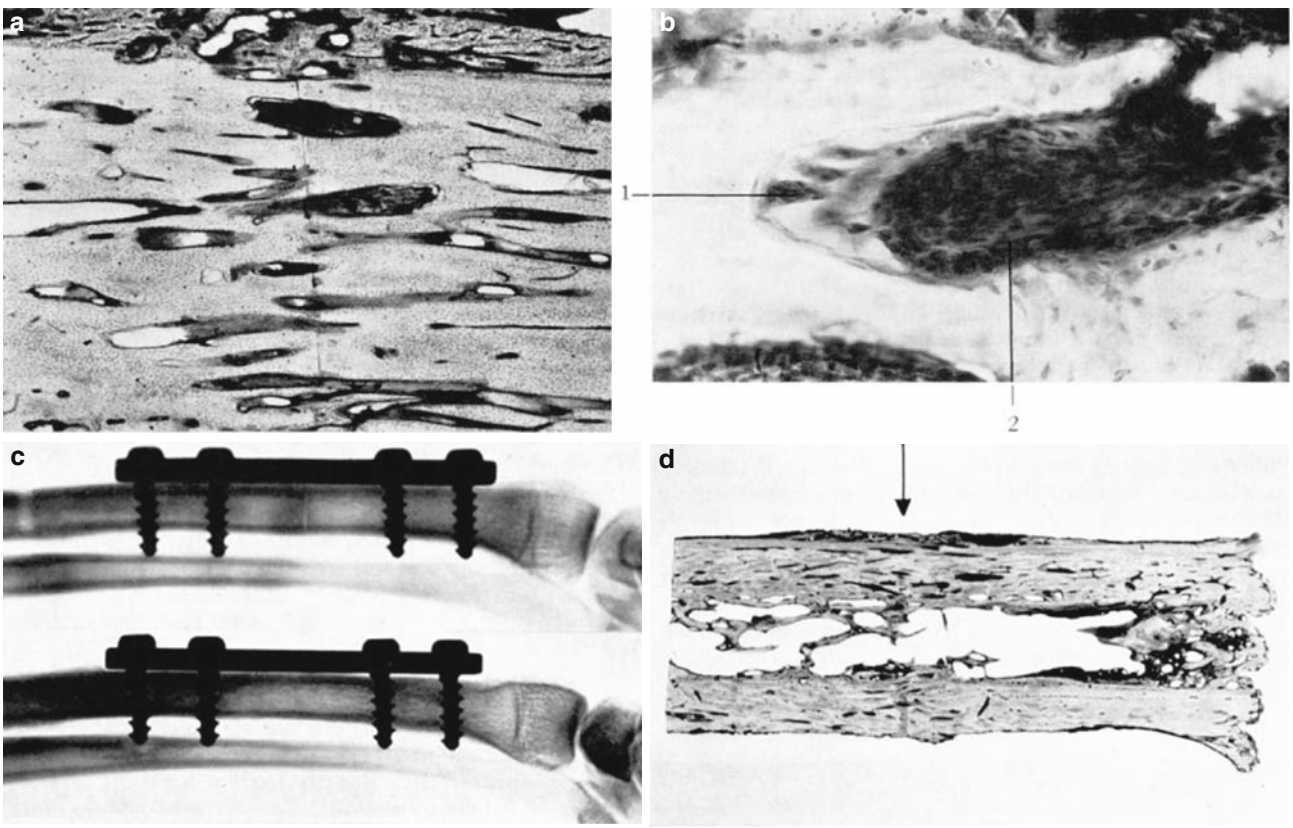

Fig. 6.8 Histological appearance of Haversian remodeling in a canine radius osteotomy model, following rigid compression plate fixation. (**a**) Direct osteon to osteon bridging without external callus at 6 weeks. (**b**) The cutting head with osteoclasts at the tip (1) and osteoblasts behind the forefront (2). (**c**) Forelimb radiographs after fixation (**C-top**) and at 6 weeks (**C-bottom**) show no significant external callus formation despite disappearance of the osteotomy line. (**d**) Ground section at 10 weeks confirms the same findings (With permission from [7])

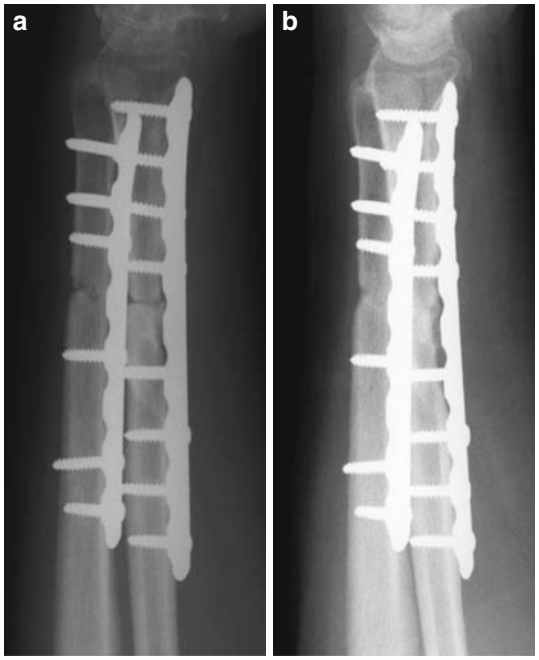

Fig. 6.9 Progression of direct healing following rigid fixation of the ulnar fracture with a limited contact dynamic compression plate is shown on lateral forearm radiographs. (**a**) The fracture lucencies are visible at 2 months post-op. (**b**) The fracture lucencies are less apparent at 4 months post-op despite the absence of significant external callus formation

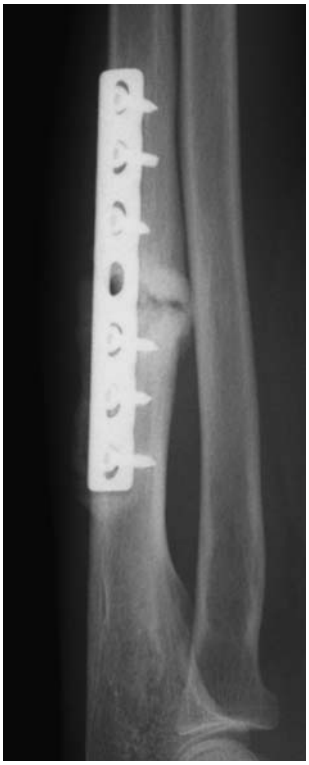

Fig. 6.10 Exuberant external callus 5 months following internal fixation with a dynamic compression plate and persistence of fracture line is shown on a lateral proximal forearm radiograph. These findings are warning signs of instability

ends, and so within a few weeks the Haversian system initiates a process of internal remodeling.

The Haversian system – or osteon – is the functional unit of the cortical bone. Each osteon is composed of six to seven concentric layers of lamellar bone and carries a layer of osteoclasts at its tip. The osteoclasts act as a cutting head by drilling a tunnel at the necrotic ends of the fracture (Figs. 6.6 and 6.7). Within a few weeks, these tunnels eventually reach the end of each fracture fragment. Behind the cutting head, there are a large number of osteoblasts that start to form new bone within the tunnels and subsequently cross the microscopic fracture gap, thus creating numerous microbridges between the bone fragments [5]. In 1963, Schenk and Willenegger [7] first demonstrated the histologic details of callus-free healing (Fig. 6.8a, b), known as *direct bone healing, osteonal remodeling, Haversian remodeling, internal remodeling* or, as first described by Danis, *soudure autogène*, or self-welding.

Radiologically, only minor changes can be observed. Following anatomical reduction, only a fine hairline lucency may be seen at the fracture interface. No significant external callus develops, but over time healing can be judged by gradual disappearance of the linear fracture lucency (Figs. 6.8c and d, 6.9). Any widening of the gap or development of hypertrophic callus, on the other hand, is a worrisome sign of instability (Fig. 6.10).

Bone Screws

Screws are strong mechanical devices which convert rotational force into linear force [5, 8, 12]. A screw is generally composed of a head, a shaft, a shank, and a tip (Fig. 6.11).

The *head* is usually round and may engage the bone or the plate. There is a recess in the head for coupling with the screwdriver.

The *shaft* is the unthreaded portion between the head and the threaded part (shank).

The *shank* is the threaded portion of the screw. Screws can be partially or fully-threaded (Figs. 6.12 and 6.13).

The *tip* may be sharp (self-tapping screw) or blunt (non-self-tapping) (Fig. 6.13).

The *thread* engages the bone. The larger the thread diameter, the larger is the purchase (hold) area of the screw in the bone (Fig. 6.11).

A *tap* is a sharp instrument used to cut threads in the bone identical to those on the screw, after a pilot hole is

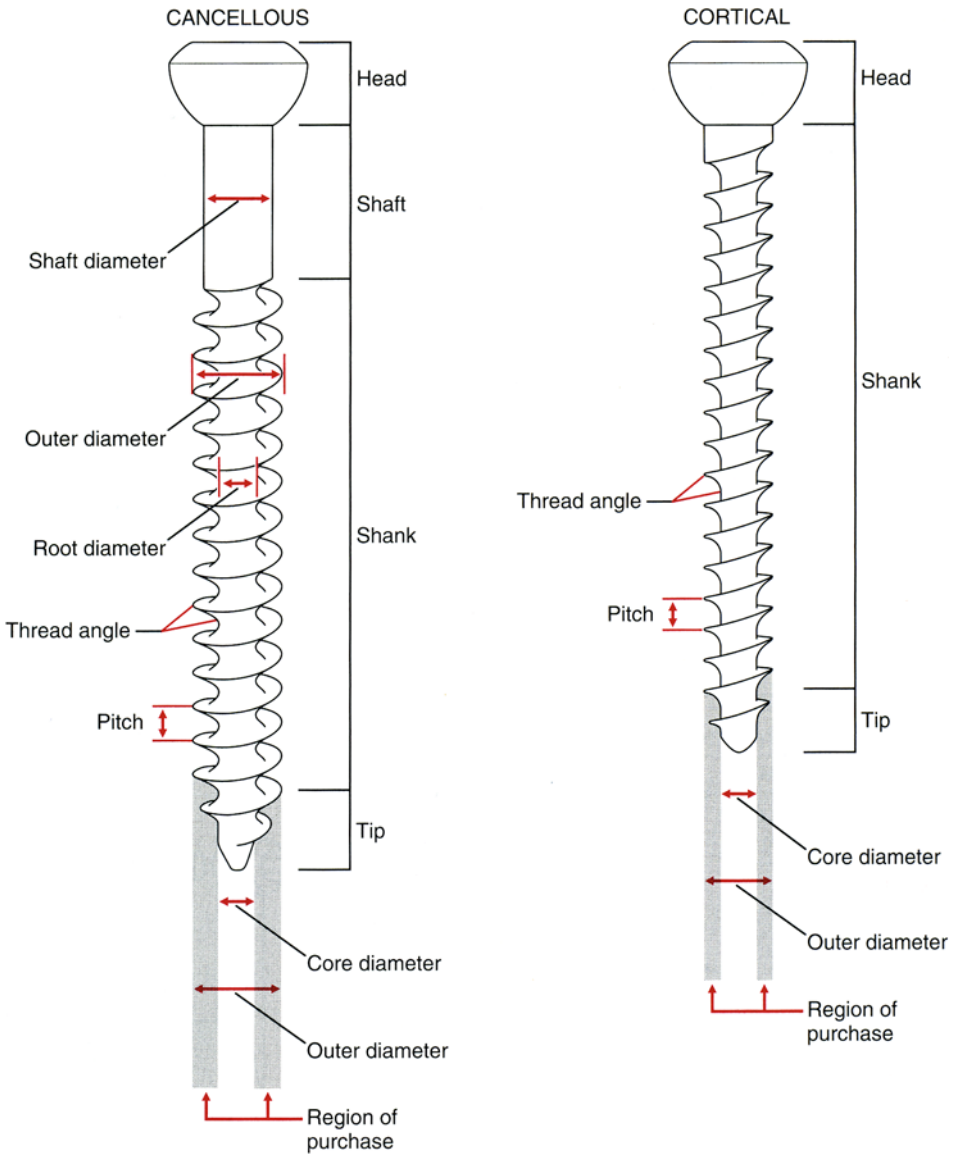

Fig. 6.11 Anatomy of bone screws (With permission from [8])

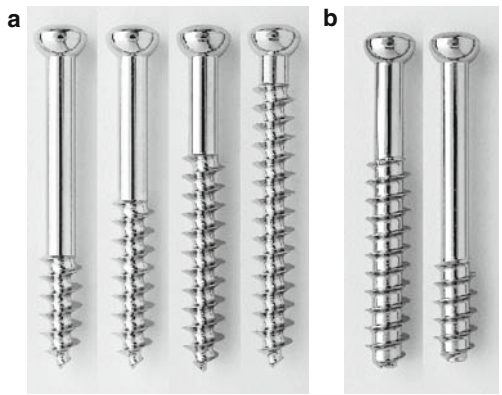

Fig. 6.12 Cancellous screws can be partially or fully-threaded, and solid (**a**) or cannulated (**b**). © Synthes, Inc. or its affiliates

Fig. 6.13 Cortex screw (*middle*) and its derivatives – shaft screw (*left*) and malleolar screw (*right*). They all have similar thread profiles. Malleolar screw has a trocar shaped tip. © Synthes, Inc. or its affiliates

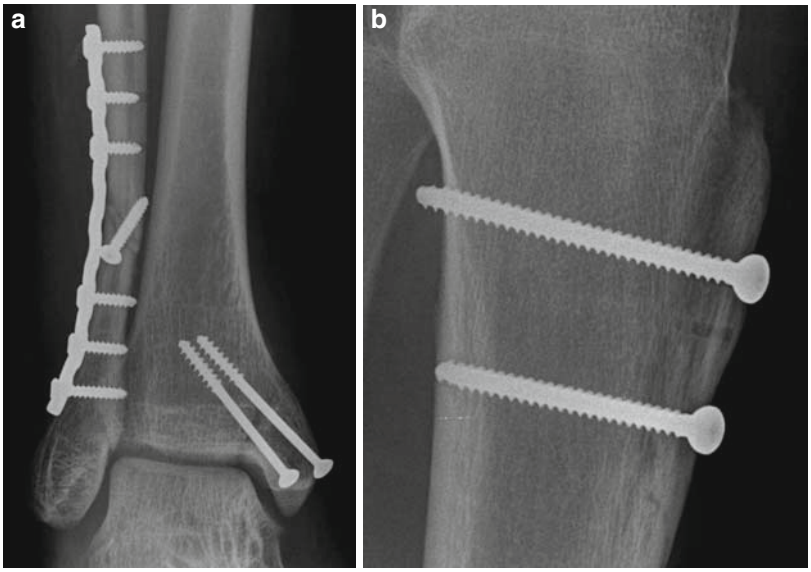

Fig. 6.14 (**a**) AP ankle radiograph showing a compression plate and cortex screws fixing the fibular fracture and two small cancellous screws fixing the medial malleolar fracture. Small cancellous screws are often preferred over malleolar screws in the medial malleolus because of their superior pull out strength. (**b**) Cortex screws are shown on a lateral tibial radiograph, fixing a tibial tuberosity osteotomy performed for distal patellar realignment surgery

drilled (Fig. 6.15). Tapping facilitates screw insertion in the pilot hole and prevents inadvertent cracks and fractures of the bone.

The *outer or thread diameter* is the largest diameter of the threads (Fig. 6.11).

The ***core*** is the root of the screw threads, from which the screws protrude. The core provides resistance to bending forces. A slight increase in core diameter significantly increases a screw's bending strength (proportional to the third power of the core radius). Core diameter also determines the size of the drill bit needed to create the pilot hole in the bone.

The *pitch* is the longitudinal distance between the two successive threads. The *lead* is the linear distance the screw advances in the bone for one complete revolution of the screw. Most orthopedic screws are single-threaded, in which case the pitch and lead are equal.

Screws can be differentiated in a variety of ways:

1. The type of the bone they engage:

    a. *Cancellous screws* have a large thread-to-core ratio and a large pitch, to increase their pull-out strength in soft cancellous bone (Figs. 6.12 and 6.14). They are used primarily in the epiphysis and metaphysis of long bones and also in the pelvis. They can be fully- or, more commonly, partially-threaded. The thread length varies. Partially-threaded cancellous screws are used in

Fig. 6.15 Cortex screw and cortex tap (**a**), and cancellous screw and cancellous tap (**b**). The threads in the tap (*right*) are identical in shape to those in the screw but are sharp. The tap also has 3 longitudinal flutes near its tip. After the pilot hole is drilled, the tap is inserted in the hole to cut threads in the pilot hole identical to those in the screw. The screw can then be inserted in the threaded hole, without risk of bone fracture. Cortex screws are shown in titanium (*left*) and stainless steel (*middle*), and in non-self-tapping (*left*) and self-tapping (*middle*) varieties. ((**b**) from [2])

Fig. 6.16 Locking head screw. © Synthes, Inc. or its affiliates

lag screw fixation (page 213) and fully-threaded cancellous screws often in plate fixation.

b. *Cortex screws* are fully-threaded and have a large core diameter, shallow threads, and a small pitch (Figs. 6.13 to 6.15). They are used in the diaphysis of long bones. The tip may be self-tapping or non-self-tapping.
c. *Shaft screws* have a cortical thread profile but are partially-threaded (Fig. 6.13). They are used in the diaphysis of long bones as lag screws. The shaft diameter of a shaft screw is larger than the shaft diameter of a similar cancellous screw and is equal to the outer thread diameter (Figs. 6.12 and 6.13).
d. *Malleolar screws*, designed for use in the medial malleolus, are also partially-threaded screws with a cortex screw thread profile, but they have a trocar tip (Fig. 6.13). Small cancellous screws are, however, preferred because of their superior pull-out strength (purchase or hold power).

2. Function [5]:

a. *Plate screws* are used to create compression between plate and bone.
b. *Lag screws*: Lag screw does not refer to a specific screw type or morphology. Rather, it is a technique to create compression between bone fragments. Both cortical and cancellous screws, and fully- and partially-threaded screws can be used to create the lag effect (page 213).
c. *Locking head screws* have threads in the screw head that lock in corresponding threads in the plate screw hole (Figs. 6.16, 6.54, and 6.55). This creates angular stability between the plate and screw. It does not, however, compress the plate to the bone.
d. *Anchor screws* are used to anchor a wire loop, such as in tension band wiring (Fig. 6.42). They are also placed temporarily in the bone for fracture reduction (Fig. 6.17).
e. A *Poller screw* is used as a fulcrum to redirect an intramedullary nail within the medullary canal and limit its motion (Fig. 6.18).

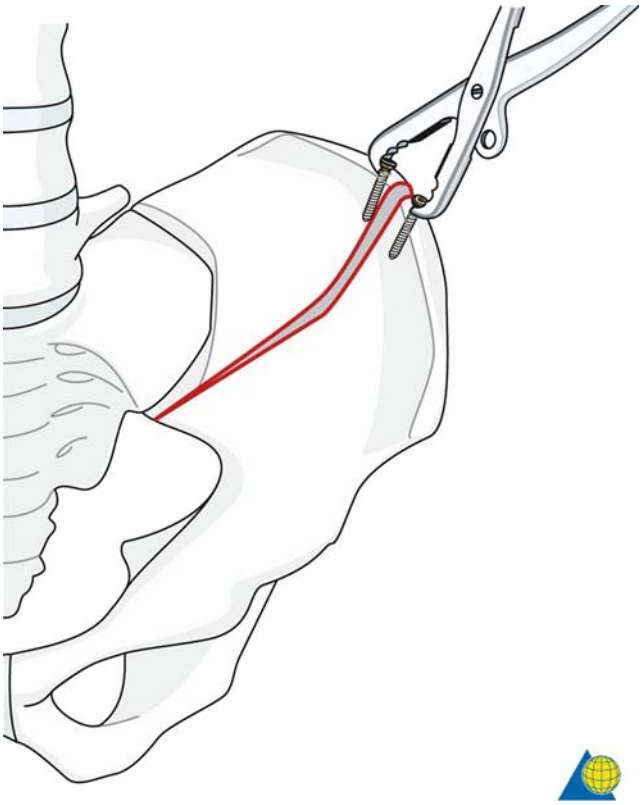

Fig. 6.17 Anchor screws are used to anchor a wire loop or are placed temporarily for fracture reduction (With permission from [15])

3. Type of recess in the head and the way they couple with the screw driver:

a. *Hexagonal recess* is the classic design in AO screws (Figs. 6.19, 6.42, and 6.71) and provides excellent coupling with a hexagonal screw driver.
b. *Philips head* (cruciate recess): mainly used in mini screws in the hand (Fig. 6.20).
c. *Slot-shaped recess*: infrequently used.

4. Cannulated vs. non-cannulated: *Cannulated* screws are hollow and can therefore be inserted percutaneously over a guide wire (Fig. 6.21).

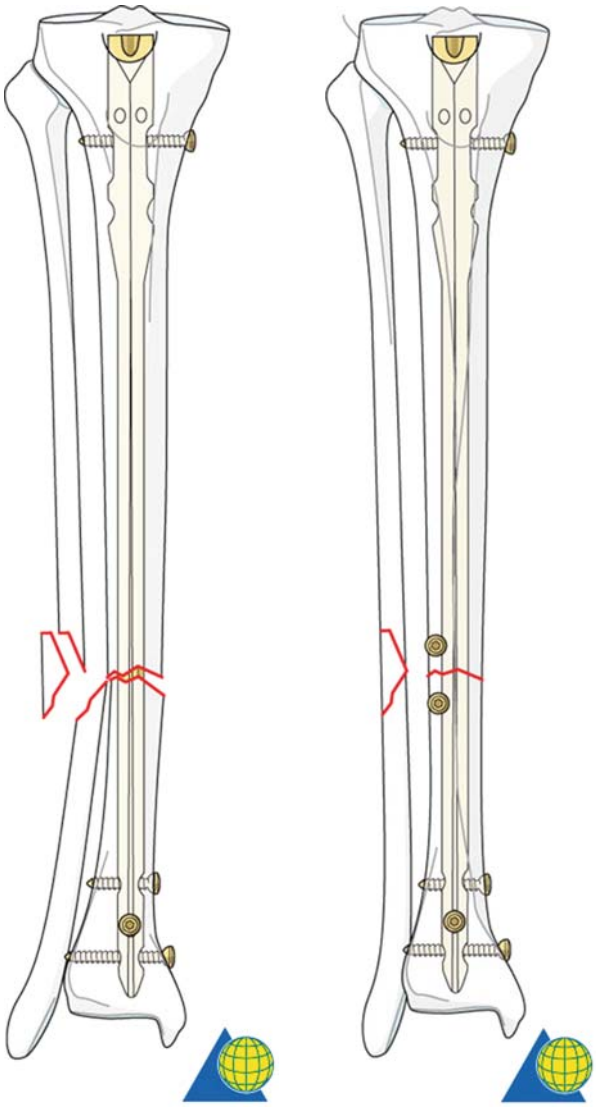

Fig. 6.18 Poller screw. Poller screws help prevent or correct malalignments and increase the stability of the intramedullary nail (With permission from [16])

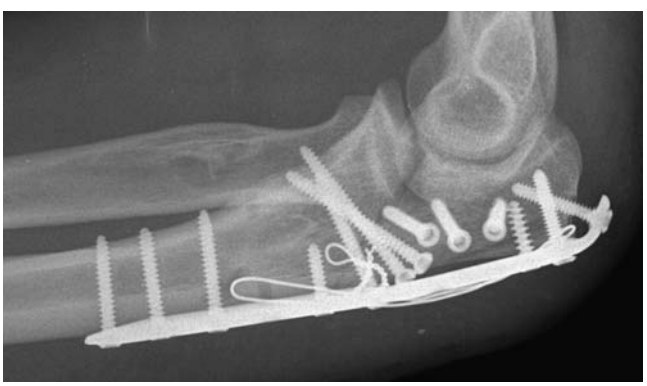

Fig. 6.19 AO screws typically couple with a hexagonal screwdriver through their hexagonal recess or socket

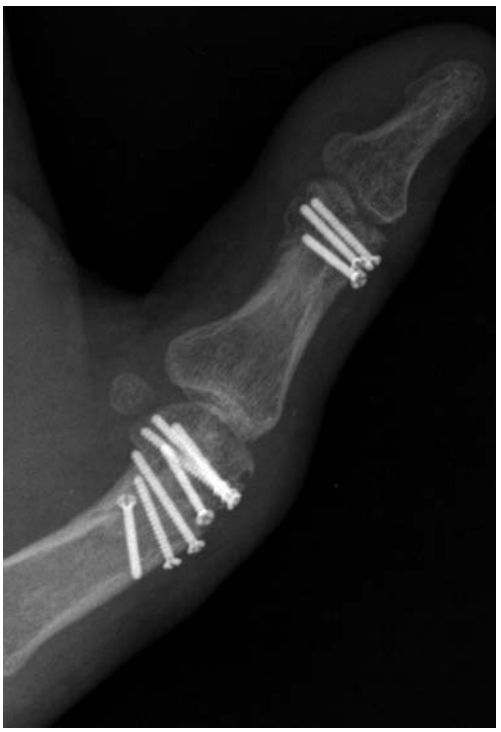

Fig. 6.20 Phillips head mini-screw with a cruciate recess

5. Headless screws:
    a. An *interference screw* is used to anchor a graft within a tunnel, most commonly used in anterior cruciate ligament reconstruction (Fig. 6.22).
    b. *Herbert screw* and its variants are headless screws mainly used to create compression in scaphoid fractures. The prototype is a partially-threaded screw with threads at each end with a differential pitch between them (Fig. 6.23a, b, d). The central non-threaded portion creates the lag effect and the differential pitch theoretically causes different rates of advancement in the two fracture fragments resulting in compression. Fully-threaded variants are also available (Fig. 6.23c).
6. *Schanz screws* are used in external fixators (Figs. 6.24, 6.65 to 6.67).

Techniques of Absolute Stability

A stable fracture is one in which there is no visible motion between the fracture fragments under physiologic loading. As previously described (page 206), a fracture with absolute stability undergoes primary bone healing without external callus formation (Figs. 6.8 and 6.9).

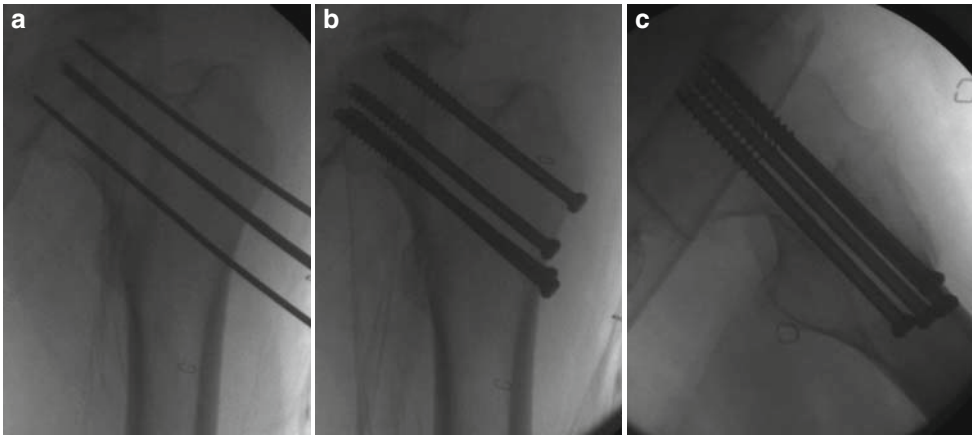

Fig. 6.21 Cannulated Screw. AP (**a** and **b**) and frog's leg lateral (**c**) hip radiographs showing cannulated screws (**b** and **c)** inserted percutaneously over guide wires (**a**). The cannulation can be recognized radiographically by a linear central lucency along the screw's length (**b** and **c)**

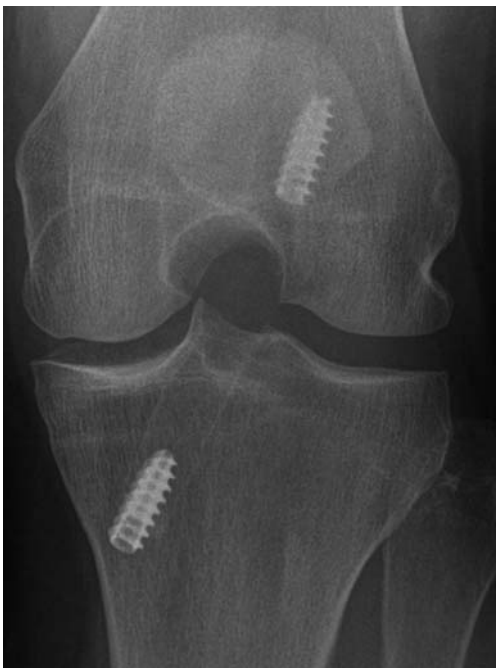

Fig. 6.22 Interference Screw. AP radiograph of the knee showing interference screws in the distal femur and proximal tibia. These screws are headless and embedded in a bone tunnel

Lag Screw Fixation

Fractures that involve the articular surfaces need anatomic reduction and absolute stability during healing to avoid articular surface incongruity [4]. Lag screw fixation, using a cancellous screw, is the major technique used in this area. The length of the screw shaft must be chosen so that the threaded part of the screw lies fully within the far bone fragment with no threads in the near fragment (Fig. 6.25). In other words, for a cancellous screw to function as a lag screw, there needs to be a "gliding hole" in the near fragment and a "threaded hole" in the far fragment. As the screw is tightened, the screw threads are anchored in the far fragment. Once the screw head engages the bone in the near fragment, the *gliding hole* in the near fragment allows free motion of the far fragment toward the near fragment, thereby closing the gap at the fracture interface and creating compression between the two fragments (Figs. 6.25 and 6.26).

Lag screw fixation does not imply any particular screw morphology; rather it refers to the technique of compressing two fracture fragments to each other. In fact, a fully-threaded screw can also function as a lag screw. In this case the near fragment is over-drilled to a size larger than the outer core diameter of the screw threads, to prevent the screw threads from engaging within the near cortex. Over-drilling in effect creates a gliding hole in the near fragment (Fig. 6.27).

Lag screw effect can also be achieved through a plate by inclining the screw (Fig. 6.28) causing interfragmentary compression.

Femoral neck fractures can be treated percutaneously with three large cannulated cancellous screws. The screws must be inserted in a parallel fashion for the lag effect to take place (Fig. 6.21). During healing of the femoral neck fracture, there is commonly resorption of the fracture ends and gradual impaction at the fracture site. The use of lag screws allows sliding and backing out of the screws in the gliding hole (Fig. 6.29). If the lag screw technique is not used correctly, impaction of fracture during healing can result in protrusion of the tip of the screw through the femoral head into the acetabulum, since sliding in the near fragment will not occur. Some examples of incorrect technique are shown in Fig. 6.30.

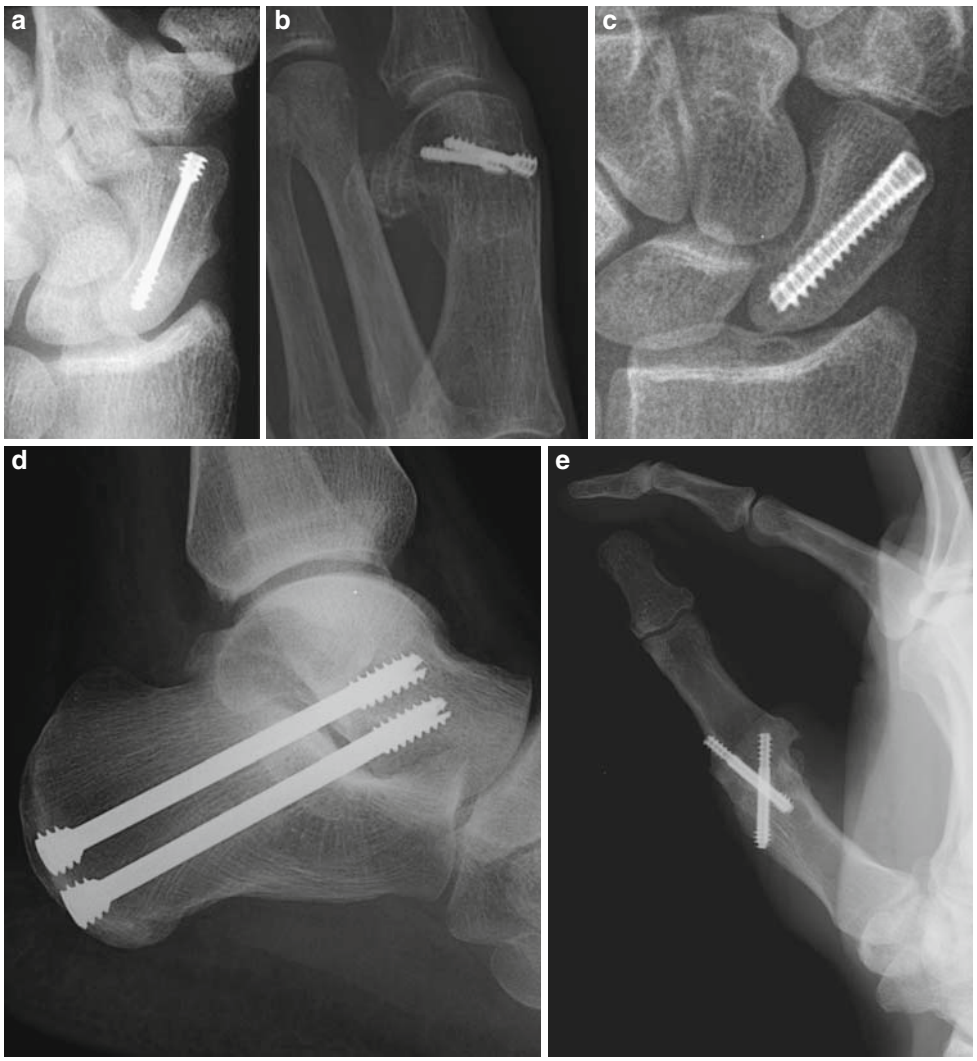

Fig. 6.23 (**a-e**) Different applications and varieties of differential pitch headless screws. Coned down ulnar-deviated PA wrist radiograph (**a**) and coned down oblique foot radiograph (**b**) showing the prototype Herbert screws. The prototype is partially threaded with threads at the two ends and a differential pitch design. Coned down PA wrist radiograph (**c**) shows a fully-threaded Acutrak screw with differential pitch. Lateral ankle radiograph (**d**) shows a large Herbert screw used in subtalar joint arthrodesis. PA radiograph (**e**) of the thumb shows two cannulated Herbert type screws used in metacapophalangeal joint arthrodesis

Compression Plates

The first generation of AO compression plates, known as Müller's round-hole plate introduced in early 1960s, is no longer in general use. This plate was an improvement over Danis' coapteur (Fig. 6.5) and created compression at the fracture site by application of an external tension device to one end of the bone (Fig. 6.31). The use of a tension device increased the operative time and the size of the surgical field and required additional periosteal stripping of the bone. In addition, screws could only be placed perpendicular or with minimal angulation relative to the plate's round holes, further limiting its application.

Dynamic Compression Plate (DCP)

The dynamic compression plate (DCP) was introduced in 1969 by Parren and featured a simple but ingenius screw hole design, allowing for axial compression by *eccentric screw insertion* (Fig. 6.32d, e) [4].

DCPs feature an oval-shaped screw hole with a sloped margin at one end in the form of an inclined and a transverse cylinder (Fig. 6.32a, b). A pilot screw is drilled and the plate is initially fixed with one screw to one of the two fracture fragments. Then, a pilot hole is drilled eccentrically within the opposite fragment and the screw is advanced within the pilot hole (Fig. 6.32f). As the screw is tightened, the screw head comes in contact with the sloped edge of the plate screw

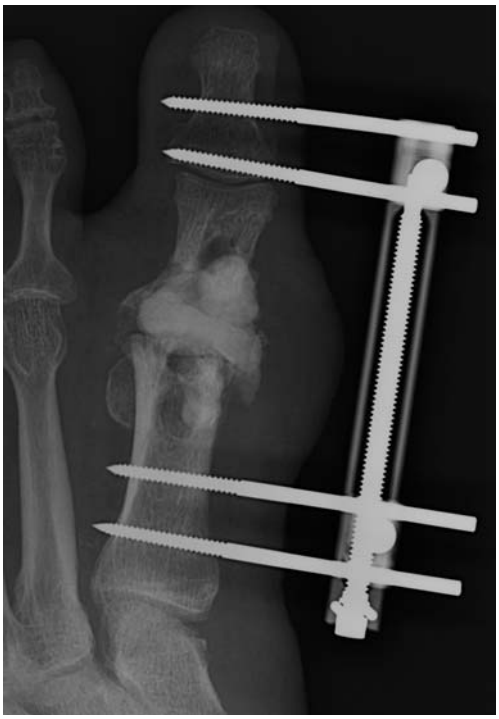

Fig. 6.24 Schanz screws are used in pin-type external fixators. An AP radiograph of the first digit shows a failed 1st MTP joint arthrodesis secondary to osteomyelitis, status post removal of plate and screws and subsequent fixation with an external fixator and interposition of antibiotic-impregnated methylmethacrylate

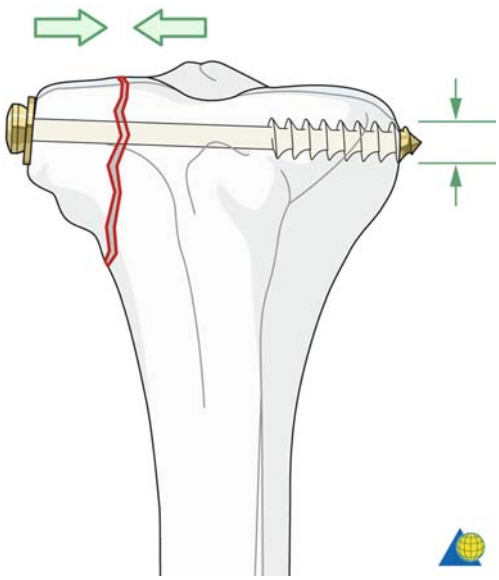

Fig. 6.25 Lag screw fixation. Compression of an intra-articular fracture using a partially threaded cancellous screw. The length of the screw shaft must be chosen so that the shank (threaded portion) of the screw lies fully within the far bone fragment. The threads pull the far fragment toward the head of the screw. The holes in the near and far fragments are called the "gliding hole" and the "threaded hole," respectively (With permission from [17])

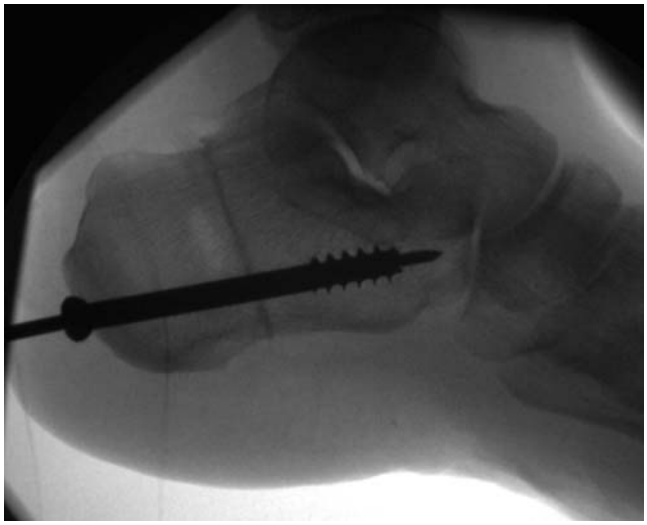

Fig. 6.26 Lag screw fixation. Lateral calcaneal radiograph showing a calcaneal osteotomy fixed with a percutaneously inserted cannulated lag screw. Note that the screw threads lie fully in the far fragment

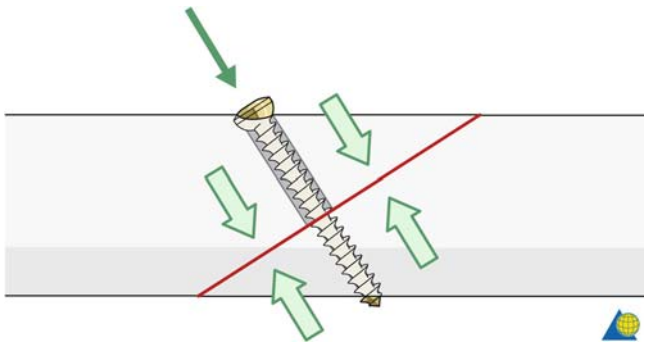

Fig. 6.27 Lag screw fixation using a fully-threaded screw. The gliding hole in the near fragment has to be slightly wider than the thread diameter of the screw, so that the screw threads do not engage the bone (With permission from [17])

hole. With further tightening the screw tends to slide down the sloped edge, like a ball rolling down a sloped cylinder (Fig. 6.32a, b, and f). Since the screw can only advance within its pilot hole, in practice this results in movement of the plate relative to the screw (Fig. 6.32d, e) which in turn, results in movement of the far bone fragment toward the near fragment, dynamically creating compression across the fracture interface [5] (Fig. 6.33).

The oval shape of the screw holes (Fig. 6.33a) has the additional benefit of allowing oblique screw insertion in oblique or complex fractures (Fig. 6.28).

Limited-Contact Compression Plate (LC-DCP)

The third generation of AO compression plates were introduced in 1989–1990 by Parren. LC-DCP has several design

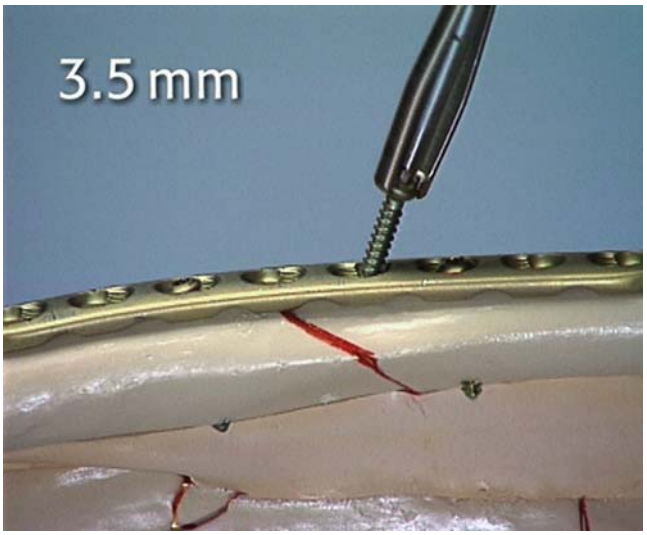

Fig. 6.28 Lag screw placed through the plate in an oblique manner, creating interfragmentary compression (With permission from [18])

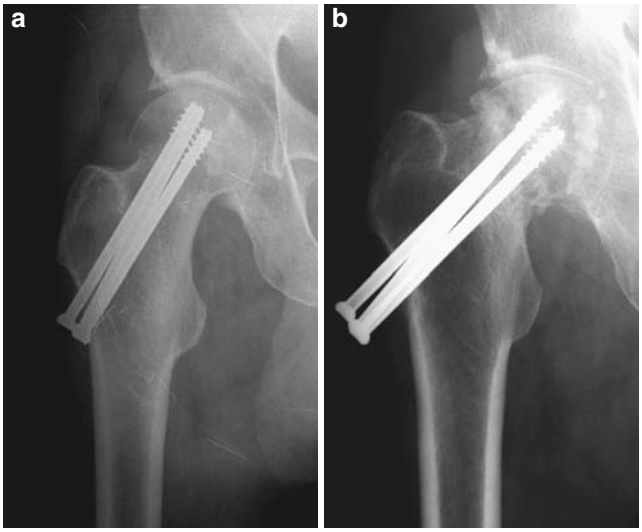

Fig. 6.29 Correct lag screw technique. AP radiograph of the hip (**a**) after fixation and (**b**) months later shows correct lag screw technique. This permits the screw to slide in the glide hole, as the fracture ends resorb and impact during healing. This technique minimizes the risk of screw extrusion through the femoral head into the acetabulum

improvements over the classic DCP. It was realized that the bone underneath the DCP undergoes resorption and develops osteoporosis, either from the stress-shielding effect of the plate or from disturbed cortical blood supply, resulting from compression of the plate to the bone. The LC-DCP features undersurface grooves in the plate (Figs. 6.34 and 6.9), limiting its contact area with the bone and therefore reducing the risk of vascular damage and osteoporosis beneath the plate. Similar to DCP, the oval-shaped holes also allow oblique screw insertion in oblique and comminuted fractures to achieve interfragmentary fixation (Fig. 6.28).

Tubular Plates

Tubular plates have a curved cross section. They include semitubular and one-third tubular plates. The curved cross section facilitates their application in long bones with a round external contour and minimal soft tissue covering, such as the lateral malleolus and the distal ulna (Figs. 6.35 and 6.36).

Plate Contouring and Reconstruction Plates

Straight plates must be contoured before application to perfectly conform to the surface of different bones with various curvatures and complex anatomy. Plate contouring is done with the help of malleable templates and bending devices

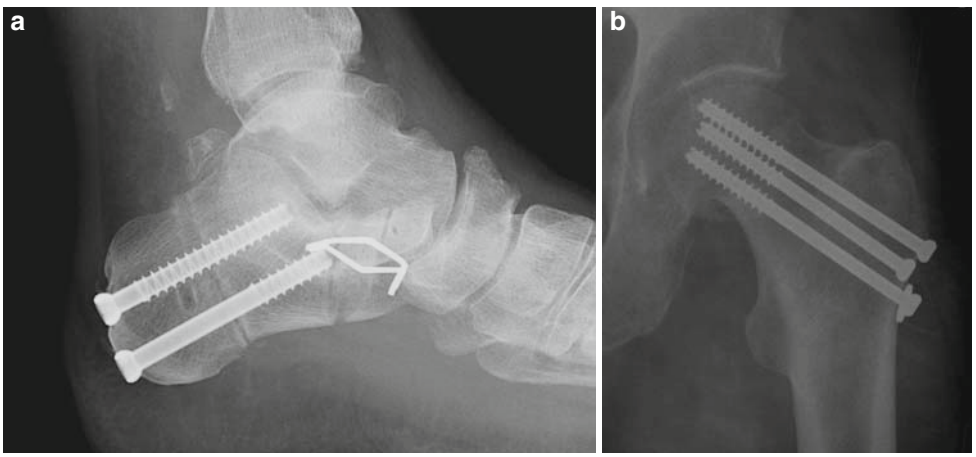

Fig. 6.30 Incorrect lag screw technique. Lateral calcaneal (**a**) and AP hip (**b**) radiographs. The screw threads should lie fully within the far fragment for the lag effect to occur. Otherwise, the glide hole will not function properly

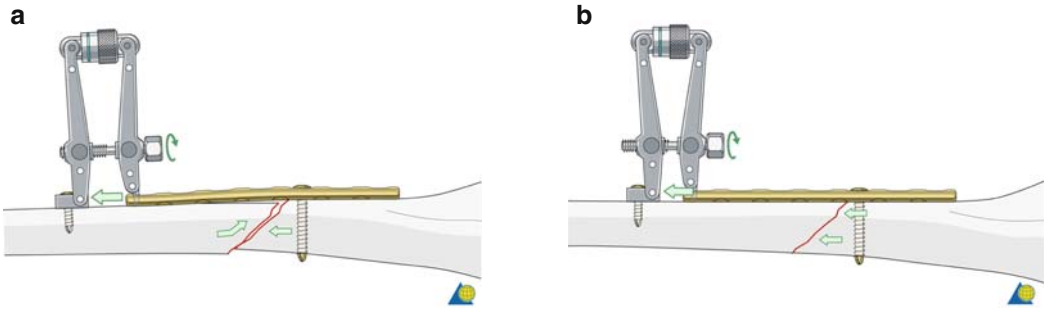

Fig. 6.31 Application of a tension device to the plate (**a**) and subsequent tensioning of the plate (**b**) creates compression of the fracture fragments (With permission from [18])

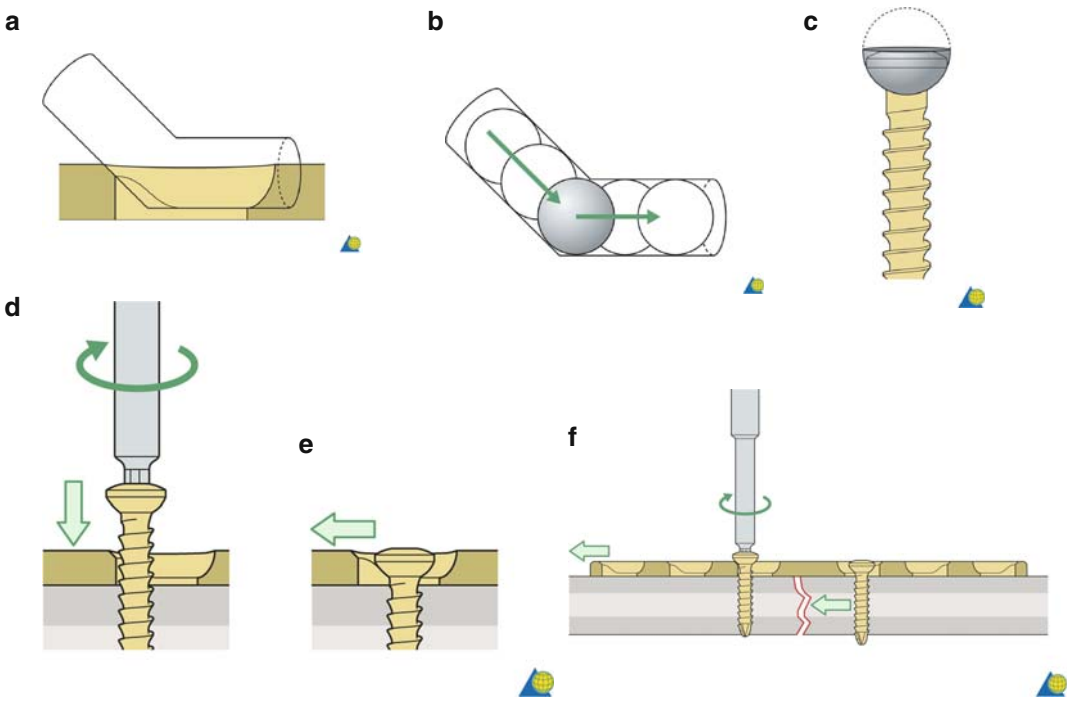

Fig. 6.32 Dynamic compression principle. (**a**) The holes in the plate are oval shaped and sloped at one end like an inclined and a transverse cylinder. (**b, c**) If the screw is inserted eccentrically, as the screw is tightened, the screw head tends to slide down the sloped edge, like a ball rolling down a sloped cylinder. (**d, e**) Since in reality the screw cannot move horizontally, the plate is moved horizontally when the screw is driven home. (**f**) Tightening of the screw results in the horizontal movement of the plate and the far fracture fragment already attached to the plate by the first screw, creating compression of the fracture fragments

such as bending pliers, bending irons, and the bending press (Fig. 6.37a–c) [5].

A plate can be twisted along its long axis with bending irons (Fig. 6.37b, d) and can be bent along its long axis with bending pliers or a bending press (Fig. 6.37c, d).

In certain areas with complicated three-dimensional bone geometry, such as in the pelvis, it often becomes necessary to contour plates in all three planes. It is, however, very difficult to bend a straight plate "on the flat," along its width or short axis (Fig. 6.37d). Contouring "on the flat" would result in elongation or tearing of the plate along its convex border and shortening or buckling along the concave border. This would result in plate failure. To solve this problem, AO has developed *reconstruction plates*.

Reconstruction plates feature deep notch or indentations along both edges of the plate, between the screw holes. Indentations permit plate contouring in all the three planes, particularly bending "on the flat" along its short axis (Fig. 6.38a, b). Contouring on the flat results in wider separation of the notches on the convex side and close approximation on the concave side without plate failure.

In addition to the pelvis and acetabulum, reconstruction plates are frequently used in the distal humerus, distal tibia, and the clavicle, where contouring "on the flat" may be necessary (Fig. 6.39). Reconstruction plate is not as strong as a compression plate, and may be further weakened by excessive contouring.

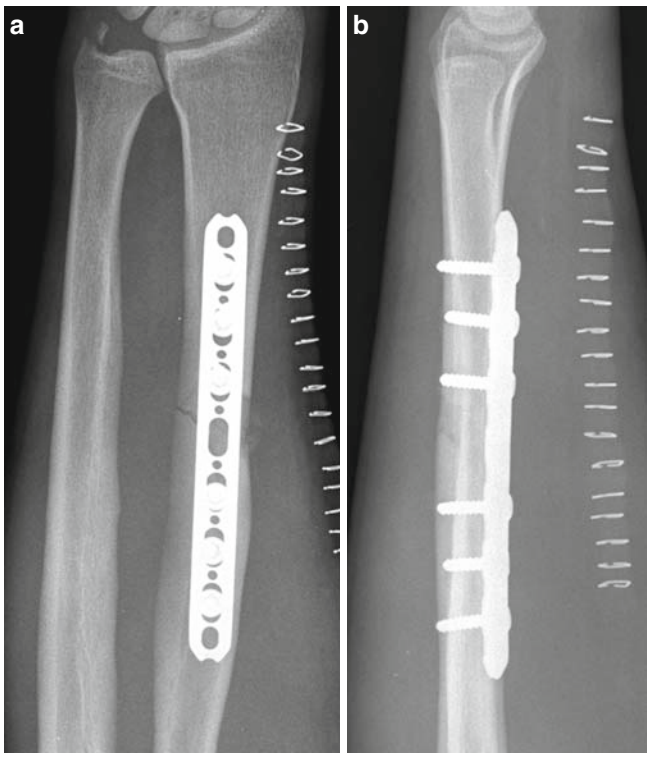

Fig. 6.33 DCP. Dynamic compression by eccentric screw insertion, shown in AP (**a**) and lateral (**b**) forearm radiographs. Oval-shaped holes also allow oblique screw insertion when necessary (Fig. 6.28)

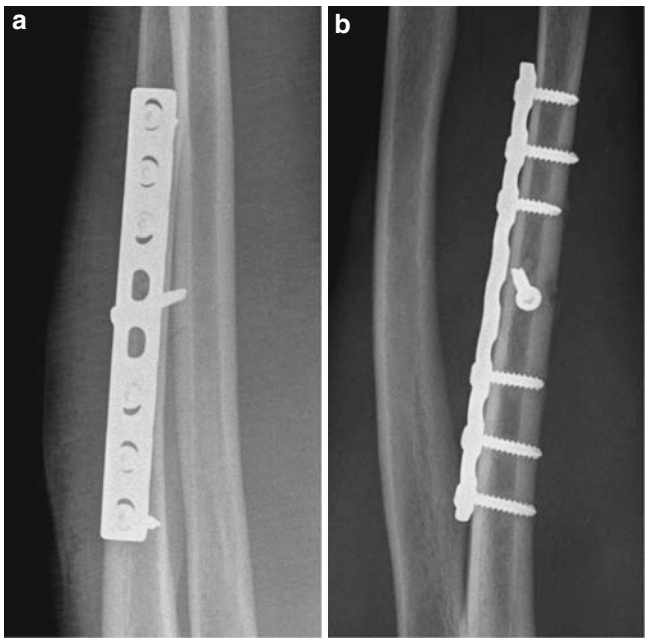

Fig. 6.34 LC-DCP. AP (**a**) and lateral (**b**) forearm radiographs. The undersurface cuts decrease the contact area between the plate and bone, compared with the older DCP, thereby reducing the risk of vascular damage (With permission from [18])

Tension Band Fixation

The *Tension Band Principle* was first explained by Frederic Pauwels [8, 9]. When a tubular structure is axially loaded, it distributes the compressive force in a uniform fashion, provided the load is applied along its central axis. On the other hand, if the load is applied eccentrically, a bending moment is created resulting in compression force on the near side and tension force on the opposite side (Fig. 6.40a). The tensile force can be neutralized by application of an unyielding band, such as a wire or a plate, to the tension side. This is called a *tension band*. Subsequent eccentric loading results in uniform compression on both sides of the fracture, converting tensile force into compressive force (Fig. 6.40b).

Tubular bones, such as the femur, are physiologically under eccentric axial loading, and therefore always have a tension side and a compression side [5, 9]. Eccentric axial loading of the femur, applied to the femoral head, results in a medial compression force and a lateral tension force (Fig. 6.41a).

Compression is critical for fracture healing. Conversely, tensile force and distraction impede bone healing. If a plate is applied to the tensile (convex) side of a fractured femur, it can function as a tension band and the tensile force can be

Fig. 6.35 One-third tubular plates shown in stainless steel (**a**) and titanium (**b**). (With permission from [18])

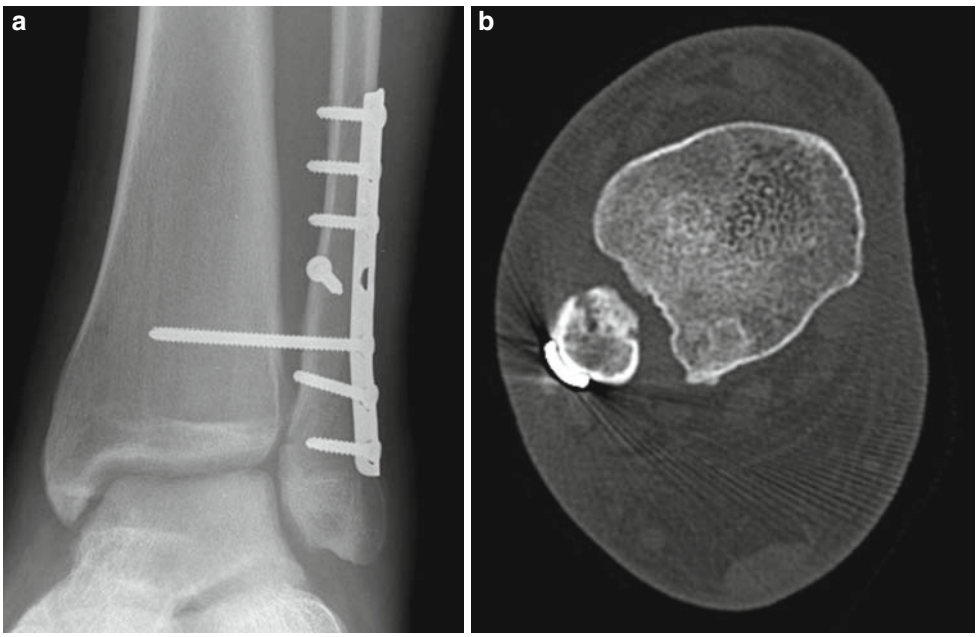

Fig. 6.36 One-third tubular plate. Mortise view of the ankle (**a**) and axial CT (**b**) show a one-third tubular plate used to fix a fibular fracture. These are useful in areas with minimal soft tissue coverage

converted to compressive force, resulting in uniform compression on both sides of the fracture (Fig. 6.41b).

Tension band wiring is used in areas where muscle pull causes constant tensile force across the fracture, such as in the patella, olecranon, and greater tuberosity (*dynamic tension band*); or where there is constant ligament pull such as in the medial malleolus (*static tension ban*d) (Figs. 6.39, 6.42–6.44). The tension band wire neutralizes the tensile force and even converts it into a compressive force. It is critical that the tension band be applied to the tension side, e.g., anterior aspect of the fracture in the patella, and posterior aspect of the fracture in the olecranon.

The tension band wire loop may be anchored to the fracture fragment with K-wires (Figs. 6.42, 6.44) or screws (Figs. 6.39, 6.42, 6.43). It is important to note that it is the wire loop, not the screws or K-wires, that exerts the tension band function. In fact, simple K-wire or screw fixation of such fractures is insufficient and will often fail (Fig. 6.45).

Angled Plates

In 1959, AO developed the angled blade plate [5] for use in the proximal and distal femur (Fig. 6.46). This is a one-piece device with a U profile in the blade portion, and a strong side plate. Its advantage is stability, and its disadvantage is difficulty of insertion. Accurate blade insertion is crucial. The 130° angled blade plate was used in the proximal femur for trochanteric and femoral neck fractures, and the 95° condylar blade plate was initially used in the distal femur for supracondylar and intercondylar fractures, and later for certain proximal femoral fractures as well (Fig. 6.46). These plates have been largely replaced by DHS and DCS, described below, in fracture treatment. They are still in use for pediatric femoral osteotomies (Fig. 6.47) and sometimes in arthrodeses (Fig. 6.48).

Current AO angled blade plates feature a cannulated blade, facilitating insertion over a guide wire (Fig. 6.49).

Compression Plates with Sliding Screws: Dynamic Hip Screw (DHS) and Dynamic Condylar Screw (DCS)

These were subsequent improvements over the angled blade plates. AO first developed the dynamic hip screw (DHS). This is a two-piece device composed of a large cannulated sliding screw that is inserted in the femoral neck and head, and a strong side plate with a fixed angle barrel (Fig. 6.50). The sliding screw articulates with the side plate through the barrel.

The DHS allows dynamic compression of the fracture with weight bearing by gradual sliding of the screw within the side plate's barrel – hence the term dynamic compression screw (Fig. 6.51). The sliding mechanism of DHS allows gradual impaction of the fracture during healing without the risk of the screw cutting through the femoral head into the

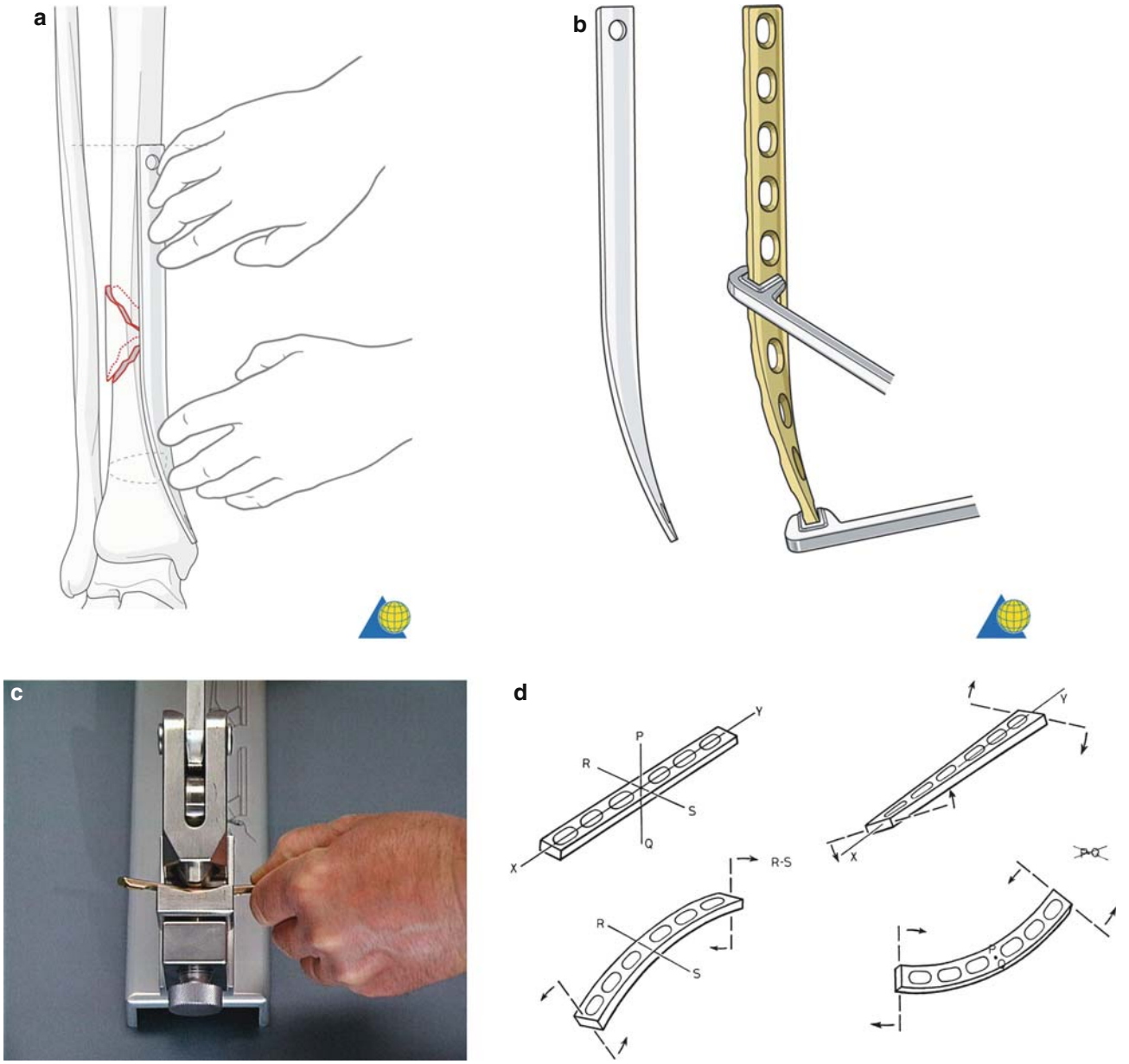

Fig. 6.37 (**a**) Malleable contouring template. (**b**) Bending iron. (**c**) Bending press. (**d**) Difficulty of contouring "on the flat" (**a**–**c** with permission from [18], **d** from [11])

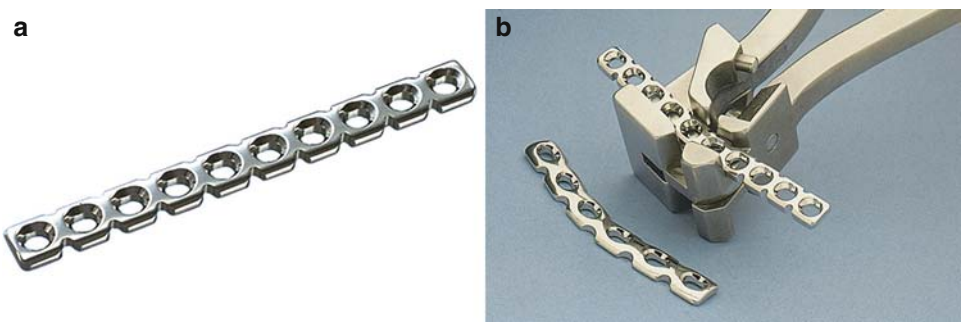

Fig. 6.38 (**a**) Reconstruction plate with its deep indentations along both edges between the screw holes. (**b**) The indentations allow contouring in all three planes, particularly contouring "on the flat," using a special bending iron (With permission from [18])

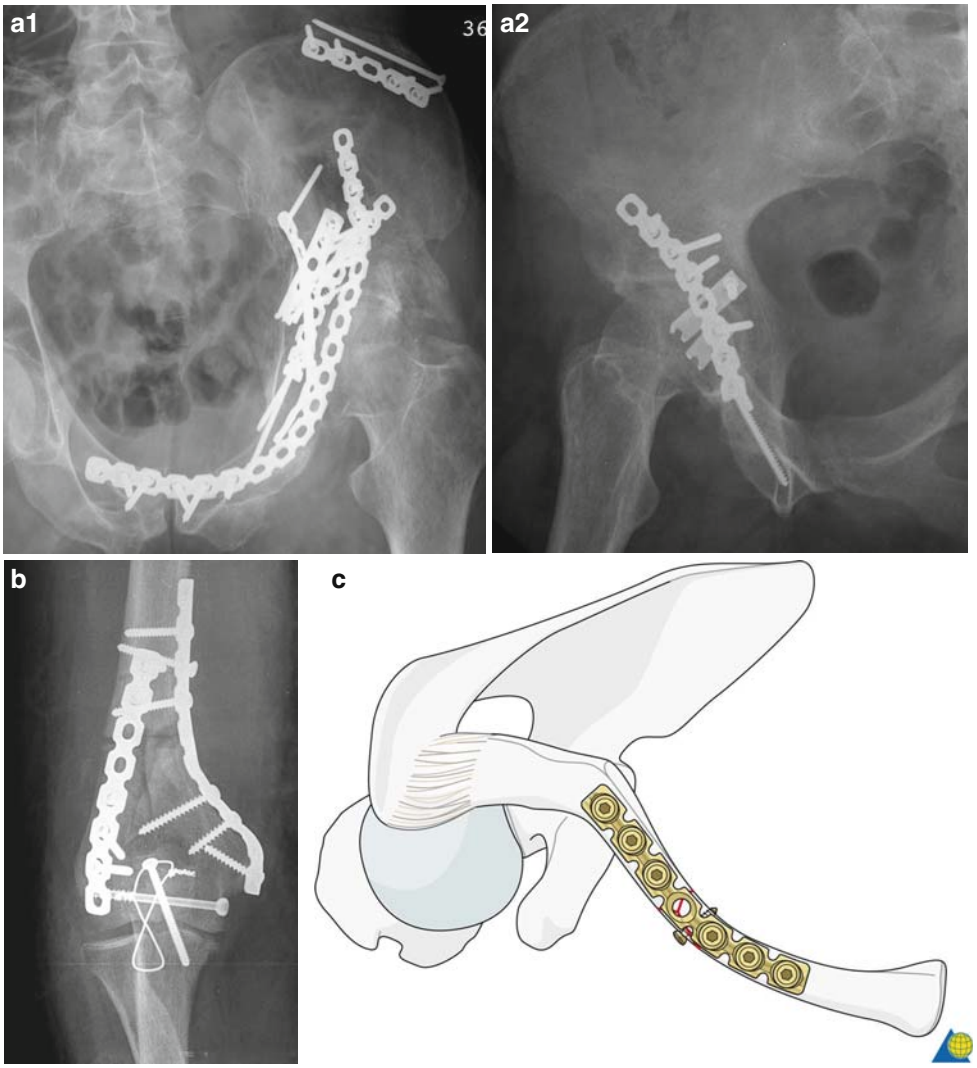

Fig. 6.39 Examples of contouring in all three planes using reconstruction plates. AP pelvic radiograph **a1**, right hip radiograph **a2**, AP elbow radiograph (**b**) and diagram of clavicular fracture fixation (**c**). Two spring hook plates are visible in **a2**. ((**c**) *w*ith permission from [18])

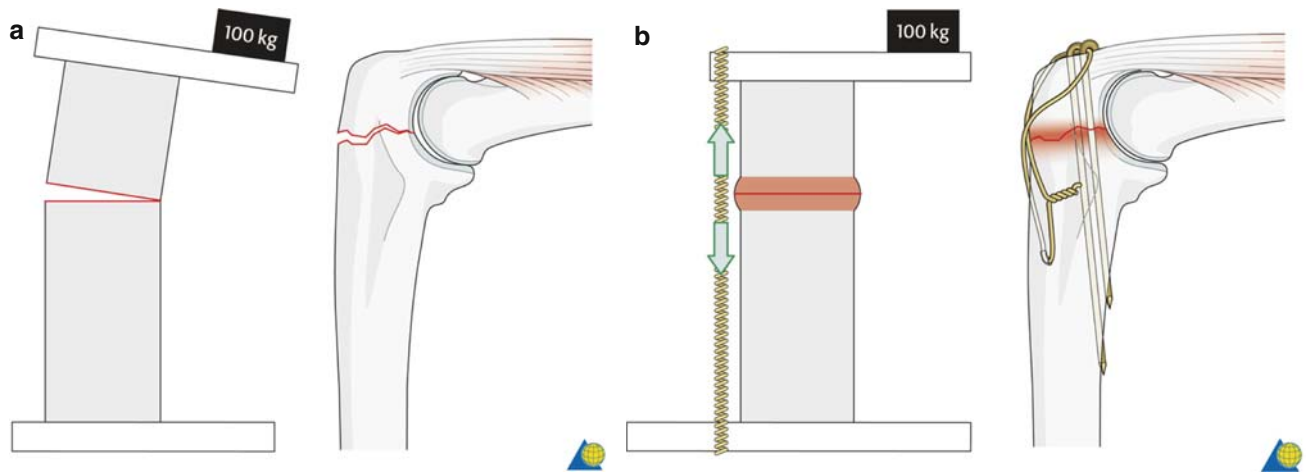

Fig. 6.40 Tension band principle. (**a**) An eccentrically loaded bone structure has a tension side and a compression side. (**b**) A tension band applied to the far cortex converts tension into compression (With permission from [19])

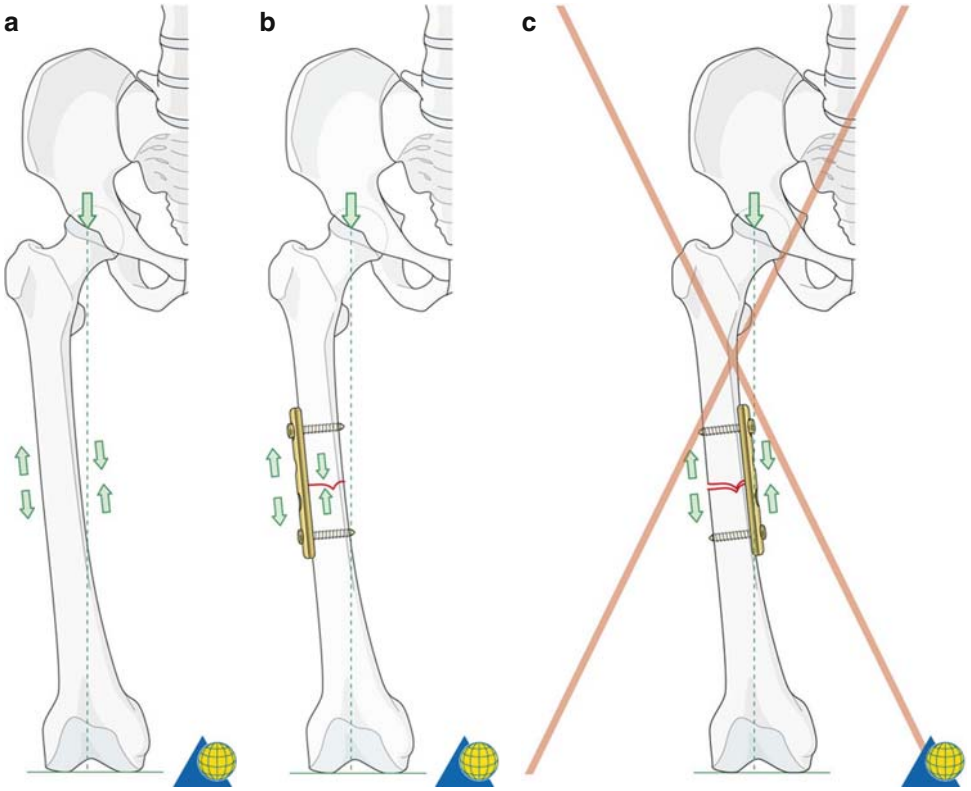

Fig. 6.41 (**a**) The mechanical axis of long bones is often not at the center of the bone. Under axial loading, the curved femur creates a bending moment with a tension force laterally (convex side) and a compression side medially (concave side). (**b**) A tension band plate applied to the lateral cortex converts tensile force into compressive force and promotes healing. Note that the plate is under tension (tension band) but the fracture is uniformly under compression. (**c**) If the plate is applied to the compression side of the fracture, a gap will form on the tension side (With permission from [19])

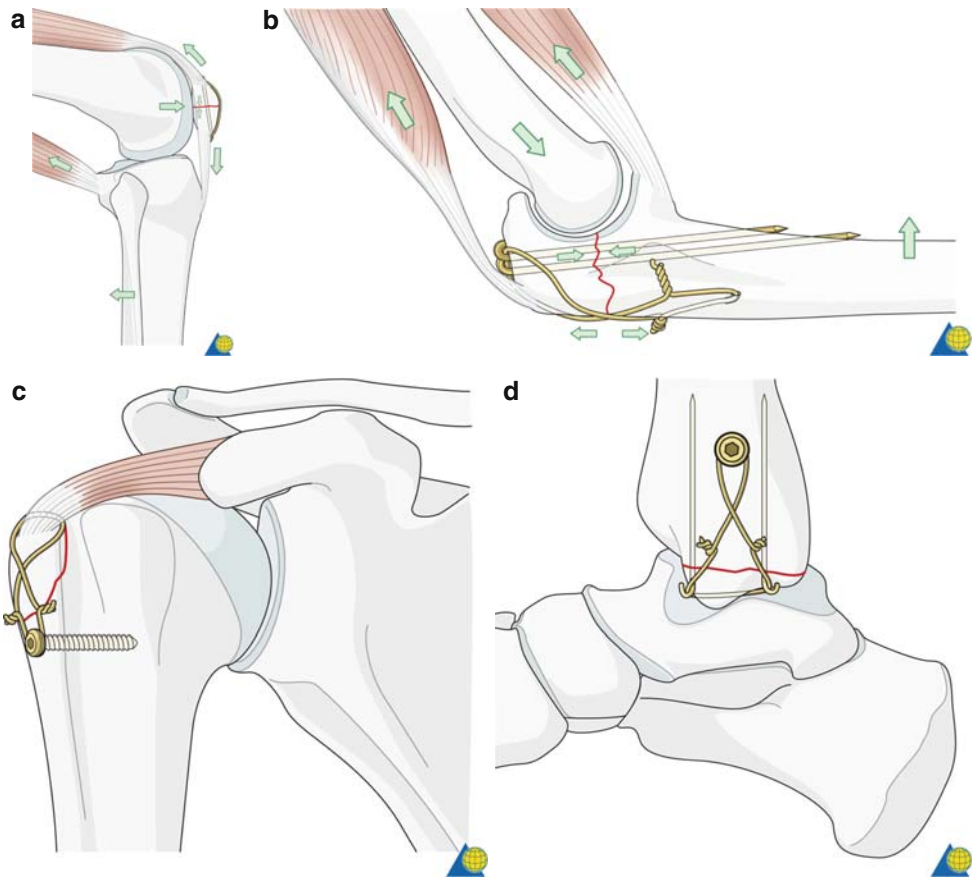

Fig. 6.42 Tension band fixation of the patellar fracture (**a**), olecrenon fracture (**b**), greater tuberosity fracture (**c**), and medial malleolus (**d**). In the patellar fracture (**a**), the figure-of-eight wire loop lies anterior to the fracture (tension side). Upon knee flexion, the tensile force between the quadriceps tendon and the tibial tuberosity that would ordinarily tend to distract the fracture fragments is converted to compressive force. The wire loop may be anchored to the bone by K-wires, as seen in (**a**) and (**b**) or by screws as seen in (**c**) and (**d**) (With permission from [19])

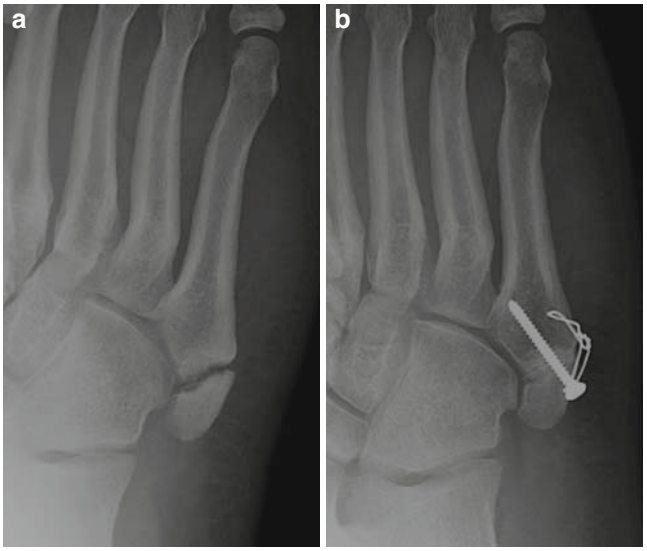

Fig. 6.43 Tension band wiring of the fifth metatarsal base fracture resulting from avulsion of the peroneus brevis tendon is an example of dynamic tension band. Oblique radiographs of the lateral foot before (**a**) and after (**b**) tension band wiring. (**a**) The fracture is not healed 5 months after trauma. (**b**) Significant interval healing has taken place 4 months following tension band wiring. Note that the wire loop, and not the screw, is the major stabilizer

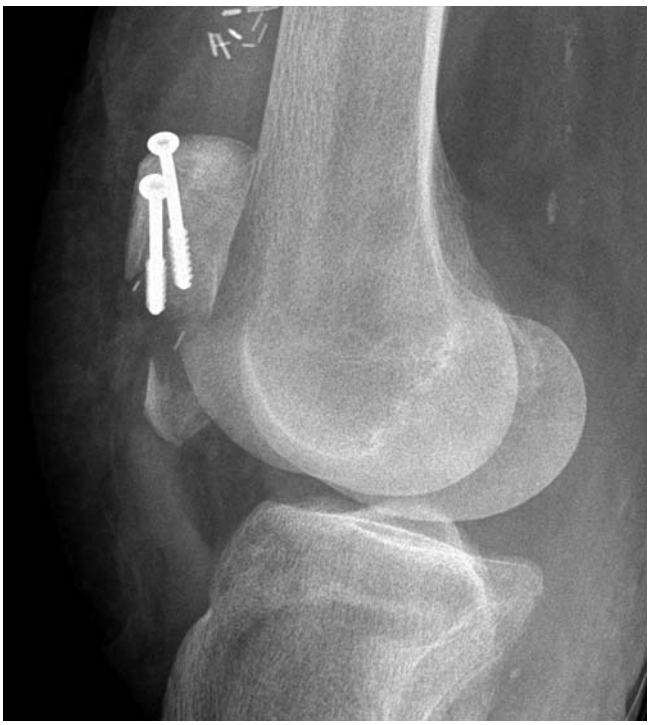

Fig. 6.45 Lateral radiograph of the knee. Simple screw or K-wire fixation of the fractures that are under tensile force, without tension band fixation, is often insufficient

acetabulum – a serious risk with the one-piece angled blade plates.

A few points have to be remembered. For the lag screw effect and sliding mechanism to function, there should be no threads at the fracture interface, and the screw thread must engage only the far fragment. In addition, since fixation with a single screw, no matter how strong and large, cannot provide sufficient rotational stability, an additional lag screw should be inserted in the femoral neck and head, cranial but parallel to the sliding screw (Fig. 6.52). Again, the threads of this screw should only be in the far fragment.

AO subsequently developed the 95° dynamic condylar screw (DCS), used both in the proximal and distal femur

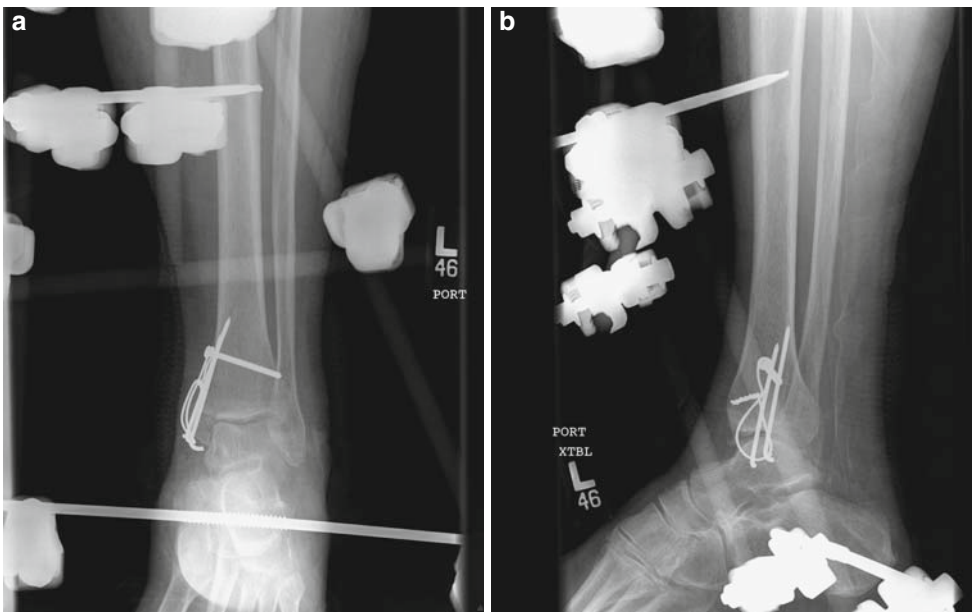

Fig. 6.44 Tension band wiring of the medial malleolus, shown in AP and lateral radiographs of the ankle (**a** and **b**), is considered a static tension band, counteracting the deltoid ligament

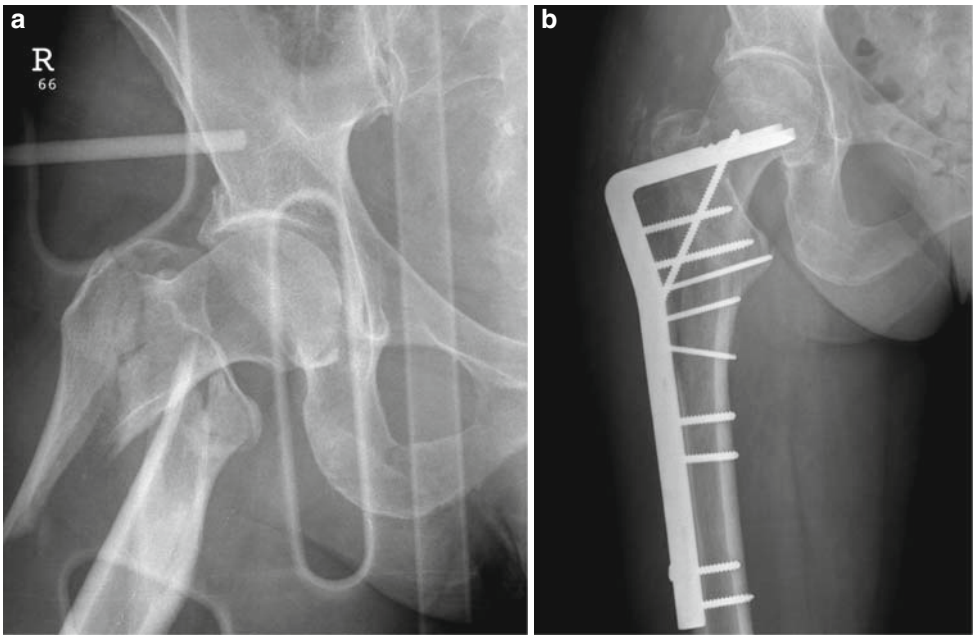

Fig. 6.46 A 95° condylar blade plate, fixing a comminuted subtrochanteric fracture. AP hip radiographs before (**a**) and after (**b**) fixation

(Fig. 6.53). It functions along the same principles as the DHS.

The DHS is the implant of choice for femoral neck and stable trochanteric fractures. Other options include angled blade plate and DCS. As discussed above, femoral neck fractures can also be fixed percutaneously with three parallel cancellous screws (Page 213, *Lag Screw Fixation*).

Locking Plates

Locking plates, introduced in 1994, are the most recent AO development in plate technology. The key difference is in the way the screws couple with the plate. The screw head and the plate screw holes have matching threads, allowing the screws to effectively bolt into the plate and bone [5] (Fig. 6.54). Locking head screws provide angular stability and create a *fixed-angle construct*, with improved fixation in osteopenic bone or highly comminuted fractures.

Unlike compression plates, locking plates do not rely on plate-to-bone compression to maintain stability. Instead, with their locked screws, they function similar to multiple small angled-blade plates that are not in contact with the bone. Thus, they are in effect non-contact plates (Fig. 6.55). The divergent and convergent orientation of the locked screws provides stability without the need to compress the plate to the bone (Fig. 6.71). Their function also resembles an external fixator, but in a submuscular location with very short pins (Page 238).

Locking compression plates (LCP) (Fig. 6.55) have combination holes that combine a dynamic compression unit hole with a locking screw hole. The combination hole provides flexibility for the plate to function as either a conventional compression plate, a locked plate, or a combination of both. In combination mode, which is most often used, the LCP can be used initially as a conventional dynamic compression plate, with as many cortex screws as needed, to creat compression across the fracture and to compress the plate to the bone. When sufficient compression is achieved, the remaining plate holes can be locked with locking head screws for additional angular stability.

Anatomically shaped LCPs are available for application in a variety of bones, including the distal femur, proximal and distal tibia, olecranon, distal humerus, and distal radius (Figs. 6.56 and 6.63).

Techniques of Relative Stability

As described earlier, anatomic reduction and rigid stable internal fixation are mandatory for optimal healing of intra-articular fractures. Diaphyseal fractures, on the other hand, can be managed with flexible fixation techniques.

Flexible fixation with *relative stability* aims to maintain fracture reduction while allowing for the mechanical stimulation to repair the fracture by callus formation [5]. Flexible fixation techniques allow some degree of motion between the fracture fragments. These techniques include intramedullary nailing, external fixation, percutaneous pinning, bridge plating, and less invasive stabilization systems (LISS).

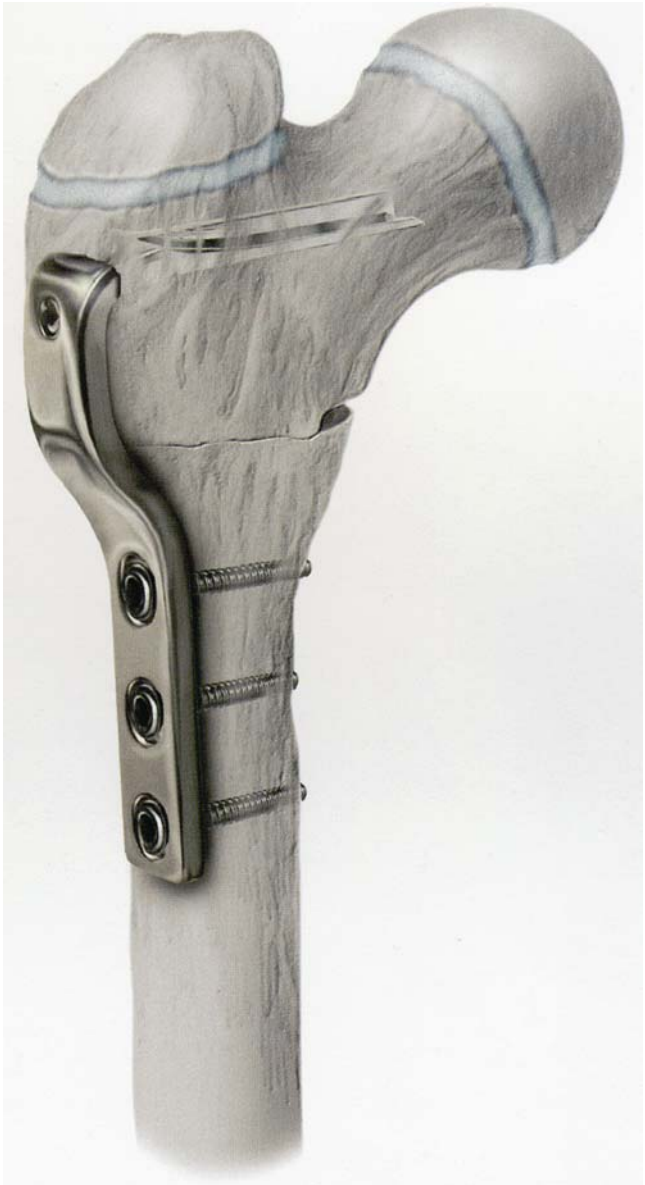

Fig. 6.47 Pediatric subtrochanteric osteotomy blade plate. Note the blade extends into the femoral neck. © Synthes, Inc. or its affiliates

Intramedullary Nailing

Early generations of intramedullary nails, including the classic Küntscher nail, were unlocked systems. Many of them had large diameters and were placed after reaming the medullary canal. Reaming was done to increase the contact area of the nail and bone, thereby improving stability. These nails, nevertheless, provided no rotational or axial (telescopic) stability in comminuted fractures. Their application was therefore limited to stable non-comminuted mid-diaphyseal fractures.

Recent advances in intramedullary nailing include development of locked systems where proximal and distal interlocking screws can be inserted through the nail with the aid of aiming devices and intra-operative fluoroscopy. These screws, inserted percutaneously through small holes or slots within the intramedullary nail, provide both rotational and axial stability and extend the indication of IM nailing to more complex and comminuted fractures and more proximal and distal fractures.

Intramedullary nailing can be performed in two modes [8]:

1. Splintage: For stable simple fractures.
2. Bridging: For unstable comminuted fractures.

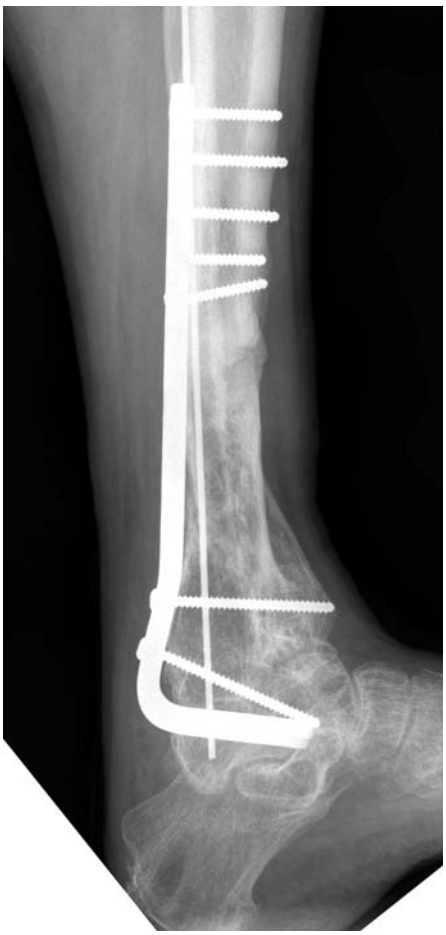

Fig. 6.48 95° condylar blade plate, fixing an ankle joint arthrodesis. Lateral radiograph of the ankle

Splintage

Splintage refers to fixation of a simple stable fracture, using either an unlocked or a dynamically locked intramedullary nail.

Unlocked intramedullary nailing: Is described above.

Dynamically-locked nails: In dynamically-locked fixation, interlocking screws or bolts are inserted at both ends of the nail, but proximally only in the oval-shaped dynamic hole, allowing a few millimeters of axial compression at the fracture (Fig. 6.57). Distally, usually two (femur) or three (tibia) interlocking screws are inserted through the round static holes that permit no play of the nail across the screw. Dynamic locking is indicated in stable fractures with at least 50% intact cortical contact between the two fracture fragments. Dynamic locking is an example of the splintage mode of fixation.

Bridging

Statically-Locked Nails: Comminuted axially-unstable fractures have to be realigned and bridged with a fixation device, in this case an intramedullary nail. A static mode of locking is necessary to maintain the axial length and prevent rotation of the fracture parts. Usually two or three proximal interlocking screws are inserted into the round static holes of the nail (Fig. 6.58). Optimally, two (femur) or three (tibia) interlocking screws should be inserted distally. The nail bends and torques by a small amount and so allows some limited motion at the fracture site. Static locking is an example of the bone bridging mode of fixation.

Dynamization

Dynamization of statically-locked nails in combination with bone grafting may be needed when a fracture is at risk of delayed union. Although not usually necessary for femoral fractures, dynamization is sometimes required to stimulate healing in the tibial fractures. Dynamization converts a bridging mode of fixation to the splinting mode.

To dynamize, one or both of the proximal interlocking screws are removed [5] (Fig. 6.59) so that no screw or only one screw in the oval-shaped dynamic hole remains. This increases the flexibility to the construct and allows axial stress to be transferred to the bone to stimulate healing. Dynamization should be performed when the fracture and the newly formed callus have gained enough stability to withstand axial forces without collapse, usually 2–3 months after the initial fixation.

Nail–Screw Systems

DHS (page 219) is the appropriate implant for femoral neck and stable intertrochanteric fractures, but is usually not strong enough to fix subtrochanteric fractures. Here the stronger intramedullary nail–screw systems are needed. Unstable intertrochanteric fractures, non-comminuted subtrochanteric fractures and high subtrochanteric fractures (within 2 cm of the lesser trochanter) can be fixed using a short proximal femoral nail (PFN) system (Fig. 6.60). Long proximal femoral nails (Fig. 6.61) are used for low or unstable subtrochanteric fractures. Configurations with single or double spiral blades are available for improved rotational stability in the femoral neck [5].

PFN is significantly stronger than the dynamic hip screw (DHS). More important, PFN has a shorter lever arm than a DHS, since it is placed more medially than a DHS, and

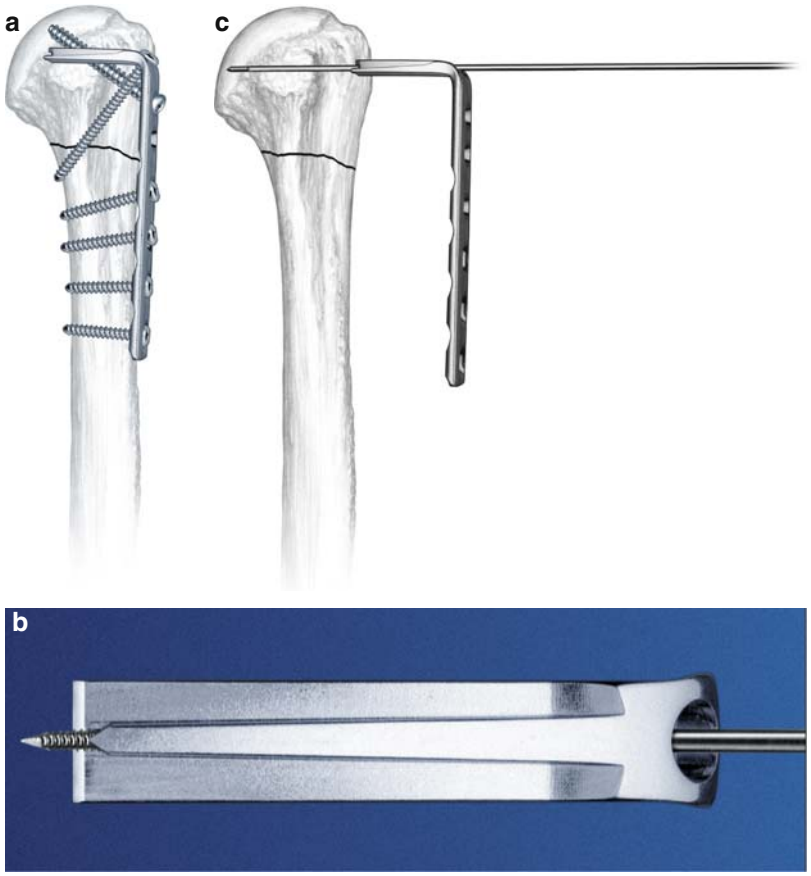

Fig. 6.49 A more recent version of AO angled blade plate. The 90° cannulated blade plate permits insertion over a guide wire for accurate blade positioning and blade length determination. © Synthes, Inc. or its affiliates

therefore is closer to the body's center of gravity. This gives the PFN a biomechanical advantage over the DHS.

While the PFN's distal interlocking screw provides axial stability, the proximal sliding screw allows gradual impaction of the fracture during healing, similar to DHS, without risk of screw cut out into the acetabulum.

Bridge Plating

Conventional compression plating with absolute stability comes at a cost. This technique employs a traditional subperiosteal approach that requires periosteal stripping and hence some loss of the vascular supply to the superficial cortical bone. While this may not be critical to bone survival in simple fractures, in highly comminuted fractures traumatic stripping of the fracture fragments from their soft tissue attachments (periosteal, muscular, etc.) may already have compromised the bone's vascular supply, so that any additional devascularization that occurs with conventional compression plating may lead to bone necrosis.

Bridge plating is a suitable technique in these circumstances (Fig. 6.62). In this technique, the plate acts as a splint fixed to the two main fragments, bridging the fracture and leaving the complex fracture zone untouched [5]. The alignment, length, and rotation are restored but, to prevent further vascular damage, no attempt is made at anatomical reduction of each individual comminuted fragment.

Most types of plates, including compression plates (LC-DCP) (Fig. 6.62), locking plates (LCP) (Fig. 6.63), and the less invasive stabilization system (LISS) (Fig. 6.71, 6.72), can be used as a bridge plate, providing splintage and relative stability. The plate has to be long enough to span the comminuted fracture zone and provide adequate stability to the main proximal and distal fragments.

Spring hook plates (Figs. 6.39A, 6.64) are a form of buttress plate that are used in comminuted posterior acetabular wall fractures. They are used when significant fragmentation precludes fixation of each of the articular fragments with a

Fig. 6.50 Components of the dynamic hip screw (DHS). The main components are a *side plate with a barrel* (**a**) that accepts the *sliding hip screw* (**b**). The small compression screw (**c**) may be inserted at the completion of the procedure through the end of the barrel into the sliding screw for added compression. © Synthes, Inc. or its affiliates

lag screw. The hooked spring plates buttress and reduce small fragments against the femoral head in an attempt to remold the acetabulum back into shape.

External Fixator

External fixators are an integral part of the emergency polytrauma management. They provide rapid fracture stabilization and prevent further damage. External fixation is also useful in cases where internal fixation is contraindicated, such as with open (compound) fractures, closed fractures with severe soft tissue damage, contaminated fractures, markedly comminuted fractures, floating joints. It is also indicated for arthrodesis, corrective osteotomy, limb lengthening, and segmental bone transport procedures.

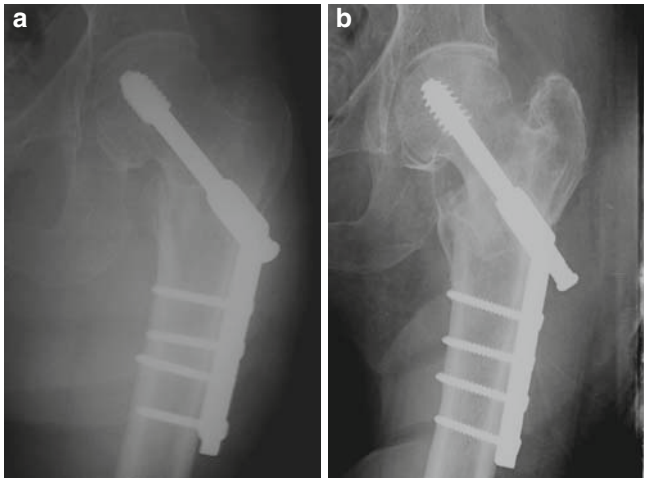

Fig. 6.51 DHS. AP hip radiographs after insertion (**a**) and after healing (**b**) of the fracture. Despite marked impaction and collapse at the fracture site in (**b**), the tip of the screw remains in the same place in the femoral head

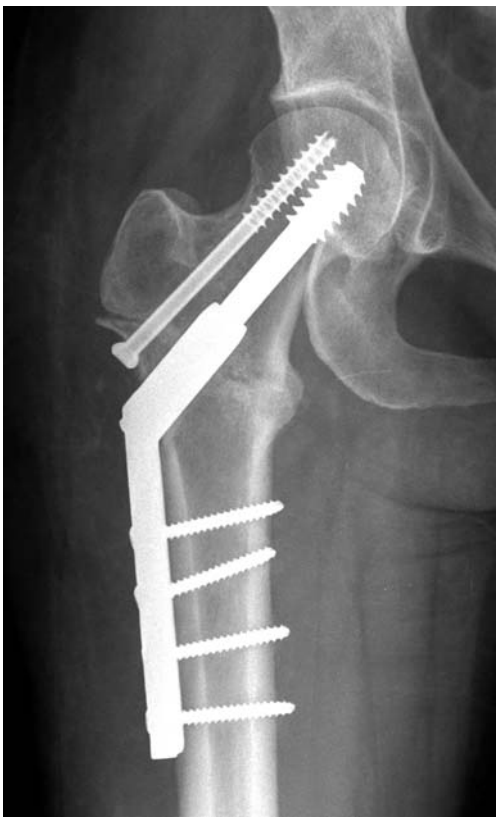

Fig. 6.52 DHS with an antirotation screw. Optimal DHS technique requires insertion of an antirotation screw for rotational stability. This screw should be inserted parallel to the sliding hip screw to allow the lag effect and gradual collapse

Fig. 6.53 Components of 95° dynamic condylar screw. The main components are a *side plate with a barrel* (**a**) that accepts the *sliding hip screw* (**b**). The small compression screw (**c**) may be inserted at the completion of the procedure through the end of the barrel into the sliding screw for added compression. © Synthes, Inc. or its affiliates

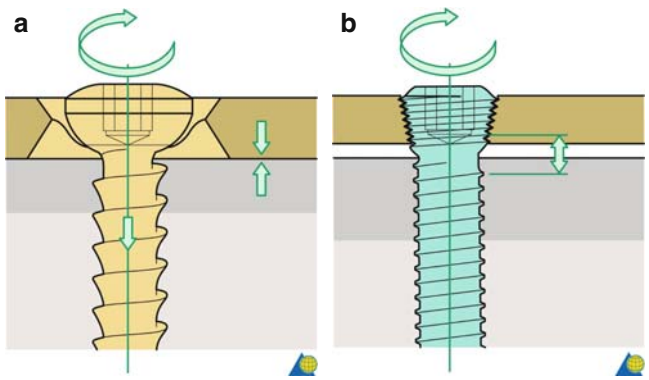

Fig. 6.54 Conventional and locking head screws. (**a**) Conventional compression screw acts by creating friction between the undersurface of the plate and bone (*arrows*). (**b**) Locking head screw acts like a bolt rather than a screw. It provides fixation by locking into position perpendicular to the plate. The plate is not compressed to the bone (*arrows*) (With permission from [17])

Types of Fixators

Three general categories of external fixators may be recognized:

1. Pin External Fixator
2. Ring External Fixator
3. Hybrid External Fixator

Pin External Fixator

The *AO tube–rod system* is a commonly used pin external fixator. In this system partially-threaded pins called Schanz screws and centrally-threaded Steinmann pins are inserted in the bone and are connected to stainless steel tubes or semi-radiopaque carbon fiber rods through metallic clamps (Figs. 6.65–6.67) [5, 22]. This is a very versatile system allowing different frame constructs including unilateral uni-

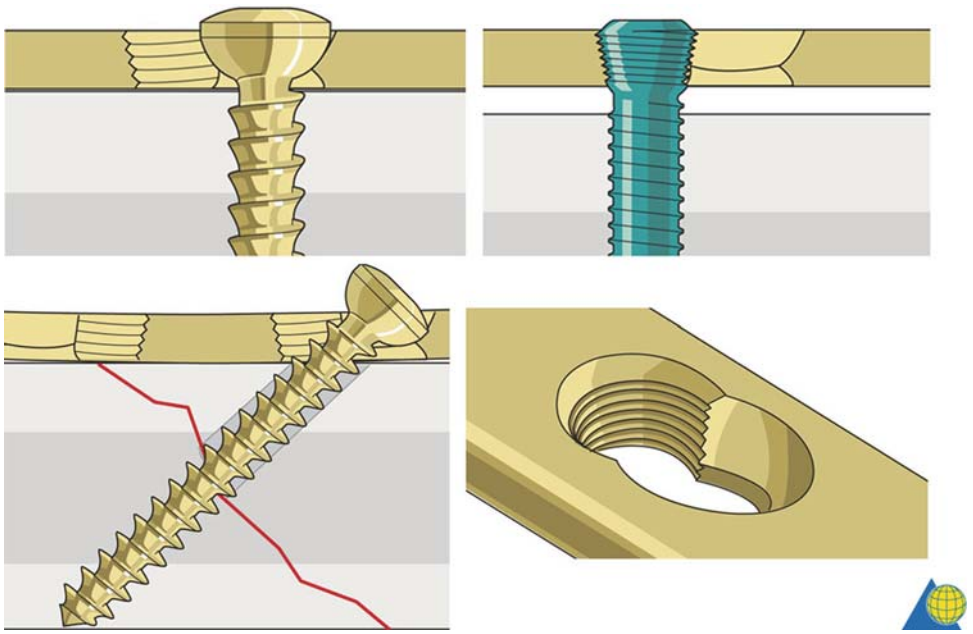

Fig. 6.55 Locking compression plates (LCP) can function both as a non-contact locking plate and/or as a compression plate. LCPs feature a combination hole. One half of the hole has the design of the standard dynamic compression plate, for conventional screws, including oblique interfragmentary lag screws, The other half is threaded and accepts the matching thread of the locking head screw, providing angular stability. Note that in locking screw mode, the plate is not in intimate contact with the plate – hence the term non-contact plating (With permission from [20])

planar, unilateral biplanar, and bilateral constructs. Unilateral frames use half pins (Schanz screws) (Fig. 6.67a–c), but bilateral frames require centrally-threaded Steinmann pins (Fig. 6.67a)

Ring External Fixator (Ilizarov Device)

The c*ircular ring fixator system* was devised in the early 1950s by an ingenius Syberian orthopedic surgeon, Gavriil Ilizarov. This system was for the most part unknown to the west until the 1980s, when Italian surgeons were confronted with patients coming from Yugoslavia with circular frames on their limbs. Rather than the thick Schanz screws, Ilizarov inserted numerous very thin pre-tensioned wires in bone and connected them to circular rings (Fig. 6.68 and 6.69). The Ilizarov frame allows multiple modes of treatment, including compression, distraction, lengthening, and bone transport, in monofocal, bifocal, and trifocal modes referring to the number of bone parts being transported.

His innovative concept is called *distraction osteogenesis* – or callus distraction. After creating a corticotomy, he applied a circular frame with tensioned wires inserted through the bone proximally and distally. After a 7-day period of compression, he gradually distracted the corticotomy site at a rate of 1 mm/day, causing progressive distraction of newly formed callus at the corticotomy. With optimal care, osteogenesis will occur at the distraction gap and the distracted callus will ossify over time.

Using his unique frame system and his discovery of distraction osteogenesis, Ilizarov successfully treated for the first time many complex and challenging conditions such as large segment bone defects, severe limb length shortenings, complex unstable fractures, difficult infected and aseptic nonunions, complex deformities, and arthrodesis. He was able to elongate, rotate, angulate, and shift segments of bones gradually relative to each other.

Ilizarov technique is now widely accepted for limb lengthening (Fig. 6.69) and for segmental bone transport in otherwise untreatable large segment bone defects.

Although amazing results can be obtained, this method is technically demanding and requires training and experience, as well as patience on the part of both the surgeon and the patient.

Hybrid External Fixator

The *hybrid external fixator* combines features of both the pin fixators and the circular ring fixators. They use thin pretensioned K-wires attached to half or three-fourth rings near the joint and thick Schanz screws and rod/tube system in the diaphyseal region. Their main indication is in fractures close to the joint in the proximal and distal tibia [5].

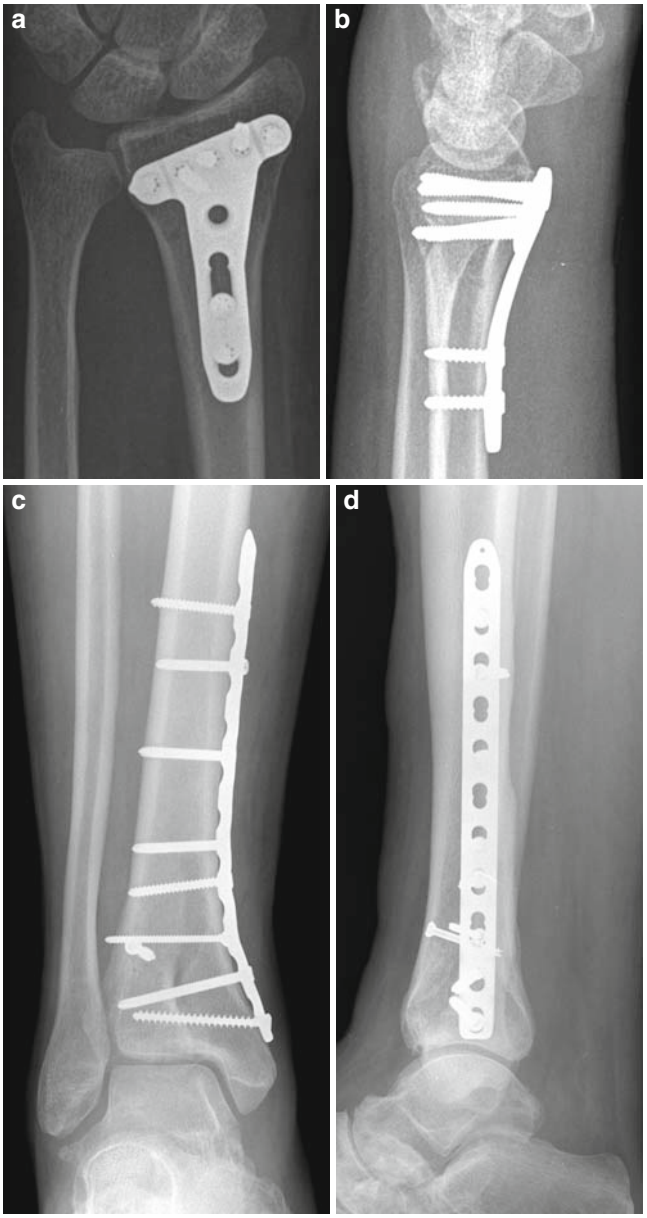

Fig. 6.56 Anatomically shaped distal radius LCP: PA (**a**) and lateral (**b**) wrist radiographs. simple LCP: AP (**c**) and lateral (**d**) ankle radiographs

Complications

Pin loosening is the most common complication of external fixators.

Pin tract infection is also a common complication of external fixators. It can lead to bone resorption and pin loosening, and formation of a ring sequestrum (Fig. 6.70). Good pin site care is essential in preventing pin tract infection.

Delayed union and nonunion are also potential complications of external fixation. To prevent this, as healing progresses, the patient is instructed to gradually increase weight-bearing in order to dynamize the construct [5].

Internal Fixator: LISS and LCP

Undesired structural changes that occur in the cortex underneath a compression plate – as a result of disturbed blood flow or stress shielding – have already been described (Page 215). Although development of limited contact dynamic compression plate (LC-DCP) with a reduced contact area between bone and plate has decreased the magnitude of these vascular changes, the LC-DCP still has to be compressed against the bone [5].

Recent development of the locking head screws and locking plates by AO brought about yet another new era in plate technology, called *non-contact plating*. A locking plate

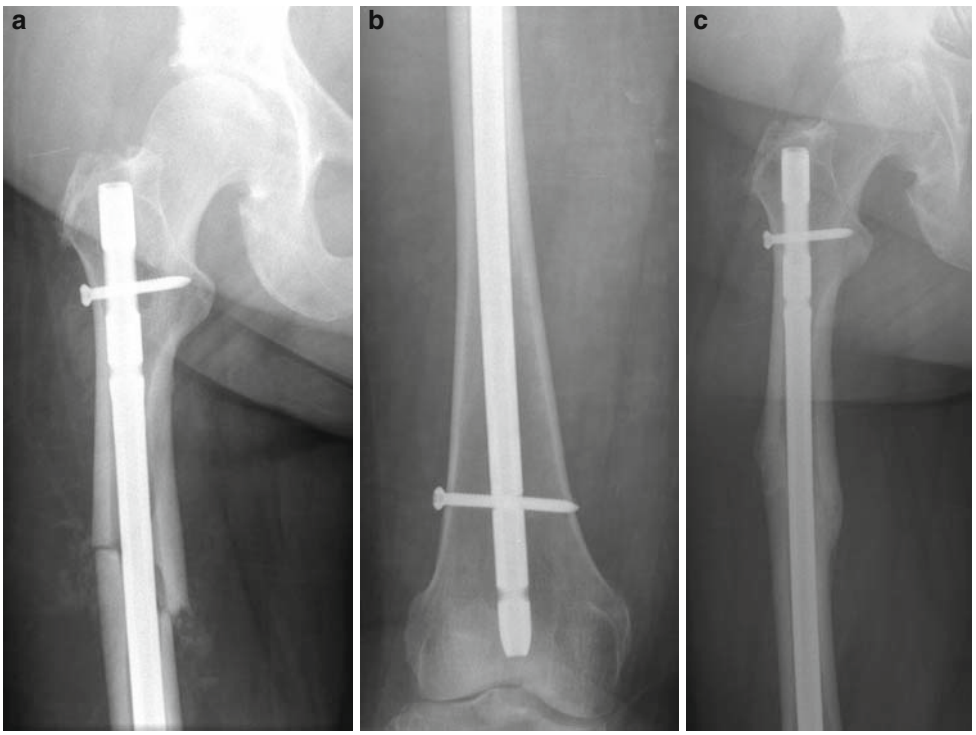

Fig. 6.57 Dynamic locking. AP radiographs of the proximal (**a**) and distal (**b**) femur immediately after nailing showing a femoral lnterlocking intramedullary nail in a dynamically-locked mode. Dynamic locking is used for stable fractures and allows axial compression at the fracture site to stimulate healing. AP radiograph 5 months later (**c**) shows solid healing

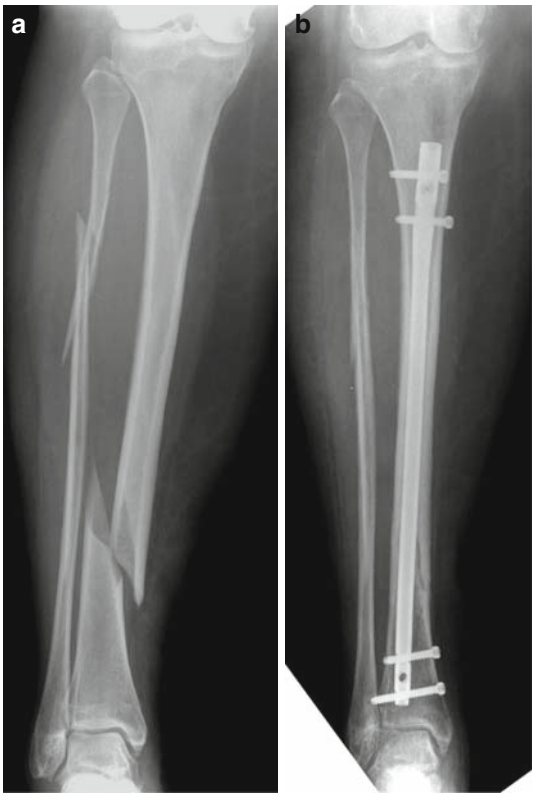

Fig. 6.58 Static locking. AP leg radiograph before (**a**) and after (**b**) placement of a statically locked intramedullary nail to fix an axially-unstable spiral distal tibial fracture. Insertion of multiple interlocking screws in the round static holes on both ends of the fracture interlocks the nail and the major proximal and distal fragments, and provides axial stability. Static locking is also indicated in comminuted fractures at risk of axial collapse. Interlocking also provides rotational stability. Static locking is an example of bone bridging mode of fixation

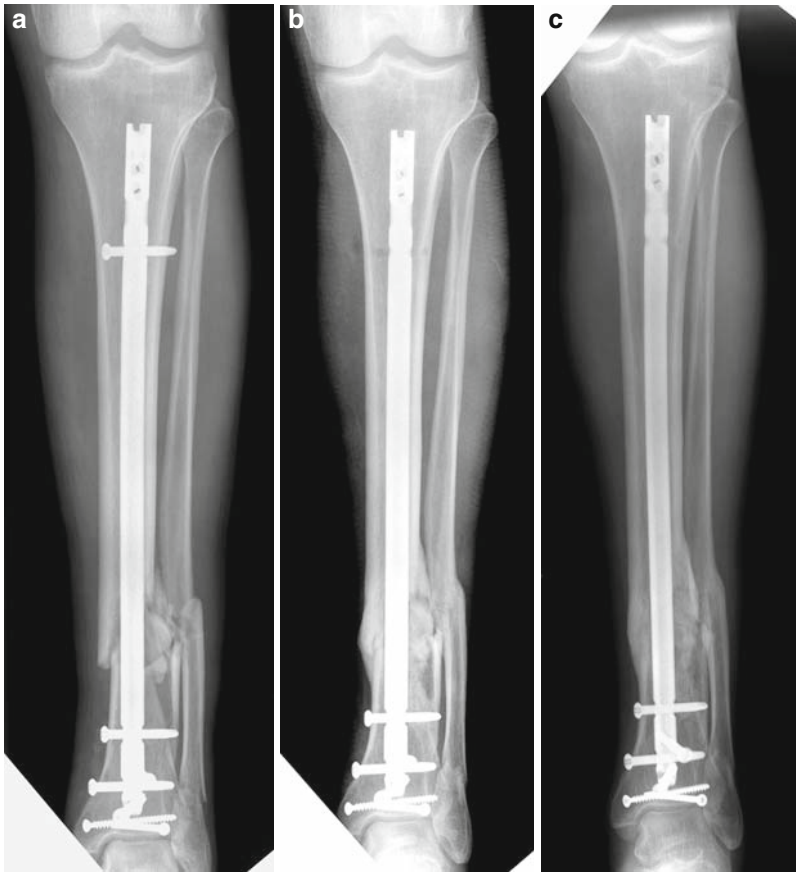

Fig. 6.59 Dynamization. AP radiographs of the left leg after static fixation (**a**), after dynamization (**b**), and 1 year later showing healing (**c**). Dynamization refers to removal of one or more proximal interlocking screws, so that no screw or only one screw in an oval-shaped dynamic hole remains. Note removal of the proximal, round hole screw in the dynamization process between (**a**) and (**b**). This allows axial stress to be transferred to the bone to stimulate healing. Dynamization should only be performed when the fracture and the newly formed callus has gained enough stability to withstand axial forces without collapse, usually after 2–3 months. Dynamization is sometimes necessary in tibial fractures when there is concern for delayed-union, but not usually in femoral fractures

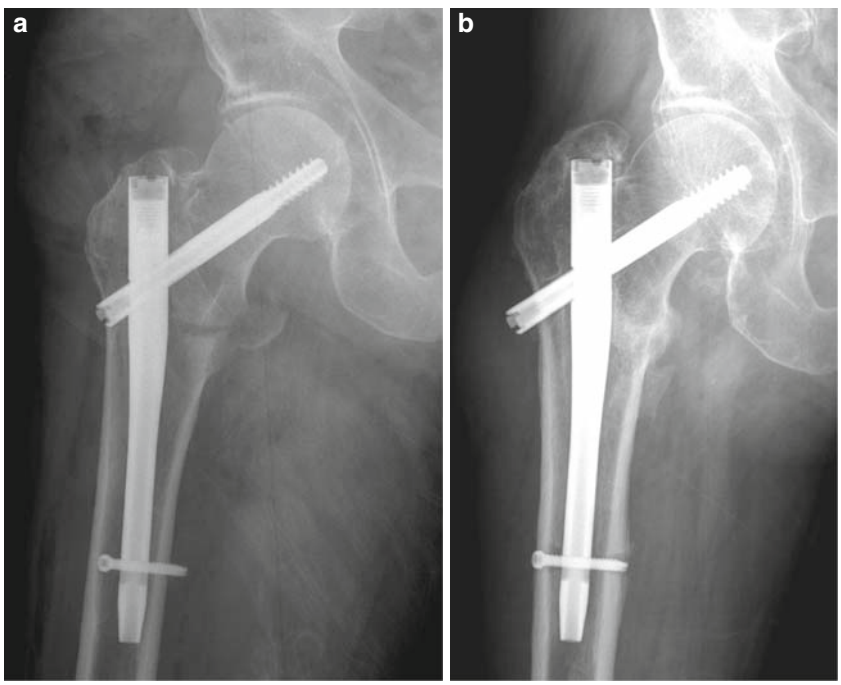

Fig. 6.60 Short PFN. AP radiograph immediately after fixation (**a**) and after healing (**b**). In simple and high subtrochanteric fractures (within 2 cm of the lesser trochanter), as seen in this case, a short PFN can be used. While the distal interlocking screw provides axial stability, the sliding screw allows impaction of the fracture during healing (similar to DHS), without risk of screw protrusion into the acetabulum. **b,** Healed high subtrochanteric fracture shows collapse and impaction of the fracture, as evidenced by sliding back of the hip screw. Note that there is no change in the position of the screw tip in the femoral head

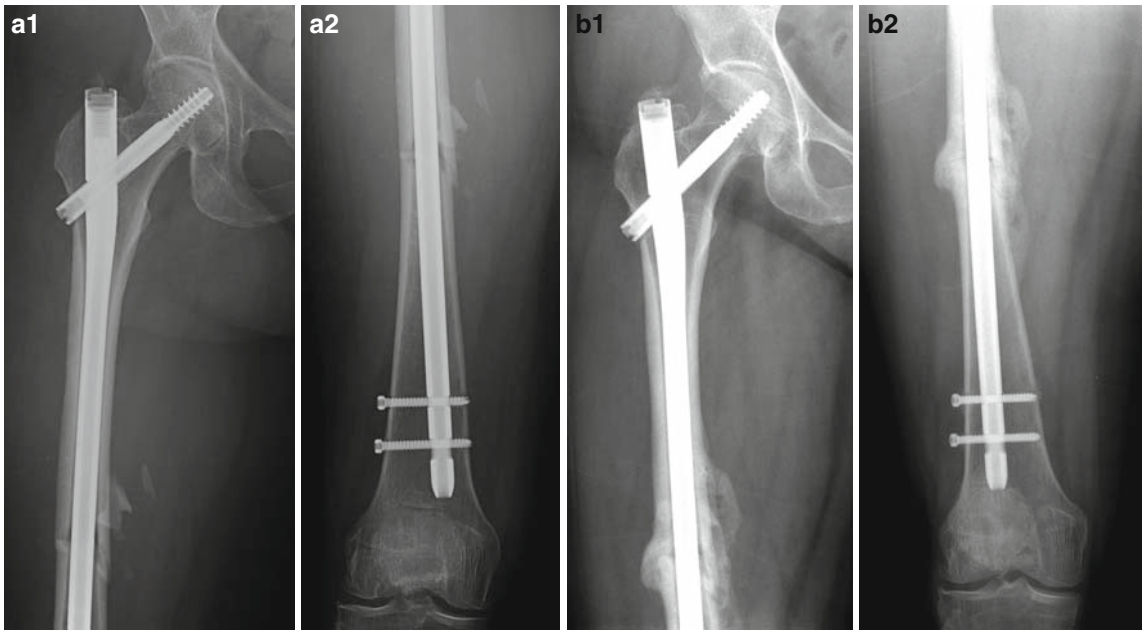

Fig. 6.61 Long PFN. AP radiographs of the femur immediately after fixation (**a1** and **a2**) and after healing (**b1** and **b2**). Although in this case a long PFN has been used to fix an unstable midshaft fracture, typically it is indicated for comminuted and low subtrochanteric fractures

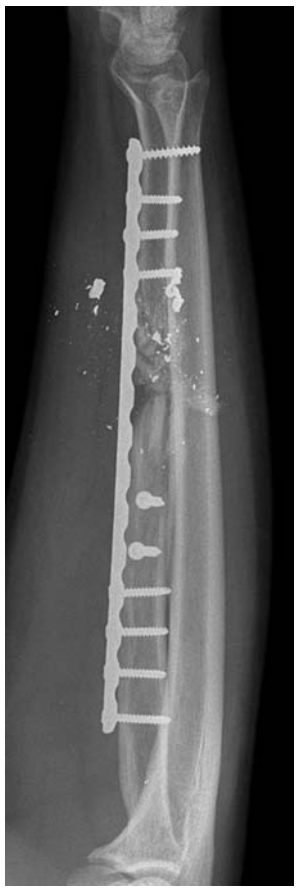

Fig. 6.62 Bridge plate. Lateral forearm radiograph showing application of a limited contact dynamic compression plate (LC-DCP) bridging a highly comminuted mid-diaphyseal fracture of the radius resulting from a gun shot injury. The fracture zone is left untouched to avoid further soft tissue damage. The plate is long enough to bridge the fracture and maintain stability of the proximal and distal fragments

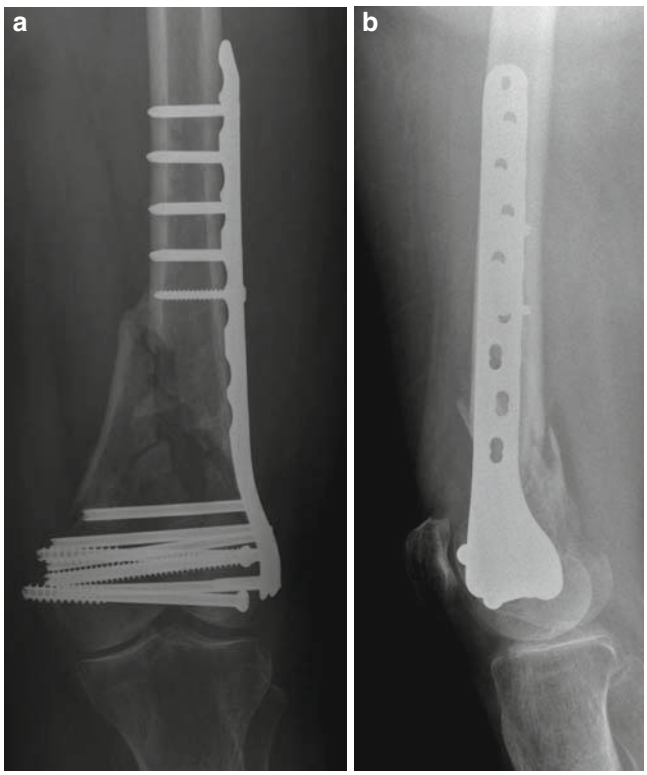

Fig. 6.63 Bridge plate. AP (**a**) and lateral (**b**) radiographs of the distal femur showing a locking compression plate (LCP) bridging a comminuted intraarticular supracondylar fracture of the femur. Note the cannulated lag screws in the epiphysis

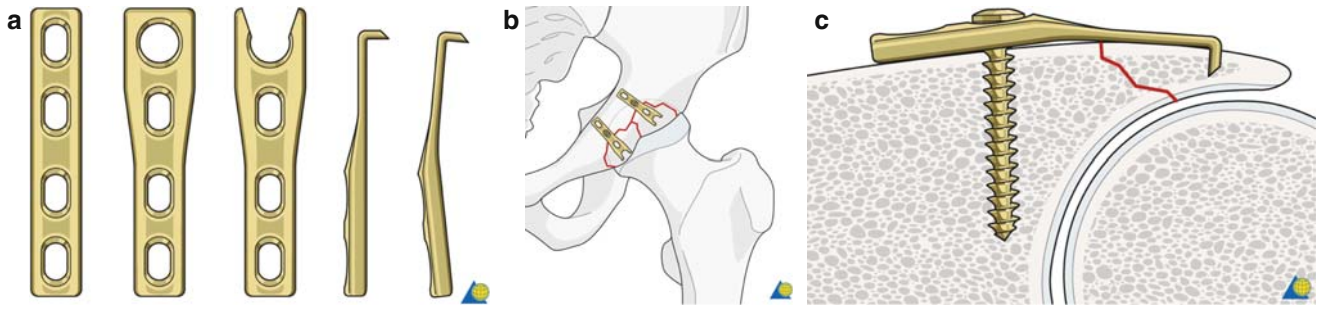

Fig. 6.64 Drawing of spring hook plates (**a**). Coronal (**b**) and cross-sectional (**c**) diagrams of a hip showing the use of spring plates to fix posterior wall acetabular fractures. Note the hook of the spring plate embedded into the fracture fragment (**c**). (With permission from [21])

Fig. 6.65 AO Schanz screws are used as half pins in monolateral frame constucts. (With permission from [22])

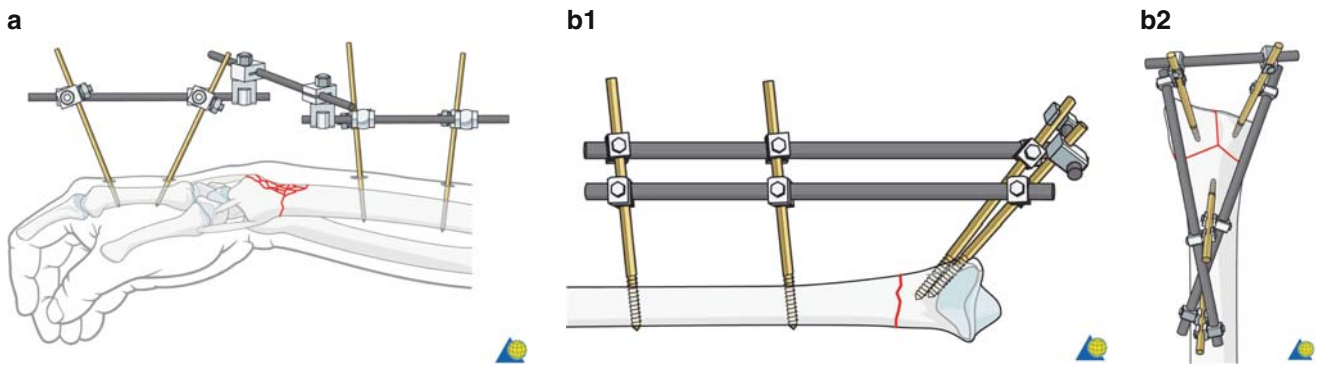

Fig. 6.66 AO tube-rod external fixator system. Diagrams of bridging (**a**) and non-bridging (**b**) external fixator fixing distal radial fractures. The bridging external fixator is fixed to bones proximal and distal to the fracture (**a**). This technique is used for fractures that are too close to the joint to insert Schanz screws in the distal fragment. Indirect reduction method using normal ligament tension (ligamentotaxis) is employed. The non-bridging fixator is applied with the Schanz screws directly in the fracture fragments (**b**). This allows direct reduction by manipulation of fragments using the fixator pins. (With permission from [23])

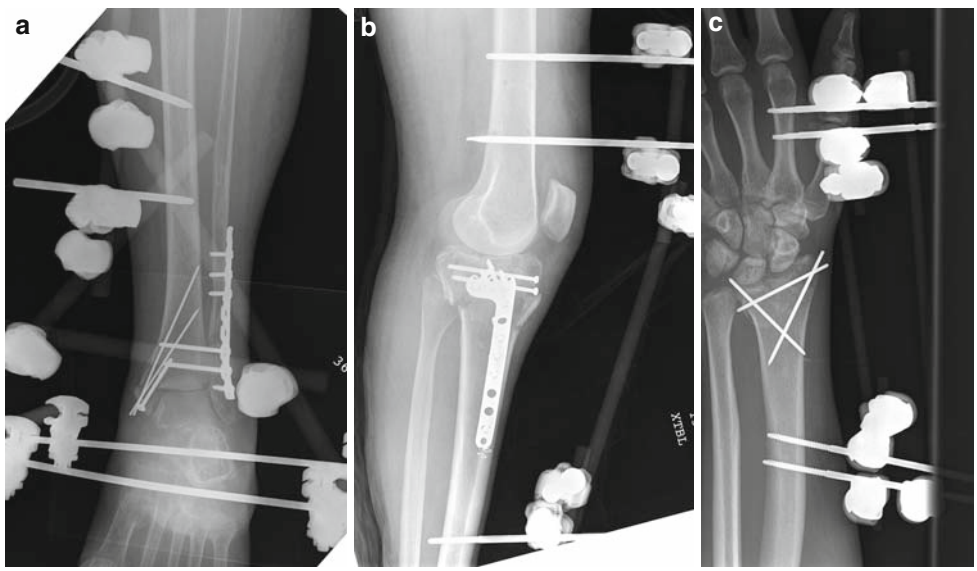

Fig. 6.67 AO tube-rod pin external fixator system. Three main components of this system are (**1**) Schanz screws, use as half pins for monolateral frame constructs (**a, b, c**) and centrally-threaded Steinmann pins, mainly inserted in the calcaneus and midfoot, to build bilateral frame constructs (**a**), (**2**) metallic clamps (**a-c**), and (**3**) stainless steel or semi-radiopaque carbon fiber rods (**a-c**)

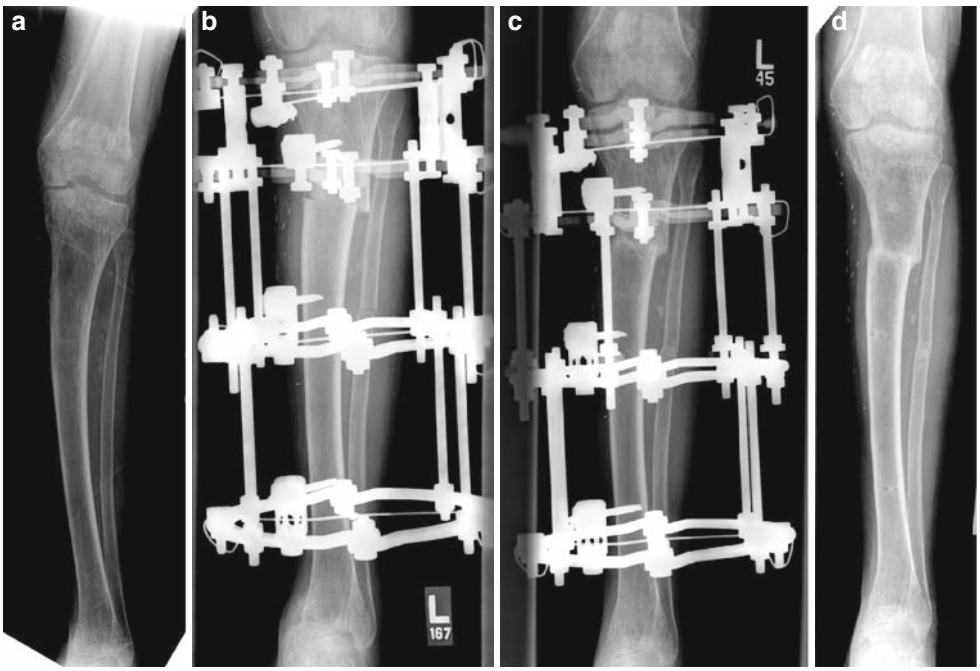

Fig. 6.68 Ilizarov ring fixator - *Monofocal Osteosynthesis in compression mode.* The fixator is used to correct valgus tibial bowing deformity. AP tibial radiograph shows valgus bowing of the tibia (**a**). AP tibial radiographs show application of an Ilizarov fixator after proximal tibial and mid fibular osteotomies (**b**) and later after healing (**c**). AP tibial radiograph (**d**) after removal of the frame shows the corrected valgus deformity and the healed osteotomies

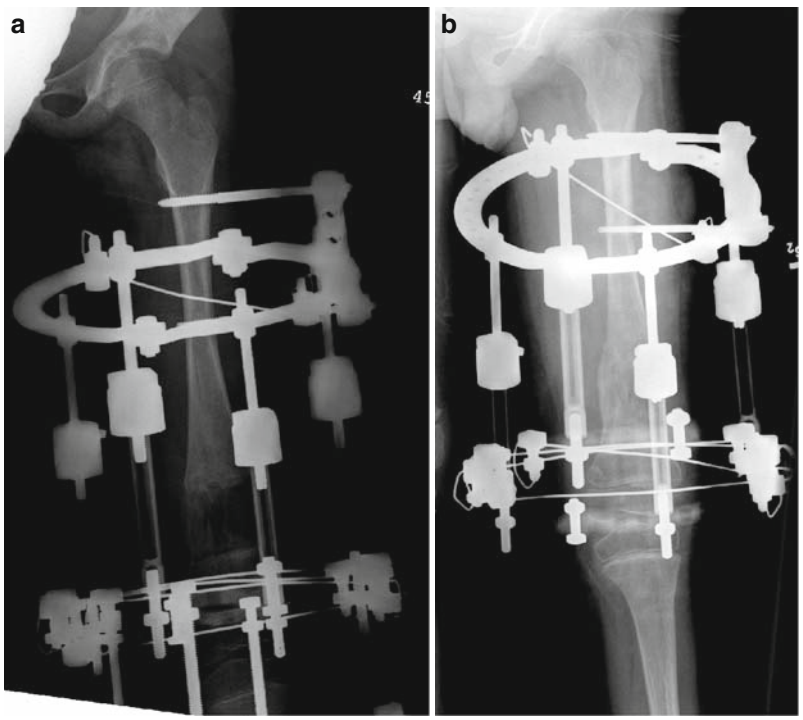

Fig. 6.69 Ilizarov ring fixator - *Monofocal Osteosynthesis in distraction mode* (distraction osteogenesis). The Ilizarov device is used to correct femoral leg length discrepancy using the distraction osteogenesis technique. AP femur radiograph (**a**) shows the frame in position with a large distal femoral corticotomy gap, and early ossification of the distracted callus. AP femoral radiograph (**b**) with the frame still in place but with the carticotomy gap now completely filled in with mature distracted callus

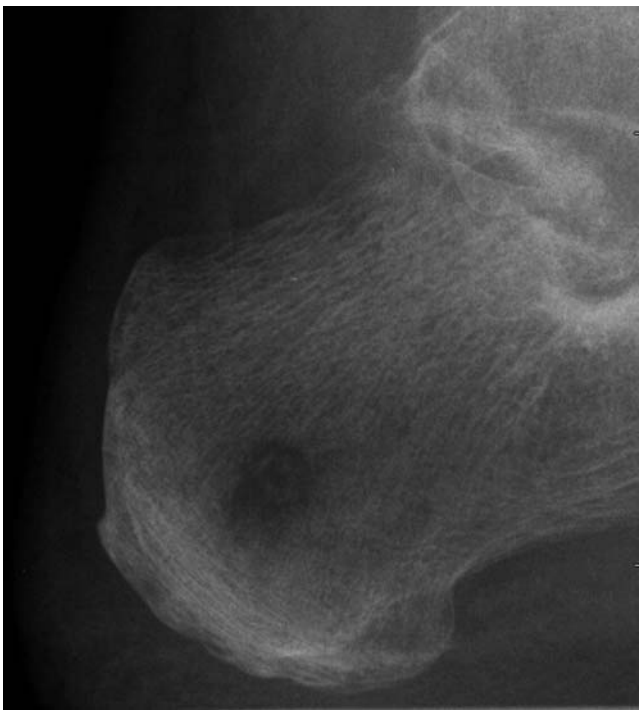

Fig. 6.70 Ring sequestrum. Lateral calcaneal radiograph showing a pin-tract sequestrum. A lytic area with poorly defined margins where a Steinmann pin once traversed the posterior calcaneus is present consistent with osteomyelitis. Note the residual ring-like sclerotic density within this lucency representing residual dead bone – the ring sequestrum – around where the pin had been. Courtesy of Jeffrey Towers, MD, Pittsburgh, PA

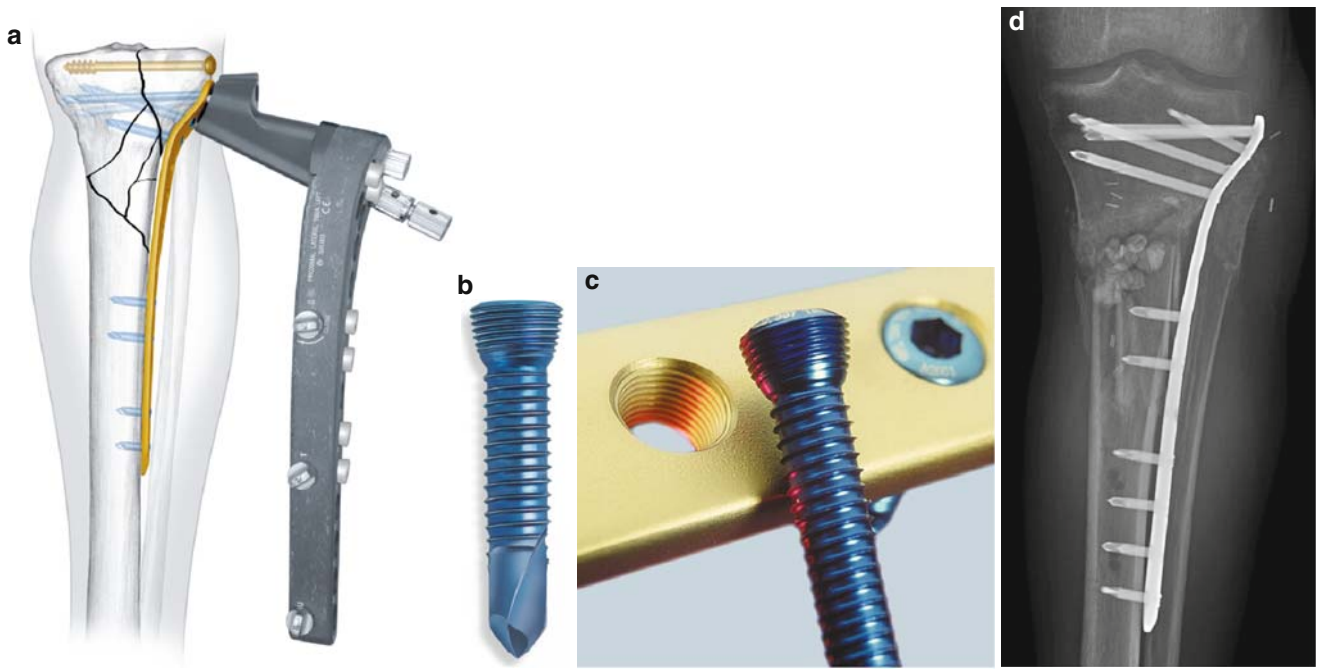

Fig. 6.71 Internal fixator: Less Invasive Stabilization System - LISS. Diagram (**a**): Anatomic shape of the plate and locked construct eliminates the need for intra-operative contouring of the plate. Percutaneous, submuscular plate insertion does not disrupt cortical blood supply. Fixed angle screws provide angular stability, and eliminate the need for additional implants to buttress the contralateral side. Note the self-tapping self-drilling unicortical locking head screws (**b–d**) and the non-contact nature of the plate (**d**). Unicortical locking screws offer angular stability and optimal purchase (hold). AP tibia radiograph (**d**) showing a LISS proximal tibia in place across a proximal tibial fracture. Although anatomically Shaped, this plate is not in contact with the tibia. (**a–c**) © Synthes, Inc. or its affiliates

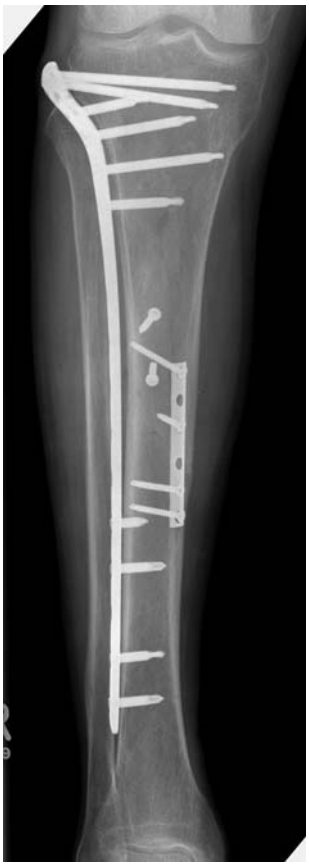

Fig. 6.72 LISS proximal tibia. AP tibial radiograph showing a healed fracture. Note the self-tapping self-drilling unicortical locking head screws and the non-contact nature of the plate

in fact functions similar to an external fixator placed in a submuscular location – hence the term *internal fixator* (Fig. 6.71).

LISS – Less Invasive Stabilization System

LISS was developed by Frigg at AO in 1994 [10]. The plates used in this method are anatomically shaped, for use in the distal femur and proximal tibia (Fig. 6.71). Fine contouring is not necessary since the plate does not need to contact the bone. Locking head screws in diverging and converging directions lock into the plate and provide angular stability and tremendous pull-out resistance. As the name implies, placing a LISS plate is a less invasive procedure. With the aid of a handle (Fig. 6.71a), the plate is inserted through a small incision in a submuscular position – rather than the subperiosteal position used in compression plates. The plate is fixed with multiple small locking screws, inserted percutaneously through small stab incisions. The screws are self-drilling and self-tapping (Fig. 6.71b–d) and can be placed unicortically, across a single cortex instead of through the entire diameter of the bone (Figs. 6.71d, 6.72).

LCP – Locking Compression Plate

Locking compression plates (LCP), developed by Wagner and Frigg in 2001 at AO, are recent refinements of the LISS [10]. The LCP has already been described in this chapter (Page 224). In brief, LCP features combination holes that combine a dynamic compression unit hole with a locking screw hole (Fig. 6.55). The combination hole provides the flexibility of the plate to function as a conventional compression plate, as a LISS, or a combination of both. Similar to LISS, LCP can be inserted percutaneously in a submuscular position.

Conclusion

The AO recently celebrated its 50th anniversary. It is ironic that a movement that revolutionized the face of fracture fixation so dramatically through development of generations of compression plating techniques has seen those techniques gradually move away from the bone's surface. First AO developed the limited contact compression plates and now has entered the era of non-contact plating. Although these techniques have moved from compression to non-compression, they remain soundly based on fundamental scientific principles.

References

1. Colton CL, Green SA, Matta JM, Colton CL. History of fracture treatment. In: Browner BD, Jupiter JB, Levine AM, Trafton PG, (Eds.), Browner: Skeletal Trauma, Basic Science, Management, and Reconstruction, 3rd ed. Philadelphia: Elsevier/WB Saunders, 2003.
2. Texhammar R, Colton C. AO/ASIF instruments and Implants. A technical manual, 2nd ed. Berlin/Heidelberg/New York: Springer-Verlag, 1994.
3. Hunter J. Experiments and observations on the growth of bones. In: Palmer JR, (Ed.), The Transactions of a Society for the Improvement of Medical and Chirurgical Knowledge. London: Longman, Rees, Orme, Brown, Breen, & Longman, 1837.
4. Rüedi TP, Murphy WM. AO Principles of Fracture Management, 1st ed. Davos, Switzerland: AO Publishing, 2000.
5. Rüedi TP, Buckley RE, Moran CG. AO Principles of Fracture Management, 2nd ed. Davos, Switzerland: AO Publishing, 2007.
6. Danis R. Théorie et Pratique de l'Ostéosynthèse. Paris: Masson, 1949.
7. Schenk R, Willenegger H. Zum histologischen Bild der sogenannten Primärheilung der Knochenkompakta nach experimentellen Osteotomien am Hund. Experientia 1963; 19:593–595.
8. Mazzocca AD, Andrew E. Caputo AE, Browner BD, Mast JW, Mendes MW. Principles of internal fixation. In: BD Browner, JB

Jupiter, AM Levine, PG Trafton (Eds.), Browner: Skeletal Trauma, Basic Science, Management, and Reconstruction, 3rd ed. Philadelphia: Elsevier/WB Saunders, 2003.
9. Pauwels F. Biomechanics of the Locomotor Apparatus, 1st ed. Berlin/Heidelberg/New York: Springer-Verlag, 1980.
10. Wagner M, Frigg R. AO Manual of fracture management. Internal fixators. Concepts and cases using LCP and LISS, 1st ed. Davos, Switzerland: AO Publishing, 2006.
11. Müller ME, Allgöwer M, Schneider R, Willenegger H. Manual of Internal Fixation. Techniques Recommended by the AO-ASIF Group, 3rd ed. Berlin/Heidelberg/New York: Springer-Verlag, 1991.
12. Browner BD, Jupiter JB, Levine AM, Trafton PG (Eds.). Browner: Skeletal Trauma, Basic Science, Management, and Reconstruction, 3rd ed. Philadelphia: Elsevier/WB Saunders, 2003.
13. Ito K, Perren SM. Biology and biomechanics in bone healing. In: Rüedi TP, Buckley RE, Moran CG, (Eds.) AO Principles of Fracture Management. 2nd ed., Davos, Switzerland: AO Publishing, 2007:9–31.
14. Kinnaert P. History of the ISS/SIC: Robert Danis, A True General Surgeon. World J Surg 2002; 26:1202–1205.
15. Gautier E, et al. Surgical reduction. In: Rüedi TP, Buckley RE, Moran CG, (Eds.) AO Principles of Fracture Management. 2nd ed., Davos, Switzerland: AO Publishing, 2007:164–187.
16. Krettek C. Intramedullary nailing. In: Rüedi TP, Buckley RE, Moran CG, (Eds.) AO Principles of Fracture Management. 2nd ed., Davos, Switzerland: AO Publishing, 2007:257–285.
17. Messmer P, et al. Screws. In: Rüedi TP, Buckley RE, Moran CG, (Eds.) AO Principles of Fracture Management. 2nd ed., Davos, Switzerland: AO Publishing, 2007: 213–225.
18. Lorich DG, et al. Plates. In: Rüedi TP, Buckley RE, Moran CG, (Eds.) AO Principles of Fracture Management. 2nd ed., Davos, Switzerland: AO Publishing, 2007: 226–247.
19. Hak DJ, Stewart RL. Tension band principle. In: Rüedi TP, Buckley RE, Moran CG, (Eds.) AO Principles of Fracture Management. 2nd ed., Davos, Switzerland: AO Publishing, 2007:248–255.
20. Sommer CP, et al. Internal fixator. In: Rüedi TP, Buckley RE, Moran CG, (Eds.) AO Principles of Fracture Management. 2nd ed., Davos, Switzerland: AO Publishing, 2007: 321–335.
21. Bartlett CS, Helfet DL. Acetabbulum. In: Rüedi TP, Buckley RE, Moran CG, (Eds.) AO Principles of Fracture Management. 2nd ed., Davos, Switzerland: AO Publishing, 2007: 718–749.
22. Höntzsch D, et al. External fixator. In: Rüedi TP, Buckley RE, Moran CG, (Eds.) AO Principles of Fracture Management. 2nd ed., Davos, Switzerland: AO Publishing, 2007:301–319.
23. Rikli DA, Campbell LA. Distal radius and wrist. In: Rüedi TP, Buckley RE, Moran CG, (Eds.) AO Principles of Fracture Management. 2nd ed., Davos, Switzerland: AO Publishing, 2007:656–677.
24. Rüedi TP, et al. AO philosophy and evolution. In: Rüedi TP, Buckley RE, Moran CG, eds. AO Principles of Fracture Management. 2nd ed., Davos, Switzerland: AO Publishing, 2007:1–6.

Chapter 7

Systematic Approach to Tumors and Focal Lesions of Bone

Shigeru Ehara and Jasvir S. Khurana

Abstract Bone neoplasms consist of mesenchymal tumors, hematopoietic tumors, and metastasis from mainly epithelial carcinomas. Also non-neoplastic bone lesions that mimic true tumors, including bone cysts and Langerhans cell histiocytosis, need to be included in the differential diagnosis. Classic analyses on tumor margin, mineralized matrix, and periosteal reaction, based on plain radiography, are important for differential diagnoses. CT provides greater morphological detail about the bone surrounding a lesion, and a similar analysis can be applied in the same way as classic radiographic margin analysis. MR imaging is particularly useful for preoperative staging of tumor extent and involvement of critical tissues such as joints, nearby neurovascular bundles, and muscles. In addition, it is particularly useful to evaluate aggressive lesions, with transcortical infiltration, a sign of highly aggressive lesions, and intertrabecular infiltration, a sign of focal infiltrative growth seen in malignant tumors. An "Aunt Minnie" approach often works, but radiologists have to approach non-specific or atypical lesions systematically.

Keywords Bone tumors • Metastases • Tumor margin • Mineralized matrix • Periosteal reaction

Introduction

Focal lesions of bone fall into two primary categories, those that are primary and those that are metastatic. Primary lesions may be neoplasms arising from the bone; related to acquired metabolic processes, e.g. brown tumors in hyperparathyroid ism or hemophilic pseudotumors; they may be related to inborn errors of metabolism, e.g. Gaucher disease or Langerhans Cell Histiocytosis or genetically induced events, e.g. fibrous dysplasia. Regardless, primary tumors of bone are rare compared with metastatic lesions. Benign primary lesions are again much more common than malignant ones. Even so, focal bone lesions represent a fascinating and exotic part of musculoskeletal pathology and imaging. Here we present a systematic approach to the analysis of focal osseous lesions that will aid the reader in arriving at the correct imaging diagnosis and improve understanding of the underlying pathology.

S. Ehara (✉)
Department of Radiology, Iwate Medical University School of Medicine, Morioka 020-8505, Japan
e-mail: ehara@iwate-med.ac.jp

Bone Tumors

Classification of Bone Tumors

Neoplasms arising from bone and bone marrow consist of three groups. The first group contains tumors that are derived from mesenchymal elements, principally bone and cartilage. This group is the main subject of this chapter. Osteosarcoma, chondrosarcoma, and their benign counterparts are included in this category. These tumors arise primarily from the bone and theoretically are curable by surgical resection.

The second group of bone tumors arises from hematopoietic cells in the marrow, for example, leukemia, malignant lymphoma, and multiple myeloma. These lesions are thought to originate from the hematopoietic stem cells. Instead of forming a focal mass lesion, they may be distributed throughout the hematopoietic bone marrow. In such widespread tumors, chemotherapy, not surgical resection, is the treatment of choice.

The last and the most common tumor group is metastasis from epithelial carcinomas. Bone, together with lung and liver, is the preferred site for carcinoma metastases. Both hematopoietic precursor tumors and metastases tend to localize in the axial skeleton where there is red marrow with high blood flow. Often, when these tumors spread to the peripheral skeleton, it is an indication that the central marrow has become fibrotic or packed with tumor. In these circumstances, new red marrow is recruited peripherally from yellow marrow to meet the organism's hematopoietic needs.

A. Bonakdarpour et al. (eds.), *Diagnostic Imaging of Musculoskeletal Diseases: A Systematic Approach*,
DOI 10.1007/978-1-59745-355-4_7,

As the peripheral marrow converts, it tends to behave identically to the normal axial red marrow, becoming a bed for new metastases or spread of infiltrating hematopoietic neoplasms.

A fourth group of lesions that needs to be considered in the differential diagnosis of neoplasms is non-neoplastic bone lesions that mimic true tumors. This group of lesions may have the characteristics of either neoplasm or inflammation.

Bone Tumor Statistics

Primary bone tumors, both malignant and benign, are rare. Primary malignant bone tumors are uncommon, constituting only 0.2% of all neoplasms [1]. Their incidence is only 0.8 in 100,000 people per year [2]. Although the exact numbers are not known, metastatic tumors in bone far outnumber primary bone tumors by as much as 50–100 times. Lung, breast, and prostate carcinomas are among the most common to metastasize to bone. The most common primary malignant bone tumor is multiple myeloma. Osteosarcoma is the most common malignant mesenchymal tumor of bone, with an incidence of 2–3 in 1,000,000 people per year. Among malignant mesenchymal tumors, osteosarcoma accounts for about 35%, chondrosarcoma about 25%, and Ewing sarcoma about 16% of newly diagnosed tumors. Precise statistics on benign bone tumors are not available, but the most common benign tumors in the pathology literature are osteochondroma.

Unlike most visceral and soft tissue sarcomas that become more prevalent at older ages, most mesenchymal bone tumors including benign ones tend to occur in a young age group during or shortly after active skeletal growth. This rule of thumb is not hard and fast, however. For example, the incidence of chondrosarcoma increases with age. Osteosarcoma has a bimodal age distribution. The first peak is in the second decade (ages 11–20) and the second peak is seen in patients older than 60. Typically, this older peak occurs in bones afflicted with Paget disease. Extremity tumors are common in young patients, but craniofacial tumors are more common in older patients.

Genetics of Bone Tumors

Advances in cytogenetic and molecular genetics have contributed greatly to the understandings of sarcomatogenesis. Genes related to oncogenesis include well-studied oncogenes and tumor suppressor genes. Characteristic fusion genes have been identified in the Ewing sarcoma/PNET group: EWS/FLI1 t(11;22) (q23;q12), EWS/ ERG t(21;22)(q22;q12), EWS/ETV1 t(7;22)(q22;q12), EWS/EIAF t(17;22)(q21;q12), EWS/FEV t(2;22) (q33;q12), EWS/ZSG inv(22)(q12q12), and FUS/ERG t(16;21)(q11;q22) [3]. Extraskeletal myxoid chondrosarcoma and synovial sarcoma have characteristic chromosomal translocations and associated fusion genes. Although genetic analysis does not replace histologic investigation, it plays an important complementary role for histological confirmation and diagnosis.

Differential Diagnosis of Solitary Bone Lesions

Classic Analyses

Margin Analysis

Evaluation of the margin of primary bone lesions has proven to be the most successful system of image analysis, and it is used for both grading and differential diagnosis. The Armed Forces Institute of Pathology (AFIP) system has become a standard of analysis (Fig. 7.1) [4]. Lesions are categorized first by the size and appearance of the lesion. Type I lesions are called geographic (IA: with sclerotic margin, IB: with partial sclerotic margin, IC: without sclerotic margin) because they occupy a single large area of the bone as though they have grown from a single expanding nidus. Type II lesions are called moth-eaten because they leave the bone with multiple small areas of luceny of varying sizes as a moth-eaten coat might appear. Type III lesions are termed permeative and appear as fine lytic lesions with indeterminate margins as if the lesion is spreading aggressively in all directions. Grade IA lesions, those surrounded by a sclerotic rim, tend to be indolent. The sclerotic rim indicates that the host bone has had time to react and wall off the lesion. Grade IB and IC lesions are localized, but active with some growth potential. Grade II and III lesions are infiltrating, consistent with aggressive lesions.

Generally long bone lesions' margins have different appearances depending upon whether they are on the epiphyseal or diaphyseal sides of the lesions. Typically, the diaphyseal margin of the lesion is less well defined because there are few trabeculae within the diaphysis of long bones and

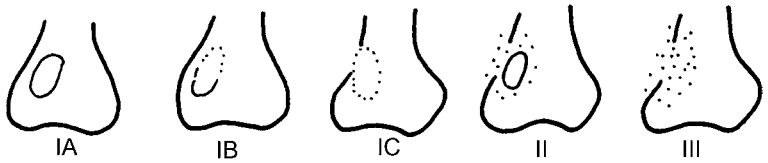

Fig. 7.1 AFIP grading system

thus little contrast with the soft tissue tumor. The epiphyseal margin, on the other hand, is usually better defined and may even have some marginal sclerosis because of the abundant trabeculae at this margin of the lesion.

Lodwick system of bone tumor classification is a system similar to the AFIP system [5]. Lodwick system uses cortical expansion of the one while the AFIP system does not. More than 1 cm cortical expansion is designated as grade IB. Partial cortical disruption is classified in Lodwick system as IA and IB. On the other hand, total cortical penetration is the characteristic of IC margin. The AFIP grading system uses the zone of transition at the margin of the lesion instead of cortical destruction. A wide zone of transition is characteristic of more aggressive lesions.

Matrix Analysis

Tumor matrix is an extracellular substance produced by some mesenchymal tumors, e.g., osteoid, chondroid, and collagen (Fig. 7.2). Osteoid and chondroid matrix may calcify or ossify in a characteristic manner permitting a specific diagnosis or at least indicating the cell line of origin of the tumor [6].

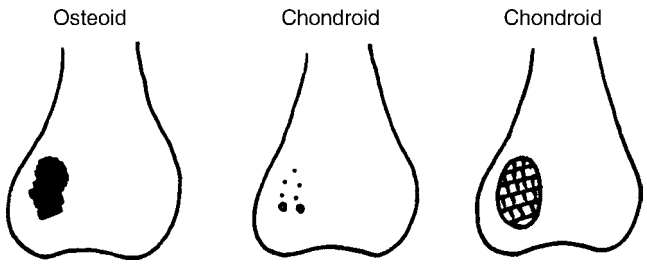

Fig. 7.2 Patterns of mineralized matrix. Chondroid matrix vs osteoid matrix

Osteoid matrix represents the product of membranous ossification and appears as amorphous or cloud-like ossification on imaging (Fig. 7.3). Bone-forming tumors, typically osteosarcoma, have this type of matrix. It is important to differentiate myositis ossificans from periosteal and parosteal osteosarcoma with osteoid matrix. The location and maturity of the ossification help to make this differential. While tumor osteoid forms in an irregular pattern throughout the tumor, ossification in myositis ossificans is organized and forms peripherally first and then matures centripetally.

Chondroid matrix represents calcification upon cartilage in chondroid tumors, such as chondromas and chondrosarcomas. Ironically, the better differentiated the cartilage formed by the tumor, the more likely it will develop a calcified matrix. Thus, the more calcified matrix a chondrous lesion has at imaging, in general, the better differentiated it will be histologically. The cartilage in chondroid tumors tends to grow in an irregular pattern that resembles a mulberry. As a result, the deposited calcium has an appearance of "O"s, "C"s, and "rings and arcs" (Fig. 7.4). Differential diagnosis of chondroid matrix includes the ossification seen in bone infarcts and osteonecrosis, and the sequestra that may be contained in Brodie abscess.

Periosteal Reaction

Focal periosteal reaction is not formed by a lesion but is a response of the native bone to heal itself and wall off the lesion. As such, its presence is a sensitive but non-specific indicator of the presence of an underlying lesion (Fig. 7.5) [7]. Since the native bone forms the periosteal new bone, biopsy of areas of periosteal reaction usually will not yield a diagnosis.

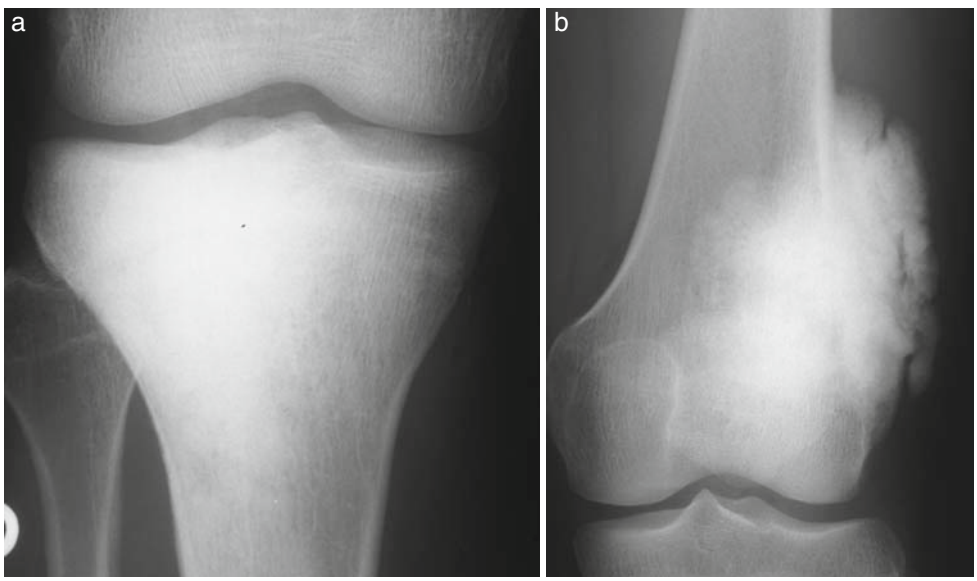

Fig. 7.3 Osteoid matrix: **a**. Amorphous intraosseous mineralization (osteosarcoma) and **b**. amorphous extraosseous and intraosseous mineralization (osteosarcoma)

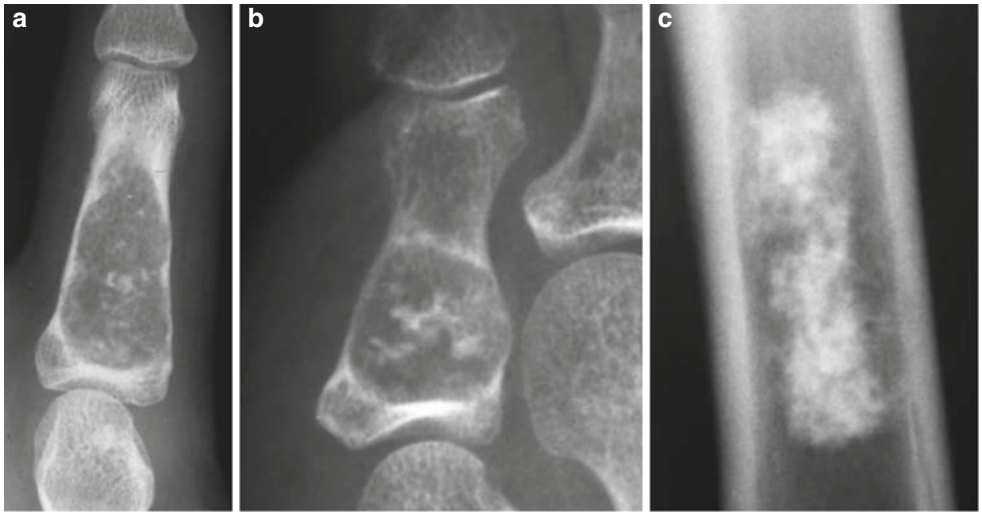

Fig. 7.4 Chondroid matrix: **a**. Punctate mineralization (enchondroma); **b**. "rings" and "arcs" mineralization (enchondroma); and **c**. dense mineralization (enchondroma)

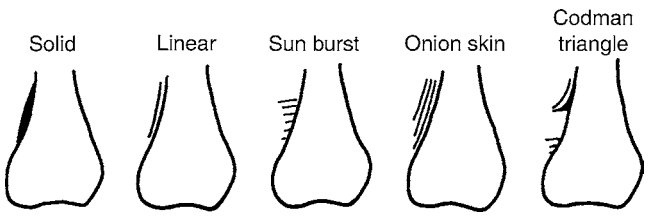

Fig. 7.5 Periosteal reaction

On the other hand, the appearance of the periosteal reaction can provide a clue to the aggressivity and growth pattern of a lesion. The thicker the periosteal new bone, the less aggressive the lesion. The more radiolucency visible radiographically within areas of periosteal reaction, the more aggressive the lesion. Thus, thin and solid linear periosteal reaction on the cortical surface is a sign of active healing. When the periosteal reaction becomes chronic, it thickens and may incorporate into the cortex to give rise to an appearance of focal cortical thickening. If the periosteal reaction shows thin layers of luceny between thicker layers of new bone in a laminated pattern (Fig. 7.6), this indicates accelerated periosteal bone growth, not alternating slow and fast growth [8].

Spiculation or sunburst reaction is a sign of a rapidly growing lesion (Fig. 7.7), forcing growth of the reactive bone perpendicular to cortex. Here, the reactive new bone is intermingled with the neoplastic process. The same is true of "onion skin" periosteal reaction, where layers of dense new bone interpose themselves between layers of tumor (Fig. 7.8). The latter are lucent and must be thicker than the layers of periosteal new bone to qualify for this description. Similarly, central interruption of the periosteal reaction by a lytic process, creating Codman triangle of periosteal new bone at the edge of the lesion, signifies that the tumor is growing rapidly and destroying previously formed reactive

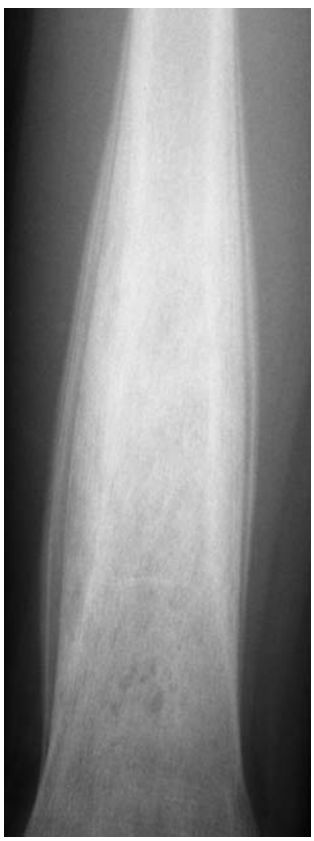

Fig. 7.6 Laminated periosteal reaction (Langerhans cell histiocytosis)

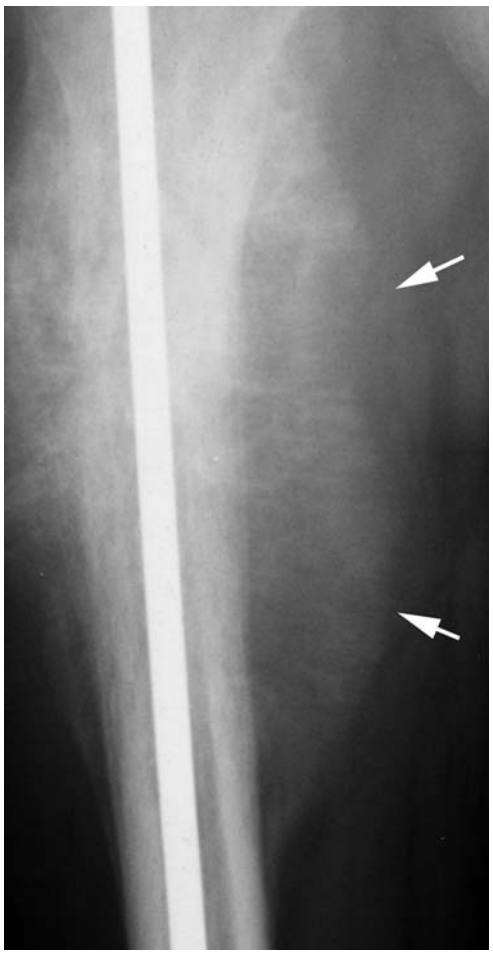

Fig. 7.7 Spiculated periosteal reaction (Ewing sarcoma). Spiculated periosteal reaction is evident medially (*arrows*)

bone. This is a sign of aggressivity and occurs with malignant tumors as well as some forms of infection (see Fig. 7.10A).

CT Analysis of Bone Tumors

CT provides greater morphological detail about the bone surrounding a lesion, and analysis can be applied in the same way as classic radiographic margin analysis [9]. A well-defined lesion within the cortex suggests indolent growth while evidence of cortical penetration, destruction, or permeation is a sign of aggressiveness (Fig. 7.9). As with radiographic analysis, CT has a grading system. Lesions contained in the bone or by periosteal new bone are grade I and represent relatively indolent processes. Lesions that partially penetrate or destroy the cortex are called grade II. Penetration of the cortex or periosteal new bone shows aggressiveness. Grade III lesions completely penetrate through the cortex but show no localized bone destruction.

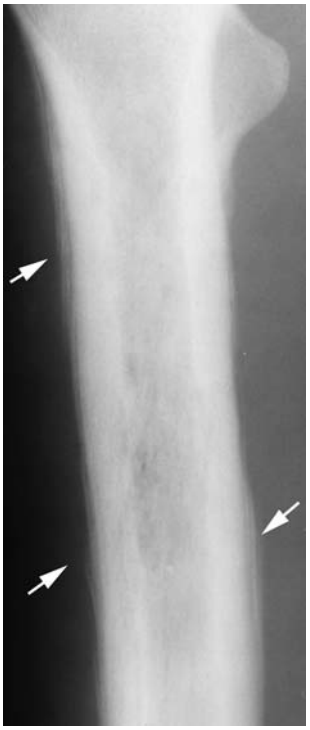

Fig. 7.8 Onionskin periosteal reaction (Ewing sarcoma). Multi-layered periosteal reaction with focal areas of interruption is noted (*arrows*)

These are highly aggressive, permeative lesions, e.g., Ewing sarcoma. CT margin analysis is particularly useful when the tumor margin is not well seen on plain radiographs. This applies particularly to lesions in the vertebrae and flat bones, such as the ilium and scapula.

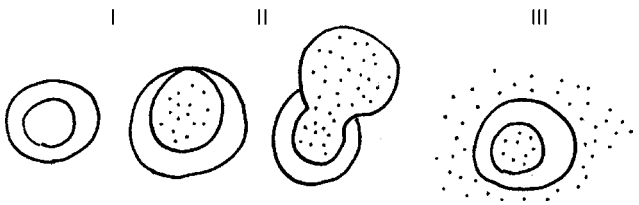

Fig. 7.9 CT grading system (concept of Brown system)

MR Imaging of Bone Tumors

MRI is exquisitely sensitive to lesions that replace marrow and destroy bone. It shows the full extent of lesions' growth into the soft tissues. Although MR is sensitive, it provides relatively few diagnostic clues to a lesion's nature (discussed below). As such, it is particularly useful for preoperative staging of tumor extent and involvement of critical tissues such as joints, nearby neurovascular bundles,

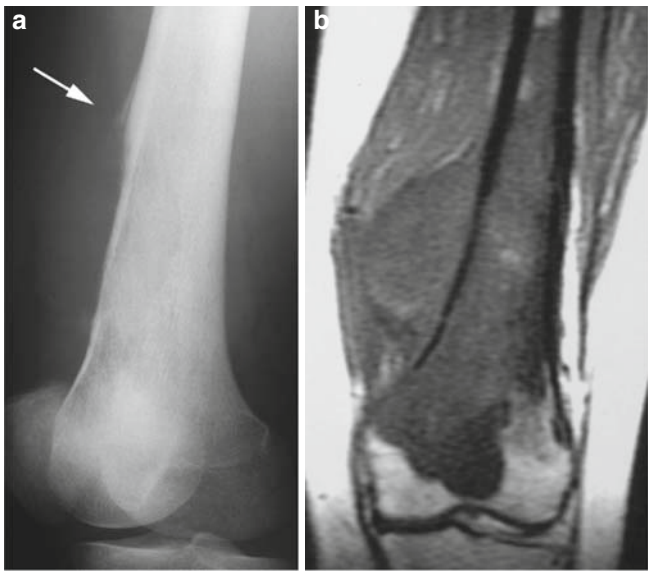

Fig. 7.10 Transcortical infiltration seen in osteosarcoma (16-year-old woman): **a**. plain radiography, oblique view and **b**. T1-weighted coronal MR image. Infiltration of the tumor through the intact cortex is evident. Codman triangle is noted (*arrow*)

and muscles. MRI is particularly useful to evaluate aggressive lesions. It depicts transcortical infiltration, a sign of highly aggressive lesions, better than CT (Fig. 7.10). MR also depicts intertrabecular infiltration, a sign of infiltrative growth seen in malignant tumors (Fig. 7.11). It also shows active tumor growth in periosteal and endosteal extension at tumor margins.

Approach to Specific Locations

Vertebral column

Two structural columns form the spine. The vertebral bodies compose the anterior column and the posterior column includes the pedicles, lamina, facet joints, and spinous processes. Hematopoietic tumors, typically multiple myeloma, and less commonly malignant lymphoma arise in vertebral bodies and epithelial tumors also commonly metastasize to the bodies. Vertebral bodies are a common site of hemangiomas; these may extend into the posterior elements as well. Giant cell tumors occur in both the anterior and posterior elements, but more commonly in the vertebral body. Some mesenchymal tumors commonly arise in the posterior columns (Fig. 7.12), typically osteoid osteoma, osteoblastoma, and aneurysmal bone cyst. In fact, over 50% of osteoblastomas arise in the spine. Chordomas are notochordal rest tumors and therefore occur only in the spine and the clivus, most commonly the sacrum, followed by the clivus and then the junction of the odontoid with the C2 vertebral body. Otherwise, most tumors have no specific predilection for any particular spinal level. Both CT and MRI show tumor extent in the spine, but MRI is more sensitive.

Chest wall

Ribs have the characteristics of both tubular and flat bones. They are common sites of metastasis. Fractures occur more commonly in ribs than metastases and for obvious reasons it

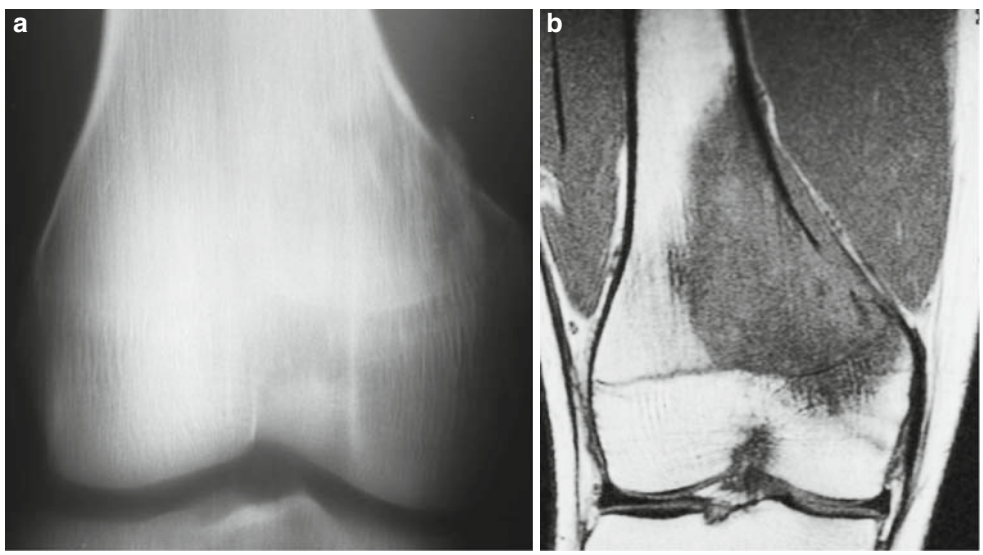

Fig. 7.11 Intertrabecular infiltration and periosteal extension in fibroblastic osteosarcoma (16-year-old man): **a** AP tomogram and **b** T1-weighted MR image. The tumor infiltrates into the intact bone trabeculae and extends along the periosteum. Sclerosis may be due to thickened trabeculae seen on tomography (©: Bunkodo)

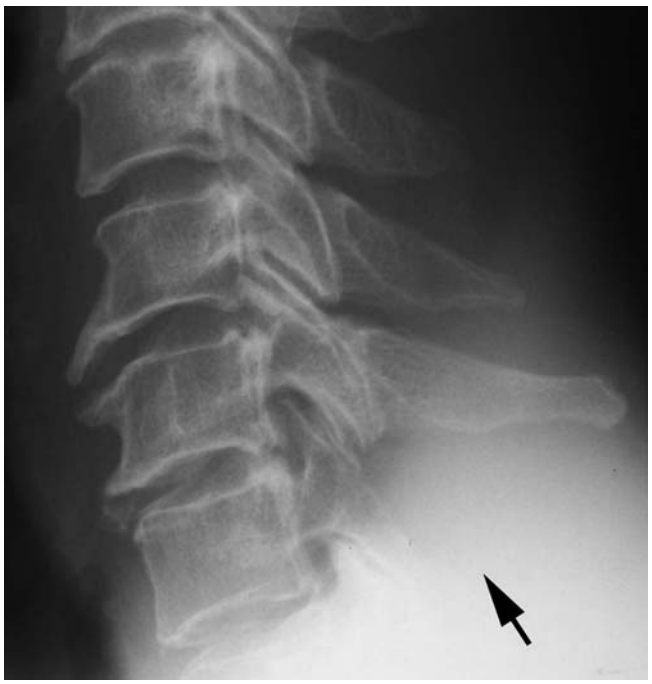

Fig. 7.12 Osteolytic metastases to the posterior element (metastasis from hepatocellular carcinoma, 65-year-old man). Spinous process of C7 is destroyed (*arrow*) (©: Medical view Co.)

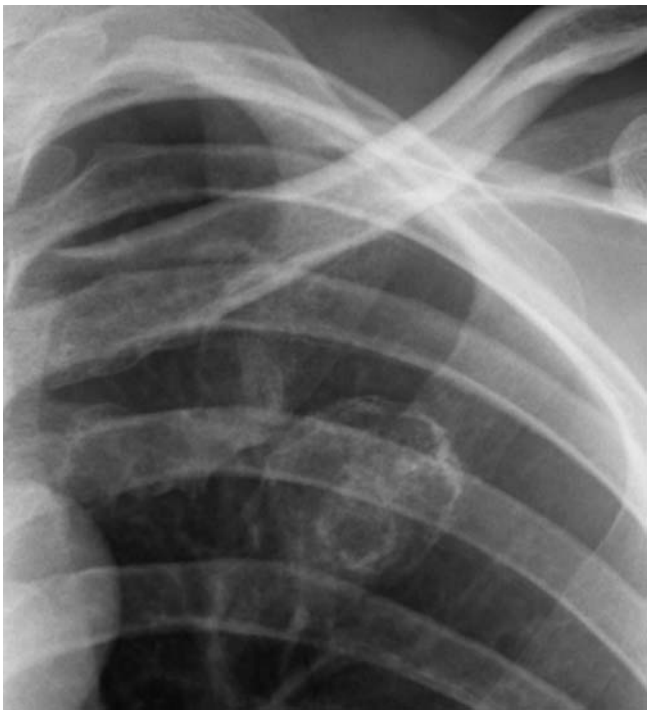

Fig. 7.13 Enchondroma of the rib. Expansive tumor is seen at the anterior edge of the rib (29-year-old man)

is important to differentiate the two. A solitary metastasis to the rib is uncommon and occurs in less than 10% of abnormal bone scans with a single rib focus.

Fibrous dysplasia is the most common benign process involving the rib. Chondroid tumors, including enchondroma and chondroblastomas, occur in any portion of the rib, but they most commonly occur anteriorly, close to costal cartilage (Fig. 7.13). Tumors arising in the sternum are usually malignant, most commonly multiple myeloma and metastases. CT and MR imaging are suitable for evaluation of the chest wall (Fig. 7.14), but here CT has hedgemony because of its rapid imaging time and hence a better visualization of smaller lesions.

Pelvis

The pelvis consists of the ilium, ischium, pubis, and sacrum, and similar to the ribs, metastases and hematopoietic tumors most often arise here. The triradiate cartilage in the acetabulum may be a site of origin of chondroid tumors. The pelvis has multiple epiphyses and apophyses making differential diagnosis difficult (Fig. 7.15). The configuration of the pelvis and overlying bowel gas on radiographs may make lesion analysis problematic, and often CT and MRI are needed for adequate diagnosis and staging.

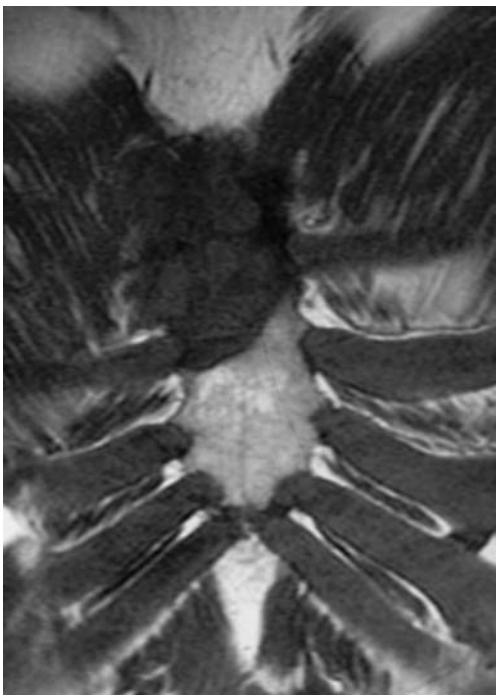

Fig. 7.14 Osteosarcoma metastases to the sternum (27-year-old man). Coronal T1-weighted image representing a low-signal lesion

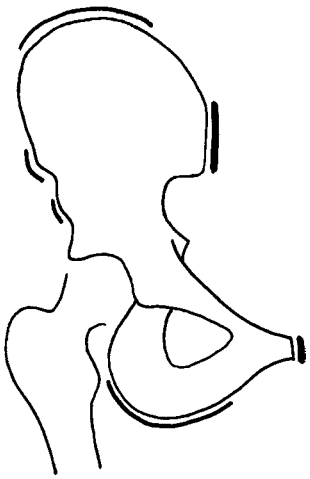

Fig. 7.15 Apophyses of the pelvis

Skull

Membranous bone forms the calvarium and the diploic space remains filled with hematopoietic marrow throughout life. Thus, hematopoietic tumors and pseudotumors, including multiple myeloma, lymphoma, and Langerhans cell histiocytosis, commonly occur here. The occipital bone lacks hematopoietic marrow, and so these disorders occur in this portion of the skull less commonly. Hemangiomas are common in the skull, second only to their incidence in the vertebrae. Fibrous dysplasia and Paget disease frequently affect the skull. Fibrous dysplasia affects both the calvarium, where it is characteristically has an ill-defined mixed appearance, and the skull base and facial bones where it may appear as a sclerotic lesion. Paget disease is more common in the cranial vault, but may occasionally affect the skull base.

Staging of Bone Tumors

There are two staging systems of bone tumors: Musculoskeletal Tumor Society system, and TNM (AJCC-UICC) system.

Musculoskeletal Tumor Society (Enneking) System

This staging system is only applicable to mesenchymal tumors, not hematopoietic tumors and is based on grades (G), tumor sites (T), and metastases (M). The grade can be benign G0, low-grade malignant G1, or high-grade malignant G2. It is the mixture of histologic, radiologic (Lodwick grading system), and clinical factors. Tumor site is classified into intracompartmental (T1) and extracompartmental (T2). Metastases can be either absent (M0) or present (M1). All lymph node metastases are included in M factor, the same as distant metastases in this system.

TNM System

The TNM system, developed by AJCC (American Joint Commission on Cancer) – UICC (International Union against Cancer) [10], has limited use in staging mesenchymal tumors. TNM stands for local tumor extent, nodal involvement, and distant metastases. Mesenchymal tumor staging using this system is as follows:

- Local tumor extent (T) (Fig. 7.16): The local tumor extent is defined as the anatomic region surrounded by a natural barrier and the tumor extent whether intracompartmental or extracompartmental is important for surgical planning (Table 7.1). Skip metastases, a separate focus in the same bone, are classified as T3, rather than M1. Skip metastases may also include separate tumor foci just across the joint [11]. CT and MR imaging are suitable for defining tumor extent in determining intra- and extracompartment tumor extension [12, 13].
  - T1 is tumor of 8 cm or less in the greatest dimension,
  - T2 is tumor more than 8 cm in the greatest dimension,
  - T3 is discontinuous tumor in the primary site (skip metastases).

- For mesenchymal tumors, nodal involvement (N) has similar implications as metastases (M). Both imply a poor prognosis. In the TNM system, only axillary and inguinal nodes are considered to be regional nodes and so less potentious than metastases [14, 15]. Occasionally, a question may arise as to whether distant foci of

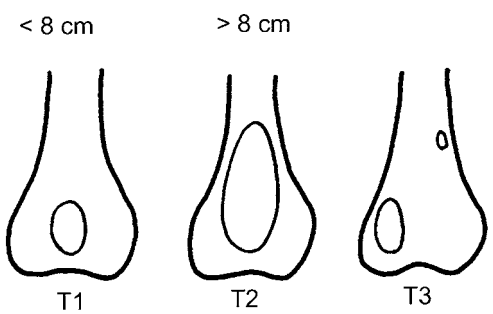

Fig. 7.16 T1-factor of bone tumors

Table 7.1 Compartment

Upper arm	Anterior, posterior
Forearm	Volar, dorsal, mobile wad
Pelvis	Each muscles
Thigh	Anterior, posterior
Calf	Anterior, lateral, deep posterior, posterior
Foot	Medial, calcaneal, lateral, interosseous (4), superficial central, deep central, skin

tumor in bone represent metastases (M stage) or multicentric primary tumor. For example, in a certain subset of patients, osteosarcomas may arise synchronously in different parts of the body.

- An additional G-factor, standing for histological grade of mesenchymal tumors, has been added to the TNM grading system in an attempt to classify cellular atypia and pyknosis. Here grade 1 stands for well differentiated and the grading becomes progressively worse to grade 4 which stands for poorly differentiated.

Imaging Evaluation of Tumor Response After Chemotherapy and RT

Plain radiography is of limited value to assess tumor healing and recurrence. Initially, the soft tissue component may regress rapidly, and periosteal reaction may become consolidated in the healing process. Nonetheless, once a large portion of the bone has been destroyed, healing and remodeling are usually slow and incomplete. Thus, it is difficult to evaluate treatment response.

MR imaging with Gd enhancement can assess treatment response in the early phase after therapy. Scar tissue may also enhance, albeit typically slowly and slightly, and confound the question of recurrent tumor. A dynamic contrast study of enhancement with time generally will show that scar tissue enhances less briskly than tumor. This test is not routinely performed clinically since it is limited to specific scan planes and cannot be done throughout the entire lesion.

Nuclear imaging can assess tumor bulk after treatment. Thallium-201 (^{201}Tl) scan is useful to assess treatment response both early on and later after therapy. Fluorine-18 fluorodeoxyglucose (^{18}F-FDG) positron emission tomography (PET) can assess treatment response in early phases of therapy (Fig. 7.17). Both modalities show treatment response before signs on CT or MR imaging become evident. Furthermore, PET/CT promises to be very useful in evaluation of tumor response to therapy. Continued research will establish a reasonable imaging protocol for bone tumor patients after therapy.

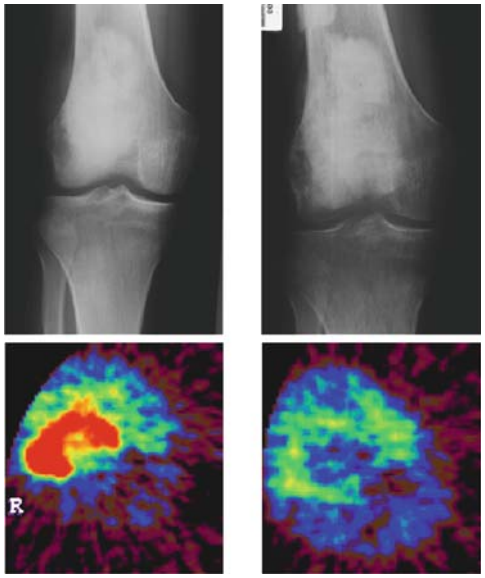

Fig. 7.17 PET for treatment response. Before and after chemotherapy for osteosarcoma. Although no significant interval changes on plain radiography is noted, decrease in the tracer uptake in the lesion is evident (courtesy of Dr. Hideo Shiraishi)

Cartilaginous Tumors

Benign Chondroma

Chondromas are benign neoplasms consisting of hyaline cartilage forming chondrocytes. They occur in any portion of a bone, but most commonly arise in metaphyses. Diaphyseal lesions are not uncommon in long tubular bones. Chondromas frequently arise in the small bones of hands and feet. They occur most often in the bone marrow (enchondroma), but may also arise on the cortical surface (periosteal chondroma). Chondromas typically arise in a young age group, 10–30 years of age, but they may be diagnosed in older patients because they are persistent, slow-growing lesions that cause few symptoms.

Enchondroma is a central well-defined lesion with variable matrix formation (Figs. 7.18 and 7.19). Typically, the matrix has a radiographic appearance of rings, arcs, and an appearance similar to chicken-wire fence. The matrix usually is distributed uniformly throughout the lesion. Thus, a localized lucent area within the lesion suggests potential malignancy, typically a low-grade chondrosarcoma.

Differentiation between benign enchondroma and low-grade chondrosarcoma represents a challenge to the pathologist and radiologist [16]. Chondromas should not cause any cortical destruction when they arise in the bone marrow of large tubular bones (Fig. 7.20), but cortical erosion and

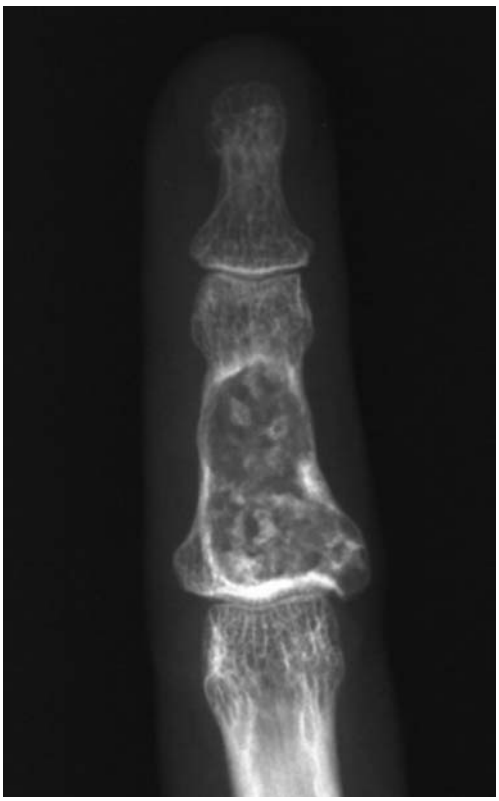

Fig. 7.18 Enchondroma, phalanx (51-year-old woman). A well-defined lytic lesion is associated with chondroid mineralization

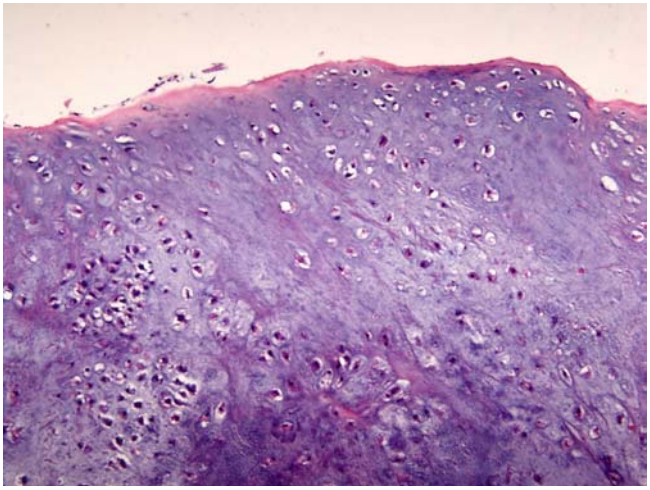

Fig. 7.18H Well-delineated lobule of cartilage from an enchondroma. The lesion is relatively hypocellular and composed of typical chondroblasts lacking atypia, mitoses, necrosis, and myxoid change

penetration may occur in benign chondroma of the small bones of the hands and feet. According to the AFIP, erosion through more than two-thirds of the cortical thickness suggests malignancy (Fig. 7.21), particularly in the large long tubular bones, e.g., femur, humerus, and tibia [17]. MR imaging typically shows abundant hydrophilic hyaline cartilage, seen as lobulated high-signal lesion characteristic of hyaline cartilage on T2-weighted fat-suppressed imaging [18] (Figs. 7.19 and 7.22). Patients with Ollier and Maffucci syndromes have multiple enchondromas, the latter also with hemangiomas, and are discussed in the section on Congenital/Hereditary Syndromes.

Periosteal chondroma (juxtacortical or parosteal chondroma, ecchondroma) is less common than enchondroma, mainly arising from the surface of metaphysis of a long bone. It is most common in proximal humerus and distal femur. Typically, it causes saucerization of the cortical margin of the metaphysis with a thin rim of sclerosis [19]

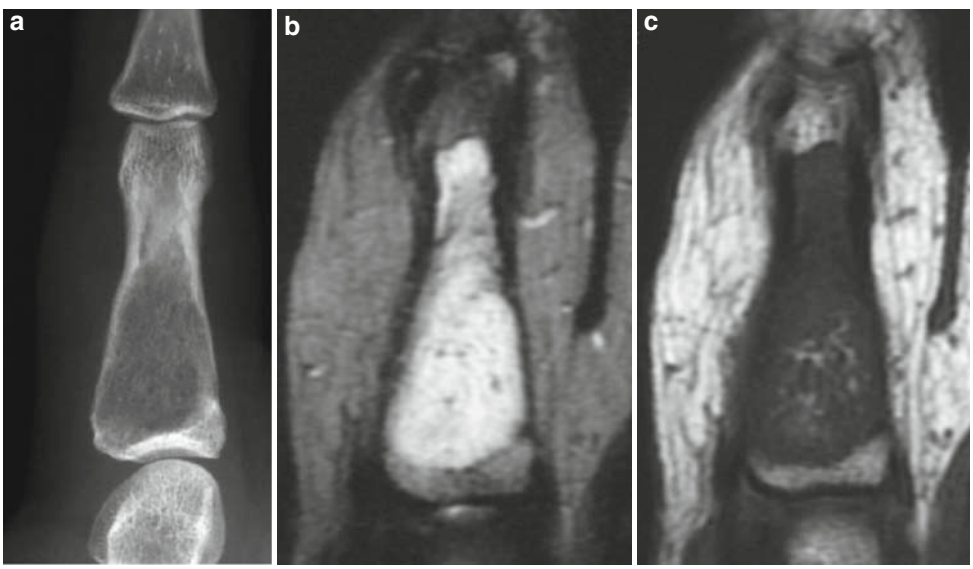

Fig. 7.19 Enchondroma, phalanx (28-year-old woman). **a**. Radiography demonstrating a well-defined lytic lesion with no mineralization. **b**. T2-weighted coronal MR image. Bright signal intensity represents hyaline cartilage. **c**. T1-weighted coronal MR image. Bright signal intensity represents fat interposition among the lobules of chondroid matrix

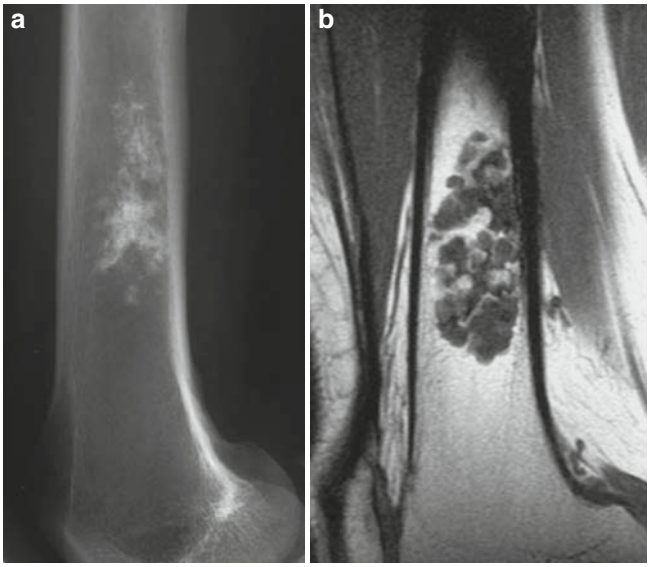

Fig. 7.20 Enchondroma, femur (60-year-old man). **a**. Lateral view. Chondroid mineralization is seen in the bone marrow of the distal femur. No cortical erosion is noted. **b**. Sagittal T1-weighted MR image. Lobules of chondroid are evident in the bone marrow

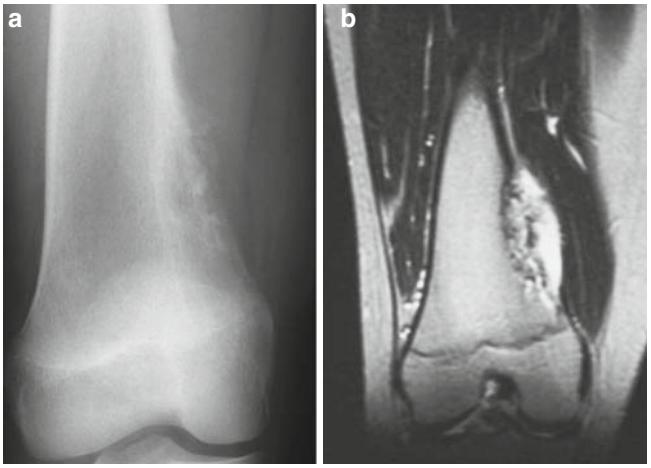

Fig. 7.22 Parosteal chondroma, femur (14-year-old woman). **a**. AP view of the knee. Cortical erosion on the surface of the distal femur. **b**. Coronal T2-weighted MR image. A bright signal lesion on the cortical surface represents hyaline cartilage growth (courtesy of Dr. Joo-Hyuk Lee)

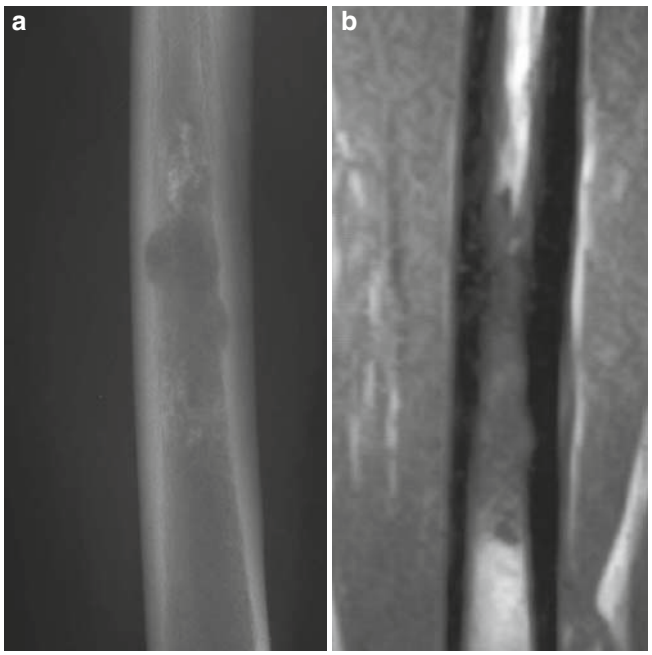

Fig. 7.21 Low-grade chondrosarcoma, femur (36-year-old woman). **a**. Lateral view of the tibial shaft. A lobulated lytic lesion is associated with erosion of the endosteal region of the cortex, and it should not be seen in the benign lesion. **b**. Sagittal T1-weighted MR images, representing a bone marrow lesion

(Fig. 7.22). It may have an irregular cortical margin and periosteal bone formation and so may simulate an aggressive lesion.

Surgical Pathology: Grossly, chondromas are mostly small (3–5 cm) well-circumscribed lesions. Periosteal chondromas may be covered in a thin shell of periosteum or reactive bone. On cut sections, chondromas are composed of semi-translucent, hyaline cartilage. Cyst formation or mucoid change is unusual, and raises the possibility that the lesion is a chondrosarcoma. Microscopically, the features of chondromas vary with the location. In general, they have a mulberry-like, lobular configuration. These lobules may be rimmed by reactive woven bone or calcification (the basis for the C's and O's of matrix on the radiologic images). Ischemic necrosis of chondrocytes may occur in calcified areas.

Enchondromas, in the tubular long bones show small chondrocytes, lying in lacunae. They have round, regular nuclei, which are barely visible at low magnification (Fig. 7.18H). Binucleated chondrocytes and necrotic foci are extremely rare. Calcification may be seen, and bone formation is often present surrounding the lobules of cartilage.

Enchondromas of the hands and feet can sometimes be alarmingly cellular. Chondrocytes may be present in clusters or even in sheets. Nucleomegaly and binucleation, as well as slight myxoid change of cartilage may be present. Permeation of the cortex of the phalanges is not a feature and signifies that the lesion is a chondrosarcoma. Benign periosteal chondromas may also show cytologic atypia, but they are well-demarcated lesions. Multiple enchondromas can also be cellular with chondrocytes tending to spindle.

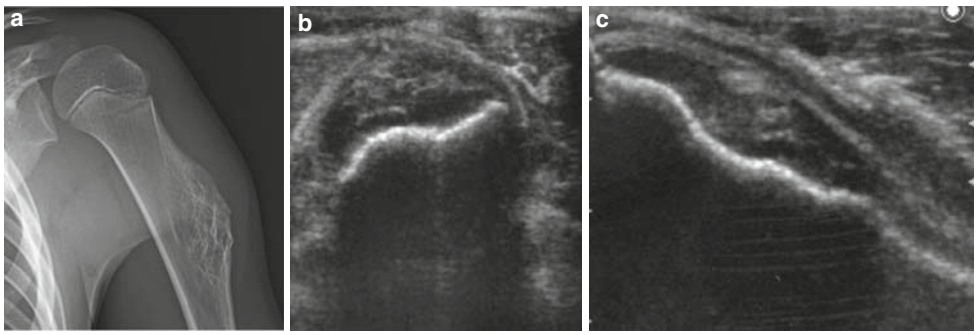

Fig. 7.23 Osteochondroma, humerus (12-year-old man). **a**. AP view of the humerus. A broad-based osseous growth is seen in the proximal humerus. **b**. Ultrasonography. Transverse scan of the exostosis represents a sonolucent cartilaginous cap. **c**. Ultrasonography. Longitudinal scan again shows a sonolucent cartilaginous cap

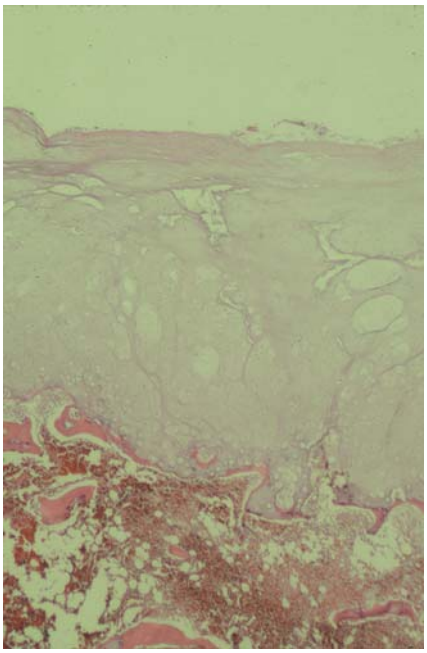

Fig. 7.23H An osteochondroma showing a thin cartilage cap lined by perichondrium on the surface. There is endochondral ossification occurring at the junction with the underlying bone and marrow

Osteochondroma

Osteochondroma is a very common lesion. Although once considered to result from aberrancies at the growth plates, they show a consistent clonal pattern of EXT gene mutation within the lesional tissue – evidence that these lesions are true neoplasms. Even so, normal physiologic signaling regulates their growth and they stop growing when the physeal plates close at skeletal maturity.

Osteochondromas show exophytic bone growth with a cartilaginous cap at its tip (Figs. 7.23 and 7.24). The exophytic bone typically connects with the host bone marrow with a neck or stalk and has a cartilaginous cap at its distal surface. Osteochondromas occur in patients younger than 20 years of age, and typically arise in the metaphysis of long tubular bones. They stop growing when normal growth plates close and the residual cartilaginous cap will be thin, approximately 1–2.5 cm, and should grow thinner as the patient ages. The attachment of an osteochondroma to the native bone can vary from a narrow stalk to broad base. Thus, they may appear as either pedunculated or sessile lesions. When osteochondromas arise from the epiphyseal ossification center, they cause an irregular region in the metaphysis of the bone (Fig. 7.25). This entity is known as Trevor disease or dysplasia epiphysealis hemimelica.

The cartilaginous caps of osteochondromas have a small tendency to undergo malignant transformation to chondrosarcoma. When this happens, the cap will thicken and become irregular. US, CT, and MR imaging all can assess the thickness of the cap accurately [20]. Irregular cartilaginous margins or a lucent zone in the lesion is a characteristic of chondrosarcoma arising in osteochondroma [21].

Osteochondromas may cause significant deformity and symptoms [22]. Because of their exophytic growth, they may cause vascular and nerve compression. Bursa may form over the end of the lesion as a complication of mechanical stress on adjacent musculature [23] (Fig. 7.26).

Subungual exostosis and turret exostosis in the phalanges are different from osteochondroma as they represent reactive ossification that forms later in life after physeal plate closure (Fig. 7.27). Multiple hereditary exostoses is a genetic condition where patients form multiple osteochondromas (see below).

Surgical Pathology: Osteochondromas usually have a well-defined bony stalk, capped by cartilage. The stalk may be narrow and pedunculated or broad. When multiple osteochondromas occur in a single patient, they tend to have broader stalks. The thickness of the cartilage cap varies with age, being greater in younger patients. In adults, the cartilage may be entirely eburnated leaving behind only residual bone. Microscopically, the chondrocytes of the base, within the cartilage cap, line up simulating a growth plate. Below this, enchondral ossification is often seen. The stalk shows a medullary cavity containing fatty or hematopoietic marrow (Fig. 7.23H).

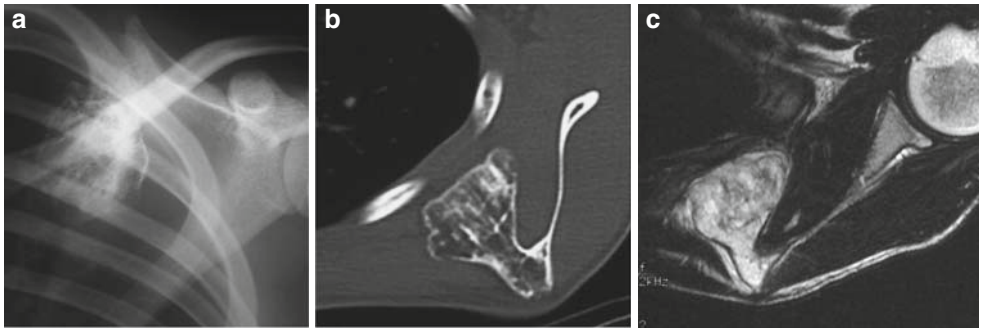

Fig. 7.24 Osteochondroma, scapula (14-year-old man). **a**. AP view of the scapula. Osseous projection is noted. **b**. CT, demonstrating osseous projection on the medial edge of the scapula. **c**. T2-weighted axial MR image. Cartilaginous cap is thin (*arrow*)

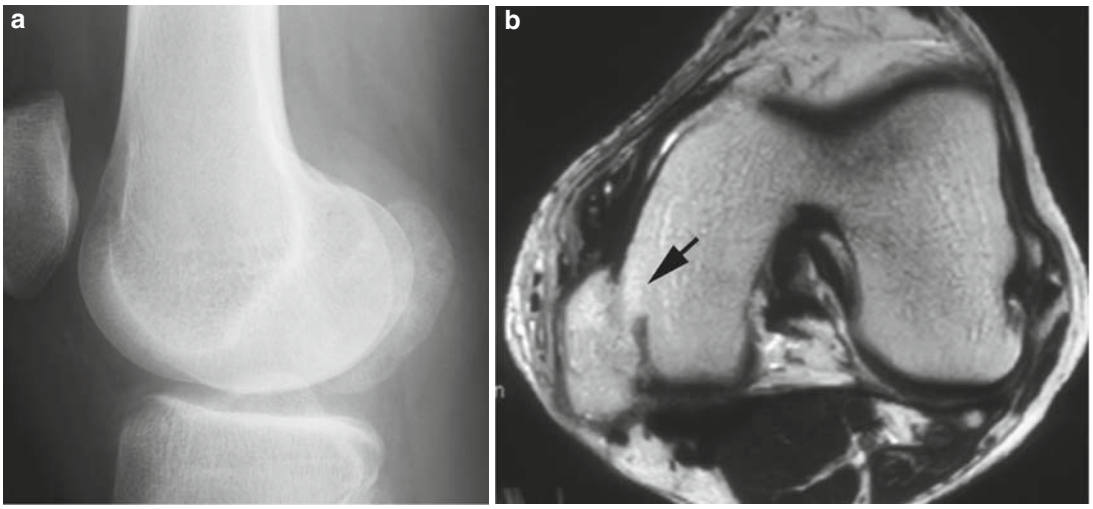

Fig. 7.25 Trevor disease (20-year-old man). **a**. Lateral view of the knee. Ossification is attached to the distal femoral epiphysis. **b**. T2-weighted axial MR image. Ossification is seen at the posterior aspect of the medial femoral condyle. Bone marrow is connected to that of the host bone, similar to osteochondroma (*arrow*)

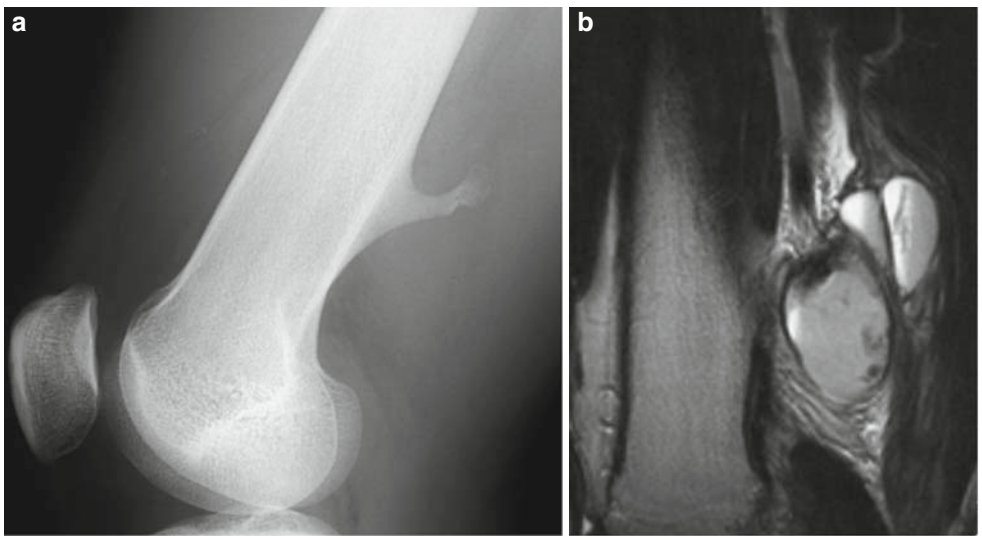

Fig. 7.26 Bursa formation of osteochondroma (19-year-old man). **a**. Lateral view of the femur. Osseous projection on the posterior aspect of the distal femur. **b**. T2-weighted sagittal MR image. A lobulated cystic lesion with fluid levels, representing hemorrhage, is present over the osseous projection (courtesy of Dr. Satoru Tazawa)

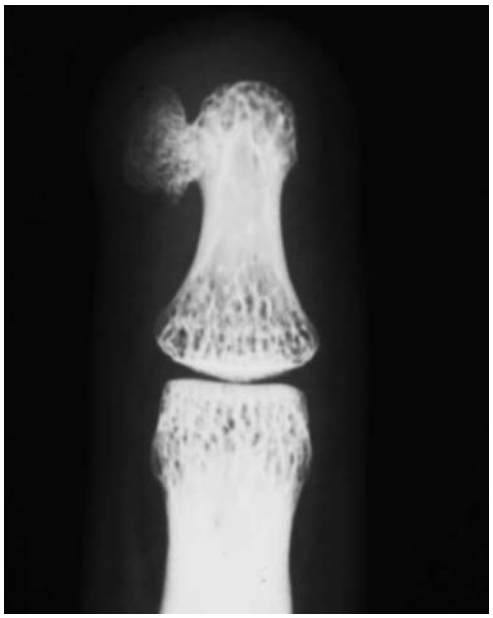

Fig. 7.27 Subungual exostosis (15-year-old woman). An osseous projection is seen in the distal phalanx. The ossification is not connected to the bone marrow of the host bone, and it is different from osteochondroma. Lateral radiograph demonstrating proliferating bone from the base of the proximal phalanx. Histologically, this proved to be BPOP. Sagittal water sensitive MR of the same lesion showing low signal in the area of proliferating bone and surrounding high signal representing cartilage

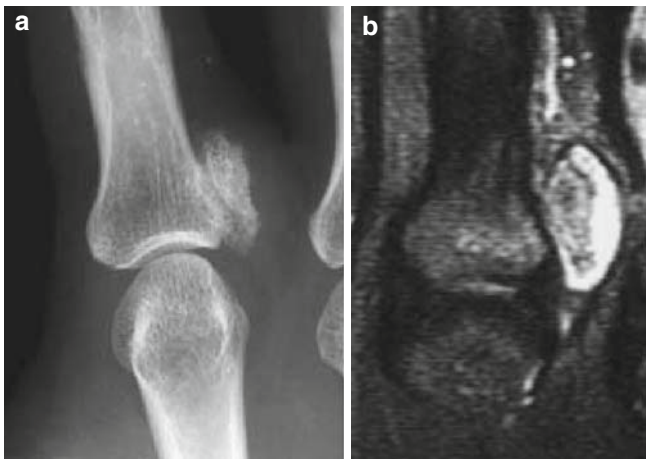

Fig. 7.28 BPOP (32-year-old-man). **a**. PA radiography. Periosteal reaction is seen adjacent to the proximal phalanx. **b**. T2-weighted coronal image. The mass is heterogeneous. Bright signal on the surface of the lesion represents rich hyaline cartilage component

It is important to exclude malignant transformation in an osteochondroma, most often to chondrosarcoma. Chondrosarcomatous cartilage is cellular, often shows prominent myxoid change, and may have wide fibrous bands that accentuate its lobular character. In secondary chondrosarcoma there is often evidence of extension of the cartilage into the soft tissues beyond the confines of the periosteum. The finding of a cartilage cap of over 2.0 cm in an adult is suspicious of a chondrosarcoma developing on an osteochondroma.

Subungual Exostoses: Specimens show proliferating fibrocartilaginous tissue resembling osseous callus. Subungual exostoses tend to show mature bone formation in an orderly pattern that points to the correct diagnosis and prevents misdiagnosis of this lesion as a sarcoma. Skin included in the biopsy or excision specimen should be assessed for excluding the rare entity of a melanoma producing an osteoblastic reaction.

Bizarre Parosteal Osteochondromatous Proliferation (BPOP, Nora lesion): This oddly named lesion is a reactive ossified lesion on the surface of the cortex of small bones of hands and feet. It was first reported by the group of Mayo Clinic in 1983 and is considered to be similar to other reactive ossification, including florid reactive periostitis and turret exostosis. It occurs mainly in small bones of hands and feet, but larger tubular bones, such as humerus and bones around the knee, are also reported. Bone–cartilage interface is irregular, and large, bizarre, binucleated chondrocytes are noted. Radiographically, it is a well-marginated periosteal ossification, which may grow over several months (Fig. 7.28a). MR imaging reveals high-signal portion, on T2-weighted images reflecting cartilagenous elements (Fig. 7.27c). The recurrence after resection is high, nearly 50% in the initial Nora report [105]

Surgical Pathology: Grossly, the lesions have a stalk and may have a well-defined cartilage cap. Microscopically, there is a mixture of cartilage, bone, and a spindle cell element. The bone may show considerable osteoblastic prominence and has a characteristic blue tinctorial quality. Fibrous tissue and osteoclast-type giant cells are also sometimes present.

Chondroblastoma

Chondroblastoma is a tumor of the epiphysis of long tubular bones. It occurs most commonly in children and adolescents before closure of the physis, but also may occur in later adult life. The lesion has a male predominance. It most commonly arises in the knee, pelvis, and shoulder. The calcaneus is also a common site. In the pelvis, chondroblastomas may arise from the region of the triradiate cartilage. Although benign, but it may recur, and rarely metastasize.

Radiological features include a well-defined lucency with sclerotic margin in the epiphysis (Fig. 7.29). Periosteal reaction is also seen on plain radiography [24]. Mineralized matrix is usually subtle and occurs in 1/3–1/4 of cases. Because of this, CT is better suited to show chondroid

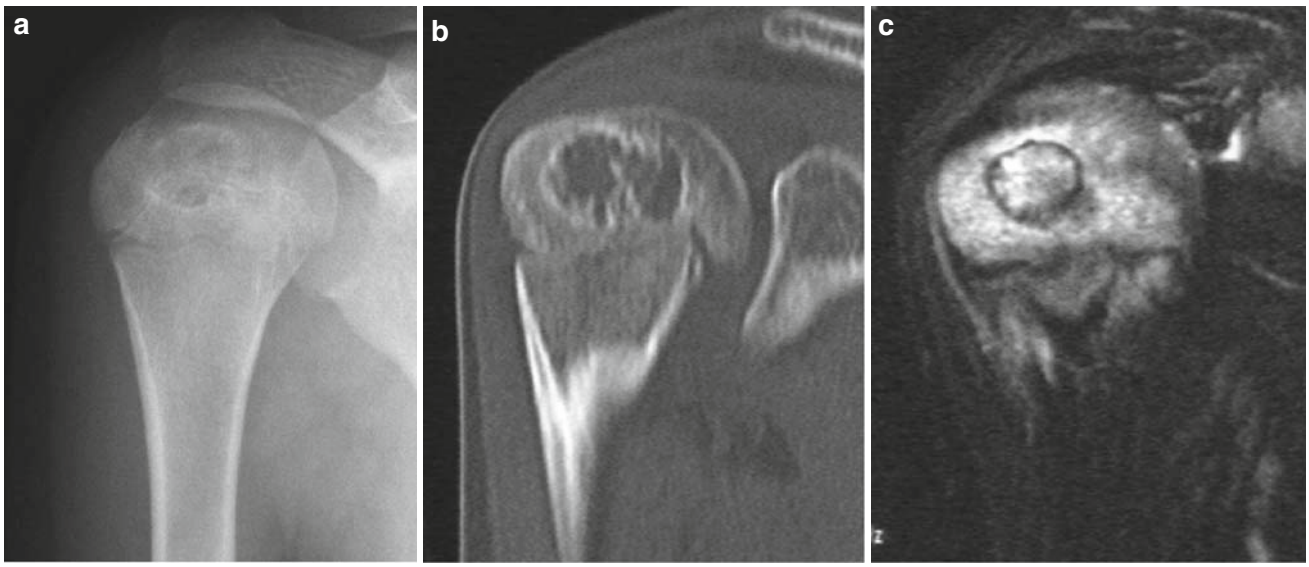

Fig. 7.29 Chondroblastoma, humerus (15-year-old man). **a**. AP view of the humerus. A well-defined mass with sclerotic margin in the proximal humeral epiphysis. **b**. CT with coronal reconstruction. A well-defined lytic change in the proximal humerus is again noted. Periosteal reaction is seen along the lateral cortex (*arrow*). **c**. T2-weighted coronal MR image. Bright signal intensity, representing reactive change, is noted around the lesion

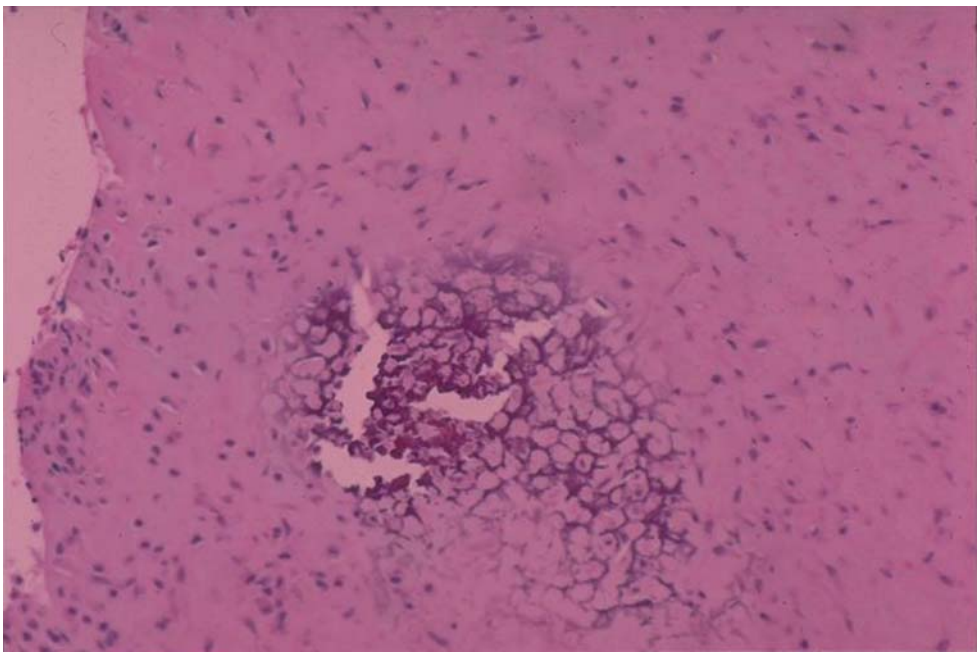

Fig. 7.29H Chicken-wire calcification in a chondroblastoma

mineralization than plain radiographs. Chondroblastoma has a high association of the secondary aneurysmal bone cyst. On MR imaging, the lesion typically shows relatively low signal intensity on T2-weighted images compared with other cartilaginous tumors, reflecting chondroblastoma's relatively higher cellular component compared to lesions predominant composed of hyaline cartilage [25]. Reactive bone marrow edema may be significant and extend into the metaphysis. This reactive marrow edema reflects tumor activity [26].

Surgical Pathology: Grossly, chondroblastomas are circumscribed lesions. A secondary aneurysmal bone cyst (ABC) may be seen within the lesion. Blue gray areas typically represent cartilage while yellow gritty areas represent calcification or secondary woven bone.

Microscopically, chondroblastomas have a spectrum of histologic appearances. This results from variable amounts of matrix within lesions, secondary changes (ABC like), and cytological variability. Chondroblasts are typically a polygonal to oval cells with sharp cytoplasmic borders, lightly staining, or clear cytoplasm. The nuclei are round to oval, with prominent grooving. Mitotic figures may be seen, but are not very frequent. Atypical mitoses are absent. Some chondroblastomas are comprised of cells that have abundant pink cytoplasm. These have been referred to as epithelioid variants. Scattered osteoclast-type giant cells may be seen in many chondroblastomas. Pigmented cells (hemosiderin-laden macrophages as well as pigmented chondroblasts) are sometimes prominent. Calcification may be found focally or more typically surrounding chondroblasts. The latter is especially true around foci of necrotic chondroblasts. The result is a characteristic "chicken-wire" pattern of calcium deposition. This feature is present in almost two-thirds of the cases in most series (Fig. 7.29H).

Chondromyxoid Fibroma

Chondromyxoid fibroma (CMF) is a rare, less than 1% of all bone tumors, cartilaginous tumor with myxoid matrix. It may arise in any age group, but two-thirds occur between the ages of 10 and 30. It is most common in the second decade. It is a benign tumor, but recurrence is frequent (Fig. 7.30). Locations typically arise eccentrically in the metaphysis of long bones, most common around the knee, and less commonly in flat bones.

Radiological features include a well-defined, septated eccentric lucency, with sclerotic and lobulated margins [27]. CMF may sometimes cause erosion of cortex. Although rarely visible on plain radiography, CT may show some calcified matrix. MR imaging often reflects the myxoid component of the tumor, showing hyperintensity on T2-weighted imaging.

Surgical Pathology: Grossly, the lesions are small, circumscribed, and lobulated. Microscopically, the tumors are lobular and contain variable amounts of fibrous tissue and cartilage. The lobules have characteristic hypercellular septae surrounding hypocellular myxoid matrix. The fibrous component is usually small and often confined to the septae separating the lobules. These septae on occasion contain blood vessels, osteoclast-type giant cells, and osteoid.

Chondrosarcoma

Chondrosarcoma is a malignant cartilaginous tumor, the third most common bone sarcoma following multiple myeloma and osteosarcoma. It may be primary or secondary. Secondary chondrosarcoma arises in solitary osteochondroma, multiple osteochondromatoses, and enchondromatosis (Ollier and Maffucci syndromes and metachondromatosis).

Chondrosarcoma is rare in patients younger than 20, and usually seen in the patients older than 30 years of age. The pelvis and shoulder girdle are common sites, accounting for two-thirds of cases. In long tubular bones, metaphyses and diaphyses are often involved. Chondrosarcomas are graded histologically as grades I, II, and III with one being most differentiated and III least differentiated. The distinction between grade I chondrosarcoma and benign chondroma

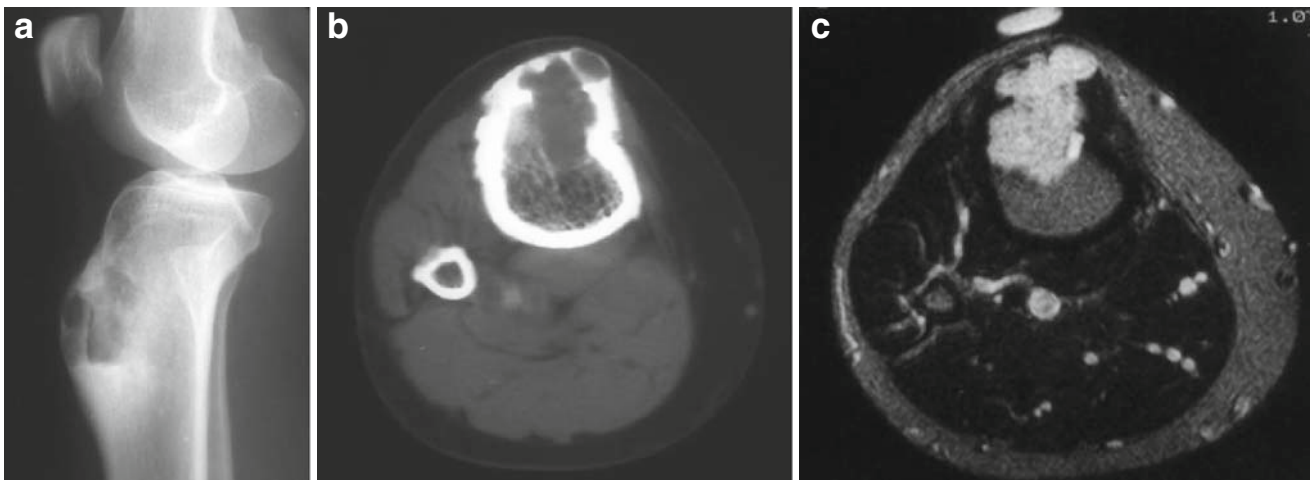

Fig. 7.30 Chondromyxoid fibroma, tibia (43-year-old woman). **a**. Lateral view of the proximal tibia. A well-defined mass with sclerotic margin at the proximal tibia. The mass is located in the anterior aspect. **b**. CT. A lobulated lytic lesion is seen on the anterior aspect with partial cortical disruption. **c**. T2-weighted axial MR image. A bright signal intensity mass with lobulation in the anterior aspect of the proximal tibia (courtesy of Dr. Takehiko Yamaguchi)

is difficult and some pathologists have adopted a grade ½ to indicate this.

There is some correlation between histological grades and imaging features. Tumors of higher histological grades tend to have fine or irregular chondroid mineralization, a larger non-mineralized component, circumferential growth, and significant areas of tumor necrosis. Tumors of lower histological grade tend to have dense ring-like mineralization, extensive mineralization, localized proliferation, and no foci of tumor necrosis [28]. Differentiation between high-grade chondrosarcoma and the chondroblastic form of osteosarcoma is also difficult. On MR imaging, a pattern of septal enhancement may help in diagnosing low-grade chondrosarcoma [29].

Although benign chondromas of small bones of hands and feet are common, chondrosarcomas are rare in these locations. As discussed above, chondroid tumors in fingers that have aggressive-looking histology or imaging features have relatively benign prognoses [30]. Permeation in the medullary canal of the phalanges is not a sign of malignancy, but invasion through the cortex is suggestive of malignancy. High-grade malignancy with metastatic potential is rare in phalangeal tumors.

Central Chondrosarcoma

Central chondrosarcoma occurs in the bone marrow and grows along the medullary canal. Low-grade tumors may be difficult to differentiate from enchondroma. They are common in the flat bones of the pelvis and shoulder girdle and around the trunk in the proximal long tubular bones, including the femur, tibia, and humerus (Fig. 7.31). Central chondrosarcomas of the craniofacial skeleton are rare. The few examples of chondrosarcomas of the skull base are controversial, and some at least are probably examples of chondroid chordoma. Cortical involvement and periosteal reaction are suggestive of malignancy. Endosteal scalloping and cortical expansion are also characteristic features of these lesions.

Surgical Pathology: High-grade chondrosarcomas are relatively straightforward to diagnose. They are composed of cellular cartilage showing extension into soft tissues and/or permeation of bone with entrapment of pre-existing trabeculae. There may be widespread mitotic activity, multinucleation of chondrocytes, and necrosis. In fact, despite obvious malignant features, the challenge in such cases may be to exclude other malignancies that have cartilage as a prominent component, such as chondroblastic osteosarcoma.

Low-grade *c*hondrosarcomas, on the other hand, can be difficult to diagnose and differentiate from benign but cellular cartilage lesions such as chondromas. Experience and long-term follow-up studies have shown that different rules apply in different locations. For example, cartilage tumors of the sternum are almost always malignant regardless of the histologic appearance. On the other hand, chondromas of the hands and feet, periosteal chondromas, enchondromas of Ollier disease and Maffuci syndrome, synovial chondromatosis and soft tissue chondromas of the hands and feet are most often benign, in spite of sometimes alarming cellularity.

Grossly, the appearance of mucus-like cartilage that runs is very suggestive of chondrosarcoma. Microscopically, chondrosarcomas are frequently lobular similar to chondro-

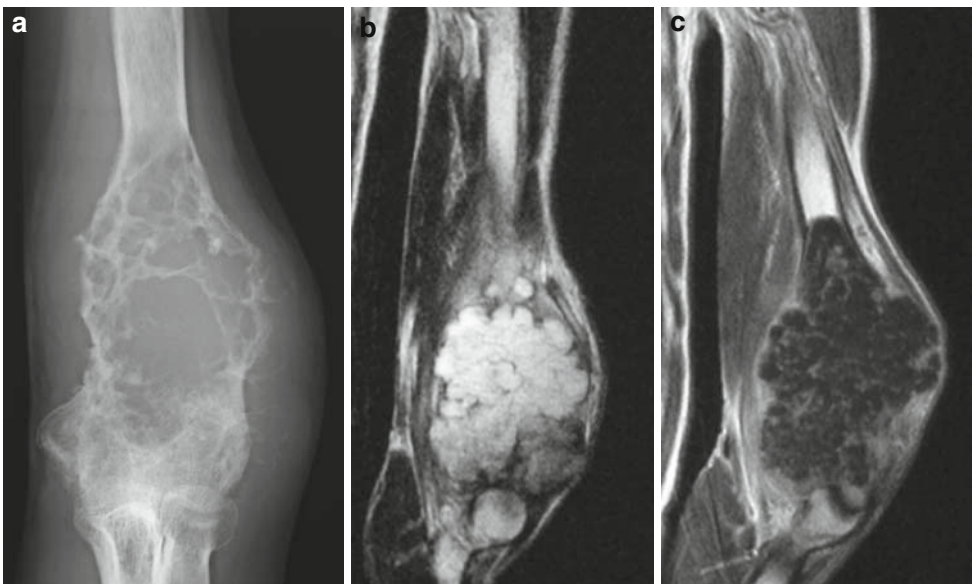

Fig. 7.31 Central chondrosarcoma, humerus (48-year-old man). **a**. AP view of the distal humerus. A lobulated lesion in the distal humerus with cortical disruption. Soft tissue extension is evident. **b**. T2-weighted coronal MR image. A bright signal intensity mass is lobulated, a typical finding of chondroid lesion. **c**. T1-weighted coronal MR image after intravenous Gd contrast. Enhancement is evident in the septae of the lobulated chondroid matrix

mas. The presence of myxoid change (a bubbly transformation of the cartilage that leads to cystification) is indicative that the lesion might be a chondrosarcoma rather than a chondroma although some phalangeal enchondromas can have myxoid change especially in patients with Ollier disease.

A low power view suggestive of infiltration or entrapment of native bone is one of the most helpful clues to separate low-grade chondrosarcoma from chondroma (Fig. 7.31H). Chondrosarcomas also tend to be more cellular than chondromas. This is especially true in the larger bones. Enchondromas of small bones can be cellular, but grow by pushing borders rather than infiltrating adjacent tissue. Thus, an infiltrative border is an important criterion to diagnose malignancy. The creation of a soft tissue mass by the tumor growing out of bone (in the absence of fracture or previous surgery) is a definite sign of malignancy.

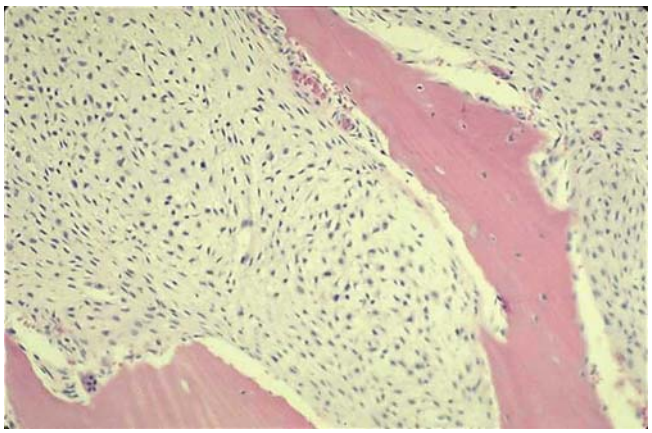

Fig. 7.31H Chondrosarcoma showing a permeative growth pattern. The tumor extends within the marrow cavity and entraps trabeculae of bone

Grading of Chondrosarcomas: The cellularity of chondrosarcomas can vary often depending upon location. Chondrocyte atypia, mitoses, and multinucleation are features to be taken into account, but no feature by itself is sufficient to be diagnostic. Chondrocyte nuclear enlargement (over 10 μm) should be noted. Techniques such as ploidy studies to differentiate between the various grades or between low-grade malignant and benign cartilages have been not very successful. Genetic studies have been very limited in number and are not conclusive or clinically useful. Since there is imperfect correlation between histologic appearance and biologic behavior of chondroid tumors, and since features such as size, location, and radiologic appearances play a major role in determining the outcome of these lesions, grading of chondrosarcoma has become somewhat subjective.

Peripheral Chondrosarcoma

Peripheral chondrosarcoma is a malignant counterpart of osteochondroma: a tumor arising from cartilaginous cap. The term should not be confused with juxtacortical or periosteal chondrosarcoma, a form of chondrosarcoma that arises on the surface (periphery) of bone. Since this name is confusing, exostotic chondrosarcoma is also used. In fact, in pathology literature and in the WHO classification of bone tumors, the term peripheral chondrosarcoma is not used, instead these lesions are included within other secondary chondrosarcomas. This type of chondrosarcoma may occur in long tubular bones (humerus and proximal femur), the pelvis, and the scapula (Fig. 7.32). The majority of peripheral chondrosarcoma is of low grade, and differentiating low-grade malignancy from benign osteochondroma may be difficult. Tumors of low histological grade are common and they tend to be large at the time of diagnosis [31]. Thick areas of cartilage first calcify, are subsequently replaced by endochondral ossification, creating a large ossified mass. Radiological features consist of osteochondroma and large soft tissue tumor of various degree of muneralization attached to it. CT and MR imaging are useful to delineate thick cartilaginous cap.

Surgical Pathology: Chondrosarcomas, especially those arising on osteochondromas, often lack an infiltrative quality, and frequently demonstrate a "pushing" border. Matrix deposition can vary from minimal to extensive. Qualitatively, it can be hyaline or myxoid. Wide fibrous septae are seen in some cases and these form a diagnostic clue in chondrosarcomas developing secondarily on osteochondromas. When chondrosarcomas supervene on a previous osteochondroma, the thickness of the cartilage cap increases, and the normal columnar arrangement of chondrocyte columns is lost. Nodules of cartilage can sometimes be found lying in the adjacent soft tissues in such instances.

Periosteal Chondrosarcoma

Periosteal chondrosarcoma is a specific type of chondrosarcoma, occurring on the cortical surface. Cortical erosion is a common feature (Fig. 7.33). The margins tend to be more irregular than periosteal chondroma [32]. Periosteal chondrosarcomas tend to be of low grade, and the prognosis is relatively good. A size larger than 5 cm is more suggestive of chondrosarcoma, and that of less than 3 cm is more likely a benign periosteal chondroma.

Clear Cell Chondrosarcoma

Clear cell chondrosarcoma is a rare low-grade chondrosarcoma with strong tendency to involve the end of long bones.

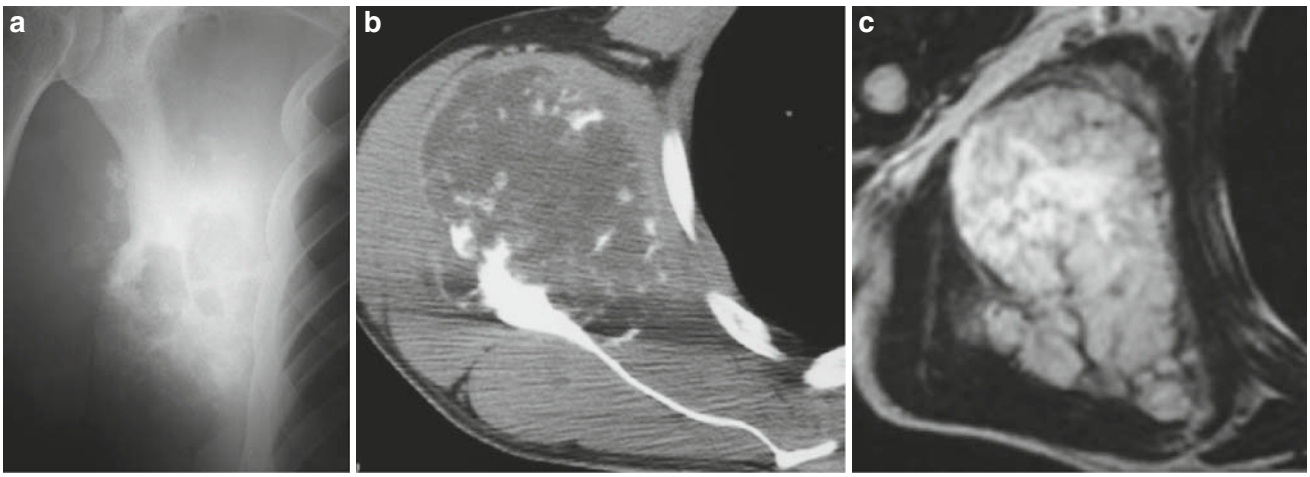

Fig. 7.32 Peripheral chondrosarcoma, scapula (36-year-old man). **a**. AP view of the scapula. A large lobulated mass arises from the lateral edge of the scapula. Irregular ossification in and around the mass. **b**. CT. A large soft tissue component attached to the scapula. Punctate mineralization represents chondroid matrix. **c**. T2-weighted axial MR image. A lobulated bright signal represents chondroid growth. Tumor extent is well depicted

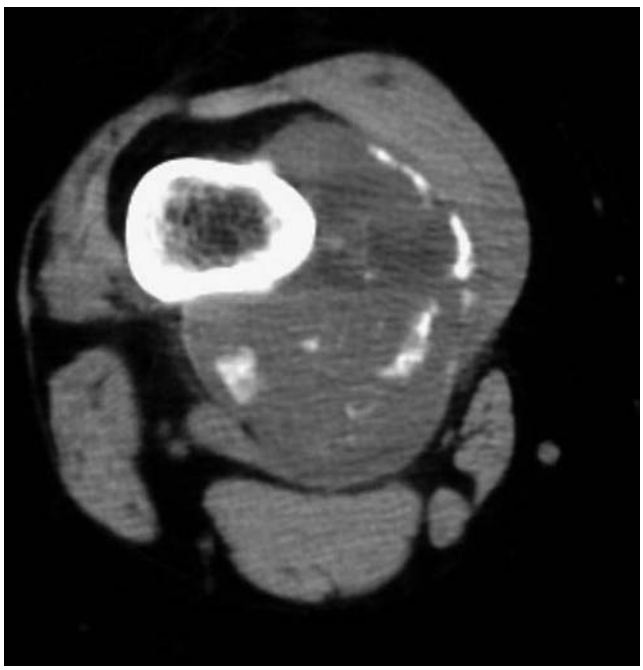

Fig. 7.33 Periosteal chondrosarcoma, femur (25-year-old woman). CT scan demonstrating a large periosteal mass contains mineralization. No intraosseous extension is noted (courtesy of Dr. Yamaguchi)

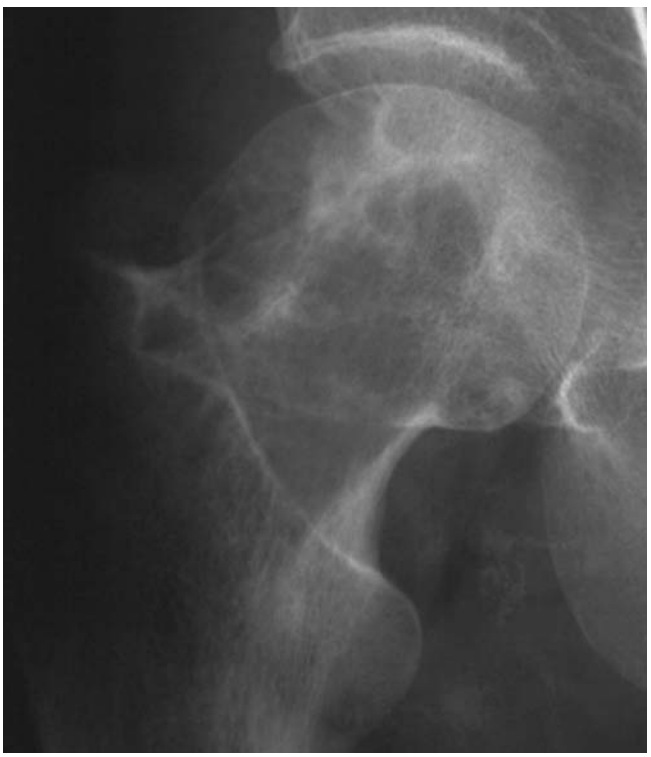

Fig. 7.34 Clear cell chondrosarcoma, femur (34-year-old man). AP view of the hip. A lobulated lytic lesion is noted in the femoral head and neck (courtesy of Dr. Kyoji Okada)

The location and imaging appearances of this lesion resemble chondroblastoma. The male to female ratio is 2.6:1. It commonly occurs in the proximal femur in the third and fourth decades of life. It appears typically as a radiolucent lesion in the end of tubular bones (Fig. 7.34). Clear cell chondrosarcoma may present as a well-defined lesion with sclerotic margins, giving it a non-aggressive appearance [33].

Surgical Pathology: Microscopically, these tumors are rich in chondrocytes with clear cytoplasm. Unlike conventional chondrosarcomas, the clear cell variant can have large numbers of multinucleated giant cells. This explains why, in the past, this tumor has been referred to as an atypical

chondroblastoma. New bone formation may occur centrally within the tumor. The dominant cell is the "clear cell" chondrocyte, with a sharp cell border and a round, vesicular nucleus, with a prominent nucleolus. Powdery cytoplasm may be aggregated near the cell border or the nuclear membrane (Fig. 7.34H). These clear cells stain for S100 protein – a feature they share with other chondroid cells. Mitotic figures are rare. Matrix is sparse and may be focally calcified. Foci of conventional (grade 1) chondrosarcoma may be present and is prominently seen in about half the cases. Foci of osteoid or metaplastic bone that are typically seen should not be confused with osteoblastoma or osteosarcoma.

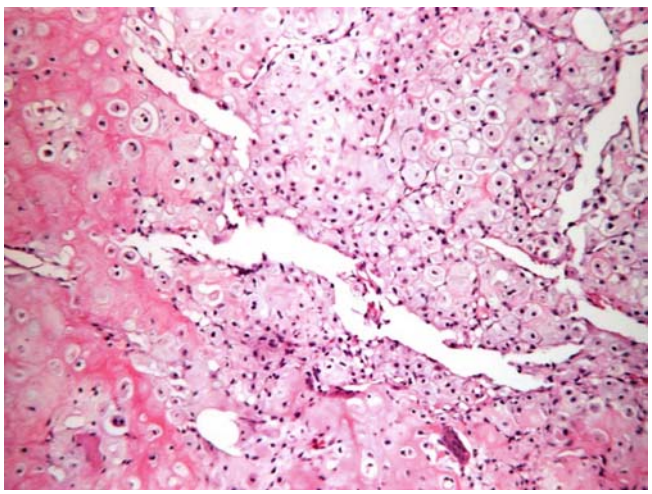

Fig. 7.34H "Clear cell" Chondrocytes in clear cell Chondrosarcoma

Mesenchymal Chondrosarcoma

Mesenchymal chondrosarcoma is a high-grade chondrosarcoma, with histologic bimorphic growth consisting of undifferentiated chondroid component and a small cell component. It typically occurs in younger patients with 60% in the second and third decades of life. Radiological findings are similar to conventional chondrosarcoma, except that infiltrating tumor growth is typical (Fig. 7.35) [34]. The prognosis is relatively poor, compared with conventional chondrosarcoma.

Surgical Pathology: Microscopically, the tumor is composed of a combination of anaplastic small stromal cells and islands of benign-appearing chondroid. The stromal cells may vary from "small, round, blue" cells to oval or very slightly spindle-shaped cells. The stromal cells are classically arranged in a hemangiopericytoma fashion (with prominent branching vessels). Interspersed within these is low-grade cartilage, which may form only a small component

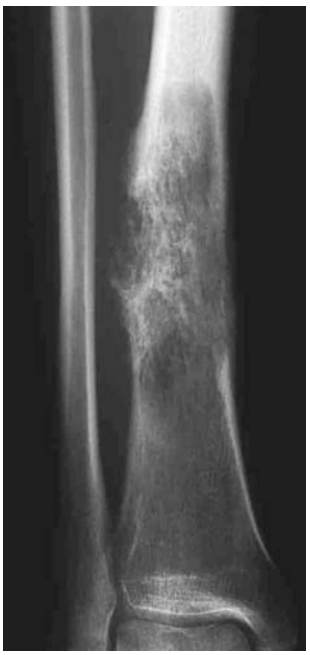

Fig. 7.35 Mesenchymal chondrosarcoma (34-year-old man). AP view of the distal tibia. An ill-defined osteolysis in the midshaft of the tibia represents a non-specific high-grade lesion. Cortical disruption is seen on the lateral aspect (courtesy of Dr. Yamaguchi)

of the neoplasm. The border between the two components is usually sharp.

Dedifferentiated Chondrosarcoma

Dedifferentiated chondrosarcoma consists of a mixed tumor including low-grade chondrosarcoma and high-grade spindle cell sarcoma (osteosarcoma, malignant fibrous histiocytoma [pleomorphic sarcoma], and other tumors). In most cases at the initial diagnosis, low-grade and high-grade components coexist. Radiographic features of dedifferentiated chondrosarcoma can be characteristic, combining areas similar to low-grade chondrosarcoma with infiltrating osteolytic areas as well (Fig. 7.36) [35]. The two components are also well documented on MR imaging by differing signal characteristics: a low-grade portion with rich hyaline cartilage having high signal on T2-weighted images and a cellular portion with relatively low signal.

Surgical Pathology: Grossly, the lesion reflects the radiologic appearances. The high-grade sarcoma and low-grade cartilage components are usually easily identified. The cartilage is generally translucent and lobular. The cartilage component is often centrally located, but it may sometimes be small and overlooked, although in some cases the reverse might be true. The high-grade sarcoma is usually tan,

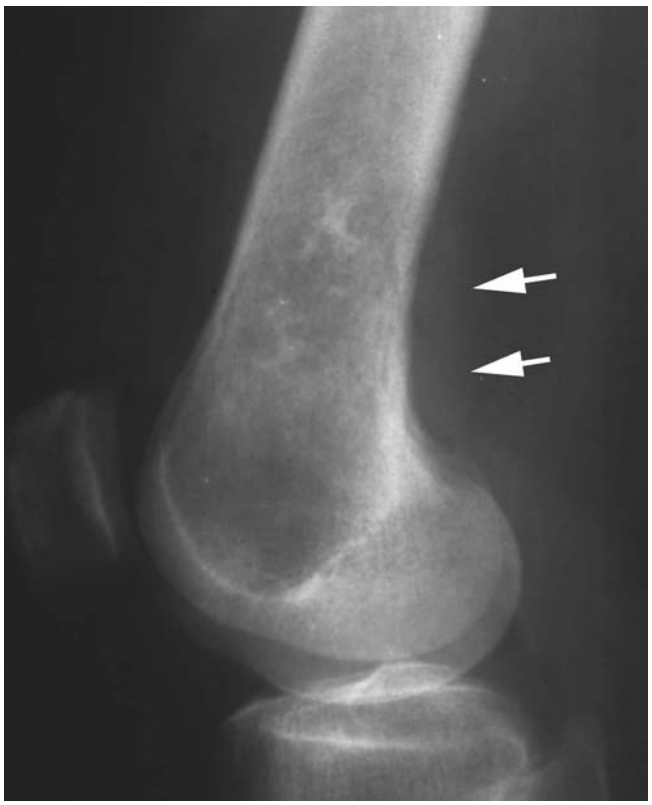

Fig. 7.36 Dedifferentiated chondrosarcoma (52-year-old woman). An ill-defined lytic lesion in the distal femur. An infiltrating soft tissue tumor is associated with the posterior aspect (*arrows*)

hemorrhagic, and focally necrotic. Microscopically, the lesion once again has two components – chondrosarcoma and a high-grade sarcoma. The chondrosarcoma component is most frequently low grade (about three-fourths are grade 1 and the remainder are grade 2). The junction between the two components is most often quite sharp. Fibrosarcoma and MFH are the most frequent supervening sarcomas, but osteosarcoma, rhabdomyosarcoma, and angiosarcoma have also been described. Some lesions may cluster, suggesting a metastatic carcinoma. It is important to distinguish this lesion from a chondroblastic osteosarcoma since the prognosis and response to chemotherapy are far worse in dedifferentiated chondrosarcoma.

Osseous Tumors

Osteoma and Bone Island (Enostosis)

Osteoma and bone island (insula compacta) are hamartomatous growths of compact bone in osseous structures usually first identified in adults, typically in the 20–40 age range. Osteoma is growth of mature bone on the surface of the calvarium and mandible ("ivory exostosis"), in the lumen of the paranasal sinuses and orbits (sinoorbital osteoma), and rarely on the surface of long tubular bones (surface osteoma of long bones). Usually no clinical significance is associated with these lesions, but pneumocephalus may occur secondary to invasion of the thin wall of the paranasal sinus, typically the frontal sinus. Well-defined osseous projection on plain radiography or CT is a typical finding (Fig. 7.37). Patients with Gardner polyposis syndrome have multiple osteomas, often throughout the skeleton (Fig. 7.38).

Bone islands are round or oblong osseous growths of compact bone within the medullary cavity of a bone. They are common, typically small, less than 1 cm, but occasionally

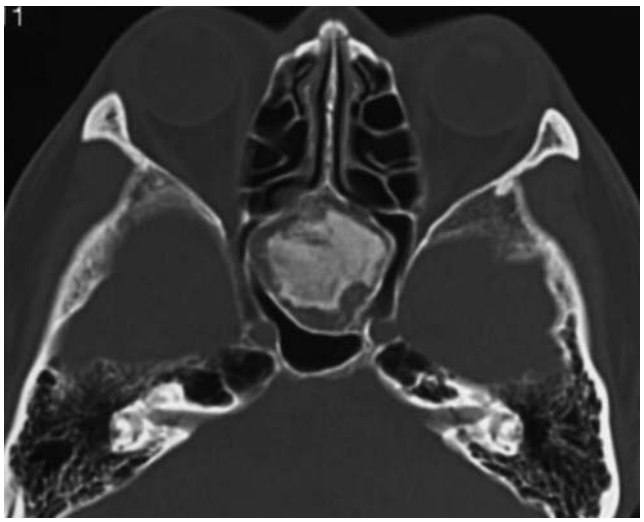

Fig. 7.37 Osteoma (48-year-old man). Dense cortical bone is present in the sphenoid sinus

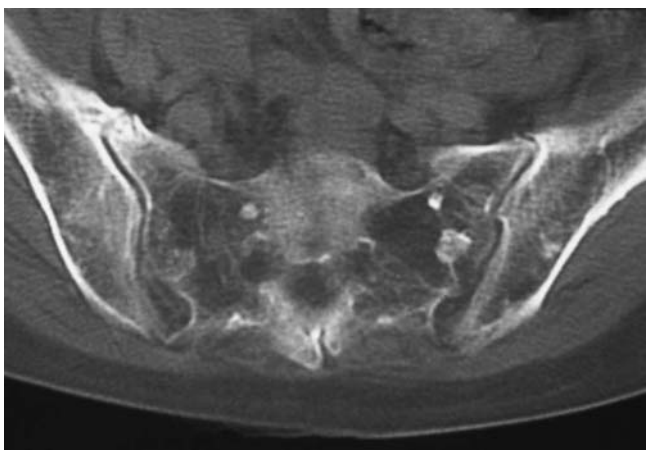

Fig. 7.38 "Ivory osteoma" of the sacrum in the patient with Gardner syndrome (51-year-old woman). Dense ossifications (*arrows*) are seen in the bone marrow of the sacrum

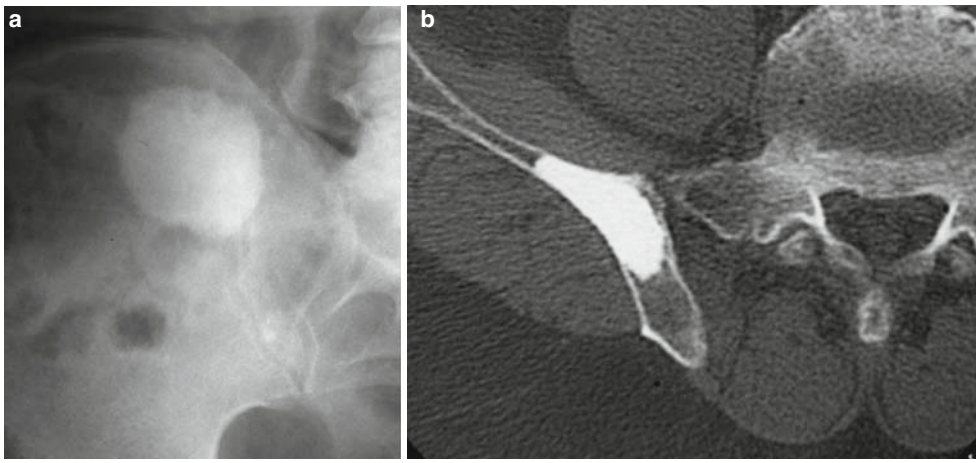

Fig. 7.39 Bone island, ilium (60-year-old man). **a**. Oblique view of the ilium. A large dense ossification in the ilium. Spiculation or fuzzy border is noted. **b**. CT. Spiculated margin, connecting to the thickened trabeculae, is typical

one may grow to 4 or 5 cm, or occupy the major portion of a vertebral body. They typically have trabeculae at their periphery creating a spiderweb-like margin at the periphery of the bone island on imaging (Fig. 7.39).

Surgical Pathology: Osteomas are composed primarily of lamellar bone, but some amount of woven bone is acceptable. A spongy variant of the osteoma has been described which contains a fibro-fatty or hematopoietic medullary component.

Osteoid Osteoma

Osteoid osteoma is a benign bone-forming neoplasm. Patients classically give a history of pain that is worse at night and is relieved by aspirin. Osteoid osteomas are treated traditionally using surgery or currently percutaneous radio-frequency (RF) ablation techniques [36], but they may regress spontaneously. Long-term medical therapy with nonsteroidal anti-inflammatory agents may palliate the patients' symptoms. Osteoid osteomas have limited growth potential and they are typically less than 2 cm in diameter. They typically occur in patients 5–30 years of age, and the male to female ratio is about 2:1. Half of these lesions occur in the femur or tibia, but they may occur in any bone, including the posterior elements of the spine.

Imaging features depend upon whether the lesion is intracortical, periosteal, or intramedullary and on whether it occurs in bone associated with a joint [37]. The typical imaging finding on radiographs and CT is that of a round radiolucency, called the nidus, surrounded by exaggerated sclerosis. The nidus represents the tumor. The sclerotic reaction is typically intense in periosteal and cortical lesions (Figs. 7.40 and 7.41). The sclerosis may make the nidus difficult to see radiographically.

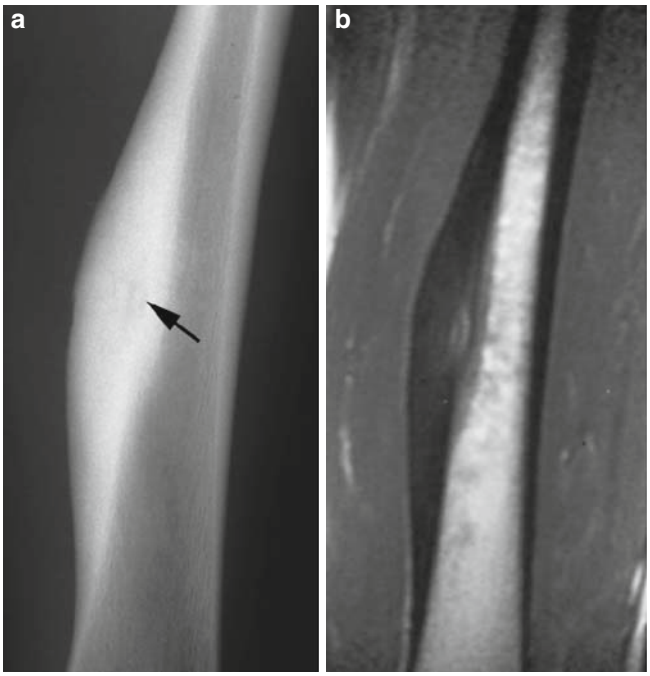

Fig. 7.40 Osteoid osteoma, femur (16-year-old man). **a**. AP view of the femur. Thick periosteal reaction is associated with a small radiolucent lesion (*arrow*). **b**. Coronal T1-weighted MR image. Reactive change in the bone marrow is extensive

Hence, CT is the study of choice to locate the radiolucent nidus of the osteoid osteoma within the surrounding sclerosis.

Osteoid osteomas that occur around joints, particularly in the femoral neck, often have little or no associated sclerosis. A lesion in a subchondral location may simulate arthritis both clinically and radiographically (Fig. 7.42). When an osteoid osteoma occurs in the posterior elements of a vertebra, it may induce painful scoliosis (Fig. 7.43). Occasionally, more than one nidus is present.

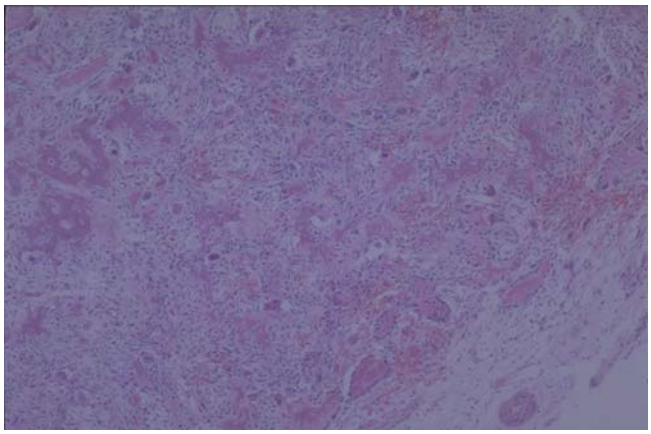

Fig. 7.40H The nidus of an osteoid osteoma shows fibrovascular tissue and bone trabeculate that are rimmed by benign-appearing osteoblasts

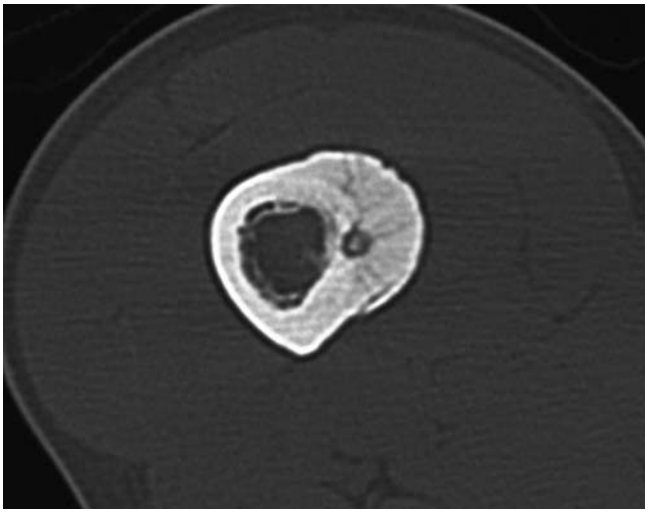

Fig. 7.41 Osteoid osteoma, femur (16-year-old man). CT scan demonstrates a nidus and thick periosteal reaction

On MR imaging, extensive reactive edema frequently occurs around the lesion, and may confound the diagnosis [38, 39]. The surrounding reactive edema is characteristic of this tumor and is considered to be caused by excretion of prostaglandin E2 by the tumor [40]. Typically younger patients have more intense reaction on MR imaging.

Differentiation from Brodie abscess is difficult on plain radiographs. MRI facilitates differentiation since Gd enhancement occurs in an osteoid osteoma, but not in Brodie abscess. Dynamic enhancement is particularly useful [41].

Surgical Pathology: An osteoid osteoma consists of a fibrovascular nidus that shows benign osteoblastic proliferation and surrounding reactive new bone. Grossly, the nidus is red, spherical, and gritty. Classically, it can almost always be "shelled" out from the surrounding bone.

Microscopically, there is a *sharp demarcation* of the nidus from the surrounding sclerotic bone. The nidus may be poorly ossified, with a richly vascularized stroma, or, it may be ossified, with calcific or lacy osteoid composed of osteoid rimmed with osteoblasts. The osteoblasts of osteoid osteomas are usually plump and active (Fig. 7.40H). They may have occasional mitoses but there should be no atypical mitotic figures. The woven bone shows prominent osteoblastic rimming. Cartilage is absent unless there has been a fracture, previous surgery, or if the lesion is intra-articular. Surrounding the nidus is sclerotic compact or spongy lamellar bone. The previously termed "giant" osteoid osteomas (larger than 2 cm) were probably examples of osteoblastomas.

Osteoblastoma

Osteoblastoma is a rare benign bone-forming tumor. It is histologically identical to osteoid osteoma, but it has greater growth potential. Differentiation from osteosarcoma

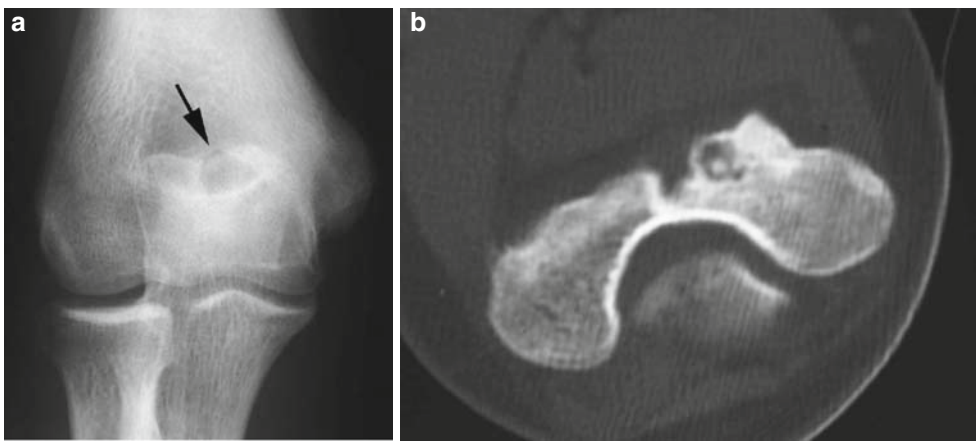

Fig. 7.42 Osteoid osteoma, elbow (15-year-old man). **a**. AP view of the elbow. A small lucent lesion is seen in the distal humerus (*arrow*). **b**. CT scan shows a small well-defined lucent lesion with a sclerotic margin (*arrow*) (courtesy of Dr. Jun Aoki)

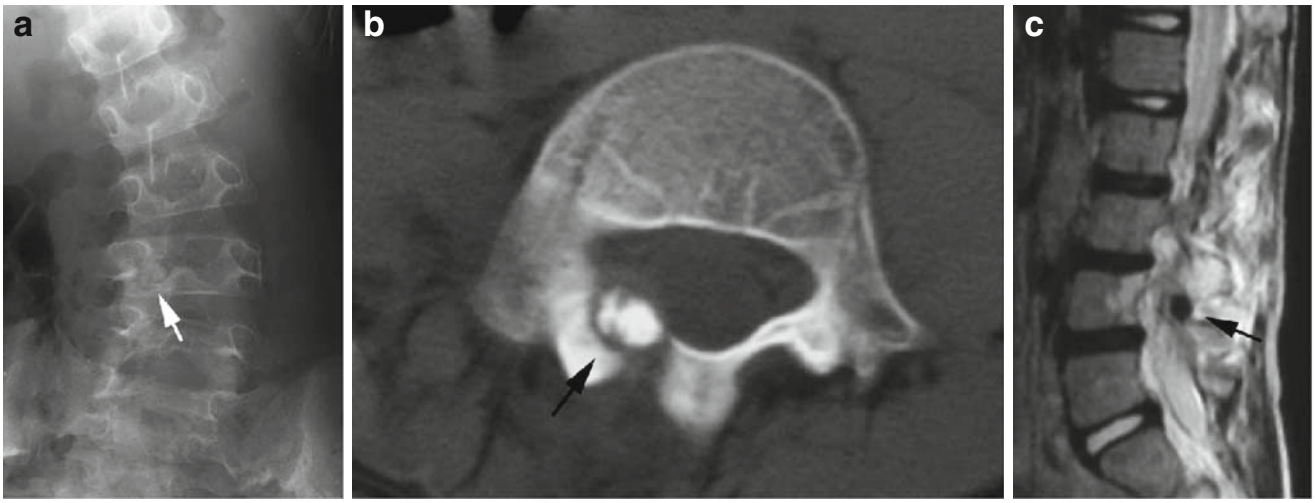

Fig. 7.43 Osteoid osteoma, lumbar spine (9-year-old man). **a**. AP view of the lumbar spine. A round density overlying the right side of L4 (*arrow*). **b**. CT. A radiolucent lesion contains a round sclerosis (*arrow*). Periosteal reaction is associated along the vertebral body. **c**. T2-weighted sagittal MR image. A round low signal in the nidus (*arrow*). An extensive reactive change is associated (©: Springer Verlag)

can be difficult both radiologically and histologically. Patients are typically 10–35 years of age, and the male to female ratio is 1:1. Clinical symptoms are non-specific, but systemic symptoms may be associated with the tumor (toxic osteoblastoma). The most common location is spine (30–40%), particularly in the posterior elements. It also occurs in hands and the long tubular bones.

Radiologically osteoblastoma is expansile with sclerotic margins. It is usually dense but may be lucent. The lesion contains various amounts of ossified matrix. One-third to one-half of the reported cases contain visible ossification. Mineralization may be punctate, resembling chondroid matrix. Periosteal reaction is present in half of the cases. In approximately one-third of cases, radiological findings are aggressive with cortical penetration [42].

Vertebral lesions are often characteristic in appearance (Fig. 7.44), but lesions in tubular bone are often challenging and definitive diagnosis is only proven at biopsy (Fig. 7.45). Reactive edema may occur in the soft tissues and bone marrow around the lesion [43]. Aggressive osteoblastoma is characterized by its histological appearance (epithelioid osteoblasts, sheet-like osteoid and osteoclastic resorption), not by radiologic features.

Surgical Pathology: Grossly, osteoblastomas are well circumscribed and typically measure 2–10 cm. Secondary cystic change (aneurysmal bone cyst) may supervene in some of these tumors.

Microscopically, they are identical to osteoid osteomas, being composed of anastomosing variably calcified bony trabeculae in a fibrovascular stroma. Some lesions are heavily mineralized, whereas others may be made of just osteoid.

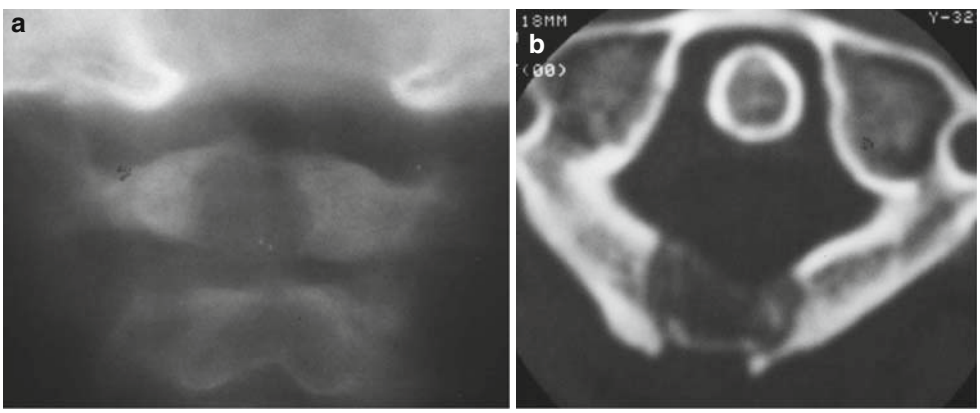

Fig. 7.44 Osteoblastoma, cervical spine (13-year-old man). **a**. AP tomography represents a well-defined lucency with no sclerotic margin. **b**. CT shows a round lucency with an ossified rim. Cortex is destroyed (courtesy of Dr. Tohru Sekiya)

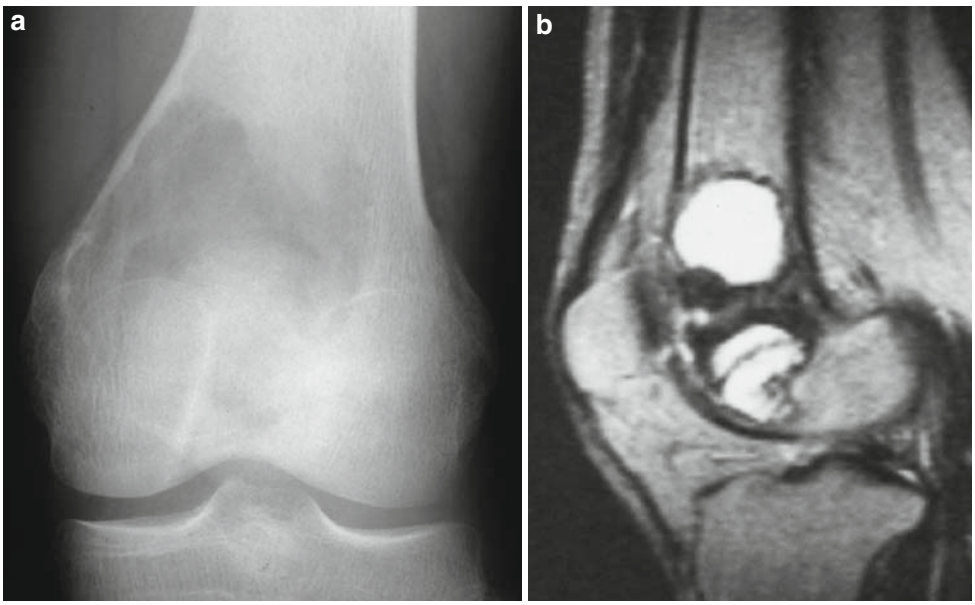

Fig. 7.45 Osteoblastoma, femur (25-year-old man). **a**. AP view of the distal femur. A well-defined lytic lesion in the distal femur. No mineralization is seen inside. **b**. Sagittal T2-weighted MR image. A heterogenous mass in the distal femoral shaft (courtesy of Dr. Hiroshi Nishimura)

There is considerable intralesional variation in trabeculum size. In the majority of cases, the trabecule are thick. In a small number, thin, lace-like trabeculae are present, raising the differential diagnosis of osteosarcoma. Plump, mitotically active osteoblasts line these trabeculae. This rimming is considered an important feature in favor of benignity. Early lesions may be rich in giant cells. Chondroid differentiation can occur but is unusual in the absence of fracture. Bizarre pleomorphic nuclei may occur in some cases. These are thought to represent a secondary degenerative change, similar to that seen in neurilemomas. In such nuclei, the nuclear features are not crisp. Secondary aneurysmal bone cyst-like change occurs in about 10% of cases.

A sub-group of *"aggressive" osteoblastomas* has also been recognized. These have been termed "malignant" osteoblastomas by some authors. These variants contain a trabecular pattern of osteoid similar to that of the "conventional" osteoblastoma; however, there is a tendency to wider and more irregular forms. There may be occasional areas of non-trabecular (lace-like) osteoid, but this component is minor. The osteoblasts present are large (almost twice the size of normal osteoblasts) and have an *epithelioid* quality. The nuclei may have a vesicular "histiocyte-like" appearance. Although many of these aggressive variants develop in patients over the age of 30 years, some have been seen in younger age groups as well. Radiologically, they are larger in size, but can occur in a variety of bones. The propensity of these tumors to recur is the reason for separating out this sub-group.

Osteosarcoma

Conventional Osteosarcoma

Osteosarcoma is the most common malignant neoplasm of bone. It arises from undifferentiated, multipotential, fibroblastic cells of bone. RB (retinoblastoma) gene and TP53 (a tumor suppressor gene) gene mutations are associated with osteosarcoma in certain familial cases. Conventional osteosarcomas consist of several subtypes based on the major histological component of the tumor such as osteoblastic, chondroblastic, fibroblastic, and fibrous-histiocytic (MFH-like). Other (non-conventional) variants of osteosarcoma are based upon a location and biological behavior and include small cell, giant-cell-rich and osteoblastoma-like osteosarcoma, intramedullary low-grade osteosarcoma, telangiactetic osteosarcoma, intracortical osteosarcoma, parosteal osteosarcoma, periosteal osteosarcoma, and high-grade surface osteosarcoma.

Histological and imaging features correlate to some extent, since chondroblastic osteosarcomas often contain areas of tumor with imaging features similar to chondrosarcoma. Most patients are 10–25 years of age, but osteosarcoma may occur in older patients, particularly those with Paget disease or who have had radiation therapy. In fact, malignant transformation of Pagetic bone accounts for the majority of the second peak of osteosarcomas seen in late adult life.

Seventy-five percent of osteosarcomas occur in the metaphysis of long tubular bones; the distal femur and proximal

tibia constitute 75% of the all osteosarcomas. Extension into the epiphysis is common and is easily visible on the plain radiographs [44]. The tumor does not occur commonly in the axial skeleton. Lesions in the spine tend to be sclerotic [45]. Radiographic features are often specific because of the presence of osteoid matrix (Figs. 7.46 and 7.47). Osteosarcoma may penetrate and destroy cortex. It often has spiculated or sunburst periosteal reaction and a soft tissue component, better identified on MR imaging.

The most common metastatic pathway for osteosarcoma is to the lungs. Thus, careful evaluation and follow-up of the chest are essential in the evaluation of patients with osteosarcoma. Skeletal metastases may occur, but it may be difficult to differentiate from multicentric osteosarcomata especially if they are present in the absence of lung or other visceral metastases.

The prognosis, once dismal, has improved greatly, thanks to advancements in chemotherapy. Five-year survival is now greater than 75%. As a result, accurate staging is getting more important for presurgical assessment.

Surgical Pathology: Osteosarcomas are often large, generally over 5 cm. Conventional osteosarcomas are (by definition) intramedullary and centered in the metaphysis. Grossly, the vast majority of osteosarcomas demonstrate penetration of the cortex, with an extraosseous soft tissue extension. Distant foci within the marrow cavity of the same bone may

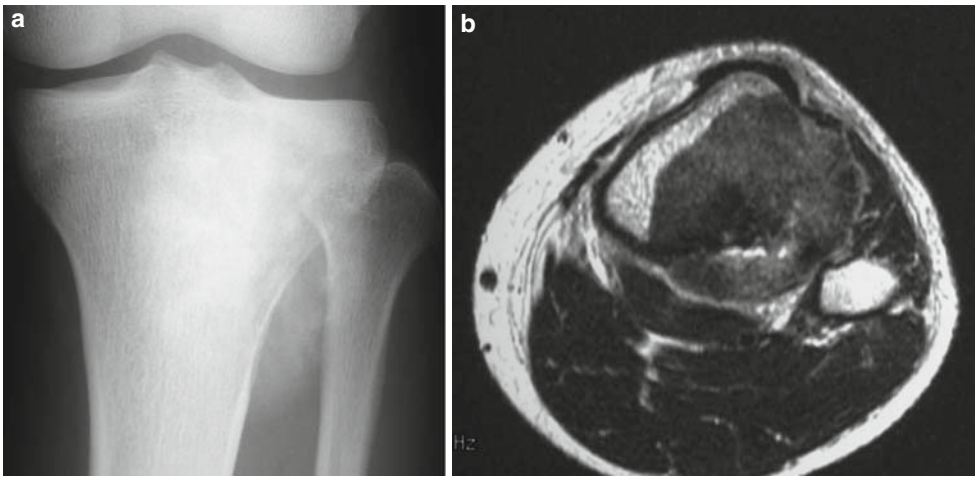

Fig. 7.46 Osteosarcoma, tibia (20-year-old man). **a**. AP view of the knee. Amorphous ossification in the proximal femur representing osteoid. **b**. T2-weighted axial MR image. An infiltrating lesion involves the bone around bone marrow

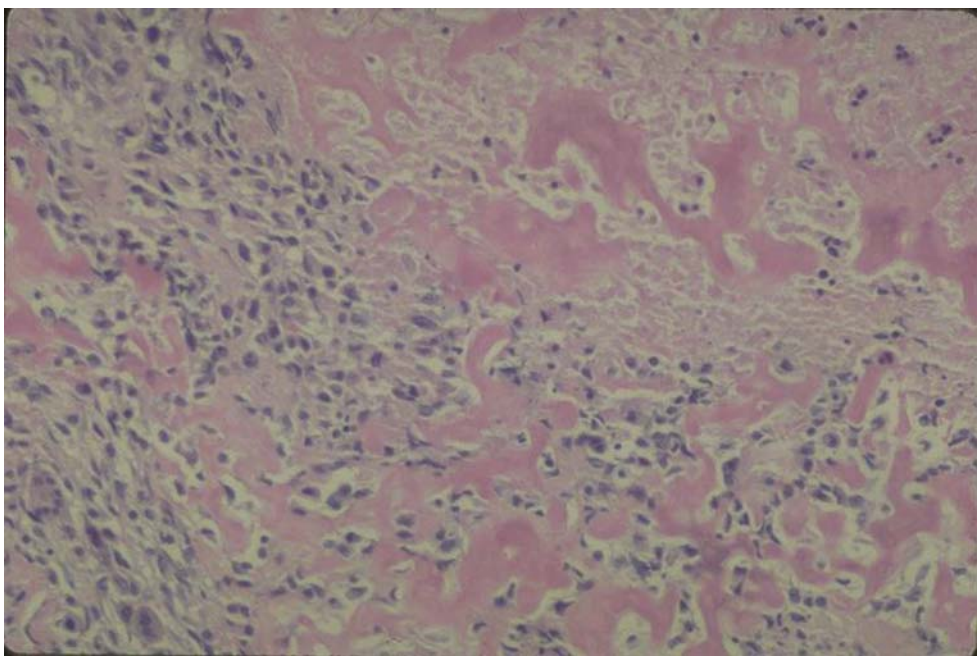

Fig. 7.46H Osteosarcoma showing lacy osteoid, necrosis, and malignant osteoblasts

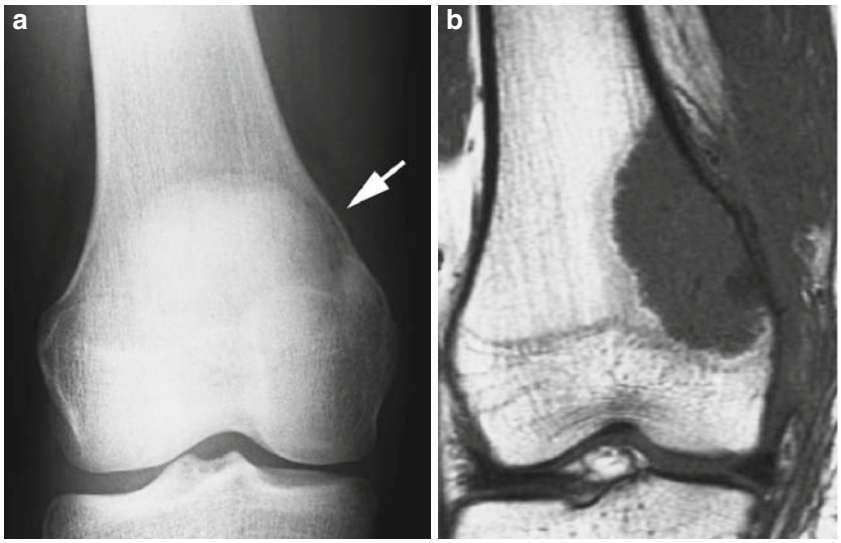

Fig. 7.47 Osteosarcoma, femur (15-year-old man). **a**. AP view of the knee. A lytic change without sclerotic margin is noted on the medial aspect of the femoral metaphysics (*arrow*). **b**. T1-weighted MR image reveals a well-defined, slightly lucent lesion

be found (at a distance from the main tumor mass) and are termed "skip" lesions or skip metastases. Skip lesions are uncommon findings but are important potential causes of recurrent disease.

The gross appearance of the tumor is variable and frequently variegated, depending upon the predominant differentiation. Thus, areas of lobular cartilaginous growth and gritty bone may be found within the same mass. Foci of hemorrhage and necrosis are common. Large blood-filled areas may represent a telangiectatic component. The periosteal reaction is frequently visible as spicules or lamellae of bone. Epiphyseal penetration is uncommon especially at the macroscopic level. Joint extension may occur, sometimes following along intra-articular ligaments (ligamentum teres in the femoral head or the cruciate ligaments in the knee). Because preoperative chemotherapy is commonly utilized, it is rare to see osteosarcomas nowadays in their native viable form.

Microscopically, osteosarcomas are high-grade, anaplastic tumors and frequently show unequivocal osteoid production (Fig. 7.46H). Osteoblastic, chondroblastic, and fibroblastic differentiation is commonly admixed. Sometimes the amount of osteoid production can be minimal or absent in otherwise typical osteosarcomas. However, such lesions may produce heavily ossified metastases, justifying the use of osteosarcoma, even though the primary tumor has little or no bone production.

The neoplastic cells of the osteosarcoma may be plasmacytoid, epithelioid, spindled, or oval. They often have marked nuclear pleomorphism, a high mitotic rate, and atypical mitotic forms. These cells are easier to identify in the areas away from the bone trabeculae or osteoid formation. Occasional osteosarcomas, however, are bland cytologically. This makes small fragmented biopsies treacherous to interpret, and the clinical context must be taken into account. Osteoid may have variable thickness and degrees of mineralization. A thin, highly mineralized pattern (the filigreed pattern) is quite suggestive of neoplastic osteoid if found. Other tumors can be very heavily ossified. Some osteosarcomas can resemble osteoblastomas, but the presence of an infiltrative border suggests the correct diagnosis.

Some osteosarcomas are composed of epithelioid-looking cells. A rosette formation may give the appearance of gland formation, and immunohistochemical markers may be positive for epithelial differentiation. Such osteosarcomas can be also seen as part of the sarcomatous component of a dedifferentiated chondrosarcoma.

Chemonecrosis of the tumor (following neo-adjuvant therapy) is important to recognize and quantitate. The appearance of the tumor after chemotherapy depends upon its original morphology. A tumor necrosis of greater than 90% is associated with a good clinical outcome.

Small Cell Osteosarcoma

Small cell osteosarcoma is a variant of high-grade osteosarcoma, histologically composed of small round cells that produce osteoid matrix. Radiological findings are non-specific, similar to conventional osteosarcoma, although a blastic change is frequent (Fig. 7.48) [46].

Surgical Pathology: The tumor is a round cell malignancy with at least focal osteoid formation. Chondroblastic differentiation occurs in about a third of cases. The small round cells may form sheets or arrange in a hemangiopericytoma-like pattern. Necrosis and mitotic figures may be seen fre-

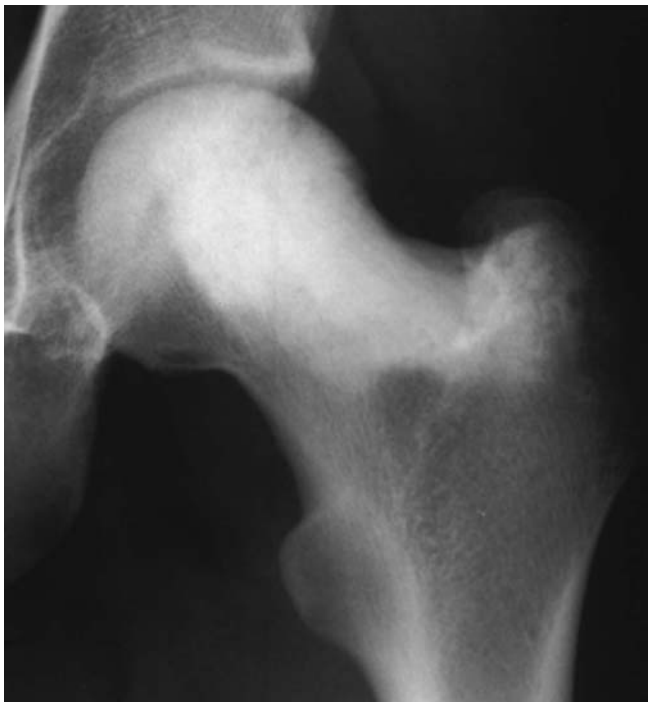

Fig. 7.48 Small cell osteosarcoma, femur (17-year-old man). A relatively well-defined sclerotic focus is seen in the proximal femur (courtesy of Dr. Kunihiko Fukuda)

quently or occasionally be rare. The majority of cases have cells with hyperchromatic rounded nuclei. Other examples have closely packed spindle-shaped cells with scant amounts of indistinct cytoplasm.

Ultrastructurally, the features are similar to those of Ewings tumor and mesenchymal chondrosarcoma and show small cells with scant cytoplasm and organelles. There are frequent free ribosomes and variable numbers of mitochondria, rough endoplasmic reticulum, Golgi, and filaments.

The characteristic t(11;22) translocation of Ewing sarcoma is not seen in small cell osteosarcoma. By molecular methods the EWS/FLI1 or EWS/ERG fusion product is absent.

Parosteal Osteosarcoma

Parosteal osteosarcoma is a distinctive type of low-grade surface osteosarcoma. Parosteal osteosarcoma appears as dense ossification spreading along the cortical surface of a bone. Typically it does not invade the bone marrow.

Parosteal osteosarcoma is most common in slightly older patients than those with conventional medullary osteosarcoma. It arises most commonly along the posterior cortex of the distal femoral metaphysis, constituting 70% in Okada's series [47], followed at a distant second by the distal radial metaphysis. Plain radiography is usually diagnostic, showing dense ossification along the outer margin of the cortex (Fig. 7.49). The inner surface of the lesion often has a non-ossified portion, representing chondroid matrix that may be confused with a histologically high-grade portion of the tumor [48]. The tumor has low recurrence and metastasis rates. The prognosis is generally good after local resection with the attached cortex, but dedifferentiation to high-grade sarcoma occurs in approximately 15% of the cases.

Surgical Pathology: Parosteal osteosarcoma typically presents as a large heavily ossified mass encircling the bone from which it arises. Sometimes it may resemble an osteochondroma because of the presence of a cartilage cap. Less ossified areas may be seen and they represent cartilage, fibrous tissue, fat, or more importantly, areas of dedifferentiation. Areas of intramedullary spread may occur in some lesions.

On microscopy, parosteal osteosarcomas typically show long narrow bone trabeculae arranged in a parallel fashion or areas of osteoid and woven bone with osteoblastic rimming separated by a fibrous stroma. The trabeculae may show maturation, resulting in lamellar bone. The spaces between the trabeculae are often filled with spindle fibroblastic tissue showing only minimal cytologic atypia (Fig. 7.49H). As many as half the lesions show cartilage. In about a third, this is present peripherally, simulating the cap of an osteochondroma. In others it is admixed with the tumor. The islands of cartilage or the cartilage cap are low grade. The columnar (physis-like) arrangement of the cartilage cap that is seen in osteochondromas is not usually present in parosteal osteosarcoma.

High-grade areas resembling conventional osteosarcomas should be interpreted as evidence of dedifferentiation, implying a worse prognosis. Unfortunately, the clinical and epidemiological profiles of patients with dedifferentiation and those without are similar. It is therefore critical to sample the lesions thoroughly to exclude this possibility.

Periosteal Osteosarcoma

Periosteal osteosarcoma is another distinctive type of predominantly chondroblastic, low-grade surface osteosarcoma. The medullary cavity is not involved. Its prognosis is better than conventional osteosarcoma but poorer than for parosteal osteosarcoma.

Periosteal osteosarcoma characteristically appears at imaging as a diaphyseal, broad-based surface lesion with cortical erosion and speculated periosteal reaction [49] (Fig. 7.50). In general, it has much less matrix than parosteal

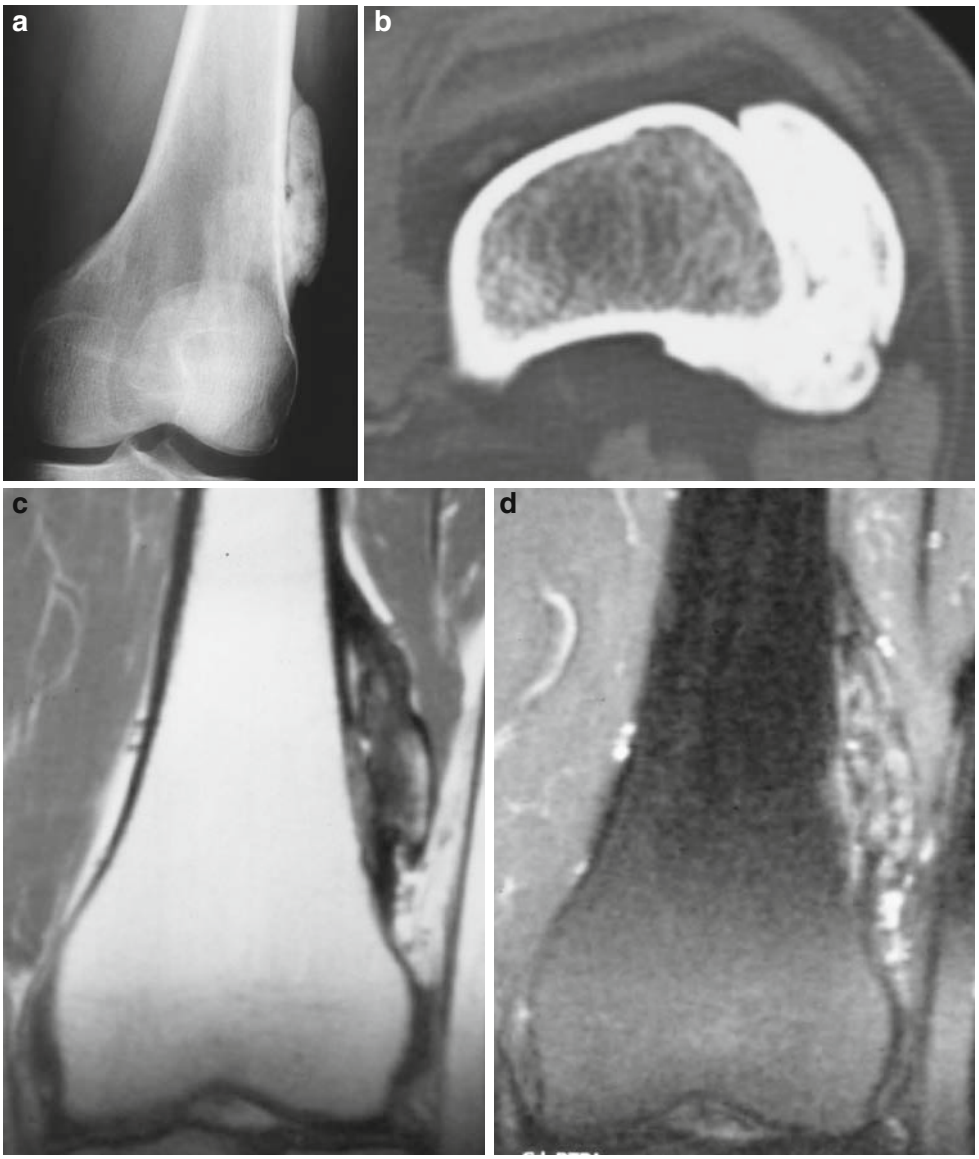

Fig. 7.49 Parosteal osteosarcoma, femur (48-year-old woman). **a**. AP view of the knee. A dense ossification on the distal femoral cortex. **b**. CT. An ossified massin the parosteal region. **c**. T1-weighted coronal MR image. A low-signal lesion corresponds to the ossified mass. **d**. T1-weighted coronal MR image with fat suppression after intravenous Gd. The ossified mass is well enhanced (courtesy of Dr. Osamu Tokuta)

osteosarcoma. CT and MR imaging are used for surgical staging.

Surgical Pathology: Grossly, these tumors are sharply demarcated, lobulated, and cartilaginous. Microscopically, they have dominant chondrosarcomatous areas (grades 2–3) with at least some focal osteoid formation. Usually, the osteoid is present in the centers of the lobules. In some cases the cartilage forms islands separated by anaplastic spindle cells. The malignant osteoid is often thin and lacy, surrounding these spindle cells. There are often broad spicules near the underlying cortex. Fibroblastic foci may be present in a minor component.

Telangiectatic Osteosarcoma

Telangiectatic osteosarcoma is a variant of osteosarcoma consisting predominantly of aneurysmal bone cyst-like blood-filled cystic regions. Three criteria are often used for diagnosis:

1. Predominantly lytic bone lesion with minimal sclerosis on radiography
2. Grossly cystic medullary mass with no or minimal solid or sclerotic component
3. Histologic features consisting of bone-forming tumor with notable blood-filled spaces separated by septae lined

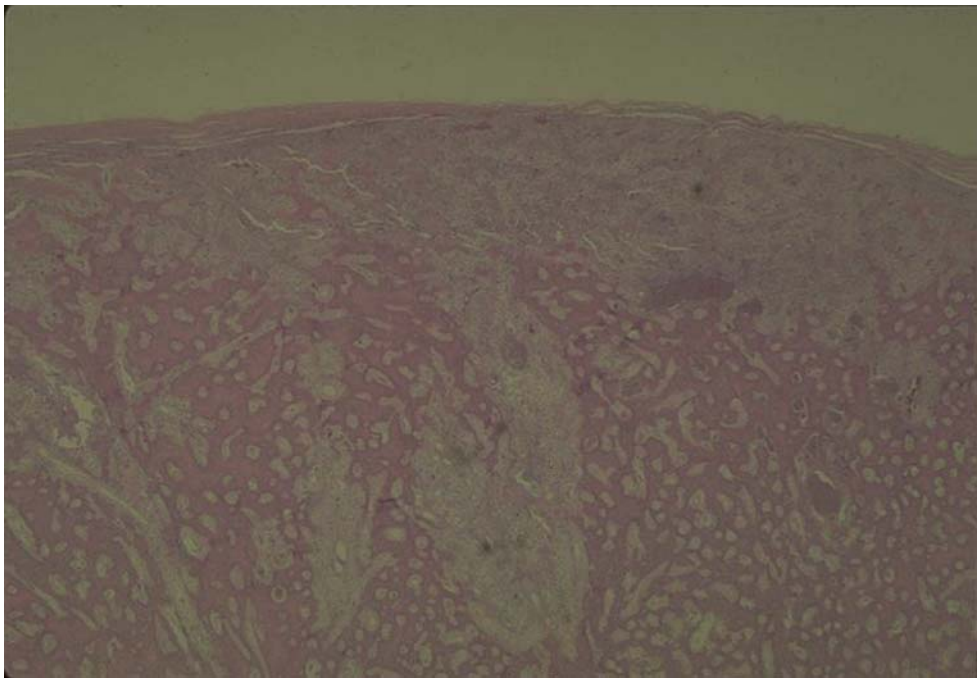

Fig. 7.49H Parosteal osteosarcoma showing abundant well formed osteoid and stroma with minimal atypia

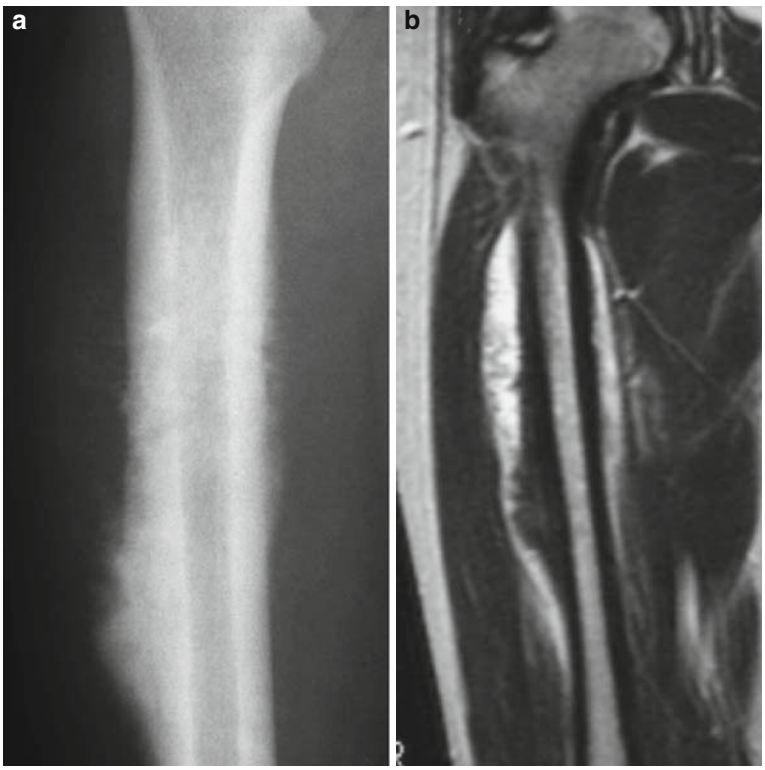

Fig. 7.50 Periosteal osteosarcoma, femur (12-year-old woman). **a**. AP view of the femur. Irregular ossification in the periosteal region. **b**. T2-weighted coronal MR image. A bright signal lesion extending along the irregular periosteal ossification (©Kanehara Shuppan)

by and/or containing malignant tumor cells with prominent nuclear atypia and limited osteoid deposition [50]

Areas of telangiectatic osteosarcoma often occur within conventional osteosarcomas. Telangiectatic osteosarcomas, however, are mainly (or exclusively) composed of dilated blood-filled spaces (Fig. 7.51). This osteosarcoma is a high-grade lesion with poor prognosis. Some have suggested that the prognosis may be similar to conventional osteosarcoma if no pathologic fracture is associated [50].

Radiographically, telangiectatic osteosarcoma is a purely lytic lesion, usually in the metaphysis of a long bone,

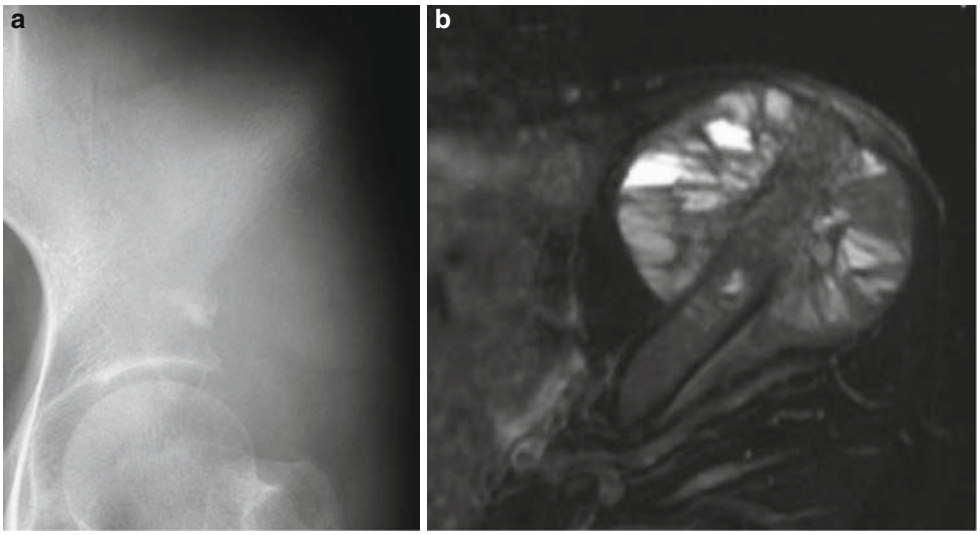

Fig. 7.51 Telangiectatic osteosarcoma, ilium (29-year-old woman). **a**. AP view of the ilium. An ill-defined lytic lesion in the acetabulum. **b**. T2-weighted axial MR image. Multi-loculated cystic lesion with fluid levels is noted

and often associated with pathologic fracture. CT and MR imaging can define the cystic component and fluid levels. Differentiation from aneurysmal bone cyst (ABC) can be difficult, but ABC tends to have sharper margins, and it may involute and become more localized with peripheral ossification.

Surgical Pathology: Grossly, the tumor may appear as a blood clot, as a hemorrhagic–necrotic mass, or as multicystic with blood-filled spaces or even resemble an aneurysmal bone cyst (ABC). Microscopically, two variants are described, corresponding to the gross appearances. These are the hemorrhagic–necrotic and the aneurysmal bone cyst-like (ABC-like) variants. In the hemorrhagic–necrotic variant, malignant cells are present, widely separated in a background of blood and necrotic debris (several levels and slides may have to be viewed in order to diagnose this variant). Osteoid matrix may be minimal.

In the second (ABC-like) variant, the low power view is that of an aneurysmal bone cyst. Necrosis is sparse or absent. It is only at high power that one begins to appreciate the overtly malignant cells within the cyst wall. Benign giant cells are present, and serve to further obscure the malignant nature of this entity. Focal delicate osteoid should be sought and contrasted with the more abundant coarse osteoid of the usual aneurysmal bone cyst.

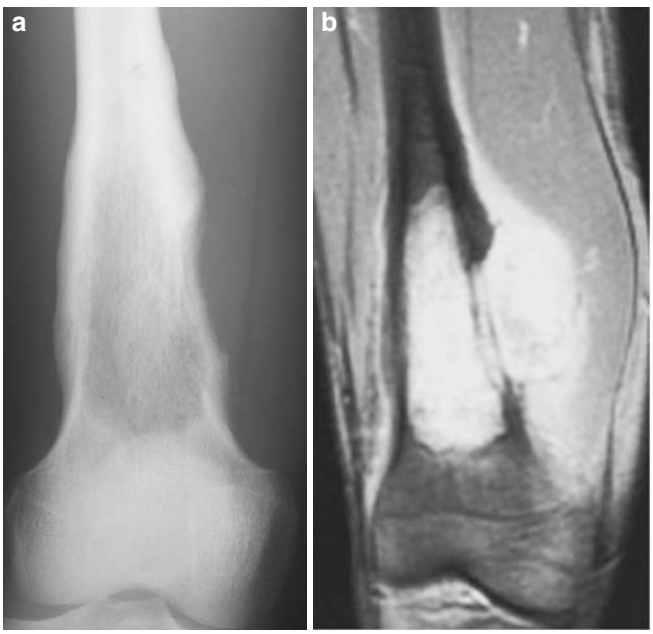

Fig. 7.52 Giant-cell-rich osteosarcoma, distal femur (24-year-old man). **a**. AP view of the femur. An ill-defined lytic lesion in the distal shaft of the femur. No mineralization is noted. **b**. T2-weighted coronal MR image revealing a bright intramedullary lesion extending into the soft tissue

Giant-Cell-Rich Osteosarcoma

Giant-cell-rich osteosarcoma also occurs in the bone marrow. Its significance is that it may be confused with giant cell tumor histologically and radiographically. The lesion is relatively well defined, and sclerosis or ossified osteoid matrix is rare (Fig. 7.52) [51].

Surgical Pathology: This variant of osteosarcoma is characterized by a proliferation of bland giant cells amidst a sarcomatous stroma. Osteoid production is usually sparse. If attention is not paid to the stromal anaplasia, an incorrect interpretation of this lesion as a giant cell tumor will result. Usually, but not always, these tumors are metaphyseal (like conventional osteosarcomas) rather than epiphyseal (like other giant cell tumors). This location gives a clue to its

true nature. Unfortunately, there are examples, where this is not the case, and some tumors have had all the x-ray features of giant cell tumors.

Low-Grade Central Osteosarcoma (Intraosseous Well-Differentiated Osteosarcoma)

Intraosseous well-differentiated osteosarcoma is a term given to an intramedullary osteosarcoma variant composed of low-grade, fibrous, and osseous tissue with only minimal cytologic atypia. Although the number of cases studied in most series is small, it is important to recognize this subtype, since the patients tend to fare much better than those with the conventional osteosarcoma. The lesion is often well circumscribed. Although some cases are similar to fibrous dysplasia histologically, their radiographic features are not. Instead, they appear as well-defined lytic lesions in the bone marrow often with localized cortical destruction [52] (Fig. 7.53).

Surgical Pathology: Microscopically, fibrous tissue and variable amounts of osteoid form the bulk of the tumor. Cartilage differentiation is infrequent. A pattern of infiltration into the pre-existing lamellar bone or fatty marrow is diagnostic. There is only slight atypia and the mitotic rate is low (1–2 per 10 high-power fields). The osteoid component may be mineralized and appear mature (lamellar). About one-third have a fibroblastic stroma that resembles a desmoid or desmoplastic fibroma. Sometimes, a fibrous dysplasia-like pattern of "Chinese alphabets"-like bone may be seen embedded in a fibrous stroma. The most important histologic finding is that of a permeative growth pattern.

High-Grade Surface Osteosarcoma

High-grade surface osteosarcoma is another variant of osteosarcoma arising upon an intact cortex. Radiography shows a lesion on the cortical surface with typically fluffy-appearing mineralization, representing the high-grade lesion [53]. These lesions are higher grade than parosteal and periosteal osteosarcomas. Imaging features may reflect the aggressive nature of the tumor (Fig. 7.54).

Surgical Pathology: Grossly, the tumors are bulky, multilobulated masses with a variegated appearance. The dense sclerosis of the parosteal and the chondroid appearance of the periosteal variants is absent. Microscopically they resemble the conventional osteosarcoma.

Osteosarcoma of the Mandible and Maxilla

Osteosarcoma of mandible is characteristically a bulky low-grade ossified tumor. Densely mineralized soft tissue mass representing low-grade osteosarcoma is a typical imaging feature (Fig. 7.55), but it varies [54]. The prognosis is usually good, different from osteosarcoma of the skull which generally has a poor prognosis. Microscopically many cases show chondroblastic differentiation and can be mistaken for chondrosarcoma. True chondrosarcomas, however, are rare in this region and better sampling often reveals diagnostic areas showing a spindle cell tumor with at least focal osteoid formation as well.

Multicentric Osteosarcomata

Multicentric osteosarcomata may occur synchronously or metachronously [55]. This syndrome occurs most commonly in teenage girls. A dominant lesion occurs in most cases. This may be the primary lesion and the other foci may be metastatic (Fig. 7.56) [56]. Synchronous tumors with no dominant lesion, typically presenting as sclerotic foci in the metaphysis, may be the only real multicentric tumor but rare.

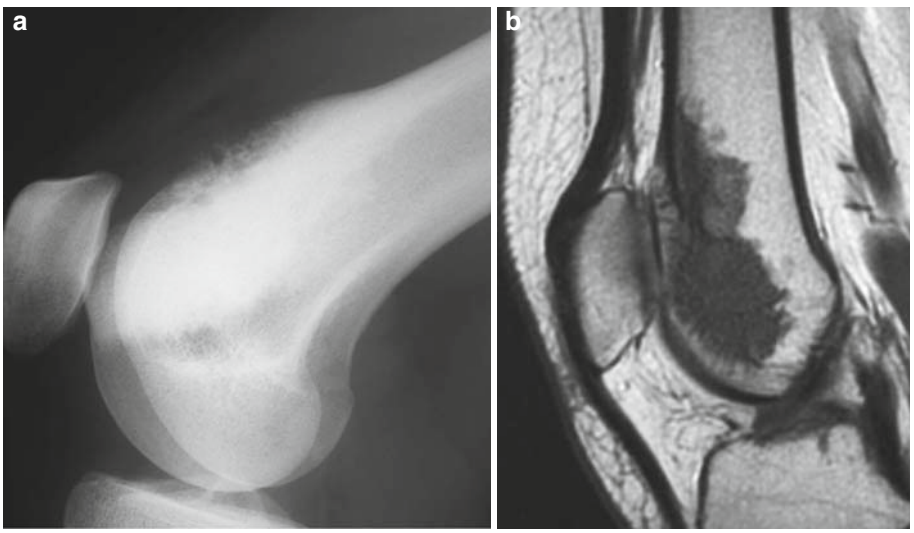

Fig. 7.53 Low-grade central osteosarcoma, tibia (23-year-old woman). **a**. Lateral view of the knee. A sclerotic lesion with fuzzy border in the proximal shaft of the tibia. **b**. T2-weighted sagittal MR image. A low signal intensity mass is localized in the medullary canal. Although the lesion is similar to fibrous dysplasia histologically, this imaging feature is more likely conventional osteosarcoma

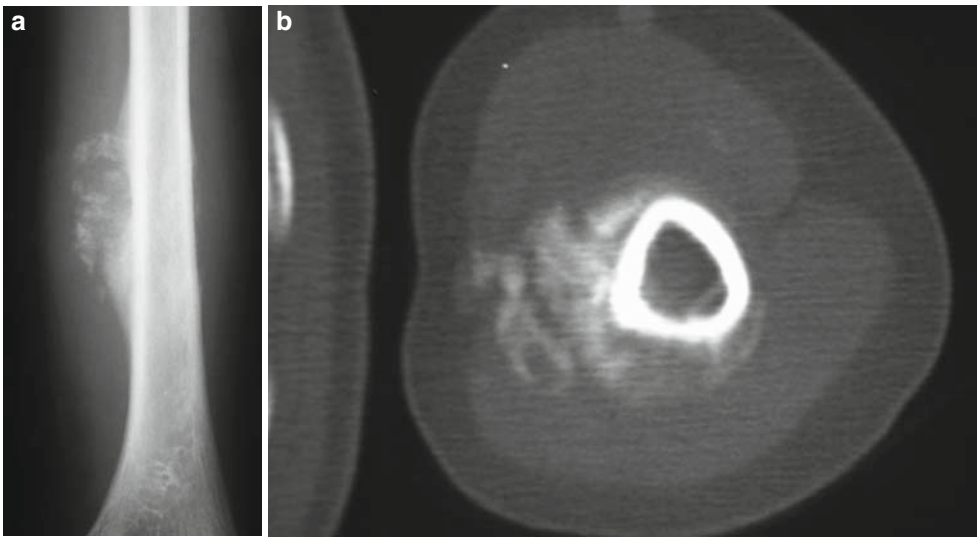

Fig. 7.54 High-grade surface osteosarcoma. **a**. AP view of the humerus. An irregular ossification is seen in the cortical surface. **b**. CT showing an ossified mass in the cortical surface (Courtesy of Dr. Okada)

Osteosarcoma Associated with Other Conditions

Osteosarcomas occur later in life in association with various disorders including Paget disease, radiation therapy, and fibrous dysplasia. Such secondary sarcomas are usually high-grade sarcomas. The prognosis is poor [57].

The exact incidence of sarcoma in Paget bone is unknown. In a case of Paget osteosarcoma, the typical radiographic finding is osteolysis developing in the sclerotic phase of the disease (Fig. 7.57).

Postradiation sarcoma occurs within a bone in the radiation field after a latent period, greater than 5 years in adults and greater than 2 years in children. Histologically, the diagnosis needs to be different from the original tumor. Advances in radiation therapy have made this a very rare lesion. Differentiation from postradiation change is important; newly developed osteolysis is often a clue to the early diagnosis. Malignant osteoid is also one of the findings of Paget osteosarcoma (Fig. 7.58).

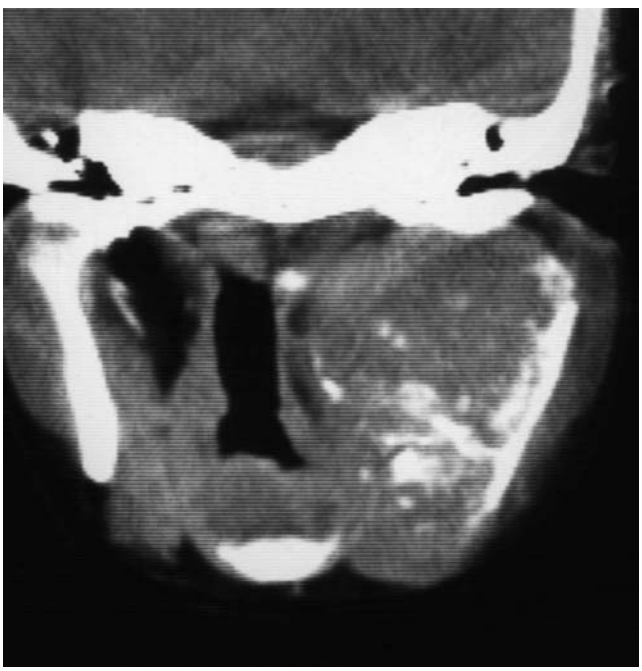

Fig. 7.55 Osteosarcoma of the mandible (31-year-old woman). Coronal CT demonstrating a large ossified mass on the medial aspect of the mandible

Fibrous and Fibrohistiocytic Tumors

Non-ossifying Fibroma and Fibrous Cortical Defects (Fibroxanthoma, Metaphyseal Fibrous Defect)

Several lesions show common histologic features such as a storiform cellular pattern, histiocyte-like giant cells, foam cells, and a polymorphic infiltrate. Such lesions are often grouped under the general heading of (non-ossifying fibroma and fibrous cortical defect), even though many such entities may be unrelated to each other or to the histiocyte cell line.

Although each of these entities have identical histology, the term non-ossifying fibroma is used to designate a larger potentially expansive lesion involving the bone marrow, and the term fibrous cortical defect is reserved for a small cortical ossification defect with minimal bone marrow involvement. Majority of the patients are young, 5–15 years old, and male

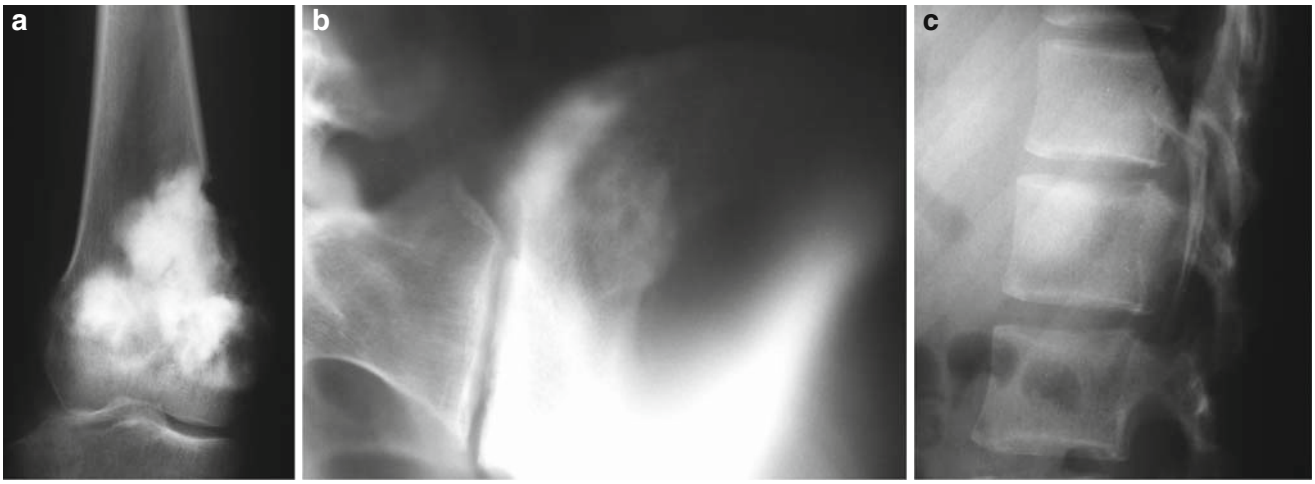

Fig. 7.56 Multicentric osteosarcomata. **a**. AP view of the distal femur, revealing a large ossified mass. **b**. AP tomogram of the pelvis shows an ossified mass. **c**. Lateral view of the lumbar spine. An ossified focus is noted. Because of the dominant lesion in the distal femur, and the distribution of the other lesions, metastasis from the distal femoral lesion is more likely (courtesy of Dr. Okada)

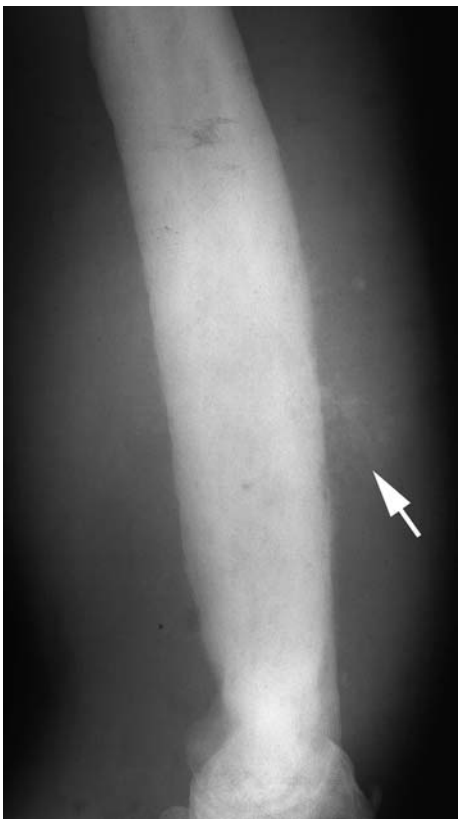

Fig. 7.57 Osteosarcoma due to Paget disease, humerus (65-year-old man). Lateral view of the humerus. Expansive and sclerotic humerus is due to Paget disease. An ossified soft tissue mass is associated in the periosteal region (*arrow*)

to female ratio approaches 1. Clinically, most patients are asymptomatic, but on occasion patients may suffer a pathologic fracture through one of these lesions.

Typically, NOFs are metaphyseal and eccentric. They may cause some cortical expansion (Fig. 7.59). They are usually lytic lesions with a well-defined sclerotic margin with a denser inner border. After adolescence, the lesion gradually scleroses inward. MR imaging shows low signal intensity on T1-weighted and T2-weighted images [58].

Both NOF and FCD tend to heal spontaneously as patients mature. Thus, treatment is usually conservative. However, if the lesion involves more than half of the diameter of a weight-bearing tubular bone, fracture may occur (Fig. 7.60) [59]. Patients with neurofibromatosis type I (Jaffe–Lichtenstein syndrome) often have multiple nonossifying fibromas.

A cortical defect in the distal posterior femoral metaphysis at the insertion of the medial head of the gastrocnemius, also called cortical desmoid, is likely not a fibrous defect but related instead to partial avulsion of the gastrocnemius muscle insertion. These typically occur in the early teenage years and heal rapidly without residual change (Fig. 7.61) [60]. Their significance, however, is that they may be confused with a surface osteosarcoma. Differentiation is essential.

Surgical Pathology: Microscopically, the lesions are predominantly fibrous, often having a storiform arrangement. Foamy histiocytes (xanthoma cells), hemosiderin-laden macrophages, and multinucleated giant cells are present in varying proportions. In the presence of fracture or in the healing phase, there may be reactive woven bone present.

Fibrous Dysplasia

Fibrous dysplasia (FD), a common bone marrow lesion, is a proliferation of spindle cells, due to a somatic mutational

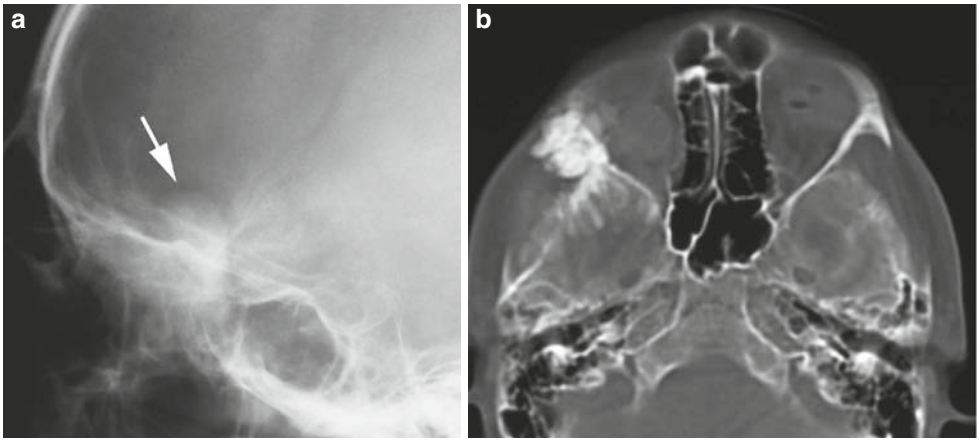

Fig. 7.58 Osteosarcoma of the skull due to radiation therapy for bilateral retinoblastoma (21-year-old man). **a**. Lateral view of the skull, showing malignant osteoid overlying the frontal region (*arrow*). **b**. CT. An ossified mass is seen in the lateral wall of the orbit and middle cranial base

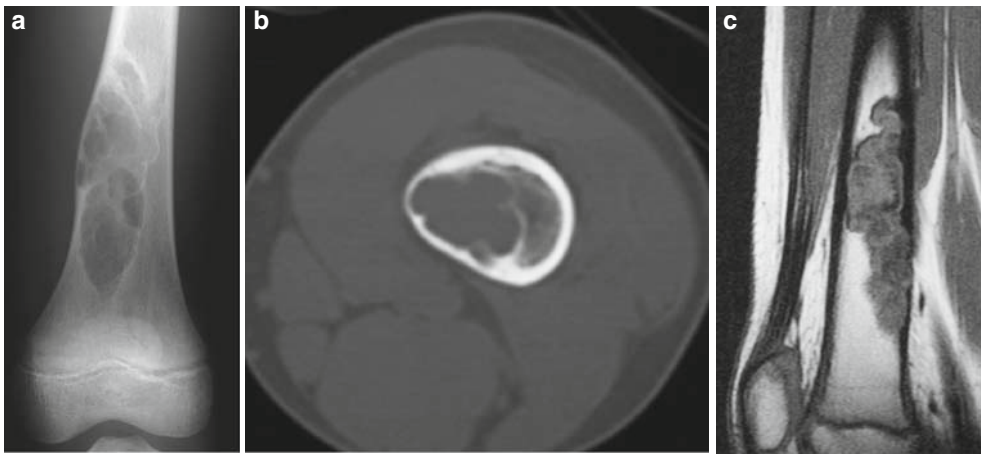

Fig. 7.59 Non-ossifying fibroma of femur (9-year-old man). **a**. AP view of the distal femur. A well-defined lytic lesion with sclerotic margin in the distal femur. **b**. CT. The lytic lesion is associated with thin sclerotic margin. **c**. T1-weighted sagittal MR image. A well-defined lesion with low signal intensity in the center and the periphery of the lesion is typical for non-ossifying fibroma

event (often an activating mutation of GNAS1 that results in the activation of G proteins). It may occur either in a mosaic pattern, early in fetal life, (McCune–Albright syndrome) or at multiplesites or even an isolated site in bone, probably later in life, and resulting in polyostotic or mono-ostotic disease FD is usually asymptomatic, often found incidentally or because of pathologic fracture. It may involve a single bone (mono-ostotic) either focally or diffusely, or multiple bones (polyostotic). When FD is polyostotic, lesions tend to occur on one side of the body or even in a single limb. In tubular bones, it typically involves the diaphysis, and extends along the long axis. In addition to tubular bones, fibrous dysplasia commonly affects the pelvis, facial bones, the calvarium, and ribs. It is the most common incidental lesion in the rib in adults.

Radiographic features are variable. Ground-glass opacity is typical and classic, but FD may be purely lytic or even densely sclerotic (Figs. 7.62, 7.63 and 7.64). Uncommonly, FD may undergo chondroid metaplasia and develop some chondroid matrix [61]. Secondary aneurysmal bone cyst also develops frequently as a complication (Fig. 7.63). If FD is diffuse and is a weight-bearing bone, it weakens the bone. This may result in a deformity of the limb as is seen in "shepherd crook" deformity of the proximal femur (Fig. 7.64). The skull is also a common site of FD, usually in the skull base and the walls of the paranasal sinuses (Fig. 7.65). It may also affect the calvarium where it may have a mixed sclerotic and lytic appearance that suggests an aggressive lesion (Fig. 7.66). There have been a few reports of malignant transformation of FD, but this is very rare, and its incidence may be close to the level of the incidental association.

Surgical Pathology: Grossly, fibrous dysplasia is firm, fibrous white, or red with a variable amount of "grittiness." Secondary cyst formation is occasionally seen. Some lesions contain grossly visible cartilage.

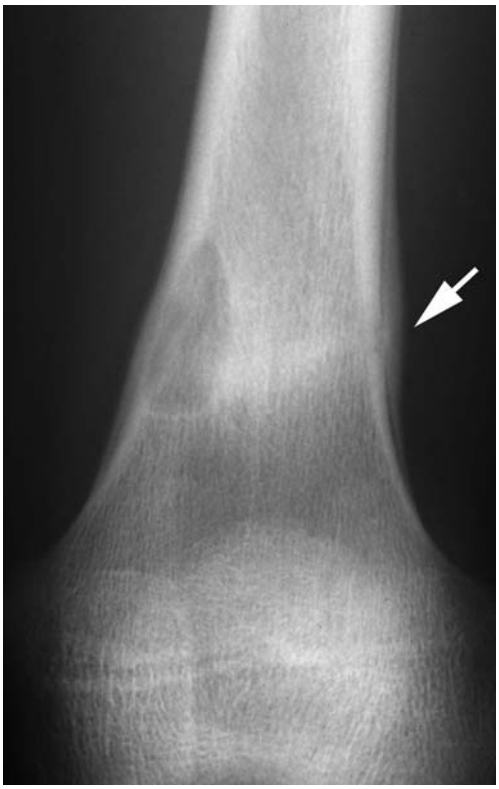

Fig. 7.60 Stress fracture through fibrous cortical defect (15-year-old man). A well-defined cortical lesion at the distal femur, consistent with fibrous cortical defect. A linear sclerosis and periosteal reaction represent stress fracture (*arrow*)

Microscopically, there are trabeculae of woven bone in a background of moderately cellular fibrous tissue. The trabeculae often obtain a variety of shapes (C's, circles, etc.) and are sometimes referred to as "Chinese letters." Osteoblasts are interspersed in the woven bone but are not conspicuous around the trabeculae (Fig. 7.62H). The fibrous stroma is highly variable in microscopic appearance. It may be highly or sparsely cellular, myxomatous, or show considerable collagenization. The fibroblasts usually have plump ovoid nuclei, but may show elongated narrow ones in some cases or in some areas. Multinucleate osteoclast-type giant cells may be present. Cartilage with peripheral enchondral ossification is sometimes present. The cartilage may be present in long islands, rounded nodules, or simulate a growth plate. Collections of foam cells are common.

Desmoplastic Fibroma

Desmoplastic fibroma is a rare non-metastasizing but locally aggressive lesion composed of cytologically typical fibroblasts in an abundantly collagenized stroma. This lesion is considered to be the bone counterpart of the soft tissue aggressive fibromatosis. Desmoplastic fibroma most commonly develops in young patients in the second and the third decades of life, and may arise in any bone. Post-therapeutic local recurrence is not unusual. The mandible is a common site of involvement.

Desmoplastic fibroma is usually central within the medullary cavity and well demarcated with a partially disrupted sclerotic margin. "Internal pseudotrabeculation" is characteristic, and seen in 90% of the cases (Fig. 7.67) [62]. T2 shortening on MR imaging causing low signal intensity on T2-weighted images may help with diagnosis [63].

Surgical Pathology: Microscopically, the tumors are hypocellular and composed of fibrous tissue resembling their soft tissue counterpart (aggressive fibromastosis). They demonstrate a proliferation of spindle cells separated by abundant collagen. Entrapped bone may be present. Soft tissue extension is commonly seen. Nucleoli and mitotic figures are inconspicuous to absent. There is often a prominent

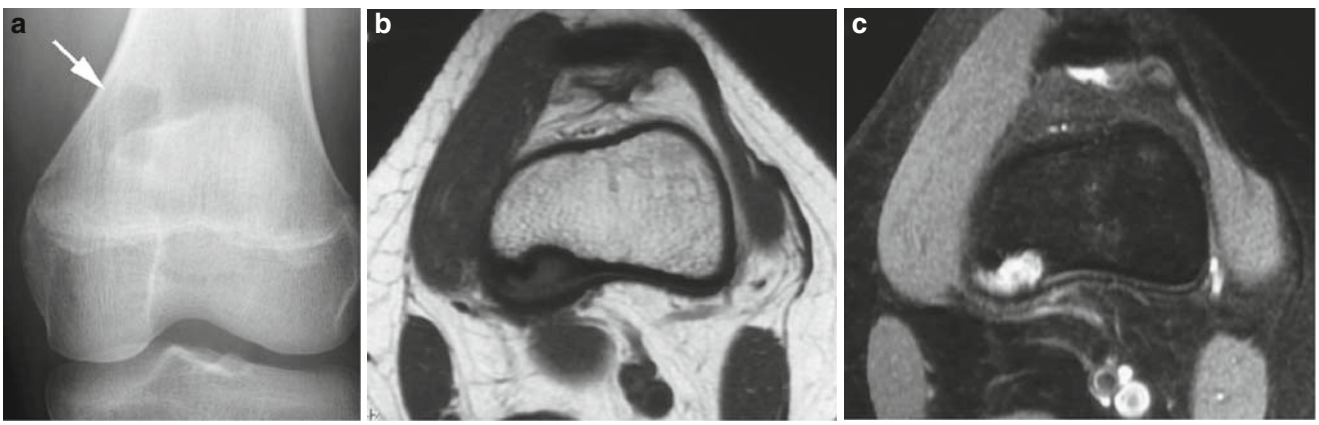

Fig. 7.61 Distal femoral cortical defect (13-year-old woman). **a**. AP view of the knee. A radiolucent lesion with partially sclerotic margin is seen in the medial aspect of the distal femur, at the origin of medial head of the gastrocnemius (*arrow*). **b**. T1-weighted axial MR image. **c**. T2-weighted axial T2-weighted MR image. The cortical defect has low signal on T1-weighted image and bright signal on T2-weighted image

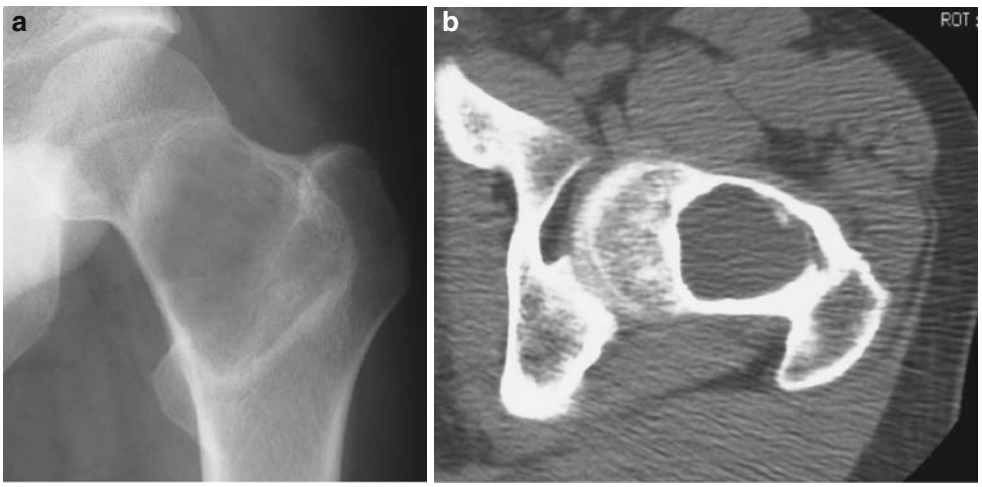

Fig. 7.62 Fibrous dysplasia, femur (24-year-old man). **a**. AP view of the hip. A well-defined lytic lesion with sclerotic margin is seen in the femoral neck. The sclerotic margin is thick, with ground-glass center. **b**. CT. A well-defined lytic lesion with sclerotic margin

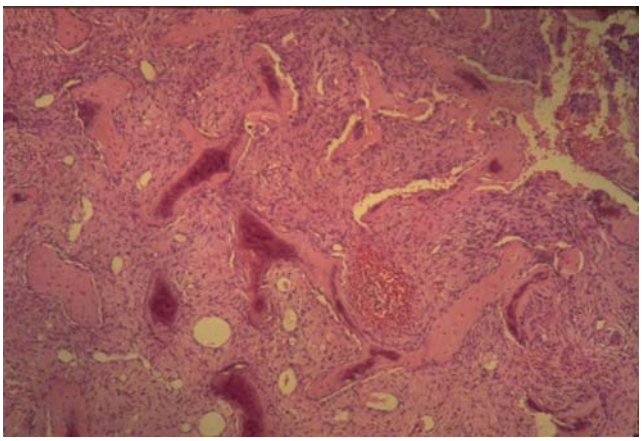

Fig. 7.62H Fibrous dysplasia showing emerging irregular bone trabeculae in a cytologically bland fibrous background

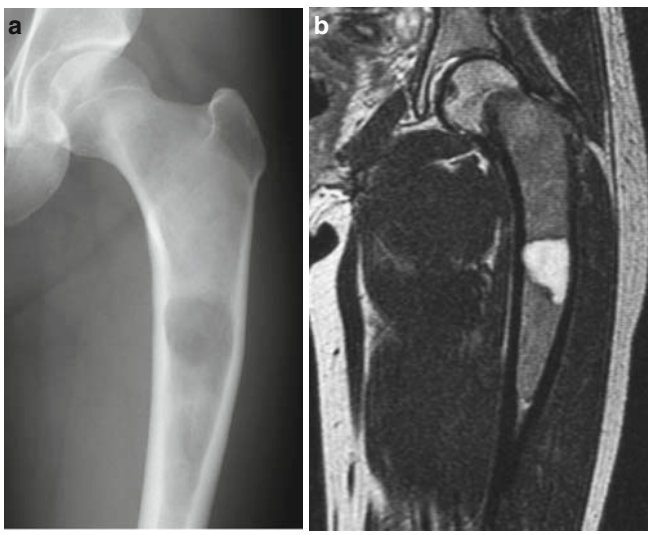

Fig. 7.63 Fibrous dysplasia, femoral shaft (24-year-old woman). **a**. AP view of the proximal femur. A long-segment ground-glass lesion in the proximal femur contains a well-defined purely lytic change. **b**. T2-weighted coronal MR image. A ground-glass portion has low signal intensity, and a bright signal intensity focus in the midshaft represents secondary cystic change

vascular component, once again, similar to the soft tissue desmoid.

Fibrosarcoma

Fibrosarcoma is a spindle cell sarcoma, and its diagnosis is often one of exclusion from other sarcomas, e.g., osteosarcoma. The patient's age at diagnosis varies between the teens and the fifties. The prognosis correlates directly with the histological grade of the tumor. Congenital and infantile fibrosarcoma are separate entities, presenting with large lytic lesions. Compared with adult fibrosarcoma, these tumors have a good prognosis.

Fibrosarcoma is difficult to characterize, and radiological features are usually non-specific [64]. The distal femur and proximal tibia are the most common sites. Generally, fibrosarcoma is a central lytic lesion in the metaphysis of a long bone without ossified matrix. The tumor may contain myxoid matrix reflected as bright signal on T2-weighted MR imaging. Fibrosarcoma usually shows an aggressive growth pattern. The lesion margin is not well defined, and the tumor often causes cortical destruction (Fig. 7.68). Occasionally, the tumor may envelop a small piece of dead bone, creating a sequestrum. This finding suggests the diagnosis.

Surgical Pathology: Grossly, the tumors vary from gray and firm to tan and soft or fleshy tumors with infiltrative

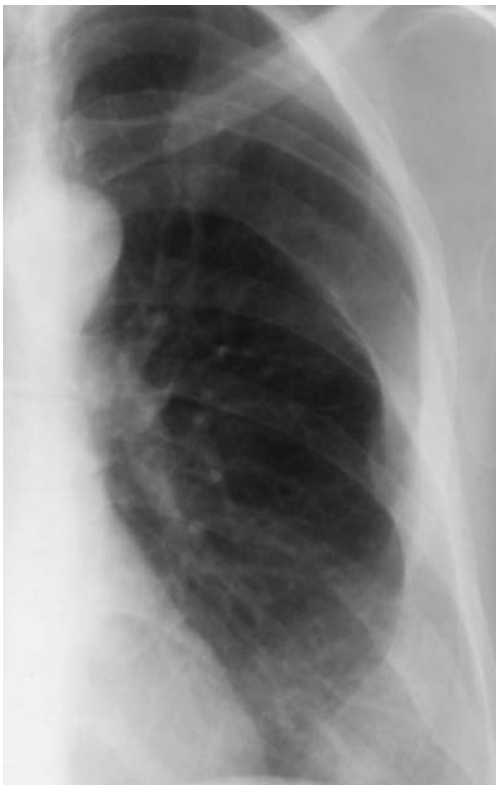

Fig. 7.64 Fibrous dysplasia, ribs (40-year-old woman). AP view of the left hemithorax. An expansive sclerotic change involves the long segment of the rib

margins. Areas of hemorrhage or necrosis may be present in high-grade tumors. Microscopically, the spectrum ranges from tumors that are heavily collagenized and difficult to separate from desmoplastic fibromas to others that are more than cellular, with bizarre, mitotically active spindle cells with considerable cytologic atypia. The spindle cells are consistently arranged in a "herring-bone" fashion of interlacing fascicles. Some tumors may be myxoid. Most tumors show evidence of cortical breakthrough.

Malignant Fibrous Histiocytoma (Pleomorphic Sarcoma)

Malignant fibrous histiocytoma (MFH) is a controversial pleomorphic sarcoma [65]. Because the tumor has no relationship to histiocytes, some authors have suggested renaming this lesion to undifferentiated pleomorphic sarcoma. However, the WHO 2002 group continued to accept the term, especially in bone lesions. Immunohistochemistry has reclassified a significant fraction of tumors, once diagnosed as MFH, to other types of sarcoma.

MFH usually occurs in an older age group. Its imaging features may be indistinguishable from fibrosarcoma, a purely lytic lesion of the metaphysis (Fig. 7.69). The findings are non-specific, but its aggressive nature is often evident radiographically. The prognosis is better than it used to be, but MFH is still a high-grade malignancy with a guarded prognosis.

Surgical Pathology: Grossly, the tumor is similar to other high-grade sarcomas, often having a variegated appearance with hemorrhage and necrosis. The margins are frequently permeative. Microscopically, these lesions have a wide range of appearances. The lesions dominated by fibrous tissue, or like soft tissue MFH, exhibit a variety of patterns such as inflammatory, myxoid, pleomorphic–storiform, hemangiopericytomatous, epithelioid. Nuclear atypia and mitotic rate can often be impressive. Multinucleated malignant giant cells are found in most examples. Histiocyte-like cells with grooved nuclei are also frequent. Fibrosis is often variable, and may be absent. Spindle cell areas with a storiform arrangement are common. Chronic inflammatory cells may often be seen.

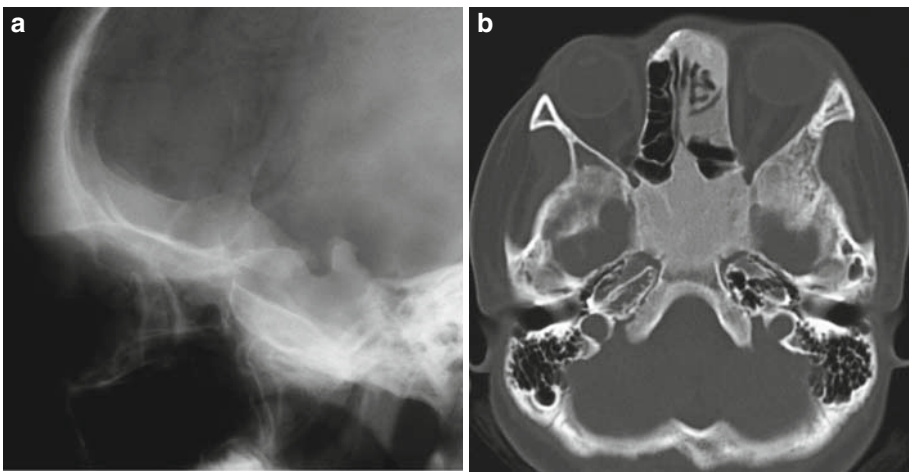

Fig. 7.65 Fibrous dysplasia, skull (15-year-old woman). **a**. Lateral view of the skull. An ill-defined sclerosis at the skull base. **b**. CT. Sclerotic change with ground-glass appearance involving the paranasal sinuses and orbit

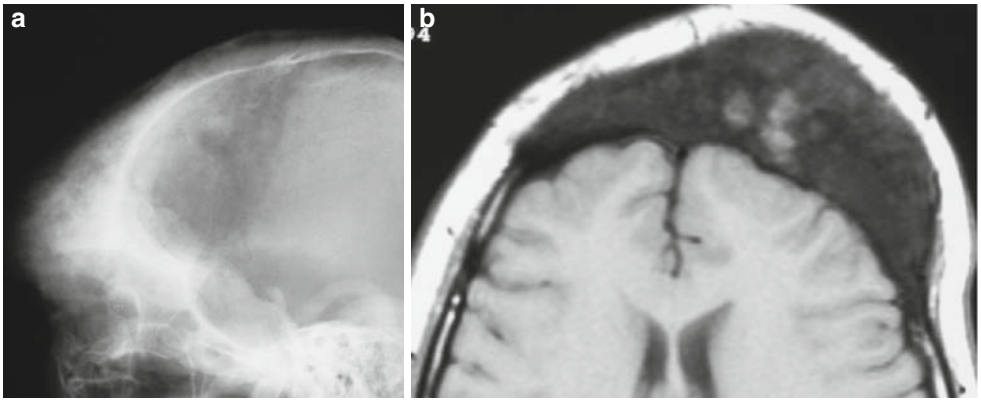

Fig. 7.66 Fibrous dysplasia, skull (22-year-old man). **a**. Lateral view of the skull. Thick and irregularly dense frontal region. Sclerosis is also seen in the skull base. **b**. T1-weighted axial MR image. Frontal bone is thick and the signal is heterogeneous

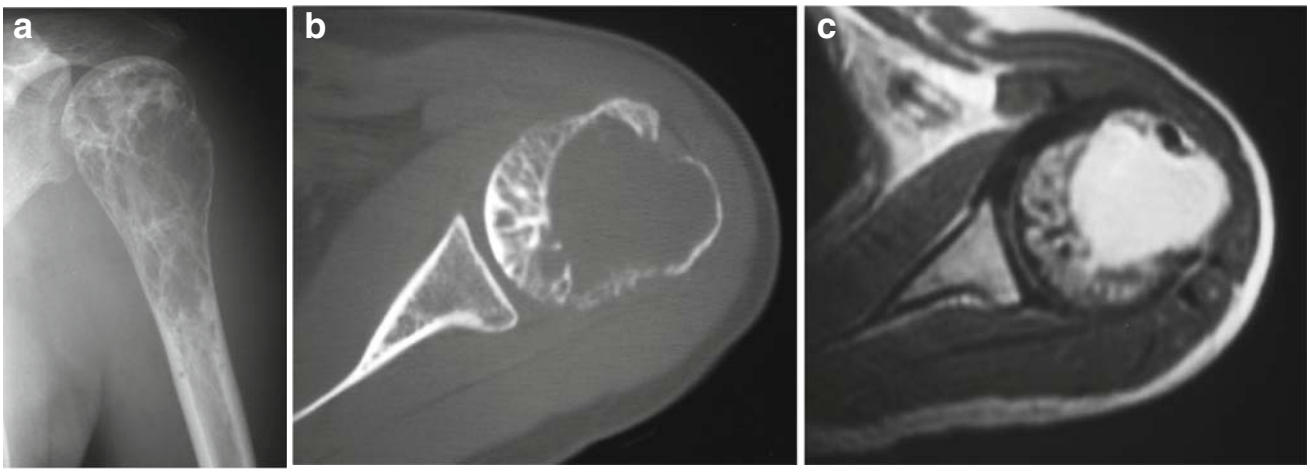

Fig. 7.67 Desmoplastic fibroma (37-year-old woman). **a**. AP view of the proximal humerus. An extensive lytic change with irregular margin in the proximal humerus. "Pseudotrabeculation" is noted. **b**. CT. A well-defined lytic portion and infiltrating portion with coarse trabeculae are noted. **c**. T2-weighted axial MR image. The lesion has bright signal (courtesy of Dr. Yamaguchi)

Vascular Tumors

The classification of vascular tumors is confusing and evolving [66]. Included in the consideration are unrelated entities such as hemangioma, intermediate-grade vascular tumors, and angiosarcoma. Also included are conditions such as angiomatosis and Gorham disease.

Hemangioma

Hemangioma is a distinctive benign vascular tumor consisting of vessels with single-layer vascular endothelium. Lymphatic channel may exist in the periosteum, but not in the bone marrow, and solitary lymphangioma of bone is considered to be extremely rare. Although this tumor arises in any age group, its peak incidence is in the 50s. Imaging features are variable depending on the location and the size of the vascular component. Vertebrae are the most common sites of osseous hemangioma, but most of these hemangiomas are actually venous malformations with a small vascular component, increased bone marrow fat, and thickened trabeculae (Figs. 7.70 and 7.71) [67]. True hemangiomas with expansive bone and soft tissue component in the vertebrae are rare, but when they do occur, can cause neurological compromise (Fig. 7.72) [68]. The second most common site for hemangiomas is the skull. These appear as ill-defined lytic lesions, and a secondary trabecular pattern perpendicular to the diploic space is typical (Fig. 7.73). Hemangiomas of tubular bones are rare and variable. Some may be lytic with variable margination; others may be sclerotic (Fig. 7.74) [69].

Hemangiomas can be multiple, and multiple hemangiomas may be seen in diffuse cystic angiomatosis and Maffucci syndrome. The former syndrome is characterized by

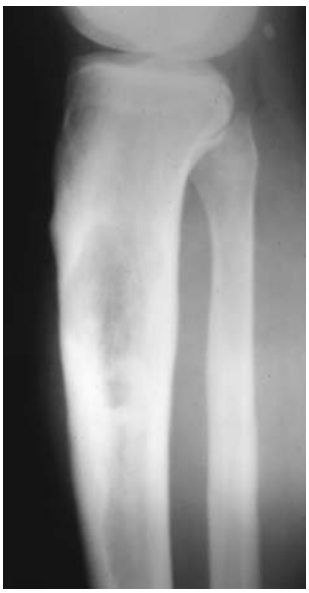

Fig. 7.68 Low-grade fibrosarcoma (42-year-old man). Lateral view of the tibia. A lytic lesion in the midshaft of the tibia. An ill-defined sclerotic change in the midshaft of the tibia

cystic expansile lesions, and may be associated with visceral involvement. The latter is the combination of hemangiomas and multiple enchondromas.

Surgical Pathology: Microscopically, hemangiomas are comprised of vascular channels, respectively, and can vary markedly in size. A loose fibrous stroma supports the vessels. Infrequently, thick-walled vessels of the arteriovenous malformation type are seen. There may be prominent aggregates of lymphocytes in lymphangiomas. A small amount of blood may be present. The vascular channels are often highlighted by vascular stains such as Factor VIII-related antigen, Ulex europus, CD 31, and CD 34. The lesions of skeletal–extraskeletal angiomatosis and Gorham disease are similar, but may be extensive and often (in angiomatosis) involving extraosseous tissues. Epithelioid hemangiomas have plump endothelial cells lining the vessels that have abundant eosinophilic cytoplasm (hob-nail cells).

Angiosarcoma (Including Hemangioendothelioma)

Angiosarcoma is a rare malignant tumor of vascular origin, consisting of vascular channels lined by single- or multilayered endothelium. Hemangioendothelioma is a term used by some authors to designate a lesion of intermediate aggressivity that may metastasize. Some use the name angiosarcoma and high-grade hemangioendothelioma to identify the same lesion. The term hemangioendothelioma is therefore somewhat problematic – a fact recognized in the last WHO consensus group that met in Lyon (WHO 2000). Angiosarcomas occur in both bone and soft tissue. They may be solitary or multiple, may be more than one contiguous bone. The prognosis has been reported to be related to the histological grade, not their multiplicity. Angiosarcomas tend to be long lesions radiographically and often give the bone a "Swiss cheese" appearance. However, overall imaging features are difficult to characterize since they may be lytic, sclerotic, or mixed lytic and sclerotic [70] (Figs. 7.75 and 7.76). In high-grade lesions, the tumor margins tend to be ill defined. The imaging features are those of aggressive tumors, but they are usually non-specific.

Surgical Pathology: Grossly, angiosarcomas are soft, red or gray, spongy focally firm, and have solid areas. Microscopically, the diagnosis is usually not difficult. There are areas of well-formed anastomosing vascular channels lined

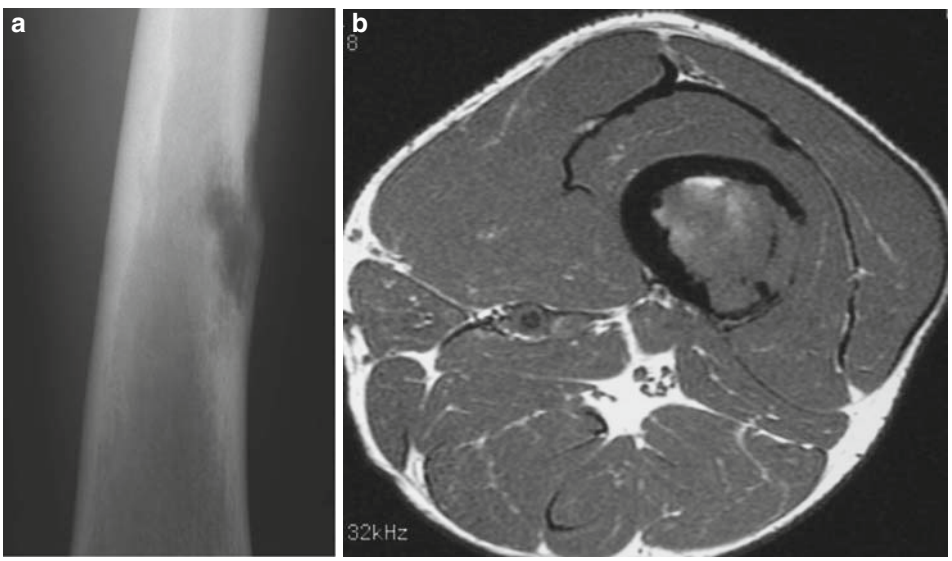

Fig. 7.69 Malignant fibrous histiocytoma (53-year-old man). **a**. AP view of the femur. An eccentric lytic lesion is noted in the midshaft of the femur. No mineralization is noted. **b**. T1-weighted axial MR image. A low-signal lesion in the medullary canal infiltrating into the cortex

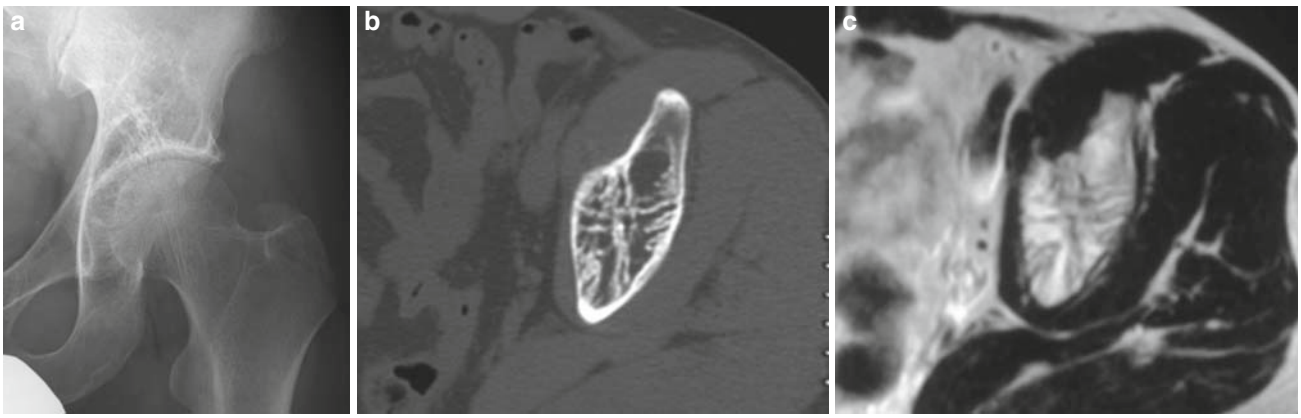

Fig. 7.70 Hamangioma of the acetabulum (48-year-old woman). **a**. AP radiography reveals a coarse trabecular pattern in the left acetabulum. **b**. CT. Coarse trabeculation and fat content of the lesion are noted. **c**. Axial T2-weighted image. Mixed fat and more bright vessels are noted.

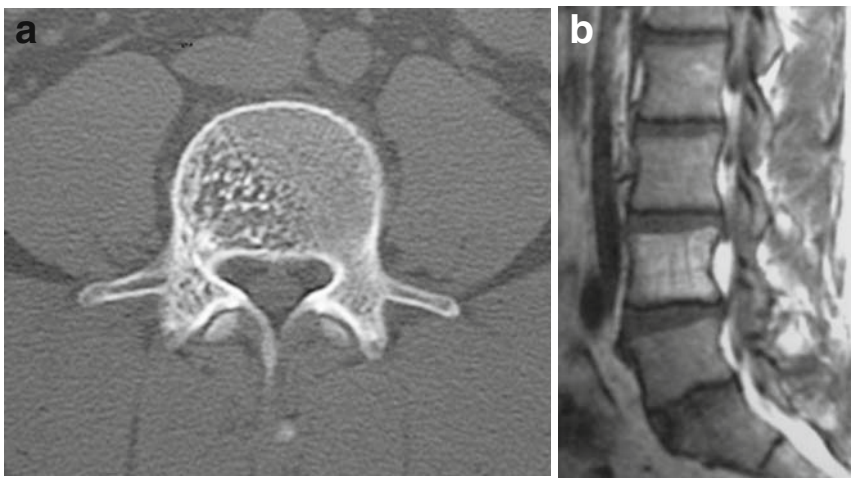

Fig. 7.71 Hemangioma of the vertebral body (47-year-old man). **a**. CT. Coarse trabeculae in the vertebral body representing hemangioma. **b**. T1-weighted sagittal image. The lesion consists of bone marrow fat

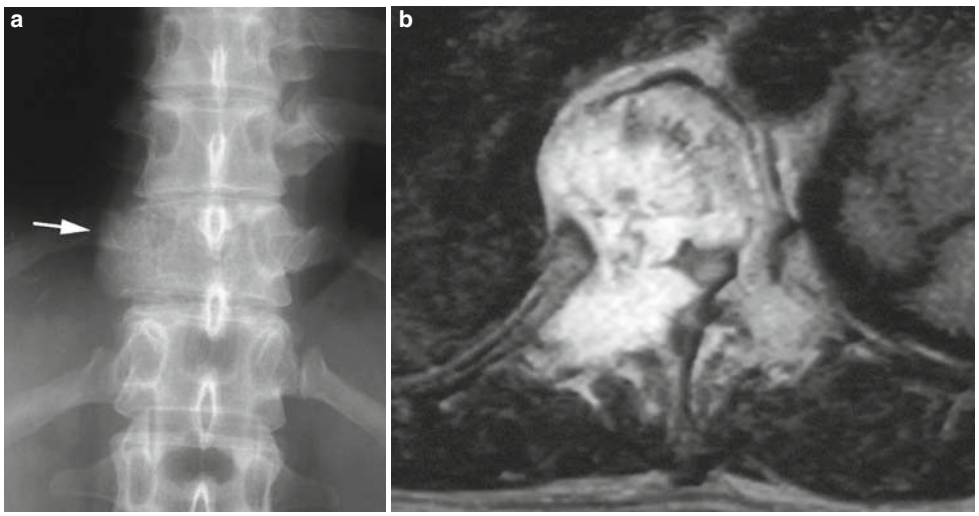

Fig. 7.72 True hemangioma of the vertebral body with expansive growth (43-year-old woman). **a**. AP view of the lumbar spine representing overgrowth of eleventh thoracic vertebra (*arrow*). **b**. T2-weighted axial MR image. An expansive growth with bright signal corresponds to hemangioma. Spinal canal is narrowed (courtesy of Dr. Shinichi Kikuchi)

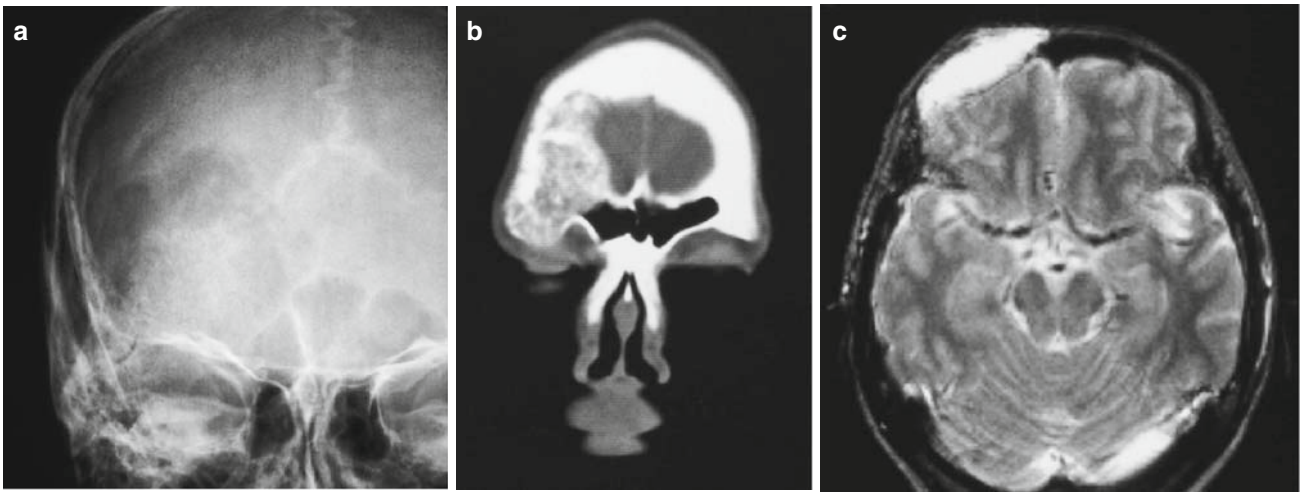

Fig. 7.73 Hemangioma of skull (48-year-old woman). **a**. AP view of the skull. An ill-defined lytic lesion in the right frontal region. A hazy high density is seen in the lytic focus. **b**. Coronal CT. The calvarium is thick with mixed lytic-sclerotic change. **c**. T2-weighted axial MR image. A bright signal intensity in the calvarium of the right frontal region

Fig. 7.74 Hemangioma of the phalanx (11-year-old man). AP view of the finger. A mixed lytic-sclerotic change is seen in the phalanx

by atypical endothelial cells, with large vesicular or hyperchromatic nuclei. There are often solid, poorly differentiated areas where the vasoformative nature may be undiagnosible. Immunohistochemically, the tumor cells are often positive for vascular markers such as CD 31, CD 34, and Factor VIII-related protein. Often epithelial markers are also positive, a potential source of misdiagnosis.

Other Mesenchymal Tumors

Cysts (Simple Bone Cyst, Aneurysmal Bone Cyst)

Simple Bone Cyst (Unicameral Bone Cyst, UBC)

Simple bone cysts are not neoplasms. They are fluid collections that result from a circulatory disturbance in the physeal portion of the bone. For unknown reasons, the hydrostatic pressure increases in this area of the bone [71]. One theory is that venous outflow obstruction is the cause. This cyst consists of a single fluid-filled cavity within the bone marrow, but false septa giving the appearance of loculation occur occasionally.

Patients are young, 3–19, and the male to female ratio is 2:1. UBCs arise most commonly in the proximal femur, tibia and humerus, and in the distal femur. These locations account for about 90% of all cases. Lesions in typical sites tend to arise in young patients, but a second group of older patients, usually in their fourth decade, also develops unicameral bone cysts. These are usually in atypical locations, including the calcaneus and juxtasacral ilium [72].

Radiologically, UBCs appear as a well-defined medullary lucency with sclerotic margin, often centrically located (Figs. 7.77 and 7.78). The closer the lesions are to their physeal plate of origin, the more likely they are to be active. Clinically, UBC is usually asymptomatic and recognized incidentally, or because they have undergone pathologic fracture. When pathologic fracture occurs, a fragment of bone from the wall may fall into the cyst creating a "fallen fragment" sign. This is considered to be a pathognomonic radiographic

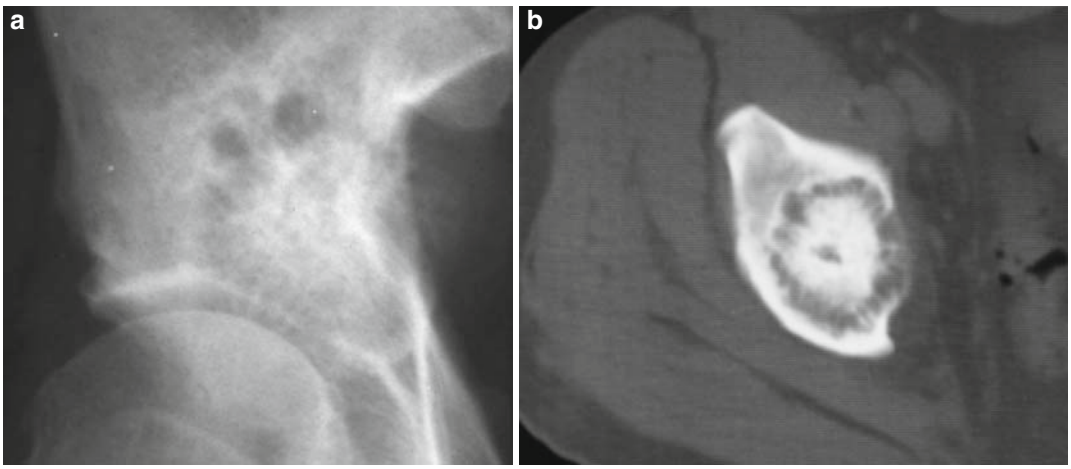

Fig. 7.75 Low-grade hemangioendothelioma, right hip (56-year-old man). **a**. AP view of the right hip. An irregular-shaped lytic lesion contains sclerotic focus (©: Kanehara Shuppan). **b**. CT. An irregular-shaped sclerotic change in a lytic focus (©: Bunkodo)

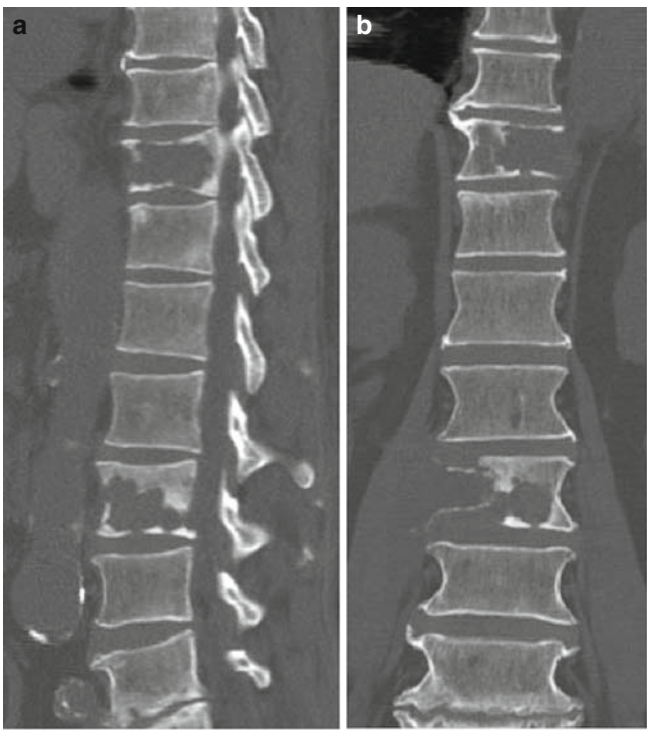

Fig. 7.76 Multicentric hemangioendothelioma of vertebrae. **a**. Sagittal CT. Well-defined purely lytic changes in the eleventh thoracic and the third lumbar vertebrae. **b**. Coronal CT revealing the two lesions. Compression fractures and cortical disruption are noted (courtesy of Dr. Yamaguchi)

finding. A fluid level on CT and MR imaging, a sign of bleeding, arises when pathologic fracture occurs. Although curettage and bone graft used to be a standard treatment, simple drainage or steroid injection may be curative.

Surgical Pathology: It is unusual to receive intact gross specimens, since these lesions are rarely resected. Curetted material consists of irregular fragments of membranous fibrovascular tissue, with reactive bone. Hemosiderin, granulation tissue, a few giant cells, or mild focal chronic inflammatory cells may be present. Some cases have pink cementum-like rounded material.

Aneurysmal Bone Cyst

Aneurysmal bone cyst (ABC) is a benign multicystic lesion of bone, which is composed of blood-filled spaces, separated by connective tissue septae containing giant cells and reactive bone. Changes similar to aneurysmal bone cysts can be seen in several other benign bone tumors and are sometimes designated as secondary aneurysmal bone cysts to distinguish from the true (or primary) cases.

Recent cytogenetic studies have suggested that primary aneurysmal bone cysts are true neoplasms and have a consistent genetic abnormality, associated with the short arm of chromosome 17 (most likely involving the coding sequence of the ubiquitin protease gene USP 6). The commonest translocation is t(16;17)(q22;p13), but there are several variations. Similar changes have been seen in solid aneurysmal bone cysts and the related entity of myositis ossificans. These genetic changes seem to be absent in secondary aneurysmal bone cysts further supporting the evidence that this is a definite pathological entity.

Patients typically are 10–30 years old at the time of diagnosis. The male to female ratio is 1:1. ABCs may occur in any bone, but the majority are distributed in the spine (25%) (usually posterior elements), in long bones (37%), in flat bones (25%), and in short tubular bones (16%).

Radiologically ABCs are lytic with rapid growth in their active phase. As they involute, sclerotic bone gradually replaces the lytic lesion. CT and MR imaging show a septated cystic mass with multiple fluid levels (Figs. 7.79 and 7.80). Fluid levels are not specific, however,

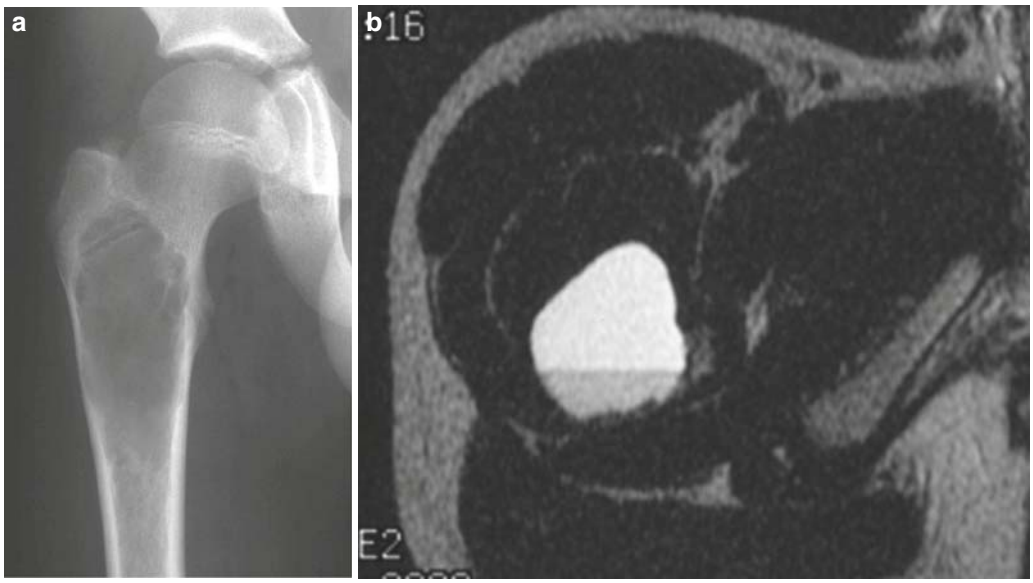

Fig. 7.77 Simple bone cyst, femur (11-year-old man). **a**. AP view of the femur. A well-defined lytic lesion in the proximal femoral metadiaphysis. **b**. T2-weighted axial MR image. A bright fluid signal with a fluid level representing traumatic change

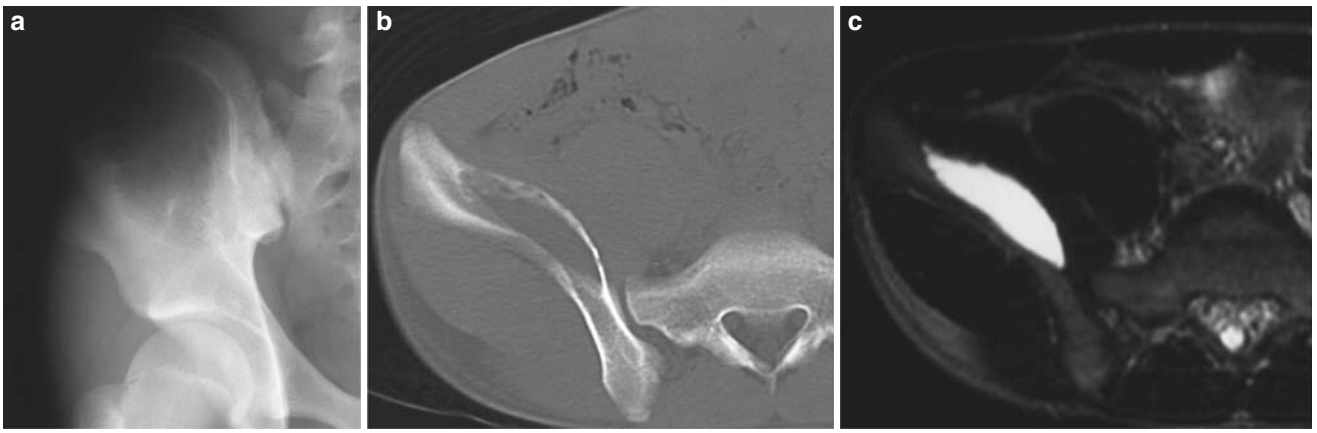

Fig. 7.78 Simple bone cyst, ilium (15-year-old woman). **a**. AP view of the pelvis. A well-defined lytic change with thin sclerotic margin. **b**. CT. A slightly expansive lytic lesion is evident in the ilium. **c**. T2-weighted axial MR image. A bright signal intensity represents fluid content

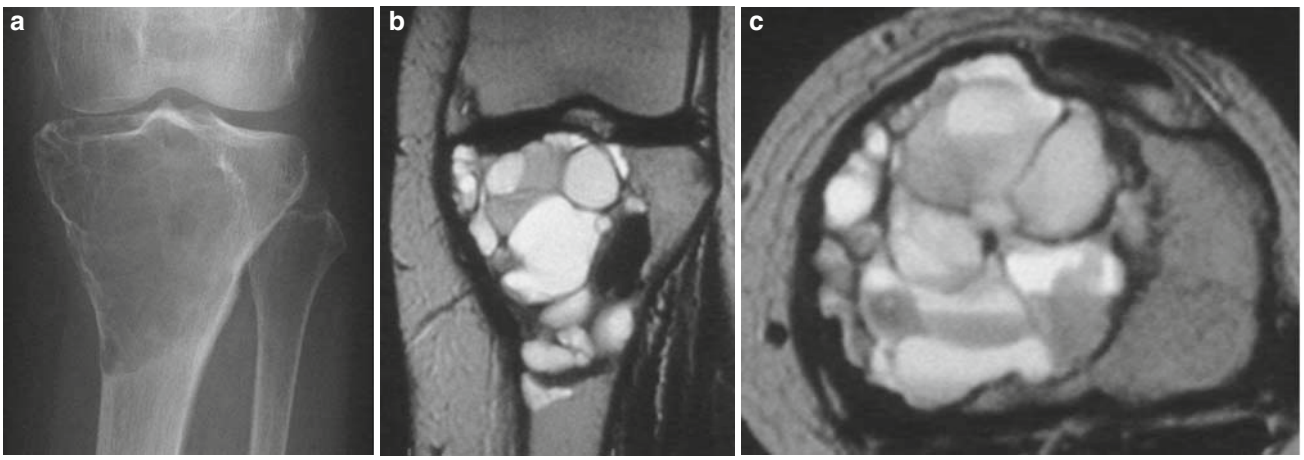

Fig. 7.79 Aneurysmal bone cyst, femur (74-year-old woman). **a**. AP view of the knee. A well-defined lytic lesion with no mineralization in the proximal tibia. **b**. T2-weighted coronal MR image. A multilocular cystic lesion with variable signal intensity is noted. **c**. T2-weighted axial MR image. Fluid levels are seen in the lesion

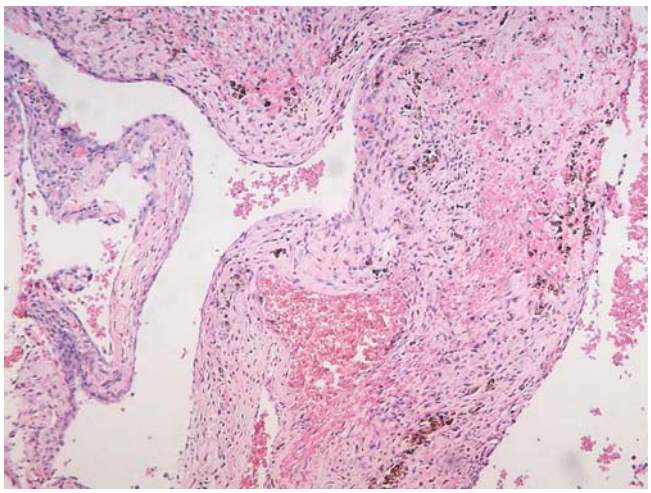

Fig. 7.79H A low-power photomicrograph of an aneurysmal bone cyst showing a hypocellular lesion with septations composed of fibroblasts and fibrocollagenous matrix

and may arise in other bone lesions, e.g., telangectatic osteosarcomas [73].

Surgical Pathology: Grossly, if intact, the lesions can be seen to have a thin osseous bony shell surrounding a honeycomb mass with cavernous vascular spaces that ooze blood like a sponge. Older cysts may have sero-sanguinous fluid rather than blood. A careful search could reveal a precursor lesion in a secondary ABC.

Microscopically, the main feature of ABC is the presence of cavernous spaces that are filled with blood but lack the smooth muscle wall and endothelial cells of blood vessels (Fig. 7.79H). The fibrous walls contain fibroblasts, osteoid, chondroid, and giant cells in varying proportions. The cysts of an ABC may invaginate into normal bone at the periphery of the lesion or extend into the soft tissue.

The fibroblastic stromal cells lack the atypia, atypical mitoses, and anaplasia that are seen in telangiactetic osteosarcomas. Osteoid may arise in a metaplastic fashion, like fibrous dysplasia, or may be surrounded by chondroid. Chondroid within these lesions may have a fibrillary or chondromyxoid quality. It may be focally calcified. Mitotic figures may be numerous, particularly in the areas of osteoid formation. Atypical mitoses, however, should not be seen. Necrosis too is generally absent, except in regions around a pathological fracture.

"Solid ABC" is a solid tumor with fibrous lined walls identical to those of an ABC [74], but it is otherwise histologically identical to giant cell reparative granuloma. Usually, no specific features to suggest ABC are present radiographically. Macroscopically, these lesions are completely solid. Microscopically, a spindle cell proliferation with a loose arrangement is seen. Giant cells occur in clusters, and are often arranged around areas of hemorrhage. Characteristically, there is abundant reactive new bone formation with osteoblastic activity similar to heterotopic ossification.

Secondary ABCs may occur in several other bone tumors, but they are most commonly associated with giant cell tumor, chondroblastoma, and fibrous dysplasia. Although difficult, imaging features may help differentiate secondary from primary ABCs [75]. Telangiectatic osteosarcomas are distinguished from aneurysmal bone cysts on the basis of careful microscopy. Their imaging features are more aggressive than standard ABCs but they contain no radiographically visible tumor bone, making it difficult to differentiate the two lesions in early phases.

Intraosseous Ganglion

An intraosseous ganglion is a small cyst containing mucinous material in subarticular bone. It is similar histologically

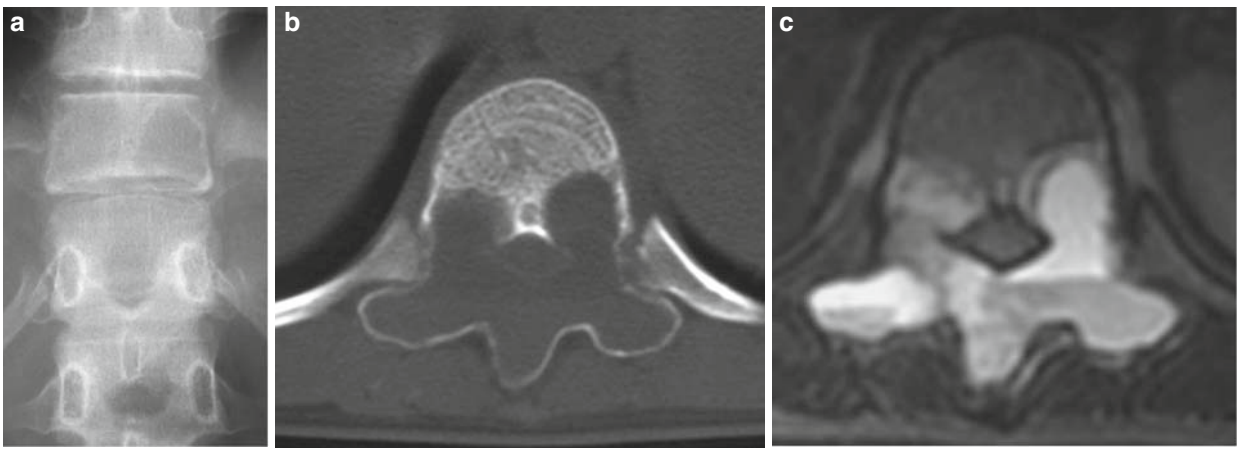

Fig. 7.80 Aneurysmal bone cyst, thoracic spine (12-year-old woman). **a**. AP view of the thoracolumbar spine. A lytic lesion in the pedicle and lamina of the thoracic vertebra. **b**. CT scan. An expansive lytic change in the lamina and pedicle of the vertebrae. **c**. T2-weighted axial MR image. Fluid levels are seen in the expansive lesion

to the subchondral cysts seen in osteoarthritis and rheumatoid arthritis, but ganglions arise in the absence of arthritis (Fig. 7.81). A ganglion is usually cystic with sclerotic margins; it may contain fluid, gas, or fibrovascular tissue. The last may show faint enhancement on MR imaging. Ganglions have been reported variously as causing symptoms [76].

Surgical Pathology: Microscopically, the tissue is mainly myxoid, mixed with fibroblasts, but the typical stellate cells of true myxomas are not seen. Fibrous tissue may be haphazardly interspersed or be arranged in the form of septa. The outer layer is often heavily collagenized.

An intraosseous pneumatocyst is a gas-containing cystic lesion arising in the juxtaarticular portion of the bone [77]. Simple bone cysts may lose fluid, and so also may be filled with gas (probably nitrogen) (Fig. 7.82). Most pneumatocysts, however, are small and close to the joint and are most likely gas-filled intraosseous ganglions. Pneumatocysts also occur in the vertebral bodies, probably secondary to spondylosis or degenerated Schmorl nodes.

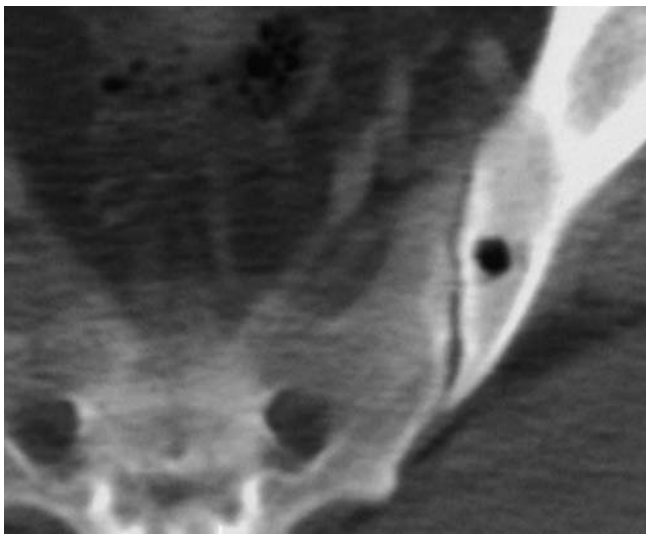

Fig. 7.82 Intraosseous pneumatocyst (24-year-old man). CT. A small round gas-containing cyst in the ilium, adjacent to the sacroiliac joint

Intraosseous Lipoma

Intraosseous lipoma most often occurs in patients 20–40 years of age. It arises in any bone, although the femur and calcaneus are the most common sites (Fig. 7.83). It is a controversial tumor. Since fat is abundantly present within normal bone marrow, histology cannot differentiate a mass of normal fat from a tumor. In addition, osteoporosis with lack of trabeculae may appear histologically as a fatty mass.

Furthermore, the fat in an intraosseous lipoma often has foci of necrosis, and this may have areas of dystrophic calcification or ossification [78]. On the other hand, a mature bone infarct typically contains fat. Thus, differentiation of an infarct from an intraosseous lipoma can be difficult. To avoid confusion with osteonecrosis, some designate intraosseous lipoma as a fat-containing mass with cortical expansion. Unfortunately, this caveat is not foolproof since a healed simple bone cyst may appear as a fatty medullary mass with cortical expansion and further not all lipomas expand bone.

On imaging, intraosseous lipomas appear as a lytic lesion with or without sclerotic margins. Mineralization and necrosis may be included in the fat. A cystic component, if present, may be either a result of necrosis or a remnant of a simple bone cyst. These lesions are diagnosed more commonly now that MR is commonplace.

Surgical Pathology: Intraosseous lipomas are composed of mature adipose tissue and so are similar to the common soft tissue counterpart, but may often show prominent areas of fat necrosis.

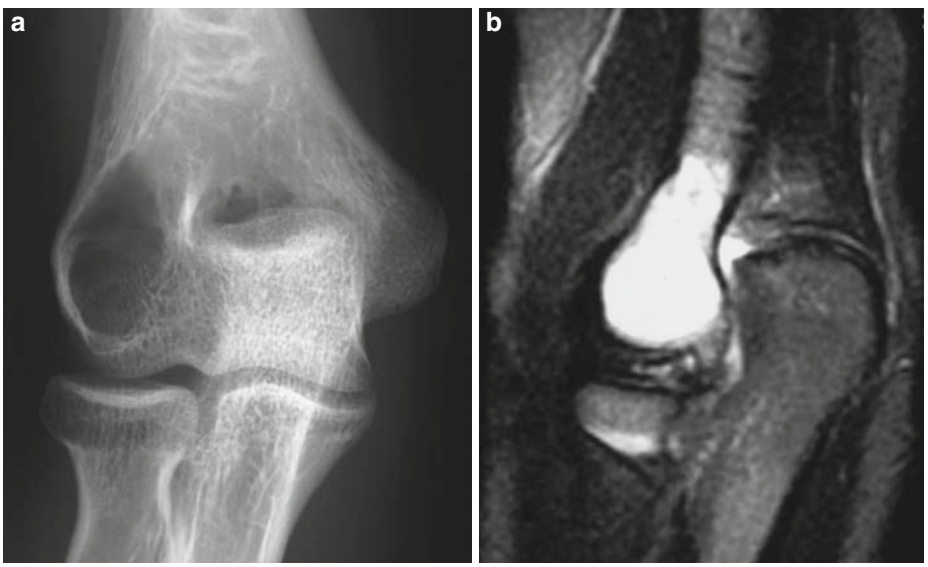

Fig. 7.81 Intraosseous ganglion, elbow (21-year-old woman). **a**. AP view of the pelvis. A well-defined lytic change is seen in the capitellum. **b**. T2-weighted coronal MR image. A bright signal intensity corresponds to fluid content

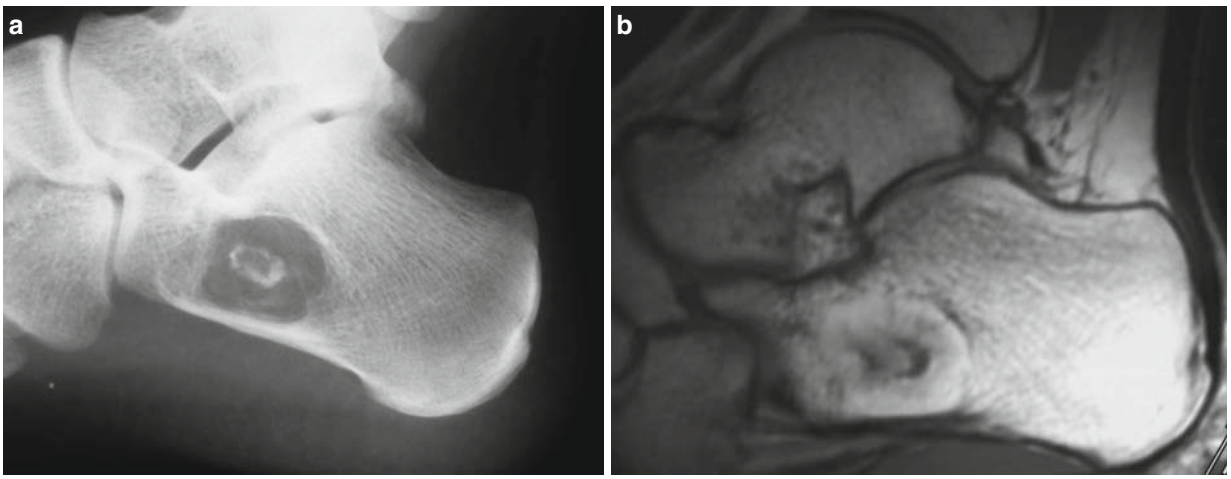

Fig. 7.83 Intraosseous lipoma, (23-year-old woman). **a**. Lateral view of the calcaneus showing a well-defined lucency containing a ring of calcification. **b**. Sagittal T1-weighted image. The mass consists of predominantly bright fat.

Giant Cell Tumor

Giant cell tumor (GCT) is a common neoplasm characterized by proliferation of round or oval mononuclear cells and osteoclast-type giant cells. It constitutes approximately 5% of all bone tumors, and typically occurs after closure of the physes at the end of tubular bones [79]. About 5% extend into the adjacent joint. GCT occurs most frequently in young adults with more than 90% of patients over the age of 20 years. GCTs in skeletally immature patients are rare, and tend to be located at the metaphysis of a tubular bone [80].

Characteristically, GCT affects women more commonly than men. The distal femur, proximal tibia, and distal radius are common sites, but they also may arise in the pelvis (particularly the sacrum), spine, ribs, and skull. Some pathologists believe that GCT of small bones of hands and feet are actually giant cell reparative granulomas. In the spine, the lesion can arise in either the vertebral bodies or the posterior elements, but it is more common in the vertebral bodies. Patients with Paget disease often develop masses that resemble GCT, but some investigators report that these lesions are giant cell reparative granulomas.

Radiologically, GCT typically appears as an eccentric lesion extending into the subarticular portion of a long tubular bone (Fig. 7.84). The lesion usually has well-defined edges without a sclerotic margin, and it contains no matrix. They may have septation or a "soap bubble" appearance caused by endosteal bone bridging at the margins of the tumor. Typically, periosteal reaction occurs only after pathological fracture or biopsy.

CT and MR imaging are suited to evaluate tumor extension, particularly soft tissue and joint extension. MR imaging is most suitable for tumor staging. Low signal on

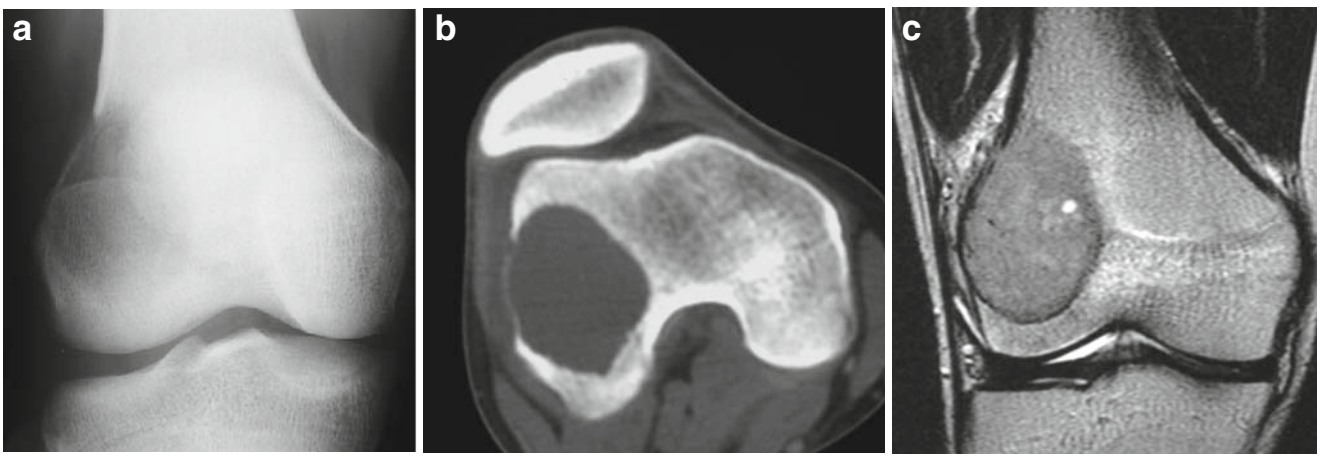

Fig. 7.84 Giant cell tumor, femur (21-year-old man). **a**. AP view of the knee. An eccentric lytic change with no sclerotic margin or mineralization in the distal femoral epiphysis and metaphysis. **b**. CT. A well-defined lytic lesion with no sclerotic margin in the distal femur. **c**. T2-weighted coronal MR image. The lesion is well defined with intermediate signal

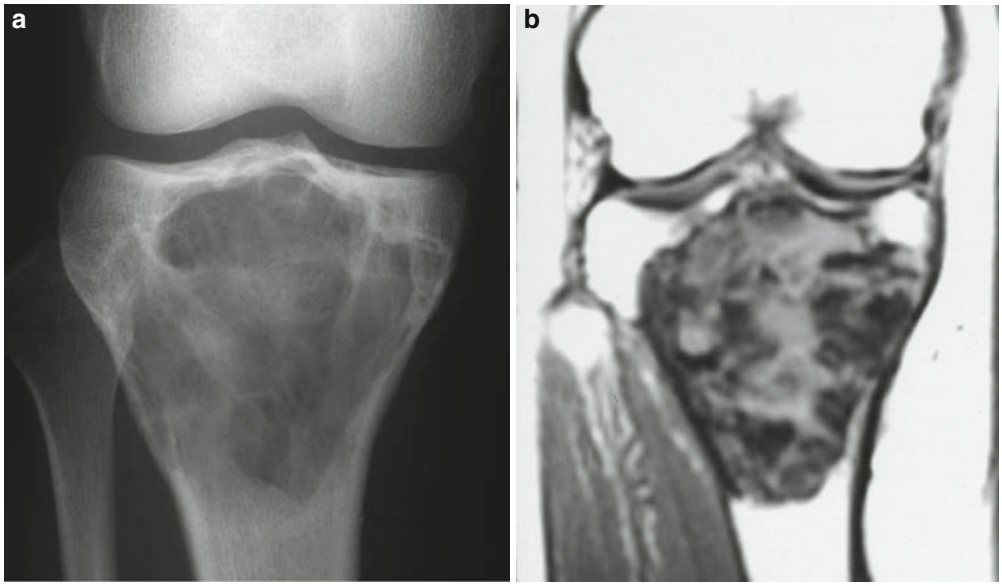

Fig. 7.85 Giant cell tumor, femur (23-year-old woman). **a**. AP view of the knee. A well-defined lytic lesion with no sclerotic margin in the center of the proximal tibial epi-metaphysis. **b**. T1-wighted coronal MR image. Low-signal foci are seen in the lesion, representing hemosiderin deposition (©: Kanehara Shuppan)

T2-weighted MR image sometimes may be significant, as it reflects hemosiderin deposition, and is a characteristic feature of GCT (Fig. 7.85) [81]. CT shows cortical thinning and erosion. In the spine and the sacrum, giant cell tumors are difficult to characterize because the lesions are purely lytic without mineralization or sclerotic margins (Fig. 7.86). Recurrence is common, although its frequency depends on the resection margin. Soft tissue recurrence and lung metastases may be associated with peripheral rim of ossification (Fig. 7.87) [82].

Surgical Pathology: Grossly, the giant cell tumors may be tan fleshy or hemorrhagic and have focal aneurysmal bone cyst-like areas. Microscopically, the diagnosis is made on the background population of stromal cells (Fig. 7.86H). These are round to oval, with nuclei resembling those of the giant cells. Occasionally, the stromal cells appear slightly spindled. Mitotic figures may be abundant with two to three per high-power field. A high mitotic rate does not correlate with outcome, however. Giant cells are numerous and diffusely distributed. They contain a few to hundreds of nuclei, which resemble the nuclei of the stromal cells. Occasional tumors may have broad bands of collagen coursing through, especially in recurrent tumors. About half the giant cell tumors contain reactive osteoid and woven bone, especially at the advancing edge of the lesion and in areas of soft tissue extension. Cartilage is distinctly uncommon in the absence of

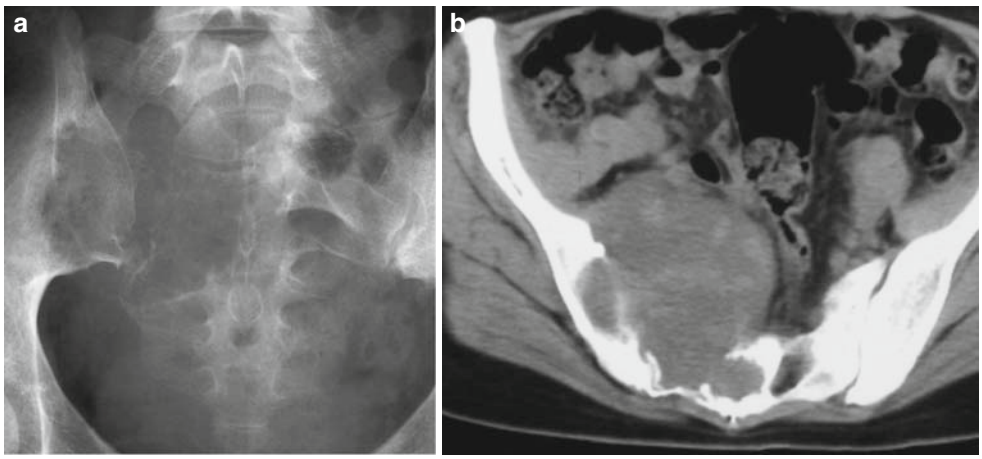

Fig. 7.86 Giant cell tumor, sacrum (26-year-old woman). **a**. AP view of the pelvis. An irregular-shaped lytic lesion is evident in the wing of the sacrum. **b**. CT. A large soft tissue density mass is seen anteriorly

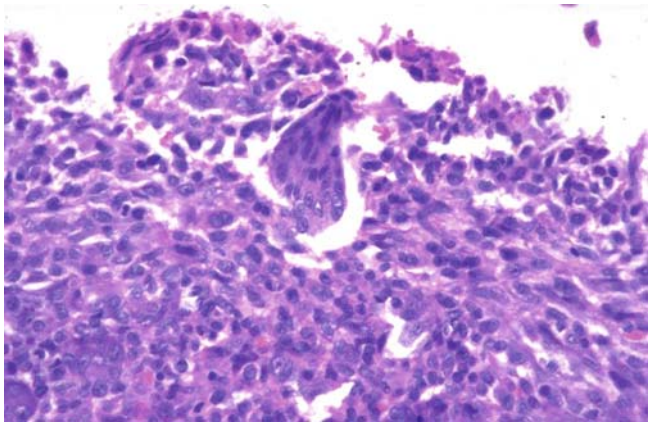

Fig. 7.86H Giant cell tumor showing multinucleate giant cells and stromal cells

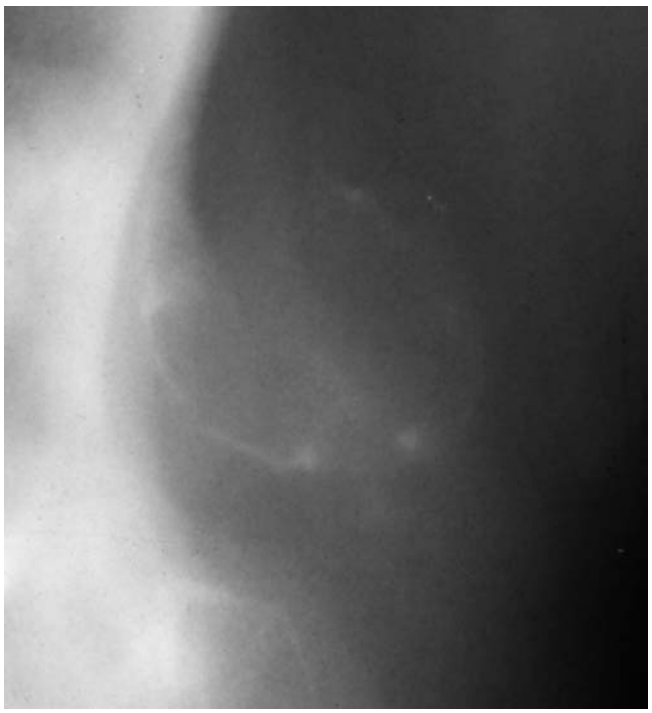

Fig. 7.87 Soft tissue recurrence of giant cell tumor (64-year-old woman). Lateral tomogram of the popliteal region revealing a rim of ossification around the recurrent soft tissue mass

fracture. Areas of infarct-like necrosis and foam cells are common.

The stroma of giant cell tumors is usually quite vascular, and up to 40% giant cell tumors are thought to have foci of intravascular invasion. This phenomenon may explain the "benign" metastases of a giant cell tumor and this phenomenon has not been associated with a more aggressive behavior. Histologic grading of giant cell tumors has not been found to correlate with metastasis, recurrence, or local aggressiveness.

The term "malignant" giant cell tumor has been used by different authors in various different ways. It has been used to designate true bone sarcomas (such as osteosarcomas or malignant fibrous histiocytomas) which are rich in giant cells. The term has also been used to describe a "dedifferentiated" giant cell tumor (a typical giant cell tumor juxtaposed with a high-grade sarcoma). Another use has been to describe giant cell tumors that have metastasized. In view of all these, the term is confusing and is best avoided.

About 1–2% of otherwise typical giant cell tumors metastasize. These are generally identical, histologically to the primary tumor. Most are detected within a year of resection, but some occur up to a decade later. There are no microscopic features to predict this phenomenon. Such metastases are indolent and amenable to resection. A sarcomatous transformation should be excluded in these cases.

Giant Cell Reparative Granuloma

Giant cell reparative granuloma is a reactive process, not a neoplasm. It is also known as a solid aneurysmal bone cyst. Lesions typically arise in the maxilla, mandible, and small bones of the head and feet. Patients with Paget disease also develop similar lesions in affected bones.

Giant cell lesions in the jaw and in the small bones, e.g., hands and feet (Fig. 7.88), are believed to be giant cell reparative granulomas, not giant cell tumor [83]. Imaging features are relatively non-specific, and in most cases, imaging cannot differentiate these lesions from giant cell tumors.

Brown Tumor of Hyperparathyroidism

Brown tumors arise in patients with hyperparathyroidism and are osteolytic lesions with abundant activated giant cells.

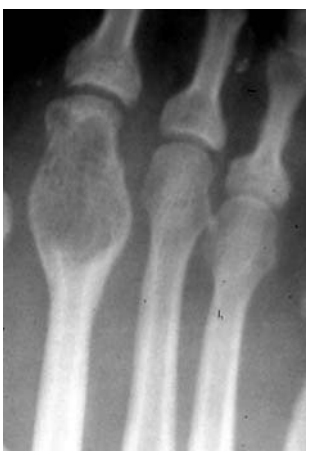

Fig. 7.88 Giant cell reparative granuloma. AP view of the foot. An expansive lytic change in the distal end of the metatarsal

They can occur in any bone. Radiological features mimic other lytic lesions, and differentiating these lesions from giant cell tumors is difficult radiologically and even histologically. Clinical and radiological evidence of hyperparathyroidism is important to make the diagnosis. Similarly, hyperparathyroidism should be excluded prior to making the diagnosis of giant cell tumor.

Surgical Pathology: The major skeletal manifestations are caused by increased bone remodeling rates, with increased bone resorption and augmented bone formation rates. Cancellous bone volume is maintained but cortices are thinner and more porous. The bones are characterized by marrow fibrosis, osteoclastic resorption, active osteoblasts on new and often incompletely mineralized lamellar bone trabeculae and rarely, "brown tumors." The latter are areas of granulation tissue, inflammatory cells, and macrophages containing hemosiderin and giant cell formation. There is virtually no bone present in the area. Occasionally cystic change may supervene. The increased osteoclastic activity is seen in subperiosteal, intracortical, endosteal, subchondral, and trabecular surfaces. Intracortical resorption is characterized by groups of osteoclasts (known as cutting cones) that tunnel through the cortex enlarging the Haversian and Volkmann canals. These channels are often expanded to 1 mm or more in some cases, and may be seen radiographically as lucent lines within the cortex. Endosteal resorption is also visible radiographically as "scalloping" of the cortex at its marrow interface. Subchondral resorption results in microfractures and joint abnormalities.

Chordoma

Chordoma is a low-grade malignancy occurring predominantly in the axial skeleton, in the region of the embryonic notochord. They have a differentiation toward (but not identical to) fetal notochord. Vestigial rests of notochord-like tissue, located in the spheno-occipital region, are sometimes found and termed ecchordosis physaliphora. A benign counterpart of the tumor, the giant notochordal rest, has been described. They occur in the spine: 60% in the sacrococcygeal region, 30% in the clivus, and the other 10% in any levels of the mobile spine, but most commonly in C2 at the junction of the odontoid with the C2 vertebral body. Chordomas arising in the mobile spine typically arises in the center of the vertebral body and have sclerotic margins (Fig. 7.91) [84]. Rarely the paravertebral soft tissues are the site of origin. Chordoma is common in male patients, between 40 and 60 years of age. It typically presents with a large soft tissue tumor destroying a portion of the axial skeleton (Figs. 7.89 and 7.90). Small bone fragments, sequestra, can be seen in the lesion on CT scan [85]. MR imaging is characteristic, with very bright signal on T2-weighted images, corresponding to vacuolated physaliferous cells. The MR signal is similar to that seen in chondroid tumors.

Chondroid chordoma in the skull base, a low-grade variant of chordoma, may be difficult to differentiate from chondrosarcoma. Prognosis depends on the local control, but local recurrence is common. Uncommonly, chordomas may metastasize to the lungs.

Benign notochordal tumor, or giant notochord remnant, is another controversial entity [86]. It typically represents an ill-defined infiltrating process on MR imaging (Fig. 7.92). It is difficult to detect using both radiography and CT unless it shows some sclerosis. No destruction of cortex, bone trabeculae, or extension into the soft tissue is noted.

Surgical Pathology: Grossly, chorodomas are lobulated, soft, myxoid masses and may mimic a chondrosarcoma. Microscopically, the lesions are lobulated and have a myxoid background (composed of hyaluronidase-resistant sulfated mucopolysaccharide). The lobules are separated by fibrous septa. The tumor frequently extends beyond the grossly identified margins. Within these lobules are cells arranged in

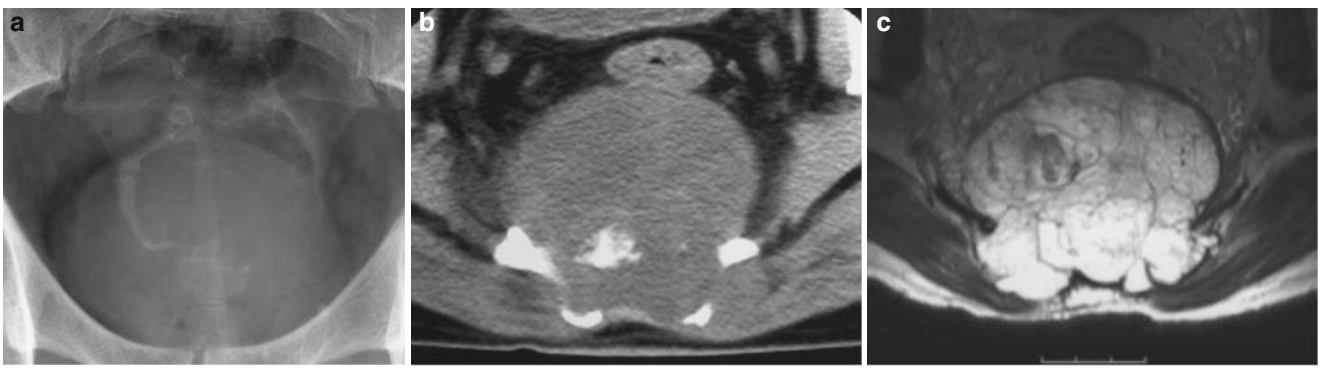

Fig. 7.89 Sacrococcygeal chordoma (48-year-old man). **a**. AP view of the pelvis reveals a lytic lesion in the sacrococcygeal region. **b**. CT. The lesion consists of soft tissue density, and contains mineralization, probably representing sequestra. **c**. T2-weighted axial image. A lobulated mass with bright signal is characteristic of chordoma

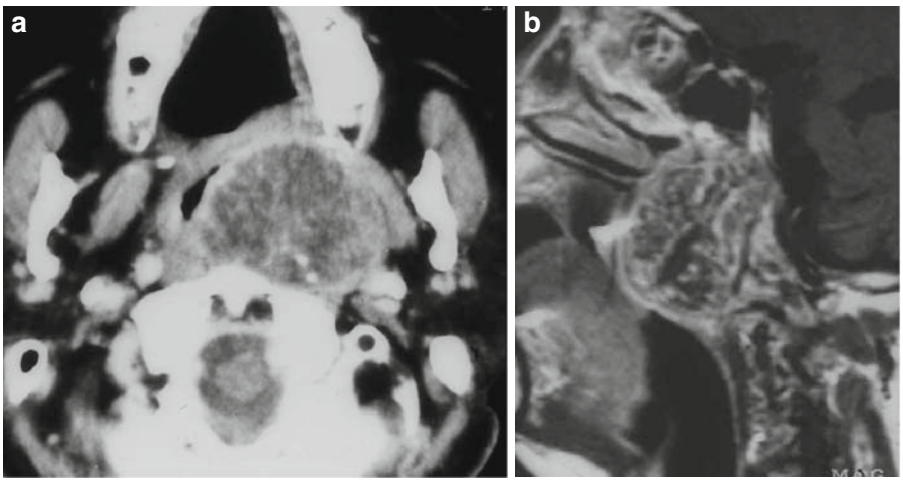

Fig. 7.90 Spheno-occipital chordoma. **a**. CT after intravenous contrast medium. A low density mass with peripheral or septal enhancement in the nasopharyngeal wall. **b**. T1-weighted sagittal MR image. The mass involves the sphenoid with Gd enhancement (courtesy of Dr. Fukuda)

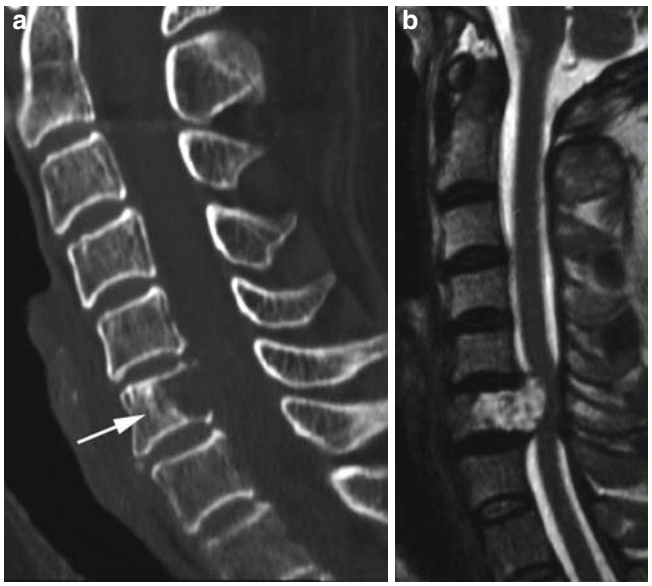

Fig. 7.91 Chordoma of mobile spine. **a**. Sagittal CT. An irregular-shaped lytic change in the posterior aspect of the sixth cervical vertebral body (*arrow*). **b**. T2-weighted sagittal MR image. A bright signal mass in the posterior aspect of the vertebral body (courtesy of Dr. Yamaguchi)

cords, sheets, or occasionally, haphazardly. At least some of these cells contain vacuolated cytoplasm (physaliphorous cells). Some cells may have abundant eosinophilic cytoplasm or may mimic signet ring cells. Nuclear pleomorphism is mild and mitotic activity low to absent. Some cases are seen with considerable "degenerative" atypia present in the tumor cells. Such lesion should not be considered as dedifferentiated.

Immunohistochemical positivity for epithelial markers is seen in the tumor cells, and corroborated by ultrastructural visualization of tonofilaments and desmosomes. These immunostains and ultrastructural features suggest the relationship to neuroectoderm. A newly recognized marker, brachyury, may be helpful diagnostically. This takes advantage of the fact that the transcription factor brachyury is involved in notochord development. Early data suggest that it might be a good marker for chordomas. The marker podoplanin (D-240) is positive in chondroid tumors but not chordoma and together with brachyury might be helpful in separating out difficult lesions such as chondroid chordoma of the skull base from chondrosarcoma. Experience with these two immunomarkers, however, is very preliminary at the time of writing.

Benign notochord tumors are well-circumscribed lesions composed of physaliphorous cells, but lacking the lobular growth pattern and the myxoid background. Immunohistochemically, they are identical to chordomas.

Osteofibrous Dysplasia and Adamantinoma

Osteofibrous dysplasia, also called ossifying fibroma or Campanacci disease, is a benign fibro-osseous tumor. Like its more malignant cousin, adamantinoma, it occurs nearly exclusively in the tibia and fibula. Osteofibrous dysplasia generally arises in children younger than 10 years of age. Radiographically, it is typically a well-defined lesion with sclerotic margins, located in the anterior cortex of the tibia (Figs. 7.93 and 7.94). It may cause anterior bowing of the tibia. Initial reports suggested that spontaneous regression during growth was the rule, but osteofibrous dysplasia may persist into the adult life. In children, recurrence after curettage is common.

Adamantinoma is a low-grade malignancy of the tibia and fibula, with epithelial differentiation. The name is derived from the histologically similar tumor in the jaw, ameloblastoma (which had previously been called adamantinoma), although the jaw ameloblastoma is currently considered to be an entirely different entity. These lesions tend to occur in an

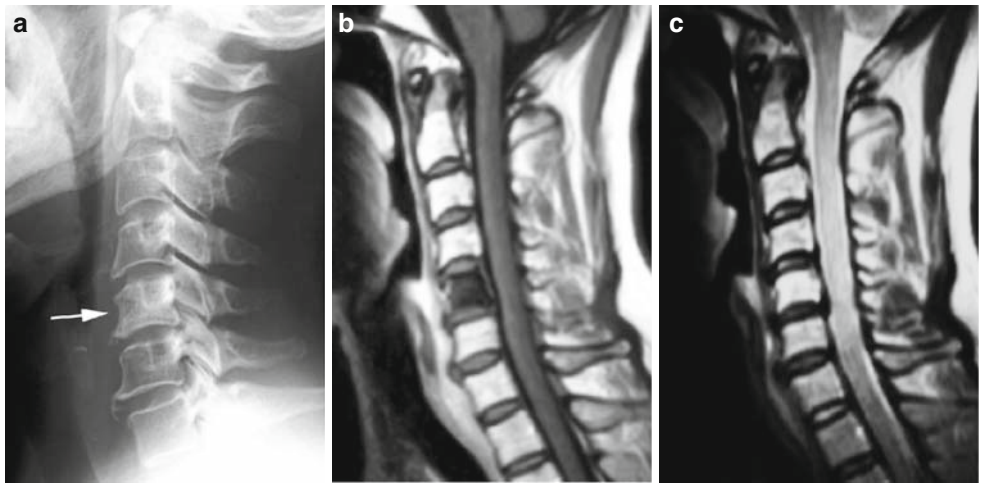

Fig. 7.92 Benign notochordal tumor (55-year-old man). **a**. Lateral view of the cervical spine. An ill-defined sclerotic change is seen in the fifth cervical vertebral body (*arrow*). **b**. T1-weighted sagittal MR image. The lesion corresponds to a low-signal intensity area. **c**. T2-weighted sagittal image. The fifth cervical vertebral body has bright signal (courtesy of Dr. Yamaguchi)

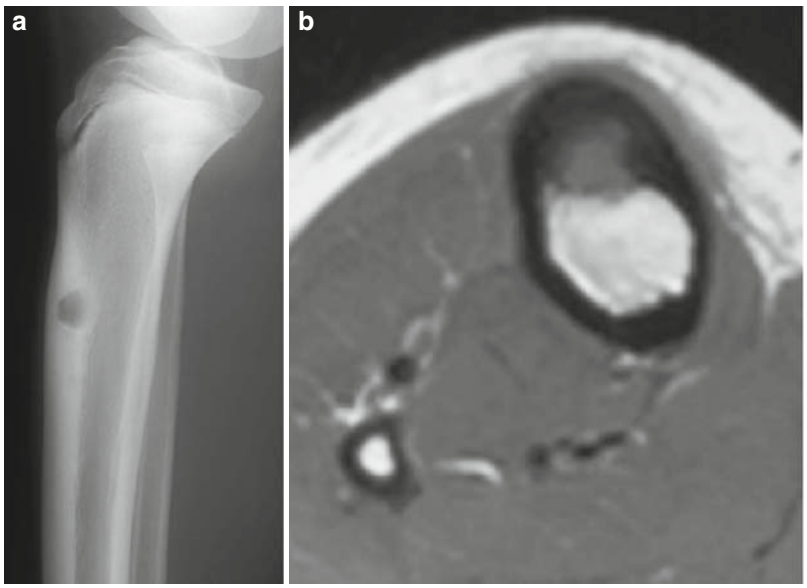

Fig. 7.93 Osteofibrous dysplasia (11-year-old woman). **a**. Lateral view of the tibia. A well-defined lytic change in the anterior cortex. **b**. T1-weighted axial image. The well-defined lesion has an intermediate signal

older age group than osteofibrous dysplasia. They typically appear as an eccentric tibial medullary lytic lesion with cortical penetration (Fig. 7.95). They contain no ossified matrix. Adamantinoma may coexist with or develop in osteofibrous dysplasia [87]. There is a poorly understood relationship between the two entities at the clinical, morphological, and genetic levels. Clinically some cases of osteofibrous dysplasia have progressed to adamantinoma, histologically some adamantinomas show areas similar to osteofibrous dysplasia, and similarly, osteofibrous dysplasia can show epithelial differentiation immunohistochemically. Genetic studies have shown trisomy of 7 and 8 (and absence of G protein stimulating mutations) in both lesions (although some cases of adamantinoma have shown additional or different changes). Differentiation between adamantinoma and osteofibrous dysplasia may be difficult in some cases. The clinical course is often unpredictable, but adamantinoma usually follows an indolent but locally aggressive course, whereas osteofibrous dysplasia is considered to be a benign condition.

Surgical Pathology of Osteofibrous Dysplasia: Grossly, the lesional tissue may be fibrous or gritty, similar to fibrous dysplasia. Microscopically, too, there is a similarity to fibrous dysplasia but the bony trabeculae show prominent osteoblastic rimming. Like fibrous dysplasia, the fibrous tissue is variably cellular and may show prominent collagenization. Focal collections of giant cells may be present, in a pattern reminiscent of giant cell reparative granuloma. Some studies have demonstrated cytokeratin-

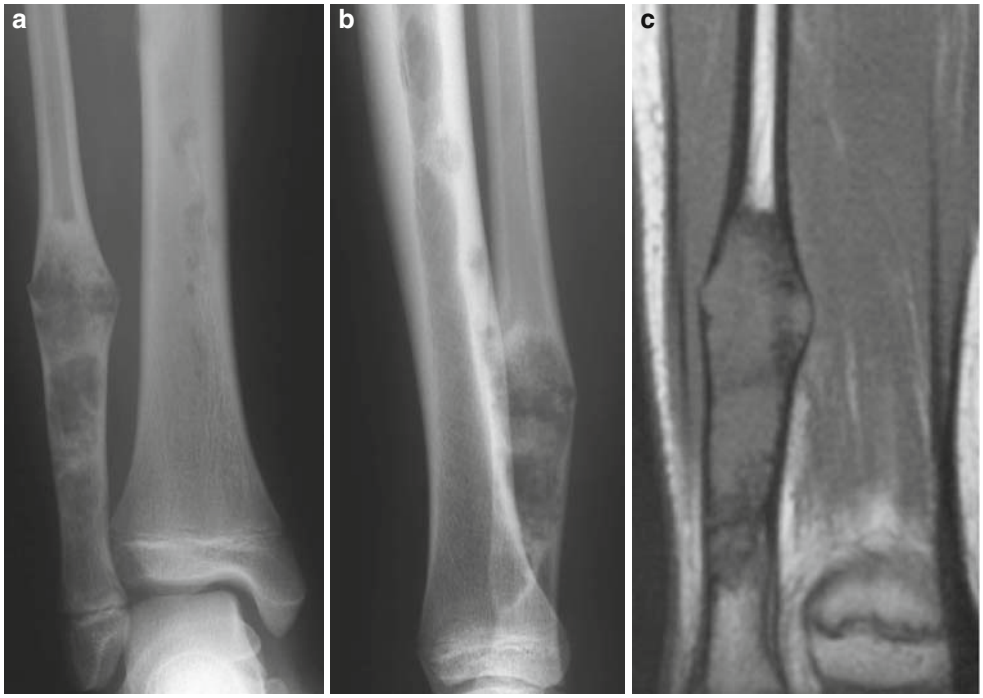

Fig. 7.94 Osteofibrous dysplasia (11-year-old woman). **a**. AP view of the tibia and fibula. A well-defined lytic lesion in the distal shaft of the fibula. Small lytic foci in the tibia are also present. **b**. Lateral view of the tibia and fibula. Lytic lesions are seen in the fibula and tibia. **c**. T1-weighted coronal MR image. An intermediate signal lesion is seen in the fibula

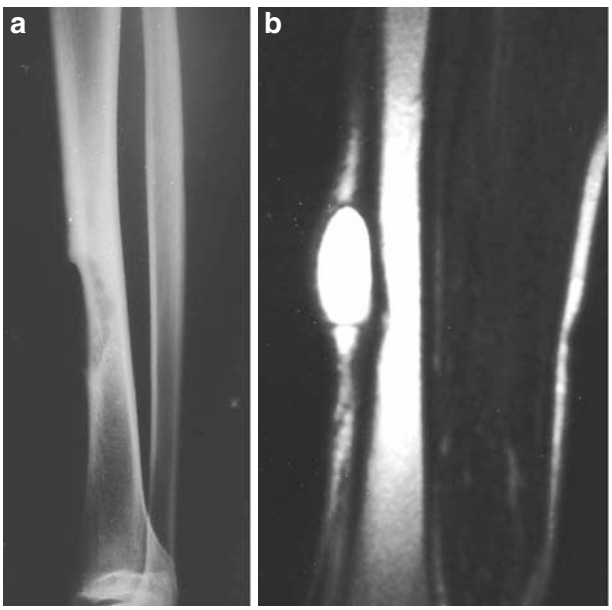

Fig. 7.95 Adamantinoma. **a**. Lateral view of the tibia. An eccentric lytic change is seen in the anterior aspect of the midshaft. **b**. T2-weighted sagittal MR image. A bright signal mass is seen in the anterior aspect of the tibia (courtesy of Dr. Kunihiko Fukuda)

positive cells in many of these cases. The latter finding has lead to speculation on whether these cases might be examples of adamantinoma with poorly developed epithelial islands.

Surgical Pathology of Adamantinoma: Grossly, the tumor is well demarcated in resection specimens. Cystic spaces and hemorrhage are common. Microscopically, the tumor consists of epithelial islands in a fibrous stroma. The nuclei of adamantinoma are usually bland and the mitotic rate is usually low in most cases. A variety of growth patterns may be evident in the epithelial component. These include spindle, basaloid, tubular, and squamoid. The spindle pattern, in particular, can be difficult to recognize as epithelial, in the absence of immunohistochemical stains. A clue, that the spindle cell proliferation is from an adamantinoma rather than fibrosarcoma, is the obvious lack of atypia. Anastamosing spaces, with the appearance of vascular channels, are seen in some cases.

Hematopoietic Tumors

Langerhans Cell Histiocytosis

Langerhans cell histiocytosis is a multi-organ systemic disorder characterized by proliferation of Langerhans cells associated with inflammatory response and rapid evolution and involution. Clonality studies have supported the idea that these lesions are true neoplasms despite the fact that some cases regress. Langerhans cell histiocytosis is generally seen in children younger than 20 years; most of the affected

children are younger than 5 years. It involves hematopoietic bone marrow, mainly in the axial skeleton, including vertebrae, pelvis, and skull. Long tubular bones of the extremities are also involved, but usually in young children.

Langerhans cell histiocytosis may progress rapidly, and later may regress spontaneously (Fig. 7.96). In the rapidly growing phase, the radiologic features are aggressive with an infiltrating process, but become better defined in the chronic or involuting phase. In the spine, vertebral bodies are commonly affected, and vertebra plana is characteristic (Fig. 7.97). In young children, the vertebral height reconstitutes spontaneously after collapse without medical intervention [88]. In tubular bones, a central lytic lesion with accompanying periosteal reaction is typical (Fig. 7.96). Langerhans cell histiocytosis affects the diploe of the calvarium and erodes the inner and outer table differentially causing a so-called "beveled edge" and "hole-in-hole" appearance on radiographs (Fig. 7.98).

The prognosis depends on the extent of disease. If the lesion is a solitary osseous eosinophilic granuloma, the prognosis is excellent. On the other hand, more aggressive forms of the disease have soft tissue organ involvement (Letterer–Siwe and Hand–Schuller–Christian disease) and the prognosis is guarded.

Surgical Pathology: Microscopically, the lesions comprise a proliferation of histiocytoid cells, with variable amounts of cytoplasm. The cell borders may be well defined or syncitium like. The nuclei have characteristic "grooves" similar to coffee beans. Multinucleated giant cells may be present. There is frequently an accompanying inflammatory response, often rich in eosinophils. Lipid-laden histiocytes are sometimes seen. Immunohistochemically, the histiocytes show characteristic positivity with S-100 protein and CD1a (similar to Langerhan's cells of the skin) and a variable staining with CD 68.

Malignant Lymphoma

Malignant lymphoma includes non-Hodgkin and Hodgkin lymphomas and accounts for only 5% of extranodal lymphomas. Primary Hodgkin lymphoma of bone is very rare. The osseous origin of lymphoma as opposed to spread of soft tissue lymphoma to bone rests on imaging at initial presentation that shows only bone is involved. Although it is rare in children before 10 years of age, patients in any age may develop an osseous lymphoma. The hematopoietic (red) bone marrow is more often involved. Radiologically, the lesion is usually lytic lesion involving a long segment of the diaphysis of a long bone (Figs. 7.99 and 7.100). Sclerotic lesions occur in less than 5% of cases (Fig. 7.101). There is no difference in the imaging features between non-Hodgkin lym-

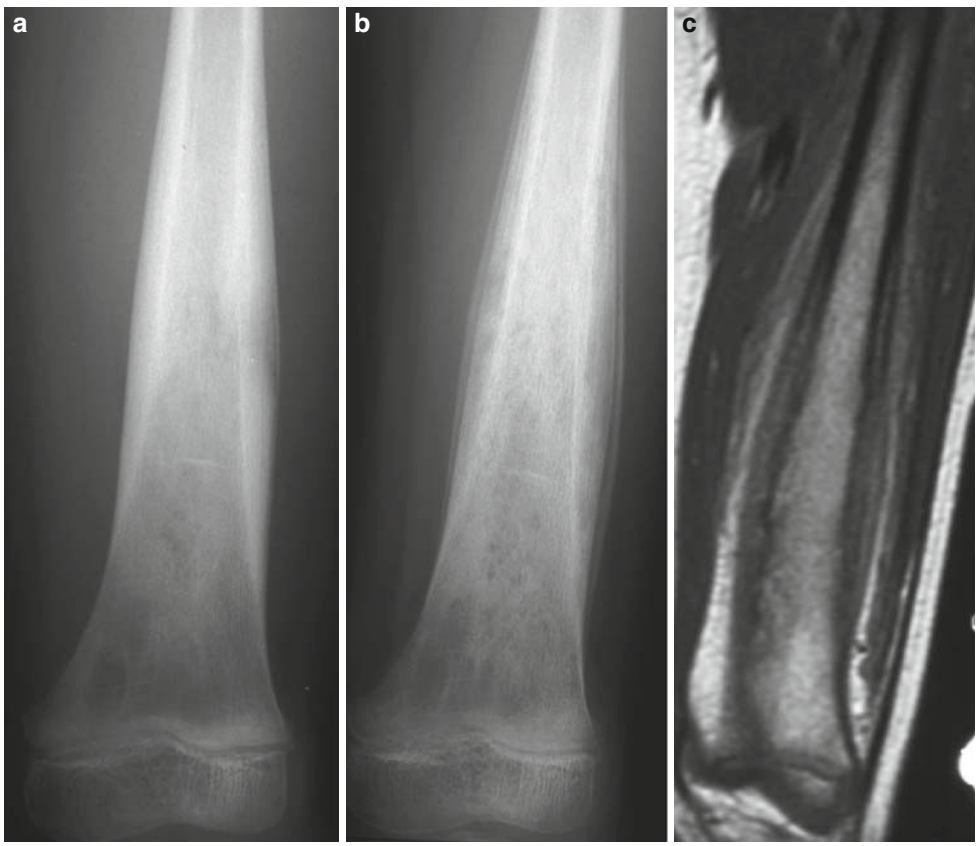

Fig. 7.96 Langerhans cell histiocytosis, femur (5-year-old woman). **a**. AP view of the femur showing periosteal reaction. **b**. AP view taken 3 weeks after Fig. 7.87a. Progression of periosteal reaction is noted. **c**. T1-weighted coronal MR image. Periosteal reaction and medullary lesion with low signal are prominent (©: Bunkodo)

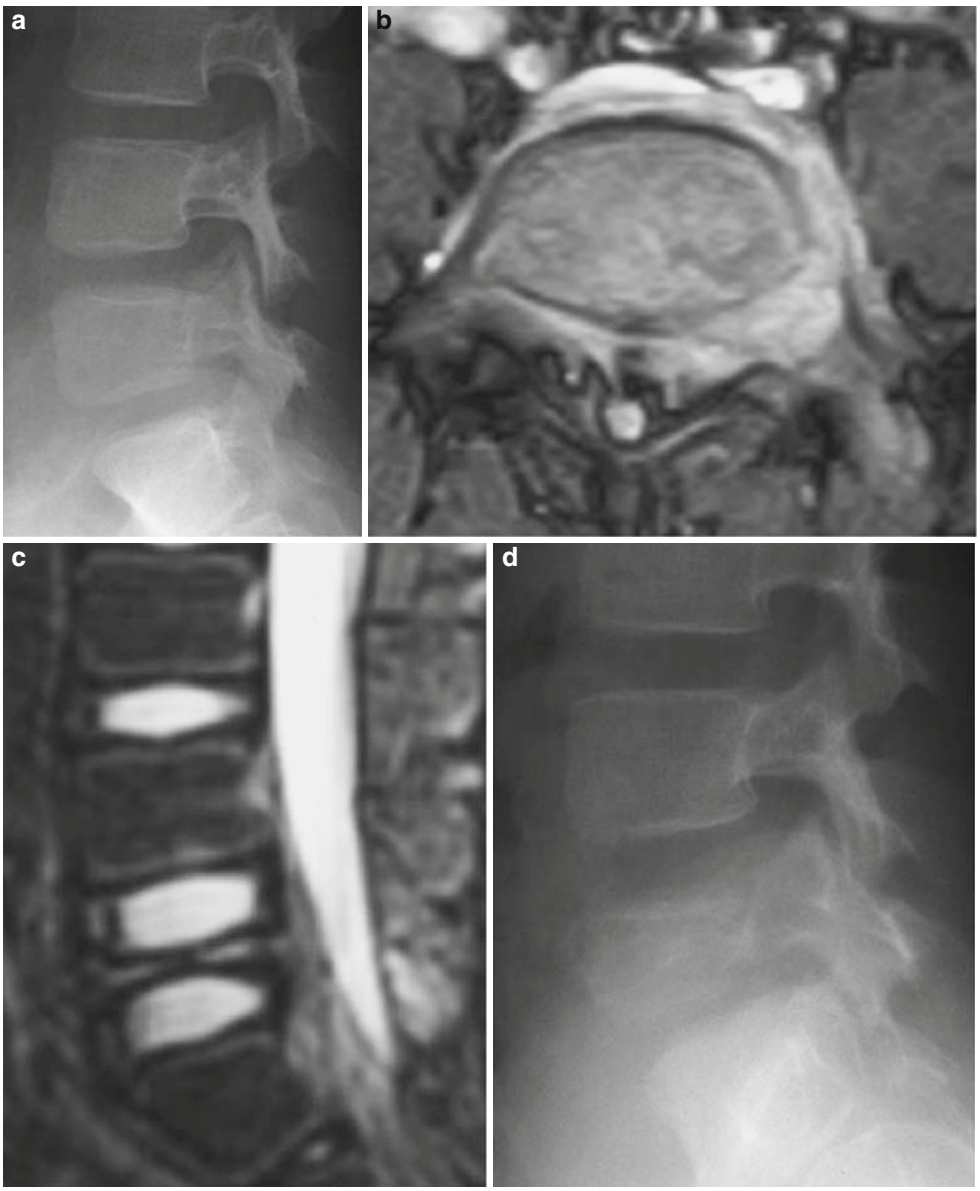

Fig. 7.97 Langerhans cell histiocytosis, lumbar spine (8-year-old man). **a**. Lateral view of the lumbar spine. An ill-defined lytic change at the fifth lumbar vertebra. **b**. T2-weighted axial MR image. An infiltrating process involves the vertebral body and adjacent soft tissue. **c**. T2-weighted sagittal MR image, taken 3 months later. Severe collapse of the vertebral body is noted. **d**. Lateral view of the lumbar spine, taken 18 months later. Recovery of the vertebral collapse is evident (©: Bunkodo)

phoma and Hodgkin lymphoma, but "ivory vertebra" has been described as a typical feature in Hodgkin lymphoma. Secondary osseous involvement is more common, occurring in 16% in Braunstein's series of lymphomas. There are no differences in the imaging features between primary and secondary lymphoma [89, 90]. Radiographic, CT, and MR imaging features are typically those of aggressive lesions (Fig. 7.99), similar to other small round cell tumors including Ewing sarcoma, but non-aggressive imaging appearance may also be noted (Fig. 7.100) [91]. MR imaging is quite sensitive to define the tumor extent. Prognosis depends on the histological grade and staging.

Surgical Pathology

Non-Hodgkin Lymphoma: The microscopic appearance is that of a lymphoid proliferation. Lesions may show a diffuse or nodular involvement. There is often considerable variability of tumor cells, a feature that helps distinguishing lymphoma from Ewing sarcoma. Some of these lesions, however, may have a fibroblastic or spindle cell component. A very rare signet ring form of lymphoma has also been described. In both these instances, immunophenotypic studies by flow cytometry or immunohistochemical stains are useful in the diagnosis. A panel to both establish the diagnosis and classify it often includes CD45 (leukocyte common antigen or

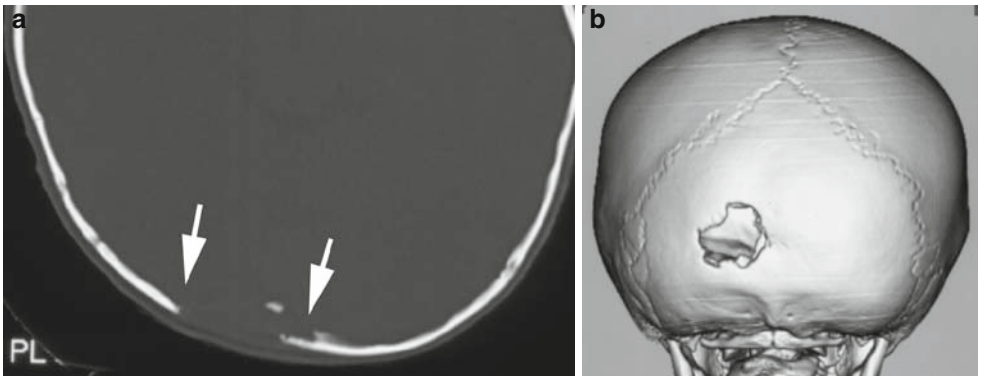

Fig. 7.98 Langerhans cell histiocytosis (3-year-old woman). **a**. CT of the occipital bone. A lytic lesion in the occipital bone. Extent of the involvement of the inner and outer tables is different. **b**. CT-3D reconstruction of the skull. A well-defined lytic change with bevelled edge (*arrows*) is noted

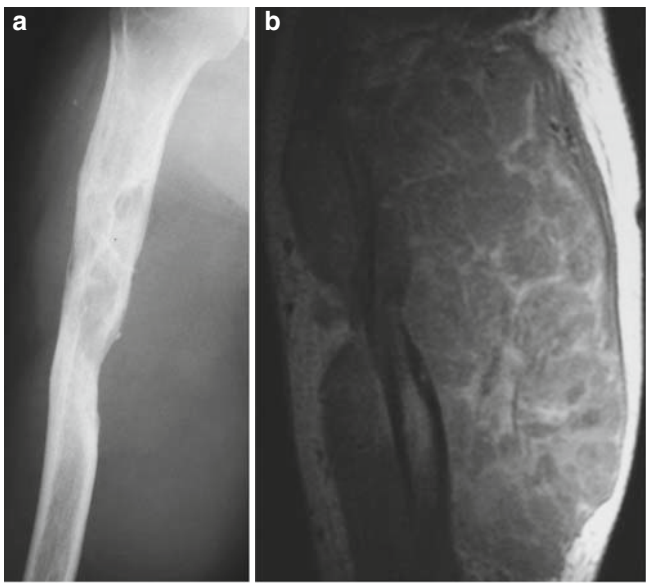

Fig. 7.99 Malignant lymphoma, humerus (64-year-old woman). **a**. AP view of the humerus. An irregular osteolysis of the humerus with a large soft tissue tumor. **b**. T1-weighted coronal MR image. An extensive soft tissue mass involving the humerus and soft tissue is noted

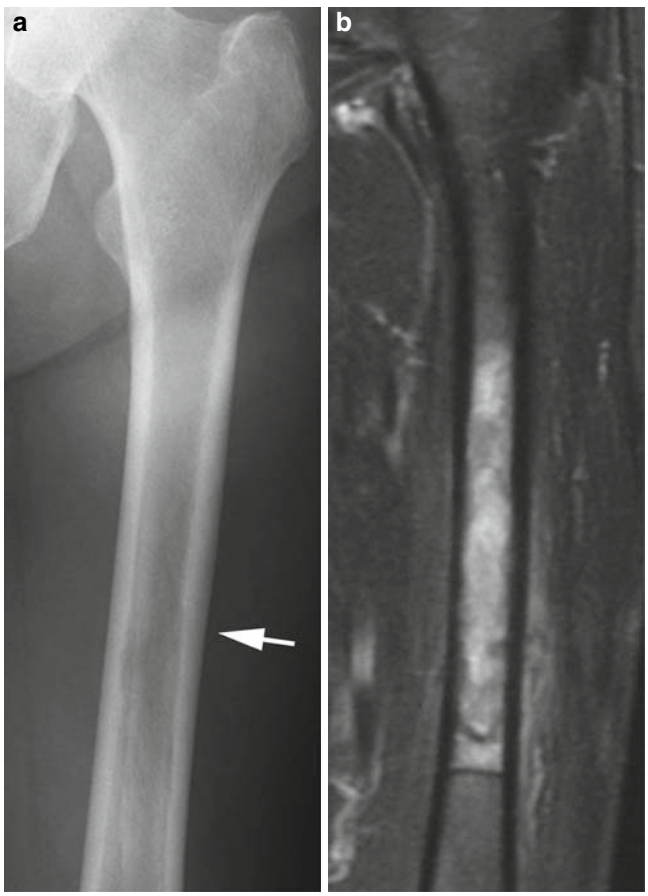

Fig. 7.100 Malignant lymphoma. Femur (68-year-old woman). **a**. AP view of the femur. An ill-defined lytic change in the midshaft of the femur (*arrow*). **b**. T2-weighted coronal MR image. A bright signal intensity lesion in the medullary canal of the femoral shaft. Periosteal reaction is associated

LCA), B- and T-cell markers, and other markers to differentiate lymphoma from its mimics such as Ewing tumor (CD99 or Mic-2).

Hodgkin Lymphoma: Microscopically, nodular sclerosing or mixed cellularity-type subtypes are the most frequently seen in lymph nodes. Immunohistochemical studies for CD15, CD30, CD45 (LCA), and PAX-5 are the most helpful.

Other Lesions: Several other hematologic entities can involve the skeleton usually, secondarily. Entities such as systemic mastocytosis or sinus histiocytosis with massive lymphadenopathy can occasionally show involvement of the bone as the first presentation. The features of most of these in bone are similar to the soft tissue counterparts.

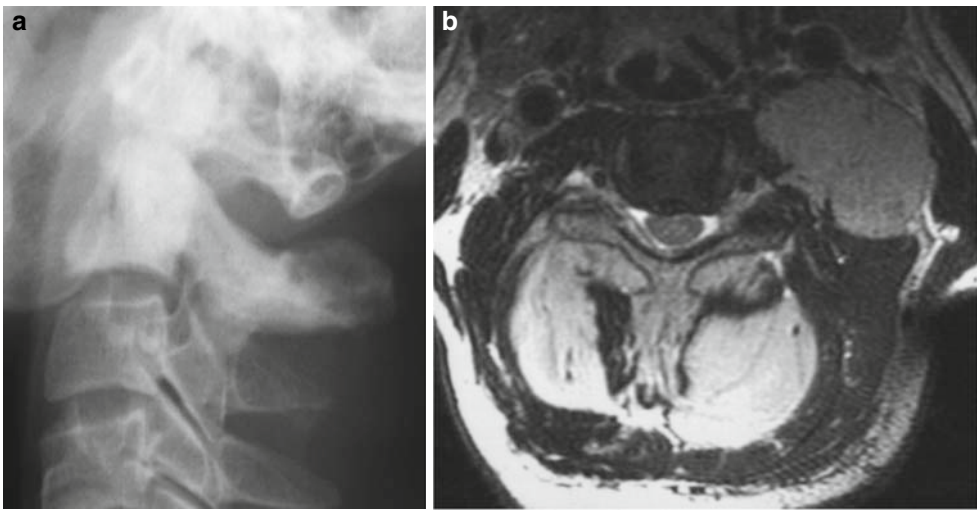

Fig. 7.101 Malignant lymphoma (52-year-old man). **a**. Lateral view of the cervical spine. A sclerotic change is seen in the second cervical vertebra. A soft tissue mass is associated. **b**. T2-weighted axial MR image. An extensive soft tissue mass involving the lamina and the spinous process (courtesy of Dr. Masashi Koyama)

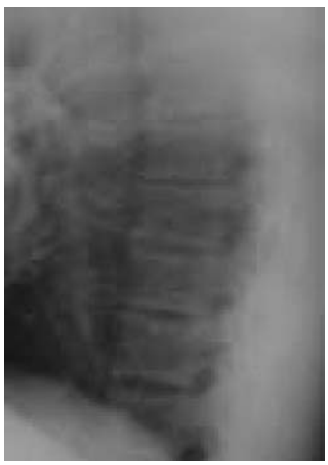

Fig. 7.102 Systemic mastocytosis. Lateral radiography of the thoracic spine. Slightly increased density with coarse but thick trabeculae is noted in the thoracic vertebrae

Mastocytosis

There are three forms of mastocytosis: urticaria pigmentosa (skin type), systemic mastocytosis, and mast cell leukemia. Mast cells, containing chemical mediators, such as histamin, heparin, and serotonin, exist widely in the soft tissue. Skeletal involvement is typically seen in systemic mastocytosis. Systemic mastocytosis is a rare proliferative disorder of fifth to eighth decades of life. Mast cells are known to stimulate fibroblastic activity in the bone marrow, and the chemical mediators, heparin and prostaglandin, induce bone resorption. Radiographically, generalized bone resorption is seen particularly in the axial skeleton, skull, pelvis, spine, and ribs. Although uncommon, generalized osteosclerosis may also be seen (Fig. 7.102). The cause of sclerosis is not known. MR imaging has been reported useful to demonstrate bone marrow infiltration.

Surgical Pathology: The diagnosis of mastocytosis requires the demonstration of multiple clusters of mast cells (preferably supported by stains such as Giemsa or mast cell tryptase). Loose or scattered mast cell proliferations are more difficult to diagnose and may require supportive genetic studies to demonstrate KIT mutations.

Leukemia

Leukemia is a neoplasm of hematopoietic bone marrow with tumor cells in the peripheral blood. Tumor cell proliferation occurs in the bone marrow, but usually no bone abnormalities are associated. Radiographic findings are non-specific. Bone resorption occurs more commonly in children, usually in the metaphyses of long bones (Fig. 7.103). Sclerosis and periosteal reaction are rare findings. A leukemic line is a radiolucent band in the metaphysis in young infants, reflecting the patient's poor general condition, not actual tumor infiltration. Although imaging studies have only limited role in the treatment of leukemia, MR imaging may help define the tumor extent in the bone marrow, and it is particularly useful to detect complications. Soft tissue tumor formation, granulocytic sarcoma, occurs occasionally, particularly after marrow transplantation in the soft tissue, and may rarely destroy bone (Fig. 7.104).

Surgical Pathology: The microscopic appearance of these tumors consists of a proliferation of blasts. Auer rods and/or azurophilic granules may be present in some myeloblasts. Immunophenotypic studies by flow cytometry or immuno-

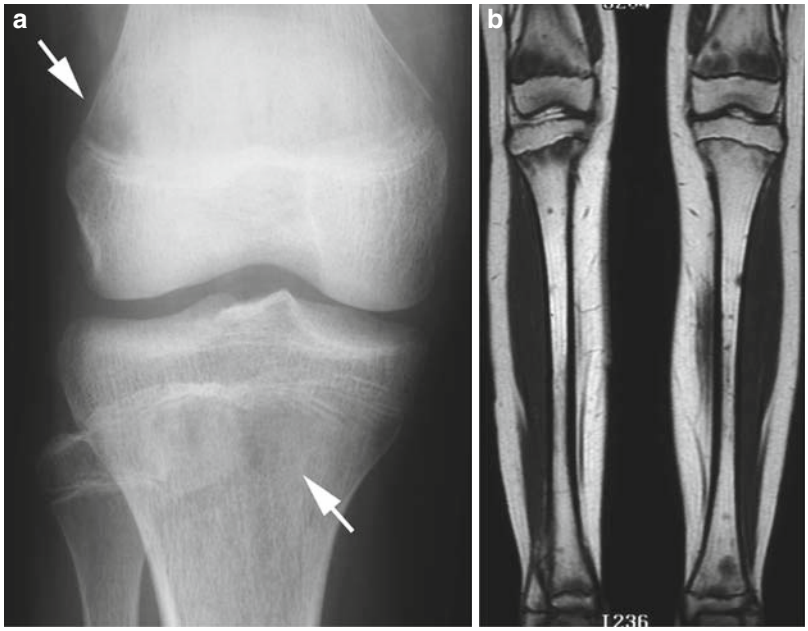

Fig. 7.103 Bone resorption of ALL (13-year-old woman). **a**. AP view of the knee. A lytic change is seen in the distal femoral and proximal tibial metaphysis (*arrows*). **b**. T1-weighted coronal MR image of the bilateral thighs. Low-signal foci in the bone marrow of the bilateral distal femora and tibiae represent leukemic infiltration (©: Tokyo-Igakusha)

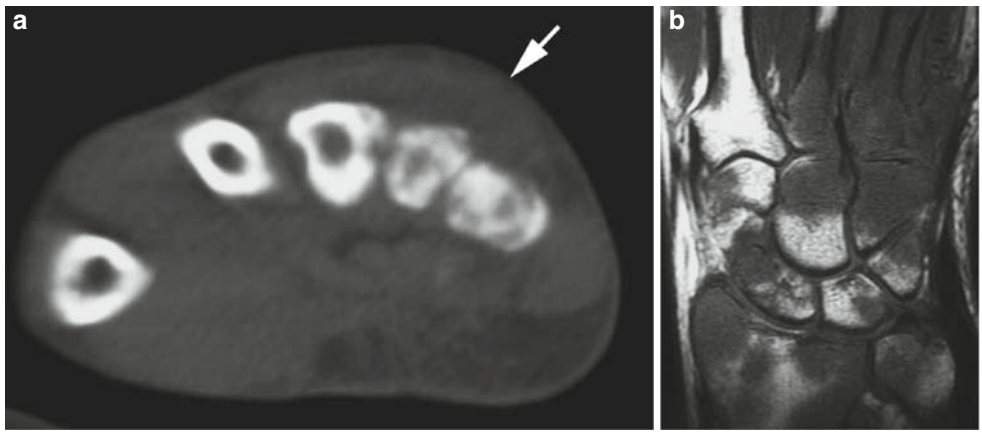

Fig. 7.104 Granulocytic sarcoma, hand (61-year-old man). **a**. CT. Osteolytic changes in the third, fourth, and fifth metacarpals, and soft tissue mass on the dorsal aspect of the wrist (*arrow*). **b**. T1-weighted coronal MR image. Bone marrow infiltration of the leukemia is seen as low-signal foci

histochemistry for myeloid and lymphoid markers and cytochemical stains (non-specific esterase) are useful. The histiological differential diagnosis includes small round cell tumors: Ewing sarcoma, metastatic neuroblastoma, small cell osteosarcoma, mesenchymal chondrosarcoma, rhabdomyosarcoma, and occasionally osteomyelitis. In problematic cases, DNA studies on snap-frozen material could be helpful.

Multiple Myeloma

Multiple myeloma is a malignancy with proliferation of plasma cell in the bone marrow. It is the most common primary malignant bone tumor and constitutes 44% of all bone sarcomas [92].

There are several clinical forms of myeloma, including multiple (50%), solitary (25%), generalized (15%, diffuse skeletal form), extraskeletal (9%, nasopharyngeal, oral cavity), and plasma cell leukemia (<1%). The disease probably affects men (about 70%) more often than women. The average age of patients at presentation is 52 years. Pain, anemia, and elevated ESR are common clinical findings, and Bence-Jones proteinemia (40–60%) and hypercalcemia (25–40%) also occur. On serum electrophoresis, the globulin fraction is abnormal (80–90%), and the tumor is classified according to the predominant immunoglobulin fraction: IgG myeloma (60%), IgA myeloma (20%), IgD myeloma (2%), and IgE and IgM myeloma (rare). As for prognosis, IgA myeloma is

better than IgG myeloma, and IgG leukemia is better than IgD myeloma.

Myeloma tends to spread through the red marrow and so the most common sites of involvement are the vertebrae (34%), ribs, skull, pelvis, and femur in the descending order of frequency. Solitary plasmacytoma most commonly occurs in the spine and represents 50% of all solitary spinal tumors. Deposition of amyloid is seen in 10–15% of cases and may cause masses radiographically. The amyloid may calcify [93].

Radiologic findings are variable (Figs. 7.105, 7.106, 7.107, and 7.108). Approximately 25% of patients have normal radiographs, 25% have only diffuse osteopenia (myeloma cells produce an osteoclastic factor, interleukin-6), and 50% develop focal lytic lesions. A soft tissue mass frequently arises adjacent to the bone. Bone scan is not helpful diagnostically since it only shows about half of myeloma lesions. While radiographic skeletal survey may be indicated, MR imaging survey (whole body MRI) and PET-CT may be better diagnostic examinations. Combined multidetector CT and MR imaging are modalities of choice for staging [94].

Osteosclerotic myeloma is rare, seen in approximately 3% of patients. POEMS (polyneuropathy, organomegaly, endocrinopathy, M-proteinemia, sclerodactyly) syndrome may be associated with sclerotic myeloma (Fig. 7.108) [95].

Surgical Pathology: Microscopically, the lesions are composed of sheets or aggregates of mature to immature, pleomorphic, or anaplastic plasma cells. Less differentiated examples may show prominent nucleoli immature or "plasmablastic" morphology. Amyloid deposition may be seen in some cases. The plasma cells are usually positive for CD38, CD56, CD79a, CD138, and an immunoglobulin light chain (κ or λ). In the very poorly differentiated or anaplastic examples, there may be difficulty in distinguishing from lymphoma and other non-hematopoietic disorders (osteomyelitis) and immunohistochemical stains to establish clonality (κ and λ) may be required.

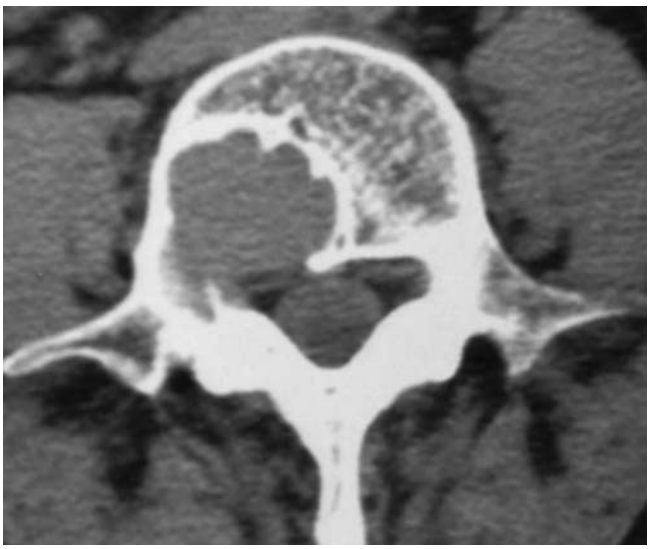

Fig. 7.106 Multiple myeloma (44-year:-old woman). CT. A well-defined mass with sclerotic margin is noted (©Iji-Shinpo)

Ewing Sarcoma and Primitive Neuroectodermal Tumor (PNET) Group

Ewing sarcoma is a primary osseous neoplasm composed of small round cells with no matrix production. It is now considered to be one of the less differentiated tumors from the group of neoplasms with neuroectodermal differentiation.

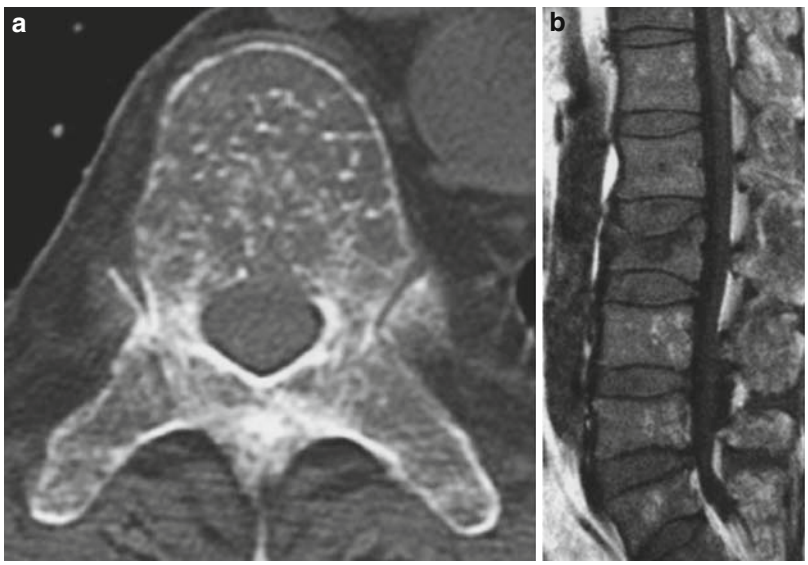

Fig. 7.105 Multiple myeloma (61-year-old man). **a**. CT. An infiltrating process in the bone marrow of the vertebral body. **b**. T1-weighted sagittal MR image. Bone marrow infiltration in the bone marrow is extensive (**b**: ©: Iji-Shinpo)

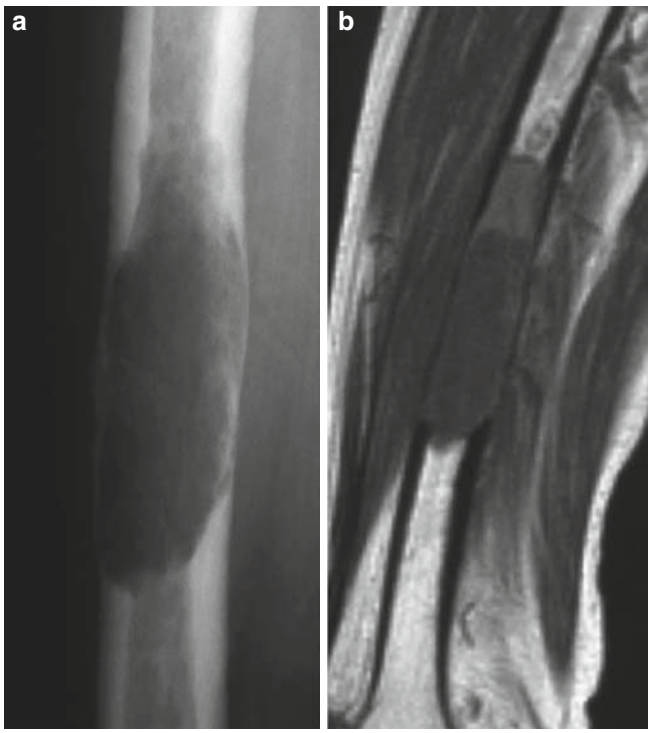

Fig. 7.107 Solitary plasmacytoma (68-year-old woman). **a**. Lateral view of the femur. A well-defined lytic lesion with slight expansion is noted. **b**. T1-weighted sagittal MR image. A well-defined lesion is noted (©: Iji-Shinpo)

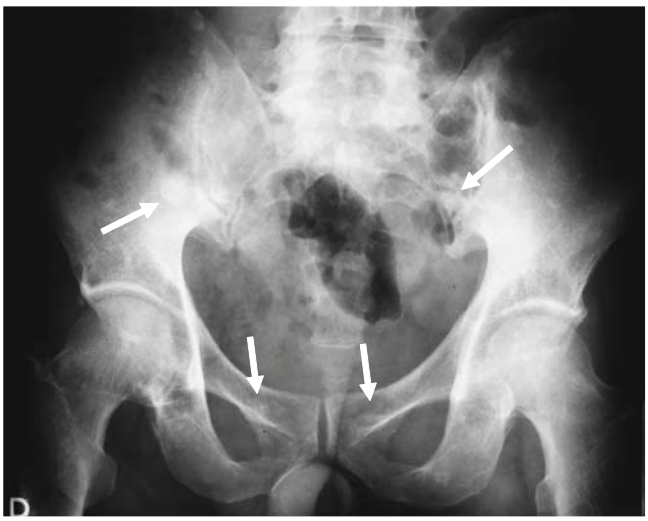

Fig. 7.108 POEMS syndrome with sclerotic multiple myeloma (53-year-old man). Multiple sclerotic foci are seen in the pelvis (arrows). (Couetesy of Hajime Fujimoto, M.D.)

Ewing sarcoma is a tumor of children and young adults, 5- to 25-year-old, uncommonly seen in infants younger than 5 years of age or older population. The pelvis and lower extremities are common sites, but the tumor may arise in any bone. It is rarely seen in small bones of hands and feet. In peripheral tubular bones, Ewing sarcoma usually involves the diaphysis.

Radiologically the lesion is typically permeative, involving bone marrow and extraosseous soft tissue (Fig. 7.109). Fine periosteal reaction, occasionally multi-layered – onion skinning, is also typical (Fig. 7.110). Cortical erosion, saucerization, is one of the findings of bone tumors due to tumor extension along the cortical surface (Fig. 7.111) [96]. Rarely, radiological features are indolent with cyst-like expansile lucency [97]. MR imaging is useful for defining the tumor extent (Fig. 7.112).

Since the advent of current chemotherapy and radiation, Ewing sarcoma's prognosis has improved significantly, and

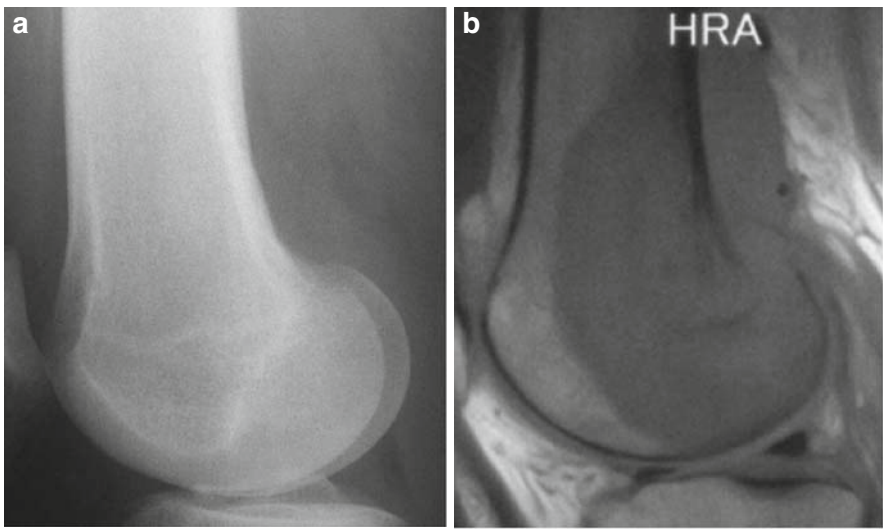

Fig. 7.109 Ewing sarcoma, femur (24-year-old man). **a**. Lateral view of the knee. No bone change is detected. **b**. T1-weighted sagittal MR image. An infiltrating process is seen in the distal femur and soft tissue

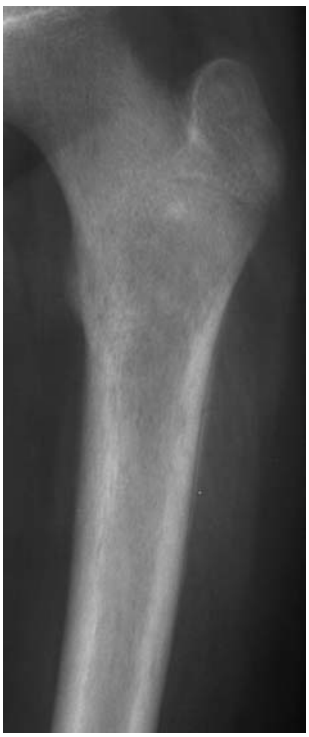

Fig. 7.110 Ewing sarcoma, femur (10-year-old woman). AP view of the femur. Fine periosteal reaction and ill-defined sclerosis are seen along the femoral cortex

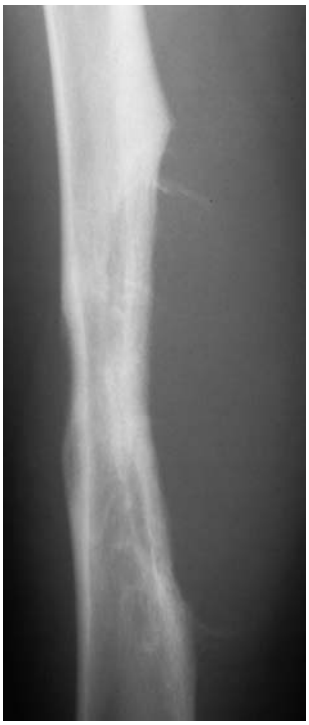

Fig. 7.111 Ewing sarcoma, femur (9-year-old woman). AP view of the femur. A periosteal tumor growth is associated with saucerization of the cortex (©: Kanehara Shuppan)

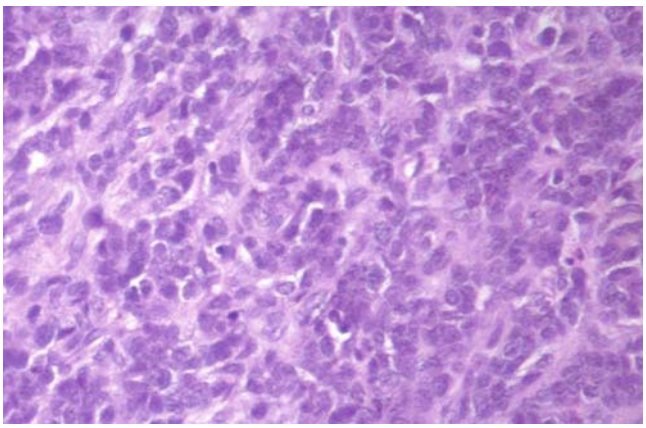

Fig. 7.110H Ewing sarcoma composed of small blue round cells

5-year survival is now more than 50% in major centers. Bone changes after such treatment on radiography are minimal and slow, and MR imaging with Gd enhancement and nuclear imaging (FDG-PET and thallium scan) may be useful for assessment after treatment.

Surgical Pathology: Grossly, the tumor may be firm or glistening, or more friable, mimicking pus. Hemorrhage and cystic change may be evident.

Microscopically, the classic form is very cellular, and consists of sheets and large nests of uniform, small, round to polygonal cells with scanty cytoplasm (Fig. 7.110H). The chromatin is finely dispersed usually with no nucleoli and a variable number of mitotic figures. Perivascular cuffing may be evident in areas of necrosis. Rosettes are seen in a small minority of cases, and may cause a misdiagnosis of the lesion as a metastatic neuroblastoma. Variants from this classic pattern include a large-cell type and a filigree pattern. In the large cell type, the cells may be larger, and cytologically may show nucleoli. The filigree pattern refers to a bi-cellular architecture, separated by stroma. Some authors recognize on morphologic basis, an "atypical" Ewing sarcoma characterized by one or more of the features – lack of glycogen, brisk (over 2 per high-power field) mitoses, neoplastic vascular formation, spindling at the periphery of the tumor, some amount of extracellular matrix, lobular architecture, or alveolar pattern.

Cytoplasmic glycogen demonstrated by the PAS stain is evident in many (but not all) cases. An immunohistochemical stain, Mic 2 (CD 99), has become available for use in formalin-fixed paraffin-embedded tissue. It shows membranous positivity in the large majority (if not all cases) of Ewing sarcoma and PNETs. This immunomarker also stains the cells from some rhabdomyosarcomas and cells

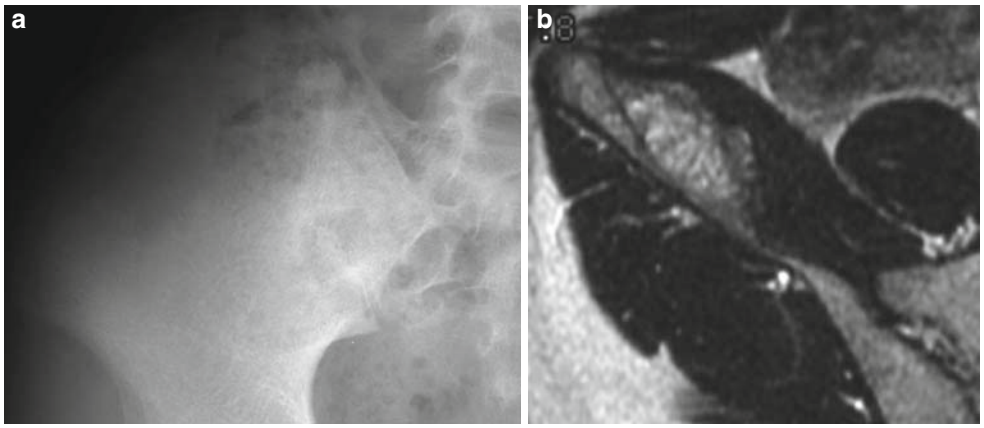

Fig. 7.112 Ewing sarcoma, ilium (11-year-old man). **a**. AP view of the ilium. An ill-defined density in the ilium. **b**. T2-weighted axial MR image. A bone marrow and periosteal lesion are evident

from acute lymphoblastic leukemia; however, these tumors tend to show cytoplasmic rather than membranous staining. Occasional cases may express weak-focal staining for cytokeratin, although an occasional case may express strong "adamantinoma-like" positivity. Neuron-specific enolase and other neural-specific markers may be positive. Leukocyte common antigen, markers of muscle and blood vessel differentiation should be absent.

Ewing sarcomas show a characteristic t(11;22) chromosomal translocation. By molecular methods, this chromosomal abnormality corresponds to the EWS/FL1 gene fusion. The EWS gene (located on chromosome 22 at q12) is translocated to the FL1 (a gene of the ETS family located on chromosome 11). This results in the formation of a chimerical protein product and is seen in about 85% of patients. A second translocation has been identified in about 15% of patients. This is the t(21;22) translocation, which fuses the EWS gene with a different member of the ETS family, the ERG gene located on chromosome 21q22. This gives a hybrid EWS/ERG product. Whether these two kinds of Ewing sarcoma behave differently clinically is unknown. These two kinds cannot be distinguished at the light microscopic level. Diagnostically, this is a convenient method of confirming or establishing the diagnosis of Ewing sarcoma in selected cases.

Metastases

Statistics

Skeletal metastases occur in 20–30% of cancer patients. Metastases are the most common bone tumor, considered 50–100 times more common than primary tumors. Their likelihood and incidence vary depending upon the type of primary tumor. The tumors that most commonly metastasize to the bones include prostate, breast, kidney, thyroid, and lung. Breast, prostate, kidney, and lung constitute 75% of all skeletal metastases. Prostate cancer constitutes 60% of metastatic epithelial tumors in men, and breast cancer constitutes 75% of metastases in women.

Surgical Pathology: The diagnosis is usually straightforward in most cases. The lesions are quite amenable to fine-needle aspiration cytology as a means of diagnosis (the method is more difficult to use in primary bone lesions since sarcomas are heterogenous). In selected cases a panel of antibodies to establish the diagnosis of metastatic carcinoma and to locate the primary origin can be helpful.

Mechanism of Metastases

Metastases occur via arterial transmission of cells into a distant intraosseous artery. When lung metastases exist, bone metastases are considered to have spread from the lung lesion, but bone metastases often arise, even when lung metastases are not present. Arterial metastases to the spine are typically located in the posterior aspect of the vertebral body, at the base of the pedicle, where many intraosseous arteries are present. As the tumor grows in this location, the radiographic contour of the pedicle is lost due to involvement at the junction between the vertebral body and the pedicle [98].

Metastasis via a venous route occurs in the vertebra through Batson venous plexus. This mechanism of metastasis arises mainly in the tumors of abdomen and pelvis. These occur at a vertebral level close to the primary lesion. These lesions are typically in the center of the vertebral body because of the distribution of the basivertebral vein.

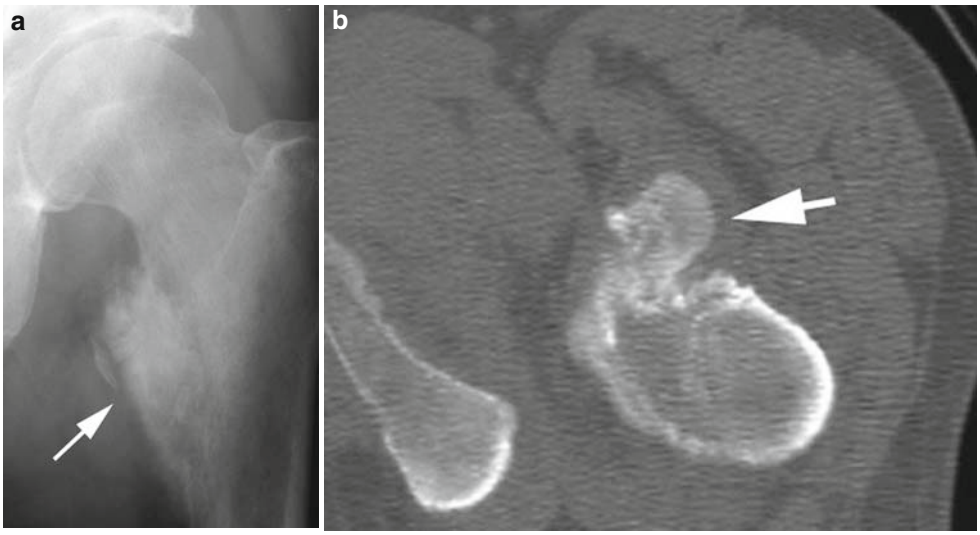

Fig. 7.113 Ossified periosteal metastasis of prostatic carcinoma (67-year-old man). **a**. AP view of the hip. An ossified soft tissue mass is seen adjacent to the lesser trochanter (*arrow*). **b**. CT. An ossified mass is again noted (*arrow*) (©: Japanese Society of Medical Imaging)

Types of Metastases

Osteolytic Metastases

Pure bone resorption on radiography is the typical feature of carcinoma metastases. The shape and margin of osteolysis vary, but most commonly large osteolytic lesions without sclerotic margins are typical on radiographs. Occasionally, a moth-eaten or permeative osteolytic pattern is noted. The osteolytic change may be subtle on radiographs. Radionuclide bone scan and MR imaging are more sensitive.

Sclerotic Metastasis

Sclerotic metastases often develop in prostate and breast carcinoma and less commonly in gastrointestinal carcinoma, bronchial adenoma, and even lung carcinoma (small cell carcinoma and adenocarcinoma). Carcinoids and medulloblastomas also can give rise to blastic metastases. On CT, sclerosis is not rare at the lesion margin in any metastases, even those with purely lytic findings on radiography. Except in the case of prostate carcinoma, most of the radiographically visible sclerosis results from reactive changes at the tumor margin. In the case of prostate carcinoma, however, stromal ossification, similar to what occurs in osteosarcoma, may be seen (Fig. 7.113).

Acrometastasis

Metastases to the limb bones are uncommon, constituting approximately 10% of metastases. These usually occur in the proximal femora and humeri. Acrometastases are hematogenous metastases occurring in the peripheral skeleton: wrists, hands, ankles, and feet. In approximately a half of acrometastases, the primary lesions are lung, with the remainder represented by a variety of tumors, including renal cell, breast, and thyroid carcinomas [99]. The phalangeal tuft is a typical site because the finger tip and glomus apparatus have relatively increased arterial blood supply. Acrometastases are usually purely lytic lesions without sclerotic margins, but this depends on the primary tumor (Fig. 7.114).

Cortical Metastasis

Occasionally hematogenous metastases develop in the cortex [100, 101]. Again, the typical primary lesion is a lung carcinoma (Fig. 7.115). A soft tissue mass may develop on the periosteal bone margin. Cortical metastases may be deceptive since they may appear radiographically as well-defined lucencies, simulating the appearance of a cyst or a benign fibrous lesion. Thus, any lytic lesion in the cortex of an older adult should be considered potentially malignant until proven otherwise.

Intertrabecular Metastasis

Some metastases may infiltrate the marrow space, spreading but not destroying the trabeculae. This is known as intertrabecular metastasis and is typically seen in early metastatic spread. Lung and hepatocellular carcinoma, however, may become extensive before destroying bone. Because the bone is intact, bone scintigraphy often fails to detect these lesions. MR imaging may be the only study to detect such

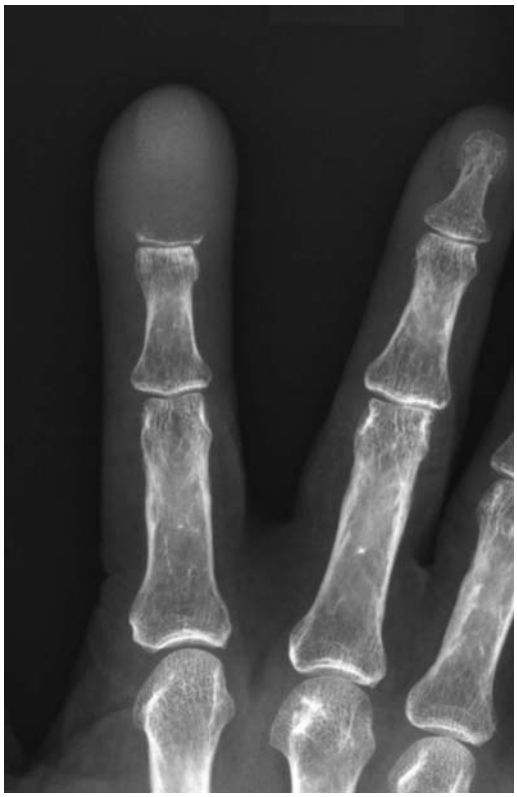

Fig. 7.114 Acrometastasis of the digit (75-year-old women). Metastasis from the endometrial carcinoma. An ill-defined lytic lesion in the distal phalanx of the index finger

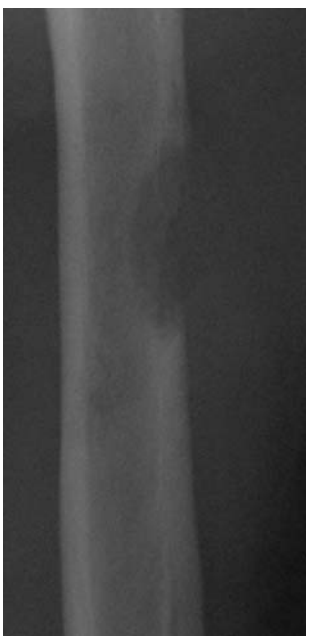

Fig. 7.115 Cortical metastasis (69-year-old man with carcinoma of lung). AP view of the femur. Cortical destruction is evident at the femoral shaft

metastases (Fig. 7.116) [102]. The role of PET has not yet been well investigated.

Congenital/Hereditary Syndromes

Enchondromatosis

Ollier disease or multiple enchondromatosis is characterized by multiple enchondromas arising in the tubular skeleton. Since these lesions develop during skeletal growth, they may cause deformity and shortening of the extremities. Two forms of Ollier disease have been documented: one is idiopathic and the other arises from an autosomal dominant mutation of the PTHR-1 gene (3p21-22). Radiographs characteristically show a striated pattern of lucencies and the metaphyses are often widened (Fig. 7.117). Maffucci syndrome is similar to Ollier disease but has multiple associated hemangiomas of the extremities, in both the soft tissues and the bone. Malignant transformation to chondrosarcoma, though possibly higher in Maffucci syndrome, is high in both diseases. Furthermore, the incidence of epithelial carcinomas also has been reported to be high in these syndromes.

McCune–Albright Syndrome

A mutation of the GNAS gene on 20th chromosome (20q3) causes McCune–Albright syndrome. The syndrome includes the triad of endocrinopathy, polyostotic fibrous dysplasia, and café-au-lait spots with margins that are irregular and resemble the coast of the State of Maine (Fig. 7.118). Precocious puberty is often associated. Secondary osseous neoplasms that arise in this syndrome include simple bone cyst, aneurysmal bone cyst, osteosarcoma, and chondrosarcoma. Fortunately, they are uncommon. Mazabroud syndrome is the association of fibrous dysplasia with intramuscular myxomas (Fig. 7.119).

Multiple Osteochondromas

Multiple hereditary osteochondromatosis is an autosomal dominant disorder caused by mutation of the EXT1 gene on the eighth or eleventh chromosome (8q24, 11p11-12). Malignant transformation is uncommon in this disease, approximating the cumulative sum of the probability of a single osteochondroma's likelihood of transforming into a chondrosarcoma.

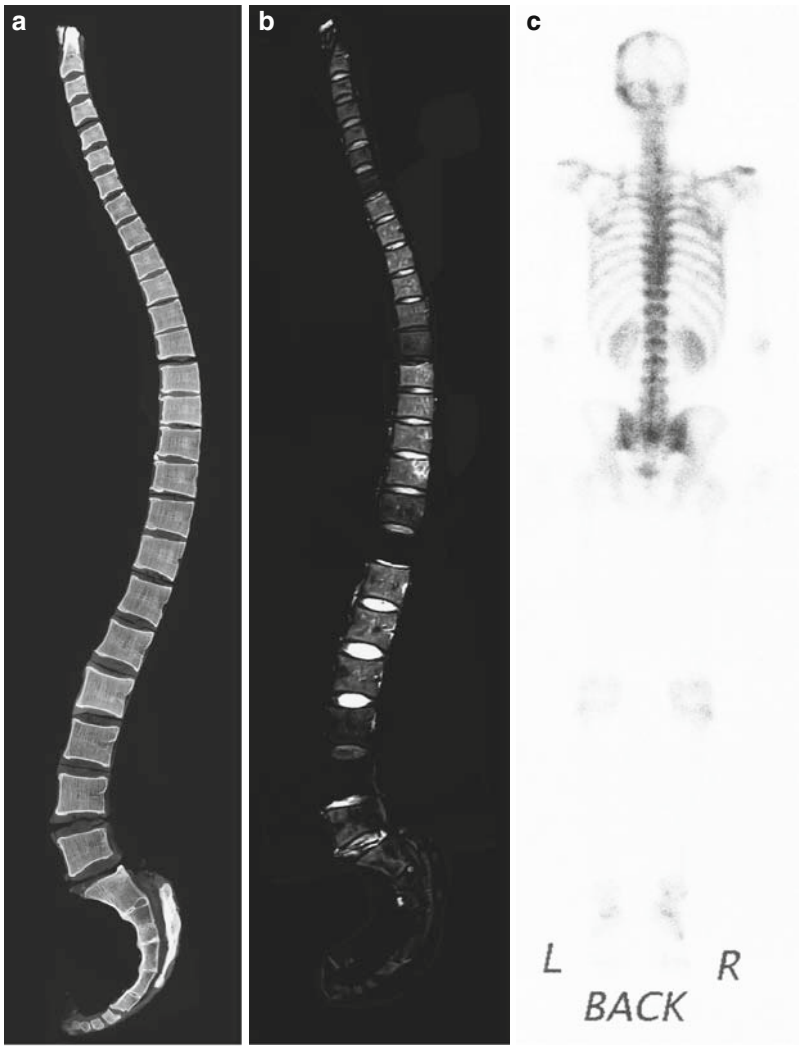

Fig. 7.116 Intertrabecular metastasis (50-year-old woman with large cell carcinoma of the lung, this patient has six lumbar vertebrae). **a**. Specimen radiography in sagittal section. Slightly sclerotic changes at T7, T8, and L3. **b**. Specimen MR in sagittal STIR section. Bright signal in the bone marrow of T1-5, T7-10, and L1-3. **c**. Tc-99m MDP scintigraphy before death. No abnormal uptake is noted (©: Japanese Society of Medical Imaging, courtesy of Dr. Yamaguchi)

Langer-Gideon syndrome (trichorhinophalangeal syndrome, type II) and Potocki–Shaffer syndrome are related syndromes associated with multiple exostoses. Characteristic faces and short stature are associated with Langer-Gideon syndrome. Deformity of extremities is common (Fig. 7.120). Secondary neoplasm occurs in 0.5–3% of cases, and chondrosarcoma is the most common.

Retinoblastoma Syndrome

Retinoblastoma syndrome is an autosomal dominant disorder caused by the RB1 gene on 13th chromosome (13q14). The primary retinoblastomas recur through the optic nerve or within the ethmoid bone or sphenoid bone. Secondary neoplasms also occur after complete remission of the retinoblastoma, most commonly osteosarcoma occurring in the field of radiation therapy after trilateral retinoblastoma (bilateral retinal lesions and pineal lesion) (Fig. 7.57).

Li Fraumeni Syndrome

Patients afflicted with this syndrome develop premature and familial occurrence of malignancies. Mutation of the TP53 or CHEK2 gene (17p13, 22q11) causes this syndrome. The incidence of osteosarcoma and rhabdomyosarcoma is high.

Rothmund–Thomson Syndrome

These patients have dermatologic disorders including erythema, abnormal pigmentation, and skin atrophy. It has autosomal recessive inheritance from a RECQL4 gene (8q24) mutation. A high incidence of malignancy, particularly osteosarcoma, has been reported in these patients.

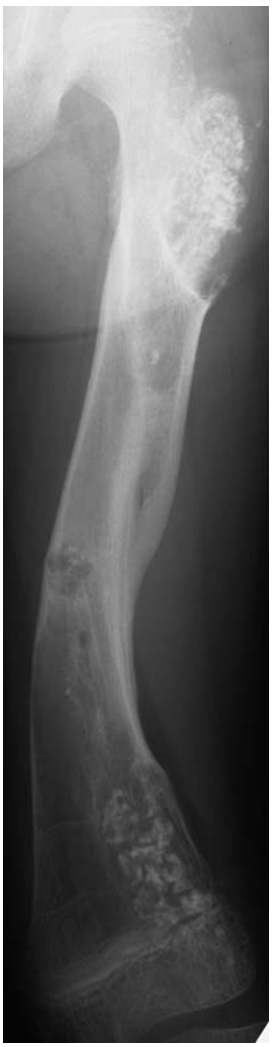

Fig. 7.117 Enchondromatosis (6-year-old man after fracture healing). AP view of the femur. Linear lucent lesions with chondroid matrix mineralization are seen in the metaphysis. Deformity is significant

Werner Syndrome

Patients with Werner syndrome show premature aging. It has autosomal recessive inheritance, via a WRN gene mutation (8p11-12). Again, a high incidence of malignancy, including bone sarcoma, has been reported.

Paraneoplastic Syndromes

Hypertrophic Osteoarhropathy

Hypertrophic osteoarthropathy is of uncertain etiology. Patients with this syndrome present with joint pain and periosteal reaction of the tubular bones of the extremities. Characteristically, the periosteal reaction is solid and extends from metaphysis to metaphysis of the long bone, sparing the epiphyseal region. It is common in the bones of the forearm, the femur, tibia, and fibula, and occasionally the metacarpals and metatarsals.

It is most commonly associated with thoracic neoplasms. Lung carcinoma is the most common cause of this syndrome, approximately 5% of the patients, and the incidence is high in mesothelioma, reported up to 50%.

PTHrP Bone Resorption

Various tumors can excrete parathyroid hormone-related peptide (PTHrP). Hypercalcemia and bone resorption, similar to hyperparathyroidism, may occur [103]. Adult T-cell lymphoma is a typical tumor associated with this type of behavior (Fig. 7.121).

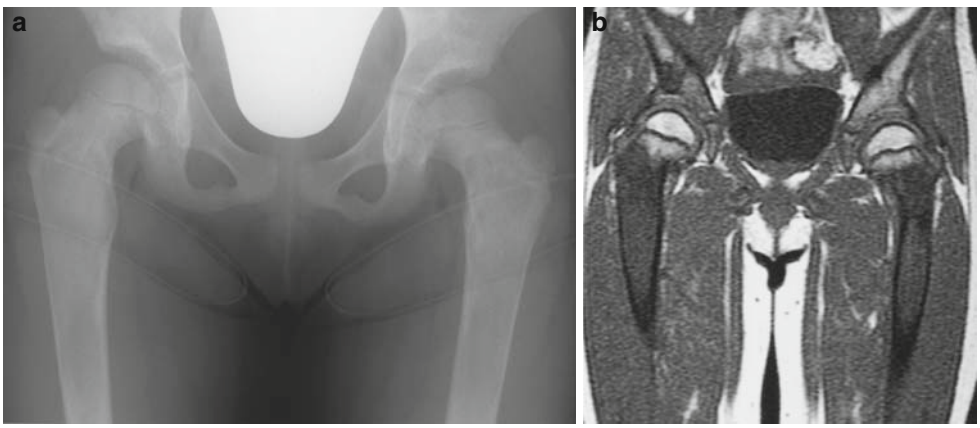

Fig. 7.118 Albright syndrome (5-year-old woman with precocious puberty). **a**. AP view of the bilateral femora. An expansile change in the bilateral femoral shaft. **b**. T1-weighted coronal MR images. Low-signal lesions in the bone marrow of the bilateral femoral shafts

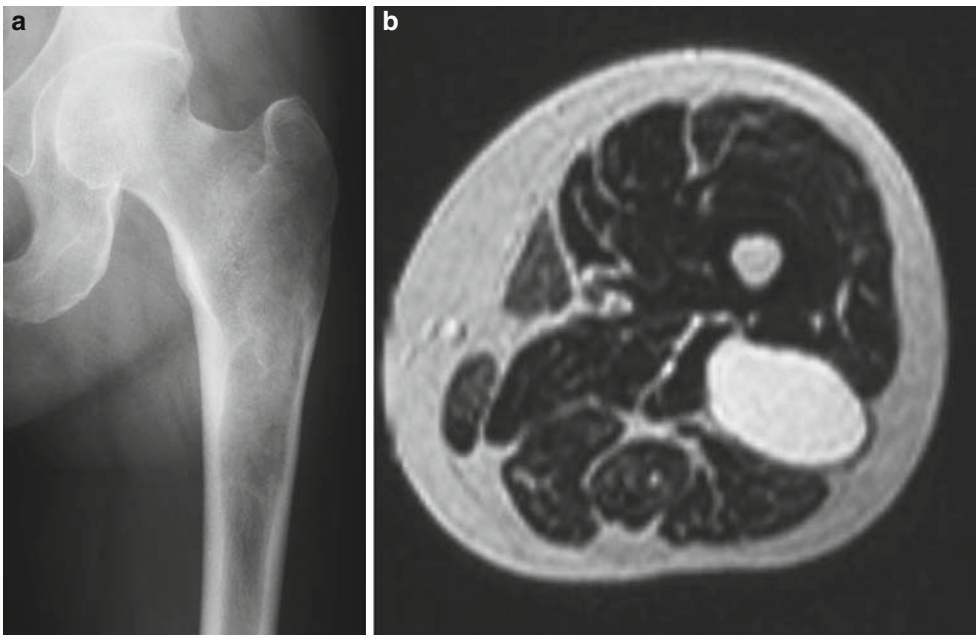

Fig. 7.119 Mazabroud syndrome (44-year-old woman). **a**. AP view of the femur. Bone marrow expansion and sclerosis are seen at the proximal femoral shaft consistent with fibrous dysplasia. **b**. T2-weighted axial MR image. A well-defined soft tissue mass with bright signal intensity, the finding compatible with myxoma

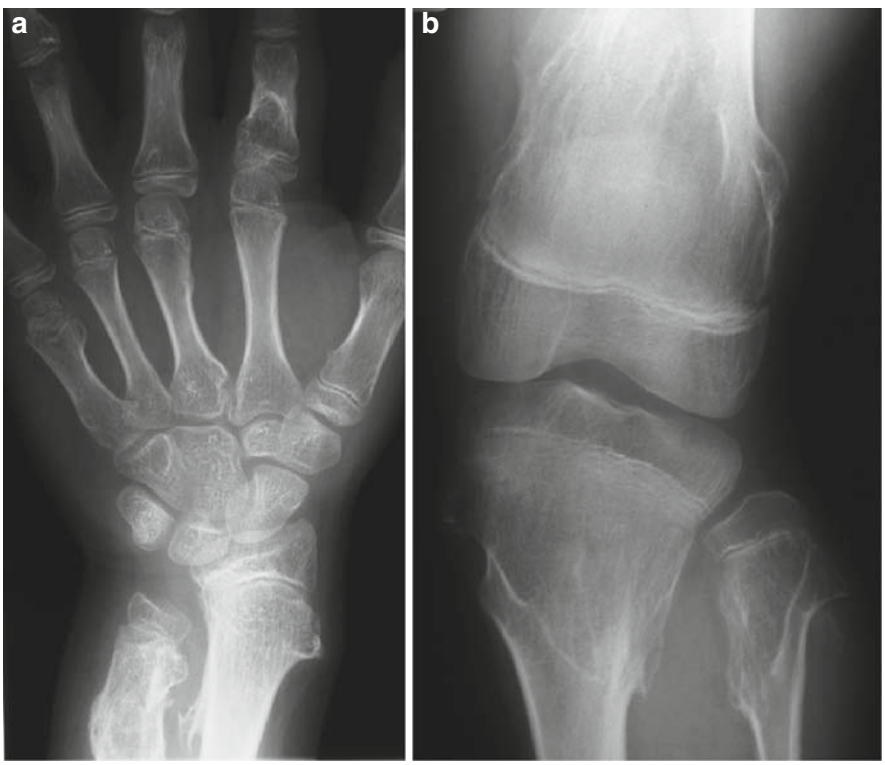

Fig. 7.120 Multiple herideditary exostosis (11-year-old male). **a**. AP view of the hand. Exostoses at the distal radius, ulna, fifth metacarpal and second and third proximal phalanges. Deformity of the wrist due to shortened ulna. **b**. AP view of the knee. Exostoses at the metaphyses. Valgus deformity is noted

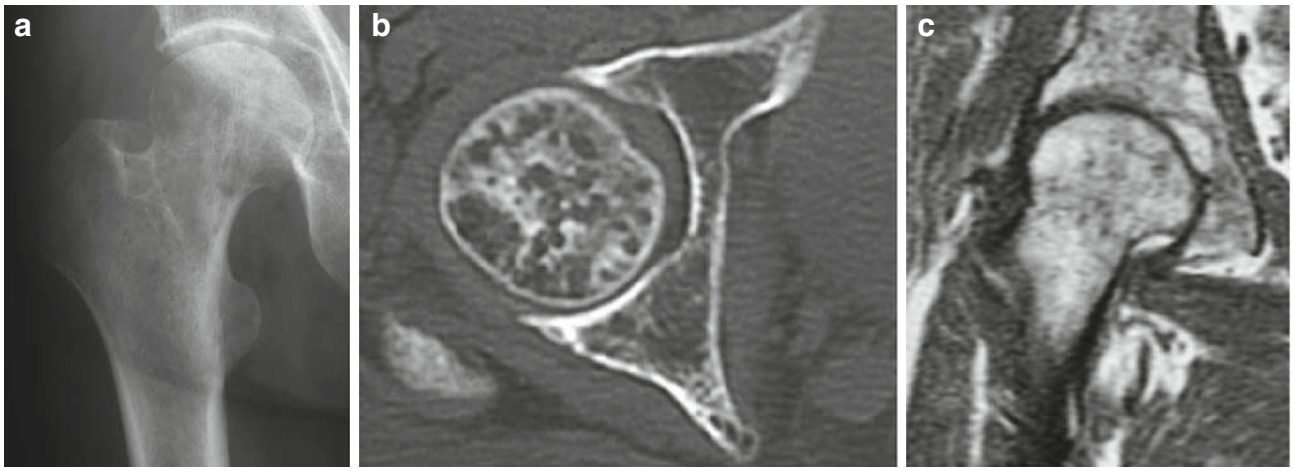

Fig. 7.121 Adult T-cell lymphoma with bone resorption (50-year-old man). **a**. AP view of the hip. Coarse bone resorption at the femoral head. **b**. CT. Coarse bone resorption is again noted. **c**. T1-weighted coronal MR image. No tumor invasion in the bone marrow is noted. The bone resorption is considered to be due to humoral factor, PTHrP

Table 7.2 Congenital and hereditary disorders related to bone tumors

Syndrome	Mode of inheritance	Gene	Locus	Associated tumors
Bloom syndrome	AR	BLM	15q26	Osteosarcoma
Li Fraumeni syndrome	AD	TP53	17p13, 22q11	Osteosarcoma
McCune–Albright syndrome	SP	GNAS1	20q13	Osteosarcoma
Multiple exostosis	AD	EXT1	8q24	Chondro- and osteosarcoma
		EXT2	11p11-12	
Ollier disease	SP	PTHR1	3p21-22	Chondrosarcoma
Retinoblastoma syndrome	AD	RB1	13q14	Osteosarcoma
Rothmund–Thomson syndrome	AR	RECQL4	8q24	Osteosarcoma
Werner syndrome	AR	WRN	8p11-12	Various sarcoma

Oncogenic Osteomalacia

Some tumors release fibroblast growth factor (FGF)-23, a hormone that promotes phosphorus loss through the renal tubules. Phosphaturic tumors typically include several different groups of benign and intermediate mesenchymal tumors, including hemangiopericytoma. These tumors are characteristically associated with mineralization on CT [104]. Once identified, tumor resection is curative (Table 7.2).

Summary

Plain radiography is the key for specific bone tumor diagnosis. Usually more than two-thirds of focal bone lesions may be diagnosed only on plain radiography. CT, MRI, and nuclear medicine studies are used primarily to stage tumors prior to therapy. If the diagnosis of benign non-aggressive tumor is made on imaging features, biopsy may not be needed, but if malignant or aggressive tumor is considered, biopsy is indicated for treatment planning. An "Aunt Minnie" approach works in some cases, but we have to approach non-specific or atypical lesions systematically, erring on the side of caution.

Further Readings

1. Dorfman HD, Czerniak B. Bone cancers. Cancer 1995; 75(Suppl 1):203–210.
2. Huvos AG. Bone Tumors: Diagnosis, Treatment and Prognosis, 2nd ed. Philadelphia, PA: WB Saunders, 1991.
3. Fletcher CD, et al. World Health Organization Classification of Tumors: Pathology and Genetics of Tumours of Soft Tissue and Bone. Lyon: IARC Press, 2002.
4. Madewell JE, Ragsdale BD, Sweet DE. Radiologic and pathologic analysis of solitary bone lesions. Part I: internal margins. Radiol Clin North Am 1981; 19:715–748.
5. Lodwick GS, Wilson AJ, Farrell C, et al. Determining growth rates of focal lesions bone from radiographs. Radiology 1980; 577–583.
6. Sweet DE , Madewell JE, Ragsdale BD. Radiologic and pathologic analysis of solitary bone lesions. Part II: matrix patterns. Radiol Clin N Am 1981; 19:785–814.
7. Ragsdale BD, Madewell JE, Sweet DE. Radiologic and pathologic analysis of solitary bone lesions. Part III: periosteal reactions. Radiol Clin N Am 1981; 19:749–784.

8. Volberg FM Jr, Whalen JP, Krook L, Winchester P. Lamellated periosteal reactions: a radiologic and histologic investigation. Am J Roentgenol 1977; 128:85–87.
9. Brown KT, Kattapuram SV, Rosenthal DI. Computed tomography analysis of bone tumors: patterns of cortical destruction and soft tissue extension. Skeletal Radiol 1986; 15: 448–451.
10. Wittekind C, Green FL, Hutter RVP et al. (Eds.). TNM Atlas: Illustrated Guide to the TNM/pTNM Classification of Malignant Tumors. Berlin: Springer, 2007.
11. Enneking WF, Kagan A. "Skip" metastasis in osteosarcoma. Cancer 1975; 36:2192–2205.
12. Panicek DM, Gatsonis C, Rosenthal DI, et al. CT and MR imaging in local staging of primary malignant musculoskeletal neoplasms: report of the Radiology Diagnostic Oncology Group. Radiology 1997; 202:237–246.
13. Atacy GS, Mahal RS, Peabody TD. Staging of bone tumors: a review with illustrative examples. Am J Roentgenol 2006; 186:967–976.
14. Musculoskeletal Tumor Society (Enneking WF). Staging of musculoskeletal neoplasms. Skeletal Radiol 1985; 13: 183–194.
15. Caceres E, Zaharia M, Tantlean E. Lymph node metastasis in osteogenic sarcoma. Surgery 1969; 65:421–422.
16. Geirnaerdt MJ, Hermans J, Bloem JL, et al. Usefulness of radiography in differentiating enchondroma from central grade 1 chondrosarcoma. Am J Roentgenol 1997; 169: 1097–1104.
17. Murphey MD, Flemming JD, Boyea SR, et al. Enchondroma versus chondrosarcoma in the appendicular skeleton: differentiating features. RadioGraphics 1988; 18:1213–1237.
18. Cohen EV, Kressel HY, Frank TS, et al. Hyaline cartilage-origin bone and soft tissue neoplasms: MR appearance and histologic correlation. Radiology 1988; 167:477–481.
19. De Santos LA, Spjut HJ. Periosteal chondroma: a radiological spectrum. Skeletal Radiol 1981; 6:15–20.
20. Hudson TM, Springfield DS, Spanier SS, et al. Benign exostoses and exostotic chondrosarcomas: evaluation of cartilage thickness by CT. Radiology 1984; 152:595–599.
21. Garrison RC, Unni KK, McLoad RA, et al. Chondrosarcoma arising in osteochondroma. Cancer 1982; 49:1890–1897.
22. Chin KR, Kharazzi FD, Miller BS, et al. Osteochondromas of the distal tibia and fibula: natural history and treatment. J Bone Joint Surg Am 2000; 82A:1269–1278.
23. El-Khoury GY, Bassett GS. Symptomatic bursa formation with osteochondroma. Am J Roentgenol 1979; 133:895–898.
24. Brower AC, Moser RP, Kransdorf MJ. The frequency and diagnostic significance of periostitis of chondroblastoma. Am J Roentgenol 1990; 154:309–314.
25. Cohen EV, Kressel HY, Frank TS, et al. Hyaline cartilage-origin bone and soft tissue neoplasms: MR appearance and histologic correlation. Radiology 1988; 167:477–481.
26. Weatherall PT, Maale GE, Mendelsohn DB, et al. Chondroblastoma: classic and confusing appearance at MR imaging. Radiology 1994; 190:467–474.
27. Wilson AJ, Kyriakos M, Ackerman LV. Chondromyxoid fibroma: radiographic appearance in 38 cases and in a review of the literature. Radiology 1991; 179:513–518.
28. Rosenthal DI, Schiller AL, Mankin HJ. Chondrosarcoma: correlation of radiological and histological grades. Radiology 1984; 150:21–26.
29. Geirnaerdt MJ, Bloem JL, Eulderink F, et al. Cartilaginous tumors: correlation of gadolinium-enhanced MR imaging and histopathologic findings. Radiology 1993; 186:813.
30. Bovee JV, van der Heul RO, Taminiau AH, et al. Chondrosarcoma of phalanx: a locally aggressive lesion with minimal metastatic potential: a report of 35 cases and a review of literature. Cancer 1999; 86:1724–1732.
31. Norman A, Sissons HA. Radiographic hallmarks of peripheral chondrosarcoma. Radiology 1984; 151:589–596.
32. Nojima T, Unni KK, McLeod RA, et al. Periosteal chondroma and periosteal chondrosarcoma. Am J Surg Path 1985; 9:666–677.
33. Kumar R, David R, Cierney G III, et al. Clear cell chondrosarcoma. Radiology 1985:154:45–48.
34. Nakashima Y, Unni KK, Shives TC, et al. Mesenchymal chondrosarcoma of bone and soft tissue: a review of 111 cases. Cancer 1986; 57:2444–2453.
35. Littrell LA, Wenger DE, Wold LE, et al. Radiographic, CT and MR imaging features of dedifferentiated chondrosarcomas: a retrospective review of 174 de novo cases. RadioGraphics 2004; 24:1397–1409.
36. Rosenthal DI, Springfield DS, Gebhardt MC, et al. Osteoid osteoma: percutaneous radio-frequency ablation. Radiology 1995; 197:451–454.
37. Edeiken J, DePalma A, Hodes PJ. Osteoid osteoma: roentgenographic emphasis. Clin Orthop 1966; 49:201–206.
38. Woods ER, Martel W, Mandell SH, et al. Reactive soft tissue mass associated with osteoid osteoma: correlation of MR imaging features with pathologic findings. Radiology 1993; 186: 221–225.
39. Assoun J, Richardi G, Railhac JJ, et al. Osteoid osteoma: MR imaging versus CT. Radiology 1994; 191:217.
40. Makley JT, Dunn MJ. Prostaglandin synthesis by osteoid osteoma. Lancet 1982; 2:42.
41. Lieu P, Chivers S, Roberts CC, et al. Imaging of osteoid osteoma with dynamic gadolinium-enhanced MR imaging. Radiology 2003; 227:691.
42. McLeod RA, Dahlin DC, Beabout JW. The spectrum of osteoblastoma. Am J Roentgenol 1976; 126:321–325.
43. Kroon HM, Schurmans J. Osteoblastoma: clinical and radiologic findings in 98 new cases. Radiology 1990; 175:783–790.
44. Norton KI, Hermann G, Abdelwahab IF, et al. Epiphyseal involvement of osteosarcoma. Radiology 1991; 180:813.
45. Ilaslan H, Sundaram M, Unni KK, et al. Primary vertebral osteosarcoma: imaging findings. Radiology 2004; 230: 697–702.
46. Edeiken J, Raymond AK, Ayala AG, et al. Small-cell osteosarcoma. Skeletal Radiol 1987; 16:621–628.
47. Okada K, Frassica FJ, Sim FH, et al. Parosteal osteosarcoma: a clinicopathologic study. J Bone Joint Surg 1994; 76A:366–378.
48. Bertoni F, Present D, Hudson T, et al. The meaning of radiolucency in parosteal osteosarcoma. J Bone Joint Surg 1985; 67A:901–910.
49. Murphey MD, Jelinek JS, Temple HT, et al. Imaging of periosteal osteosarcoma: radiologic-pathologic correlation. Radiology 2004; 233:129–138.
50. Weiss A, Khoury JD, Hoffer FA, et al. Telangictatic osteosarcoma: the St. Jude Children's Research Hospital experience. Cancer 2007; 109:1627–1637.
51. Bathurst N, Sanerkin N, Watt I. Osteoclast-rich osteosarcoma. Br J Radiol 1986; 59:667–673.
52. Andresen KJ, Sundaram M, Unni KK, et al. Imaging features of low-grade central osteosarcoma of long bones and pelvis. Skeletal Radiol 2004; 33:373–379.
53. Okada K, Unni KK, Swee RG, et al. High grade surface osteosarcoma: a clinicopathologic study of 46 cases. Cancer 1999; 85:1044–1054.
54. Bertoni F, Dallera P, Bacchini P, et al. The Instituto Rizzoli-Beretta experience with osteosarcoma of the jaw. Cancer 1991; 68:1555–1563.

55. Amstutz HC. Multiple osteogenic sarcoma: metastatic or multicentric? Cancer 1969; 24:923–931.
56. Hopper KD, Moser RP, Haseman DB, et al. Osteosarcomastosis. Radiology 1990; 175:233–239.
57. Mankin HJ, Hornicek FJ. Paget's sarcoma: a historical and outcome review. Clin Orthop 2005; 438:97–102.
58. Jee WH, Choe BY, Kang HS, et al. Nonossifying fibroma: characteristics at MR imaging with pathologic correlation. Radiology 1998; 209:197.
59. Arata MA, Peterson HA, Dahlin DC. Pathological fractures through non-ossifying fibromas: review of Mayo Clinic experience. J Bone Joint Surg 1981; 63A:980–983.
60. Resnick D, Greenway G. Distal femoral cortical defect, irregularities, and excavations. Radiology 1982; 143: 345–354.
61. Ishida T, Dorfman HD. Massive chondroid differentiation in fibrous dysplasia of bone (fibrocartilaginous dysplasia). Am J Surg Path 1993; 17:924–930.
62. Crim JR, Gold RH, Mirra JM, et al. Desmoplastic fibroma of bone: radiographic analysis. Radiology 1989; 172: 827–832.
63. Frick MA, Sundaram M, Unni KK, et al. Imaging findings in desmoplastic fibroma of bone: distinctive T2 characteristics. Am J Roentgenol 2005; 184:1762–1767.
64. Taconis WK, van Rijsseel TG. Fibrosarcoma of long bones: a study of the significance of areas of malignant fibrous histiocytoma. J Bone Joint Surg 1985; 67B:111–116.
65. Dahlin DC, Unni KK, Matsuno T. Malignant fibrous histiocytoma: fact or fancy? Cancer 1977; 39:1508–1516.
66. Unni KK, Ivins JC, Beabout JW, et al. Hemangioma, hemangiopericytoma, and hemangioendothelioma (angiosarcoma) of bone. Cancer 1971; 27:1403–1414.
67. Ross JS, Masaryk TJ, Modic MT, et al. Vertebral hemangiomas: MR imaging. Radiology 1987; 165:165–169.
68. Baker ND, Greenspan A, Neuwirth M. Symptomatic vertebral hemangiomas: a report of four cases. Skeletal Radiol 1986; 15:458–463.
69. Kenan S, Abdelwahab IF, Klein MJ, et al. Hemangiomas of the long tubular bone. Clin Orthop 1992; 280:256–260.
70. Wenger DE, Wold LE. Malignant vascular tumor of bone: radiologic and pathologic features. Skeletal Radiol 2000; 29:619–631.
71. Chigira M, Maehara S, Arita S, et al. The aetiology and treatment of simple bone cysts. J Bone Joint Surg 1983; 65: 633–637.
72. Norman A, Schiffman M. Simple bone cysts: factors of age dependency. Radiology 1977; 124:779–782.
73. Tsai JC, Dalinka MK, Fallon MD, et al. Fluid-fluid level: a nonspecific finding in tumors of bone and soft tissue. Radiology 1990; 175:779–782.
74. Sanerkin NG, Mott MG, Roylance J. An unusual intraosseous lesion with fibroblastic, osteoclastic, osteoblastic, aneurismal and fibromyxoid elements: "solid" variant of aneurismal bone cyst. Cancer 1983; 51:2278–2286.
75. Bonakdarpour A, Levy WM, Aegerter E. Primary and secondary aneurismal bone cyst: a radiological study of 75 cases. Radiology 1978; 126:75–83.
76. Magee TH, Rowedder AM, Degnan GG. Intraosseous ganglion of the wrist. Radiology 1995; 195:517–520.
77. Ramirez H Jr, Blatt ES, Cable HF, et al. Intraosseous pneumatocyst of the ilium. Radiology 1984; 150:503–505.
78. Milgram JW. Intraosseous lipomas: radiologic and pathologic manifestations. Radiology 1988; 167:155–160.
79. Dahlin DC. Giant cell tumor of bone: highlights of 407 cases. Am J Roentgenol 1985; 144:955–960.
80. Kransdorf MJ, Sweet DE, Buetow PC, et al. Giant cell tumor in skeletally immature patients. Radiology 1992; 184:233.
81. Aoki J, Tanikawa H, Ishii K, et al. MR findings indicative of hemosiderin in giant-cell tumor of bone: frequency, cause, and diagnostic significance. Am J Roentgenol 1996; 166:145–148.
82. Cooper KL, Beabout JW, Dahlin DC. Giant cell tumor: ossification of soft tissue implants. Radiology 1984; 153:597–602.
83. Glass TA, Mills SE, Fechner RE, et al. Giant-cell reparative granuloma of the hands and feet. Radiology 1983; 149:65–68.
84. Ducou le Pointe H, Bruqieres P, Chevailer X, et al. Imaging if chordomas of mobile spine. J Neuroradiol 1991; 18:267–276.
85. Smith J, Ludwig RL, Masrcove RC. Sacrococcygeal chordoma: a clinicopathological study of 60 patients. Skeletal Radiol 1987; 16:33–44.
86. Yamaguchi T, Suzuki S. Ishiiwa H, et al. Benign notochordal cell tumors: a comparative histological study of benign notochordal cell tumors, classic chordomas, and notochordal vestiges of fetal intervertebral discs. Am J Surg Path 2004;28: 756–761.
87. Sweet DE, Vinh TN, Devaney K. Cortical osteofibrous dysplasia of long bone and its relationship to adamantinoma: a clinicopathologic study of 30 cases. Am J Surg Path 1992; 16:282–290.
88. Sartoris DJ, Parker RB. Histiocytosis X: rate and pattern of resolution of osseous lesions. Radiology 1984; 152:679–684.
89. Braunstein EM. Hodgkin disease of bone: radiographic correlation with the histologic classification. Radiology 1980; 137:643–646.
90. Braunstein EM, White SJ. Non-Hodgkin lymphoma of bone. Radiology 1980; 135:59–63.
91. Heyning FH, Kroon HM, Hogerdoorn PC, et al. MR imaging characteristics in primary lymphoma of bone with emphasis on non-aggressive appearance. Skeletal Radiol 2007; 36: 937–944.
92. Unni KK, Inward CY, Bridge JA, et al. Tumors of Bones and Joints (AFIP Atlas of Tumor Pathology). Washington, DC: ARP, 2005.
93. Reinus WR, Kyriakos M, Gilula LA, et al. Plasma cell tumors with calcified amyloid deposition mistaken for chondrosarcoma. Radiology 1993; 189:505–509.
94. Mahnken AH, Wildberger JE, Gehbauer G, et al. Multidetector CT of the spine in multiple myeloma: comparison with MR imaging and radiography. Am J Roentgenol 2002; 178: 1429–1436.
95. Resnick D, Greenway GD, Bardwick PA, et al. Plasma-cell dyscrasia with polyneuropathy, organomegaly, endocrinopathy, M-proteinemia, and skin changes: the POEMS syndrome. Radiology 1981; 140:17–22.
96. Shapeero LG, Vanel D, Sundaram M, et al. Periosteal Ewing sarcoma. Radiology 1994; 191:825.
97. Reinus WR, Gilula LA. Radiology of Ewing's sarcoma: intergroup Ewing's sarcoma study (IESS). RadioGraphics 1984; 9:929–944.
98. Algra PR, Heimans JJ, Valk J, et al. Do metastases in vertebra begin in the body or pedicles? Am J Roentgenol 1992; 158:1275–1279.
99. Healey JH, Turnbull ADM, Miedema B, et al. Acrometastases: a study of twenty nine patients with osseous involvement of the hands and feet. J Bone Joint Surg 1986; 68A: 743–746.
100. Coerkamp EG, Kroon HM. Cortical bone metastases. Radiology 1988; 169:525–528.

101. Hendrix RW, Rogers LF, Davis TM Jr. Cortical bone metastases. Radiology 1991; 181:409–413.
102. Yamaguchi T, Tamai K, Yamato M, et al. Intratrabecular pattern of tumors metastatic to bone. Cancer 1996; 78:1388–1394.
103. Ohuchida T, Nishitani H, Kamikawaji N, et al. "Adult T-cell leukemia/lymphoma" with bone demineralization. Skeletal Radiol 1985; 14:194–197.
104. Folpe AL, Fanberg-Smith JC, Billings SD, et al. Most osteomalacia-associated mesenchymal tumors are a single histopathologic entity: an analysis of 32 cases and comprehensive review of the literature. Am J Surg Path 2004; 28:1–30.
105. Nora FE, Dahlin DC, Beabout JW. Bizarre parosteal osteochondromatous proliferations of the hands and feet. Am J Surg Path 1983; 7:245–250.

Chapter 8

Systematic Approach to Tumors and Tumor-Like Conditions of Soft Tissue

Theodore T. Miller, Carolyn M. Sofka, Paul Zhang, and Jasvir S. Khurana

Abstract "Soft tissue tumors represent a relatively common problem for musculoskeletal radiologists. This chapter reviews the classification of soft tissue tumors and the clinical, histological, and imaging features of the most common benign and malignant soft tissue tumors. It also discusses the advantages and disadvantages of various modalities to evaluate these lesions."

Keywords World Health Organization (WHO) • Positron emission tomography (PET) • Standardized uptake value (SUV) • Dynamic contrast enhancement • Resistive index • Extended field of view sonography • Lipoma • Liposarcoma • Nodular fasciitis • Elastofibroma • Myositis ossificans • Fibromatosis • Desmoid • Fibrosarcoma • Fibrohistiocytic • Pigmented villonodular synovitis (PVNS) • Dermatofibrosarcoma protuberans (DFSP) • Glomus • Rhabdomyosarcoma • Hemangioma • Arterivenous malformation • Hemangioendothelioma • Angiosarcoma • Schwannoma • Neurofibroma • Malignant peripheral nerve sheath tumor (MPNST) • Myxoma • Synovial sarcoma • Ganglion cyst • Hematoma

Introduction

The imaging analysis of soft tissue masses is a common task for musculoskeletal radiologists. Benign soft tissue tumors are much more common than malignant ones, but the radiology and pathology literature differs on the exact proportions. The World Health Organization classifies soft tissue tumors according to their cell of origin (Table 8.1) and subdivides them into benign, intermediate, and malignant lesions, based on histologic features of cellularity, cellular pleomorphism, and mitotic activity. This classification is ever changing as immunohistochemistry and molecular genetics delve deeper into the origins of these various processes.

The imaging evaluation of a suspected soft tissue mass should begin with radiographs because they often provide clues to the nature of the abnormality. For example, a radiolucent mass indicates a fatty tumor, the presence of phleboliths indicates a vascular lesion, and peripheral mineralization suggests myositis ossificans. Usually, however, more advanced imaging is required, both for the purpose of tissue characterization and for the demonstration of the local extent of the lesion for staging and surgical planning.

Computed tomography (CT) scanning is excellent for the evaluation of mineralization within a mass and for the evaluation of adjacent bone erosion. Otherwise, the CT density of most masses is usually not helpful because with the exception of lipomas and other fat-containing tumors, they have non-specific soft tissue attenuation. The combination of multi-detector scanners and advanced workstations produce multi-planar reconstructed images in a fraction of the time that it takes to perform an MR examination, but the soft tissue contrast of CT does not equal that of MR imaging.

Magnetic resonance (MR) imaging is the workhorse for evaluation of soft tissue masses. Its anatomic delineation and soft tissue contrast are unequaled. MRI can occasionally provide a diagnosis of tumor type based on signal characteristics, such as the uniform fatty signal appearance of a lipoma, the serpiginous appearance of fatty and vascular elements within a hemangioma, or the demonstration of phleboliths in a vascular malformation. Unfortunately, most soft tissue tumors have a non-specific appearance that is low to intermediate signal intensity on T1-weighted sequences and intermediate to high signal intensity on T2-weighted sequences. The primary reason for obtaining an MR imaging examination is for surgical staging and determination of the anatomic location and extent of a lesion.

Intravenous gadolinium contrast generally cannot distinguish benign from malignant lesions but can give an indication of tumor vascularity and confirm the cystic nature of a ganglion. Moreover, intravenous contrast can be helpful for outlining cystic or necrotic portions of a solid mass, which

T.T. Miller (✉)
Department of Radiology and Imaging, Hospital for Special Surgery, Weill Medical College of Cornell University, New York, NY, USA
e-mail: millertt@hss.edu

A. Bonakdarpour et al. (eds.), *Diagnostic Imaging of Musculoskeletal Diseases: A Systematic Approach*,
DOI 10.1007/978-1-59745-355-4_8,

Table 8.1 World Health Organization classification of soft tissue tumors

Adipocytic tumors
- **Benign**
  - Lipoma
  - Lipomatosis
  - Lipomatosis of nerve
  - Lipoblastoma/lipoblastomatosis
  - Angiolipoma
  - Myolipoma
  - Chondroid lipoma
  - Extrarenal angiomyolipoma
  - Extraadrenal myolipoma
  - Spindle cell/pleomorphic lipoma
  - Hibernoma
- **Intermediate (locally aggressive)**
  - Atypical lipomatous tumor/well-differentiated liposarcoma
- **Malignant**
  - Well-differentiated liposarcoma
  - Dedifferentiated liposarcoma
  - Myxoid liposarcoma
  - Pleomorphic liposarcoma
  - Mixed-type liposarcoma

Fibroblastic/myofibroblastic tumors
- **Benign**
  - Nodular fasciitis
  - Proliferative fasciitis
  - Proliferative myositis
  - Myositis ossificans
  - Ischemic fasciitis
  - Elastofibroma
  - Fibrous hamartoma of infancy
  - Myofibroma/myofibromatosis
  - Fibromatosis colli
  - Juvenile hyaline fibromatosis
  - yInclusion body fibromatosis
  - yFibroma of tendon sheath
  - Desmoplastic fibroblastoma
  - Mammary-type myofibroblastoma
  - Calcifying aponeurotic fibroma
  - Angiomyofibroblastoma
  - Cellular angiofibroma
  - Nuchal-type fibroma
  - Gardner fibroma
  - Calcifying fibrous tumor
  - Giant cell angiofibroma
- **Intermediate (locally aggressive)**
  - Superficial fibromatosis (palmar/plantar)
  - Desmoid-type fibromatosis
  - Lipofibromatosis
- **Intermediate (rarely metastasizing)**
  - Solitary fibrous tumor – hemangiopericytoma
  - Inflammatory myofibroblastic tumor
  - Low-grade myofibroblastic sarcoma
  - Myxoinflammatory fibroblastic sarcoma
  - Infantile fibrosarcoma

Table 8.1 (Continued.)

- **Malignant**
  - Adult fibrosarcoma
  - Myxofibrosarcoma (formerly myxoid MFH)
  - Low-grade fibromyxoid sarcoma/hyalinizing spindle cell tumor
  - Sclerosing epithelioid fibrosarcoma

So-called Fibrohistiocytic Tumors
- **Benign**
  - Giant cell tumor of tendon sheath
  - Diffuse-type giant cell tumor
  - Benign fibrous histiocytoma
- **Intermediate (rarely metastasizing)**
  - Plexiform fibrohistiocytic tumor
  - Giant cell tumor of soft tissues
- **Malignant**
  - Pleomorphic undifferentiated pleomorphic sarcoma
  - Giant cell undifferentiated pleomorphic sarcoma
  - Inflammatory undifferentiated pleomorphic sarcoma
  - Dermatofibrosarcoma protuberans (a tumor of the skin)

Smooth muscle tumors
- **Benign**
  - Angioleiomyoma
  - Deep leiomyoma
  - Genital leiomyoma
- **Malignant**
  - Leiomyosarcoma

Pericytic (perivascular) tumors
- **Benign**
  - Glomus tumor (and variants)
  - Myopericytoma
- **Malignant**
  - Malignant glomus tumor

Skeletal muscle tumors
- **Benign**
  - Rhabdomyoma
  - Adult type
  - Fetal type
- **Malignant**
  - Embryonal rhabdomyosarcoma (including spindle cell, botryoid, and anaplastic types)
  - Alveolar rhabdomyosarcoma (including solid and anaplastic types)
  - Pleomorphic rhabdomyosarcoma

Vascular tumors
- **Benign**
  - Hemangiomas (capillary, cavernous, arteriovenous, venous)
  - Epithelioid hemangioma
  - Angiomatosis
  - Lymphangioma
- **Intermediate (locally aggressive)**
  - Kaposiform hemangioendothelioma
  - Intermediate (rarely metastasizing)
  - Retiform hemangioendothelioma
  - Papillary intralymphatic angioendothelioma
  - Hemangioendothelioma
  - Kaposi sarcoma
- **Malignant**

Table 8.1 (Continued.)

Epithelioid hemangioendothelioma
Angiosarcoma
Chondro-osseous tumors
Benign
Soft tissue chondroma
Malignant
Mesenchymal chondrosarcoma
Extraskeletal osteosarcoma
Peripheral nerve sheath tumors
Benign
Schwannoma (also called neurilemoma)
Neurofibroma
Malignant
Malignant peripheral nerve sheath tumor
Tumors of uncertain differentiation
Benign
Intramuscular myxoma
Juxta-articular myxoma
Angiomyxoma
Pleomorphic hyalinizing angiectatic tumor
Intermediate (rarely metastasizing)
Angiomatoid fibrous histiocytoma (formerly angiomatoid MFH)
Ossifying fibromyxoid tumor
Mixed tumor/myoepithelioma/parachordoma
Malignant
Synovial sarcoma
Epithelioid sarcoma
Alveolar soft part sarcoma
Clear cell sarcoma of soft tissue
Extraskeletal myxoid chondrosarcoma
Primitive neuroectodermal tumor/extraskeletal Ewing tumor
Desmoplastic small round cell tumor
Extrarenal rhabdoid tumor
Malignant mesenchymoma
Neoplasms with perivascular epithelioid cell differentiation (PEComa)

should be avoided during needle biopsy since the yield will be non-diagnostic. In addition, contrast may occasionally show solid components to lesions thought completely cystic on non-contrast imaging. Thus, it may change the imaging differential diagnosis.

Dynamic contrast enhancement, in which the degree of enhancement of a particular region of tumor is measured over time, can determine the vascularity of a solid soft tissue mass and can be used to monitor the effectiveness of chemotherapy. It cannot reliably distinguish benign from malignant masses because of the overlap of vascularity between different types of lesions.

Sonography is useful for determining whether a mass is cystic or solid, an occasional diagnostic dilemma on MR images. Doppler sonography can be helpful to determine the vascularity of a lesion. Malignant lesions tend to have much more internal vascularity than benign ones, and the vessels are often tortuous and irregular in contour, but overlap among lesions exists and thus vascularity is also not a reliable indicator of malignancy. Resistive indices, too, greatly overlap between benign and malignant masses and are not reliable for distinguishing benign from malignant lesions. The advent of extended field-of-view sonography allows for visualization of the entire extent of a mass and the surrounding structures, rivaling MRI's ability to demonstrate a large anatomic overview, and the dynamic real-time capability of sonography makes it the ideal modality for guiding needle biopsy of soft tissue lesions.

Positron emission tomography (PET) scanning can be used for the evaluation of lymphoma and melanoma, which are depicted as foci of increased metabolic activity. Other soft tissue tumors have also been investigated using PET in an attempt to distinguish benign from malignant masses based on the standardized uptake value (SUV) of metabolic activity. Although there is an overall statistically significant difference in the SUV of benign and malignant masses, there is sufficient overlap between the two groups of tumors as to make this imaging technique limited in its usefulness in the diagnostic work-up of a lesion. Instead, PET may be more worthwhile for the follow-up surveillance of a lesion after treatment.

Besides imaging examinations, certain clinical information may aid in the imaging diagnosis of a soft tissue mass:

1. Location – Some masses have typical locations. For example, a small mass on the plantar aspect of the foot is most likely a plantar fibroma, a small mass around the wrist, hand, and fingers is most likely a ganglion cyst, a mass near the scapula is most likely an elastofibroma, masses around the knee are most likely meniscal cysts or bursae, masses around the glenohumeral joint are most likely perilabral cysts or ganglia, and those around the ankle are likely to be ganglia or distended joint recesses. In addition, some tumors have predilections for certain anatomic compartments, such as skin (dermatofibroma/dermatofibrosarcoma, pilomatrixoma), subcutaneous (lipoma, nodular fasciitis), intermuscular (synovial sarcoma, lipoma, nerve sheath tumors, myositis ossificans), and intramuscular (lipoma, pleomorphic sarcoma, liposarcoma, rhabdomyosarcoma, lipoma).
2. Clinical history – Information regarding the development or patient's awareness of a mass can be helpful. A history of blunt trauma in the presence of vague ossific matrix in the soft tissues suggests myositis ossificans or evolving hematoma formation; a history of anticoagulation and rapid development also suggest hematoma formation, or a history of gout brings tophus formation to mind.
3. Physical examination – Some masses are soft, such as lipoma or hemangioma; some are firm, such as fibromas and desmoids; some characteristically feel larger on examination than on imaging, such as fibromas, and some

are painful, such as nodular or proliferative fasciitis and nerve sheath tumors.

Regardless of the ability to make a specific diagnosis or even distinguish between benign and malignant lesions, the radiologist's role is to stage the mass and aid pre-operative planning by describing the anatomic compartment and location of the mass, the size of the mass, involvement of adjacent neurovascular structures, and any bone or joint involvement.

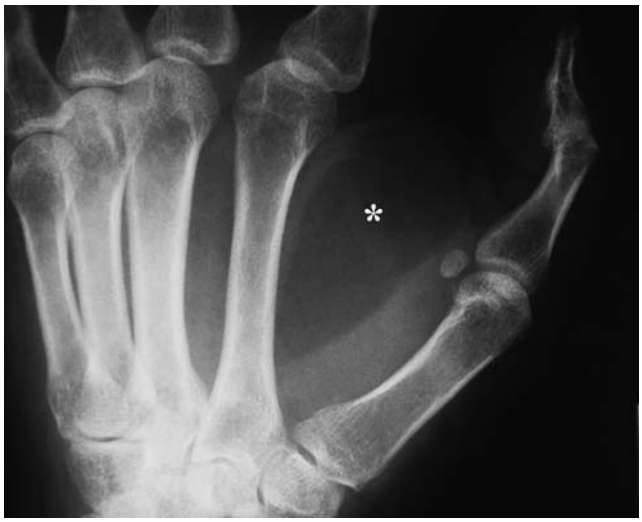

Fig. 8.1 Lipoma. Oblique radiograph of the hand shows a radiolucent mass (∗) in the thenar eminence and first web space

Adipocytic Tumors

Benign

Lipoma

Lipoma is the most commonly encountered soft tissue tumor. Although histologically identical to typical subcutaneous or deep fat, it is a neoplastic process which is independent of the body's metabolic regulation of fat stores. Thus, even an emaciated person can have a lipoma, and often a patient first notices the mass after losing weight. Lipomas are classified as superficial when they occur in the subcutaneous tissue and deep when they occur anywhere else. Superficial lipomas are soft, usually painless masses most often located in the neck, back, and shoulder regions, where they tend to be less than 5 cm in size. Deep lipomas are more common in the lower extremities and can be inter- or intramuscular, or may infiltrate the adjacent musculature. Lipomas are multiple in up to 15% of cases, with a male predominance and a familial association.

Radiographs and CT show a mass with fatty (radiolucent) density or attenuation (Figs. 8.1 and 8.2). Sonographically, a lipoma is a well-demarcated mass which usually has homogenous fine echoes, but it can be hypoechoic or hyperechoic compared to adjacent subcutaneous tissues (Fig. 8.3).

MR imaging shows a homogeneously fatty mass which is iso-intense to subcutaneous fat and is well delineated from the adjacent subcutaneous fatty tissue by a pseudocapsule, although sometimes the pseudocapsule is not visible. Lack of a demarcated capsule is particularly encountered in the subcutaneous lesions, where a distinction from adjacent fat can be difficult. Thin low signal intensity septae may be present within the lipoma but the lipoma should be otherwise uniformly high signal intensity on the T1WI sequences and uniformly low signal intensity on fat-suppressed fast spin echo T2WI sequences (Figs. 8.4 and 8.5). In fact, on all sequences the signal should follow that of normal adjacent fat. The septae should be less than 2 mm thick and usually do not enhance with contrast but occasionally may show mild enhancement. Although a benign lipoma rarely may have thick septae (>2 mm) or an internal region of non-fatty signal intensity (caused by fat necrosis or occasional benign mesenchymal elements), these lesions must be regarded as potentially malignant, and biopsied in one of the non-fatty regions. The variants of lipoma, such as lipoblastoma, spindle cell/pleomorphic lipoma, angiolipoma, myolipoma, lipoma of nerve (formerly called fibrolipomatous hamartoma), and chondroid lipoma also show non-fatty mesenchymal components, making their imaging distinction from liposarcoma difficult in some cases.

Surgical Pathology: Lipomas are typically composed of fully matured adipose tissue. Variable amounts of myxoid, chondroid, and fibrous tissue can be seen in some cases and hence the names – myxoid lipoma, chondroid lipoma, and fibrolipoma, respectively (Fig. 8.1H). By definition, lipoma should not show immature adipose tissue. However, lipoblasts can be encountered in chondroid lipoma. These lipoblasts are vacuolated cells arranged in clusters in the myxoid stroma.

Spindle cell lipomas are composed of bland, short spindle cells associated with thick rope-like collagen fibers with variable amounts of myxoid stromal change and only variable amounts of fat. Mast cells, plasma cells, and lymphocytes are seen in some cases. Angiolipomas have prominent blood vessels within the fat, many containing fibrin thrombi. Pleomorphic lipomas are related to spindle cell lipomas and are characterized by the presence of hyperchromatic floret-like multinucleated giant cells in addition to the short spindle cells. Myxolipomas have a myxoid background within an otherwise benign lipoma.

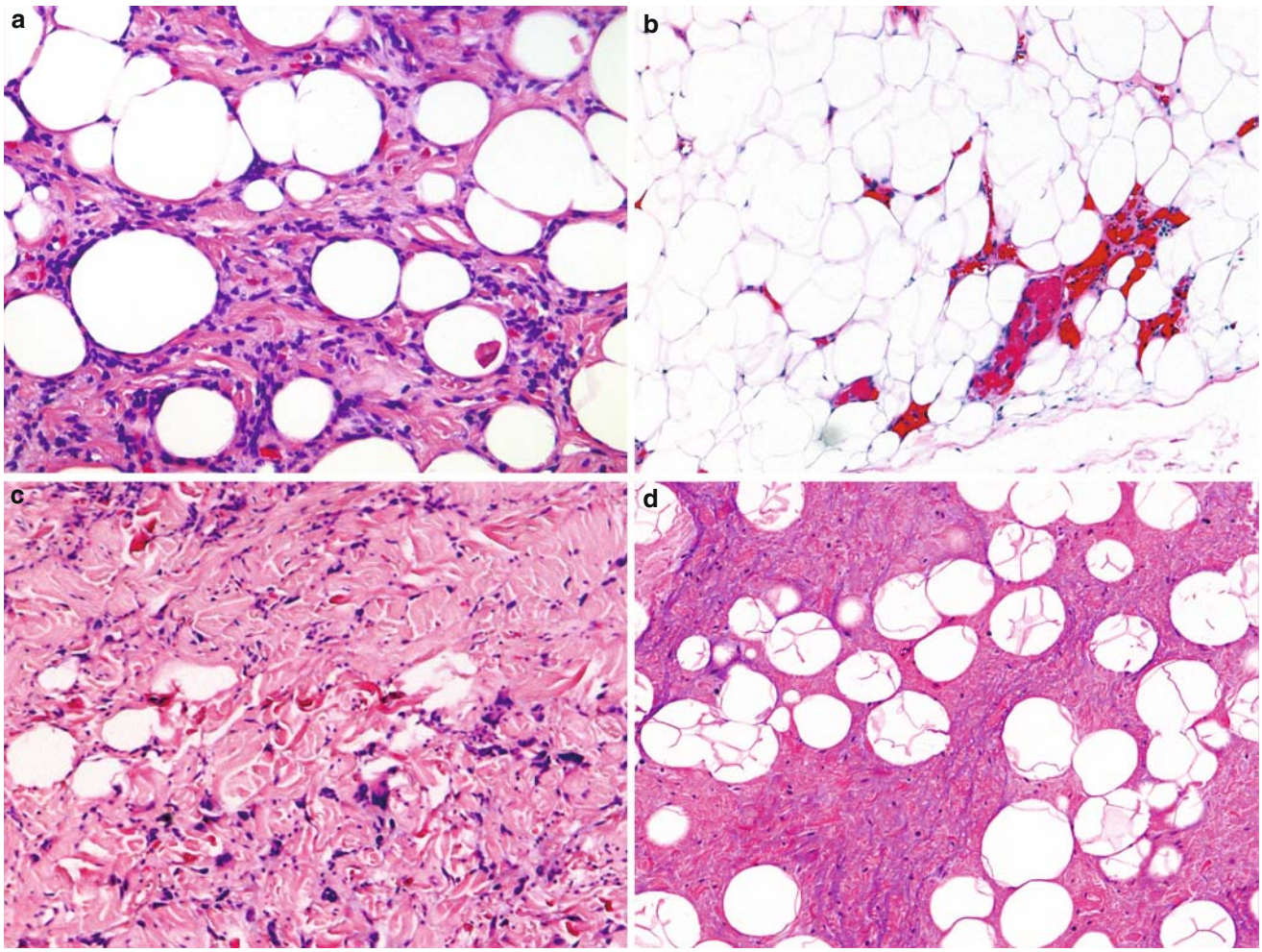

Fig. 8.1H (**a**) Spindle cell lipoma showing bland spindle cells in fibrous background with some adipocytes. (**b**) Angiolipoma showing capillary-type vascular element in background of otherwise typical lipoma. (**c**) Pleomorphic lipoma showing pleomorphic cells in a fibrous background similar to that in spindle cell lipoma with few adipocytes. (**d**) Myxolipoma showing increased paucicellular myxoid matrix in a lipoma

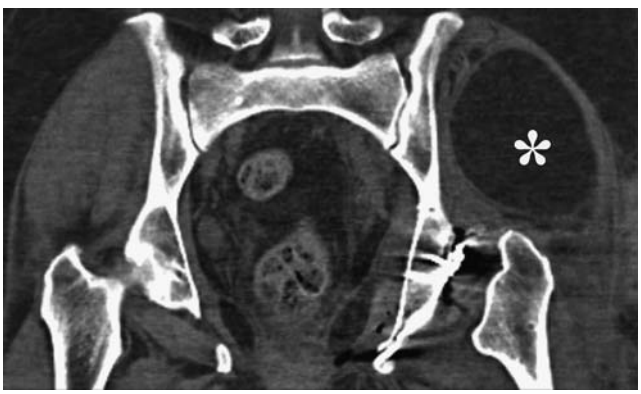

Fig. 8.2 Lipoma. Coronally reformatted CT image of the pelvis shows a large lipoma (∗) in the inter-muscular space between the gluteus medius and minimus muscles. Notice that it has the same density as subcutaneous fat and deep pelvic fat

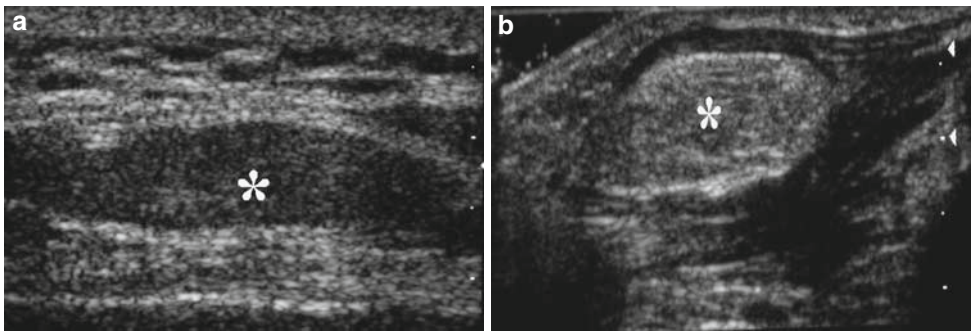

Fig. 8.3 Sonographic appearance of lipomas. (**a**) Longitudinal sonographic image shows a hypoechoic mass (∗). (**b**) Longitudinal sonographic image of a different patient shows a hyperechoic appearance (∗)

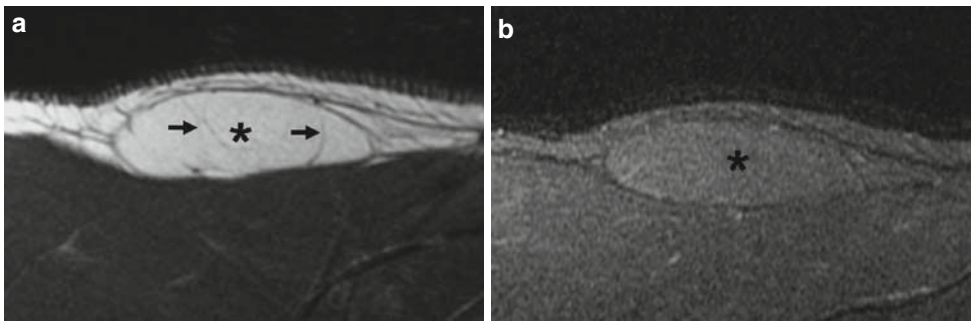

Fig. 8.4 Lipoma. (**a**) A well-circumscribed homogenously high signal intensity lipoma (∗) is present in the subcutaneous tissue. Note the thin septations (*arrows*). (**b**) Corresponding fat-suppressed T2WI sequence shows the uniform suppression of the fat signal intensity (∗)

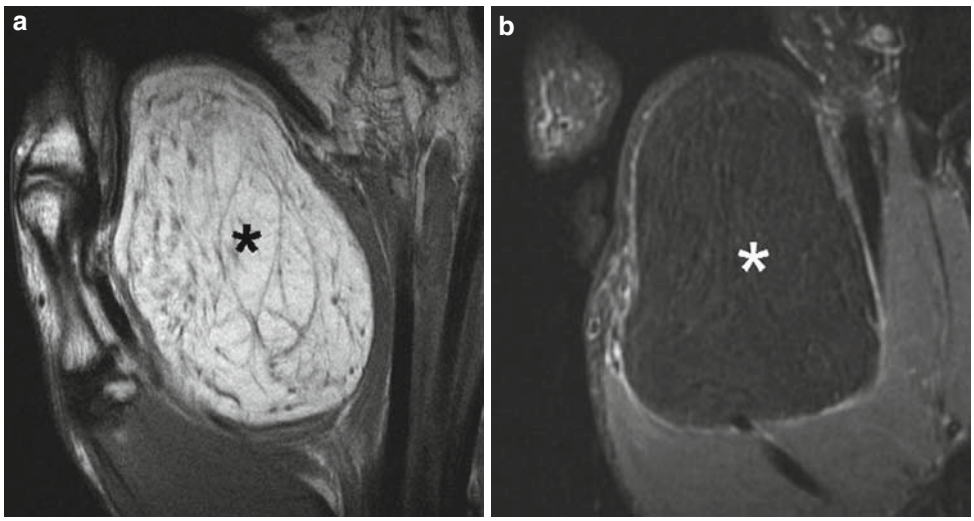

Fig. 8.5 Lipoma. (**a**) Coronal T1WI sequence shows a large fatty mass (∗). Numerous septations are presented within it, but they measure less than 2 mm. (**b**) Corresponding fat-suppressed T2WI image shows uniform suppression of the lipoma (∗)

Lipomatosis

Lipomatosis is a diffuse overgrowth of mature adipose tissue that involves both superficial and deep tissue, unlike a solitary lipoma which only affects a single location even though it may be infiltrating. Several different types of lipomatosis have been described based on the clinical and anatomic presentations.

Diffuse lipomatosis usually affects children less than 2 years old, predominantly involves the limbs, and may have osseous hypertrophy of the affected limb but does not cause lipomatosis of local nerves. Macrodystrophia lipomatosa, on

the other hand, also presents in childhood but is associated with lipomatosis of the nerve.

Lipomatosis of the nerve used to be called intraneural lipoma or fibrolipomatous hamartoma, and is most common in the upper extremity, most often involving the median nerve at the wrist, followed in frequency by the ulnar nerve. The lower extremity is much less often involved. Patients complain of pain and loss of sensation or paresthesias, and macrodactyly is present in up to two-thirds of cases. Unlike other forms of lipomatosis, in which the fatty tissue has a typically bland fatty appearance on MR imaging, lipomatosis of the nerve shows a characteristic appearance of fatty enlargement of the nerve with low signal neural fascicles running through it (Fig. 8.6).

Multiple symmetric lipomatosis usually affects middle-aged men and is associated with alcoholism; there is painless deposition of fat in the upper body, usually the neck, upper chest and back and arms. In contrast, adiposa dolorosa (also called "Dercum disease") predominantly affects obese post-menopausal women, and is characterized by deposition of fat around the pelvis, hips and knees. Unlike the other forms of lipomatosis, adiposa dolorosa is painful, and the patients complain of tenderness, motor weakness, and fatigability.

Surgical Pathology: The histologic features of all types of lipomatosis are identical and characterized by completely normal appearing mature adipose tissue replacing and entrapping the surrounding normal tissues, structures, or organs.

Lipoblastoma

Lipoblastoma is a benign fatty tumor of children, most often occurring in the subcutaneous tissue of the extremities of children less than 3 years old. It resembles fetal adipose tissue histologically. Its appearance is indistinguishable from myxoid liposarcoma, however, this latter tumor is extraordinarily rare before age 10. Lipoblastoma shows both fatty and mesenchymal signal characteristics on MR imaging (Fig. 8.7a–c). The mixed signal intensity may mimic a liposarcoma, but liposarcoma is extremely rare in children. The diffuse form of this tumor is called lipoblastomatosis. Treatment is surgical but these tumors may recur in up to 25% of cases if resection is incomplete.

Surgical Pathology: Lipoblastomas are tumors that morphologically resemble myxoid liposarcomas of adults. They are rich in plexiform (chicken-wire type) vasculature, have a myxoid background, and have a variable number of lipoblasts. They are biologically benign lesions.

Cytogenetics is quite helpful in distinguishing lipoblastomas from other adipocytic tumors. Translocations involving *HAS2/PLAG1* and *COL1A2/PLAG1* are characteristic found with lipoblastomas. *HAS2* is located at 8q24, *PLAG1* at 8q12 and *COL1A2* at 7q22. Additional copies of chromosome 8 are often times seen with lipoblastomas as well.

Hibernoma

Hibernomas are tumors of brown fat, usually intermixed with mature (white) fat. They are most common in sites of normal brown fat deposition, such as the periscapular region, mediastinum, and thorax. They may be up to 10 cm in size and are discovered most often in people in their twenties. The brown fat component has a non-specific mesenchymal appearance on MR imaging and markedly enhances with contrast [Fig. 8.7d–e]. On sonography, it is hyperechoic with respect to surrounding muscle and may be very vascular. This vascular mesenchymal appearance can mimic a liposarcoma.

Surgical Pathology: Hibernomas are composed of lobules of polygonal brown fat cells that have abundant multivacuolated, eosinophic cytoplasm with a small central nucleus. Cytogenetic analyses have shown recurrent 11p13 and11p13-21 structural rearrangements. These sites house the *MEN1* gene and the *PPP1 (PPP1CA)* gene.

Malignant

Liposarcoma

Liposarcoma is the most common malignant soft tissue tumor in adults, and tends to occur in the extremities. It has five different histologic subtypes including well-differentiated, myxoid/round cell, dedifferentiated, pleomorphic, and mixed types, representing a spectrum of histology and behavior, with the well-differentiated subtype being the least aggressive and the pleomorphic subtype being a highly aggressive metastasizing malignancy. Despite the use of "lipo-" in the name, the amount of tissue with fatty signal intensity within these masses is quite variable, with some masses being predominantly fatty while others have no discernable fat at all. In fact, some liposarcomas appear similar to other soft tissue malignancies because of their paucity of fat on imaging and histology.

It must be stressed that the presence of any non-fatty component (other than thin septations) within an otherwise fatty mass should be suspicious for liposarcoma (Figs. 8.8 and 8.9), keeping in mind that benign lipomas may occasionally have non-fatty elements and even foci of calcification.

Well-differentiated liposarcomas are the most common subtype, usually occur in people in their fifties and sixties, and are most common in the lower extremities, especially

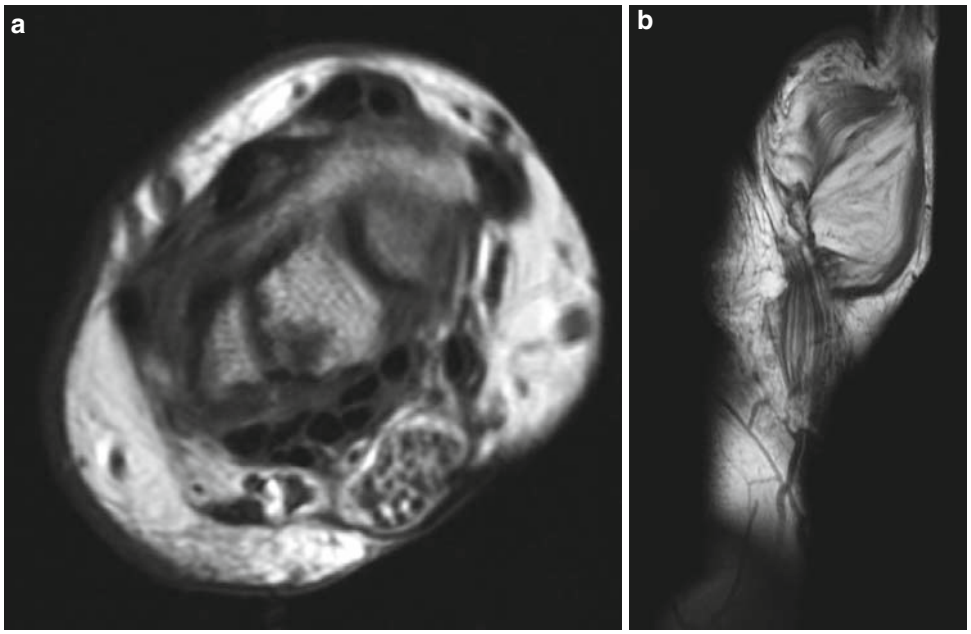

Fig. 8.6 Lipomatosis of the median nerve in a 50-year-old woman. T1W axial (**a**) and T1W coronal (**b**) MR images show an enlarged median nerve (∗) with fat interposed among the fascicles. In addition, there is a lipoma of the opponens pollicis muscle belly (#) (case courtesy of Dr. William Reinus.)

the thigh, followed by the retroperitoneum. These tumors are also called "atypical lipomatous tumor," a term that is often used when these lesions are in the extremities because the term sounds too innocuous for lesions in the retroperitoneum. Well-differentiated liposarcomas do not have the metastatic potential of the other histologic subtypes of this tumor but can be locally aggressive, especially when they occur in the retroperitoneum where complete excision is also more difficult. They can be distinguished from benign lipomas because their internal septations are much thicker (> 2 mm) and more nodular than their benign counterparts. The septations enhance moderately to markedly with contrast, and these tumors tend to be larger (greater than approximately 10.0 cm) than benign lipomas (Fig. 8.10). Up to one-third of well-differentiated liposarcomas have foci of mineralization. Any fatty tumor in the mediastinum or retroperitoneum should be considered a well-differentiated liposarcoma regardless of the presence of septations or non-fatty elements.

Myxoid/round cell liposarcoma is the second most common subtype of liposarcoma and occurs in a wide age range of patients. Myxoid liposarcoma and round cell liposarcoma are now considered two opposite ends of histologic spectrum of a group of liposarcomas with identical karyotype. Its peak prevalence is about 10 years younger (forties and fifties) than that of well-differentiated liposarcomas. The most common location is the thigh and popliteal fossa of the knee. These tumors are usually intermuscular, i.e., deep rather than subcutaneous, and the patient presents with a large painless mass. The CT and MR imaging appearance reflects the relative proportions of myxoid and round cell components in the lesion; lesions that are predominantly myxoid will have a "cyst-like" appearance (bright signal on T2-weighted images (T2WI)) but the presence of any fatty element within this mass, any mural nodularity, or any enhancement with intravenous contrast should be the clue that the mass is a neoplasm and not a cyst (Fig. 8.11). Lesions with mixed round cell and myxoid elements have a more heterogeneous appearance. In contrast to myxoid liposarcomas, benign myxomas are intramuscular, and have adjacent muscle atrophy and surrounding edema.

Surgical Pathology: Four kinds of liposarcomas are recognized – atypical lipomatous tumors/well-differentiated liposarcomas, myxoid/round cell liposarcomas, pleomorphic liposarcomas, and dedifferentiated liposarcomas (Fig. 8.10H).

Surgical Pathology of Atypical Lipomatous Tumor/Well-Differentiated Liposarcoma: These tumors are slightly lobulated and fleshy yellow to white on cut surface. There are four histologic types of well-differentiated liposarcoma: lipoma-like, sclerosing type, inflammatory type and spindle cell type.

Lipoma-like liopsarcoma usually preserves the lobulated architecture that is composed of relatively mature adipocytes. There are, however, variable numbers of atypical adipocytes

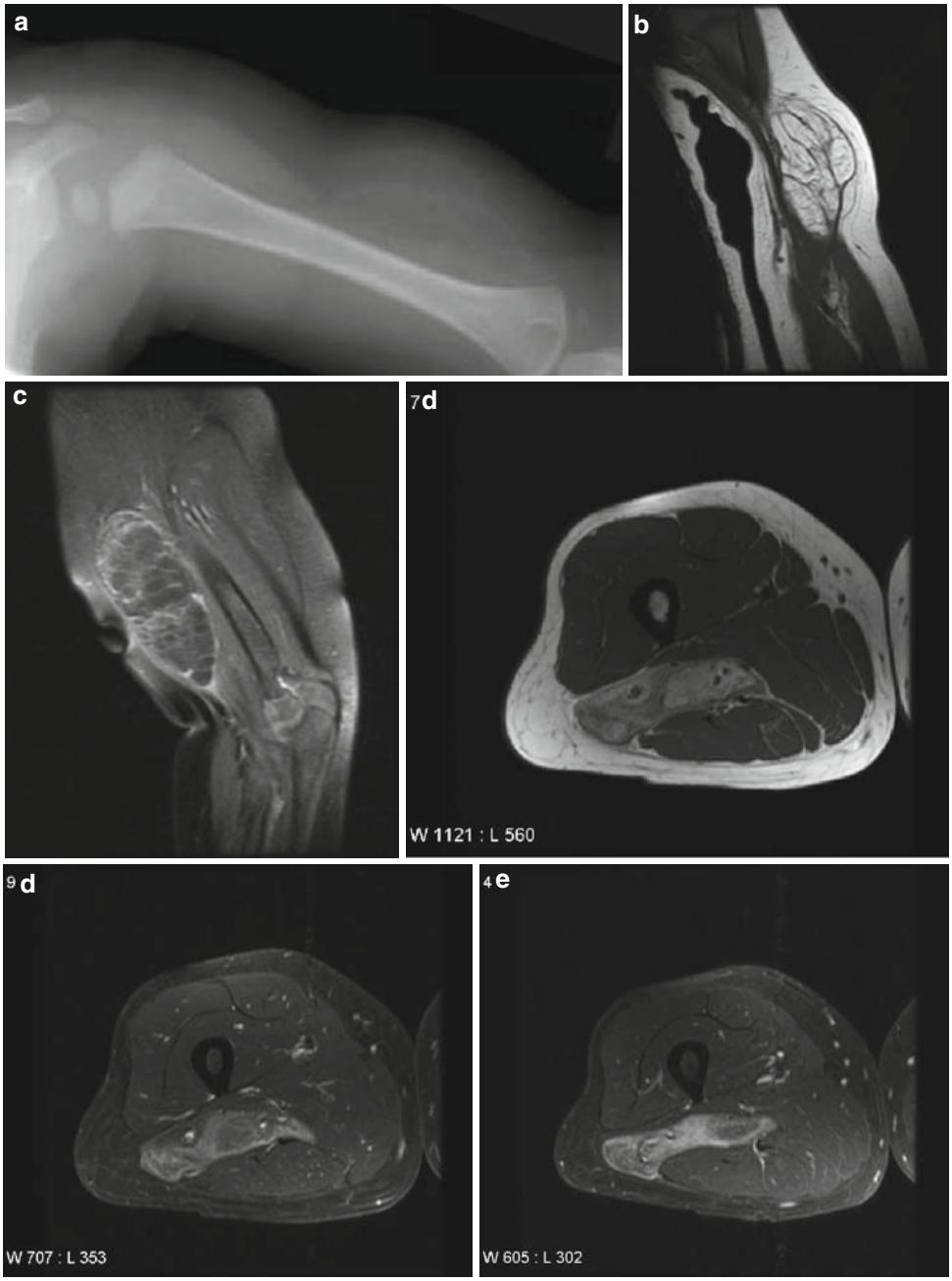

Fig. 8.7 Lipoblastoma in a 1-month-old infant. Anteroposterior radiograph (**a**) shows a fat density mass along the lateral aspect of the arm. Off-axis coronal T1W (**b**) and fat-saturated T2W (**c**) MR images show a predominantly fatty mass with multiple septations. Note that this mass has a very similar appearance to a well-differentiated liposarcoma, but these occur in an older age group. (**d, e**) Hibernoma. Axial T1, FST2, and FS T1 post-gadolinium images through a hibernoma of the lateral thigh show a bright mass on T1 with poor suppression on T2 and heterogeneous intense enhancement. Note that the degree of fat suppression on FST2 can be highly variable (case courtesy of Dr. William R. Reinus)

with enlarged, irregular and hyperchromatic nuclei scattered within the lesion. In sclerosing type, there are hyperchromatic stromal cells seen within fibrous septa or in a hyaline fibrous stroma which sometimes dominates the tumor with little lipogenic areas. The tumor can also be dominated by chronic inflammatory infiltrates composed of lymphoplasmacytic cells (inflammatory type of well-differentiated liposarcoma). The spindle cell variant is the least common type of well-differentiated liposarcoma and it is characterized by the presence of bland spindle cells

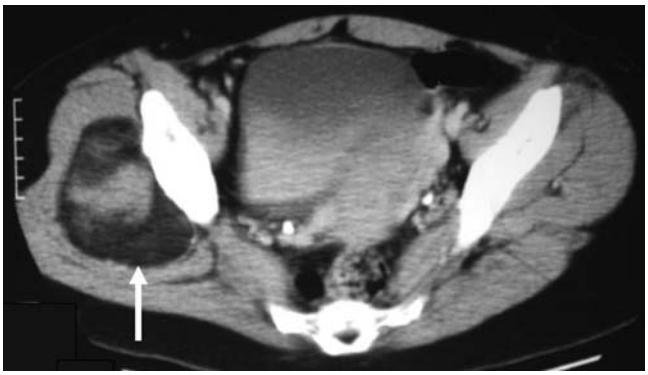

Fig. 8.8 Liposarcoma. Axial CT scan through the pelvis shows a large fatty mass (*arrow*) arising deep to the gluteus minimus muscle. Note the soft tissue density within the mass

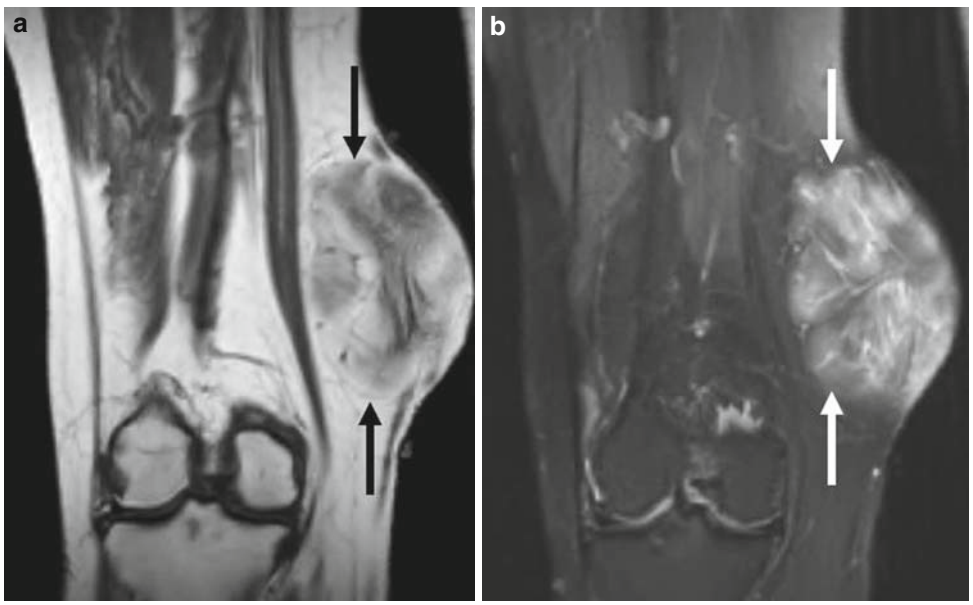

Fig. 8.9 Liposarcoma. (**a**) Coronal T1WI image Through the distal thigh shows a large mass (*arrow*) with mixed fatty and soft tissue signal intensity. (**b**) Corresponding fat-suppressed T2WI coronal image shows heterogeneous low and high signal intensity within the mass (*arrow*) (case courtesy of Dr. William Reinus)

in myxoid fibrous background associated with lipoma-like liposarcoma. Although lipoblasts can be seen in all forms of well-differentiated liposarcoma, they are rare in most cases.

Surgical Pathology of Myxoid/Round cell liposarcoma: These tumors are typically multinodular, tan, and gelatinous on cut surface in tumors with myxoid histologic features and are white fleshy in tumors with round cell features.

The well-differentiated end of the histologic spectrum is represented by myxoid phenotype. The tumor cells are individually scattered in a myxoid stroma with a slightly increased cellularity in the periphery of the lobules. Mitotic figures are rare. There are rich delicate arborising, short branching capillary vessels in a myxoid stroma in pattern referred as "chicken wire" under low magnification. Accumulation of amorphous mucin-like material in myxoid stroma forms variable-sized confluent pools (microcysts).

On the other end of the spectrum, the poorly differentiated tumors are represented by round cell phenotype that is characterized by closely packed primitive round cells with higher

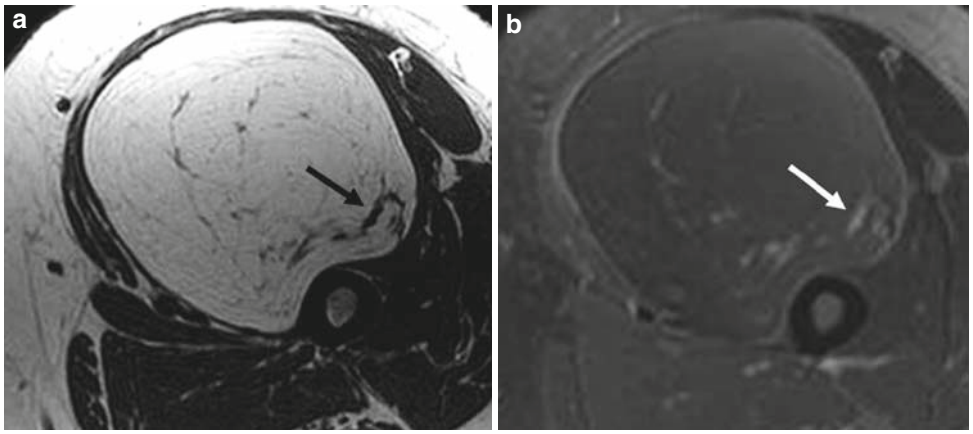

Fig. 8.10 Well-differentiated liposarcoma (atypical lipoma) (**a)** Axial T1WI image through the thigh shows a large fatty mass with thick septation (*arrow*). (**b)** Corresponding fat-suppressed T2WI image shows almost uniform fat suppression but high signal intensity of the thick septation

nucleo-cytoplasmic ratio and active mitotic activity. There is little or complete lack of myxoid stroma in the round cell areas.

Most tumors, however, show both myxoid and round cell features.

Surgical Pathology of Pleomorphic Liposarcoma: Pleomorphic liposarcoma is usually firm, multinodular, and white to yellow in gross appearance. Histologically, it is characterized by presence of numerous pleomorphic cells, many of which show cytoplasmic multivacuolation indenting the nuclei (lipoblasts). There are many other less pleomorphic cells which are spindle to round in shape and have similar hyperchromatic nuclei in a fibrous background. Mitotic figures are frequent and tumor necrosis is common.

Surgical Pathology of Dedifferentiated Liposarcoma: Nodules or areas with tan-grey or heterogeneous cut surface distinctly different from the adjacent soft, fleshy, and yellow well-differentiated liposarcoma are frequently seen in gross examination. The histologic hallmark of dedifferentiation is the presence of non-lipogenic neoplastic elements which are usually abrupt juxtaposition to the well-differentiated liposarcoma in the background. The most commonly seen non-lipogenic element is fibrosarcomatous with variable myxoid and pleomorphic features. However, chondroblastic, osteogenic, myogenic, angiomatous, and neural elements can be seen as well. The dedifferentiated elements can be histologically high or low grade. Not infrequently, the dedifferentiated component occupies majority of the tumor mass and only very small portion of well-differentiated liposarcoma can be found in the periphery of the specimen and could be misinterpreted as normal fat. Careful search for atypical cells in the remnant of "normal appearing fat" adjacent to dedifferentiated area is the key for a proper diagnosis.

Fibrous Lesions

Benign

Nodular Fasciitis

Nodular fasciitis represents an idiopathic rapid proliferation of benign fibroblasts. Histologically, it has three different cell subtypes (myxoid, cellular, and fibrous) that affect the tumor's appearance on MR imaging. Typically it is approximately 2.0 cm in size. Approximately half of the cases occur in the subcutaneous fat, especially of the forearm. The remaining cases may arise from muscle, intermuscular fascia, or from deep fat. The masses typically are low signal intensity on T1-weighted sequences with varying degrees of heterogeneous high signal intensity on T2-weighted sequences, an appearance often strikingly similar to peripheral nerve sheath tumors. Their rapid growth, occasional heterogeneous and ill-defined appearance on MR imaging, and histologic demonstration of fibroblast proliferation may lead to a misdiagnosis of sarcoma, but any rapidly appearing mass in the subcutaneous tissue of the forearm should raise the consideration of this benign process.

Surgical Pathology: Nodular fasciitis might appear to be circumscribed grossly with grey-white firm mass, sometimes with central cystic change on cut surface. Histologically, it is a non-encapsulated nodular or stellate lesion characterized by a proliferation of fusiform or stellate-shaped stromal cells with plump spindle nuclei. The stromal cells are arranged loosely in a haphazard pattern in a myxoid matrix. Extravasated red cells, chronic inflammatory cells, and osteoclast-like giant cells are frequently seen. In some

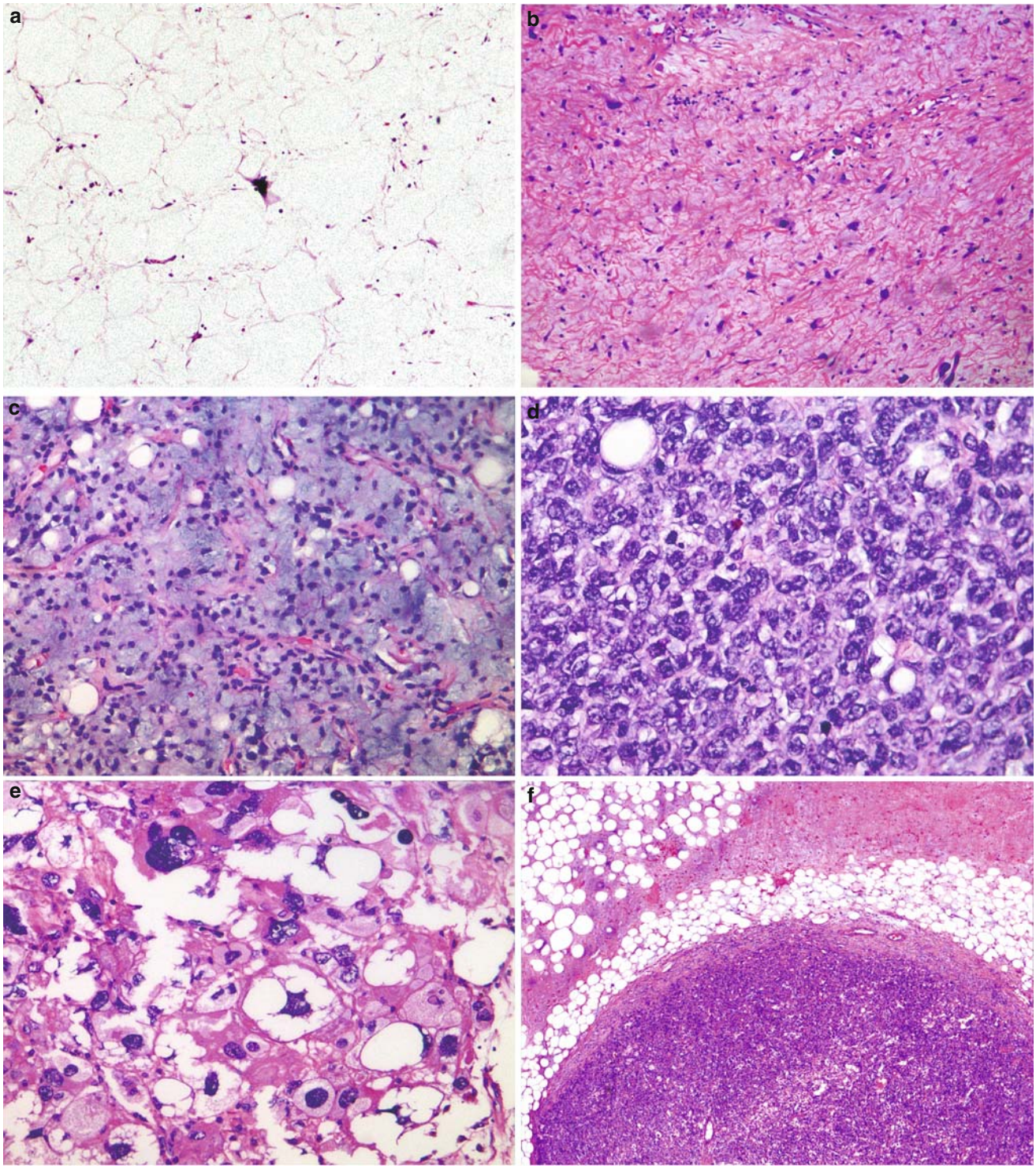

Fig. 8.10H (**a**) Lipoma-like WD liposarcoma with rare large atypical cells in lipoma-like background. (**b**) Sclerosing WD liposarcoma with many large atypical cells in fibrous sclerosing background with little lipogenic element. (**c**) Myxoid liposarcoma with round tumor cells loosely scattered in a myxoid background associated with many delicate fine vessels in a "chicken-wire" pattern. (**d**) Round cell liposarcoma with packed round tumor cells with little myxoid matrix and vasculature. (**e**) Pleomorphic liposarcoma with bizarre large tumor cells, many of them showing lipogenic activity as pleomorphic lipoblasts with spider-like nucleus. (**f**) Dedifferentiated liposarcoma with juxtaposition of poorly differentiated, non-lipogenic element (*low half*) to well-differentiated, lipogenic element of the tumor (*upper half*)

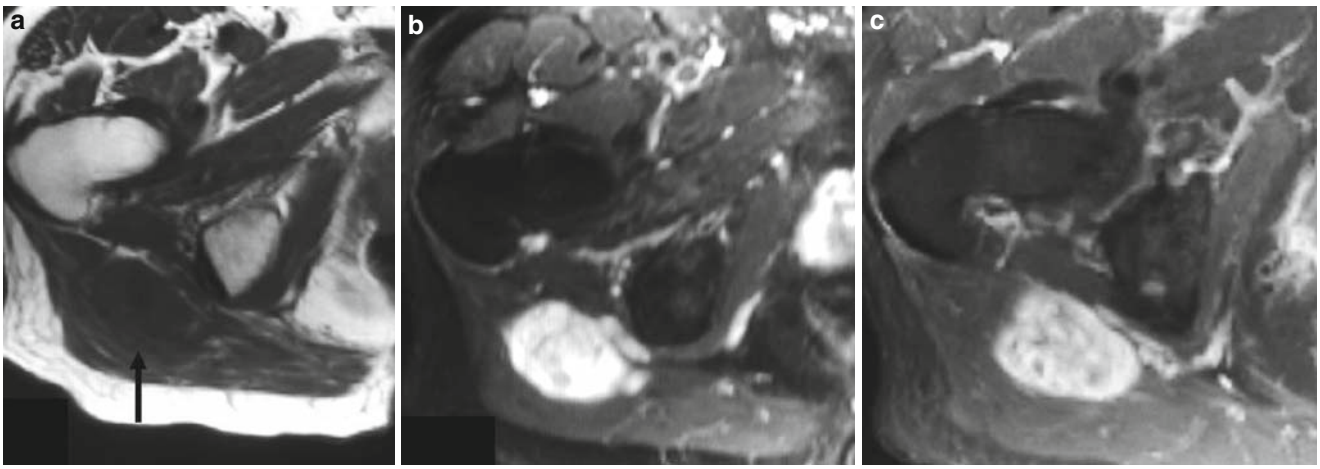

Fig. 8.11 Myxoid liposarcoma. (**a)** Axial T1WI image shows a uniformly low signal intensity mass (*arrow*) within the gluteus maximus muscle. (**b)** Corresponding fat-suppressed T2WI image shows heterogeneous high signal intensity in the mass. (**c)** Fat-suppressed T1WI image after intravenous administration of contrast shows heterogeneous high signal enhancement (case courtesy of Dr. William R. Reinus)

cases keloid-like collage deposition can be seen focally or even prominently.

Elastofibroma

Elastofibroma is a fibrous mass that typically arises at or near the inferior angle of the scapula. The patient may complain of vague scapular pain, a snapping or grinding sensation when they move their arm, or may have a frank mass on their back. The elastofibroma has soft tissue density on CT scanning, signal characteristics on MR imaging, and echogenicity characteristics sonographically all of which mimic muscle (Fig. 8.12). Some evidence suggests that these lesions are not true neoplasms but reactive lesions related to chronic friction of the scapula against the chest wall.

Surgical Pathology: The lesion is an ill-defined, rubbery white mass, characterized microscopically by hyalinized collagenous stroma and abundant large coarse, intensively eosinophic fibers that can be fragmented into variable lengths and globules. Elastic stain highlights a dense core and irregular serrated margins in these fibers.

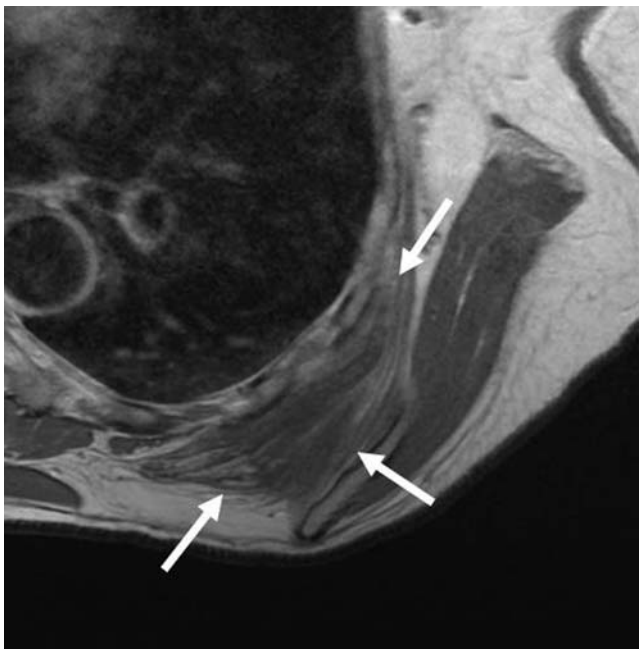

Fig. 8.12 Elastofibroma. Axial T1WI image through the scapular region shows a large heterogeneous mass (*arrows*) with a striated appearance similar to adjacent normal muscle

Myositis Ossificans

Myositis ossificans is a post-traumatic inflammation of the soft tissues that goes on to ossify. The name is actually a misnomer since the process usually occurs in the fascia between muscles rather than in the muscles themselves, and sometimes the trauma is so negligible as to not be remembered by the patient. In the first few weeks after trauma, the patient may complain of pain, and radiographs may show blurring of the fat plains around the lesion. MR imaging at this stage shows a mass-like process which is low signal intensity on T1-weighted images and heterogeneously high signal intensity on T2-weighted images with surrounding edema, mimicking a malignant soft tissue tumor, particularly in children in whom rhabdomyosarcoma is a consideration (Fig. 8.13). The extensive soft tissue edema surrounding myositis ossificans is a clue to the diagnosis, since other tumors have

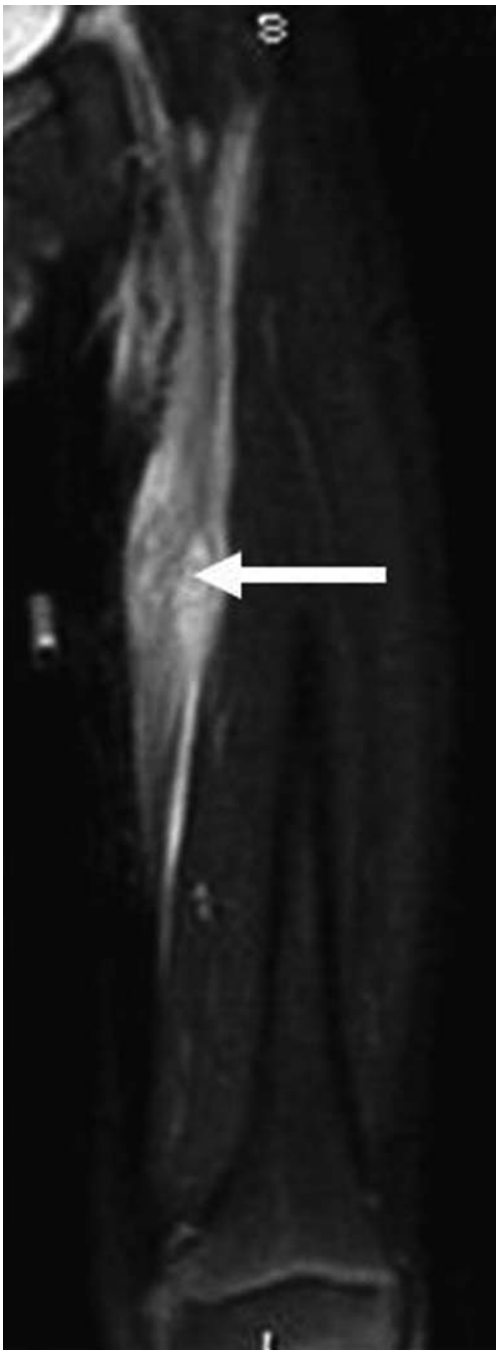

Fig. 8.13 Myositis ossificans. Coronal fat-suppressed T2WI image through the thigh of a teenager shows a central area of heterogeneous high signal intensity (*arrow*) with marked intramuscular edema proximally and distally

little if any surrounding edema. As the lesion matures over the ensuing 4–8 weeks, it develops faint peripheral mineralization and ossification, detected by CT scanning earlier than plain radiographs. The radiographic demonstration of the peripheral or "zonal" distribution of mineralization suggests the correct diagnosis. On MR imaging the mineralization will appear as peripheral foci of low signal intensity on all pulse sequences. Mature lesions have the signal intensity of fat on all pulse sequences and the natural history for these lesions is to slowly contract. Some lesions that are adjacent to long bones sometimes may appear to reabsorb into the bone.

Surgical Pathology: The histological features of myositis ossificans mirror the radiological features and show a prominent zonation with more mature reactive woven bone found peripherally and more immature fibroblastic-type tissue found centrally. A biopsy from the center of the lesion, therefore, taken out of context of the clinical and radiological findings can be incorrectly interpreted as a fibroblastic neoplasm or sarcoma.

Intermediate (Locally Aggressive)

Fibromatoses

The fibromatoses are a group of tumors composed of fibroblasts in a collagenous stroma, and are classified according to whether they are superficial or deep. They arise from fascia between muscles and from within muscles and have various appearances, none of which is characteristic. Some lesions may appear as discrete masses and some have a poorly defined, infiltrative appearance, but even the seemingly well-defined masses show microscopic invasion of the surrounding tissues. The MR signal intensity is also variable, depending on the histology, usually being heterogeneously low to intermediate signal intensity on T1-weighted imaging (T1WI) and heterogeneously high signal intensity on T2WI, but may also have high signal intensity on T1WI or may have low signal intensity on both pulse sequences (Fig. 8.14). Sonographically these lesions are usually heterogeneously hypoechoic.

Dupuytren fibromatosis is a superficial fibrotic process involving the flexor tendons of the hand. Dynamic sonography may show restricted motion of the tendons through the areas of fibrosis.

The plantar fibroma is a typically small mass that arises from the plantar fascia of the foot. The patient may complain of plantar foot pain, but if small, the mass will not be palpable. It is typically oval to fusiform in appearance and has low to intermediate signal intensity on all MR imaging pulse sequences, with prominent contrast enhancement (Fig. 8.15). Sonographically it is hypoechoic, with or without internal vascularity on Doppler imaging. When large, these fibromas rarely may extend deep to the plantar fascia and it is important to note if the fibroma has penetrated the fascia to involve the deep muscle compartments of the foot. When multiple plantar fibromas form, the disease is known as

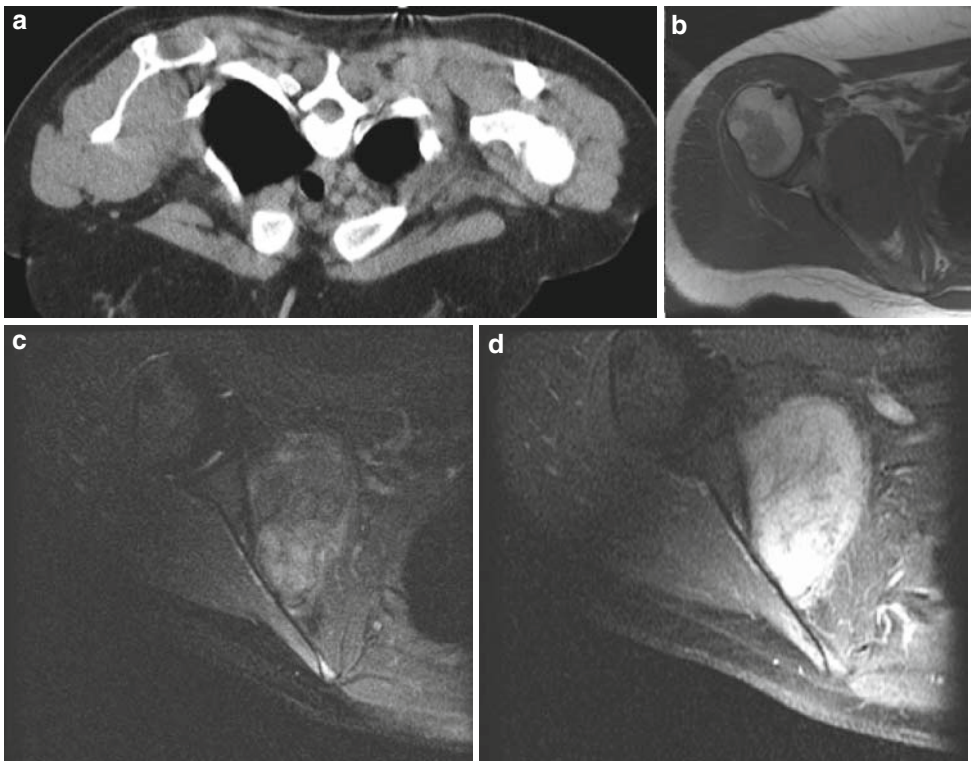

Fig. 8.14 Fibroma in a 41-year-old woman. Axial CT (**a**), T1W (**b**), T2W fat-saturated (**c**), and post-gadolinium T2W FS images show a well-circumscribed mass anterior to the scapula with moderately well-defined margins, low signal on T1W, higher heterogeneous signal on T2W and avid enhancement after gadolinium administration (case courtesy of Dr. William Reinus)

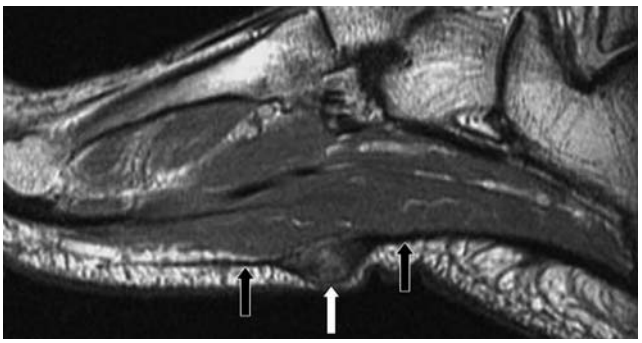

Fig. 8.15 Plantar fibroma. Sagittal proton density image shows a by and large low signal intensity mass with mild heterogeneity and higher signal (*white arrow*) within the plantar fascia (*black arrows*)

plantar fibromatosis or "Ledderhose disease." Some believe that it is related to Dupuytren contractures in the hand.

A desmoid tumor is an aggressive form of fibromatosis, most often encountered in early adulthood and more common in women. It is associated with the familial adenomatous polyposis syndromes, with up to one-third of patients with Gardner syndrome having desmoids. Outside of the abdominal cavity it arises from muscle or overlying fascia/aponeurosis, with the most common locations being the shoulder, back and chest wall, and proximal thigh/hip region. The musculature of the anterior abdominal wall is also a typical location. These tumors are usually large (up to 10 cm) and fusiform in shape, with partially ill-defined or stellate margins (Fig. 8.16). They tend to be isointense to muscle on T1WI and heterogeneously high signal intensity on T2WI sequences, and they enhance with intravenous contrast. These tumors are locally aggressive and invasive, and have a propensity for recurrence after surgery although a small percentage of theses tumors spontaneously regress. Their metastatic potential is small.

Surgical Pathology: The histologic hallmarks of fibromatoses are proliferation of bland and uniform fibroblastic-type stromal cells. These cells are typically spindle or fusiform in shape within a very characteristic wavy

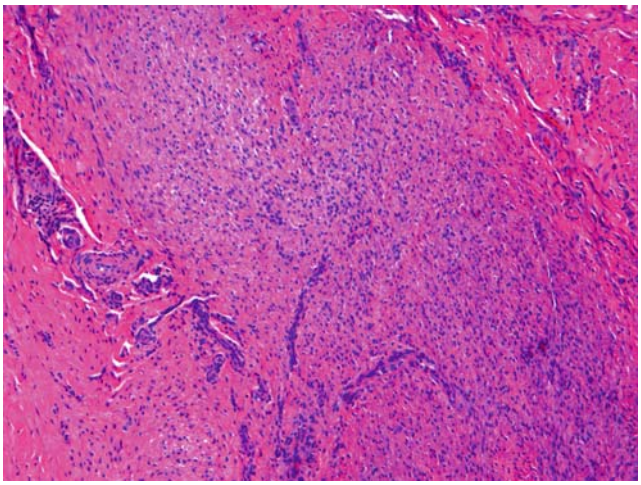

Fig. 8.15H Plantar fibromatosis showing a relatively hypocellular, cytologically bland fibroblastic proliferation

collagenous stromal matrix. Nuclear accumulation of beta-catenin has been reported by some authors within the lesional cells of deep fibromatosis but not superficial fibromatosis (Figs. 8.15H and 8.16H).

Malignant

Fibrosarcoma

Adult fibrosarcoma is a malignant tumor of fibroblasts representing approximately 5% of all soft tissue sarcomas. The majority of cases of fibrosarcoma involve patients between the ages of 40 and 70 years and usually arise in the proximal extremities, specifically the thigh and knee, or trunk. Clinical presentation is usually a painless mass. Fibrosarcomas typically appear on MR imaging as heterogeneous, predominantly low signal intensity lesions on T1WI, with variable enhancement after contrast administration, and a heterogeneous high signal intensity appearance on T2WI sequences. There are variants of fibrosarcoma, most often subcategorized based on the degree of myxoid components present. The presence of myxoid components often alters the imaging appearance of these lesions. Low-grade fibromyxoid sarcoma, for example, is a rare, slow-growing, malignant neoplasm often demonstrating intralesional variable-sized nodules both on ultrasound and MRI, with some of the nodules often exhibiting a "target-like" appearance. Similarly, myxoinflammatory fibroblastic sarcoma also demonstrates a central multinodular appearance within a fairly well-circumscribed mass lesion with heterogeneous enhancement pattern, post-contrast administration corresponding to areas of myxoid matrix (Fig. 8.17). Fibrosarcomas are seen as heterogeneous solid masses at sonography.

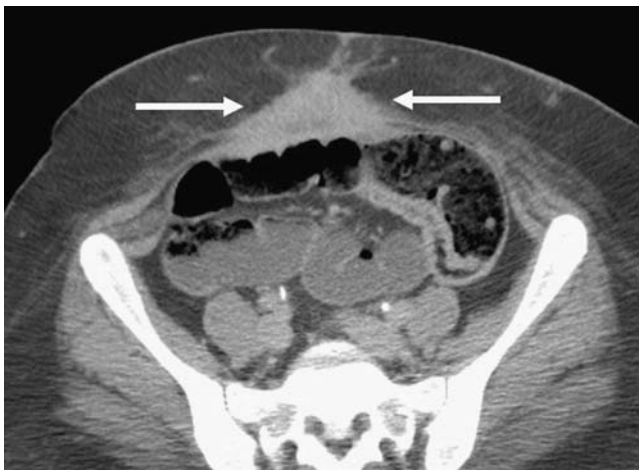

Fig. 8.16 Desmoid tumor. Axial CT scan through the lower abdomen shows a soft tissue mass (*arrows*) within the musculature of the interior abdominal wall with infiltration into the subcutaneous fat and musculature

Surgical Pathology: Fibrosarcoma is usually a solid white to tan firm mass. Histologically, it is composed of relatively uniform spindle cells characteristically arranged in fascicles running at different directions (Fig. 8.17H). At low magnification, a classic herringbone pattern is seen, with the groups of parallel running fascicles intersection at an angle. The tumor cells have fusiform and hyperchromatic nuclei with variable-sized nucleoli. Mitotic figures are frequent and necrosis is variable.

Immunohistochemically, fibrosarcomas are typically positive for vimentin and variably positive for smooth muscle actin. Immunostains are performed primarily to exclude other spindle cell sarcomas, such as synovial sarcoma or

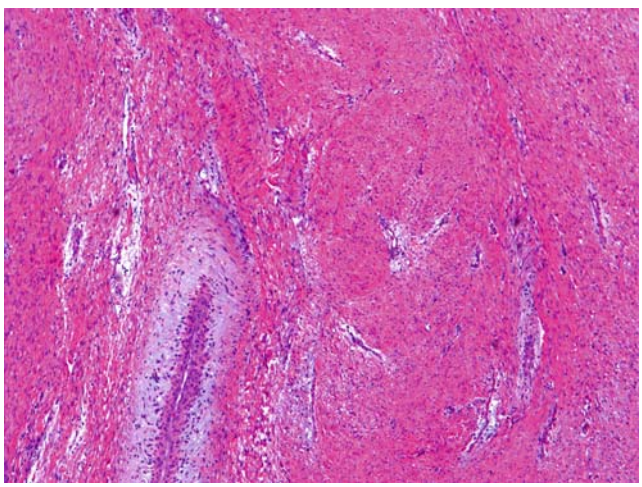

Fig. 8.16H Desmoid tumor (aggressive fibromatosis) showing hypocellular bland fibroblasts with collagenous background containing prominent vessels

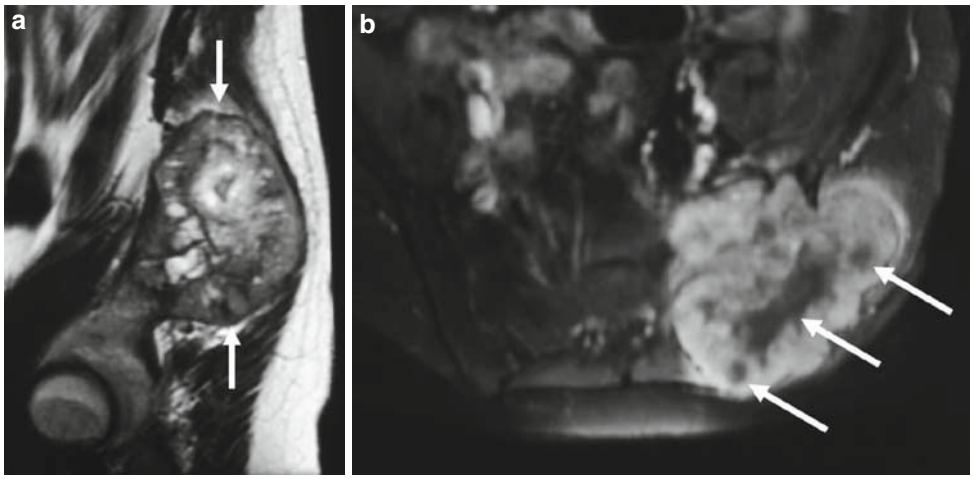

Fig. 8.17 Fibrosarcoma. (**a**) Sagittal T2WI MR image through the pelvis shows a large mass (*arrows*) arising from the gluteus maximus muscle with nodular heterogeneous high signal intensity. (**b**) Axial fat-suppressed T1WI image after the intravenous administration of contrast shows generalized high signal intensity enhancement with focal nodular areas of non-enhancing necrosis. The mass is destroying the ilium (case courtesy of Dr. William Reinus)

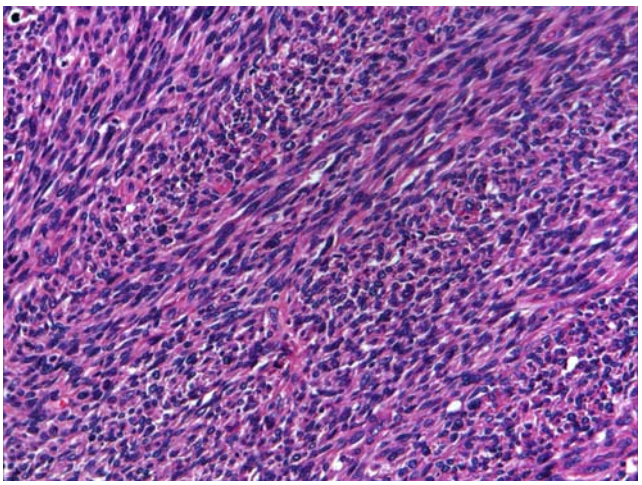

Fig. 8.17H A markedly hypercellular spindle cell proliferation with bland but mitotically active cells arranged in fascicles characteristic of a fibrosarcoma

malignant peripheral nerve sheath tumor, both of which may also have a focal herringbone pattern.

Fibrohistiocytic Lesions

Benign

Giant Cell Tumor of Tendon Sheath

Giant cell tumor of tendon sheath (GCTTS) is an idiopathic hypervascular proliferation of the synovium, histologically identical to pigmented villonodular synovitis (which occurs within joints), and it may represent a focal extra-articular form of the same disease. GCTTS tends to arise from tendon sheaths and most commonly occurs in the hands. The mass is usually less than 3 or 4 cm in size and on MR imaging has variable signal intensity on T2-weighted sequences depending on the amount of hemosiderin deposition within it (Fig. 8.18). This lesion may enhance strongly. Sonographically, GCTTS may appear as a homogeneous mildly echogenic mass with fine internal echoes and some degree of vascularity on color or power Doppler.

Surgical Pathology: The tumors are lobulated and circumscribed. Microscopically they have variable numbers of multinucleated giant cells, macrophages including foam cells, hemosiderin-laden macrophages, and mononuclear round or slightly spindled stromal cells. Mitoses may be occasional

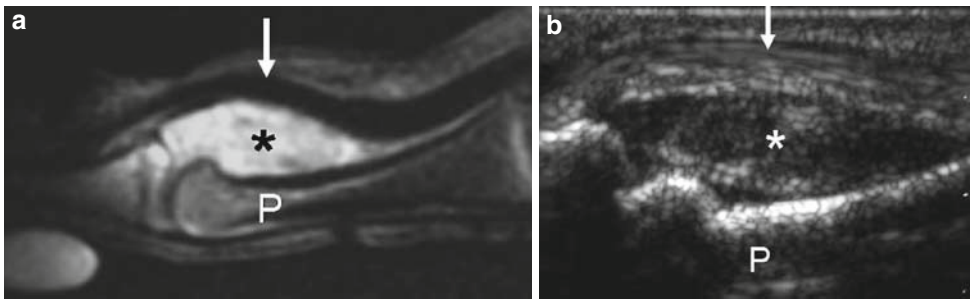

Fig. 8.18 Giant cell tumor of tendon sheath. (**a**) Sagittal fat-suppressed T2WI image of a finger shows a heterogeneously high signal intensity mass (∗) interposed between the flexor tendons (*arrow*) and the phalanx (P). (**b**) Corresponding longitudinal sonographic image shows a heterogeneously echogenic tumor (∗) between the flexor tendons (*arrow*) and phalanx (P)

or frequent. Necrosis is not usually seen. The mononuclear cells are often positive for CD 68 and smooth muscle actin. The multinucleate cells also express CD 68 and may express tartrate-resistant acid phosphatase, but immunostains are rarely needed for diagnosis. The diffuse type of giant cell tumor is also known as pigmented villonodular synovitis. Both lesions have shown a translocation t(1,2)(p11;q35-36); however, the diffuse type (PVNS) sometimes shows only trisomies of chromosome 5 and 7. The diffuse type of giant cell tumor may be difficult to completely excise surgically and recurrences are frequent.

Malignant

Malignant Fibrous Histiocytoma (Undifferentiated Pleomorphic Sarcoma)

Malignant fibrous histiocytoma (MFH) was first described in the early 1960s, but has now been reclassified as an undifferentiated pleomorphic sarcoma that has giant cell and inflammatory subtypes. It may merely represent a heterogeneous group of sarcomas that are not otherwise specified, rather than being a distinct entity. Two other previously described subtypes of MFH are now recognized as distinct entities and have been reclassified. The previous myxoid subtype of MFH has been reclassified into the fibroblastic/myofibroblastic category as myxofibrosarcoma and has a better prognosis than the other three types of MFH even though 35% of these lesions metastasize. The angiomatoid type of MFH found predominantly in children has been reclassified as a tumor of uncertain differentiation and is now called angiomatoid fibrous histiocytoma. MFH was formerly considered to be the most common type of malignant soft tissue tumor. The current counterpart undifferentiated pleomorphic sarcoma is not the most common, because of reclassification of lesions once called MFH.

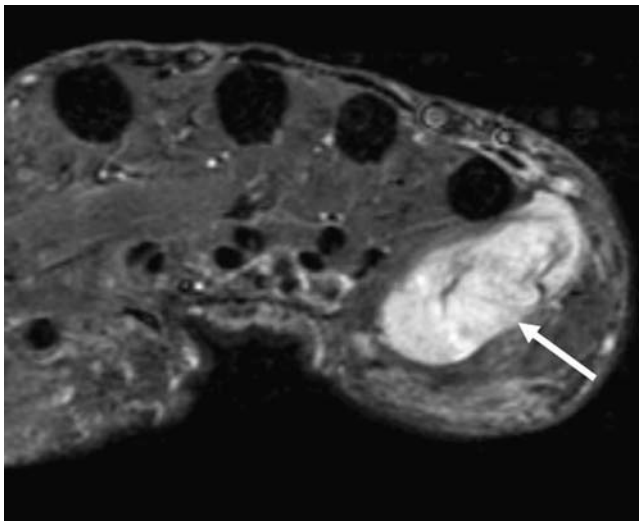

Fig. 8.19 Myxoid pleomorphic undifferentiated sarcoma (malignant fibrous histiocytoma). Axial fat-suppressed T2WI image through the hand shows a heterogeneously high signal intensity mass (*arrow*)

Pleomorphic sarcomas tend to arise from skeletal muscle, most commonly in the lower extremity, followed by the upper extremity, and retroperitoneum and are more common in men than women. Peak age of incidence is 50–70 years. They tend to be large tumors, on the order of 10 cm. Almost half the cases metastasize, usually to the lungs, and they have a propensity for local recurrence after resection. Metaplastic ossification may sometimes occur in the periphery of these lesions but in general they have a non-specific appearance on MR imaging of heterogeneous low signal intensity on T1-weighted sequences and heterogeneous high signal intensity on T2-weighted sequences (Fig. 8.19). They tend to be well defined due to a pseudocapsule and have adjacent edema that dissects up and down the affected muscle but which does not violate compartmental boundaries.

Surgical Pathology: The tumors tend to be large and heterogeneous on cut surface with necrosis and hemorrhage. Histologically, it is characterized by proliferation of

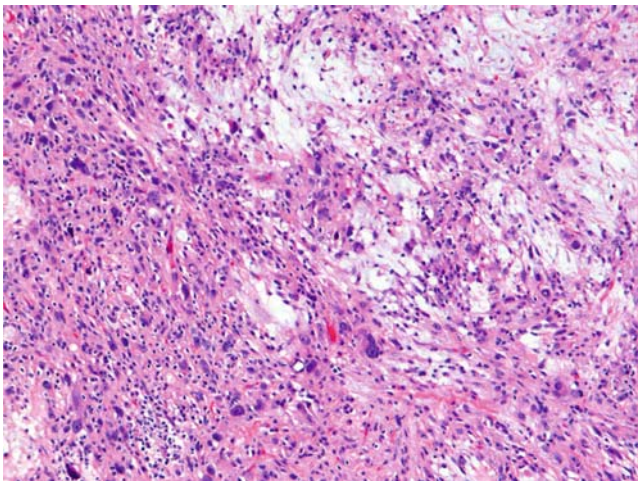

Fig. 8.19H Malignant fibrous histiocytoma/pleomorphic sarcoma showing a moderately cellular high-grade sarcoma with pleomorphic mononuclear giant cells in a background of spindle cells with a slightly storiform pattern. Xanthoma cells (histiocytes) are also seen

significantly pleomorphic neoplastic cells (Fig. 8.19H). The morphology of tumor cells ranges from spindle, polygonal, to bizarre giant mononuclear or multinucleated cells. Areas with more spindle cell features can show a storiform pattern. Many tumors also contain numerous osteoclast-like multinucleated giant cells (giant cell MFH) and some are overwhelmed by extensive inflammatory infiltrates composed of histiocytes, neutrophils, eosinophils, lymphocytes, and plasma cells (inflammatory MFH). The tumor cells usually are positive for vimentin and variably for CD68, neither of which is specific for pleomorphic undifferentiated sarcoma. Instead, the use of immunohistochemical staining is mainly to exclude other tumors in the differential diagnosis.

Dermatofibrosarcoma Protuberans

Dermatofibrosarcoma protuberans (DFSP) is a malignant fibrohistiocytic tumor arising from the dermis, typically occurring over the trunk, followed in frequency by the upper and lower extremities, of teenagers to middle-aged adults. It presents as slow-growing painless skin nodule, sometimes with discoloration and sometimes exophytic, and usually does not undergo imaging evaluation because of its typical clinical presentation. Small series of the MR imaging appearance of this tumor have been reported, describing a well-defined, albeit sometimes, irregularly shaped mass in the cutis and subcutaneous tissue, which is low to intermediate signal intensity on T1-weighted images, mixed to uniform high signal intensity on T2-weighted sequences, and patchy to homogeneous enhancement with contrast. These lesions rarely penetrate through the deep subcutaneous tissue and have a low propensity for metastasis, but can recur locally.

Surgical Pathology: DFSP is grossly tan-white and firm mass mainly centered in deep dermis and subcutaneous tissue. Histologically, the tumor is composed of monotonous fibroblast-like spindle cells arranged in uniform storiform pattern throughout the lesion with little intervening collagenous stroma. The tumor cells have slender nuclei and scant cytoplasm. One to five percent of the cases contain melanin pigment and these pigmented variants are called Bednar tumor. High-grade transformation (usually into a fibrosarcoma or pleomorphic sarcoma) occurs in small number of the cases, particularly in recurrent cases. The immunoprofile of DFSP is CD34 positive and Factor XIIIa and D2-40 negative.

Perivascular Tumors

Benign

Glomus Tumor

A glomus tumor is a benign lesion arising from elements of the neuromyoarterial glomus. These lesions usually are located about the distal phalanx in the hand but have also been found in the lower extremities and the pre-coccygeal soft tissues. Most subungual lesions occur in women between the ages of 20 and 40 years. Clinically, lesions present as a small red-blue nodule with point tenderness and occasional episodic radiating pain often caused by temperature changes. Rare cases of multiple glomus tumors (glomangiomatosis) are on record and are often associated with an autosomal dominant inheritance pattern.

Radiographic findings are usually limited to a non-specific soft tissue mass about the tuft of the digit, with associated extrinsic indolent erosion of the subjacent distal phalanx. On MR imaging, these lesions are typically homogeneously hyperintense on T2-weighted images and enhance fairly homogeneously after contrast administration. On ultrasound, glomus tumors have been described as typically hypoechoic. The vascularity of these lesions can also be demonstrated with color or power Doppler, further aiding in diagnosis.

Surgical Pathology: Glomus tumors are typically composed of glomus-like cells and variable amounts of vascular spaces. The glomus-like cells are uniform round to ovoid epithelioid cells which are considered to be modified smooth muscle cells. The tumor nuclei have bland chromatin pattern with absent or inconspicuous nucleoli. Mitotic activity is usually inconspicuous. The glomus-like cells form nests and trabeculae cuffing around thin-walled, capillary-sized

vessels. According to the proportion of these two components, glomus tumors can be subcategorized as solid glomus tumor and glomangioma. In some cases, cells with more smooth muscle differentiation are present and are referred to as glomangiomyoma. Tumors with large size (>2 cm), deep location, moderate to high nuclear grade, increased mitotic rate (>5/10 high-power fields), and presence of atypical mitotic figure are considered malignant. Tumors with only one of the above malignant features other than nuclear pleomorphism are considered as glomus tumors of uncertain malignant potential. Immunohistochemically, the tumors are positive for actin and vimentin.

Skeletal Muscle Tumors

Malignant

Rhabdomyosarcoma

Rhabdomyosarcoma is the most common malignant soft tissue tumor in children, but it can also occur in adults. In addition to a rapid growing mass, the clinical presentation of a rhabdomyosarocoma is usually related to mass effect on adjacent organs and structures. While it arises from skeletal muscle, its most common location in children is actually in the head and neck and around the urinary bladder in the space of Retzius. In adults, these tumors occur in the extremities where they appear as an intramuscular mass (Fig. 8.20). Histologically, there are three subtypes: (1) embryonal, occurring most frequently in children; (2) alveolar, occurring in older children and young adults; and (3) pleomorphic, occurring in adults. The lesions tend to have a non-descript aggressive appearance on MRI with poorly defined margins and heterogeneous low signal intensity on T1-weighted sequences and heterogeneous high signal intensity on T2-weighted sequences.

Embryonal rhabdomyosarcoma accounts for three-fourths of all rhabdomyosarcomas and primarily occurs in children younger than 15 years old. It typically affects the head and neck region, paratesticular area, urinary tract, and biliary tract. There are two variants of embryonal rhabdomyosarcomas: botryoid and spindle cell variants. Botryoid type occurs in mucosa of the head and neck, biliary tract, and urinary tract of young children. Spindle cell rhabdomyosarcomas are rare and typically occur in the scrotal soft tissue and may occur in the head and neck or as a pleuro-pulmonary blastoma of the lung.

Alveolar rhabdomyosarcoma most commonly occurs in deep soft tissue of limbs, and less commonly in paranasal sinuses, paraspinal, and perineal regions. It can occur at all ages but are seen more often in older children or young adults.

Pleomorphic rhabdomyosarcoma is extremely rare and occurs almost always in adults older than 45 years old. In order to diagnose this variant, other sarcomas with rhabdomyoblastic differentiation must be excluded. It usually affects the deep soft tissue of the lower extremities.

Surgical Pathology: Rhabdomyosarcomas are poorly circumscribed, fleshy and tan mass. Embryonal rhabdomyosarcomas show a diverse histologic appearance. The tumor cells can be round, spindle and/or strap shape with hyperchromatic and vesicular nuclei. The cytoplasm of the tumor cells can be scant and amphophilic to abundant fibrillary eosinophilic dependent upon the degree of myoid differentiation. Many untreated embryonal rhabdomyosarcomas are dominated by primitive undifferentiated round rhabdomyoblasts with rare strap cells or cells with cross-striation. Tumor cells are usually arranged haphazardly with alternating hypercellular and myxoid hypocellular zones. After treatment (chemotherapy), however, the tumor cells tend to show maturation into a more myoid differentiation.

Botryoid rhabdomyosarcoma presents as a polypoid mass on the mucosal surface. Histologically, it is composed of round to spindle rhabdomyoblasts with a more myxoid and hypocellular pattern except the submucosal region where there is increased cellularity (cambium layer). Spindle cell variant is composed of monotonous spindle rhabdomyoblasts arranged in whorls or fascicles. The spindle rhabdomyoblasts are typically fusiform with moderate amount of bright eosinophilic cytoplasm sometimes with cross-striation.

Alveolar rhabdomyosarcoma is typically a round cell sarcoma characterized by an alveolar growth pattern. The alveolar pattern is resulted from loss or lack of extracellular matrix within a nest of round rhabdomyoblasts. Sometimes this characteristic alveolar pattern is not apparent in some tumors which show solid sheets or nests of tumor cells and are referred to solid variant of alveolar rhabdomyosarcoma. In rare cases, mixed typical alveolar pattern and embryonal features are seen.

Pleomorphic rhabdomyosarcoma is characterized by numerous large and pleomorphic rhabdomyoblasts which can be globoid, spindle, and tadpole in shape with hyperchromatic nuclei and abundant eosinophilic cytoplasm. Although the tumor cells have a rhabdoid appearance in general, cross-striation is extremely hard to find and identification of striated muscle differentiation usually requires either ultrastructural examination or immunohistochemical evaluation.

Immunohistochemically, rhabdomyoblastic cells are positive for myogenic markers, such as desmin, common muscle actin myoD, myogenin, and myoglobin. Myogenin staining pattern is usually diffuse in alveolar rhabdomyosarcoma and spotty in embryonal rhabdomyosarcomas. Alveolar rhabdomyosarcomas have a characteristic and diagnostically

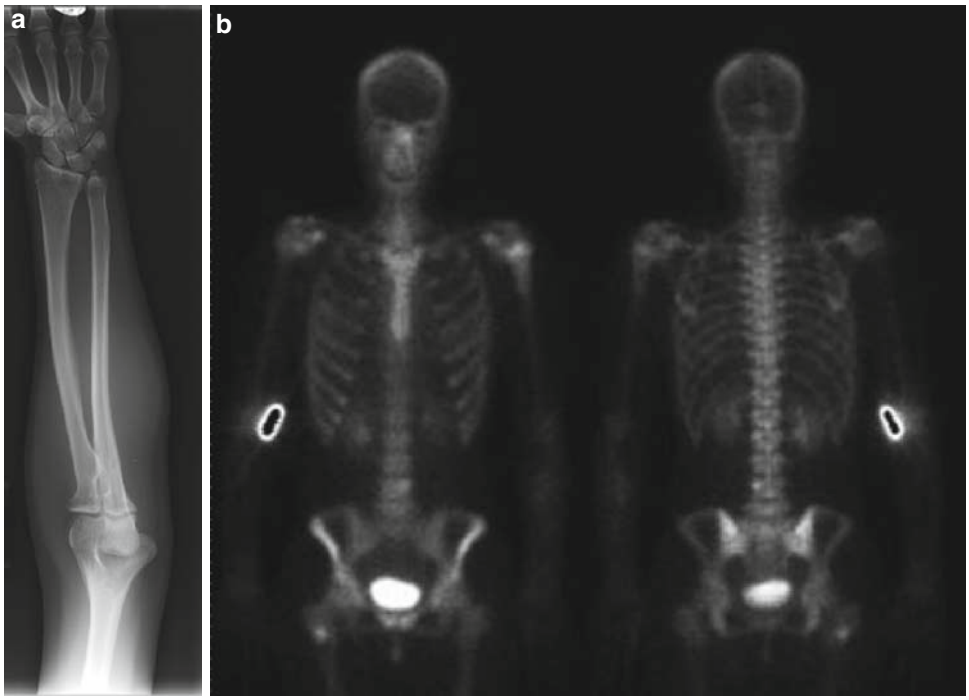

Fig. 8.20 Embryonal rhabdomyosarcoma in a 25-year-old woman. Anteroposterior plain radiograph (**a**) shows a well-delineated soft tissue mass in the forearm. The bone scan (**b**) shows abnormally increased uptake in the mass (case courtesy of Dr. William Reinus)

useful cytogenetic profile. The t(2;13)(q35;q14) translocation can be cytogenetically detected in approximately 60% of alveolar rhabdomyosarcoma. This translocation juxtaposes the *Pax3* gene on 2q35, a transcription factor functional during early neuromuscular development, to *FKHR* gene (*FoxO1A*) on 13q14, a member of the forkhead family of transcription factors A less common variant of the translocation, fusing *Pax7* gene, located on 1p36, to *FKHR*, and resulting in a t(1;13)(p36;q14) translocation, has also been associated with alveolar rhabdomyosarcoma. A third t(2;2)(q35;p23) translocation fusing *Pax3* to *NCOA1* (nuclear receptor co activator) gene has also been recently identified.

Vascular Tumors

Benign

Hemangiomas and Arteriovenous Malformations

Vascular malformations can be classified as venous, cavernous, or capillary hemangiomas and arteriovenous malformations. Lesions can also be classified as high or low flow, depending on their arterial feeding vessels. Vascular malformations are usually located in either the subcutaneous tissue or within muscles, and less commonly in the intermuscular fascia or even the synovium of joints. If they are subcutaneous, they may discolor the overlying skin. Patients may present with pain, if the mass is deep-seated, or with a palpable mass that may mildly wax and wane in size. Soft tissue hemangiomas are the most common soft tissue tumor of infancy and childhood.

The diagnosis of cavernous hemangioma or AV malformation can be made when phleboliths are visible on radiographs, present in up to 30% of cases (Fig. 8.21a, b). Sonography shows the serpiginous vascular channels and power Doppler demonstrates flow within them; the phleboliths are echogenic with posterior acoustical shadowing.

MR imaging of cavernous hemangiomas shows a typical lace-like or lobulated appearance of interposed high signal intensity fatty elements and low signal intensity vascular elements on T1WI sequences whose appearance sometimes has been likened to a "bag of worms." Capillary hemangiomas have a more uniform and solid appearance on both MR imaging and sonography since the vascular channels are smaller and these lesions tend not to have visible fat. Calcified phleboliths may be seen on MR imaging as oval signal voids. Gradient echo imaging may show blooming from hemosiderin deposition as well as accentuating the presence of small phleboliths while 3D-MR angiography is helpful for identifying areas of vascular flow. Rarely, soft tissue hemangiomas may display fluid–fluid levels, probably because of

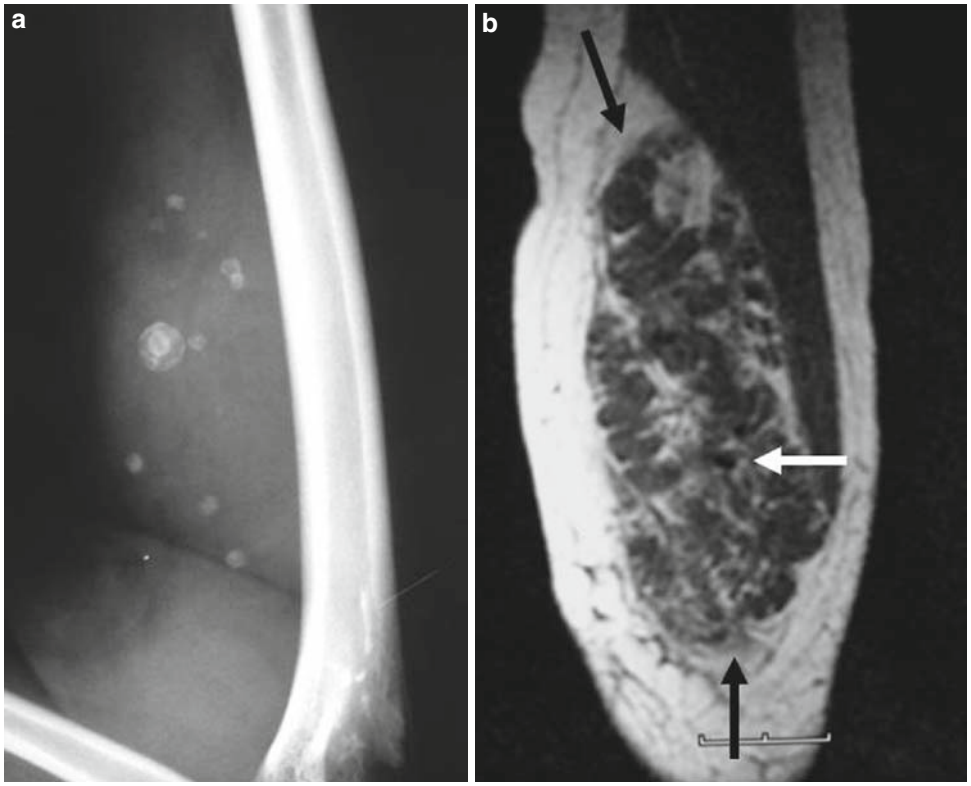

Fig. 8.21 Soft tissue hemangioma. (**a**) Lateral radiograph of the arm shows numerous phleboliths of varying size associated with a soft tissue mass. (**b**) Corresponding longitudinal T1WI MR image through the arm shows a large mass (*black arrows*) with a "bag of worms" serpiginous mixture of fatty and vascular elements. One of the phleboliths (*white arrow*) is visualized as a focal area of low signal intensity

Table 8.2 Fluid–fluid levels

Benign
Hematoma
Hemangioma
ABC of soft tissue
Malignant
Synovial sarcoma
Angiosarcoma
Myxofibrosarcoma
Sarcoma not-otherwise-specified

sluggish flow with pooling of blood and consequent layering of red cells. This finding is non-specific, however, since it may be found in as many as 3% of soft tissue tumors and bone tumors, including both benign and malignant processes (Table 8.2). Benign soft tissue hemangiomas may violate anatomic compartmental boundaries.

Surgical Pathology: Hemangiomas may be of the capillary or cavernous type (Fig. 8.21H). Both show vessels or vascular spaces lined by cytologically bland and mitotically quiescent endothelial cells. Immunohistochemically, markers such as CD 31, CD 34 and Factor VIII related antigen are expressed by the lesional cells lining the vascular spaces. In lymphangiomas D2-40 (podoplanin) is also positive. Sometimes the lesions occur in a characteristic location (intramuscular angiolipoma and synovial hemangioma) or show a characteristic morphology (lobular capillary hemangioma or pyogenic granuloma), epitheloid hemangioma or spindle cell hemangioendothelioma (which was previously thought to be of borderline malignancy and hence the designation of hemangioendothelioma rather than hemangioma). Rare cases show a diffuse involvement (angiomatosis) which can pose considerable difficulties in the surgical management. Arteriovenous malformations are composed of twisted or tangled medium or large caliber vessels and abnormal veins with a thickened intima and media.

Intermediate

Several new entities are recognized as vascular tumors of intermediate malignancy including tufted angioma (kaposiform hemangioendothelioma), retiform hemangioendothelioma (hobnail hemangioendothelioma), papillary intralymphatic angioendothelioma (PILA or Dabska tumor), composite hemangioendothelioma, polymorphous hemangioendothelioma, and giant cell angioblastoma. Differentiating radiological characteristics of these lesions, other than identification of tubular, serpentine vessels that can suggest the diagnosis of an angiomatoid tumor, are insufficient to

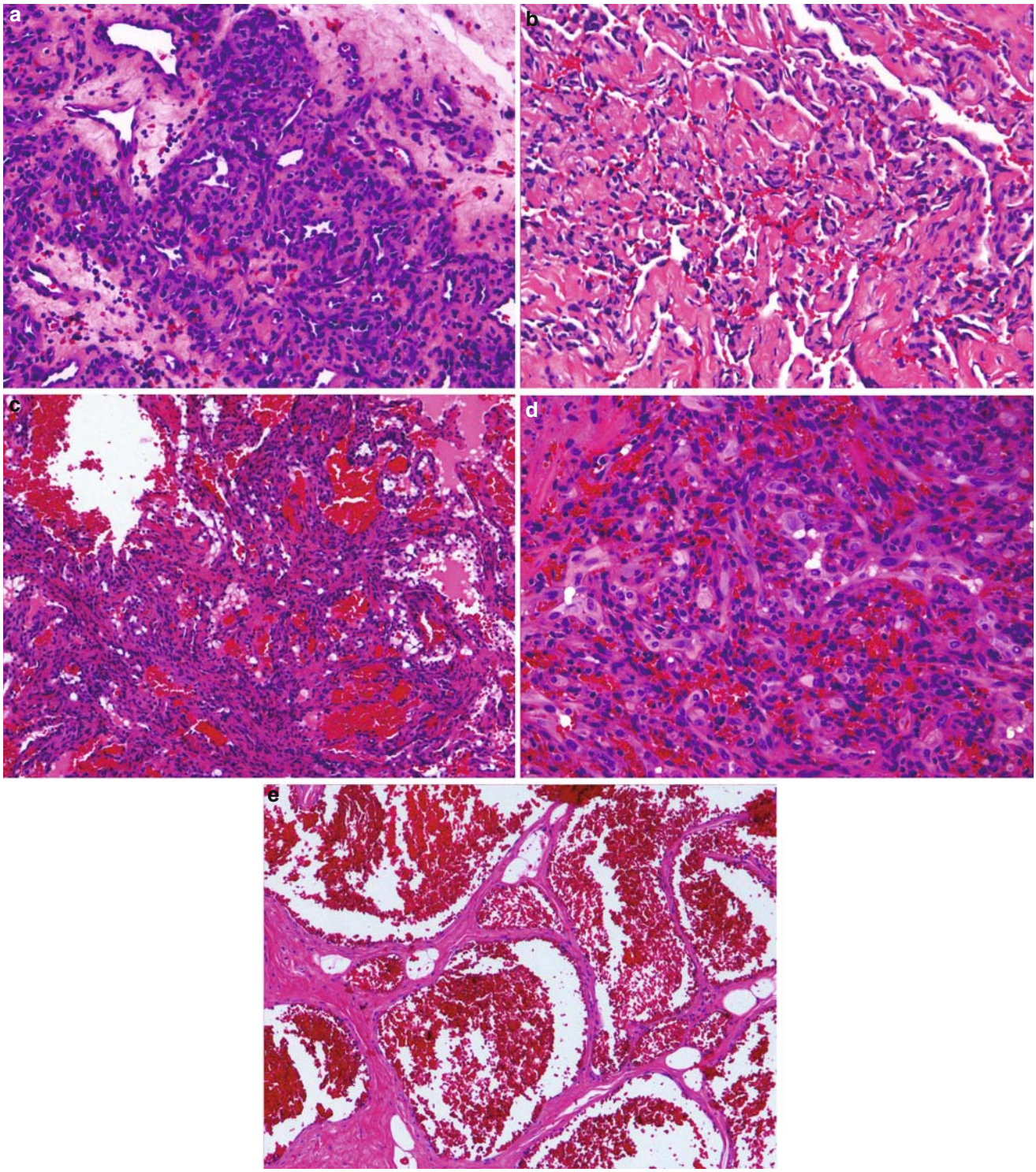

Fig. 8.21H (**a**) Capillary hemangioma showing growth of benign capillary vessels in a lobular pattern. (**b**) Masson hemangioma showing the characteristic papillary endothelial proliferation around fibrinoid cores. (**c**) Spindle cell hemangioma showing bland spindle cells between the well-formed vein-like vascular spaces. (**d**) Epithelioid hemangioma showing small vascular spaces lined by epithelioid endothelial cells with rich inflammatory cells. (**e**) Cavenous hemangioma showing relatively uniformed, packed thin-walled large vascular spaces filled with blood

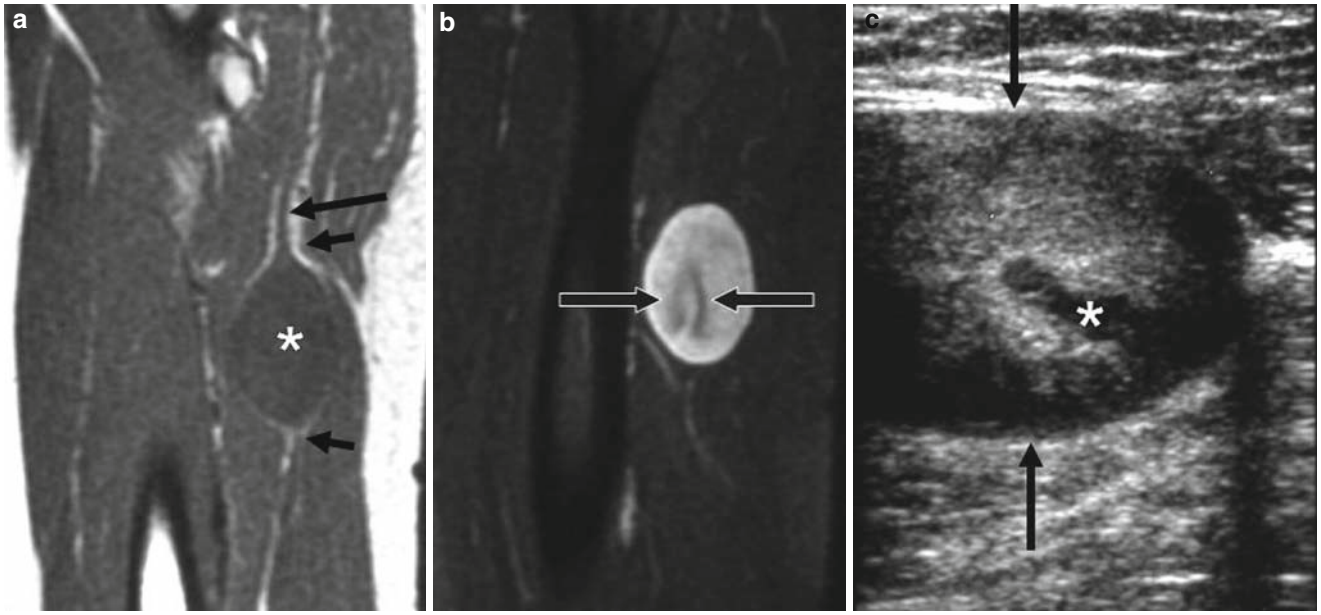

Fig. 8.22 Benign peripheral nerve sheath tumor. (**a**) Sagittal T1WI image through the thigh shows a fusiform tumor (∗). The sciatic nerve (*large arrow*) can be seen entering the mass proximally. The "split fat" sign is present proximally and distally (*short arrows*). (**b**) Corresponding fat-suppressed T2WI MR image shows the heterogeneous high signal intensity appearance of the mass with a central low signal intensity "target sign" (*arrows*). (**c**) Corresponding longitudinal sonographic image shows the heterogeneously echogenic mass (*arrows*) with a central hypoechoic target (∗) with surrounding mild hyperechogenicity

merit discussion. Frequently, these tumors arise multifocally. Generally, the literature suggests that sonography shows a heterogeneous lesion, with central anechoic spaces thought to represent areas of hemorrhage. The ability to demonstrate arteriovenous shunting with duplex Doppler ultrasound indicates that the tumor is a vascular lesion.

Kaposi Sarcoma

Kaposi sarcoma (KS), first described in the middle of the nineteenth century, is a multicentric malignant vascular tumor of unknown etiology arising from endothelial cells. Lesions arise in the oral mucosa, skin, lymph nodes, GI tract, lungs, liver, spleen, and bone. Four clinical patterns of this disease occur: classical, African-endemic, AIDS-related, and the iatrogenic form (seen in post-transplant patients or those undergoing immunosuppressive therapy). All forms of this sarcoma have been shown to be associated with herpesvirus 8 infection.

Classical KS, found predominantly in men of Eastern European and Italian ancestry, is the most benign form. Patients generally die from unrelated causes. The African-endemic form of the disease is more aggressive. Patients have cutaneous lesions that may extend to the deep soft tissues and also invade bone. AIDS-related Kaposi sarcoma of soft tissue and bone is the most common neoplasm in the HIV-positive population, ultimately developing in 25–30% of AIDS patients. The MR imaging appearance of KS is nonspecific, with low signal intensity on T1WI and high signal intensity on T2WI.

Surgical Pathology: The histologic features of KS are the same in all four forms. In early stage (patch stage) skin disease, there is a subtle increase in slightly irregular vascular channels. The endothelial cells lining the vascular spaces are flat with little atypia. There are variable numbers of poorly formed vascular channels recognized as slit-like spaces lined by attenuated or spindle endothelial cells in a dissecting pattern of growth in dermis. Variable numbers of lymphocytes, plasma cells, and extravasated red blood cells are seen around the vascular or slit-like spaces. In the later plague stage, the histologic features of the patch stage become exaggerated. The lesion is usually slightly raised and the slit-like spaces and spindle cell component of the lesion become more obvious. There are more siderophages and hyaline globules as a result of red blood cell destruction. Finally, the lesion develops into a nodular stage that is characterized by even more dominant slit-like spaces and spindle cell proliferation in intersecting fascicles. The lesional cells show mild nuclear pleomorphism and frequent mitotic figures. The spindle cells and endothelial cells of the KS are positive for lymphatic endothelial markers, such as D2-40 (podoplanin) in addition to CD34 and CD31. The lesional cells are also positive for HHV-8.

Malignant

Angiosarcoma

Angiosarcoma is a rare but aggressive soft tissue tumor. While most other aggressive soft tissue sarcomas arise from the deep muscle compartments of the extremities, angiosarcoma tends to involve the skin and superficial soft tissue. Deep tumors, however, can be seen as can visceral tumors, such as angiosarcoma of breast, body cavity, lung, liver, or spleen. An association between radiation, chemicals such as Thorotrast, arsenic, and vinyl chloride as well as chronic lymphedema and development of angiosarcomas has been reported. In addition, angiosarcoma is one of several tumors that can produce a phosphaturic peptide and so present with oncogenic osteomalacia as an associated paraneoplastic syndrome.

Radiographically, soft tissue calcifications and erosion of subjacent bone can occur but are uncommon. Similar to other vascular lesions, sonography shows a heterogeneous lesion with central anechoic areas due to hemorrhage, and Doppler imaging can identify areas of arteriovenous shunting.

MR imaging may show serpentine blood vessels and the signal characteristics of these vessels can be either low signal intensity or high signal intensity on T2WI images depending on the speed of blood flow. Angiosarcomas may have fluid–fluid levels, and foci of fat are notably absent in more aggressive lesions. Angiosarcomas enhance heterogeneously after gadolinium administration, and dilated vascular spaces may show persistent enhancement in the delayed phase due to blood pooling.

Surgical Pathology: Angiosarcoma is typically composed of irregular anastomosing vascular channels lined by atypical endothelial cells. The tumor is characterized by a dissecting growth pattern. The endothelial cells may form intraluminal tufts and papillary proliferations. Mitotic figures are present but not always numerous. In some very well-differentiated angiosarcomas, the histologic appearance might simulate that of hemangioma. In these cases, the histologic feature that distinguishes angiosarcoma from hemangioma is infiltrative growth at low magnification. When the lesion is less differentiated, the neoplastic endothelial cells become more epithelioid or more spindled with less or no vascular channel formation. Nuclear pleomorphism and mitotic figures are more obviously apparent. In very poorly differentiated lesions there are scant vascular channels. In some cases cells with intracytoplasic lumina sometimes containing red blood cells might be the only evidence suggestive of endothelial origin of the tumor. Endothelial markers such CD34, CD31, and Factor VIII-related antigen are positive in majority of the well-differentiated cases and only variably positive in poorly differentiated cases. Some angiosarcomas are also positive for D2-40 suggesting a lymphatic endothelial differentiation in these cases.

Peripheral Nerve Sheath Tumors

Benign

Benign peripheral nerve sheath tumors include Schwannomas (also called neurilemmomas) that arise from the Schwann cells that surround nerve axons and benign tumors of the axons called neurofibromas. These two types of tumors often are not able to be differentiated from each other with imaging, although the Schwannoma theoretically has an eccentric location and the neurofibroma has a central location relative to the nerve axon. When small, these lesions have a non-specific appearance on MR imaging, consisting of low to intermediate signal intensity on T1WI sequences that becomes usually uniform high signal intensity on T2WI sequences. Larger lesions may demonstrate a central longitudinal "target" or "sickle" sign of centrally located low signal intensity within a high signal periphery on T2WI, reflecting the histologic composition of Antoni A and Antoni B fibers. The tumors will enhance with gadolinium contrast with varying homogeneity, depending on their size. Sonographically they appear as a well-circumscribed echogenic mass, with or without a sonographic target sign, or as a hypoechoic mass with posterior acoustic enhancement, mimicking a cyst but Doppler imaging will demonstrate internal vascularity. The clue to the correct diagnosis with either MR imaging or sonography is that these tumors occur in the expected course of a nerve, with or without demonstration of a nerve entering and exiting the mass on either end of it (Fig. 8.22). Benign neurogenic tumors may also demonstrate a "split fat" sign on MR imaging, representing the splaying of intermuscular fat at the proximal and distal aspects of the tumor. The term "ancient Schwannoma" refers to a Schwannoma that exhibits calcification and cystic necrosis.

Most neurogenic tumors occur as isolated events, but there are two distinct clinical and genetic syndromes in which neurogenic tumors are a major feature. Type 1 neurofibromatosis ("peripheral" NF or "Von Recklinghausen disease") is due to a defect in chromosome 17. The disease is autosomal dominant, but up to half of all cases result from a spontaneous mutation, and it is present in as many as 1 in 3,000 live births. These patients may have multiple individual neurofibromas or may have large sheet-like "plexiform neurofibromas," which can run in a lumpy fashion along the course of the nerve and may insinuate into muscle (Fig. 8.23). Plexiform neurofibromas may have a heterogeneous appearance on MR imaging, particularly when large, and have reported

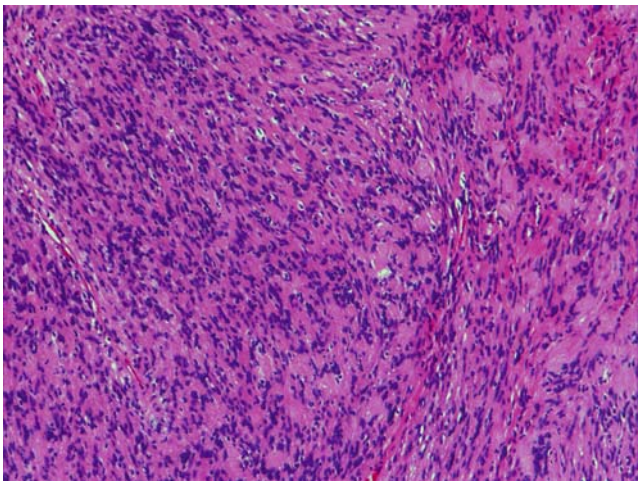

Fig. 8.22a Schwannoma showing typical Verocay bodies

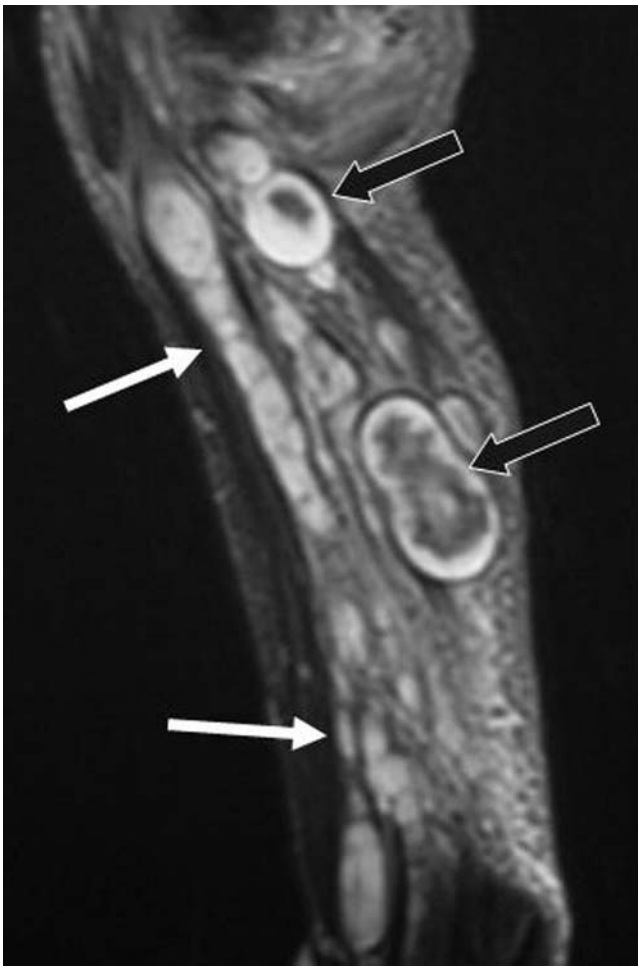

Fig. 8.23 Neurofibromatosis (NF1). Sagittal fat-suppressed T2WI MR image through the thigh shows plexiform neurofibromas (*white arrows*). Some of the neurofibromas have target signs (*black arrows*)

incidences of 5–15% of malignant degeneration into malignant peripheral nerve sheath tumors, particularly when they are located within the retroperitoneal space.

Other features of the NF-1 involve the skin, eyes, and skeleton. The cutaneous manifestations are freckling in the axilla and groin and cafe-au-lait spots. These spots have smooth borders (coast of California), in contrast to the irregular margins (coast of Maine) of the cafe-au-lait spots of McCune–Albright syndrome in fibrous dysplasia. To be considered as potentially having NF-1, the adult patient must have six or more spots measuring 15 mm or more in diameter. Prepubescent patients must only have six or more lesions larger than 5 mm in diameter. Ocular involvement includes optic gliomas and "Lisch nodules" which are hamartomas of the iris.

The gamut of skeletal involvement in NF1 extends from the head to the legs: absence of the greater and lesser wings of the sphenoid cause the "harlequin" appearance of the face on AP radiographs; the ribs may be thin and twisted ("ribbon" ribs) or may have indentations along their inferior aspects due to pressure by adjacent neurofibromas; the spine may have a sharp-angled scoliosis, scalloping of the posterior aspects of the vertebral bodies, or enlargement of the neural foramina due to "dumb-bell" shaped neurofibromas within them; the tibia may have anterior bowing or a pseudarthrosis, and the fibula may be hypoplastic or absent.

"Central" neurofibromatosis (NF-2) patients have a deletion of a portion of chromosome 22 and frequently develop bilateral acoustic Schwannomas. These patients rarely develop neurofibromas and may have multiple Schwannomas elsewhere as well as a high incidence of meningiomas and ependymomas. Recently, some have proposed changing the name of this entity to Schwannomatosis or MISME syndrome. The latter is an acronym for multiple inherited Schwannomas; meningiomas, and ependymomas. These patients also have a higher incidence of gliomas than the general population.

Surgical Pathology: Schwannoma is usually an encapsulated mass eccentrically associated with a nerve. Histologically, it is composed of nodular or multinodular growth of spindle cells that have angulated or comma-shaped nuclei with fine chromatin, and ill-defined eosinophilic fibrillary cytoplasm. The cellularity alternates from areas to areas with variable myxoid to hyaline stromal changes. In the cellular areas (Antoni A areas), the cells are arranged in short fascicles, swirls and/or palisading pattern (Verocay bodies) (Fig. 8.22H). The hypocellular areas (Antoni B areas) are characterized by myxoid and variable fibro/hyaline stroma. Various degenerative/reactive changes, such as hemorrhage, hemosiderin deposition, organizing thrombi, inflammatory infiltrate, xanthomatous infiltrate, pseudocyst formation, calcification, necrosis, hyalinized thick-walled vessels, and presence of pleomorphic and hyperchromatic nuclei are commonly seen. Lesions with uniformly hypercellular areas

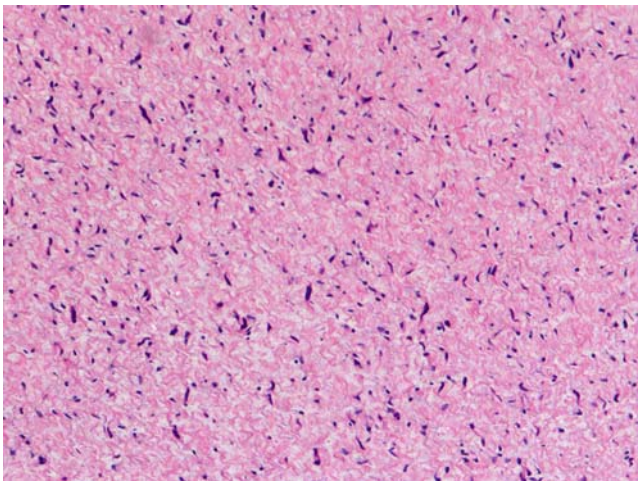

Fig. 8.23H Neurofibroma showing a proliferation of cells with a wavy nucleus in a slightly fibrillary eosinophilic background

without Antoni B areas are called cellular Schwannoma. Although mitotic activity is very scant in conventional Schwannoma, increased mitotic activity is common in cellular Schwannoma. However, there are no atypical mitotic figures or significant nuclear atypia. Immunohistochemically, Schwannoma is strongly positive for S100, D2-40, and NSE but negative for neurofilament.

Neurofibromas can be an encapsulated fusiform mass (localized neurofibroma) or a plexiform mass (plexiform neurofibroma) derived from a nerve. It can also show diffuse growth without capsule (diffuse neurofibroma). Histologically, it is proliferation of Schwann cells, fibroblasts, and perineurial cells in fascicular, whorling, storiform, and/or haphazard pattern. Concentric structures resembling pacinian bodies are seen in some cases (pacinian neurofibroma). The Schwann cells are admixed with numerous fibroblast-like spindle cells in abundant fibrocollagenous stroma with variable myxoid, inflammatory or xanthomatous change. In plexiform neurofibroma, the nerve sheath proliferation is primarily confined within the perineurium of numerous disorganized nerve fascicles. Scattered hyperchromatic pleomorphic cells and increased cellularity (cellular neurofibroma) are seen in some cases, however, mitotic activity is rare or absent. Immunohistochemically, the Schwann cells in neurofibroma are positive for S100. Entrapped axons, if present, are positive for neurofilament.

Malignant

Malignant peripheral nerve sheath tumors (MPNST) most often arise from malignant transformation of plexiform neurofibromas in type 1 neurofibromatosis. Previous radiation therapy is the second most common cause of transformation of neurofibroma to neurofibrosarcoma. Malignant neurofibrosarcomas arising from benign neurofibromas tend to be larger than their benign counterparts, tend to lack the target sign and split-fat sign, and may have surrounding soft tissue edema.

Surgical Pathology: MPNST usually is a circumscribed nodular/multinodular mass with pseudocapsule. The cut surface is grey-tan with variable necrosis and hemorrhage. The tumor may arise from a nerve trunk or a pre-existing neurofibroma, the residua of which can be seen in some but not all cases. Histologically, high-grade MPNST exhibits various morphologies but little peripheral nerve sheath differentiation while low-grade lesions can show features bordering with cellular Schwannoma and cellular neurofibroma but with more significant cellular crowding, larger nuclei, and hyperchromasia. More typically, it is composed of proliferating oval to spindle cells with nuclei that are wavy or angulated with tapered ends and a coarse chromatin pattern. The cells have a scant to moderate amount of weakly eosinophilic, poorly defined cytoplasm and grow in fascicles, whorls, or rarely rosettes, and they may show a palisading pattern. The cellularity varies sharply from area to area. Mitotic activity is high with variable numbers of atypical mitotic figures. Geographic necrosis is common with perivascular tumor preservation in high-grade lesions. A hemangiopericytomatous vascular pattern can be seen focally. Pleomorphism is not a common feature but can be seen focally. Various divergent differentiation, such as osteogenic, chondroblastic, rhabdomyoblastic, vascular, and epithelial differentiations can be seen in some tumors. MPNST with rhabdomyosarcomatous differentiation is called malignant Triton tumor. The tumor cells can also become epithelioid focally or diffusely (epithelioid MPNST). Unlike benign nerve sheath tumors, the MPNSTs are either negative or only focally positive for S100. The tumor can also react with various markers related to its divergent differentiation. Epithelioid variant can show focal to diffuse cytokeratin reactivity. Melanocytic markers, such as HMB45 and melan-A are usually negative.

Tumors of Uncertain Differentiation

Benign

Intramuscular Myxoma

Myxomas are composed of scattered spindle-shaped fibroblasts in a very myxoid stroma. Excluding so-called cardiac myxomas (likely a separate entity), they most commonly occur in the appendicular skeletal muscle, usually of the

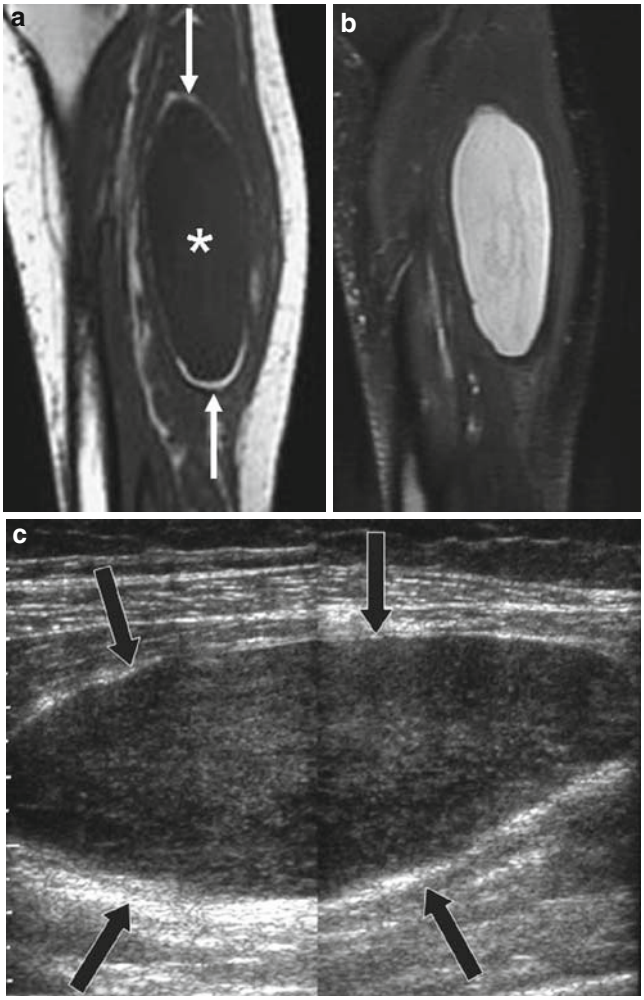

Fig. 8.24 Intramuscular myxoma. (**a**) Sagittal T1WI MR image through the calf shows a large oval uniformly low signal intensity mass (∗). Notice the rind of high signal intensity fat (*arrows*) which is typical for this tumor. (**b**) Corresponding fat-suppressed T2WI MR image shows a heterogeneously high signal intensity mass. (**c**) Corresponding longitudinal sonographic image shows a heterogeneously hypoechoic mass with a thin rind of hyperechoic fat (*arrows*).

thigh or shoulder. They average about 7 cm in diameter, but can be as much as three times that size. When small they may have the homogenous MR imaging appearance of a cyst, but they are solid tumors despite their low signal intensity on T1-weighted sequences and high signal intensity on T2-weighted sequences (Fig. 8.24). When large they may have a heterogeneous appearance on all pulse sequences, may heterogeneously enhance with contrast, and may have surrounding edema, thus giving a more aggressive appearance. A clue to the lesion's correct identity, however, is a thin rind of fat, dubbed the "bright rim sign", present in 70–80% of cases, which may be discontinuous or intermittent, and which represents atrophy of the adjacent compressed skeletal muscle. Sonographically, myxomas have a heterogeneous hypoechoic appearance, and when large may show internal vascularity on Doppler imaging. A peripheral hyperechoic rim is usually visualized due to the rind of adjacent atrophic tissue, corresponding to the "bright rim sign" on MRI (Fig. 8.24). CT shows a hypodense mass compared to the adjacent muscle. The lesions do not calcify. The combination of myxomas and polyostotic fibrous dysplasia is called "Mazabraud syndrome" (Fig. 8.25).

Surgical Pathology: Myxomas have a gelatinous and slimy appearance grossly. Microscopically, they are composed of uniform bland spindle and stellate-shaped cells with tapering, weak eosinophilic and fibrillary cytoplasm scattered in abundant myxoid matrix. Lesions with diffusely increased cellularity have been called cellular myxoma. Regardless of the cellularity, mitoses, nuclear atypia, and necrosis should not be present in myxoma.

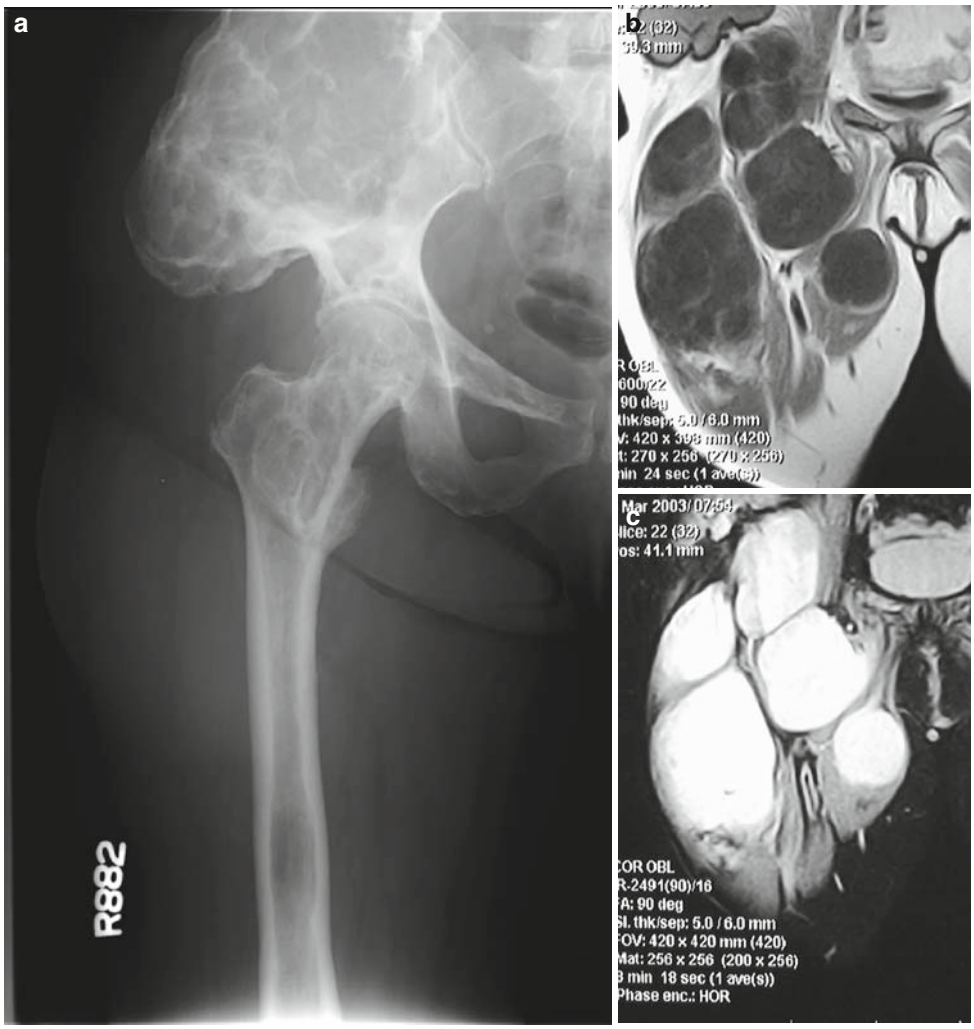

Fig. 8.25 Mazabraud syndrome. Polyostotoic fibrous dysplasia of bone and myxoma of the anterior thigh in a 61-year-old woman. AP radiographs of the right hip and proximal femur (**a**) shows numerous lytic lesions with well-defined margins and either a bubbly or oval appearance proven to represent polyostotic fibrous dysplasia. Coronal T1W (**b**) and T2W fat-saturated images (**c**) show a multilocular mass in the anterior thigh involving the quadriceps muscle. The mass, though solid, has very high signal on T2W sequences giving a false impression of a cyst (case courtesy of Dr. William Reinus)

Malignant

Synovial Sarcoma

Despite its name, synovial sarcoma (also called "synovioma") does not arise from synovium. It can occur anywhere in the body but most cases occur in the extremities near and around joints, with less than 10% of these tumors actually arising within the joint itself. It tends to affect children and young adults (up to approximately 40 years of age) and is the second most common malignant *soft tissue* tumor in children, after rhabdomyosarcoma. Half of all patients die within 5 years of diagnosis, with common sites of metastasis being lung, lymph nodes, and bone. Typically, the tumor presents as a painless mass.

Approximately 30% of the cases show dystrophic calcification on radiographs or CT imaging. Large masses have a well-defined multilobulated appearance, sometimes with internal septations, and heterogeneous signal intensity on MR imaging. These large tumors may also show fluid–fluid levels (Fig. 8.26). When small, this tumor has a more homogeneous appearance, sometimes mimicking that of a ganglion cyst, and thus may be mistakenly interpreted as benign unless contrast is given or sonography performed to show the solid nature of the tumor.

Surgical Pathology: Synovial sarcoma typically is a circumscribed multinodular mass with tan or grey cut surface.

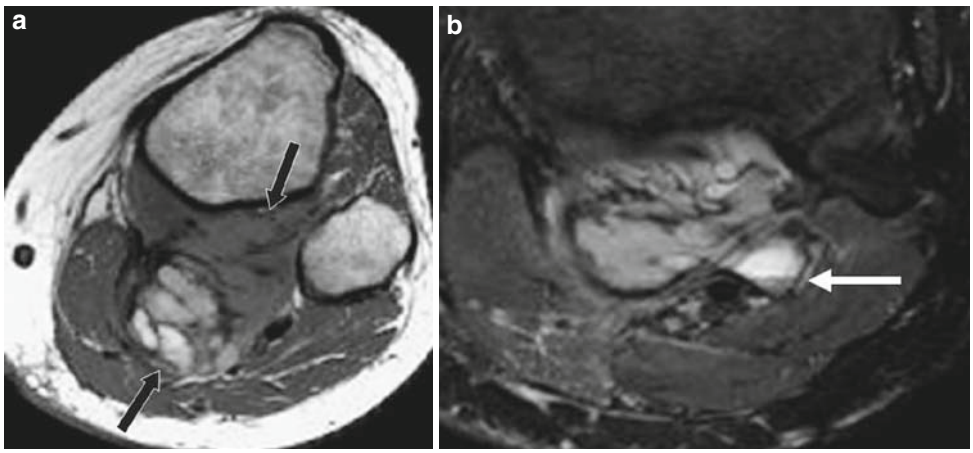

Fig. 8.26 Synovial sarcoma. (**a**) Axial T1WI image through the proximal leg shows a large mass (*arrows*) posterior to the tibia with heterogeneously high and low signal intensity. (**b**) Corresponding fat-suppressed T2WI image at a slightly different location in the mass shows a fluid-fluid level (*arrow*)

They can be either biphasic or monophasic. The typical biphasic variant is characterized by proliferation of neoplastic cells exhibiting both epithelial and spindle cell phenotypes (Fig. 8.26H). The epithelial cells may form glandular structures or solid nests and have abundant cytoplasm and oval nuclei. Between the epithelial elements, there are proliferation of spindle cells which have scant cytoplasm and indistinct cell borders. In rare cases, the epithelial component can be very overwhelming with very little spindle cell component. The monophasic variant is composed of only short spindle cells which are monotonous and form vague fascicular, whorling, and rarely palisading patterns. Extracellular matrix is usually scant except for variable myxoid matrix in the less cellular areas alternating with hypercellular areas. Calcification is present in some cases. The presence of a hemangiopericytoma-like vascular pattern is common but usually focal. Immunohistochemically, both epithelial and spindle cells are positive for cytokeratin and EMA. In addition, synovial sarcoma is frequently positive for CD 99 and bcl-2. Focal S100 reactivity is present in one-third of cases.

Cytogenetically both monophasic and biphasic synovial sarcomas share a recurrent reciprocal t(X;18)(p11.2;q11.2) translocation. This translocation fuses the *SYT* gene on chromosome 18q11 to either of three homologous genes on Xp11, *SSX1, SSX2,* and rarely *SSX4.* Early data had suggested that there might be a relationship between the type of fusion transcript and the histologic subtype (with *SYT–SSX1* associated mostly with biphasic and *SYT–SSX2* with monophasic types) as well as with prognosis, with a significantly better metastasis-free survival associated with the *SYT–SSX2* subtype. But there have been some contradictory reports and this issue is not completely settled. Detection of *SYT–SSX* fusion (often by PCR methods) is an important tool diagnostically.

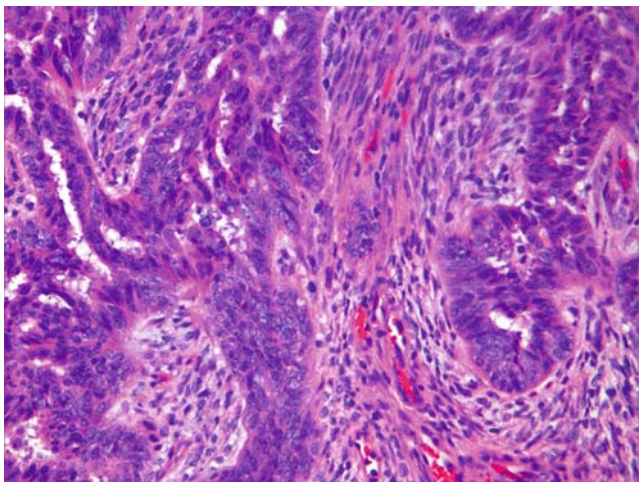

Fig. 8.26H Biphasic synovial component with malignant epithelial and spindle cell elements

Miscellaneous Lesions

Benign

Ganglion Cyst

Ganglion cysts are the most common benign soft tissue mass, and are usually encountered around the wrist, hand, and fingers, and ankle or foot. When superficial, they can present as firm hard masses. They tend to arise near tendons and may represent a focal degenerative or post-traumatic process of the tendon sheath. Dynamic sonographic scanning during flexion and extension of the digits, if the ganglion is located in a finger or toe, can demonstrate whether the mass is tethered to the tendon. Histologically, ganglion cysts

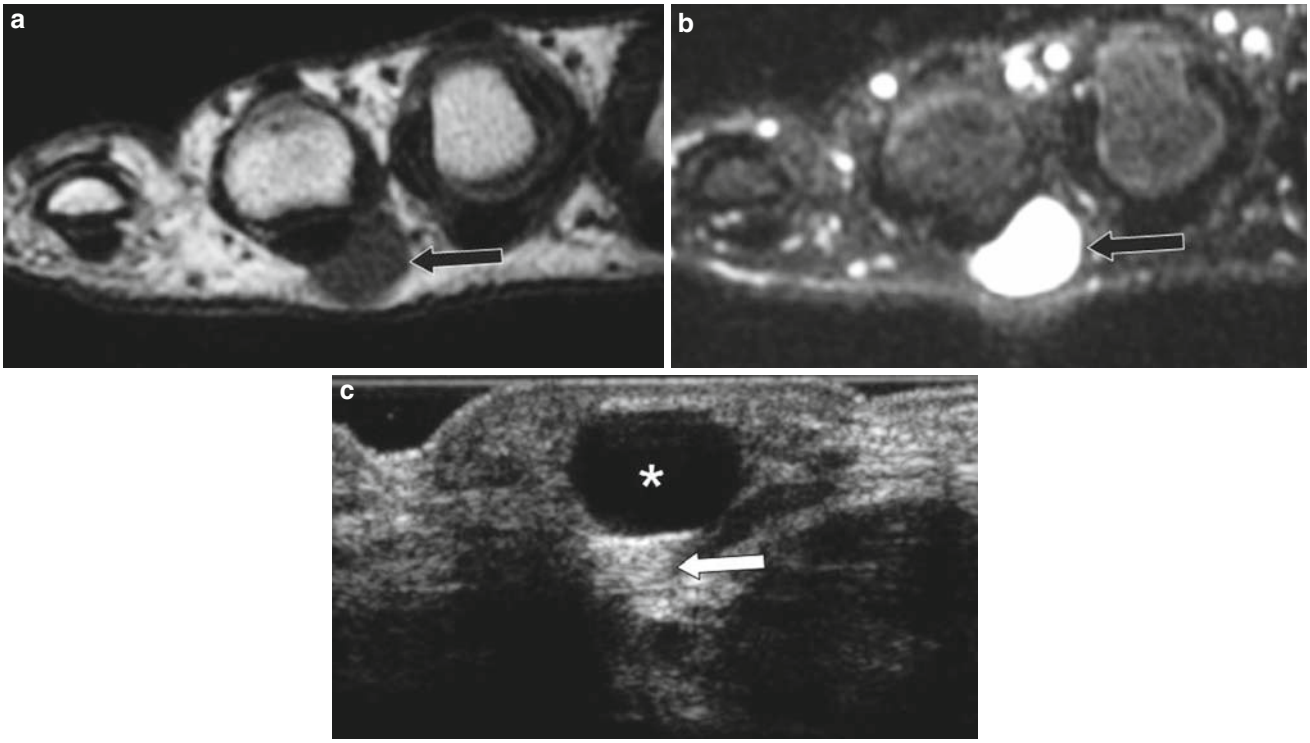

Fig. 8.27 Ganglion cyst. (**a**) Short access T1WI image through the forefoot shows a well-circumscribed low signal intensity mass (*arrow*) in the subcutaneous fat adjacent to the flexor tendon. (**b**) Corresponding fat-suppressed T2WI image shows the uniform high signal intensity of the cyst (*arrow*). (**c**) Corresponding short access sonographic image shows the anechoic cyst (∗) with imperceptible walls and echogenic posterior acoustic enhancement (*arrow*)

have a thin fibrous wall lined with flat cells. Radiographs may show a bump or focal soft tissue density in the contour of the affected region, since the cyst has the same water density as muscle. Similarly, CT may show a water density mass which may be difficult to distinguish from muscle as they may have similar density.

MR imaging shows a well-defined mass which is uniformly low signal intensity on T1-weighted sequences and homogeneously high signal intensity on T2-weighted sequences (Fig. 8.27). The thin cyst wall will enhance after intravenous contrast administration, but the internal fluid will not. Ganglion cysts are usually round or oval, but may be elongated and may insinuate between tendons or small bones of the hands and feet.

Sonography is the preferred method of evaluation of suspected ganglia since it is rapidly performed and can immediately distinguish a cystic from solid mass. The cyst is typically completely anechoic, with a thin wall and posterior acoustic enhancement (Fig. 8.27). Cysts containing thick walls, internal septations, or debris are not uncommon, however, especially if they have sustained repetitive trauma causing fibrosis and hemorrhage. This heterogeneous atypical appearance may be misleading, but the clinical history and location should suggest the proper diagnosis.

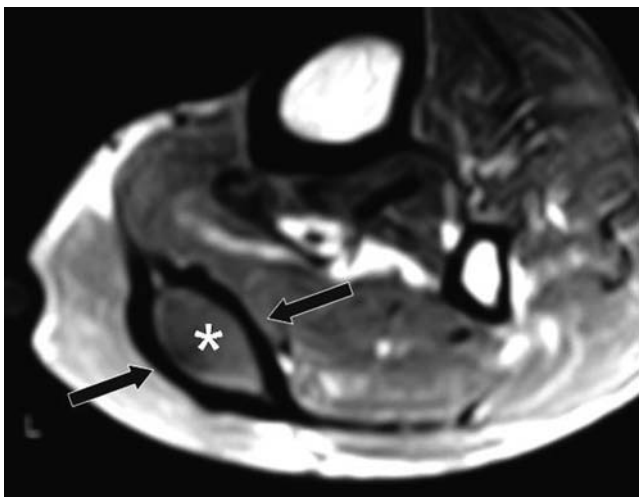

Fig. 8.28 Chronic hematoma. Axial T1WI MR image through the calf shows a heterogeneous appearing hematoma (∗). Note the markedly thickened low signal intensity wall (*arrows*) due to chronic deposition of hemosiderin

Ganglia can sometimes be clinically occult, meaning that they are not palpable or visible on physical examination. These occult ganglia usually occur around the wrist or in the foot and can be a cause of pain. Both MR imaging

and sonography can show these cysts, but sonography has the additional benefit of being able to guide percutaneous aspiration.

Hematoma

Hematomas are commonly encountered during MR imaging of a suspected mass. They typically occur in the lower extremity, particularly the calf, usually as a result of superficial tear of the gastrocnemius, plantaris, or soleus muscles during athletic activity. They can also occur spontaneously in patients on anticoagulation therapy. With a large sudden hemorrhage, the patient's hematocrit may drop. When a hematoma is present one should search carefully for an adjacent traumatic process or, in the absence of trauma or overuse, a possible soft tissue malignancy.

Blood in the musculoskeletal system does not behave in the same predictable fashion as a hematoma in the brain, and regardless of their time course most musculoskeletal hematomas have a heterogeneous appearance on MR imaging, with both high and low signal intensity regions on T1- and T2-weighted sequences. They also commonly have an appearance similar to simple fluid collections. Hematomas often have heterogeneous echogenicity on sonography. Musculoskeletal hematomas usually resorb gradually and ultimately resolve, but occasionally they become walled off by fibrous tissue and do not regress. The wall of these chronic hematomas may be thick and low signal intensity due to peripheral deposition of hemosiderin from the breakdown of the red cells (Fig. 8.28).

Morton Neuroma

Morton neuroma is not a neoplasm but rather is a mass-like scarring of the plantar interdigital nerve. It is an idiopathic process, though repetitive micro-trauma, such as from sports or wearing high-heeled or tight shoes, may contribute. The mass typically occurs between the second and third or third

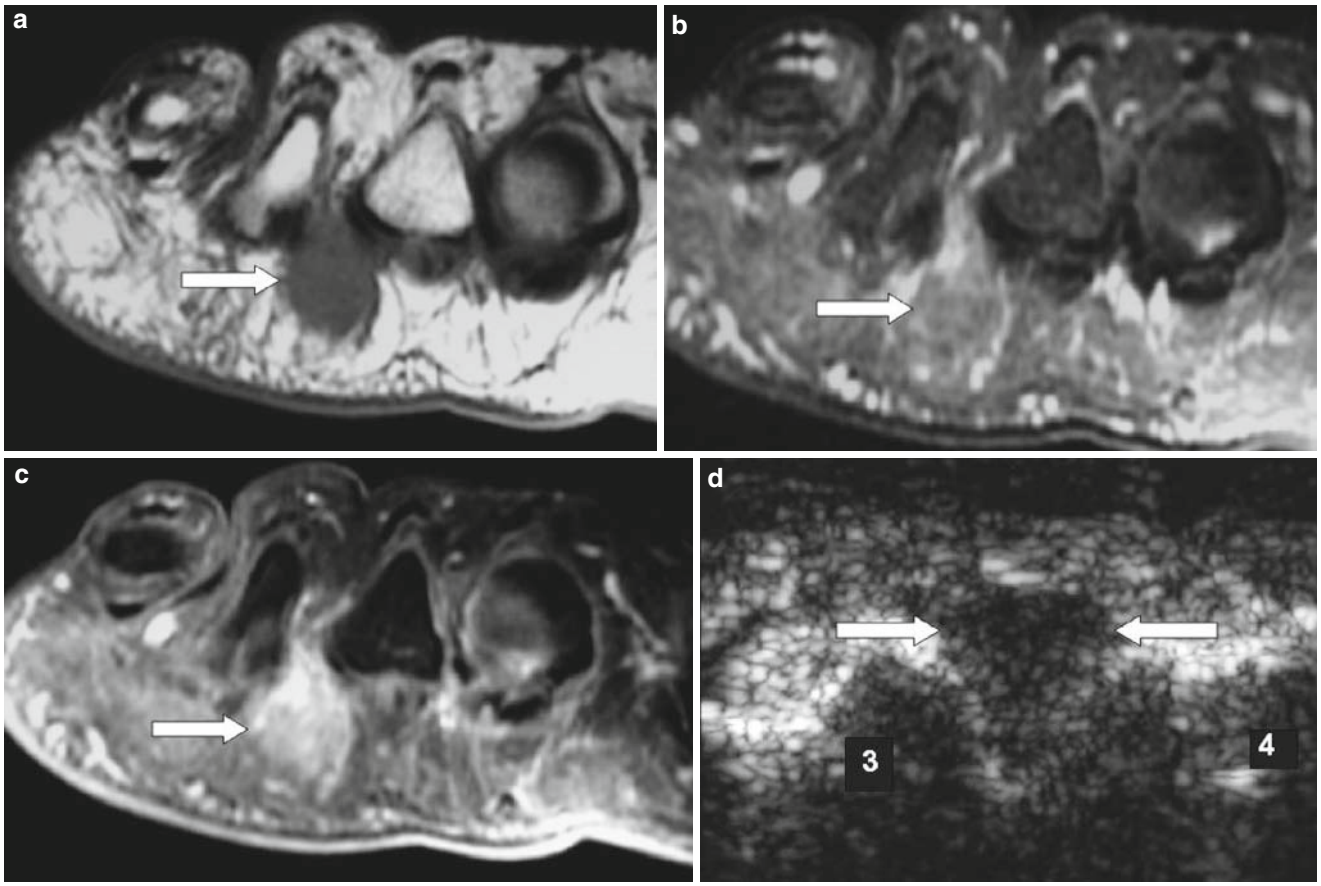

Fig. 8.29 Morton neuroma. (**a**) Short axis T1-weighted MR image of the forefoot shows a homogeneously low signal intensity mass (*arrow*) in the plantar aspect of the third webspace. (**b**) On a corresponding short axis fat-suppressed T2-weighted MR image the mass (*arrow*) is low signal intensity, distinguishing it from a ganglion cyst. (**c**) Corresponding short axis fat-suppressed T1-weighted MR image after intravenous contrast administration shows heterogeneous intermediate enhancement of the mass (*arrow*). (**d**) Corresponding short-axis sonographic image shows a hypoechoic mass (*arrows*) with faint internal echoes insinuating itself between the third (3) and fourth (4) metatarsal heads

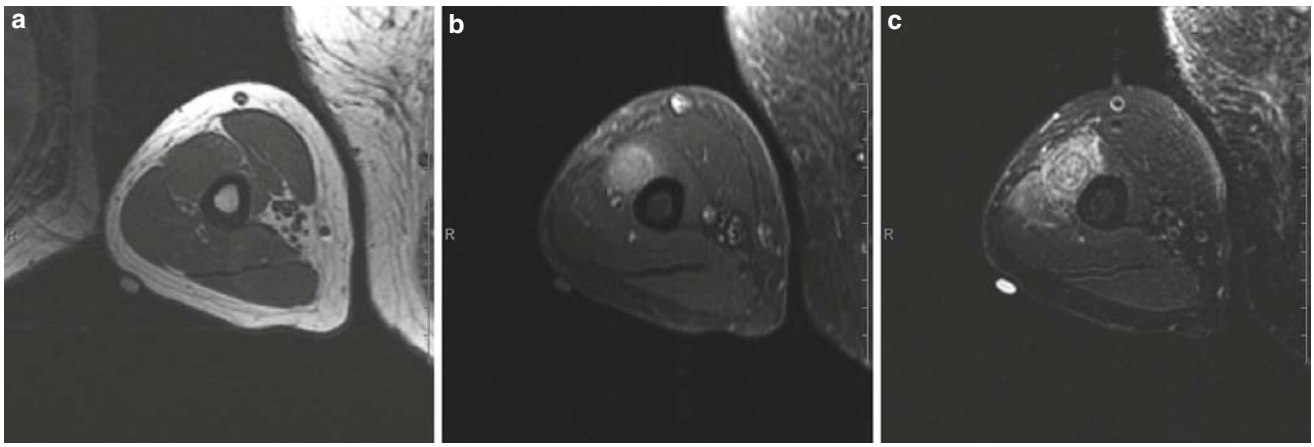

Fig. 8.30 Metastasis to muscle: 47-year-old woman with lung cancer complaining of pain in her arm. Axial T1WI (**a**), T2W fat-suppressed (**b**), and T1W fat-suppressed MR images after intravenous gadolinium (**c**) show a well defined heterogeneously enhancing mass in the brachioradialis muscle (case courtesy of Dr. William Reinus)

and fourth metatarsal heads, and more than one metatarsal interspace can be affected at the same time. They may or may not be symptomatic, but when symptomatic, pain occurs when standing or walking and can be elicited by palpation. Morton neuroma is typically low to intermediate signal intensity on both T1- and T2-weighted sequences and may be round or dumbbell shaped if large. They have variable enhancement (Fig. 8.29). Sonographically they are demonstrated as hypoechoic masses (Fig. 8.29). Sonography has the advantage of being able to demonstrate which neuromas are symptomatic by performing palpation during sonography, as well as being able to guide percutaneous injection of steroid for therapeutic relief.

Malignant

Soft Tissue Metastases

Not all malignant soft tissue masses are primary. Melanoma commonly metastasizes to muscle, and lung cancer, because of its overwhelming prevalence, will also occasionally spread to distant soft tissue (Fig. 8.30). Lymphoma may also have soft tissue masses.

Conclusion

The imaging evaluation of soft tissue masses can be challenging. While some masses have characteristic imaging features, most do not. Nonetheless, a differential diagnosis can be generated based on the location of the mass and the age of the patient. In these indeterminate cases the radiologists' role is to provide a differential diagnosis and delineate the anatomic location and extent of the mass prior to biopsy or excision.

Suggested Readings

General Imaging of Tumors

1. Fletcher CDM. The evolving classification of soft tissue tumours: an update based on the new WHO classification. Histopathology 2006; 48: 3–12
2. Vilanova JC, Woertler K, Narváez JA, Barceló J, Martínez SJ, Villalón M, Miró J. Soft-tissue tumors update: MR imaging features according to the WHO classification. Eur Radiol 2007; 17: 125–138
3. Adler RS, Bell DS, Bamber JC, et al. Evaluation of soft-tissue masses using segmented color Doppler velocity images: preliminary observations. AJR 1999; 172: 781–788.
4. Belli P, Costantini M, Mirk P, Maresca G, Priolo F, Marano P. Role of color Doppler sonography in the assessment of musculoskeletal soft tissue masses. J Ultrasound Med 2001; 19(12): 823–830
5. Capelestegui A, Astigarraga E, Fernandez-Colon G, et al. Masses and pseudomasses of the hand and wrist: MR findings in 134 cases. Skeletal Radiol 1999; 28: 498–507.
6. Erlemann R, Reiser MF, Peters PE, et al. Musculoskeletal neoplasms: static and dynamic Gd-DTPA-enhanced MR imaging. Radiology 1989; 171: 767–773.
7. Fletcher BD, Hanna SL, Fairclough DL, Gronemeyer SA. Pediatric musculoskeletal tumors: use of dynamic, contrast-enhanced MR imaging to monitor response to chemotherapy. Radiology 1992; 184: 243–248.
8. Hwang S, Adler RS. Sonographic evaluation of musculoskeletal soft tissue masses. Ultrasound Q 2005; 21(4): 259–270.

9. Kaushik S, Miller TT, Nazarian LN, Foster WC. Spectral Doppler sonography of musculoskeletal soft tissue masses. J Ultrasound Med 2003; 22(12): 1333–1336.
10. Kransdorf MJ. The use of gadolinium in MR evaluation of musculoskeletal tumors. Top Magn Reson Imaging 1996; 8: 15–23.
11. Kransdorf MJ. Benign soft-tissue tumors in a large referral population: distribution of specific diagnoses by age, sex, and location. AJR 1995; 164: 395–402.
12. Kransdorf MJ. Malignant soft-tissue tumors in a large referral population: distribution of diagnoses by age, sex, and location. AJR 1995; 164: 129–134.
13. Lang P, Johnston JO, Arenal-Romero F, Gooding CA. Advances in MR imaging of pediatric musculoskeletal neoplasms. Magn Reson Imaging Clin N Am 1998; 6: 579–604.
14. May DA, Good RB, Smith DK, Parsons TW. MR imaging of musculoskeletal tumors and tumor mimickers with intravenous gadolinium: experience with 242 patients. Skeletal Radiol 1997; 26: 2–15.
15. Seale KS, Lange TA, Monson D, Hackbarth DA. Soft tissue tumors of the foot and ankle. Skeletal Radiol 1997; 26(10): 619–621.
16. Verstraete KL, De Deene Y, Roels H, et al. Benign and malignant musculoskeletal lesions: dynamica contrast-enhanced MR imaging-parametric "first class" images depict tissue vascularization and perfusion. Radiology 1994; 192: 835–843.
17. Hamada K, Tomita Y, Ueda T, Enomoto K, Kakunaga S, Myoui A, Higuchi I, Yoshikawa H, Hatazawa J. Evaluation of delayed 18F-FDG PET in differential diagnosis for malignant soft-tissue tumors. Ann Nucl Med 2006; 20: 671–675.
18. Aoki J, Watanabe H, Shinozaki T, Takagishi K, Tokunaga M, Koyama Y, Sato N, Endo K. FDG-PET for preoperative differential diagnosis between benign and malignant soft tissue masses. Skeletal Radiol 2003; 32: 133–138.
19. Parsons III TW, Frink SF, Campbell SE. Musculoskeletal neoplasia: helping the orthopaedic surgeon establish the diagnosis. Semin Musculoskelet Radiol 2007; 11: 3–15.
20. Keenan S, Bui-Mansfield LT. Musculoskeletal lesions with fluid-fluid level: a pictorial essay. J Comput Assist Tomogr 2006; 30: 517–524.
21. Van Dyck P, Vanhoenacker FM, Vogel J, Venstermans C, Kroon HM, Gielen J, Parizel PM, Bloem JL, De Schepper AM. Prevalence, extension and characteristics of fluid-fluid levels in bone and soft tissue tumors. Eur Radiol 2006; 16(12): 2644–2651.
22. Coindre JM. Grading of soft tissue sarcomas review and update. Arch Pathol Lab Med 2006; 130: 1448–1453.
23. Goodwin RW. O'Donnell P, Saifuddinb A. MRI appearances of common benign soft-tissue tumours. Clin Radiol 2007; 62: 843–853.
24. Papp DF, Khanna AJ, McCarthy EF, Carrino JA, Farber AJ, Frassica FJ. Magnetic resonance imaging of soft-tissue tumors: determinate and indeterminate lesions. J Bone Joint Surg Am 2007; 89: 103–115.
25. Stacy GS, Nair L. Magnetic resonance imaging features of extremity sarcomas of uncertain differentiation. Clin Radiol 2007; 62: 950–958.
26. Ilaslan H, Sundaram M. Advances in musculoskeletal tumor imaging. Orthop Clin N Am 2006; 37: 375–391.
27. Collin F, Gelly-Marty M, Bui Nguyen Binh M, Coindre JM. Soft tissue sarcomas: current data in the field of pathology. Cancer Radiother 2006; 10(1–2): 7–14.
28. Blacksin MF, Ha DH, Hameed M, Aisne SR. Superficial soft-tissue masses of the extremities. RadioGraphics 2006; 26: 1289–1304.
29. Beaman FD, Kransdorf MJ, Andrews TR, Murphey MD, Arcara LK, Keeling JH. Superficial soft-tissue masses: analysis, diagnosis, and differential considerations. RadioGraphics 2007; 27: 509–523.

Adipocytic Tumors

1. Arkun R, Memis A, Akalin T, Ustunn EE, Sabah D, Kandiloglu G. Liposarcoma of soft tissue: MRI findings with pathologic correlation. Skeletal Radiol 1997 Mar; 26: 167–172.
2. Bush CH, Spanier SS, Gillespy T 3rd. Imaging of atypical lipomas of the extremities: report of three cases. Skeletal Radiol 1988; 17: 472–475.
3. Einarsdottir H, Soderlund V, Larsson O, et al. 110 subfascial lipomatous tumors. MR and CT findings versus histopathological diagnosis and cytogenetic analysis. Acta Radiol 1999; 40: 603–609.
4. Hardes J, Scheil-Bertram S, Hartwig E, Gebert C, Gosheger G, Schulte M. Sonographic findings of hibernoma: a report of two cases. J Clin Ultrasound 2005; 33(6): 298–301.
5. Hosono M, Kobayashi H, Fujimoto R, et al. Septum-like structures in lipomas and liposarcoma: MR imaging and pathologic correlation. Skeletal Radiol 1997; 26: 150–154.
6. Kransdorf, MJ, Moser RP, Meis JM, Meyer CA. Fat-containing soft tissue masses of the extremities. RadioGraphics 1991; 11: 81–106.
7. Kransdorf MJ, Bancroft LW, Peterson JJ. Imaging of fatty tumors: distinction of lipoma and

well differentiated liposarcoma. Radiology 2002; 224: 99–104.
8. Munk PL, Janzen DL, Connell DG, et al. Lipoma and lipsarcoma: evaluation using CT and MR imaging. AJR 1997; 169: 589–594.
9. Murphy WD, Hurst GC, Duerk JL, et al. Atypical appearances of lipomatous tumors on MR images: high signal intensity with fat-suppression STIR sequences. JMRI 1991; 1: 477–480.
10. Murphey MD, Carroll JF, Flemming DJ, Pope TL, Gannon FH, Kransdorf MJ. Benign musculoskeletal lipomatous lesions. RadioGraphics 2004; 24: 1433–1466.
11. Pang AK, Hughes T. Magnetic resonance imaging of lipomas and liposarcoma: potential of short tau inversion recovery as a technique of fat suppression. Australas Radiology 2000; 44: 412–416.
12. Sung MS, Kang HS, Suh JS, et al. Myxoid liposarcoma: appearance at MR imaging with histologic correlation. RadioGraphics 2000; 1007–1019.
13. Bancroft LW, Kransdorf MJ, Peterson JJ, O'Connor MI. Benign fatty tumors: classification, clinical course, imaging appearance and treatment. Skeletal Radiol 2006; 35: 719–733.
14. Murphey MD, Arcara LK, Fanburg-Smith J. Imaging of Musculoskeletal Liposarcoma with Radiologic-Pathologic Correlation. RadioGraphics 2005; 25: 1371–1395.
15. Drevelegas A, Pilavaki M, Chourmouzi D. Lipomatous tumors of soft tissue: MR appearance with histological correlation. Eur J Rad 2004; 50: 257–267.

Fibroblastic Tumors

1. Aust NZ. Nodular fasciitis and related pseudosarcomatous lesions of soft tissues. J Surg 1996; 66: 22–25.
2. Bernstein KE, Lattes R. Nodular (poseuosarcomatous) fasciitis, a nonrecurrent lesion: clinicopathologic study of 134 cases. Cancer 1982; 49: 1668–1678.
3. Koh SH, Choe HS, Lee IJ, Park HR, Bae SH. Low-grade fibromyxoid sarcoma: ultrasound and magnetic resonance findings in two cases. Skeletal Radiol 2005; 34(9): 550–554.
6. Polat P, Kantarci M, Alper F, et al. Nodular fasciitis of the breast and knee in the same patient. AJR 2002; 178: 1426–1428.
7. Pritchard DJ, Sim FH, Ivins JC, et al. Fibrosarcoma of bone and soft tissues of the trunk and extremities. Orthop Clin North Am 1977; 8: 869–881.
8. Pritchard DJ, Soule EH, Taylor WF, Ivins JC. Fibrosarcoma: a clinicopathologic and statistical study of 199 tumors of the soft tissues of the extremities and trunk. Cancer 1974; 33: 888–897.
9. Quinn SF, Erickson SJ, Dee PM, et al. MR imaging in fibromatosis: results in 26 patients with pathologic correlation. AJR 1991; 156: 539–542.
10. Scott SM, Reiman HM, Pritchard DJ, Ilstrup DM. Soft tissue fibrosarcoma. A clinicopathologic study of 132 cases. Cancer 1989; 64: 925–931.
11. Wang XL, De Schepper AMA, Vanhoenacker F, et al. Nodular fasciitis: correlation of MRI findings and histopathology. Skeletal Radiol 2002; 31: 155–161.
12. De Smet AA, Norris MA, Fisher DR. Magnetic resonance imaging of myositis ossificans: analysis of seven cases. Skeletal Radiol 1992; 21: 503–507.
13. Kransdorf MJ, Meis JM, Jelinek JS. Myositis ossificans: MR appearance with radiologic-pathologic correlation. AJR 1991; 157: 1243–1248.
14. Parikj J, Hyare H, Saifuddin A. The imaging features of post-traumatic myositis ossificans, with emphasis on MRI. Clin Radiol 2002; 57: 1058–1066.
15. Tateishi U, Hasegawa T, Onaya H, Satake M, Arai Y, Moriyama N. Myxoinflammatory fibroblastic sarcoma: MR appearance and pathologic correlation. AJR 2005; 184: 1749–1753
16. Kreuzberg B, Koudelova J, Ferda J, Treska V, Spidlen V, Mukensnabl P. Diagnostic problems of abdominal desmoid tumors in various locations. Eur J Radiol 2007; 62: 180–185.
17. Dinauer PA, Brixey, CJ, Moncur JT, Fanburg-Smith JC, Murphey MD. Pathologic and MR imaging features of benign fibrous soft-tissue tumors in adults. RadioGraphics 2007; 27: 173–187.
18. Vandevenne JE, De Schepper AM, De Beuckeleer L, Van Marck E, Aparisi F, Bloem JL, Erkorkmaz Z, Brijs S. New concepts in understanding evolution of desmoid tumors: MR imaging of 30 lesions. Eur Radiol 1997; 7(7): 1013–1019.
19. McCarville MB, Hoffer FA, Adelman CS, Khoury JD, Li C, Skapek SX. MRI and biologic behavior of desmoid tumors in children. AJR 2007; 189(3): 633–640.
20. Hosalkar HS, Fox EJ, Delaney T, Torbert JT, Ogilvie CM, Lackman RD. Desmoid tumors and current status of management. Orthop Clin N Am 2006; 37: 53–63.
21. Naylor MF, Nascimento AG, Sherrick AD, McLeod RA. Elastofibroma dorsi: radiologic findings in 12 patients. AJR 1996; 167: 683–687.
22. Robbin MR, Murphey MD, Temple HT, Kransdorf MJ, Choi JJ. Imaging of musculoskeletal fibromatosis. RadioGraphics 2001; 21: 585–600.

Fibrohistiocytic Tumors

1. Jelinek JS, Kransdorf MJ, Shmookler BM, et al. Giant cell tumor of the tendon sheath: MR findings in nine cases. AJR 1994; 162: 919–922.
2. Middleton WD, Patel V, Teefey SA, Boyer MI. Giant cell tumors of the tendon sheath: analysis of sonographic findings. AJR 2004; 183(2): 337–9
3. Miller TT, Hermann G, Abdelwahab IF, et al. MRI of malignant fibrous histiocytoma of soft tissue: analysis of 13 cases with pathologic correlation. Skeletal Radiol 1994; 23: 271–275.
4. Munk PL, Sallomi DF, Janzen DL, et al. Malignant fibrous histiocytoma of soft tissue imaging with emphasis on MRI. J Comput Assist Tomogr 1998; 22: 819–826.
5. Randall RL, Albritton KH, Ferney BJ, Layfield L. Malignant fibrous histiocytoma of soft tissue: an abandoned diagnosis. Am J Orthop 2004; 33: 602–608.
6. Dei Tos AP. Classification of pleomorphic sarcomas: where are we now? Histopathology 2006; 48: 51–62.
7. Kransdorf MJ, Meis-Kindblom JM. Dermatofibrosarcoma protuberans: radiologic appearance. AJR 1994; 163: 391–394.
8. Torreggiani WC, Al-Ismail K, Munk PL, Nicolaou S, O'Connell JX, Knowling MA. Dermatofibrosarcoma protuberans: MR imaging features. AJR 2002; 178: 989–993.

Pericytic Tumors

1. Drape JL, Idy-Peretti I, Goettmann S, et al. Subungual glomus tumors: evaluation with MR imaging. Radiology 1995; 195: 507–515.
2. Fornage BD. Glomus tumor in the fingers: diagnosis with ultrasound. Radiology 1988; 167: 183–185.
3. Kneeland JB, Middleton WD, Matloub HS, et al. High resolution MR imaging of glomus tumor. J Comput Assist Tomogr 1987; 11: 351–352.
4. Matloub HS, Muoneke VN, Prevel CD, et al. Glomus tumor imaging: use of MRI for localization of occult lesions. J Hand Surg 1992; 17A: 472–475.
5. Mathis WH, Schulz MD. Roentgen diagnosis of glomus tumors. Radiology 1948; 51: 71–76
6. Schiefer TK, Parker WL, Anakwenze OA, Amadio PC, Inwards CY, Spinner RJ. Extradigital glomus tumors: a 20 year experience. Mayo Clin Proc 2006; 81(10): 1337–1344.

Vascular Tumors

1. Bach AD, Walgenbach KJ, Horch RE. Hemangiosarcoma of the left hand in a patient with the rare combination of Maffucci's and Stewart Treves syndrome. Vasa 2000; 29(1): 71–73.
2. Coldwell DM, Baron RL, Charnsangavej C. Angiosarcoma: diagnosis and clinical course. Acta Radiol 1989; 30: 627–631.
3. Choi JJ, Murphey MD. Angiomatous skeletal lesions. Semin Musculoskel Radiol 2000, 4(1): 103–112.
4. Kim EY, Ahn JM, Yoon HK, et al. Intramuscular vascular malformations of an extremity: findings on MR imaging and pathologic correlation. Skeletal Radiol 1999; 28: 515–521.
5. Lorigan JG, David CL, Evans HL. Wallace S. The clinical and radiologic manifestations of hemangiopericytoma. AJR 1989; 153: 345–349
6. Murphy MD, Fairbarin KJ, Parman LM, Baxter KG, Parsa MB, Smith WS. Musculoskeletal angiomatous lesions: radiologic-pathologic correlation. RadioGraphics 1995; 15: 893–917
7. Nakazono T, Kudo S, Matsuo Y, Matsubayashi R, Ehara S, Narisawa H, Yonemitsu N. Angiosarcoma associated with chronic lymphedema (Stewart-Treves syndrome) of the leg: MR imaging. Skeletal Radiol 2000; 29(7): 413–416
8. Suh JS, Hwang G, Hahn SB. Soft tissue hemangiomas: MR manifestations in 23 patients. Skeletal Radiol 1994; 23: 621–625.
9. Teo ELHJ, Strouse PJ, Hernandez RJ. MR imaging differentiation of soft tissue hemangiomas from malignant soft tissue masses. AJR 2000; 174: 1623–1628.
10. Theumann NH, Bittoun J, Goettman S, et al. Hemangiomas of the fingers: MR imaging evaluation. Radiology 2001; 218: 841–847.
11. Restrepo CS, Lemos DF, Gordillo H, Odero R, Varghese T, Tiemann W, Rivas FF, Moncada R, Gimenez CR. Imaging findings in musculoskeletal complications of AIDS. RadioGraphics 2004; 24 (4): 1029–1049.

Peripheral Nerve Sheath Tumors

1. Beggs, I. Sonographic appearances of nerve tumors. J Clin Ultrasound 1999; 27: 363–368.
2. Chen W, Jia JW, Wang JR. Soft tissue diffuse neurofibromas: sonographic findings. J Ultrasound Med 2007; 26(4): 513–518.
3. King AD, Ahuja AT, King W, Metreweli C. Sonography of peripheral nerve tumors of the neck. AJR 1997; 169: 1695–1698.
4. Lin J, Martel W. Cross-sectional imaging of peripheral nerve sheath tumors: characteristic signs on CT, MR imaging, and sonography. AJR 2001; 176: 75–82.

5. Martinoli C, Bianchi S, Derchi LE. Ultrasonography of peripheral nerves. Semin Ultrasound CT MR 2000; 21: 205–213.
6. Reynolds DL Jr, Jacobson JA, Inampudi P, Jamadar DA, Ebrahim FS, Hayes CW Sonographic characteristics of peripheral nerve sheath tumors. AJR 2004; 182(3): 741–744.
7. Koga H, Matsumoto S, Manabe J, Tanizawa T, Kawaguchi N. Definition of the target sign and its use for the diagnosis of schwannomas. Clin Orthop Relat Res 2007; 464: 224–229.
8. Van Herendael BH, Heyman SRG, Vanhoenacker FM, De Temmerman G, Bloem JL, Parizel PM, De Schepper AM. The value of magnetic resonance imaging in the differentiation between malignant peripheral nerve-sheath tumors and non-neurogenic malignant soft-tissue tumors. Skeletal Radiol 2006 35: 745–753.

Tumors of Uncertain Differentiation

1. Bancroft LW, Kransdorf MJ, Menke DM, et al. Intramuscular myxoma: characteristic MR imaging features. AJR 2002; 178: 1255–1259.
3. Girish G, Jamadar DA, Landry D, Finlay K, Jacobson JA, Friedman L. Sonography of intramuscular myxomas: the bright rim and bright cap signs. J Ultrasound Med 2006; 25(7): 865–869
4. Jones BC, Sundaran M, Kransdorf MJ. Synovial sarcoma: MR imaging findings in 34 patients. AJR 1993; 161: 827–830.
5. McCarville MB, Spunt, SL, Skapek SX, Pappo, AS. Synovial sarcoma in pediatric patients. AJR 2002; 179: 797–801.
6. Morton MJ, Berquist TH, McLeod RA, et al. MR imaging of synovial sarcoma. AJR 1991; 156: 337–340.
7. Murphey MD, McRae GA, Fanburg-Smith JC, et al. Imaging of soft tissue myxoma with emphasis on CT and MR and comparison of radiologic and pathologic findings. Radiology 2002; 225: 215–224.
8. van Rijswijk CSP, Hogendoorn PCW, Tanminiau AHM, Bloem JL. Synovial sarcoma: dynamic contrast-enhanced MR imaging features. Skeletal Radiol 2001; 30: 25–30.
9. Luna A, Martinez S, Bossen E. Magnetic resonance imaging of intramuscular myxoma with histological comparison and a review of the literature. Skeletal Radiol 2005; 34: 19–28.

Miscellaneous Lesions

1. Breidahl WH, Adler RS. Ultrasound-guided injection of ganglia with coricosteriods. Skeletal Radiol 1996; 25: 635–638.
2. Sofka CM, Adler RS, Ciavarra G, Pavlov H Ultrasound-guided interdigital neuroma injections: short term clinical outcomes after a single percutaneous injection – preliminary results. HSS Journal: the Musculoskeletal Journal of Hospital for Special Surgery 2007; 3(1): 44–49.
3. Terk MR, Kwong P K Suthar M, Horvath BC, Colletti PM. Morton neuroma: evaluation with MR imaging performed with contrast enhancement and fat suppression. Radiology 1993 Oct; 189: 239–241.
4. Williams JW, Meaney J, Whitehouse GH, Klenerman L, Hussein Z. MRI in the investigation of Morton's neuroma: which sequences? Clin Radiol 1997 Jan; 52: 46–49.
5. Zanetti M, Ledermann T, Zollinger H, Hodler J. Efficacy of MR imaging in patients suspected of having Morton's neuroma. AJR 1997 Feb; 168: 529–532.
6. Unger HR Jr, Mattoso PQ, Drusen MJ, Neumann C H Gadopentetate-enhanced magnetic resonance imaging with fat saturation in evaluation of Morton's neuroma. J. Foot Surg 1992 May–Jun; 31: 244–246.
7. Glockner JF, White LM, Sundaram M, McDonald. Unsuspected metastases presenting as solitary soft tissue lesions: a fourteen-year review. Skeletal Radiol 2000; 29: 270–274.

Chapter 9

Imaging Approach to Hemoglobinopathies

Avneesh Chhabra and William R. Reinus

Abstract Hematologic disorders of the skeleton produce radiologic appearances related to marrow infiltration and/or replacement. These include common findings, such as osteopenia with trabecular prominence, growth disturbances, and extramedullary hematopoiesis. Most entities also manifest with various typical imaging features and appear in characteristic distributions, which aids in their differentiation and clinical management. In this chapter, we will discuss imaging appearances of sickle cell disease, thalassemia, and other rare causes of anemia.

Keywords Sickle cell disease • Thalassemia • Anemia • Red marrow reconversion • Extramedullary hematopoiesis

Introduction

Hematologic disorders of the skeleton either infiltrate or replace normal marrow. Preferentially, these diseases first affect red (hematopoietically active) marrow and ultimately will involve yellow (hematopoietically inactive) marrow as the disease progresses and yellow marrow is recruited back to red marrow. Congenital diseases, including the hemoglobinopathies, will prevent the normal physiologic red to yellow conversion of marrow as the red cell half-life will be short requiring increased reticulocyte formation.

Thus, it is important to recall the normal physiologic sequence of red marrow conversion to yellow marrow that occurs during the first two decades of life. Normal conversion of red to yellow marrow progresses in sequence from appendicular skeleton to axial skeleton and within the appendicular skeleton, from distal to proximal. The epiphyses and apophyses are the first to convert to yellow marrow, followed by diaphyses and ultimately the metaphyses. This process is complete by the late teens. Curvilinear areas of residual subchondral red marrow can be seen in femoral and humeral epiphyses. When pathologic processes infiltrate the marrow space, reconversion of yellow to red marrow tends to occur in just the opposite direction. Many of the conditions discussed in this chapter can be expected to lead to marrow reconversion.

In hematological diseases, chronic red marrow reconversion, expansion, and reticulocytosis cause secondary bone resorption and remodeling that becomes detectable on plain radiographs. Common findings include osteopenia with trabecular prominence, growth disturbances, and extramedullary hematopoiesis. Some entities manifest typical imaging features and occur in characteristic distributions that aid diagnosis. Other findings may result from complications, such as super infection, ischemic necrosis, and secondary arthritis.

Sickle Cell Disease (SCD)

Sickle cell disease manifests clinically as a spectrum of conditions related to the patient's genetic zygosity for production of hemoglobin S (Hbs) in the red blood cells (RBCs). Hbs contains an abnormal beta chain in which a single valine replaces a glutamine in the 6th position of the beta chain of the globin. This predisposes the RBCs to deform (sickle) under hypoxic conditions. Sickling causes increased viscosity of blood leading to vaso-occlusion and tissue ischemia. Complications such as infections and osteonecrosis are common.

Sickle cell disease occurs almost exclusively in blacks. Roughly 8% of the black population in the United States is heterozygous for production of Hbs, an asymptomatic or minimally symptomatic condition known as sickle trait. Approximately 0.15% of the black population is homozygous for the gene and develops full-blown sickle cell disease. Sickle cell disease is prevalent in other ethnic groups as well

A. Chhabra (✉)
Department of Radiology, Johns Hopkins School of Medicine, Baltimore, MD, USA
e-mail: avneesh28@yahoo.com

A. Bonakdarpour et al. (eds.), *Diagnostic Imaging of Musculoskeletal Diseases: A Systematic Approach*,
DOI 10.1007/978-1-59745-355-4_9, © Springer Science+Business Media, LLC 2010

as blacks, including those from Mediterranean area, the Arabian Peninsula, and the Indian subcontinent.

The abnormally shaped red cells lead to increased viscosity of the blood and decreased flow in small vessels. As a result, patients are prone to painful ischemic episodes known as "sickle cell crises." Often these crises commence suddenly and without warning. They are more likely to occur, however, when the temperature is cold or the patient is dehydrated. Ischemia and its ultimate result, infarction, can occur in any tissue, including organs and bone, although some tissues are more predisposed than others. Typically patients will infarct their spleens by their late teenage years. Their loss of their spleen and its "C" protein production predisposes them to infections.

The abnormally shaped red cells have a shortened half-life and are trapped prematurely by the reticuloendothelial system. As a result, patients with SCD have high red cell turnover. This high red cell turnover, in turn, causes anemia, reticulocytosis, marrow reconversion, and pigment gallstones. The chronic anemia of SCD leads to high output cardiac failure. This, combined with small vessel cardiac ischemia, causes cardiomegaly.

Patients present with clinical features of anemia, such as weakness, malaise, shortness of breath, and hepatosplenomegaly. Ischemia commonly leads to painful "sickle cell crises." Half of all patients with SCD experience a painful crisis by about 5 years of age. Young infants with the disease are usually asymptomatic during the first few months of life because of continued and prolonged fetal hemoglobin production. Crises can present with acute chest syndrome, bone and joint pain, hand foot syndrome (HFS), and abdominal pain. HFS is a self-limiting ischemic dactilitis of hands and feet, common between 6 months and 2 years of age and rarely seen after 6–7 years of age. It may be extremely difficult to differentiate ischemia from infection since both may show soft tissue swelling, patchy lytic–sclerotic appearance in the bones and periostitis radiographically. Multiple site involvement and bilateral osseous involvement are much more common in HFS than osteomyelitis, aiding in the differential.

Sickle cell disease is painful and debilitating. Patients suffer from severe anemia, recurrent infections, and painful ischemic crises. While once uniformly fatal by the third decade of life, better understanding of the disease's behavior and its causes has greatly improved survival. Today, patients can survive into their fifth and even their sixth decades.

Radiographic findings are a direct result of the pathophysiology of the disease. They occur in both the axial and appendicular skeleton in early years of life, especially with the involvement of hands and feet where blood flow is slowest and body temperature is lowest. In older children, changes predominate in axial skeleton due to fatty conversion of the bones in the digits.

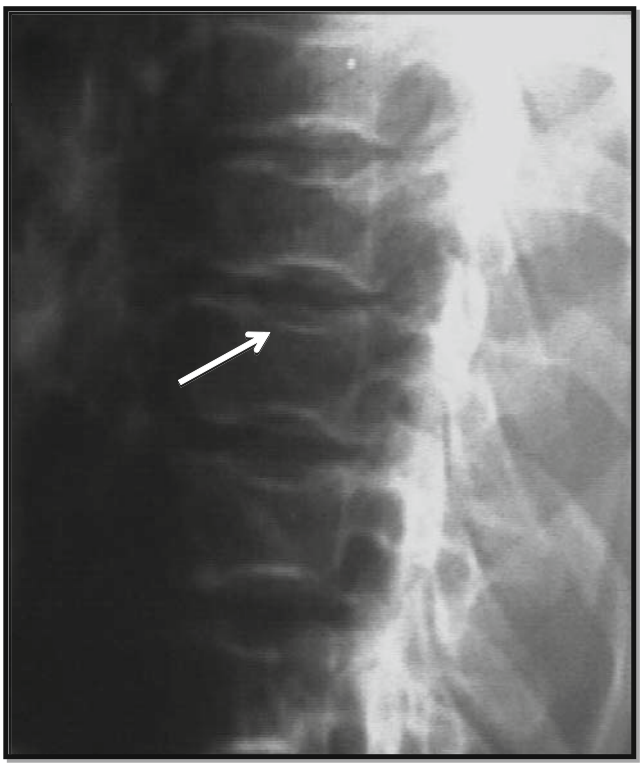

Fig. 9.1 Lateral thoracic spine in a patient with SCD shows diffuse osteopenia with H-shaped vertebral deformity due to central end plate infarcts (*arrow*)

The most common radiologic features result from red marrow hyperplasia, leading to cortical thinning and trabecular prominence in long bones, diploic widening of the skull with relative sparing of the occipital bone, and osteopenia in vertebral bodies (Fig. 9.1) as well as growth disturbances leading to shortening of long bones. Changes in the skull can cause a so-called hair-on-end appearance of the diploic space. A similar radiographic appearance in the calvarium may also be seen in patients with thalassemia major. Thalassemia patients also have failure of sinus development leading to "chipmunk facies" (Figs. 9.11 and 9.13).

Other characteristic features of SCD result from ischemia and osteonecrosis occurring throughout the skeleton. Multiple small infarcts lead to reactive sclerosis throughout the skeleton, causing dense-appearing bones on radiographs. Larger scale infarction in the developing skeleton can lead to skeletal deformities, including H-shaped vertebrae caused by ischemia of central portion of the growth plate (Fig. 9.1), tibiotalar slant (from partial talar epiphyseal infarction (Fig. 9.2)), Madelung deformity (from partial distal radial epiphyseal infarction (Fig. 9.3)), bone within bone appearance (Fig. 9.4), epiphyseal infarcts in femoral and humeral heads (Figs. 9.5 and 9.6), and HFS.

Infarctions manifest with an ill-defined zone of radiolucency that subsequently evolves into arc-like subchon-

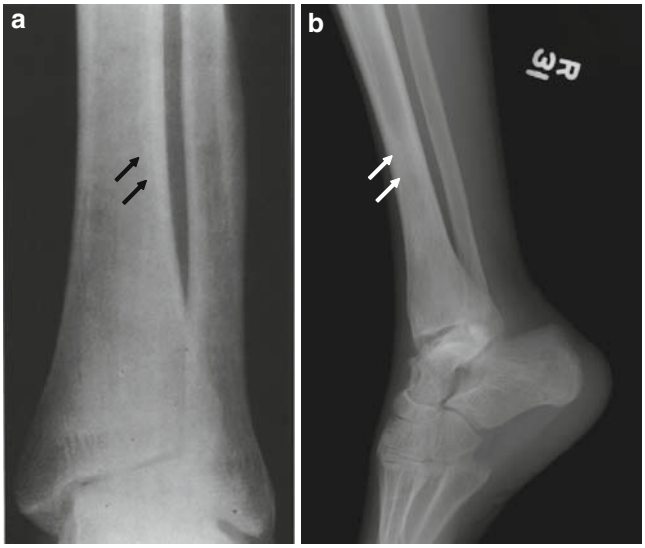

Fig. 9.2 AP (**a**) and lateral (**b**) ankle radiographs in SCD with distal tibial epiphyseal and talar dome infarcts and consequent tibiotalar slant. Also note focal distal tibial diaphyseal sclerosis consistent with additional medullary infarct (*arrow*)

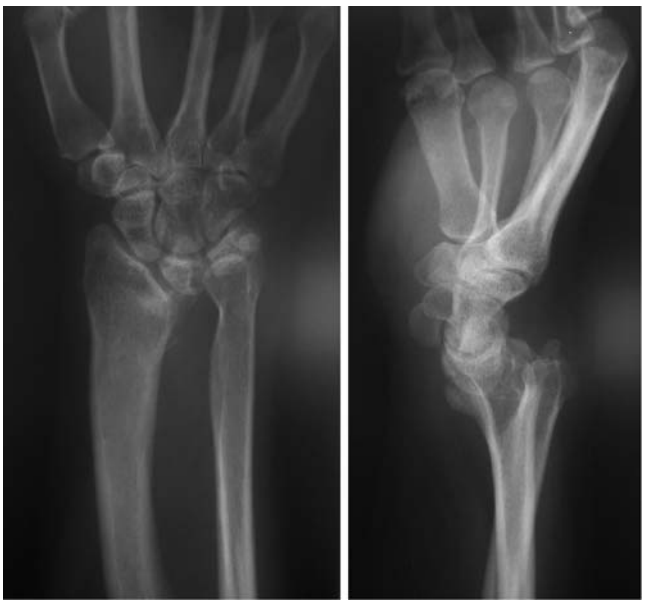

Fig. 9.3 Madelung deformity due to developmental abnormality of distal radial and ulnar epiphyses. There is V-shaped radiocarpal space with dorsal subluxation of ulna and triangular appearance of carpus (case courtesy Dr. K Nakhoda, MD)

dral and serpigineous intramedullary areas or patchy lucent and sclerotic areas (see Chapter 4 on osseous ischemia and Figs. 9.6, 9.7, and 9.8). A peripheral rim of sclerosis is often seen, especially with medullary bone infarcts (Fig. 9.8). If cortical, subperiosteal new bone may form leading to thickening of the cortex or layered new bone along the inner surface of the cortex causing "bone-within-bone" appearance (Fig. 9.4). On CT, an infarct initially manifests as disruption of the normal trabecular architecture and may be difficult to detect. In epiphyseal osteonecrosis, subsequent radiographs show subchondral lucent areas (*crescent sign*, Fig. 9.6a) and, finally, flattening of the articular surface (Figs. 9.5, 9.6, and 9.7). Over time, osteoarthritis may occur and in weight-bearing joints, such as the hip, joint replacement may be necessary (Fig. 9.7a).

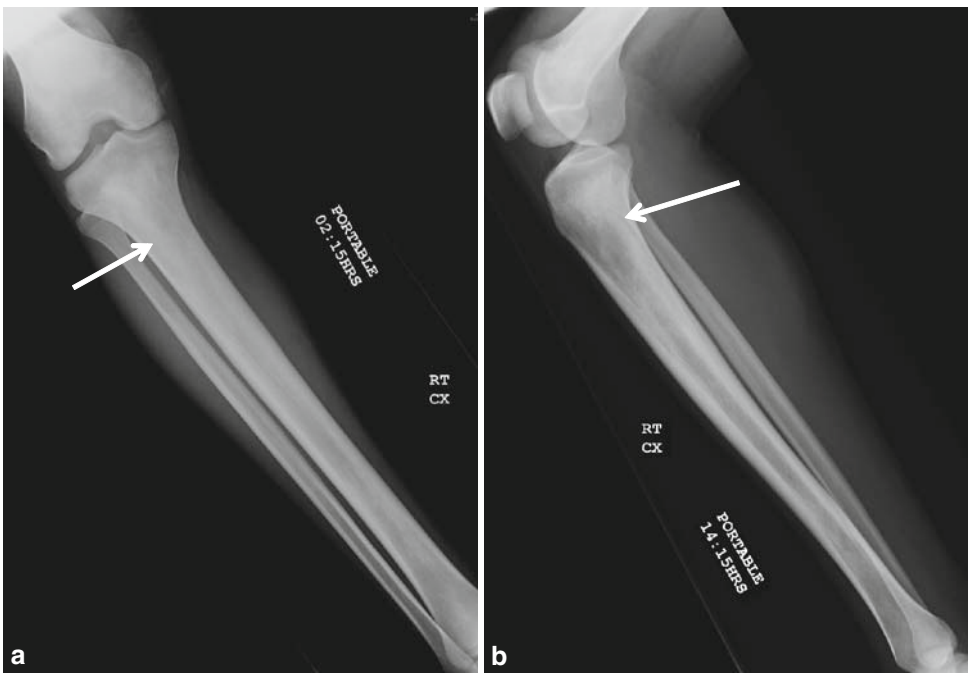

Fig. 9.4 Young boy with SCD. AP (**a**) and lateral (**b**) views of right leg show elongated area of sclerosis in proximal tibial metaphysis (*arrows*) related to medullary infarction, simulating bone within appearance (case courtesy Dr. E. Smergel, MD)

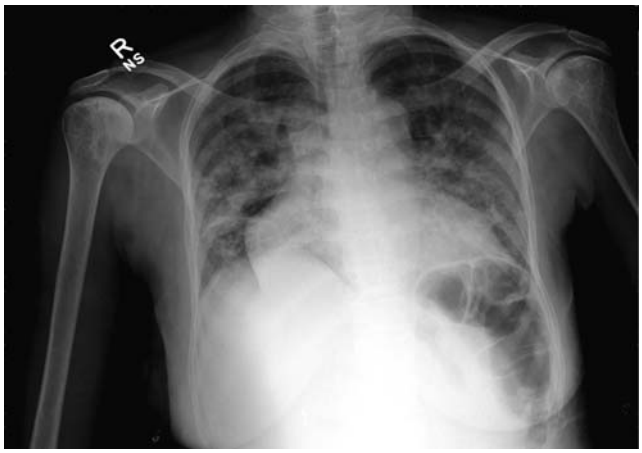

Fig. 9.5 AP chest radiograph in SCD with bilateral humeral epiphyseal infarcts leading to sclerosis and of humeral heads. Also note cardiomegaly and pulmonary congestion from high-output cardiac failure. The gas-filled splenic flexure of the colon is immediately under the left hemidiaphragm as a result of splenic infraction. The patient has had a cholecystectomy because of pigmented gallstone-induced cholecystitis

Salmonella osteomyelitis occurs with higher incidence in patients with sickle cell disease than in the unaffected population. For unknown reasons, symmetrical osseous involvement occurs frequently with salmonella osteomyelitis. The clinical picture may be atypical for osteomyelitis and hence difficult to distinguish from a typical sickle cell crisis caused by ischemia or microinfarction. Bone infarction is estimated to be at least 50 times more common than osteomyelitis in sickle cell disease. Indium leukocyte and technitium sulfor colloid scans may help differentiate infection from infarction in SSD.

Other radiographic findings in SCD may be encountered during skeletal survey as a result of sickle cell pathophysiology. These include cardiomegaly (Fig. 9.5), congestive cardiac failure, pulmonary artery hypertension, cholelithiasis, posterior mediastinal mass of extramedullary hematopoiesis, and splenic calcifications (autosplenectomy). Typically, extramedullary hematopoiesis occurs between the T8 and L2 levels of the spine, but it can arise anywhere, particularly as an intrapelvic mass.

Nuclear Imaging

Radionuclide bone scans with Tc99m MDP usually show heterogeneous uptake in the axial and appendicular skeleton, especially in peri-articular distribution related to previous episodes of bone infarction. There is often increased uptake as well as enlargement of both kidneys and spleen (Fig. 9.9). During the ischemic crisis, bone scan may show areas of decreased radiopharmaceutical activity in areas of acute

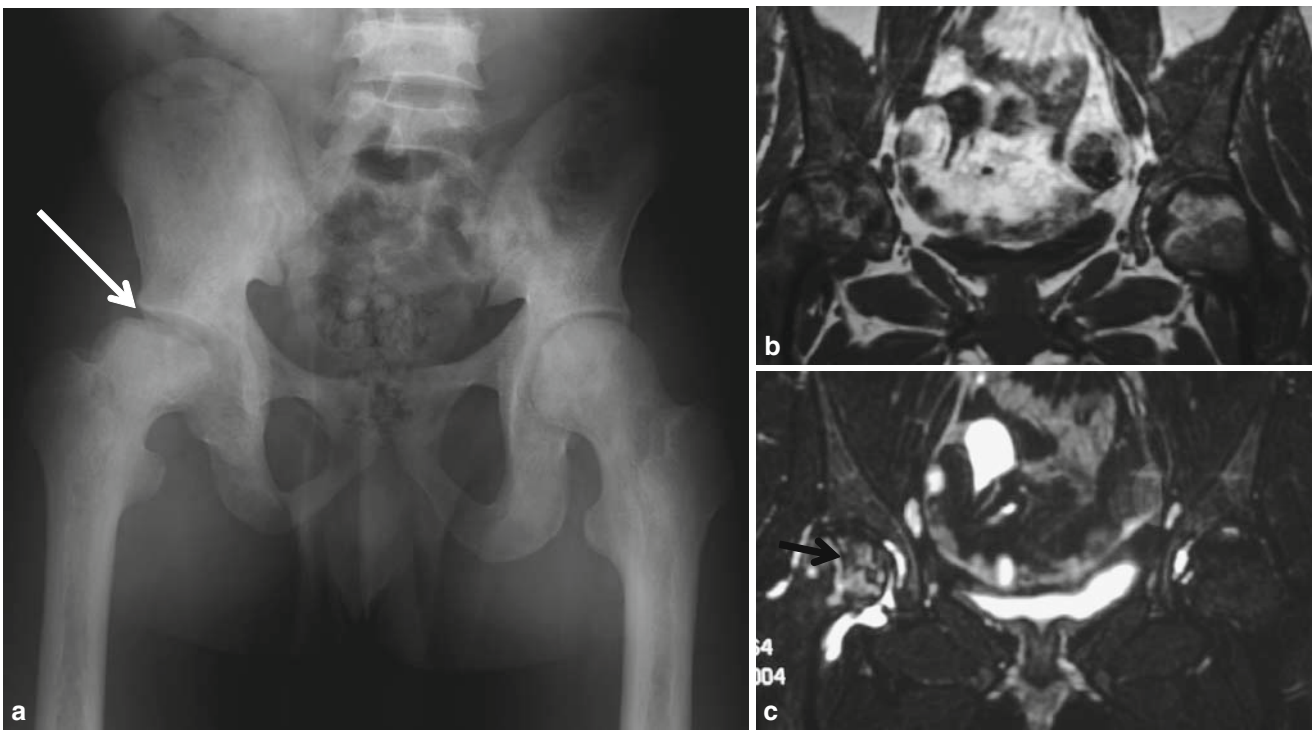

Fig. 9.6 AP pelvis (**a**), coronal T1W (**b**), and coronal fat-saturated T2W (**c**) images show bilateral femoral epiphyseal infarcts and marrow reconversion. Note crescent sign in right femoral head (*arrow*) with advanced collapse. Double ring sign (*white arrow*) is seen on T2W MRI (**c**)

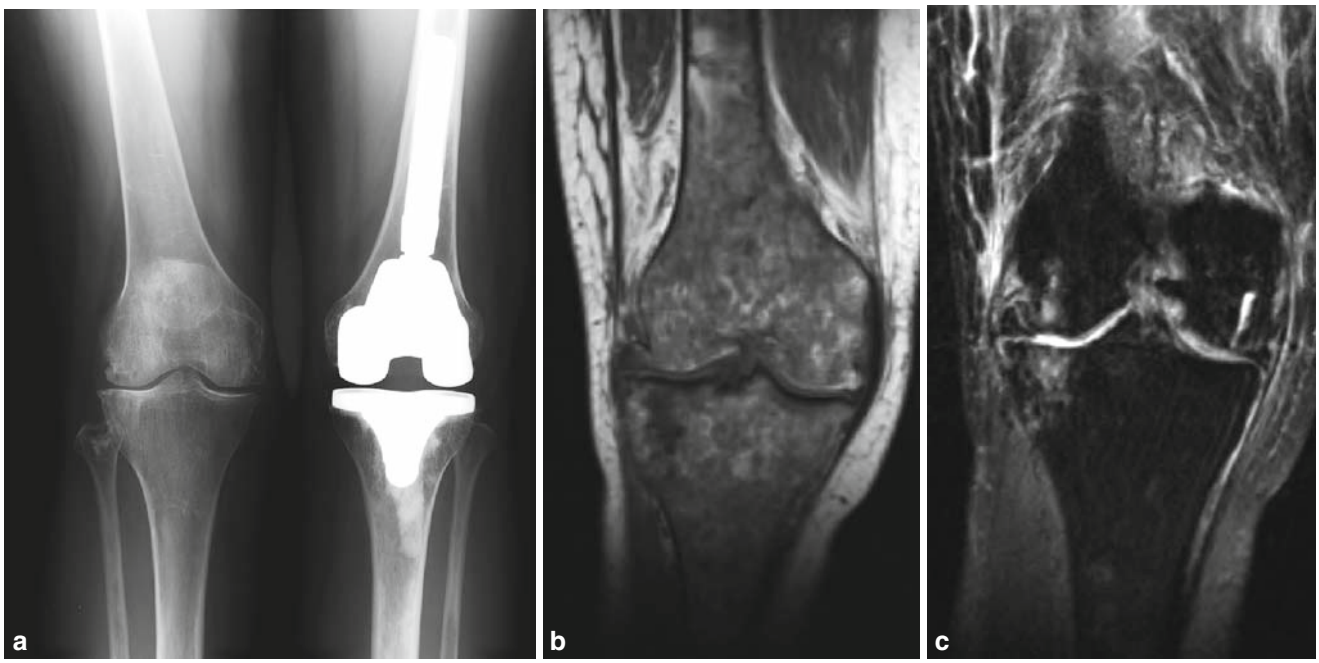

Fig. 9.7 AP knee radiograph (**a**), T1W (**b**), and T2W (**c**) coronal MR images of a 53-year-old woman with long-standing SCD. Note epiphyseal infarcts in distal femur and lateral tibial plateau. There is diffuse T1W (**b**) and T2W (**c**) marrow signal hypointensity consistent with marrow reconversion and secondary hemosiderosis. There is articular cartilage loss of the lateral tibiofemoral compartment with secondary OA. Left knee prosthesis is in expected position

infarction. Over the ensuing days to weeks, activity increases as a result of reactive bone formation, which persists for several months. A combination of Tc99m MDP and T99m sulfur colloid scan may help to differentiate symptomatic bone infarction from infection. Osteonecrosis shows disproportionately smaller area of activity on Tc99m MDP bone scan compared with Tc99m sulfur colloid marrow scan. In osteomyelitis this differential activity does not occur. Alternatively, an indium-labeled WBC scan may be performed. These studies show preferential uptake in the areas of infection with relatively little or no activity in the areas of infarction.

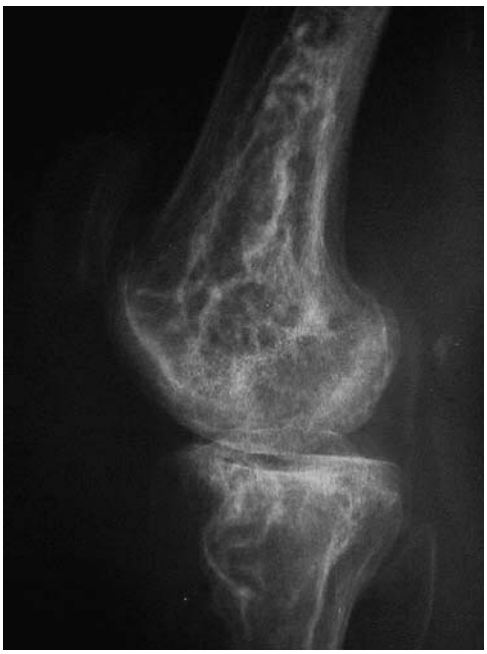

Fig. 9.8 Lateral knee radiographs showing epiphyseal and medullary bone infarcts in a case of SCD. Note serpigineous and arc-like sclerotic margin of infarcts

Magnetic Resonance Imaging

MRI is extremely sensitive to bone marrow changes. Normal muscle and intervertebral discs provide a reference to distinguish red marrow from pathologically infiltrated marrow. Normal red marrow still contains substantial fat (~40%) and so the signal intensity of appendicular red marrow is iso- to hyperintense to muscle, and normal vertebral marrow is hyperintense to adjacent intervertebral disc on T1-weighted (T1W) images. The signal intensity (SI) on fat-saturated fluid-sensitive (T2-weighted (T2W) or inversion recovery) images is mildly T2 hyperintense. There may be very mild enhancement on postcontrast images.

Substantial red marrow reconversion occurs in sickle cell disease (Fig. 9.5b, c) and other anemias. Reconversion begins in the calvarium and progresses to vertebrae, ribs, sternum, and pelvis followed ultimately by reconversion in the extremities. In appendicular skeleton, the marrow progresses from

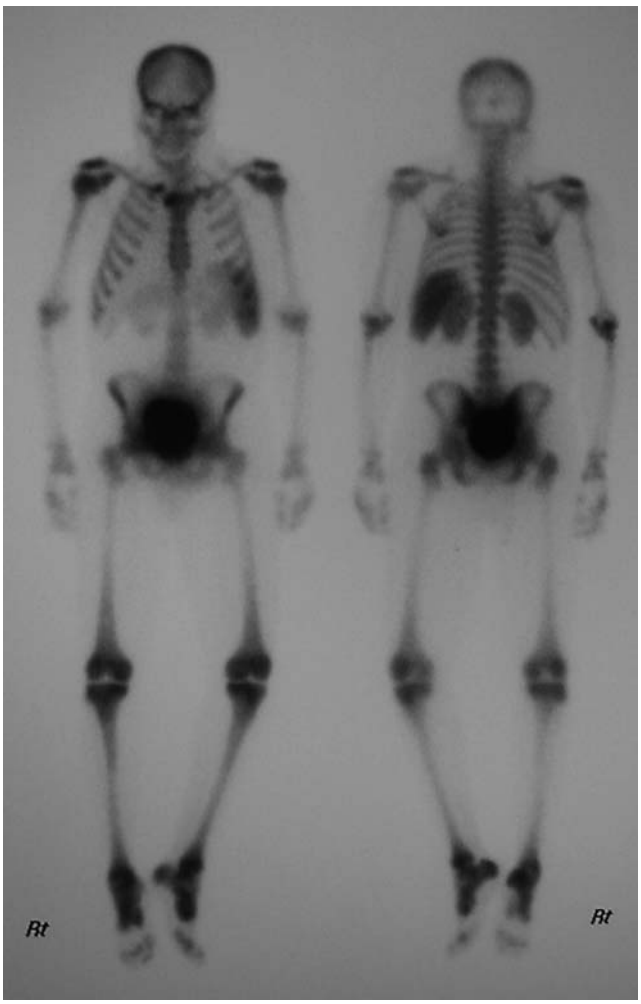

Fig. 9.9 Whole-body Tc99MDP images in anterior and posterior projections in a case of SCD. There is increased peri-articular uptake and abnormal bilateral renal cortical and splenic uptake along with splenomegaly. A common appearance (case courtesy Dr. K Nakhoda, MD)

proximal to distal. The epiphyses are spared unless extreme needs are present. The signal intensity also changes to iso- to hypointense to both muscle and intervertebral disc signal on T1W images and iso- to hyperintense to these tissues on T2W images.

MR imaging, especially with fat-saturated fluid-sensitive sequences, is very sensitive for detection of early marrow edema and infarction. Infarction may be detected as early as a few days after the ischemic insult as an area of high signal intensity on T2W and inversion recovery images, with or without abnormal periosteal reaction and soft tissue edema. Over time, these areas will become low signal intensity on all MR images as fibrosis and sclerosis replace the infarcted region (Figs. 9.6, and 9.7). Vaso-occlusion may occur in muscle tissue, leading to edema and myonecrosis. Fluid collections including hematomas and fat necrosis may occur in soft tissues.

Sometimes, the marrow reconversion is heterogeneous, which may make it difficult to distinguish it from neoplastic marrow infiltration. Increasing T2 hyperintensity, marked postgadolinium enhancement, and cortical disruption with or without the presence of soft tissue mass should suggest pathologic marrow infiltration rather than reconversion related to marrow hyperplasia. Focal neoplastic lesions can also be differentiated from foci of red marrow using chemical shift MR imaging technique. Unlike neoplastic foci, red marrow shows significant signal loss on out-of-phase images as compared with in-phase images.

Thalassemia

Thalassemia is an autosomal recessive condition characterized by reduced rate of synthesis of the globin chains of hemoglobin resulting in microcytic hypochromic type of hemolytic anemia. Both α and β chain hemoglobin mutations may cause thalassemia. The alpha thalassemias involve mutations of the genes *HBA1* and *HBA2* or deletions from the 16p chromosome. They result in decreased α-globin chain production, resulting in an excess of β chains in adults and excess γ chains in newborns. Beta thalassemias are caused by mutations in the *HBB* gene on chromosome 11. A δ chain form of the disease has been reported among the 3% of the population with δ chain hemoglobin. As a result of these mutations, patients have an imbalance of normal α and β chain production. This imbalance results in the formation of inherently unstable hemoglobin tetramers of one chain or another instead of two α and two β chains.

Thalassemia is particularly prevalent among Mediterranean people, including Greece, southern Italy, and the Maldives. Heterozygosity for thalassemia occurs in 2.5% of Italian Americans and about 10% of Greek Americans. There are major, minor, and intermedia clinical variants of thalassemia, depending on the zygosity of the patient and hence the severity of the α and β chain imbalance, resulting in varying degrees of anemia severity. Beta thalassemia, also known as Cooley anemia, is the most common form of the disease in the United States, but only about 800–1,000 patients in this country have homozygous beta thalassemia. These patients are concentrated on the East Coast, mainly between Boston and New York.

Clinical symptoms vary from none in thalassemia trait to severe symptoms of anemia in thalassemia major. Patients are pale and listless, have dark urine, jaundice, delayed growth and puberty, and enlarged spleen, liver, and heart.

Radiologically, beta thalassemia major causes the most findings, and they occur in both axial and appendicular skeleton, especially hands and feet in early years of life and axial and proximal appendicular skeleton in adults. Common

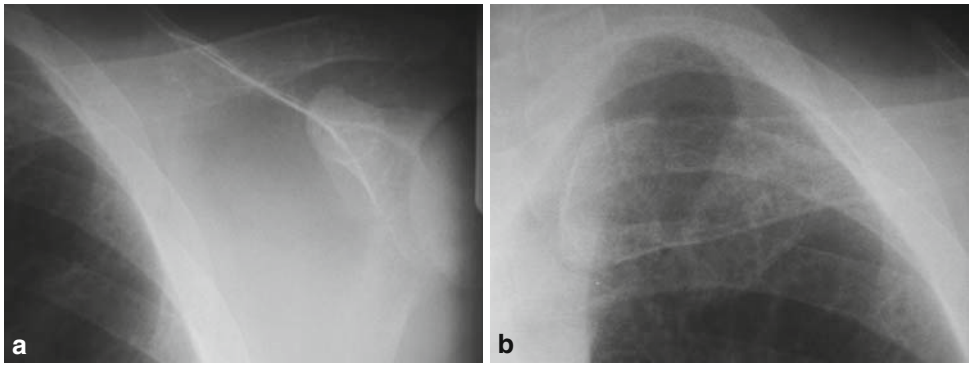

Fig. 9.10 Thirty-four-year-old man with thalassemia major. AP views of left upper chest show changes of marrow expansion with cortical thinning and trabecular prominence

radiologic features include cortical thinning and resorption of cancellous bones (Fig. 9.10), diploic space widening of the calvarium with relative sparing of occipital bone (Fig. 9.11), and osteopenia in vertebral bodies (Fig. 9.12b) as well as growth disturbances leading to shortening of long bones.

Generally, beta thalassemia major causes greater marrow expansion than does sickle cell disease. As a result, there may be bulbous expansion of the ribs and deposits of extramedullary hematopoiesis may be noted paravertebrally, extending on both sides of the spine (Fig. 9.12a). A typical rib-within-rib appearance (Fig. 9.12a) may be seen as an elongated density within anterior portions of the ribs, less commonly seen in sickle cell disease. Marked hair-on-end appearance of the skull (Fig. 9.13), no or delayed pneumatization of paranasal sinuses, dental malalignment, lateral displacement of orbits, dental protrusion and malalignment rodent or "chipmunk" facies (Figs. 9.11 and 9.13), and modeling deformity of long bones (Erlenmeyer flask deformity) also seen in other marrow infiltrating diseases such as Gaucher disease and osteopetrosis, may all occur as a result of marrow space expansion in this disease. Patients also have increased incidence of spontaneous fractures and premature fusion of their long bone epiphyses. The epiphyseal fusion may involve only a segment of the physis rather than its entire width, manifesting as an area of focal sclerosis at the

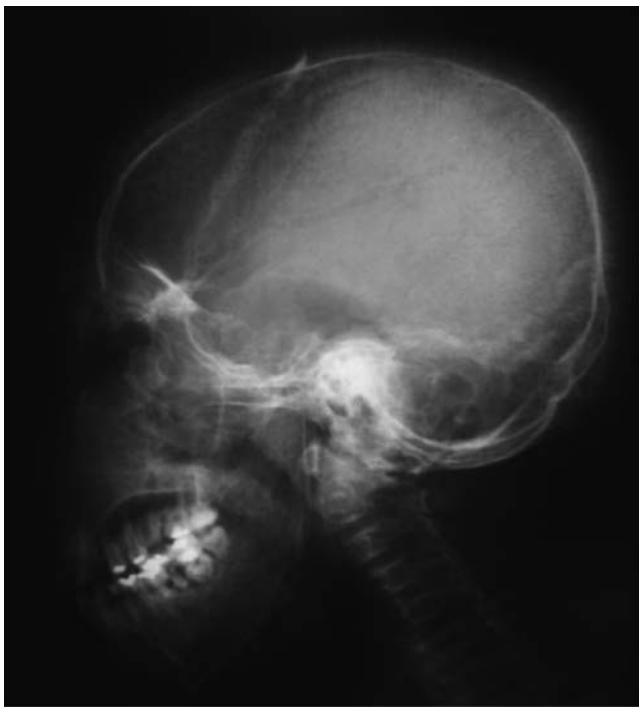

Fig. 9.11 Lateral skull from a patient with thalassemia major showing diploic widening with relative sparing of the occipital bone. Also note dental malocclusion and underpneumatized paranasal sinuses with rodent facies

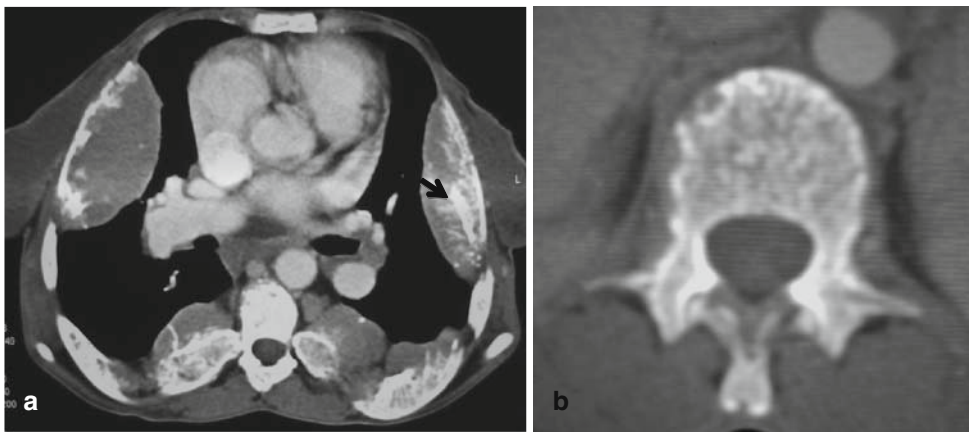

Fig. 9.12 Forty-year-old woman with thalassemia intermedia. CECT images through lower chest show expansion of multiple ribs with bilateral paravertebral areas of extramedullary hematopoiesis (*white arrows*). Also note rib-within-rib appearance in the left lower rib (*black arrow*). Osteopenia of the upper lumbar vertebra in the same patient (**b**)

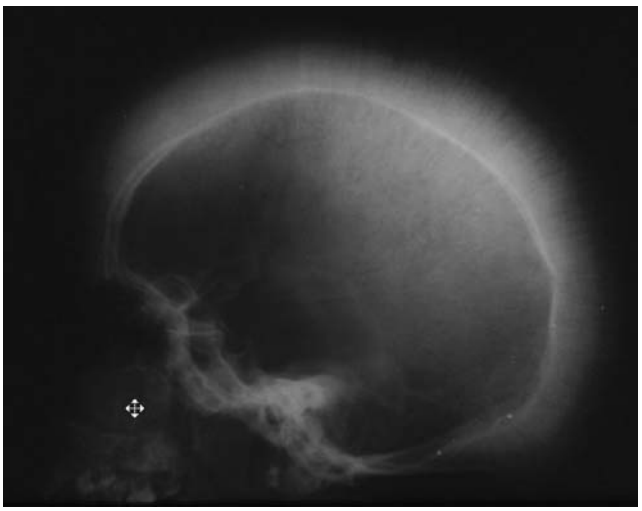

Fig. 9.13 Lateral view of skull in a thalassemia major patient shows hair-on-end appearance. Also note underpneumatization of paranasal sinuses

site. This eccentric fusion leads to partial premature physeal fusion, deformity and abnormal tilt of the epiphysis. In the upper arm, it may be seen as varus deformity of humerus with consequent shortening of the upper arm. Madelung deformity in the wrist and tibiotalar slant at the ankle joint may also occur.

Other findings encountered may be related to complications of the disease, such as secondary hemochromatosis-related arthropathy, particularly in the metacarpophalangeal joints, knees, and hips. Patients may also develop desferoxamine-induced bone dysplasia as a result of chelation therapy. This rare disorder manifests as flattening of the thoracic and lumbar vertebral bodies, metaphyseal osseous defects, widened growth plates, and genu valgum. Gout or CPPD arthropathy may also be seen late in the disease process.

MR imaging especially with gradient echo sequences is helpful to assess the severity of iron deposition and response to chelation therapy. Iron deposition results in hypointense signal intensity relative to skeletal muscle on GRE images in liver, heart, and spleen due to magnetic susceptibility. As in sickle cell disease, marrow reconversion is also seen in a characteristic distribution.

Soft tissue masses related to extramedullary hematopoiesis, hand, feet, and rib involvement, Erlenmeyer flask deformity of long bones, and hair-on-end appearance of skull occur more commonly in thalassemia than in sickle cell disease. Osteonecrosis/bone infarctions, H-shaped vertebrae, and infections occur more frequently in sickle cell disease.

Mixed Hemoglobinopathies

Sickle cell disease and thalassemia do not occur always in pure form but may combine with other inherited hemoglobin abnormalities. In mixed hemoglobinopathies, there is mixed inheritance of genes of different abnormal hemoglobin chains. These include rare diseases such as sickle cell hemoglobin C (SC) disease (clinically similar to SCD but with splenomegaly instead of splenic infarction), sickle cell thalassemia, sickle cell hemoglobin D (SD) disease, hemoglobin E/thalassemia (common in Cambodia, Thailand, and parts of India), and hemoglobin C/thalassemia.

The skeletal changes, in general, are less severe and appear at older age in sickle cell variants than in the sickle cell disease. Skull changes are particularly uncommon. Vertebral osteopenia, H-shaped deformity, and epiphyseal osteonecrosis are the most common findings encountered.

Iron Deficiency Anemia

Skeletal changes are usually mild in iron deficiency anemia and dominate in axial skeleton. Skull changes are most common, manifesting as osteopenia, occasional diploic widening, and coarsened trabeculations. Similar changes are also seen in nonspherocytic hemolytic anemias, such as pyruvate kinase deficiency and G6PD deficiency anemia. Hair-on-end appearance has been reported in iron deficiency anemia but is extremely rare.

Fanconi Aplastic Anemia

Fanconi anemia usually manifests as pancytopenia with many other associated anomalies, such as abnormal skin pigmentation, renal anomalies, dwarfism, developmental dysplasia of hip, Klippel–Feil deformity, and clubfoot. Skeletal anomalies are some of the initial manifestations of the disease and may point to the diagnosis. Unilateral or bilateral radial ray defects in the form of constriction of bones, hypo- or aplasia of radius, metacarpal or phalanges of thumb are common. Similar changes occur in Holt–Oram syndrome (Fig. 9.14), congenital biliary dysplasia, and the synphalangism syndromes, including Apert, Carpenter, and Pfeiffer syndromes. Other conditions with radial ray anomaly include THAR syndrome (thrombocytopenia with absent radius). In THAR syndrome, pancytopenia is uncommon, prognosis is better, radial anomalies are almost invariably bilateral, and the thumb is always present.

Secondary causes of aplastic anemia are myriad, including drugs, such as chloramphenicol, phenylbutazone, and gold, radiation, viral infections, and thymoma. MR imaging of the spine in Fanconi or other causes of aplastic anemia will show fatty marrow conversion and upon treatment with one or a combination of colony stimulating factor, erythropoietin, blood transfusions, etc., MR imaging will show red marrow reconversion, especially at the vertebral end plates.

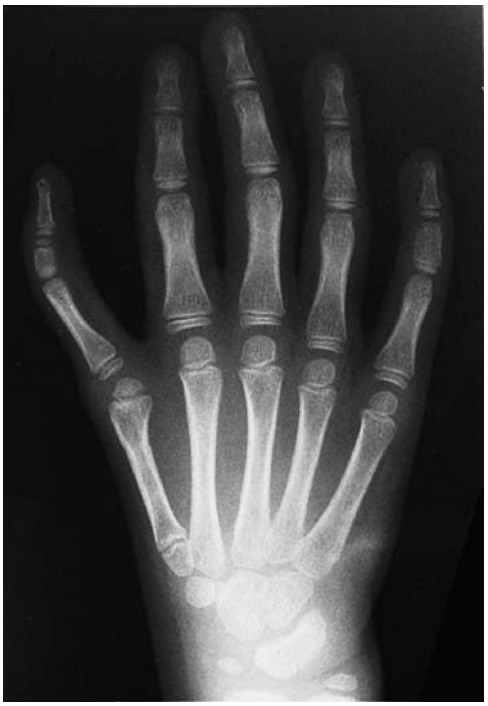

Fig. 9.14 Case of Holt–Oram syndrome with radial ray anomaly (triphalangeal thumb)

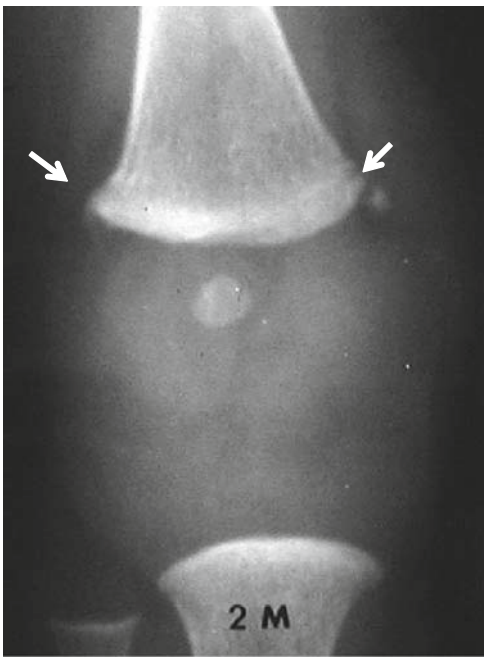

Fig. 9.15 Two-month-old boy with Menkes disease shows corner lesions (*arrows*) similar to battered baby syndrome (case courtesy Dr. E. Smergel, MD). Note that Menkes disease or congenital copper deficiency has radiological similarities to scurvy

Hereditary Spherocytosis

It is a hemolytic anemia caused by abnormal osmotic fragility related to an unusual spherical shape of red blood cells (RBCs). It arises most commonly in northern Europeans. These abnormally shaped cells are sequestered and destroyed in the spleen leading to anemia, jaundice, and splenomegaly. As the disease is often not detected until adulthood, skeletal changes are usually evident in skull and vertebrae in the form of marrow hyperplasia, osteopenia, and coarsened trabeculations. Extramedullary hematopoiesis has been reported in paravertebral and pelvic locations. The disease may improve following splenectomy.

Copper Deficiency

Copper is a trace element required by many enzymes in metabolic function. Nutritional deficiency may be seen in premature newborns or patients on long-term total parenteral nutrition without copper supplementation. The deficiency leads to anemia and manifests as osteoporosis, metaphyseal irregularity, and fractures. Menkes syndrome (MS), an X-linked neurodegenerative disorder, is also associated with abnormal distribution of copper in body cells. It is caused by a mutation in *ATP7A* gene. Menkes and Wilson disease genes have 55% amino acid identity. In MS, copper accumulates in small intestine and kidneys, while the brain and other tissues have unusually low levels. Clinical manifestations include seizures, developmental delay, failure to thrive, subnormal body temperature, and strikingly peculiar kinky hairs. Radiologic findings include osteoporosis, metaphyseal flaring, corner lesions similar to battered baby syndrome (Fig. 9.15), epiphyseal fragmentation, especially in humerus and femur, and increased incidence of fractures.

Myelofibrosis

Also referred to as agnogenic myeloid metaplasia, myelofibrosis is a disease of the elderly, commonly seen in the sixth–eighth decade of life. The disease is characterized by bone marrow replacement related to abnormal proliferation of marrow stem cells and progressive fibrosis/sclerosis leading to pancytopenia. The degree of fibrosis dictates the severity of disease process. It is commonly primary/idiopathic or may occur secondary to a variety of neoplastic (advanced leukemia/lymphoma/polycythemia vera, metastases) infections such as TB, radiation, toxins. The primary variety demonstrates JAK 2 mutation on Val 617 Phe locus in 50% of the cases. Radiographically, the changes are most pronounced in axial and proximal appendicular skeleton. A traid of pancytopenia, splenomegaly, and diffuse osteosclerosis is characteristic (Fig. 9.16).

Radiographically, the changes are most pronounced in axial and proximal appendicular skeleton. A triad of pancytopenia, splenomegaly, and diffuse osteosclerosis is characteristic. Although diffuse osteosclerosis is

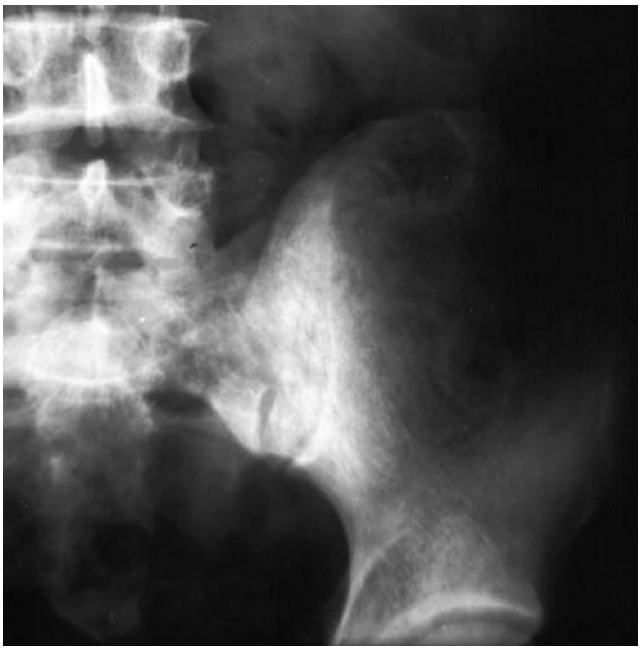

Fig. 9.16 AP radiograph of the left hemipelvis in a 50-year-old anemic woman with myelofibrosis. Note the patchy diffuse sclerotic changes in the medullary cavity of the hemipelvis and spine

typical, some cases may show normal or decreased bone density. Extramedullary hematopoiesis manifests as hepatosplenomegaly and bilateral paravertebral masses similar to thalassemia. Other findings may include hemarthrosis, polyarthritis, and secondary gouty arthritis. MRI shows changes of red marrow reconversion and increased T2W signal intensity in active cellular phase. With progressive fibrosis, the marrow signal intensity becomes hypointense on all sequences. MRI of the skeleton provides a comprehensive assessment of the pattern and extent of fibrosis and allows for correlation with biopsy findings.

The differential diagnosis includes leukemia/lymphoma, mastocytosis, renal osteodystrophy, and fluorosis. Lymphoma, leukemia, and mastocytosis are usually patchy and are usually not that widespread. Mastocytosis is also associated with nodular small intestinal mucosal thickening and systemic manifestations of urticaria, diarrhea, bronchospasm, and flushing related to excessive serotonin production by mast cells. Renal osteodystrophy is distinguished by the presence of other accompanying changes of secondary hyperparathyroidism and osteomalacia. Fluorosis can also be differentiated by additional presence of enthesopathic changes, ligament calcifications, and periostitis.

Further Readings

1. Moseley JE. Skeletal changes in the anemias. Semin Roentgenol. 1974 Jul; 9(3): 169–184.
2. Sebes JI, Diggs LW. Radiographic changes of the skull in sickle cell anemia. AJR Am J Roentgenol. 1979; 132: 373–377.
3. Keeley K, Buchanan GR. Acute infarction of long bones in children with sickle cell anemia. J Pediatr. 1982; 101: 170–175.
4. Feldman F, Zwass A, Staron RB, Haramati N. MRI of soft tissue abnormalities: a primary cause of sickle cell crisis. Skeletal Radiol. 1993; 22: 501–506.
5. Bonnerot V, Sebag G, de Montalembert M, et al. Gadolinium-DOTA enhanced MRI of painful osseous crises in children with sickle cell anemia. Pediatr Radiol. 1994; 24: 92–95.
6. Babhulkar SS, Pande K, Babhulkar S. The hand-foot syndrome in sickle-cell haemoglobinopathy. J Bone Joint Surg Br. 1995; 77: 310–312.
7. Smith JA. Bone disorders in sickle cell disease. Hematol Oncol Clin North Am. 1996; 10: 1345–356.
8. Deely DM, Schweitzer ME. MR imaging of bone marrow disorders. Radiol Clin North Am. 1997; 35: 193–212.
9. Marlow TJ, Brunson CY, Jackson S, Schabel SI. "Tower vertebra": a new observation in sickle cell disease. Skeletal Radiol. 1998; 27: 195–198.
10. Burnett MW, Bass JW, Cook BA. Etiology of osteomyelitis complicating sickle cell disease. Pediatrics. 1998; 101: 296–297.
11. Frush DP, Heyneman LE, Ware RE, Bissett GS. MR features of soft-tissue abnormalities due to acute marrow infarction in five children with sickle cell disease. AJR Am J Roentgenol. 1999; 173: 989–993.
12. Umans H, Haramati N, Flusser G. The diagnostic role of gadolinium enhanced MRI in distinguishing between acute medullary bone infarct and osteomyelitis. Magn Reson Imaging. 2000; 18: 255–262.
13. Skaggs DL, Kim SK, Greene NW, Harris D, Miller JH. Differentiation between bone infarction and acute osteomyelitis in children with sickle-cell disease with use of sequential radionuclide bone-marrow and bone scans. J Bone Joint Surg Am. 2001; 83-A:1810–1813.
14. Lonergan GJ, Cline DB, Abbondanzo SL. Sickle cell anemia. RadioGraphics. 2001; 21: 971–994.
15. Bahebeck J, Atangana R, Techa A, Monny-Lobe M, Sosso M, Hoffmeyer P. Relative rates and features of musculoskeletal complications in adult sicklers. Acta Orthop Belg. 2004; 70: 107–111.
16. Palestro CJ, Love C, Tronco G, et al. Combined labeled leukocyte and technetium 99m sulfur colloid bone marrow imaging for diagnosing musculoskeletal infection. Radiographics. 2006; 26:859–70.
17. Ejindu VC, Hine AL, Mashayekhi M, Shorvon PJ, Misra RR. Musculoskeletal manifestations of sickle cell disease. RadioGraphics. 2007 JulA-ug; 27(4): 1005–21.
18. Caffey J. Cooley's anemia: a review of the roentgenographic findings in the skeleton: Hickey lecture, 1957. Am J Roentgenol Radium Ther Nucl Med. 1957 Sep; 78(3): 381–91.
19. Sfikakis P, Stamatoyannopoulos G. Bone changes in thalassemia trait. Acta Haematol. 1963; (Basel) 29: 193–201.
20. Korsten J, Grossman H, Winchester PH, et al. Extrameduhary hematopoiesis in patients with thalassemia anemia. Radiology. 1970; 95: 257–263.
21. Exarchou E, Politou C, Vretou E, Pasparakis D, Madessis G, Caramerou A. Fractures and epiphyseal deformities in beta-thalassemia. Clin Orthop Relat Res. 1984 Oct; 189: 229–233.
22. Brill PW, Winchester P, Giardina PJ, Cunningham-Rundles S. Deferoxamine-induced bone dysplasia in patients with thalassemia major. AJR Am J Roentgenol. 1991 Mar; 156(3): 561–565.
23. Aviña-Zubieta JA, Galindo-Rodriguez G, Lavalle C. Rheumatic manifestations of hematologic disorders. Curr Opin Rheumatol. 1998 Jan; 10(1): 86–90.

24. Chourmouzi D, Pistevou-Gompaki K, Plataniotis G, Skaragas G, Papadopoulos L, Drevelegas A. MRI findings of extramedullary haemopoiesis. Eur Radiol. 2001; 11(9): 1803–1806.
25. Chan YL, Pang LM, Chik KW, Cheng JC, Li CK. Patterns of bone diseases in transfusion-dependent homozygous thalassaemia major: predominance of osteoporosis and desferrioxamine-induced bone dysplasia. Pediatr Radiol. 2002 Jul; 32(7):492–497.
26. Hazza a AM, Al-Jamal G. Radiographic features of the jaws and teeth in thalassaemia major. Dentomaxillofac Radiol. 2006 Jul; 35(4): 283–288.
27. Barton CJ, Cockshott WP. Bone changes in hemoglobin SC disease. Am J Roentgenol Radium Ther Nucl Med. 1962 Sep; 88: 523–532.
28. Reynolds J, Pritchard JA, Ludders D, et al. Roentgenographic and clinical appraisal of sickle cell betathalassemia disease. Am J Roentgen.1973; 118: 378–400.
29. Moseley JE. Skull changes in chronic iron deficiency anemia. Am J Roentgen.1961; 85: 649–652.
30. Agarwal KN, Dhar N, Shah MM, Bhardwaj OP. Roentgenologic changes in iron deficiency anemia. Am J Roentgenol Radium Ther Nucl Med. 1970 Nov; 110(3): 635–637.
31. Juhl JH, Wesenberg RL, Gwinn JL. Roentgenographic findings in Fanconi s anemia. Radiology.1967 Oct; 89(4): 646–653.
32. Kaplan PA, Asleson RJ, Klassen LW, Duggan MJ. Bone marrow patterns in aplastic anemia: observations with 1.5-T MR imaging. Radiology. 1987 Aug; 164(2): 441–444.
33. Rabinowitz, JG, Moseley JE, Mitty HA, et al. Trisomy 18, esophageal atresia, anomalies of the radius, and congenital hypoplastic thrombocytopenia. Radiology.1967; 89: 488–491.
34. De Backer AI, Zachée P, Vanschoubroeck IJ, Mortelé KJ, Ros PR, Kockx MM. Extramedullary paraspinal hematopoiesis in hereditary spherocytosis. JBR-BTR. 2002 AugS-ep; 85(4): 206–208.
35. Soler R, Pombo F, Rodríguez E, Cobas A, Lago CF, Torres JP. MR findings in hereditary spherocytosis. Comput Med Imaging Graph. 1995 MarA-pr; 19(2): 247–250.
36. Halfdanarson TR, Kumar N, Li CY, Phyliky RL, Hogan WJ. Hematological manifestations of copper deficiency: a retrospective review. Eur J Haematol. 2008 Jun; 80(6): 523–531. Epub 2008 Feb 12.
37. Aoki T. Wilson s disease and Menkes disease. Pediatr Int. 1999 Aug; 41(4): 403–404.
38. Bacopoulou F, Henderson L, Philip SG. Menkes disease mimicking non-accidental injury.Arch Dis Child. 2006 Nov; 91(11): 919.
39. Tefferi A, Lasho TL, Schwager SM, Steensma DP, Mesa RA, Li CY, Wadleigh M, Gary Gilliland D. The JAK2(V617F) tyrosine kinase mutation in myelofibrosis with myeloid metaplasia: lineage specificity and clinical correlates. Br J Haematol. 2005 Nov; 131(3): 320–328.
40. Pettigrew JD, Ward HP. Correlation of radiologic, histologic, and clinical findings in agnogenic myeloid metaplasia. Radiology. 1969 Sep; 93(3): 541–548.
41. Cloran F, Banks KP. AJR teaching file: Diffuse osteosclerosis with hepatosplenomegaly. AJR Am J Roentgenol. 2007 Mar; 188(3): S18–S20.
42. Shaver RW, Clore FC. Extramedullary hematopoiesis in myeloid metaplasia. AJR Am J Roentgenol. 1981 Oct; 137(4): 874–876.

Chapter 10

Imaging Approach to Musculoskeletal Infections

William R. Reinus

Abstract As with other organs in the body, the musculoskeletal system is subject to infection. Although the most common infection in the United States is pyogenic osteomyelitis, virtually all types of infectious agents infect the musculoskeletal system, including viruses, pyogenic bacteria, mycobacteria, spirochetes, and fungi. Infection can cause both acute and chronic forms of disease, each with their own imaging characteristics. This chapter reviews the major forms of infection encountered in both the bones and the muscles, presenting the salient clinical and imaging features. Various modalities used to identify and follow infections are described. In addition, although not proven, Paget disease will be discussed in this chapter because of the mounting evidence that this represents a chronic viral infection of bone.

Keywords Osteomyelitis • Septic arthritis • Discitis • Brodie abscess • Garre disease • Sequestrum • Involucrum • Paget disease • Syphilis • *Staphylococcus aureus* • *Streptococcus pneumoniae* • *Neisseria gonorrhea* • Fungus • Coccidiomycosis • Histoplasmosis • Cryptococcus • Blastomycosis • Sarcoidosis • Pyomyositis • Madura foot necrotizing fasciitis • Meleney ulcer • Fournier gas gangrene • Leprosy • Poliomyelitis • Parsonage–Turner syndrome

Introduction

The musculoskeletal system, as with other organ systems, is subject to infection not only from bacteria but also from viruses and fungi. In the United States, the overwhelming majority of infections are pyogenic in nature. Tuberculosis follows a distant second. Fungal bone infection is uncommon in most parts of this country and viral infections, although known, are now being categorized further and recognized for what they are.

Infecting agents may attack the bone and cause osteomyelitis or attack the soft tissues and cause cellulitis, myositis, fasciitis, or abscess. They may also affect the joints and cause septic arthritis or discitis. Septic arthritis is discussed in the chapter on arthritis (Chapter 11). Cellulitis, of course, is generally evident clinically and not the province of radiology. Osteomyelitis, myositis, fasciitis, and deep abscess, on the other hand, often require imaging for diagnosis.

To this end there are many available modalities, each with their own specific utility. For example, MRI is essential to diagnose soft tissue infections such as myositis, and it is highly sensitive for the diagnosis of osteomyelitis. In the correct clinical setting, plain radiographs are highly specific for identification of osteomyelitis, though not as sensitive as MRI. Radiographs, on the other hand, have very little utility in diagnosing soft tissue infection. Nuclear medicine offers a panoply of techniques to localize and diagnose infection. The two most commonly employed today are three-phase technetium-99^{m} bone scans and indium-111-labeled white cell scans. Nuclear medicine competes favorably with MRI in diagnosing osteomyelitis, often at a lower cost to the patient. On the other hand, MRI shows the anatomy and pathology in greater detail and with greater specificity. Ultrasound also has a role, albeit limited, in diagnosing soft tissue musculoskeletal infection, particularly in identifying abscesses in smaller anatomic parts and in guiding abscess aspiration in some cases. Computed tomography may also have a role in guiding aspiration but otherwise has only a limited role in the diagnosis of musculoskeletal infections. MRI has better soft tissue definition and sensitivity for bone destruction than CT; it does not radiate the patient with X-rays and avoids the use of iodinated contrast agents. Occasionally, CT may also be useful to image sites where plain radiographs have difficulty showing detail such as the sternoclavicular joints (Fig. 10.1).

W.R. Reinus (✉)
Musculoskeletal Radiology Temple University, Temple University School of Medicine, Philadelphia, PA 19140 USA
e-mail: reinusw@tuhs.temple.edu

A. Bonakdarpour et al. (eds.), *Diagnostic Imaging of Musculoskeletal Diseases: A Systematic Approach*,
DOI 10.1007/978-1-59745-355-4_10, © Springer Science+Business Media, LLC 2010

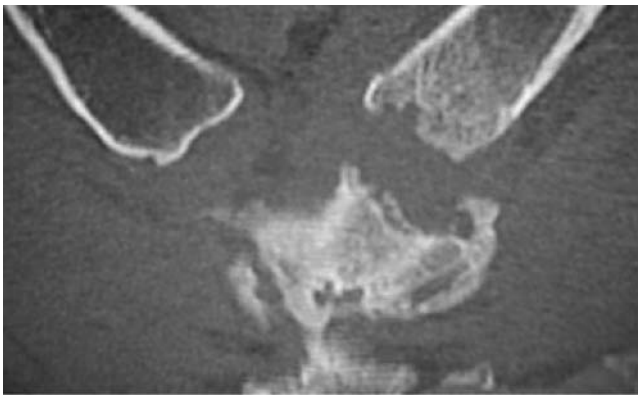

Fig. 10.1 CT reconstruction of the sternoclavicular joint showing septic arthritis on the left and osteomyelitis of the manubrium sternum. Note the destroyed cortex of the proximal left clavicle compared with the right and the destruction of the manubrium

Acute Pyogenic Osteomyelitis

When considering the diagnosis of osteomyelitis, there are two distinct populations: the pediatric and the adult population. In children, the main pathway of bone infection is hematogenous, accounting for 90–95% of osteomyelitis. On the other hand approximately 85–90% of adult osteomyelitis results from direct penetration of both the skin and subcutaneous fascia. Those adults in whom hematogenous infection is the pathway are often from particular populations such as intravenous drug abusers and patients with bacterial endocarditis where there are exceedingly large intravascular inocula of bacteria. The relatively greater competence of the immune system in adults over children is thought to be the main difference that accounts for the different pathways of infection between the two populations.

Not only do these populations have different pathways to infection but also as a consequence different bones will be affected most commonly and even different portions of the bone will be affected. Since pediatric infections are usually hematogenous, bone infection in these patients is most common in the areas of slowest flow within the most rapidly growing bones, i.e., femur (27%), tibia (22%), humerus (12%), and hands and feet (13%). This means that pediatric osteomyelitis will be most common in the subphyseal metaphysis of rapidly growing bones (Fig. 10.2). The infection also may start in the diaphysis or even in the epiphysis (Fig. 10.3). This latter location is more common than once thought.

On the other hand, adult osteomyelitis will be most common where skin ulcers tend to develop. This will primarily be in those body parts that are most subject to pressure trauma and that have the poorest blood flow, e.g., the feet in diabetics (Fig. 10.4) and the pelvis in paraplegics. In fact, the prevalence of osteomyelitis in adult patients who have penetrating wounds to the feet is about 16%, and this number jumps to 30–40% in diabetics. Those adults who do suffer from hematogenously spread osteomyelitis have a tendency to have a high rate of vertebral and sternoclavicular infection (Fig. 10.1). Even so, one may reasonably infer that a typical adult without a penetrating soft tissue ulcer, whether from anoxic or neuropathic tissue break down or from direct trauma, is unlikely to have osteomyelitis (Figs. 10.5, 10.6, and 10.7).

As already suggested, patients' immune competence will also play a role in determining the likelihood of developing osteomyelitis. Conditions that hamper the immune system predispose to development of osteomyelitis, including diabetes mellitus, sickle cell disease, AIDS, IV drug abuse, alcoholism, chronic steroid use, chronic joint disease, orthopedic prostheses, recent orthopedic surgery, and open fractures.

Infectious Agent

Although *Staphylococcus aureus* is overwhelmingly the most common infecting agent of bones, the patient's age and the condition of the immune system predispose to different varieties of bacterial infection. In neonates *Enterobacter* and streptococcus A and B are also common causes of infection. As children age, *Haemophilus influenza* and *Kingella* species become common and streptococcus B disappears as an etiologic agent. In adults, *Enterobacter*, streptococcus A, and *Haemophilus* infections are uncommon and *Kingella kingae* is virtually unseen. On the other hand, *Pseudomonas aeruginosa* infection occurs in adults, particularly in intravenous drug abusers. Underlying diseases may also influence the type of infection. For example, patients with sickle cell disease have a high incidence of salmonella-induced osteomyelitis.

Clinical Aspects of Diagnosis

As with pathophysiologic features of osteomyelitis, patients' clinical symptoms also tend to divide according to age. Younger patients may present with systemic complaints such as lethargy and fatigue. They may or may not have fever and anorexia. Neonates may show pseudoparalysis of the affected limb. Adults may also complain of systemic symptoms, but they will also often have skin ulcer with accompanying swelling and inflammation, including erythema, heat, pain, and loss of function.

Regardless of age, lab parameters can also help make the diagnosis. Although only 25% of patients have markedly

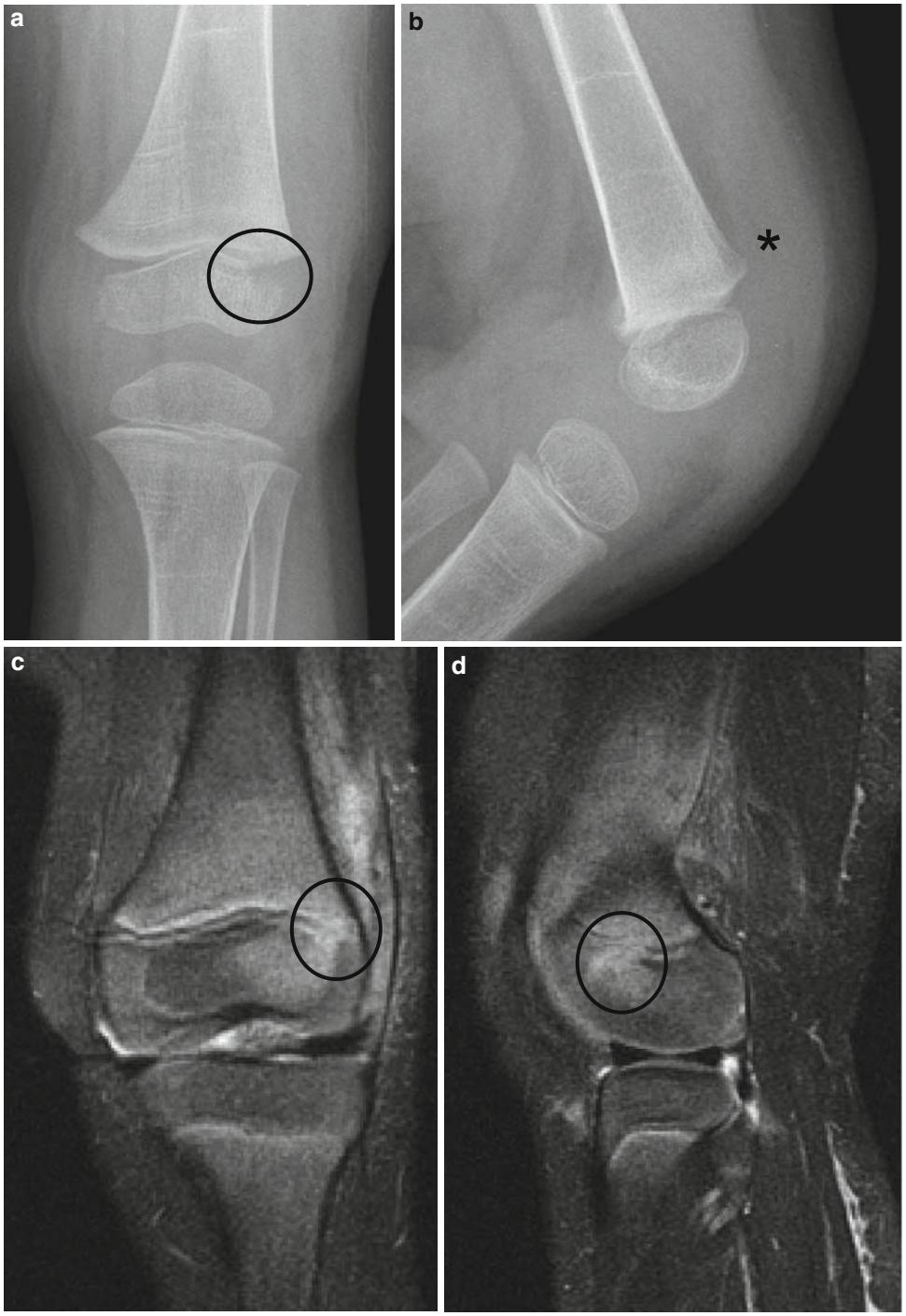

Fig. 10.2 AP (**a**) and lateral (**b**) radiographs and T2-weighted fat-suppressed coronal (**c**) and T2-weighted fat-suppressed sagittal (**d**) MR image of the left knee in a pediatric patient with osteomyelitis. Note the destruction of bone in both the metaphysis and epiphysis of the lateral aspect of the distal femur in (**a**), (**c**) and (**d**) (*circles*). A large joint effusion is noted in (**b**) (∗)

elevated white blood cell counts, acute phase reactants – erythrocyte sedimentation rate (ESR) and C-reactive protein (CRP) – are also generally elevated. Of these two reactants, the CRP is most reliable as it is elevated in 98% of cases and tracks most closely the state of the infection. Nonetheless, both ESR and CRP are non-specific and may be elevated in other diseases.

Culture is, of course, important in cases of suspected osteomyelitis. These should include both bone and blood cultures; the latter are positive in between 30 and 60% of

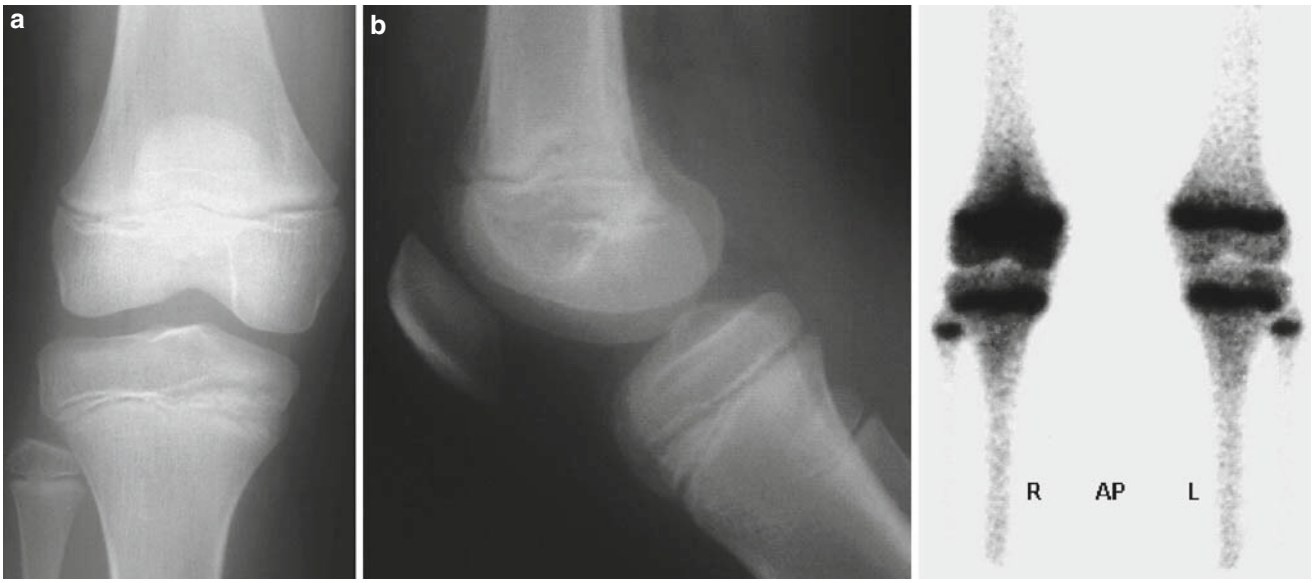

Fig. 10.3 AP (**a**) and lateral (**b**) radiographs of the right knee and an anterior projection for a Tc99m radiopharmaceutical bone scan in a pediatric patient showing abnormal activity in the right epiphysis related to early osteomyelitis. The radiographs show no abnormality

patients with osteomyelitis. Not only can culture confirm the diagnosis but is also useful to determine the appropriate antibiotic therapy. Gram stain is only positive in about one-third of bone or joint aspirates.

Radiological Pathophysiology

Pediatric Osteomyelitis

Radiological findings correspond to the underlying pathophysiology of the infection. The subphyseal bone has slow flow vessels with arteriolar loops and venous lakes. In pediatric patients there are few phagocytes in the zone of hypertrophy thus presenting the immature bone's weakest point of defense against infection. Bacteria can pass into the osseous interstitium through gaps in the capillary endothelium in the subphyseal bone. Here they cling to type II collagen. As they multiply, the body mounts an inflammatory response to the foreign antigens, and lymphocytes release octeoclast activating factor. This, in turn, causes osteoclasts to resorb bone. Simultaneously bacteria secrete lytic enzymes that directly destroy bone. These phenomena are visible in pediatric patients on radiographs as osteolysis around the physeal plate (Fig. 10.2) or on bone scan as abnormal radiopharmaceutical tracer uptake (Fig. 10.3).

Shortly after the lytic process commences, the resulting bone destruction leads to altered biomechanical stresses and changes in the reduction/oxidation potential within and around the area of infection within the bone. These phenomena eventually lead to osteoblast activation and bone remodeling that is visible on radiographs as areas of new bone formation and sclerosis (Figs. 10.8, 10.9,and 10.10).

If left untreated, the infection will spread via Volkmann canals and the Haversian system. Since pediatric periosteum is less well adherent to the bone than is adult periosteum, this spread leads to subperiosteal pus formation and cortical destruction. The cortical destruction will engender periosteal new bone formation (Fig. 10.11) as the bone remodels in competition with the destructive process. Alternatively, soft tissue infection adjacent to the bone may also cause periosteal new bone formation even though there is no actual osteomyelitis (Fig. 10.12). Thus, periosteal reaction is not specific and alone does not indicate the presence of osteomyelitis. The periosteal new bone may become rather prominent as the reparative process attempts to wall off the infection. If the infection is aggressive, however, as most pyogenic infections are, it may destroy the central portion of the periosteal new bone creating a triangular appearance known as Codman triangle (Fig. 10.11). This appearance is more common with malignancies of bone than with infection, especially today with effective antibiotic therapy. As the infection spreads through into the subperiosteal region, it may extend into the joint and cause septic arthritis (Fig. 10.7) or may penetrate into the surrounding soft tissues where it may cause an abscess.

As the infection becomes chronic, the periosteal envelope of new bone forming around the infected bone will attempt to wall off the infection leading to a radiographic appearance of a bone forming around the infection, an *involucrum* (Figs. 10.13 and 10.14). Simultaneously, the tracts that

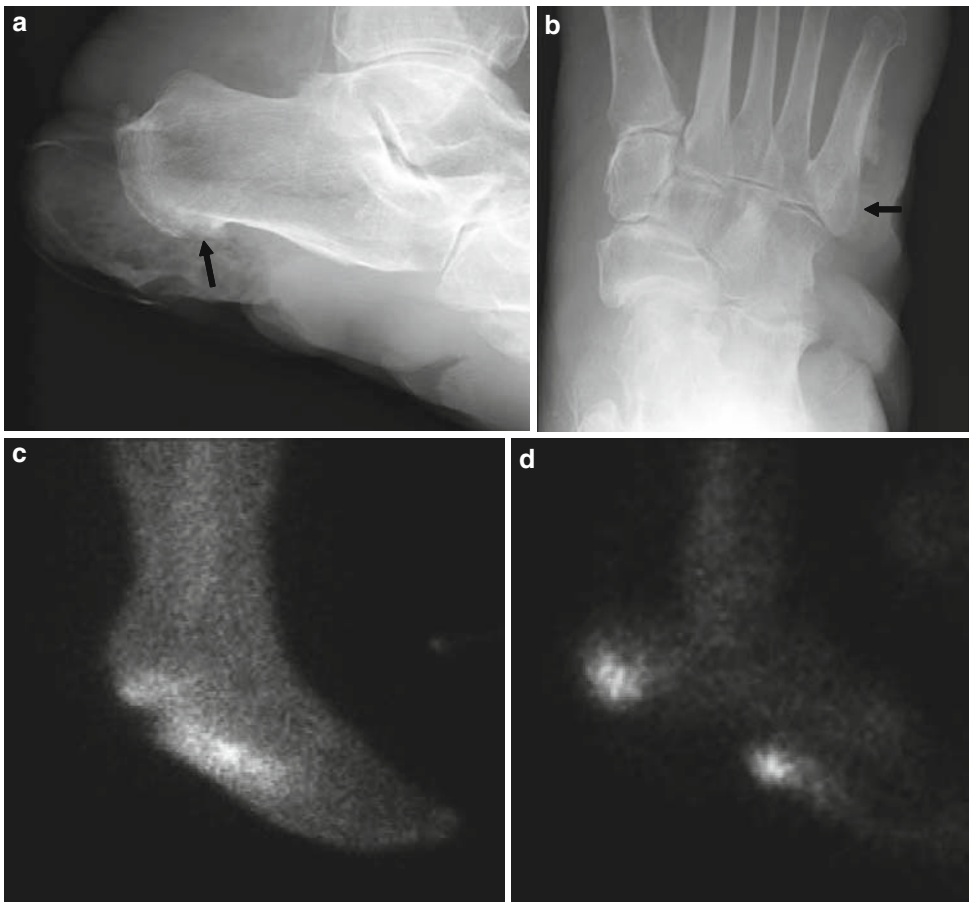

Fig. 10.4 Lateral (**a**) and oblique (**b**) radiograph of the hind foot and lateral projection from the blood pool phase (**c**) and from the delayed phase (**d**) of a technetium-99m bone scan in an adult diabetic with osteomyelitis of the calcaneus subjacent to a soft tissue ulcer. The inferior cortex of the calcaneus deep to the ulcer has been destroyed (**a**) (*arrow*). The bone scan shows increased blood pool activity in the soft tissues (**b**) and increased activity in the bone (**c**) on the delayed phase, both consistent with the infection. Note the second area of abnormal activity in the region of the fifth metatarsal base also related to osteomyelitis with subtle cortical destruction as shown in (**b**) (*arrow*) and adjacent periosteal reaction

originally allowed passage of the bacteria into the subperiosteal bone enlarge and form a direct communication between the medullary cavity of the bone and the surrounding soft tissues. These become visible as *cloacae* (Figs. 10.8, 10.9, 10.10, and 10.14).

Simultaneously, the destruction that is ongoing within the infected bone may isolate small fragments of bone. The infection and inflammatory response also elevate the pressure within the bone leading to decreased venous return and bone infarction. These processes lead to pieces of dead bone within infected bone known as *sequestra* or *sequestrations* (Figs. 10.14 and 10.15). Sequestrations are important for the radiologist to identify since they must be removed in order for the infection to be cured. Although plain radiographs may show sequestra, CT is the most sensitive technique for their identification and should be considered in cases of refractory chronic osteomyelitis (Fig. 10.16).

Adult Osteomyelitis

Adult osteomyelitis follows much the same pathways as pediatric osteomyelitis except that it usually starts in the soft tissues and spreads to bone through the cortex. Because the periosteum adheres to the bone more closely in adults than children, there is less chance of subperiosteal spread of infection. Instead, infection tends to propagate directly from the infecting source. Nonetheless, if bone adjacent to a joint is involved, the infection can lead to septic arthritis (Fig. 10.7). Obversely septic arthritis may lead to extension of the infection into the adjacent bones. As with pediatric cases, adult chronic osteomyelitis also is prone to develop large-scale sclerosis mixed with areas of destruction (Figs. 10.8, 10.9, and 10.10). Sequestration, Codman triangles, cloacae, and involucra are also possible and have the same implications (Figs. 10.8, 10.9, 10.10, 10.13, 10.14, and 10.15).

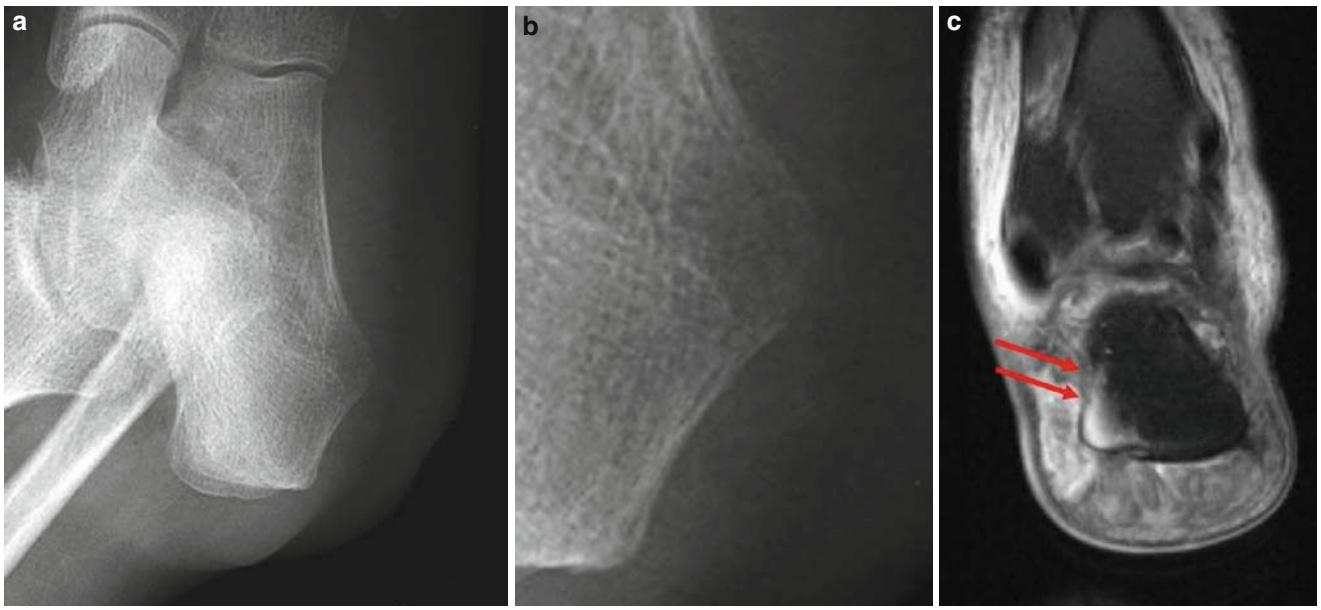

Fig. 10.5 Oblique radiograph (**a**), detail (**b**), and coronal T2-W fat-suppressed MR (**c**) of patient with early osteomyelitis showing subtle cortical destruction (*arrows*)

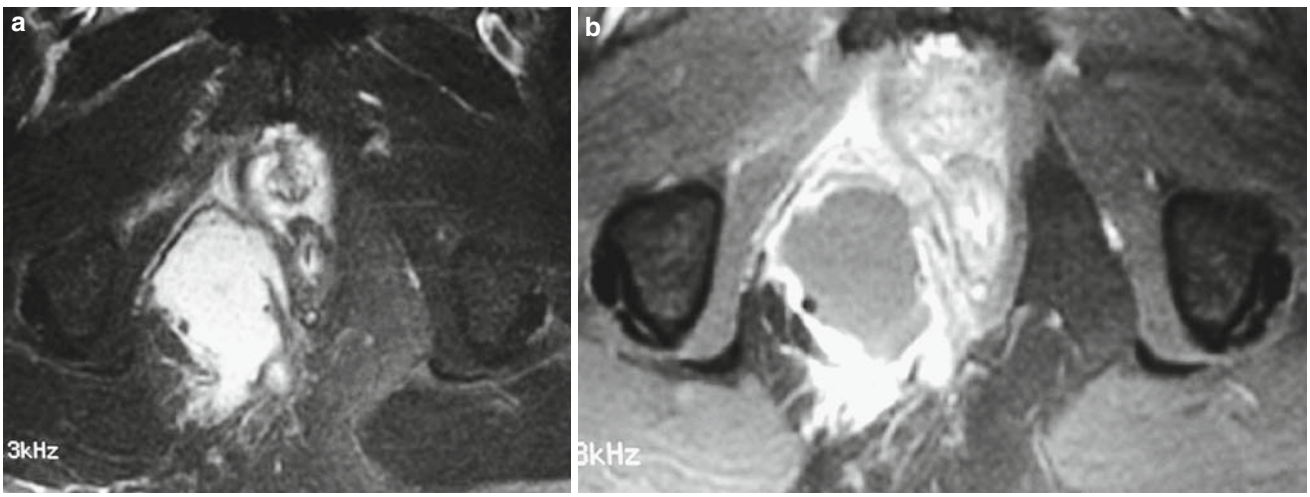

Fig. 10.6 Axial T2-weighted fat-suppressed (**a**) and T1-weighted fat-suppressed post-gadolinium (**b**) MR images showing a perirectal abscess in the right ischiorectal fossa. Note the high fluid signal on T2 imaging (**a**) that shows peripheral enhancement on T1 after contrast administration

Often acute osteomyelitis will continue to smolder despite antibiotic therapy and patients will have flares of acute osteomyelitis superimposed on chronic disease. In chronic osteomyelitis, the bone becomes thickened, irregular, and deformed. Sinuses may drain for extended periods of time. Low-grade infections can smolder on, in a chronic fashion, resolve and heal or undergo acute relapses. Relapses are caused by and in turn contribute to debilitation, malnutrition, and reduced immunity.

Joint contractures and scarring may occur. In pediatric cases, epiphyseal destruction may cause malaligned limbs if partial or shortening if complete. Epiphyseal hyperemia is an infrequent but dramatic cause of limb lengthening. Special problems in orthopedic practice involve treating osteomyelitis in the presence of foreign material (either orthopedic hardware or a fragment of sequestrum).

Radiological Diagnosis of Acute Osteomyelitis

The radiographic diagnosis of acute osteomyelitis depends on two factors. One is the *clinical setting* in which the studies are obtained. The other is imaging identification of *cortical destruction*, however, subtle it may be. Other findings

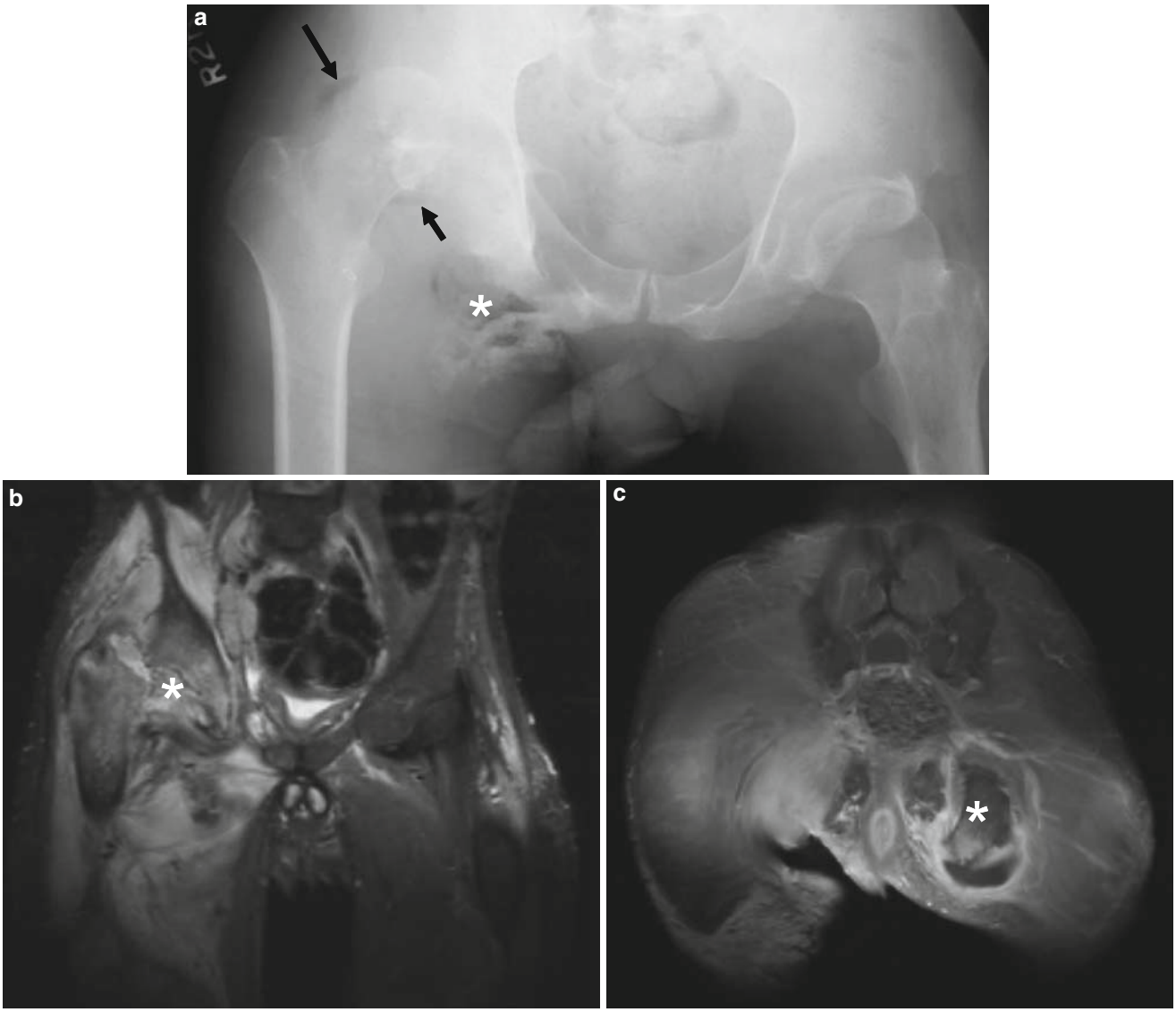

Fig. 10.7 Pelvic radiograph (**a**) and 6 weeks later a T2-weighted fat-suppressed (**b**) and fat-suppressed T1-weighted post-intravenous gadolinium (**c**) coronal MR showing gross osteomyelitis and destructive septic arthritis of the right hip (∗) and both ischial tuberosities in a paraplegic. Note the gas in the soft tissues inferior to the left ischial tuberosity related to a large decubitus ulcer. The right hip is dislocated and has gas within the joint from communication from the ulcer (**a**) (*arrows*). On the left note the low signal abscess with enhancing margins in (**c**) inferior to the destroyed ischial tuberosity (∗)

are ancillary and non-specific. For example, periosteal reaction may be present in a number of circumstances, including venous insufficiency or cellulitis without osteomyelitis. Similarly, many disease entities, not simply osteomyelitis, cause marrow space edema. Thus seeing marrow edema on MRI is not sufficient to make the diagnosis. Even marrow enhancement after contrast administration is not specific.

Both plain radiographs and MR show cortical destruction to advantage. The difference between the two modalities is their sensitivity. Generally, although soft tissue swelling may be visible within a few days, radiographs show no osseous changes until 10–14 days after infection of the bone. This is because substantial bone must be destroyed to begin seeing cortical destruction on plain radiographs (Figs. 10.5 and 10.17). MR, on the other hand, is sensitive to early cortical loss and will show changes in 1–2 days after infection. Normal cortex appears as dark signal on all sequences in MR because it has no free protons that the imager can perturb. The moment only a few free protons, usually from water, permeate the cortex, it will develop signal and appear as though it has been destroyed (Figs. 10.5 and 10.18). Conversely, MRI's high sensitivity to cortical permeation is

exactly the feature that makes it contraindicated as a study to evaluate tumor deposits in bone for orthopedic significance. Instead, CT with its high accuracy at depicting calcium is much better suited to the job of evaluating structural integrity of bone.

Gadolinium is routinely employed in cases of suspected osteomyelitis. The administration of MR contrast agents has little to do with diagnosing osteomyelitis *per se*. Instead, gadolinium is used to evaluate the viability of the bone and hence discover the presence of a sequestrum, a fragment of devitalized bone (Fig. 10.15). In addition, gadolinium may make soft tissue abscesses more conspicuous (Fig. 10.19), particularly smaller ones.

In patients with chronic osteomyelitis, flares of superimposed acute osteomyelitis may occur. As with de novo diagnoses of acute osteomyelitis, the only radiographic finding useful to determine the presence of acute disease is evidence of new cortical destruction. In fact, it is expected that patients with chronic osteomyelitis will have large areas of sclerosis and periosteal new bone formation (Fig. 10.20). Thus, a careful search for subtle areas of cortical destruction in patients with suspected flares of acute infection superimposed on chronic osteomyelitis is warranted.

Surgical Pathology of Chronic Osteomyelitis

Grossly, an infected bone may contain sequestrated necrotic bone, new bone (involucrum), and draining sinuses. Necrotic bone is usually surrounded by granulation tissue (the sequestrum). Separation of the sequestrum generally takes months to complete. This necrotic bone is usually of cortical origin, since the cancellous bone is much more easily absorbed and replaced by viable bone. The bone surrounding a focus of chronic osteomyelitis is often dense, and is referred to as the "involucrum". The involucrum is often of periosteal origin. The involucrum frequently has several openings or "cloacae" through which exudate, bone debris, and sequestra exit and pass through sinus tracts to the surface. Constant destruction of the neighboring soft tissues leads to scarring and squamous metaplasia of the sinus tract. This is a further impediment to resolution. Persistent infection in a localized area is a rare cause of secondary squamous cell carcinoma, which may develop in a long-standing sinus. Equally infrequent is the systemic secondary amyloidosis, which may develop in long-standing chronic osteomyelitis.

The microscopic diagnosis of chronic osteomyelitis is usually straightforward. Sometimes, however, the inflammatory infiltrate is often sparse and may mimic the normally found elements of the marrow space. Microscopic recognition of the sequestrum can be very helpful if the diagnosis of infection is in doubt. The sequestrum is recognized by virtue of its anucleate nature; often the edges are jagged owing to the action of proteolytic enzymes and osteoclastic action.

Discitis

When it comes to acute infection, intervertebral discs pose a slightly different pathophysiologic situation compared with bones. Since discs are avascular, they tend to become infected from seeding of the small vessels adjacent to the disc space. Once seeded, however, the absence of blood supply makes them ideal culture media for invading pyogenic organisms. The result is that the discs are rapidly destroyed and the infection spreads quickly to adjacent endplates leading to a characteristic imaging appearance. While multiple levels may be involved (Fig. 10.21), the infection usually is confined to one disc level and the two adjacent vertebral bodies. Typically on radiographs, the infected disc space is narrowed and destroyed as are the adjacent endplates (Figs. 10.21 and 10.22). While CT may be useful in evaluation of disc-centered infection, MR is currently the preferred modality. MR is more sensitive than either radiographs or CT and may show disease before other modalities become positive. MRI shows edema within and gadolinium contrast enhancement of the disc and the adjacent infected bone (Fig. 10.21, and 10.22). MR is also useful to show adjacent spread of disease, both around the vertebral body and into the spinal canal (Fig. 10.22e–g). Radiopharmaceutical scans – technetium bone scans and indium leukocyte scans – show abnormally increased radiotracer uptake at the infected levels.

Brodie Abscess

Occasionally, the body will succeed in limiting a bone infection to a localized area within the bone. This can lead to formation of an abscess within the medullary canal of the bone. As with osteomyelitis in general, *S. aureus* is the most commonly isolated organism from these abscesses, but oddly about half of them are sterile when cultured.

Radiographically, these lesions appear as well-defined lytic lesions with broad sclerotic margins (Figs. 10.23 and 10.24). Bone scans and indium scans generally show increased activity in the area of the abscess (Fig. 10.25). As these lesions are more common in younger patients in whom the origin of the infection is hematogenous, they may be confused radiologically with osteoid osteoma (Fig. 10.26), which occurs in a similar age group.

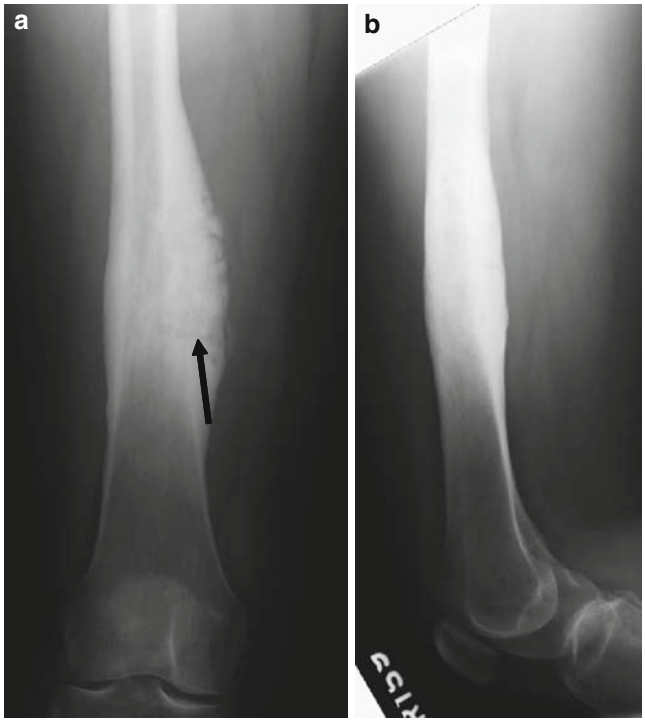

Fig. 10.8 AP (**a**) and lateral (**b**) radiographs of the right femur in a patient with ongoing osteomyelitis showing marked sclerosis, periosteal new bone formation, and a lucent track within the medial sclerosis consistent with a cloaca (*arrow*). The patient had a sinus on his skin that was draining purulent material

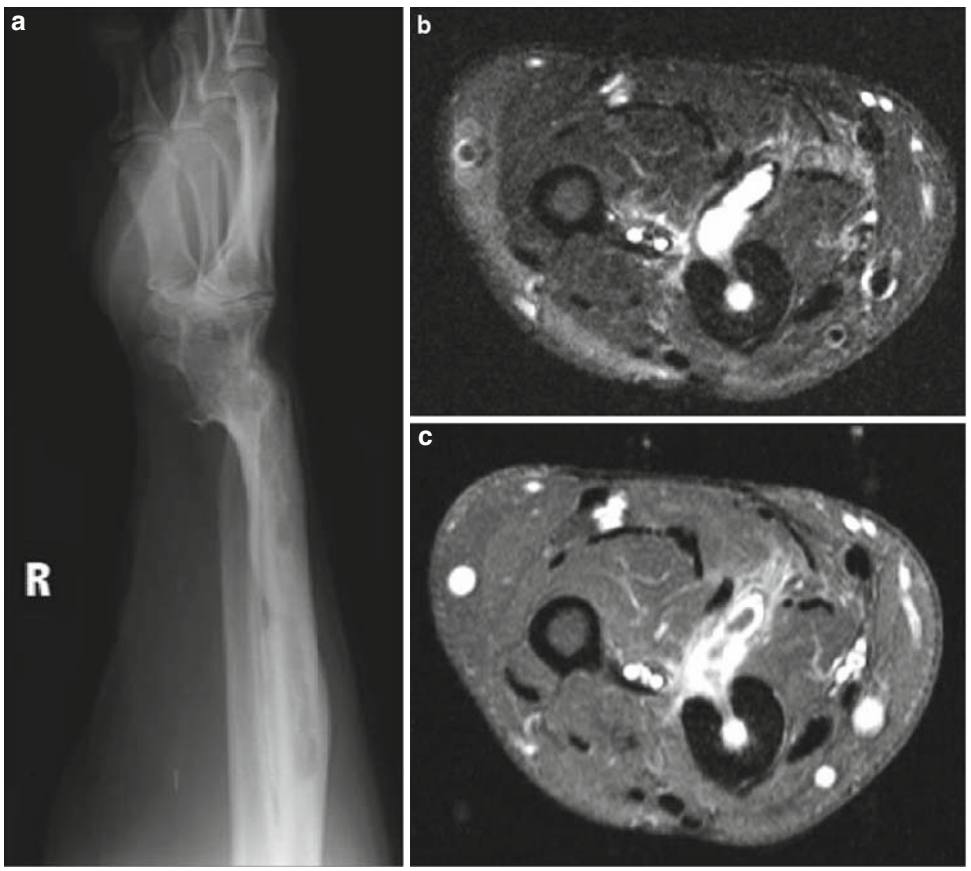

Fig. 10.9 Lateral forearm radiograph (**a**), T2-weighted fat-suppressed (**b**) and T1-weighted fat-suppressed post-gadolinium (**c**) axial MR images showing chronic osteomyelitis and cloaca with abscess extending from the bone into the soft tissues. Note the sclerotic reaction around the infection in the bone on the radiograph (**a**)

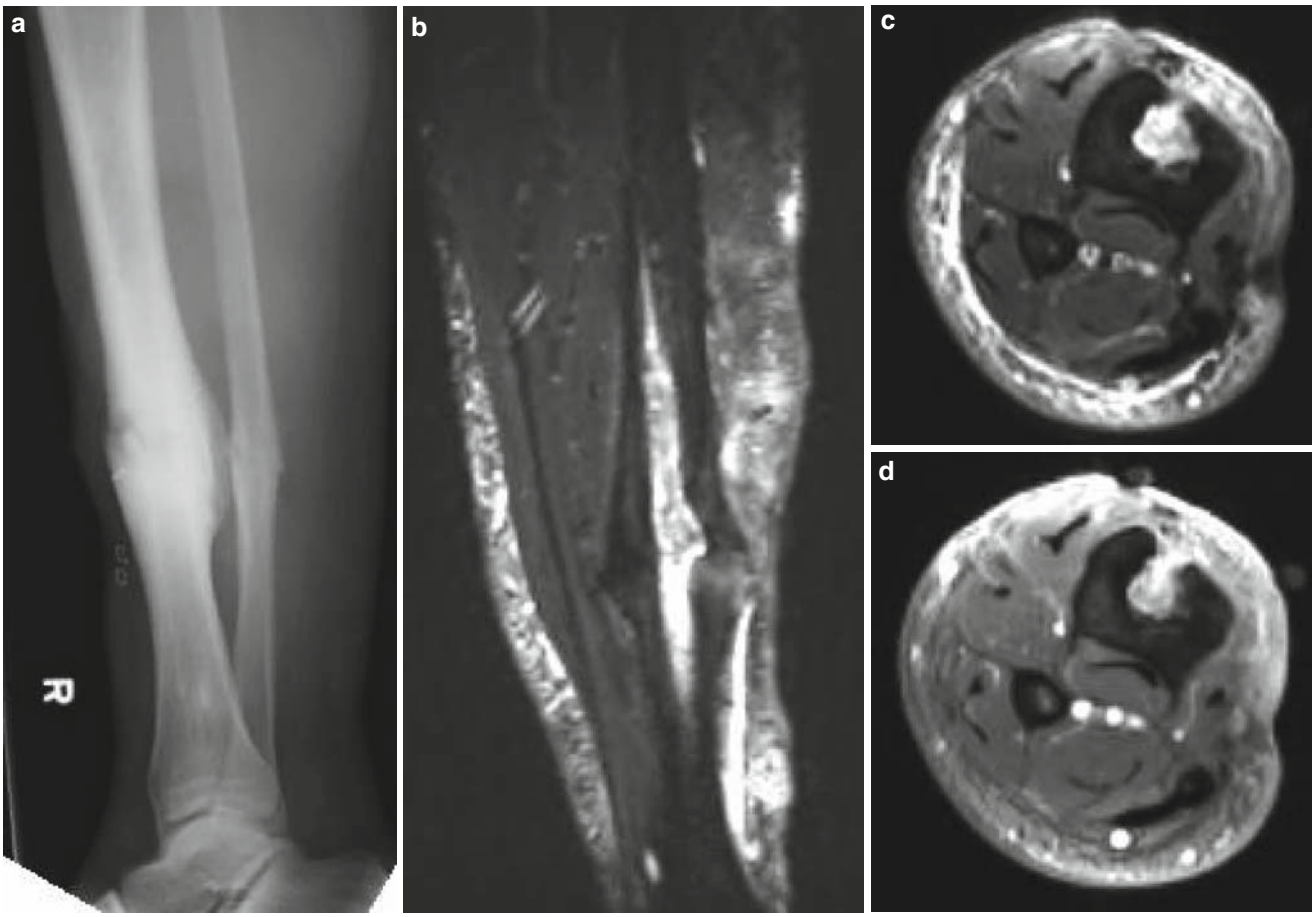

Fig. 10.10 Lateral radiograph (**a**) of the tibia and coronal (**b**) and axial (**c**) T2W fat-suppressed and T1W fat-suppressed post-contrast axial (**d**) MR images showing chronic osteomyelitis with sclerosis, an intramedullary abscess and a cloaca

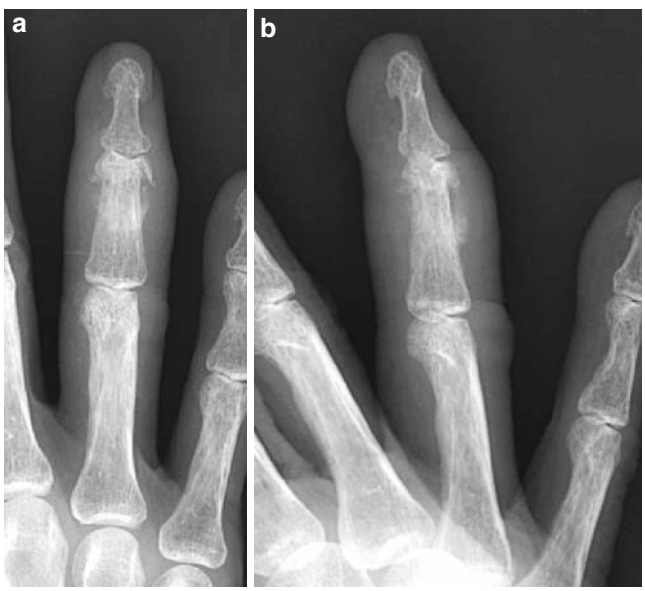

Fig. 10.11 PA (**a**) and oblique (**b**) radiograph of the third digit in a patient with acute osteomyelitis showing cortical destruction, periosteal new bone and Codman triangles

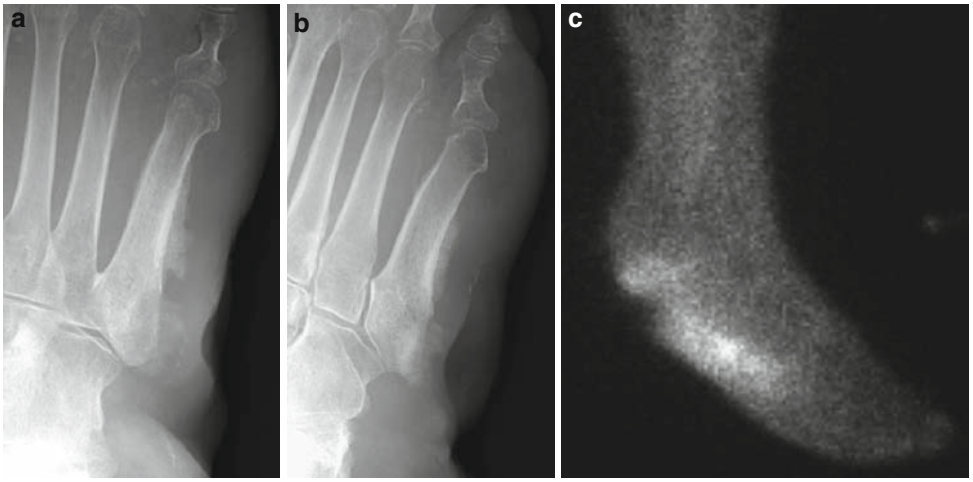

Fig. 10.12 PA (**a**) and oblique radiograph (**b**) and immediate static blood pool image (**b**) from a technetium-99m bone scan (**c**) in a patient with osteomyelitis of the proximal fifth metatarsal and diffuse periosteal reaction. Note the ulcer and soft tissue swelling along the lateral aspect of the foot. The periosteal reaction extends distal to the area of osteomyelitis and alone might only result from the soft tissue infection. Note that it has formed a Codman triangle

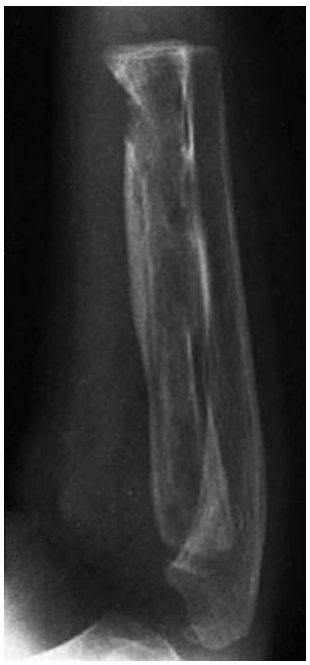

Fig. 10.13 Forearm radiograph in a 6-year-old patient showing new bone enveloping the infected bone. This new bone is known as an involucrum and represents an attempt to limit the infection with new and healthy bone

Garre Disease

Garre disease is a rare form of osteomyelitis seen primarily in patients under the age of 25. It presents as a focally sclerosing disease of bone (Fig. 10.27). Patients complain of continuous dull pain in the area. Although the etiology is incompletely understood, most believe that this represents a low-grade chronic osteomyelitis. The anterior tibia and the mandible are most commonly affected but the disease may occur anywhere in the skeleton.

Imaging Utility

Imaging generally plays two roles in suspected bone infection. The first is diagnosis. Imaging is very useful to diagnose osteomyelitis, discitis, and soft tissue abscess. On the other hand, in cases where the diagnosis is clear, as in bone exposed to air through an ulcer, imaging findings add little and may even confuse the clinical picture. The second role for imaging in osteomyelitis is following the patient's disease for healing or progression. More often than not, the clinical circumstances provide information regarding the patient's status, but imaging may be required when questions arise.

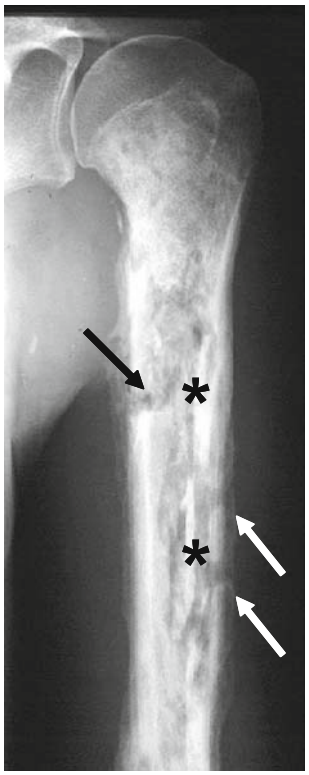

Fig. 10.14 AP radiograph of the proximal humerus in a patient with long-standing osteomyelitis showing sclerosis, sequestrum (∗), cloaca (*arrows*), and involucrum all in one radiograph

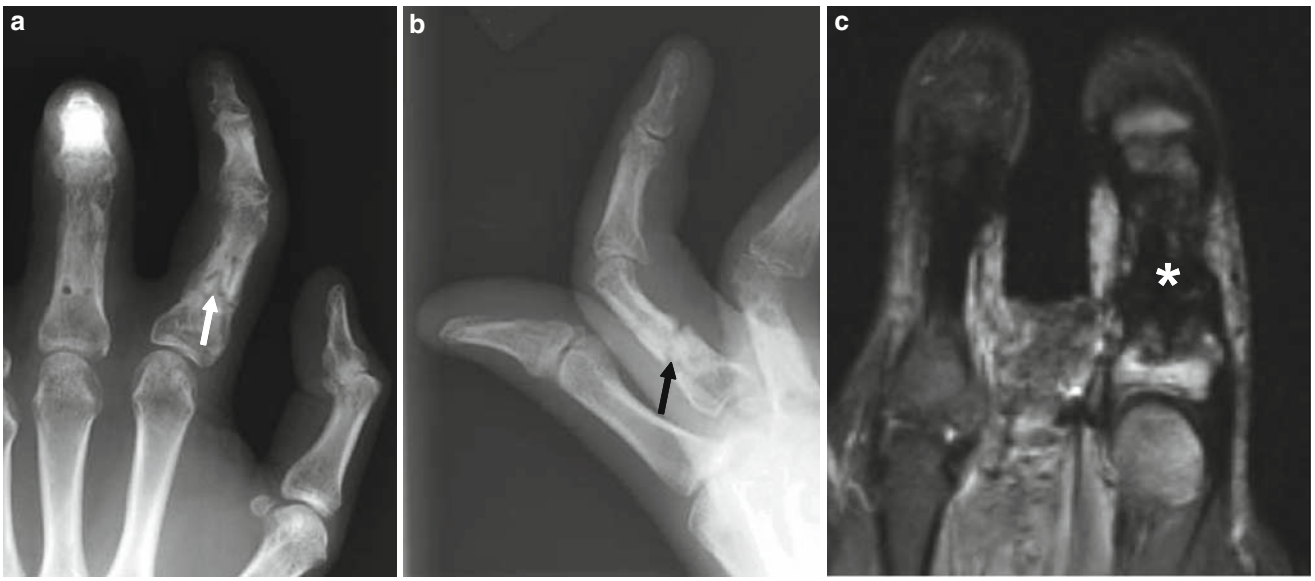

Fig. 10.15 AP (**a**) and lateral (**b**) radiographs and coronal T1W fat-suppressed post-gadolinium coronal MR image (**c**) of the left hand in a patient with chronic osteomyelitis and a fracture of the proximal phalanx of the second digit. Note the small sclerotic density within the medullary cavity (*arrows*). This represents a sequestrum and must be removed in order to cure the infection. On the MR scan the medullary cavity is not enhanced, indicating avascular bone (∗)

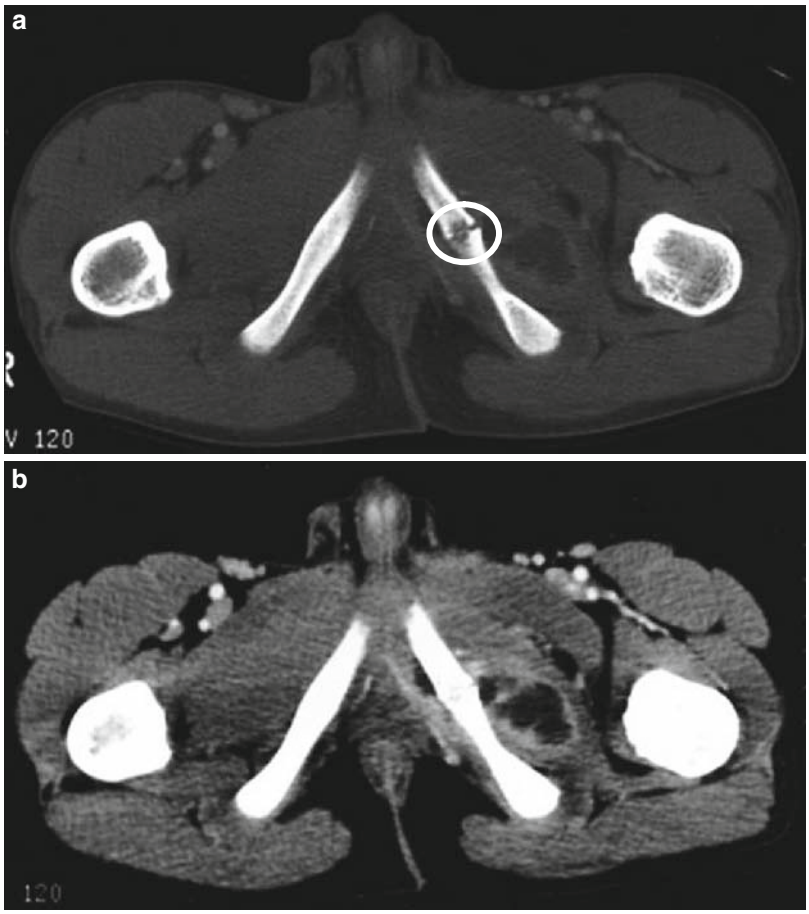

Fig. 10.16 Axial CT post-intravenous contrast bone (**a**) and soft tissue (**b**) windows showing a small sequestrum (*circle*) in the left inferior ischial ramus and an adjacent soft tissue abscess

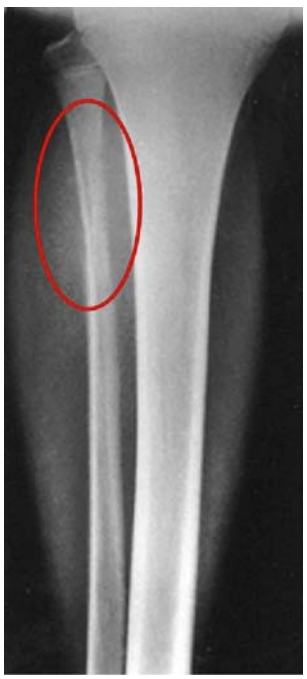

Fig. 10.17 AP radiograph of the proximal tibia and fibula showing early cortical destruction of the fibular diaphysis from osteomyelitis (red oval).

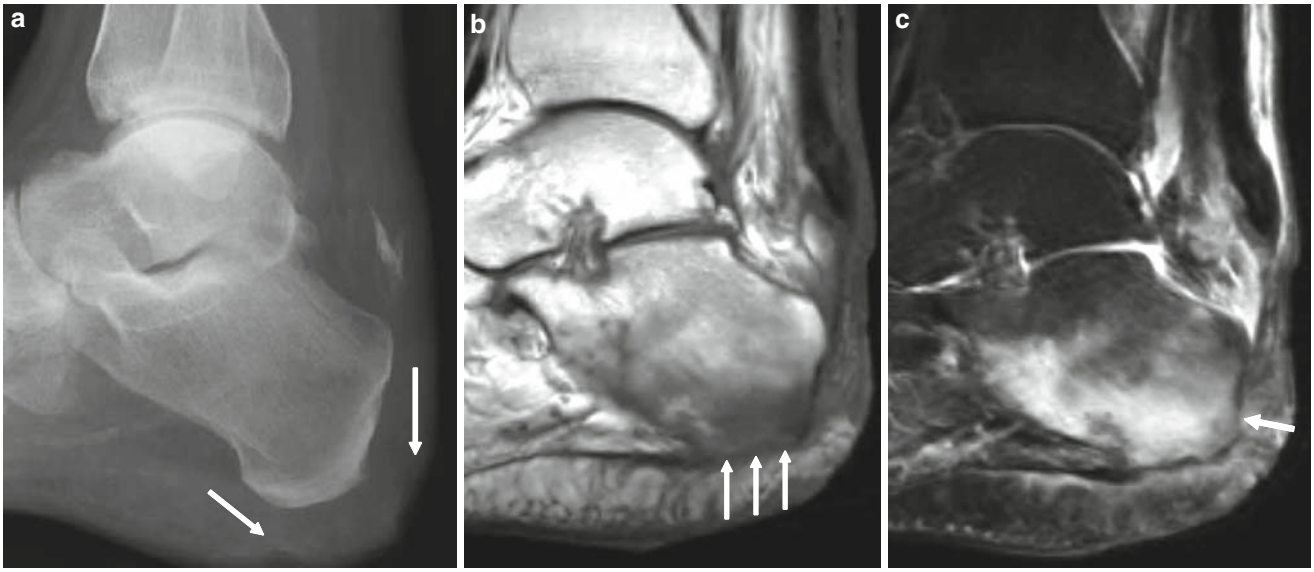

Fig. 10.18 Lateral radiograph of the ankle (**a**) and sagittal T1-weighted (**b**) and T2-weighted fat-suppressed (**c**) MR images showing acute osteomyelitis on MR but not on the radiograph. The radiograph (**a**) shows soft tissue ulceration inferior and posterior to the calcaneus (*arrows*) but no evidence of cortical destruction. The MR, on the other hand, shows the absence of cortex on the calcaneus inferiorly on the T1-weighted image (**b**) and posteriorly on the T2-weighted image (**c**) (*arrows*). Note the calcification in the region of the distal Achilles tendon and the thinning visible on MR in this region. The patient suffered from a chronic Achilles tendon tear

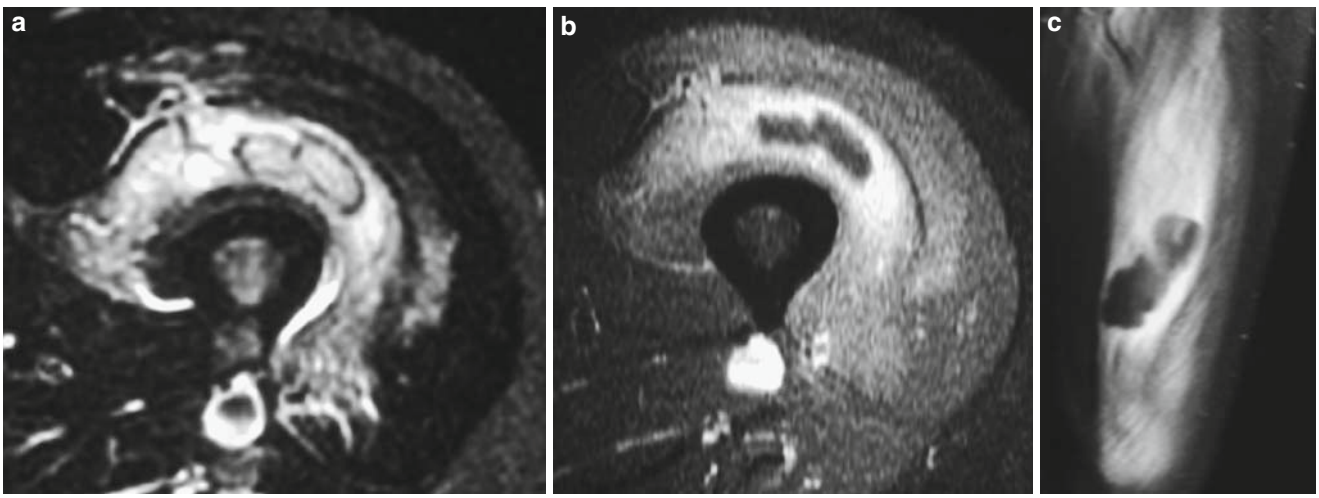

Fig. 10.19 Axial T2-weighted fat-suppressed (**a**), T1-weighted fat-suppressed post-gadolinium axial (**b**) and coronal (**c**) images showing a vastus intermedius abscess. Note that the abscess is easily separated from the surrounding edema on the post-gadolinium images because the fluid within the abscess is avascular and therefore non-enhancing

The large array of imaging studies available to diagnose and follow osteomyelitis can cause confusion among imagers and clinicians alike. Not only does the array of available modalities have differing sensitivities and specificities (Table 10.1) but they vary widely in cost as well (Table 10.2). Furthermore tests vary with regard to ancillary findings and the anatomic detail they are capable of displaying.

Given the available data, most institutions initiate evaluations for pyogenic osteomyelitis with plain radiographs (Figs. 10.3a, b and 10.4a, b), unless it is possible to probe a wound to bone in which case the bone is assumed to be infected. While some argue for three/four-phase bone scan (Fig. 10.4c, d), indium scan or bone and indium scans in combination, increasingly the tendency has been to use MRI for cases where osteomyelitis is suspected but radiographs are non-diagnostic. This practice has arisen largely because of the time savings and improved anatomic detail offered by MRI over nuclear studies (Fig. 10.5). MR, for example, can identify and demarcate abscesses while bone scan cannot (Figs. 10.6, 10.9, 10.10 and 10.19).

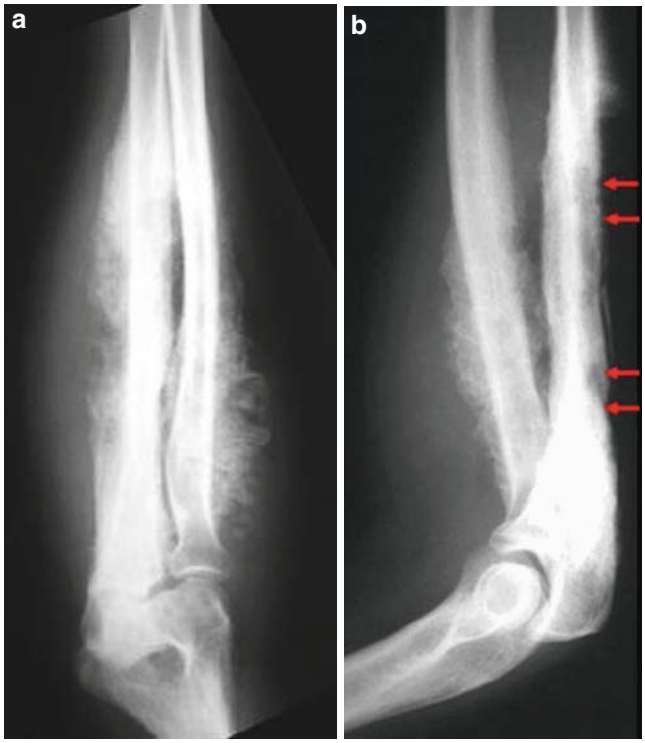

Fig. 10.20 AP (**a**) and lateral radiograph (**b**) of a patient with acute osteomyelitis superimposed on chronic osteomyelitis. Note the areas of cortical destruction (*arrows*) in the posterior cortex of the ulna indicating acute osteomyelitis

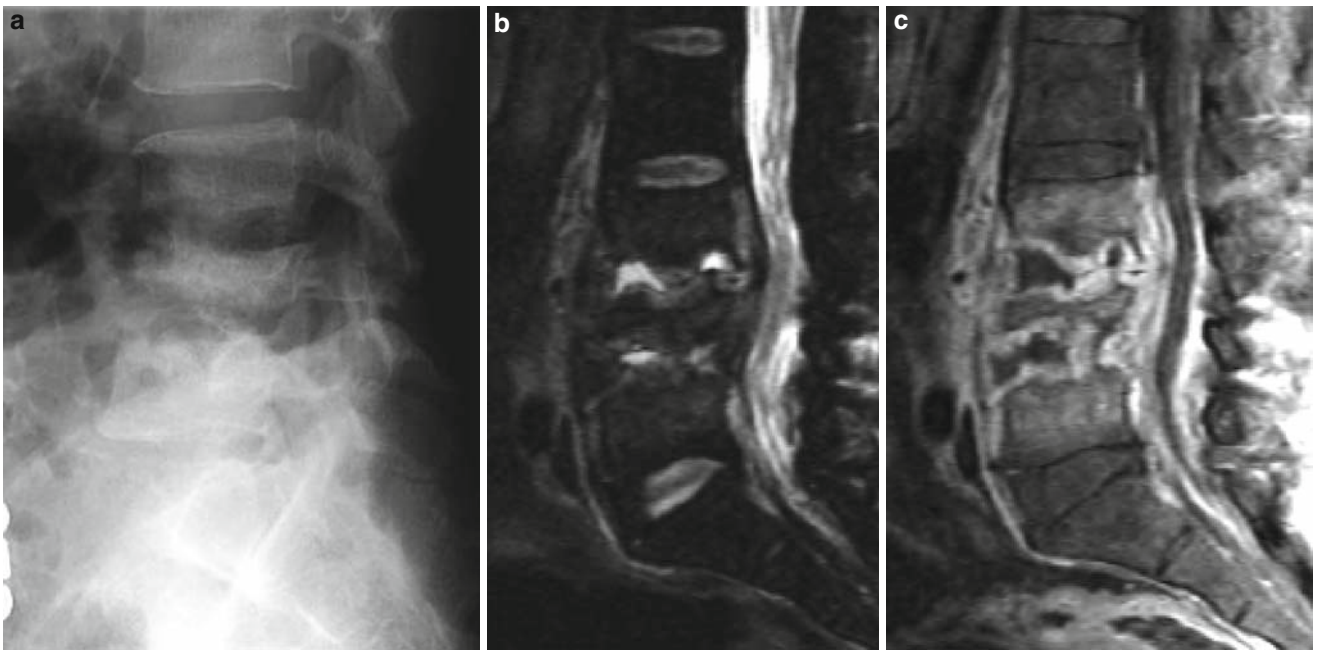

Fig. 10.21 Lateral radiograph (**a**), T2W FS (**b**) and T1W FS post-Gd (**c**) sagittal MR images of the lumbar spine show destruction of the L34 and L45 osseous endplates (**a**) and the disc levels (**a–c**) with involvement of the adjacent soft tissues (**b**) and (**c**) in a patient with discitis. Note the bright enhancement in (**c**) that wraps entirely around the cauda equine and the non-enhancing fluid (pus) within the disc spaces

The diagnosis of osteomyelitis may be difficult in patients with neuropathic arthropathy. Unfortunately, both diseases are common complications of diabetes mellitus. Similarly, discriminating between acute infarction and osteomyelitis can present difficulties in patients with sickle cell disease. In these cases, clinical information, laboratory values (CRP), and indium leukocyte scans alone or in combination with bone scans can help make the diagnosis. Infarction and neu-

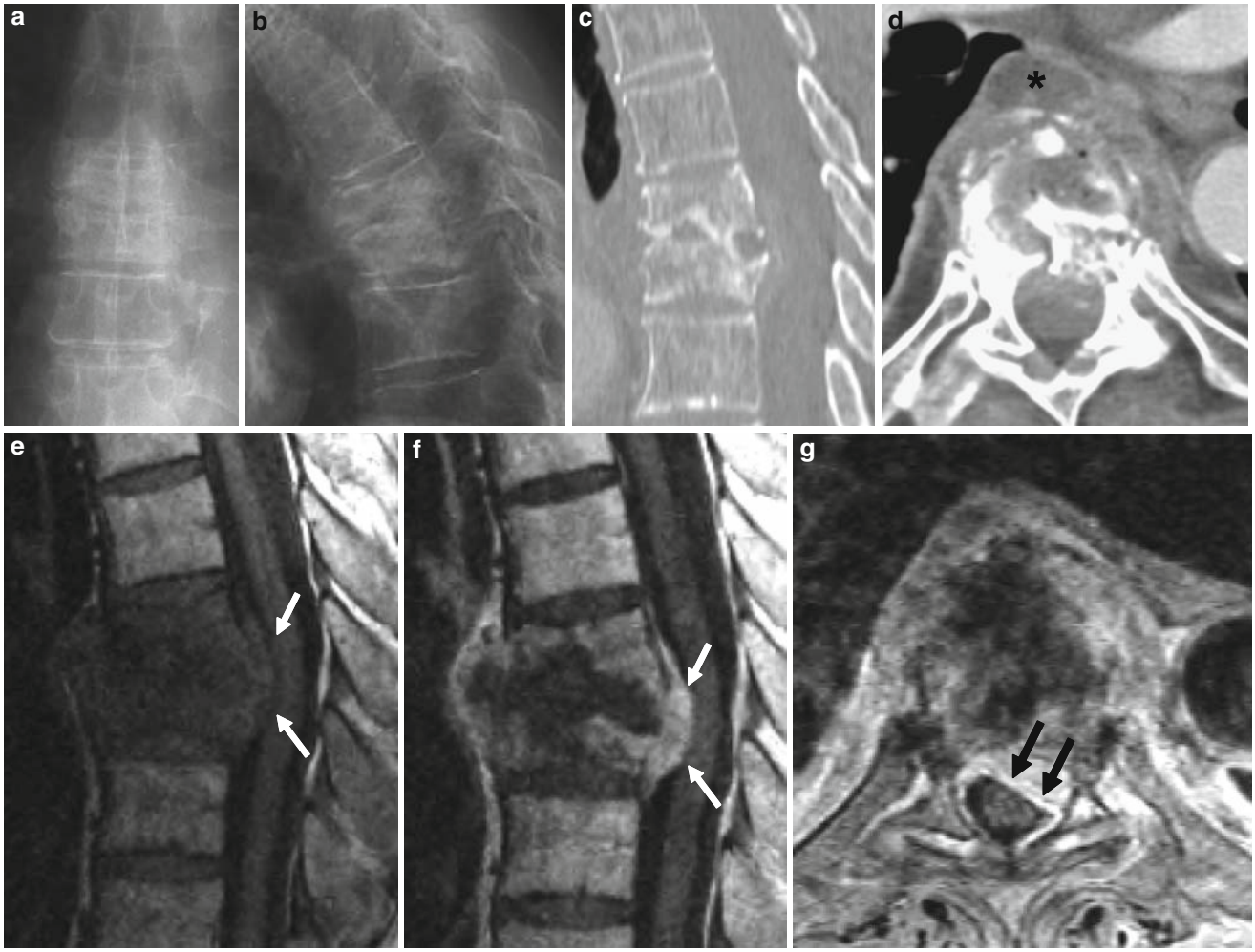

Fig. 10.22 AP (**a**) and lateral radiograph (**b**) with sagittal (**c**) and axial (**d**) CT and sagittal T1W (**e**) and T1W post-Gd (**f**) and axial T1W post-Gd (**g**) images in a patient with discitis. The radiographs (**a** and **b**) show marked destruction of the T9-10 disk and adjacent endplates. The CT (**c** and **d**) confirms these findings and in addition shows a prevertebral abscess (∗). Note that the spinal canal is not well evaluated. The MR images (**e**–**g**) show not only the disc destruction but also extension into the spinal canal with impingement on the spinal cord (*arrows*)

Table 10.1 Sensitivity and specificity of diagnostic tests for osteomyelitis

Test	Sensitivity	Specificity
Radiograph	54% (22–93%)	80% (50–94%)
BS	91% (69–95%)	46% (38–100%)
Indium scan	86% (45–100%)	84% (67–89%)
BS/indium scan	88% (73–100%)	82% (55–91%)
MRI	92% (29–100%)	84% (78–89%)
Probe to bone	66%	85%

From: Grayson et al. JAMA 1995 Mar 1; 273(9): 721–723.
Data obtained by varying methods and not always comparable.
Dependent on the use of bone biopsy to diagnose the disease.

Table 10.2 Cost of diagnostic tests for osteomyelitis

Procedure	Cost (1994)
Bone probe	$0
Plain film	$120
BS	$550
Gallium scan	>$1000
Indium scan	>$1000
MRI	>$1000

ropathic arthropathy should have minimal if any inflammatory component and therefore will not show as much activity on indium scans as acute osteomyelitis, particularly if there is differential activity between bone and indium scans in patients with neuropathic arthritis.

Spirochetal Osteomyelitis

The most common form of spirochetal osteomyelitis is congenital syphilis (*Treponema pallidum*), although pinta and yaws also may cause bone infection. Transplacental spread of spirochetes from mother to the fetus causes congenital syphilis. Long bones, such as the tibia, and the calvarium are typically affected. Congenital syphilis has manifests as

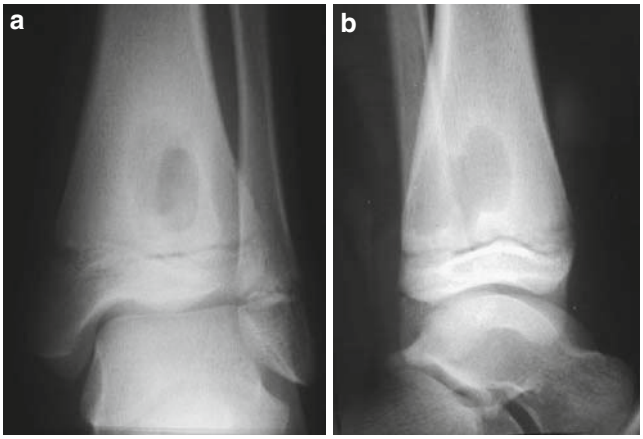

Fig. 10.23 AP (**a**) and lateral (**b**) radiographs of the ankle showing a well-defined lytic lesion in the distal tibia with broad surrounding sclerosis typical of a Brodie abscess

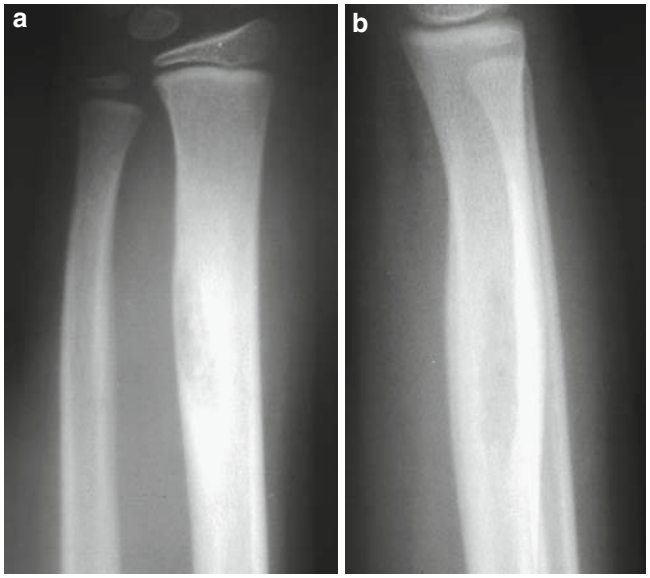

Fig. 10.24 AP (**a**) and lateral (**b**) radiographs of the distal radius showing a well-defined lytic lesion with broad surrounding sclerosis typical of a Brodie abscess

either periostitis or metaphysitis. With periostitis, there is subperiosteal new bone formation along the diaphysis of long bones, causing enlargement of the diaphysis. In the tibia this causes a saber shape, known as a saber shin deformity. With metaphysitis, the juxtaepiphyseal metaphysis resorbs separating the epiphysis from the metaphysis.

Early Congenital Syphilis (Parrot's Pseudoparalysis)

Skull, nasal bones, and long bones are the favored sites of congenital syphilis. The neonate is irritable, with a tender limb. Other stigmata of syphilis may be present such as snuffles, keratitis, skin or mucous lesions, and positive serology.

Histologically, the osseous metaphyseal medulla is invariably involved. This causes disordered enchondral ossification, wide epiphyseal plates, increased accumulation of calcified cartilage, and a propensity to fracture at this site. Healing frequently occurs by a few months of age, along with reactive periosteal new bone.

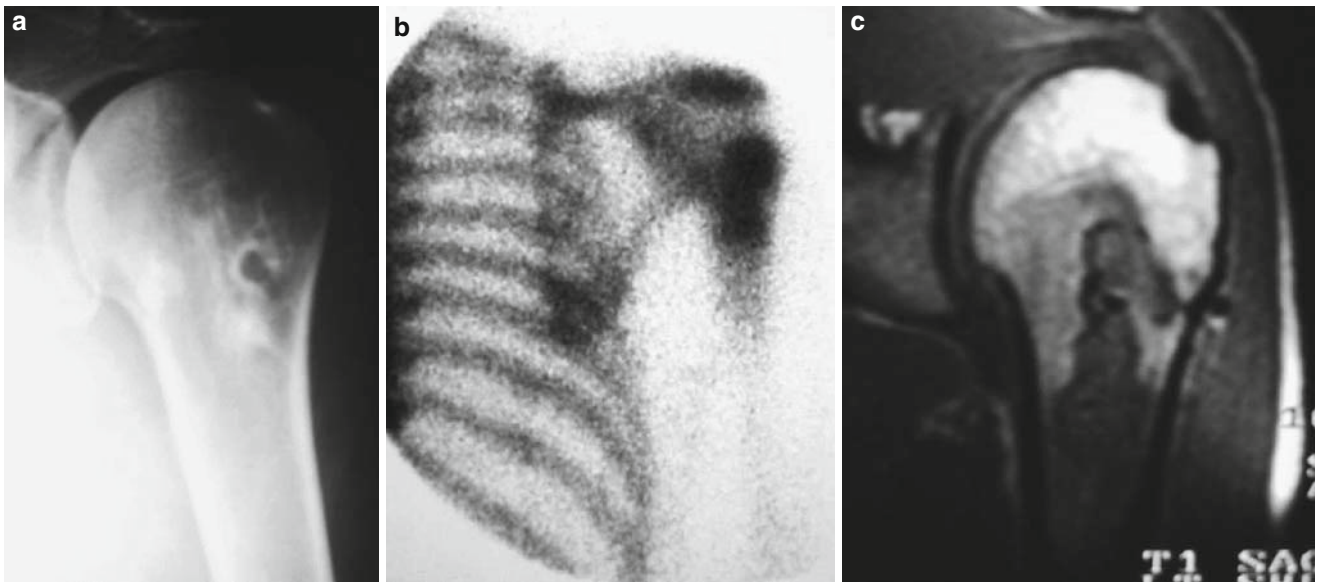

Fig. 10.25 AP externally rotated shoulder radiograph (**a**), radiopharmaceutical bone scan (**b**), and T1-weighted coronal MR image (**c**) showing a proximal humeral Brodie abscess

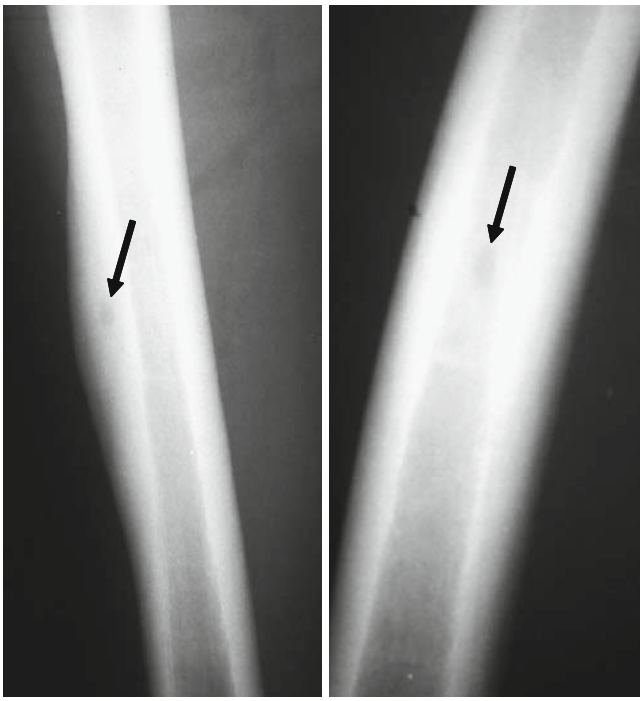

Fig. 10.26 Details from AP (**a**) and lateral (**b**) radiographs of the femur showing an intracortical osteoid osteoma (*arrows*). The lesion resembles a Brodie abscess radiographically. Note the marked sclerosis surrounding the lytic nidus that is the actual lesion

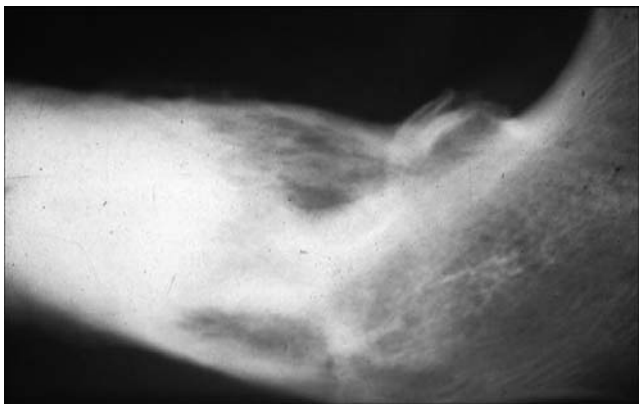

Fig. 10.27 Detail lateral radiograph of the elbow showing sclerosis and enlargement of the distal humerus in a patient with Garre disease

Late Congenital Syphilis

This is the tertiary form of congenital syphilis. It occurs around the second or third year of life. Periosteal new bone is the hallmark of this stage, but occasionally destructive gummatous lesions may be seen. Syphilitic dactylitis (spina ventosa syphilitica) refers to periosteal new bone formation causing enlargement of the tubular bones of the hands. Additional stigmata such as Hutchinson triad – interstitial keratitis of the cornea, labyrinthine deafness, and gapped notched incisors – or central nervous system involvement may be present. Between 8 and 18 years of age, Clutton joints (symmetrical syphilitic synovitis) may be seen.

Adult Syphilitic Osteomyelitis

Usually a manifestation of tertiary syphilis, adult syphilitic osteomyelitis, is rare in the United States. Syphilitic osteomyelitis presents with gumma formation within the bones causing punched-out lytic lesions.

Chronic Granulomatous Osteomyelitis

Both fungi and mycobacteria can infect bone. Tuberculous infection is relatively common in the United States, but today other fungal infections are comparatively unusual. When the latter occur, it is likely that the host is immune compromised, but rarely fungal osteomyelitis has been reported in immune-competent hosts. Today, *Candida* (*Candida albicans*) and *Aspergillus* (*Aspergillus fumigatus*) are the most common fungal agents infecting bone and disk in the United States. Coccidiomycosis (*Coccidiodes immitis* and *Coccidiodes posadasii*) may also be seen, particularly in the western United States (Fig. 10.28). Blastomycosis (*Blastomyces dermatitidis*), although typically infecting the skin and lungs, involves bone in between 10 and 25% of infected patients. Histoplasmosis relatively commonly infects bone in parts of Africa but is primarily a parenchymal disease in the United States. Other forms of the disease are common in the Middle East. As with tuberculous osteomyelitis, the course is usually indolent and as a result osteomyelitis is often not considered until later in the course of the disease.

Tuberculous Osteomyelitis

Bone involvement arises in about 2% of patients with tuberculosis and results from hematogenous spread from a primary site. Despite this, bone involvement is usually seen clinically 6 months to 3 years after the primary infection. In fact, half of the patients with skeletal involvement have no clinical pulmonary involvement. Thus, the absence of pulmonary tuberculosis does not exclude tuberculosis as the cause of osseous infection.

Tuberculous osteomyelitis is relatively uncommon in the United States compared with some developing Asian countries, e.g., India and compared with pyogenic osteomyelitis

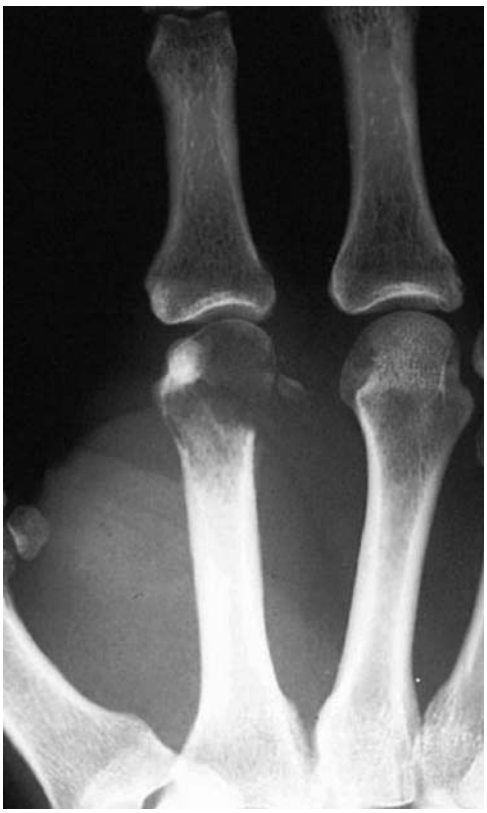

Fig. 10.28 AP radiographs of the second metacarpal in a patient with coccidiomycosis osteomyelitis. The metacarpal head cortex is destroyed medially and the proximal margin of the lesion shows permeation into the metacarpal (case courtesy of Dr. John Hunter, University of Washington)

overall. As with other chronic granulomatous infections, tuberculosis typically has an indolent course related to its inability to produce proteolytic enzymes. About half of the tuberculous disease affecting the skeleton in this country involves the spine, Pott disease. The remainder typically affects large joints such as the knee and hip. Tuberculous arthritis of both synovial joints and the spine is discussed further in the chapter on arthritis and other diseases of joints (Chapter 11). Infection of bone without joint involvement is uncommon but does occur (Figs. 10.29 and 10.30).

For purposes of description, tuberculous disease pathologically traditionally has been divided into "granular" and "exudative" types. Grossly, the disease is characterized by reactive tissue, which can be extensive in the exudative forms or sparse in the granular (dry) forms. In reality, both forms overlap.

The characteristic histological findings of tuberculous osteomyelitis are those of a granulomatous inflammation, often with Langhan-type giant cells. Special stains reveal organisms, which fluoresce with auramine–rhodamine and are acid-fast with the Ziehl–Neelson stain or one of its modifications such as the Kinyoun. It must be remembered that giant cells are common in the marrow space. Foreign body giant cells, osteoclasts, and megakaryocytes should not be confused with a tubercular reaction. Looking for epithelioid histiocytes and granuloma formation should help in establishing the correct diagnosis. Organisms should be sought, since fungi can have a granulomatous reaction similar to tuberculosis. Mycobacteria other than tuberculosis can infect the bone. Culture is generally needed to speciate the organisms.

Acid-fast organisms may be sparse, and special methods to confirm the diagnosis include tests based on the polymerase chain reaction technology as well as culture methods. The emergence of BACTEC instruments has improved the yield and turn-around time of the latter method.

Management is based upon multi-drug chemotherapy along with the appropriate surgical approach. The latter is dependent upon the site and clinical situation. For example, vertebral tuberculosis may be treated with drugs alone, but if associated with a progressive neurologic deficit or a rapidly developing cauda equina syndrome, then surgical intervention must be considered. Several different types of operations are described depending upon the location and type of the infection.

Sarcoidosis

While generally considered a disease of unknown etiology, it has many similarities to tuberculosis. The disease causes non-caseating granulomas that in other respects resemble the caseating granulomas of tuberculosis. Although long thought to be caused by an occult infection, possibly tuberculosis, this never has been definitively proven. Today there is immune and empirical evidence that the disease is in fact the result of infection or an immune response to infection, either active or past. Even so, sarcoidosis remains classified as a disease caused by a deranged immune response to an unknown antigen, not necessarily infectious in nature, e.g., pine pollen.

Although sarcoidosis most commonly affects the thorax with adenopathy and interstitial lung disease, it involves the skeleton in between 5 and 10% of cases. Conversely, it is estimated that between 80 and 90% of patients with osseous sarcoidosis have disease manifestations elsewhere, typically in the mediastinum and lungs. Most osseous sarcoidosis is asymptomatic. As with pulmonary sarcoidosis, there is no definite gender predilection, but racially, blacks are affected about 10 times more frequently than whites.

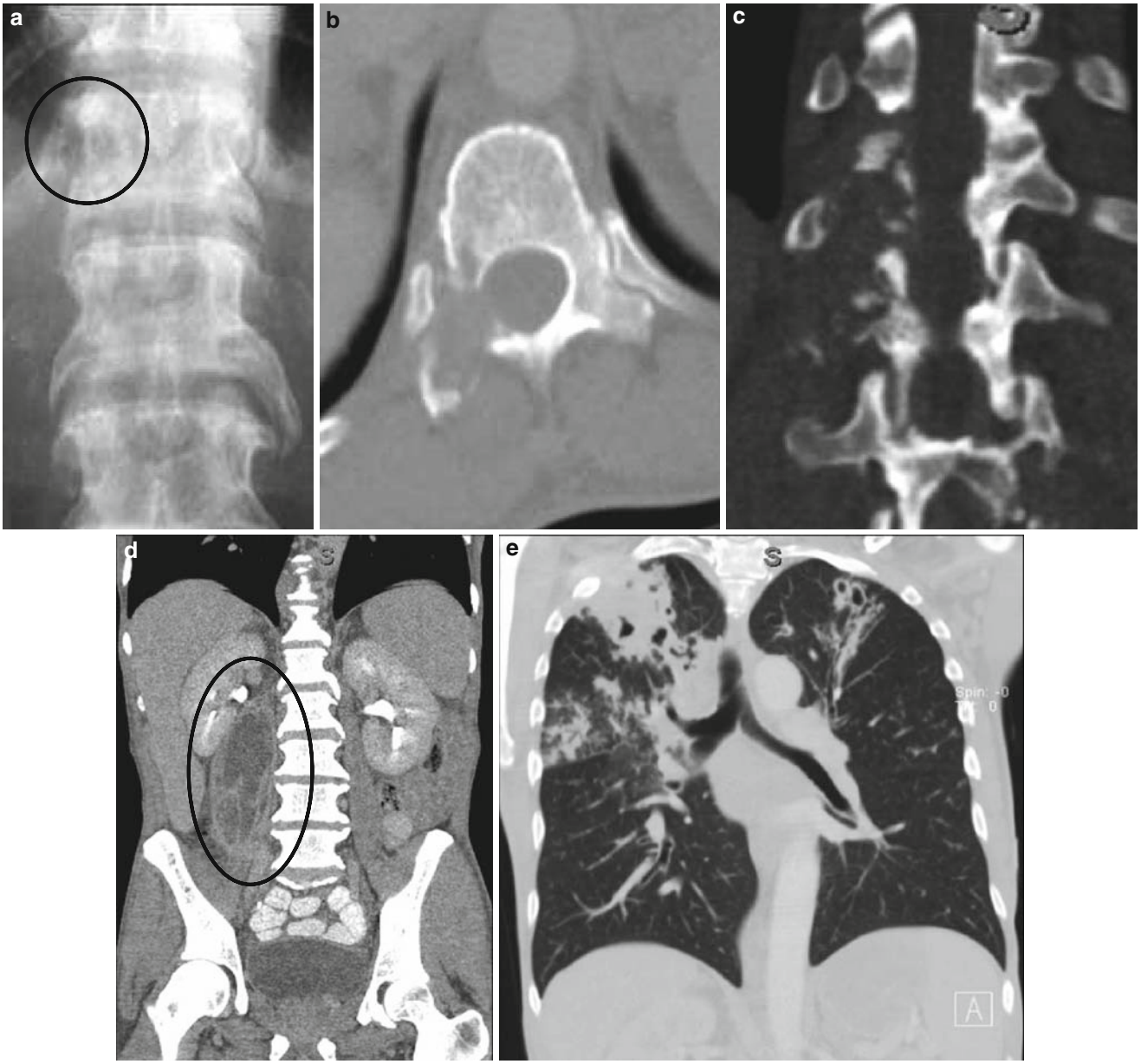

Fig. 10.29 AP lumbar spine radiograph (**a**), CT bone window through T12 (**b**), coronal reconstruction through the lumbar spine posterior elements (**c**), CT reconstruction with a soft tissue window through the psoas muscles (**d**), and coronal reconstruction of the chest with a lung window (**e**) in a patient with tuberculous osteomyelitis. The right pedicle of T12 has been destroyed (*circle*) (**a**–**c**) by the infection and there is a large right psoas abscess (*oval*) (**d**). The image of the thorax shows bilateral upper lobe cavitary infiltrates and right parahilar fullness from adenopathy from the patient's pulmonary tuberculosis

The radiographic appearance of osseous sarcoidosis depends upon location. Most commonly it occurs in the small long bones of the hands and feet. Here, sarcoidosis typically appears radiographically as focal punched-out lesions (Fig. 10.31) or gives a lacy interstitial pattern (Fig. 10.32), the former from formation of intraosseous granulomas and the latter from infiltrating disease. Rarely the disease may progress to a destructive form with cortical loss (Fig. 10.33), but unlike most destructive processes with this type of appearance, periosteal reaction is unusual. Another uncommon form is localized or generalized osteosclerosis (Fig. 10.34). This form of the disease may appear long after the pulmonary manifestations have been arrested.

Tuberous sclerosis, although a phakomatosis, may develop punched-out lytic lesions in the digits that resemble those of sarcoidosis. This is the result of fibrous tubers forming within the bone marrow. This disease is discussed in more detail in the chapter on bone dysplasias (Chapter 13).

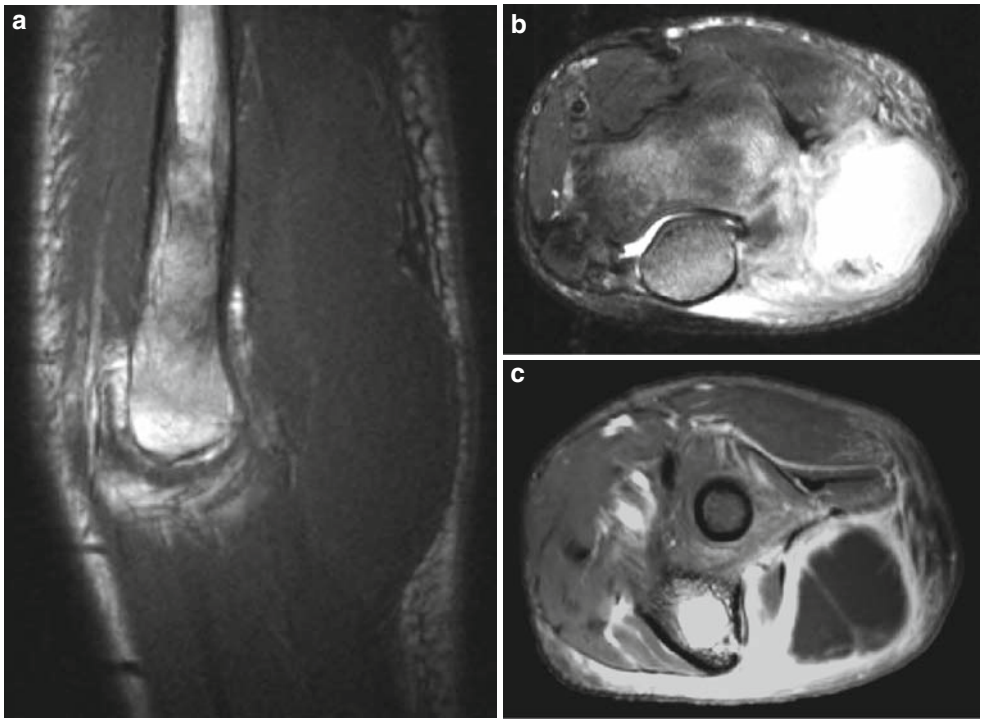

Fig. 10.30 T1-weighted sagittal (**a**), T2-weighted fat-suppressed (**b**), and T1-weighted fat-suppressed post-gadolinium (**c**) axial MR images of the elbow showing tuberculous osteomyelitis with destruction of the posterolateral humeral condyle and abscess in the adjacent soft tissues

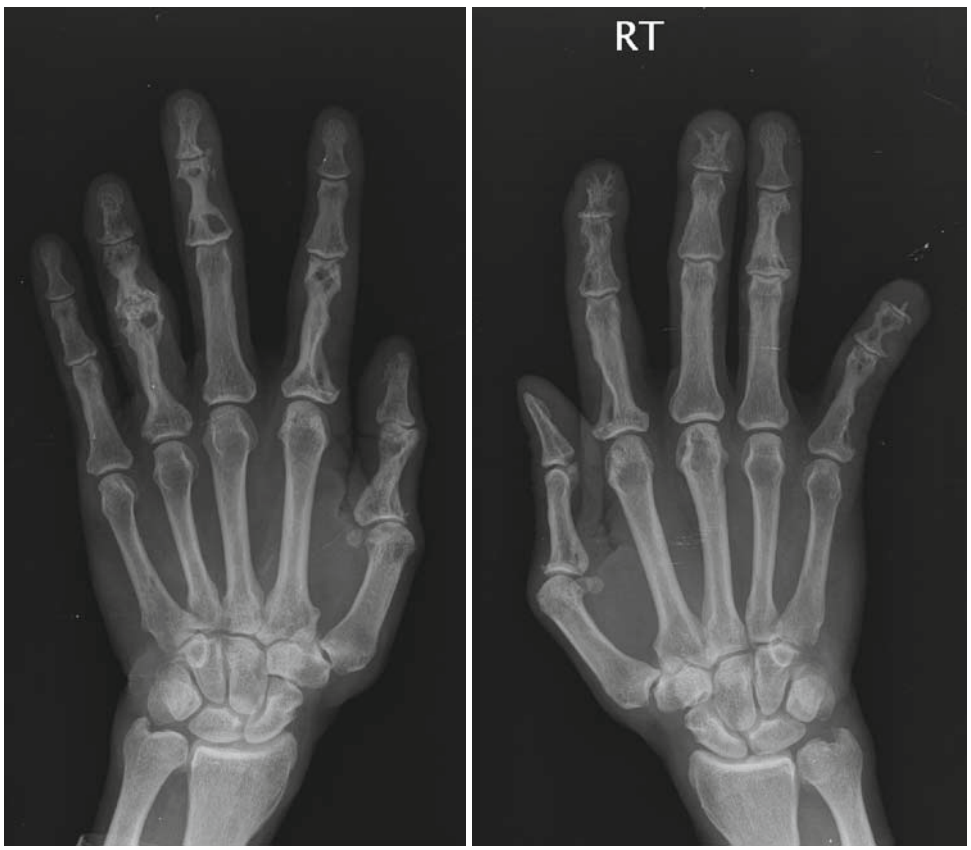

Fig. 10.31 PA radiographs of the hands show multiple punched-out lytic lesions caused by sarcoidosis in the digits. In addition there is saucerization of the radial aspect of the proximal phalanx of the second digit of the left hand and the ulnar aspect of the proximal phalanx of the right hand. This is the result of soft tissue granulomas adjacent to bone. Acroosteolysis is also present involving the tufts of the second through fifth digits of the right hand, another finding in sarcoidosis

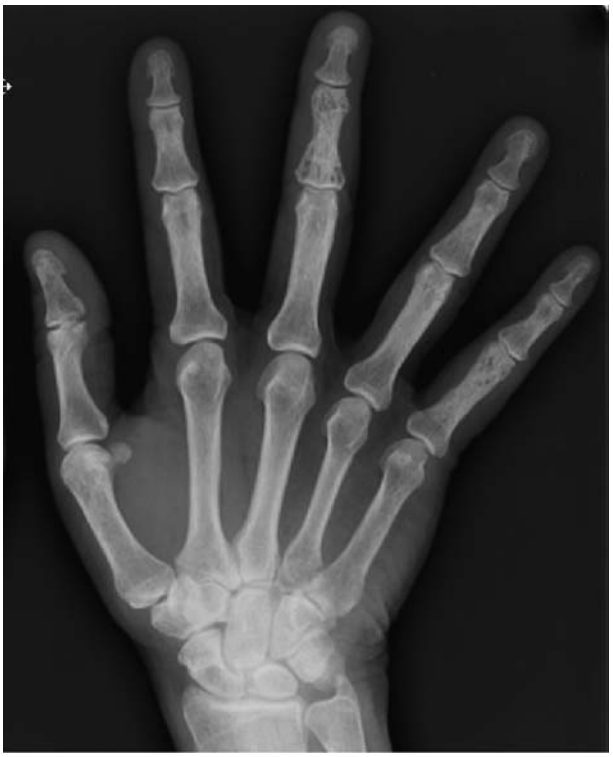

Fig. 10.32 PA radiograph of the right hand shows lacy appearing trabeculae caused by infiltrating sarcoidosis in the third middle and fifth proximal phalanges (images courtesy of Dr. John Hunter, University of Washington)

Viral Osteomyelitis

Until now, little has been known concerning viral infection of bone. Both rubella and cytomegalovirus have been identified as capable of causing osseous changes in the newborn period from intrauterine fetal infection (Fig. 10.35). These entities are now uncommon, especially since the advent of rubella vaccine and awareness of the importance of avoiding maternal exposure during pregnancy. Similarly, Caffey disease, although a disease of unknown etiology, has been suggested by some to be a viral infection. In mid-twentieth century Caffey disease was a relatively common cause of diffuse and painful periostitis of infants usually less than 5 months of age (Fig. 10.36). For unknown reasons, it has now all but disappeared.

Paget Disease

On the other hand, Paget disease, traditionally classified as a disease of unknown etiology, is coming to be regarded as a chronic viral infection of bone. Paramyxovirus nucleocapsids are present in pagetic osteoclasts – giant osteoclasts with more than 100 nuclei (Fig. 10.37) that are responsible for causing the rapid bone resorption in this disease. These nucleocapsids are not found in other non-pagetic osteoclasts (Fig. 10.37). The nucleocapsids found in both the nuclei and cytoplasm of pagetic osteoclasts strongly resemble measles virus.

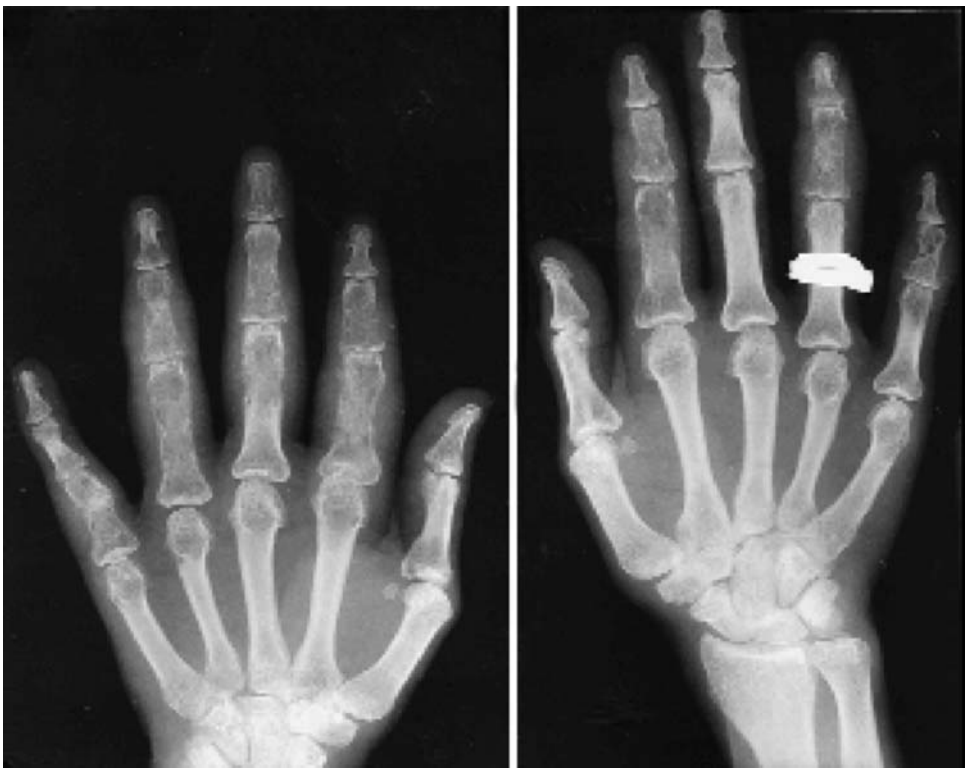

Fig. 10.33 PA views of the hands show destructive lesions in multiple phalanges secondary to sarcoidosis

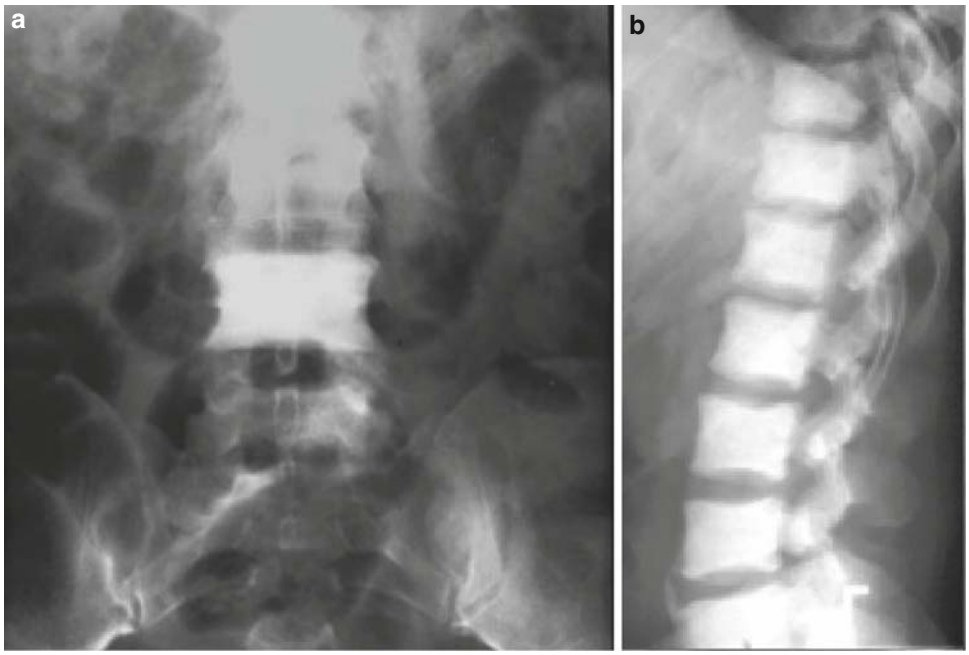

Fig. 10.34 (**a**) AP radiograph of the inferior lumbar spine showing a sclerotic L4 vertebral body caused by sarcoidosis. This is in the differential of ivory vertebral body. (Case courtesy of Ramesh Kaul, MD.) (**b**) Lateral radiograph of the lumbar spine shows sclerosis of multiple vertebral bodies, posterior elements, and the superior sacrum from sarcoidosis. Sclerotic sarcoidosis lesions may also be diffuse and are most common in the spine

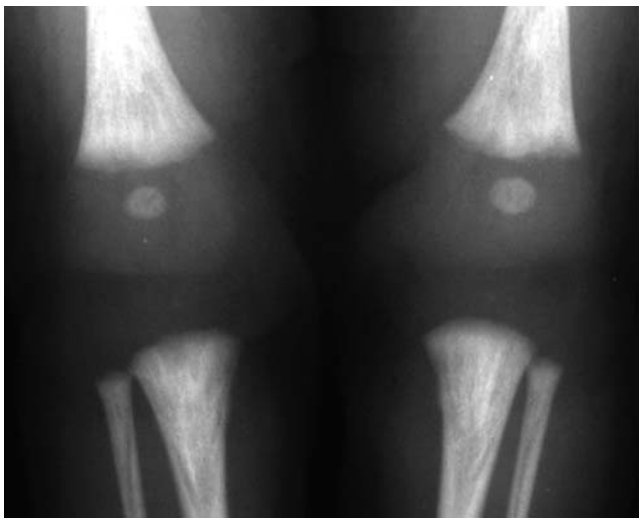

Fig. 10.35 AP radiograph of the knees of a patient with neonatal rubella showing "celery stalking." This striking appearance is related to intrauterine fetal infection

Other evidence that suggests Paget disease is infectious is that the disease tends to start at one end of a long bone or the juxtaarticular region of a flat bone and proceeds systematically along the length of the bone. Generally, the disease moves through a bone at a rate of about 1–1½ cm annually. It may affect a single bone (monostotic) or multiple bones (polyostotic). While Paget disease may affect any bone, the pelvis, femur, tibia, spine, and skull are most commonly affected. Allograft from Pagetic bone transplanted into an unaffected bone will induce the disease in the recipient bone.

The most commonly held theory today is that Paget disease represents recurrence of measles virus as a slow virus infection of osteoclasts in a genetically prepared host, i.e., one with an immune system susceptible to infection. The reason that it appears that there is an immune component in the recrudescence of Paget disease is that the disease is prominent in individuals of Anglo-Saxon descent and virtually unheard of in Asians. The disease has the highest incidence in England, Western Europe, United States, Australia, and New Zealand. Scandinavia, China, Japan, and India, on the other hand, have the lowest.

Paget disease becomes more prevalent as individuals age. It is seen in less than 1% of individuals less than 40 years of age. The prevalence increases to between 3 and 5% in the 50- to 70-year age group. By age 80 and older about 10% of the target population is affected.

Most cases are asymptomatic, but when Paget disease is symptomatic, patients complain either of bone pain or of complications resulting from Paget-induced bone enlargement including sensineural hearing loss from neuroforaminal stenosis, enlarging hat size, skeletal deformity, and secondary osteoarthritis. Patients typically have markedly elevated serum alkaline phosphatase levels and urine hydroxyproline levels.

Paget disease has four defined radiographic phases: lytic, mixed, sclerotic, and malignant transformation. The first three of these are the direct result of the pathophysiology of the disease. As pagetic osteoclasts form in the affected bone, they rapidly resorb bone creating a lytic wave front in the bone with abnormal lytic bone behind and normal unaffected bone ahead. In the skull this creates an appearance of

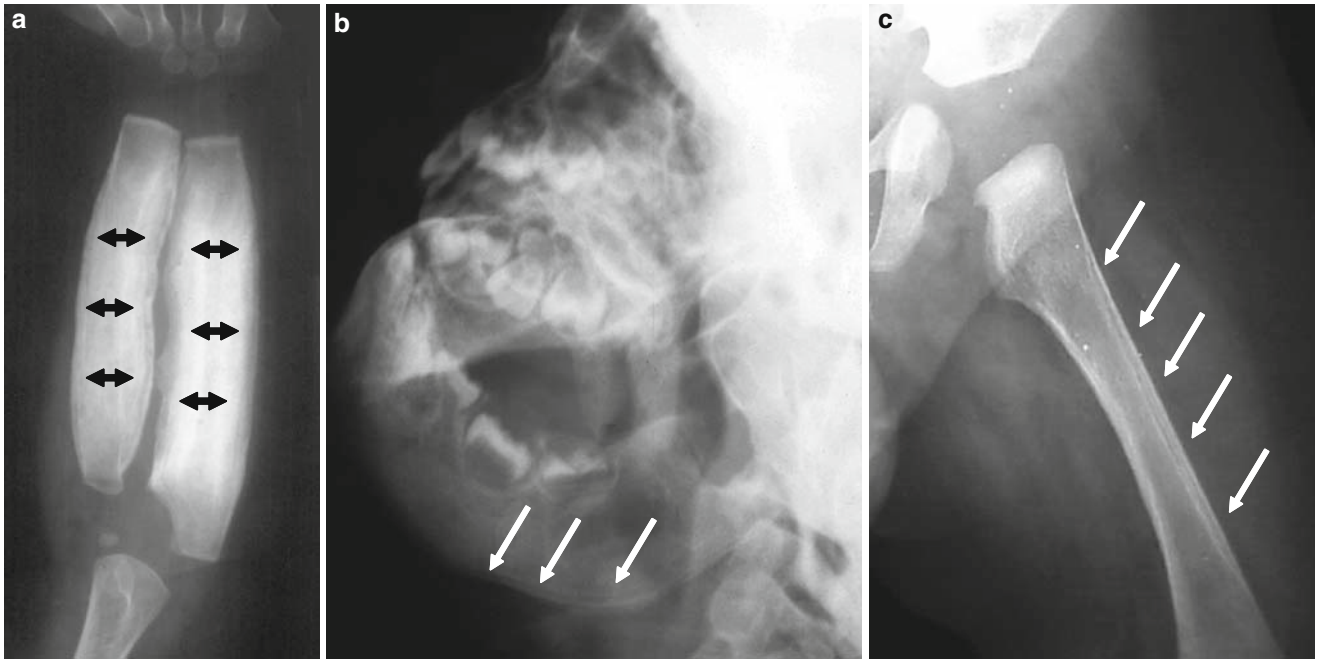

Fig. 10.36 AP radiograph of the forearm (**a**), the mandible (**b**), and left femur (**c**) of an infant with Caffey disease showing diffuse periosteal reaction along the shafts of the long bones and the mandible (*arrows*)

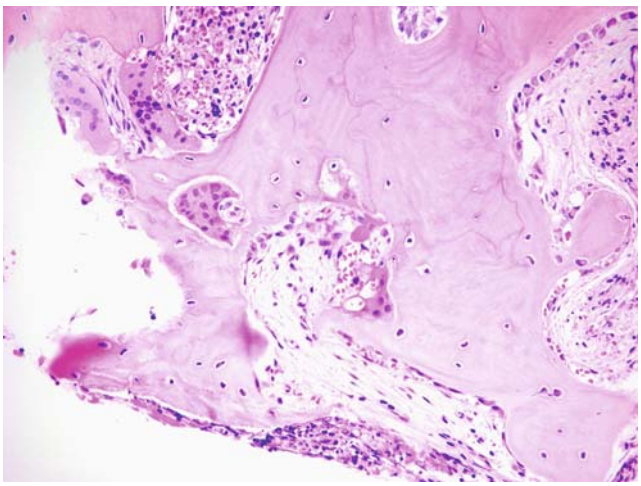

Fig. 10.37 Paget disease showing prominent osteoclastic and osteoblastic activity with a fibrotic and vascular marrow space along with trabeculae showing mosaic bone with prominent cement lines

osteoporosis circumscripta (Fig. 10.38). In long bones this creates a "blade of grass" or "flame" sign (Fig. 10.39). On radiopharmaceutical bone scan, the leading edge of the disease is highly active (Fig. 10.38c). Surprisingly, this phase may be difficult to detect on CT despite its high sensitivity to changes in bone density (Fig. 10.38b).

As the disease progresses, osteoblasts activate to remodel the demineralized bone. These enter a competition with the osteoclasts so that much of the primary woven bone that they produce is never converted to secondary lamellar bone. This produces the mixed phase with both lytic and sclerotic areas. Radiopharmaceutical bone scans show markedly increased activity (Fig. 10.40) during this and the early sclerotic phase of the disease until it finally burns out later in the course of the disease.

As more osteoblasts are recruited the bone begins to show the full sclerotic and most commonly visualized phase of the disease. Three radiographic findings typify this third phase: bone enlargement, thickened cortex, and coarse trabeculae (Figs. 10.41 and 10.42). In the skull this phase is manifest as a "cotton wool" skull (Fig. 10.43) with enlargement of the skull and multiple areas of spherical density resembling cotton balls. In the spine, the vertebral bodies and the posterior elements are equally affected. Affected vertebral bodies show enlargement and coarse cortices creating a picture frame effect (Fig. 10.44). Occasionally, the entire body may become sclerotic giving an ivory vertebra appearance (Fig. 10.45). This may also be seen in other diseases such as sclerotic metastases from prostate or breast cancer, Hodgkin disease and sarcoidosis of bone.

As mentioned, the rapidly remodeling bone is primarily woven bone and hence more malleable than lamellar bone. This leads not only to enlargement but also to bowing deformities in the weight bearing long bones (Fig. 10.46) and changes in shape of the skull. The latter changes manifest themselves as enlarging hat size, a deformity of the calvar-

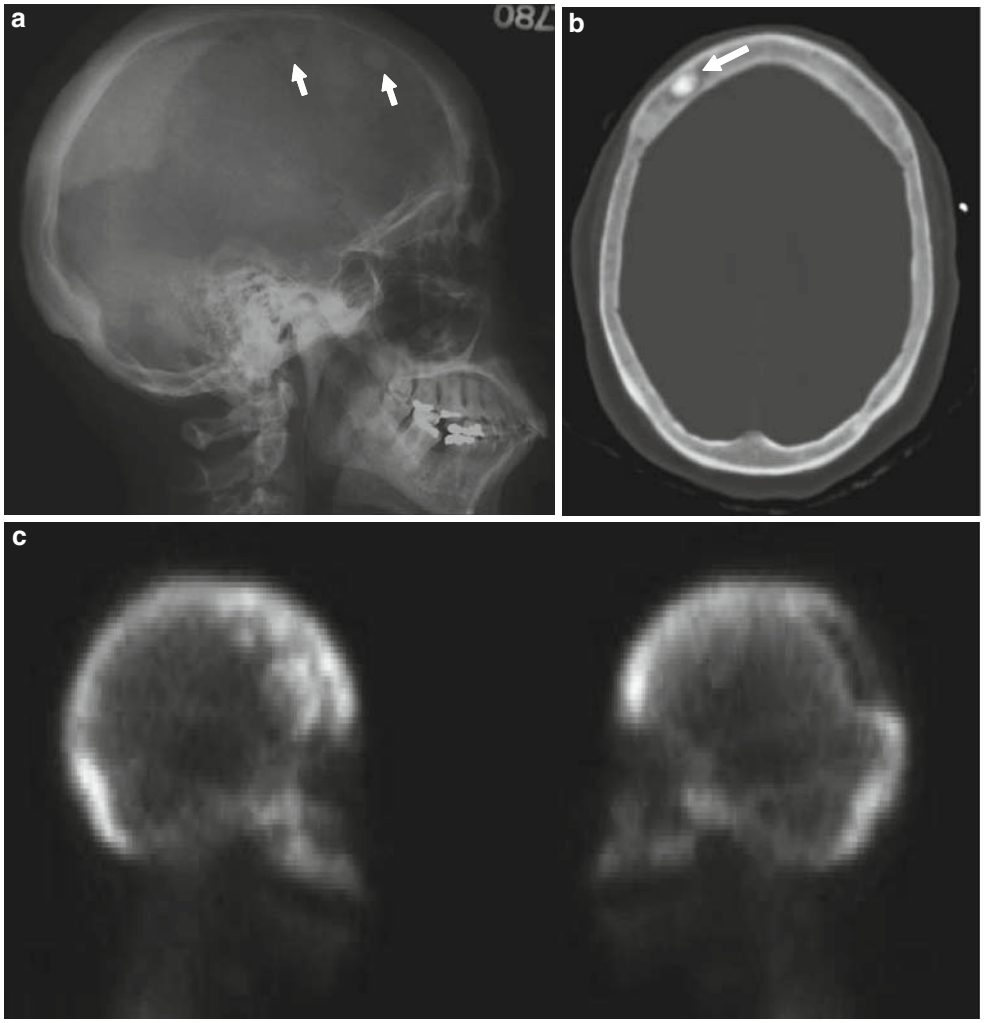

Fig. 10.38 Lateral skull radiograph (**a**), bone-windowed CT image (**b**), and bone scan (**c**) of a patient with Paget disease showing osteoporosis circumscripta. On the radiograph, note the sharp demarcation between the normal bone posteriorly and reabsorbed bone anteriorly. Further note the small areas of density in the frontal bone (*arrows*) as the disease enters the mixed phase where active remodeling occurs. While this last finding is obvious on the CT (*arrow*), the osteoporosis circumscripta is difficult to detect. The bone scan images show the advancing wave front of resorption and the active remodeling in the frontal bone to advantage

ium known as a "Tam O'Shanter skull" resembling the Scottish hat of that name, basilar invagination and narrowing of the neuroforamina leading to compressive cranial neuropathies. Furthermore, the long bones begin to form pseudofractures that form perpendicular to the cortex of the bone typically along its convexity (Fig. 10.46). These pseudofractures are also known as Looser zones or Milkman fractures.

With chronicity, there is a chance that Paget disease will progress to the fourth phase of the disease: malignant transformation. As with other chronic infections, Paget disease with its high cell turnover rate is thought to potentiate neoplastic transformation. Paget disease accounts for the majority of cases of osteosarcoma seen in later life, typically seventh decade (Fig. 10.47). Other tumors also occur, including chondrosarcoma and malignant fibrous histiocytoma.

Infection of Muscle, Fascia, and Nerves

Myositis and Abscess

Besides cellulitis, which is primarily a clinically diagnosed disease, radiologists often are called upon to evaluate patients with soft tissue infections. These include myositis, pyomyositis, abscess, and fasciitis. Unlike osteomyelitis, muscle abscesses and pyomyositis most commonly arise from hematogenous spread of bacteria during episodes of bacteremia that are not necessarily associated with sepsis. The most common organisms cultured from these abscesses are *S. aureus* or mixed anaerobic bacteria.

Today, overwhelmingly the modality of choice for evaluation of muscle inflammation is MRI. CT with iodinated

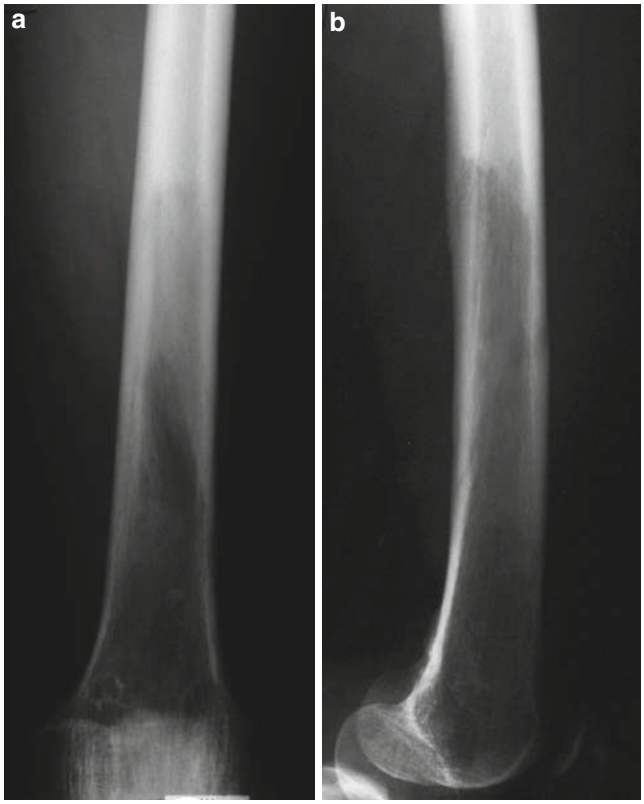

Fig. 10.39 AP (**a**) and lateral (**b**) radiograph of the femur showing a "flame sign" or "blade of grass sign" – a sharp demarcation of Paget disease with the reabsorbed bone distally and the normal bone proximally

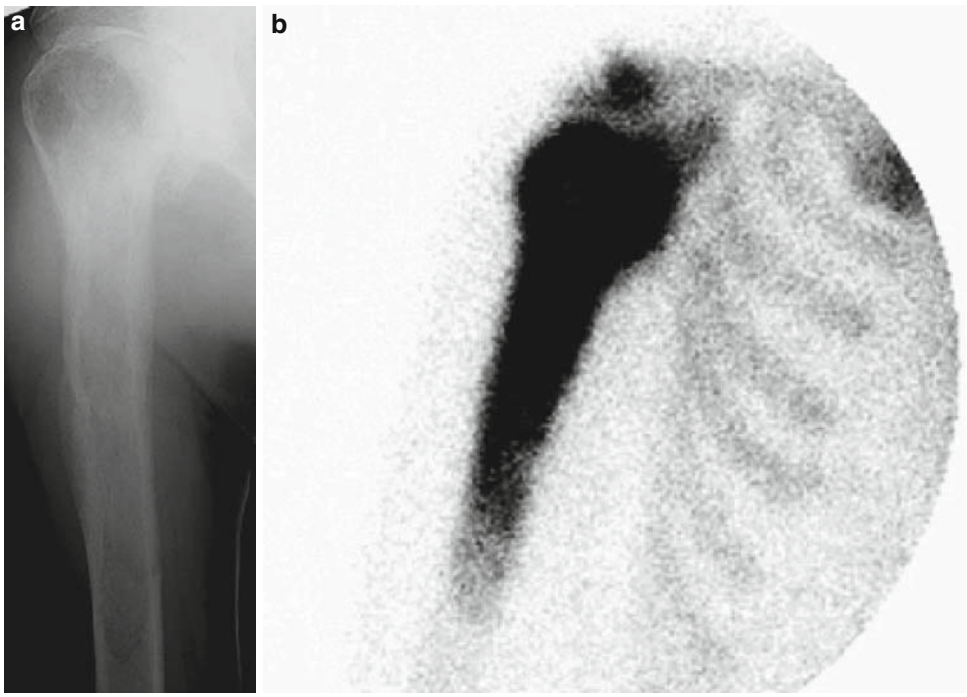

Fig. 10.40 AP radiograph (**a**) and anterior projection of a radiopharmaceutical bone scan (**b**) from a patient with stage 2–3 Paget disease. Note the cortical thickening, trabecular coarsening, and bone enlargement (**a**) correlating with the marked activity on the bone scan (**b**)

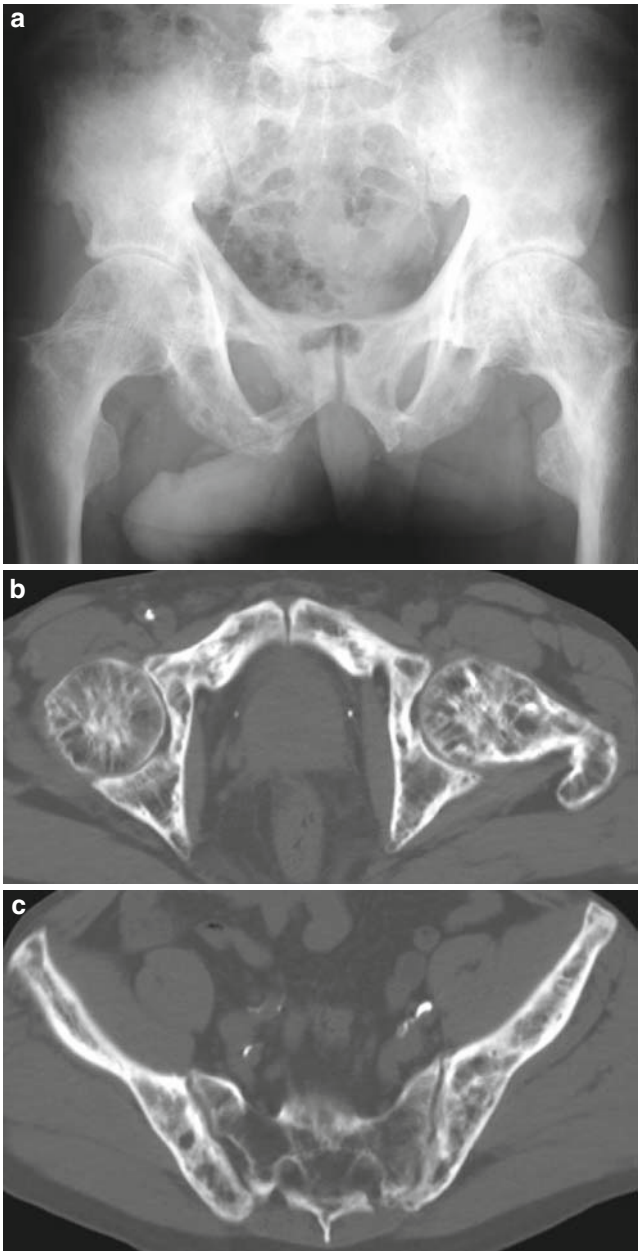

Fig. 10.41 AP pelvis radiograph (**a**) and CT images (**b**) and (**c**) showing Stage 3 Paget disease. Note the bone enlargement, thickened cortices, and coarsened trabeculae

contrast may be useful for abscess identification (Fig. 10.48), but its decreased sensitivity compared with MRI, its use of x-radiation, and the possibility of allergic reaction to intravenous contrast make it a second choice examination. On the other hand, MR has proven adept at identification of abscesses of both large scale (Fig. 10.19) and small scale as is seen in pyomyositis (Fig. 10.49). In all cases, whether on CT or MRI, an abscess appears as a well-defined fluid density or signal structure with an enhancing rim after administration of contrast. Identification of edema without these criteria may be consistent with myositis or phelgmonous change but does not represent an abscess. This distinction is important, particularly in the case of large abscesses where drainage may be contemplated. In consideration of the differential diagnosis, it is important to realize that such abscesses are not always pyogenic but may arise in chronic granulomatous infection, particularly tuberculosis (Fig. 10.50).

Madura Foot

First described in Madura India in 1842, Madura foot represents a fungal infection of the deep tissues of the foot

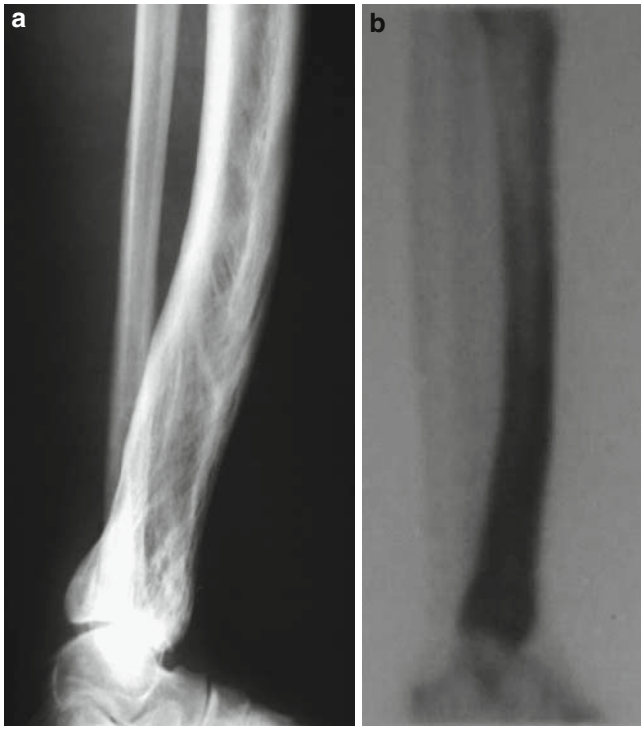

Fig. 10.42 Lateral radiograph (**a**) and lateral projection from a radiopharmaceutical bone scan (**b**) showing stage 3 Paget disease

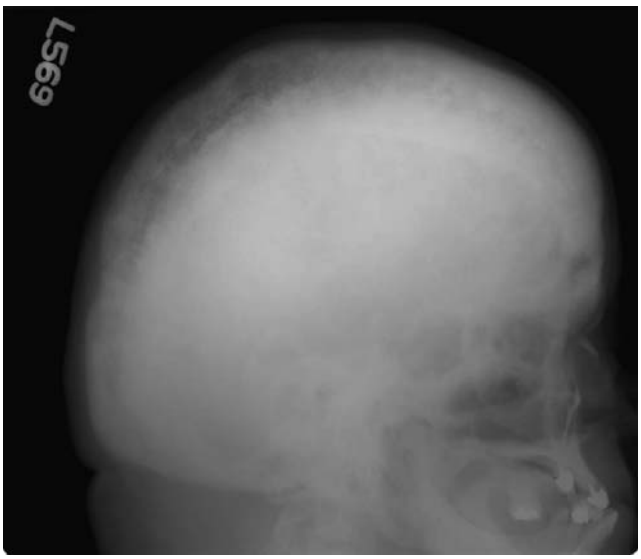

Fig. 10.43 Lateral skull radiograph in a patient with stage 3 Paget disease showing diffuse "cotton wool skull" with thickening of the calvarium including the diploic space and the inner and outer tables. Note the early cotton wool changes in Fig. 10.38

by the filamentous bacterium, actinomycetes (60%), or true fungi (40%). It presents as a mass in the foot in subtropical regions, including the southern United States, and is known as a mycetoma. The lesion may spread to the bone and cause a highly destructive osteomyelitis reminiscent of an infected neuropathic foot (see Chapter 11). Today, with better imaging technology, it is more likely to be appreciated in its soft tissue phase (Fig. 10.51). The disease has also been recognized in immunocompromised patients in non-tropical zones.

Fasciitis

Fasciitis represents infection and inflammation of the deep fascia. It is becoming more common as immunosuppression

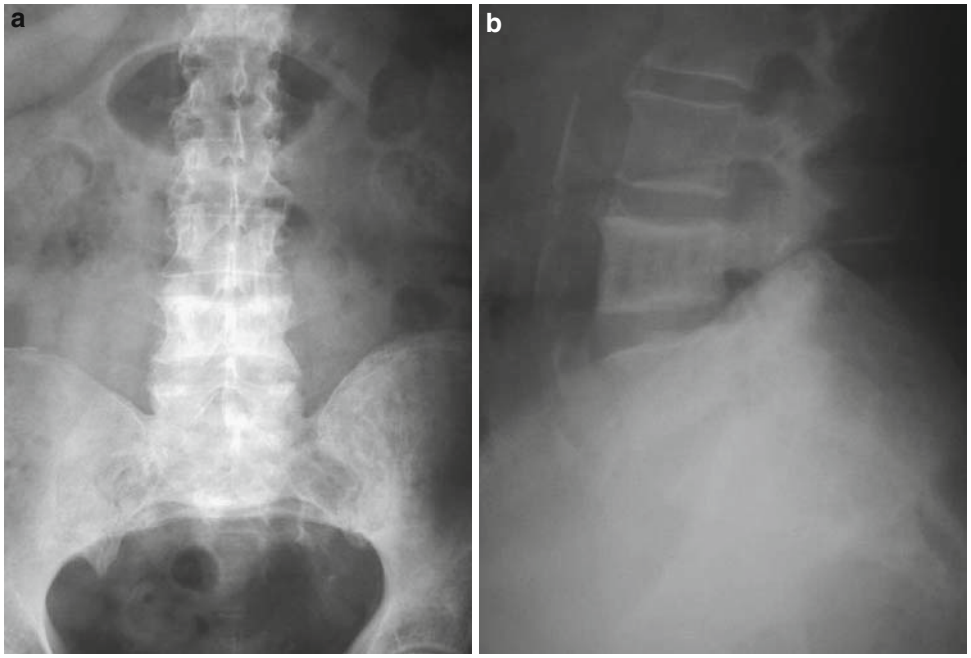

Fig. 10.44 AP (**a**) and lateral (**b**) lumbar spine radiograph in a patient with stage 3 Paget showing involvement of L4 with coarsened trabeculae and thickening of the cortex as well as mild enlargement

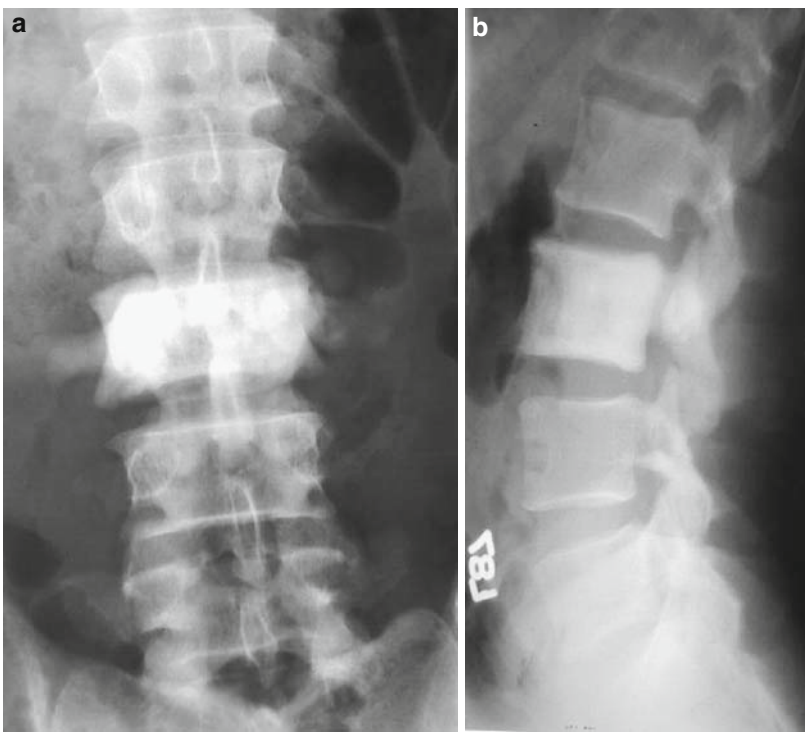

Fig. 10.45 AP (**a**) and lateral (**b**) lumbar spine radiograph in a patient with stage 3 Paget. The L3 vertebral body is sclerotic, enlarged, and has a thickened cortex creating a "picture frame" appearance. Note the marked sclerosis giving an "ivory vertebra" appearance. Other entities that may cause an ivory vertebra appearance include blastic metastases, Hodgkin lymphoma, and rarely Pott disease and sarcoidosis. In Paget disease, the particular findings often allow an absolute diagnosis without differential

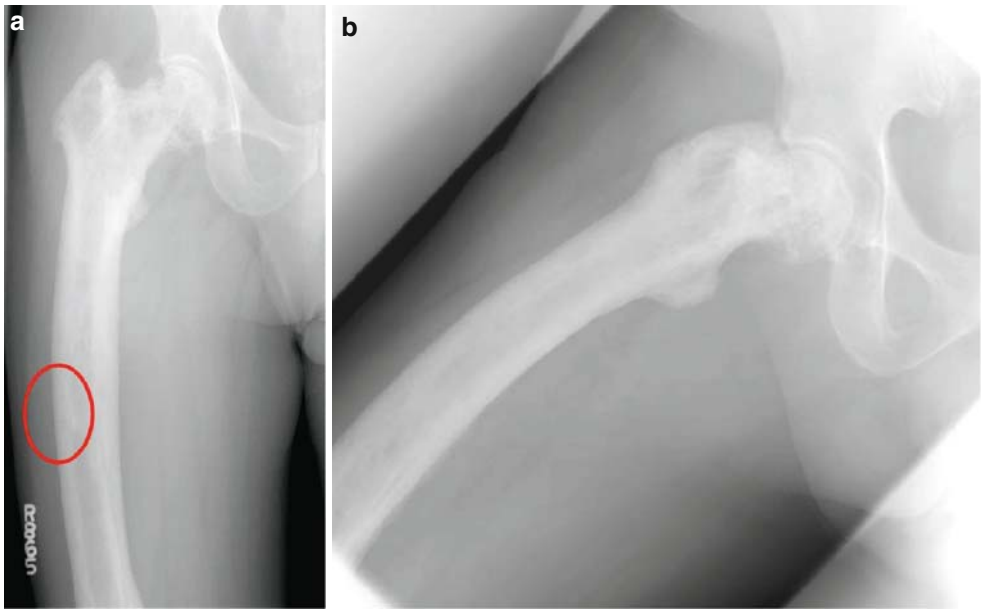

Fig. 10.46 AP (**a**) and frog's leg lateral (**b**) images of the proximal right femur showing stage 3 Paget disease and a pseudofracture (*oval*). Pseudofractures, also called Looser zones and Milkman lines, are characteristically along the convexity of the bone in Paget disease

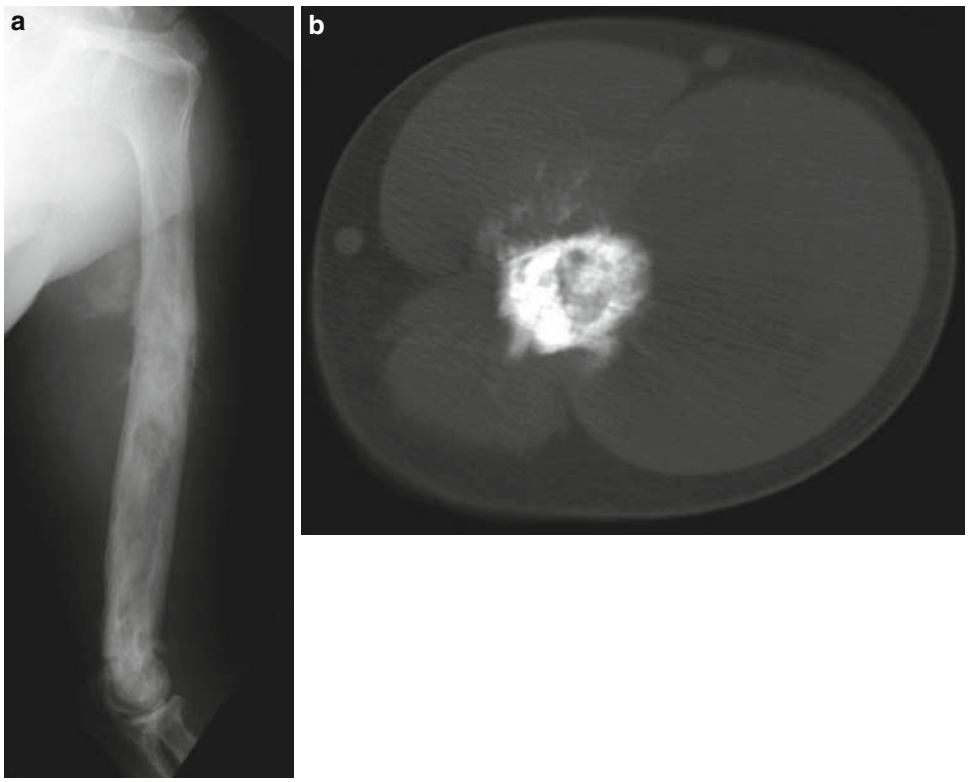

Fig. 10.47 AP humeral radiograph (**a**) and bone-windowed CT image (**b**) showing osteosarcoma forming in Paget disease. The mid-humeral diaphysis shows speculated periosteal new bone formation along with areas of new bone in the medial soft tissues and lytic lesions within the humerus. These findings are all atypical for Paget disease and suggest malignant transformation

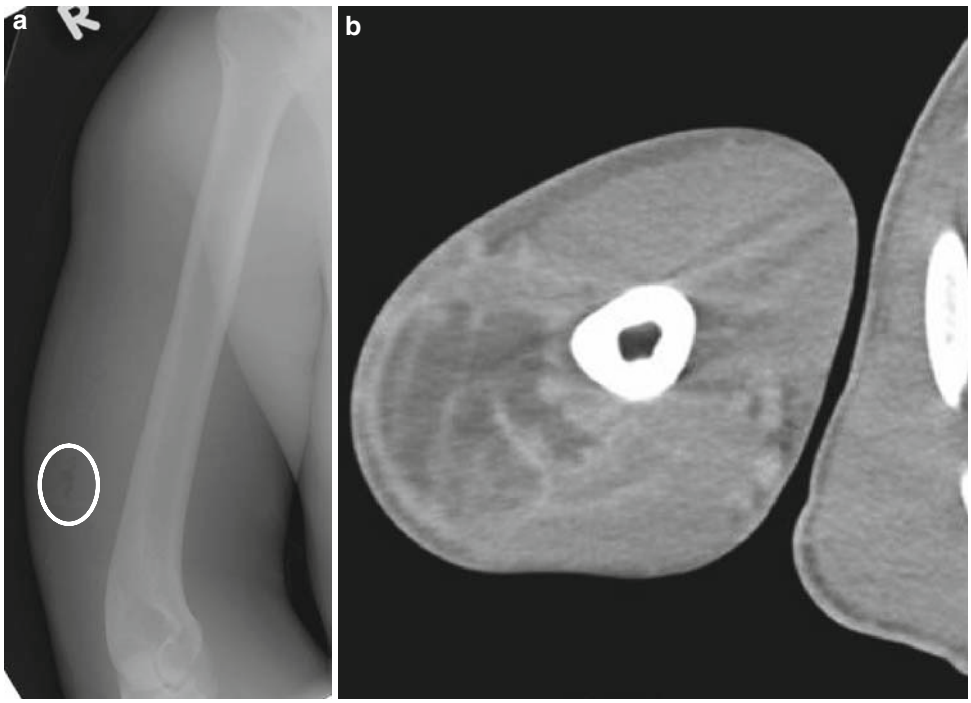

Fig. 10.48 AP radiograph (**a**) of the right humerus and soft tissue CT image after contrast (**b**) showing a small focus of air in the soft tissues (**a**) and a large peripherally enhancing abscess (**b**)

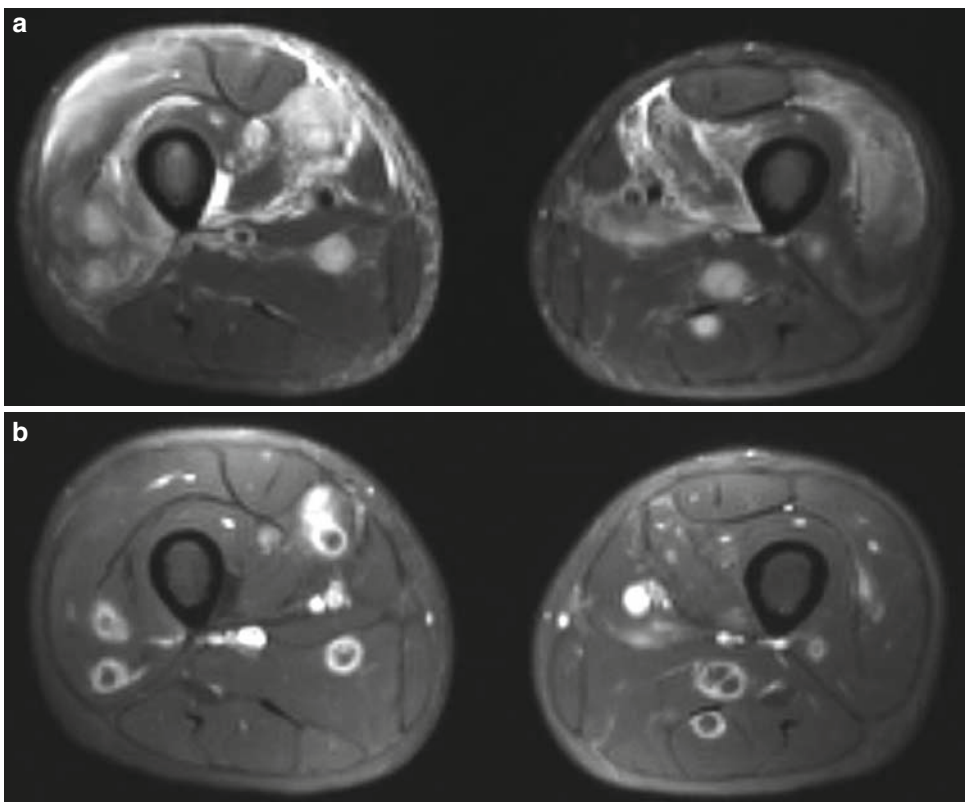

Fig. 10.49 Axial T2-weighted fat-suppressed (**a**) and T1-weighted fat-suppressed post-gadolinium **(b)** images showing multiple intramuscular micro-abscesses

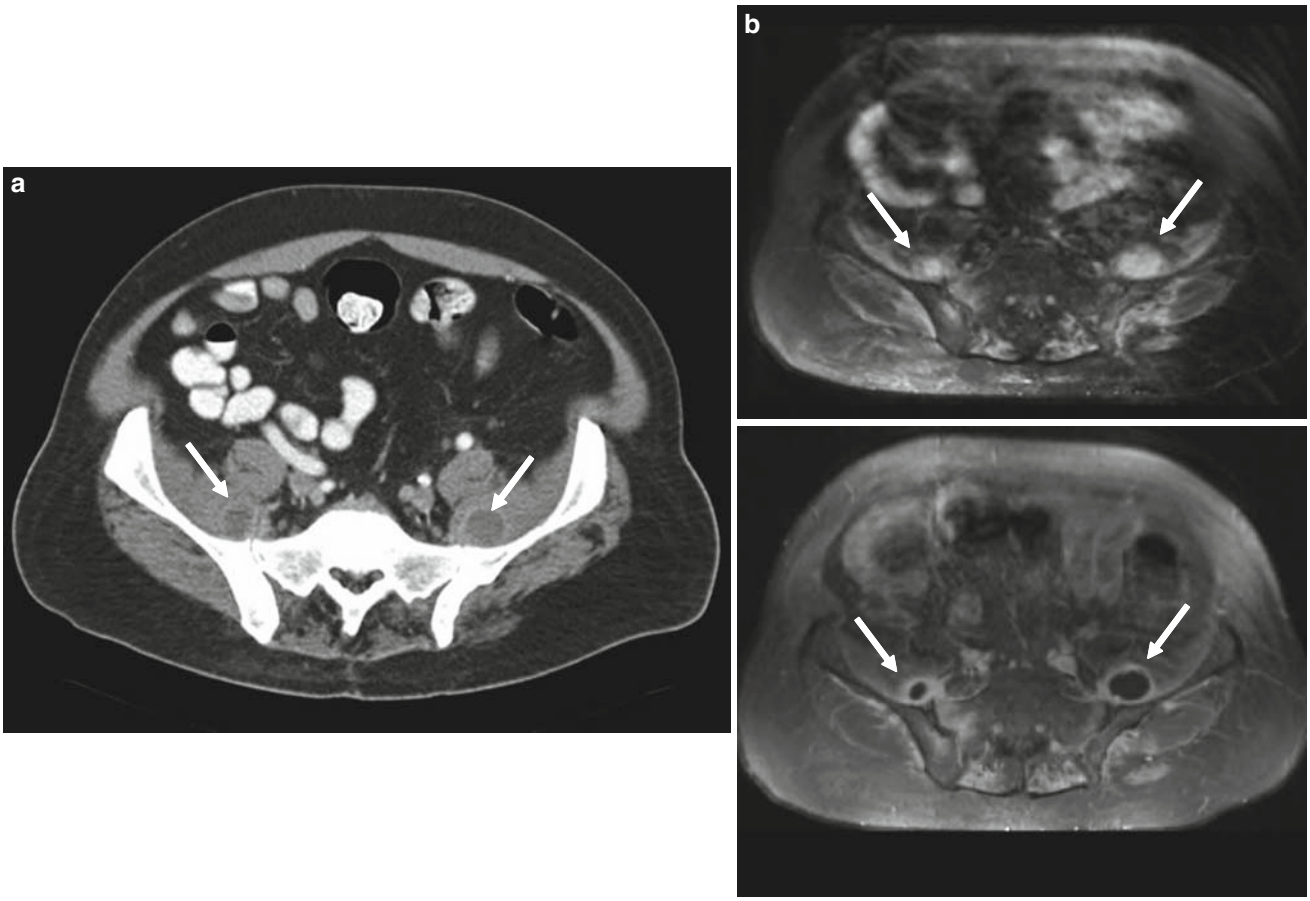

Fig. 10.50 Axial post-contrast CT image (**a**) and axial T2-weighted fat-suppressed (**b**) and T1-weighted fat-suppressed post-gadolinium MR images showing typical bilateral psoas abscesses from tuberculosis (*arrows*)

related to AIDS, diabetes mellitus, transplants, and chemotherapy for neoplasms increases in the population. Clinically, fasciitis is usually apparent as the patient is acutely ill with fever and high white cell counts; the extremity is markedly swollen and may have subcutaneous gas (subcutaneous emphysema) causing crepitus. As a result, the diagnosis is generally made clinically.

Radiologists may be called upon to stage the extent of disease and evaluate for the presence of localized abscess. Plain radiographs generally show swelling and may show subcutaneous emphysema (Fig. 10.52), but otherwise are not particularly useful. CT and MRI, on the other hand, are useful for evaluation of the soft tissues as discussed above (Figs. 10.53, 10.54, and 10.56). Gadolinium administration may help to demarcate areas of necrosis since they will not enhance. Currently, no radiographic examination can reliably diagnose acute compartment syndromes. This can only be done clinically using manometry and at times Doppler ultrasound. MR may show edema and enlargement of the involved compartment, but it is not the test of choice and is much more expensive than compartment manometry.

Two forms of fasciitis deserve particular attention. These include necrotizing fasciitis and Fournier gas gangrene. Necrotizing fasciitis, also known as hemolytic streptococcal gangrene, Meleney ulcer, acute dermal gangrene, hospital gangrene, and suppurative fasciitis, is a fulminant infection of the soft tissues caused by streptococcus A, *S. aureus*, and anaerobic species – including *Bacteroides, Clostridium, Peptostreptococcus,* Enterobacteriaceae, coliforms, *Proteus, Pseudomonas,* and *Klebsiella*. Often the streptococcal and staphylococcal species are the initiating organisms and the anaerobes superinfect the area. Necrotizing fasciitis is life-threatening and requires immediate attention. Here radiographs may show severe subcutaneous emphysema and swelling (Fig. 10.55).

Fournier gangrene is a fulminant necrotizing fasciitis of the perineum and is polymicrobial in etiology. It was described in the nineteenth century by French dermatologist Jean Alfred Fournier. The disease is about 10 times more common in men than women possibly because women have better perineal lymphatic drainage. Typically, the perineum and scrotum are massively swollen and show subcutaneous

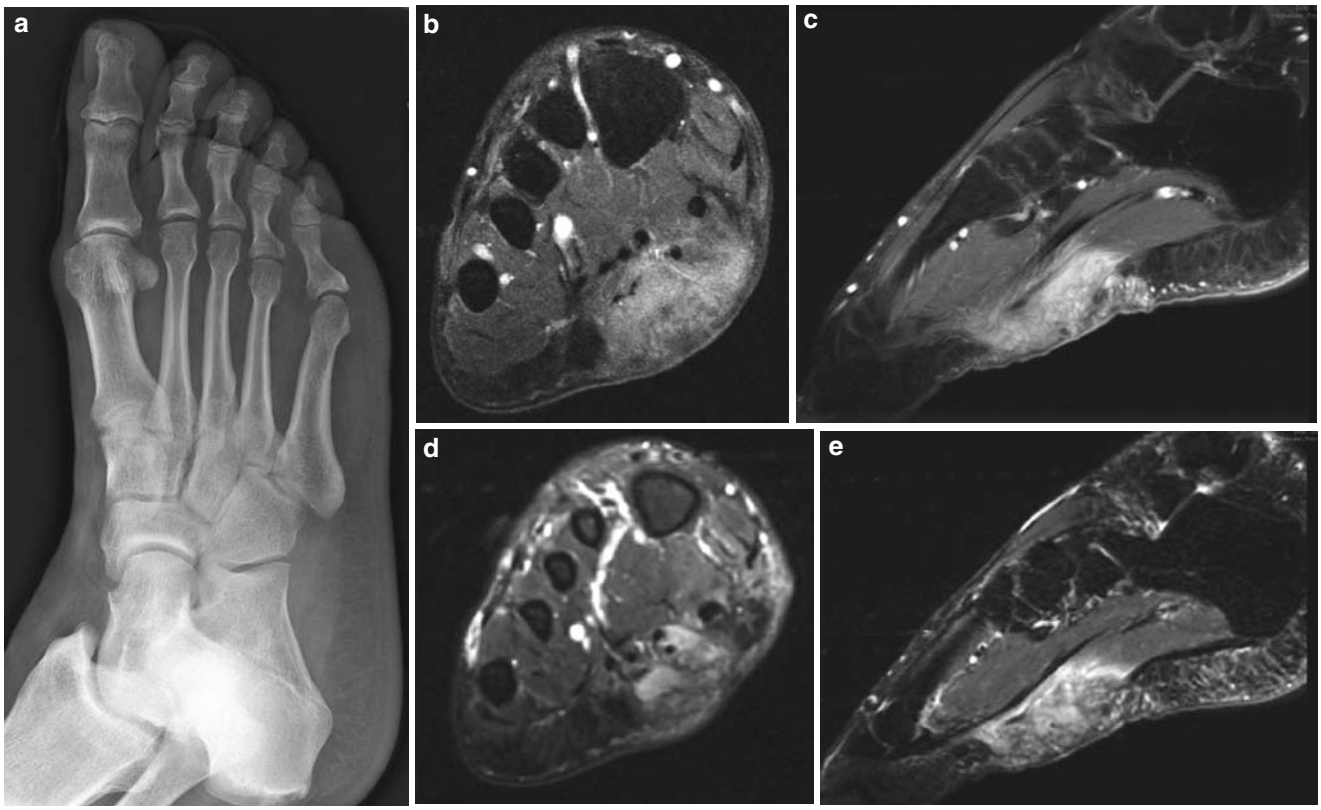

Fig. 10.51 Oblique right foot radiograph (**a**), sagittal IR (**b**), short axis (**c**) T2-weighted fat-suppressed and sagittal (**d**) and short axis (**e**) T1-weighted fat-suppressed post-gadolinium MR images showing a uniformly enhancing soft tissue mass in the plantar aspect of the forefoot in a patient with Madura foot. The mass is invading the plantar musculature and bowing the plantar soft tissues (images courtesy of Dr. John Hunter, University of Washington)

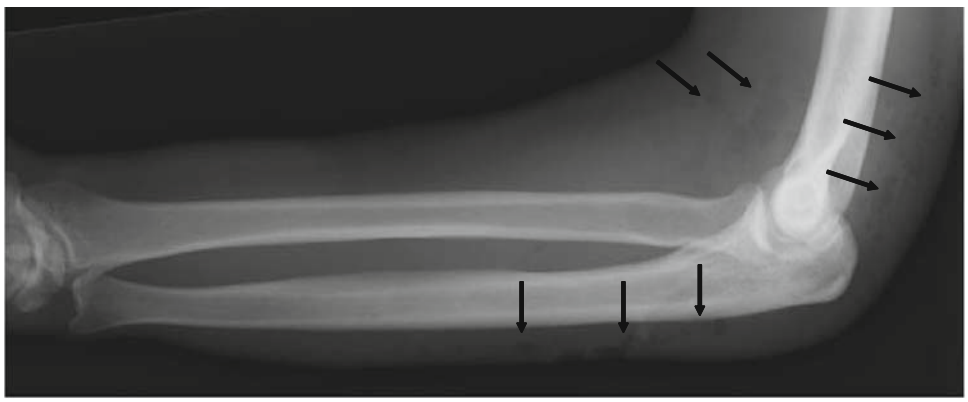

Fig. 10.52 Lateral forearm radiograph showing dorsal soft tissue swelling and gas (*arrows*) in a patient with necrotizing fasciitis

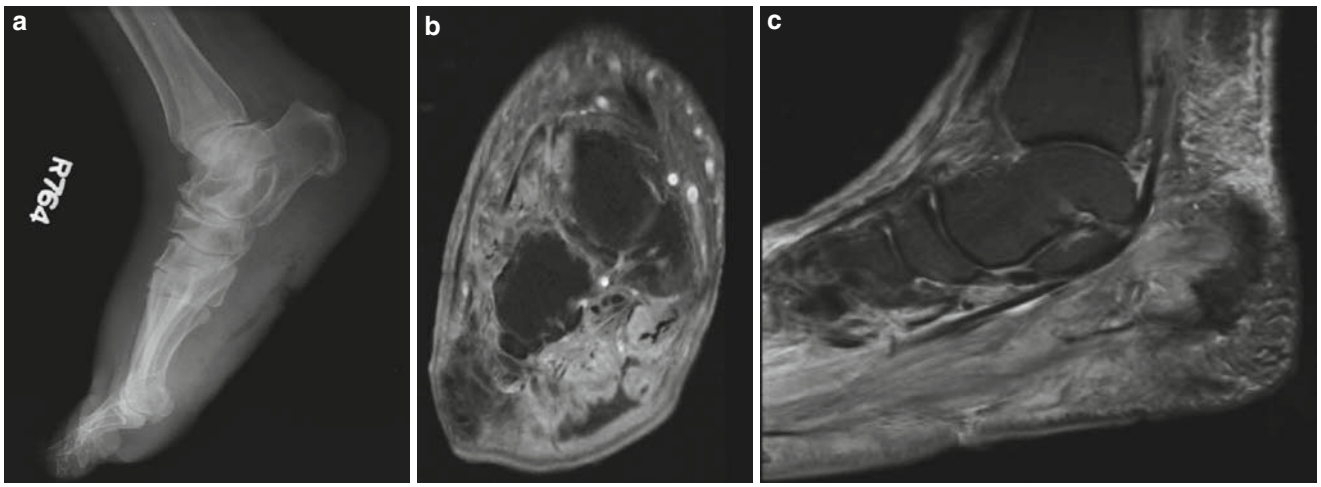

Fig. 10.53 Lateral foot radiograph (**a**) and short axis (**b**) and sagittal (**c**) T2-weighted fat-suppressed images in a patient with fasciitis of the plantar tissue of the foot. Gas tracks along the plantar fascia on the radiograph. The MR images show severe plantar and milder diffuse soft tissue edema and inflammation (high signal on T2W)

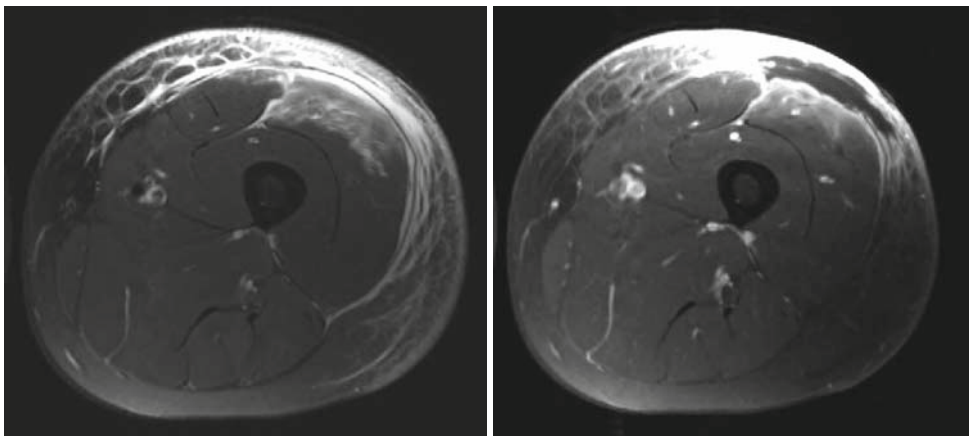

Fig. 10.54 Axial T2-weighted fat-suppressed (**a**) and T1-weighted fat-suppressed post-gadolinium images of a thigh in a patient with fasciitis and abscess formation in the subcutaneous tissues

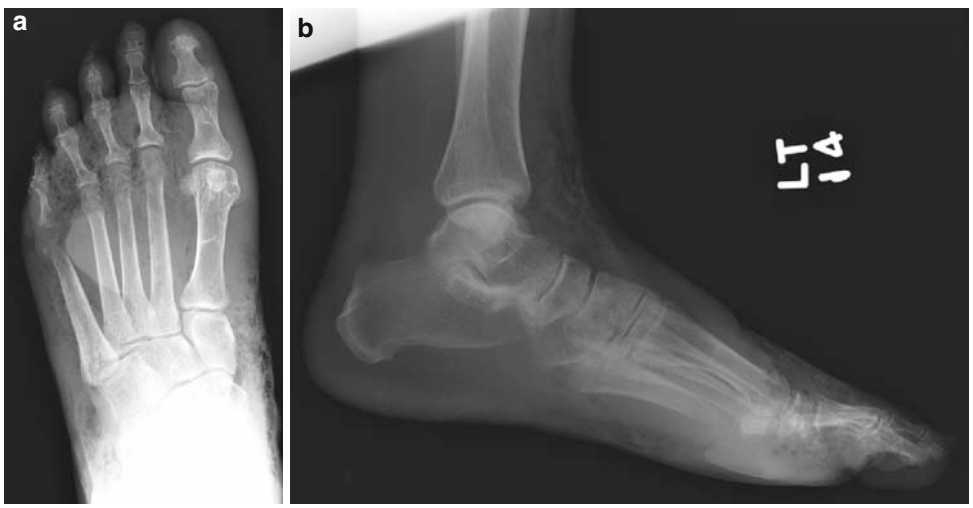

Fig. 10.55 AP (**a**) and lateral (**b**) views of the foot show marked soft tissue swelling and subcutaneous emphysema in this patient with necrotizing fasciitis. Note the destruction of the fifth metatarsal head and the base of the proximal phalanx on the fifth digit consistent with osteomyelitis

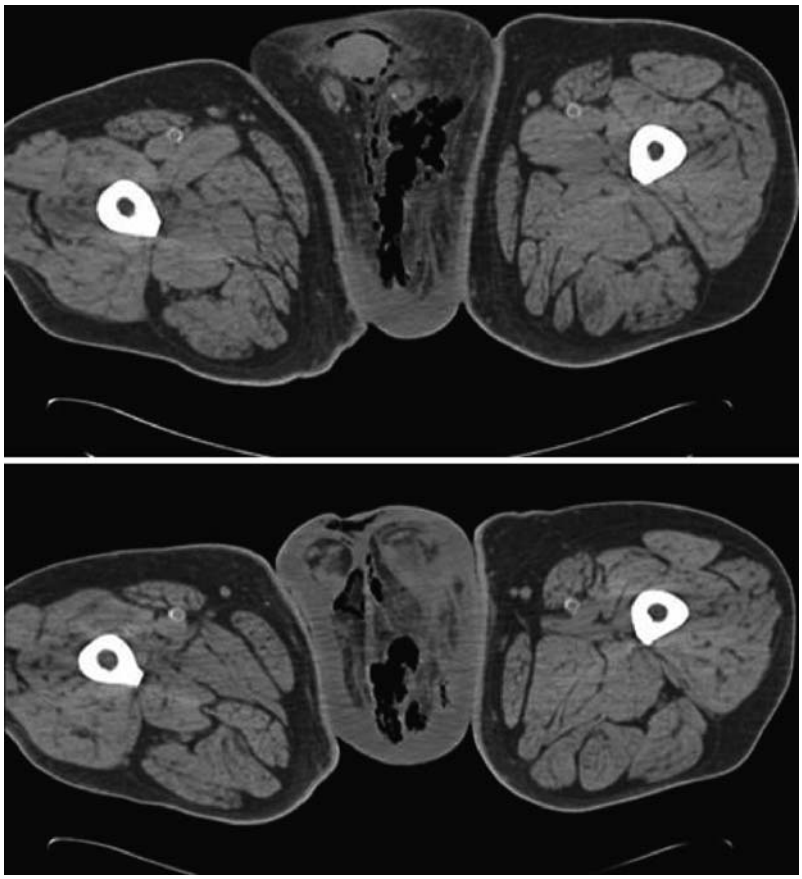

Fig. 10.56 CT images through the perineum in a patient with Fournier gas gangrene. Note the massive scrotal gas and swelling

emphysema and areas of necrosis (Fig. 10.56). Today, even with effective antibiotic therapy, Fournier gas gangrene still has a mortality rate as high as 25–40.

Infection of Peripheral Nerves

Some infections primarily affect the peripheral nerves and as a result cause prominent musculoskeletal findings at imaging. A few of these deserve mention.

Leprosy

Leprosy is an infection of the skin and peripheral sensory nerves by Hansen bacillus, *Mycobacterium leprae*. Leprosy occurs rarely in the United States. Only about 150 new cases occur annually, mostly in the southern states. On the other hand, every year about 500,000–700,000 new cases are reported worldwide, particularly in South America. While imaging is not particularly useful for diagnosis of the infection in the nerves, the sequelae of the infection are characteristic in the correct clinical setting.

The loss of sensory nerves for patients with leprosy means a loss of proprioception and increased susceptibility to unrecognized trauma. The acral skeleton is most affected. As a result, patients will have radiographs that strongly resemble the changes of neuropathic arthritis. They will often show a licked candy cane appearance to their metatarsals and phalanges (Fig. 10.57). In addition, patients are prone to superimposed pyogenic infections because of the loss of sensation. Thus, radiographs should be evaluated for osteomyelitis as well as the lepromatous changes.

Poliomyelitis

Unlike leprosy, polio affects the motor neurons in the anterior horn of the spinal cord and the brainstem resulting in flaccid paralysis. The disease is the result of an RNA enterovirus infection and is spread via an oral–fecal route. The incidence of new polio infection in the United States is very small,

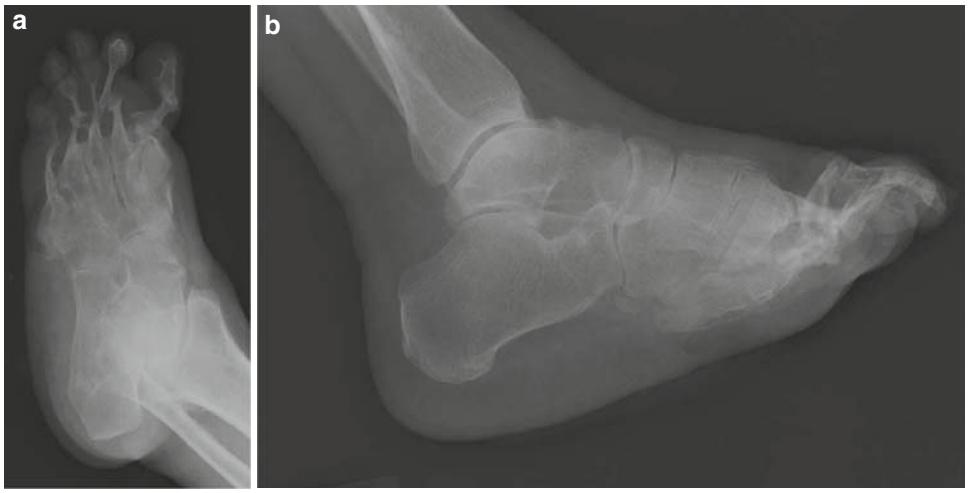

Fig. 10.57 AP (**a**) and lateral (**b**) foot radiographs in a patient with leprosy. Note the marked distortion of the bones and joints giving a "licked candy stick" appearance along with disorganization and dislocation of the joints. Essentially this is a neuropathic arthropathy that results from the sensory nerve involvement in this disease

fewer than 10 cases annually, thanks to an aggressive vaccination program. Most of these cases actually occur as complications of the vaccination itself.

The disease causes marked muscle tissue wasting. This is visible on plain radiographs and other imaging modalities as fatty replacement of the muscles (Fig. 10.58). Further, when the disease strikes the patient at a young age, the bones fail to model appropriately because of the absence of normal stresses from weight bearing. This results in gracile appearing long bones. The findings of polio on radiographs strongly resemble those of the muscular dystrophies, but differential diagnosis is rarely a problem clinically.

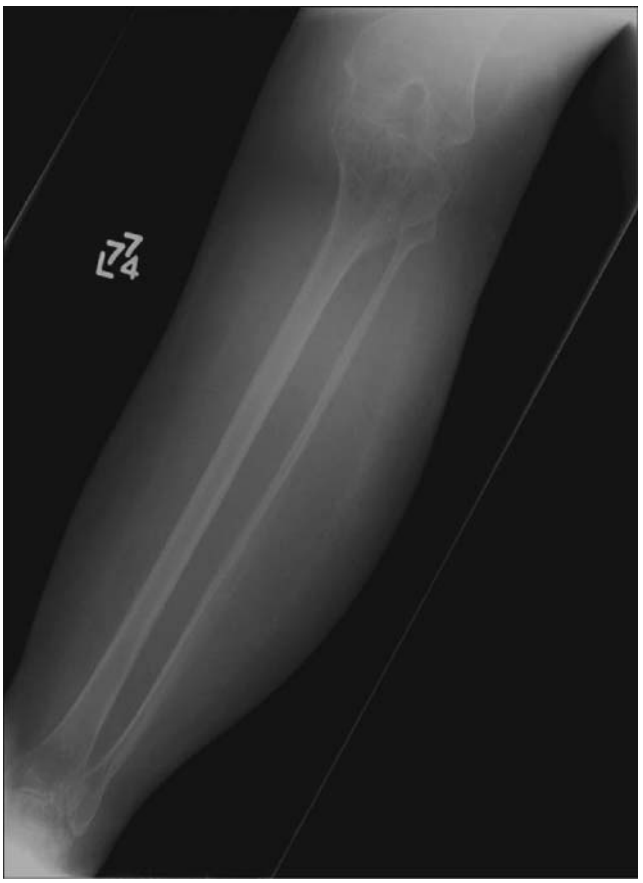

Fig. 10.58 AP calf radiograph in a patient with poliomyelitis. The muscles have been completely replaced by fat and the bones are thin and gracile. The latter finding results from lack of weight bearing during childhood when the bones are growing

Parsonage–Turner Syndrome

Parsonage–Turner syndrome is thought to be a viral neuritis that affects primarily the suprascapular nerve. The disease appears in epidemics usually associated with known viral epidemics that affect other parts of the body such as the upper respiratory tract. It has a relatively benign course and is self-limiting but patients may take as long as 2 years from initial infection to recover. Parsonage–Turner is clinically significant because patients present with complaints related to their rotator cuffs and are often suspected of a rotator cuff tear. MRI obtained to exclude a rotator cuff tear shows acute denervation atrophy of the supraspinatus and infraspinatus muscles with edema in their distribution (Fig. 10.59). The deltoid and teres minor muscles may be involved if the disease affects the axillary nerve.

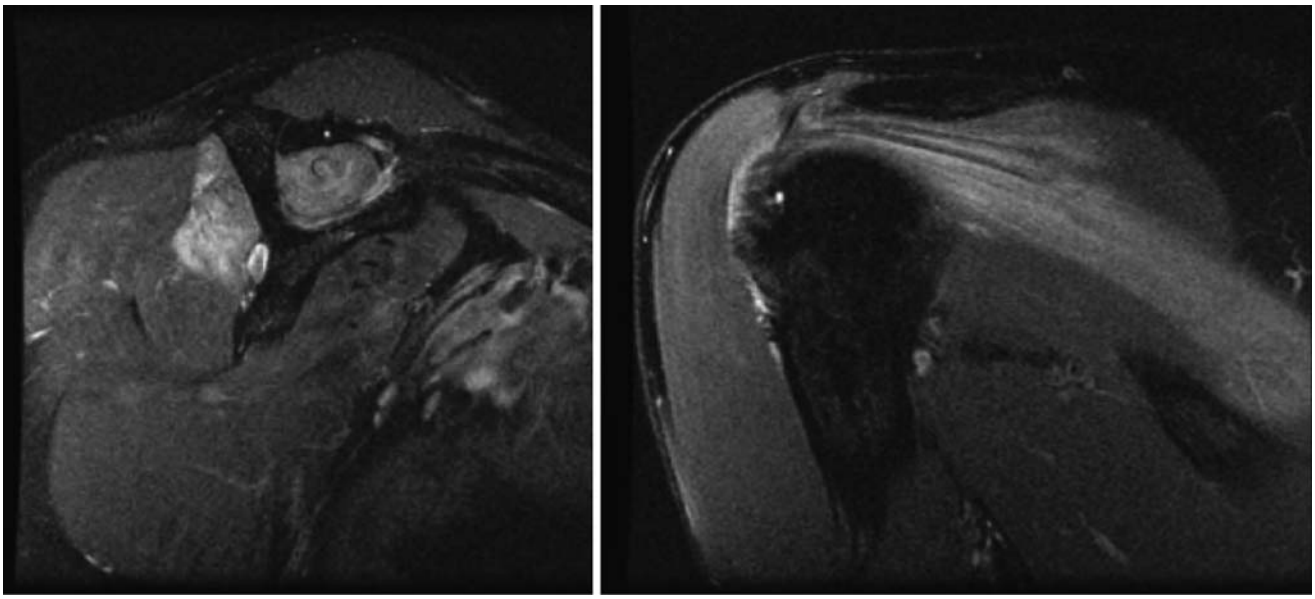

Fig. 10.59 Off-axis sagittal (**a**) and off-axis coronal T2-weighted fat-suppressed MR images of the shoulder in a patient with Parsonage–Turner syndrome. Note the edema in the supraspinatus and infraspinatus muscles while the teres minor and subscapularis muscles are spared

Further Readings

Osteomyelitis, Pyogenic

1. Abernethy LJ, Lee YC, Cole WG: Ultrasound localization of subperiosteal abscesses in children with late-acute osteomyelitis. J Pediatr Orthop 1993 Nov–Dec; 13(6): 766–768.
2. Adatepe MH, Powell OM, Isaacs GH, et al.: Hematogenous pyogenic vertebral osteomyelitis: diagnostic value of radionuclide bone imaging. J Nucl Med 1986 Nov; 27(11): 1680–1685.
3. Alazraki NP: Radionuclide imaging in the evaluation of infections and inflammatory disease. Radiol Clin North Am 1993 Jul; 31(4): 783–794.
4. Azouz EM: Computed tomography in bone and joint infections. J Can Assoc Radiol 1981 Jun; 32(2): 102–106.
5. Babcock DS, Kaufman RA: Ultrasonography and computed tomography in the evaluation of the acutely ill pediatric patient. Radiol Clin North Am 1983 Sep; 21(3): 527–550.
6. Becker W: Imaging osteomyelitis and the diabetic foot. Q J Nucl Med 1999 Mar; 43(1): 9–20.
7. Biviji AA, Paiement GD, Steinbach LS: Musculoskeletal manifestations of human immunodeficiency virus infection. J Am Acad Orthop Surg 2002 Sep–Oct; 10(5): 312–320.
8. Carek PJ, Dickerson LM, Sack JL: Diagnosis and management of osteomyelitis. Am Fam Physician 2001 Jun 15; 63(12): 2413–2420.
9. Chandnani VP, Beltran J, Morris CS, et al.: Acute experimental osteomyelitis and abscesses: detection with MR imaging versus CT. Radiology 1990 Jan; 174(1): 233–236.
10. Das De S, Bose K: Acute pyogenic bone and joint infections. Ann Acad Med Singapore 1987 Apr; 16(2): 252–255.
11. Datz FL: Indium-111-labeled leukocytes for the detection of infection: current status. Semin Nucl Med 1994 Apr; 24(2): 92–109.
12. De Winter F, van de Wiele C, Vogelaers D, et al.: Fluorine-18 fluorodeoxyglucose-position emission tomography: a highly accurate imaging modality for the diagnosis of chronic musculoskeletal infections. J Bone Joint Surg Am 2001 May; 83-A(5): 651–660.
13. De Winter F, Vogelaers D, Gemmel F, Dierckx RA: Promising role of 18-F-fluoro-D-deoxyglucose positron emission tomography in clinical infectious diseases. Eur J Clin Microbiol Infect Dis 2002 Apr; 21(4): 247–257.
14. Demharter J, Bohndorf K, Michl W, Vogt H: Chronic recurrent multifocal osteomyelitis: a radiological and clinical investigation of five cases. Skeletal Radiol 1997 Oct; 26(10): 579–588.
15. Deysine M, Rafkin H, Teicher I, et al.: Diagnosis of chronic and postoperative osteomyelitis with gallium 67 citrate scans. Am J Surg 1975 Jun; 129(6): 632–635.
16. Dirschl DR, Almekinders LC: Osteomyelitis. Common causes and treatment recommendations. Drugs 1993 Jan; 45(1): 29–43.
17. Dirschl DR: Acute pyogenic osteomyelitis in children. Orthop Rev 1994 Apr; 23(4): 305–312.

18. Erdman WA, Tamburro F, Jayson HT, et al.: Osteomyelitis: characteristics and pitfalls of diagnosis with MR imaging. Radiology 1991 Aug; 180(2): 533–539.
19. Firooznia H, Rafii M, Golimbu C, Sokolow J: Computerized tomography of pelvic osteomyelitis in patients with spinal cord injuries. Clin Orthop 1983 Dec; (181): 126–131.
20. Fletcher BD, Scoles PV, Nelson AD: Osteomyelitis in children: detection by magnetic resonance. Work in progress. Radiology 1984 Jan; 150(1): 57–60.
21. Gold R: Radiographic diagnosis of osteomyelitis. Pediatr Infect Dis J 1995 Jun; 14(6): 555.
22. Gold RH, Tong DJ, Crim JR, Seeger LL: Imaging the diabetic foot. Skeletal Radiol 1995 Nov; 24(8): 563–571.
23. Graham GD, Lundy MM, Moreno AJ, Frederick RJ: The role of Tc-99m MDP and Ga-67 citrate in predicting the cure of osteomyelitis. Clin Nucl Med 1983 Aug; 8(8): 344–346.
24. GrossT, Kaim AH, Regazzoni P, Widmer AF: Current concepts in posttraumatic osteomyelitis: A diagnostic challenge with new imaging options. J Trauma. 2002; 52: 1210–1219.
25. Guhlmann A, Brecht-Krauss D, Suger G, et al.: Chronic osteomyelitis: detection with FDG PET and correlation with histopathologic findings. Radiology 1998 Mar; 206(3): 749–754.
26. Harvey J, Cohen MM: Technetium-99-labeled leukocytes in diagnosing diabetic osteomyelitis in the foot. J Foot Ankle Surg 1997 May–Jun; 36(3): 209–214; discussion 256.
27. Isobe Z, Utsugi T, Ohyama Y, et al.: Recurrent pyogenic vertebral osteomyelitis associated with type 2 diabetes mellitus. J Int Med Res 2001 Sep–Oct; 29(5): 445–450.
28. Ivancevic V, Dodig D, Livakovic M, et al.: Comparison of three-phase bone scan, three-phase 99m-Tc-HM-PAO leukocyte scan and 67-gallium scan in chronic bone infection. Prog Clin Biol Res 1990; 355: 189–198.
29. Jacobson AF, Gilles CP, Cerqueira MD: Photopenic defects in marrow-containing skeleton on indium-111 leucocyte scintigraphy: prevalence at sites suspected of osteomyelitis and as an incidental finding. Eur J Nucl Med 1992; 19(10): 858–864.
30. JohnsonJE, Kennedy EJ, Shereff MJ, et al.: Prospective study of bone, indium-111-labeled white blood cell, and gallium-67 scanning for the evaluation of osteomyelitis in the diabetic foot. Foot Ankle Int 1996 Jan; 17(1): 10–16.
31. Jurriaans E, Singh NP, Finlay K, Friedman L: Imaging of chronic recurrent multifocal osteomyelitis. Radiol Clin North Am 2001 Mar; 39(2): 305–327.
32. Kaim AH, Gross T, von Schulthess GK: Imaging of chronic posttraumatic osteomyelitis. Eur Radiol 2002 May; 12(5): 1193–1202.
33. Kak V, Chandrasekar PH: Bone and joint infections in injection drug users. Infect Dis Clin North Am 2002 Sep; 16(3): 681–695.
34. Kang B, Zhu TB, Du JY, et al.: Sonographic diagnosis of acute hematogenous osteomyelitis in the early stage. J Tongji Med Univ 1994; 14(1): 61–64.
35. Kattapuram TM, Treat ME, Kattapuram SV: Magnetic resonance imaging of bone and soft tissue infections. Curr Clin Top Infect Dis 2001; 21: 190–226.
36. Kern EB: Suppurative (bacterial) sinusitis. Postgrad Med 1987 Mar; 81(4): 194–198, 203–210.
37. Kharbanda Y, Dhir RS: Natural course of hematogenous pyogenic osteomyelitis (a retrospective study of 110 cases). J Postgrad Med 1991 Apr; 37(2): 69–75.
38. Larcos G, Antico VF, Cormick W, et al.: How useful is ultrasonography in suspected acute osteomyelitis? J Ultrasound Med 1994 Sep; 13(9): 707–709.
39. Ledermann HP, Kaim A, Bongartz G, Steinbrich W: Pitfalls and limitations of magnetic resonance imaging in chronic posttraumatic osteomyelitis. Eur Radiol 2000; 10(11): 1815–1823.
40. Lichtenstein M, Andrews J, Scales R: Localization of osteomyelitis with 99mtechnetium sulphur colloid. Aust N Z J Surg 1983 Aug; 53(4): 339–342.
41. Lipman BT, Collier BD, Carrera GF, et al.: Detection of osteomyelitis in the neuropathic foot: nuclear medicine, MRI and conventional radiography. Clin Nucl Med 1998 Feb; 23(2): 77–82.
42. Lobo J, McKee M: Musculoskeletal images. Chronic osteomyelitis. Can J Surg 2003 Feb; 46(1): 47–479.
43. Lopes TD, Reinus WR, Wilson AJ: Quantitative analysis of the plain radiographic appearance of Brodie's abscess. Invest Radiol 1997 Jan; 32(1): 51–58.
44. Loredo R, Metter D: Imaging of the diabetic foot. Emphasis on nuclear medicine and magnetic resonance imaging. Clin Podiatr Med Surg 1997 Apr; 14(2): 235–264.
45. Lupi L, Bighi S, Limone GL, et al.: The role of computed tomography in chronic osteomyelitis. Rays 1987 Sep–Dec; 12(3): 27–29.
46. McAfee JG, Samin A: In-111 labeled leukocytes: a review of problems in image interpretation. Radiology 1985 Apr; 155(1): 221–229.
47. Meller J, Koster G, Liersch T, et al.: Chronic bacterial osteomyelitis: prospective comparison of (18)F-FDG imaging with a dual-head coincidence camera and (111)In-labelled autologous leucocyte scintigraphy. Eur J Nucl Med Mol Imaging 2002 Jan; 29(1): 53–60.
48. Morrey BF, Peterson HA: Hematogenous pyogenic osteomyelitis in children. Orthop Clin North Am 1975 Oct; 6(4): 935–951.
49. Oyen WJ, van Horn JR, Claessens RA, et al.: Diagnosis of bone, joint, and joint prosthesis infections with

In-111-labeled nonspecific human immunoglobulin G scintigraphy. Radiology 1992 Jan; 182(1): 195–199.
50. Palestro CJ, Mehta HH, Patel M, et al.: Marrow versus infection in the Charcot joint: indium-111 leukocyte and technetium-99m sulfur colloid scintigraphy. J Nucl Med 1998 Feb; 39(2): 346–350.
51. Palestro CJ: The current role of gallium imaging in infection. Semin Nucl Med 1994 Apr; 24(2): 128–141.
52. Peters AM: The utility of [99mTc]HMPAO-leukocytes for imaging infection. Semin Nucl Med 1994 Apr; 24(2): 110–127.
53. Piazza P, Comoretto M, Lutman M: [Computed tomography in acute inflammation of the orbit]. Radiol Med (Torino) 1994 Mar; 87(3): 235–239.
54. Propst-Proctor SL, Dillingham MF, McDougall IR, Goodwin D: The white blood cell scan in orthopedics. Clin Orthop 1982 Aug; (168): 157–165.
55. Quinn SF, Murray W, Clark RA, Cochran C: MR imaging of chronic osteomyelitis. J Comput Assist Tomogr 1988 Jan–Feb; 12(1): 113–117.
56. Rachinsky I, Agranovich S, Lantsberg S: Imaging of bone to skin sinus tract from osteomyelitis of the femur by Tc-99m HMPAO leukocyte scintigraphy. Clin Nucl Med 2002 Dec; 27(12): 891–892.
57. Riebel TW, Nasir R, Nazarenko O: The value of sonography in the detection of osteomyelitis. Pediatr Radiol 1996; 26(4): 291–297.
58. Robinson CB, Higginbotham-Ford EA: Determination of sequestrum activity by SPECT with CT correlation in chronic osteomyelitis of the head and neck. J Otolaryngol 1986 Oct; 15(5): 279–281.
59. Sartoris DJ: The role of radiology in orthopaedic sepsis. Orthop Rev 1987 Apr; 16(4): 271–286.
60. Sato T, Indo H, Kawabata Y, et al.: Scintigraphic evaluation of chronic osteomyelitis of the mandible in SAPHO syndrome. Dentomaxillofac Radiol 2001 Sep; 30(5): 293–295.
61. Sayle BA, Fawcett HD, Wilkey DJ, et al.: Indium-111 chloride imaging in chronic osteomyelitis. J Nucl Med 1985 Mar; 26(3): 225–229.
62. Schauwecker DS, Park HM, Mock BH, et al.: Evaluation of complicating osteomyelitis with Tc-99m MDP, In-111 granulocytes, and Ga-67 citrate. J Nucl Med 1984 Aug; 25(8): 849–853.
63. Schauwecker DS: Osteomyelitis: diagnosis with In-111-labeled leukocytes. Radiology 1989 Apr; 171(1): 141–146.
64. Seltzer SE: Value of computed tomography in planning medical and surgical treatment of chronic osteomyelitis. J Comput Assist Tomogr 1984 Jun; 8(3): 482–487.
65. Stokkel MP, Takes RP, van Eck-Smit BL, et al.: The value of quantitative gallium-67 single-photon emission tomography in the clinical management of malignant external otitis. Eur J Nucl Med 1997 Nov; 24(11): 1429–1432.
66. Taneja K, Mittal SK, Marya SK, et al.: Acute osteomyelitis: early diagnosis by ultrasonography. Australas Radiol 1992 Feb; 36(1): 77–79.
67. Tehranzadeh J, Wang F, Mesgarzadeh M: Magnetic resonance imaging of osteomyelitis. Crit Rev Diagn Imaging 1992; 33(6): 495–534.
68. Tehranzadeh J, Wong E, Wang F, Sadighpour M: Imaging of osteomyelitis in the mature skeleton. Radiol Clin North Am 2001 Mar; 39(2): 223–250.
69. Tumeh SS, Aliabadi P, Seltzer SE, et al.: Chronic osteomyelitis: the relative roles of scintigrams, plain radiographs, and transmission computed tomography. Clin Nucl Med 1988 Oct; 13(10): 710–715.
70. Tumeh SS, Aliabadi P, Weissman BN, McNeil BJ: Chronic osteomyelitis: bone and gallium scan patterns associated with active disease. Radiology 1986 Mar; 158(3): 685–688.
71. Urso S, Pacciani E, Fariello G, et al.: [Nonspecific osteomyelitis in childhood and adolescence. The contribution of imaging diagnosis]. Radiol Med (Torino) 1995 Sep; 90(3): 212–218.
72. White LM, Schweitzer ME, Deely DM, Gannon F: Study of osteomyelitis: utility of combined histologic and microbiologic evaluation of percutaneous biopsy samples. Radiology 1995 Dec; 197(3): 840–842.
73. Wiest PW, Hartshorne MF: Chronic osteomyelitis: clarification of nuclear medicine findings by fusion scans. Clin Nucl Med 2001 Mar; 26(3): 233–226.
74. Wing VW, Jeffrey RB Jr, Federle MP, et al.: Chronic osteomyelitis examined by CT. Radiology 1985 Jan; 154(1): 171–174.
75. Wolf G, Aigner RM, Schwarz T: Diagnosis of bone infection using 99m Tc-HMPAO labelled leukocytes. Nucl Med Commun 2001 Nov; 22(11): 1201–1206.
76. Wong AL, Sakamoto KM, Johnson EE: Differentiating osteomyelitis from bone infarction in sickle cell disease. Pediatr Emerg Care 2001 Feb; 17(1): 60–63; quiz 64.
77. Yang DC, Ratani RS, Mittal PK, et al.: Radionuclide three-phase whole-body bone imaging. Clin Nucl Med 2002 Jun; 27(6): 419–426.
78. Yuh WT, Corson JD, Baraniewski HM, et al.: Osteomyelitis of the foot in diabetic patients: evaluation with plain film, 99mTc-MDP bone scintigraphy, and MR imaging. Am J Roentgenol 1989 Apr; 152(4): 795–800.
79. Zhuang H, Alavi A: 18-fluorodeoxyglucose positron emission tomographic imaging in the detection and monitoring of infection and inflammation. Semin Nucl Med 2002 Jan; 32(1): 47–59.

80. Zhuang H, Duarte PS, Pourdehand M, et al.: Exclusion of chronic osteomyelitis with F-18 fluorodeoxyglucose positron emission tomographic imaging. Clin Nucl Med 2000 Apr; 25(4): 281–284.

Brodie Abscess

1. Andrew TA, Porter K: Primary subacute epiphyseal osteomyelitis: a report of three cases. J Pediatr Orthop 1985 Mar–Apr; 5(2): 155–157.
2. Blyth MJ, Kincaid R, Craigen MA: The changing epidemiology of acute and subacute haematogenous osteomyelitis in children. J Bone Joint Surg Br 2001 Jan; 83(1): 99–102.
3. Bogoch E, Thompson G, Salter RB: Foci of chronic circumscribed osteomyelitis (Brodie's abscess) that traverse the epiphyseal plate. J Pediatr Orthop 1984 Mar; 4(2): 162–169.
4. Brailsford JF: Brodie's abscess and its differential diagnosis. Br Med J 1938; 2: 119.
5. Brodie BC: An account of some cases of chronic abscess of the tibia. Med Chir Trans 1832; 17: 239.
6. Brodie BC: Pathological and Surgical Observations on the Diseases of the Joints. 4th ed. London: Longman, etc; 1836.
7. Craigen MA, Watters J, Hackett JS: The changing epidemiology of osteomyelitis in children. J Bone Joint Surg Br 1992 Jul; 74(4): 541–545.
8. Dangman BC, Hoffer FA, Rand FF, O'Rourke EJ: Osteomyelitis in children: gadolinium-enhanced MR imaging. Radiology 1992 Mar; 182(3): 743–747.
9. Dormans JP, Drummond DS: Pediatric hematogenous osteomyelitis: new trends in presentation, diagnosis, and treatment. J Am Acad Orthop Surg 1994 Nov; 2(6): 333–341.
10. Ezra E, Khermosh O, Assia A, et al.: Primary subacute osteomyelitis of the axial and appendicular skeleton. J Pediatr Orthop B 1993; 1: 148–152.
11. Ezra E, Wientroub S: Primary subacute haematogenous osteomyelitis of the tarsal bones in children. J Bone Joint Surg Br 1997 Nov; 79(6): 983–986.
12. Gamble JG, Rinsky LA: Kingella kingae infection in healthy children. J Pediatr Orthop 1988 Jul–Aug; 8(4): 445–449.
13. Garre C: Ueber besondere formen und folgenzustaende der akuten infektioesen osteomyelitis. Beitraege zur klinischen Chirurgie (Brun's) 1893; 10: 241.
14. Gledhill RB: Subacute osteomyelitis in children. Clin Orthop 1973 Oct; 96: 57–69.
15. Gonzalez-Lopez JL, Soleto-Martin FJ, Cubillo-Martin A: Subacute osteomyelitis in children. J Pediatr Orthop B 2001 Apr; 10(2): 101–104.
16. Green NE: Osteomyelitis of the epiphysis. In: Uhthoff HK, Wiley JJ, eds. Behavior of the Growth Plate. New York: Raven Press; 1988: 323–329.
17. Green NE, Beauchamp RD, Griffin PP: Primary subacute epiphyseal osteomyelitis. J Bone Joint Surg Am 1981 Jan; 63(1): 107–114.
18. Grey AC, Davies AM, Mangham DC, et al.: The 'penumbra sign' on T1-weighted MR imaging in subacute osteomyelitis: frequency, cause and significance. Clin Radiol 1998 Aug; 53(8): 587–592.
19. Hamdy RC, Lawton L, Carey T, et al.: Subacute hematogenous osteomyelitis: are biopsy and surgery always indicated? J Pediatr Orthop 1996 Mar–Apr; 16(2): 220–223.
20. Harris NH, Kirkaldy-Willis WH: Primary subacute pyogenic osteomyelitis. J Bone Joint Surg Br 1965; 47: 526–532.
21. Hoffman EB, de Beer JD, Keys G, Anderson P: Diaphyseal primary subacute osteomyelitis in children. J Pediatr Orthop 1990 Mar–Apr; 10(2): 250–254.
22. Jones NS, Anderson DJ, Stiles PJ: Osteomyelitis in a general hospital. A five-year study showing an increase in subacute osteomyelitis. J Bone Joint Surg Br 1987 Nov; 69(5): 779–783.
23. Kandel SN, Mankin HJ: Pyogenic abscess of the long bones in children. Clin Orthop 1973 Oct; 96: 108–117.
24. King DM, Mayo KM: Subacute haematogenous osteomyelitis. J Bone Joint Surg Br 1969 Aug; 51(3): 458–463.
25. Kozlowski K: Brodie's abscess in the first decade of life. Report of eleven cases. Pediatr Radiol 1980 Sep; 10(1): 33–37.
26. Letts RM: Subacute osteomyelitis in children. In: Current Concepts of Infections on Orthopaedic Surgery. Berlin/Heidelberg: Springer-Verlag; 1985: 141–149.
27. Letts RM: Subacute osteomyelitis and the growth plate. In: Uhthoff HK, Wiley JJ, eds. Behavior of the Growth Plate. New York: Raven Press; 1988: 331–338.
28. Lindenbaum S, Alexander H: Infections simulating bone tumors. A review of subacute osteomyelitis. Clin Orthop 1984 Apr; (184): 193–203.
29. Lundy DW, Kehl DK: Increasing prevalence of Kingella kingae in osteoarticular infections in young children. J Pediatr Orthop 1998 Mar–Apr; 18(2): 262–267.
30. Mahboubi S: CT appearance of nidus in osteoid osteoma versus sequestration in osteomyelitis. J Comput Assist Tomogr 1986 May–Jun; 10(3): 457–459.
31. Martin RF: Subacute osteomyelitis: is surgical treatment always indicated? In: Morin B, ed. 7th Ste Justine Paediatric Orthopaedic Review Course. Montreal: Becotte A Inc; 1994: 299–304.
32. Miller WB Jr, Murphy WA, Gilula LA: Brodie abscess: reappraisal. Radiology 1979 Jul; 132(1): 15–23.

33. Nixon GW: Hematogenous osteomyelitis of metaphyseal-equivalent location. Am J Roentgenol 1978; 130: 123–129.
34. Rasool MN: Primary subacute haematogenous osteomyelitis in children. J Bone Joint Surg Br 2001 Jan; 83(1): 93–98.
35. Roberts JM, Drummond DS, Breed AL, Chesney J: Subacute hematogenous osteomyelitis in children: a retrospective study. J Pediatr Orthop 1982 Aug; 2(3): 249–254.
36. Robertson DE: Primary acute and subacute localized osteomyelitis and osteochondritis in children. Can J Surg 1967 Oct; 10(4): 408–413.
37. Roddie ME, Peters AM, Osman S etal: Osteomyelitis. Nucl Med Commun 1988; 9: 713–717.
38. Ross ER, Cole WG: Treatment of subacute osteomyelitis in childhood. J Bone Joint Surg Br 1985 May; 67(3): 443–448.
39. Season EH, Miller PR: Multifocal subacute pyogenic osteomyelitis in a child. A case report. Clin Orthop 1976 May; (116): 76–79.
40. Speers DJ, Nade SM: Ultrastructural studies of adherence of *Staphylococcus aureus* in experimental acute hematogenous osteomyelitis. Infect Immun 1985 Aug; 49(2): 443–446.
41. Stephens MM, MacAuley P: Brodie's abscess. A long-term review. Clin Orthop 1988 Sep; (234): 211–216.
42. Trueta J: The three types of acute hematogenous osteomyelitis, a clinical and vascular study. J Bone Joint Surg Br 1959; 41: 671–680.
43. Trueta J, Morgan JD: The vascular contribution to osteogenesis. Studies by the injection method. J Bone Joint Surg Br 1960; 42: 97–109.
44. Turpin S, Lambert R: Role of scintigraphy in musculoskeletal and spinal infections. Radiol Clin North Am 2001 Mar; 39(2): 169–189.
45. Wiles P: Essentials of Orthopaedics. London: J & A Churchill Ltd; 1951.

Chronic Granulomatous Osteomyelitis

1. Cimerman M, Gunde-Cimerman N, Zalar P, Perkovic T. Gemur osteomyelitis due to a mixed fungal infection in a previously healthy man. J Clin Microbiology, 1999 May; 37(5): 1532–1535.
2. Davidson PT, Le HQ: Musculoskeletal tuberculosis. In: Schlossberg D, ed. Tuberculosis and Nontuberculous Mycobacterial Infections. 4th ed. Saint Louis, MO: W B Saunders; 1999; 204–220.
3. Davies AG. The bone changes of Madura foot; observations on Uganda Africans. Radiology. 1958 Jun; 70(6): 841–847.
4. Engin G, Acuna B, Acuna G, Tunaci M. Imaging of extrapulmonary tuberculosis. RadioGraphics. 2000; 20: 471–488.
5. Harisinghani MG, McLoud TC, Shepard JO, Ko JP, Shroff M, Mueller PR. Tuberculosis from head to toe. RadioGraphics. 2000; 20: 449.
6. Martini M, Adjrad A, Boudjemaa A. Tuberculous osteomyelitis. A review of 125 cases. Int Orthop. 1986; 10(3): 201–207.
7. Ridley N, Shaikh MI, Remedios D, Mitchell R: Radiology of skeletal tuberculosis. Orthopedics 1998 Nov; 21(11): 1213–1220.
8. Rubin SA. Tuberculosis and atypical mycobacterial infections in the 1990s. RadioGraphics 1997; 17: 1051.
9. Watts HG, Lifeso RM: Tuberculosis of bones and joints. J Bone Joint Surg Am 1996 Feb; 78: 288–298.
10. Williams RL, Fukui MB, Meltzer CC, Swarnkar A, Johnson DW, Welch W. Fungal spinal osteomyelitis in the immunocompromised patient: MR findings in three cases. AJNR Am J Neuroradiol 1999 March; 20: 381–385.

Sarcoidosis

1. Fernandes SR, Singsen BH, Hoffman GS: Sarcoidosis and systemic vasculitis. Semin Arthritis Rheum. Aug 2000; 30(1): 33–46.
2. Cohen NP, Gosset J, Staron RB, Levine WN: Vertebral sarcoidosis of the spine in a football player. Am J Orthop. Dec 2001; 30(12): 875–877.
3. Sharma OP, Mihailović-Vučinić V: Clinical features and treatment of bone sarcoidosis. CPD Rheumatology 2001; 2(2): 40–46.
4. Waanders F, van Hengel P, Krikke A, Wesseling J, Nieboer P: Sarcoidosis mimicking metastatic disease: a case report and review of the literature. Netherlands J Medicine 2006; 64(9): 342–345.
5. Silver HM, Shirkhoda A, Simon DB: Symptomatic osseous sarcoidosis with findings on bone scan. Chest 1978; 73; 238–241.
6. James DG, Neville E, Carstairs LS: Bone and joint sarcoidosis. Semin Arthritis Rheum 1976; 6(1): 53–81.
7. Neville E, Carstairs LS, James DG: Bone sarcoidosis. Ann N Y Acad Sci 1976; 278: 475–487.
8. Vinnicombe S, Heron C, Wansbrough-Jones M: Dense bones. Br J Radiol 1992; 65(779): 1049–1050.
9. Shaikh S, Soubani AO, Rumore P, Cantos E, Jelveh Z: Lytic osseous destruction in vertebral sarcoidosis. N Y State J Med 1992; 92: 213–214.
10. Cutler SS, Sankaranarayan G: Vertebral sarcoidosis. JAMA 1978; 240: 557–558.

11. Rua-Figueroa, Gantes MA, Erausquin C, Mhaidli H, Montesdeoca A: Vertebral sarcoidosis: clinical and imaging findings. Semin Arthritis Rheum 2002; 31(5): 346–352.
12. Aberg C, Ponzo F, Raphael B, Amorosi E, Moran V, Kramer E: FDG positron emission tomography of bone involvement in sarcoidosis. Am J Roentgenol 2004; 182(4): 975–977.
13. ATS/ERS/WASOG Committee: Statement on Sarcoidosis. Am J Respir Crit Care Med 1999; 160: 736–755.

Paget's Disease

1. Adami S, et al.: Effects of two oral doses of alendronate in the treatment of Paget's disease of bone. Bone 1994; 15: 415–417.
2. Alvarez L, et al.: Discriminate value of biochemical markers of bone turnover in assessing the activity of Paget's disease. J Bone Miner Res 1995; 10: 458–465.
3. Frame B, Marel GM: Paget disease: a review of current knowledge. Radiology 1981; 141: 21–24.
4. Gabel GT, Rand JA, Sim FH: Total knee arthroplasty for osteoarthrosis in patients who have Paget's disease of bone at the knee. J Bone Joint Surg 1991; 73–A: 739–744.
5. Hadjipavlou A, Lander P: Paget's disease of the spine. J Bone Joint Surg 1991; 73–A: 1376–1381.
6. Hoyland JA, Freemont AJ, Sharpe PT: Interleukin-6, IL-6 receptor, and IL-6 nuclear factor gene expression in Paget disease. J Bone Miner Res 1994; 9: 75–80.
7. Kaplan FS, Singer FR: Paget's disease of bone: pathophysiology, diagnosis and management. J Am Acad Ortho Surg. 1995; 3: 336–344.
8. Ludkowski P, Wilson-MacDonald J: Total arthroplasty in Paget's disease of the hip. Clin Ortho Rel Res 1990; 255: 160–167.
9. Lyles KW, et al.: Functional and mobility impairments associated with Paget's disease of bone. J Am Geriatrics Soc 1995; 43: 502–506.
10. Mills BG, et al.: Multinucleated cells formed in vitro from Paget's bone marrow express viral antigens. Bone 1994; 15: 443–448.
11. Morales-Piga AA, et al.: Frequency and characteristics of familial aggregation of Paget's disease of bone. J Bone Miner Res. 1995; 10: 663–670.
12. Murphy WA, Whyte MP, Haddad Jr. JG: Healing of lytic Paget bone disease with diphosphonate therapy. Radiology 1980; 134: 635–637.
13. Paget J: On a form of chronic inflammation of bones. Med Chir Trans 1877; 60: 37–63.
14. Reddy SV, et al.: Detection of measles virus nucleocapsid transcripts in circulating blood cells from patients with Paget's disease. J Bone Miner Res 1996; 11: 1602–1607.
15. Resnick D: Paget's disease of bone: current status and a look back to 1943 and earlier. Am J Roentgenol 1988; 150: 249–256
16. Roberts MC, Kressel HY, Fallon MD, Zlatkin MB, Dalinka MK: Paget disease: MR imaging findings. Radiology 1989; 173: 341–345.
17. Roodman GD: Paget's disease and osteoclast biology. Bone 1996; 19: 209–212.
18. Seret P, et al.: Sarcomatous degeneration in Paget's bone disease. J Cancer Res Clin Oncol 1987; 113: 392–399.
19. The Paget Foundation, 200 Varick Street, Suite 1004, New York, NY 10014-4810; 212–229–1582; (fax) 212–229–1502.
20. Wallace K, et al.: Skeletal response to immobilization in Paget's disease of bone. Clin Ortho Rel Res 1996; 328: 236–240.

Myositis and Fasciitis

1. Becker M, Zbaren P, Hermans R, Becker CD, Marchal F, Kurt AM, Marre S, Rufenacht DA, Terrier F: Necrotizing fasciitis of the head and neck: role of CT in diagnosis and management. Radiology 1997; 202: 471–476.
2. Cumming MJ, Levi CS, Ackerman TE: US case of the day. Fournier gangrene. RadioGraphics 1994; 14: 1423–1424.
3. Fan CM, Whitman GJ, Chew FS: Radiologic-Pathologic Conferences of the Massachusetts General Hospital. Necrotizing fasciitis of the scrotum (Fournier's gangrene) [clinical conference]. Am J Roentgenol 1996; 166: 1164.
4. Fleckenstein JL, Burns DK, Murphy FK, Jayson HT, Bonte FJ: Differential diagnosis of bacterial myositis in AIDS: evaluation with MR imaging. Radiology 1991; 179: 653–658.
5. Fugitt JB, Puckett ML, Quigley MM, Kerr SA: Necrotizing fasciitis. RadioGraphics 2004; 24: 1472–1476.
6. Grayson DE, Abbott RM, Levy AD, Sherman PM: Emphysematous infections of the abdomen and pelvis: a pictorial review. RadioGraphics 2002; 22: 543–561.
7. Hernandez RH, Keim DR, Chenevert TL, Sullivan DB, Aisen AM: Fat-suppressed MR imaging of myositis. Radiology 1992; 182: 217–219.
8. Loh NN, Ch'en IY, Cheung LP, Li KC: Deep fascial hyperintensity in soft-tissue abnormalities as revealed by T2-weighted MR imaging. Am J Roentgenol 1997; 168: 1301–1304.
9. May DA, Disler DG, Jones EA, Balkissoon AA, MAnaster BJ: Abnormal signal intensity in skeletal muscle at

MR imaging: patterns, pearls, and pitfalls. RadioGraphics 2000; 20: 295S–315S.
10. Rajan DK, Scharer KA: Radiology of Fournier's gangrene. Am J Roentgenol 1998; 170: 163–168.
11. Restrepo CS, Lemos DF, Gordillo H, Odero R, Varghese T, Tiemann W, Rivas FF, Moncada R, Gimenez CR. Imaging findings in musculoskeletal complications of AIDS. RadioGraphics 2004; 24: 1029–1049.
12. Schmid MR, Kossmann T, Duewell S: Differentiation of necrotizing fasciitis and cellulitis using MR imaging. Am J Roentgenol 1998; 170: 615–620.
13. Steinbach LS, Tehranzadeh J, Fleckenstein JL, Vanarthos WJ, Pais MJ: Human immunodeficiency virus infection: musculoskeletal manifestations. Radiology 1993; 186: 833–838.
14. Wysoki MG, Santora TA, Shah RM, Friedman AC: Necrotizing fasciitis: CT characteristics. Radiology 1997; 203: 859–863.

Leprosy

1. Andreisek G, Crook DW, Burg D, Marincek B, Weishaupt D. Peripheral neuropathies of the median, radial, and ulnar nerves: MR imaging features. RadioGraphics 2006; 26: 1267–1287.
2. Enna CD, Jacobson RR, Rausch RO: Bone changes in leprosy: a correlation of clinical and radiographic features. Radiology 1971; 100: 295–306.
3. Jones EA, Manaster BJ, May DA, Disler DG: Neuropathic osteoarthropathy: diagnostic dilemmas and differential diagnosis. RadioGraphics 2000; 20: 279S–293S.
4. Newman H, Casey B, Du Bois JJ, Gallagher T: Roentgen features of leprosy in children. Am J Roentgenol 1972; 114: 402–410.
5. Ward RJ, Zawodniak LJ, Blake MA, Eustace SJ: Musculoskeletal case of the day. Tuberculoid leprosy. Am J Roentgenol 1999; 173: 798.

Parsonage–Turner Syndrome

1. Gaskin CM, Helms CA: Parsonage–Turner syndrome: MR imaging findings and clinical information of 27 patients. Radiology 2006; 240: 501–507.
2. HelmsCA, Martinez S, Speer KP: Acute brachial neuritis (Parsonage–Turner syndrome): MR imaging appearance–report of three cases. Radiology 1998; 207: 255–259.

Chapter 11

Systematic Approach to Arthropathies

William R. Reinus

Abstract Arthritis is, by definition, a disease confined to the joints. Many arthropathies result from systemic diseases. The goal of this chapter is to provide a systematic approach to the analysis and classification of arthritis. Arthropathies can be divided into four basic categories: productive, destructive, both productive and destructive, and those that only affect the ligaments surrounding joints. The major and common entities causing each of these types of arthritis is discussed from the point of view of pathophysiology and diagnosis. Appropriate imaging modalities are reviewed.

Keywords Arthritis • Septic arthritis • Rheumatoid arthritis • Psoriatic arthritis • Reactive arthritis • Reiter syndrome • Ankylosing spondylitis • Spondyloarthropathy of inflammatory bowel disease • Multicentric reticulohistiocytosis • Dermatolipoid arthritis • Amyloid arthropathy • Osteoarthritis • Acromegaly • Hemochromatosis • Calcium pyrophosphate dehydrate deposition disease • Juvenile rheumatoid arthritis • Juvenile chronic arthritis • Hemophilia • Ochronosis • Alkaptonuria • Wilson disease • Gout • Neuropathic arthritis • SAPHO syndrome • Pigmented villonodular synovitis • Erosive osteoarthritis • Still disease • Systemic lupus erythematosus • Jaccoud arthropathy • Haglund disease • Scleroderma • Osteochondromatosis • Chondromalacia patella

Introduction

The number of pathologic processes that affect joints, their hyaline cartilage and fibrocartilage, their synovium or the synovium of tendon sheaths is extensive. All arthritides, however, share certain features in common. They are by definition joint centered. As such they are expected to cause some narrowing of the affected joint space(s) and changes in the bones surrounding the joint space in more or less equal proportions. If only the bone on one side of a joint is affected, then the disease in question is unlikely to be arthritis. A typical example of such a case is avascular necrosis (AVN) adjacent to a joint – for example, in the femoral head (see Chapter 4).

There are three basic types of joints in the human body. The most common of these are synovial joints – joints with a synovial lining deep to the joint capsule and hyaline cartilage covering the apposing ends of the bones (Fig. 11.1). These joints permit free movement within a defined range. They permit uninhibited motion while at the same time having the ability to transfer loads comfortably across the joint space. All synovial joints arise from the same model that is combined into different forms to permit the required motion (*vide infra*).

The second most common type of joint is the synchondroidal joint. These joints have no synovium or hyaline cartilage, but instead join two bones together via a fibrocartilage disk. This type of joint permits only minimal motion and can be thought of as the expansion joints of the body, very similar to those built into bridges and other architectural structures to accommodate the need for expansion and contraction under varying environmental conditions. Typical examples of synchondroidal joints include the intervertebral disks and the symphysis pubis.

The least common type of joint is the pseudo-synovial joint. Here, two bones articulate without a true joint capsule but have only a bursa between the apposed ends of the bones. The atlantoaxial joint is typical of this type of joint. The odontoid articulates with anterior arch of C1, the first cervical segment with a bursa interposed between the two. A second bursa is also interposed posteriorly between the transverse ligament of C1, which holds the odontoid in place, and the odontoid itself. As can be surmised from the name, this type of joint functions very much the same way that true synovial joints function. That is it permits free motion in a defined plane. Further, these joints may have ligamentous supporting structures similar to true synovial joints. They are not, however, derived from the universal model from which all true

W.R. Reinus (✉)
Musculoskeletal Radiology Temple University, Temple University School of Medicine, Philadelphia, PA, USA
e-mail: reinusw@tuhs.temple.edu

A. Bonakdarpour et al. (eds.), *Diagnostic Imaging of Musculoskeletal Diseases: A Systematic Approach*,
DOI 10.1007/978-1-59745-355-4_11,

synovial joints are derived. For all intents and purposes, these joints function as and are affected by pathological processes in a similar manner to true synovial joints.

As mentioned, synovial joints take their form from a particularly simple model and vary according to depth and combination with other simple joints to form the necessary shape to meet the functional demands of the body at that location. The metacarpophalangeal joints with their mildly convex metacarpal heads and concave proximal ends of the proximal phalanges may be thought of as the simplest synovial joint. As needs require, the depth of the concavity of the joint and size of the convexity of the joint may adapt to different functions. Consider the hip joint with its large ball-like femoral head and deeply concave acetabulum. Alternatively, the joints may simply enlarge in surface area as in the case of the shoulder joint with its large mildly concave glenoid fossa and the convex portion of the joint that has shifted from the end over to the medial side of the proximal end of the humerus.

Joints may combine in form to accomplish more complicated types of motion. The elbow joint is a good example of such a combination, combining a shallow dish-like articulation between the humerus and radius with a deep hinge-like articulation between the humerus and ulna, to allow pronation and supination, and flexion and extension at the same articulation. Finally, the same simple joint model may adsorb to bone surfaces ultimately defining the shape of the bones and allowing for complex motions as occurs in the wrist.

In all synovial joints, the basic biomechanical function of the hyaline cartilage is twofold. Hyaline cartilage is a combination of mucopolysaccharide intermixed with hyaluronic acid cartilage fibrils. This creates a sponge-like substance that when compressed exudes a highly viscous and slippery material. The hyaline cartilage's first and major function is to secrete and store this mucopolysaccharide material which functions to reduce shear forces on the apposing bones, with or without a load, and permits the joint to move easily. The second function of the hyaline cartilage sponge is to absorb a small portion of the acute changes in the forces across the joint and maintain pressure homeostasis. The major fraction of this shock absorber function falls to the trabecular bone as it forms an architectural truss specific to the orientation of the stresses across the joint. The biomechanical characteristics of trabecular bone are considered further in the chapter on trauma (Chapter 5).

Diseases that cause arthritis tend to affect joints in four main ways. The first relates to chondrocyte death, leading to loss of hyaline cartilage. In the second, abnormal biomechanics leads to abnormal wear of the apposing hyaline cartilage. In the third, deposition of foreign materials within the substance of the hyaline cartilage structure weakens the structure and leads to its loss. The final mechanism is one of inflammatory destruction of the hyaline cartilage and underlying bone as the result of synovitis and release of inflammatory cells and cytokines into the joint space. The first three mechanisms give rise to a form of osteoarthritis, while the last leads to inflammatory arthritis. In synchondroidal joints, degeneration of the fibrocartilage leads to loss of the normal function during biomechanical stresses.

In all types of osteoarthroses, the first step in developing arthritis is loss of the articular cartilage covering of the apposing bones. Once this occurs, the bones begin to rub against one another, instead of gliding along the mucopolysaccharide layer created by the hyaline cartilage. This rubbing with increased friction leads to reactive new bone formation in the subchondral plate. The new bone is visible both pathologically and on radiographs as reactive subchondral bone formation. The loss of hyaline cartilage leads to a decrease in the sponge-like action of the hyaline cartilage and creates abnormal stresses across the joint. These stresses ultimately lead to new bone formation around the joint in an attempt to increase the joint's surface area and return the forces across the joint to their former levels. This new bone is a form of osteophyte and occurs along the margins of the joints. Abnormal stresses on the internal structures of the joints related to ligamentous laxity or abnormal biomechanics may also cause osteophytes in regions of capsular and ligamentous insertions, so-called traction osteophytes. Thus, the *sine qua non* for the diagnosis of osteoarthritis – whether primary or secondary – is the trio of joint space narrowing, subchondral sclerosis, and osteophyte formation about a joint.

Inflammatory processes generally cause irregular destruction of the tissues within the joint, leading to erosions in the hyaline cartilage and cortical surfaces. Depending on the severity and duration of the process, the joint may be destroyed, ankylose, or ultimately go on to develop osteoarthritis related to its underlying loss of articular cartilage. These processes tend to affect not only the synovium of joints but also other synovial-lined structures. Thus, it is quite common to see bursae and tendon sheaths develop inflammatory changes associated with the underlying pathology. The archetypal inflammatory arthropathies are septic arthritis and rheumatoid arthritis.

From a radiological point of view, then, there are two main types of arthritis: those that are productive, the osteoarthroses, and those that are destructive, the inflammatory arthropathies. Some arthropathies, either simultaneously or sequentially, induce both destructive and productive changes. This leads to a radiographic class of arthropathies that appear both productive and destructive. Since inflammatory arthropathies affect tendons and bursae, not only can they cause alignment abnormalities at the joints, but in a few diseases tendon inflammation may be the predominant pathology. This creates a final small radiographic class of "arthropathies," where the joints become misaligned but otherwise are normal radiographically.

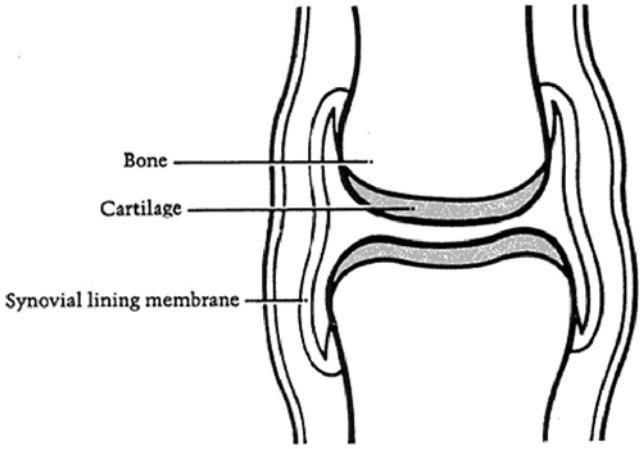

Fig. 11.1 Schematic of typical synovial joint. Hyaline cartilage demarcated in gray. Note the bare areas in the margins of the joint where hyaline cartilage does not cover

Image Analysis

The classic analysis of the imaging features of arthropathies involves careful evaluation of several radiographic findings. These include the **S**oft tissues surrounding the joint, the **A**lignment of the joint, the **B**ones, the **C**artilage spaces, and the **D**istribution of involvement. To this list, we may also add **E**xtraordinary findings. These points of analysis create the pneumonic **SABCDE** for analysis of arthritis Taken as a whole, the radiographic findings in the soft tissues, bones, cartilage spaces, and alignment abnormalities determine the radiographic class of arthritis: destructive, productive, both, or neither. The distribution of involved joints and the extraordinary findings are most useful to narrow the diagnosis within the designated class.

Soft Tissue

The soft tissues may show three different findings: swelling, masses, and wasting related to chronic inflammation or disuse. Typically active arthropathies will have an accompanying joint effusion that may show as capsular swelling about affected smaller joints (Fig. 11.2) or effusions in large joints. Aggressive inflammatory arthropathies such as some forms of psoriasis cause diffuse swelling about affected digits, also called sausage digits (Fig. 11.3)

Destructive arthropathies in their advanced stages may lead to a severely incapacitating deformity known as arthritis mutilans (Fig. 11.4). This deformity, also known as *main en lorgnette* or Marie–Léri syndrome, shows a peculiar clinical feature of extreme mobility of the joints so that the digits may be extended and shortened like a telescope. Arthritis mutilans is most commonly a product of rheumatoid arthritis, psoriatic arthritis, Reiter syndrome, multicentric reticulohistiocytosis (MRH), and juvenile chronic arthritis. It may also be seen in extremely rare disorders such as congenital insensitivity to pain and Thevenard syndrome (congenital sensory and autonomic neuropathy with acroulceration).

Three arthritides cause focal masses – either near the affected joint(s) or in remote locations. Gout is the most common of these and here tophaceous masses are often located adjacent to joints (Fig. 11.5) but may also occur remotely in

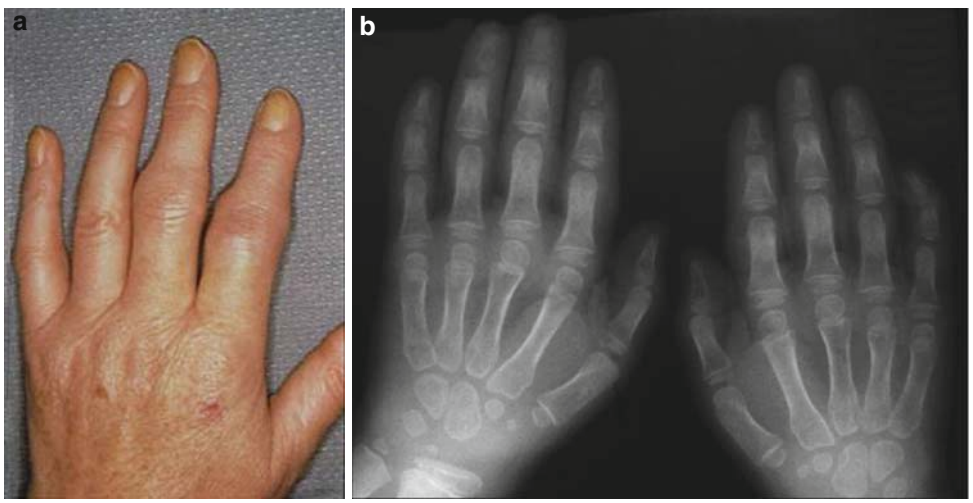

Fig. 11.2 Capsular swelling (**a**) is prominent about the second and third proximal interphalangeal joints of this adult hand. Similar changes are noted around the second and third metacarpophalangeal joints and the third proximal interphalangeal joint of the radiograph of the juvenile hand in (**b**)

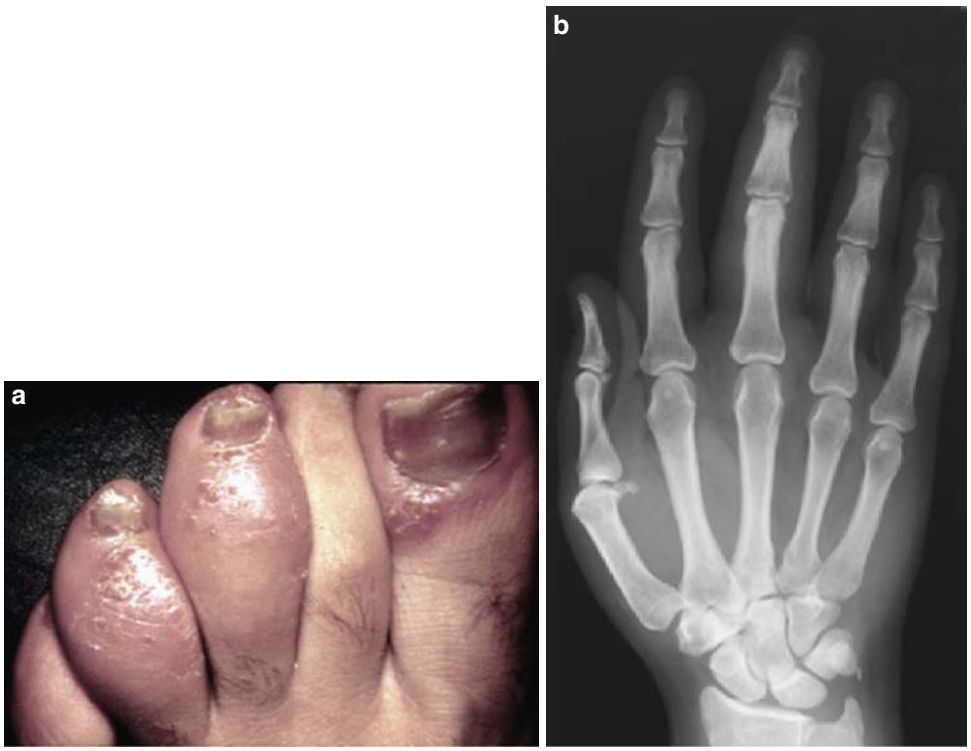

Fig. 11.3 (**a**) Sausage digits of the toes in psoriasis. (**b**) PA radiograph of the hand showing sausage third digit

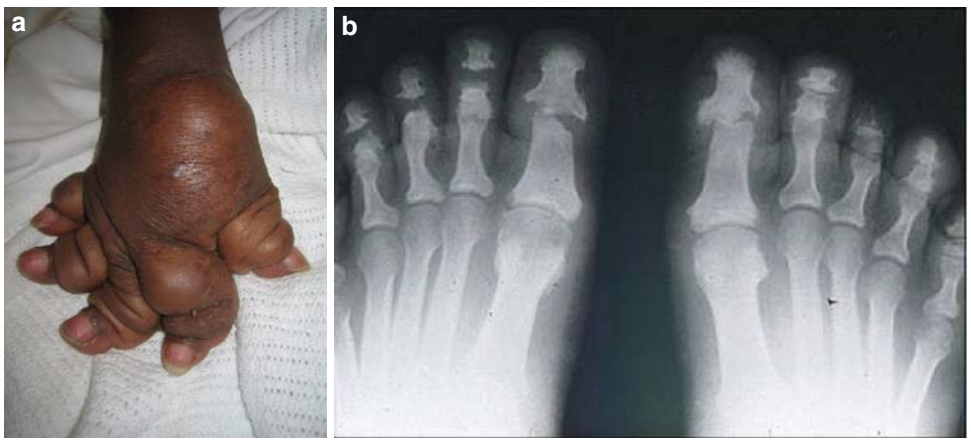

Fig. 11.4 Arthritis mutilans in hand (**a**) and radiograph of a foot (**b**). Note the severe destruction of the bones, particularly the second to fourth distal interphalangeal joints related to the aggressive inflammatory arthropathy

tendons or even within bones, the latter causing lytic lesions on plain radiographs. These masses, because of their high urate content, may be slightly dense compared with the surrounding soft tissues. The other two diseases rheumatoid arthritis and MRH also cause localized masses or nodules. Masses resulting from the rheumatoid arthritis most commonly arise on extensor surfaces and at biopsy show inflammatory granulomas (Fig. 11.6). Masses related to MRH may be numerous, often contain xanthomatous material and occur on the face, particularly around the eyes, and extremities (Fig. 11.7).

Systemic lupus erythematosis (SLE) and Jaccoud arthropathy are the most common arthropathies to cause soft tissue atrophy, particularly along the thenar and hypothenar eminences of the hand. This atrophy creates a subtle yet characteristic appearance of loss of the convexity of the margins of these eminences on posteroanterior (PA) radiographs of the hands (Fig. 11.8).

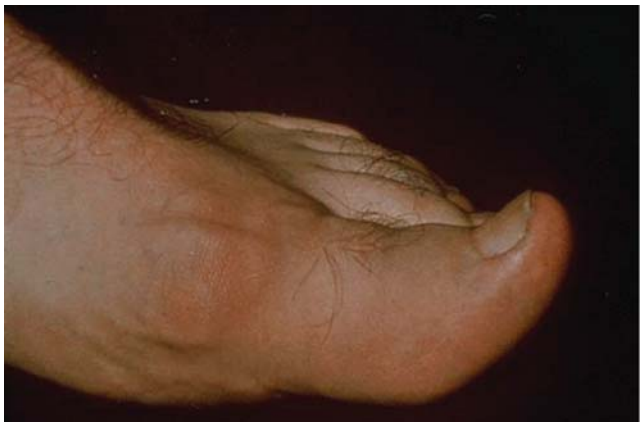

Fig. 11.5 Inflamed mass adjacent to the first metatarsophalangeal joint in a man with gout

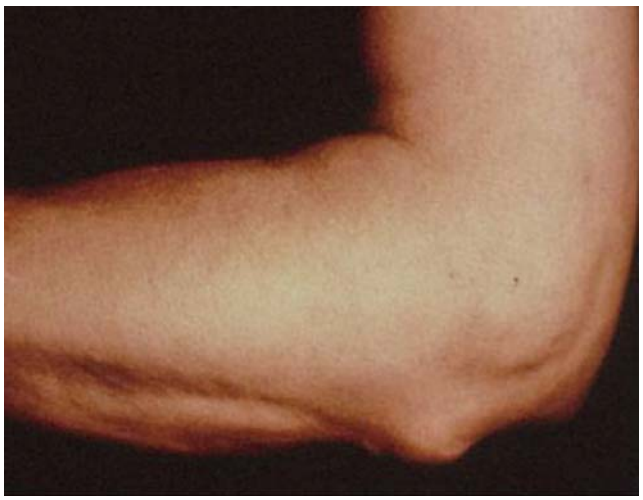

Fig. 11.6 Rheumatoid nodule along the extensor surface of a forearm

Alignment

Many inflammatory arthropathies may cause laxity of the ligaments and tendons around a joint so that several alignment deformities may arise, including individual joint subluxations and dislocations. In addition, abnormal tendonous pull may cause ulnar deviation or drift of the digits. Abnormalities of the extensor mechanisms of the digits may lead to swan neck and boutonnière deformities. In typical ulnar drift, the metacarpophalangeal joints of the hands sublux medially toward the ulna giving a swept appearance to the digits (Fig. 11.8b). This abnormality is most common in long-standing rheumatoid arthritis but occurs in other inflammatory polyarthropathies as well.

Swan neck and boutonnière deformities arise from an imbalance of the forces on the proximal (PIP) and distal (DIP) interphalangeal joints of the digits related to synovial proliferation and inflammation. In the case of a swan neck deformity, the lateral bands of extensor mechanism ultimately subluxate laterally, whether from inflammatory shortening of these bands or rupture of the superficial flexor digitorum tendon. These changes lead to hyperextension at the PIP joint and hyperflexion at the DIP joint (Fig. 11.9).

The opposite occurs in a boutonnière deformity – hyperflexion at the PIP joint and hyperextension at the DIP joint (Fig. 11.10). In this deformity, synovial proliferation in the PIP joint causes inflammatory weakening of the extensor mechanism resulting in flexion at the PIP. Subsequently, as with swan neck deformities, the lateral bands subluxate volarly. The oblique retinacular ligaments shorten resulting in hyperextension of the DIP joint. Swan neck deformities are much more incapacitating than boutonnière deformities as the flexed DIP joints impede the patient's manual dexterity.

Bones

Depending upon the arthropathy, the bones may become osteopenic, sclerotic, or may develop periosteal reaction. Periarticular osteopenia is particularly common in early rheumatoid arthritis and results from the increased blood flow about the joint and within the ends of the bones related to the synovial inflammation. The increased blood flow within and around the bone ends will lead to resorption and ultimately osteoporosis. This manifests itself as periarticular osteopenia on radiographs (Fig. 11.11).

As arthropathies progress, not only inflammatory arthropathies but also productive arthropathies, patients become progressively incapacitated. To avoid pain or simply because of an inability to use an extremity effectively, patients develop diffuse disuse osteoporosis. This finding is usually reflected as diffuse osteopenia on radiographs. Thus, it is common to see patients with long-standing RA and OA with diffuse osteopenia on their radiographs.

On the other hand, patients with psoriatic arthritis and a few other less common arthropathies may develop bone sclerosis in the some phalanges early in the course of their disease. This gives an appearance known as an ivory phalanx (Fig. 11.12). Sclerosis may also occur in other bones such as the sternum associated with sternoclavicular joint inflammation. The exact cause of this sclerosis is obscure but potentially it is related to disease-specific cytokines that promote osteoblastic activity. In RA, older patients have a tendency to develop sclerosis of their distal phalanges and tufts. This may simply be a relative phenomenon related to the osteoporosis

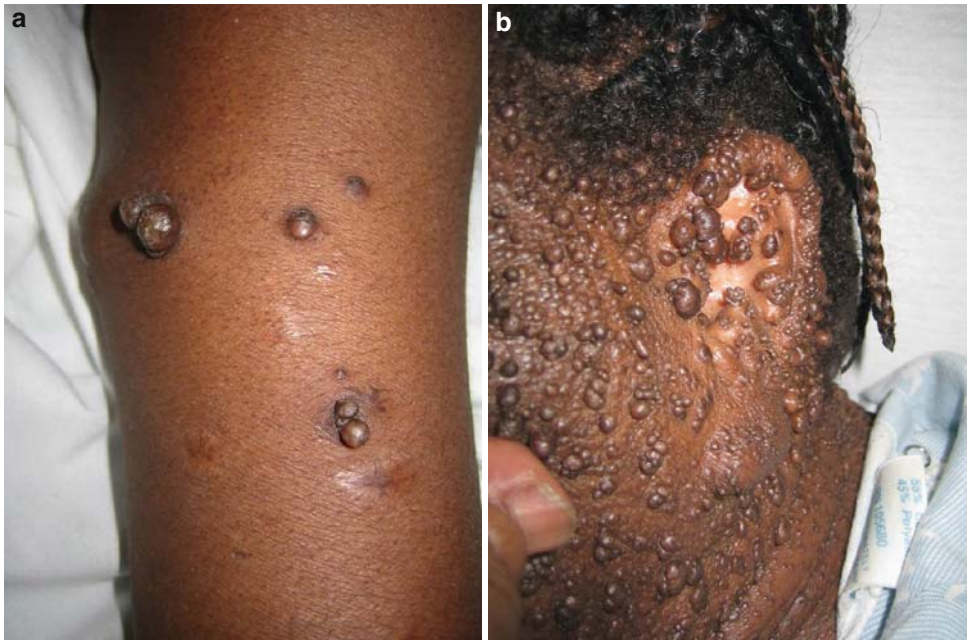

Fig. 11.7 Skin lesions on the forearm (**a**) and face (**b**) of a patient with multicentric reticulohistiocytosis

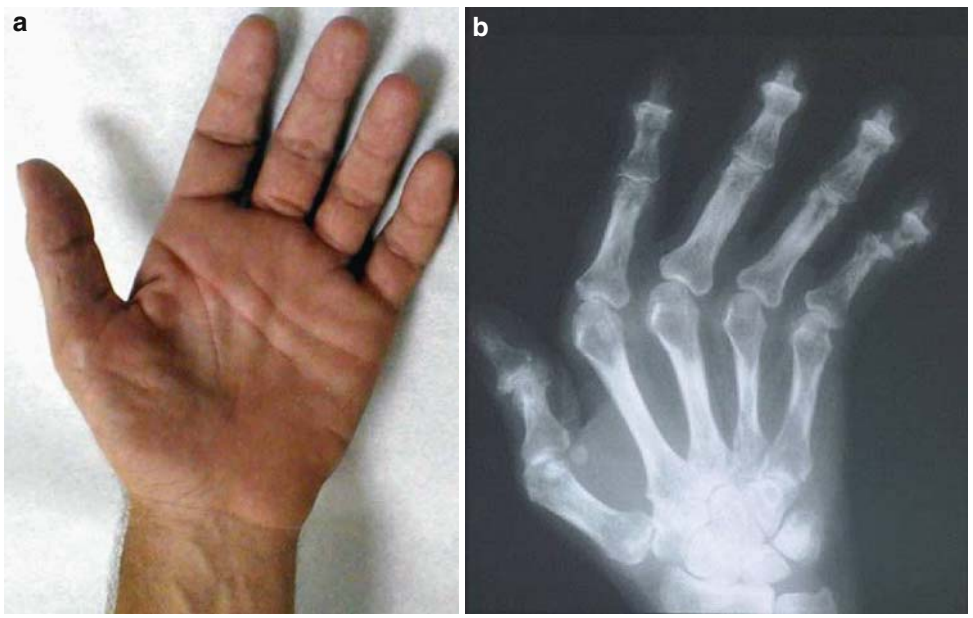

Fig. 11.8 Photograph of the hand of a patient (**a**) and posteroanterior radiograph of the hand (**b**) of another patient with SLE. Note in (**a**) atrophy of both hypothenar eminences and the left thenar eminence is striking in comparison with the normal right thenar eminence. In (**b**) note loss of convexity of the margins of the thenar and hypothenar eminences as well as the ulnar deviation of the metacarpophalangeal joints

of the remainder of the skeleton, but it may be quite striking radiographically.

Periosteal reaction may also occur along the diaphysis of bones, affected by inflammatory arthropathies, particularly psoriatic arthritis and Reiter disease (Fig. 11.13). In addition, many inflammatory arthropathies cause inflammation in tendon insertions and aponeuroses. This may cause postinflammatory new bone formation around these insertions resulting in radiographically apparent enthesopathy. This last finding also occurs commonly as a senile process in older patients and as such is nonspecific.

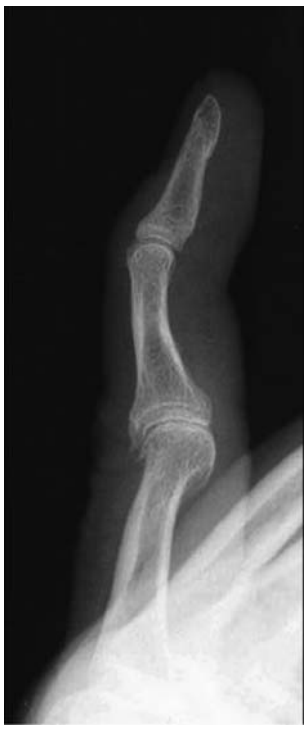

Fig. 11.9 Swan neck deformity showing hyperextension at the PIP and hyperflexion at the DIP

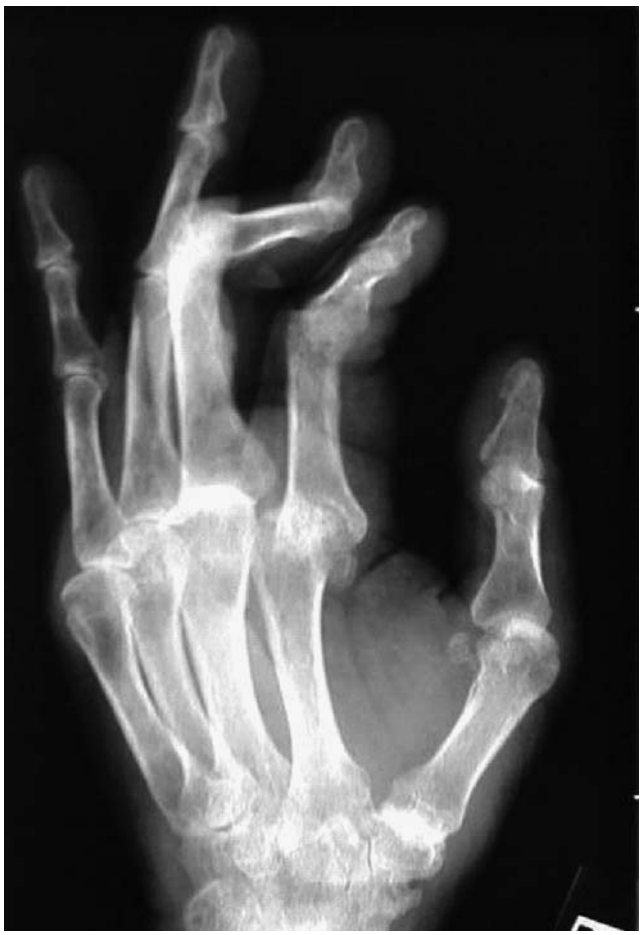

Fig. 11.10 Boutonnière deformity showing hyperflexion at the PIP and hyperextension at the DIP

Cartilage Spaces

In the end, all arthropathies will cause joint space narrowing. The pathophysiology of the narrowing relates to the underlying pathology of the particular disease. Some diseases, e.g., RA, cause initial marginal erosive disease early on (Fig. 11.18 and 11.19) while others show uniform erosive changes, e.g., erosive osteoarthritis (Fig. 11.21). Some cause joint space narrowing early and progressively, e.g., osteoarthritis, while others show relative preservation of the joint space until later in the disease, e.g., multicentric reticulohistiocytosis (Fig. 11.16). Further, different arthropathies typically affect different portions of the joint, e.g., weight-bearing surfaces (Fig. 11.17) versus the entire articular surface (Figs. 11.14 and 11.15) or early changes in the periarticular region of the joint as in RA (Fig. 11.18). These differences lead to different patterns of narrowing in different joints. Finally, the ability to visualize articular cartilage directly with MRI further aids the analysis of the joint space. Ultimately, the information gleaned from the analysis of the cartilage space in terms of the pattern and progression of joint space loss is very useful in making a diagnosis.

Inflammatory arthropathies tend to be destructive and as such show erosions along the joint margins within the cartilage space. Depending upon the underlying condition, the types of erosions and the severity with which they affect the joint vary in appearance and provide another clue to diagnosis. For example, RA because of its relapsing and remitting nature typically will cause marginal erosions of joints of different ages that also vary in their progression toward the central portion of the joint (Fig. 11.19). Psoriatic arthritis in its more aggressive forms is more likely to result in pencil-in-cup deformity of the joint than RA (Fig. 11.20). Erosive osteoarthritis tends to show gull-wing shaped erosions all the way across the joint at once since the hyaline cartilage is generally completely lost early on in the disease as a result of its osteoarthritic component (Figs. 11.21).

Some erosions may have a smoother appearance related to frequent periods of remission with periods of new bone formation and healing, e.g., RA (Fig. 11.22). Other diseases may give rise to irregular erosions, presumably related to a course that is more relentless and unremitting, e.g., psoriatic arthritis (Fig. 11.23).

Some arthropathies show erosions first in the bare areas of the joint where there is no hyaline cartilage. Early on in the disease, this gives rise to periarticular erosions because the erosions arise at the edges of the joint space (Figs. 11.18 and 11.19). Other arthropathies may show paraarticular as

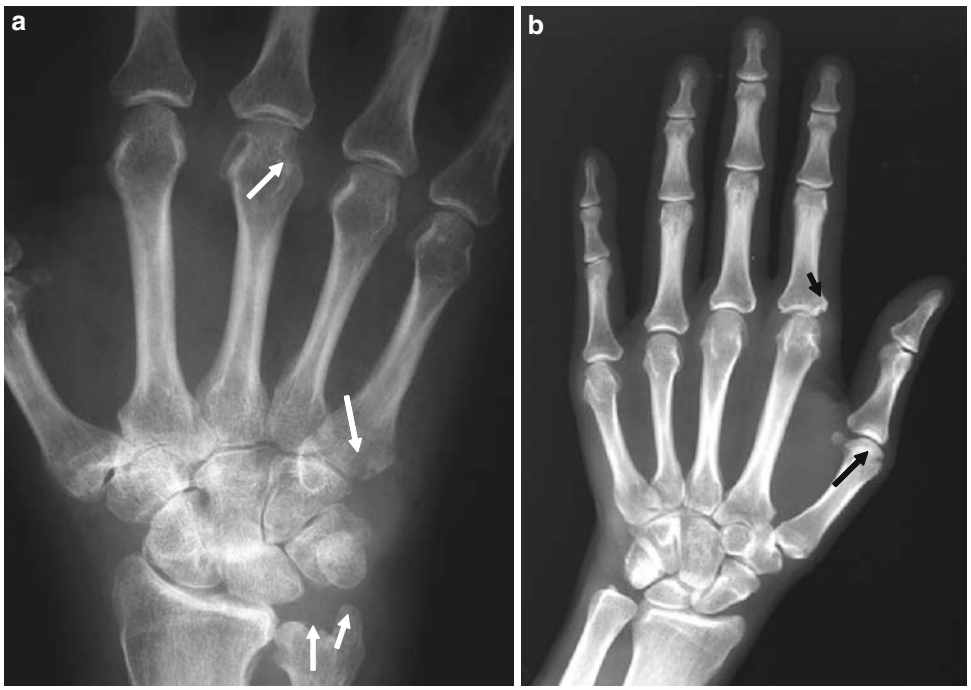

Fig. 11.11 PA radiographs of the right hand (**a**) and the left hand (**b**) in another patient showing periarticular osteopenia involving the bone surrounding metacarpophalangeal joints. Note the erosive changes in multiple joints (*arrows*)

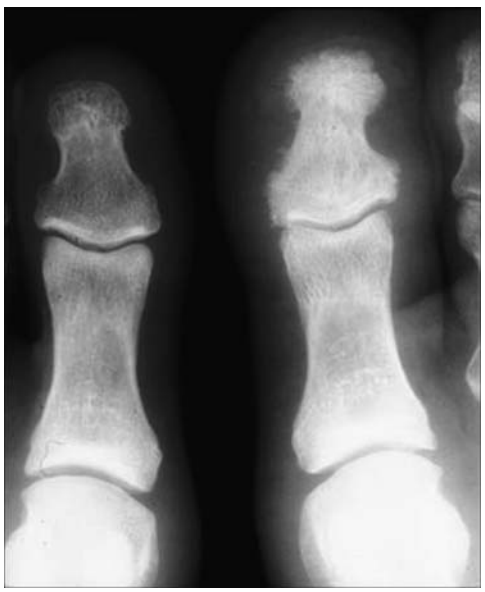

Fig. 11.12 Ivory phalanx in psoriatic arthritis

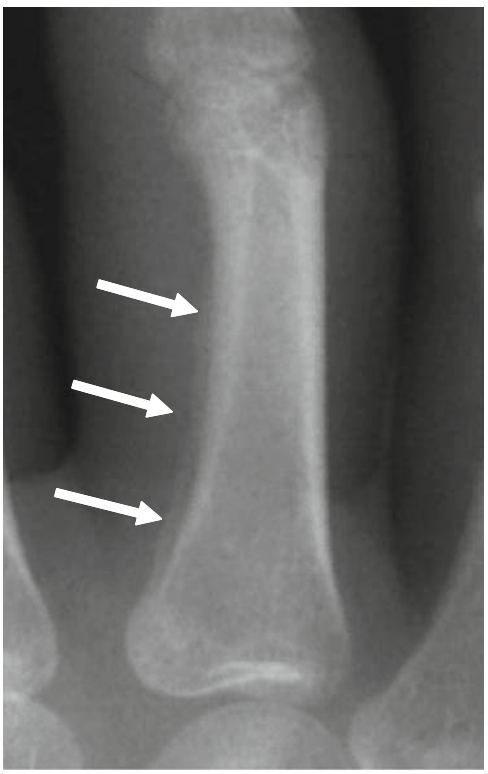

Fig. 11.13 Periosteal reaction in psoriatic arthritis (*arrows*)

well as articular erosions, e.g., gout. In this disease, erosions may start juxtarticularly in the region of endarterial flow in the metaphysis and give rise to a peculiar clasp-like erosion with overhanging edges (Fig. 11.24), so-called Granger overhanging edges. Whether these erosions actually arise from initial deposition of urate crystals within the metaphysis or adjacent to the bone is debatable. According to the former theory, the urate deposition within the slow flow area gives rise to an intraosseous tophus that slowly and concentrically

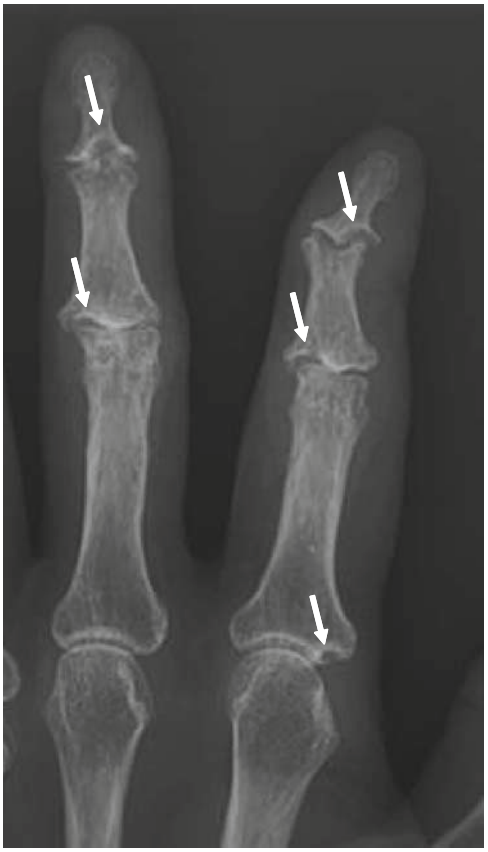

Fig. 11.14 Regular, smooth-bottomed erosions in a patient with rheumatoid arthritis (*arrows*)

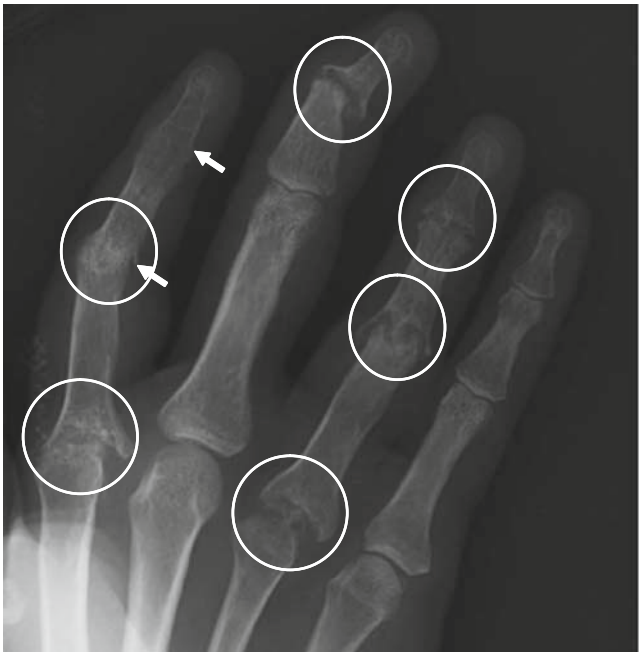

Fig. 11.15 Irregular and large erosions in a patient with psoriatic arthritis (*circles*). Note the fusion of the second DIP and the near fusion of the second PIP (*arrows*). This latter finding is common in psoriatic arthritis

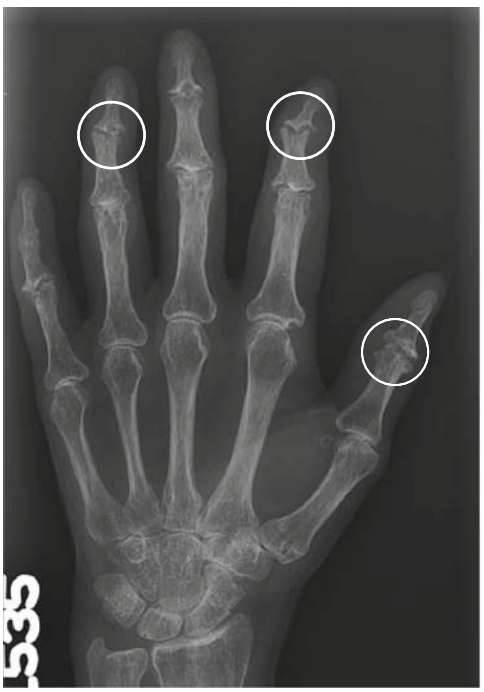

Fig. 11.16 Erosions with preserved joint space in multicentric reticulohistiocytosis (*circles*). Other erosions are more advance and have caused joint space narrowing

accretes more urate and inflammatory cells until it perforates the cortex. In the latter theory, the urate is deposited adjacent to the cortex and over time erodes into the bone while at the margins the bone adds reactive mineral to finally give the clasp-like appearance.

Some diseases lead to total obliteration of the cartilage space and ankylosis, e.g., psoriatic arthritis (Figs. 11.23 and 11.25). This radiographic finding must be tempered by the fact that in some cases, the therapy of choice is to surgically ankylose the joint. Regardless, analysis of the degree and the type of joint space changes, whether narrowing alone or narrowing in combination with erosive or destructive change, can be very helpful in diagnosing the underlying pathology.

Other conditions lead to deposition of calcium within the cartilage structures, both hyaline and fibrocartilage, within the joint. This phenomenon, known as chondrocalcinosis, may be seen in a host of conditions (Table 11.4). These are primarily metabolic conditions that affect the calcium/phosphorus solubility product in or around the joint, e.g., hyperparathyroidism, or diseases that lead to deposition of foreign materials within the cartilage itself, e.g., hemochromatosis, alkaptonuria (ochronosis), calcium pyrophosphate deposition disease.

The final and yet essential analysis of the cartilage space requires an understanding of the remitting and relapsing

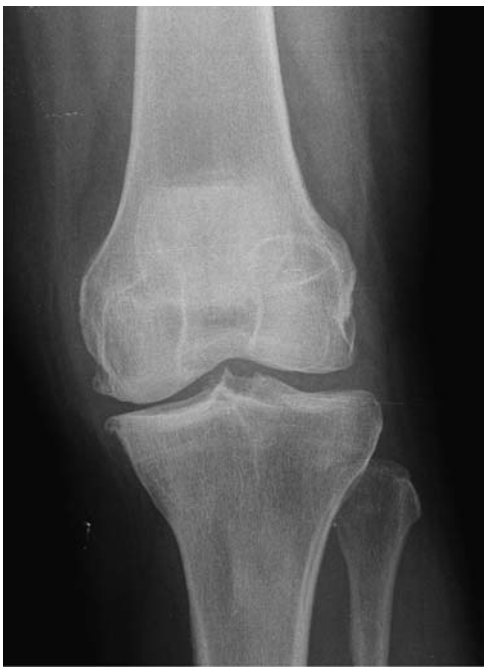

Fig. 11.17 Osteoarthritis of the knee showing medial joint space narrowing with a normal lateral compartment joint space

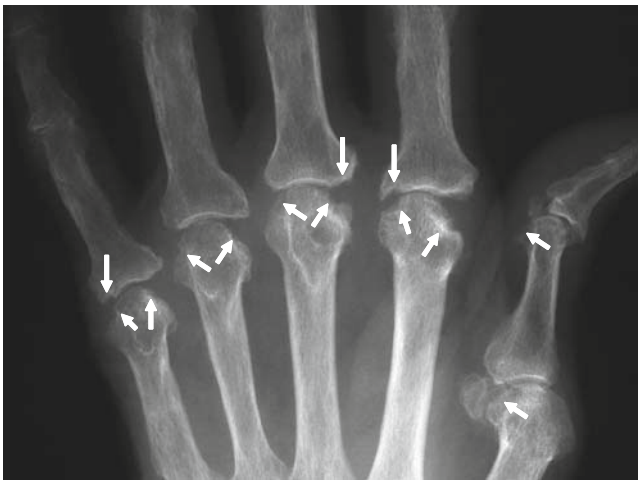

Fig. 11.18 PA radiograph of the hands in a patient with RA showing numerous periarticular erosions (*arrows*)

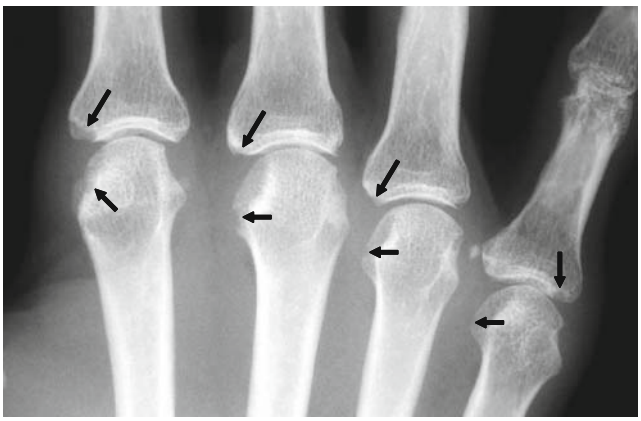

Fig. 11.19 Rheumatoid arthritis, earlier than in Fig. 11.18, with erosions of different ages and activity (*arrows*)

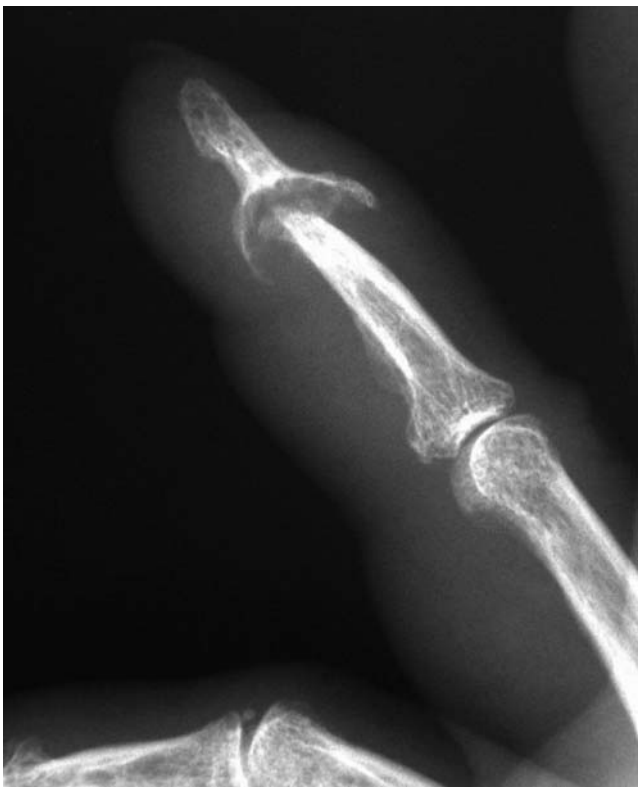

Fig. 11.20 Lateral radiograph showing pencil-in-cup deformity of the DIP of the third digit in psoriatic arthritis

nature of many of the inflammatory arthropathies. During remissions, the destruction within the joint space undergoes some repair and healing. During relapses, new areas of destruction form (Figs. 11.18 and 11.19). Thus the radiographic appearance of the cartilage space will be the integrated result of the competition between the disease process and the body's attempt at healing. This competition has several implications. First, the fewer the number and length of periods of remission, the worse the destruction will be. This means that more constant disease should give more irregular appearing erosions as mentioned above.

Second, erosive changes may be detected long before actual deep pitting of the cortex is evident. Radiographically subtle areas of cortical loss, particularly in the periarticular portions of the joint, may be detected much earlier in the disease than actual erosion (Figs. 11.19 and 11.26). This has an appearance akin to small holes within the cortical line giving

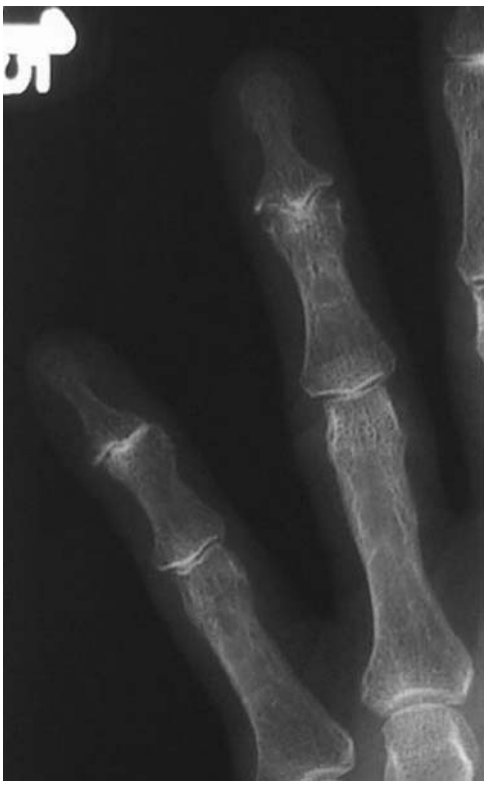

Fig. 11.21 PA radiographs showing gull-wing erosion of the third DIP and diffuse erosion of the second DIP in a patient with erosive osteoarthritis

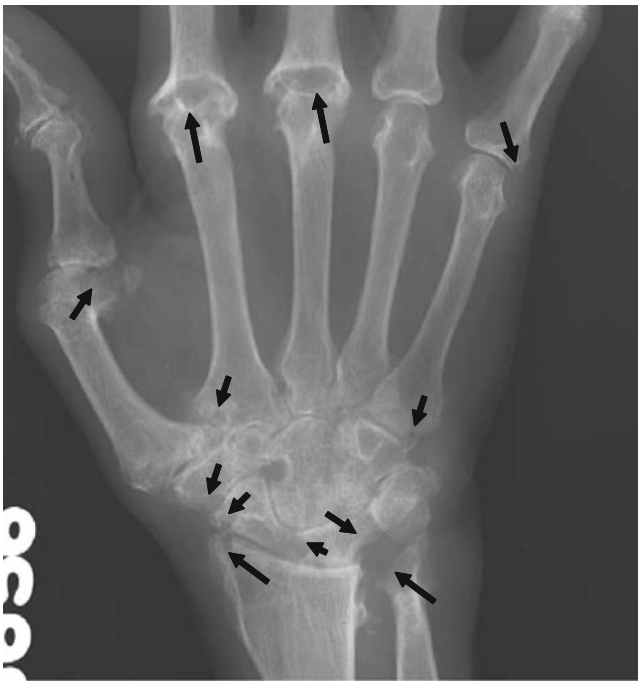

Fig. 11.22 PA radiograph of the right wrist in a patient with RA showing multiple advanced, but smooth, erosions consistent with periods of destruction and healing (*arrows*)

a dot–dash appearance. For this reason, this appearance is known as a Morse code cortex (Figs. 11.19 and 11.26).

Third, as immune competence declines with age, the expectation is that many of the rheumatologic diseases that cause arthritis should have longer period of remission, leaving the patient with a biomechanically abnormal joint that will be prone to secondary osteoarthritis (*vide infra*).

Fourth, between periods of active disease there will be periods of bone remodeling. During that time, the erosions of active disease will heal and start to develop cortex at their bases. Thus, using this finding on radiographs along with other hints such as the presence of capsular swelling, one can make a gross determination of the activity of disease at a given joint space.

Finally, the more the destruction at the joint, the less the healing process can repair the damage during periods of remission. Even when destruction is mild, the healing process often leaves telltale signs that the underlying process was one of a destructive arthritis and not osteoarthritis. Besides the relative absence of osteophytes, the pattern of residual healing differs from the subchondral sclerosis present in osteoarthritis. The former will leave irregularities in the contour of the articular surface of the joint's cortex as well as the endosteal surface. The result is that secondary

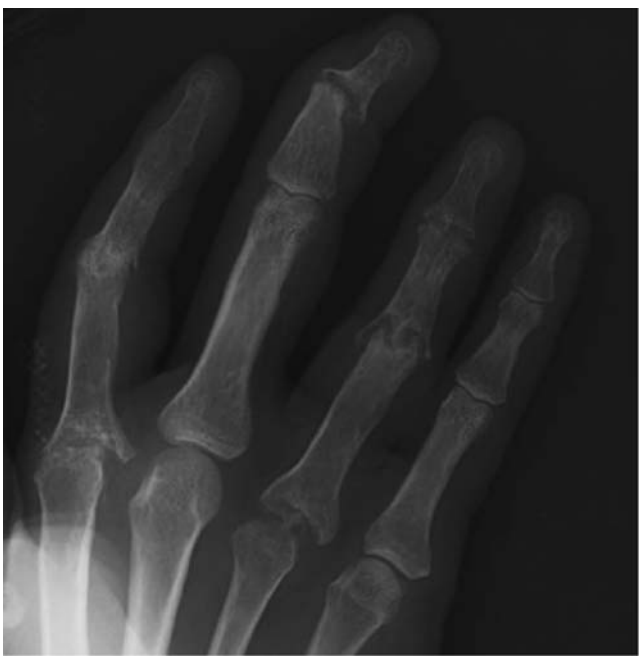

Fig. 11.23 PA radiograph of the digits of the right fingers in a patient with psoriatic arthritis showing irregular erosions consistent with prolonged periods of inflammation. Note the PIP of the fourth digit showing Mickey Mouse ear erosions, often associated with psoriatic arthritis. Also note the ankylosis of the DIP of the second digit

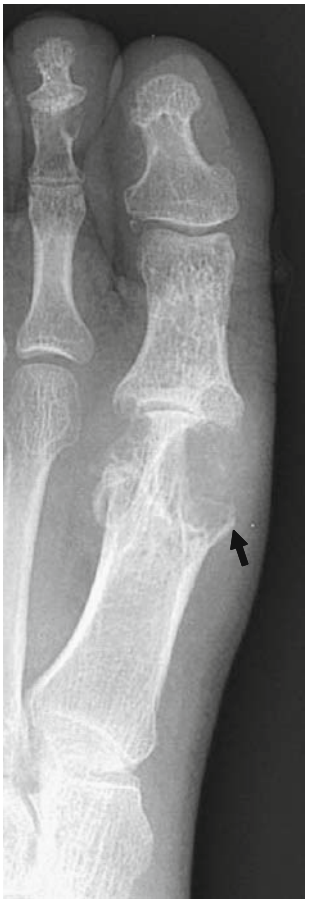

Fig. 11.24 PA radiograph of the foot showing paraarticular erosions of the distal first metatarsal secondary to gout. Note the clasp shape appearance to this erosion and the Granger overhanging edge (*arrow*)

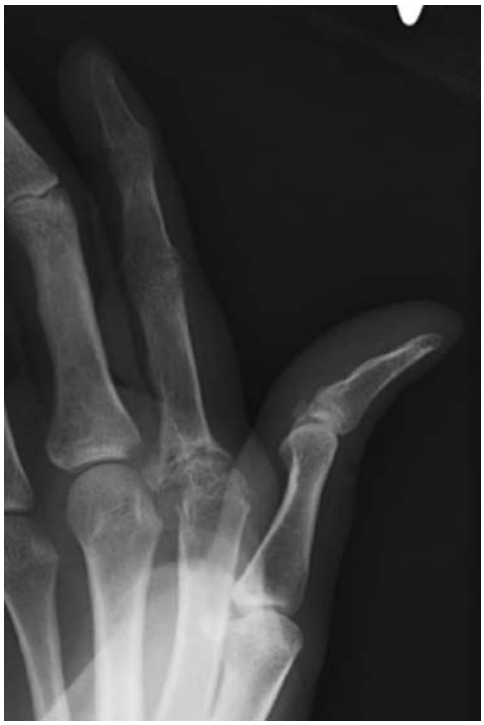

Fig. 11.25 PA radiograph of the second digit showing noniatrogenic fusion of the PIP and DIP related to psoriatic arthritis. Marked erosive change is present at the second MCP

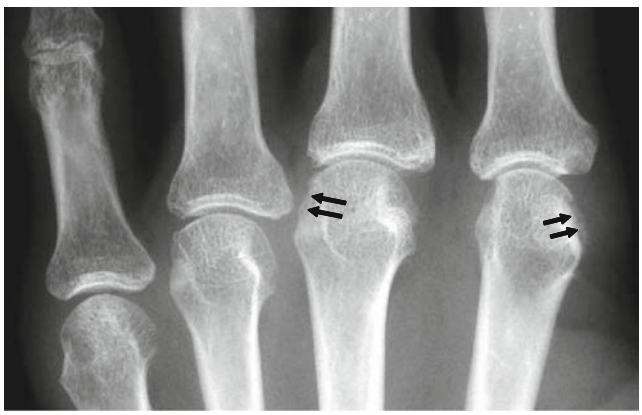

Fig. 11.26 PA radiograph of the MCPs of the left hand showing early erosions. Note subtle early cortical loss along the radial aspect of the head of the second and third metacarpal (*arrows*) at the articular margin

osteoarthritis related to prior inflammatory disease will often show some mild, "fuzzy" appearing joint surfaces that suggest healing from prior inflammation.

Distribution

Once the soft tissues, joint alignment, bone characteristics, and cartilage spaces have been evaluated, the class of arthropathy, i.e., destructive, productive, both, or neither, is generally apparent. Narrowing the differential down within the class of arthropathies requires two additional pieces of information, the distribution of joints affected and any distinguishing radiographic, clinical, or laboratory findings.

Different arthropathies have predilections to involve different joints. Intimate knowledge of these predilections is useful for making a diagnosis. Of course, the spondyloarthropathies tend primarily to affect the spine, but so does ochronosis. Gout, on the other hand, tends to affect acral parts of the skeleton where the local body temperature is likely to go down with inactivity and where daily accumulation of fluid tends to resorb overnight. Relatively poor acral circulation means lower tissue temperatures that in turn lead to a lower solubility product for urate. Further, resorption of fluid overnight from dependent tissues leads to concentration of urate most prominently in the feet.

Symmetry of involvement provides important clues to the diagnosis since some arthropathies have a tendency to affect the body more symmetrically than others, e.g., RA. Some

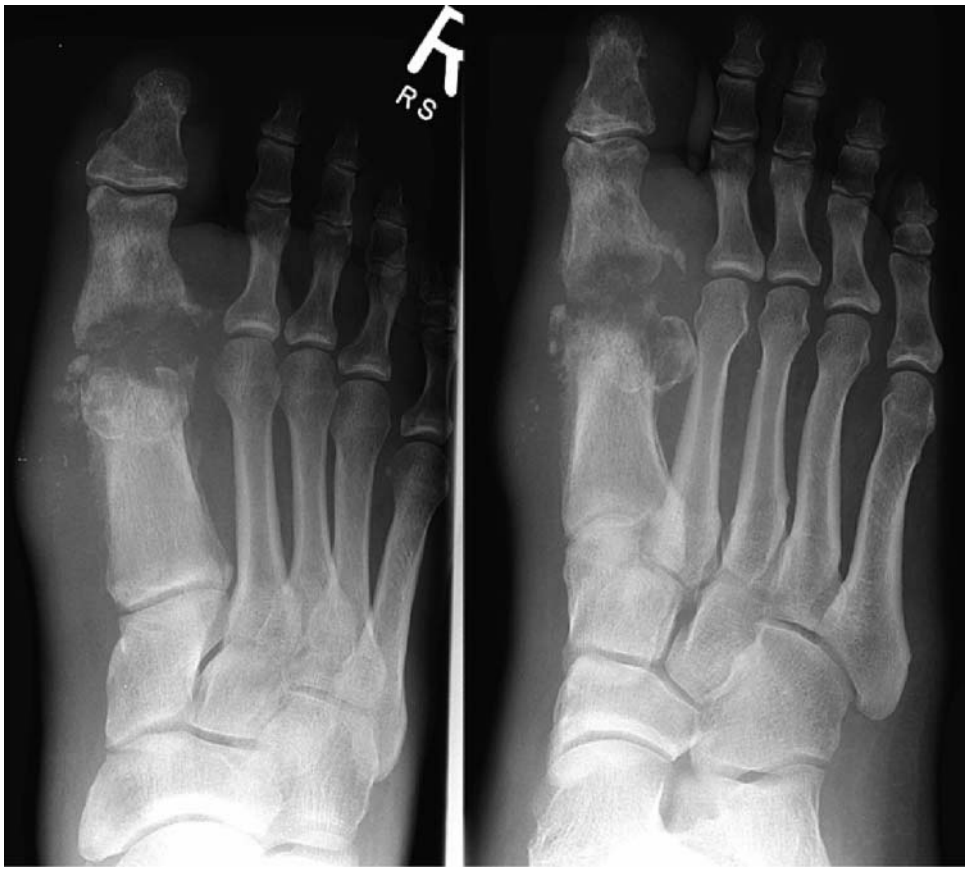

Fig. 11.27 Septic arthritis of the MTP of the first digit with joint space destruction and marked soft tissue swelling (Case courtesy of Dr. John Hunter.)

tend to be very asymmetric, e.g., psoriatic arthritis and Reiter disease. In addition, different arthritides affect different sets of joints. For example, some have a predilection for carpal bones and tarsal bones, e.g., RA or amyloid arthropathy. Others, e.g., psoriatic arthritis and erosive osteoarthritis, have a greater tendency to affect the small joints of the hands and feet. Spondyloarthropathies often affect the sacroiliac joints – some symmetrically and others asymmetrically – while some arthropathies, e.g., RA, rarely affect these joints. Last but certainly not least, some arthropathies, particularly purulent septic arthritides and to a lesser extent gout, tend to affect a single joint (Fig. 11.27) as opposed to the majority of arthropathies which tend to affect multiple joints. In fact, an arthritis that affects a single joint or causes disk-centered destruction should be considered an infection until proven otherwise, particularly in a patient without gout.

Thus, a bilaterally symmetric destructive arthropathy involving the carpi and the metacarpophalangeal joints strongly suggests RA. Productive arthritis involving the patellofemoral joint out of proportion to other compartments of the knee joint should raise the possibility that the patient suffers from calcium pyrophosphate dihydrate deposition arthropathy (CPPD), not primary osteoarthritis. Similarly, a productive arthritis that involves primarily the second and third metacarpophalangeal joints and shows large radial hook-like osteophytes suggests the possibility of hemochromatosis.

Extraordinary Findings

Demographics, clinical history, and laboratory data contribute to narrowing the radiographic diagnosis. It is expected that certain arthropathies will affect certain populations, predominantly one gender or the other, and have their onset at certain ages (Table 11.1). In addition, peculiarities of the radiographic appearance and distribution of some arthropathies help to narrow the differential and lead to definitive diagnosis. For example, the presence of spontaneous joint ankylosis or the presence of an ivory phalanx is strongly suggestive of psoriatic arthritis. Chondrocalcinosis is frequently, but not always, present in CPPD. Atlantoaxial subluxation is common in RA but unusual in psoriatic arthritis and Reiter disease. Interstitial lung disease is

Table 11.1 Common ages of onset of arthropathies

Age group	Age of onset	Disorder
Young (< 20 years)	< 20 years	Juvenile chronic arthritis Hemophilia Septic arthritis
Middle (> 20 years)	Onset 15–35 years) Young adults 25–55 years	Ankylosing spondylitis Reiter syndrome Enteropathic arthropathies Rheumatoid arthritis Psoriatic arthritis
Older patients (> 55 years)	> 55 years	Osteoarthritis Septic arthritis (diabetes) DISH CPPD

common in some of the conditions associated with arthritis, e.g., RA and ankylosing spondylitis.

Productive Arthropathies

Osteoarthritis

Osteoarthritis is by far and away the most common form of arthritis in the United States followed by rheumatoid arthritis and gout in about equal proportions as distant seconds (Fig. 11.28). All of the many remaining arthropathies comprise only a small, but important, portion of clinical arthropathies. We will discuss the important and relatively common of these diseases.

Osteoarthritis (OA), also known by many derivative names including degenerative joint disease (DJD), has two principle forms: primary and secondary. Traditionally, the former has been thought to be the result of aging and wear and tear on a joint while the secondary forms of the disease have a known pathology that leads to loss of the articular cartilage and so arthritis (Table 11.2). Primary osteoarthritis, although seen in younger patients, becomes more common as patients age to the point that it may affect at least one joint in all patients over the age of 65 years. Over 80% of patients over the age of 75 years have clinically symptomatic OA. It affects women about twice as often as men, but this ratio depends upon the joint in question. For example, women have OA of the small joints of the hand much more frequently than men, but hip OA is equally common between the genders. Racial differences also exist. For example, OA of the hip is more common in Caucasians than in Blacks and Asians.

Overall, OA is most common in the major weight-bearing joints, the hip, the knee, and to a lesser degree the ankle. It is also common in the frequently used small joints of the hands and wrists, particularly the first carpometacarpal joint at the base of the thumb. Often the dominant hand is more severely affected than the nondominant hand. The facet joints of the cervical and lumbar spine are also commonly affected. The shoulder and elbow are relatively spared.

Table 11.2 Classification of osteoarthritis

Primary osteoarthritis	
Secondary osteoarthritis	
Trauma	Hemophilia
Neuropathic	Ochronosis
CPPD	Homocysteinuria
AVN	Porphyria
Acromegaly	Neuromuscular disease
Hemochromatosis	

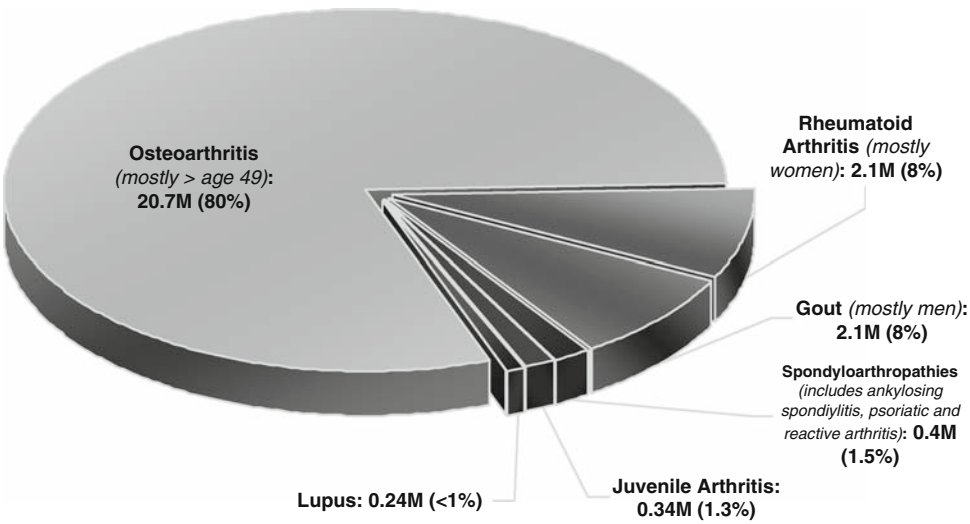

Fig. 11.28 Prevalence of common arthropathies. Many arthropathies are too uncommon to affect the chart

Clinically patients with OA complain of joint pain, crepitus, and stiffness after periods of inactivity. Normally, the pain is relieved by rest, but late in the disease pain may be constant. OA is not relentless in its symptoms. It undergoes relative periods of symptomatic improvement and worsening, related to periods of reactive synovitis and development of joint effusion.

Advanced disease is often accompanied by weakness from disuse atrophy of muscles. Further, the pain that these patients experience causes patients to shift their weight-bearing to avoid discomfort. This, along with increasingly poor vestibular function in elderly patients, contributes to instability in older patients and helps to explain the high incidence of falls in this age group. The combination of falls and worsening osteoporosis in this age group leads to a high incidence of fracture.

As OA progresses, the joints begin to show clinical enlargement. In the fingers, these enlarged areas are known as Heberden and Brouchard nodes as the distal and proximal interphalangeal joints enlarge respectively. With enlargement of the facet joints in the spine, the neuroforamina may become encroached resulting in radiculopathy, development of spinal stenosis or anterior subluxation of one vertebral body on another (spondylolisthesis).

Recent evidence suggests that primary OA is actually genetically inherited and not merely related to wear and tear on a joint although the latter may abet the onset of the disease. A number of researchers have discovered abnormalities within the synovial fluid of primary OA patients and their kinships that suggest deficient nutrition of the chondrocytes in the hyaline cartilage layer. Since chondrocytes in this cartilage have no direct blood supply but instead obtain their nutrition from diffusion of the synovial fluid within the joint, it appears that this might be a cause of primary OA. Other abnormalities have been found that suggest abnormal collagen formation in hyaline cartilage. Among these is a point mutation in the cDNA cloning for type II collagen, suggesting that chondrocyte function may be impaired in some patients with primary OA. Thus, the etiology of primary OA may be more complicated and multifactorial than previously thought. Indeed, it may actually be more than one disease. Simultaneously, this new information suggests that one day effective preventative therapies may become available for this common ailment.

All forms of OA, whether primary or secondary, have a common etiologic pathway that commences with loss of the hyaline cartilage within the joint. The causes of the cartilage loss vary and include:

- poor chondrocyte nutrition as in primary OA,
- poor cartilage formation and maintenance by chondrocytes, also as in primary OA,
- oovergrowth of the thickness of the cartilage beyond the diffusion coefficient of synovial fluid as in acromegaly,
- direct biomechanical alteration of the forces across the joint that lead to acute or at times chronic cartilage loss as may occur with trauma,
- deposition of foreign material with the cartilage that leads to weakening and subsequent sloughing of the overlying cartilage layer as in hemochromatosis, homocysteinuria, ochronosis, or CPPD to name a few,
- loss of proprioception as occurs in neuropathic arthropathy, leading to chronic repetitive trauma on the joints.

Once enough hyaline cartilage loss has occurred, the normal shear reduction function of the cartilage is lost. This leads to bone-on-bone apposition across the joint and stimulates new bone formation in two critical locations. The first is the subchondral plate of the joint where eburnation takes place in response to the loss of the hyaline cartilage and the resulting alterations in pressure across the joint. Second, the body attempts to return the pressure across the joint back to its homeostatic set point through development of peripheral osteophytes. As a result, joints affected by long-term OA will have large osteophytes giving the appearance of a productive arthritis. All of these changes occur in the absence of significant or prolonged inflammation. As a result, the blood flow to the periarticular bone is not increased and there is no tendency to develop periarticular osteoporosis.

Thus, the hallmarks of the radiographic diagnosis of OA are joint space narrowing, subchondral sclerosis, and osteophytes (Figs. 11.17, 11.29 and 11.30) against a background of normally mineralized bone. Typically, joint space nar-

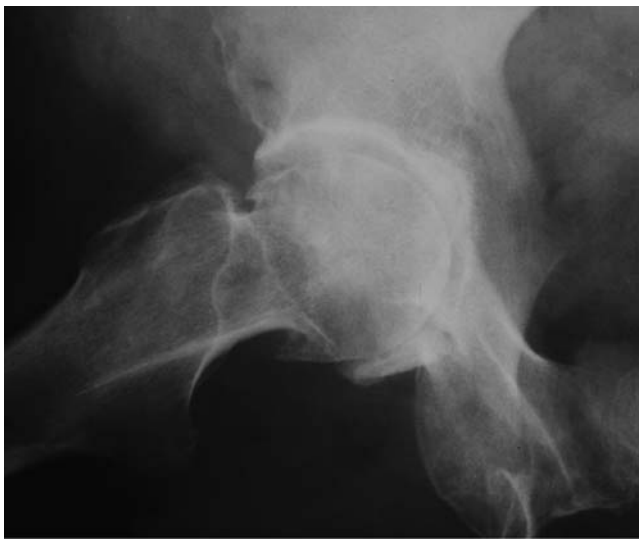

Fig. 11.29 Osteoarthritis of the hip with joint space narrowing, subchondral sclerosis, and osteophyte formation

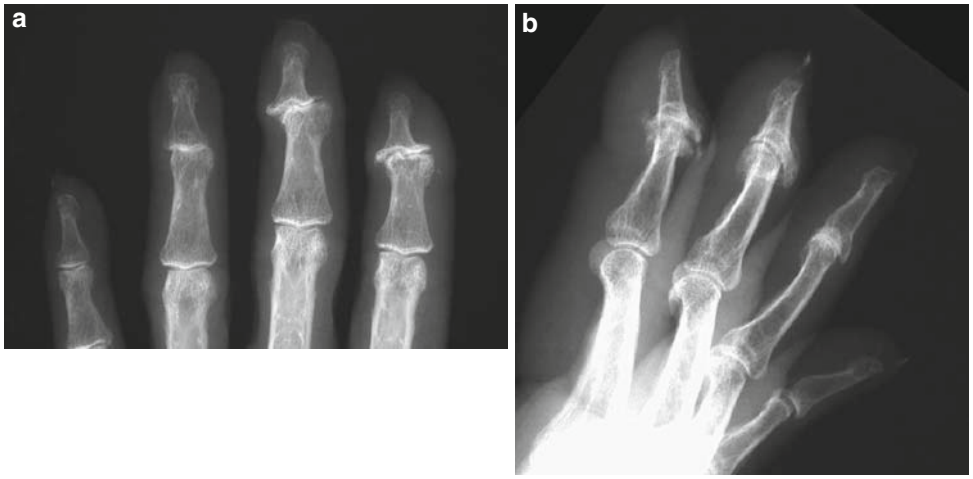

Fig. 11.30 PA (**a**) and lateral (**b**) radiographs of the digits showing marked joint space narrowing, subchondral sclerosis, and osteophytes of the second, third, and fourth digits

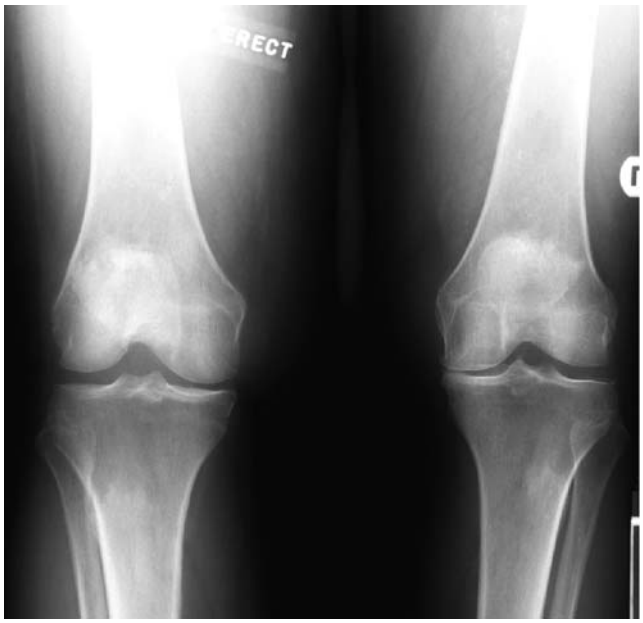

Fig. 11.31 AP view of knees with weight-bearing to show true degree of joint space narrowing. Note the marked medial compartment narrowing on the left and to a lesser extent on the right. The normal valgus carrying angle (5–8°) has been lost

rowing should precede the latter two features radiographically, but it may be imperceptible when images are obtained without weight-bearing or compressive forces across a joint. Hence, whenever a diagnosis of OA is suspected, it is advisable to obtain at least one weight-bearing view of the joint (Fig. 11.31).

Over time, patients with OA will develop subchondral cysts in their affected joints that are visible radiographically as lucencies (Fig. 11.32). These are more typically seen in large joints such as the hip, the knee, or the ankle and much less commonly seen in smaller joints such as the first carpometacarpal joint. Most believe that these cysts form as a result of small fissures that form in the denuded articular cortex, allowing the higher pressure within the joint space to communicate with the lower pressure marrow space. This results in gradual erosion of the marrow space and pseudocyst formation. Eventually, these cysts may corticate along their margins.

An unusual form of OA has been described in which there is rapid destruction of a joint without evidence of inflammation (Fig. 11.33). The entire joint may be destroyed over a period of months. This variant occurs more frequently in women than in men and is usually seen in elderly patients. The hip is most frequently involved, and the disease is usually unilateral. The major differential for this type of OA is septic arthritis. The latter must be excluded before making this diagnosis.

Secondary Osteoarthritis

As indicated, many diseases result in secondary osteoarthritis. We will discuss the more common of these here.

Neuropathic Arthritis

Neuropathic arthritis is an extreme form of posttraumatic osteoarthritis. Instead of resulting from an isolated traumatic event with or without a posttraumatic deformity, this arthropathy represents continuous and ongoing trauma. In neuropathic arthropathy, the involved joints lack proprioception and in some cases deep sensation as well. As a result, joint movement is not inhibited and tends to cause unintentional repetitive minor trauma. Ultimately, this constant

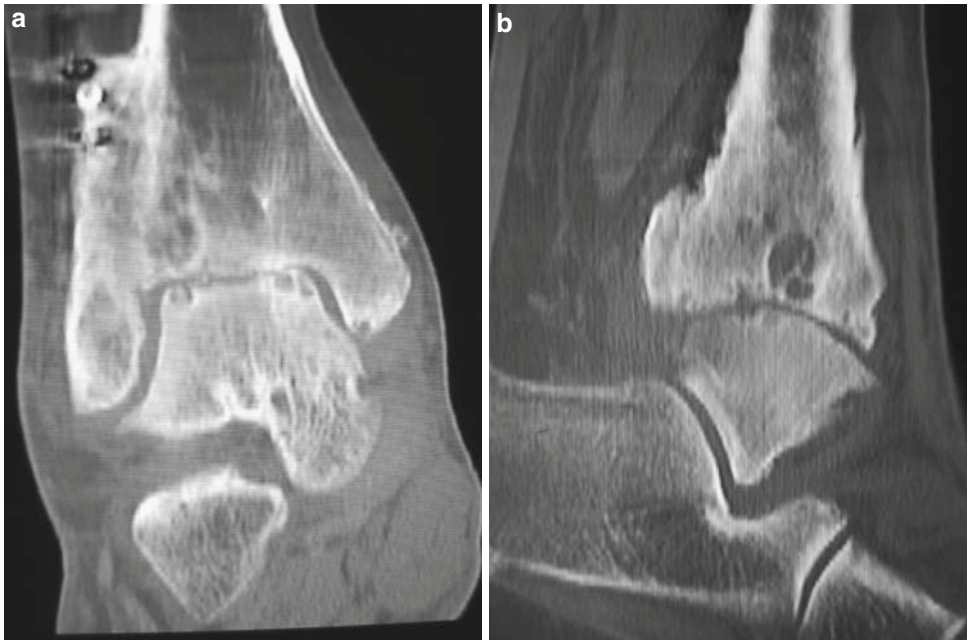

Fig. 11.32 Coronal (**a**) and sagittal (**b**) CT reconstructions of an ankle showing subchondral lucencies in osteoarthritis consistent with subchondral cysts. Note that some of these have well-developed cortication indicating chronicity

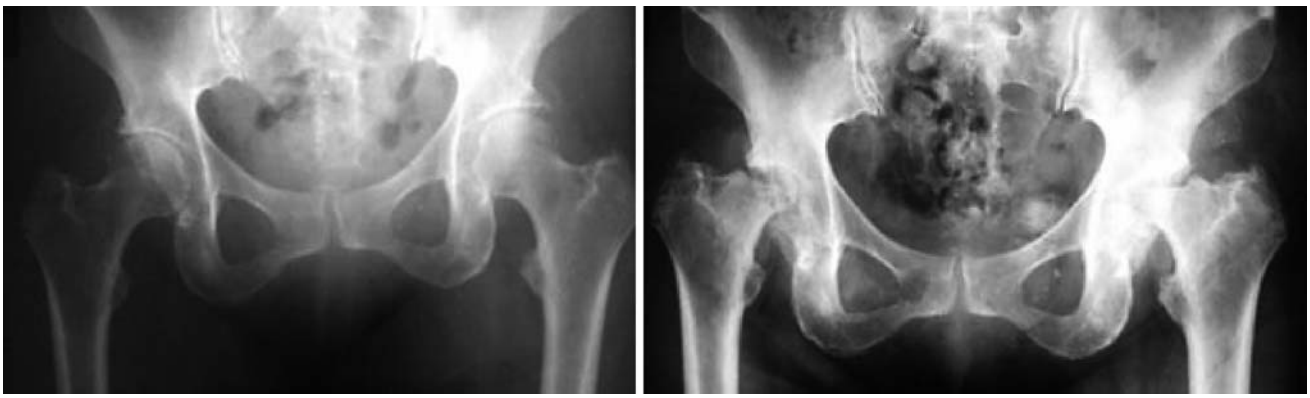

Fig. 11.33 AP views of the pelvis showing rapid destruction over both hips, period of 4 months

trauma causes repetitive fracture and fragmentation of the joint which in turn leads to loss of articular cartilage and initiation of the process that gives rise to OA.

The radiographic hallmark of neuropathic arthritis is one of "osteoarthritis with a vengeance." Not only will affected joints show narrowing, sclerosis, and osteophytes, but they will show these with such exuberance that the appearance is one of marked increased **D**ensity about the joint, **D**isorganization of the joint structures, **D**ebris surrounding and within the joint, **D**estruction of the joint surfaces and **D**islocation of the joint (Figs. 11.34 and 11.35). This collection of "**D**" word descriptors should bring the diagnosis to mind. The fact that joints affected by neuropathic arthropathy may show disorganization and destruction may be confusing and suggest a destructive arthritis rather than a productive one. Thus, the viewer must be vigilant to make the diagnosis, especially since neuropathic arthritis may range widely from a purely productive arthropathy to one that resembles an aggressively destructive process. Because of this, septic arthritis with or without osteomyelitis is often in the differential diagnosis of neuropathic arthritis, particularly in the diabetic foot.

Neuropathic arthritis may arise from a number of causes, each of which has a predilection for certain joints (Table 11.3). All of these diseases affect the nervous system and, whether from infection of the nervous system, interrupted neuronal pathways, ischemic conduction abnormalities, or other causes, result in loss of proprioception. Those conditions that affect upper motor neurons are more likely to cause a hypertrophic form of arthritis, while those that affect the peripheral nerves are more likely to cause an atrophic form of the disease where the amount of disorganization and

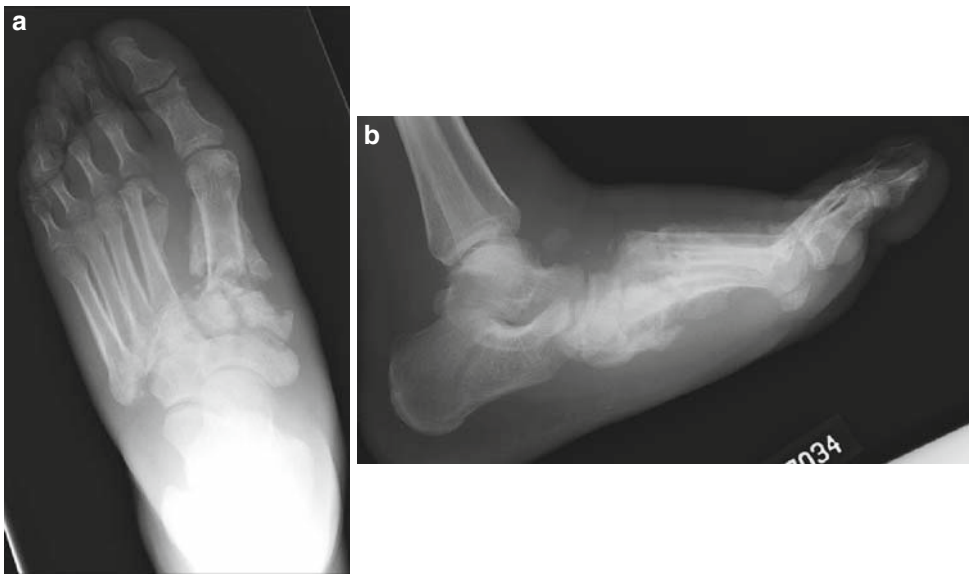

Fig. 11.34 AP (**a**) and lateral (**b**) views of a foot with midfoot neuropathic arthritis showing disorganization, debris, density, and dislocation. The patient has diabetes. Note the rocker bottom foot deformity

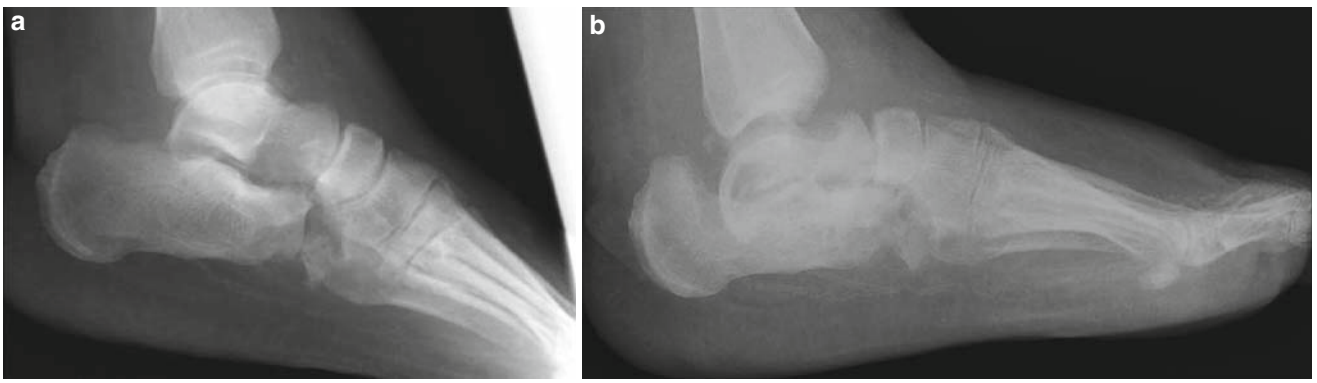

Fig. 11.35 Early midfoot (**a**) and late hindfoot (**b**) neuropathic changes in the hind and midfeet in patients with diabetic neuropathic arthritis

production is less prominent (Figs. 11.36 and 11.37). As this form progresses, it may give rise to symmetrical enlargement of the joint with an appearance more typical of neuropathic arthritis (Fig. 11.37). Syphilis was once a major cause of neuropathic arthritis in developed countries but now is rarely seen (Fig. 11.38).

The overwhelming majority of neuropathic arthritis in the United States today is the result of diabetes and affects the feet and ankles and to a lesser degree the knees in these patients. Neuropathic arthritis affects about 1 in 700 diabetics and usually has its onset in the fifth or sixth decades of life. Its occurrence appears to be inversely related to how well the patient's diabetes is controlled.

Similarly, the vast majority of adult osteomyelitis and septic arthritis (>90 %) occurs in diabetic patients with cutaneous ulceration. Thus, the cross section of these two diseases is similar. Typically most diabetic foot osteomyelitis occurs around the first and fifth metatarsal heads, the proximal interphalangeal joints, the cuboid, the lateral malleolus, and the posteroinferior calcaneus. On the other hand, neuropathic arthropathy is more typically centered in the midfoot

Table 11.3 Diseases associated with neuropathic arthritis and commonly affected joints

Disease	Joints involved
Syphilis	Lumbar spine, hips, knees
Diabetes	Midfoot, ankles, knees
Syringomyelia	Shoulders
Charcot marie tooth	Large joints
Meningomyelocoele	Hips, knees
Leprosy	Small joints of feet >> hands
Spina bifida	Hips, knees
Paraneoplastic sensory neuropathy	Large joints
Congenital insensitivity to pain	Diffuse

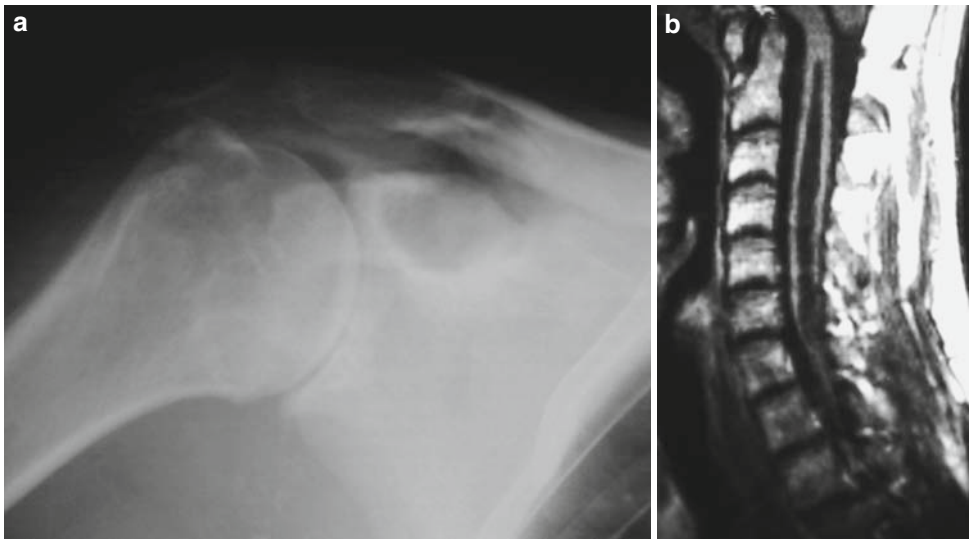

Fig. 11.36 AP shoulder (**a**) and sagittal T1-weighted MRI (**b**) showing atrophic neuropathic arthritis and a large syrinx. In **a**, the glenohumeral joint has narrowed and shows subchondral sclerosis, but there is no fragmentation or dislocation

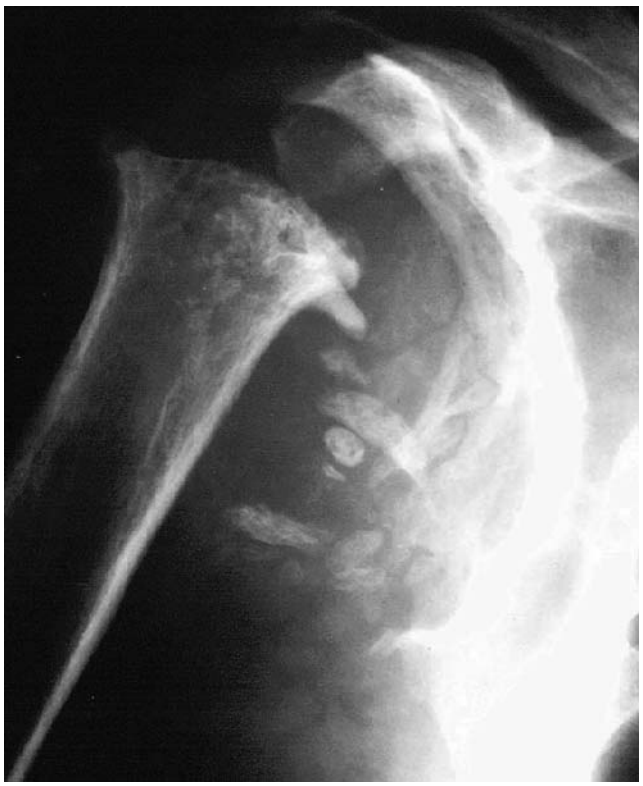

Fig. 11.37 AP of the right shoulder showing late neuropathic arthropathy with marked enlargement of the joint and debris

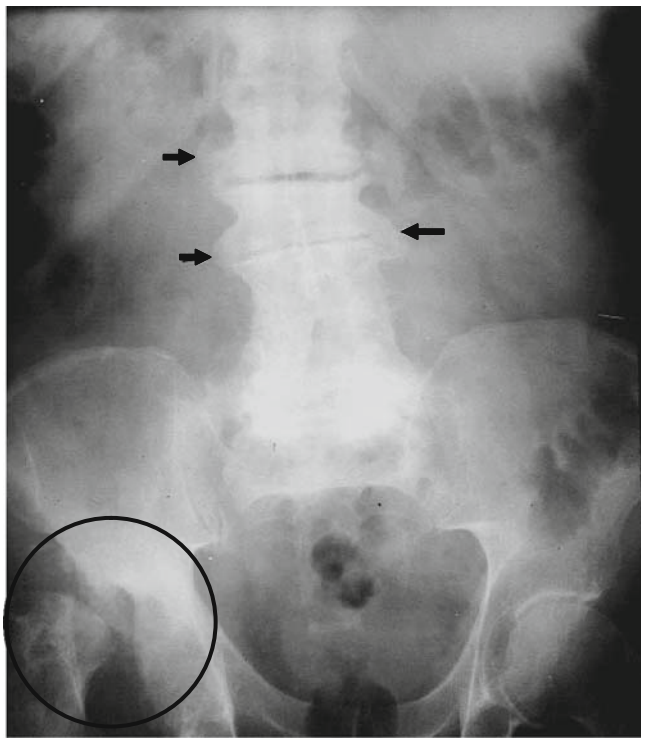

Fig. 11.38 AP lumbar spine in a patient with syphilitic neuropathic arthritis showing marked osteophytes in the lumbar spine (*arrows*) and destruction, dislocation, and debris around the right hip (*circle*)

in diabetes (Fig. 11.34). The presence of ulceration and/or disease in locations typical of infection should increase the suspicion of infection as opposed to neuropathic arthropathy. It should be remembered, however, that patients with neuropathic arthritis of the foot will tend to develop rocker bottom deformities of their feet. These deformities allow abnormal pressures on the insensate diabetic foot and lead to ulceration in atypical locations. Thus, infection – septic arthritis and osteomyelitis – often may complicate neuropathic arthritis.

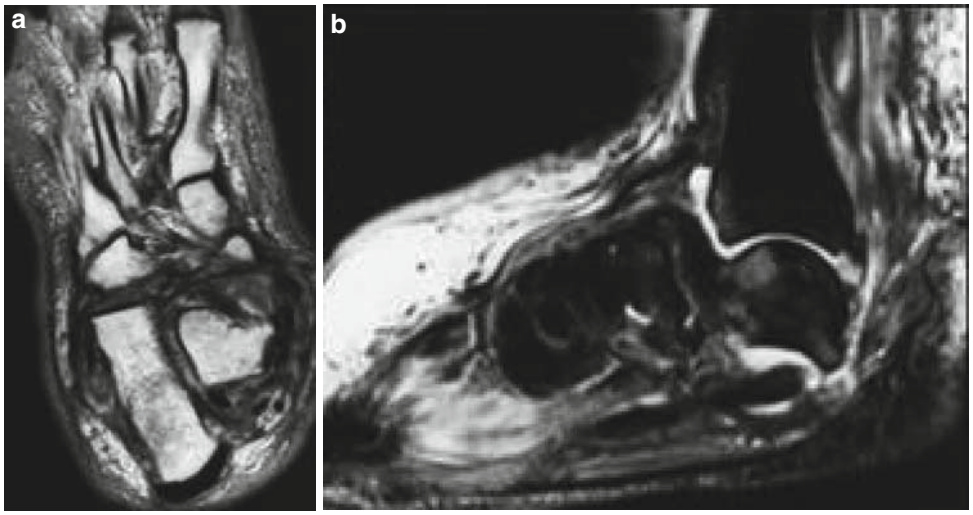

Fig. 11.39 T1-weighted long axis (**a**) and T2-weighted sagittal (**b**) of a diabetic's foot with severe neuropathic arthritis. No cortical destruction is present, only edema and disorganization. Note the marked soft tissue swelling along the dorsum of the foot (**b**). The differential of neuropathic arthritis is often infection as both are common in diabetics and can present similar appearances

MRI may also be helpful at making this crucial distinction as it is able to show the soft tissues to advantage, including the presence of abscesses and draining ulcers (Fig. 11.39). It also shows the true epicenter of disease – joint centered versus bone centered. Even so, no imaging method alone can distinguish completely between neuropathic arthritis and septic arthritis.

Calcium Pyrophosphate Dihydrate Deposition Arthropathy (CPPD)

In calcium pyrophosphate dihydrate deposition arthropathy (CPPD), there is excess calcium and pyrophosphate solute with the joint such that crystal precipitates out into the joint spaces and is deposited within the synovium and articular cartilage. This material causes an inflammatory reaction within the joint that leads to destruction of the articular cartilage and a symptomatic joint effusion. Aspiration of the joint will reveal positively birefringent rod-shaped crystals within the fluid (Fig. 11.40).

Clinically, CPPD affects a similar population to that of OA. It becomes more prevalent with age and affects about 5% of the population. Unlike OA, there is no reported gender predominance. CPPD also behaves very similarly to OA, causing joint pain, stiffness after prolonged rest, and crepitus. It also has a tendency to present with occasional flares where patients develop acute inflammation in the joint, swelling from a joint effusion, and erythema. This presentation may be very similar to gout and has been referred to clinically as pseudogout. It is important to point out, however, that CPPD and pseudogout are not synonymous terms. While CPPD refers to a pathologic diagnosis, pseudogout refers to a clinical presentation. As such, the latter is not confined to CPPD but refers to any disease that presents with a single, acutely swollen, and hot joint. Other causes include septic arthritis, hemophilia, hyperparathyroidism, hemochromatosis, hypothyroidism, hypomagnesemia, and hypophosphatsia.

While inflammation is intermittent in CPPD, the damage to the cartilage is permanent and ultimately this leads to an arthropathy that closely resembles OA (Fig. 11.41). It differs, however, in that the inflammatory component may also contribute to some radiographically identifiable erosion at the joint surfaces, particularly in the radioscaphoid joint (Fig. 11.42).

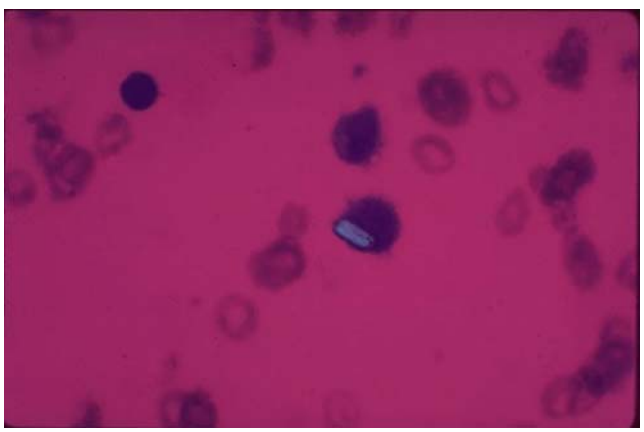

Fig. 11.40 Calcium pyrophosphate crystals viewed under semi-polarized light at 400× magnification

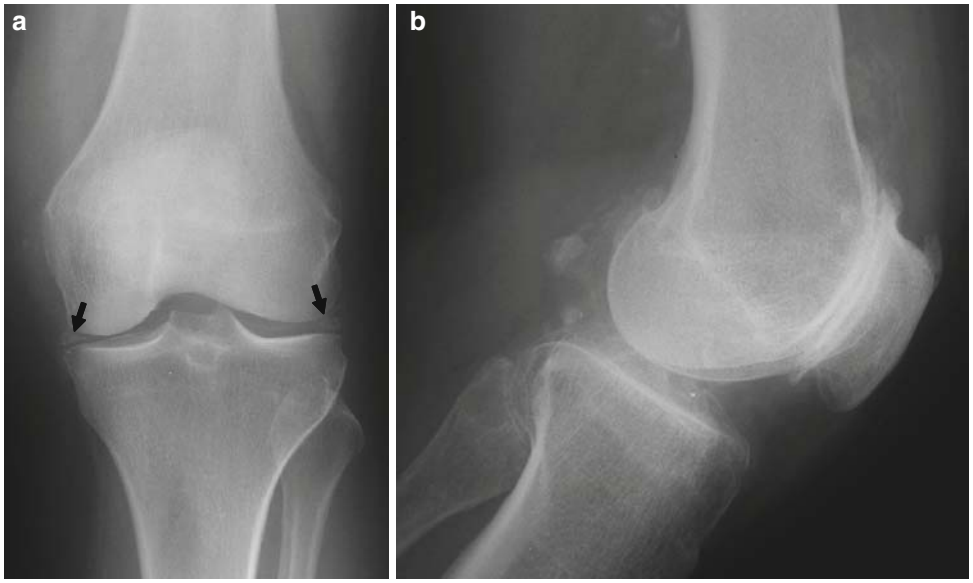

Fig. 11.41 AP (**a**) and lateral (**b**) radiograph of the knee showing productive arthropathy of CPPD. Chondrocalcinosis, though not an essential feature of the disease, is visible outlining the menisci (*arrows*) in both the medial and lateral compartments

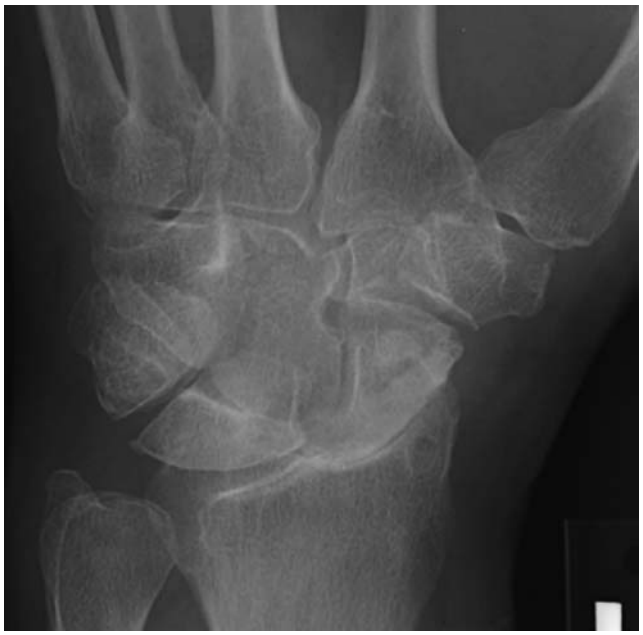

Fig. 11.42 CPPD arthropathy with erosive changes at the radioscaphoid joint

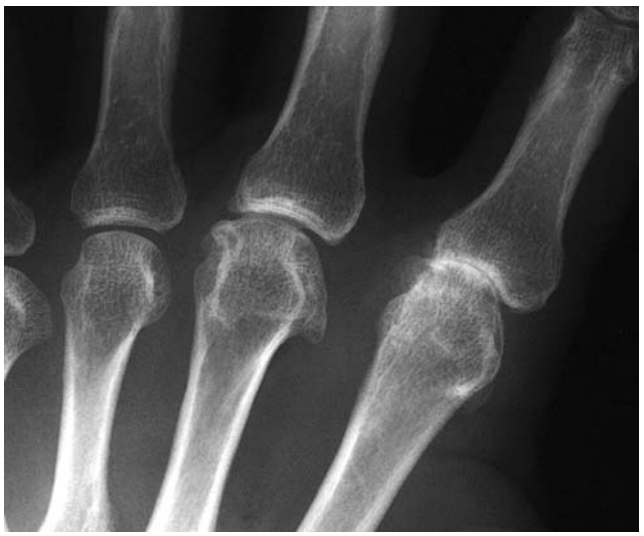

Fig. 11.43 CPPD arthritis of the second and third MCP joints showing joint space narrowing, subchondral sclerosis, and osteophytes indistinguishable from that of OA

In addition, CPPD has a predilection for certain joints that differ from the typical distribution of OA. These include the radioscaphoid joint, the scaphotrapeziotrapezoidal (STT) joint, the metacarpophalangeal joints (particularly the second and third) (Fig. 11.43), the patellofemoral joint (Fig. 11.44), and the talonavicular joint. Long-standing CPPD may lead to collapse of the carpus, giving a radiographic appearance similar to a post-traumatic SLAC (scapholunate advanced collapse) wrist (Fig. 11.45).

The deposition of calcium pyrophosphate within the articular structures, primarily the hyaline cartilage and the meniscal fibrocartilage, can become radiographically visible (Figs. 11.41 and 11.46). This phenomenon, known as chondrocalcinosis, is not unique to this disease. In fact, chondrocalcinosis is a nonspecific finding that may be seen in a number of different diseases, including hemochromatosis and

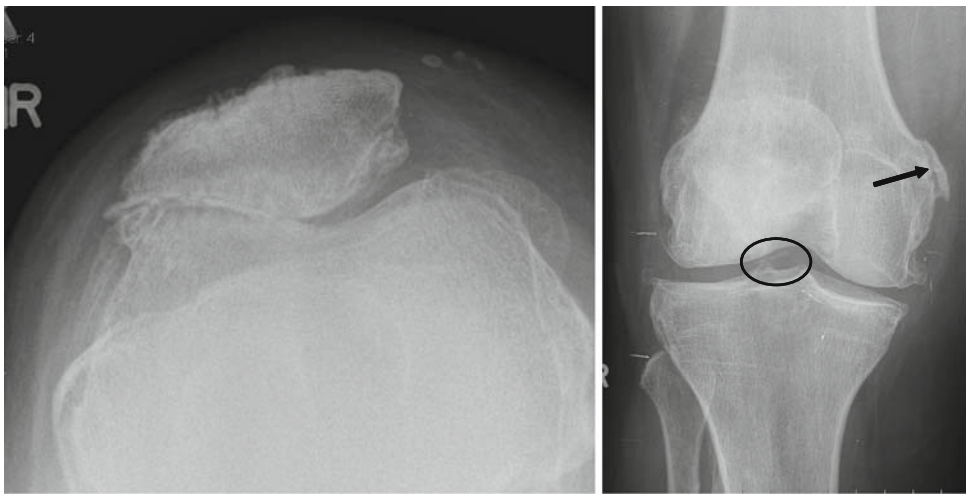

Fig. 11.44 CPPD showing disproportionate narrowing of the patellofemoral joint compared with the medial and lateral compartments of the knee. Note the chondrocalcinosis in the femoral notch (*oval*) consistent with a diagnosis of CPPD and the Pellegrini–Stieda suggesting prior medial collateral ligament injury (*arrow*)

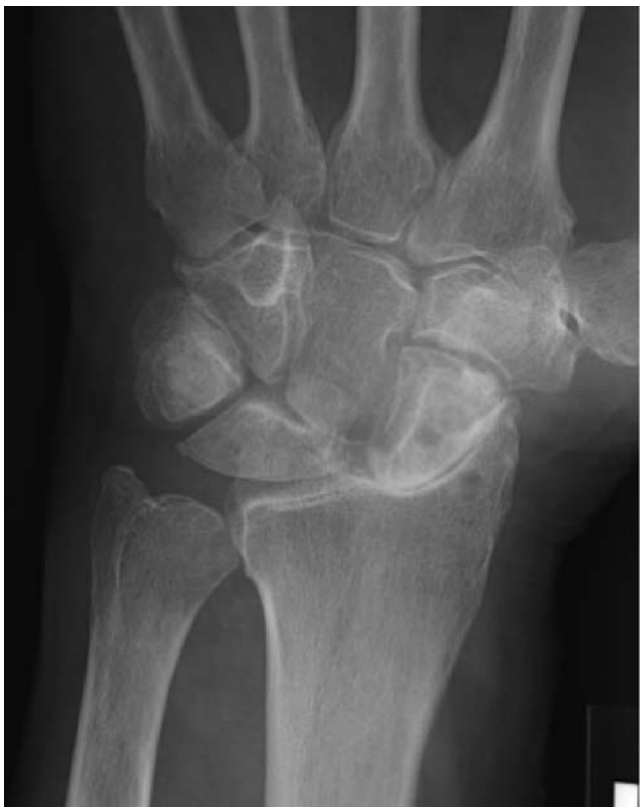

Fig. 11.45 CPPD with widening of the scapholunate joint space and migration of the capitate into the proximal row similar to a post-traumatic scapholunate (SLAC) wrist

hyperparathyroidism (Table 11.4). On the other hand, its presence is not required to make any of the diagnoses listed in the table.

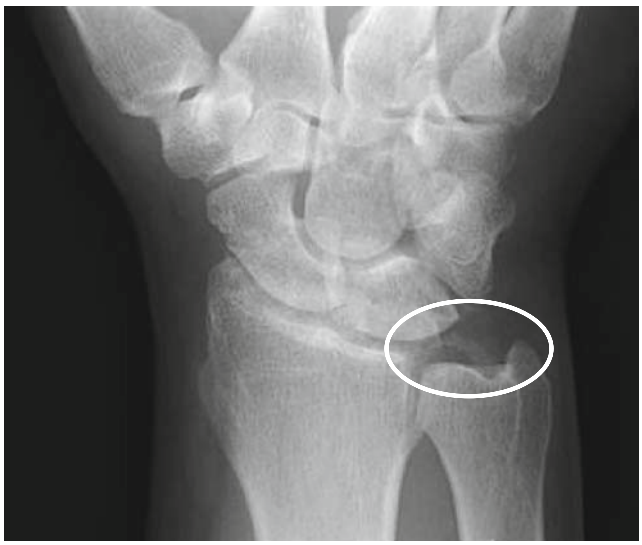

Fig. 11.46 Chondrocalcinosis of the triangular fibrocartilage complex (TFCC) caused by CPPD (*oval*)

Table 11.4 Conditions associated with chondrocalcinosis.

Wilson disease
Hemochromatosis
Idiopathic
Parathyroid disease (hyperparathyroidism)
Amyloid
DJD (osteoarthritis) & CPPD
Ochronosis
Gout

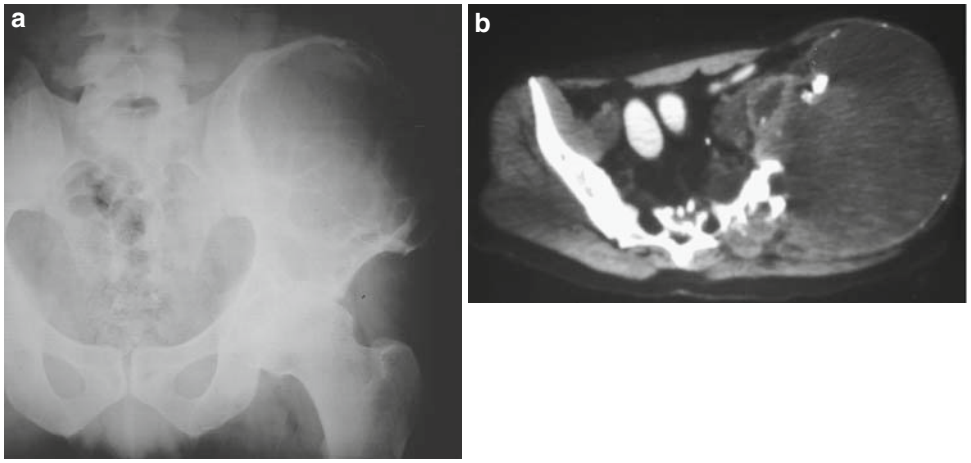

Fig. 11.47 AP radiograph (**a**) and image from a CT of the left iliac bone showing a large bubbly lesion representing a hemophiliac pseudotumor

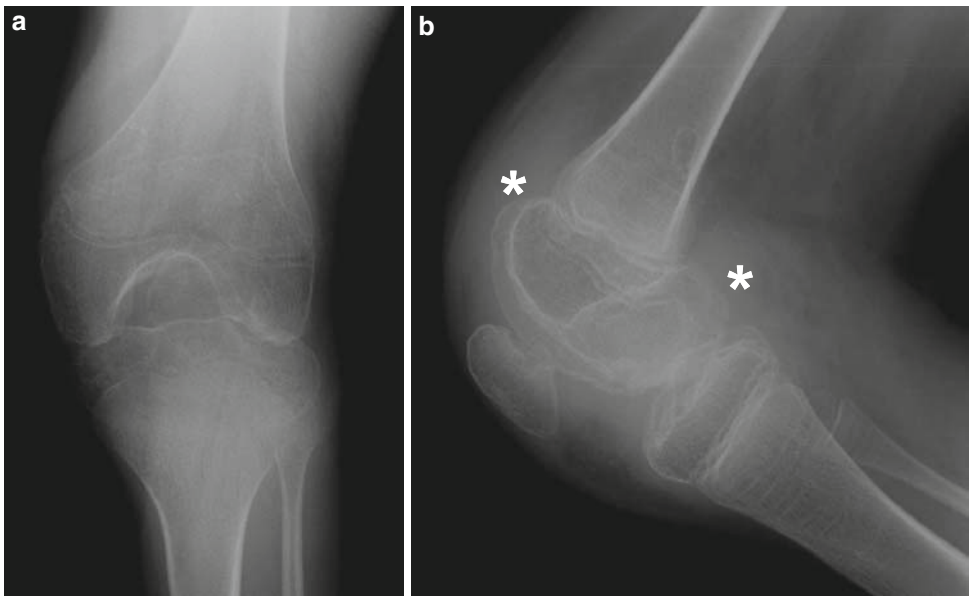

Fig. 11.48 AP radiograph (**a**) and lateral (**b**) of a child's knee with hemophilia. Note the enlargement of the epiphysis and widening of the femoral notch. Also note the hyperdense effusion (∗) related to recurrent hemorrhage

Hemophilia

Hemophilia is one of the oldest recorded diseases. It affects about 400,000 people worldwide and 20,000 in the United Sates. This bleeding diathesis actually represents two separate diseases: hemophilia A, a lack of clotting factor VIII, and hemophilia B or Christmas disease, resulting from a lack of clotting factor IX. Both are sex-linked diseases, making women asymptomatic carriers of the gene. Until the development of clotting factor replacement therapy, life expectancy for patients with hemophilia was around 11 years. Since the 1980s, replacement therapy has lengthened patients' lives to 50 or even 60 years.

Hemophilia is a serious disease where minor trauma permits life-threatening bleeding not only with external injuries but also into the body's potential spaces. Joints undergo continual minor daily trauma and so are prone to bleeding. In fact, hemarthroses occur in 75–90% of patients with hemophilia. The knees, ankles, and elbows are the joints most commonly affected. For obscure reasons, joints distal to the elbow and ankle are rarely affected, and hemarthroses diminish or disappear altogether as patient's age. Patients may also develop hemorrhage into their marrow space, resulting in pseudotumors of bone (Fig. 11.47). These are generally isolated lytic lesions with well-defined margins that may be confused radiographically with other true neoplastic lesions of bone.

Recurrent hemorrhage into a target joint leads to immediate inflammation and eventual deposition of ferritin within the joint. As episodes of hemorrhage begin around the age

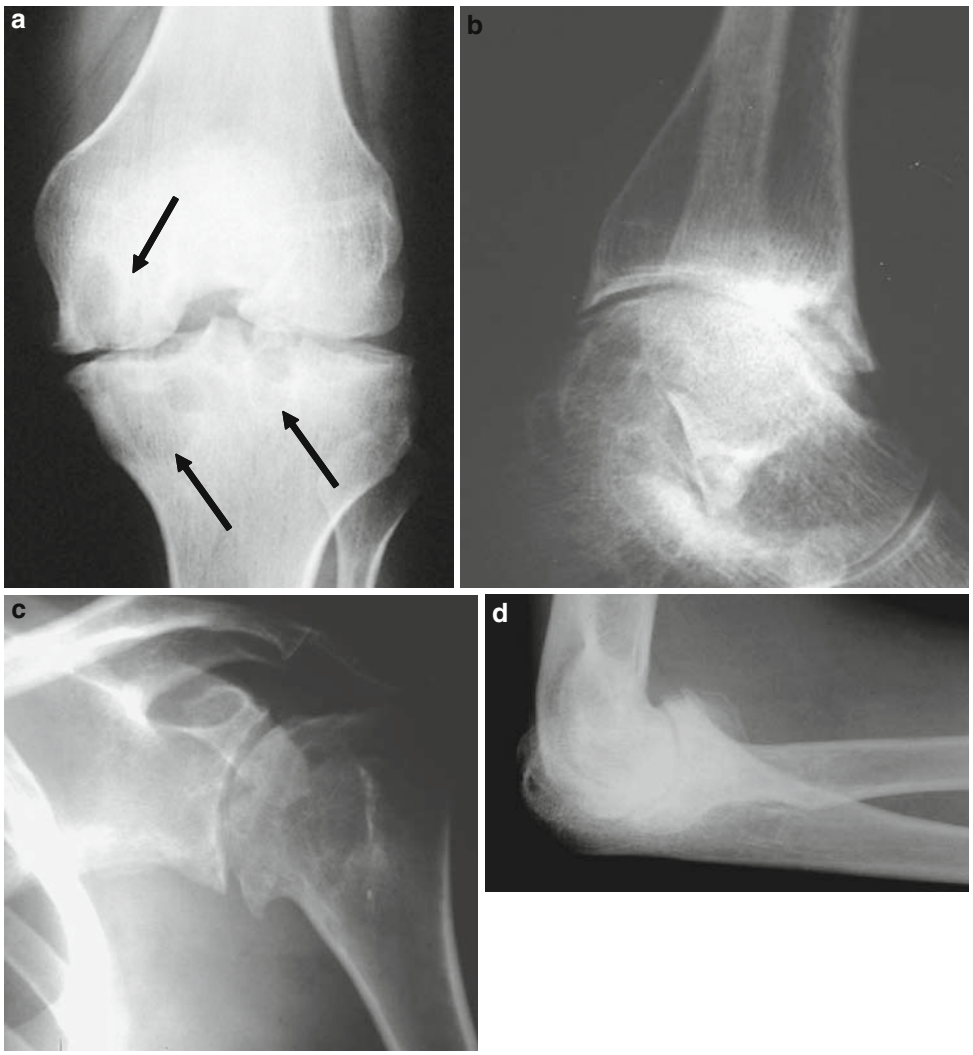

Fig. 11.49 Advanced hemophilic arthritis in knee (**a**), ankle (**b**), shoulder (**c**), and elbow (**d**). Note that it resembles closely routine osteoarthritis except that hemorrhagic subchondral cysts (*arrows*) may be more prominent in this disease than routine OA

of 2 years, the inflammation and increased blood flow to the bone around the joint will become apparent as local overgrowth on the adjacent epiphyses (Fig. 11.48) and early leg length discrepancies with the involved leg becoming longer than the uninvolved leg. Overgrowth of the femoral condyles leads to widening of the intercondylar notch, and overgrowth of the patella causes the appearance of squaring of its inferior pole. This last finding is evident in about 20–30% of juvenile patients with hemophilia. Similar hyperemic changes from inflammation in children with juvenile chronic arthritis (JCA) may also lead to epiphyseal overgrowth. Thus, JCA is a major radiological differential of hemophilic arthritis.

With recurrent hemorrhage and ferritin deposition, the tissues within and around the joint of hemophiliacs develop some increased density relative to the adjacent soft tissues on radiographs from the iron within the ferritin (Fig. 11.48). Further, as patients age, the recurrent bouts of inflammation ultimately lead to premature closure of the patient's physeal plates around the affected joint. This means that, once the patient reaches adulthood, an affected leg may be shorter than an unaffected leg. If the epiphyses close unevenly, the joints may develop deformities, e.g., Madelung deformities in the wrist or tibiotalar slant in the ankle. In addition, the chronic inflammation may lead to scarring in the soft tissues and flexion deformities about the target joint.

The appearance of hemophilic arthritis in the adult is essentially the result of the effect of ferritin deposition in the hyaline cartilage, lining the articular surfaces of the joint. As expected, the ferritin within the hyaline cartilage leads to sloughing of the cartilage and thus secondary osteoarthritis (Fig. 11.49). Subchondral cysts, often blood filled and related to recurrent intraosseous hemorrhage, figure prominently in adult hemophiliac osteoarthritis. MRI shows intraarticular hemosiderin to good effect (Fig. 11.50).

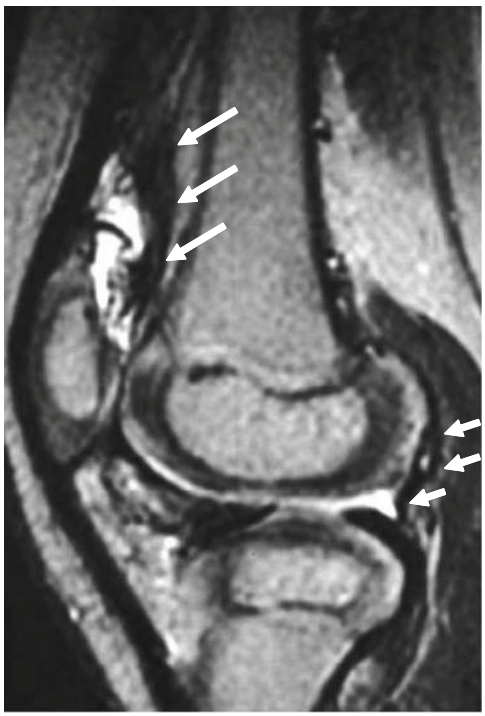

Fig. 11.50 Sagittal T1-weighted fat suppressed image from a knee of a child with hemophilia and recurrent hemorrhage. Note the thickened synovium (*arrows*) with nearly absent signal related to hemosiderin deposition from the recurrent hemorrhage

Hemochromatosis

Hemochromatosis has two major forms, one an autosomal recessive genetic inborn error of metabolism and the other an acquired form from exogenous iron overload as might result from hemolytic anemias or among the Bantu who use iron cookware exclusively. The genetic form of the disease results from a point mutation C282Y and causes defective HFE protein. This in turn leads to low transferrin and high levels of cellular iron saturation. Iron is deposited in many organs, most prominently the liver (Fig. 11.51), spleen, pancreas, brain, joints, and skin – 90% of patients have hyperpigmentation.

The genetic form of the disease is most common among northern Europeans and is more common in men than women. Symptoms may not appear for 30–50 years. This protean disease may have disastrous consequences, however. These include iron-induced cirrhosis and a high rate of hepatocellular carcinoma, type I diabetes secondary to pancreatic destruction of the islet cells in the pancreas, cardiomyopathy, and pituitary apoplexy.

Often the arthropathy becomes evident before other organ involvement and may be seen in as many as 50% of patients with hemochromatosis. Joint involvement may manifest itself as chondrocalcinosis (*vide supra*) or osteoarthritis. Similar to CPPD, hemochromatosis has a predilection for the second and third metacarpophalangeal joints (Fig. 11.52). Unlike CPPD, hemochromatosis arthropathy has a tendency to cause large "hook-like" osteophytes from the radial aspect of the metacarpal heads (Fig. 11.53). Although a relatively uncommon disease, it is prudent to suggest the diagnosis with the appropriate radiographic findings because the joint involvement may be a sentinel finding of the disease. Thus, diagnosing hemochromatosis from its radiographic musculoskeletal manifestations may be lifesaving.

Ochronosis

Ochronosis is a rare autosomal recessive genetic disease with over 70 described mutations that lead to ineffective homogentisic acid oxidase in the pathway of tyrosine catabolism. Lack of this enzyme leads to excessive production of homogentisic acid (*ortho-meta*-dihydroxyphenylacetic acid). This material is rapidly cleared by the kidneys and only a small amount remains in the tissues, but eventually it begins to accumulate, particularly in tissues with high cartilage content, i.e., synovial joints,

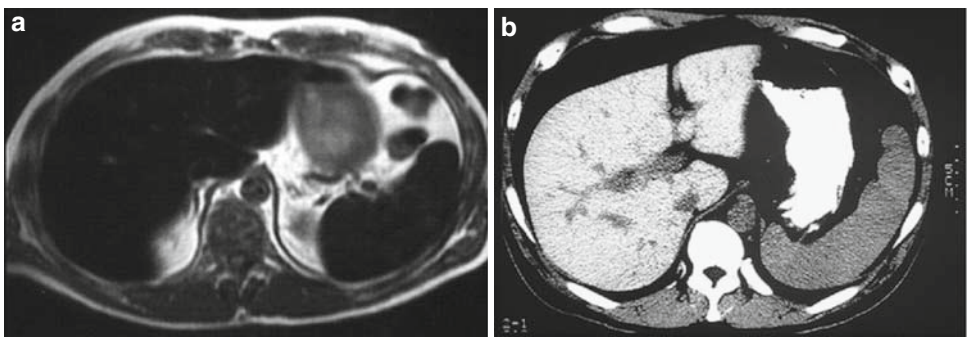

Fig. 11.51 T1-weighted MR of liver and spleen (**a**) showing marked loss of signal from hemosiderin deposition within the reticuloendothelial cells in these organs. CT scan image of the liver at the same level shows marked hyperdensity of the liver relative to the spleen

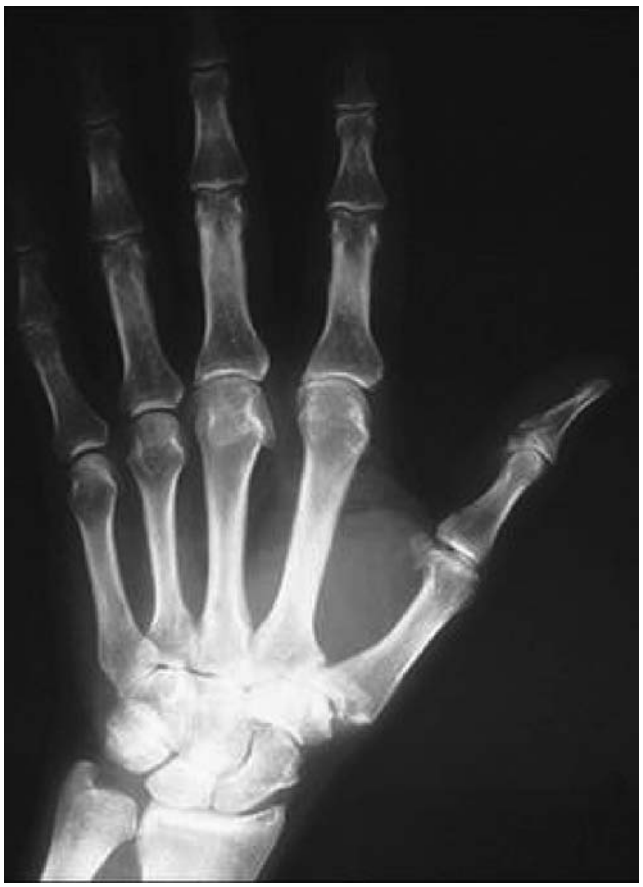

Fig. 11.52 PA radiograph of a hand with arthritis of the second and third MCP joints related to hemochromatosis. Note the resemblance to routine OA and CPPD arthropathy. The joints are narrow and marginal osteophytes are present

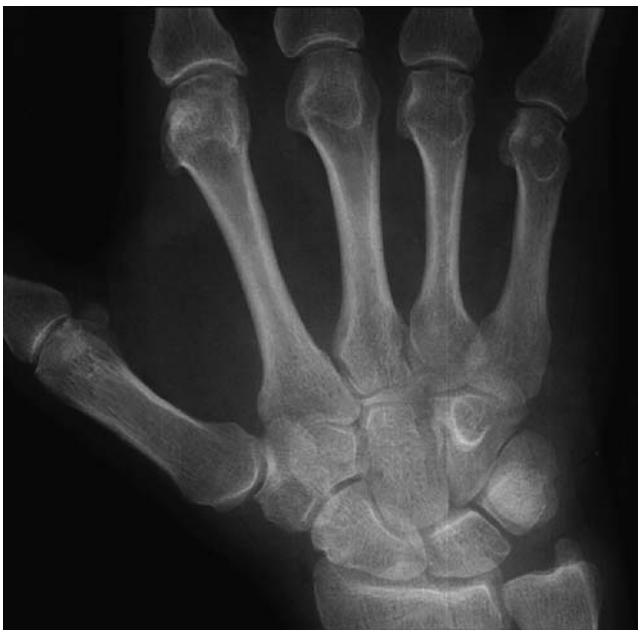

Fig. 11.53 PA radiograph showing arthritis of hemorochromatosis involving the second through the fourth MCP joints. Note the large hook-like osteophyte from the radial aspect of the second metacarpal head. This has been suggested as being a helpful diagnostic differentiating finding from CPPD arthritis

intervertebral disk spaces, the sclera of the eye, and the pinna of the ear.

Homogentisic acid is reactive on exposure to air and will oxidize into a black polymer. As a result, the typical first hint that the patient is afflicted with the disease will be black staining of the diapers by oxidized homogentisic acid excreted in the urine.

The eventual soft tissue accumulation of homogentisic acid, usually in the fourth decade of life, results in pigmentation changes and calcification in a number of structures. The synovial joints show chondrocalcinosis on radiography. The intervertebral disks calcify (Fig. 11.54a) as does the pinna of the ear (Fig. 11.55). The deposition of homogentisic acid leads to degeneration of the substrate tissues and produces secondary osteoarthritis and spondylosis (Fig. 11.54). Although life span is normal in this disease, patients will often have undergone joint replacement in their sixth decade and start to develop back problems with pain in their fourth decade that require surgical stabilization. The sclera begins to show a slate grey pigmentation from oxidized homogentisic acid accumulation in the sixth decade as well.

Destructive (Inflammatory) Arthropathies

Rheumatoid Arthritis

Rheumatoid arthritis (RA), as with many of the rheumatologic diseases, is a multisystem disease. The hallmark of RA is that it causes an inflammatory arthritis of varying severity. While officially listed as a disease of unknown etiology, certain epidemiologic and cell biologic evidence has suggested potential causes of this disease.

Rheumatologic diseases have a prevalence among Native Americans that is 5–7 times that of Caucasian Americans. Epidemiologic studies of Native American populations have shown that onset of new disease tends to come in outbreaks and to follow recent viral epidemics. In addition, the rheumatologic manifestations of disease in this population tend to show crossover among the classically described rheumatologic diseases. Finally, there is a prevalence of certain HLA markers in this population that appears to track down the western North American continent from the Aleutian land bridge into the southwestern United States and beyond. Nearly 60% of US patients with RA carry the

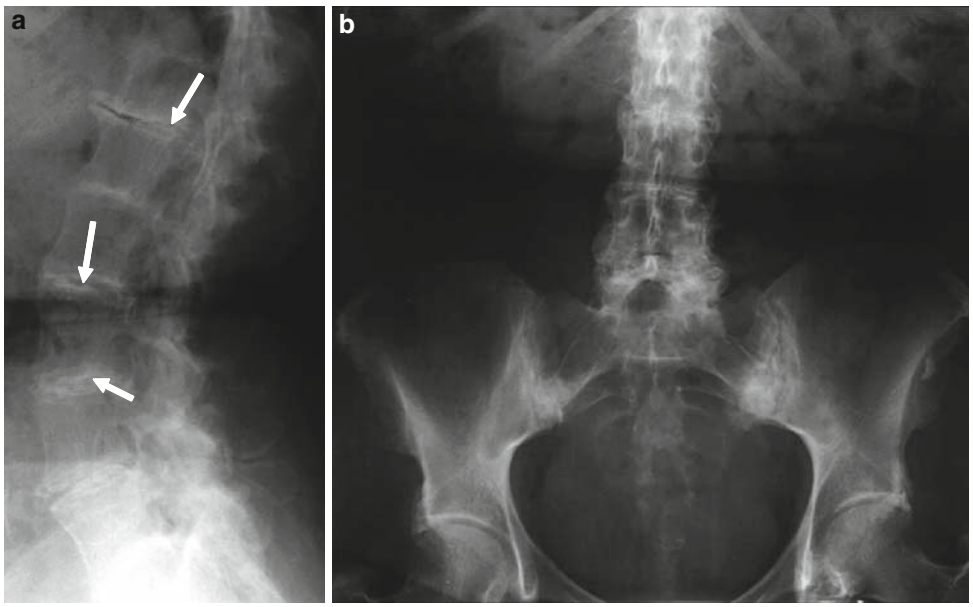

Fig. 11.54 Lateral (**a**) and AP (**b**) radiograph of the lumbar spine from a patient with ochronosis. Note the severe degenerative disk disease and the calcification in numerous disk spaces (*arrows*)

Fig. 11.55 Radiograph showing calcification within the pinna of the ear in a patient with ochronosis

so-called shared epitope of the HLA–DR4 cluster. In southern Europe, there is a high prevalence of HLA–DR1 cluster which also carries this shared epitope and confers risk for RA. Sequencing genes from families with RA has suggested the presence of several susceptibility genes and several resistance genes. These observations have led some to propose that rheumatologic diseases in general and RA in particular are abnormal cross-reactive antigenic responses to infectious agents in prepared hosts. That is to say that an autoimmune response against native tissues develops after viral infection. This response is facilitated by high susceptibility in certain populations with discrete overlapping HLA markers.

The inflammatory cascade that results from this apparent tissue misidentification is complicated and still only partially understood. Nonetheless, the disease causes inflammation in multiple tissues, including medium and small arteries, mesothelium, and synovium. Within joints and other synovial-lined structures, this gives rise to pannus formation. Thus, rheumatoid arthritis is a systemic, multi-organ disease that involves the lungs, the pleura, the myocardium, and of course the synovial and pseudo-synovial joints. Newer therapies are directed at interrupting the inflammatory cascade in RA. Most prominent in the current armamentarium of pharmaceuticals for treating RA are tumor necrosis factor-α (TNF-α) antagonists. It is hoped that this class of agents will prevent progression of disease as opposed to simply ameliorating symptoms.

RA tends to occur more in women than men in a ratio of about 2–3:1. The disease may appear at any time during life but has its peak incidence between 35 and 50 years of age. The majority of patients afflicted with RA (75%) have intermittent disease with flares and periods of remission in their joints. Another 20% have chronic mild ongoing inflammation, and about 5% will have severe progressive deforming disease. Since the severity and behavior of RA varies from patient to patient and is often insidious in onset, diagnosis can be difficult. The American College of Rheuma-

Table 11.5 American College of Rheumatology Criteria for diagnosis of rheumatoid arthritis.

1. Morning stiffness: This occurs in and around the joints and lasts at least 1 hour before maximal improvement.
2. Arthritis of three or more joint areas: At least three joint areas simultaneously have soft tissue swelling or fluid (not bony overgrowth) observed by a physician. The 14 possible areas are right and left proximal interphalangeal (PIP), metacarpophalangeal (MCP), wrist, elbow, knee, ankle, and metatarsophalangeal (MTP) joints.
3. Arthritis of hand joints of at least one area swollen in a wrist, MCP, or PIP joint
4. Symmetric arthritis with simultaneous involvement of the same joint areas on both sides of the body: Bilateral involvement of PIPs, MCPs, and MTPs is acceptable without absolute symmetry.
5. Rheumatoid nodules: Subcutaneous nodules are present over bony prominences or extensor surfaces or in juxtaarticular regions.
6. Serum RF: Abnormal amounts of serum RF are demonstrated by any method for which the result has been positive in fewer than 5% of healthy control subjects.
7. Radiographic changes typical of RA on posteroanterior hand and wrist radiographs, which must include erosions or unequivocal bony decalcification localized in or most marked adjacent to the involved joints: Osteoarthritic changes alone do not qualify.
These criteria are intended as a guideline for classification of patients. A patient may be diagnosed as having RA if 4 of the 7 conditions above are met.
To count: The first 4 conditions must be present for at least 6 weeks. A physician must observe criteria 2–5.

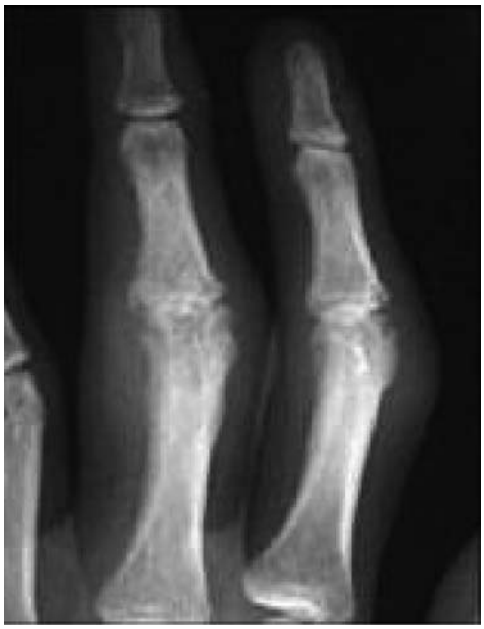

Fig. 11.56 Oblique radiograph of the third and fourth PIPs showing erosions and periarticular swelling in RA

tology has established a set of clinical criteria to establish the diagnosis (Table 11.5). Even so, newer serologic markers besides rheumatoid factor that have the promise of increasing the accuracy of early diagnosis of RA are becoming known. Chief among these is anti-cyclic citrullinated peptide (CCP). This marker, alone or in combination with rheumatoid factor, promises clinical diagnostic accuracies for RA of around 95%.

RA is a disease with many different clinical subtypes and imaging characteristics. All share certain features, including symmetry and inflammation. The inflammation tends to occur episodically with periods of remission. RA is one of three of the more common arthropathies, including gout and multicentric reticulohistiocytosis, that give rise to nodules. In the case of RA, the nodules tend to occur along the extensor surfaces (Fig. 11.6). These are more common with chronic disease and pathologically represent granulomas. More commonly, RA causes radiographically apparent soft tissue swelling, primarily around joints (Fig. 11.56). MRI is more sensitive than radiographs for the detection of capsular swelling (Fig. 11.57). In addition, MRI is very useful for detecting involvement of tendon sheaths and other synovial-lined spaces (Fig. 11.58).

As inflammation progresses in RA, the joints develop misalignments. The metacarpophalangeal joints in the hands develop ulnar drift (Fig. 11.59). Heavily affected joints may subluxate or dislocate entirely (Figs. 11.59 and 11.62d). To a lesser extent, the metatarsophalangeal joints in the feet develop a similar lateral deformity. The PIP and DIP joints are also subject to alignment abnormalities. These are a combination of the architectural instability from the internal joint destruction within the joint and inflammation and scarring of the extensor mechanisms in the digits. These lead to characteristic deformities. The boutonnière deformity (Fig. 11.10) has fixed flexion deformity at the PIP and hyperextension at the DIP. Swan neck deformities have hyperextension at the PIP and flexion at the DIP (Figs. 11.9 and 11.60). This last deformity is perhaps the most crippling because it leaves the digit nearly useless.

Unlike many of the inflammatory arthropathies, RA causes inflammation not only within a joint but also in the bone surrounding the joint. The result is that the bone adjacent to the inflamed joint often will lose bone mineral and may appear as osteopenic on radiographs (Fig. 11.11). While this finding is highly touted as being part of RA, it may be difficult to use in practice because these patients are often older and already diffusely osteopenic. Moreover, as the disease progresses, whether from continued inflammation or disuse of the affected part, the bones tend to become diffusely osteopenic (Figs. 11.61).

The inflammation in RA causes prominent synovitis and pannus formation. MRI is exceptionally sensitive for detection of synovial proliferation (Figs. 11.57 and 11.58) and further for detection of active inflammation, particularly after administration of a gadolinium contrast agent (Fig. 11.58).

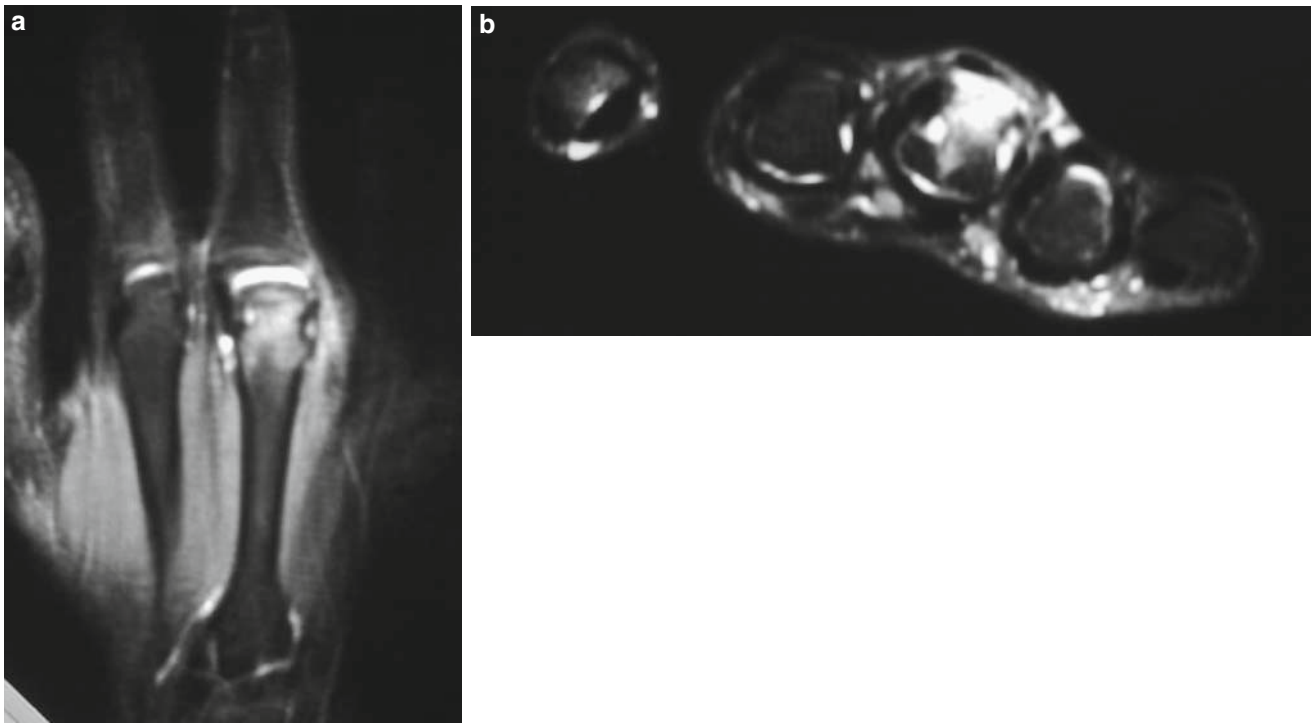

Fig. 11.57 T2-weighted fat suppressed coronal (**a**) and axial (**b**) image showing joint effusion in the third MCP and edema within the marrow of the third metacarpal head in early RA

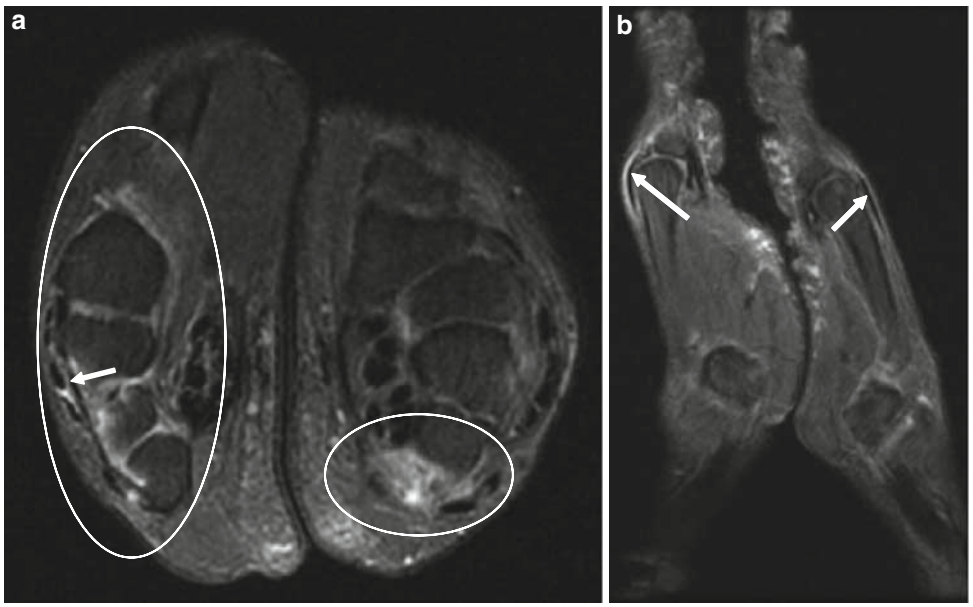

Fig. 11.58 Axial (**a**) and sagittal (**b**) T1-weighted fat suppressed MR images, obtained after intravenous gadolinium administration, showing synovitis of the wrist joint (*ovals*) and extensor tenosynovitis (*arrow*)

The general progression of the joint-centered disease follows a peripheral to central course radiographically even though the entire joint is undergoing destruction during bouts of inflammation. The reasons that changes are first apparent in the periphery of the joint are first that the margins of the joint have no hyaline cartilage over the cortex, and so radiographic bone erosion will become apparent there first. Second, a small annular organelle in the joint margin reabsorbs synovial fluid under normal conditions. This reabsorption creates a natural flow of fluid toward the joint margins and

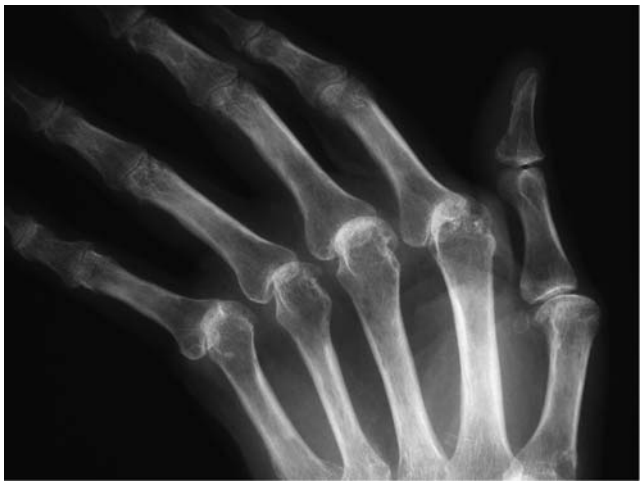

Fig. 11.59 PA radiograph of the hand showing ulnar deviation with dislocation of the second, third, and fifth MCP joints and severe subluxation of the fourth MCP joint. This last MCP maintains some degree of parallelism of the articular surfaces while the others do not, indicating that it has not entirely dislocated

becomes a collecting site for inflammatory cells. The result is that the earliest joint space findings in RA will be marginal erosive changes (Fig. 11.63).

As the disease progresses and the hyaline cartilage in the more central portion of the joint is lost, the erosions tend to move toward the central portion of the joint (Fig. 11.64). At the same time, the involvement of the joint with its concomitant cartilage destruction leads to uniform and progressively severe joint space narrowing (Fig. 11.65). Some erosive change leads to subchondral cyst formation (Fig. 11.66). In fact, there is a form of RA, know as robust RA, that shows prominent cystic changes and fewer erosions (Fig. 11.67). This form of the disease tends to affect men more than women and has a more benign course, in general, than typical erosive RA.

Early erosive change may be difficult to detect, especially if the viewer is not alert to subtle cortical loss known as dot–dash or Morse code cortex (Fig. 11.63). This represents the earliest radiographically detectable findings. In addition, certain regions, e.g., the styloid process of the ulna, tend to show changes early in the disease, perhaps, because tenosynovitis often may precede joint inflammation (Fig. 11.68). In fact, as mentioned, MRI may show inflammatory changes long before osseous erosion is apparent. Although MRI may easily show erosive disease (Fig. 11.69), it is likely that its important clinical role, now that TNF-α antagonist medictions are available, will be detection of early synovial changes (Figs. 11.57 and 11.58) before osseous destruction is apparent.

With one prominent exception, severe joint destruction from adult RA typically does not lead to pathologic ankylosis of the involved joints. That exception is the wrist where

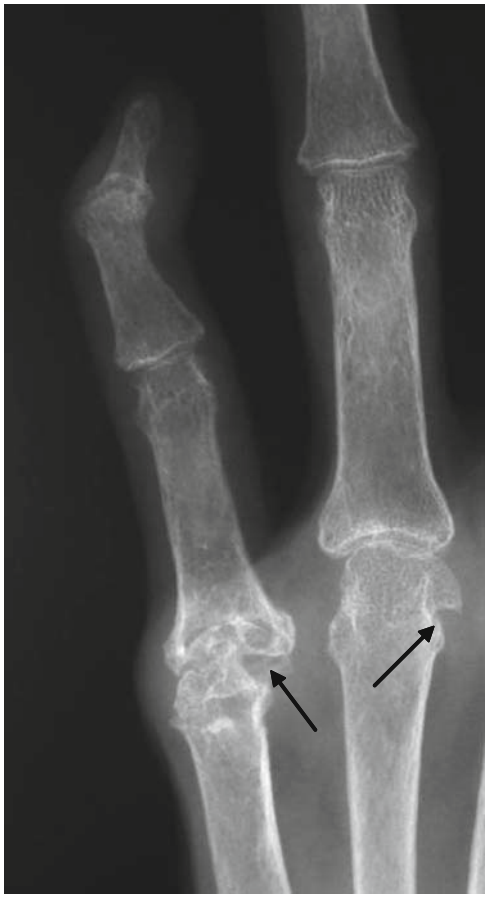

Fig. 11.60 PA radiograph of the fourth and fifth digit showing a swan neck deformity of the fifth digit (hyperextension at the PIP and flexion at the DIP joints) and joint space narrowing and erosions of the fourth and fifth MCP joints (*arrows*)

severe long-standing disease often leads to bone ankylosis (Fig. 11.70).

RA affects the metacarpophalangeal joints, the wrist, the knees (Fig. 11.71), the subtarsal joint, and the metatarsophalangeal joints in more than 80% of patients (Fig. 11.72). It affects the hips (Fig. 11.73), shoulders and acromioclavicular joints (Figs. 11.74, 11.75 and 11.76), elbows (Fig. 11.77), the ankle and subtalar joints (Fig. 11.78), and the cervical spine, particularly the atlantoaxial joint (Figs. 11.79, 11.80 and 11.81) in about 50% of patients. The temporomandibular joints and the sternoclavicular joints are affected in about a third of patients. The sacroiliac joints, on the other hand, are involved in less than 5% of patients, a distinguishing feature from the spondyloarthropathies.

Typically the distribution of erosive changes in RA is symmetrical. When one hip is involved, it is likely that the other will be as well and to a similar degree. The distribution of joint involvement in one hand and wrist will closely mirror the other. The one exception to this rule is in paralyzed patients where, for unknown reasons, the disease tends not to involve the paralyzed limb.

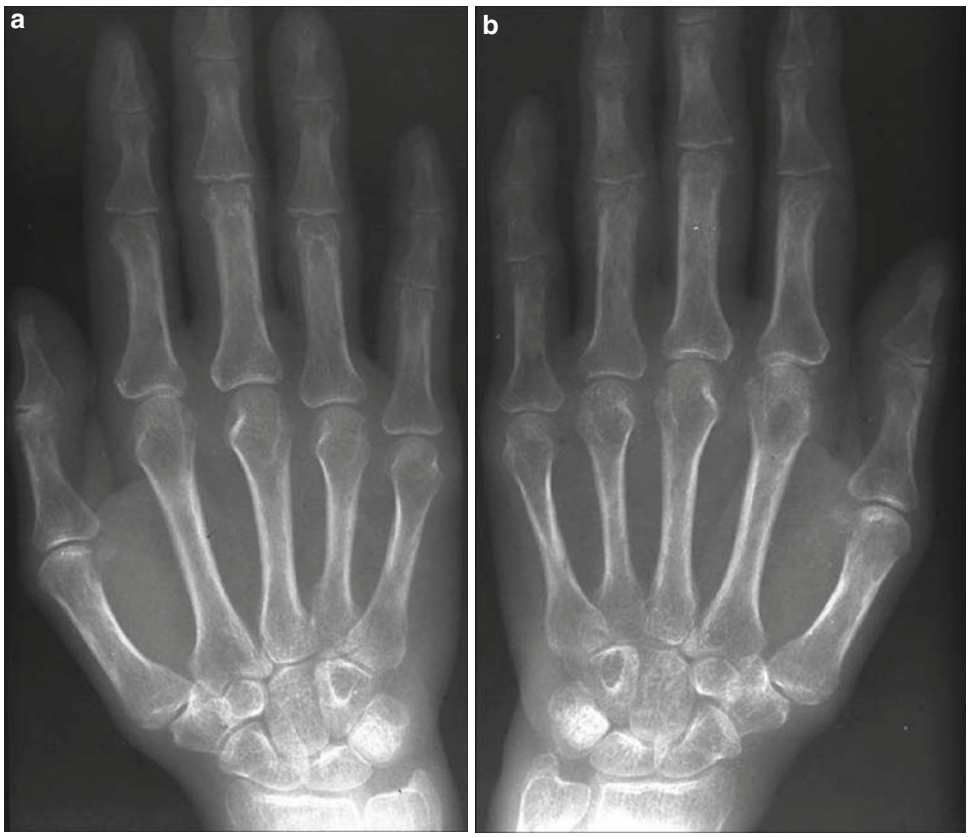

Fig. 11.61 PA radiographs of a patient with early rheumatoid arthritis showing profound periarticular osteopenia

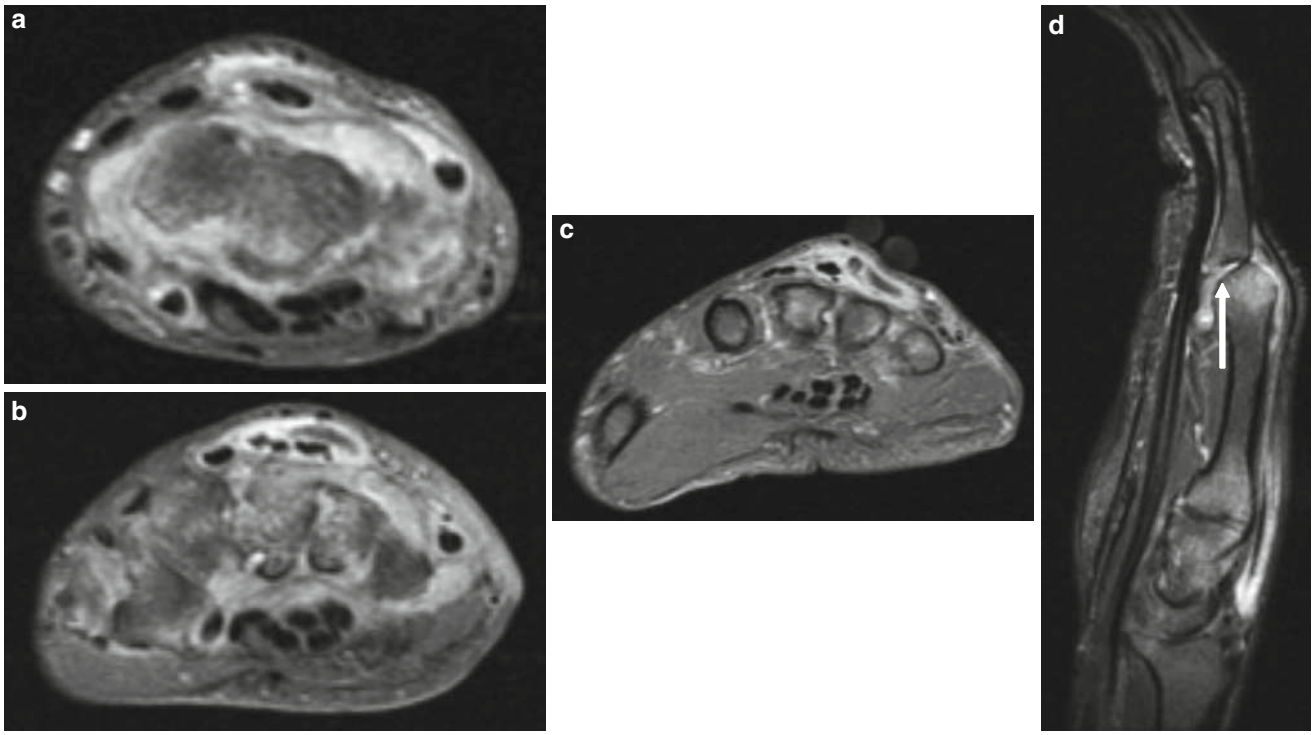

Fig. 11.62 Three axial (**a–c**) and a single sagittal (**d**) T1-weighted fat suppressed MR images after administration of gadolinium of a wrist in a 38-year-old woman showing marked synovial enhancement of the carpal joint and multiple tendon sheaths. Note the volar subluxation of the third MCP joint (*arrow*)

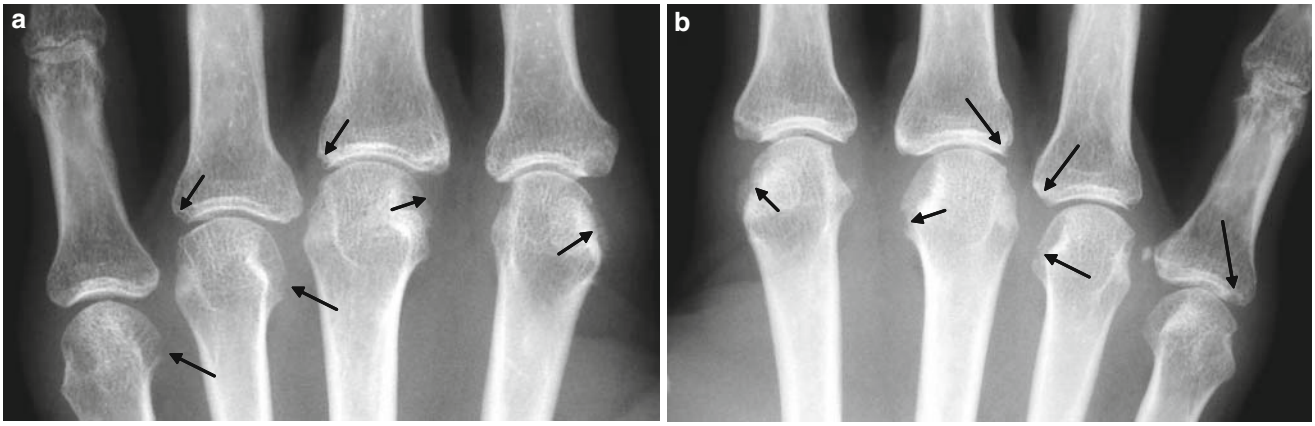

Fig. 11.63 PA views of the left (**a**) and right (**b**) MCP joints of a patient with early RA and multiple early peripheral joint erosions. While some of the erosions present here are easily seen, others are very subtle as in the radial aspect of the right second and fifth and the left second metacarpal heads (*arrows*)

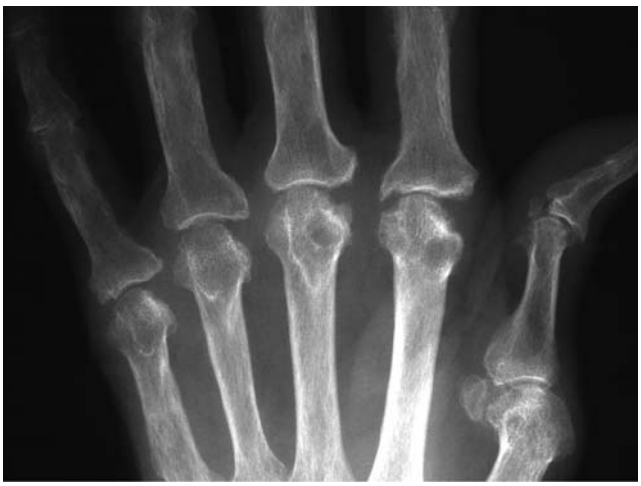

Fig. 11.64 PA radiograph of the left hand in a patient with moderate erosive disease and somewhat more advanced than in Fig. 11.63

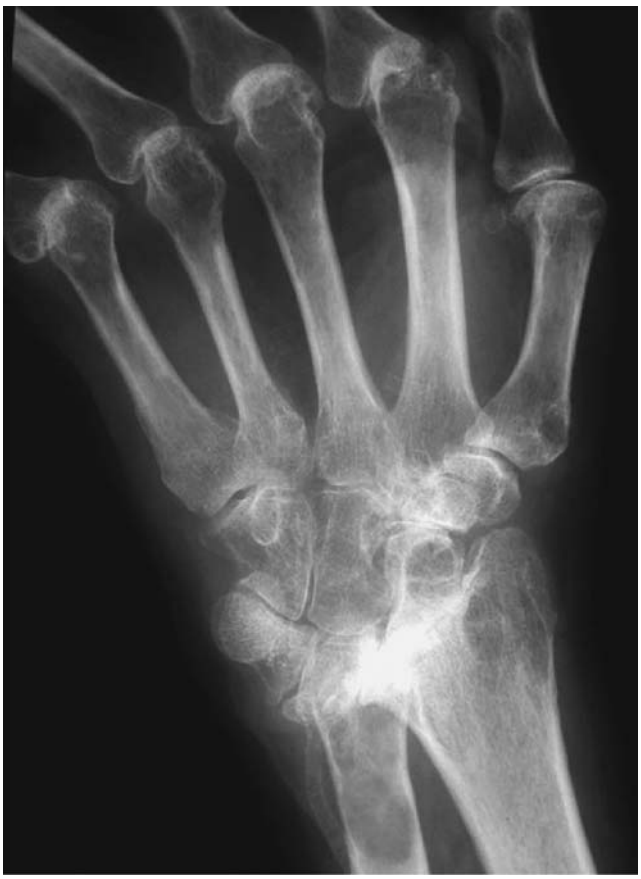

Fig. 11.65 PA radiograph of the left wrist showing moderately severe erosions, uniform joint space narrowing and early subluxation of the second through fifth MCPs. Note the severe narrowing and erosion of the radiocarpal joint space with ulnar translocation of the carpus on the radius

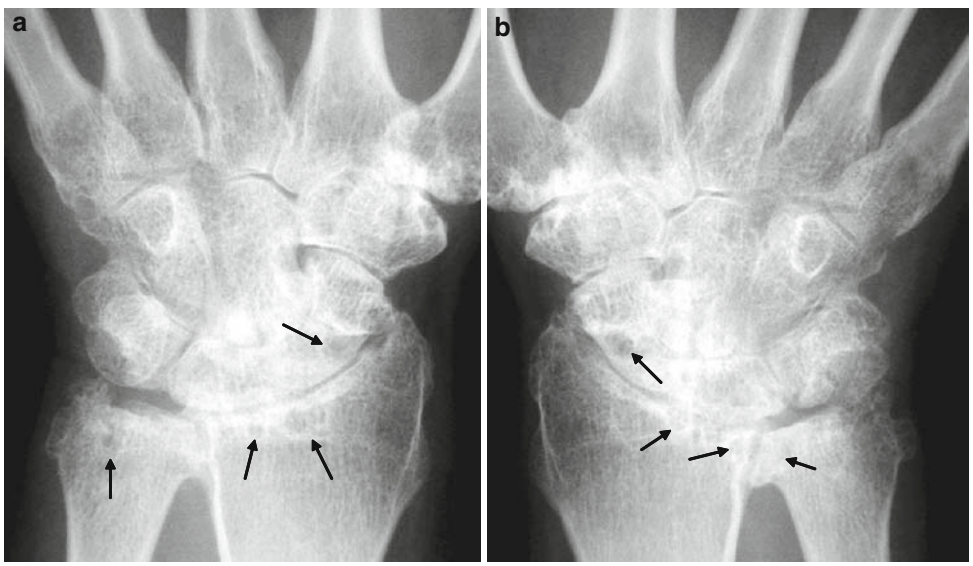

Fig. 11.66 PA radiographs of the left (**a**) and right (**b**) wrists showing severe joint space narrowing and subchondral lucencies consistent with cyst formation (*arrows*) in RA

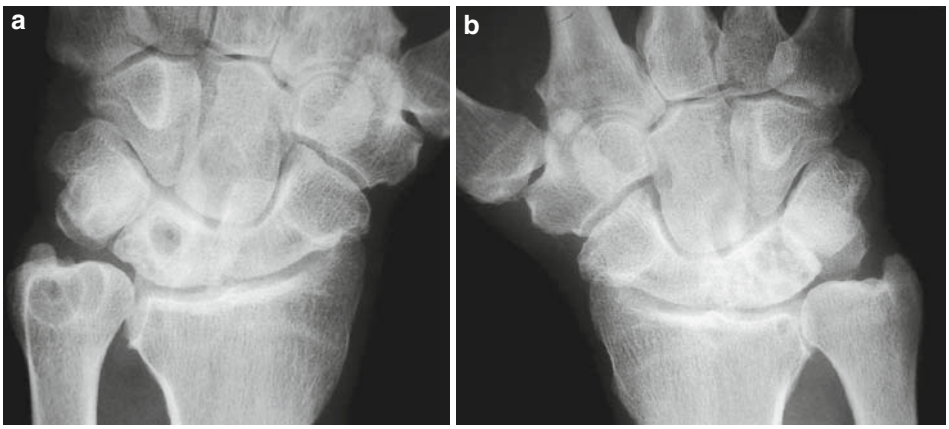

Fig. 11.67 PA radiographs of the left (**a**) and right (**b**) wrist showing prominent subchondral cyst formation and relatively few erosions in a patient with robust RA. Note the sclerosis of the right lunate. The patient also had early avascular necrosis of the lunate (Kienböck's disease)

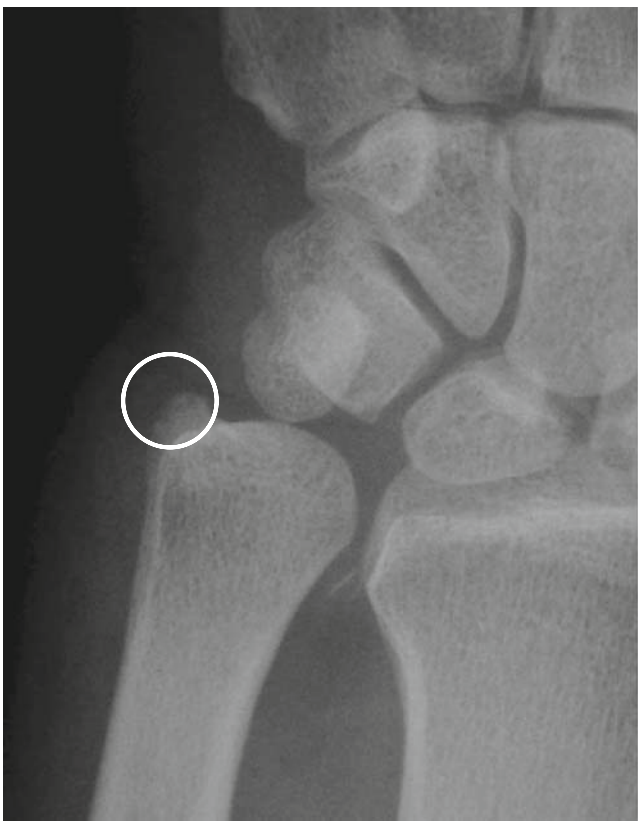

Fig. 11.68 PA radiograph showing early erosion of the ulnar styloid in RA (*circle*)

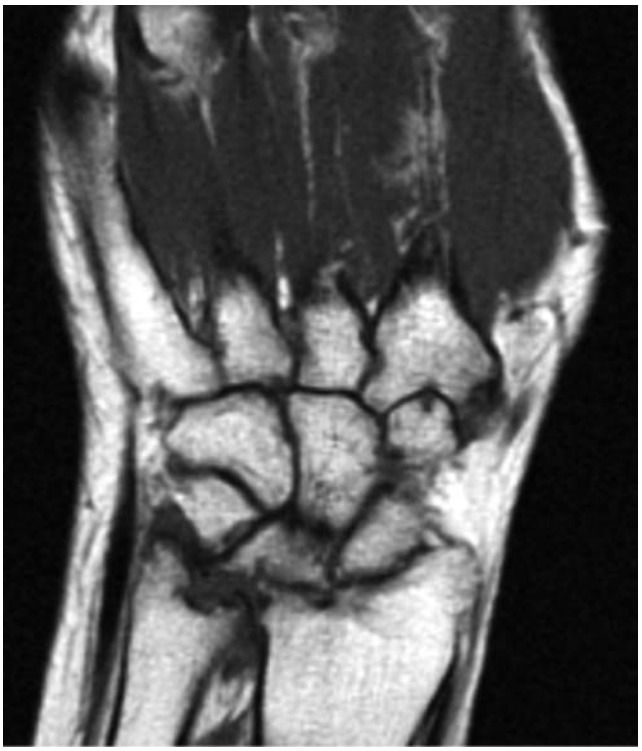

Fig. 11.69 T1-weighted coronal MR image of the wrist in a patient with RA showing marked erosive changes and partial collapse of the radioscaphoid and distal radioulnar joints

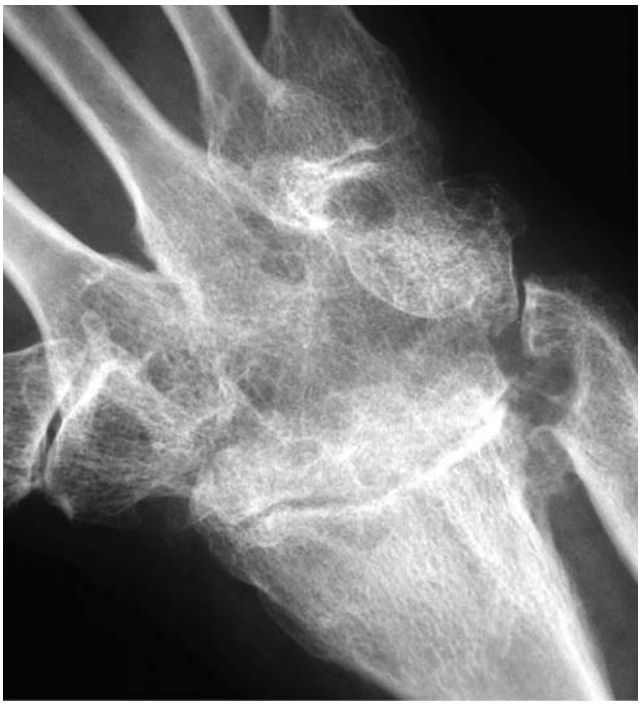

Fig. 11.70 PA radiograph from a patient with severe RA of the wrist with ankylosis of the carpal bones

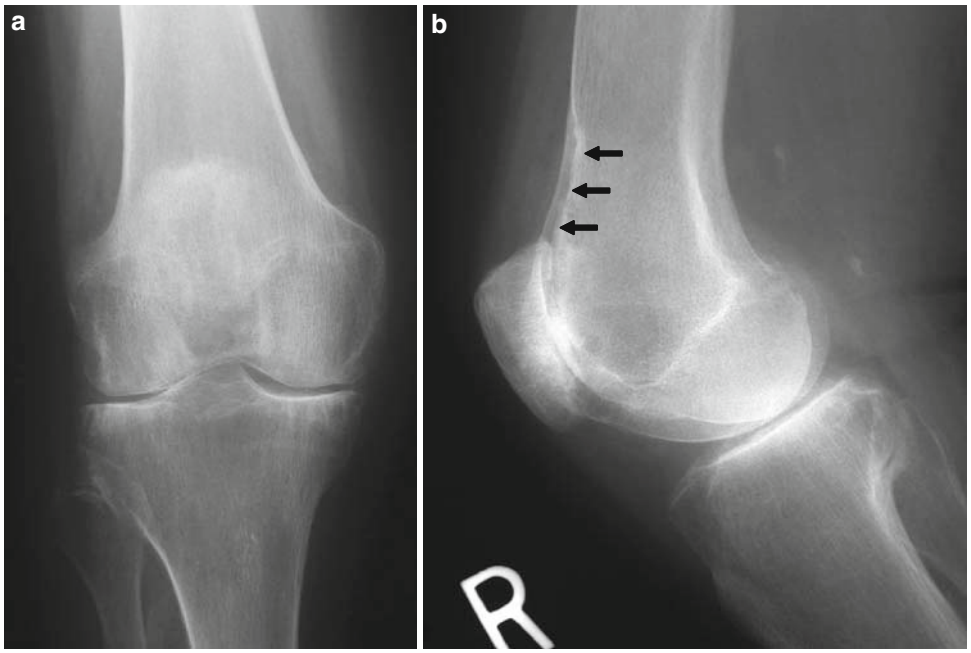

Fig. 11.71 AP (**a**) and lateral (**b**) radiograph of the right knee in a patient with RA showing joint space narrowing without osteophyte formation, subtle cortical irregularity typical of large joint disease. Note the saucerization of the anterior femur (*arrows*) just superior to the patella. This represents "pressure" erosion often noted in locations where bursae or joint recesses abut bone. The inflammation in the bursa, abetted by the motion of the patella, has caused this bone remodeling

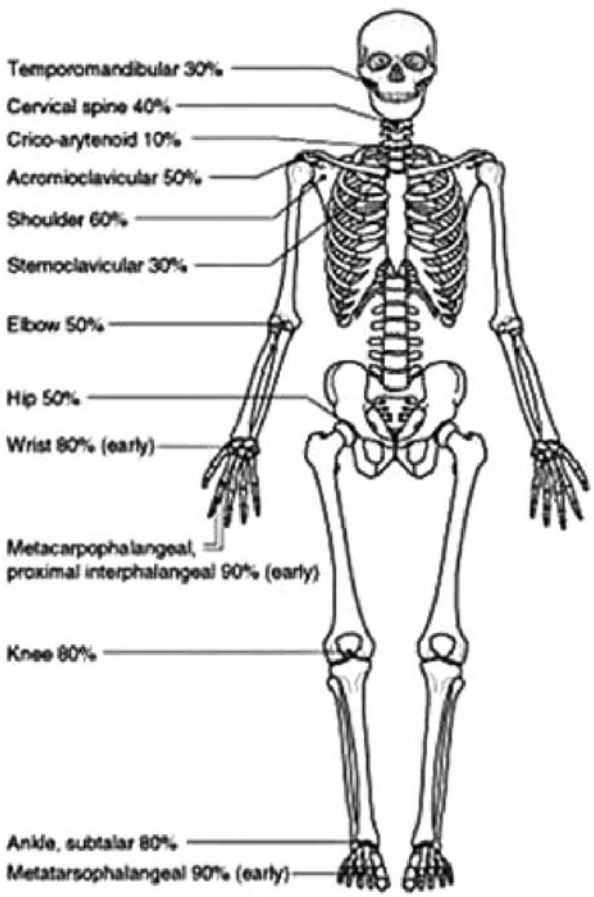

Fig. 11.72 Schematic showing frequency distribution of joint involvement with RA

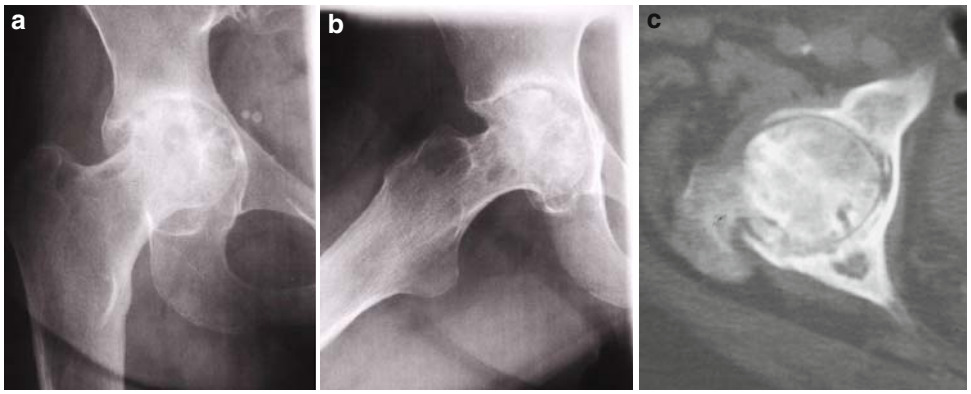

Fig. 11.73 AP (**a**), frog's leg lateral (**b**), and CT image of the hip with RA. The hip joint is narrowed along the axis of the femoral neck. The joint space has multiple erosions and cortical irregularity consistent with inflammatory disease. The medial wall of the acetabulum is slightly convex into the pelvis, consistent with remodeling and giving an appearance of protrusio acetabuli

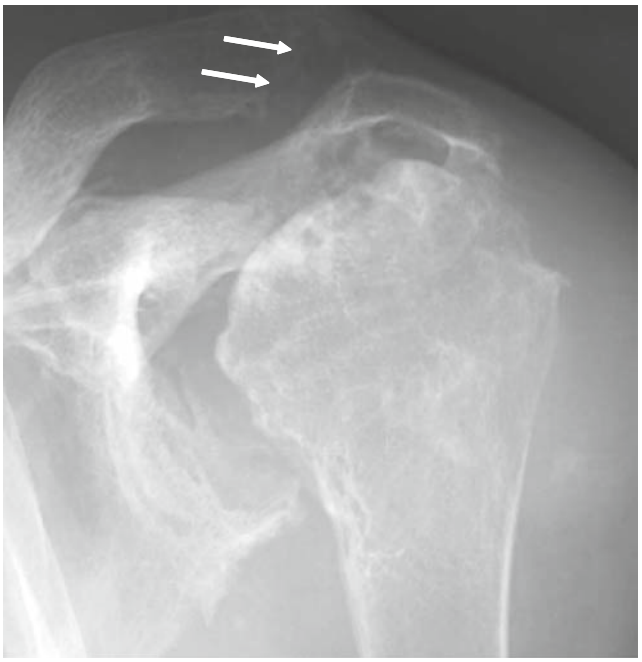

Fig. 11.74 AP radiograph of the shoulder in a patient with advanced RA showing erosive changes involving the glenohumeral joint and the distal end of the clavicle (*arrows*). This latter finding, when bilateral, is suggestive of RA or hyperparathyroidism. In this case, the changes in the glenohumeral joint make the diagnosis of RA

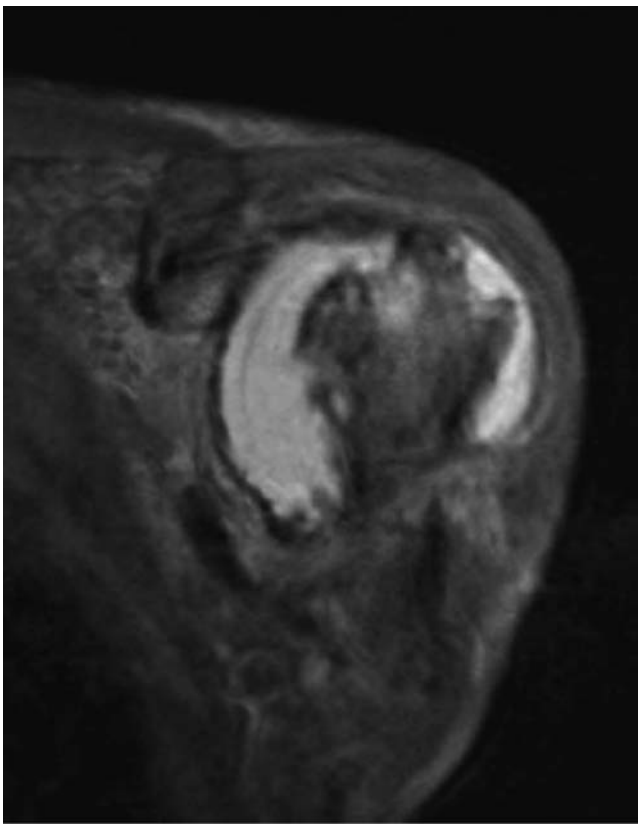

Fig. 11.75 Coronal T2-weighted fat suppressed MR image of a patient with RA showing complete loss of the rotator cuff, marked erosive changes in the glenohumeral joint and at the greater tuberosity and a joint effusion

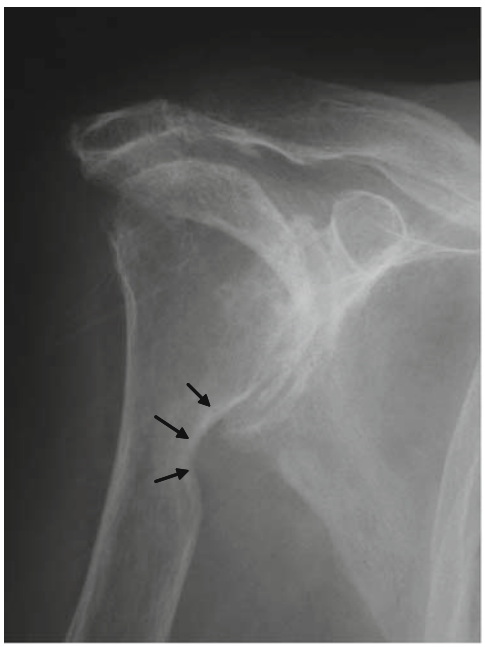

Fig. 11.76 AP radiograph of a patient with RA showing a large pressure erosion (*arrows*) of the medial humerus. As in the knee, this saucerization is caused by the inflammation in the adjacent recess abetted by the impingement of the superiorly subluxed humerus against the inferior glenoid. The superior subluxation of the humerus is the result of inflammatory tearing of the rotator cuff

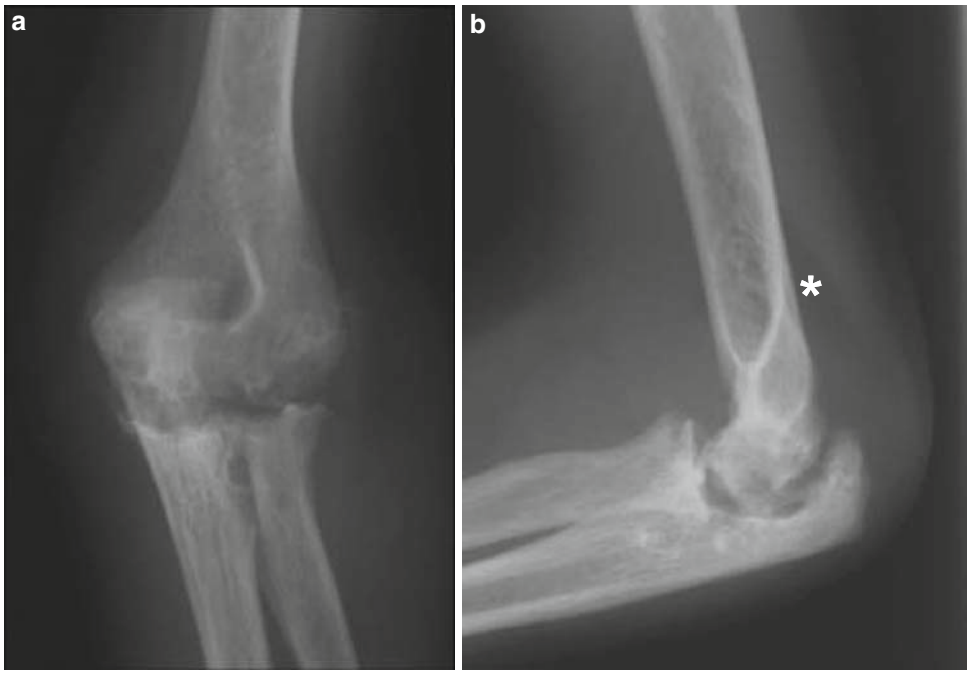

Fig. 11.77 AP (**a**) and lateral (**b**) radiograph of the elbow in RA showing severe erosive changes in the radial head, ulna, and distal humeral joint surface. Note the large effusion as indicated by the visible posterior fat pad (∗) on the lateral image

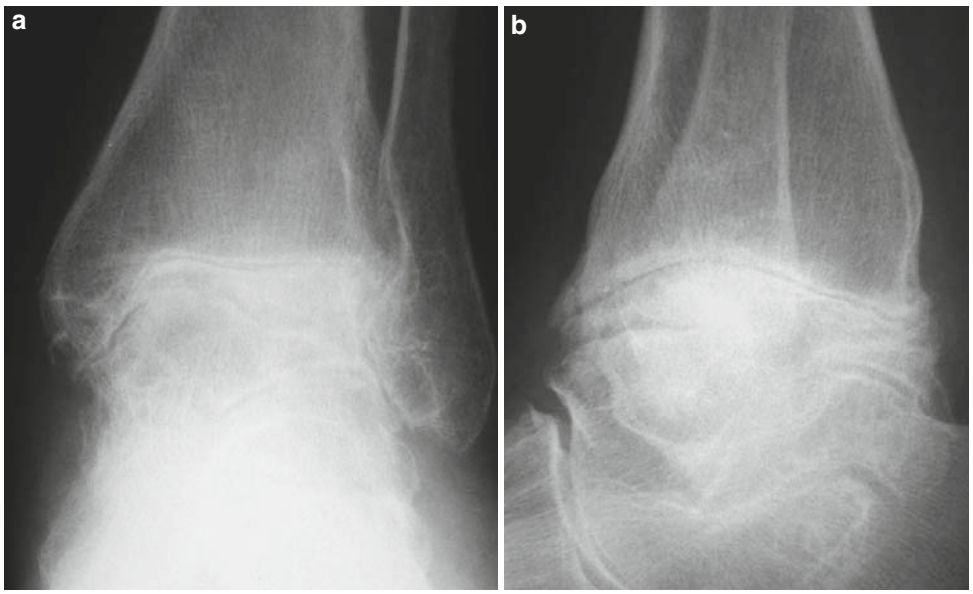

Fig. 11.78 AP (**a**) and lateral (**b**) radiograph of the ankle in RA showing uniform joint space narrowing without significant osteophyte formation. The articular cortices show irregularities consistent with erosions. A pressure erosion is present in the distal medial fibula adjacent to the distal lateral tibia (**a**). The tibia shows some mild periosteal reaction (**b**), a finding that is unusual for RA

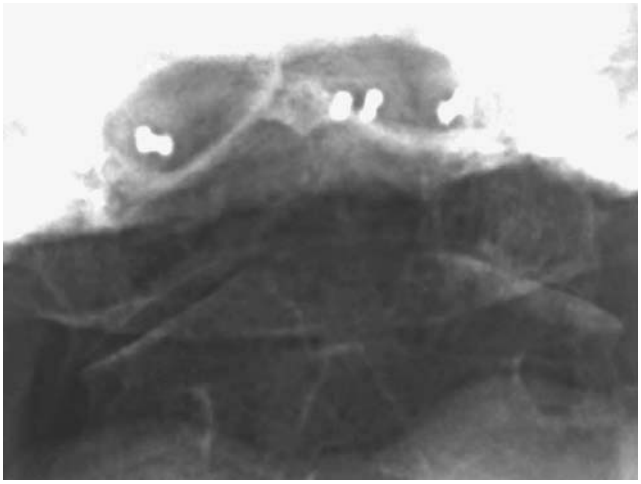

Fig. 11.79 Open mouth view of the cervical spine showing poor visualization of the odontoid secondary to severe erosion

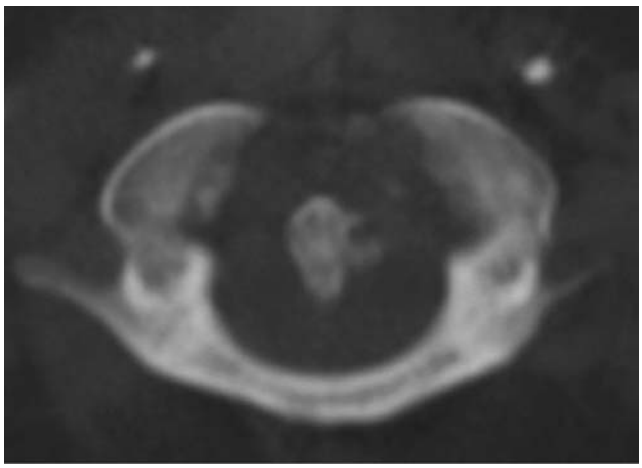

Fig. 11.80 CT scan image at the level of the odontoid in RA. The odontoid is eroded and displaced posteriorly into the center of the ring of C1 indicating post-inflammatory rupture of the posterior transverse ligament. This indicates instability and is potentially life threatening

As a result, some typical patterns of disease emerge. Bilaterally symmetric erosive arthropathy involving the wrists and the metacarpophalangeal joints is most common in RA (Figs. 11.61, 11.63 and 11.66). Bilateral glenohumeral erosive arthritis with acromioclavicular (AC) joint arthropathy, the latter giving the radiographic appearance of distal clavicular resorption, is a common pattern detected on routine chest radiographs. Among the most life-threatening findings of disease is development of atlantoaxial subluxation from erosive changes to the odontoid and inflammation-induced laxity of the posterior transverse ligament at this joint (Table 11.6 and Fig. 11.81). All cervical spine studies in patients with RA should be examined for atlantoaxial subluxation since about 10% of these patients will develop cord compression related to this problem.

Finally, certain findings help to limit the differential. The presence of nodules, particularly in a characteristic location suggests RA. Rice bodies form in some joints involved by RA (Fig. 11.82). These are fibrin globules, once most commonly seen in tuberculous arthritis, but now most commonly seen in RA and less commonly in other seronegative arthritides. RA may also cause erosive changes at the superior margins of the ribs related to inflammation of the insertions of the accessory muscles of respiration. Appropriate systemic organ involvement, including the lungs and heart, may also suggest the diagnosis. On the other hand, some findings militate against a diagnosis of RA. As mentioned, sacroiliac joint involvement is uncommon in RA. Similarly, adult RA uncommonly involves the thoracic and lumbar spines. Ankylosis also occurs rarely in RA except in the carpus. Periosteal reaction, while common in psoriatic arthritis, is rare in RA. Thus, with careful attention to detail, the correct choice of imaging modalities, it is possible not only to diagnose the RA but to estimate its activity in each involved joint.

Juvenile Chronic Arthritis (JCA)

Once called juvenile rheumatoid arthritis (JRA), this classification has expanded to include virtually all childhood inflammatory arthropathies (Table 11.7). Included are JRA and Still's disease (seronegative chronic arthritis), representing about 70% of patients, juvenile ankylosing spondylitis (may be impossible to distinguish radiographically from the adult form), psoriatic arthritis or inflammatory bowel disease, and finally juvenile onset adult type RA.

By definition, the most common form of JCA, seronegative JRA, has its onset before age 16. As with adult RA, it affects girls more often than boys in a 2:1 ratio. It is also seen more frequently in Caucasian children than Black children. It often resolves with age but may leave significant residual joint damage. JRA has three main forms: pauciarticular, polyarticular, and Still's disease.

The pauciarticular form is the most common type of JRA and has two clinical subtypes: type I which is more common in girls and established by a positive ANA serum laboratory examination and type II which is seen in older HLA-B27 positive children, mostly boys. It has its onset generally before age 8. Pauciarticular JRA, by definition, has fewer than five joints affected, and these are generally large joints, such as the hips or knees.

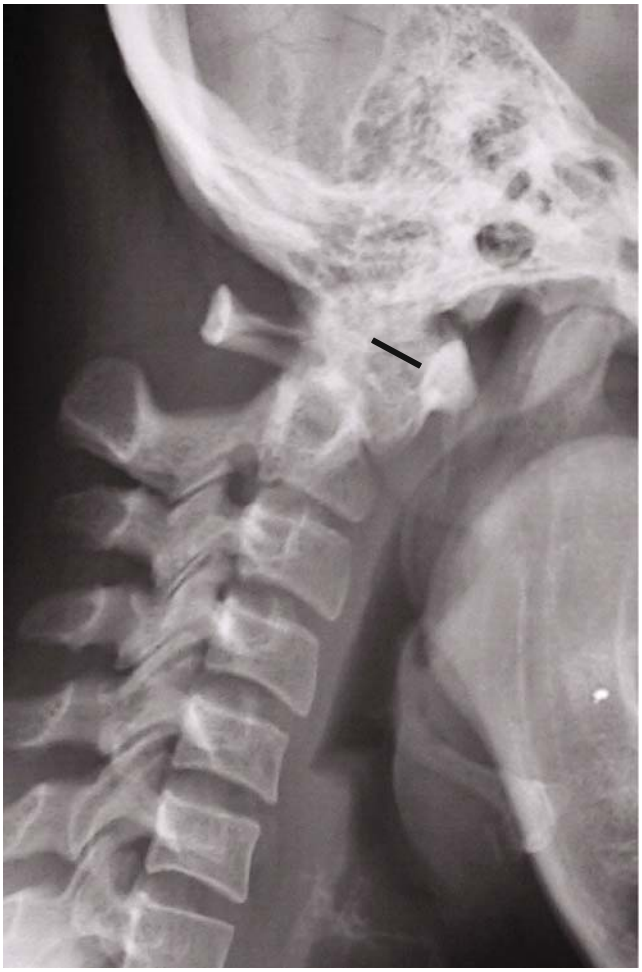

Fig. 11.81 Lateral flexion radiograph of the C1–C2 levels showing atlantoaxial subluxation (atlantoaxial distance greater than 3 mm) in a patient with RA (*line*). This serious complication may be life threatening

The radiographic findings in this form of the disease may be difficult to distinguish from a joint involved by hemophilia. Radiographs may show periarticular soft tissue swelling, osteopenia, periosteal new bone formation, and overgrown epiphyses (Fig. 11.83). As with hemophilia, the knee may show widening of intercondylar notch and squaring of the inferior pole of the patella. The inflammation may eventually lead to premature skeletal maturation. This in turn causes leg length discrepancies and small vertebral bodies (Fig. 11.84). The inflammation may also cause irregular physeal closure. This can give an appearance of tibiotalar slant in the ankle from premature fusion of one side of the distal tibial epiphysis or Madelung's deformity in the wrist (Fig. 11.85) from premature closure or the ulnar aspect of the distal radial epiphysis. Erosions are often a late fining in JRA and unlike adult RA, joint fusion may be a prominent complication in severe cases (Figs. 11.84, 11.86, 11.87 and 11.9). As with adult RA, atlantoaxial subluxation may be a problem (Fig. 11.84).

Table 11.6 Causes of atlantoaxial subluxation.

Arthritis:
Rheumatoid arthritis (~50%)
Juvenile chronic arthritis
Psoriatic arthritis
Ankylosing spondylitis (late feature in 2%)
Systemic lupus erythematosis (SLE)
Congenital:
Down syndrome (20–30%)
Morquio's syndrome
Atlanto-occipital fusion
Congenital absence/hypoplasia of dens
Infection:
Retropharyngeal abscess/quincy
Sympathetic inflammatory ligamentous relaxation
Trauma:
Fracture
Ligament rupture

The polyarticular form of the disease involves more than five joints and is generally seronegative when its onset is in younger children, but in older children it is often seropositive and indistinguishable from adult RA. Most commonly, polyarticular JRA has its onset in the teens and accounts for one third to one half of patients with JCA. Unlike the pauciarticular form, polyarticular RA generally affects smaller joints such as the wrist and metacarpophalangeal (MCP) joints (Fig. 11.88). As with adult RA, its distribution is generally symmetric (Fig. 11.88). It is also more likely than pauciarticular JRA to persist into adulthood. MRI and radiopharmaceutical bone scan may help evaluate early disease in both pauciarticular and polyarticular JRA (Fig. 11.89 and 11.90).

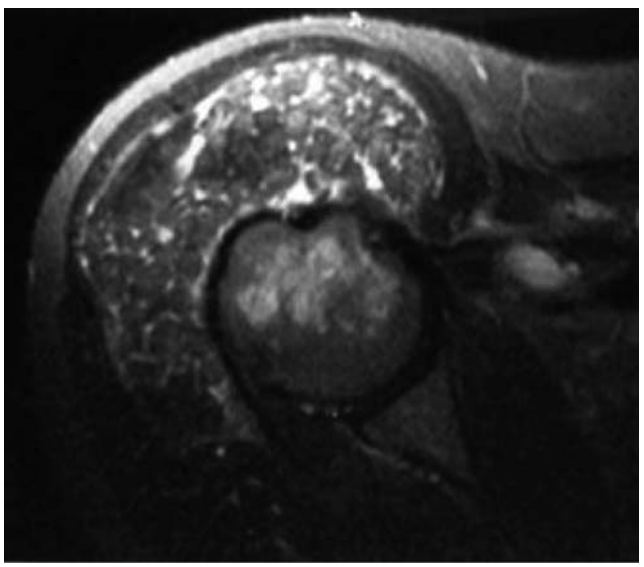

Fig. 11.82 T2-weighted MR of the shoulder showing a large joint effusion with innumerable small rice bodies, seen as low signal filling defects within the effusion

Table 11.7 Classification of juvenile chronic arthritis.

	Pauciarticular	Polyarticular	Systemic	Juvenile spondylitis	Seropositive
Median age of onset (years)	2	3	5	10	12
% JCA patients	40	20	10	20	10
Gender ratio	F>M	F>M	F=M	F<M	F>M
ANA (%)	60	25	No	No	60
Rheumatoid factor (%)	No	No	No	No	100
Chronic uveitis (%)	30	10	No	No	No
HLA	DR5	None	None	B27	DR4
Prognosis (severe)	10%	20%	30%	Mild, but spondylitis later	75%

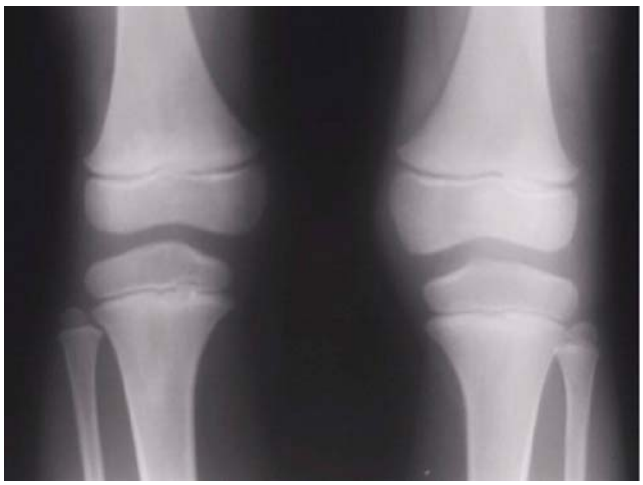

Fig. 11.83 AP radiograph showing epiphyseal overgrowth of the left distal femoral and proximal tibial epiphyses relative to the right in a patient with JRA. Note also the soft tissue swelling about the knee related to inflammation and effusion

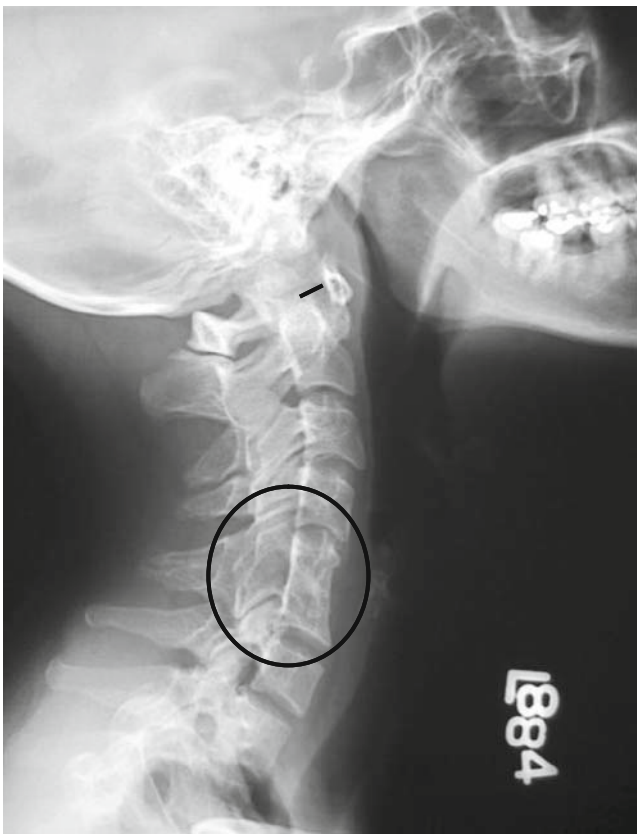

Fig. 11.84 Lateral cervical spine radiograph in a patient with JRA showing small fused C5 and C6 and atlantoaxial subluxation. Note the complete anterior and posterior element fusion of C5 and C6 (*oval*) with small anteroposterior diameter of the vertebral bodies at the level of fusion. Also note the increased atlanto-odontoid distance (*line*)

Still's disease is the most serious form of JRA. It not only affects the joints but has systemic manifestations including fever and diffuse lymphadenopathy. It affects multiple organ systems including the heart and pericardium, the pleura, and the spleen.

All patients with JRA complain of swollen, stiff, and painful joints, especially in the morning or after a nap. The affected joints show warmth and redness. They often complain of fatigue, decreased appetite, poor weight gain and show slow growth. The children may have ocular inflammation.

Septic Arthritis

Pyogenic septic arthritis is a devastating disease and one that should not be missed. About 20% of cases are afebrile. White blood cell count and sedimentation rate are unreliable predictors of disease. Currently, the C-reactive protein appears to correlate best with the presence of infection. The most common causative organism, whether hematogenously borne or from direct penetration, is *Staphylococcus aureus* followed closely by *Neisseria gonococcus*. Typically, septic arthritis affects a single joint, but about 15–20% of cases may be polyarticular. The knee, hip, and shoulder are the most commonly affected joints (Fig. 11.91). Septic arthritis is a therapeutic emergency since enzymatic destruction of the joint by the infecting organism can be extremely rapid

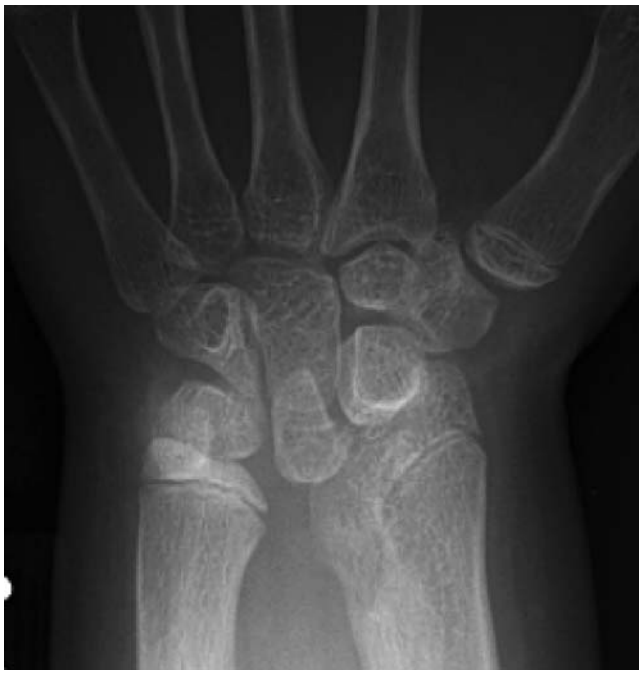

Fig. 11.85 PA radiograph of a juvenile wrist showing premature closure of the medial portion of the distal radial physis with resulting Madelung's deformity. The carpal angle, formed by intersections of the line tangential to the proximal surfaces of the scaphoid and lunate and the line tangential to the proximal surfaces of the triquetrum and lunate, is decreased with a Madelung's deformity. The normal carpal angle is 130°

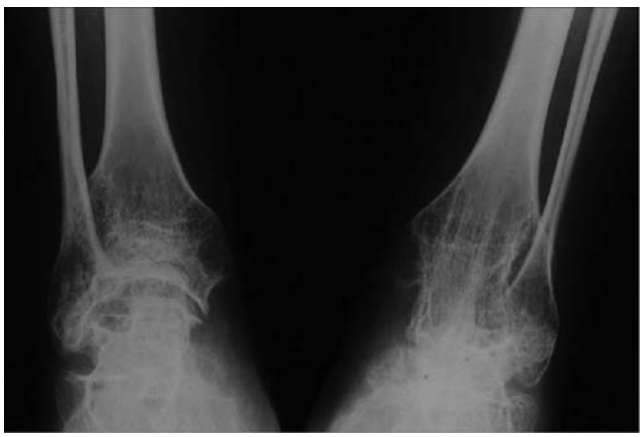

Fig. 11.86 AP radiograph of ankles in patient with JRA showing tarsal bone fusion, including the tibiotalar and subtalar joints on the left and the subtalar joint on the right

(Fig. 11.92). In the setting of suspected septic arthritis, whether in a child or an adult, the diagnostic test of choice is joint aspiration. This direct and comparatively safe test allows relatively accurate differentiation among pyogenic arthritis, viral arthritis, crystal-induced arthritis, e.g., gout or CPPD, and hemorrhage. No imaging examination permits this degree of differentiation and only forestalls the

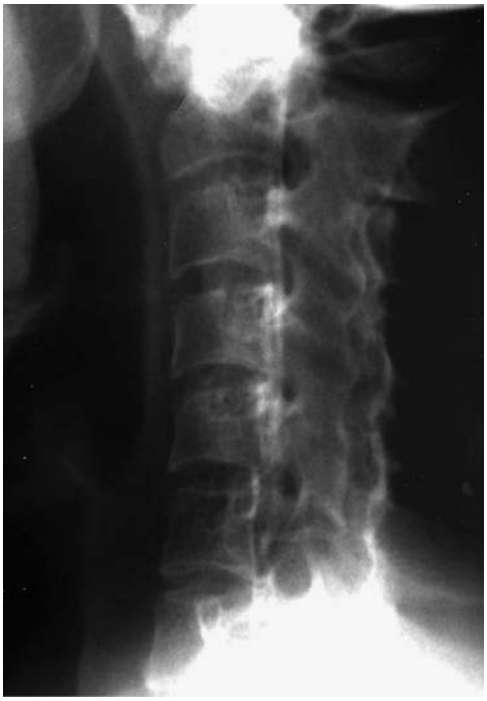

Fig. 11.87 Lateral cervical spine radiograph in a patient with RA showing complete fusion of the posterior masses of the cervical spine with sparing of the vertebral bodies anteriorly

inevitable. In fact, absence of a joint effusion does not exclude septic arthritis. Therefore, imaging also cannot be used to exclude this disease (Fig. 11.93).

There are times when septic arthritis may have been overlooked clinically. In this case, the radiologist needs to be able to correctly suggest the diagnosis from imaging findings. Radiographs will show a rapidly moving destructive arthropathy localized to a single or in some cases a few joints (Fig. 11.92). MRI will show similar findings but earlier than radiographs, and it will also show to good effect surrounding soft tissue edema, (Figs. 11.93 and 11.94) abscesses, osteomyelitis and bone marrow edema.

Similarly, infected disks often show characteristic findings. Typical pyogenic discitis starts in the disk space and spreads to adjacent vertebral bodies (Fig. 11.95). While a few other diseases, notably amyloid discitis and chronic pseudoarthrosis in ankylosing spondylitis – so-called Anderrson or Romanus lesion – may cause a similar appearance the most common etiology of this finding is pyogenic discitis. The clinical concern for patients with discitis is epidural spread of disease and hence an MRI should be done in any patient where neurologic signs suggest extension into the spinal canal. As with other forms of septic arthritis, pyogenic discitis may be rapidly progressive.

Acute viral (aseptic) arthritis is common in the pediatric population. Typical viral agents include parvovirus B-19,

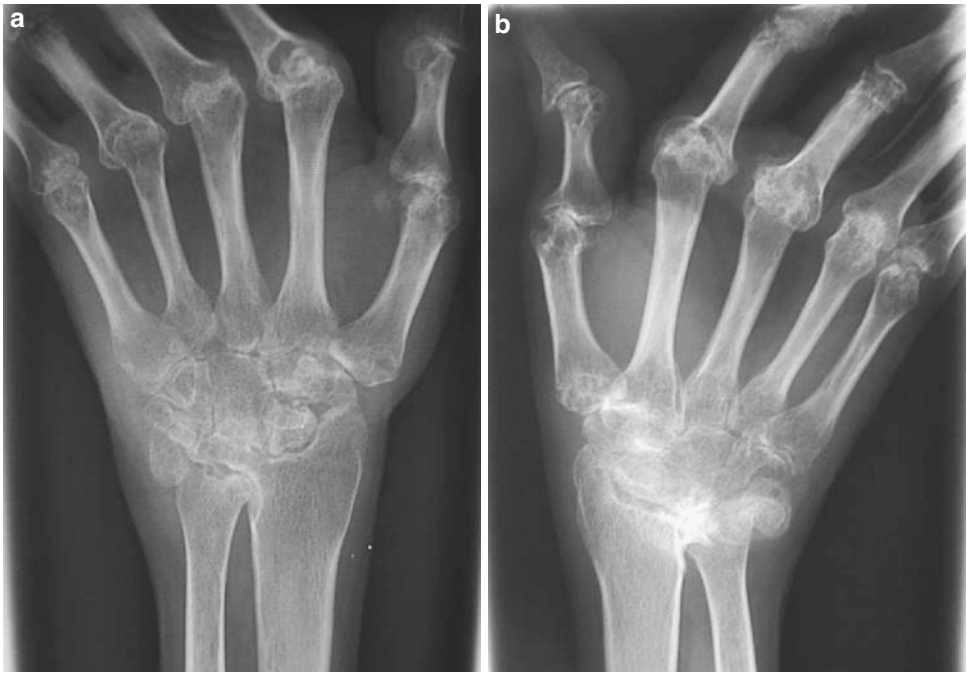

Fig. 11.88 PA radiographs of the left (**a**) and the right (**b**) wrists in seropositive JRA. Severe erosive disease is present symmetrically in the carpi and the MCPs that is virtually indistinguishable from adult RA

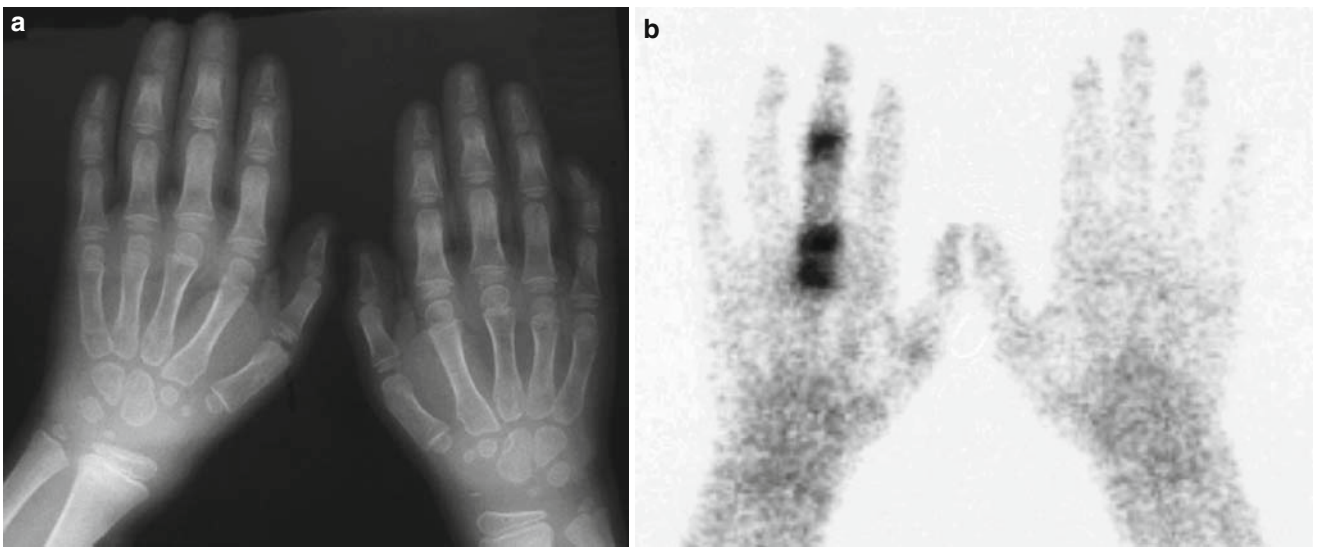

Fig. 11.89 (**a**) PA radiographs of the hands and bone scan image (**b**) in a patient with JRA showing only subtle soft tissue swelling of the third digit of the left hand, but obvious abnormal radiopharmaceutical activity involving the MCP and PIP of that hand on the bone scan image

rubella, hepatitis B and C, acute HIV infection, Epstein–Barr virus, and mumps virus. Patients often have a history of a prodrome or a rash. Some patients will have a history of contact with another ill child. The illness may present with a polyarthritis that mimics RA or affect a single joint and present identically to pyogenic arthritis. Unlike either RA or pyogenic arthritis, generally viral arthritis is benign and self-limiting, unless associated with a systemic disease.

Gonococcus is a common cause of septic arthritis among younger, sexually active adults. Presentation is typically a sexually active individual with a flu-like syndrome lasting over 5–7 days and associated with chills and fever. Genital lesions are often asymptomatic so the absence of this finding does not preclude the disease. The patient may have erythematous skin lesions or even pustules. The patient may complain of migratory arthralgias that eventually settle into a

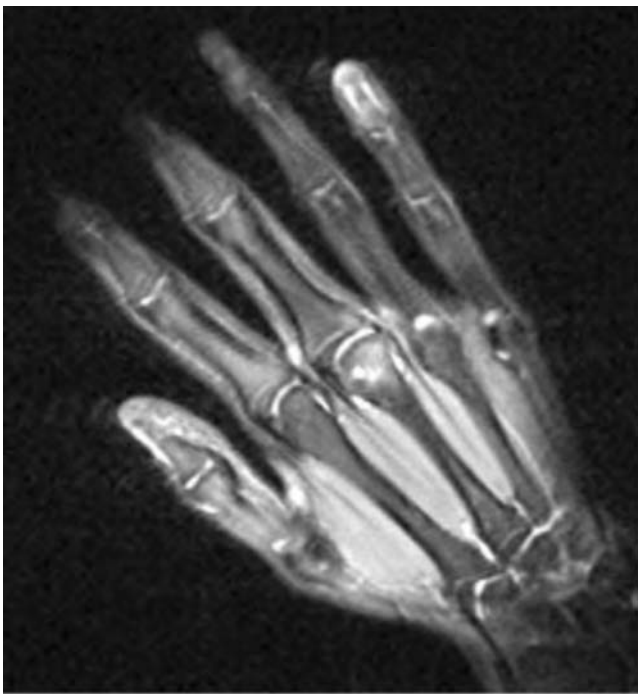

Fig. 11.90 T2-weighted coronal image of the hand of a patient with JRA showing abnormal signal in the third MCP metacarpal head and to a lesser extent in the ulnar aspect of the base of the proximal phalanx

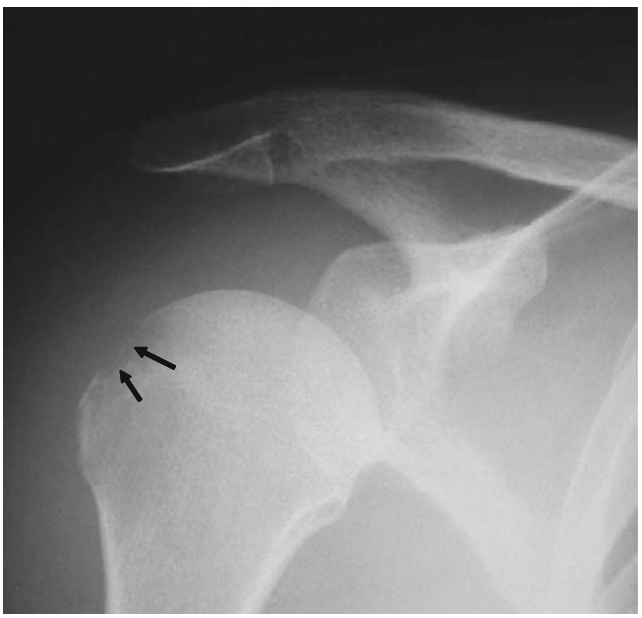

Fig. 11.91 AP radiograph showing early septic arthritis of the shoulder. The humeral head is inferiorly displaced by a large joint effusion. The cortex of the superior aspect of the greater tuberosity has been destroyed by the infection (*arrows*) consistent with development of osteomyelitis

persistent monoarthritis. Again, joint aspiration is the diagnostic procedure of choice, although other imaging modalities may show destructive changes and MR may show synovitis and erosions (Fig. 11.96).

Tuberculosis causes the most common form of chronic granulomatous septic arthritis. This differs from typical pyogenic arthritis by its absence of rapid joint destruction. Instead, it tends to cause a more indolent arthropathy characterized by marginal joint erosions, osteopenia surrounding the joint, and gradual development of joint space narrowing (Fig. 11.97). This triad of findings is known as Phemister's triad.

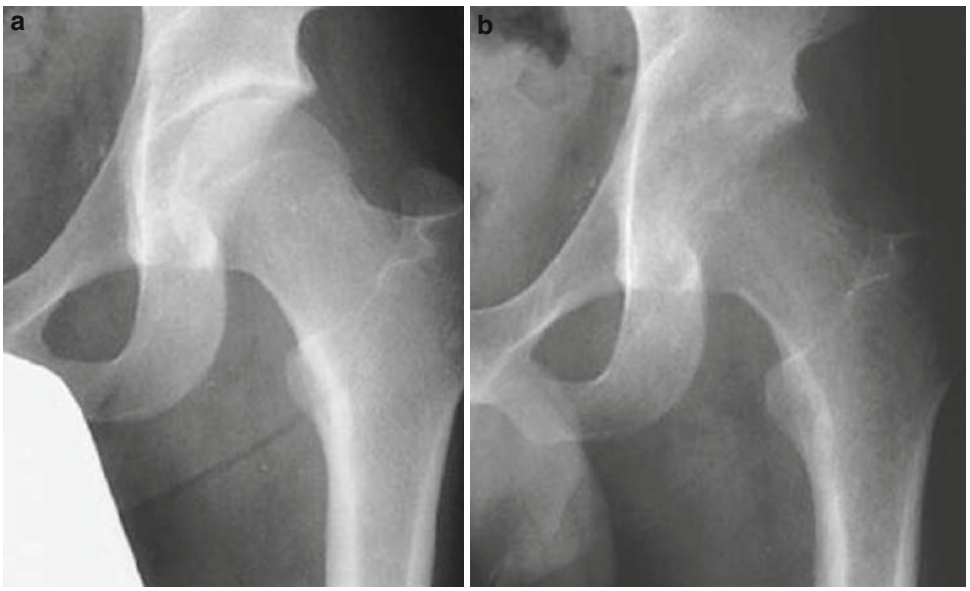

Fig. 11.92 AP radiograph of the hip at presentation (**a**) and 48 hours later (**b**) showing rapid progressions of septic arthritis. Note the development of periarticular osteopenia and joint space narrowing with some loss of the cortical definition of the acetabular and femoral head cortex

Once common in the United States, tuberculous arthritis is now rare in most practices. When it does occur, it is most common in the spine (Pott's disease) accounting for 50% of cases, followed by the hip (Fig. 11.97), knee, and tarsal joints (Fig. 11.98). Pott's disease typically starts paravertebrally and then extends into the joint space, often associated with a large paraspinal or psoas abscess (Fig. 11.99). These may drain by fistulization to the skin. MR has become the imaging method of choice for staging this problem.

Gout

Gout is one of the oldest recognized arthropathies, having been described with uncanny accuracy by Thomas Sydenham in 1683. Today, it remains a common problem in the United States affecting about 2 million individuals, roughly the same number as are afflicted by RA. Primary gout is predominantly a disease of adult men with a 4:1 male to female ratio. In fact, gout is the major cause of inflammatory arthritis in men over the age of 30. When it does occur in women, they are usually postmenopausal.

In general, gout arises from precipitation of urate crystals in the joint spaces, the marrow, and the soft tissues. The first causes an inflammatory arthropathy within the joint, the second causes intraosseous tophi that may lead to paraarticular erosive changes, and the last causes soft tissue tophi and inflammatory masses.

Gout develops when uric acid precipitates out and crystallizes in the tissues, at a level that exceeds 6.8 mg/dL, with slight variation for temperature and pH of the local tissue environment. High concentrations of uric acid may result from underexcretion or from overproduction of uric acid. The former, known as primary gout, accounts for 90% of cases. Overproduction most commonly results from high rates of tissue degradation as one may see in patients on chemotherapy for neoplasms or myeloproliferative diseases, chronic renal insufficiency, diuretics, or ethanol abuse. This form of gout is secondary and accounts for only 10% of patients. Some rare enzymatic deficiencies result in overproduction of uric acid. These include patients with Lesch–Nyhan syndrome (hypoxanthine–guanine phosphoribosyl transferase deficiency) and Von Gierke's disease (fructose-1-phosphate aldolase deficiency) and patients with PP-ribose-P synthetase variants.

Generally patients have hyperuricemia for years before symptoms occur. Seventy-five percent of attacks of gout occur in the lower extremities. About half of gouty attacks occur in the great toe, a condition known as podagra. Other joints involved by gout include the tarsal joints, ankles, knees, fingers, wrists, and elbows, roughly in that order of frequency. Soft tissue tophi occur in elbows, fingers, toes, auricles, and Achilles tendons. Gout also affects the urinary tract where hyperconcentraion of uric acid in the kidneys leads to uric acid stones. These are not radio-opaque.

Attacks usually begin in the wee hours of the night and are self-limited, lasting from a few days to a few weeks. Good pathophysiological reasons exist for this pattern. At night the body temperature decreases resulting in a lower solubility product for uric acid. This phenomenon is most prominent in the acral portions of the body, i.e., the hands and feet.

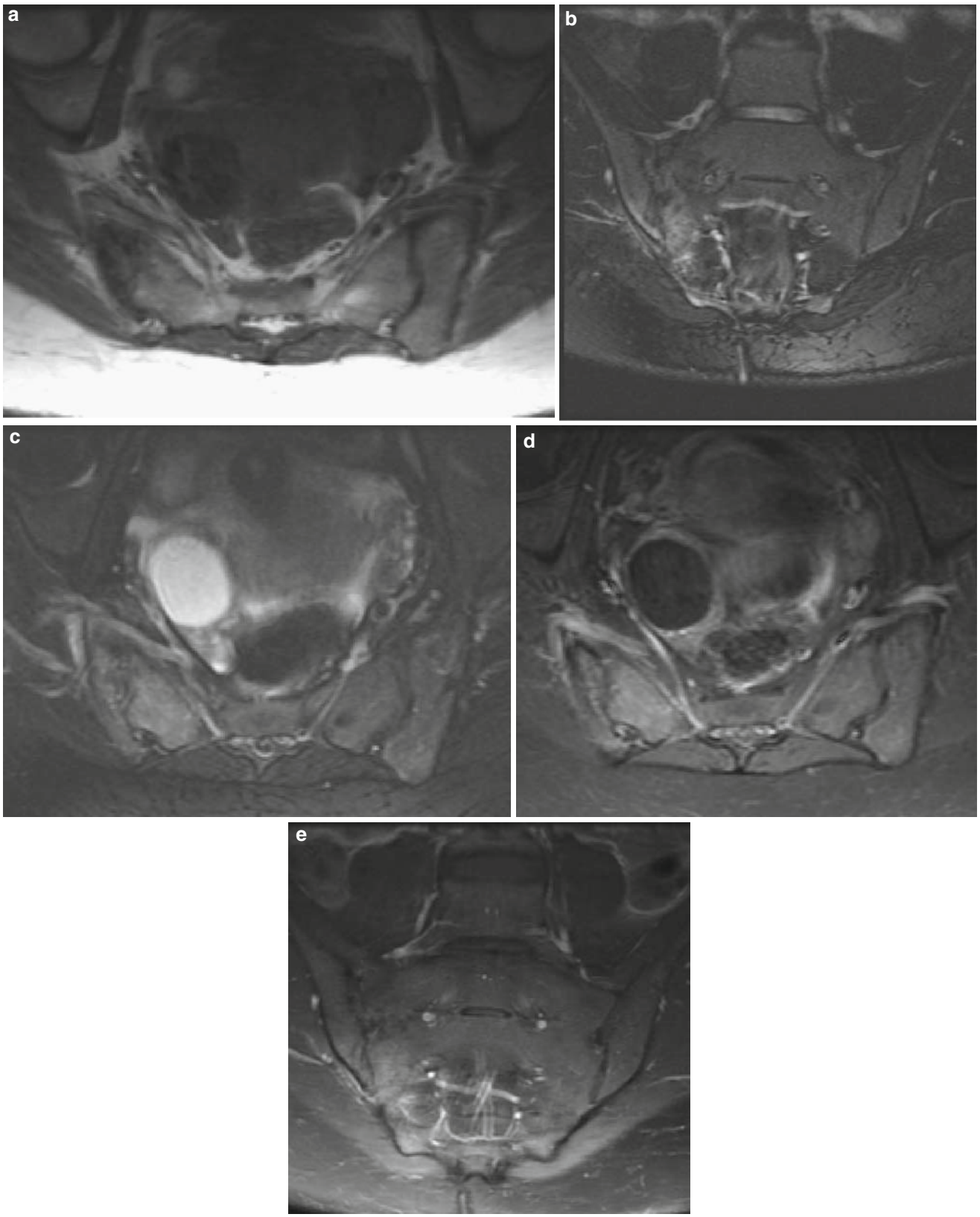

Fig. 11.93 T1W axial (**a**), T2W coronal (**b**), axial (**c**), T1W fat-uppressed postgadolinium coronal (**d**), and axial (**e**) images showing early right sacroiliac joint septic arthritis in an intravenous drug user with *Staphylococcus aureus* septic arthritis involving multiple joints and complaining of recent onset of right sacroiliac joint pain. Note the destruction of the cortices on both sides of the joint with marrow edema and enhancement consistent with septic arthritis. Images show no significant joint fluid

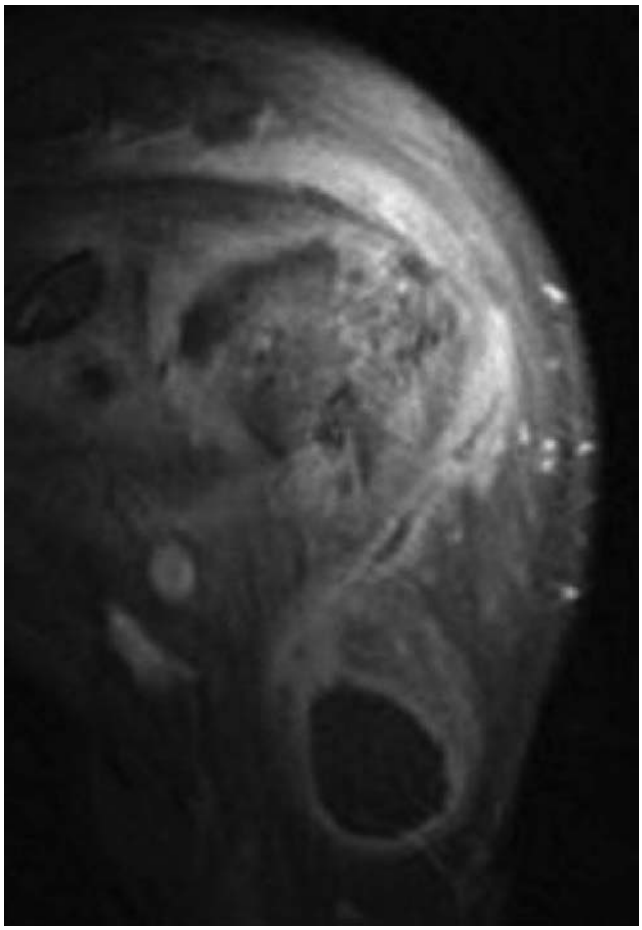

Fig. 11.94 T1-weighted fat suppressed coronal image of the shoulder after administration of intravenous gadolinium showing a deltoid abscess in a patient with septic arthritis of the shoulder. Note the enhancement of the tissues in the shoulder joint as well as around the abscess inferiorly

In addition, during normal daytime activities, fluid tends to collect in the interstitium of the tissues of the lower extremities. At night this interstitial fluid reabsorbs, concentrating the uric acid left behind. The combination of temperature-induced lower uric acid solubility and reabsortion of fluid from the tissues in the feet, causing high concentrations of uric acid, lead to late night precipitation of uric acid crystals. This, in turn, causes an inflammatory response arousing the patient from sleep with acute pain. In the long term, this process leads to tophus formation and bone destruction.

Aspiration of joints inflamed with gout shows high counts of neutrophils and monosodium urate crystals. Under polarized light, the latter appear as negatively birefringent crystals (Fig. 11.100). Histologically, tophi show collections of these crystals surrounded by chronic inflammatory cells.

Radiographic findings in gout include soft tissue swelling and increased density within the tissues from formation of tophi that consist of Ca++ urate crystals and early endosteal erosion from tophus formation within the bone as well (Fig. 11.101). Later in the disease, the joint space narrows. The inflammatory response causes both typical marginal periarticular erosions, adjacent to the joint (Fig. 11.102), and paraarticular erosions at a remote location from the joint (Fig. 11.24) to form. These erosions often have a characteristic overhanging edge, known as a Granger's overhanging edge (Figs. 11.24 and 11.102). While gout most commonly affects the first MTP of the feet, it may affect other joints, particularly the tarsal joints (Fig. 11.102b), the carpus, and the hand (Fig. 11.103).

The reason that some erosions in gout have this paraarticular location and the peculiar overhanging edges relates to the pathophysiology of the disease. One theory suggests that the inflammatory masses forming in the tissues adjacent to the joints slowly erode their way into the bone margin, while the bone itself grows around the collection forming a clasp-like lesion. Another theory is that the urate collects within the endarterial region of the bone – the intrameduallary paraarticular portion of the bone. The collection slowly accretes mass spherically and erodes the bone from its endosteal surface outward. This process may cause the clasp-like appearance seen on radiographs.

Crystals may collect in bursae as well as within joints. This may cause recurrent bursitis with secondary calcifications (Fig. 11.104). Intraosseous tophi cause lesions with a well-defined, small zone of transition within bone (Fig. 11.105). Without appropriate history, these may be confused with other focal lesions of bone.

MRI of gouty arthritis shows inflammatory changes with synovitis and erosions (Fig. 11.106). This is not particularly useful diagnostically. On the other hand, it is a powerful technique to show soft tissue tophi (Fig. 11.107). These appear as low signal on T1-weighted images and as varying signal intensity on T2-weighting, depending upon the amount of calcification and active inflammation.

Psoriatic Arthritis

Most patients experience psoriasis purely as a skin disease with a silver-red scale-like rash predominantly on the extensor surfaces of the extremities and sometimes "oil stain" discoloration and pitting of the nails. In about 5–8% of patients with psoriasis, the disease causes an inflammatory arthritis. The latter may range from relatively mild to one that is severe, progressive, and deforming. The arthritis may precede the rash (~15%), and so the radiologist cannot rely on a history of psoriatic skin rash to make the diagnosis. Instead, in these cases, radiologists may be instrumental in identifying the patient's disease.

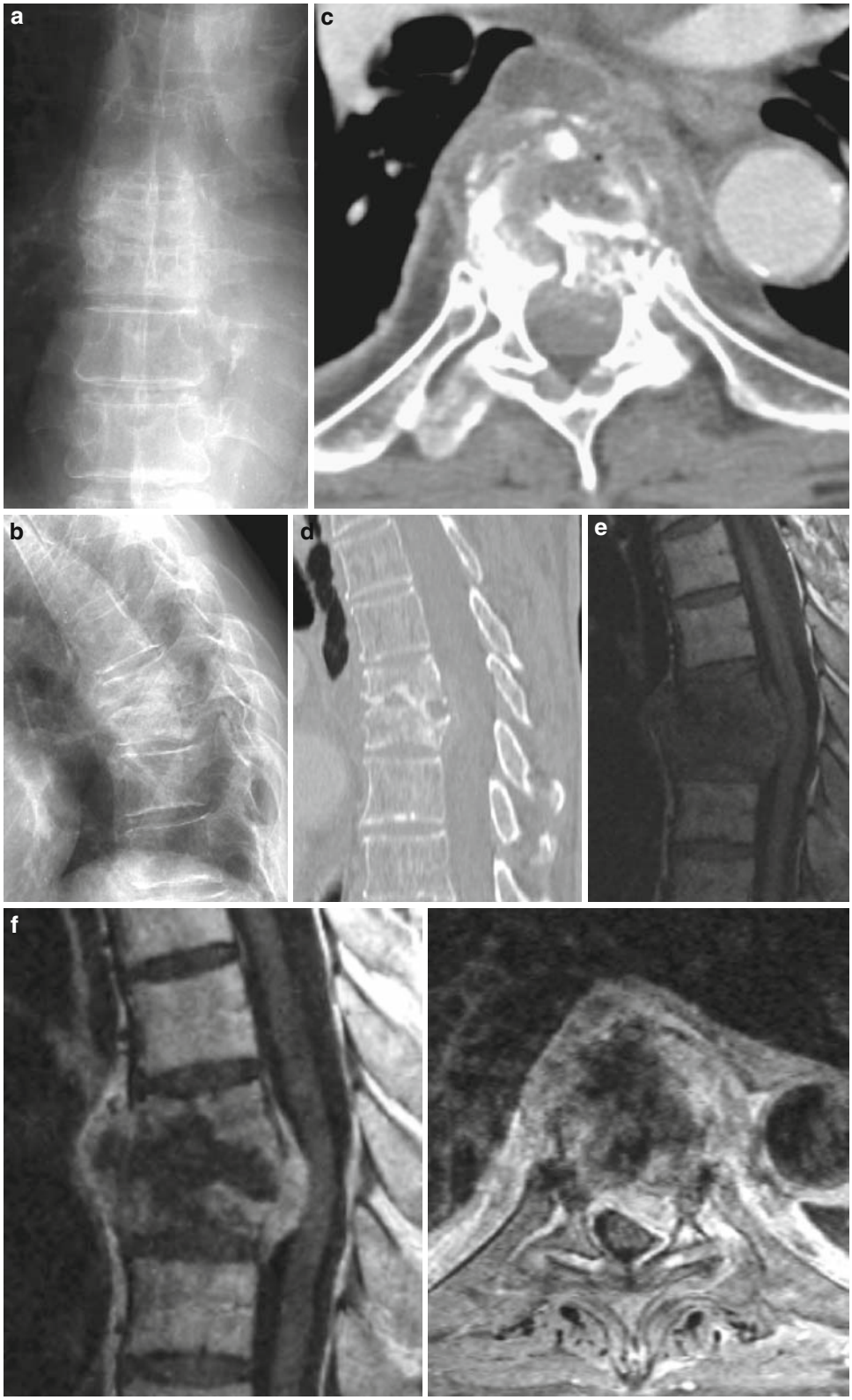

Fig. 11.95 AP (**a**), lateral B radiographs, axial (**c**) and sagittal CT reconstruction (**d**), T1 fat suppressed sagittal MR pre- (**e**) and postgadolinium (**f**), and axial T1-weighted fat suppressed postgadolinium MR showing discitis at T8–T9. Note the epidural spread of disease

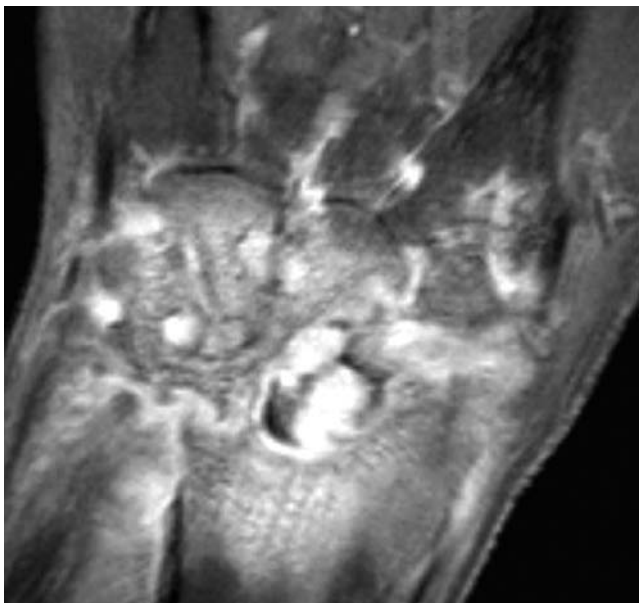

Fig. 11.96 T1-weighted coronal fat suppressed MR image of a wrist with gonococcal septic arthritis after intravenous gadolinium showing diffuse synovial enhancement and erosions

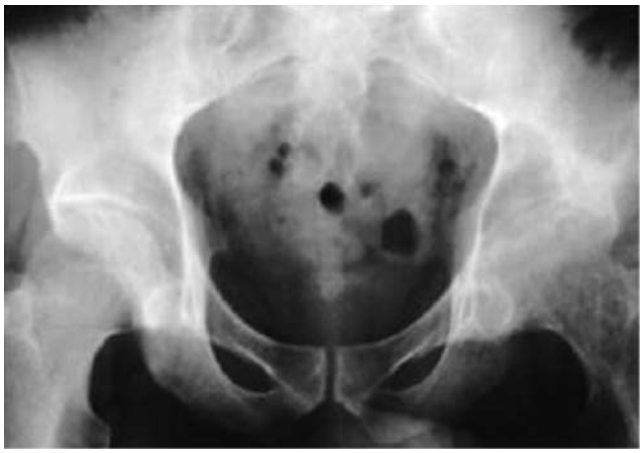

Fig. 11.97 AP pelvic radiograph in a patient with tuberculous arthritis of the left hip showing periarticular osteopenia, marked joint space narrowing and peripheral erosions – Phemister's triad

Psoriatic arthritis, unlike RA, shows little osteopenia but instead may have bone sclerosis, periosteal proliferation, and typically a more distal and asymmetric distribution. Five basic patterns of psoriatic arthritis have been described:

1. Asymmetric distal oligoarthritis involving the small joints of the digits (55–70%);
2. Asymmetric DIP arthritis, often with paronychial swelling and nail changes (5–10%);
3. Sacroiliitis and spondylitis (5%);
4. Symmetric polyarthritis that resembles RA (10–30%);
5. Arthritis mutilans with severe opera glass hand deformity ("main en lorgnette") (3–5%).

Of these, the asymmetric oligoarthritis is most common; the mutilans form of the disease is the least common.

In the common form of psoriatic arthritis, the soft tissues around the involved joints may be diffusely swollen, causing an appearance known as a sausage digit (Fig. 11.108). The nails may show pitting and "oil stain" pinkish discoloration, particularly in the small joint distal joint form of the disease. The former may be visible on radiographs; the latter is not. Typically this arthropathy affects the small joints of the hands and to a lesser extent the feet (PIP and DIP) followed by the sacroiliac joints and the spine. Alignment abnormalities may occur in this arthritis, but they are not as common as in RA. The bones may show some periosteal reaction (Fig. 11.13) and sclerosis (Fig. 11.109). Typically they also may show areas of enthesopathy – new bone proliferation in areas of tendon insertion (Fig. 11.110).

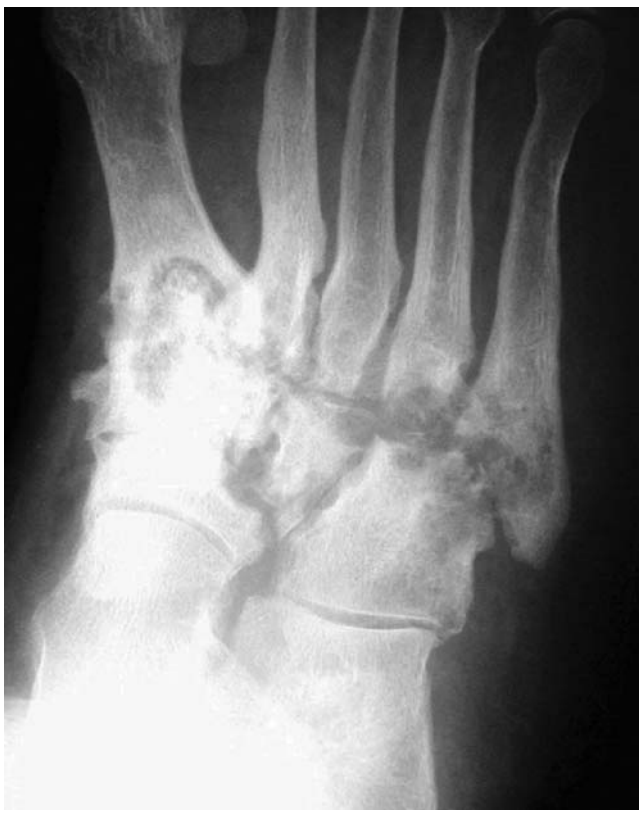

Fig. 11.98 Oblique radiograph of the midtarsal joints in a patient with tuberculous arthritis. Unlike typical tuberculous arthritis, this patient's foot shows evidence of marked destruction along the Lis Franc joint (tarsometatarsal joint)

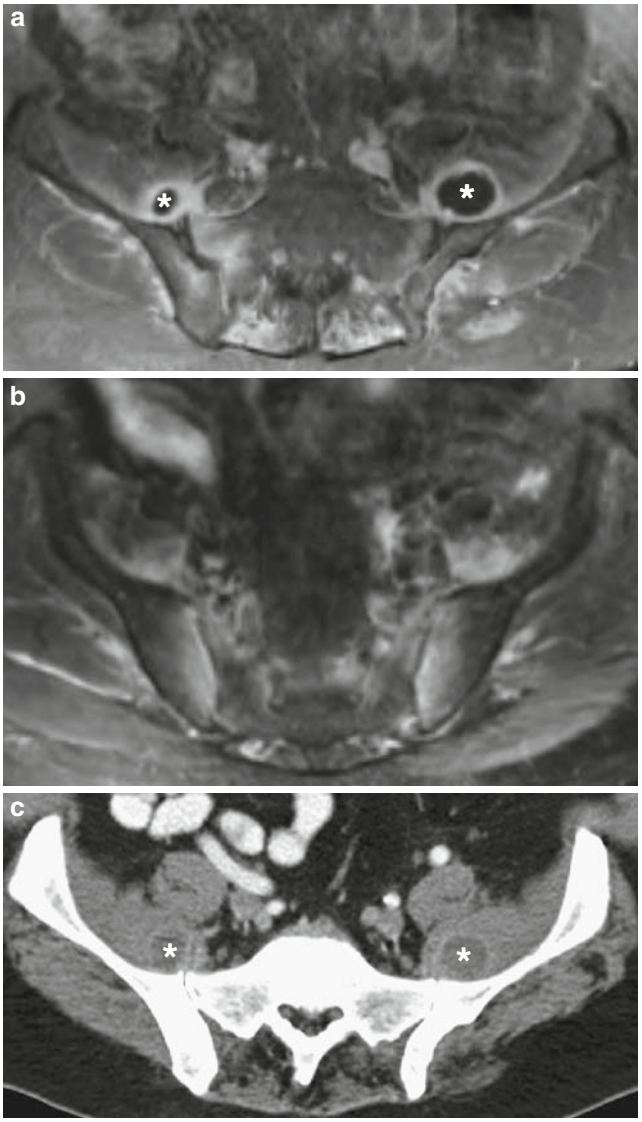

Fig. 11.99 Axial T1-weighted fat suppressed postgadolinium (**a**), axial T2-weighted fat suppressed (**b**), and CT scan image of the pelvis (**c**), showing bilateral tuberculous psoas abscesses (∗) (**a** and **c**) and psoas inflammation with bilateral sacroiliac septic arthritis

As with RA, erosive changes tend to start at the margins of the joint synovial joint spaces and progress centrally (Fig. 11.108, 11.23 and 11.25). Some erosions in psoriasis, however, may become more prominent centrally and preserve the joint space giving a "Mickey Mouse ear" appearance to the joint (Fig. 11.111, 11.23). Over time, continued erosion and destruction of the bone and joint space may lead to a "pencil-in-cup" appearance (Fig. 11.112). Further, the bones may spontaneously ankylose (Figs. 11.23 and 11.25), a phenomenon that is rarely observed in adult RA except in the carpus. Cortical erosion may occur in regions where there is active bursal inflammation, particularly about the plantar and dorsal aspects of the calcaneus (Fig. 11.110).

Psoriatic arthritis is among a group of diseases associated with a spondyloarthritis. Four diseases – anklyosing spondylitis, spondyloarthropathy of inflammatory bowel disease, psoriasis, and reactive arthritis – commonly may cause an arthritis that primarily affects the sacroiliac (SI) joints and the spinal column. In each of these diseases, this pattern is typically seen in patients who are HLA-B27 positive (Table 11.8). In all, the SI joints are usually first affected, followed by spine involvement. In the first two, the disease typically affects the SI joints symmetrically, while in the latter two, the arthritis tends more often to affect them asymmetrically (Fig. 11.113). As the disease progresses, the SI joints may fuse and the syndesmophyte formation also progresses, leaving the patient with a rigid back and marked decreased range of motion. The rate of progression is variable.

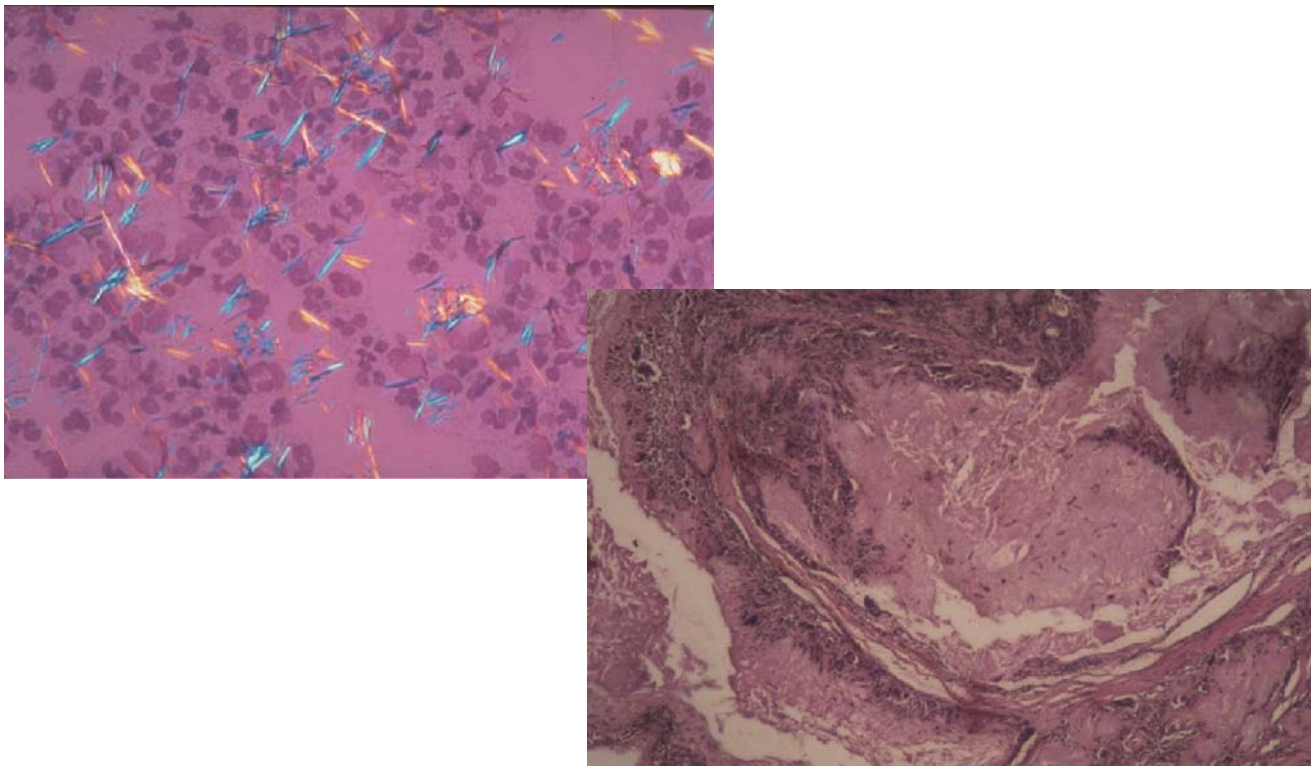

Fig. 11.100 Needle-shaped crystals of uric acid viewed under semi-polarized light with a red compensator. Crystals that are parallel to the axis are seen in blue, those perpendicular are seen in yellow. This pattern is called negative birefringence

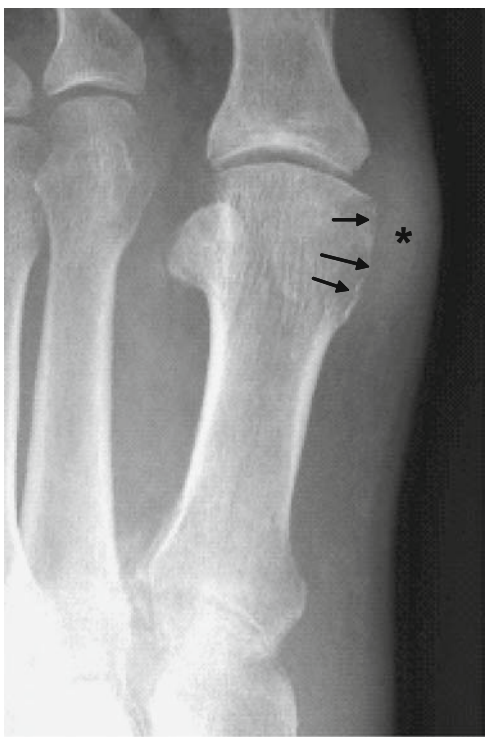

Fig. 11.101 AP radiographic detail of the first MTP showing tophus in the medial soft tissues (∗) and endosteal erosive changes (*arrows*) in the medial aspect of the metatarsal head

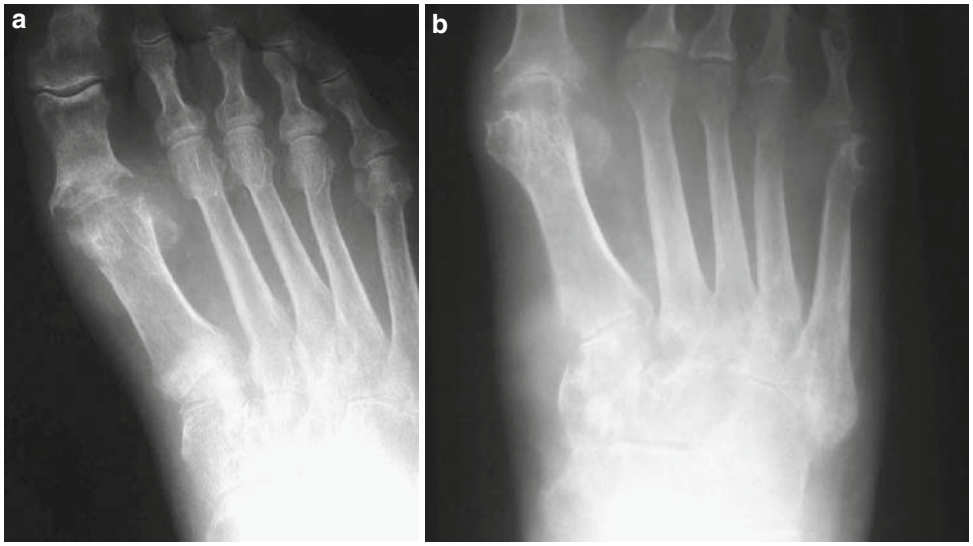

Fig. 11.102 PA radiographs of the first MTP joint and the midfoot in two different patients (**a**) and (**b**) showing advanced periarticular erosive changes of gout in. Note the overhanging edges giving the erosions a clasp-like appearance in the majority of the joints and the density of the tissues related to the presence of Ca++ urate

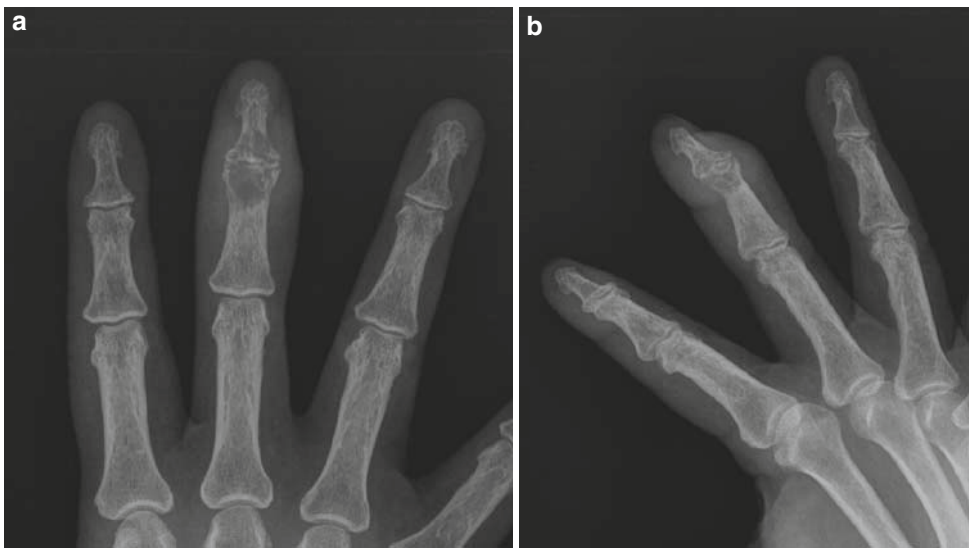

Fig. 11.103 Oblique (**a**) and PA (**b**) detail radiographs of the hand in a patient with gout showing soft tissue swelling related to tophus and DIP narrowing with lytic changes within the proximal aspect of the distal phalanx and distal aspect of the middle phalanx. This last finding may result from inflammation and osteopenia or intraosseous tophi

All of the spondyloarthropathies cause syndesmophytes – superoinferiorly oriented ossification along the margin of the spine. Syndesmophytes may be distinguished radiographically from osteophytes in that the latter have a prominent transverse component while the former do not. In psoriasis, the syndesmophytes are also generally asymmetric and spotty in distribution (Fig. 11.114). They are classically described as being nonmarginal in appearance; that is, they appear as thicker areas of ossification that run from the midsection of one vertebral body to the midsection of the next.

Reactive Arthritis

Originally called Reiter's syndrome and described by Hans Reiter in 1916, this rare syndrome is now called reactive arthritis (ReA). It is five times more common in men than women and occurs primarily in patients aged 18–40. Over 75% of patients with this disease are HLA-B27 positive. Reactive arthritis has an incidence that is roughly 30 times higher in urban areas (1:1000/year) than rural ones (3.5:100,000/year).

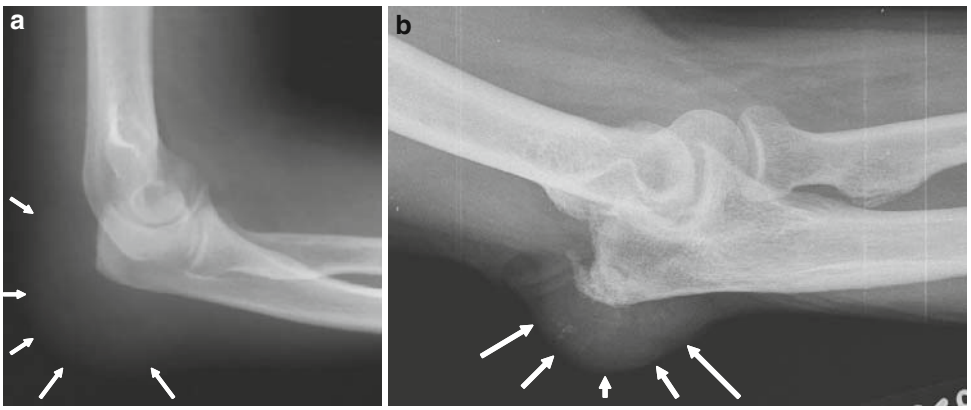

Fig. 11.104 Lateral radiographs of the elbow in two patients (**a**) and (**b**) showing olecrenon bursitis (*arrows*). Note the calcifications within the bursa in (**b**)

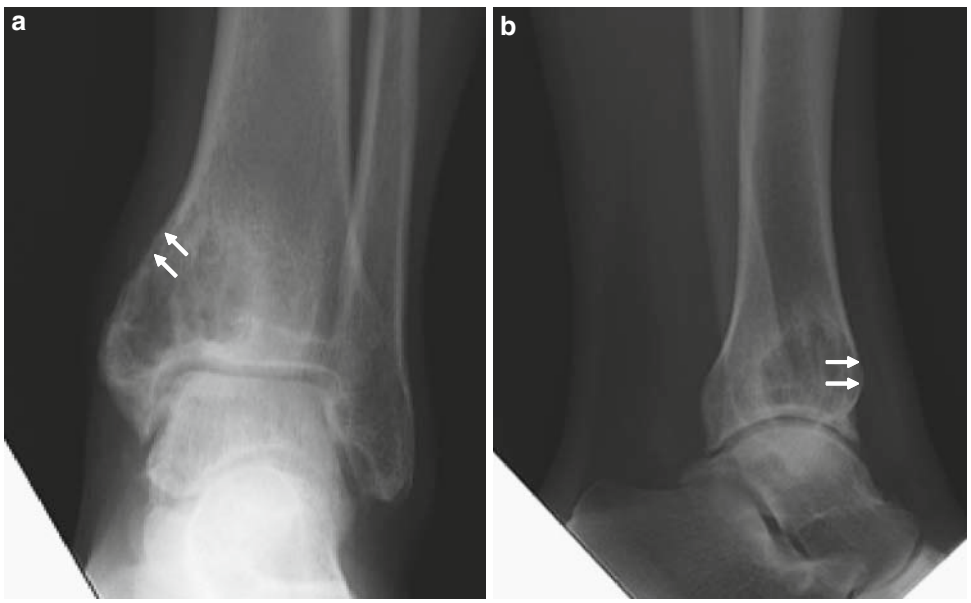

Fig. 11.105 AP (**a**) and lateral (**b**) radiographs of intraosseous tophus in the tibia. Note the endosteal erosion of the cortex (*arrows*) related to the tophus

Bauer and Engleman formalized the syndrome in 1942 into a series of ailments that may be seen either synchronously or metachronously. The diagnosis may be challenging in patients with metachronous disease. The syndrome consists of inflammatory arthritis, conjunctivitis, urethritis or cervicitis, circinate ballanitis, and keratoderma blenorrhagicum. The last is a rash that occurs on the soles of the feet and the palms of the hands and resembles pustular psoriasis. Patients may also have apthous ulcers on their palates and Achilles tendonitis. The majority of male patients (80%) will have prostatitis.

The name of the disease was changed from Reiter's syndrome to ReA because it is now thought to be reactive to other antigenic stimuli, similar to the hypothetical etiology of RA. In the case of ReA, several bacterial triggers have been identified, including shigella, salmonella, *Yersinia enterocolitica*, *Chlamydia trachomatis*, *Campylobacter jejuni*, and Lymphogranuloma *venereum*. In all instances, the belief is that a cross-reactive immune response to the bacterial antigens is responsible for the clinical manifestations of the syndrome. Around 1–2% of patients with sexually transmitted disease (STD) and urethritis will eventually be diagnosed as having ReA. The same is true for a similar proportion of patients with shigellosis.

Radiographically the arthritis of ReA is virtually indistinguishable from psoriatic arthritis. ReA causes a bilateral asymmetric and distal arthritis with fusiform digital swelling, peripheral erosions, bone proliferation, and enthesopathy. It even causes an asymmetric spondyloarthropathy that is virtually identical to psoriatic spondyloarthropathy. As a result,

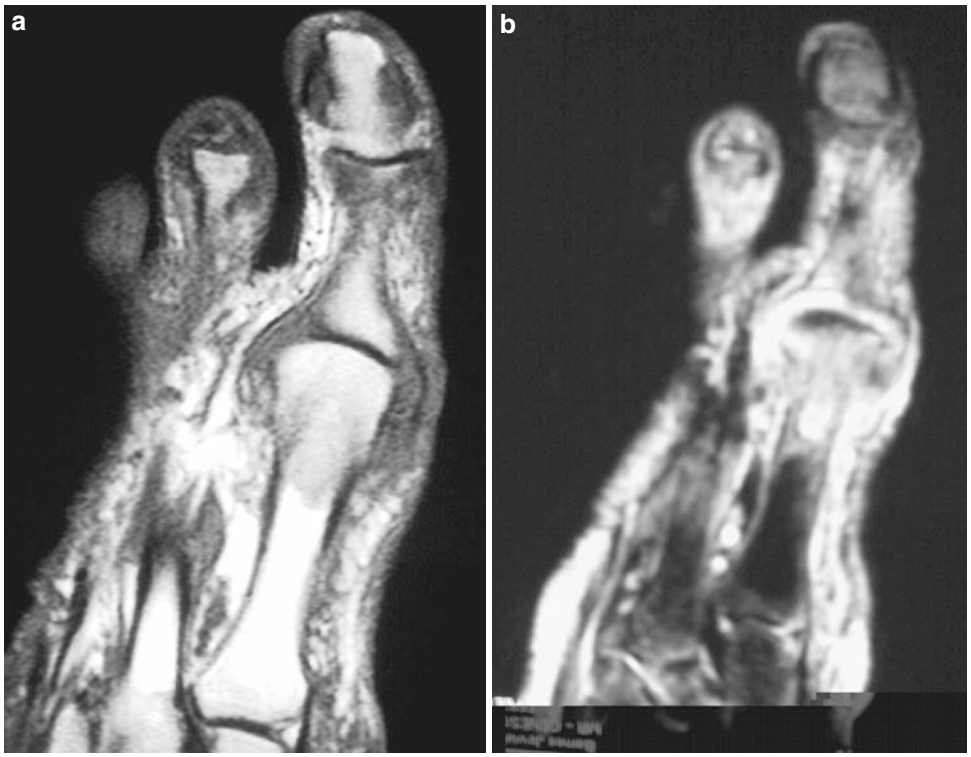

Fig. 11.106 T1-weighted (**a**) and T2-weighted fat suppressed (**b**) MRI images of a patient with gout showing edema and synovitis involving the first MTP

a wise rule of thumb is that whenever psoriasis arises in a differential diagnosis, it is a prudent to also include ReA.

ReA differs from psoriasis in the frequency with which joints are involved. ReA involves the feet, ankles, and knees most frequently. The hands, hips, and SI joints are much less frequently involved. When it involves the feet, the MTP joints and the calcanei are involved more frequently than the distal small joints.

Ankylosing Spondylitis

The adult form of ankylosing spondylitis (AS), also know as Marie Strümpell disease, is the most common of the spondyloarthropathies and has the highest association with the HLA-B27 antigens (Table 11.8). As with many arthropathies, it is a systemic disease that not only affects the spine and SI joints but also causes aortitis and aortic insufficiency late in the disease in about 5–10% of patients, rare upper lobe predominant interstitial restrictive pulmonary disease (1%), and iridocyclitis (25%) or uveitis (20%). About 10% of AS patients will develop secondary amyloidosis. Conversely, about 30–50% of patients presenting with acute anterior uveitis will ultimately be diagnosed with AS.

AS is insidious in onset and usually begins between ages 16 and 45, although 10% of patients may have had an earlier onset in a juvenile form of the disease. It progresses to significant disability in about 20% of those affected. Clinically, it affects men about three times more often than women, but radiographic survey studies have shown an equal prevalence, suggesting that women are less symptomatic. As with other rheumatic diseases, AS is more common in Native Americans and less common in Blacks.

Patients complain of low back pain, morning stiffness, and fatigue. They may have intermittent fever. Typically, AS starts in the SI joints and slowly ascends the spine, but this pattern may be observed less frequently in women than men. About 30% of patients will have peripheral manifestations of the disease including tendonitis and a large joint arthropathy that is indistinguishable from RA.

The radiographic findings of AS depend upon the stage of the disease. Early findings include a bilaterally symmetric erosive arthropathy of the SI joint (Fig. 11.115). This generally starts in the inferior synovial portion of the joint and early on spares the superior fibrous joint. As the disease progresses, the entire joint space will be involved and ultimately the joints will fuse.

Early on, the spine may show ivory corners (Fig. 11.116) related to inflammation and reactive bone formation in the

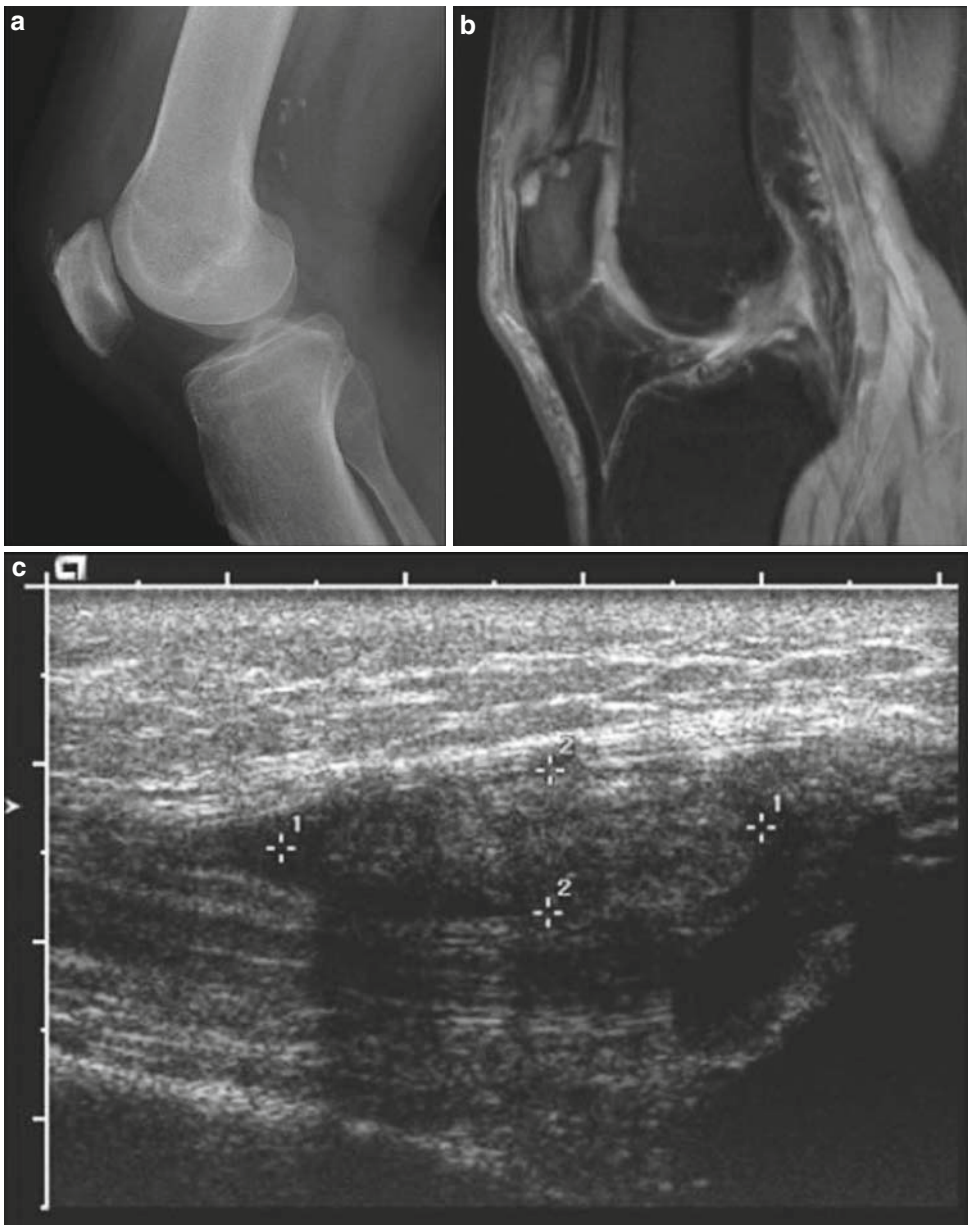

Fig. 11.107 Lateral radiograph (**a**), lateral T2-weighted MR image (**b**), and sagittal ultrasound image (**c**), showing avascular gouty tophus within the quadriceps tendon. (Case courtesy of Dr. Antoni Parellada, Diagnostic Imaging, Philadelphia, PA)

ring apophyses of the vertebral bodies. As the disease progresses, the inflammation will erode the margins of the vertebral bodies (Romanus lesion) while simultaneously the longitudinal ligaments calcify and then ossify, as new bone is laid down along the anterior margin of the vertebral bodies. This leads to a loss of the concavity of the anterior vertebral bodies and an appearance of "squaring" (Figs. 11.116 and 11.117). Just as new bone develops in the longitudinal ligaments, similar changes occur in the paradiscal ligaments leading to syndesmophyte formation. Unlike the syndesmophytes of psoriasis and reactive arthritis, the syndesmophytes in AS are generally symmetric and marginal – extending only along the ligament from one vertebral margin to the next (Fig. 11.118). At the same time that inflammation is occurring in the ligaments around the spine and the apophyses of the vertebral body margins, the facet joints undergo a synovial inflammatory arthritis. Early on this will cause erosions in the facet joints; later it will lead to bone fusion (Fig. 11.119). Similarly, an inflammatory bursitis may develop in the bursae surrounding the odontoid process. This will cause erosions in the odontoid and laxity of the posterior transverse ligament at this level. This later phenomenon may lead to ligamentous laxity and secondary atlantoaxial subluxation, similar to that which is seen in RA (Table 11.6).

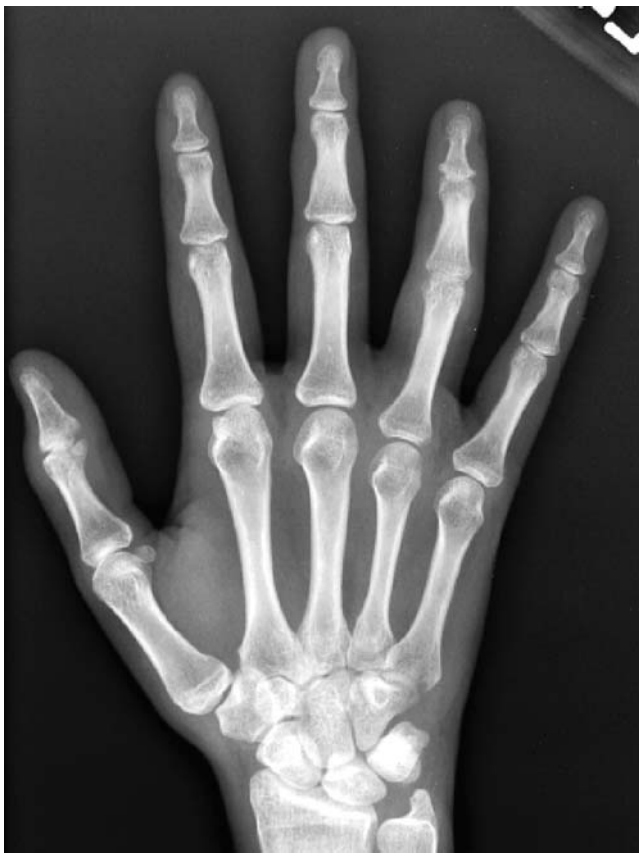

Fig. 11.108 PA radiograph of the right hand showing swelling of the fourth digit consistent with a sausage digit and joint space narrowing with erosions in the fourth PIP

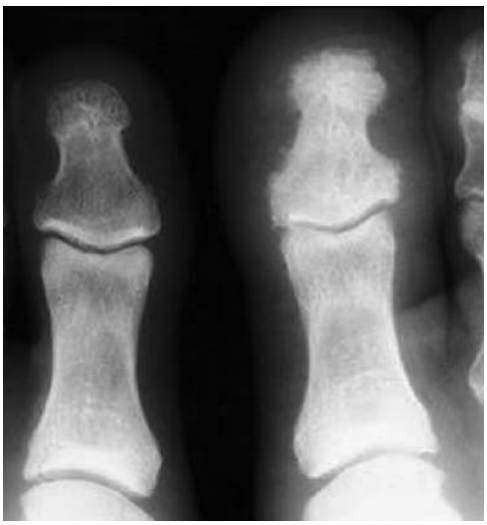

Fig. 11.109 PA radiograph detail of the great toes in a patient with psoriatic arthritis showing swelling and an ivory phalanx of the right great toe

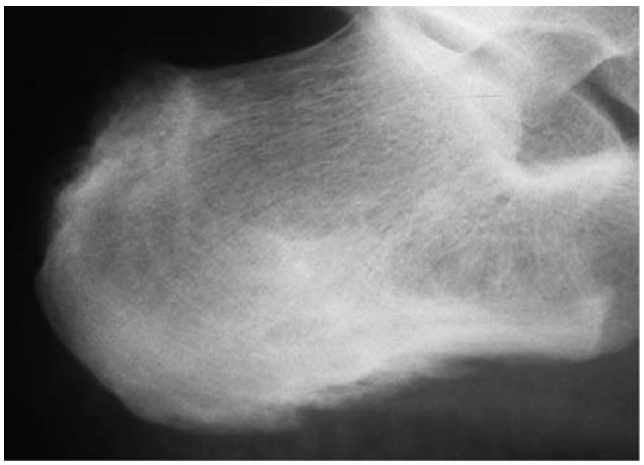

Fig. 11.110 Lateral radiograph of the calcaneus showing bursal erosion of the plantar and dorsal surfaces of the calcaneus along with enthesopathic changes in a patient with psoriatic arthritis

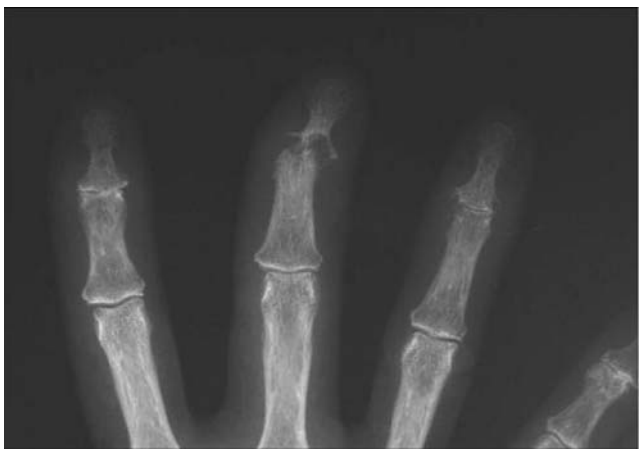

Fig. 11.111 Detail PA radiograph of the fingers of the right hand in a patient with psoriasis showing Mickey Mouse ear erosion of the third DIP

While inflammation and destruction are the hallmarks of early disease, bone fusion characterizes late AS. The patients develop fixed kyphosis with a chin-on-chest posture (Fig. 11.120), and their spines and SI joints show characteristic changes. The SI joints fuse (Fig. 11.121), and the syndesmophytes and other ligamentous ossification become continuous, creating the appearance of a "bamboo spine" (Fig. 11.122). Fusion of the posterior facet joints may give rise to a "trolley track" sign on AP images of the spine (Fig. 11.123). The loss of mobility inevitably leads to loss of mineral and osteoporosis, seen as osteopenia on imaging. With this the vertebral bodies may take on a ballooned appearance (Fig. 11.124).

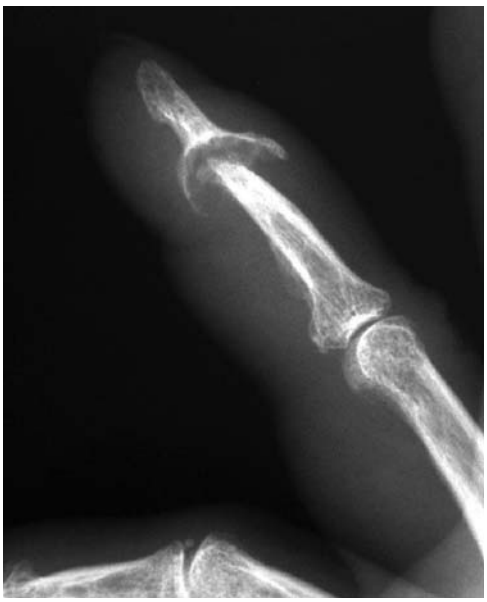

Fig. 11.112 Lateral radiograph detail of the third digit in a patient with psoriasis showing "pencil-in-cup" deformity

Sudden return of mobility is a sign of fracture through the fused bone mass and is an acute emergency as the mobility implies spinal instability. These fractures will appear as so-called chalk stick type of fractures (Fig. 11.125), having a transverse orientation relative to the long axis of the spine. They are most common where the spine normally reverses its curvature and therefore experiences the greatest shear stress, i.e., the cervicothoracic and throacolumbar junctions. Sometimes these fractures may go undiagnosed, and the patient may develop a pseudoarthrosis of the spine that affects both the anterior and posterior columns of the spine. This lesion, known as an Andersson or Romanus lesion (Fig. 11.126), may resemble discitis except that the posterior elements are also involved.

Patients with AS (~30%) are prone to painful tendinous inflammation elsewhere in the body, leading to ossification in the tendon insertions in various areas of the body. Most believe that recurrent biomechanical stress and micro-tearing of the tendon insertions lead to inflammation around these insertions. The inflammation and enthesopathy are most common around the iliac crests, the ischial tuberosities, around the large joints (Fig. 11.127), and the calcaneus.

As mentioned, about 30% of AS patients may also develop, usually later in the disease, a large joint arthropathy that resembles RA, but that, unlike RA, may also go onto ankylosis (Fig. 11.128). The hips and knees are most commonly affected. Finally, AS may cause bursal inflammation, not only around the odontoid but elsewhere in the body. Around the calcaneus, this may lead to Achilles tendonitis and plantar fasciitis. It may also cause visible erosions in the bone adjacent to bursae, particularly at the posterior calcaneus (Fig. 11.129).

Table 11.8 Prevalence of HLA-B27 positivity in selected populations.

Population	Positive (%)
Healthy Whites	8
Healthy Blacks	4
Ankylosing spondylitis (Whites)	92
Ankylosing spondylitis (Blacks)	50
Reactive arthritis	60–80
Psoriasis with spondyloarthropathy	60
Inflammatory bowel disease with spondyloarthropathy	60
Acute anterior uveitis, isolated	50
Undifferentiated spondyloarthropathy	20–25

Spondyloarthropathy of Inflammatory Bowel Disease (IBD)

Crohn's disease and less commonly ulcerative colitis patients may develop a spondyloarthropathy that is virtually indistinguishable radiographically from AS. As with psoriasis, the patients' manifestation of the arthropathy may precede other organ involvement, and as such, the radiologist may play an important role in early recognition of the disease.

In a small percentage of patients, the spondyloarthropathic complaints and manifestations do not fall into one of the above well-defined classifications. These patients are classified as having an undifferentiated spondyloarthropathy.

SAPHO Syndrome

SAPHO takes its name not from the Greek word "saphos," but from a constellation of conditions that create an acronym: **S**ynovitis, **A**cne fulminans, **P**ustulosis palmaris, **H**yperostosis, and **O**steitis of the anterior chest wall. It is not a single disease but a collection of different entities that are loosely associated with the syndrome: pustulotic arthro-osteitis (PAO), chronic recurring multifocal osteomyelitis (CRMO), sternocostoclavicular hyperostosis, multifocal osteomyelitis, and sclerosing osteitis of the clavicle. These diseases tend to affect children and young adults.

This group of diseases is thought to be related to the spondyloarthropathies, and at least one study has shown that about one third of patients with SAPHO syndrome have spine-related changes at the discovertebral junctions and in the sacroiliac joints. Others have postulated that the disorders that comprise SAPHO syndrome represent an abnormal immune response to infective agents, similar to

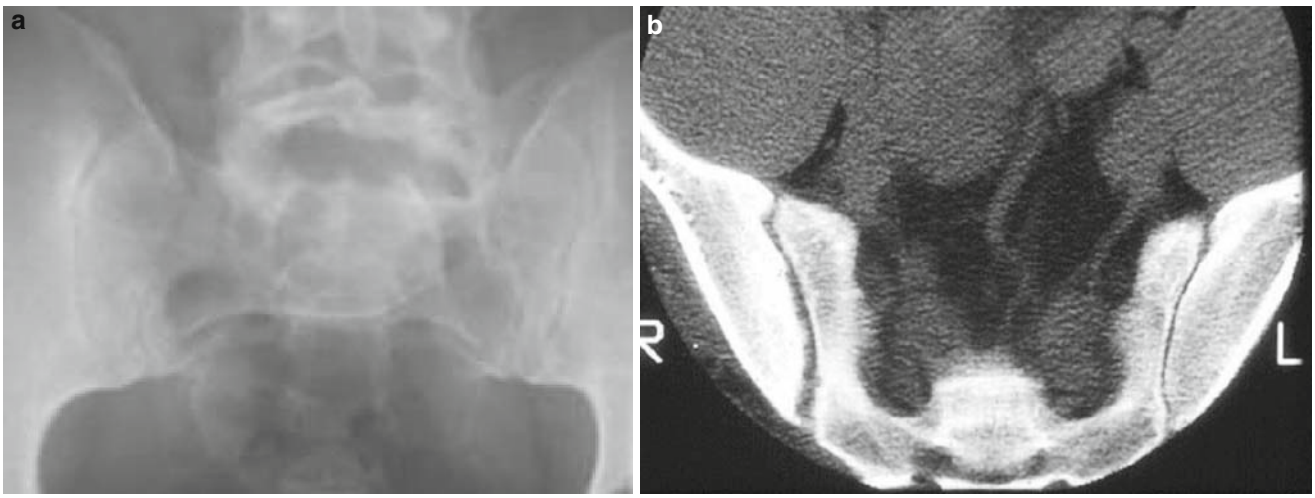

Fig. 11.113 Detail AP radiograph of the SI joints (**a**) and CT scan (**b**) in a patient with psoriasis showing asymmetric erosion of the right SI joint

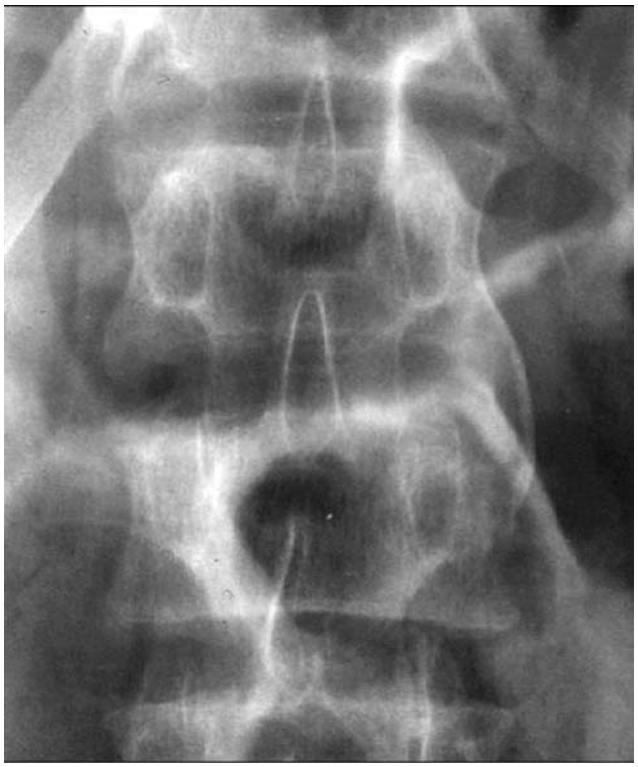

Fig. 11.114 Detail AP radiograph of the lumbar spine in a patient with psoriasis showing an asymmetric nonmarginal syndesmophyte on the left at L1–L2

current hypotheses for the etiology of rheumatoid arthritis. A definite infectious etiology has not been shown, even in cases of recurrent osteomyelitis. In many patients, there is a family history of psoriasis, perhaps explaining why the lesions on the palms of the hands and soles of the feet resemble pustular psoriasis. In most patients, the disease is self-limited and resolves without sequelae.

Multicentric Reticulohistiocytosis (MRH)

Also called lipoid dermatoarthritis, this rare disease causes a polyarticular inflammatory arthritis. The majority of cases (~90%) occur in Caucasians and in women two to three times as often as men. Its onset is usually in the late fourth or early fifth decade. Patients with this disease have

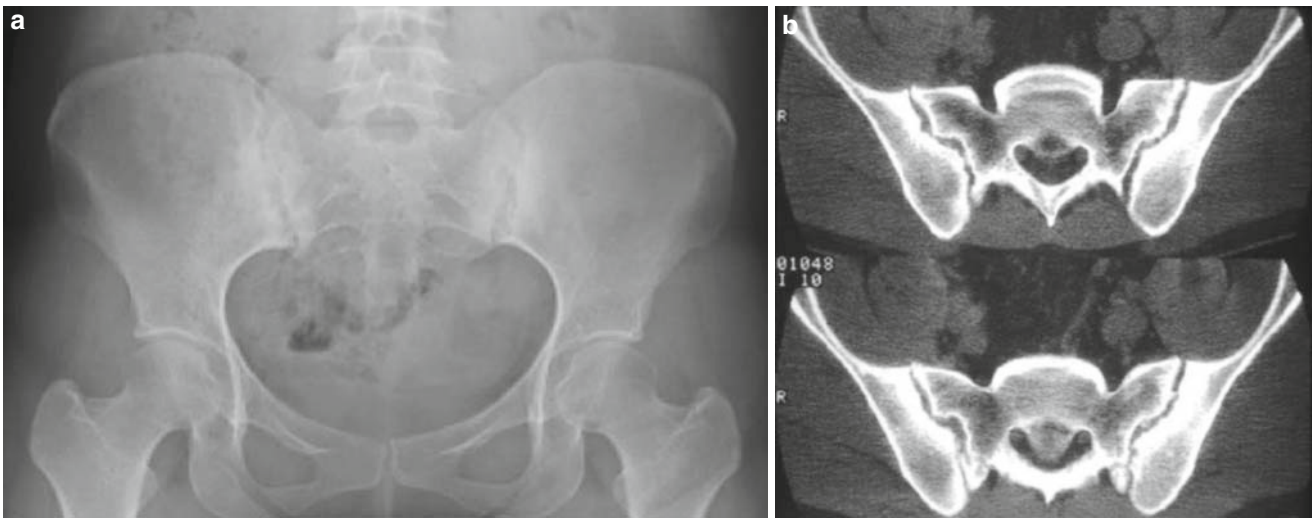

Fig. 11.115 AP radiograph (**a**) and CT images (soft tissue window) (**b**) of a patient with AS showing erosive changes of the SI joints symmetrically as is typical in AS

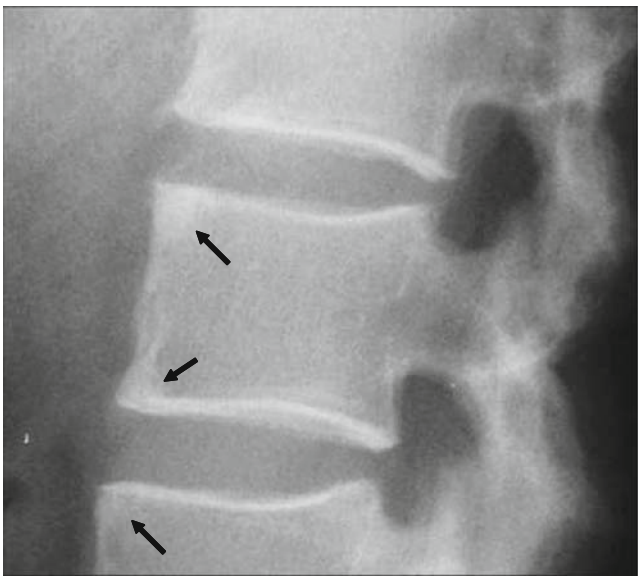

Fig. 11.116 Detail lateral radiograph of the lumbar spine in a patient with AS showing squaring and "ivory corner" signs (*arrows*), reactive sclerosis in the region of the ring apophysis of the vertebral body related to inflammation

reddish brown papulonodular skin lesions that occur on the face and extremities (Fig. 11.7). The lesions range in size from a few millimeters to several centimeters in diameter. Histologically the nodules show an eosinophilic and histiocytic proliferation. It is possible for these lesions to resolve spontaneously. Some have observed that new lesions may develop after minor trauma (Koebner phenomenon).

MRH may be paraneoplastic as about 30% of patients have an underlying malignancy, and in ~70% of cases the development of MRH precedes the diagnosis of malignancy. This observation is unreliable, however, because of the rare nature of the disease.

The hands (Fig. 11.130) are most commonly affected in MRH, followed by knees, shoulders (Fig. 11.131), wrists (Fig. 11.132), hips, ankles, elbows, feet, and spine. When the arthritis involves the hands, it resembles psoriatic arthritis in that it typically involves the DIP and to a lesser extent the PIP joints and shows no periarticular osteopenia. Unlike psoriasis, however, MRH arthritis is usually bilaterally symmetric and does not lead to ankylosis. The erosions tend to be sharply marginated (Figs. 11.130, 11.131 and 11.132). MRH may progress rapidly, and distressingly, about 45% of patients with this disease will develop arthritis mutilans (Fig. 11.4).

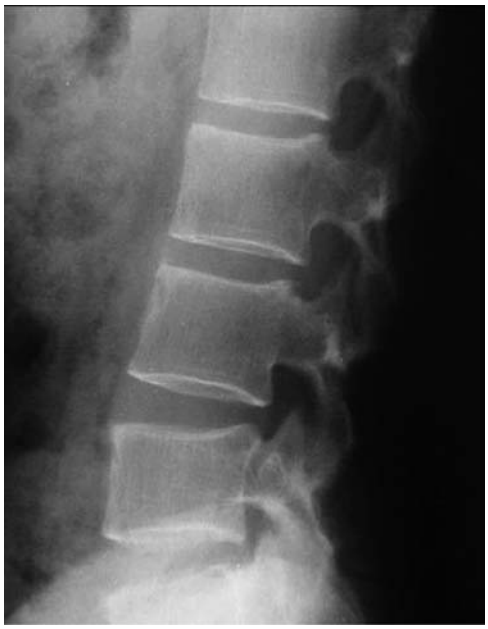

Fig. 11.117 Detail lateral radiograph of the lumbar spine in a patient with AS showing squaring (loss of the normal concave anterior surface) of the vertebral bodies

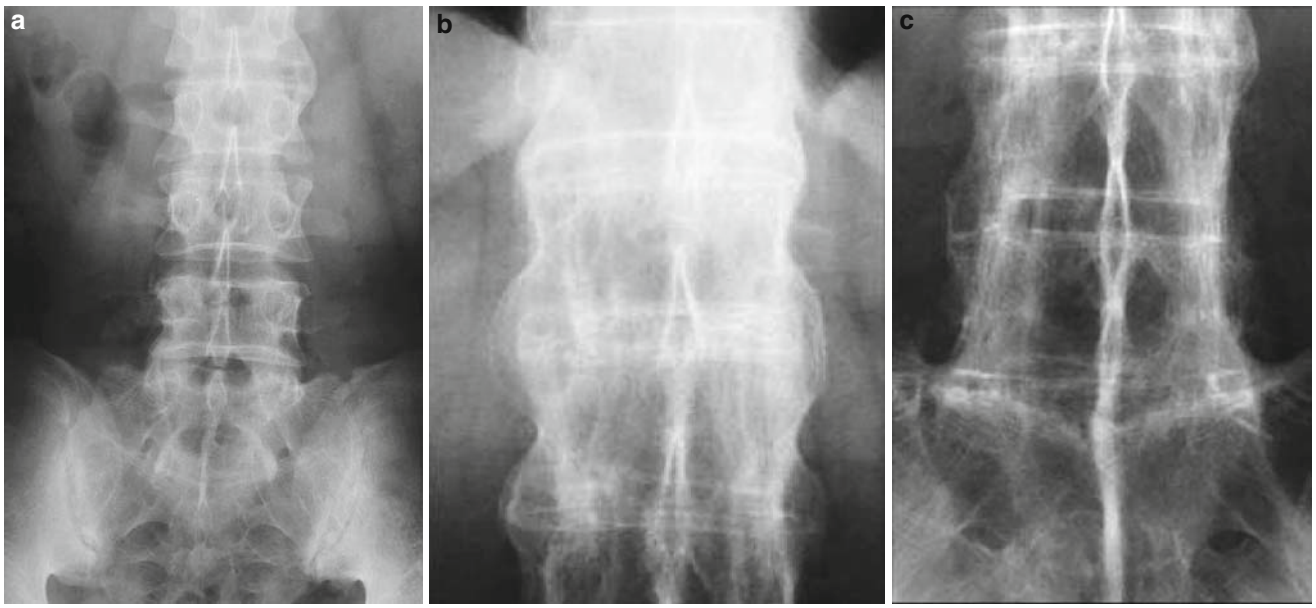

Fig. 11.118 Detail AP radiographs (**a**–**c**) of the lumbar spine in three patients with AS showing syndesmophytes in progressive stages of the disease from early to late

Amyloid Arthritis

The frequency of amyloid arthritis has increased with the use of long-term dialysis. The arthritis is usually caused by the deposition of β2-microglobulin in the joints. Occasionally this arthritis may arise in other diseases that produce either β2-microglobulin or light chain amyloid such as multiple myeloma.

Amyloid arthritis is most common in the spine, wrists, and large joints. In the spine, it causes disk-centered destruction, typically in the cervical spine, that may resemble infectious

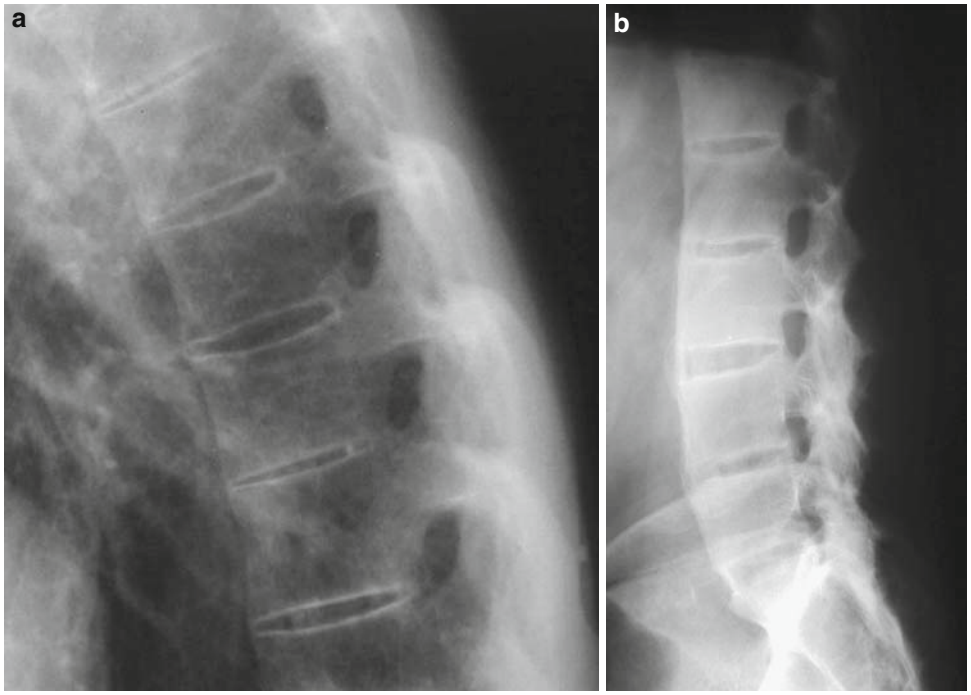

Fig. 11.119 Detail lateral radiograph of the thoracic spine (**a**) and the lumbar spine (**b**) in patients with AS showing fusion of the posterior elements as well as changes in the vertebral bodies

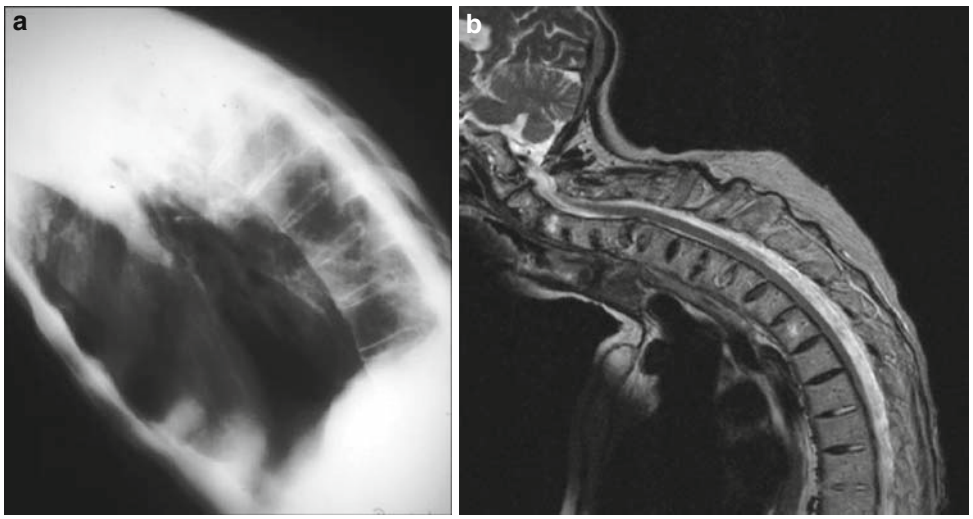

Fig. 11.120 Lateral chest radiograph (**a**) and sagittal T2-weighted MR image of two patients with late stage AS showing fixed kyphosis of the thoracic spine

discitis (Fig. 11.133). In the synovial joints, amyloid arthritis causes large lytic lesions that resemble cystic (robust) RA (Fig. 11.134). The deposits cause low to intermediate signal on both T1- and T2-weighted MRI sequences (Fig. 11.135). Therapy for this disease is centered on treatment of the cause of the underlying amyloidosis and palliation.

Pigmented Villonodular Synovitis (PVNS)

PVNS is an uncommon benign proliferative disease of the synovium that arises most frequently in patients aged 20–50 years. Pathologically, the synovial nodules of PVNS are identical to that seen in giant cell tumors of tendon sheath

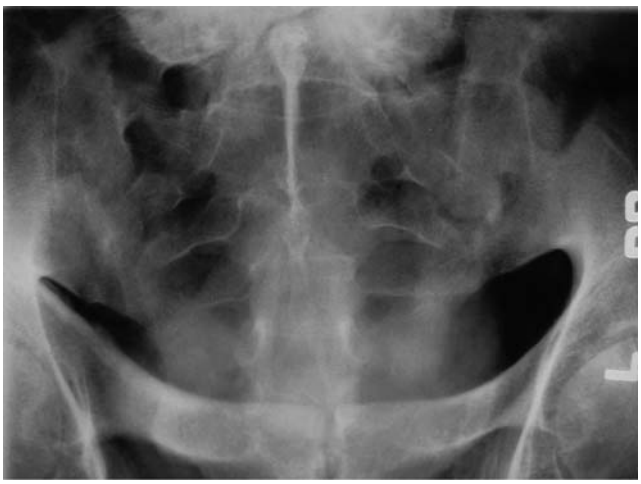

Fig. 11.121 AP radiographic detail of the sacroiliac joints in a patient with AS showing bilateral complete fusion

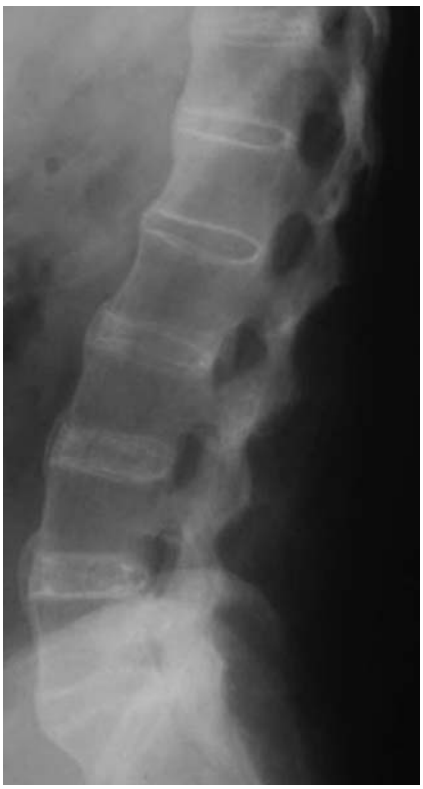

Fig. 11.122 Lateral radiograph the lumbar spine in a patient with AS syndesmophytes and ligamentous ossification creating a bamboo spine appearance

(Fig. 11.136). This disease may affect the synovium of the joints, bursae, and tendon sheaths and is most common in the hips, knees, and ankles. Typically it causes diffuse nodular changes throughout the joint but rarely may give rise to

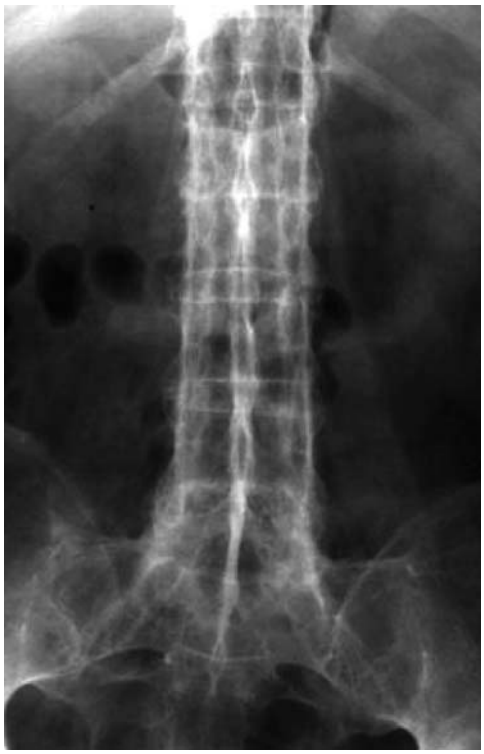

Fig. 11.123 AP radiograph the lumbar spine in a patient with AS syndesmophytes and ligamentous ossification creating a trolley track appearance

a focal nodular form. The proliferative nodules have a tendency to bleed, and over time, hemosiderin is deposited in the joint giving rise to characteristic pigmentation of the nodules and a "crankcase oil" appearance of the affected joint fluid.

Early in the disease, the nodules may cause pain and recurrent hemarthroses, saucerized erosions, and subchondral cysts on either side of the joint. Radiographically, these phenomena are seen as hyperdense effusions (Fig. 11.137) and smooth corticated saucerizations (Fig. 11.138) with relative preservation of the joint space. MRI has proven very useful to make the diagnosis because of the paramagnetic effects of hemosiderin. MRI shows joint effusion with dark signal lining the synovium and internal structures of the joint (Fig. 11.137 and Fig. 11.139). This material shows susceptibility effects on gradient echo imaging, resulting in "blooming" of the low signal (Fig. 11.139). Calcification is rare in cases of PVNS, and if present, alternative diagnoses should be considered, particularly synovial cell sarcoma (Fig. 11.140).

Treatment usually consists of synovectomy, but the disease has a tendency to recur, requiring placement of a joint prosthesis. If left untreated, PVNS will eventually cause hyaline cartilage destruction and secondary osteoarthritis.

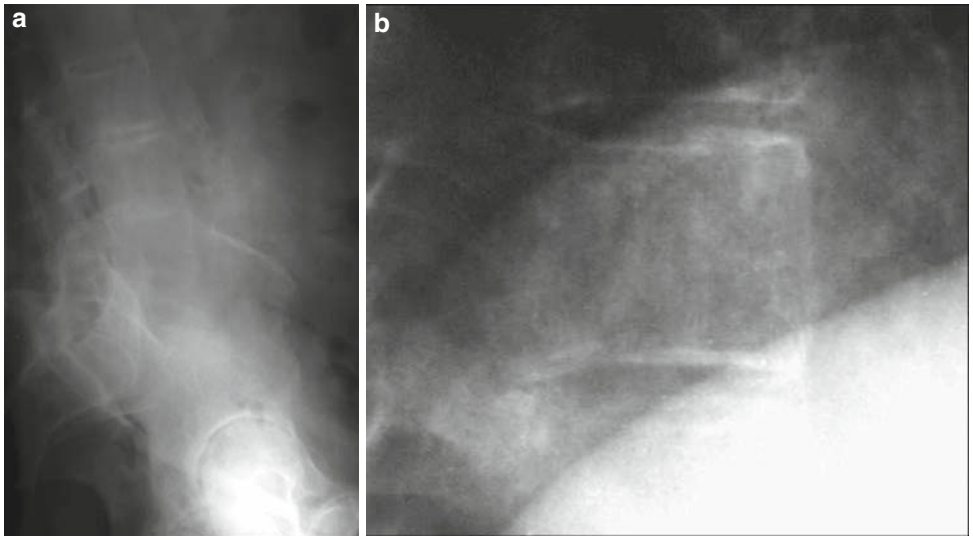

Fig. 11.124 Lateral lumbar radiograph (**a**) and detail from another patient (**b**) showing ballooning of the vertebral bodies and severe osteopenia. Note the severe osteopenia and also the erosion of the hip joints (**a**) consistent with AS involvement of other large joints

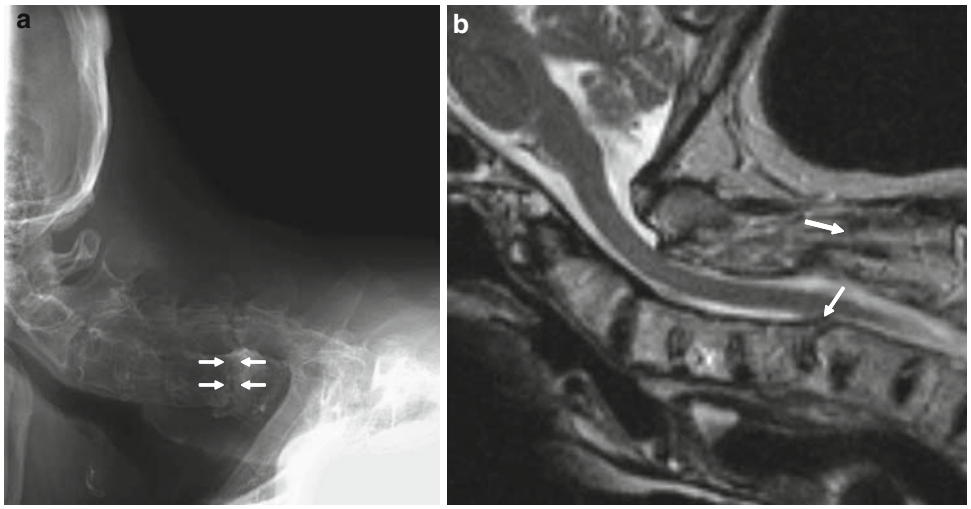

Fig. 11.125 Lateral cervical spine radiograph (**a**) and T2-weighted sagittal MR of a patient with AS and sudden new movement in the lower cervical spine. Images reveal a fracture through the previously fused C5–C6 disk space and posterior elements (*arrows*)

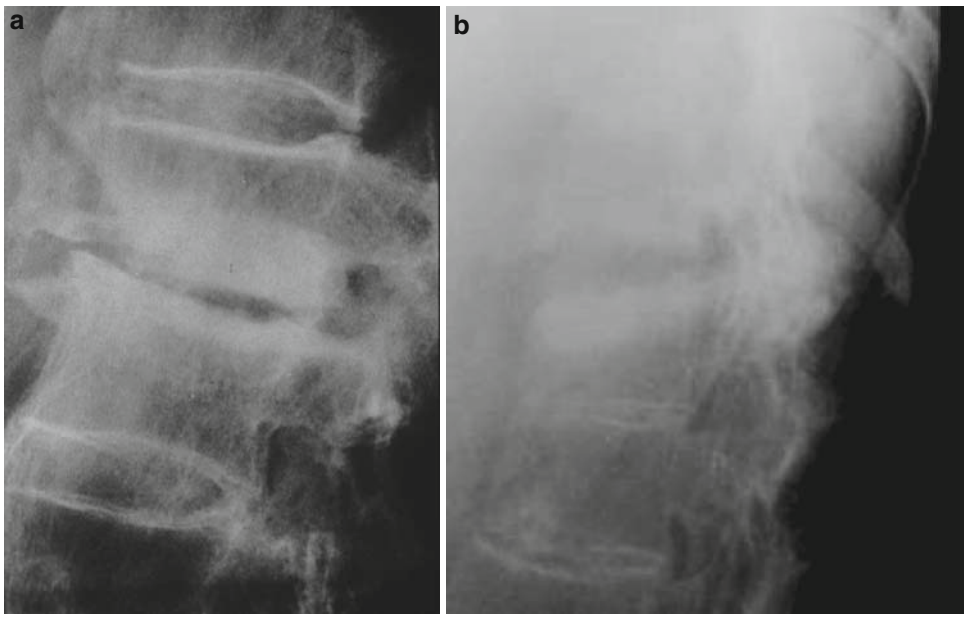

Fig. 11.126 Lateral lumbar radiograph detail showing a chronic pseudoarthrosis (Andersson/Romanus lesion) through the L2–L3 disk level (**a**) and the T12–L1 disk level (**b**) in patients with AS

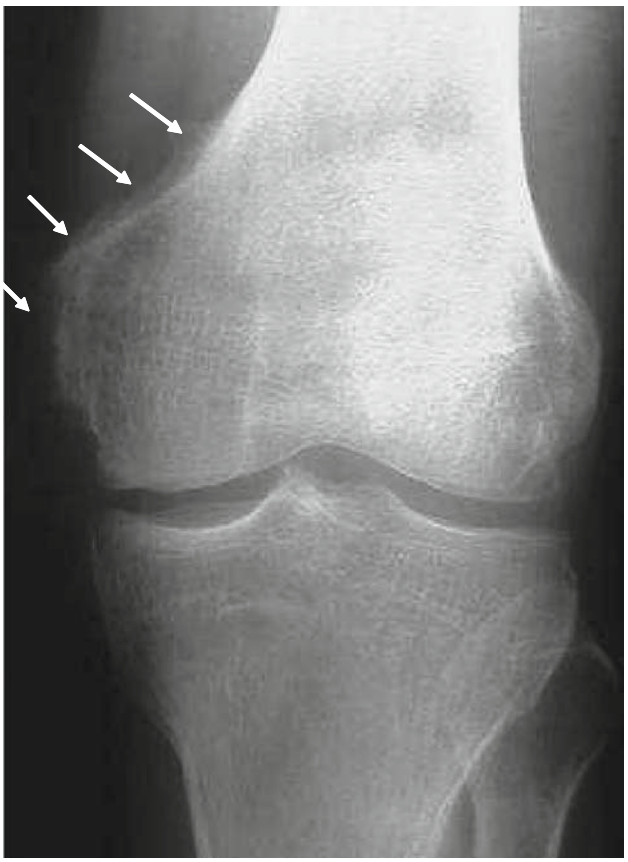

Fig. 11.127 AP radiograph of the knee showing enthesopathic changes medially from the region of the adductor tubercle of the femur. Note the productive bone formation in this area (*arrows*)

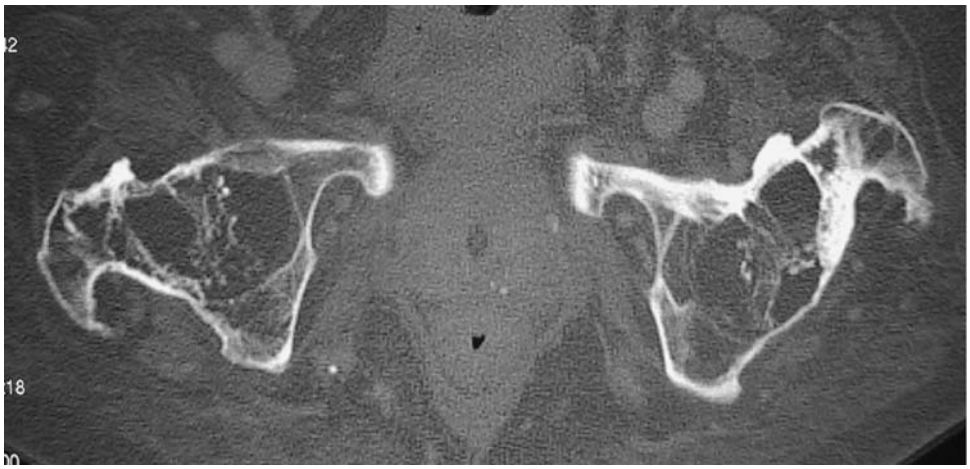

Fig. 11.128 CT image showing complete fusion of the hips bilaterally in another patient with advanced AS and large joint arthritis

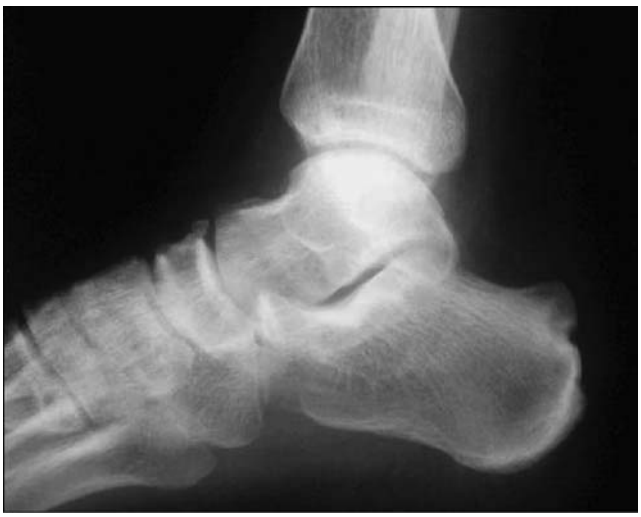

Fig. 11.129 Lateral radiograph of the calcaneus from a patient with AS showing dorsal bursal erosions from bursitis. Note that these erosions now have cortex along their bases indicating that they are not currently active

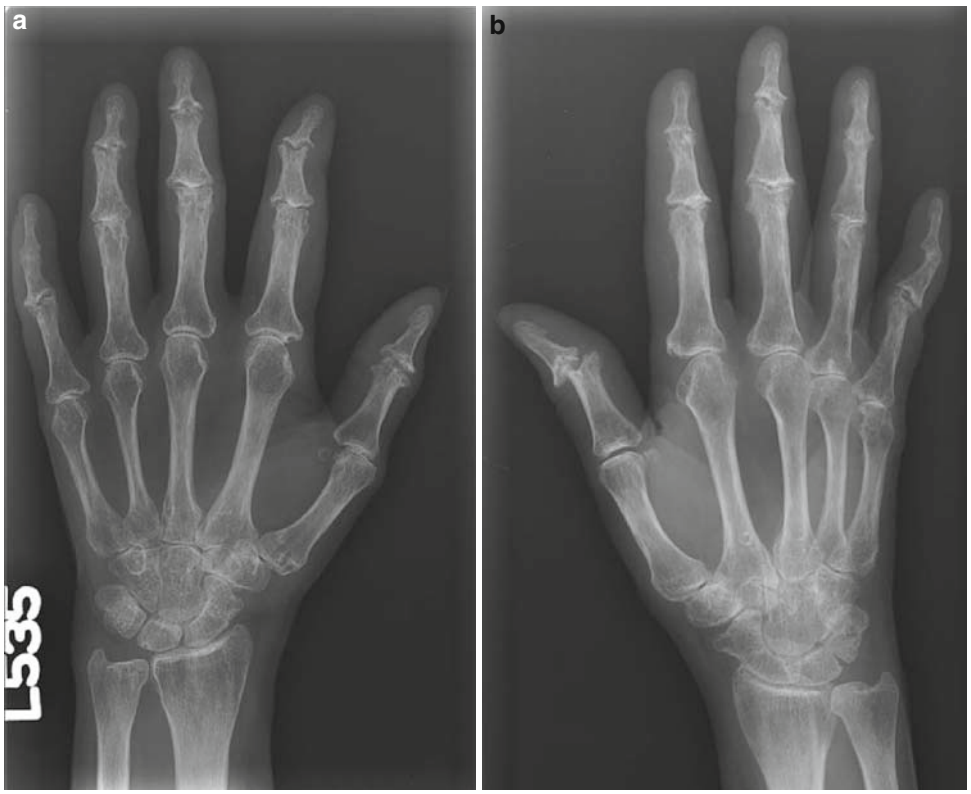

Fig. 11.130 PA radiographs of the left (**a**) and right (**b**) hands of a patient with MRH showing symmetrical distal erosive arthritis with relative joint preservation

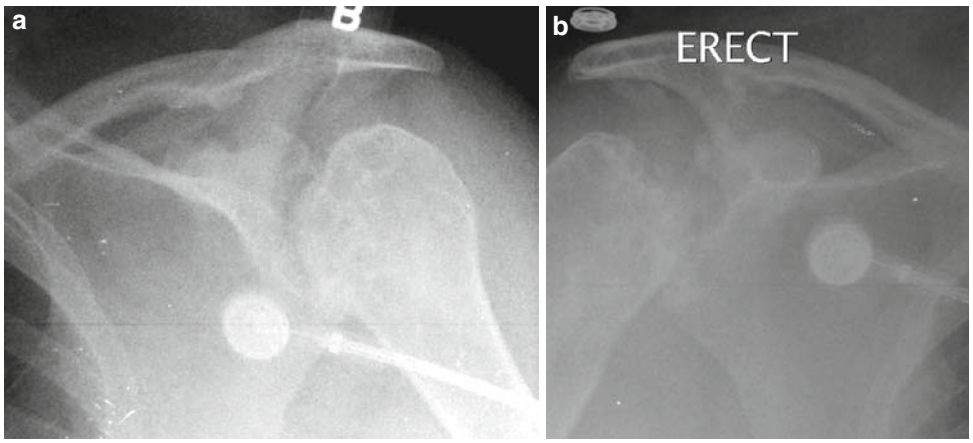

Fig. 11.131 AP radiographs of the left (**a**) and right (**b**) shoulders in a patient with MRH showing server erosive arthropathy of the glenoheumeral joints

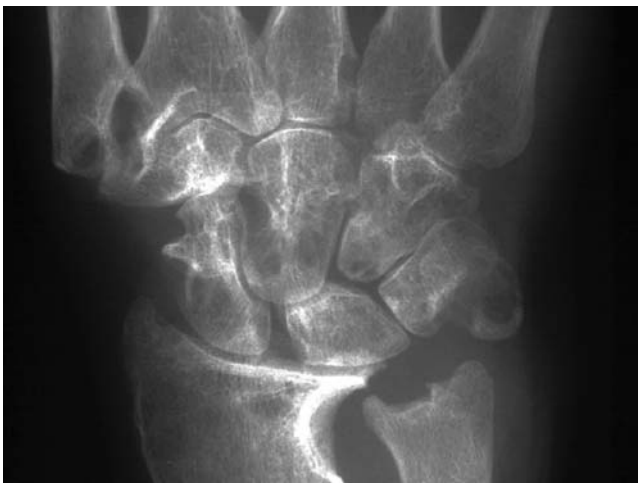

Fig. 11.132 PA radiograph of the left wrist showing severe erosive arthropathy of MRH. Note the presence of large erosions and subchondral cysts, reminiscent of robust RA, gout or amyloid arthropathy *(vide infra)*

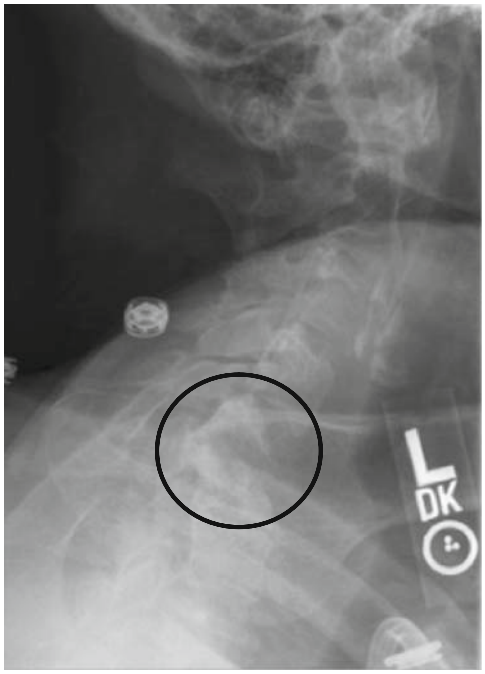

Fig. 11.133 Lateral cervical spine showing amyloid spondyloarthropathy at C5–C6 (*circle*) in a patient on long-term dialysis. Note the destructive nature of the disease and its focality resembling infectious discitis

Productive and Destructive Arthropathies

This class of arthropathies shows both erosive and productive changes together in the same joint. Erosive osteoarthritis is the prototype of this type of arthritis. This imaging pattern also becomes manifest in cases of old burned-out destructive arthropathies where, for reasons of altered biomechanics, the joints develop secondary osteoarthritis superimposed on old inflammatory changes within the joint. Gout, too, though typically destructive, may give an appearance of a combination of destruction and production. In part, this may, be the result of bone production in the healing phase between acute attacks, the loss of hyaline cartilage to synovitis, and bone production induced by urate. On the other side of the coin, neuropathic arthritis may cause so much joint disintegration that it may appear destructive as well as productive.

Erosive Osteoarthritis

This form of osteoarthritis is most common in older women in their seventh and eighth decades of life. The hands are most often affected. Erosive osteoarthritis is often confused with psoriatic arthritis because of its similar distribution and destructive nature (Fig. 11.141). As with psoriasis, erosive OA may lead to bone ankylosis across joints. Two features can help differentiate this arthropathy. First, as with typical OA, the first carpal metacarpal joints are typically involved in erosive OA. This finding may be unreliable, however, since many older patients with other arthropathies will also have OA involving this joint. The second distinguishing feature of erosive OA is that erosions in this disease do not start at the periphery of the joint. This is because the hyaline cartilage already has been lost to the underlying OA, leaving the cortical surface exposed to the inflammatory synovitis. As a result, the bone across the joint is exposed to the inflammatory synovitis. This results in joint erosions that give the joint an appearance like a seagull in flight. These are known as "gull-wing" erosions (Fig. 11.142). As with other inflammatory arthropathies, severe cases rarely may progress to arthritis mutilans (Fig. 11.143). Often, the radiographic appearance of erosive OA combined with the appropriate demographics allows the radiologist to suggest it as the first differential diagnosis.

Nondestructive and Nonproductive Arthropathies

Although these diseases do not actually cause morphological alterations in joint architecture and hence technically are not arthropathies, a few conditions are traditionally placed in this category. These include the joint-related abnormalities of systemic lupus erythematosis (SLE), scleroderma, Ehlers Danlos syndrome, agammaglobulinemia, and those abnormalities associated with rheumatic heart disease, also known as Jaccoud's arthropathy.

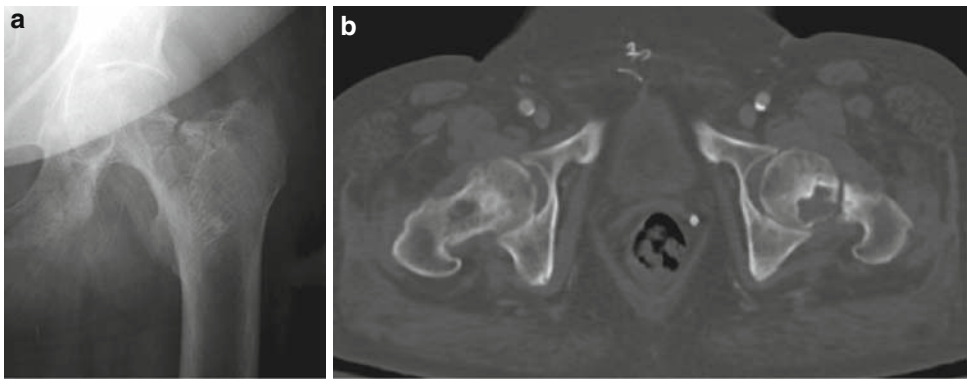

Fig. 11.134 AP radiograph (**a**) and image from a CT (**b**) showing a pathological fracture of the hip with a large lytic collection of amyloid

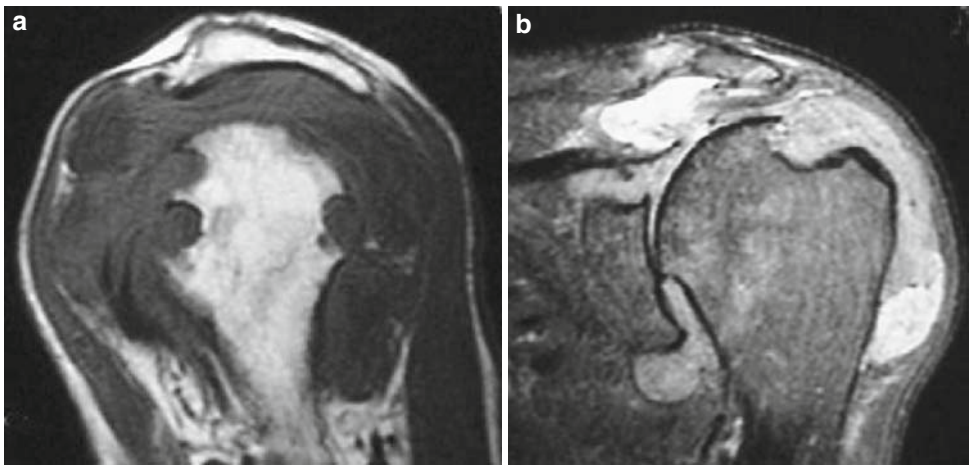

Fig. 11.135 T1-weighted sagittal (**a**) and T2-weighted fat suppressed coronal (**b**) images of the shoulder showing large amyloid masses that are low in signal intensity on both sequences

Systemic Lupus Erythematosus (SLE)

SLE is a common multisystem disease with a prevalence of about 1 in 2000 people, typically women of childbearing age. It has a higher prevalence in African Americans than Caucasians, but oddly is rare in Africans. It is a multisystem disease affecting the skin with a malar rash and photosensitivity, the oral and nasopharyngeal mucosa with aphthous ulcers, serous tissue with pleuritis and pericarditis, the kidneys with nephritis, the CNS with cerebritis, the myeloproliferative system with depressed cell production, the immune system with abnormal antibodies and, of course, the musculoskeletal system with a nonerosive and nonproductive arthritis (10%).

Patients with SLE develop myopathy and inflammation in the tendons of their hands, ligamentous laxity, and swelling about their joints. The laxity allows the patients to develop marked ulnar deviation in their MCP joints and subluxations and dislocations in the small joints of the hands and feet (Fig. 11.144). Remarkably, these subluxations are easily reduced temporarily so that a patient may appear abnormal on one radiographic study and completely normal on the next. The joint spaces are usually uninvolved, however. Inflammation in their muscles leads to eventual soft tissue wasting, particularly in their thenar and hypothenar eminences (Fig. 11.144). Less frequently they develop soft tissue calcifications similar to those seen in scleroderma or dermatomyositis (Fig. 11.145).

Jaccoud's Arthropathy

Joint involvement is common during acute rheumatic fever (50–70%). Manifestations range from arthralgias to inflammatory arthritis with swollen, erythematous, and tender joints. The larger joints are most often involved. The arthritis usually subsides within a few weeks of treating the disease. Rarely, the patients may develop periarticular fibrosis and

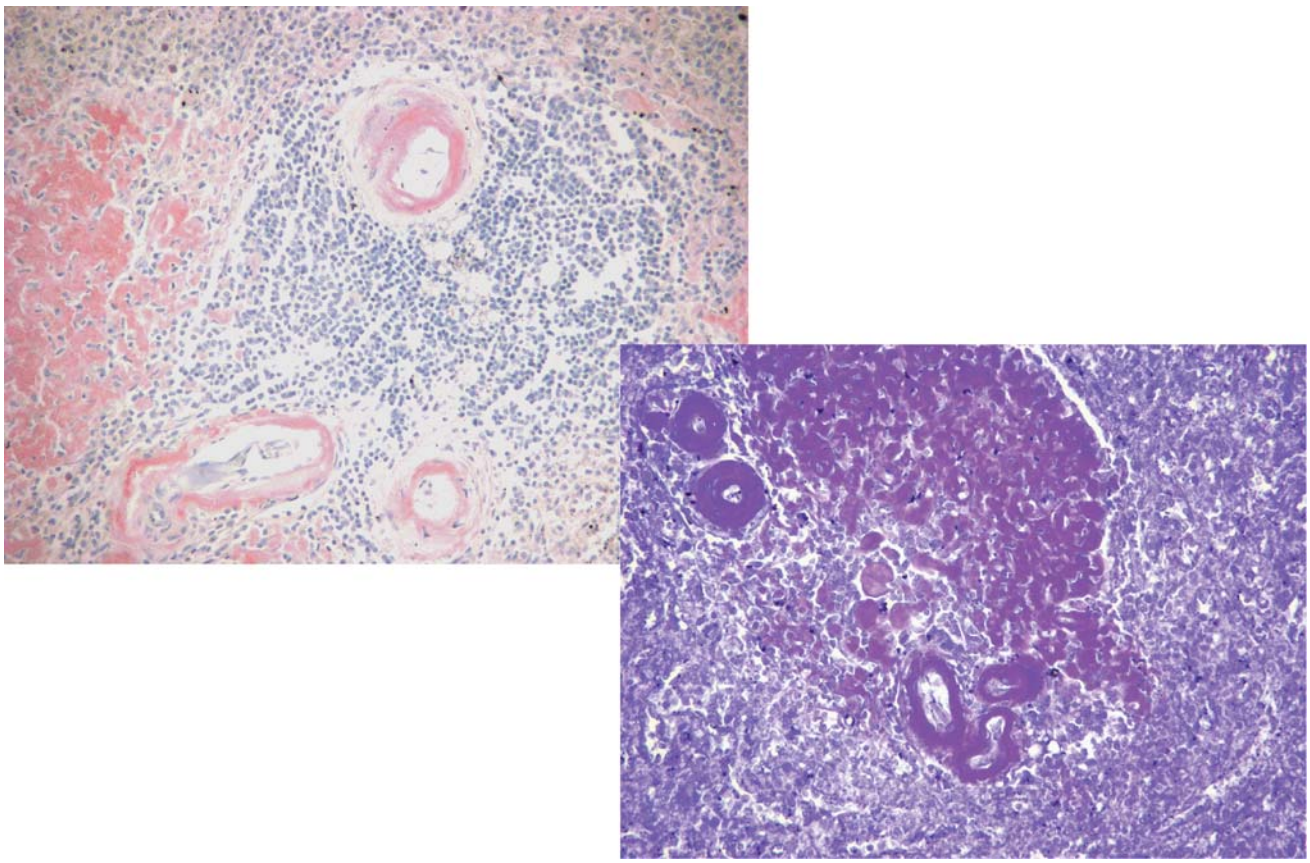

Fig. 11.136 Amyloid. There is deposition of amyloid around vessels as well as within the parenchyma of this spleen. It is highlighted by Congo red stain (*top left*) where it stains red and crystal violet stains (*bottom right*) where it stains with a magenta color

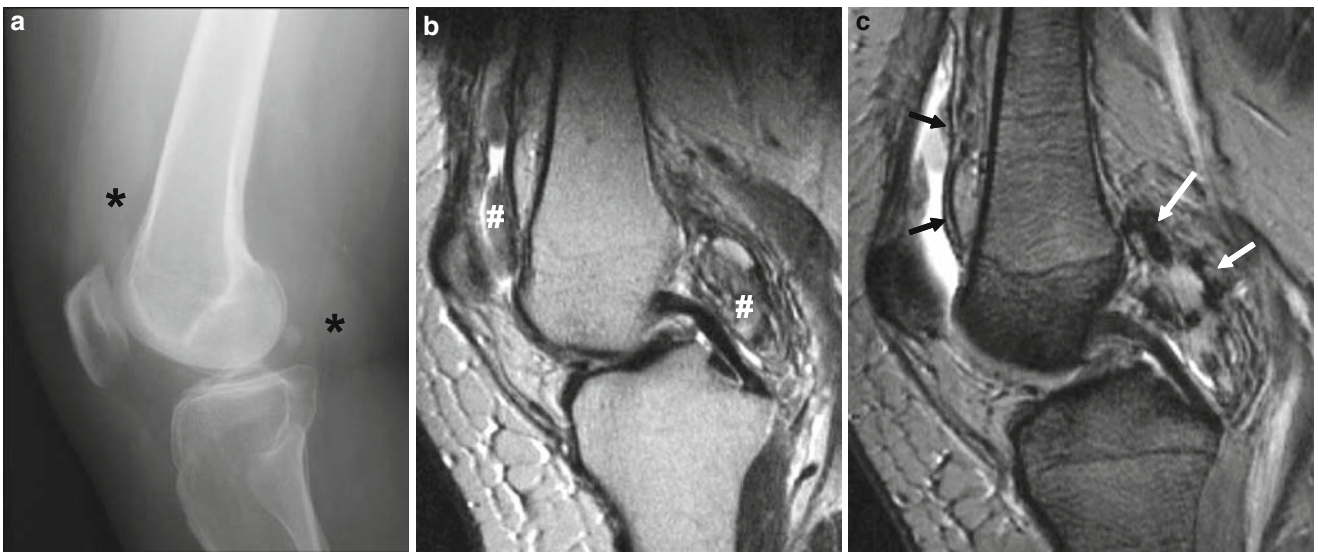

Fig. 11.137 Lateral radiograph (**a**), sagittal PD MR image (**b**), and sagittal T2-weighted fat suppressed image of the knee in a patient with PVNS showing hyperdense effusion (∗) (**a**), soft tissue nodules (#) and hemosiderin tattooing of the capsule (*arrows*)

ligamentous laxity that resembles SLE arthritis radiographically (Fig. 11.146). This phenomenon was described by the French physician Sigismond Jaccoud and now is known as Jaccoud's arthritis.

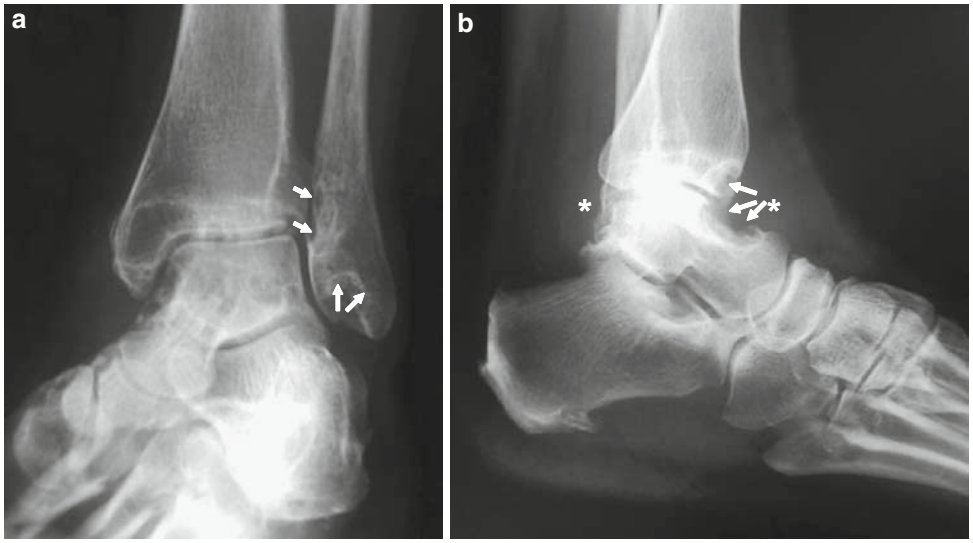

Fig. 11.138 Lateral (**a**) and AP (**b**) radiographs of the ankle in a patient with PVNS showing large saucerizations of the bone (*arrows*) indicating chronic pressure erosion from an external process and a dense effusion compatible with chronic exudation of blood products into the joint space (∗)

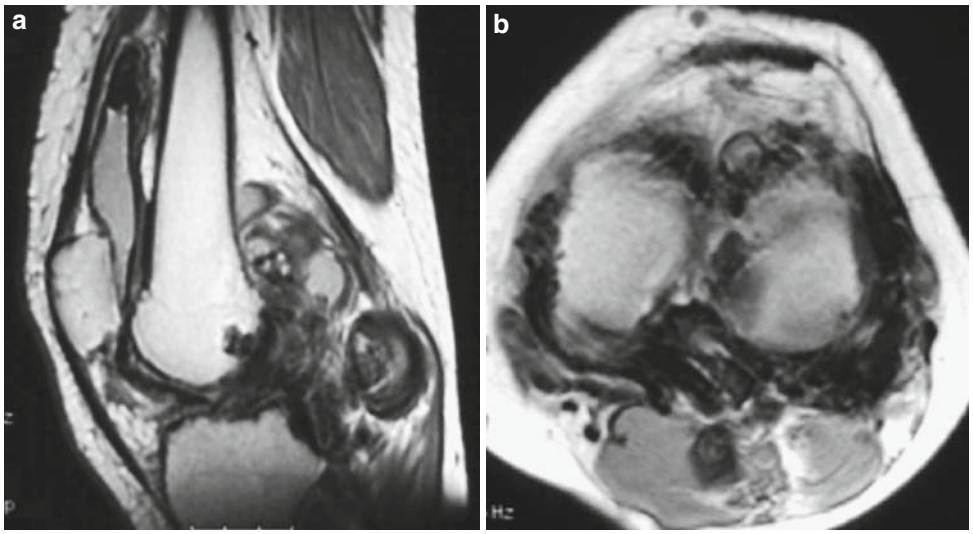

Fig. 11.139 Sagittal (**a**) and axial (**b**) GRE image of the knee in a patient with PVNS showing dark paramagnetic blooming of the signal from hemosiderin

Miscellaneous Joint-Related Conditions

Though not actually arthropathies a few conditions warrant discussion in this chapter. These are conditions that occur either around joints or bursae, i.e., diffuse idiopathic skeletal hyperostosis, Haglund's disease, and scleroderma or within the joint space, with the potential to lead to arthritis, i.e., synovial chondromatosis and chondromalacia patella.

Diffuse Idiopathic Skeletal Hyperostosis (DISH)

Diffuse skeletal hyperostosis (DISH), also known as Forestier's disease and senile ankylosing spondylitis, is a common disease of ligamentous and tendinous ossification. Depending upon where the ossification develops, the disease may cause a variety of complaints or be entirely asymptomatic.

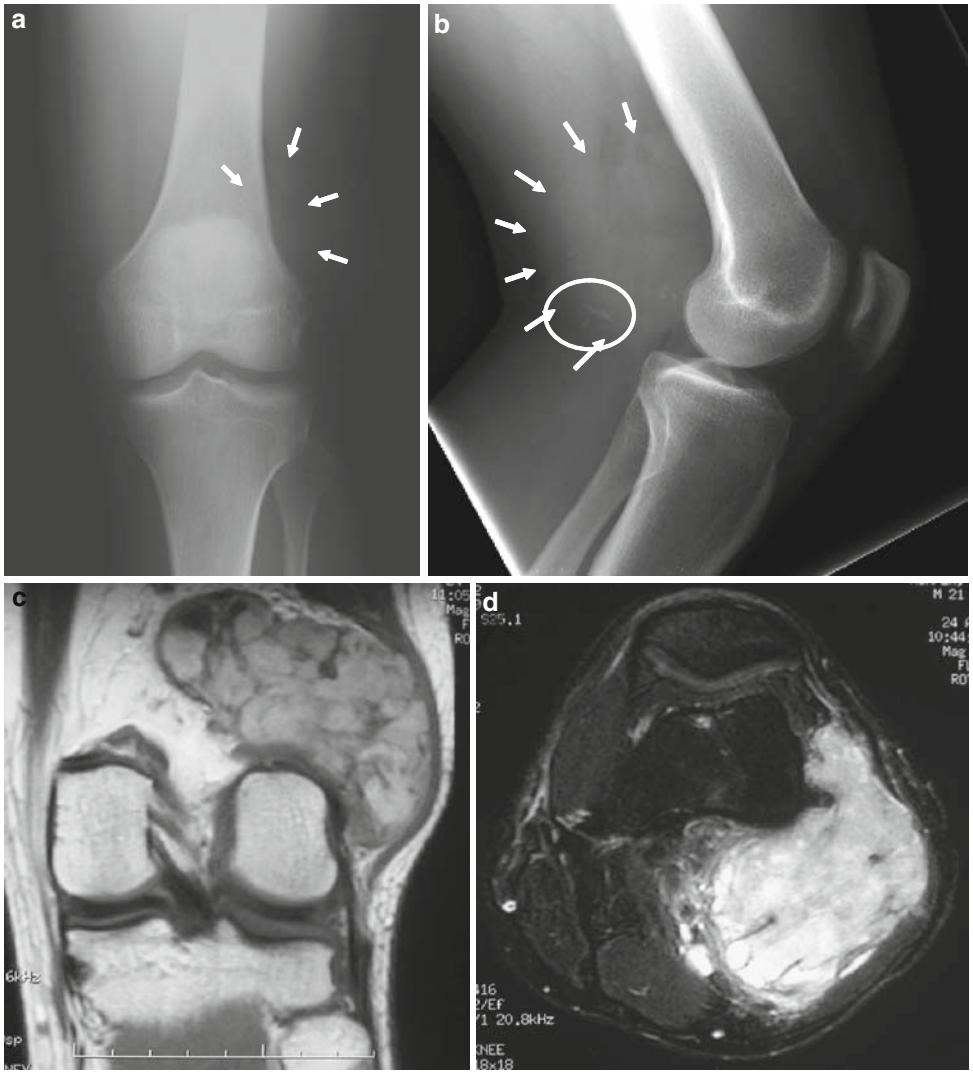

Fig. 11.140 AP (**a**) and lateral (**b**) radiographs and coronal T1-weighted (**c**) and axial T2-weighted fat suppressed (**d**) MR images of a patient with synovial cell sarcoma posterolaterally around the distal femur (*arrows*). Note the calcification (*oval*) in the soft tissues posteriorly in (**b**) as well as the asymmetry of the soft tissue density that help to distinguish this lesion from PVNS

Most commonly the disease affects the spine with prominent anterior longitudinal ligament ossification. Radiographic diagnosis depends on specific criteria of bridging anterior osteophytes over three contiguous disk levels with normal height disk spaces. While these criteria are specific, it is clear that there are patients with DISH who have lesser degrees of ossification. Typical involvement of the thoracic or lumbar spine is asymptomatic and frequently identified on lateral chest radiographs, cervical or lumbar spine studies (Fig. 11.147). On the other hand, prominent osteophytes may develop in the cervical spine and impinge the esophagus causing dysphagia (Fig. 11.148). DISH also affects the ligaments around large joints and may cause prominent ossification in these areas as well (Fig. 11.149). Rarely, this may be so progressive as to cause limitation of motion around the involved joints.

Another disease, now called ossification of the posterior longitudinal ligament (OPLL), has been described recently. Although first noted in Asians, it has now been recognized in other races as well. Most now believe that this condition is a variant of DISH. The posterior longitudinal ligament ossifies and thickens (Fig. 11.150) in OPLL, most commonly in the cervical and upper thoracic spines. As a result, patients with the disease present with long-tract neurological complaints. Therapy is decompressive laminectomy (Fig. 11.150b).

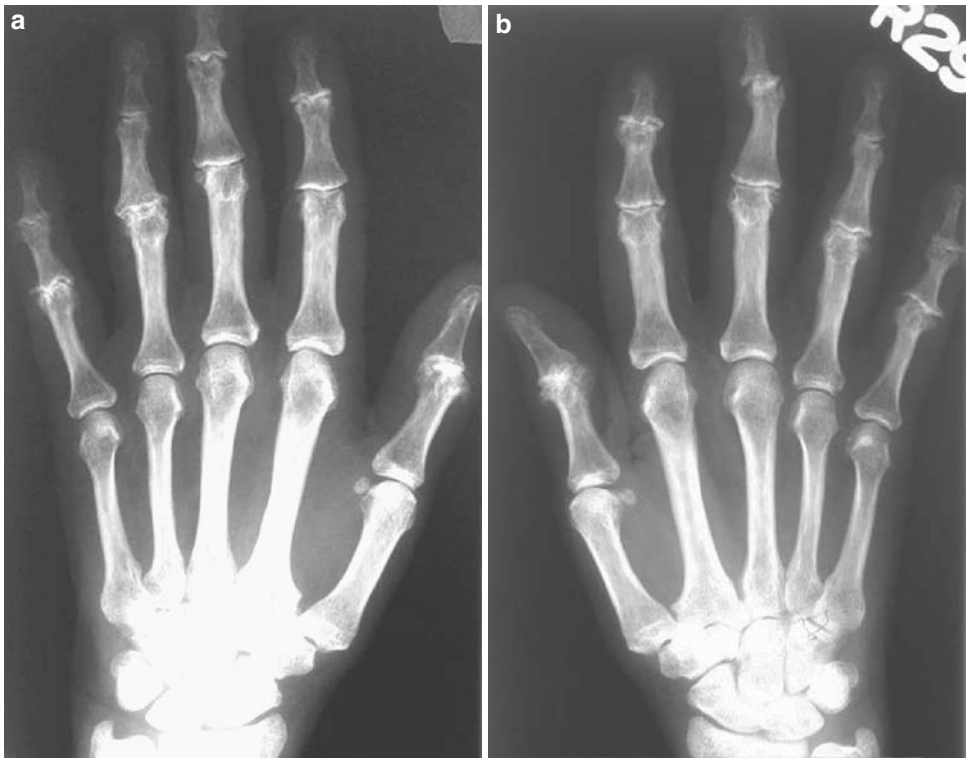

Fig. 11.141 PA radiographs of the left (**a**) and right (**b**) hands in a patient with erosive OA show severe destructive changes in the DIP and PIP joints that could be confused with psoriatic arthritis. The joints also show osteophytes that help to suggest the diagnosis

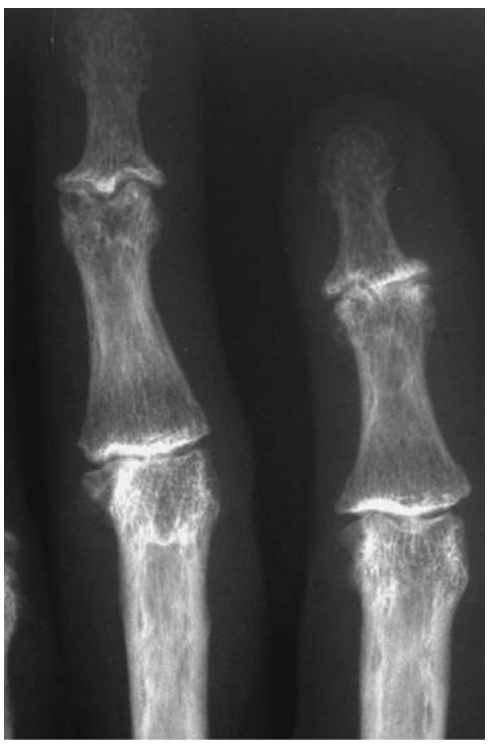

Fig. 11.142 Typical gull-wing erosion of erosive OA in the third DIP joint along with other lesser erosive changes in other joints

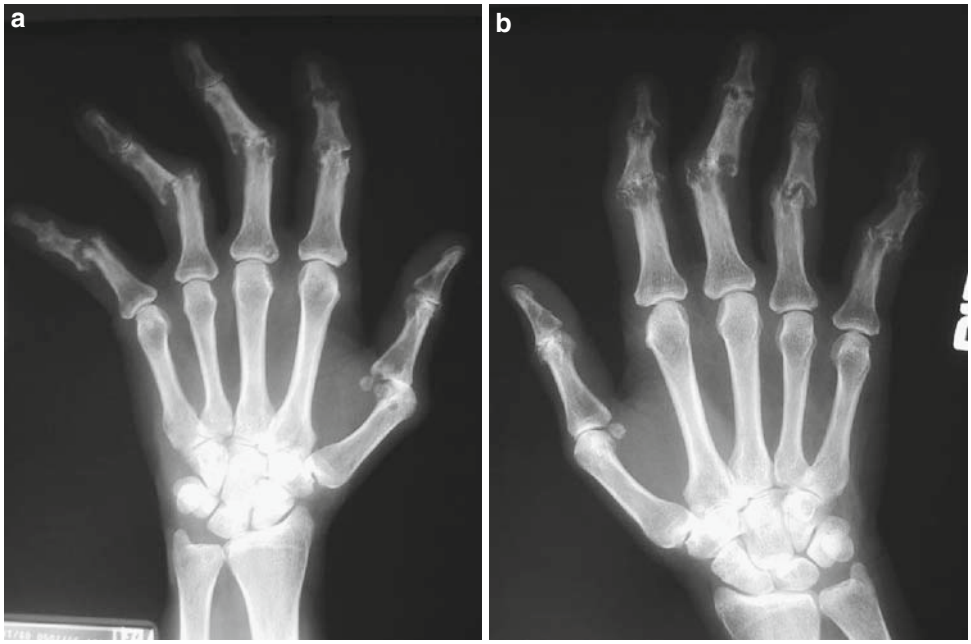

Fig. 11.143 AP radiographs of the left (**a**) and right (**b**) hand showing severe destructive changes related to erosive OA causing arthritis mutilans

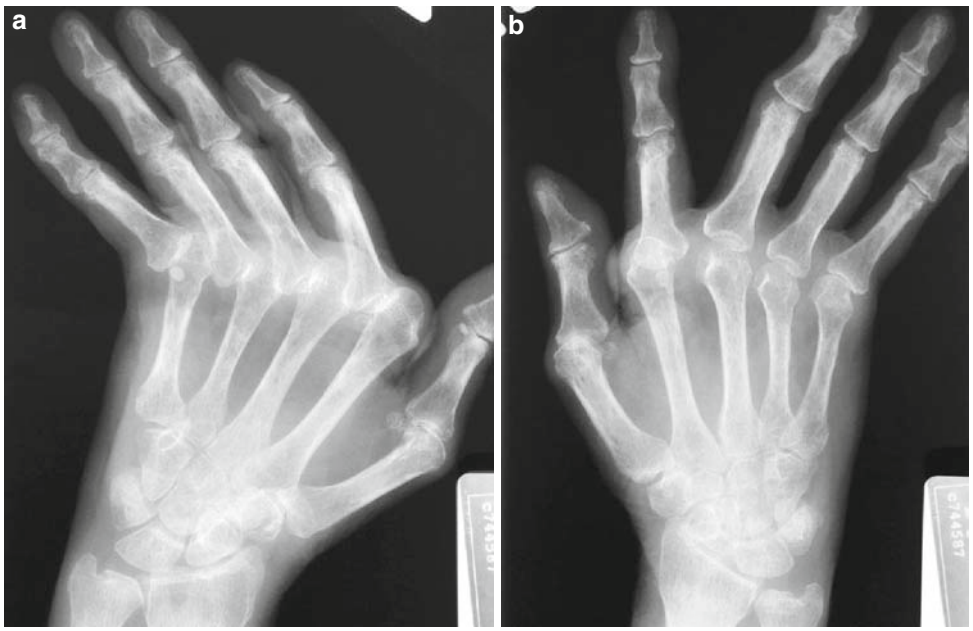

Fig. 11.144 AP radiographs of the left (**a**) and right (**b**) hand in a patient with SLE showing bilateral MCP joint ulnar deviation, subluxations, and dislocations. Note also the atrophy of the soft tissues of the thenar and hypothenar eminences giving a straight or concave appearance instead of their normal convex appearance. This finding is typical or SLE arthropathy

Haglund's Disease

Also known as a pump bump, Haglund's disease represents retrocalcaneal bursitis related to footwear, involving the precalcaneal subtendinous bursa, the post-calcaneal Achilles bursa, or both. Ladies pumps and athletic footwear may cause compression of the retrocalcaneal bursae and subsequent bursitis with pain and inflammation in the Achilles tendon resulting in a palpable bump in this region (Fig. 11.151). Prominence of the posterior superior calcaneus, Haglund deformity, may contribute to the pathogenesis of the disease.

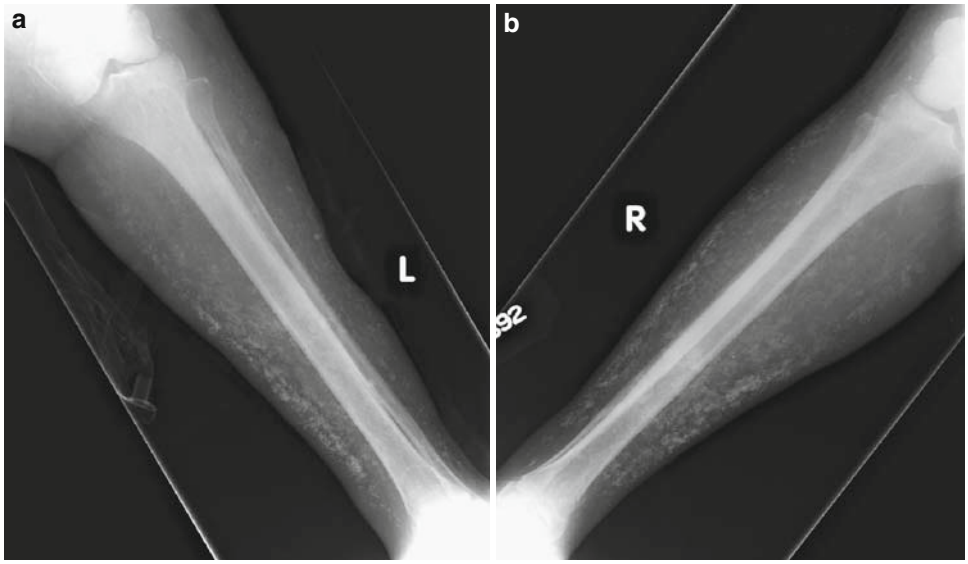

Fig. 11.145 AP radiographs of the left (**a**) and right (**b**) tibiae and fibulae in a patient with SLE showing marked subcutaneous soft tissue calcification. This has a similar appearance to that seen in dermatomyositis and mixed connective tissue disease

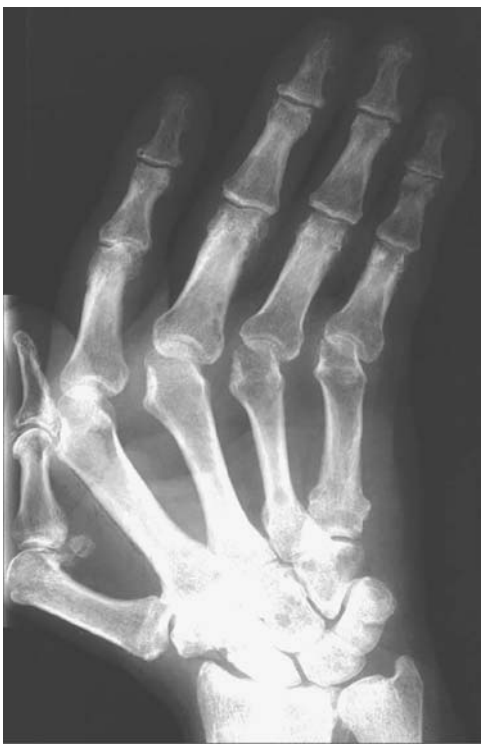

Fig. 11.146 AP radiograph right hand showing MCP joint ulnar deviation, subluxation, and soft tissue wasting in a patient with Jaccoud's arthropathy. This condition is virtually indistinguishable radiographically from SLE arthropathy radiographically

Scleroderma

Scleroderma, or progressive systemic sclerosis, results from inflammation and progressive tissue fibrosis and excessive production and deposition of types I and III collagens. It typically involves the dermis, but it may also involve the gastrointestinal tract, particularly the esophagus and colon and the lungs, where it may cause basilar interstitial fibrosis (Fig. 11.152).

About half of the patients afflicted by scleroderma will complain of arthralgias, but generally, these patients do

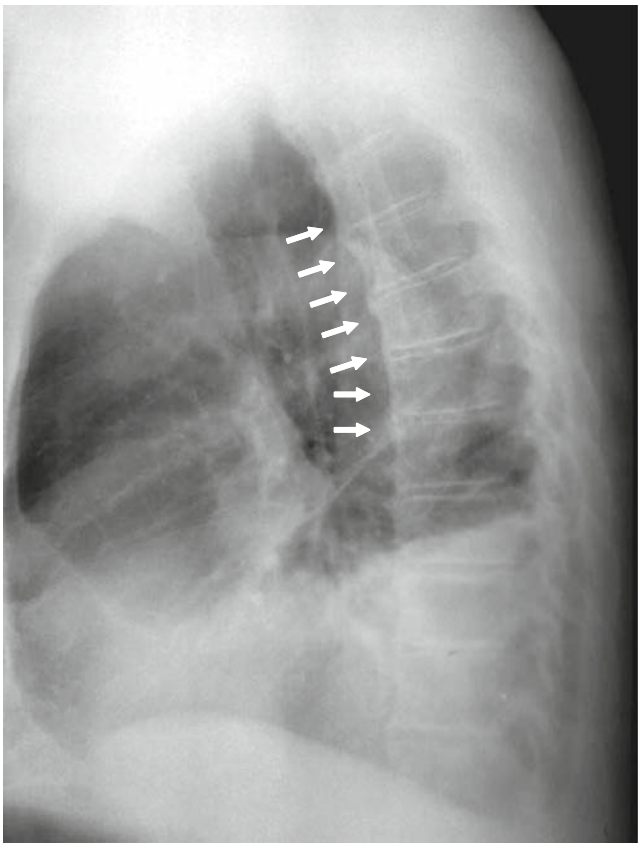

Fig. 11.147 Lateral chest radiograph showing flowing anterior longitudinal ligament ossification (*arrows*) over several levels with normal appearing disk spaces

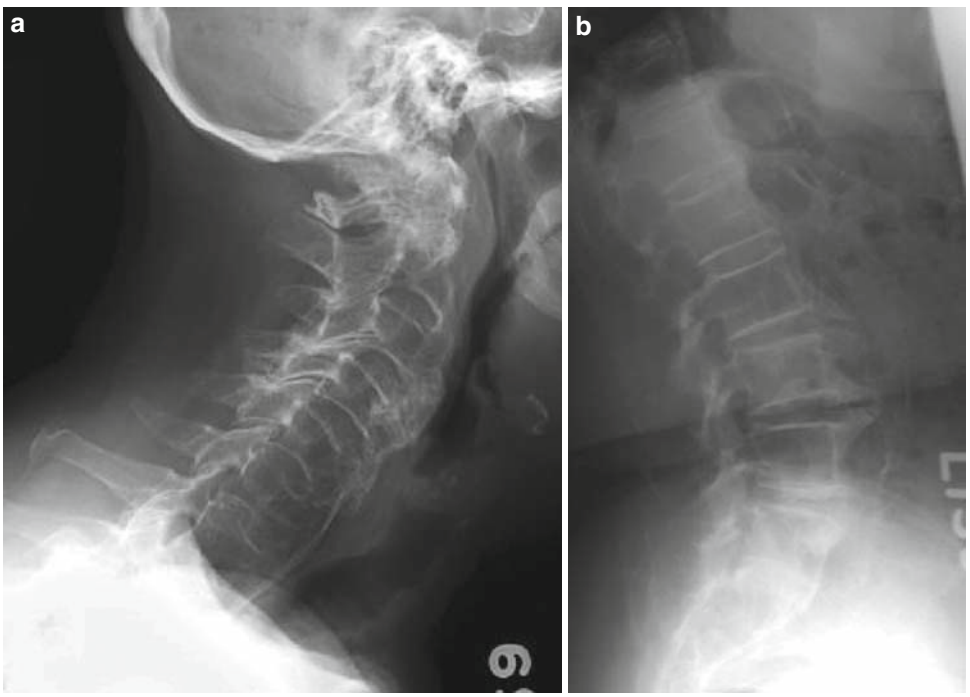

Fig. 11.148 Lateral radiograph of the cervical (**a**) and lumbar spine (**b**) showing marked osteophytes without underlying disk disease. Note that the anterior osteophytes bridge all the consecutive disk levels in the cervical spine making diagnostic criteria for DISH

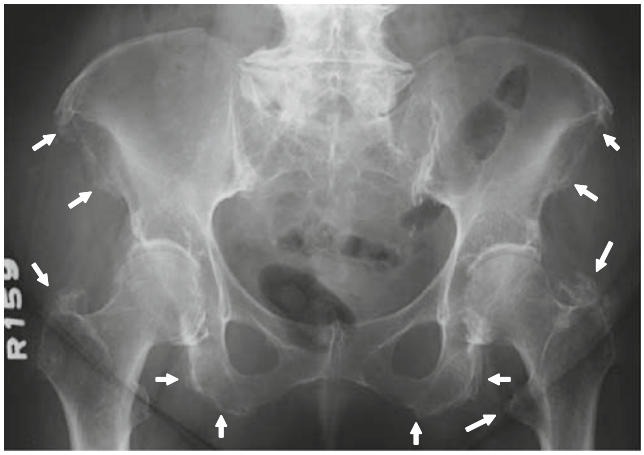

Fig. 11.149 AP pelvic radiograph from a patient with DISH showing marked and diffuse enthesopathy (*arrows*) and large osteophytes at the L45 level

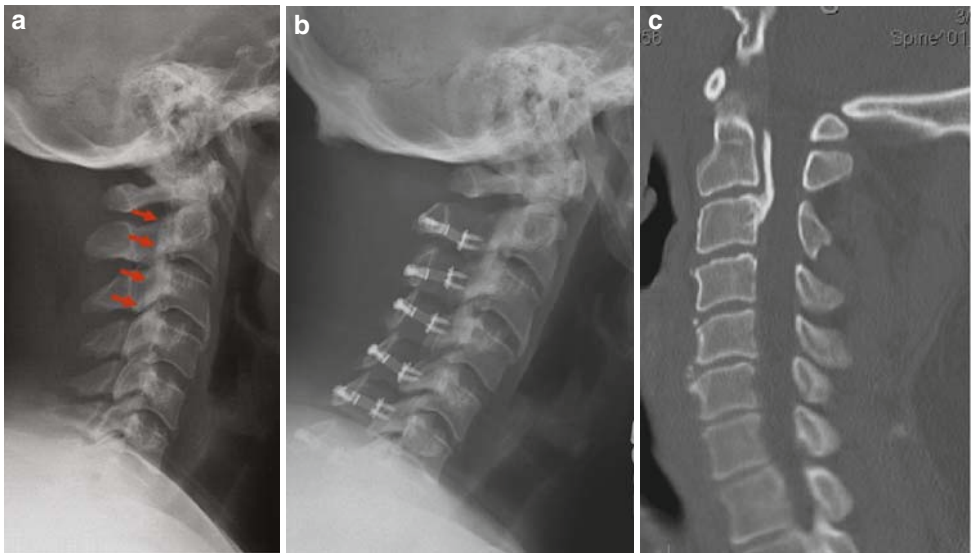

Fig. 11.150 Lateral cervical spine radiograph before (**a**) and after decompressive laminectomy (**b**) in a patient with OPLL showing ossification of the posterior longitudinal ligament extending from C2 through C4 (*arrows*) and a sagittal CT reconstruction (**c**) in another patient with OPLL at the C1–C3 level

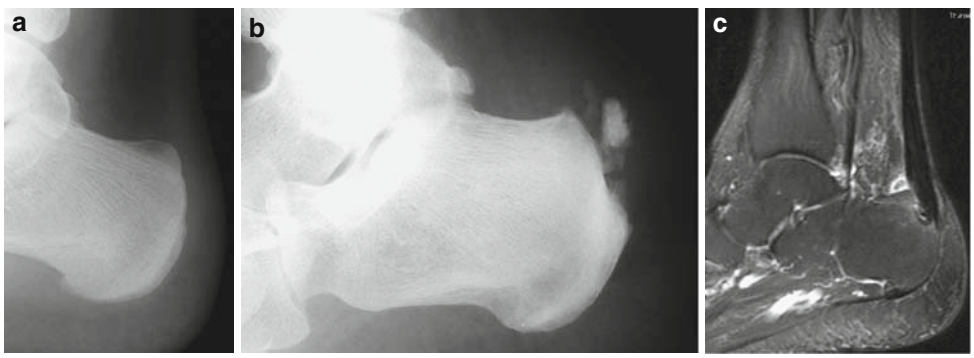

Fig. 11.151 Lateral radiograph of the calcaneus (**a**) and (**b**) and sagittal T2-weighted fat suppressed MR image (**c**) showing soft tissue prominence at the Achilles tendon insertion related to Haglund's disease (**a**) and more severe disease with reactive bone formation in the bursae (**b**). The MR (**c**) shows mild subtendinous bursitis with edema in the posterosuperior portion of the calcaneus and thickening of the distal Achilles tendon at its insertion

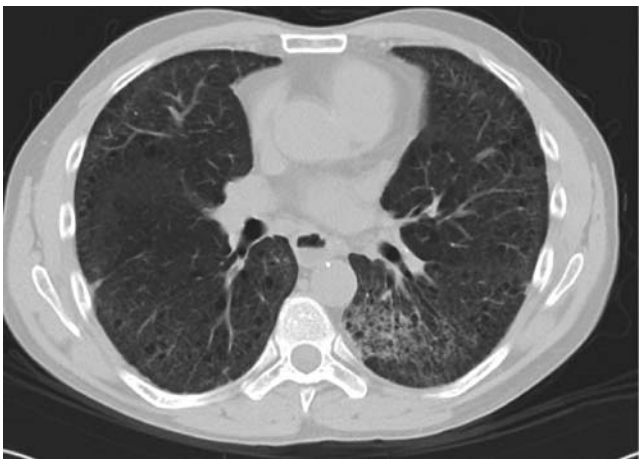

Fig. 11.152 Lung windowed CT image showing bibasilar fibrosis in a patient with scleroderma. Note the focal variation in the involvement in different lobes

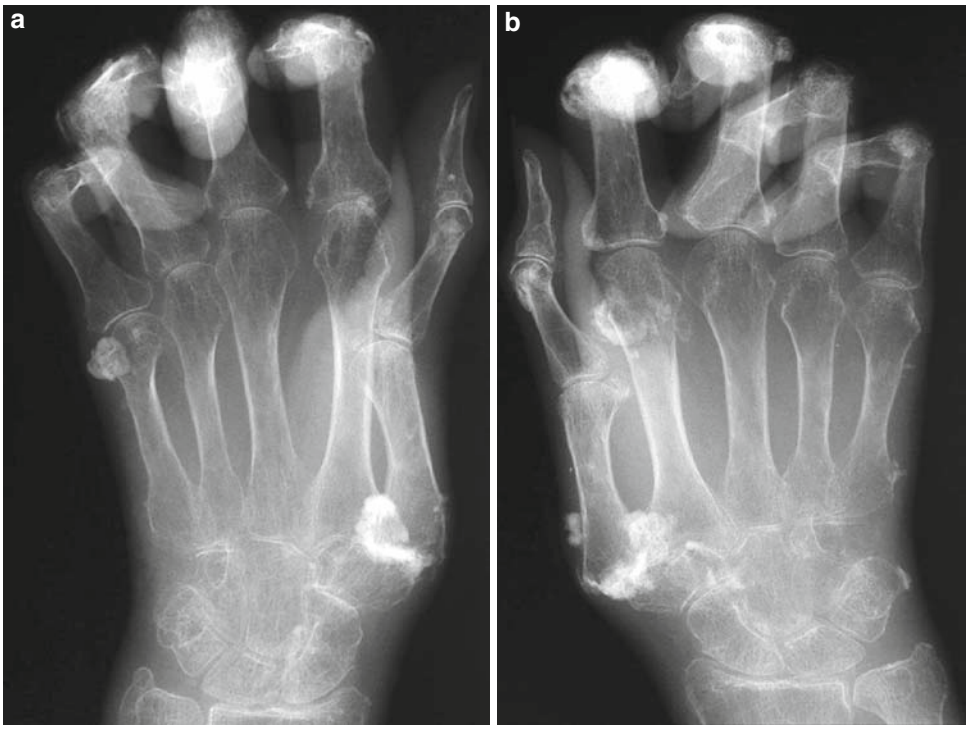

Fig. 11.153 PA radiographs of the left (**a**) and right (**b**) hands of a patient with scleroderma showing periarticular calcifications and flexion deformities

not develop an inflammatory arthritis. They do, however, develop periarticular calcifications (Fig. 11.153) along with skin tightening, flexion deformities, and loss of normal surface skin folds (Fig. 11.154).

Patients with scleroderma may also develop acroosteolysis of the tufts of their digits (Fig. 11.154). Acroosteolysis is associated with a number of diseases and occurs in two variants. One is the type seen in scleroderma where the tufts erode away as is typically seen in scleroderma. The other is band-like (Fig. 11.155). Each has a different differential that can be useful in radiological diagnosis (Table 11.9). The etiology of each type varies with disease but is generally either related to decreased blood supply as is seen in scleroderma and thermal injury or related to hormonal hyperactivity or toxin as is the case in hyperparathyroidism and polyvinylchloride exposure respectively.

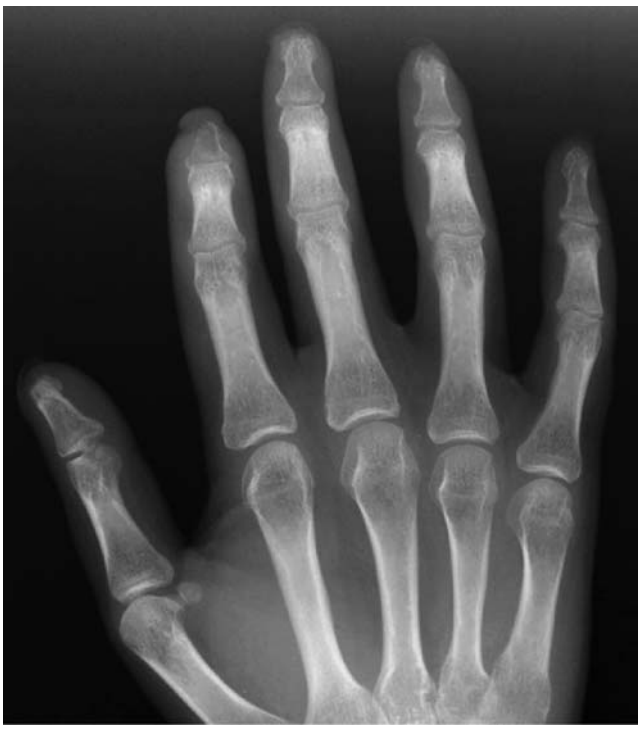

Fig. 11.154 PA radiograph of the right hand from a patient with scleroderma showing skin tightening with loss of skin folds and acroosteolysis of the first through fourth tufts

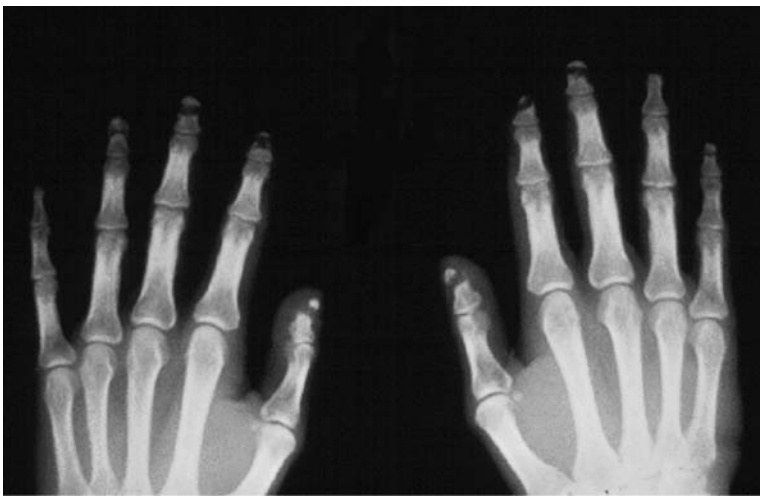

Fig. 11.155 Band-like acroosteolysis in a patient with polyvinyl chloride exposure

Osteochondromatosis

Loose bodies, small osteochondral fragments within a joint space, may arise in one of two ways. The first is the result of trauma breaking off a small piece of bone or bone together with its overlying cartilage into the joint. Instead of undergoing osteonecrosis, the fragment may obtain adequate nourishment from the synovial fluid and grow.

Table 11.9 Acroosteolysis differential diagnosis

Terminal	Band-like
Scleroderma	Polyvinylchloride exposure
Hyperparathyroidism	Hyperparathyroidism
Thermal injury	Hajdu–Cheney syndrome
Epidermolysis bullosum	Rothmund–Thomson syndrome
Hypertrophic pulmonary osteoarthropathy	Focal pressure trauma (e.g. excessive guitar playing)
Cyanotic congenital heart disease	
Progeria	
Snake venom	
Common in bold	

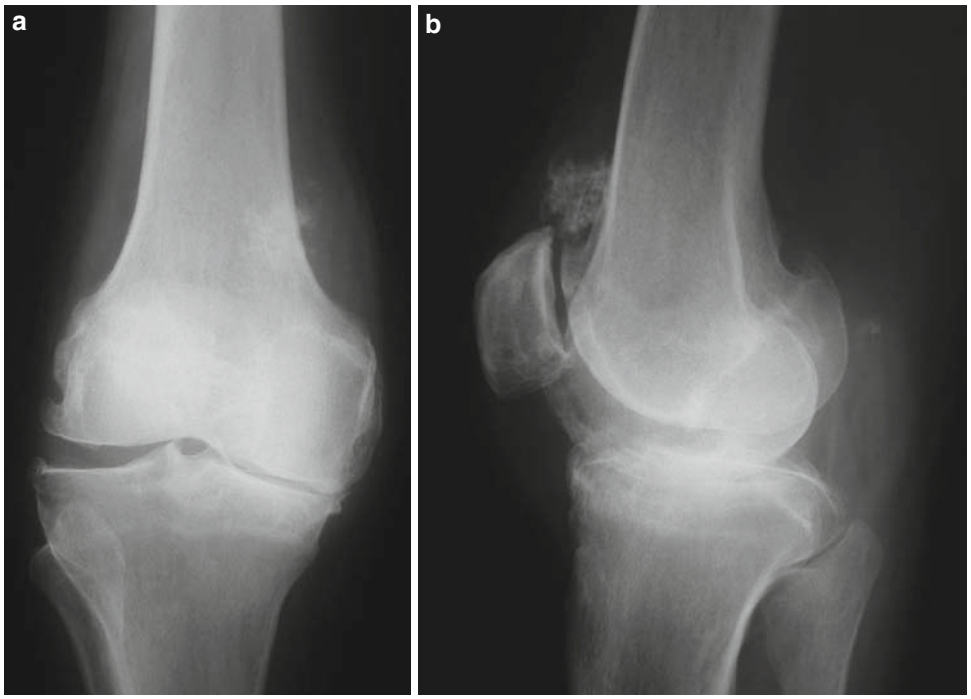

Fig. 11.156 AP (**a**) and lateral (**b**) radiographs of a patient's right knee showing a large osteochondral body in the region of the suprapatellar bursa

Generally, osteochondral bodies from trauma are few in number and may be relatively large in size with irregular margins (Fig. 11.156).

The other main cause of osteochondromatosis is synovial metaplasia. The reasons that this occurs are obscure. The process typically involves only one joint. In this case, the synovium develops numerous foci of cartilaginous metaplasia. These grow into nodules and begin to ossify and separate off the synovium into the joint. Typically this process afflicts younger aged patients and occurs most frequently in the knees, shoulders, elbows, and ankles. Radiographs show numerous small calcified and ossified bodies within the joint and its recesses (Fig. 11.157).

Chondromalacia Patella

Chondromalacia patella occurs in younger patients and is a form of chondrolysis. The patellar cartilage surface becomes softened and may develop fissures or be lost altogether. The Outerbridge classification is generally used to grade its severity (Table 11.10). MRI has become a useful tool to evaluate the hyaline cartilage in joints in general and on the posterior aspect of the patella in particular (Fig. 11.158). Most believe that chondromalacia patella is the final common pathway to a number of problems, including trauma, patellar tracking abnormalities, chronic muscle imbalance about the knee, and patellar hypermobility.

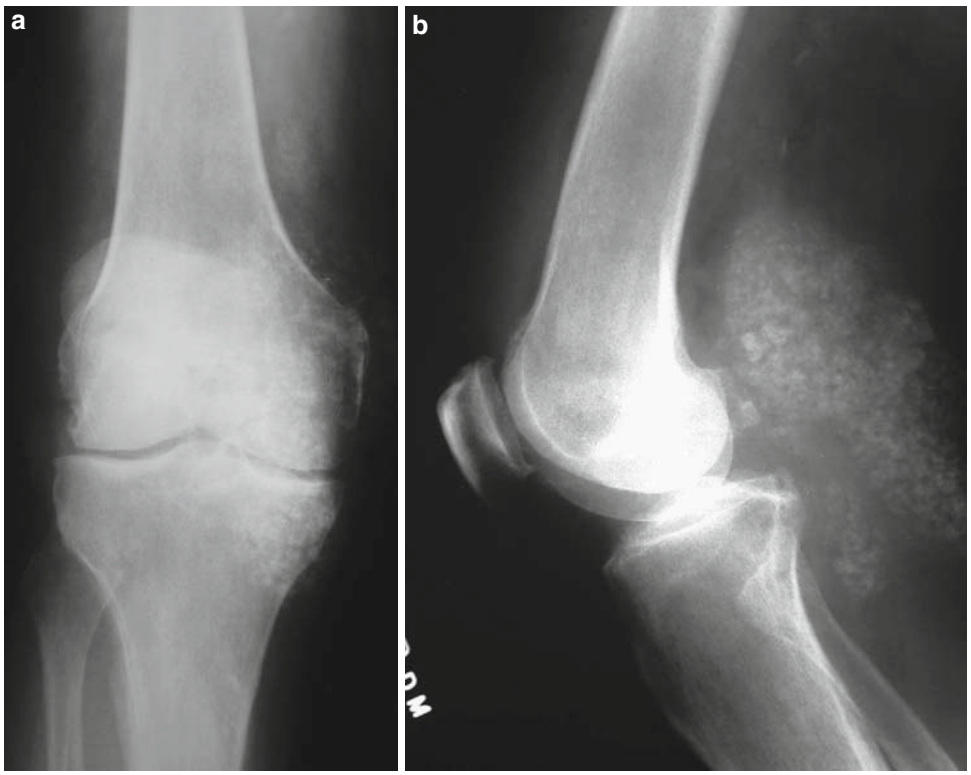

Fig. 11.157 AP (**a**) and lateral (**b**) radiographs of a patient's right knee showing multiple osteochondral bodies arising from synovial metaplasia within a Baker's cyst posterior to the knee

Table 11.10 Outerbridge grading of chondromalacia patella

Grade	Description
I	Softening and swelling
II	Mild fissuring
III	Fibrillation ("crab meat" appearance)
IV	Cartilage loss to bone

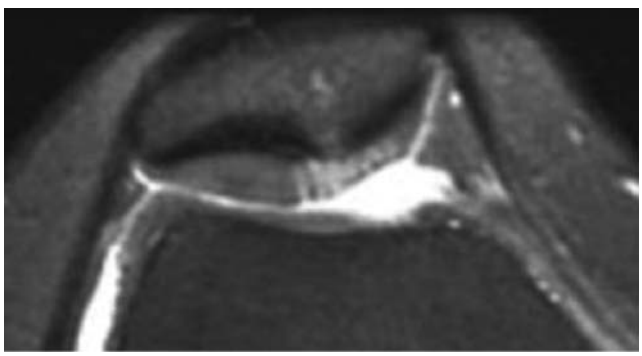

Fig. 11.158 Axial T2-weighted MR image of a patient's knee showing chondromalacia of the inominate ridge and a portion of the medial facet of the patella with fissuring

Further Readings

Primary Osteoarthritis

1. Belhorn LR, Hess EV: Erosive osteoarthritis. Semin Arthritis Rheum 1993 Apr; 22(5): 298–306.
2. Bijkerk C, Houwing-Duistermaat JJ, Valkenburg HA, Meulenbelt I, Hofman A, Breedveld FC, Pols HA, van Duijn CM, Slagboom PE: Heritabilities of radiologic osteoarthritis in peripheral joints and of disc degeneration of the spine. Arthritis Rheum 1999; 42: 1729–1735.
3. Buckland-Wright C, Verbruggen G, Haraoui PB: Imaging: radiological assessment of hand osteoarthritis. In: Osteoarthritis Cartilage 2000; 8(A): 55–56.
4. Bullough PG: The geometry of diarthrodial joints, its physiologic maintenance, and the possible significance of age-related changes in geometry-to-load distribution

and the development of osteoarthritis. Clin Orthop 1981 May; 156: 61–66.
5. Burkitt HG, Stevens A, Lowe JS: Skeletal system. In: Basic Histopathology. 3rd ed. New York, NY: Churchill Livingstone; 1996: 260.
6. Christensen SB: Localization of bone-seeking agents in developing, experimentally induced osteoarthritis in the knee joint of the rabbit. Scand J Rheumatol 1983; 12(4): 343–349.
7. Felson DT, Lawrence RC, Dieppe PA, Hirsch R, Helmick CG, Jordan JM, Kington RS, Lane NE, Nevitt MC, Zhang Y, et al.: Osteoarthritis: new insights. Part 1: the disease and its risk factors. Ann Intern Med 2000; 133: 635–646.
8. Hamerman D: The biology of osteoarthritis. N Engl J Med 1989; 320(20): 1322–1330.
9. Hirsch R, Lethbridge-Cejku M, Hanson R, Scott WW, Jr., Reichle R, Plato CC, Tobin JD, Hochberg MC: Familial aggregation of osteoarthritis: data from the Baltimore Longitudinal Study on Aging. Arthritis Rheum 1998; 41: 1227–1232.
10. Hoaglund FT, Yau AC, Wong WL: Osteoarthritis of the hip and other joints in southern Chinese in Hong Kong. J Bone Joint Surg Am 1973 Apr; 55(3): 545–557.
11. Howell DS: Pathogenesis of osteoarthritis. Am J Med 1986; 80(4B): 24–28.
12. Jewell FM, Watt I, Doherty M: Plain radiographic features of osteoarthritis. In: Brandt KD, Doherty M, Lohmander LS, eds. Osteoarthritis. New York, NY: Oxford University Press; 1998: 217–237.
13. Jonsson H, Manolescu I, Stefansson SE, et al.: The inheritance of hand osteoarthritis in Iceland. Arthritis Rheum 2003; 48: 391.
14. Kellgren JH, Moore R: Generalized osteoarthritis and Heberden's nodes. Br Med J 1952; 1: 181–187.
15. Kellgren JH: Osteoarthritis in patients and populations. Br Med J 1961; 2: 1–6.
16. Kujala UM, Leppavuori J, Kaprio J, Kinnunen J, Peltonen L, Koskenvuo M: Joint-specific twin and familial aggregation of recalled physician diagnosed osteoarthritis. Twin Res 1999; 2: 196–202.
17. Lee P, Rooney PJ, Sturrock RD: The etiology and pathogenesis of osteoarthrosis: a review. Semin Arthritis Rheum 1974 Spring; 3(3): 189–218.
18. Mankin HJ: The reaction of articular cartilage to injury and osteoarthritis (first of two parts). N Engl J Med 1974 Dec 12; 291(24): 1285–1292.
19. Miller EJ, Vanderkorst JK, Sokoloff L: Collagen of human articular and costal cartilage. Arthritis Rheum 1969; 12: 21.
20. Murray RO: The aetiology of primary osteoarthritis of the hip. Br J Radiol 1965 Nov; 38(455): 810–824.
21. Neustadt DH: Intra-articular therapy. In: Moskowitz RW, Howell DS, Altman RD, et al., eds. Osteoarthritis. 3rd ed 2001: 393–409.
22. Phadke K: Regulation of metabolism of the chondrocytes in articular cartilage – an hypothesis. J Rheumatol 1983 Dec; 10(6): 852–860.
23. Radin EL, Paul IL: Response of joints to impact loading. I. In vitro wear. Arthritis Rheum 1971 May–Jun; 14(3): 356–362.
24. Radin ER, Paul IL, Rose RM: Pathogenesis of primary osteoarthritis. Lancet 1972 Jun 24; 1(7765): 1395–1396.
25. Recht MP, Kramer J, Marcelis S: Abnormalities of articular cartilage in the knee: analysis of available MR techniques. Radiology 1993 May; 187(2): 473–478.
26. Reginato AM, Olsen BR. The role of structural genes in the pathogenesis of osteoarthritic disorders. Arthritis Res 2002; 4: 337–345.
27. Resnick D, Niwayama G: Degenerative disease of extraspinal locations. In: Resnick D, ed. Diagnosis of Bone and Joint Disorders. 3rd ed 1995: 1263–1371.
28. Roberts J, Burch TA: Osteoarthritis prevalence in adults by age, sex, race, and geographic area. Vital Health Stat 1 1966 Jun; 11(15): 1–27.
29. Rosenberg A: Bones, joints, and soft tissue tumors. In: Cotran R, Kumar V, Collins T, ed. Pathologic Basis of Disease. 6th ed 1999: 1246–1248.
30. Sharma L: Epidemiology of osteoarthritis. In: Moskowitz RW, Howell DS, Altman, RD, et al., eds. Osteoarthritis. 3rd ed 2001: 3–27.
31. Spector TD, Cicuttini F, Baker J, Loughlin J, Hart D: Genetic influences on osteoarthritis in women: a twin study. Br Med J 1996, 312: 940–943.
32. Veys E, Verbruggen G: Evolution and prognosis of osteoarthritis. In: Reginster JY, Pelletier JP, Martel-Pelletier J, et al., eds. Osteoarthritis 1999: 312–313.
33. Zanetti M, Bruder E, Romero J: Bone marrow edema pattern in osteoarthritic knees: correlation between MR imaging and histologic findings. Radiology 2000 Jun; 215(3): 835–840.

Secondary Osteoarthritis

1. Aliabadi P, Nikpoor N, Alparslan L. Imaging of neuropathic arthropathy. Semin Musculoskelet Radiol 2003 Sep; 7(3): 217–225.
2. Arnold WD, Hilgartner MW: Hemophilic arthropathy. Current concepts of pathogenesis and management. J Bone Joint Surg Am 1977 Apr; 59(3): 287–305.

3. Atkins CJ, McIvor J, Smith PM: Chondrocalcinosis and arthropathy: studies in haemochromatosis and in idiopathic chondrocalcinosis. Q J Med 1970 Jan; 39(153): 71–82.
4. Bar-On E, Floman Y, Sagiv S, et al.: Orthopaedic manifestations of familial dysautonomia. A review of one hundred and thirty-six patients. J Bone Joint Surg Am 2000 Nov; 82-A(11): 1563–1570.
5. Bernabeu-Taboada D, Martin-Hervas C: Sonography of haemophilic joints. In: Rodriguez-Merchan E, ed. The Haemophilic Joints: New Perspectives. Malden, England: Blackwell; 2003: 30–35.
6. Beutler A, Rothfuss S, Clayburne G: Calcium pyrophosphate dihydrate crystal deposition in synovium. Relationship to collagen fibers and chondrometaplasia. Arthritis Rheum 1993 May; 36(5): 704–715.
7. Bloomgarden ZT: American Diabetes Association 60th Scientific Sessions, 2000: the diabetic foot. Diabetes Care.2001 May; 24(5): 946–951.
8. Bywaters EG, Hamilton EB, Williams R: The spine in idiopathic haemochromatosis. Ann Rheum Dis 1971 Sep; 30(5): 453–465.
9. Chen C, Chandnani VP, Kang HS: Scapholunate advanced collapse: a common wrist abnormality in calcium pyrophosphate dihydrate crystal deposition disease. Radiology 1990 Nov; 177(2): 459–461.
10. Currey HL: Pyrophosphate arthropathy and calcific periarthritis. Clin Orthop 1970; 71: 70–80.
11. Deirmengian CA, Lee SG, Jupiter JB: Neuropathic arthropathy of the elbow. A report of five cases. J Bone Joint Surg Am 2001 Jun; 83-A(6): 839–844.
12. Devendra D, Farmer K, Bruce G, et al.: Diagnosing osteomyelitis in patients with diabetic neuropathic osteoarthropathy. Diabetes Care 2001 Dec; 24(12): 2154–2155.
13. Doherty M, Hamilton E, Henderson J: Familial chondrocalcinosis due to calcium pyrophosphate dihydrate crystal deposition in English families. Br J Rheumatol 1991 Feb; 30(1): 10–15.
14. Ea HK, Liote F: Calcium pyrophosphate dihydrate and basic calcium phosphate crystal-induced arthropathies: update on pathogenesis, clinical features, and therapy. Curr Rheumatol Rep 2004 Jun; 6(3): 221–227.
15. Fisher AA, Davis MW: Alkaptonuric ochronosis with aortic valve and joint replacements and femoral fracture: A case report and literature review. Clin Med Res 2004; 2: 209–215.
16. Garrod AE: The incidence of alkaptonuria: a study in chemical individuality. Lancet 1902; 2: 1616–1620.
17. Genant HK: Roentgenographic aspects of calcium pyrophosphate dihydrate crystal deposition disease (pseudogout). Arthritis Rheum 1976 May–Jun; 19(3): 307–328.
18. Gerster JC, Baud CA, Lagier R. Tendon calcifications in chondrocalcinosis. A clinical, radiologic, histologic, and crystallographic study. Arthritis Rheum 1977 Mar; 20(2): 717–722.
19. Gerster JC, Lagier R, Boivin G: Olecranon bursitis related to calcium pyrophosphate dihydrate crystal deposition disease. Arthritis Rheum 1982 Aug; 25(8): 989–996.
20. Gerster JC, Vischer TL, Fallet GH: Destructive arthropathy in generalized osteoarthritis with articular chondrocalcinosis. J Rheumatol 1975 Sep; 2(3): 265–269.
21. Halverson PB, Cheung HS, Johnson R: Simultaneous occurrence of calcium pyrophosphate dihydrate and basic calcium phosphate (hydroxyapatite) crystals in a knee. Clin Orthop 1990 Aug; 257: 162–165.
22. Halverson PB, McCarty DJ: Patterns of radiographic abnormalities associated with basic calcium phosphate and calcium pyrophosphate dihydrate crystal deposition in the knee. Ann Rheum Dis 1986 Jul; 45(7): 603–605.
23. Ishikawa K, Masuda I, Ohira T: A histological study of calcium pyrophosphate dihydrate crystal-deposition disease. J Bone Joint Surg Am 1989 Jul; 71(6): 875–886.
24. Jones AC, Chuck AJ, Arie EA: Diseases associated with calcium pyrophosphate deposition disease. Semin Arthritis Rheum 1992 Dec; 22(3): 188–202.
25. Jones EA, Manaster BJ, May DA, Disler DG: Neuropathic osteoarthropathy: diagnostic dilemmas and differential diagnosis. Radiographics 2000 Oct; 20 Spec No: S279–S293.
26. Kapila A, Lines M: Neuropathic spinal arthropathy: CT and MR findings. J Comput Assist Tomogr 1987 Jul–Aug; 11(4): 736–739.
27. Kaushik S, Erickson JK, Palmer WE: Effect of chondrocalcinosis on the MR imaging of knee menisci. Am J Roentgenol 2001 Oct; 177(4): 905–909.
28. Keller JM, Macaulay W, Nercessian OA: New developments in ochronosis: review of the literature. Rheumatol Int 2005; 25: 81–85.
29. Koop I, Loreck D, Krause A: Diabetic neuropathic arthropathy. Arthritis Rheum 1999 Apr; 42(4): 806.
30. Ling D, Murphy WA, Kyriakos M: Tophaceous pseudogout. Am J Roentgenol 1982; 138(1): 162–165.
31. Major NM, Helms CA, Genant HK: Calcification demonstrated as high signal intensity on T1-weighted MR images of the disks of the lumbar spine. Radiology 1993 Nov; 189(2): 494–496.
32. McCarty DJ: Diagnostic mimicry in arthritis patterns of joint involvement associated with calcium pyrophosphate dihydrate crystal deposits. Bull Rheum Dis 1975; 25: 804–809.
33. Menkes CJ, Simon F, Delrieu F: Destructive arthropathy in chondrocalcinosis articularis. Arthritis Rheum 1976 May–Jun; 19(3): 329–348.

34. Mizutani H, Ohba S, Mizutani M: Tumoral calcium pyrophosphate dihydrate deposition disease with bone destruction in the shoulder. CT and MR findings in two cases. Acta Radiol 1998 May; 39(3): 269–272.
35. Noonan KJ, Didelot WP, Lindseth RE: Care of the pediatric foot in myelodysplasia. Foot Ankle Clin 2000 Jun; 5(2): 281–304, vi.
36. Nuss R, Kilcoyne RF, Geraghty S: MRI findings in haemophilic joints treated with radiosynoviorthesis with development of an MRI scale of joint damage. Haemophilia 2000 May; 6(3): 162–169.
37. Nuss R, Kilcoyne RF: Diagnosis by imaging of haemophilic joints. In: Rodriguez-Merchan E, ed. The Haemophilic Joints: New Perspectives. Malden, England: Blackwell; 2003: 24–29.
38. O'Brien W, La Du BN, Bunim JJ: Biochemical, pathological and clinical aspects of alcaptonuria, ochronosis and ochronotic arthropathy: review of the world literature (1584–1962). Am J Med 1963; 34: 813–838.
39. Okazaki T, Saito T, Mitomo T: Pseudogout: clinical observations and chemical analyses of deposits. Arthritis Rheum 1976 May–Jun; 19(3): 293–305.
40. Palestro CJ, Mehta HH, Patel M, et al.: Marrow versus infection in the Charcot joint: indium-111 leukocyte and technetium-99m sulfur colloid scintigraphy. J Nucl Med 1998 Feb; 39(2): 346–350.
41. Pettersson H, Ahlberg A, Nilsson IM: A radiologic classification of hemophilic arthropathy. Clin Orthop 1980 Jun; 149: 153–159.
42. Phornphutkul C, Introne WJ, Perry MB: Natural history of alkaptonuria. N Engl J Med 2002; 347: 2111–2121.
43. Pritzker KP: Calcium pyrophosphate dihydrate crystal deposition and other crystal deposition diseases. Curr Opin Rheumatol 1994 Jul; 6(4): 442–447.
44. Rachow JW, Ryan LM, McCarty DJ: Synovial fluid inorganic pyrophosphate concentration and nucleotide pyrophosphohydrolase activity in basic calcium phosphate deposition arthropathy and Milwaukee shoulder syndrome. Arthritis Rheum 1988 Mar; 31(3): 408–413.
45. Resnick D, Pineda C: Vertebral involvement in calcium pyrophosphate dihydrate crystal deposition disease. Radiographic-pathological correlation. Radiology 1984 Oct; 153(1): 55–60.
46. Resnik CS, Resnick D: Crystal deposition disease. Semin Arthritis Rheum 1983 May; 12(4): 390–403.
47. Richards AJ, Hamilton EB: Destructive arthropathy in chondrocalcinosis articularis. Ann Rheum Dis 1974 May; 33(3): 196–203.
48. Roosendaal G, Lafeber FP: Blood-induced joint damage in hemophilia. Semin Thromb Hemost 2003 Feb; 29(1): 37–42
49. Saffar P: Chondrocalcinosis of the wrist. J Hand Surg [Br] 2004 Oct; 29(5): 486–493.
50. Sampson HW, Trzeciakowski JP: Intervertebral disk mineralization in progressive ankylosis mice. Bone Miner 1990 Jul; 10(1): 71–77.
51. Schumacher HR Jr, Bonner H, Thompson JJ: Tumor-like soft tissue swelling of the distal phalanx due to calcium pyrophosphate dihydrate crystal deposition. Arthritis Rheum 1984 Dec; 27(12): 1428–1432.
52. Schumacher HR, Holdsworth DE: Ochronotic arthropathy. I. Clinicopathologic studies. Semin Arthritis Rheum 1977 Feb; 6(3): 207–246.
53. Sofka CM, Adler RS, Cordasco FA: Ultrasound diagnosis of chondrocalcinosis in the knee. Skeletal Radiol 2002 Jan; 31(1): 43–45.
54. Sommer TC, Lee TH: Charcot foot: the diagnostic dilemma. Am Fam Physician 2001 Nov 1; 64(9): 1591–1598.
55. Stucki G, Hardegger D, Bohni U: Degeneration of the scaphoid-trapezium joint: a useful finding to differentiate calcium pyrophosphate deposition disease from osteoarthritis. Clin Rheumatol 1999; 18(3): 232–237.
56. Zaka R, Williams CJ: Genetics of chondrocalcinosis. Osteoarthritis Cartilage 2005 Sep; 13(9): 745–750.

Rheumatoid Arthritis

1. American College of Rheumatology Extremity Magnetic Resonance Imaging Task Force. Extremity magnetic resonance imaging in rheumatoid arthritis: report of the American College of Rheumatology Extremity Magnetic Resonance Imaging Task Force. Arthritis Rheum 2006 Apr; 54(4): 1034–1047.
2. Boden SD, Dodge LD, Bohlman HH, Rechtine GR: Rheumatoid arthritis of the cervical spine. A long-term analysis with predictors of paralysis and recovery. J Bone Joint Surg Am 1993 Sep; 75(9): 1282–1297.
3. Cassar-Pullicino VN: The Spine in Rheumatological Disorders. Imaging 1999; 11: 104–118.
4. Chen TS, Crues JV 3rd, Ali M, Troum OM: Magnetic resonance imaging is more sensitive than radiographs in detecting change in size of erosions in rheumatoid arthritis. J Rheumatol 2006 Aug 1; 33(10): 1957–1967.
5. Drosos AA, Lanchbury JS, Panayi GS, Moutsopoulos HM: Rheumatoid arthritis in Greek and British patients. A comparative clinical, radiologic, and serologic study. Arthritis Rheum 1992 Jul; 35(7): 745–748.
6. Dvorak J, Grob D, Baumgartner H, et al.: Functional evaluation of the spinal cord by magnetic resonance imaging in patients with rheumatoid arthritis and instability of upper cervical spine. Spine 1989 Oct; 14(10): 1057–1064.

7. Fujiwara K, Fujimoto M, Owaki H, et al.: Cervical lesions related to the systemic progression in rheumatoid arthritis. Spine 1998 Oct 1; 23(19): 2052–2056.
8. Garrod AB: Nature and Treatment of Gout and Rheumatic Gout. London: Walton and Maberly; 1859.
9. Gilkeson G, Polisson R, Sinclair H, et al.: Early detection of carpal erosions in patients with rheumatoid arthritis: a pilot study of magnetic resonance imaging. J Rheumatol 1988 Sep; 15(9): 1361–1366.
10. Guermazi A, Taouli B, Lynch JA, Peterfy CG: Imaging of bone erosion in rheumatoid arthritis. Semin Musculoskelet Radiol 2004 Dec; 8(4): 269–285.
11. Hamilton JD, Johnston RA, Madhok R, Capell HA: Factors predictive of subsequent deterioration in rheumatoid cervical myelopathy. Rheumatology (Oxford) 2001 Jul; 40(7): 811–815.
12. Hunter DJ, Conaghan PG: Imaging outcomes and their role in determining outcomes in osteoarthritis and rheumatoid arthritis. Curr Opin Rheumatol 2006 Mar; 18(2): 157–162.
13. Janssen H, Weissman BN, Aliabadi P, Zamani AA: MR imaging of arthritides of the cervical spine. Magn Reson Imaging Clin N Am 2000 Aug; 8(3): 491–512.
14. Jevtic V, Watt I, Rozman B, et al.: Contrast enhanced Gd-DTPA magnetic resonance imaging in the evaluation of rheumatoid arthritis during a clinical trial with DMARDs. A prospective two-year follow-up study on hand joints in 31 patients. Clin Exp Rheumatol 1997 Mar–Apr; 15(2): 151–156.
15. Konig H, Sieper J, Wolf KJ: Rheumatoid arthritis: evaluation of hypervascular and fibrous pannus with dynamic MR imaging enhanced with Gd-DTPA. Radiology 1990 Aug; 176(2): 473–477.
16. Neva MH, Kauppi MJ, Kautiainen H, et al.: Combination drug therapy retards the development of rheumatoid atlantoaxial subluxations. Arthritis Rheum 2000 Nov; 43(11): 2397–2401.
17. Papadopoulos IA, Katsimbri P, Katsaraki A, et al.: Clinical course and outcome of early rheumatoid arthritis. Rheumatol Int 2001 Jul; 20(5): 205–210.
18. Pellicci PM, Ranawat CS, Tsairis P, Bryan WJ: A prospective study of the progression of rheumatoid arthritis of the cervical spine. J Bone Joint Surg Am 1981 Mar; 63(3): 342–350.
19. Poleksic L, Zdravkovic D, Jablanovic D, et al.: Magnetic resonance imaging of bone destruction in rheumatoid arthritis: comparison with radiography. Skeletal Radiol 1993 Nov; 22(8): 577–580.
20. Reiser MF, Bongartz GP, Erlemann R, et al.: Gadolinium-DTPA in rheumatoid arthritis and related diseases: first results with dynamic magnetic resonance imaging. Skeletal Radiol 1989; 18(8): 591–597.
21. Roche CJ, Eyes BE, Whitehouse GH: The rheumatoid cervical spine: signs of instability on plain cervical radiographs. Clin Radiol 2002 Apr; 57(4): 241–249.
22. Singson RD, Zalduondo FM: Value of unenhanced spin-echo MR imaging in distinguishing between synovitis and effusion of the knee. AJR Am J Roentgenol 1992 Sep; 159(3): 569–571.
23. Solau-Gervais E, Legrand JL, Cortet B, Duquesnoy B, Flipo RM: Magnetic resonance imaging of the hand for the diagnosis of rheumatoid arthritis in the absence of anti-cyclic citrullinated peptide antibodies: a prospective study. J Rheumatol 2006 Sep; 33(9): 1760–1765.
24. Sugimoto H, Takeda A, Hyodoh K: Early-stage rheumatoid arthritis: prospective study of the effectiveness of MR imaging for diagnosis. Radiology 2000 Aug; 216(2): 569–575.
25. Tehranzadeh J, Ashikyan O, Dascalos J: Advanced imaging of early rheumatoid arthritis. Radiol Clin North Am 2004 Jan; 42(1): 89–107.
26. Wakefield RJ, Kong KO, Conaghan PG, et al.: The role of ultrasonography and magnetic resonance imaging in early rheumatoid arthritis. Clin Exp Rheumatol 2003 Sep–Oct; 21(5 Suppl 31): S42–S49.
27. Weissman BN, Aliabadi P, Weinfeld MS, et al.: Prognostic features of atlantoaxial subluxation in rheumatoid arthritis patients. Radiology 1982 Sep; 144(4): 745–751.
28. Winfield J, Young A, Williams P, Corbett M: Prospective study of the radiological changes in hands, feet, and cervical spine in adult rheumatoid disease. Ann Rheum Dis 1983 Dec; 42(6): 613–618.
29. Yao L, Magalnick M, Wilson M, Lipsky P, Goldbach-Mansky R. Periarticular bone findings in rheumatoid arthritis: T2-weighted versus contrast-enhanced T1-weighted MRI. AJR Am J Roentgenol 2006 Aug; 187(2): 358–363.

Juvenile Chronic Arthritis

1. Azouz EM: Arthritis in children: conventional and advanced imaging. Semin Musculoskelet Radiol 2003 Jun; 7(2): 95–102.
2. Babyn P, Doria AS: Radiologic investigation of rheumatic diseases. Pediatr Clin North Am 2005 Apr; 52(2): 373–411, vi.
3. Buchmann RF, Jaramillo D. Imaging of articular disorders in children. Radiol Clin North Am 2004 Jan; 42(1): 151–168, vii.
4. Cohen PA, Job-Deslandre CH, Lalande G, Adamsbaum C: Overview of the radiology of juvenile idiopathic arthritis (JIA). Eur J Radiol 2000 Feb; 33(2): 94–101.

5. Dressler F: Juvenile rheumatoid arthritis and spondyloarthropathies. Curr Opin Rheumatol 1998 Sep; 10(5): 468–474.
6. Faingold R, Saigal G, Azouz EM, Morales A, Albuquerque PA: Imaging of low back pain in children and adolescents. Semin Ultrasound CT MR 2004 Dec; 25(6): 490–505.
7. Feldman BM: Treating children with arthritis: towards an evidence-based culture. J Rheumatol Suppl 2005 Jan; 72: 33–35.
8. Graham TB, Blebea JS, Gylys-Morin V, Passo MH: Magnetic resonance imaging in juvenile rheumatoid arthritis. Semin Arthritis Rheum 1997 Dec; 27(3): 161–168.
9. Graham TB: Imaging in juvenile arthritis. Curr Opin Rheumatol 2005 Sep; 17(5): 574–578.
10. Guglielmi G, De Serio A, Leone A, Agrosi L, Cammisa M: The lumbar spine: imaging in rheumatic disease. Rays 2000 Jan–Mar; 25(1): 49–62.
11. Hashkes PJ, Laxer RM: Medical treatment of juvenile idiopathic arthritis. JAMA 2005 Oct 5; 294(13): 1671–1684.
12. Johnson K, Gardner-Medwin J: Childhood arthritis: classification and radiology. Clin Radiol 2002 Jan; 57(1): 47–58. (Erratum in: Clin Radiol 2002 Apr; 57(4): 323.)
13. Kleinman PK, Spevak MR. Advanced pediatric joint imaging. Radiol Clin North Am 1990 Sep; 28(5): 1073–1109. (Erratum in: Radiol Clin North Am 1991 Mar; 29(2): preceding 179.)
14. Lamer S, Sebag GH: MRI and ultrasound in children with juvenile chronic arthritis. Eur J Radiol 2000 Feb; 33(2): 85–93.
15. Miller ML. Use of imaging in the differential diagnosis of rheumatic diseases in children. Rheum Dis Clin North Am 2002 Aug; 28(3): 483–492.
16. Pepmueller PH, Moore TL. Juvenile spondyloarthropathies. Curr Opin Rheumatol 2000 Jul; 12(4): 269–273.
17. Petty RE, Southwood TR, Manners P, Baum J, Glass DN, Goldenberg J, He X, Maldonado-Cocco J, Orozco-Alcala J, Prieur AM, Suarez-Almazor ME, Woo P: International League of Associations for Rheumatology. International League of Associations for Rheumatology classification of juvenile idiopathic arthritis: second revision, Edmonton, 2001. J Rheumatol 2004 Feb; 31(2): 390–392.
18. Reed MH, Wilmot DM: The radiology of juvenile rheumatoid arthritis. A review of the English language literature. J Rheumatol Suppl 1991 Dec; 31: 2–22.
19. Reiff AO. Developments in the treatment of juvenile arthritis. Expert Opin Pharmacother 2004 Jul; 5(7): 1485–1496.
20. Reiter MF, Boden SD: Inflammatory disorders of the cervical spine. Spine 1998 Dec 15; 23(24): 2755–2766.
21. Sawhney S, Magalhaes CS. Paediatric rheumatology – a global perspective. Best Pract Res Clin Rheumatol 2006 Apr; 20(2): 201–221.
22. Southwood TR, Woo P. Juvenile chronic arthritis. Baillieres Clin Rheumatol 1995 May; 9(2): 331–353.
23. Tse SM, Laxer RM. Juvenile spondyloarthropathy. Curr Opin Rheumatol 2003 Jul; 15(4): 374–379.
24. Wihlborg C, Babyn P, Ranson M, Laxer R. Radiologic mimics of juvenile rheumatoid arthritis. Pediatr Radiol 2001 May; 31(5): 315–326.

Septic Arthritis

1. Almeida A, Roberts I: Bone involvement in sickle cell disease. Br J Haematol 2005 May; 129(4): 482–490.
2. Blickman JG, van Die CE, de Rooy JW: Current imaging concepts in pediatric osteomyelitis. Eur Radiol 2004 Mar; 14(4): L55–L64.
3. Chatha DS, Cunningham PM, Schweitzer ME: MR imaging of the diabetic foot: diagnostic challenges. Radiol Clin North Am 2005 Jul; 43(4): 747–759, ix.
4. Frick SL: Evaluation of the child who has hip pain. Orthop Clin North Am 2006 Apr; 37(2): 133–140, v.
5. Greenspan A, Tehranzadeh J: Imaging of infectious arthritis. Radiol Clin North Am 2001 Mar; 39(2): 267–276.
6. Ho G Jr: Bacterial arthritis. Curr Opin Rheumatol 2001 Jul; 13(4): 310–314.
7. Kothari NA, Pelchovitz DJ, Meyer JS: Imaging of musculoskeletal infections. Radiol Clin North Am 2001 Jul; 39(4): 653–671.
8. Learch TJ, Farooki S: Magnetic resonance imaging of septic arthritis. Clin Imaging 2000 Jul–Aug; 24(4): 236–242.
9. Learch TJ: Imaging of infectious arthritis. Semin Musculoskelet Radiol 2003 Jun; 7(2): 137–142.
10. Mellado JM, Perez del Palomar L, Camins A, Salvado E, Ramos A, Sauri A: MR imaging of spinal infection: atypical features, interpretive pitfalls and potential mimickers. Eur Radiol 2004 Nov; 14(11): 1980–1989.
11. Mitchell DH, Howden BP: Diagnosis and management of Staphylococcus aureus bacteraemia. Intern Med J 2005 Dec; 35(2): S17–S24.
12. Mohana-Borges AV, Chung CB, Resnick D. Monoarticular arthritis. Radiol Clin North Am 2004 Jan; 42(1): 135–149.
13. Restrepo CS, Lemos DF, Gordillo H, Odero R, Varghese T, Tiemann W, Rivas FF, Moncada R, Gimenez CR:

Imaging findings in musculoskeletal complications of AIDS. Radiographics 2004 Jul–Aug; 24(4): 1029–1049.
14. Ross JJ, Shamsuddin H. Sternoclavicular septic arthritis: review of 180 cases. Medicine (Baltimore) 2004 May; 83(3): 139–148.
15. Sawlani V, Chandra T, Mishra RN, Aggarwal A, Jain UK, Gujral RB: MRI features of tuberculosis of peripheral joints. Clin Radiol 2003 Oct; 58(10): 755–762.
16. Schweitzer ME, Morrison WB: MR imaging of the diabetic foot. Radiol Clin North Am 2004 Jan; 42(1): 61–71, vi.
17. Shirtliff ME, Mader JT: Acute septic arthritis. Clin Microbiol Rev 2002 Oct; 15(4): 527–544.
18. Siva C, Velazquez C, Mody A, Brasington R: Diagnosing acute monoarthritis in adults: a practical approach for the family physician. Am Fam Physician 2003 Jul 1; 68(1): 83–90.
19. Street J, Lenehan B, Mulcahy D, McGuinness A: Pelvic girdle sepsis in childhood. An illustrative case of the difficulty in diagnosis. Acta Orthop Belg 2005 Jun; 71(3): 361–365.
20. Turpin S, Lambert R: Role of scintigraphy in musculoskeletal and spinal infections. Radiol Clin North Am 2001 Mar; 39(2): 169–189.
21. Waagner DC: Musculoskeletal infections in adolescents. Adolesc Med 2000 Jun; 11(2): 375–400.
22. Wilson DJ: Soft tissue and joint infection. Eur Radiol 2004 Mar; 14(3): E64–E71.
23. Wong-Chung J, Bagali M, Kaneker S: Physical signs in pyomyositis presenting as a painful hip in children: a case report and review of the literature. J Pediatr Orthop B 2004 May; 13(3): 211–213.

Pott's Disease

1. Davidson PT, Le HQ: Musculoskeletal tuberculosis. In: Schlossberg D, ed. Tuberculosis and Nontuberculous Mycobacterial Infections. 4th ed. Saint Louis, MO: W B Saunders; 1999; 204–220.
2. Jung NY, Jee WH, Ha KY, et al.: Discrimination of tuberculous spondylitis from pyogenic spondylitis on MRI. AJR Am J Roentgenol 2004 Jun; 182(6): 1405–1410.
3. Jutte PC, Van Loenhout-Rooyackers JH: Routine surgery in addition to chemotherapy for treating spinal tuberculosis. Cochrane Database Syst Rev 2006; CD004532.
4. Leibert E, Haralambou G: Spinal tuberculosis. In: Rom WN and Garay S, eds. Tuberculosis. Lippincott, Williams and Wilkins 2004; 565–577.
5. Lifeso RM, Weaver P, Harder EH: Tuberculous spondylitis in adults. J Bone Joint Surg Am 1985; 67: 1405–1413. Moon MS: Tuberculosis of the spine. Controversies and a new challenge. Spine 1997 Aug 1; 22: 1791–1797.
6. Moorthy S, Prabhu NK: Spectrum of MR imaging findings in spinal tuberculosis. AJR Am J Roentgenol 2002 Oct; 179(4): 979–983. Pertuiset E, Beaudreuil J, Liote F, et al. Spinal tuberculosis in adults. A study of 103 cases in a developed country, 1980–1994. Medicine (Baltimore) 1999 Sep; 78(5): 309–320.
7. Pott P: The chirurgical works of Percivall Pott, F.R.S., surgeon to St. Bartholomew's Hospital, a new edition, with his last corrections. 1808. Clin Orthop Relat Res 2002 May; 398: 4–10.
8. Ridley N, Shaikh MI, Remedios D, Mitchell R: Radiology of skeletal tuberculosis. Orthopedics 1998 Nov; 21(11): 1213–1220.
9. Sharif HS, Morgan JL, al Shahed MS, al Thagafi MY: Role of CT and MR imaging in the management of tuberculous spondylitis. Radiol Clin North Am 1995 Jul; 33(4): 787–804.
10. Watts HG, Lifeso RM: Tuberculosis of bones and joints. J Bone Joint Surg Am 1996 Feb; 78: 288–298.

Gout

1. Choi MH, MacKenzie JD, Dalinka MK: Imaging features of crystal-induced arthropathy. Rheum Dis Clin North Am 2006 May; 32(2): 427–446, viii.
2. Gentili A, Sorenson S, Masih S: MR imaging of soft-tissue masses of the foot. Semin Musculoskelet Radiol 2002 Jun; 6(2): 141–152.
3. Gentili A: Advanced imaging of gout. Semin Musculoskelet Radiol 2003 Sep; 7(3): 165–174.
4. Gentili A: The advanced imaging of gouty tophi. Curr Rheumatol Rep 2006 Jun; 8(3): 231–235.
5. Liote F, Ea HK: Gout: update on some pathogenic and clinical aspects. Rheum Dis Clin North Am 2006 May; 32(2): 295–311, vi.
6. Monu JU, Pope TL Jr: Gout: a clinical and radiologic review. Radiol Clin North Am 2004 Jan; 42(1): 169–184.
7. Olsen KM, Chew FS: Tumoral calcinosis: pearls, polemics, and alternative possibilities. Radiographics 2006 May–Jun; 26(3): 871–885.
8. Sheldon PJ, Forrester DM, Learch TJ. Imaging of intraarticular masses. Radiographics 2005 Jan–Feb; 25(1): 105–119.
9. Uri DS, Dalinka MK: Imaging of arthropathies. Crystal disease. Radiol Clin North Am 1996 Mar; 34(2): 359–374, xi.

Psoriatic Arthritis

1. Evangelisto A, Wakefield R, Emery P: Imaging in early arthritis. Best Pract Res Clin Rheumatol 2004 Dec; 18(6): 927–943.
2. Healy PJ, Helliwell PS: Classification of the spondyloarthropathies. Curr Opin Rheumatol 2005 Jul; 17(4): 395–399.
3. Kane D, Pathare S: Early psoriatic arthritis. Rheum Dis Clin North Am 2005 Nov; 31(4): 641–657.
4. Klecker RJ, Weissman BN: Imaging features of psoriatic arthritis and Reiter syndrome. Semin Musculoskelet Radiol 2003 Jun; 7(2): 115–126.
5. McGonagle D: Imaging the joint and enthesis: insights into pathogenesis of psoriatic arthritis. Ann Rheum Dis 2005 Mar; 64(2): ii58–60.
6. McQueen F, Lassere M, Ostergaard M: Magnetic resonance imaging in psoriatic arthritis: a review of the literature. Arthritis Res Ther 2006; 8(2): 207. Epub 2006 Mar 23.
7. Ory PA, Gladman DD, Mease PJ: Psoriatic arthritis and imaging. Ann Rheum Dis 2005 Mar; 64(2): ii55–57.
8. Ritchlin CT: Pathogenesis of psoriatic arthritis. Curr Opin Rheumatol 2005 Jul; 17(4): 406–412.
9. van der Heijde D, Sharp J, Wassenberg S, Gladman DD: Psoriatic arthritis imaging: a review of scoring methods. Ann Rheum Dis 2005 Mar; 64(2): ii61–64.

Reactive Arthritis

1. Braun J, Sieper J: The sacroiliac joint in the spondyloarthropathies.Curr Opin Rheumatol 1996 Jul; 8(4): 275–287.
2. Grigoryan M, Roemer FW, Mohr A, Genant HK: Imaging in spondyloarthropathies. Curr Rheumatol Rep 2004 Apr; 6(2): 102–109.
3. Healy PJ, Helliwell PS: Classification of the spondyloarthropathies. Curr Opin Rheumatol 2005 Jul; 17(4): 395–399.
4. Klecker RJ, Weissman BN: Imaging features of psoriatic arthritis and Reiter syndrome. Semin Musculoskelet Radiol 2003 Jun; 7(2): 115–126.
5. Lin WY, Wang SJ, Lan JL: Evaluation of arthritis in Reiter's disease by bone scintigraphy and radiography. Clin Rheumatol 1995 Jul; 14(4): 441–444.
6. Olivieri I, Barozzi L, Padula A, De Matteis M, Pavlica P: Clinical manifestations of seronegative spondylarthropathies. Eur J Radiol 1998 May; 27(1): S3–S6.

Ankylosing Spondylitis and Other Spondyloarthropathies

1. Albu A, Parasca I, Talu S, Poanta L: Ankylosing spondylitis – a systemic disease. Rom J Intern Med 2004; 42(4): 685–694.
2. Braun J, Golder W, Bollow M, Sieper J, van der Heijde D: Imaging and scoring in ankylosing spondylitis. Clin Exp Rheumatol 2002 Nov–Dec; 20(6 Suppl 28): S178–S184.
3. Braun J, van der Heijde D: Imaging and scoring in ankylosing spondylitis. Best Pract Res Clin Rheumatol 2002 Sep; 16(4): 573–604.
4. Francois RJ, Braun J, Khan MA: Entheses and enthesitis: a histopathologic review and relevance to spondyloarthritides. Curr Opin Rheumatol 2001 Jul; 13(4): 255–264.
5. Grigoryan M, Roemer FW, Mohr A, Genant HK: Imaging in spondyloarthropathies. Curr Rheumatol Rep 2004 Apr; 6(2): 102–109.
6. Jarvik JG, Deyo RA: Diagnostic evaluation of low back pain with emphasis on imaging. Ann Intern Med 2002 Oct 1; 137(7): 586–597.
7. Levine DS, Forbat SM, Saifuddin A: MRI of the axial skeletal manifestations of ankylosing spondylitis. Clin Radiol 2004 May; 59(5): 400–413.
8. Luong AA, Salonen DC: Imaging of the seronegative spondyloarthropathies. Curr Rheumatol Rep 2000 Aug; 2(4): 288–296.
9. Maksymowych WP: Ankylosing spondylitis – at the interface of bone and cartilage. J Rheumatol 2000 Oct; 27(10): 2295–2301.
10. Ory PA: Radiography in the assessment of musculoskeletal conditions. Best Pract Res Clin Rheumatol 2003 Jun; 17(3): 495–512.
11. Sieper J, Braun J, Rudwaleit M, Boonen A, Zink A: Ankylosing spondylitis: an overview. Ann Rheum Dis 2002 Dec; 61(3): iii8–18.
12. Unsal E, Arici AM, Kavukcu S, Pirnar T: Andersson lesion: spondylitis erosiva in adolescents. Two cases and review of the literature. Pediatr Radiol 2002 Mar; 32(3): 183–187.
13. van der Heijde D, Landewe R: Imaging in spondylitis. Curr Opin Rheumatol 2005 Jul; 17(4): 413–417.
14. Vinson EN, Major NM: MR imaging of ankylosing spondylitis. Semin Musculoskelet Radiol 2003 Jun; 7(2): 103–113.
15. Zochling J, Braun J: Assessment of ankylosing spondylitis. Clin Exp Rheumatol 2005 Sep–Oct; 23(5 Suppl 39): S133–S141.

Multicentric Reticulohistocytosis

1. Baghestani S, Khosravi F, Dehghani Zahedani M, Mahboobi AA: Multicentric reticulohistiocytosis presenting with papulonodular skin eruption and polyarthritis. Eur J Dermatol 2005 May–Jun; 15(3): 196–200.
2. Liu YH, Fang K: Multicentric reticulohistiocytosis with generalized systemic involvement. Clin Exp Dermatol 2004 Jul; 29(4): 373–376.
3. Suga K, Ogasawara N, Motoyama K, Hara A, Matsunaga N, Muto T: Ga-67 scintigraphic findings in a case of multicentric reticulohistiocytosis. Clin Nucl Med 2002 Feb; 27(2): 144–145.
4. Yamada T, Kurohori YN, Kashiwazaki S, Fujibayashi M, Ohkawa T: MRI of multicentric reticulohistiocytosis. J Comput Assist Tomogr 1996 Sep–Oct; 20(5): 838–840.

Amyloid Arthropathy

1. Sheldon PJ, Forrester DM, Learch TJ: Imaging of intraarticular masses. Radiographics 2005 Jan–Feb; 25(1): 105–119.
2. Mellado JM, Salvado E, Camins A, Ramos A, Merino X, Calmet J, Sauri A: Fluid collections and juxta-articular cystic lesions of the shoulder: spectrum of MRI findings. Eur Radiol 2002 Mar; 12(3): 650–659.
3. Danesh FR, Klinkmann J, Yokoo H, Ivanovich P: Fatal cervical spondyloarthropathy in a hemodialysis patient with systemic deposition of beta2-microglobulin amyloid. Am J Kidney Dis 1999 Mar; 33(3): 563–566.
4. Boutin RD, Weissman BN. MR imaging of arthritides affecting the shoulder. Magn Reson Imaging Clin N Am 1997 Nov; 5(4): 861–879.
5. Stabler A, Heuck A, Reiser M: Imaging of the hand: degeneration, impingement and overuse. Eur J Radiol 1997 Sep; 25(2): 118–128.
6. Timsit MA, Bardin T: Metabolic arthropathies. Curr Opin Rheumatol 1994 Jul; 6(4): 448–453.
7. Ferraro FA, Winalski CS, Weissman BN: Magnetic resonance imaging of arthritides affecting the shoulder. Magn Reson Imaging Clin N Am 1993 Sep; 1(1): 157–170.

Pigmented Villonodular Synovitis (PVNS)

1. Al-Nakshabandi NA, Ryan AG, Choudur H, Torreggiani W, Nicoloau S, Munk PL, Al-Ismail K: Pigmented villonodular synovitis. Clin Radiol 2004 May; 59(5): 414–420.
2. Bancroft LW, Peterson JJ, Kransdorf MJ: Cysts, geodes, and erosions. Radiol Clin North Am 2004 Jan; 42(1): 73–87.
3. Cotten A, Demondion X, Boutry N, Chastanet P, Delfaut E: Imaging of synovial lesions, neoplastic or non-neoplastic. J Radiol 2000 Mar; 81(3 Suppl): 381–389.
4. DiCaprio MR, Damron TA, Stadnick M, Fuller C: Pigmented villonodular synovitis of the elbow: a case report and literature review. J Hand Surg [Am] 1999 Mar; 24(2): 386–391.
5. Hantes ME, Basdekis GK, Zibis AH, Karantanas AH, Malizos KN: Localized pigmented villonodular synovitis in the anteromedial compartment of the knee associated with cartilage lesions of the medial femoral condyle: report of a case and review of the literature. Knee Surg Sports Traumatol Arthrosc 2005 Apr; 13(3): 209–212. Epub 2004 Jan 29.
6. Helpert C, Davies AM, Evans N, Grimer RJ: Differential diagnosis of tumours and tumour-like lesions of the infrapatellar (Hoffa's) fat pad: pictorial review with an emphasis on MR imaging. Eur Radiol 2004 Dec; 14(12): 2337–2346.
7. Kaneko K, Nakahara D, Tobe M, Iwase H, Inoue Y, Ohbayashi O, Kurosawa H. Pigmented villonodular synovitis of the ankle in an adolescent. Int Orthop 2000; 24(4): 234–237.
8. Llauger J, Palmer J, Monill JM, Franquet T, Bague S, Roson N: MR imaging of benign soft-tissue masses of the foot and ankle. Radiographics 1998 Nov–Dec; 18(6): 1481–1498.
9. Masih S, Antebi A: Imaging of pigmented villonodular synovitis. Semin Musculoskelet Radiol 2003 Sep; 7(3): 205–216.
10. Mohana-Borges AV, Chung CB, Resnick D: Monoarticular arthritis. Radiol Clin North Am 2004 Jan; 42(1): 135–149.
11. Ofluoglu O: Pigmented villonodular synovitis. Orthop Clin North Am 2006 Jan; 37(1): 23–33.
12. Saxena A, Perez H: Pigmented villonodular synovitis about the ankle: a review of the literature and presentation in 10 athletic patients. Foot Ankle Int 2004 Nov; 25(11): 819–826.
13. Sheldon PJ, Forrester DM, Learch TJ. Imaging of intraarticular masses. Radiographics 2005 Jan–Feb; 25(1): 105–119.

Erosive Osteoarthritis

1. Ehrlich GE: Erosive osteoarthritis: presentation, clinical pearls, and therapy. Curr Rheumatol Rep 2001 Dec; 3(6): 484–488.

2. Greenspan A. Erosive osteoarthritis. Semin Musculoskelet Radiol 2003 Jun; 7(2): 155–159.
3. Stabler A, Heuck A, Reiser M: Imaging of the hand: degeneration, impingement and overuse. Eur J Radiol 1997 Sep; 25(2): 118–128.

Systemic Lupus Erythematosus and Jaccoud's Arthropathy

1. Cronin ME: Musculoskeletal manifestations of systemic lupus erythematosus. Rheum Dis Clin North Am 1988 Apr; 14(1): 99–116.
2. Primack SL, Muller NL: Radiologic manifestations of the systemic autoimmune diseases. Clin Chest Med 1998 Dec; 19(4): 573–586, vii.

Diffuse Idiopathic Skeletal Hyperostosis

1. Cammisa M, De Serio A, Guglielmi G: Diffuse idiopathic skeletal hyperostosis. Eur J Radiol 1998 May; 27(1): S7–S11.
2. Sreedharan S, Li YH: Diffuse idiopathic skeletal hyperostosis with cervical spinal cord injury – a report of 3 cases and a literature review. Ann Acad Med Singapore 2005 Apr; 34(3): 257–261.
3. Trojan DA, Pouchot J, Pokrupa R, Ford RM, Adamsbaum C, Hill RO, Esdaile JM: Diagnosis and treatment of ossification of the posterior longitudinal ligament of the spine: report of eight cases and literature review. Am J Med 1992 Mar; 92(3): 296–306.

Haglund's Disease

1. Segesser B, Goesele A, Renggli P: The Achilles tendon in sports. Orthopade 1995 Jun; 24(3): 252–267.

Scleroderma

1. Akesson A, Fiori G, Krieg T, van den Hoogen FH, Seibold JR: Assessment of skin, joint, tendon and muscle involvement. Clin Exp Rheumatol 2003; 21(3 Suppl 29): S5–S8.
2. Chroni E, Paschalis C, Stergiou T, Vlahanastasi C, Andonopoulos AP: Multiple sclerosis in the course of systemic sclerosis. Ann Rheum Dis 2002 Feb; 61(2): 188.
3. Hanlon R, King S: Overview of the radiology of connective tissue disorders in children. Eur J Radiol 2000 Feb; 33(2): 74–84.
4. Kane D, Grassi W, Sturrock R, Balint PV: Musculoskeletal ultrasound – a state of the art review in rheumatology. Part 2: Clinical indications for musculoskeletal ultrasound in rheumatology. Rheumatology (Oxford) 2004 Jul; 43(7): 829–838.
5. Olsen NJ, King LE Jr, Park JH: Muscle abnormalities in scleroderma. Rheum Dis Clin North Am 1996 Nov; 22(4): 783–796.
6. Soubrier MJ, Dubost JJ, Sauvezie BJ: POEMS syndrome: a study of 25 cases and a review of the literature. French Study Group on POEMS Syndrome. Am J Med 1994 Dec; 97(6): 543–553.

Osteochondromatosis

1. Cho KH, Park BH, Yeon KM: Ultrasound of the adult hip. Semin Ultrasound CT MR 2000 Jun; 21(3): 214–230.
2. Crotty JM, Monu JU, Pope TL Jr: Synovial osteochondromatosis. Radiol Clin North Am 1996 Mar; 34(2): 327–342, xi.
3. Knoeller SM: Synovial osteochondromatosis of the hip joint. Etiology, diagnostic investigation and therapy. Acta Orthop Belg 2001 Jun; 67(3): 201–210.
4. Oviedo A, Simmons T, Benya E, Gonzalez-Crussi F: Bizarre parosteal osteochondromatous proliferation: case report and review of the literature. Pediatr Dev Pathol 2001 Sep–Oct; 4(5): 496–500.
5. Roulot E, Le Viet D: Primary synovial osteochondromatosis of the hand and wrist. Report of a series of 21 cases and literature review. Rev Rhum Engl Ed 1999 May; 66(5): 256–266.
6. Ryan RS, Harris AC, O'Connell JX, Munk PL: Synovial osteochondromatosis: the spectrum of imaging findings. Australas Radiol 2005 Apr; 49(2): 95–100.
7. Sheldon PJ, Forrester DM, Learch TJ. Imaging of intraarticular masses. Radiographics 2005 Jan–Feb; 25(1): 105–119.

Chondromalacia Patella

1. Christian SR, Anderson MB, Workman R, Conway WF, Pope TL: Imaging of anterior knee pain. Clin Sports Med 2006 Oct; 25(4): 681–702.
2. McAlindon TE. Regional musculoskeletal pain. The knee. Baillieres Best Pract Res Clin Rheumatol 1999 Jun; 13(2): 329–344.

Chapter 12

Imaging of Prostheses

Sayed Ali and William R. Reinus

Abstract This chapter covers relevant aspects of imaging of prostheses. Initially, a brief historical review is given, as well as a description of the relevant terminology in the radiology of prostheses. This is followed by an in-depth discussion of the composition of current prostheses, including individual designs. The indications and contraindications are then outlined. The preoperative and postoperative evaluation of images follows, with a description of the various measurements, including angles that are relevant to the radiologist and orthopedist. Finally, a description of the immediate and delayed complications that are encountered, including the pathogenesis of these complications, completes the chapter.

Keywords Alloys • Cement • Polyethylene liner • Particle disease • Liner wear • Creep • Revision arthroplasty • Fractures • Dislocations • Aseptic loosening • Infective loosening • Heterotopic ossification

Introduction

Joint replacement surgery is the second most common orthopedic surgical procedure in the United States, the most common being fracture fixation. The most commonly replaced joints are the hips and the knees, and less commonly the shoulder and elbow joints. Arthroplasties of the wrist and ankle are uncommon since arthrodesis generally has a better clinical outcome. In this chapter, we give a brief historical perspective on prostheses, discuss the indications and contraindications for arthroplasty, the basic technique of joint replacement surgeries, the prosthetic components including their structural components and the preoperative and postoperative radiologic evaluation of prostheses including complications.

S. Ali (✉)
Department of Radiology, Temple University School of Medicine, Philadelphia, PA 19140 USA
e-mail: saychink@yahoo.com

Historical Perspective

Before the introduction of artificial joints, the management of the painful or nonfunctional joint included joint arthrodesis (fusion), osteotomy and ostectomy, nerve division, and joint debridement – to remove large osteophytes, heterotopic bone, calcium deposits, loose bodies, and diseased cartilage in the attempt to smooth the joint surfaces. Early attempts at resurfacing joints were directed at the hip and included such diverse and esoteric materials as chromatized pig bladder and gold. In 1925 Dr. Smith-Peterson from Boston used glass to cover the femoral head in the form of a mold, but the results of this early arthroplasty were disappointing, providing only limited pain relief and early hardware failure.

A chromium–cobalt alloy was introduced in 1933 and was deemed to be well suited for joint resurfacing. Although this alloy was strong, the use of mold arthroplasty did not bring about significant pain relief, and limitation of movement continued to be a major problem. Nonetheless, this alloy has stood the test of time and continues to be the preferred alloy used in arthroplasties today.

In the 1940s Fred Thompson of New York and Austin Moore of South Carolina developed replacements for the femoral head. These hemiarthroplasties consisted of a single component with a ball and stem. The patient's femoral head was excised and the stem of the prosthesis was placed into the femoral medullary canal. These prostheses were not cemented into place and loosening was a major problem. In addition, these only replaced the femoral head; the osteoarthritic or diseased acetabulum was not resurfaced.

Acrylic cement was introduced in France by Drs. Jean and Robert Judet in the 1930s. Loosening, however, remained a major problem. Dr. Edward Haboush from the Hospital for Joint Diseases in New York used the acrylic to help reduce the incidence of loosening. This was the first "cemented" hip prosthesis, and the concept of a cemented joint became widely accepted by surgeons as a means of anchoring prosthetic devices.

A. Bonakdarpour et al. (eds.), *Diagnostic Imaging of Musculoskeletal Diseases: A Systematic Approach*,
DOI 10.1007/978-1-59745-355-4_12,

The major revolution in hip arthroplasties began in the 1950s with Dr. John Charnley of England, who designed the first total hip arthroplasty. He eventually used polyethylene as the liner for the acetabulum with remarkable success. He changed the cement from acrylic to polymethylmethacrylate (PMMA), which was already being used in dental practice, to keep the metal femoral component and polyethylene acetabular liner firmly attached to the bone. The Charnley prosthesis is still recognized internationally as the prototypical total hip arthroplasty. Since then, total hip replacements (THR) have undergone numerous design revisions, but the basic principle remains the same.

The cement surrounding arthroplasties has a propensity to fail after a period of time causing the prostheses to loosen. Some more modern prostheses use sintered surfaces where small fissures in the metallic surface of the prosthesis allow for bone in-growth into the prosthesis (Fig. 12.1). This in-grown bone then serves to fix the prosthesis in place and replaces the need for cement. With the success of total hip replacement, over 100,000 procedures are performed annually in the United States.

Knee arthroplasties present their own set of challenges because of the knees' complex movement, the physics of their hinge-like action, and complex ligamentous anatomy. After many design attempts, the total condylar prosthesis was introduced by Insall at the Hospital for Special Surgery in New York in 1973. It concentrated on reproducing internal knee mechanics instead of simply reproducing normal knee movements. Ranawat et al. reported a rate of survivorship in these prostheses of 94% at 15 years of follow-up. Subsequently cruciate retaining prostheses were introduced, providing for more natural kinematics allowed by the retention of the posterior cruciate ligament. These prostheses permitted patients to have a better gait, especially climbing and descending stairs. Even so, cruciate resecting (or cruciate sacrificing) prostheses are also in common use (Fig. 12.2c).

Terminology

Knowledge of the various general types of prostheses and their design principles is important, but the myriad available prosthetic names are not important to remember. The following terms are firmly embedded in the surgical and radiological:

Constraint: This is the resistance of a prosthesis to a particular degree and direction of motion, e.g., in the anteroposterior or axial direction. A fully constrained prosthesis shows minimal motion in a particular direction, whereas an unconstrained prosthesis allows full motion in a particular direction. A constrained prosthesis typically has a component that physically joins the prosthetic components together, e.g., a hinged elbow prosthesis which has minimal medial–lateral motion, but full anterior–posterior motion (Fig. 12.3). An unconstrained prosthesis relies on the surrounding muscles, ligaments, tendons, and joint capsule for stability with no physical connection between the prosthetic parts. Semi-constrained prostheses, as the name suggests, are intermediate between constrained and non-constrained prostheses.

Conformity: This refers to the area of contact of the articulation. A fully conforming prosthesis has full articular contact. A non-conforming prostheses has limited or no articular contact. With increasing conformity, there is a larger contact area and so more intrinsic stress wear.

Modularity: Prostheses have multiple components or modules, e.g., stems, wedges, and other parts can be added to the basic prostheses, to allow for variations in patient anatomy (Fig. 12.4). These can be assembled by the surgeon intraoperatively to make a custom-fit prostheses.

Custom fit: Some prostheses are designed preoperatively or perioperatively to suit the particular needs of the patient,

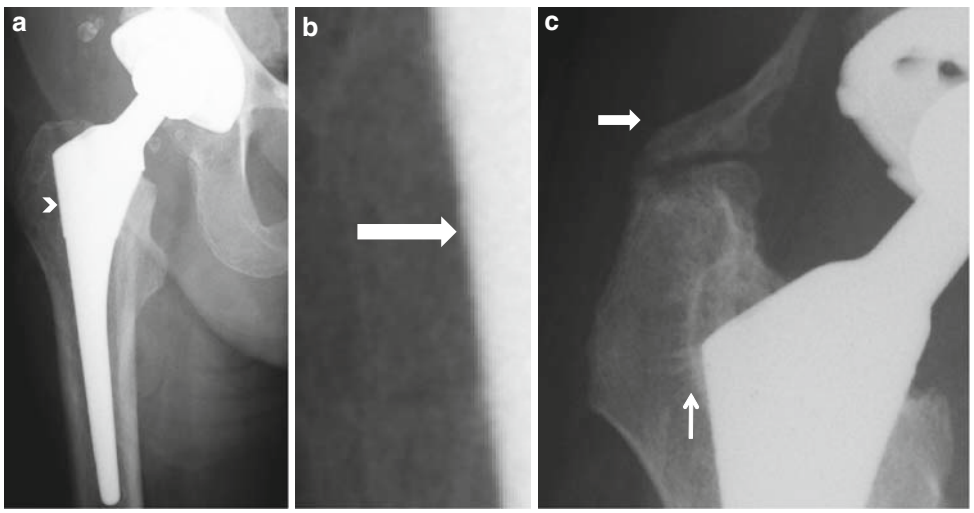

Fig. 12.1 AP hip radiographs. (**a**) Normal uncemented right hip prostheses with a sintered femoral stem (*arrowhead*). (**b**) Magnified image of the sintered (*fissured*) margin (*thick long arrow*). (**c**) Spot welds in a different patient (*arrow*) caused by bone in-growth in a sintered prostheses. Note heterotopic ossification (*thick arrow*)

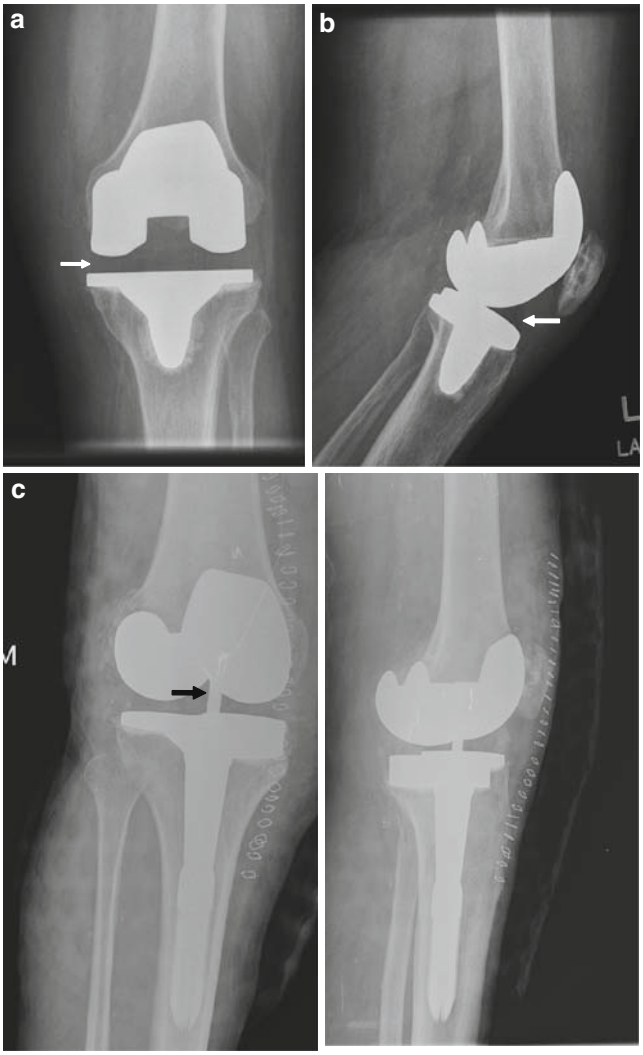

Fig. 12.2 AP (**a**) and lateral (**b**) radiographs of knee showing a normal three-part knee prosthesis with a cemented tibial component and non-cemented femoral component. The *lateral view* shows the normal knee prosthesis, and its high molecular weight polyethylene patellar component. *Arrows* show the polyethylene tibial tray. (**c**) Cruciate resecting prostheses with a post (*arrow*) that provides stability in place of the PCL. Note long-stemmed tibial component

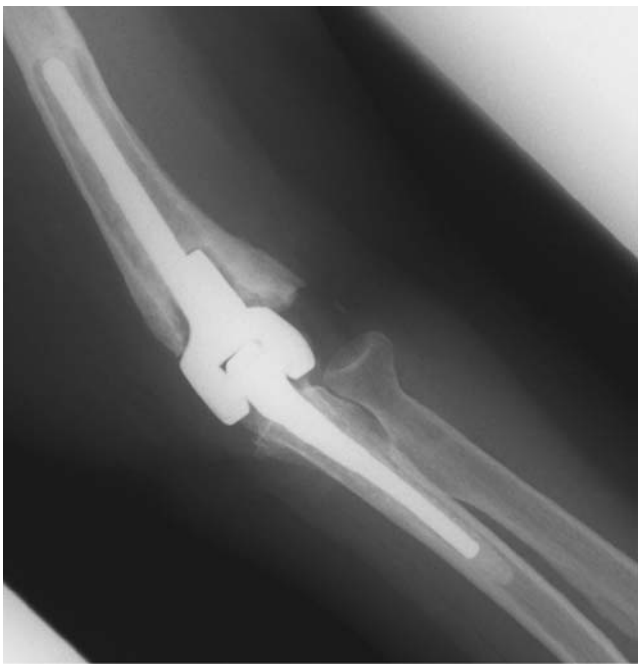

Fig. 12.3 DePuy total elbow arthroplasty. This is a hinged constrained prostheses and are more prone to loosening. Note the extensive humeral periprosthetic lucency consistent with loosening

and take into account the anatomy of the joint as well as the patient's postoperative functional requirements. Modularity is obviously important in the design of a custom-fit prosthesis (Fig. 12.5).

Cement: This is the material used to anchor the prosthesis into the medullary cavity of the bone (Fig. 12.6). Cement has no adhesive properties and is not a glue. Fixation is achieved by physical interdigitations with the rough surfaces of the bone and prosthesis and by pressure from expansion of the polymerizing cement within the bone cavity, not by chemical bonding. Polymethylmethacrylate (PMMA) is the most widely used cement. It comes as a monomer powder and polymerizes in an exothermic reaction on exposure to water. Most cement is barium impregnated to make it radiopaque postoperatively.

Press fit: Cementless prostheses encourage bone to grow directly into the prostheses. The prosthetic surface is roughened or sintered to increase surface area and is coated with a substance such as hydroxyapatite or bone morphogenic protein, which encourages the bone to grow and adhere to the surface. Radiologically, this bone ingrowth may be seen as "spot welds" with linear bands of new bone at the sintered surface (Fig. 12.1c). A hybrid prosthesis is one where cement is used for one component and press fit for the other. The most common type of hip prosthesis used in North America is hybrid, with a cementless acetabular and cemented femoral component. Removal of a cementless prosthesis is technically easier, and does not involve as much bone loss at the time of surgery. This preservation of bone stock is important if revision arthroplasty becomes necessary.

Subsidence is the gradual inferior or longitudinal displacement (sinking in) of a prosthetic component and is a sign of loosening. It is not unusual to see subsidence of 1–2 mm of the femoral component of a THR, but subsidence of greater than 4–5 mm should raise concern for loosening (Figs. 12.9 and 12.32a). In hip prosthses, subsidence may be confined to the femoral component or may include both the femoral component and the cement. Subsidence in the acetabulum manifests as protusio acetabuli, with medial migration of the acetabular component (Figs. 12.9 and 12.32a).

Fig. 12.4 Modularity. The components of a total knee prostheses: (**a**) tibial tray, (**b** and **c**) femoral condylar component, and (**d**) polyethylene tibial insert

Liner wear refers to irregular and asymmetric wear of a polyethylene component of a prosthesis. This results in loss of congruity and normal function of the prosthesis and may cause pain (Fig. 12.10). Liner wear most commonly occurs in hip prostheses.

Creep refers to gradual molding of a metallic component onto the polyethylene liner, for example, the femoral component into the acetabular liner. Creep should not be confused with liner wear, since creep is a normal phenomenon that typically occurs within the first 12–18 months after surgery, whereas liner wear typically occurs after 18 months. In addition, creep is usually superior/medial narrowing, and wear is superior/lateral. Gradual and minimal narrowing of the distance between the metallic components is visible radiographically. Further thinning after 18 months should raise the suspicion for liner wear (Fig. 12.10).

Stress Shielding is the phenomenon of bone resorption around the prosthesis, typically the stem of the prosthesis (Fig. 12.9). The material of the prosthesis is stiffer than the native bone and as a result transmits the entire load across the portion of the skeleton containing the prosthesis. The bone is thus shielded from stress and tends to resorb. Modern prostheses are designed to counter this phenomenon. If stress shielding occurs, it may lead to prosthetic loosening.

Types of Arthroplasties

Total joint arthroplasty: All parts of the joint are resurfaced.

Hemiarthroplasty: One side of the joint is replaced, e.g., the femoral head with a preserved native acetabulum in a hip hemiarthroplasty. This may be a unipolar or bipolar hemiarthroplasty (Figs. 12.7 and 12.12).

Fig. 12.5 Custom fit. The parts are initially assembled intraoperatively, so that the correct fit is achieved

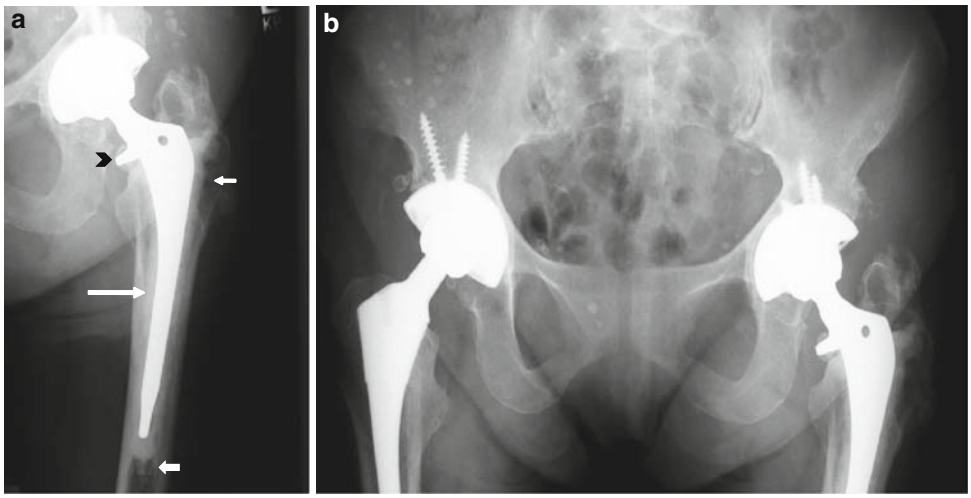

Fig. 12.6 AP radiograph of the left hip. (**a**) Cemented left prostheses with particle disease. Cement is shown (*long arrow*). Extensive lucency at the greater trochanter (*short arrow*) is the result of particle disease. Note the cement restrictor (*thick arrow*) and collar (*arrowhead*). The pelvic radiograph (**b**) shows the normal right side

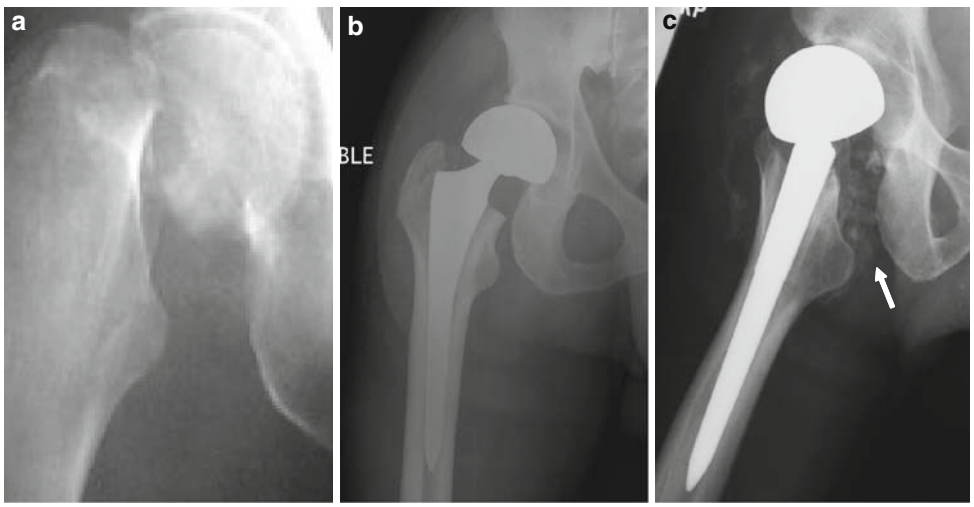

Fig. 12.7 AP hip radiographs (**a**) showing displaced subcapital fracture of the right femoral neck (Garden IV) (**b**) treated with a bipolar hip hemiarthroplasty. Note the intact native acetabulum. (**c**) Subsequent development of class III heterotopic ossification (*arrow*)

Revision or replacement arthroplasty: Loose or infected prostheses need to be replaced. Loose prostheses are typically replaced in patients (less than 60 years) with active lifestyles. The replacement prostheses are usually long-stemmed devices, which seat deeper into the bone (Fig. 12.8). This is necessary because of stress shielding and loss of bone stock from the original arthroplasty (Fig. 12.9).

Resurfacing hip arthroplasty: The femoral neck is left intact, and the head is resurfaced with a metallic or ceramic component. This procedure is typically reserved for younger active patients, with good bone stock (Fig. 12.13) and may be used in either a hemiarthroplasty or total hip replacement.

Osteocapsular arthroplasty: This technique involves removal of osteophytes, intra-articular loose bodies, and inflamed synovium, and involves reshaping and remodeling of deformed bone. It is particularly useful when there are large osteophytes and capsular contracture. Although this is similar in many ways to joint debridement, it is a relatively new technique.

Materials

Polyethylene: The material is used as a liner in most prostheses. It is typically radiolucent on radiographs but has a cloudy white appearance on visual examination. It may be used alone, e.g., high molecular weight polyethylene for patella resurfacing, or interposed between metallic surfaces as in the hip. It has a relatively high risk of wear when compared to the metallic components, but newer designs show greater wear resistance (Figs. 12.2a, b and 12.4d).

Alloys are combinations of different metals used in the metallic components of the prostheses. Typically these are combinations of chromium and cobalt or chromium–cobalt with titanium, although pure titanium also is used. These chromium/cobalt alloys show much less wear than the polyethylene liner, and the risk of osteolysis from particulate disease is also less than with polyethylene. Different alloys can be used in a single joint arthroplasty. For example, the most commonly used knee prostheses use

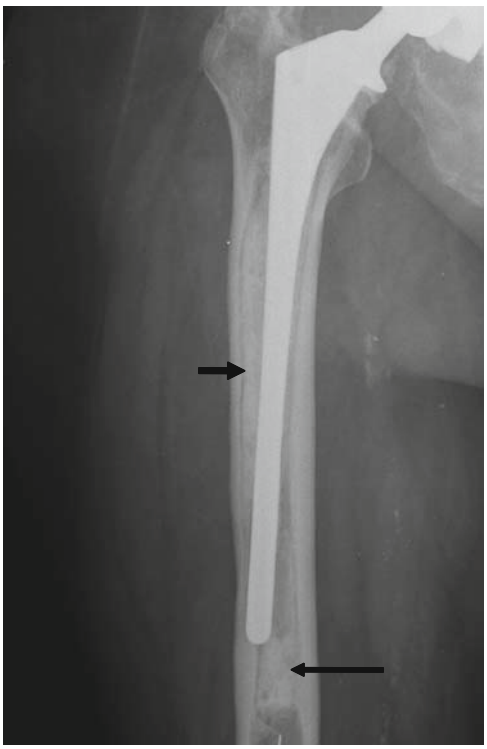

Fig. 12.8 AP radiographs of the right hip showing a long-stemmed femoral revision arthroplasty in varus position and displacement from cement (*long arrow*). Note the irregular pericemental lucency along the cement–bone interface consistent with loosening (*short arrow*)

a chromium–cobalt–molybdenum femoral component and a titanium–aluminum–vanadium tibial component with a high molecular weight polyethylene patellar component.

Ceramics can be used as an alternative to metal alloys. Typically alumina is used. Ceramics are more brittle than metal alloys and can crack or fissure, but they have a lower incidence of polyethylene liner wear (Fig. 12.10). A commonly performed knee replacement uses a ceramic surface-oxidized zirconium femoral component, a titanium alloy tibial component, and a high molecular weight polyethylene patellar component.

Carbon (pyrolytic carbon) has been used in small joint implants with reasonable success and low complication rates. It has also been incorporated into composites of larger implants.

Prosthetic Designs

Metal-on-polyethylene is the most commonly used prosthetic design. The differences in density of the two components results in a low coefficient of friction, and simulate normal joints. The typical lifespan of this design is 15–20 years.

Metal-on-metal prostheses were the initial design and had a high failure rate due to friction. This was replaced by metal on polyethylene, but regained popularity when polyethylene particles were linked to osteolysis. The newer metal-on-metal designs have a similar lifespan to metal on polyethylene (15–20 years).

Ceramic-on-ceramic prostheses initially had problems with cracking and fissuring of the surfaces, but this has been eliminated in current designs. These prostheses typically last about 15 years and are more commonly used in Europe than the United States.

Silicone spacers are typically reserved for very small joints affected by rheumatoid arthritis or osteoarthritis, e.g., the metacarpophalangeal or metatarsophalangeal joints and

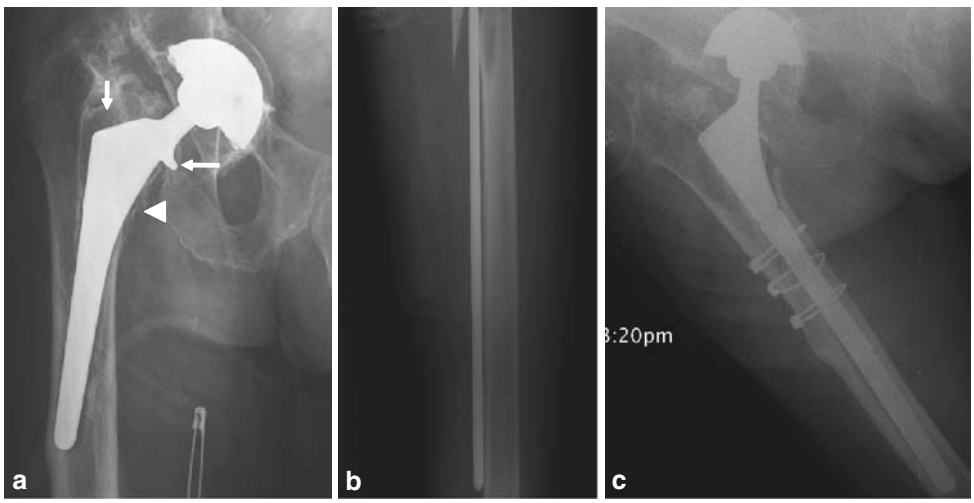

Fig. 12.9 AP hip radiograph (**a**) showing acetabuli protusio. Note the extreme varus migration of the right femoral stem with resulting weakening and remodeling of the lateral femoral cortex. Note the collar (*arrow*) at the calcar with stress shielding inferiorly (*arrowhead*) and subsidence (*small arrow*). Coned-down AP femoral radiograph (**b**) shows that the weakened lateral cortex fractured intraoperatively during revision arthroplasty. AP hip radiograph (**c**) shows that the prosthesis was revised with a long-stemmed revision arthroplasty, and the fracture was fixed with cables

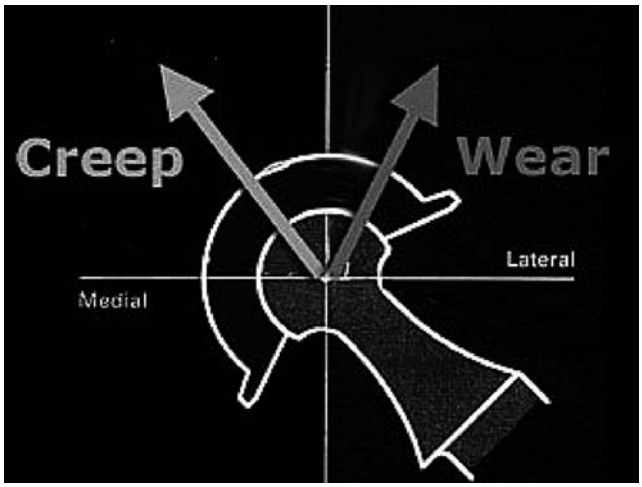

Fig. 12.10 Diagram showing liner wear vs creep. Liner wear occurs in the superior lateral direction, while creep typically occurs superomedially

less commonly the proximal interphalangeal joints. They are inserted between the bones to reduce friction and decrease wear on the articular cartilage. Strengthening of the surrounding tendons and ligaments helps to maintain alignment and stability, and these prostheses also appear to induce encapsulation possibly through foreign body reaction, further increasing stability. Silicone spacers often have titanium grommets, where the diseased end of the bone and cartilage is resected and the grommet is inserted into the bones with a silicone spacer in between (Fig. 12.11).

Occasionally, this material may induce a silastic or silicone arthropathy. This is a foreign body reaction to silicone particles wearing off of the spacer. Radiologically, this is seen as osteolysis and erosive change at the joint, usually the metatarsophalangeal joint.

Individual Designs

Most of the remaining discussion will apply to hip, knee, and shoulder prostheses which are the most common prosthses employed today.

Hip Prostheses

There are three basic types of hip prostheses in current US orthopedic practice: unipolar hemiarthroplasty, bipolar hemiarthroplasty, and total hip arthroplasty.

Unipolar hip arthroplasties are used in older patients with a lower life expectancy, typically in patients with subcapital Garden III and IV fractures, and transcervical fractures (Fig. 12.12). These prostheses are press fit or cemented, with a femoral head component size that matches the acetabulum (fully conforming) and articulate with the articular cartilage of the acetabulum directly. This is the least invasive hip prosthesis and is therefore appropriate for patients with increased surgical risks and limited lifestyles.

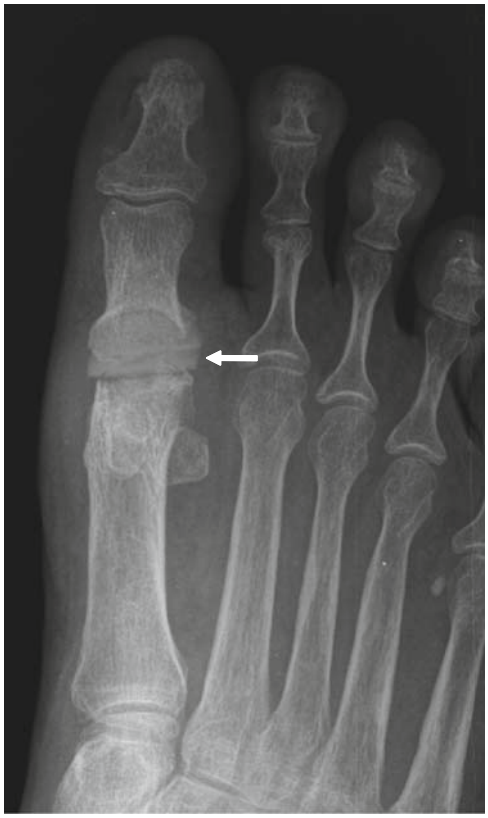

Fig. 12.11 Arthroplasty of the first metatarsophalangeal joint with silicone spacer (*arrow*). This prosthesis has no titanium grommet

A bipolar hip prosthesis is also a hemiarthroplasty, resurfacing only the femoral side of the hip (Fig. 12.7). It consists of a femoral component with a small head within a larger cup that simulates the native acetabulum. The latter is custom fit to match the native acetabulum (which is not resurfaced). The objective of this prosthesis is to increase mobility so that the larger cup component moves within the native acetabulum and the femoral head component (the small ball) moves within the cup. Because of the increased mobility, these bipolar prostheses are less prone to dislocation and causes less acetabular articular cartilage wear than unipolar prostheses. They are typically recognized on radiographs by the large cup mostly obscuring the small femoral ball, and preservation of the native acetabulum.

Over 100,000 total hip replacements are performed annually in the United States. These consist of two basic components, one replacing the femoral head and the other resurfacing the native acetabulum (Fig. 12.6). These prostheses

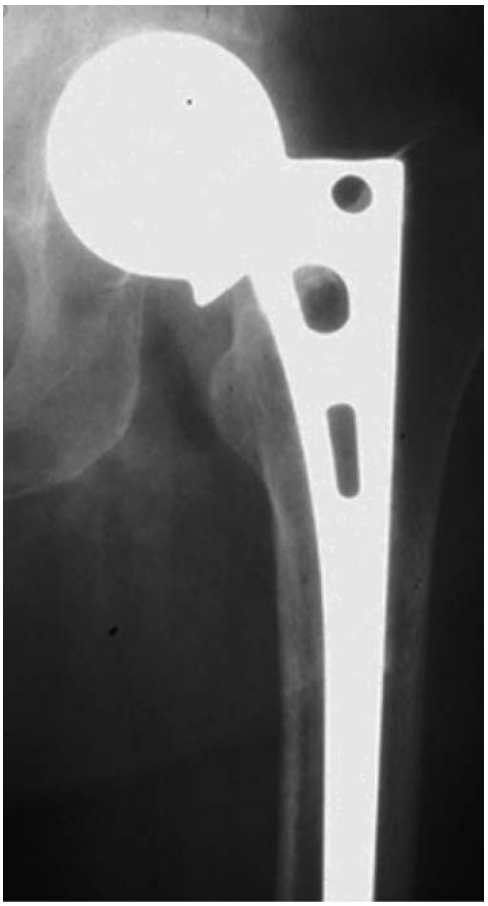

Fig. 12.12 AP left hip radiograph showing a unipolar hip arthroplasty. Note the native acetabulum

are modular with a sizable femoral head and stem and acetabular cup and liner. They are custom fit at the time of surgery. The modularity allows greater flexibility in design, but disengagement and fretting (a form of corrosion) at the interfaces are trade-offs for the increased size flexibility. Cementless designs are currently more popular than cemented prostheses.

With current cement techniques, a polyethylene cement restrictor may be placed into the femoral canal to prevent unrestricted migration of cement distally (Figs. 12.6 and 12.8). A small polyethylene centering device may be fitted onto the tip of the femoral component to be sure that the femoral stem is centered in the femoral canal. These two components provide for uniform cement fill around the prosthesis with fewer air bubbles and gaps. This improves prosthetic longevity.

A cementless acetabular component is typically fully porous coated in contrast to a cementless femoral component, which may be either partially coated proximally or fully porous coated. The cementless acetabular component can also be fixed with screws into the iliac bone, especially if there is significant loss of bone stock. Cemented acetabular components are required in patients with severe osteoporosis, a history of prior radiation with loss of bone stock, patients requiring bone grafting or in a revision arthroplasty where the original prosthesis has caused loss of bone stock.

Cementless femoral stems are preferred in younger patients because they have better life expectancy than cemented prostheses and are generally easier to revise than cemented prostheses. The femoral component may have a collar abutting the resected femoral calcar to attempt to reduce the chance of stress shielding as a complication of prosthesis placement (Fig. 12.6).

A resurfacing arthroplasty may be a hemiarthroplasty or total hip replacement. The surface of the femoral head is replaced either with a metallic or ceramic component (Fig. 12.13). These prostheses are typically used in younger active patients with osteoarthritis and good bone stock. The femoral neck is preserved, which is important for later revision to more conventional arthroplasties. Thinning of the femoral neck, possibly from stress shielding, has been reported with the use of these prostheses and this in turn has a reported 1.25% incidence of resulting femoral neck fracture.

Knee Prostheses

Total knee replacement involves resurfacing the femoral condyles, tibial plateaus, and the patella (Fig. 12.2a, b). The patella is typically resurfaced with high molecular weight polyethylene alone but this component may also be metal backed. Femoral components are of varying design but most resurface the femoral condyles and trochlear sulcus with

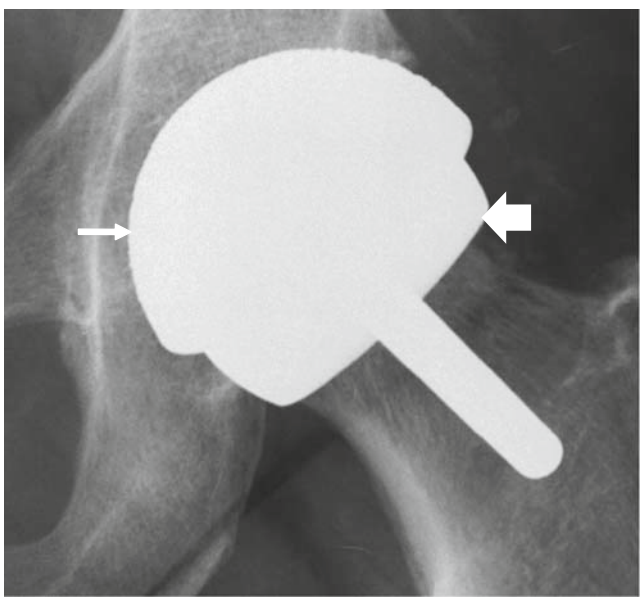

Fig. 12.13 AP view of hip showing a resurfacing total hip arthroplasty. The femoral neck is preserved and the head is resurfaced with a metallic component (*thick arrow*). The acetabulum also has been replaced in this patient (*thin arrow*)

metallic or ceramic/metal components. The tibial component is usually a metal-backed polyethylene tray, but may be polyethylene alone. The components may be cemented or non-cemented. The tibial component may be fixed with screws into the proximal tibia.

Unicompartmental knee arthroplasties are used for younger patients with severe medial or lateral compartment osteoarthritis and alteration of the knee carrying angle from its normal 5–8º of valgus (Fig.12.14a). An alternative to unicondylar arthroplasty is a tibial wedge osteotomy: a triangular wedge of bone is removed from the proximal tibia, usually the medial side, and the knee is realigned back into valgus (opening wedge osteotomy). A wedge of tissue (usually bone graft) is then placed into this space to maintain valgus alignment (Fig. 12.14b). Alternatively, a triangular wedge can be removed from the lateral tibia without placement of a spacer or graft (closing wedge osteotomy) to reduce exaggerated varus angulation caused by medial compartment osteoarthritis. The objective of these procedures is to delay having to do a total arthroplasty, which is a more invasive procedure.

Tricompartmental knee prostheses can be subdivided broadly into posterior cruciate sparing or sacrificing prostheses. (The anterior cruciate ligament is typically sacrificed.) In the United States, cruciate sparing prostheses are more commonly used. As previously mentioned, gait and stability when ascending or descending stairs appear to be slightly better with cruciate retaining prostheses. Cruciate resecting prostheses can generally be recognized by a large box in the femoral component on the lateral film. This box articulates with a post in the polyethylene tray, in order to provide posterior stability (Fig. 12.2c).

Ankle Prostheses

With the advent of second-generation arthroplasties, the success rate has improved somewhat and there has been renewed interest in replacing the ankle joint. Even so, ankle arthrodesis remains the modality of choice when treating the painful ankle joint.

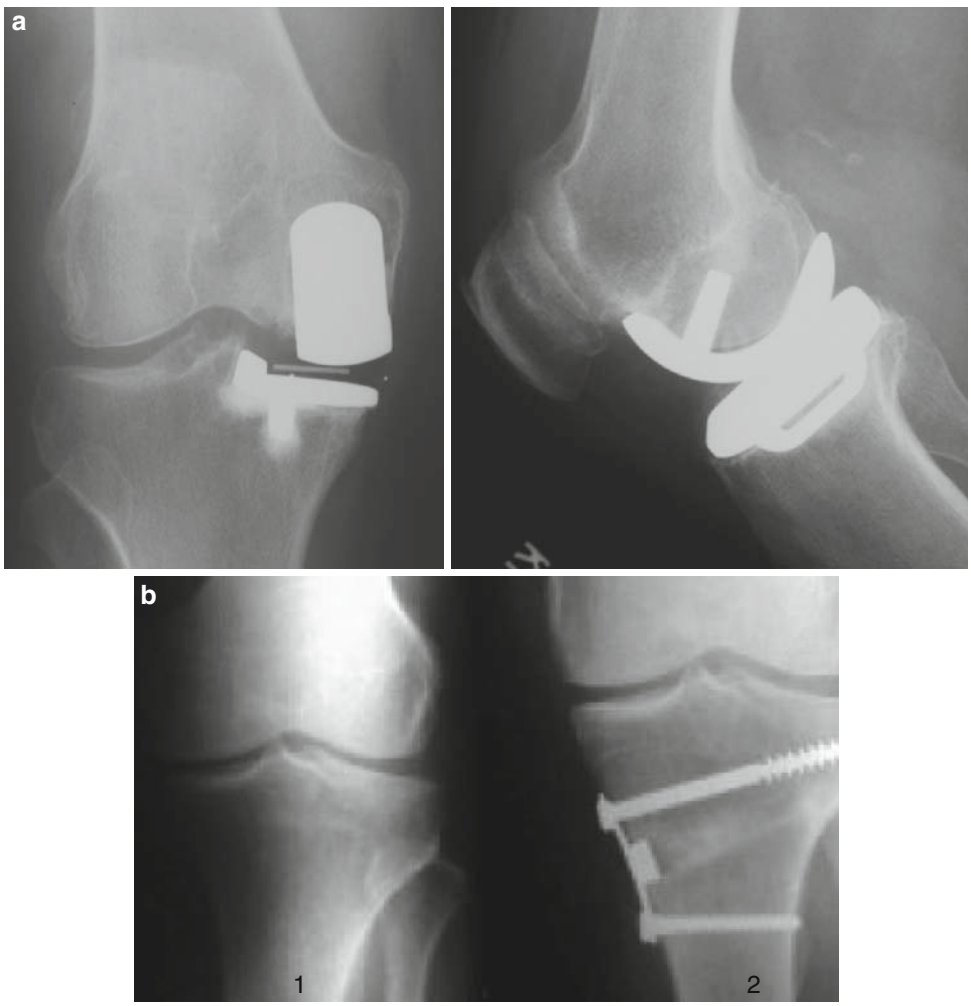

Fig. 12.14 AP and lateral radiographs (**a**) showing a unicompartmental medial knee arthroplasty. Preoperative and postoperative radiographs (**b**) showing medial compartment osteoarthritis with genu varus (**1**), treated by opening wedge osteotomy (**2**) to realign knee back into valgus

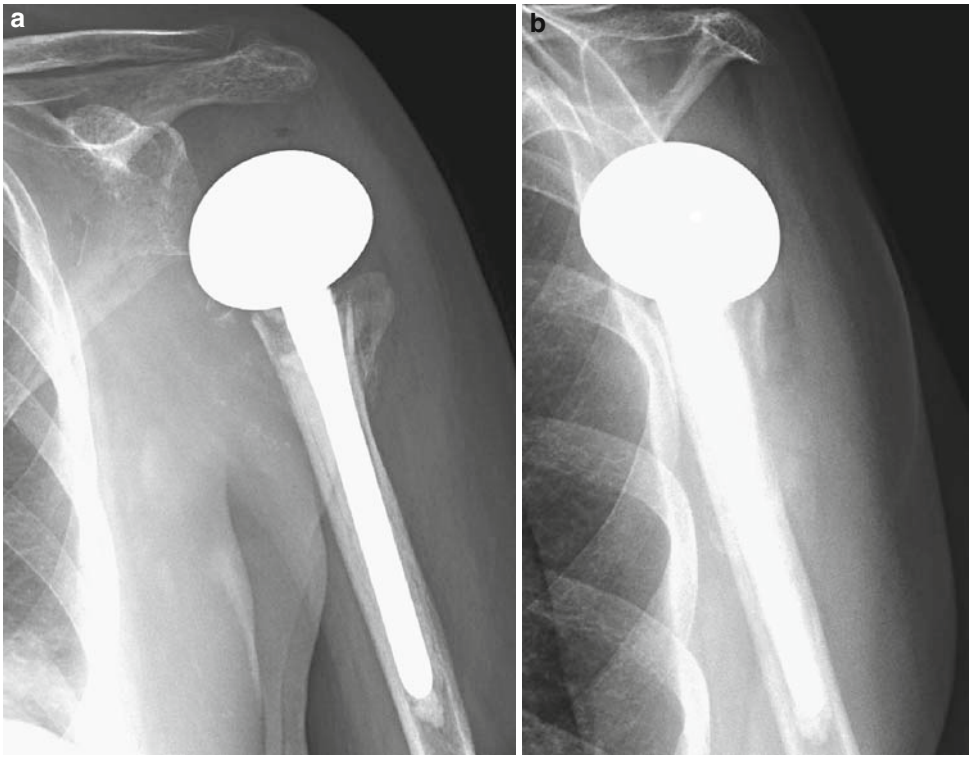

Fig. 12.15 (**a**) AP radiograph of the left shoulder showing a DePuy shoulder hemiarthroplasty. Note intact native glenoid. (**b**) Transcapular Y view of a DePuy shoulder hemiarthroplasty in good position. Bone fragment posteriorly was from the original fracture

Shoulder Prostheses

Shoulder replacement procedures include hemiarthroplasty (Fig. 12.15), total joint replacement (Fig. 12.16), and more recently a reverse shoulder arthroplasty (Fig. 12.17). Typically a hemiarthroplasty is performed for fractures or in patients with a severe rotator cuff tear, where the glenoid is relatively normal. In a total shoulder arthroplasty, usually done for osteoarthritis, the humeral component articulates with either a metallic or polyethylene glenoid. Because these prostheses are usually held in place by the surrounding rotator cuff and musculature, they are semi-constrained or unconstrained and so have a higher risk of dislocation when compared to hip prostheses.

A reverse shoulder arthroplasty, Delta reverse ball and socket design (Fig. 12.17), is used mainly in older patients with severe rotator cuff disease, especially those with rheumatoid arthritis who have exhausted all other means of repair. The change in the fulcrum of the joint permits the deltoid to move the shoulder. Unfortunately, this design creates a relatively high risk of shoulder dislocation, especially in patients who have the reverse arthroplasty placed as a revision procedure.

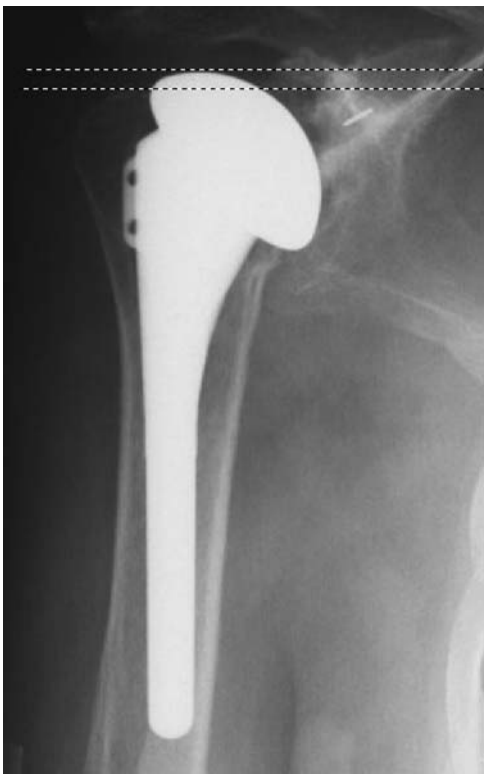

Fig. 12.16 AP radiograph of the shoulder showing a DePuy total shoulder arthroplasty with non-cemented humeral metallic component and a polyethylene glenoid component. A *line* drawn through the top of the prosthetic head should lie above the greater tuberosity to avoid risk of impingement. There is satisfactory positioning in this example

Elbow Arthroplasty

Hemiarthroplasties are no longer performed because of poor outcomes. The most common arthroplasty of the

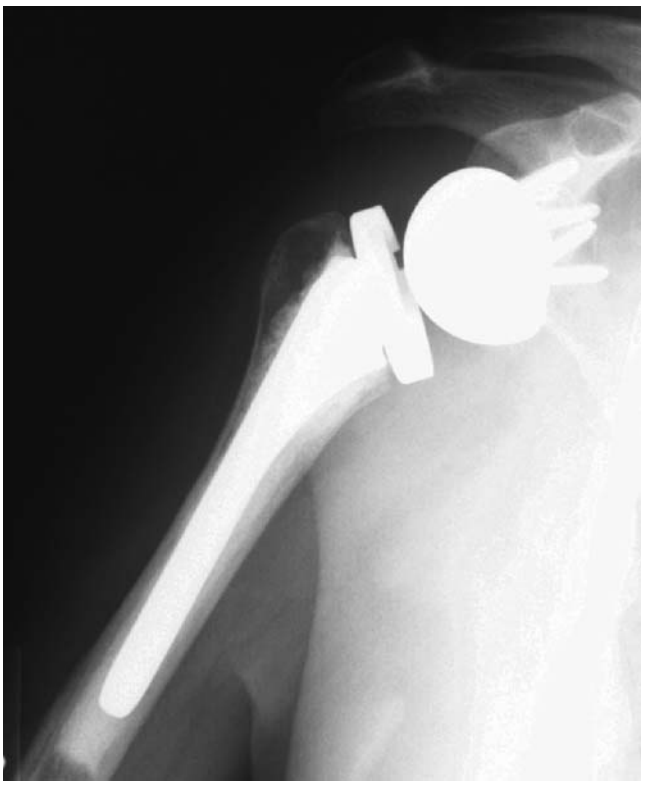

Fig. 12.17 AP radiograph of the shoulder showing a reverse shoulder arthroplasty (Delta) used in patients with severe rotator cuff disease such as seen in rheumatoid arthritis. The glenoid is replaced with a ball and the humeral head with a slightly concave component, the reverse of normal anatomy

elbow is a total elbow arthroplasty. These may be unconstrained, semi-constrained, or constrained. At our institution, hinged constrained prostheses are performed most commonly (Fig. 12.18). Unconstrained prostheses have stemmed ulnar and humeral components that articulate by a polyethylene component. Stability is provided by the surrounding muscles, ligaments, and tendons. As with any other unconstrained prostheses, the major complications with these prostheses are subluxations and dislocations.

Constrained prostheses have rigid hinges that connect the humeral component to the ulnar component. These connections are through a bushing or separate polyethylene piece. As part of the procedure, the radial head is often resected, proximal to the annular ligament. Because of the increased stresses on constrained prostheses, their major complication is loosening.

Semi-constrained prostheses connect the humeral and ulnar components with an axle and bushing system. They are less constrained in the coronal plane (varus–valgus), compared with constrained prostheses. This design helps to alleviate some of the rigid stresses of the constrained prostheses and reduces the problem of loosening associated with the less flexible constrained prostheses.

Isolated replacement of the radial head with a prosthesis may be performed for severely comminuted radial head fractures (Fig. 12.19).

Wrist and Hand Joint Prostheses

Wrist arthroplasty has been problematic and so management of the painful hand and wrist typically has been by a partial or total arthrodesis. Recent advances in prosthetic devices have alleviated some of the problems associated with the older wrist prosthetics. Most commonly, wrist arthroplasty is performed in patients with rheumatoid arthritis (Fig. 12.20), but other indications include severe primary or post-traumatic osteoarthritis. Individual carpal bone replacement with silastic prostheses has been used for trauma or avascular necro-

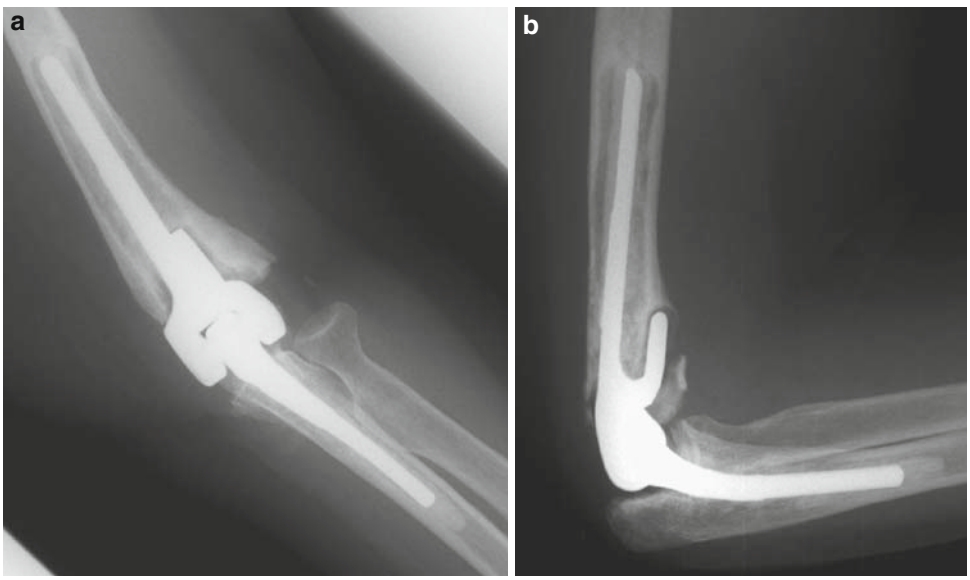

Fig. 12.18 AP (**a**) and lateral (**b**) radiographs of a DePuy total elbow arthroplasty. This is a hinged constrained prostheses and so more prone to loosening. The radial head is preserved in this patient. Extensive irregular periericement lucency is visible around the humeral component suggesting loosening has occurred

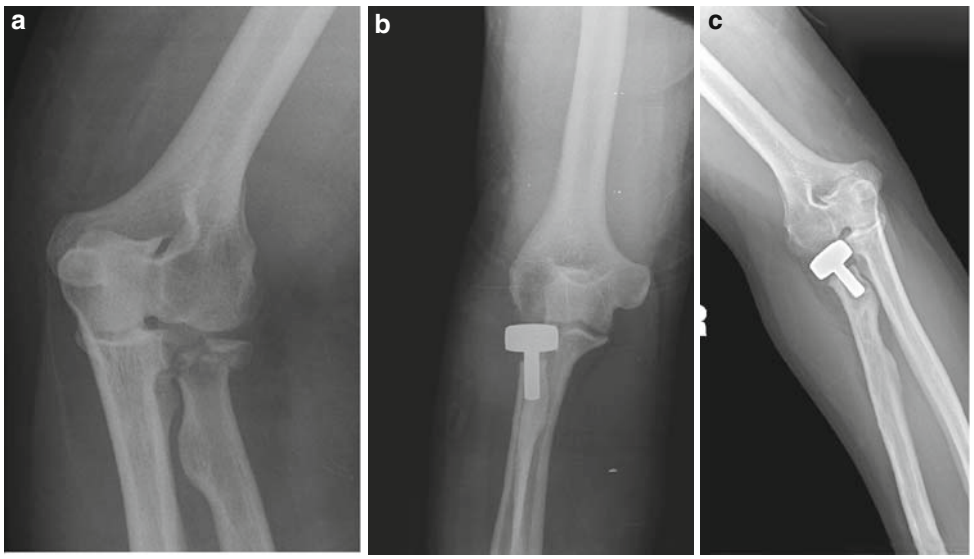

Fig. 12.19 AP oblique radiograph of the elbow: (**a**) a highly comminuted radial head fracture and (**b**) treatment with excision of the head and insertion of a radial head prosthesis. The radial prostheses subsequently loosened as is evident by the extensive periprosthetic lucency and angulation of the device (**c**)

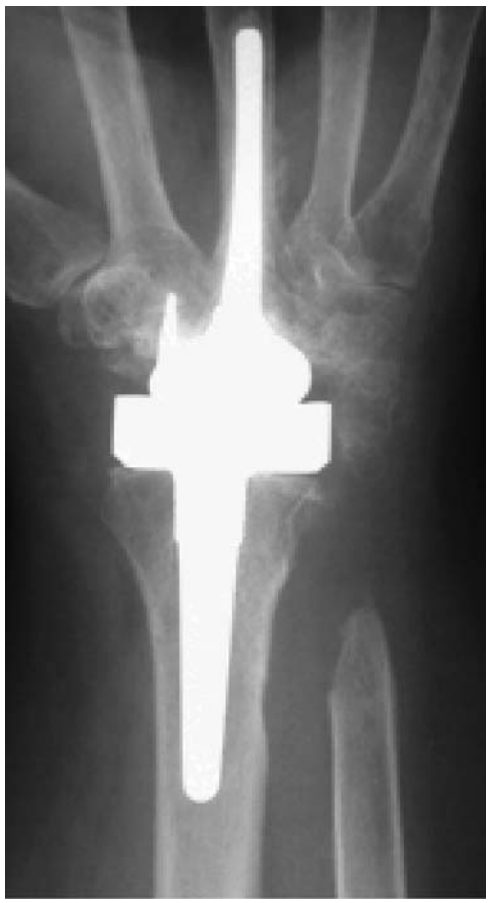

Fig. 12.20 AP wrist radiograph showing a total wrist arthroplasty. Note that the distal stem is in the third metacarpal which is the center of rotation of the wrist. The distal ulna has been resected

sis. Since most of these prostheses are made with MR compatible silicone components, these can be evaluated postoperatively with MR scans, except when combined with titanium grommets which does result in some susceptibility artifact. Specific contraindications to wrist replacement include lack of motor and sensory function, severe chronic volar and ulnar subluxation, and the need for weight bearing on the wrist joint, e.g., patients using a walker or walking stick. These activities place abnormal stress on the prostheses and may lead to loosening.

In the hands the most commonly performed arthroplasties are of the metacarpophalangeal and interphalangeal joints, typically in patients with rheumatoid arthritis.

Indications and Contraindications to Arthroplasty

Indications for joint replacements vary from joint to joint, the patient's status, and the patient's pathology, e.g., arthritic vs traumatic. Regardless, several general indications are accepted. These include severe osteoarthritis limiting mobility and interfering with quality of life, posttraumatic arthropathy, rheumatoid arthritis and other inflammatory arthritis, avascular necrosis, congenital deformities, and severe fracture deformities not amenable to adequate surgical realignment after closed or open reduction and fixation.

Contraindications are typically general in nature, but there are a few specific contraindications for individual joints. The most commonly accepted general contraindications for joint replacements are localized or generalized sepsis. A prosthesis placed in an infected joint is certain to fail. Placement of a prosthesis in a septic patient increases morbidity and mortality. Other accepted general contraindications include severe vascular insufficiency, paralysis, severe obesity (especially in total hip and knee replacements), and a history of prior arthrodesis.

Patient Considerations

Age is one of the most important factors in determining the timing and choice of a prosthesis. Joint replacement is preferred for patients 65 years and older, especially in the hip and knee where weight-bearing forces can limit the lifespan of these prostheses. Joint replacement in younger patients sets up future problems as patients are likely to outlive the lifespan of the prosthesis. Each prosthetic revision is more difficult than the one before and the new prosthesis is likely to have a shorter lifespan. Thus, younger patients are advised to undergo a longer course of conservative treatment. When replacements are unavoidable, less invasive techniques are preferred. For example, a younger patient with single compartment osteoarthritis in the knee is more likely to undergo a unicompartmental arthroplasty or tibial wedge osteotomy rather than a total knee replacement. Furthermore, joint replacements last longer in older patients, presumably because of less active lifestyles as people age.

Pain that interferes with quality of life, including sleep and activity and that has not responded to conservative therapy (typically NSAIDS and joint injections for 3–6 months, or longer in younger patients) is an indication for arthroplasty.

Gender is also important. Ten-year survival of knee prostheses is 93% in women and 88% in men, likely related increased mobility and increased weight in male patients. Revision rates were 30% higher in women than men, which is partly due to the longer lifespan of women.

Patient weight is an important factor particularly in hip and knee replacements. Severe obesity is associated with reduced prosthetic lifespan, including polyethylene liner wear which is accelerated in obese patients. There is a direct association between acetabular component failure and a patient weight exceeding 180 lbs.

The indication for joint replacement also impacts longevity. Patients treated with a Charnley hip prosthesis for advanced rheumatoid arthritis have a significantly higher prosthesis survival rate at 25 years (92%) compared to 66% in patients who received an arthroplasty for congenital hip dysplasia.

Preoperative Imaging

Preoperative imaging is essential for planning of the surgical procedure. The objective is to assess the severity of the disease process, underlying bone stock, review the pertinent anatomy, and plan the surgical technique both in terms of approach and selecting the best prostheses for the involved joint. Preoperative imaging is also used to template the prosthesis, i.e., choose the appropriate type and size of the prosthesis, determine component position and orientation, and to prevent limb length discrepancies.

CT scanning (not a CT scanogram) is not routinely performed but is useful in assessing the extent of cystic disease in osteoarthritis. Assessment of bone stock can be performed by plain films or CT. In addition, a CT scanogram could be obtained to assess for leg length discrepancy.

MRI is rarely used for preoperative planning, but may be useful in cases of avascular necrosis to assess severity and to determine bilaterality. More often, MRI is used to determine the etiology of hip pain and is subsequently reviewed prior to surgery.

Postoperative Imaging

Ideally, postoperative imaging of the knee and shoulder should be performed with fluoroscopic assistance since assessment of the tibial, patellar, and glenoid components may be difficult using conventional radiography. For other joints, routine radiography should be adequate. The frequency of postoperative imaging is determined according to the surgeon's preference and the particular institution but typically an immediate postoperative diagnostic study is obtained as soon as clinically feasible, and subsequently at 3, 6, and 12 months. Subsequent radiographs are obtained at the surgeon's discretion or if complications are suspected. CT and MRI are compromised by the presence of large amounts of metal and so have a limited role in postoperative prosthetic evaluation.

Hips

AP and lateral views of the hips are sufficient in most instances to evaluate the acetabular and femoral components. Both views should include the entire femoral stem, cement that extends around the tip of the prostheses, cement restrictor, and several centimeters of bone below the replacement. On the AP film, the acetabular component should be angled 45° to the ischial line and this is known as the inclination angle (Fig. 12.21 and 12.30b). On the lateral film, the acetabular component should be anteverted 15° although some surgeons prefer a greater degree of anteversion (Fig. 12.22). Anteversion can also be measured by CT (Fig. 12.22b, c).

The arthroplasty's center of rotation should be determined. This is measured from the center of the head of the femoral component to the ischial teardrop and should be bilaterally symmetrical. The femoral component should be aligned with the femoral shaft or in slight valgus (Fig. 12.23). Varus positioning is to be avoided because of the risk

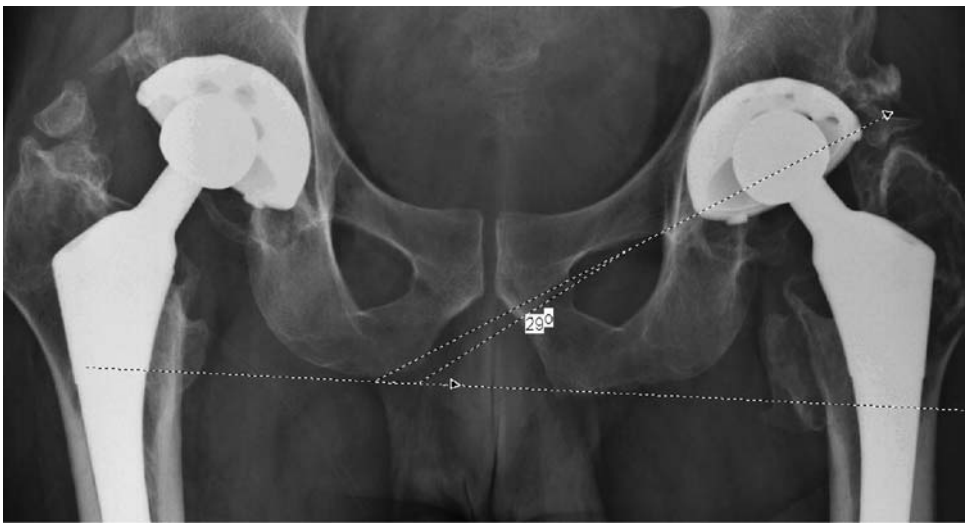

Fig. 12.21 The angle of inclination is measured by taking a line through the diameter of the acetabular component of the prosthesis and measuring its intersecting angle with a line tangenting the two ischial tuberosities. In this example it is 29°, less than the desired 45°

of migration of the stem through the cortex (Fig. 12.9). The femoral component should be positioned symmetrically within the acetabular component. A line from the prosthetic femoral head to Kohler line (ilioischial line) or from the medial wall of the acetabular component to the ilioischial line should be used to assess for acetabular protrusion (Fig. 12.30).

Normal Postoperative Changes

Several postoperative changes may occur that are considered normal postoperative findings and should not be confused with pathology. These include cortical hypertrophy especially distally; partial and complete pedestal at the tip of the femoral prosthesis (Fig. 12.24); non-progressive smooth radiolucent lines of less than 2 mm thickness (Fig. 12.25); and subsidence of less than 2 mm. Spot welds are sclerotic lines at the sintered femoral component from new bone ingrowth (Fig. 12.1).

Cement herniation may occur through small defects in the medial wall of the acetabulum (Fig. 12.26). They are mostly asymptomatic, but rare complications may include neurovascular encasement, bladder burn, and bowel fistulas. Cement herniation from the femoral component is much less common and raises the suspicion for fracture especially intraoperative fractures.

Knees

Fluoroscopically assisted visualization of knee prostheses is the preferred method of evaluating the postoperative knee, as the joint spaces and prosthetic components are better profiled. Otherwise, standing full-length AP, standing AP, and lateral and patellar (Merchant) views are obtained.

The tibial tray should cover at least 85% of the tibial articular surface and preferably be flush with and mirror the size of the native plateau (Fig. 12.27a), although some newer designs have a smaller tibial tray with the polyethylene liner covering the native plateau. Slight displacement of the tray laterally with a mild lateral overhang is acceptable, but medial displacement away from the articular surface should be avoided as there is the risk of irritation of and resulting pes anserine bursitis. The tibial tray should be 90° to the long axis of the tibia on the AP and lateral films (Fig. 12.27b, c).

The femoral component should be in valgus (97–98°) to the long axis of the femoral shaft on the AP film. The femoral–tibial carrying angle should be anatomical (5–8° of valgus). On the lateral film, the femoral component should be 90° to the femoral shaft (Fig. 12.27d). Again, the condylar component should mirror the size of the native femoral condyles, and the anterior aspect should sit flush against and be parallel to the anterior cortex of the distal femur. If the condylar component is too large, there may be limitation of prosthetic movement, whereas an undersized condylar component may lead to instability and notching of the anterior femoral cortex. This last may predispose to fracture (Fig. 12.28).

The patellar component should be centered between the condyles of the femoral components without significant tilt (Fig. 12.29). The height of the polyethylene component of the patellar resurfacing should be the same as the distance from the native tibial plateau to the patella, i.e., the approximate length of the patella tendon. To avoid risk of increased wear, the thickness of the patella/polyethylene component should not exceed the total thickness of the native patella.

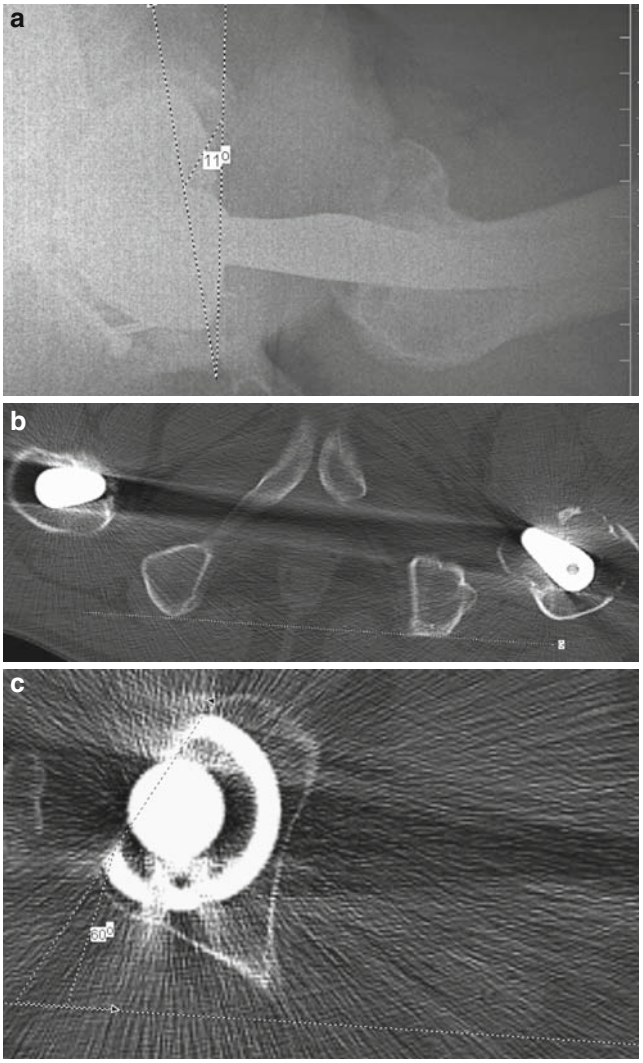

Fig. 12.22 (**a**) Lateral radiograph of a hip with a total hip arthroplasty. The acetabular cup shows 11° of anteversion (normal ≈15°). Note the posterior position of the femoral head. This may be the result of liner wear or dislocation. (**b**) Anterversion measured using CT. A *line* (**A**) is drawn through the ischial tuberosities. (**c**) The *line* through the ischial tuberosities is propagated superiorly to the level of the prosthesis, and the degree of anteversion of the cup is measured (30°)

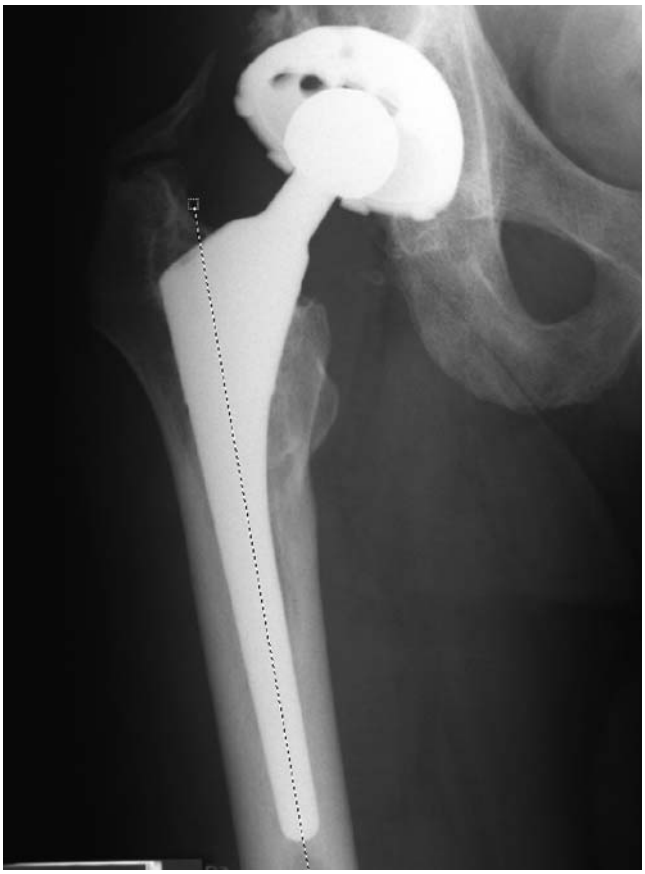

Fig. 12.23 AP radiograph of the right hip. Long axis of the femoral stem should be along the long axis of the femur as in this example or in slight valgus

Shoulders

Typically, routine postoperative shoulder evaluation includes AP internal and external rotation views and a transcapular "Y" or axillary view. It is important to assess for the risk for postoperative impingement. This is done by drawing a horizontal line tangenting the superior aspect of the greater tuberosity on the AP external rotation film (A), and another tangenting the superior aspect of the humeral component of the prosthesis (B). If B lies inferior to A, there is a risk of impingement. This may be the result of poor operative positioning or postoperative subsidence (Fig. 12.16).

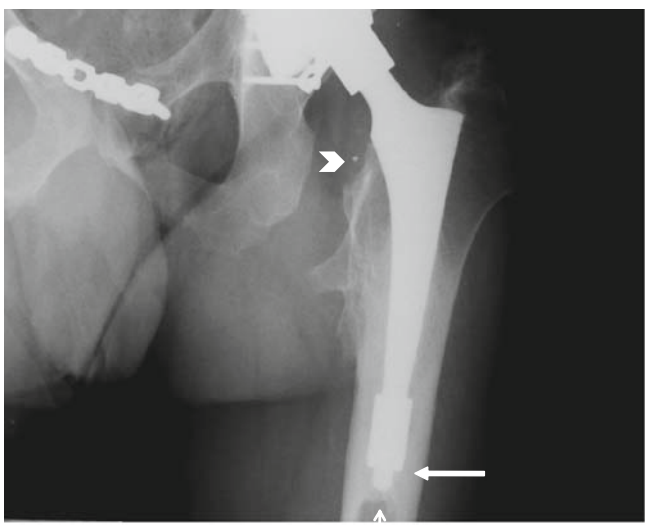

Fig. 12.24 AP radiograph of a left hip non-cemented arthroplasty showing cortical hypertrophy (*long arrow*) and pedestal formation at tip (*short arrow*). Note bead shedding (*arrowhead*)

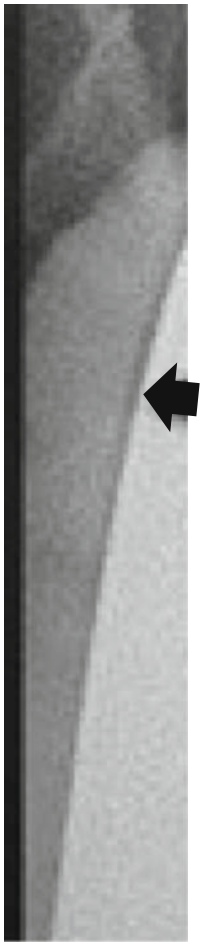

Fig. 12.25 Magnification view shows the normal thin radiolucent line at cement–prostheses interface (black arrow). It should measure less than 2 mm

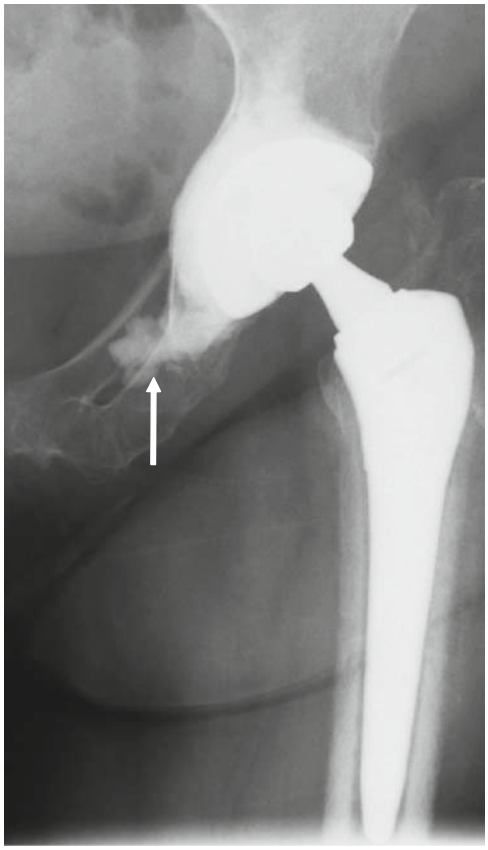

Fig. 12.26 AP radiograph of the hip showing cement extrusion (*arrow*) from the cemented acetabular component. This is typically asymptomatic

Complications

Complications can be divided into general complications and complications that are specific to a particular joint prosthesis. Complications can also be divided into early or late complications. Early complications can be further divided into medical problems related to the patient's immediate postoperative course and immediate hardware complications. Discussion in this section will be mainly confined to hardware complications. Some complications seem to occur more frequently in patients undergoing revision arthroplasty, e.g., wound infection and neurovascular injury.

General Complications

Perioperative complications include infection, hemorrhage and wound breakdown, intraoperative fractures, anesthetic problems, and renal, cardiovascular, pulmonary (especially deep venous thrombosis and pulmonary embolism) electrolyte, and other medical problems.

Deep venous thrombosis (DVT) is a major risk and may lead to pulmonary embolism. Asymptomatic deep vein thrombosis has been reported in up to 50% of patients who receive total knee arthroplasty. Postoperative ultrasonography or venography can diagnose DVT.

Precautions including early mobilization, thromboembolic disease stockings, foot pumps, and perioperative anticoagulation are essential. Low molecular weight heparin (LMWH) is the drug of choice for prophylaxis. Warfarin (Coumadin) 10 mg the night prior to surgery, followed by a daily dose that maintains the international normalized ratio (INR) at 1.5–2 for 8 weeks, is also satisfactory.

Postoperative infection is uncommon, and the incidence of infection is significantly reduced with the use of perioperative antibiotics. Neurovascular injury is also uncommon. The risk of vascular injury is increased with prolonged tourniquet time. In addition, transient nerve paralysis and rarely permanent paralysis appears to be at least in part due to prolonged tourniquet time.

Complications Specific to Arthroplasties

This section will discuss complications specific to arthroplasties and will be of a general nature as typically the etiology

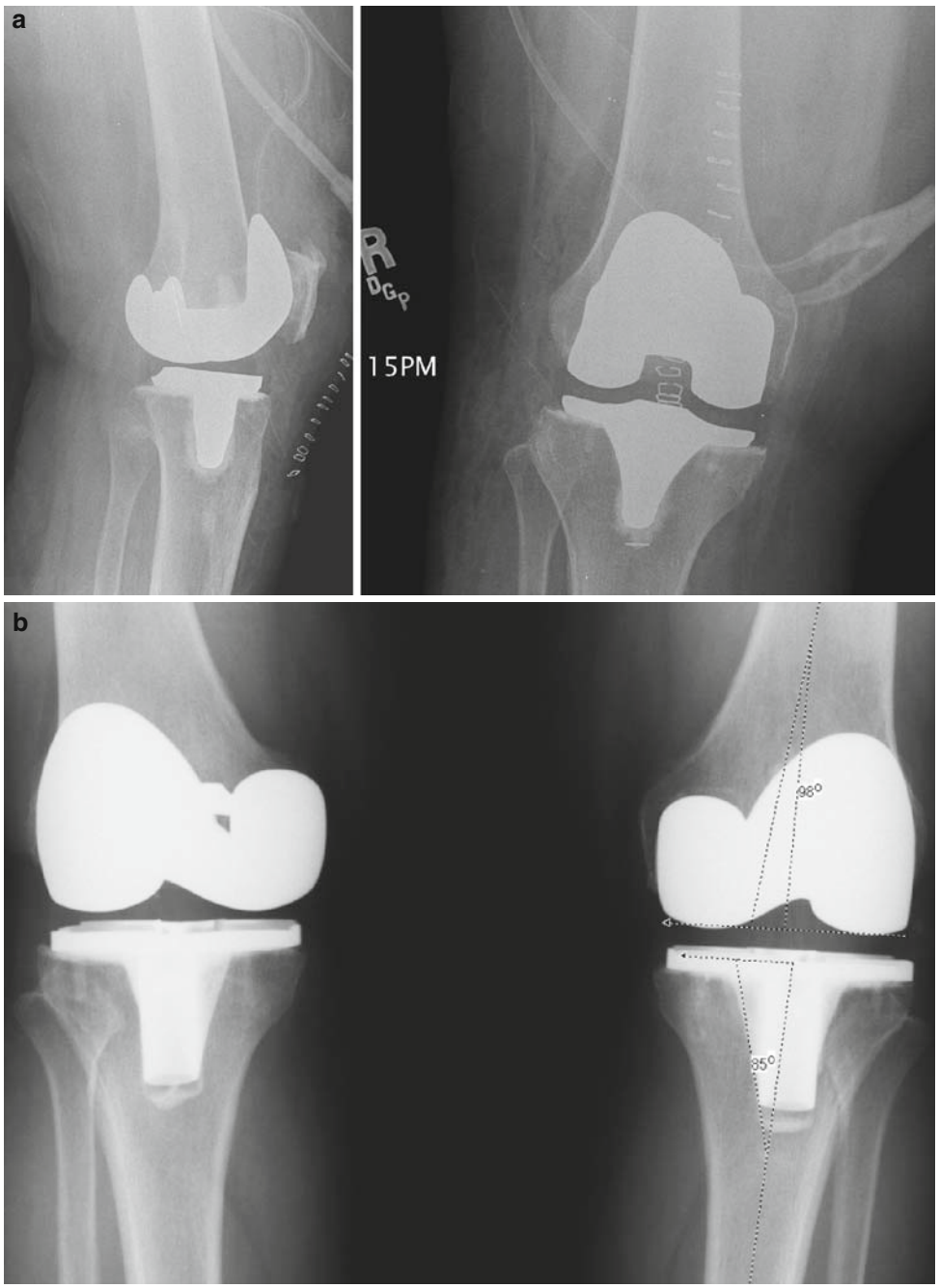

Fig. 12.27 (**a**) Lateral and AP radiographs show undersized tibial component. AP radiograph of the knees (**b**) showing normal positioning of the femoral condyle on the AP film (98°), with mild varus positioning of the left tibial tray (85°). The right prosthesis is also in slight varus, but less than the left. AP radiograph of the knees (**c**) showing excess varus positioning of both tibial trays, *left* greater than *right*. As desired, the tibial trays are flush with the native plateaus. Lateral radiograph of the knee (**d**) shows that the positions of tibial tray and femoral component are acceptable at 88° to the long axis of the tibia and 93° to the long axis of the femur, respectively. Both should be ≈ 90°

and radiographic appearance is the same for most joints. When necessary, reference is made to specific joints to highlight a particular point.

Most of the follow-up imaging of prostheses is with diagnostic radiographs. CT is mainly used to evaluate for occult fractures, assess the severity of fractures, and assess for loosening and particle disease. Nuclear medicine studies are extremely useful, especially a Tc-99^{m} MDP study combined with Indium-labeled WBC and Technetium-99^{m} sulfur colloid to differentiate between aseptic and infective prosthetic loosening. MRI is limited in the evaluation of prostheses, because of the extensive magnetic susceptibility artifact associated with metal.

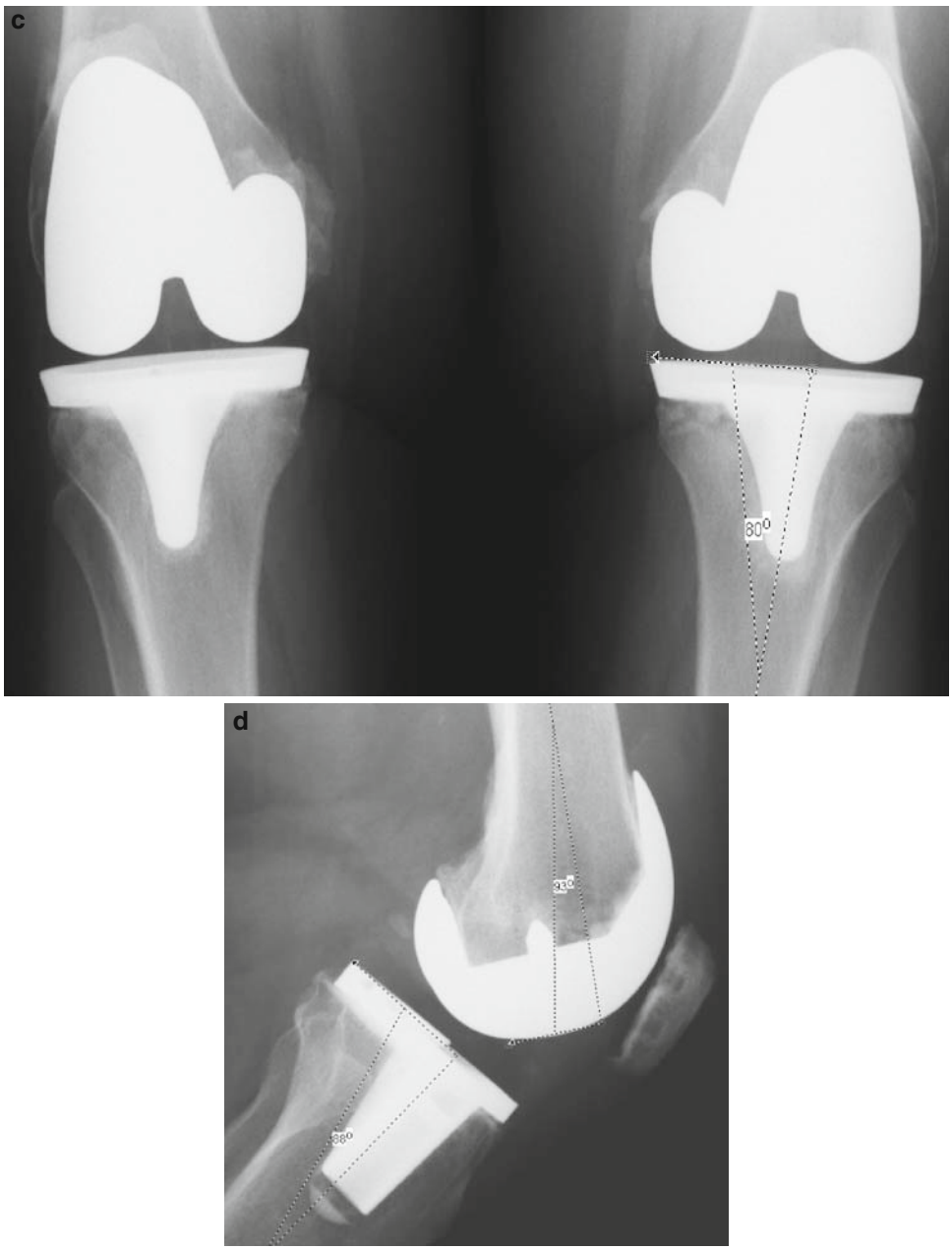

Fig. 12.27 (Continued)

Prosthetic Complications

Prosthetic may develop multiple complications, and, once again, these can be subdivided into early and delayed types.

Early Prosthetic Complications

Immediate complications include fractures (usually of the bone, but uncommonly of the prostheses or surrounding cement) and dislocation of the prostheses. Other local postoperative complications such as hematoma are not specific to arthroplasties.

Fractures

Bone fractures usually occur in osteoporotic patients, and these typically occur at the tip of the stem where load transfers from the prosthesis to the native bone (Fig. 12.9). Fractures are more common in revision procedures, likely because bone stock is decreased in these patients and removal of the old prosthesis may require large amounts of force.

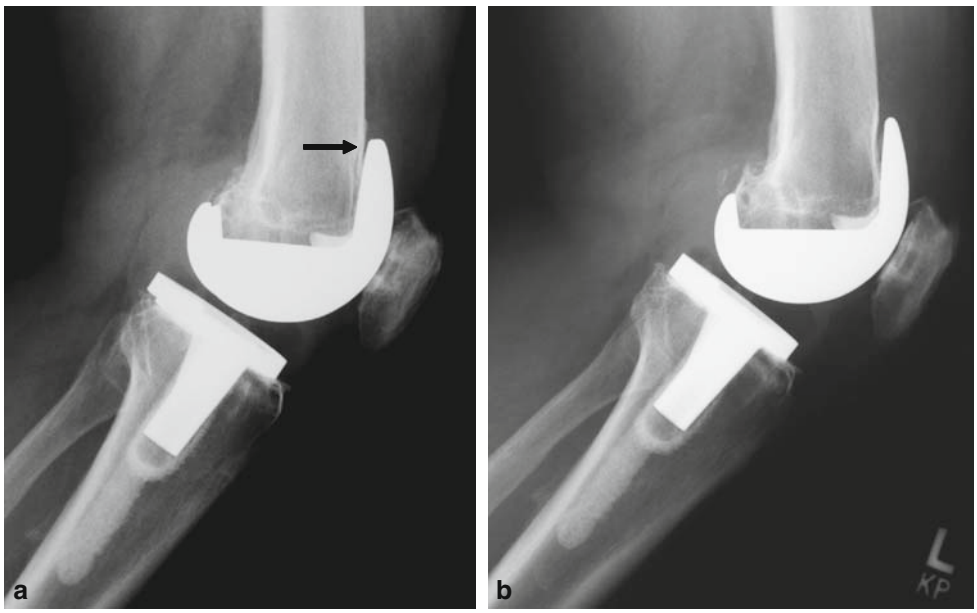

Fig. 12.28 Lateral radiographs of the knee in the same patient (**a**) and (**b**) 6 months apart showing gradual remodeling of the anterior femoral cortex from an undersized femoral component

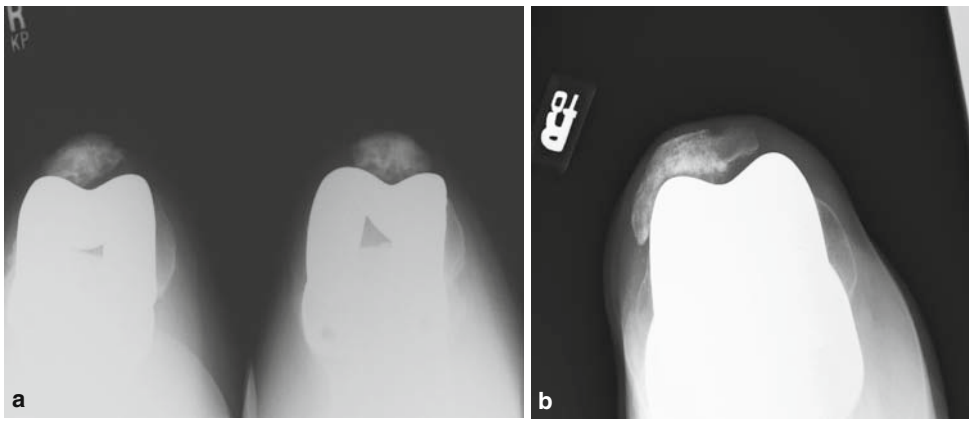

Fig. 12.29 Merchant views of the patellae in two patients (**a** & **b**) showing normal centering of the *left* patella resurfacing with tilt of the *right*. This leads to eventual remodeling of the patella with loosening and subluxation of the component as has occurred in the patient in (**b**)

Fractures of the prosthesis and cement rarely occur early after prosthesis placement, but instead tend to occur later from repetitive stress.

Dislocation or Subluxation

Dislocation or subluxation of prostheses may occur in the immediate postoperative period, or as a delayed complication. These complications occur in up to 3% of patients as an early complication (Figs. 12.30 and 12.34). The major factors predisposing to dislocation/subluxation include poor muscle tone and trauma. The use of a posterior approach in hip replacement has a higher incidence of dislocation as compared to the lateral approach. Dislocation may be related to difficulty in positioning prosthetic components. For example, in the hip, difficulty in aligning the acetabular component in patients with hip dysplasia or in severe osteoarthritis predisposes to dislocation.

In the hips, most dislocations are posterior, superior, and lateral. Radiographically, the dislocated prostheses lie superolateral to the acetabular component, and the femur is adducted (Fig. 12.30). Anterior dislocation, where the prosthetic femoral head lies anterior, inferior, and medial and the femur is abducted, is much less common.

Retained Surgical Material

While uncommon, surgical material including needles, gauze, other orthopedic hardware such as forceps and cutters can be left behind (Fig. 12.31). Close attention to the postoperative radiographs should be made to exclude retained devices. It is imperative that an intraoperative radiograph be taken when needles, gauze, or other hardwares are not accounted for in the final intraoperative count. This has medicolegal implications.

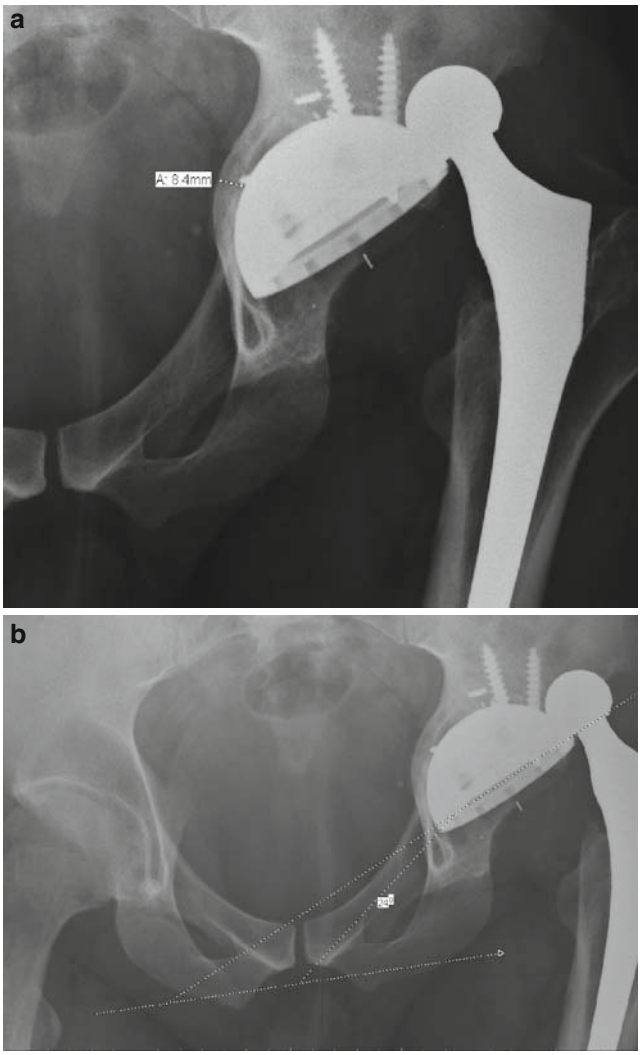

Fig. 12.30 AP hip radiograph (**a**) shows superolateral dislocation of the femoral component. Also note the acetabuli protusio. (**b**) This patient had a reduced angle of inclination of the acetabular cup (24°). Usually an increased inclination of greater than 55° predisposes to dislocation. In this case the degree of anteversion (not shown) was reduced, and this predisposed the patient to dislocation

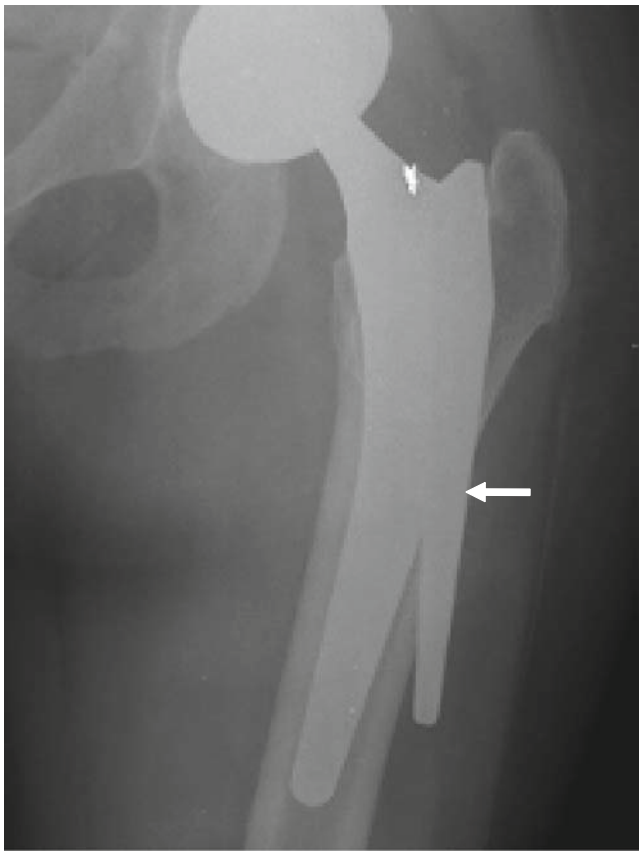

Fig. 12.31 AP radiograph of the hip showing a retained cutter (*arrow*) discovered years after the initial surgery

Delayed Prosthetic Complications

Fractures and Dislocations

Acute bone fractures were described above. Delayed fractures including stress fractures can occur, especially in the osteoporotic patient. As noted above, fractures tend to occur around the tip of the stem (Figs. 12.9 and 12.32). In the knee, there is also an increased risk of fractures in the anterior femoral cortex due to pressure from the tip of the femoral component, especially if it is too small, as it abuts the anterior femoral cortex. Remodeling of the anterior femoral cortex is often seen on the lateral radiograph, and due caution should be taken when assessing this area to make sure there is no cortical penetration or erosion of the cortex (Figs. 12.28 and 12.36a). Bone chips have sometimes been placed between the femoral condylar component and anterior femoral cortex to decrease the risk of fracture through the remodeled cortex. Varus positioning of the femoral stem in a hip prostheses alters the weight-bearing mechanics and increases the risk of loosening or periprosthetic fractures at the tip of the stem (Fig. 12.32).

Stress or insufficiency fractures are a recognized cause of late-onset pelvic pain after a successful hip arthroplasty. The rationale for this is that prior to arthroplasty the patient's condition has led to decreased mobility and disuse osteoporosis. After arthroplasty, the patient's mobility increases, putting increased stress on the osteoporotic bone. This leads to insufficiency fractures, usually in the pubic rami and in the sacrum. These stress fractures are usually readily detected with a radionuclide bone scan or MRI.

Prosthetic component fractures are uncommon now that the metallurgy of prosthetics has improved. Newer alloys, such as chromium–cobalt, titanium-6-aluminum-4-vanadium, and high strength stainless steel, rarely fracture. Metal or other prosthetic component failure, including in temporary devices such as spacers, can still occur with severe

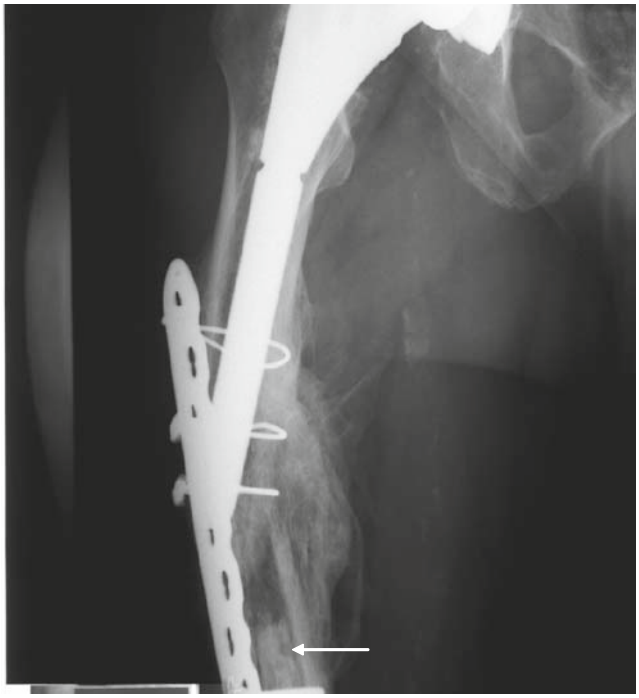

Fig. 12.32 Coned-down AP radiograph of the hip showing a healed fracture at the level of the tip of the femoral stem reduced with a side plate and cerclage wires. The fracture has healed with varus deformity. Note cement fracture (*arrow*)

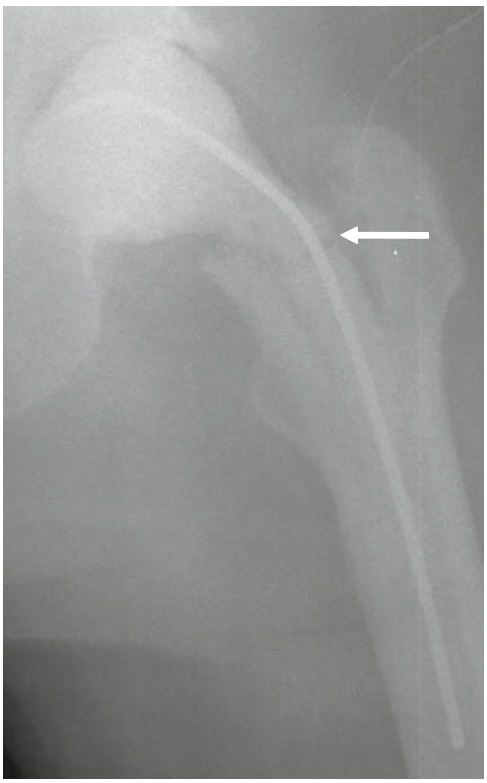

Fig. 12.33 AP radiograph of the left hip. The infected prostheses were removed and an antibiotic impregnated spacer was placed into the cavity while the infection was treated. The spacer is broken (*arrow*)

trauma or a malpositioned device that is subject to abnormal stresses (Fig. 12.33).

Cement fractures or breakage can occur but is uncommon with modern cement techniques. These may occur with shift of the femoral component in a hip prosthesis or after a bone fracture (Fig. 12.32). Transverse fractures of cement near the distal femoral stem arise in up to 1.5% of total hip replacements, usually associated with mild subsidence. If the separation of the cement fracture fragments is less than 4 mm, this is not usually associated with hardware failure and is usually asymptomatic. Fracture of the cement, if it is going to occur, is usually evident by the 6-month postoperative radiographs. This complication is not symptomatic in the majority of cases and tends to occur in patients with good postoperative functional recovery. Slight subsidence of the prosthesis in the fractured cement bed appears to result in a new and final position of stability. A small minority of patients during the first 6 postoperative months may have pain in the thigh as a result of cement fracture.

Prosthetic dislocation can occur as a delayed complication, usually in semi- or non-constrained prostheses where prosthetic stability depends on the integrity of the surrounding soft tissues (Fig. 12.34). If the surrounding muscles, ligaments, and tendons are weak, this predisposes to subluxation and dislocation. Therefore adequate muscle strengthening postoperatively with physical therapy is essential.

Component Loosening

Aseptic loosening is the most common cause for revision of an arthroplasty. It typically occurs more than 2 years after prosthesis placement, but timing is highly variable. Loosening results from mechanical stress at the component interfaces or breakdown of the cement–bone or prostheses–bone interface from migration of wear particles. Therefore, loosening may occur at the cement–bone, prostheses–cement, or prostheses–bone interface depending on whether the prosthesis is cemented or not. It is not uncommon to see periprosthetic or pericemental lucency – from interposition of blood or fibrous tissue, poor cement packing, or movement of the prostheses before the cement has polymerized – on the postoperative radiograph. This is considered normal if it is smooth, less than 2 mm in width, and non-progressive from one study to another. Progression of this lucency by more than 1 mm or irregular lucency is worrisome for loosening (Fig. 12.8).

Migration of a prosthetic component, subsidence, component rotation, or increasing varus orientation in a hip prostheses is also indicative of loosening (Figs. 12.8 and 12.9). Development of 5 mm or more prosthetic subsidence is felt to be highly suggestive of loosening. Typically, subsidence is

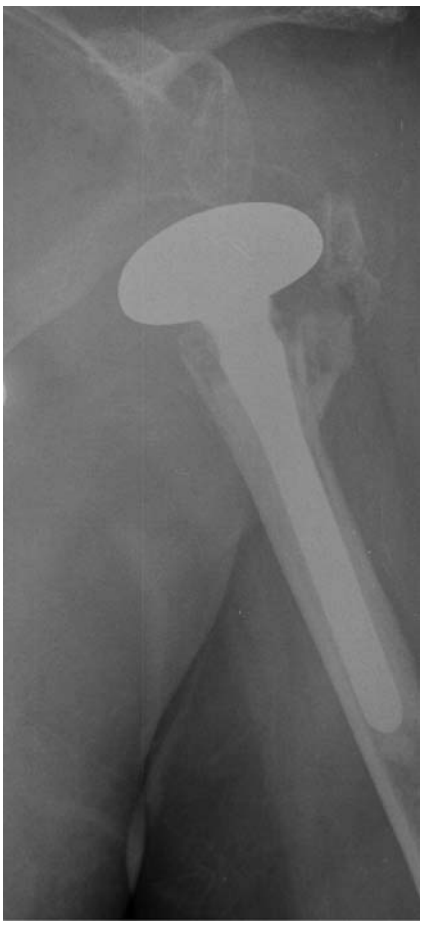

Fig. 12.34 AP radiograph of the left shoulder showing anterior inferior dislocation of the shoulder hemiarthroplasty in the immediate postoperative period

measured from the tip of the greater trochanter to the neck and shoulder of the prostheses. Alternatively, subsidence can be measured from the tip of the greater trochanter to the tip of the femoral stem. Subsidence of the acetabular component is referred to as protusio acetabuli with gradual medial migration of the acetabular cup beyond the ilioischial line (Fig. 12.9). Sequential medial migration can be detected on serial radiographs.

Pedestal formation is development of sclerosis at the tip of the prosthesis and is also suggestive of loosening. It is the motion of the loosened prostheses that stimulates this bone formation (Fig. 12.24). Mild sclerosis (pedestal) at the tip can be normal due to the distribution of the weight-bearing forces, but extensive sclerosis is more significant.

Other signs of loosening include fracture of the cement, although as previously discussed, most cement fractures especially if not separated by more than 4 mm, are asymptomatic and not indicative of loosening. Finally, bead shedding in non-cemented prostheses – fragmentation of the metallic component into tiny beads – is also indicative of loosening (Fig. 12.24).

Infection and Infective Loosening

Infective loosening of prostheses is a serious complication that is reported to occur in up to 4% of patients undergoing total hip arthroplasty. Radiologically, it is important to differentiate infective loosening from aseptic loosening, as clinical management differs. Aseptic loosening is typically managed as a one-step revision procedure. Infective loosening requires a two-step procedure and antimicrobial therapy. Here, the first step is removal of the prostheses and placement of a methylmethacrylate spacer with or without local antibiotics, followed by a revision arthroplasty after the infection has resolved (Fig. 12.33, 12.35). Infection is typically seen within the first 2 years of surgery, but sometimes may occur later if there is a remote site of infection that leads to hematogenous seeding of the prostheses.

Radiologically, distinction between septic and aseptic loosening can be challenging. Several imaging features may help distinguish the two problems. The presence of bone destruction, irregular periprosthetic lucency, and periosteal reaction suggest infective loosening. Lucency that extends completely around the prostheses is also more suggestive of infection while more focal lucency at the prosthetic tip suggests aseptic loosening (Figs. 12.8 and 12.19). Soft tissue swelling and air in the tissues, of course, suggest infection.

Several techniques have been used to help differentiate between septic and aseptic loosening:

(1) Joint aspiration is one technique that definitively diagnoses septic arthritis. Aspiration is usually performed under fluoroscopic guidance with a large gauge needle. If the tap is negative, however, infection is not excluded and capsular or periprosthetic bone biopsy may be attempted to improve the diagnostic yield. Intraoperative frozen section of the periprosthetic bone at the time of revision arthroplasty is reliable. If the bone is positive for infection, a two-stage procedure is performed compared with the one-stage procedure used in aseptic loosening.
(2) Ultrasound is useful to detect joint effusions, soft tissue fluid collections, and in some cases synovial hypertrophy and inflammation (aided by the use of color and power Doppler). The more advantageous use of ultrasound, however, is to guide intervention such as joint aspiration.
(3) Nuclear medicine studies are extremely useful in the evaluation prosthetic complications. A radionuclide bone scan using Technetium 99^{m} MDP is sensitive for detecting both infection or aseptic loosening, as both will show increased uptake on delayed images, but it is nonspecific since it cannot differentiate between the two diagnoses. Focal uptake at the tip of the prostheses is a

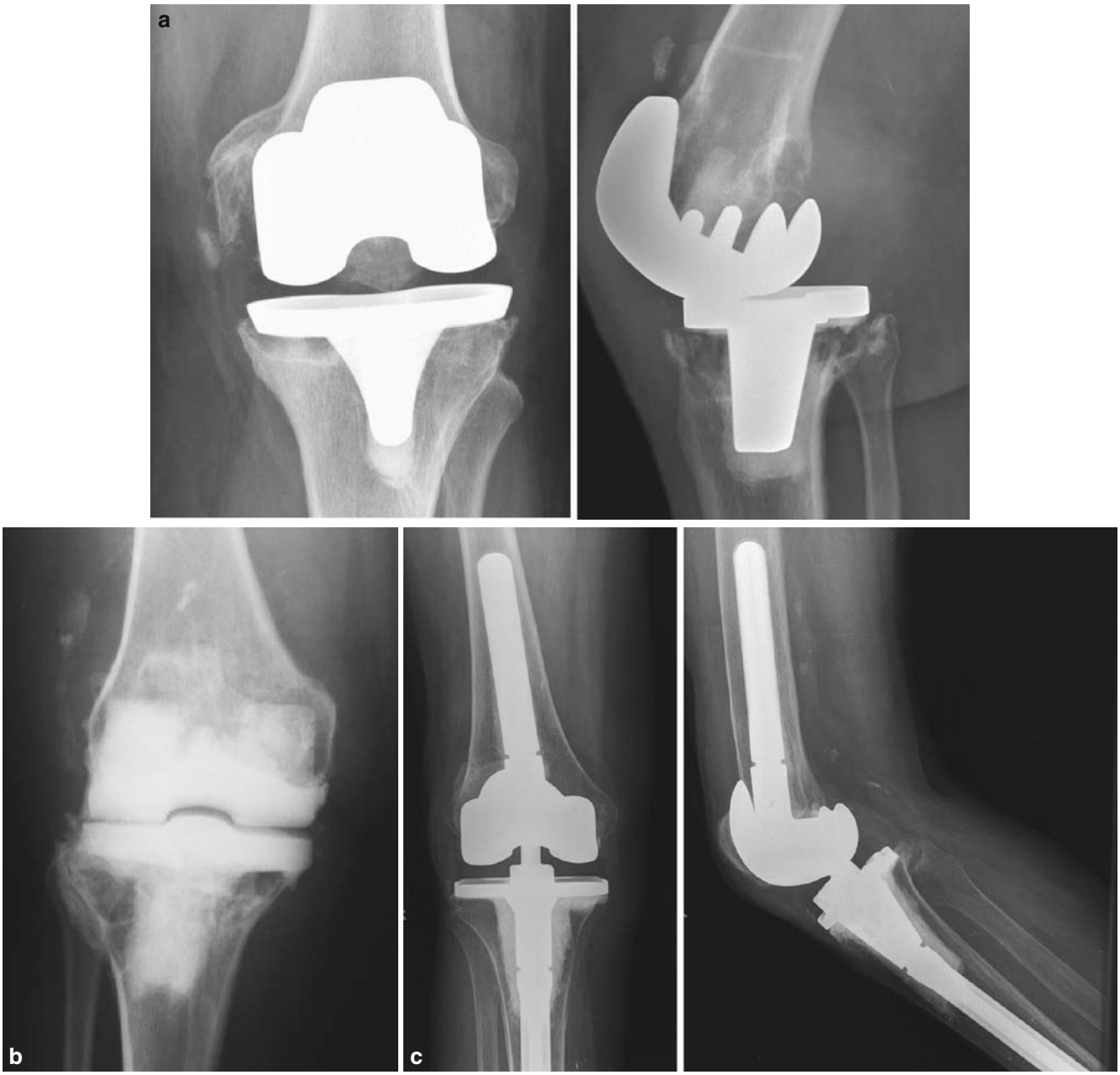

Fig. 12.35 AP and lateral radiographs of the left knee (**a**) showing marked periprosthetic lucency around the femoral component and tibial tray consistent with infective loosening. There is mild posterior subluxation of the tibia on the lateral radiograph. AP radiograph of the right knee (**b**). An infected prosthesis was removed and an antibiotic methacrylate spacer was placed while the infection was treated. AP and lateral radiographs of a right knee (**c**) showing subsequent placement of a long-stemmed revision arthroplasty after an infection was treated

sign of loosening in a cemented prosthesis but less reliable in uncemented prostheses. The blood pool images may also show increased activity in both loosening and infection. It should be noted that the bone scan usually shows increased activity around the prosthesis for 6–12 months after surgery, and sometimes for up to 2 years because of continued postoperative reparative osteoblastic activity. Interpretation, therefore, can be problematic. A negative bone scan excludes both loosening and infection.

Additional agents have been used to increase the diagnostic specificity of bone scans. Bone scan combined with Indium-111-labeled white blood cells has a low sensitivity and specificity, but both are increased when a Tc-99^{m} sulfur colloid marrow scan is done in addition to eliminate the effect of uptake of normal marrow white blood cells. Marrow reconversion normally occurs at the tip of prostheses and becomes more prominent in loose prostheses. Not only infected marrow but also this reconverted marrow has a large number of white

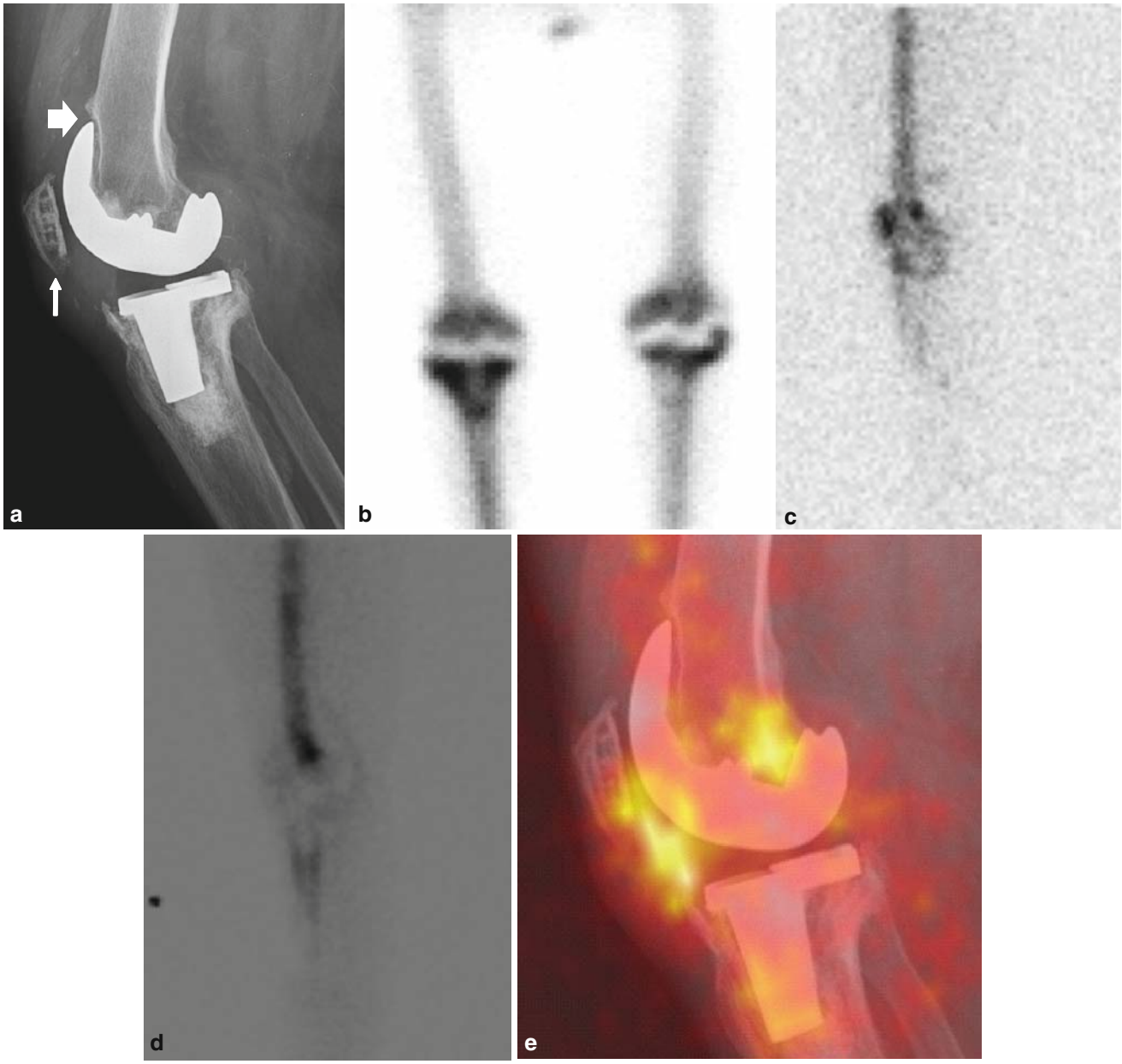

Fig. 12.36 Lateral radiograph of the knee. (**a**) Lateral view showing periprosthetic lucency around the tibial component with mild fragmentation of the lower pole patella (*arrow*). Note the deep anterior femoral notch from undersized femoral component (*large arrow*). Tc-99m MDP images (**b**) from the same patient showing uptake around the tibial and to a lesser extent the femoral components of the right knee prostheses. SPECT images (not shown) also showed uptake at the patella. Lateral image (**c**) from an In-111-labeled WBC study shows focal uptake of white blood cells anteriorly and posteriorly. A lateral image from a sulfur colloid scan (**d**) shows intense focal activity posteriorly that is consistent with marrow conversion. No anterior focus of uptake is visible on the sulfur colloid scan. This suggests that the anterior focus on the In111 WBC scan is caused by infection. Fused PET image with a lateral plain radiograph (**e**) shows that the uptake of In-111 WBC anteriorly corresponds to the mildly fragmented lower pole patella and soft tissues inferior to the patella. This is consistent with an infected patellar component and osteomyelitis of the patella

blood cells that will be apparent on an Indium scan. On the other hand, reconverted marrow will accumulate sulfur colloid but infection will not. So the accumulation of indium-labeled white cells and sulfur colloid will be seen in marrow reconversion, but septic loosening will show only uptake of indium-labeled WBC (Figs. 12.36 and 12.37). These studies are time-consuming, however, and involve multiple steps.

Gallium scanning is also sensitive but again nonspecific as there may be uptake in other aseptic inflammatory

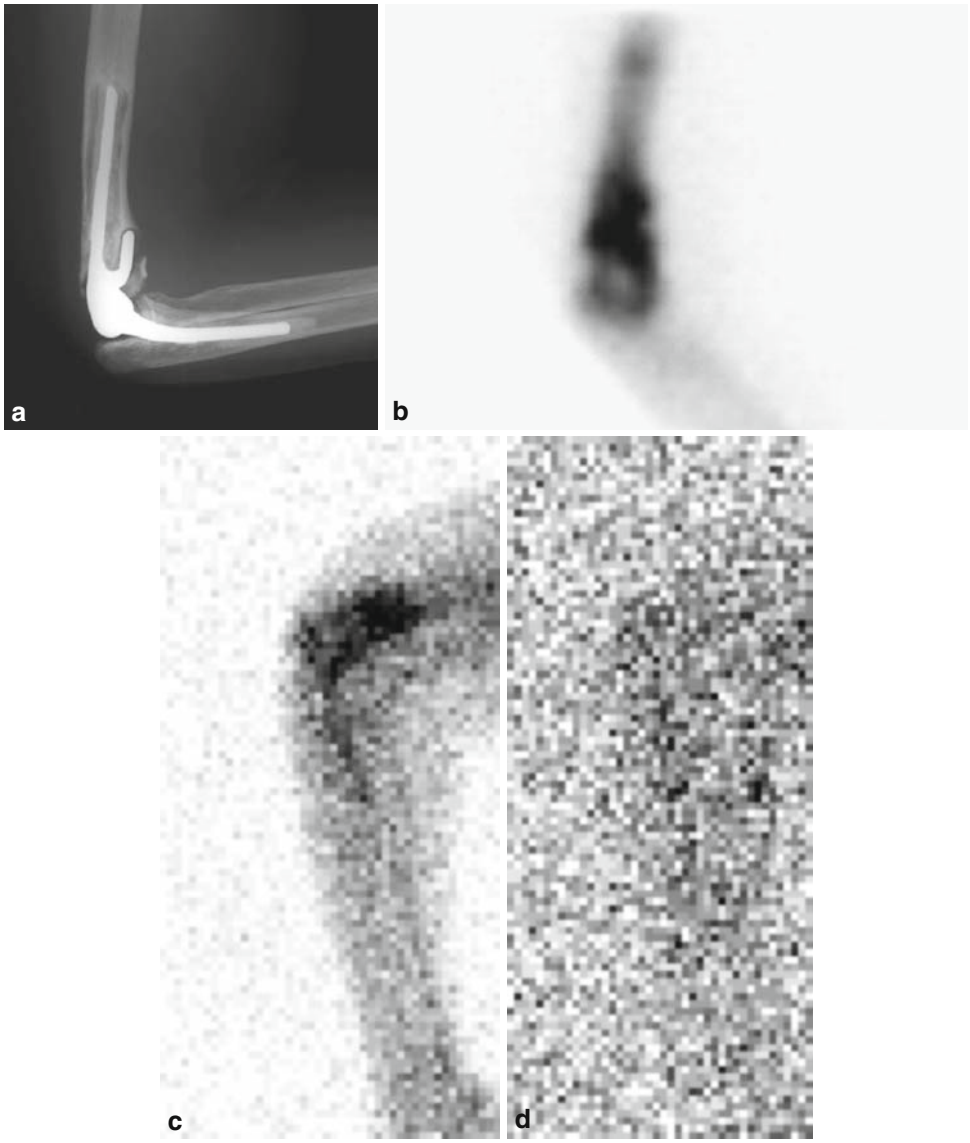

Fig. 12.37 Lateral elbow radiograph (**a**) shows extensive lucency around the humeral component. A Tc-99m MDP bone scan (**b**) shows focal uptake around the humeral component. This could be either from aseptic or septic loosening of the prosthesis. A sulfur colloid scan (**c**) shows diffuse uptake around the humeral component that could represent either marrow reconversion or infection. The In111 WBC scan (**d**) shows no abnormal activity. Thus, these findings are consistent with aseptic loosening

conditions. Anti-granulocyte scintigraphy with $TC99^{m}$-labeled monoclonal antibodies has been shown to be effective in discriminating prosthetic infection after total joint arthroplasty with a reported sensitivity of 83% and specificity of 80%.

F18-fluorodeoxyglucose PET scans have been reported to be effective in differentiating infection from aseptic loosening. Infection shows more intense uptake compared with aseptic loosening. Recent studies have concluded that PET offers no benefit over standard three-phase bone scans.

(4) Arthrography has been used to diagnose periprosthetic loosening. Joint aspiration for bacterial culture to exclude infection should be performed during the procedure prior to injection of contrast into the prosthetic pseudo-joint. Accumulation of contrast material into the periprosthetic lucency suggests either loosening or infection. Contrast accumulation around the acetabular component is nonspecific.

Particle Disease

Particle disease is a form of osteolysis that is caused by the host response to the release of liner and other wear particles into the joint space. Macrophages in the pseudo-joint space ingest these wear particles and fuse together to form foreign body giant cells. These giant cells in turn release cytokines such as prostaglandins and interleukins that recruit cells to differentiate cells into osteoclasts, leading to lytic areas around the prosthesis. The higher the wear particle load, the greater the intensity of the host response. Particle size is important. Particles between 0.2 and 7 μm in diameter

appear to stimulate the greatest macrophage response. Histologically, the lytic lesions are filled with inflammatory and fibrous tissue.

Particle disease occurs most commonly in hip prostheses but it also occurs in other joints. Symptoms and outcome depend on the severity of the disease process. Mild disease is asymptomatic and clinically inconsequential, but more severe reaction may result in loosening of the prostheses, requiring revision arthroplasty.

Radiologically, particle disease appears as multiple well-defined lytic lesions with or without a sclerotic rim on one or both sides of a prosthesis (Figs. 12.6, 12.26, 12.38). On CT scan these lytic lesions most often can be seen to communicate with the joint (Fig. 12.38d). On MRI, the lytic lesions which are mainly inflammatory and fibrous tissue appear isointense to skeletal muscle on T1- and T2-weighted image sequences. Contrast causes mild enhancement at the margins of the lytic areas. These signal characteristics help differentiate particle disease from infection which is typically hyperintense on T2-weighted images.

Pseudobursae

Pseudobursae occur in up to 43% of total hip replacements where they are particularly common. Typically, these bursae arise around the greater and lesser trochanters and also at the lateral acetabular margin. These are not true bursae and so they communicate with the prosthetic pseudo-joint of hip. Thus, arthrography will confirm their presence.

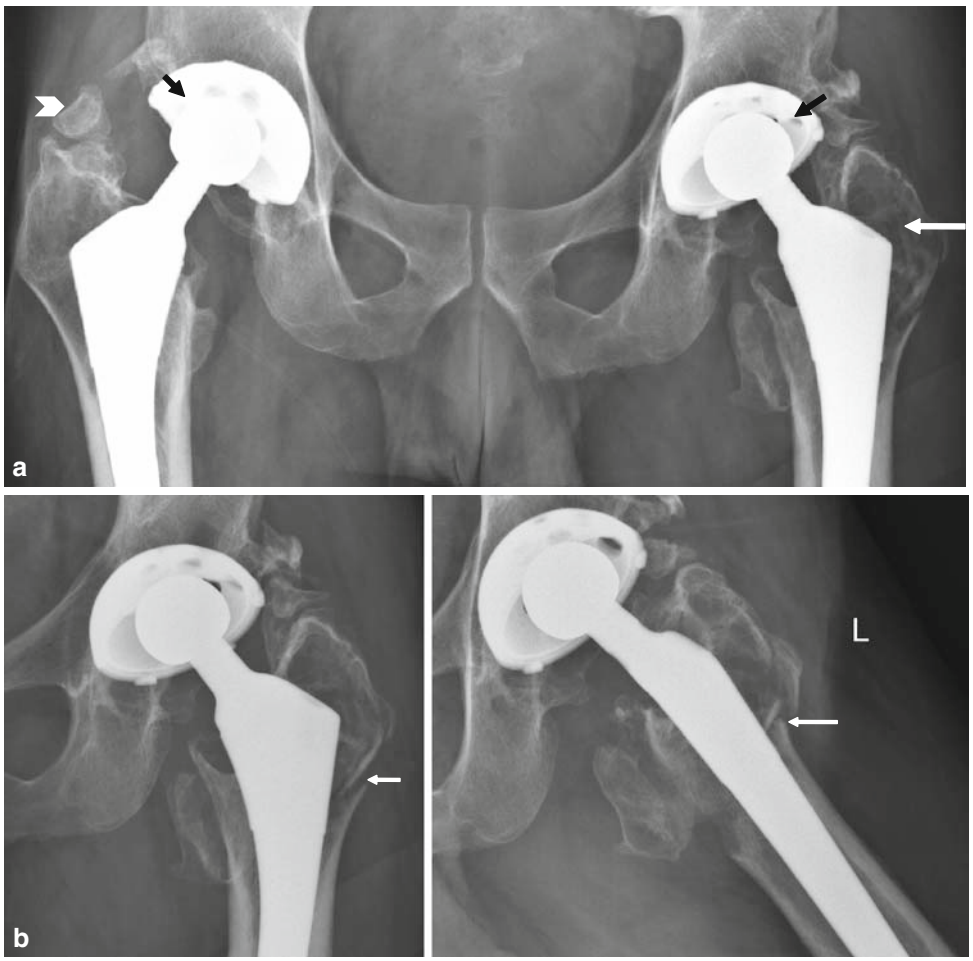

Fig. 12.38 AP pelvic radiograph (**a**) showing bilateral liner wear (*short arrows*), particle disease (*long arrow*), and heterotopic bone (*arrowhead*). AP and frog lateral radiographs in the same patient (**b**) show extensive lucency around the acetabular and femoral components of the prosthesis, consistent with particle disease, and a pathological intertrochanteric fracture (*arrows*). Coronal reformatted CT image (**c**) shows bilateral polyethylene liner wear with narrowing of the superior lateral liner. The periprosthetic lytic areas are consistent with particle disease. Axial CT scan (**d**) shows particle disease with well-defined lytic lesions communicating into the hip joint (*arrowhead*). The *small arrow* shows volume averaging of the margin of the acetabular component

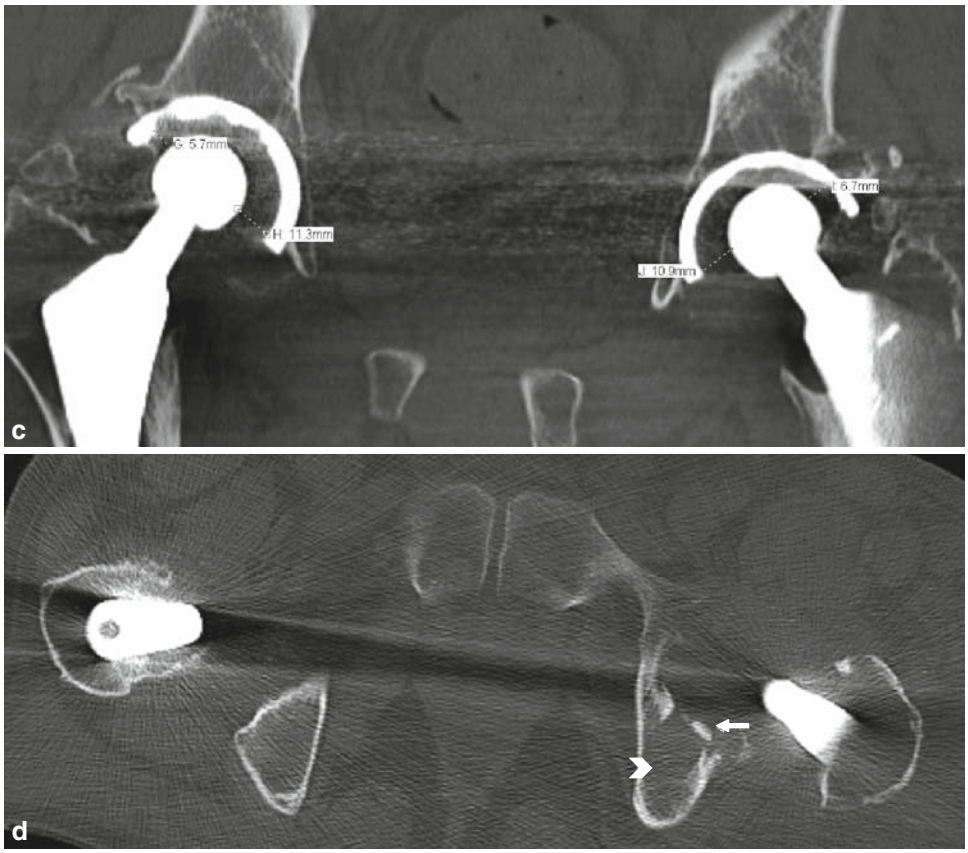

Fig. 12.38 (Continued)

Heterotopic Bone Formation

Heterotopic ossification (HO) around a prosthesis is a common complication after an arthroplasty procedure. HO occurs in up to 50% of patients with total hip replacements, but can occur around any prosthetic joint. One-third of these patients who develop heterotopic bone will be symptomatic.

Radiologically the onset of heterotopic bone is variable but occurs anywhere from 2 to 8 weeks postoperatively. It is much more common in men, patients with a history of diffuse idiopathic skeletal hyperostosis (DISH) (Fig. 12.39), ankylosing spondylitis, and post-traumatic arthritis. A history of prior heterotopic bone formation also increases the risk.

The pathophysiology of heterotopic bone is not clearly defined. The proposed etiology is that bone morphologic

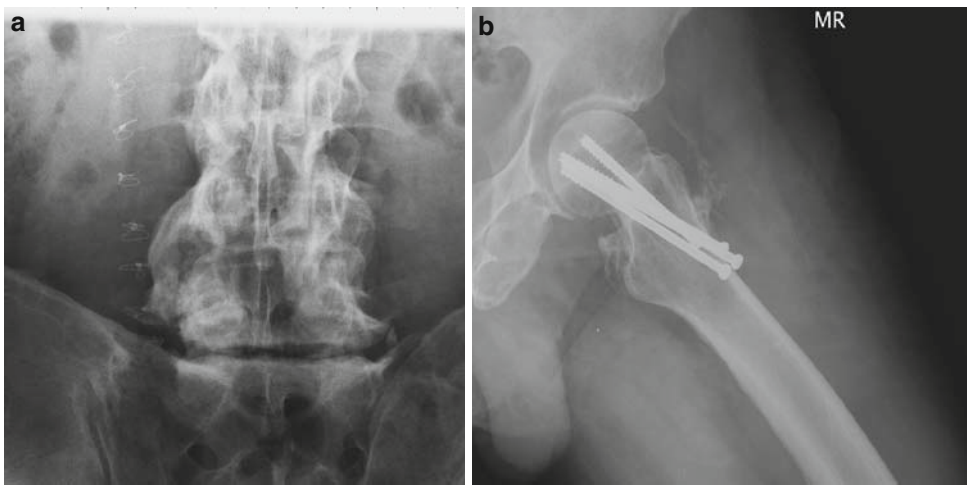

Fig. 12.39 AP lower lumbar spine radiograph (**a**) shows changes of DISH. Frogs leg lateral radiograph of the hip (**b**) shows Brooker II heterotopic ossification. Patients with DISH are more prone to develop heterotopic ossification

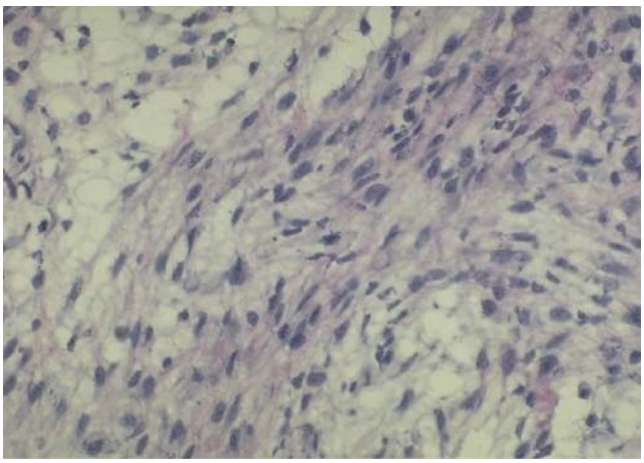

Fig. 12.40 Hypercellular central portion with active mitosis in this patient with heterotopic ossification may be mistaken by even the experienced pathologist for a sarcoma. Clinical correlation and sequential imaging are important

protein (BMP) induces mesenchymal precursor cells to differentiate into cartilage and bone-forming cells. A role for prostaglandin E in the development of HO has been shown as well. Hence, anti-prostaglandins such as indomethacin have been used for both prevention and therapy of HO. Radiotherapy using external beam radiation, 700 rads in one dose or 1000 rads in four divided doses, has been used to treat HO. Some surgeons use prophylactic perioperative radiation 700–800 rads within 48–72 h of the procedure. Surgical removal, if attempted, should be delayed until at least 6 months after onset of HO formation to allow the bone to mature. Otherwise, the risk of recurrence is high.

Clinically, patients with HO present with a painful palpable mass that gradually becomes nontender, smaller, and firmer. If the disease progresses, patients may develop limitation of motion in the involved joint. It should be noted that even after biopsy, the marked cellularity and new bone formation seen in these lesions may mislead even experienced bone pathologists to misdiagnose HO as an osteogenic sarcoma (Fig. 12.40). Since biopsy may also exacerbate the heterotopic bone formation process, biopsy should be avoided.

HO is easily seen on radiographs and CT. As heterotopic bone is starting to form, MRI shows a heterogeneously increased T2 signal with mass effect and surrounding soft tissue edema that can simulate a neoplastic process. These areas often show early intense heterogeneous uptake of intravenous gadolinium. Over weeks to months, these lesions take on MR characteristics compatible with mature bone.

Three-phase bone scan using technetium 99^{m} methylene diphosphonate is useful in diagnosing early heterotopic bone formation. Scans may be positive 2–4 weeks before mineralization is detected by plain radiographs. In early stages of HO, the dynamic (angiographic) and blood pool phases show radiopharmaceutical activity. The delayed phase of the bone scan typically shows activity after 7–10 days. When present and in the appropriate clinical setting, delayed phase uptake can be diagnostic (Fig. 12.41).

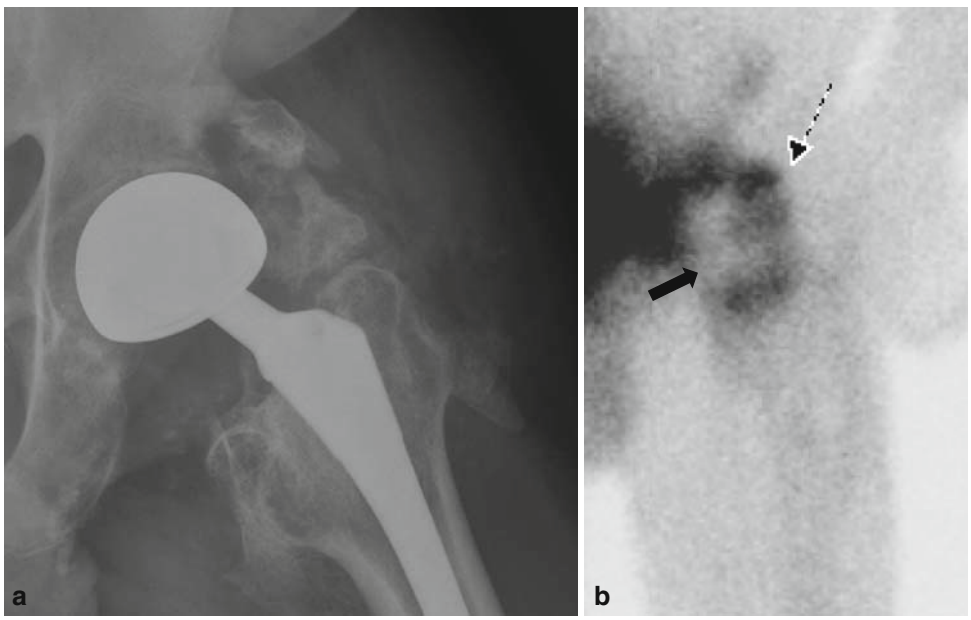

Fig. 12.41 (**a**) Extensive left heterotopic ossification (Brooker III). (**b**) Uptake of Tc-99m MDP by the heterotopic ossification (*dotted arrow*). Note the photopenic prosthesis medially (*thick arrow*)

Suggested Reading

1. Berquist TH. Imaging of joint replacement procedures. Radiol Clin North Am 2006; 44: 419–437
2. Marmery H, Ostlere S. Imaging of prosthetic joints. Imaging, September 1, 2007; 19(3): 299–309
3. Keogh CF, Munk PL, Gee R, Chan LP, Marchinkow LO. Imaging of the painful hip arthroplasty. Am J Roentgenol, January 1, 2003; 180: 115–120
4. Frick MA, Collins MS, Adkins MC. Postoperative imaging of the knee. Radiol Clin N Am 2006; 44: 367–389
5. Eustace S, Shah B, Mason M. Imaging orthopedic hardware with an emphasis on hip prostheses. Orthopedic Clin N Am January 1, 1998; 29(1): 67–84
6. Steinberg DR, Steinberg ME et al. The early history of arthroplasty in the United States. Clin Ortho Relat Res, May 2000; 374: 55–89
7. White SP, Blom AW, Lee M, Smith EJ. The crescent sign: dissociation of the polyethylene liner from a modular acetabular component in total hip arthroplasty. Skeletal Radiol 2005; 34: 620–624
8. Taljanovic MS, Jones MD, Hunter TB, Benjamin JB, et al. Joint arthroplasties and prostheses. RadioGraphics 2003; 23: 1295–1314
9. White LM, Kim JK, Mehta M, Merchant N, Schweitzer ME, et al. Complications of total hip arthroplasty: MR imaging-initial experience. Radiology 2000; 215: 254–262
10. Ostlere S, Soin S. Imaging of prosthetic joints. Imaging 2003; 15: 270–285.
11. Bestic JM, Peterson JJ, DeOrio JK, Bancroft LW, Berquist TH, Kransdorf MJ. Postoperative evaluation of the total ankle arthroplasty. Am J Roentgenol 2008; 190: 1112–1123
12. Berquist TH. Imaging Atlas of Orthopedic Appliances and Prostheses. New York: Raven Press; 1995
13. Mahomed NN, Barrett J, Katz JN, et al. Epidemiology of total knee replacement in the United States Medicare population. J Bone Joint Surg [Am] 2005; 87–A: 1222–1228
14. Anderson T, Montgomery F, Carlsson A. Uncemented STAR total ankle prostheses. J Bone Joint Surg [Am] 2003; 85–A: 1321–1329
15. Kumar S, Sperling JW, Haidukewych GH, et al. Periprosthetic humeral fractures after shoulder arthroplasty. J Bone Joint Surg [Am] 2004; 86–A: 680–689
16. Miura H, Matuda S, Mawatari T, et al. The oblique posterior femoral condylar radiographic view following total knee arthroplasty. J Bone Joint Surg [Am] 2004; 86–A: 47–51
17. Berger RA, Meneghini M, Jacobs JJ, et al. Results of unicompartmental knee arthroplasty at a minimum of ten years follow up. J Bone Joint Surg [Am] 2005; 87–A: 999–1006
18. Berquist TH, Bender CE, Maus TP, et al. Pseudobursae: a useful finding in patients with painful hip arthroplasty. Am J Roentgenol 1987; 148: 103–106
19. Morrey BF. Complications of elbow replacement surgery. In: Morrey BF, (ed). The Elbow and Its Disorders, Philadelphia: W.B. Saunders; 2000, pp. 667–77
20. Lyons CW, Berquist TH, Lyons JC, et al. Evaluation of radiographic findings in painful hip arthroplasties. Clin Orthop 1985; 195: 239–251
21. Gruen TA, McNeice GM, Anstutz HC. "Modes of Failure" of cemented stem-type femoral components: a radiographic analysis of loosening. Clin Orthop Related Res 1979; 141: 17–27
22. Madarezo EG, Judson S, Pasternak H. Late infections of total joint prostheses: a review and recommendations for prevention. Clin Orthop 1988; 229: 131–142
23. Harris WH, Schiller AL, Scholler JM, Freiberg RA, Scott R. Extensive localized bone resorption in the femur following total hip replacement. J Bone Joint Surg 1976; 58: 612–618
24. Quinn J, Joyner C, Triffitt JT, Athanasou NA. Polymethylmethacrylate-induced inflammatory macrophages resorb bone. J Bone Joint Surg Br 1992; 74: 652–658
25. Maus TP, Berquist TH, Bender CE, Rand JA. Arthrographic study of painful total hip arthroplasty: refined criteria. Radiology 1987; 162: 721–727
26. Love C, Tomas MB, Marwin SE, Pugliese PV, Palestro CJ. Role of nuclear medicine in diagnosis of the infected joint replacement. RadioGraphics 2001; 21: 1229–1238
27. Rubello D, Borsato N, Chierichetti F, Zanco P, Ferlin G. Three-phase bone scintigraphy pattern of loosening in uncemented hip prostheses. Eur J Nucl Med 1995; 22: 299–301
28. Joh TN, Mujtaba M, Chen AL, et al. Efficacy of combined technetium-99m sulfur colloid/indium-111 leukocyte scans to detect infected total hip and knee arthroplasties. J Arthroplasty 2001; 16: 753–758
29. Larikka MJ, Ahonen AK, Junila JA, et al. Improved method for detecting knee replacement infections based on extended combined 99m Tc-white blood cell/bone imaging. Nucl Med Commun 2001; 22: 1145–1150
30. Zhuang H, Duarte PS, Pourdehnad M, et al. The promising role of 18F-FDG PET in detecting infected lower limb prosthesis implants. J Nucl Med 2001; 42: 44–48
31. Holt GE, Dennis DA. The role of patellar resurfacing in total knee arthroplasty. Clin Orthop 2003; 416: 76–83
32. Berry DJ. Recognizing and identifying osteolysis around total knee arthroplasty. Instr Course Lect 2004; 53: 261–264

33. Goodman S, Lidgren L. Polyethylene wear in knee arthroplasty: a review. Acta Orthop Scand 1992; 63: 358–364
34. Chun KA, Ohashi K, Bennett DL, et al. Patellar fractures after total knee arthroplasty. J Bone Joint Surg [Am] 2002; 84–A: 532–540
35. Tharani R, Nakasone C, Vince KG. Periprosthetic fractures after total knee arthroplasty. J Arthroplasty 2005; 20(2): 27–32
36. Roberts C, Ekelund A, Renfree K, Liu P, Chew F. Radiologic assessment of reverse shoulder arthroplasty. RadioGraphics 2007; 27: 223–235
37. Raphael B, Haims A, Wu J, Katz L, White L, Lynch K. MRI Comparison of periprosthetic structures around zirconium knee prostheses and cobalt chrome prostheses. Am J Roentgenol 2006; 186: 1771–1777
38. von Knoch M, Berry D, Harmsen W, Morrey B. Late dislocation after total hip arthroplasty. J Bone Joint Surg [Am] 2002; 84: 1949–1953
39. Bezwada HP, Nazarian D. Acetabular wear in total hip arthroplasty. eMedicine http://www.emedicine.com/orthoped/TOPIC371.HTM. July 26, 2004
40. Schmalzried TP, Callaghan JJ. Wear in total hip and knee replacements. J Bone Joint Surg [Am] Jan 1999; 81(1): 115–136

Chapter 13

Systematic Approach to Skeletal Dysplasias with Emphasis on Non-lethal Disorders

Akbar Bonakdarpour

Abstract Dysplasias are defects arising during the prenatal stage of development that continue expression in postnatal life and may be primary or secondary. Primary skeletal dysplasias result from mutated genes and are expressed in mesenchymal tissues. Secondary dysplasias result from extraosseous factors causing developmental abnormalities of the skeletal system. As knowledge of clinical medicine, molecular biology, and genetics advance, the number of known skeletal dysplasias has been growing by leaps and bounds. Radiology plays a major role in caring for these patients. This chapter provides an overview of the more common and/or more interesting skeletal dysplasias that a radiologist may encounter in practice, emphasizing the non-lethal disorders. The latest nosology and classification of skeletal dysplasias was introduced in 2006 comprising 37 groups and each group has between 2 and 23 entities. This classification is the basis of our presentation. However, various entities are discussed in alphabetical order to make it easier for the readers to refer to specific disorders. Achondroplasia is the most common non-lethal skeletal dysplasia and the most common lethal entity is thanatophoric dysplasia. *Four categories of helpful hints are described to make learning and remembering skeletal dysplasias easier for the readers.*

Keywords Skeletal dysplasias • Achondroplasia • Achondrogenesis • Asphyxiating thoracic dysplasia • Chondrodysplasia punctata • Chondroectodermal dysplasia • Cleidocranial dysplasia • Craniostenosis • Diaphyseal dysplasia (Progressive) • Diastrophic dysplasia • Dysplasia epiphysealis hemimelica • Enchondromatosis • Endosteal hyperostosis • Fibrodysplasia ossificans progressiva • Fibrous dysplasia • Gaucher disease • Hyperphosphotasia • Hypophosphatasia • Hypophosphatemic rickets • Infantile cortical hyperostosis • Marfan syndrome • Melorrheostosis • Metaphyseal dysplasia • Craniometaphyseal dysplasia • Metaphyseal chondrodysplasia • Metatropic dysplasia • Mucopolysaccharidoses • Mucolipidoses • Multiple epiphyseal dysplasia • Blount disease • Multiple hereditary cartilaginous exostoses • Neurofibromatosis • Pseudarthrosis • Osteogenesis imperfecta • Osteolysis • Osteopathia striata • Osteopetrosis • Osteopoikilosis • Pseudoachondroplasia • Pyknodysostosis • Spondyloepiphyseal dysplasia • Spondyloepimetaphyseal dysplasia • Spondylometaphyseal dysplasia • Thanatophoric dysplasia • Tuberous sclerosis complex

Introduction

General diagnostic radiologists and even most musculoskeletal radiologists rarely encounter bone dysplasias in their practice. Furthermore, as knowledge of clinical medicine, molecular biology, and genetics advance, the number of known skeletal dysplasias has been growing by leaps and bounds. There were more than 243 dysplasias listed in 1997 classification and 372 in 2006 nosology and classification [1] (Tables 13.1and 13.2). This is more than 50% increase in less than a decade. Many of these are extremely rare and as a result, discussion of the diagnostic imaging is not essential for a general musculoskeletal radiology book. *Aegerter and Kirkpatrick, two pioneers in the field of musculoskeletal pathology and radiology, pointed out, "The modern literature is replete with single or one-family case reports of an infinite variety of anomalies which may or may not involve the skeleton* [2]*."* Therefore, only a limited number of selected disorders that in our opinion are of relative importance will be discussed in this chapter.

Although, genetic and molecular studies have increasing importance in the management of these disorders, radiology still plays a major role in caring for these patients. Thus, some familiarity with diagnostic imaging of dysplasias is essential to the practice of general, musculoskeletal, and pediatric radiology. This chapter provides an overview of

A. Bonakdarpour (✉)
Department of Radiology, Temple University School of Medicine, Philadelphia, PA, USA
e-mail: akbarbonakdarpour@yahoo.com

A. Bonakdarpour et al. (eds.), *Diagnostic Imaging of Musculoskeletal Diseases: A Systematic Approach*,
DOI 10.1007/978-1-59745-355-4_13,

Table 13.1 Modified nosology and classification of genetic skeletal disorders 2006 Revision [1][a]

		Name of disorders				
Number and name of groups	Inheritance	MIM	Locus	Gene	Protein	MIM
1. FGFR3 group						
Thanatophoric dysplasia type 1 (TD1)	AD	187600	4p16.3	FGFR3	FGFR3	134934
Thanatophoric dysplasia type 2 (TD2)	AD	187601	4p16.3	FGFR3	FGFR3	134934
Achondroplasia	AD	100800	4p16.3	FGFR3	FGFR3	134934
2. Type 2 collagen group						
Achondrogenesis type 2 (ACG2; Langer-Saldino)	AD	200610	12q13.1	COL2A1	Type 2 collagen	120140
Spondyloepiphyseal dysplasia congenita (SEDC)	AD	183900	12q13.1	COL2A1	Type 2 collagen	120140
Spondyloepimetaphyseal dysplasia (SEMD) Strudwick type	AD	184250	12q13.1	COL2A1	Type 2 collagen	120140
3. Type 11 collagen group						
4. Sulfation disorders group						
Achondrogenesis type 1B (ACG1B)	AR	600972	5q32-33	DTDST	SLC26A2 sulfate transporter	606718
Diastrophic dysplasia (DTD)	AR	222600	5q32-33	DTDST	SLC26A2 sulfate transporter	606718
5. Perlecan group						
6. Filamin group						
Larsen syndrome	AD	150250	3p14.3	FLNB	Filamin B	603381
7. Short-rib dysplasia (with or without polydactyly) group						
Chondroectodermal dysplasia (Ellis-van Creveld)	AR	225500	4p16	EVC1	EvC gene 1	604831
			4p16	EVC2	EvC gene 2	607261
Asphyxiating thoracic dysplasia (ATD; Jeune)	AR	208500				
8. Multiple epiphyseal dysplasia and pseudoachondroplasia group						
Pseudoachondroplasia (PSACH)	AD	177170	19p12-13.1	COMP	COMP	600310
Multiple epiphyseal dysplasia (MED) type 1 (EDM1)	AD	132400	19p13.1	COMP	COMP	600310
Multiple epiphyseal dysplasia (MED) type 2 (EDM2)	AD	600204	1p32.2-33	COL9A2	Collagen 9 alpha-2 chain	120260
Multiple epiphyseal dysplasia (MED) type 3 (EDM3)	AD	600969	20q13.3	COL9A3	Collagen 9 alpha-3 chain	120270
Multiple epiphyseal dysplasia (MED) type 5 (EDM5)	AD	607078	2p23-24	MATN3	Matrilin 3	602109
Multiple epiphyseal dysplasia (MED) type 6 (EDM6)	AD	120210	6q13	COL9A1	Collagen 9 alpha-1 chain	120210
Multiple epiphyseal dysplasia (MED), other types						
Familial hip dysplasia (Beukes)	AD	142669				
9. Metaphyseal chondrodysplasias In 2006 classification this group is named metaphyseal dysplasia which has been modified [3].						
Metaphyseal chondrodysplasia, schmid type (MCS)	AD	156500	6q21-22.3	COL10A1	Collagen 10 alpha-1 chain	120110
Cartilage-Hair-Hypoplasia (CHH; metaphyseal chondrodysplasia, McKusick type)	AR	250250	9p13	RMRP	RNA component of RNAse H	157660
Metaphyseal chondrodysplasia, Jansen type	AD	156400	3p22-21.1	PTHR1	PTH/PTHrP receptor 1	168468

Table 13.1 (Continued)

Number and name of groups	Inheritance	Name of disorders MIM	Locus	Gene	Protein	MIM
Metaphyseal chondrodysplasia, Spahr type	AR	250400	4q35			
10. Spondylometaphyseal dysplasias (SMD)						
11. Spondylo-epi(-meta)physeal dysplasias (SE(M)D)						
Metatropic dysplasia (various forms)	AD/AR	156530				
SED tarda, X-linked (SED-XL)	XLR	313400	Xp22	SEDL	Sedlin	300202
12. Severe spondylodysplastic dysplasias						
Achondrogenesis type 1A (ACG1A)	AR	200600				
13. Moderate spondylodysplastic dysplasias (brachyolmias)						
14. Acromelic dysplasias						
15. Acromesomelic dysplasias						
16. Mesomelic and rhizo-mesomelic dysplasias						
17. Bent bones dysplasias						
18. Slender bone dysplasia Group						
19. Dysplasias with multiple joint dislocations						
Pseudodiastrophic dysplasia	AR	264180				
20. Chondrodysplasia punctata (CDP) Group						
CDP Conradi-Hünermann type (CDPX2)	XLD	302960	Xp11	EBP	Emopamil-binding protein	300205
CDP X-linked recessive, brachytelephalangic type (CDPX1)	XLR	302950	Xp22.3	ARSE	Arylsulfatase E	300180
21. Neonatal osteosclerotic dysplasias						
Caffey disease (including infantile and attenuated forms)	AD	114000	17q21-22	COL1A1	Collagen 1, alpha-1 chain	120150
Caffey disease (severe variants with prenatal onset)	AR	114000				
22. Increased bone density group (without modification of bone shape)						
Osteopetrosis, severe neonatal or infantile forms	AR	259700	11q13	TCIRG1	Subunit of ATPase proton pump	604592
	AR		16p13	CLCN7	Chloride channel	602727
	AR		6q21	GL (OSTM1)	Grey lethal/ Osteopetrosis associated transmembrane protein	607649
Osteopetrosis, intermediate form	AR	259710	16p13	CLCN7	Chloride channel pump	602727
Osteopetrosis with renal tubular acidosis	AR	259730	8q22	CA1	Carbonic anhydrase 1	114800
Osteopetrosis, late-onset form type 1	AD	166600	11q13.4	LRP5	Low density lipoprotein receptor-related protein 5	603506
Osteopetrosis, late-onset form type 2	AD	166600	16p13	CLCN7	Chloride channel pump	602727
Pyknodysostosis	AR	265800	1q21	CTSK	Cathepsin K	601105
Osteopoikilosis	AD	155950	12q14	LEMD3	LEM domain-containing 3	607844

Table 13.1 (Continued)

Number and name of groups	Inheritance	Name of disorders MIM	Locus	Gene	Protein	MIM
Melorheostosis with osteopoikilosis	AD	155950	12q14	LEMD3	LEM domain-containing 3	607844
Melorheostosis						
Osteopathia striata with cranial sclerosis	XLD	166500				
23. Increased bone density group with metaphyseal and/or diaphyseal involvement						
Craniometaphyseal dysplasia, autosomal dominant type	AD	123000	5p15.2-14.2	ANKH	Homolog of mouse ANK (ankylosis) gene	605145
Diaphyseal dysplasia Camurati–Engelmann	AD	131300	19q13	TGFbeta1	Transforming growth factor beta 1	190180
Diaphyseal dysplasia Camurati–Engelmann, type 2						
Osteoectasia with hyperphosphatasia (Juvenile Paget disease)	AR	239000	8q24	OPG	Osteoprotegerin	602643
Endosteal hyperostosis, Van Buchem type	AR	239100	17q12-21	SOST	Sclerostin	605740
Craniometaphyseal dysplasia, autosomal recessive type	AR	218400	6q21-22			
24. Decreased bone density group						
Osteogenesis imperfecta type 1	AD	166200	17q21-22	COL1A1 COL1A2	Collagen 1, alpha-1 chain	120150
		166240	7q22.1		Collagen 1, alpha-2 chain	120160
Osteogenesis imperfecta type 2	AD	166210	17q21-22	COL1A1 COL1A2	Collagen 1, alpha-1 chain	120150
			7q22.1		Collagen 1, alpha-2 chain	120160
Osteogenesis imperfecta type 3	AD	259420	17q21-22	COL1A1 COL1A2	Collagen 1, alpha-1 chain	120150
			7q22.1		Collagen 1, alpha-2 chain	120160
Osteogenesis imperfecta type 3, recessive, alpha-2 chain deficient	AR	203760	7q22.1	COL1A2	Collagen 1, alpha-2 chain	120160
Osteogenesis imperfecta, recessive, unlinked to COL1A1 and COL1A2	AR	259440				
Osteogenesis imperfecta type 4	AD	166220	17q21-22	COL1A1 COL1A2	Collagen 1, alpha-1 chain	120150
			7q22.1		Collagen 1, alpha-2 chain	120160
Osteogenesis imperfecta type 5	AD					
Osteogenesis imperfecta type 6						
Osteogenesis imperfecta type 7 (rhizomelic form)	AR		3p22-p24.1	CRTAP	Cartilage-associated protein	605497
25. Defective mineralization group						
Hypophosphatasia, perinatal lethal and infantile forms	AR	241500	1p36.1-p34	ALPL	Alkaline phosphatase, tisssue non-specific (TNSALP)	171760
Hypophosphatasia, adult form	AD	146300	1p36.1-p34	ALPL	Alkaline phosphatase, tisssue non-specific (TNSALP)	171760
Hypophosphatemic rickets	XLD	307800	Xp22	PHEX	X-linked hypophosphatemia membrane protease	300550
Hypophosphatemic rickets	AD	193100	12p13.3	FGF23	Fibroblast growth factor 23	605380
Hypophosphatemic rickets with hypercalciuria	AR		9p	SLC34A3	Sodium-phosphate cotransporter	
26. Lysosomal storage diseases with skeletal involvement (dysostosis multiplex group)						
Mucopolysaccharidosis type 1H /1S	AR	607014	4p16.3	IDA	alpha-1-Iduronidase	252800

Table 13.1 (Continued)

Number and name of groups	Inheritance	Name of disorders MIM	Locus	Gene	Protein	MIM
Mucopolysaccharidosis type 2	XLR	309900	Xq27.3-28	IDS	Iduronate-2-sulfatase	309900
Mucopolysaccharidosis type 3A	AR	252900	17q25.3	HSS	Heparan sulfate sulfatase	605270
Mucopolysaccharidosis type 3B	AR	252920	17q21	NAGLU	N-Ac-beta-D-glucosaminidase	252920
Mucopolysaccharidosis type 3C	AR	252930	8p11-q13	(GNAT)	Ac-CoA:alpha-glucosaminide N-acetyltransferase	
Mucopolysaccharidosis type 3D	AR	252940	12q14	GNS	N-Acetylglucosamine 6-sulfatase	607664
Mucopolysaccharidosis type 4A	AR	253000	16q24.3	GALNS	Galactosamine-6-sulfate sulfatase	253000
Mucopolysaccharidosis type 4B	AR	253010	3p21.33	GLBI	beta-Galactosidase	230500
Mucopolysaccharidosis type 6	AR	253200	5q13.3	ARSB	Arylsulfatase B	253200
Mucopolysaccharidosis type 7	AR	253220	7q21.11	GUSB	beta-Glucuronidase	253220
Mucolipidosis II (I-cell disease)	AR	252500	4q21-23	GNPTA	N-Acetylglucosamine 1-phosphotransferase	607840
Mucolipidosis III (Pseudo-Hurler polydystrophy)	AR	252600	4q21-23	GNPTA	N-Acetylglucosamine 1-phosphotransferase	607840
27. Osteolysis group						
Torg–Winchester syndrome	AR	259600 277950	16q13	*MMP2*	Matrix metalloproteinase 2	120360
28. Disorganized development of skeletal components group						
Cherubism	AD	118400	4p16	SH3BP2	SH3 domain-binding protein 2	602104
Fibrous dysplasia, polyostotic form	SP	174800	20q13	GNAS1	Guanine nucleotide-binding protein, alpha-stimulating activity subunit 1	139320
Multiple cartilaginous exostoses 1	AD	133700	8q23-24.1	EXT1	Exostosin-1	608177
Multiple cartilaginous exostoses 2	AD	133701	11p12-11	EXT2	Exostosin-2	608210
Multiple cartilaginous exostoses 3	AD	600209	19p			
Fibrodysplasia ossificans progressiva (FOP)	AD, SP	135100	2q23-24	ACVR1	Activin A (BMP type 1) receptor	102576
Dysplasia epiphysealis hemimelica (Trevor)	SP	127800				
Enchondromatosis (Ollier)	SP	166000				
Enchondromatosis with hemangiomata (Maffucci)	SP	166000				
29. Cleidocranial dysplasia group						
Cleidocranial dysplasia	AD	119600	6p21	RUNX2	Runt related transcription factor 2	600211
30. Craniosynostosis syndromes and other cranial ossification disorders						
Apert syndrome	AD	101200	**10q26.12**	FGFR2	Fibroblast growth factor receptor 2	176943
31. Dysostoses with predominant craniofacial involvement						
32. Dysostoses with predominant vertebral and costal involvement						
Klippel–Feil anomaly with laryngeal malformation	AD	148900				
33. Patellar dysostoses						
34. Brachydactylies (with or without extraskeletal manifestations) (23 forms)						

Table 13.1 (Continued)

Number and name of groups	Inheritance	Name of disorders MIM	Locus	Gene	Protein	MIM
35-Limb hypoplasia – reduction defects group						
De Lange syndrome	AD	122470	5p13.1	*NIPBL*	Nipped-B-like	608667
Fanconi anemia	AR	227650	(several)	*(several)*		
Holt–Oram syndrome	AD	142900	12q24.1	*TBX5*	T-box gene 5	601620
36. Polydactyly syndactyly triphalangism group						
37. Defects in joint formation and synostoses						
Approximate total number of disorders	**372**					

[a]A number of entities included in 2006 nosology have no MIM, locus, gene, and protein.
MIM: Mendelian Inheritance in Man.
Locus: The specific place on a chromosome where a gene is located.
Gene: A basic unit of hereditary material made of DNA.
Protein: The end product of a gene: A large molecule composed of one or more chains of amino acids in a specific order.

the more common and/or more interesting skeletal dysplasias that a radiologist may encounter in practice, emphasizing the non-lethal Disorders.

Skeletal dysplasias are a heterogeneous group of diseases, characterized by abnormal bone and cartilage development. Genetic inheritance may be autosomal recessive, autosomal dominant, x-linked recessive, or x-linked dominant. An increasing number of skeletal dysplasias have known molecular bases [1].

Disturbances in skeletal development are divided into three main groups [3]:

- *Dysostosis* – malformation of bones singly or in combination (monostotic or polyostotic).
- *Disruptions* – secondary malformation of bones caused by toxic substances or infectious agents affecting the embryo for a limited time, e.g., thalidomide and rubella embryopathies. These factors cause secondary, acquired malformations of the skeleton. They may be considered to be secondary dysostoses but are not true dysplasias [3].
- *Dysplasias* are defects arising during the prenatal stage of development that continue expression in postnatal life: Spranger et al. [3] further divide dysplasias into two main subgroups:

  Primary skeletal dysplasias: Primary skeletal dysplasias result from mutated genes and are expressed in mesenchymal tissues.

  Secondary dysplasias: Secondary dysplasias result from extraosseous factors causing developmental abnormalities of the skeletal system. Examples include endocrine disturbances [4] such as congenital hypothyroidism causing cretinism or skeletal manifestations of eunuchoidism and ovarian agenesis. We will include several important secondary dysplasias such as neurofibromatosis and Gaucher disease in this chapter.

Skeletal dysplasia is not synonymous with dwarfism. Although some dysplasias are associated with short stature, others are not, e.g., progressive diaphyseal dysplasia (Camurati–Engelmann disease). Some authors consider developmental skeletal abnormalities dysplasias if a patient has short stature with disproportion between the size of the acral and the axial skeleton. Dwarfism, on the other hand, is proportional and may result from endocrine or metabolic disorders, osseous genetic encoding errors, or extraskeletal genetic effects (secondary dysplasia) [4].

The latest nosology and classification of skeletal dysplasias was introduced in 2006 [1] by "The International Working Group on Bone Dysplasias" (IWGBD). In this classification, skeletal dysplasias are divided into groups (families) of disorders based on a combination of clinical–radiological findings, etiologic and pathogenic similarities, genetics, and whether DNA, RNA, or protein defects are involved. This classification is better organized and more scientifically oriented than previous classifications. This classification adapts clinical, radiological, and molecular information, to create a practical and accurate nosology comprising 37 groups. Each group has between 2 and 23 entities (Table 13.2). This IWGBD classification has taken significant influence from "Rubin's approach in classifying bone dysplasias" [5].

Although this nosology makes understanding and teaching skeletal developmental abnormalities easier, it is far from perfect and will need refinement in the future. Some disorders fit into more than one group, for example, osteogenesis imperfecta (OI) with its seven subtypes is classified in group

Table 13.2 Number of diseases in each group based on 2006 classification

Group name	Number of entities in group
1. FGFR3 group	6
2. Type 2 collagen group	10
3. Type 11 collagen group	4
4. Sulfation disorders group	6
5. Perlecan group	2
6. Filamin group	8
7. Short-rib dysplasia (SRP) (with or without polydactyly) group	7
8. Multiple epiphyseal dysplasias and pseudoachondroplasia group	8
9. Metaphyseal dysplasias	8
10. Spondylometaphyseal dysplasias (SMD)	4
11. Spondylo-epi(-meta)physeal dysplasias (SE(M)D)	17
12. Severe spondylodysplastic dysplasias	5
13. Moderate spondylodysplastic dysplasias (brachyolmias)	2
14. Acromelic dysplasias	15
15. Acromesomelic dysplasias	5
16. Mesomelic and rhizo-mesomelic dysplasias	11
17. Bent bones dysplasias	4
18. Slender bone dysplasias	8
19. Dysplasias with multiple joint dislocations	3
20. Chondrodysplasia punctata (CDP) group	11
21. Neonatal osteosclerotic dysplasias	5
22. Increased bone density group (without modification of bone shape)	15
23. Increased bone density group with metaphyseal and/or diaphyseal involvement	20
24. Decreased bone density group	19
25. Defective mineralization group	8
26. Lysosomal storage diseases with skeletal involvement (dysostosis multiplex group)	21
27. Osteolysis group	8
28. Disorganized development of skeletal components group	20
29. Cleidocranial dysplasia group	3
30. Craniosynostosis syndromes and other cranial ossification disorders	16
31. Dysostoses with predominant craniofacial involvement	7
32. Dysostoses with predominant vertebral and costal involvement	9
33. Patellar dysostoses	4
34. Brachydactylies (with or without extraskeletal manifestations)	19
35. Limb hypoplasia – reduction defects group	28
36. Polydactyly syndactyly triphalangism group	20
37. Defects in joint formation and synostoses	5
Approximate total number of known dysplasias	372

24 (dysplasias with decreased bone density). It is true that in OI there is diminished bone density, but the bones are also slender, similar to group 18 (the osteodysplastic slender bone group). *Some other diseases do not completely fit their classification. Osteopetrosis, the most important member of group 22 (increased bone density group without modification of bone shape), has failure of modeling of metaphyseal regions causing deformity.* Patients with osteopetrosis have Erlenmeyer flask deformity of distal femur and similar deformities in metaphyses of other long bones. Spranger et al. [3] have classified this disease as a skeletal dysplasia with increased bone density and tubular undermodeling that better defines osteopetrosis.

In *2006 classification Group 9, metaphyseal dysplasia, may be confused with Pyle disease in group 23. Therefore, we prefer the term metaphyseal chondrodysplasia for this group as stated in reference* [3] *or metaphyseal dysostosis as stated in reference* [2]. *Furthermore, some of the disorders in this classification, currently, do not have specific locus, gene, and protein.* Examples are all of disorders in groups 10, 12, and 13, enchondromatosis, Maffucci, and Trevor diseases in group 28, as well as several other entities in this group and some other groups.

Nevertheless, with the explosion of knowledge about the cell biology and the genetics of skeletal dysplasias, older classifications and nomenclature can no longer be utilized

and the 2006 classification is the best available at this time. Since the IWGBD classification [1] is extensive and includes many extremely rare diseases, we will present a simpler modification of this classification for reference (Table 13.1).

Helpful Hints for Learning and Remembering Bone Dysplasias

1. **Learn descriptive terminologies in skeletal dysplasias**:

   A. Many of the entities under discussion have at least two names. A name based on descriptive Greek or Latin terminologies using clinical, pathophysiological, and radiological findings will be easier to remeber. Many dysplasias also have proper name(s) referring to the person(s) who first described the entity. Occasionally the first descriptor is not uniformly accepted by various authors, especially if reports were made in different languages. As a result, some dysplasias have multiple names.
   B. Descriptive radiological abnormalities such as universal vertebra plana in Morquio disease or "marble bones" in osteopetrosis remind you the major radiological finding(s).

2. **Remember pictures of patients with bone dysplasias**. "A picture is worth a thousand words." Recalling pictures makes remembering radiologic images easier, for example, pigeon breast and knocked knees in Morquio disease. Disproportionate shortening of extremities compared to axial skeleton and saddle nose are readily visible and easily remembered in pictures of achondroplastics. In a picture of a patient with diastrophic dysplasia, the findings of a crooked body, hitch hacker thumb, mushroom ears, knee dislocation, and club feet help to remember radiological findings.
3. **Consider the pathophysiology, anatomic location of abnormalities in addition to descriptive names and terminology in different dysplasias**. The following examples may be helpful:

   - *Multiple hereditary cartilaginous exostoses* indicates the multiplicity, cartilaginous, and hereditary nature of this entity better than the term osteochondromatosis.
   - *Acrocephalosyndactylism* is easier to understand and remember than Apert disease and the three other variations in this group.
   - *Multiple epiphyseal dysplasia* refers to changes in multiple epiphyses.
   - *Metaphyseal dysplasia* denotes changes primarily are in metaphyses.
   - *Progressive diaphyseal dysplasia* will be easier to remember than Camurati–Engelmann disease.
   - *Spondylometaphyseal dysplasia* denotes changes are predominantly in spine and metaphyses.
   - *Spondyloepimetaphyseal dysplasia* denotes major involvements are in the spine, epiphyses and metaphyses.
   - *Chondrodysplasia punctata* is a better name than stippled epiphyses.
   - *Cleidocranial dysplasia* involves the clavicles and skull, but the name *cleido-cranio-pubic dysplasia* is more informative since most patients also have pubic aplasia or hypoplasia.
   - *Rhizomelic dysplasia* refers to short proximal limb bones, e.g., humerus and femur.
   - *Mesomelic dysplasia* refers to shortening of the middle bones, e.g., radius, ulna, tibia, and fibula.
   - *Acromelic dysplasia* refers to shortening of the distal limb bones, e.g., metacarpals, metatarsals, and phalanges.
   - *Acromesomelic dysplasia* refers to shortening of both the middle and distal limb bones.
   - *Micromelia* is shortening of the entire limb.
   - *In short trunk dysplasias* there is disproportionate shortening of the trunk compared with the extremities, e.g., metatropic dysplasia.
   - *Disproportionate short limb rhizomelic dysplasia* denotes a dysplasia where the extremities are short compared with the spine and the humeri and femurs are disproportionately short: such as achondroplasia.

4. **Skeletal aplasias, hypoplasias and malformations are numerous and only a few interesting examples will be mentioned in anatomic regions** [3, 6]. **The upper extremity anomalies** [6];

   - *Congenital pseudarthrosis of the clavicle*.
   - *Congenital undescended scapula* (Sprengel deformity).
   - *Congenital dislocation of the radial head*.
   - *Radioulnar synostosis (almost always proximal)*,
   - *Radial dysplasia* is often bilateral (60% total aplasia, 20% partial aplasia, and radial hypoplasia is diminution in size of radius). This anomaly may be associated with other disorders [6]. The acronym VATER is referring to vertebral-anal-tracheo-esophageal-radial and renal anomalies. TAR syndrome refers to thrombocytopenia and absent radius.
   - *Ulnar dysplasia* is rarely bilateral (ulnar hypoplasia with distal ulnar epiphysis present, partial aplasia with distal epiphysis absent that is the most common form and total aplasia).
   - *Madelung deformity of the wrist* (short bowed radius and long ulna giving a triangular appearance to the

proximal carpal bones and lunate between the radius and ulna, with dorsal but reducible ulnar dislocation).
- *Carpal coalition* is most common between the lunate and triquetrum. The second most common coalition is between the capitate and hamate.
- *Amputations, syndactyly, and polydactyly* of hand may be seen.
- *Macrodactyly* (macrodystrophia lipomatosa). There is unilateral focal giantism of one or two digits, most marked in distal digit. Both bone and soft tissues are enlarged. There is increased adipose tissue. Neural enlargement may be present.
- *Pectoral aplasia-dysdactyly* is also known as (Poland syndrome).
- *Holt-Oram syndrome* [3]: This is an autosomal dominant trait (group 35-limb hypoplasia reduction defects group in 2006 classification). The radiological findings of this interesting entity will be briefly described:

  (A) *Hand:* thumb anomalies (digitized, absent, hypoplastic, abnormal plane); finger anomalies (clinodactyly, syndactyly, absent, hypoplastic).
  (B) *Carpal bones*: delayed ossification or absence, hypoplastic, fused, irregular, extracarpal (os centrale), enlarged, bipartite.
  (C) *Forearm and humerus*: radial hypoplasia or aplasia, ulnar hypoplasia or aplasia, radioulnar synostosis, humeral hypoplasia, or aplasia.
  (D) *Shoulder and chest*: hypoplastic or broad clavicle, hypoplastic glenoid fossa, Sprengel deformity, and deficiency of pectoral muscles.
  (E) *Congenital cardiovascular anomalies*: atrial septal defect 60%, hypoplastic peripheral vasculature, and patent ductus arteriosus.

The Pelvic Anomalies [6]:

- Developmental dysplasia of the hip (DDH) – DDH may be diagnosed before ossification of the proximal femoral epiphysis by ultrasonography. After calcification, radiography is easier to demonstrate subluxation or dislocation of the femur and shallow acetabulum.
- *Sacral agenesis* – The entire sacrum may be absent or partial sacral agenesis may be present.

The Lower Extremity Anomalies [6]:

- *Proximal femoral focal deficiency (PFFD)* – There is dysgenesis of variable potions of the femur. There may be only a mild femoral shortening or moderate to major femoral hypoplasia in which case only a small stub of the femur is formed [6].
- *Tibial dysplasia* – Tibial aplasia or hypoplasia is less common than fibular dysplasias.
- *Fibular dysplasia* – Fibular dysplasia ranges from fibular aplasia (fibular hemimelica) to minimal hypoplasia.
- *Congenital tibial and fibular bowing* may be present.
- *Congenital subluxation and hyperextension of the knee* is another lower extremity anomaly.

The Foot Anomalies [6]:

- *Congenital clubfoot (Congenital talipes equinovarus*) – This entity is seen in 1 to 4:1000 births [6]. Talipes refers to talus. In extreme cases of equinovarus the patient practically walks on his ankle.
  The term talipes has also been used to define other congenital abnormalities of the foot in which the patient does not walk on the ankle (such as talipes varus, talipes calcaneovalgus, talipes equinovalgus, and talipes calcaneovarus). The word equine means horse.
- *Hindfoot valgus and planovalgus foot*
- *Congenital vertical talus*
- *Cavus foot* – Refers to increased plantar arch of the foot.
- *Forefoot abduction (towing-in)* – May be due to metatarsus adductus and adductovarus.
- *Hallux valgus* – The first metatarsal is short and adducted. The normal angle between the first metatarsal and proximal phalanx, in adolescence, is 14°–16°.
- *Congenital tarsal coalition* – Coalition may be fibrous, cartilaginous, or bony. The most common sites are talocalcaneal (60%) and calcaneonavicular (30%). Talar beak is strongly suggestive of tarsal coalition.

The Spinal Anomalies [6]:

Scoliosis is lateral curvature of the spine in coronal plain. The curve is identified by the level of apex, end vertebrae, and the side of convexity. The apex is the most laterally displaced (rotated) vertebra and the vertebrae at the ends of the curvature are called the end vertebrae. The most common form is the idiopathic scoliosis which is seemingly of spontaneous origin. Other types of scoliosis are due to known etiologies such as congenital spinal anomaly, neuromuscular disease, or irritative, traumatic, metabolic, or extraspinal causes. Scoliosis may be associated with neuroectodermal or mesodermal disorders or skeletal dysplasias.

Scoliosis is measured by the angle drawn between the apical vertebra and the upper and lower end vertebrae. In PACS the angle can be measured digitally.

Kyphosis is either due to increased thoracic kyphosis beyond the normal limits or reversal of cervical or lumbar lordosis.

Lordosis is either related to reversal of thoracic kyphosis or increased lordosis of the cervical or lumbar spine beyond the normal limits.

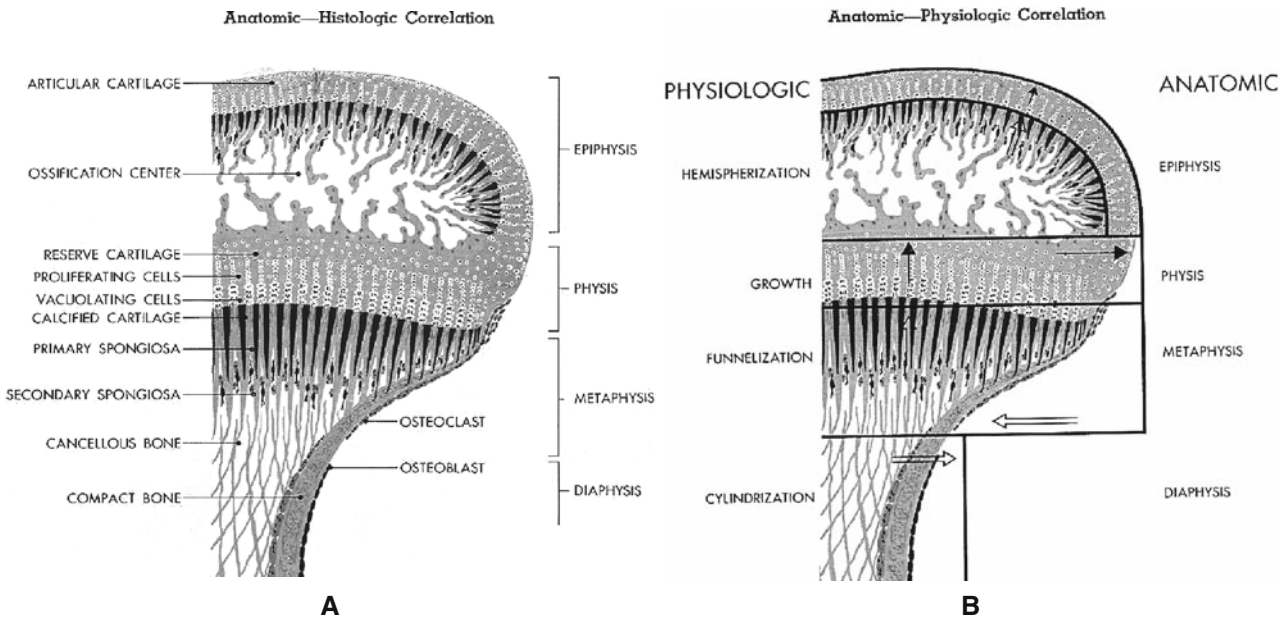

Fig. 13.1 Correlation of structure, physiology, and histology of growing long bones. **a** Correlates the anatomy to histology of the end of the long growing bone and the mechanism of metaphyseal modeling. **b** Compares the physiology of the end of the long growing bone to the anatomic segments namely, the epiphysis, physis, metaphysis and diaphysis. (Modified from Philip Rubin [5]).

Kyphosis and lordosis are measured with the same method used for scoliosis. Normal values vary in different reports, but are in the range of 21°–33° for thoracic scoliosis and 31°–50° for lumbar lordosis [6].

Kyphoscoliosis is when kyphosis and scoliosis coexist.

- *Dysraphism* refers to failure of midline vertebral structures. Open (uncovered) is seen when the dysraphism is clinically evident. Meningocele and myelomeningocele are examples of open dysraphism.
  Closed or (occult) dysraphism is when dysraphic changes are covered with skin, such as failure of midline fusion, duplication (diplomyelia and diastematomyelia), and several other forms.
- *Klippel–Feil syndrome* – At present this terminology is used to describe any form of cervical spine fusion.

Bone Development and Growth

The embryology, development, and modeling of bones are discussed in Chapter 1. The anatomy, physiology, and histology of growing long bones are shown in (Fig. 13.1a and b). Rubin Dynamic Classification of Bone Dysplasias [5], although not universally accepted, is helpful for understanding and teaching of radiology of bone dysplasias. Rubin has divided the growing bone into a number of zones. He includes the articular cartilage and the osseous epiphyseal center in one zone which he calls the epiphysis. In the second zone, which he calls physis; Rubin includes only the physeal growth plate. The terms metaphysis and diaphysis are used with their conventional meanings. He proposed that most and perhaps all the dysplasias are caused by an alteration in one or more of these zones.

In order to make the chapter easier to access and review, selected prototypes and more common entities, both with and without a known genetic basis, will be included in our brief discussion.[1] Several secondary dysplasias will be also added (Table 13.3).

Achondroplasia (MIM 100800) Group 1

Achondroplasia is the most common non-lethal skeletal dysplasia [7].

The most common lethal skeletal dysplasias are thanatophoric dysplasia, achondroplasia (severe cases), osteogenesis imperfecta (infantile and neonatal forms),

[1] Note: Readers interested in further information on various additional dyasplasias are encouraged to refer to "Taybi and Lachman radiology of Syndromes, Metabolic Disorders, and Skeletal Dysplasias 5th ed., Mosby 2007" [7] and "Spranger JW, Brill PW, and Poznanski A; Bone Dysplasias an Atlas of Genetic Disorders of Skeletal Development 2nd ed, Oxford University Press 2002:" [3], and other Text books available, as well as electronic references.

Table 13.3 Alphabetical order of selected entities included in this chapter

Name	Name
Achondroplasia	Melorrheostosis
Achondrogenesis	Metaphyseal dysplasia and craniometaphyseal dysplasia
Asphyxiating thoracic dysplasia	Metaphyseal chondrdysplasia
Chondrodysplasia punctata	Metatropic dysplasia
Chondroectodermal dysplasia	Mucopolysaccharidoses and mucolipidoses
Cleidocranial dysplasia	Multiple epiphyseal dysplasia and Blount disease
Craniostenosis	Multiple hereditary cartilaginous exostoses
Diaphyseal dysplasia (Progressive)	Neurofibromatosis and pseudarthrosis
Diastrophic dysplasia	Osteogenesis imperfecta
Dysplasia epiphysealis hemimelica	Osteolysis
Enchondromatosis (ollier/maffucci)	Osteopathia striata
Endosteal hyperostosis	Osteopetrosis
Fibrodysplasia ossificans progressiva	Osteopoikilosis
Fibrous dysplasia	Pseudoachondroplasia
Gaucher disease	Pyknodysostosis
Hyperphosphotasia (osteoectasia with hyperphosphotasia)	Spondyloepiphyseal dysplasia
Hypophosphatasia	Spondyloepimetaphyseal dysplasia
Hypophosphatemic rickets	Spondylometaphyseal dysplasia
Infantile cortical hyperostosis (Caffey disease)	Thanatophoric dysplasia
Marfan syndrome	Tuberous sclerosis complex

and achondrogenesis (types I and II). Thanatophoric dysplasia and acohondrogenesis account for 62% of lethal dysplasias [4].

Achondroplasia is inherited via autosomal dominant transmission. As a result, marriage to a genetically normal spouse means a 50% chance of parenting normal offspring [2]. Despite this mode of inheritance, most cases are the result of spontaneous mutations.

Clinical findings: Achondroplasia is a disproportionate short limb rhizomelic dwarfism. The head (calvarium) appears large in relation to body, and the nose has a saddle appearance (Fig. 13.2). Patients may have a thoracolumbar kyphosis in infancy. The buttocks are prominent in children (Fig. 13.2a). The hands have a trident appearance. Affected individuals have normal intelligence.

On average, achondroplastics attain height of about 50 in. Because of the rhizomelia, their finger tips reach only to the hip instead of the mid-thigh region as in normal individuals. The legs become bowed in older individuals as a result of the load placed on the abnormally soft bones (Fig. 13.2b).

This dysplasia exists in all degrees of severity. It may be so severe that it is diagnosed in utero and the patient may not survive gestation. In its more typical form, patients are phenotypically obvious. There also are patients with lesser degrees of involvement. Their stature may be almost normal

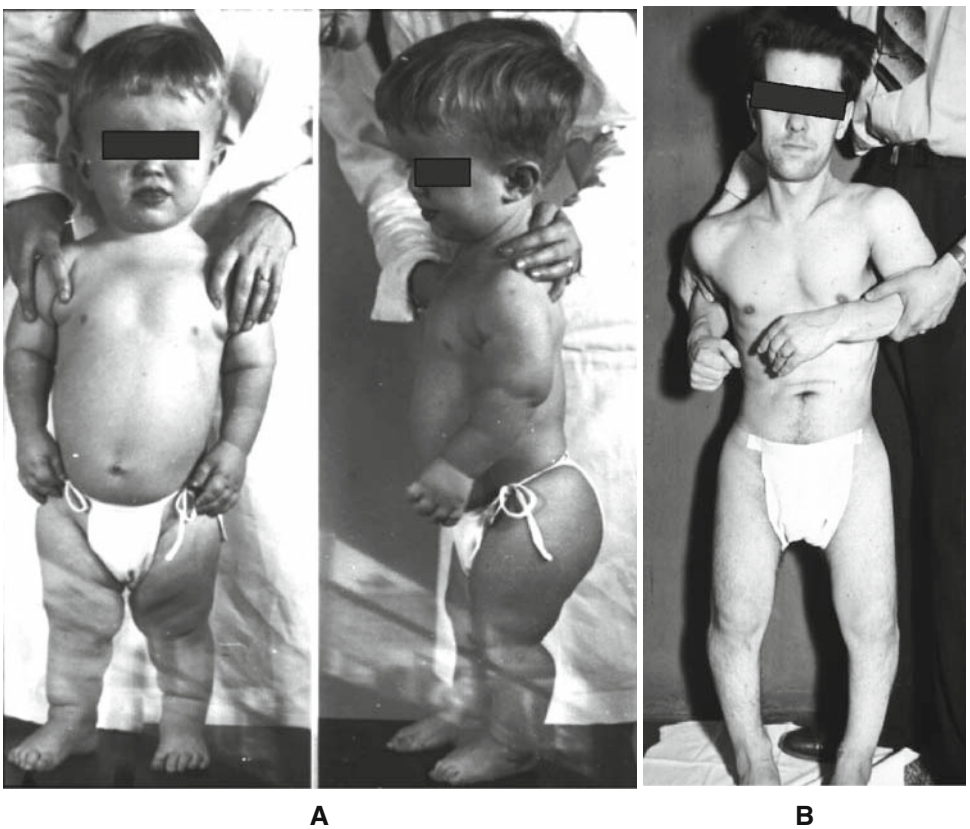

Fig. 13.2 Achondroplasia. **a** is a child with relatively large head, saddle nose, brachycephaly, and disproportionately short extremities compared with the axial skeleton. **b** is an adult achondroplast showing dwarfism, relatively large head, saddle nose, short extremities, and bowed legs

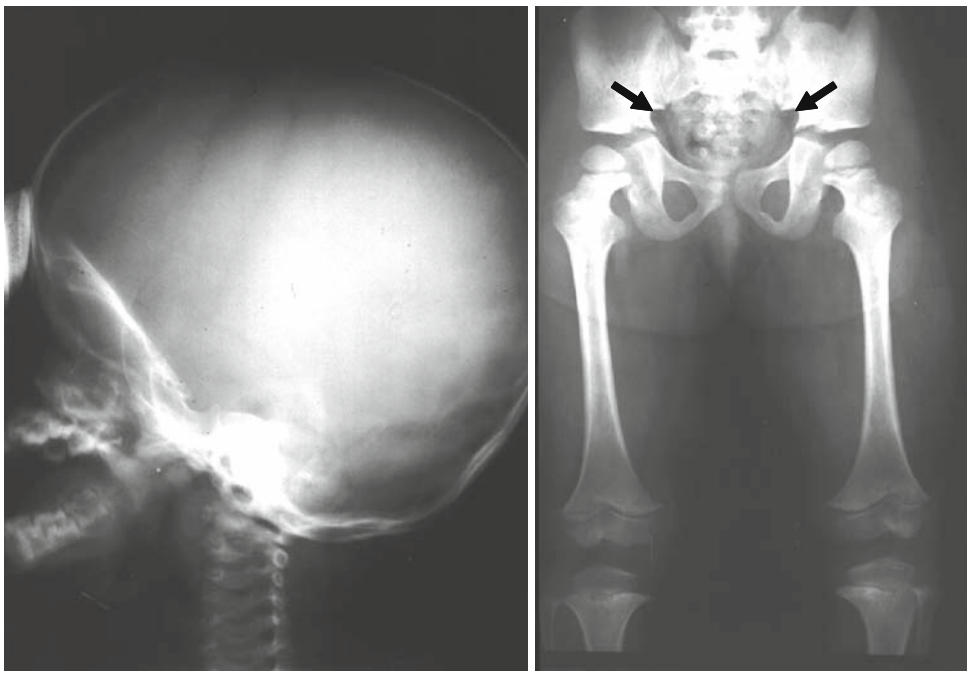

Fig. 13.3 Achondroplasia. **a** Lateral radiograph of an infant skull shows shortening of the base giving the impression of apparent enlargement of the calvarium. **b** AP radiograph of the pelvis, femurs, and knee. The sacrum articulates low on the ilia. Disturbed growth at the inferior ilia has caused short ilia and flat acetabular roofs. Note small appearing sciatic notches (*arrows*). Overall, the pelvis is small, and the pelvic bowl resembles a "champagne glass." The femurs are short with normal girth. The metaphyses of femurs and tibias reveal flaring. Bone density is normal

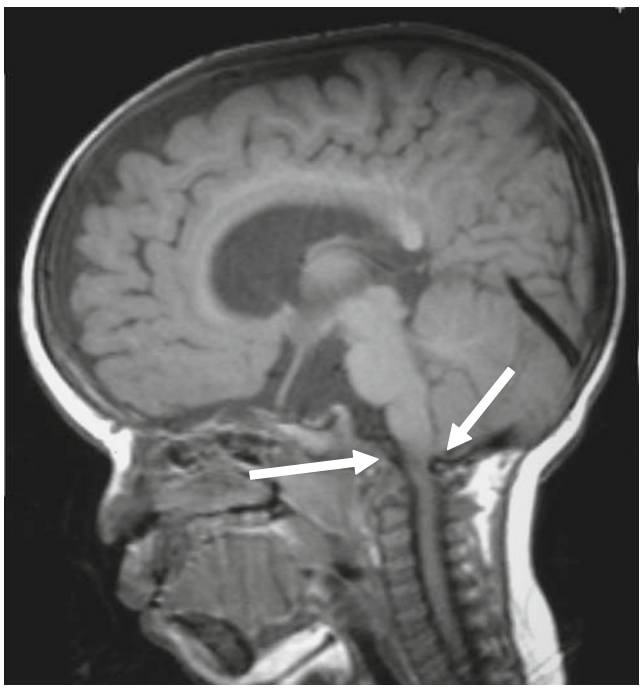

Fig. 13.4 Achondroplasia. Sagittal T1W MRI of another infant. There is shortening of the base of the skull, narrowing of the foramen magnum (*arrows*) causing indentation of the posterior brain stem. The sella turcica is shallow. The posterior fossa contents are unremarkable. The suprasellar cistern is prominent with elongation of the optic chiasm. Note the relative small size of the facial bones compared to the calvarium. Courtesy of Dr Eleanor Smergel, St Christopher's Hospital, Philadelphia

and only a radiographic skeletal survey shows the stigmata of the condition.

Radiological manifestations: Achondroplasts have diminished enchondral bone growth that results in short bones. Intramembranous bone growth is normal, and so the bones have normal girth. The radiological manifestations of achondroplasia are present in all enchondrally formed bones but are most marked in the skull, long bones, spine, and pelvis.

The skull shows apparent enlargement of the cranial vault and frontal bossing. There is decreased bone growth at the sphenooccipital synchondrosis causing shortening of the base of the skull. Shortening of the skull base results in saddle nose (Figs. 13.3and 13.4). There is narrowing of the foramen, magnum that may cause indentation of the posterior brain stem that is best demonstrated by brain MRI (Fig. 13.4). As in some other diseases, patients may have numerous sutural bones in the lambdoid suture known as Wormian bones (named after Olaus Worm, a Danish anatomist).

The spine is approximately normal in length. The interpedicle distance from the first lumbar vertebra through the fifth decreases progressively (Fig. 13.5b) instead of increasing as is seen in normal individuals. In addition, the pedicles are short and thick throughout the spine causing congenital spinal stenosis. The posterior aspects of the vertebral bodies develop marked individual concavities likely related to CSF pulsation in the stenotic canal. CT and MRI (Fig. 13.6) demonstrate the small spinal canal and multiple protruding inter-vertebral discs, a phenomenon more

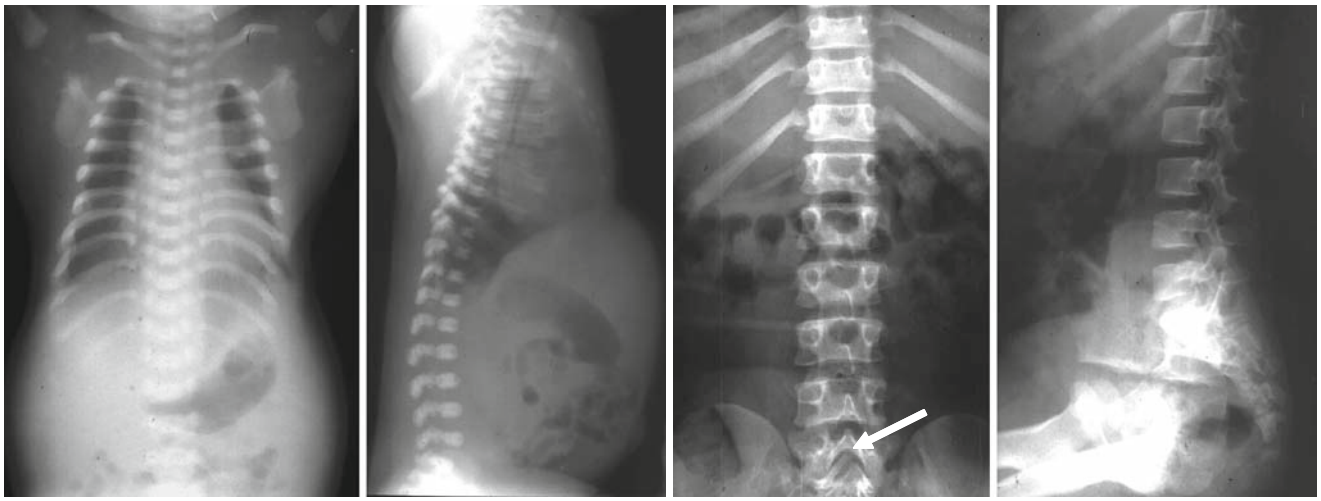

Fig. 13.5 Achondroplasia. Anteroposterior (AP) and lateral radiographs of the chest of an infant show short ribs and small vertebrae giving a false impression of widened intervertebral disc spaces. **b** Adult lumbar spine, AP radiograph shows progressive decrease of the interpediculate distances from L1 to L5 (*arrow*). In the lateral radiograph short pedicles and narrowing of the spinal canal are readily appreciated

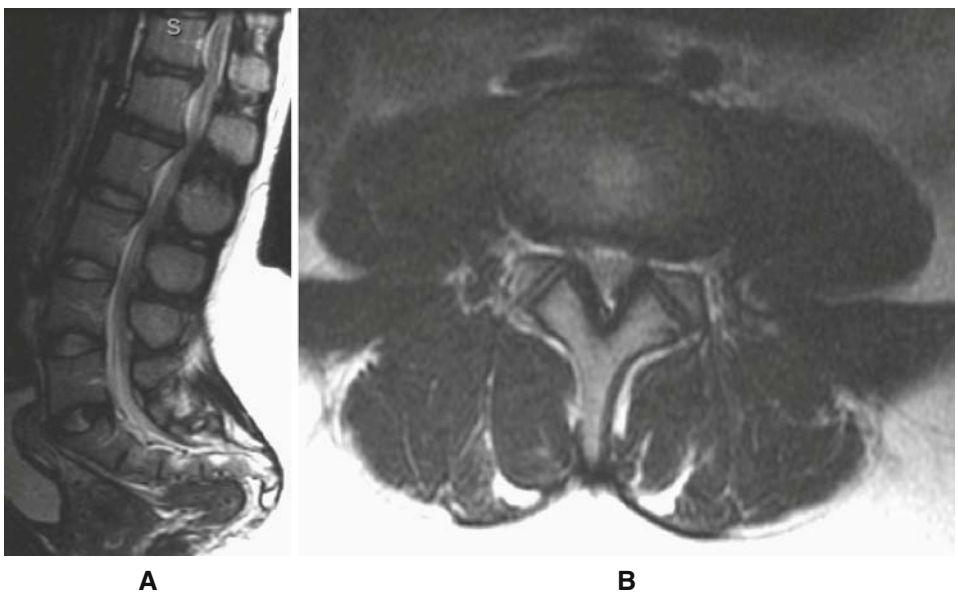

Fig. 13.6 Achondroplasia in an adult. **a** and **b** are Sagittal and axial T2 weighted MR images of the lumbar spine showing significant narrowing of the spinal canal. The sagittal image reveals marked decreased AP diameter of the spinal canal and the axial image reveals circumferential central canal stenosis. Courtesy of Dr Leslie Grissom, Alfred I. DuPont Hospital for Children, Wilmington, DE

commonly seen in older children and adults. The intervertebral discs show either normal or increased thickness. Lumbar lordosis becomes evident and marked with weight-bearing. The ribs frequently fail to grow to normal length, producing a flattened and narrow chest (Fig. 13.5a).

The bones of the pelvis also are affected. Disturbed growth at the lower end of the iliac bones causes a small and deformed pelvis, flat often irregular acetabular roofs, and small sciatic notches (Fig. 13.3b). The ischia and pubic bones are short and broad. The pelvic bowl has a characteristic "champagne glass" appearance on radiographs.

The bones of the extremities are short. The proximal bones, i.e., humerus and femur, are affected more than distal ones (rhizomelia). The ends of bones may flare (Fig. 13.3b). The zone of provisional calcification and the epiphyseal center may be relatively smooth in outline, or the epiphyseal

plate may be irregular and partially enclose the epiphyseal center. Bowing of the bones of the lower extremity is common as is cortical thickening at the sites of muscle attachment. The fibula is often longer than the tibia, causing inversion of the foot. The radius is typically longer than the ulna. The tubular bones of the hands and feet are short and appear broad. Because the fingers tend to be broader at their proximal ends, divergence of the fingers occurs when the hand is open, the "trident hand." The fourth and fifth fingers form one line of the trident, the second and third another, and the thumb another.

Prognosis: If an achondroplast survives the trauma of childbirth, he stands a good chance of living well into adult life. As the patient ages, spinal stenosis and secondary spondylosis often will lead to worsening neurological complaints from pressure on the cord and spinal nerves. Backache, sciatica, paresthesias, and even paraplegia may develop. Disc herniation may add to these difficulties.

Differential diagnosis: The following entities are in the differential diagnosis of achondroplasia:

- Achondrogenesis.
- Hypochondroplasia.
- Metatropic dysplasia.
- Pseudoachondroplasia.
- SADDAN (severe achondroplasia, developmental delay, and acanthosis nigricans).
- Thanatophoric dysplasia

Achondrogenesis, as the name implies, is caused by failure of cartilage formation. The extremities are extremely short, the vertebral bodies are hypoplastic but have intact intervertebral discs. The ribs are short making the thorax very small (Fig. 13.7). These patients generally do not survive.

Hypochondroplasia (FGFR3), (MI146000) Group 1 is similar to achondroplasia, but the changes are much less severe.

Metatropic dysplasia resembles achondroplasia in the neonatal period (Fig. 13.46). At maturity the limbs have grown more than would be expected for achondroplasia, and the trunk has shortened because of progressive kyphoscoliosis. Thus, eventually the extremities appear to be disproportionately long for the trunk, just the opposite of achondroplasia.

Pseudoachondroplasia patients have short limbs and a disproportionately long trunk. The skull is normal. Kyphosis and scoliosis may be present. A constant finding is central beaking (togging) of vertebral bodies. They have poor epiphyseal ossification, knock-knees (genu valgum) or bow legs, and hypermobility of all of their joints except the elbows [3].

SADDAN (severe achondroplasia, developmental delay, and acanthosis nigricans), as the name indicates, is a severe form of achondroplasia with developmental delay and acanthosis nigricans, a diffuse velvety acanthosis with gray, brown, or black pigmentation, chiefly in axillae and other body folds.

Thanatophoric dysplasia. The osseous changes in thanatophoric dysplasia are similar to achondroplasia but more severe: vertebrae are flatter and long bones are shorter (Fig. 13.82). These patients, as the name implies, do not survive.

Achondrogenesis (MIM 200600, 600972, and 200610) Group 12

Achondrogenesis is characterized by extreme osseous deformity, hydropic appearance, death at or soon after birth and autosomal recessive transmission. The extremities are extremely short; the vertebral bodies are small with intact intervertebral discs; and the ribs are short making the thorax very small. This condition has been divided into types IA, IB, and II. Achondrogenesis 1A is included in group 12 of 2006 classification [1] (severe spondylodysplastic dysplasias). Achondrogenesis type IB is in group 4 (sulfation disorders group). Type II is in group 2 (type 2 collagen group).

These patients have virtual absence of ossification of the vertebral bodies (Fig. 13.7) [2].

Asphyxiating Thoracic Dystrophy (Jeune Syndrome) (MIM 208500) Group 7

In 1955 Jeune et al. reported two infant siblings who died of respiratory distress associated with a small and relatively immobile thorax [2]. This rare, potentially lethal congenital dysplasia of autosomal recessive inheritance is characterized by an underdeveloped thorax (Fig. 13.8a) and micromelia (Fig. 13.8b, c), with respiratory and renal pathology. Respiratory manifestations vary widely from pulmonic underdevelopment leading to respiratory failure and death in 60–70% of patients, to mild disease with few if any respiratory symptoms. Intrinsic renal disease and interstitial fibrosis may be encountered in this group of patients [2]. Patients often have retinal degeneration. A form of this dysplasia has been described in which the thoracic deformity is mild and the patients grow into childhood.

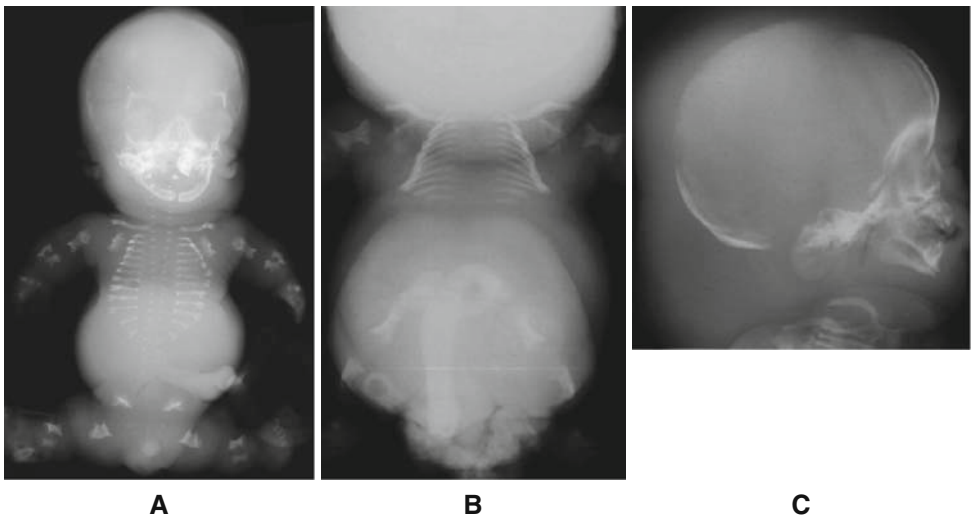

Fig. 13.7 Achondrogenesis. **a**: Type 1 – The extremities are very short similar to achondroplasia, but the spine is significantly underdeveloped. **b** and **c**: Type 2 – Similar to type 1, but the spine is not developed at all. The skull is similar to achondroplasia, but the abnormalities are more pronounced and no spinal ossification is seen. Courtesy of Dr Ralph Lachman, Professor Emeritus UCLA

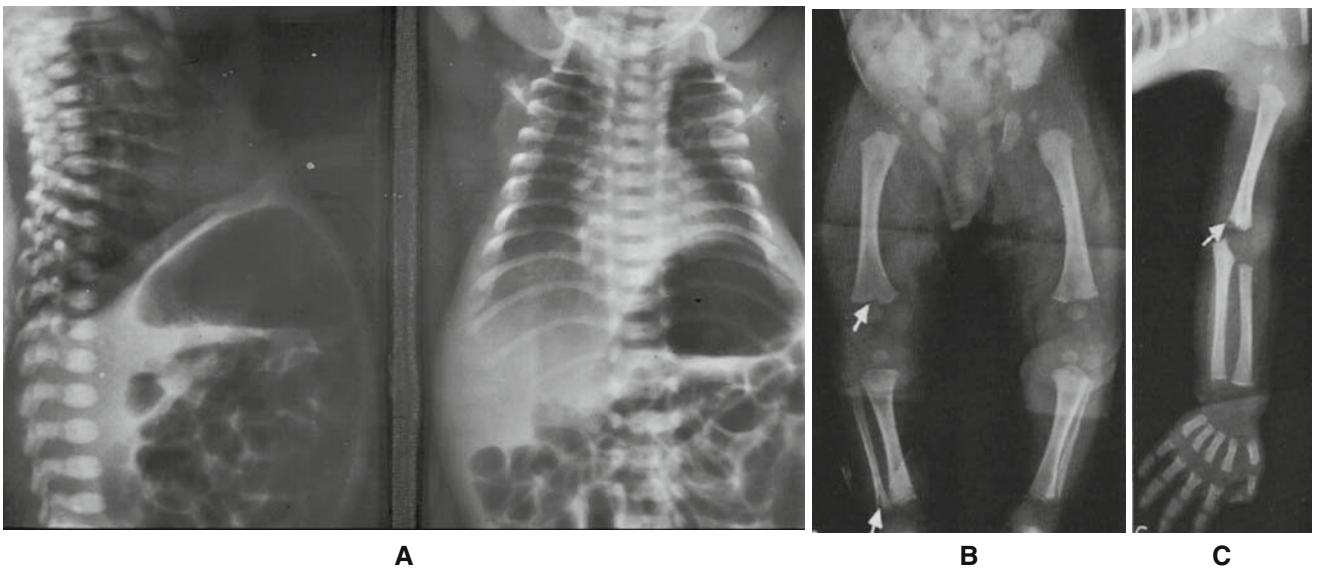

Fig. 13.8 Asphyxiating Thoracic Dysplasia. **a**: AP and lateral radiographs of the chest show short ribs causing shortening of the AP diameter of the chest. The spine is straight; the interpediculate distances are normal. **b** and **c**: AP radiographs of the pelvis, upper, and lower extremities show broad and flat roof of the acetabulae and peculiar notches in the metaphyses of many of the long bones (*arrows*)

Radiographically, these patients show very short ribs and variable degrees of shortening of the long tubular bones with peculiar notching of the metaphyses (arrows Fig. 13.8b, c). The limbs show variable micromelia (Fig. 13.8b, c) and short digits with bulbous terminal phalanges and occasional postaxial (ulnar) polydactyly of the hands and feet. Cone-shaped epiphyses in the hands are usually present, but this finding is non-specific and so not diagnostically useful.

The ilium in the young infant is short in its inferosuperior dimension with a broad acetabular roof (Fig. 13.8b) in which there is apt to be a large V-shaped notch. Spine and skull are normal.

Chondrodysplasia punctata (IMM 302960, 302950, 308050, 215100, 222765, 600121118651) Group 20

Several types of chondrodysplasia punctata (CDP) have been reported in group 20. Chondrodysplasia punctata is a better terminology for this group than dysplasia epiphysealis punctata or stippled epiphysis, because calcification is present not only in unossified epiphyseal centers, but also in unossified cartilaginous centers of small bones of hands and feet (Fig. 13.9). Milder forms may be overlooked at birth as

Fig. 13.9 Chondrodysplasia punctata. Note punctate stippling in the ossification centers of the feet. Punctate stippling is seen not only in secondary epiphyseal ossification centers of the metatarsals (*short arrow*), but also in primary ossification centers of the tarsal bones (*long arrows*). Therefore the term "stippled epiphyses" is not correct, because the primary ossification centers of tarsal bones are not epiphyses

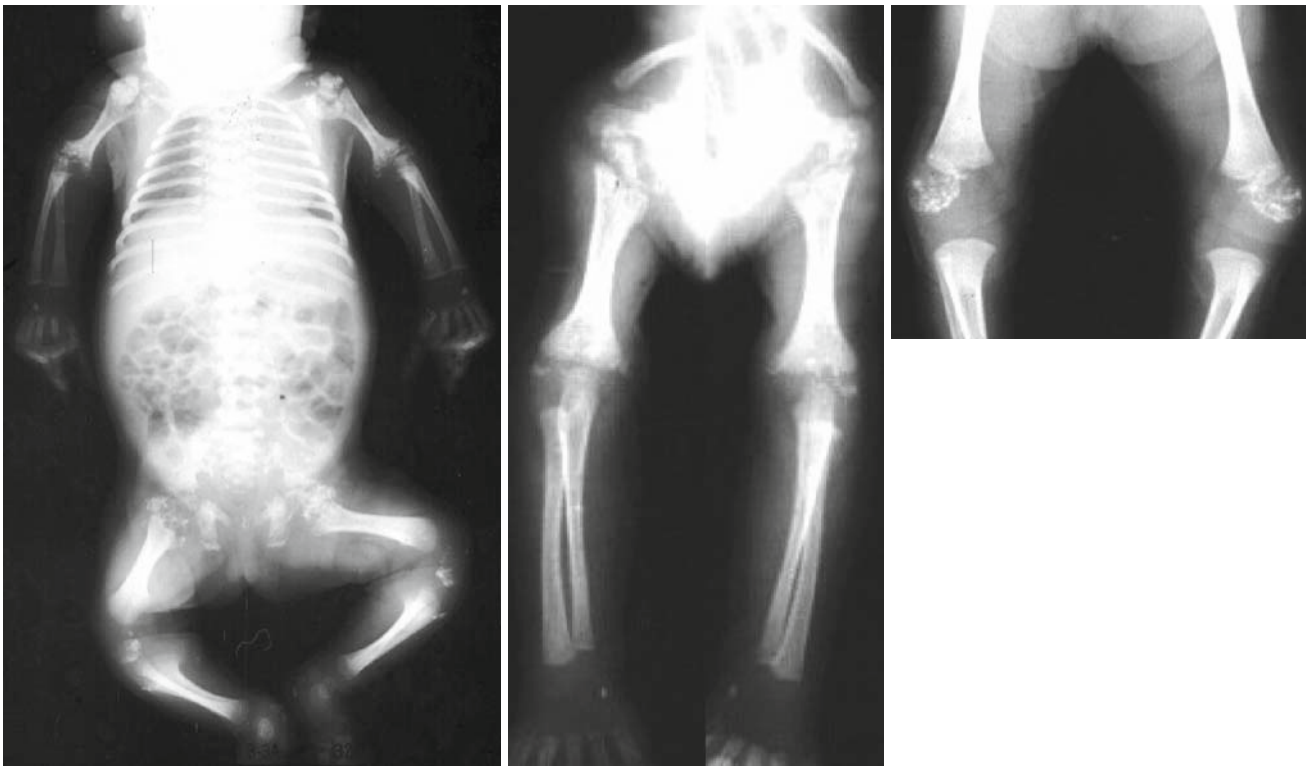

Fig. 13.10 Chondrodysplasia punctata. AP radiographs of the body (**a**), upper extremities (**b**), and the knees (**c**). Punctate dystrophic calcifications of the epiphyses and the primary ossification centers are seen in all of the images, but better demonstrated in the knees. The rhizomelic nature of dysplasia is best seen in **b**

dwarfism is lacking in these cases and the stippled areas may merge into normal appearing epiphyseal osseous centers, sometimes as early as 2 years of age [2].

In severe forms of the disease, infants are frequently stillborn or die of associated anomalies or intercurrent disease within the first year [2]. In moderately severe forms, the osseous nucleus may fail to mature, leaving the epiphysis as a bulbous mass of stippled cartilage [2] (Fig. 13.10).

In Conradi-Hunnermann type of CDP (MIM 302960), the punctate calcifications may be asymmetric [3]. In the rhizomelic form of CDP (IMM 215100, 222765, 600121), the punctate calcifications most commonly form at the end of long bones and are sparse in the spine [3]. Growth of the affected bones often is retarded. The stippling usually disappears by the age of 3–5. In these patients, the diagnosis should be made on the basis of secondary signs of growth

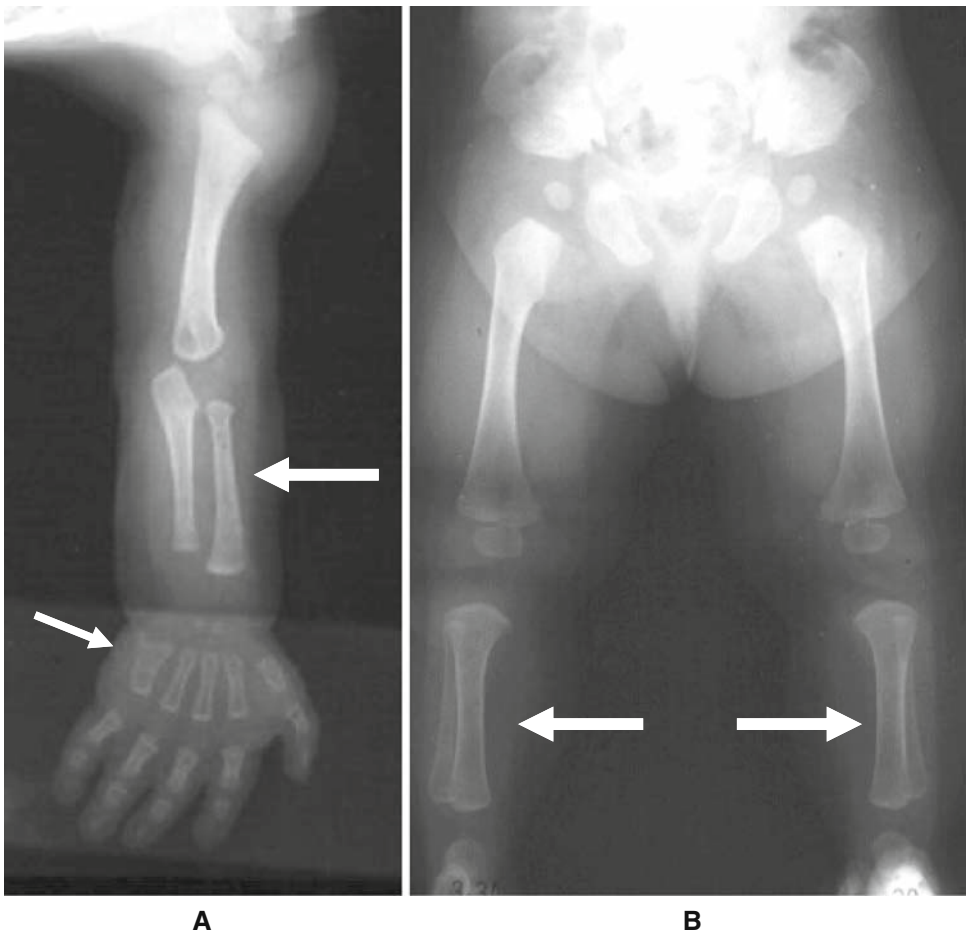

Fig. 13.11 Chondroectodermal dysplasia. The bones of the extremities are short, but the radius, ulna, as well as tibia and fibula are relatively shorter than humerus and femur (mesomelic dwarfism) (*arrows*). A rudimentary metacarpal is present (*small arrow*)

impairment, such as angulation of bone ends, cone epiphyses, and other deformities [3]. Calcifications may be seen in nasal septum, trachea, and larynx [2].

Chondroectodermal Dysplasia (Ellis-van Creveld Disease) (MIM 225500) Group 7

Ellis-van Creveld (EVC) syndrome has autosomal recessive inheritance. About 200 cases were reported in 1994. McKusick reported 89 cases in 2000. The incidence is 0.9 per 100,000 births and is high in Amish populations.

Patients with EVC exhibit ectodermal dysplasia, chondrodysplasia, ulnar (postaxial) polydactyly, and congenital cardiac anomalies. The cardiac anomalies appear in approximately 60% of cases and include common atria (40%), interatrial and interventricular septal defects, large vessel transposition, and patent ductus arteriosus. These patients usually have cyanosis at birth and in the past would die shortly thereafter in congestive heart failure. Modern cardiac surgery has expanded their life span greatly.

The ectodermal dysplasia is visible as small, distorted and friable nails, defective dentition and, rarely, alopecia. The upper lip is often short and bound down to the anterior portion of the gums by a thick and short frenulum.

Chodroectodermal dysplasia manifests as dwarfing of the extremities (Fig. 13.11), synostosis of the calvarial sutures, failure of normal skeletal growth, and deformity of the tubular bones. A defect in the lateral aspect of the proximal portion of the tibia causes genu valgum. The distal segments of the limbs manifest greater shortening (acromelic dwarfism) than do the proximal segments (Fig. 13.11). EVC often shows carpal bone fusions, the most common of which is between the hamate and capitate bones (Fig. 13.12b). Polydactyly, typically along the ulnar (postaxial) aspect of the hand (Fig. 13.12a), has been constant, appearing more often in the hands than in the feet.

Cleidocranial Dysplasia (MIM 119600) Group 29

More than 1,000 cases had been reported up to 2004. We prefer to call this entity cleido-cranio-pubic dysplasia, because most cases have associated pelvic dysplasia as well as dysplasia of the skull and clavicles. It is a developmental

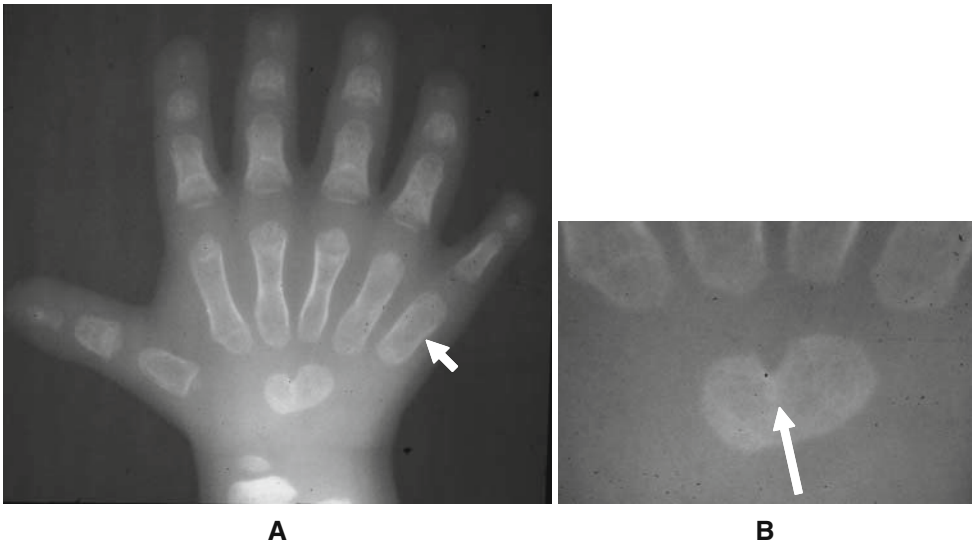

Fig. 13.12 Chondroectodermal dysplasia. This is a different patient with chondroectodermal dysplasia. **a** shows ulnar polydactyly (*Short arrow*) and fusion of the capitate and hamate in this case. **b** Magnified view of the wrist better shows the capitohamate fusion (*arrow*)

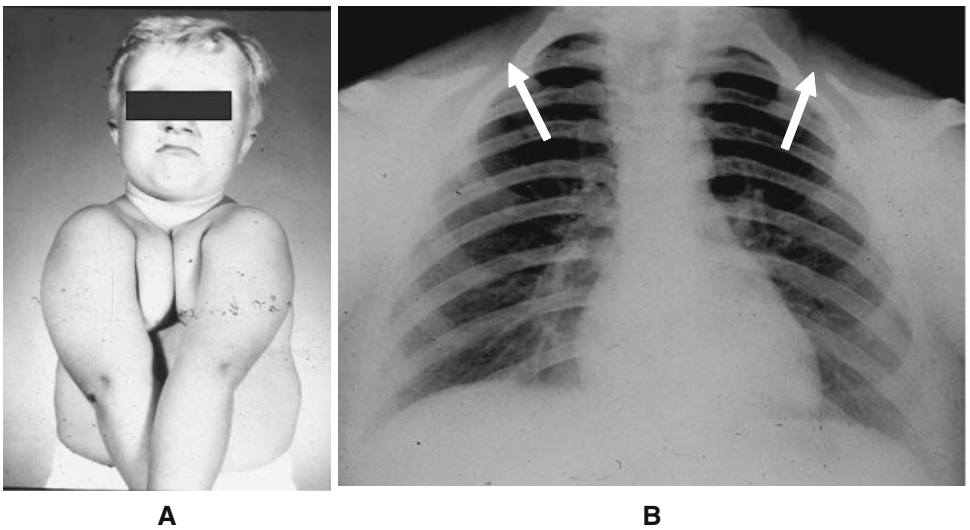

Fig. 13.13 Cleidocraniopubic dysplasia. **a** In photograph of a patient with the disease, the shoulders show significant hypermobility related to hypoplasia of the clavicles. **b**: PA chest radiograph shows absence of medial two thirds of both clavicles (*arrows*)

disturbance of the skeleton in which a wide variation of deformities occurs involving numerous bones, particularly those in the midline or adjacent to the midline. There is almost always involvement of the skull and the clavicles or both. About 60% show pubic dysplasia.

The typical patient has a large head, a small face, drooping shoulders, and a narrow chest. The patient has hypermobility of the shoulders as a result of dysplastic clavicles (Fig. 13.13a). There is a marked brachycephaly with widening of the interparietal diameter that makes the skull to appear excessively broad. The foramen magnum is larger than normal and slants forward and downward; the mandible is prognathic. The maxilla is underdeveloped as are the other bones that compose the face. As a result, the paranasal sinuses are small. The palate is narrow, sometimes cleft, and high arched. The frontal and parietal bones are prominently bossed. The principal skull sutures are greatly delayed in closing. The metopic suture may persist throughout life although in normal patients it closes in the first weeks of life. Wormian bones commonly develop from secondary centers within the suture membranes (Fig. 13.14b).

The clavicle arises from three separate ossification centers, and any or all of them may fail to form in this disease. Thus, there is great variation in the development of the clavicle (Figs. 13.13b and 13.14a). In a small percentage of cases it is absent entirely. The scapula is small and often winged. These abnormalities allow great mobility of the shoulders (Fig. 13.13a). One or both sides may be involved. In the latter instance the patient may be able to approximate the shoulders until the tips of the acromial processes touch beneath his chin.

The pelvis (Fig. 13.15) is underdeveloped and opens anteriorly with muscular contractions causing extrophy of the bladder. The pubic symphysis often fails to fuse. The sacrum

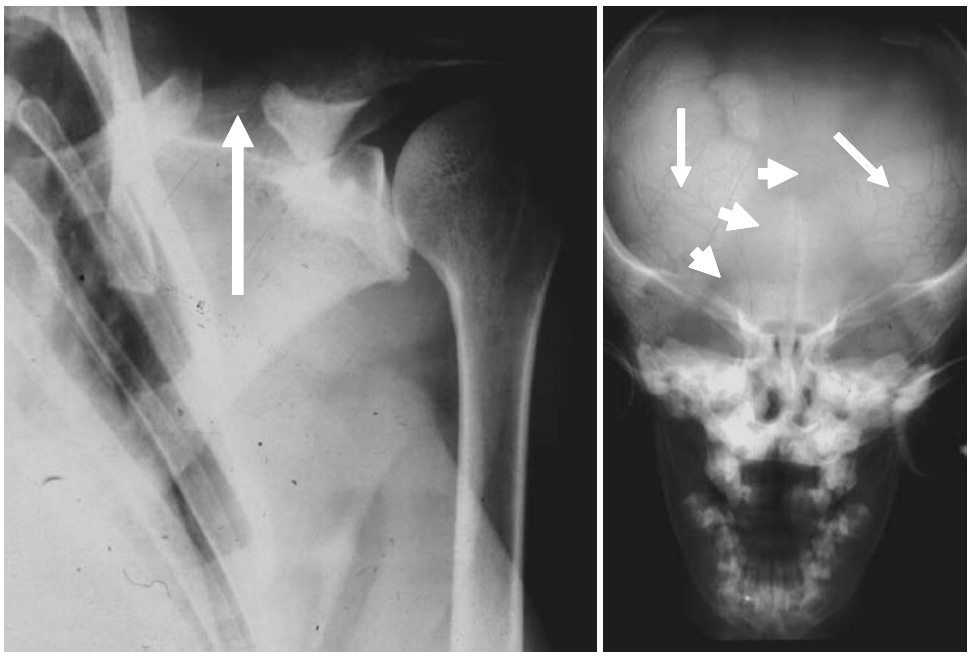

Fig. 13.14 Cleidocraniopubic dysplasia. **a**: AP shoulder radiograph shows absence of the middle portion of the left clavicle (*long arrow*). **b** The skull of a 6-month-old baby shows widely patent sutures and anterior fontanelle (*short arrows*) as well as numerous ossification centers, the Wormian bones (*arrows*)

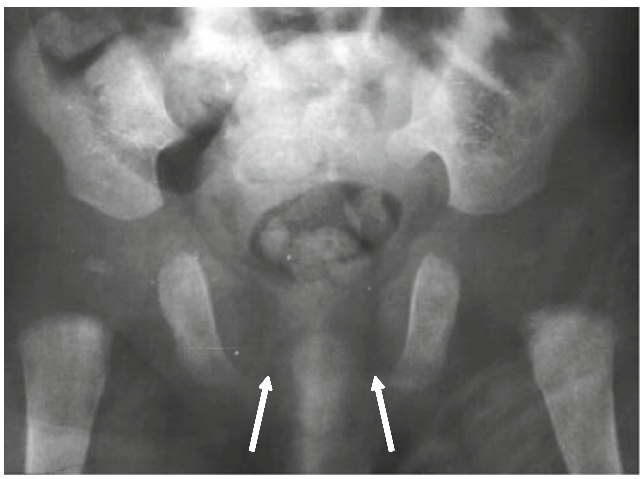

Fig. 13.15 Cleidocraniopubic dysplasia. This is the same patient as in Fig. 13.14b. The pelvis in this 6-month-old baby shows that the pubic bones are not ossified, consistent with failure of midline ossification seen in this disease (*arrows*). The proximal epiphyseal centers of the femurs are tiny

and coccyx are poorly formed; the latter is sometimes absent. The large bones of the arm are less frequently involved but occasionally the radius fails to attain proper length, causing abduction of the wrist.

The neck of the femur may be deformed resulting in coxa vara. Poorly developed vertebrae with fusion defects of the spinous processes and laminae may cause lordosis, scoliosis, or kyphosis.

There is marked disturbance in formation of the teeth. The deciduous teeth are usually normal though often delayed in eruption. Patients may have multiple supernumerary teeth.

Disturbance in dentition and difficulties in gait from femoral neck deformity are the commonest causes of clinical complaint. Persistence of sutures and the absence of normal clavicles causes little or no disability.

Craniostenosis Syndromes and Other Cranial Ossification Disorders

Group 30 of 2006 revision of Nosology and Classification of Genetic Skeletal Disorders includes 16 entities with craniosynostosis or other cranial dysostoses [1].

Apert Syndrome (Acrocephalosyndactylism MIM 101200) Group 30

This is an uncommon, congenital disturbance in the growth of bone and soft tissue affecting, as the name suggests, the head, the hands, and the feet. The

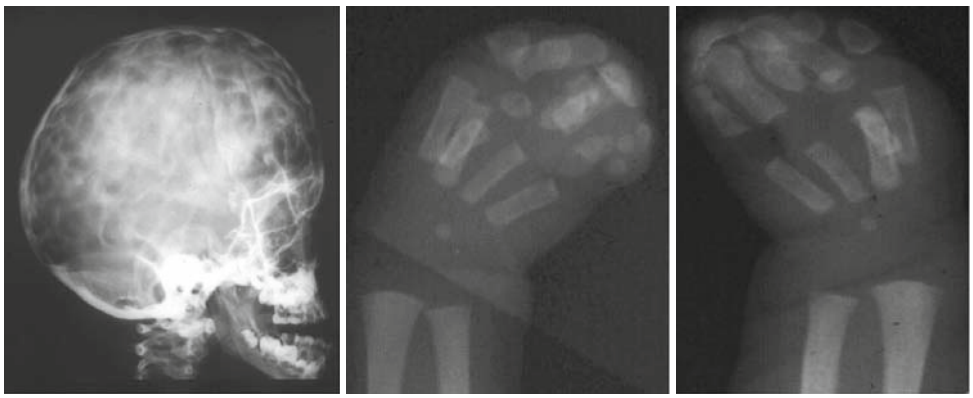

Fig. 13.16 Craniostenosis (Apert syndrome). (**a**) is a lateral radiograph revealing decreased AP diameter and increased height of the skull. The cranial vault is more convex than normal. This results from earlier premature closure of the coronal and lambdoidal sutures relative to the sagittal suture (craniostenosis). The skull is decreased in size (acrocephaly). The term turricephaly may be used for the appearance of the skull in this case. The convolutional markings are very prominent secondary to increased intracranial pressure, caused by the enlarging brain. The plains of the face and back of the skull are parallel. **b** and **c** PA radiographs of both hands show syndactyly, in this case, of all digits of both hands, hence the name "acrocephalosyndactyly"

prevalence of Apert syndrome is reported as15.5 in 1,000,000 births [7].

The head is vertically elongated and peaked, but short in AP diameter, the highest point varying between the anterior and posterior fontanelles (Fig. 13.16a). The dome slopes sharply, front and back. The face is usually considerably widened. The planes of the face and the back of the skull, which is often flush with the neck, are flattened and remarkably parallel.

The cause of this malformation is premature synostosis of the cranial bones. Impaired mental development is reported in a few cases. In some instances hydrocephalus develops. Increased intracranial pressure may cause disturbance in vision, one of the outstanding symptoms of the condition. The eyes are displaced forward so that their transverse axes diverge and slant downward. Patients often complain of strabismus.

Fusion defects occur in the maxilla, mandible, and posterior palate, which may be narrow and high-vaulted. The teeth do not develop normally. The mandible has been reported to be prognathic in some cases and recessive in others.

Syndactylism is the other prominent feature of the syndrome (Fig. 13.16b, c). It may be complete or partial, typically between metacarpals and between metatarsals. Synostoses between the phalanges of different digits may occur, and there may be failure of interphalangeal joint formation in some digits. Similar syndromes have been described, including Pfeiffer and Carpenter syndrome. These have varying degrees of digital involvement.

Progressive Diaphyseal Dysplasia (Camurati–Engelmann Disease) (MIM 131300) Group 23

In 1922 Camurati and later in 1929 Engelmann described a condition with pain in the extremities and thickening of the diaphyseal cortices in the long bones that progressed over time. Ribbing in 1949 described very similar alterations in the skeletons of four siblings under the title of hereditary multiple diaphyseal sclerosis, believing it to be a different entity, but his patients represented Camurati–Engelmann disease (progressive diaphyseal dysplasia).

Children with Camurati–Engelmann disease often present with a shuffling or waddling gait. Movement, in some cases, causes pain, and there may be periods when the limbs are tender. Typically, the musculature is underdeveloped, likely from lack of activity. The muscles are small, flabby, and weak (Fig. 13.17a). The disease usually first involves the femur and tibia. The mid-diaphyseal cortices thicken both endosteally and periosteally [7]. Over time, the cortical thickening progresses toward the metaphyses. The disease spreads to involve not only the long and short tubular bones, but also the flat bones of the trunk, skull, and face (Figs. 13.17b, c and 13.18a, b). The long bones become mildly fusiform as their diaphyses thicken (Fig. 13.18a). Multiple areas of gross cortical thickening appear in many of the flat bones.

The head enlarges and develops prominent frontal bossing. The cranial bones are thick and dense. This is most pronounced in the base of the skull. Neurological symptoms develop from foraminal stenosis that leads to cranial

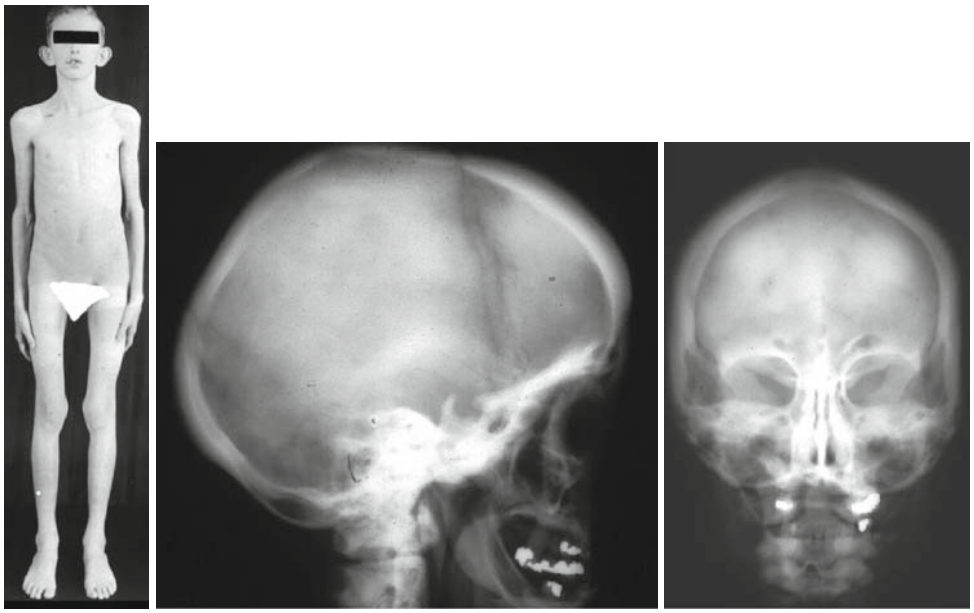

Fig. 13.17 Diaphyseal dysplasia. **a** The long bones are elongated. There is decreased muscle mass and subcutaneous fat. **b** and **c** are radiographs of another patient, a 32-year-old woman, with the disease. The calvarium shows thickening and increased density of bones, which appear denser in the base of the skull. The appearance of the skull should not be confused with osteopetrosis. Please see Fig. 13.18 (a) that shows only diaphyseal sclerosis of the humerus. The ends of humerus have normal density without failure of modeling in contrast to osteopetrosis

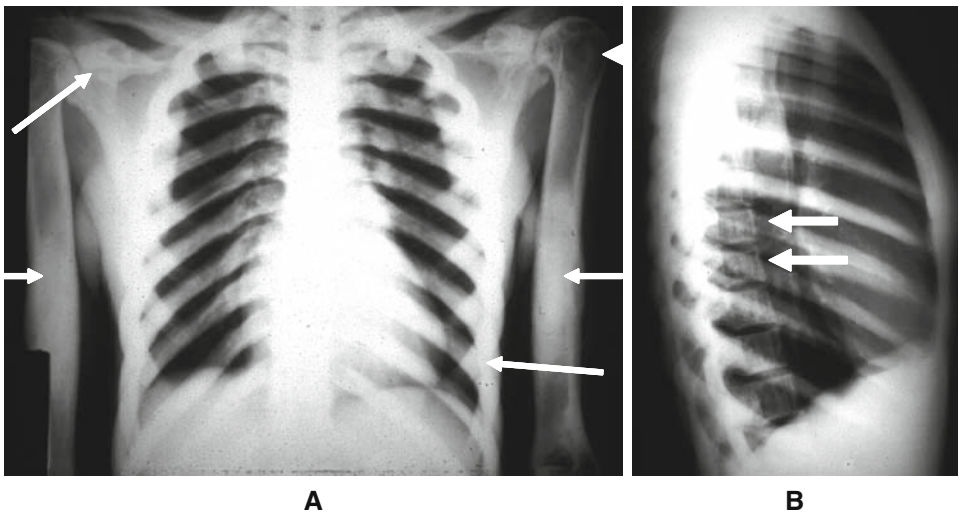

Fig. 13.18 Diaphyseal dysplasia. **a** and **b** belong to the same case as in Fig. 13.18. **a** is PA view of the chest showing increased density of the bones (*long arrows*). The humeral diaphyses show significant increased density (*short arrows*), but the humeral ends have normal density (*left arrow head*) and appearance, hence the name diaphyseal sclerosis. There is no failure of modeling of the long bones. **b**: Lateral view of the chest showing increased bone density. The vertebral bodies show characteristic coarse, dense vertical sclerotic striations (*arrows*)

nerve impingement. The spine may show dense vertical striations similar to hemangioma, but in diaphyseal dysplasia the striations are generalized and coarser than in hemangiomas (Fig. 13.18b).

Diastrophic Dysplasia (MIM 222600) Group 4

The word diastrophic derives from a Greek root meaning distorted. In this crooked dysplasia, patients have mushroom-like deformity of the ears, hitch hiker thumb, scoliosis, dislocation of knees and elbows, and club foot deformity (Fig. 13.19a, b, c, d, and e). Diastrophic dysplasia is a recessively inherited [2, 3, and 7]. It is particularly common in Finland where 1–3% of the population is a carrier. The gene responsible for diastrophic dysplasia, *DTDST*, codes for a sulfate transporter protein and has been mapped to distal end of chromosome bands 5q31-q34. Mutations in *DTDST* gene cause three other recessively inherited conditions: multiple epiphyseal dysplasia, atelosteogenesis type 2, and achondrogenesis type 1B.

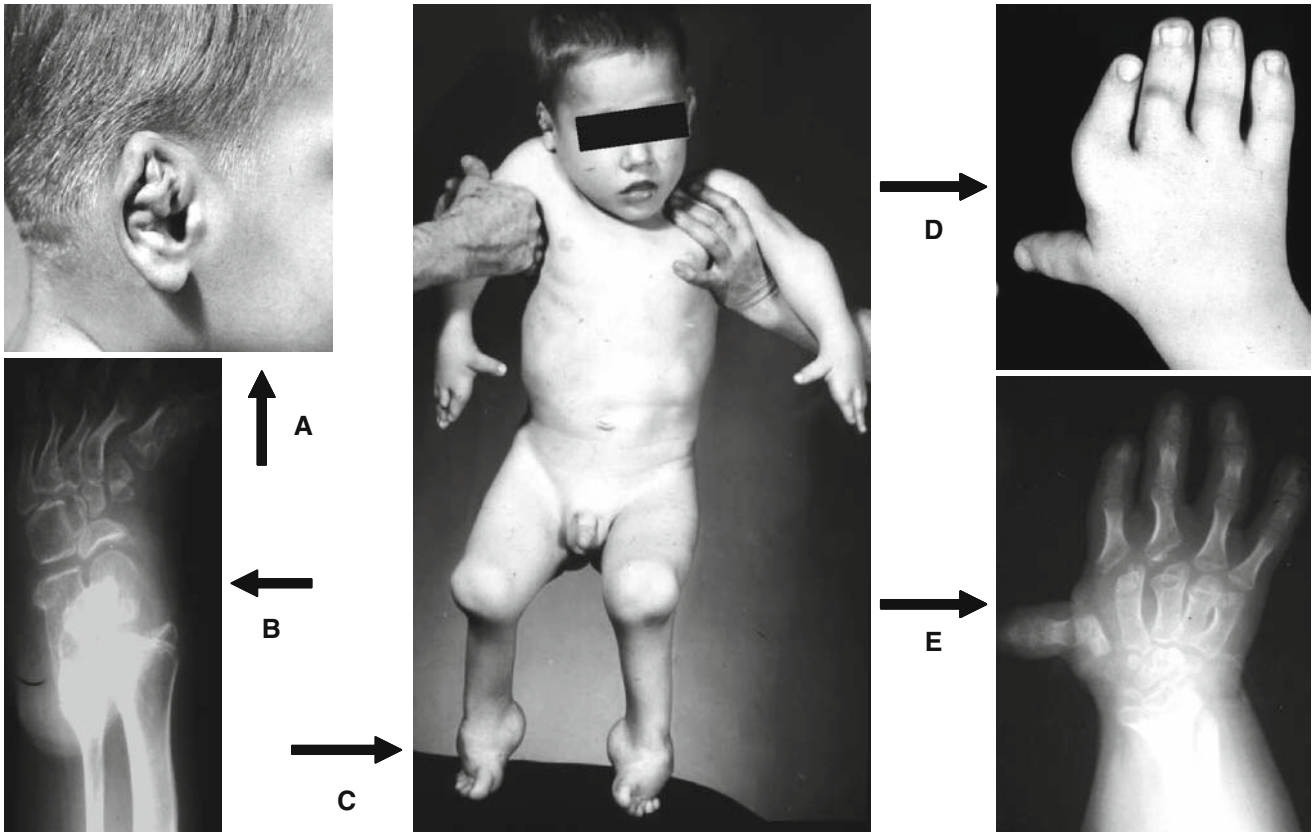

Fig. 13.19 Diastrophic dysplasia. **a** Cauliflower ear. **b** Radiograph of a club foot deformity. **c**: Picture of diastrophic dwarf. Note club feet, hitch hiker thumbs and dislocation of elbow and knees**. d** and **e** Show hitch hiker thumb

Radiological manifestations: The radiologic features of patients with diastrophic dysplasia depend in some measure on the age of the patient. If dislocations are not present at birth, they soon appear, as do flexion contractures. Similarly, the spine may be straight at birth but scoliosis or kyphosis soon develops (Fig. 13.20a, b, and c). Hypoplasia of cervical vertebral bodies has been described (Fig. 13.20c). The distance between pedicles in the lumbar spine is generally described as normal or constant throughout in contrast to the progressive narrowing described in achondroplasia.

The bones of the hands are broad and short with particular shortening of the first metacarpal so that the thumb is at a right angle to the other digits, the hitch hiker thumb (Fig. 13.19c, d and e). There is a similar deformity of the great toe and a severe equinovarus deformity (Figs. 13.19b and 13.20d). The long bones are short and broad and their epiphyseal centers flat and abnormal in shape. The appearance of the epiphyseal centers of the tubular bones of the hands and feet is delayed, but the ossification centers of the carpus and tarsus show accelerated maturation. Deformities of the hands and feet (Figs. 13.19c, d, and e and 13.20d) in association with a normal skull and vertebral bodies (until the latter becomes distorted as a consequence of scoliosis) are diagnostic of diastrophic dysplasia.

Since the underlying defect in diastrophic dysplasia is one of chondrogenesis, abnormalities occur not only in the skeletal system but other highly calcified tissues as well. The cartilage of the ear may calcify or ossify. Deficiency of tracheal cartilage results in lack of rigidity which may cause respiratory distress, particularly in infants.

Dysplasia Epiphysealis Hemimelica (Trevor disease) MIM 127800, Group 28

This disturbance of normal bone growth gives rise to ossified protrusions, resembling osteochondromas, from the margin of long bone epiphyses [2] (Fig. 13.21). No hereditary factor has been demonstrated [3, 1]. This dysplasia often affects only a single epiphysis, most commonly the talus, the distal femoral and the proximal tibial epiphyses, in that order of frequency.

The patients usually present during childhood when the protruding epiphyseal mass interferes with joint function and so causes symptoms. Patients may develop a leg length discrepancy because of premature closure of the affected

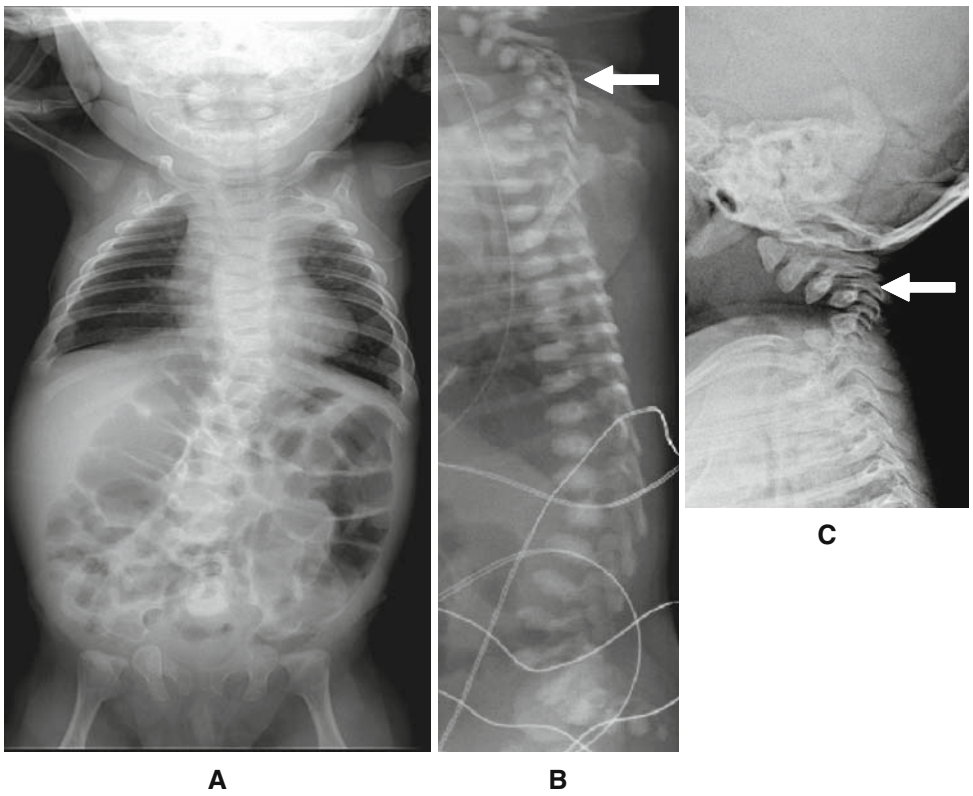

Fig. 13.20 Diastrophic dysplasia. **a** and **b** are AP and lateral views of the thoracolumbar and **c** is the lateral view of the cervical spine. Moderate levoscoliosis of the thoracolumbar and minimal dextroscoliosis of the lumbar spine are present. Marked kyphosis of the cervicothoracic spine is seen (*arrows*). Courtesy of Dr Leslie Grissom, DuPont Institute, Wilmington, Delaware

physeal plate causing the affected limb to be shorter than the other one.

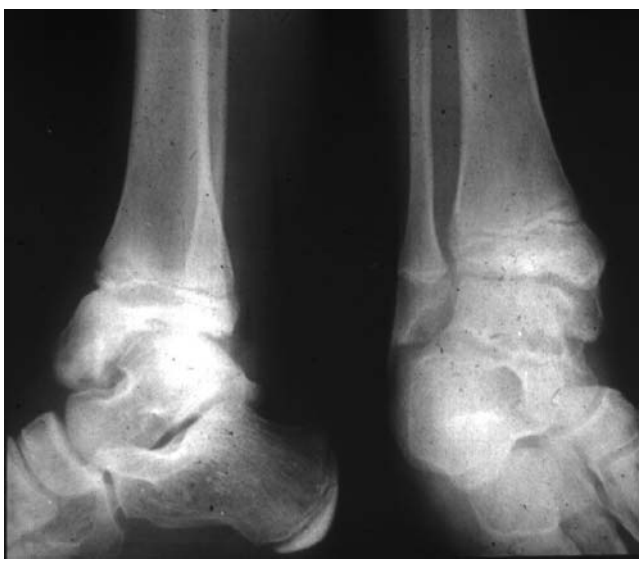

Fig. 13.21 Dysplasia Epiphysealis Hemimelica (Trevor disease). AP and lateral radiographs of the ankle show significant hypertrophy of the medial malleolus

Enchondromatosis (Ollier Disease), MIM 166000, Group 28

Enchondromatosis or "Ollier disease" designates those cases in which there are multiple enchondromas entirely or predominantly in one side of the skeleton (Fig. 13.22a). It is essentially a hamartomatous proliferation of cartilage cells within the metaphyses of several bones, causing thinning of the overlying cortices and distortion of length growth. The lesions may be observed at birth. Maffucci reported an association of enchondromatosis and multiple cavernous hemangiomas, now known as "Maffucci Syndrome."

In the more florid instances of enchondromatosis an obvious impairment of bone growth becomes apparent, usually seen as unequal growth of the lower extremities. If the enchondromas grow aggressively, the overlying cortex may be thinned and "expanded" producing characteristic "trumpeting." The cortex may be weakened to the point of

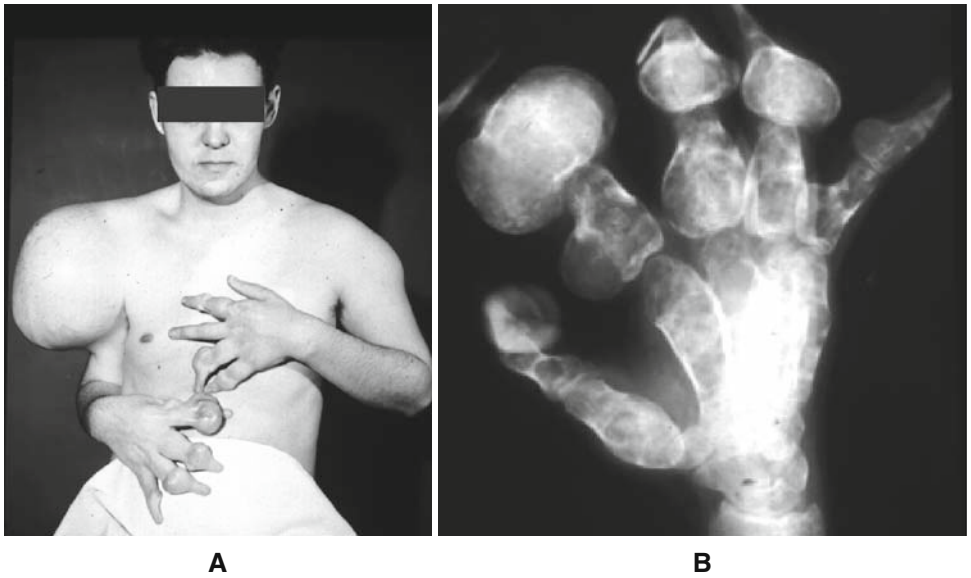

Fig. 13.22 Enchondromatosis. **a** Picture shows bilateral, but asymmetrical involvement of the bones. **b** Radiograph of the right hand shows non-uniform density of the bones related to enchondromas, in some areas resembling the ground glass appearance of fibrous dysplasia with increased girth of bones that is most marked in the middle and proximal phalanges of the second, third, and fourth fingers. Endosteal scalloping is noted in several bones. There is no cortical destruction or periosteal reaction to indicate malignancy

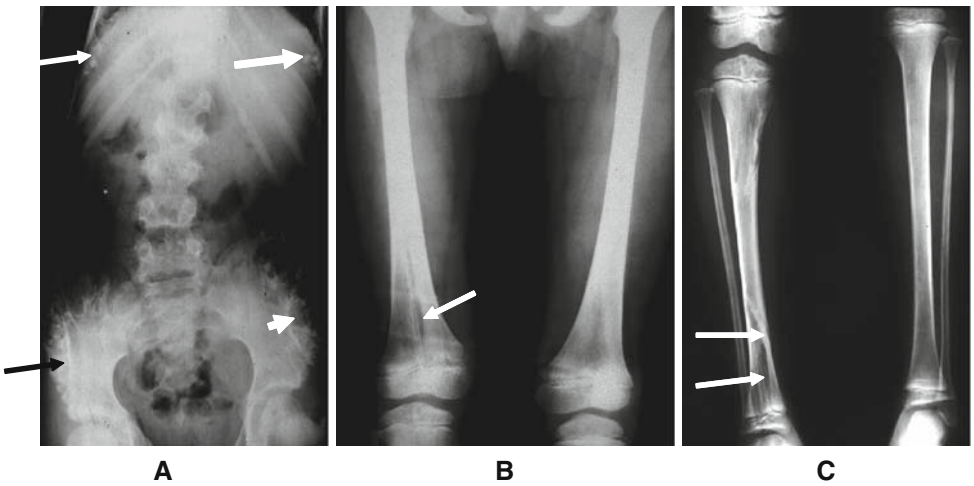

Fig. 13.23 Enchondromatosis. **a** AP view of the abdomen shows asymmetrical extensive involvement of the flat bones of the pelvis, and the lower ribs, L5 (*arrows*) shows spotty calcifications. The enchondroma in the left iliac bone is similar to fibrous dysplasia (*arrow head*). **b** and **c** show only right sided involvement. The longitudinal metaphyseal radiolucencies in the right femur and tibia should not be confused with osteopathia striata, in which longitudinal striations are dense and not radiolucent

pathologic fracture, in some cases this is the initial symptom of the disease. Pain is rare unless fracture has occurred or unless growth of a lesion reactivates in later life, a sign of malignant transformation.

Metachondromatosis is similar to enchondromatosis, but both enchondromas and osteochondromas are present. Unlike typical osteochondromas, those in metachondromatosis cluster in the hands and feet and tend to point toward rather than away from the adjacent joint [3].

Radiological manifestations: Enchondromas are radiolucent, sometimes with popcorn calcifications that tend to become more prominent in older patients. The lesions of enchondromatosis may be globular and expand bone, particularly the small bones of the hands and feet (Fig. 13.22b). In long bones, the lesions involve the metaphysis and extend into the diaphysis. The most rapidly growing ends of the long bones seem to be most affected. The involved long bone is apt to be short, and in the area of the lesion, broad and often bowed. The epiphyses are spared and involvement of the spine and skull is uncommon. Flat bones and ribs are often involved (Fig. 13.23a).

At times, the only manifestation of Ollier disease may be the presence of narrow, radiolucent, longitudinal streaks extending into the shaft from the metaphysis. This type of enchondromatosis, at first glance, may be confused with osteopathia striata. In osteopathia striata dense longitudinal densities are present, but in enchondromatosis longitudinal changes are radiolucent (Figs. 13.23b, c and 13.67).

Malignant transformation of enchondromas may be difficult to recognize. The presence of cortical destruction and periosteal reaction is indicative of malignancy. Malignant transformation in Maffucci syndrome is higher than enchondromatosis and has been repoterted to be between 20% to 30% [9, 10].

Spotty calcification in enchondromas must be differentiated from calcified medullary (diaphyseal) bone infarcts. Infarcts often reveal a bone-within-the-bone appearance. Calcified infarctions are non-continuous and give the impression of rotten pipes, but enchondromatous calcifications have a spotty or popcorn appearance and sometimes the calcifications can be counted.

Prognosis: The patient with enchondromatosis stands a substantially greater chance of developing a malignant cartilaginous tumor than the normal individual. Therefore, all known lesions should be periodically surveyed and any reactivation of growth in adult life should be regarded as malignant neoplasm until proven otherwise. Painful lesions without trauma must be approached in the same manner. The incidence of malignancy has been reported to be between 5% to 30% of cases [14].

Endosteal Hyperostosis, Hyperostosis Corticalis Generalisata (MIM 239100, Van Buchem Type) (MIM 144750, Worth type) (MIM 269500, Sclerosteosis) Group 23

In 1955 Van Buchem and Hadders described what they believed to be a new pathologic entity and called it "hyperostosis corticalis generalisata," in which the diaphyseal cortices of the long bones are uniformly thickened. In 1962 Van Buchem and colleagues reported seven additional cases [7]. The condition, now generally referred to as Van Buchem disease, is inherited as an autosomal recessive [1, 2]. Throughout skeleton the diaphyseal cortices are wide; the cortices of the ribs and clavicles are thick. There is a dramatic sclerosis of the skull and mandible with pressure effect on emerging nerves leading to facial paralysis, deafness, and blindness. The serum alkaline phosphatase is elevated [2].

Worth disease is similar to Van Buchem disease except that it is inherited as an autosomal dominant; the sclerosis is generally less impressive and the patients do not develop neural foraminal stenosis. The jaw is markedly prognathic and patients generally have a torus palatinus. This disease is prominent among Afrikaners in South Africa.

Sclerosteosis occurs in Afrikaners, but similar to Van Buchem disease, is inherited as an autosomal recessive. The phenotype is very similar to Van Buchem disease in that the bone sclerosis is marked and patients develop severe neuroforaminal encroachment. In distinction from Van Buchem disease, patients with sclerosteosis have syndactyly of the second and third fingers from birth [3].

Fibrodysplasia Ossificans Progressiva (Myositis Ossificans Progressiva MIM 135100) Group 28

Fibrodysplasia ossificans progressiva (FOP), previously known as myositis ossificans progressiva (MOP) is a rare, inherited disorder of connective tissue that causes a variety of skeletal and extraskeletal abnormalities (Fig. 13.25). These can be detected radiographically.

Typically FOP presents in the first few years of life (nearly 50% by age 2). FOP is characterized both by progressive ossification of connective tissue and muscle and by digital anomalies. All striated muscles are involved except those in the middle ear, the tongue, the diaphragm, and the heart. Almost all patients have microdactyly of the great toes and/or hallux valgus (Fig. 13.26d). Short thumbs are the next most commonly reported digital anomaly. The presence of anomalies of either the great toe or thumb is considered essential for diagnosis by some authors [11].

Initially, patients develop doughy, soft-tissue nodules. Often, there is an association between the development of the soft tissue lesions and trauma. Early nodules commonly arise in the neck and cause torticollis. The nodules resolve in a few days, leaving a doughy area that may either resolve entirely or may ossify over the following few months. Characteristically the course is one of remission and relapse with development of nodular swellings and progressive ossification of muscle and connective tissues.

The ectopic ossification in this disease may bring to mind a variety of conditions including traumatic myositis ossificans (Fig. 13.24) and heterotopic ossification of paraplegia.

The progressive ossification caused by FOP decreases the patients' mobility, making them almost living pillars of stone [11] (Figs. 13.25 and 13.26). Fusion of the posterior neural arches of the cervical spine may be seen in FOP and should not be confused with cervical changes in chronic juvenile arthritis and Klippel-Feil syndrome. No ossified fibrodysplastic changes are present in these two other entities.

Fibrous Dysplasis (Polyostotic Form MIM 174800) Group 28

It appears that this condition was first recognized as an entity in 1922 when Weil reported it in German literature. Since then fibrous dysplasia has been reported under different names by multiple authors. In 1938, Lichtenstein pro-

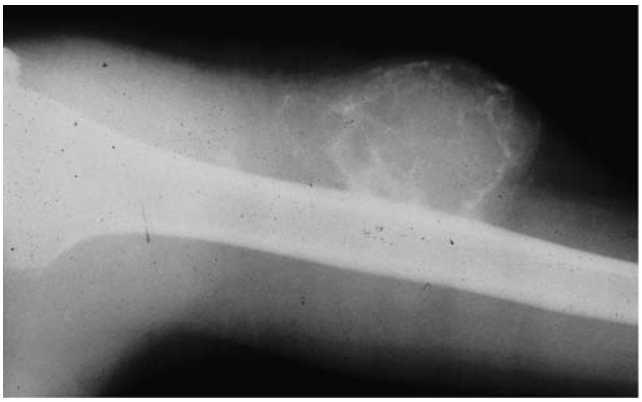

Fig. 13.24 Traumatic myositis ossificans of the left upper arm. Note juxtacortical heterotopic ossification with mainly peripheral ossification. This is in contrast to parosteal osteosarcoma that typically has an irregular contour and disorganized central calcification and/or ossification

posed the name "fibrous dysplasia" or "polyostotic fibrous dysplasia" when multiple bones are involved.

Fibrous dysplasia of bone is a disturbance in postnatal cancellous bone maintenance. Normal bone undergoing physiologic lysis is replaced by an abnormal proliferation of fibrous tissue. The process is therefore slow to develop, frequently requiring years to produce clinical lesions or cause cortical weakening. Since the inability to produce normal bone involves only the cancellous and never intramembranous bone formation, fibrous dysplasia thins the cortex from within, but the bones are always covered with a shell, however thin, of normal adult compacta [2].

Skeletal involvement in fibrous dysplasia is predominantly unilateral (Fig. 13.27a, b). All types of bones are affected though there is a slight predilection for the large bones of the extremities. Fibrous dysplasia is apt to begin in the metaphysis and progress toward the middiaphysis.

Pathologic fracture, caused by endosteal cortical thinning may bring the disease to medical attention. Osseous deformities, often involving the skull, are the second most common presenting complaint. Fibrous dysplasia may involve the orbit, causing exophthalmos, the maxilla, or the mandible (Fig. 13.27a). Pain is uncommon until osseous infractions and deformity make weight-bearing difficult.

In fibrous dysplasia about a third of cases develop pigmented, non-elevated skin patches, and they may be extensive. These lesions usually occur on the trunk, have an irregular geographic outline and vary from a few millimeters in diameter to the size of one′s palm or larger. They have a café-au-lait or chestnut color. The epidermis and underlying corium are normal in texture and consistency.

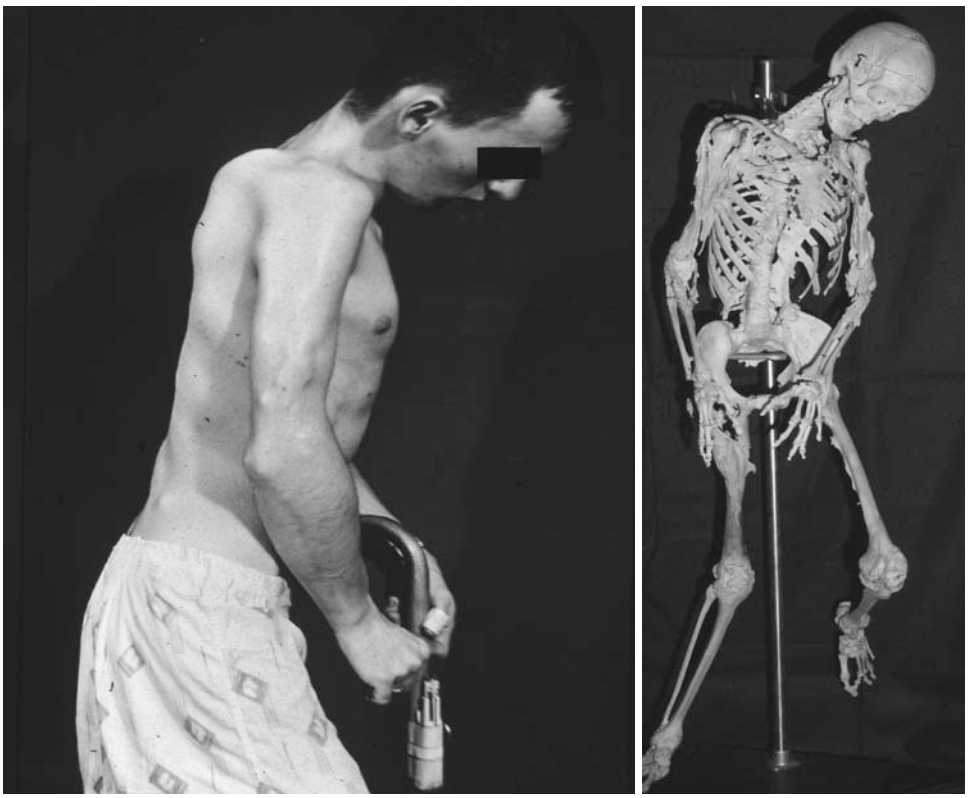

Fig. 13.25 Fibrodysplasia ossificans progressiva (FOP). **a** Photograph of a patient when the disease was moderately advanced. Note the irregular contours of the arms and back caused by ossified masses. Ossified muscles of the neck cause rigidity of the spine. **b** Skeleton of the same patient showing markedly advanced FOP

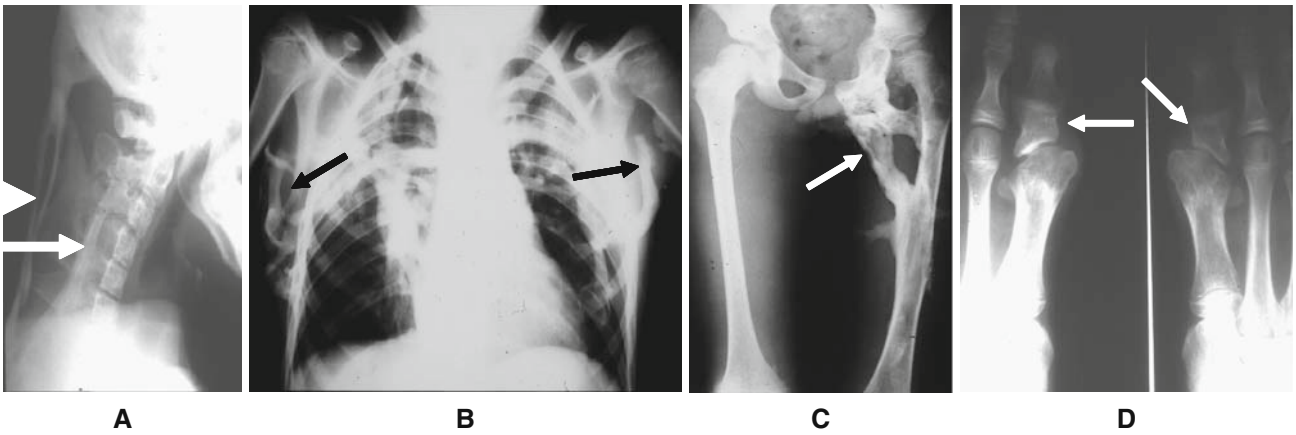

Fig. 13.26 Fibrodysplasia ossificans progressiva. **a** and **b** are the same case as Fig. 13.25 **.** Lateral radiograph of the cervical spine **a** shows soft tissue ossification extending from the occiput to the upper dorsal spine (*arrow head*). There is fusion of the facet joints and posterior arches (*arrow*). This finding simulates juvenile chronic arthritis, but calcified masses and foot abnormalities in FOP (*arrows*) in **d** help to differentiate the two entities. **b** Thorax shows pillars of ossified muscle extending to the arms (*arrows*). **c** A 10-year-old male shows progress of ossification immobilizing the joints and deforming the bones of the left pelvis and the hips (*arrow*). **d** AP radiograph shows small great toes bilaterally (microdactyly) with misshapen phalanges (*arrows*). This characteristic finding makes diagnosing FOP possible before development of soft tissue ossification

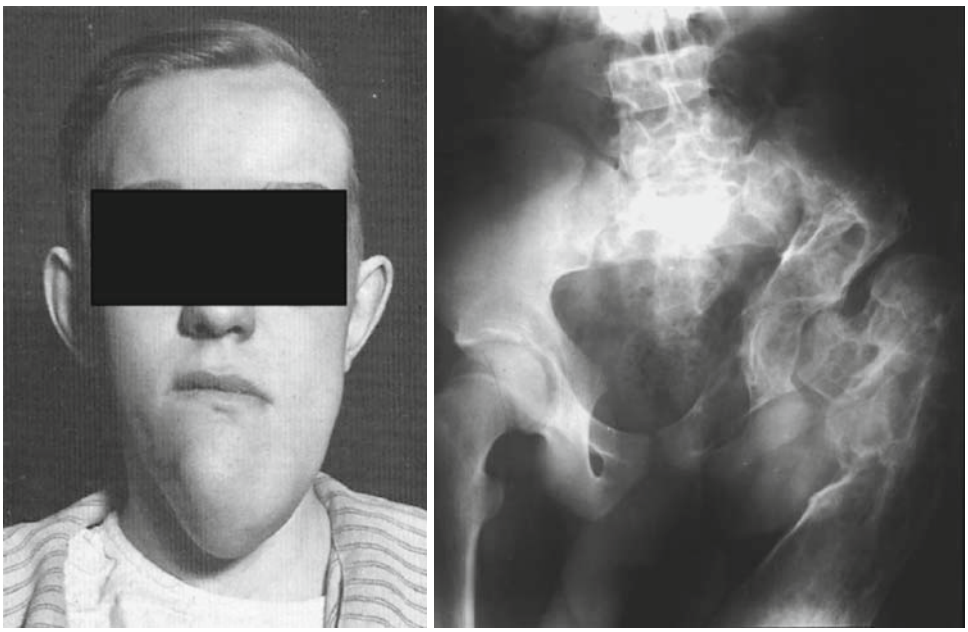

Fig. 13.27 Fibrous dysplasia. **a** Shows an asymmetric involvement. The mandible and bones of the orbit are common sites of disease. **b** AP pelvic radiograph of the same patient showing involvement of the left pelvis and left femur. The femur shows thinning of the cortex, "shepherd crook deformity" and typical "ground glass" appearance

McCune–Albright syndrome MIM (174800): McCune–Albright Syndrome includes polyostotic fibrous dysplasia, sexual precocity, and café-au-lait spots. The last are usually present at birth. Sexual precocity occurs in 50% of affected girls and is generally diagnosed by 4 years of age. Polyostotic fibrous dysplasia becomes apparent in 50% of patients by 8 years [7]. On occasion, other endocrine abnormalities such as hyperparathyroidism [12], hyperthyroidism, diabetes mellitus, and Cushing disease may be associated with this syndrome.

Mazabraud syndrome is fibrous dysplasia with intramuscular myxomas. It is more common in women.

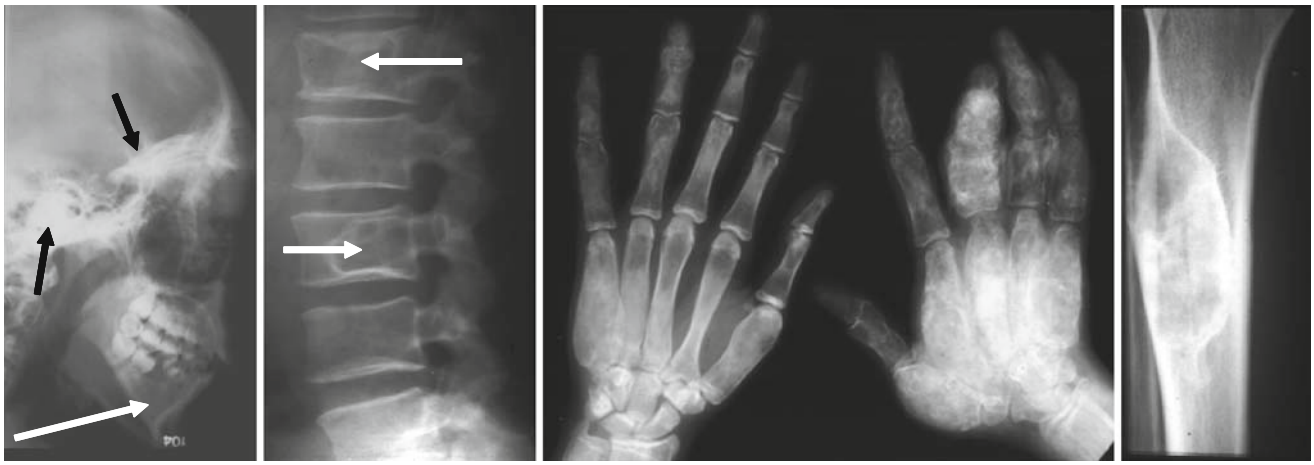

Fig. 13.28 Fibrous dysplasia. **a** The base of the skull is dense (*arrows*) Density in the sphenoid should not be confused with sphenoid ridge meningioma (*arrow*). Note mandibular enlargement (*long arrow*). **b** L1 and L3 show typical benign appearing changes. There is central decreased density with sclerotic borders. **c** Both hands are involved with foci of fibrous dysplasia. Some of these resemble enchondromatosis (compare with Fig. 13.23b). **d** The tibia shows a monostotic fibrous dysplasia with ground glass density and minimal medial expansion of the tibia. This is typical of focal disease, the lesion is sharply delineated with sclerotic borders and grand glass density

Cherubism, MIM 118400: Group 28 is fibrous dysplasia of the mandible and less commonly the maxilla. There is unilateral or bilateral painless expansion of the mandible associated with dental complications. Cherubism often undergoes spontaneous regression after puberty. In these cases residual spotty sclerotic changes remain at the site of previous involvement [7].

Radiological manifestations: The lesions of fibrous dysplasia may be radiolucent or somewhat opaque depending on the amount of irregular, microscopic masses of bone that exist within the fibrous matrix (Figs. 13.27 and 13.28). The lesions often have a "ground glass appearance." Individual lesions may not be always sharply delineated. As the process advances, lesions become lobular and scalloped in outline (Figs. 13.27b and 13.28c) and the margins become sharply defined. Even lesions that erode and expand the cortex are nevertheless covered by a layer of bone because periosteal bone formation is normal. Weight-bearing long bone deformities, including bowing and, in severe disease, telescoping are common. The proximal femur, if extensively involved, may show the so-called "shepherd crook deformity" (Fig. 13.27b). This deformity is not pathognomonic, however, since it may be also observed in other diseases such as chronic osteomyelitis and proximal focal femoral deficiency.

Manifestations of fibrous dysplasia in the cranial vault are similar to that elsewhere in the body. The base of the skull, sphenoid, ethmoid, and maxillary bones may be involved, but fibrous dysplasia in these bones may have an atypical appearance. They may show marked thickening and sclerosis that often extends superiorly into the frontal bone (Fig. 13.28a). When the base of skull is involved, fibrous dysplasia should not be confused with sphenoid ridge meningioma.

The main differential diagnosis of fibrous dysplasia is with Paget disease. Fibrous dysplasia involves medullary bone and causes thinning of the cortex (Figs. 13.27b and 13.28b). Cortical bone otherwise appears normal. There is a central relatively uniform lucency that creates a ground glass appearance with a sharp sclerotic border in the medullary cavity. In contrast, Paget disease causes cortical thickening and coarsening of the trabecular pattern. In the spine fibrous dysplasia and Paget disease both cause a picture frame appearance of vertebral bodies, but lesions of fibrous dysplasia are radiolucent. In the hands and feet, fibrous dysplasia and enchondromatosis may show a similar appearance, but other skeletal lesions help to differentiate one from the other (Fig. 13.28c).

If the lesions of fibrous dysplasia begin in early childhood are multiple and progress throughout adolescence, skeletal deformity is apt to be advanced. On the other hand, if the lesion is solitary (Fig. 13.28d) and first noted during adolescence, the patient may be virtually asymptomatic. The progress of the disease is slow and usually arrests at the time of skeletal maturation. Some lesions are detected during adulthood, often incidentally. None of these is apt to produce serious skeletal damage. Malignant transformation has been reported in fibrous dysplasia from 0.4% to 1% of cases.

Gaucher Disease (MIM 230800, 230900 and 231000)

Gaucher disease or cerebroside lipidosis clinically manifests in three types. The mode of inheritance of Gaucher disease is autosomal recessive [7, 13].

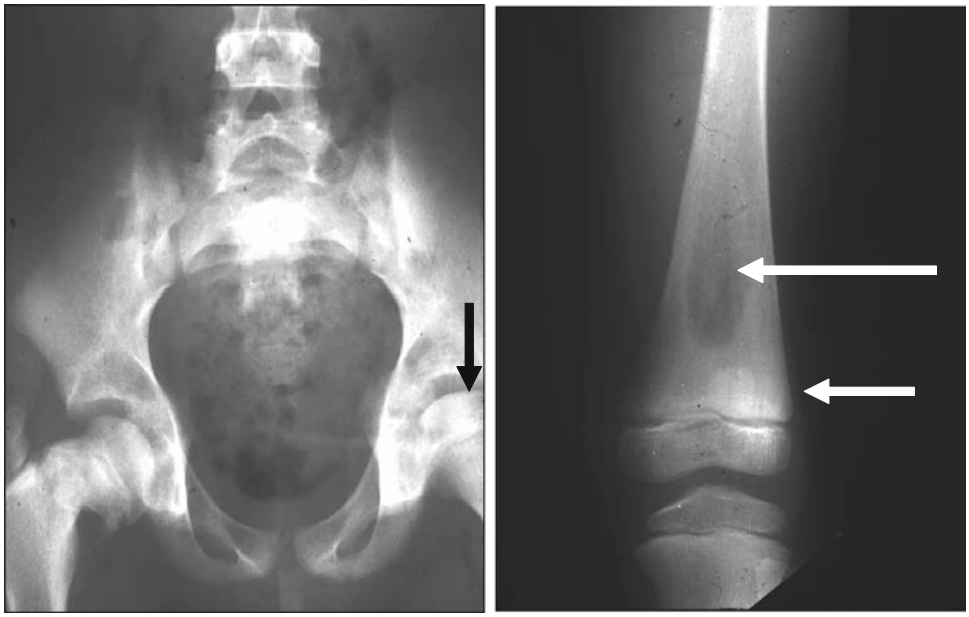

A B

Fig. 13.29 Gaucher disease. **a** The Pelvis shows early ischemic necrosis of the left proximal femoral epiphysis (*arrow*). There is a healing pathologic fracture through a lesion in the right femoral neck. **b** AP view of the left lower femur shows failure of modeling "Erlenmeyer flask deformity" of the distal femoral metaphyses (*arrow*). There is a sharply delineated lucency in the distal femoral diaphysis (*long arrow*). See Fig. 13.72a for description of bone modeling

Type 1: (MIM 230800): About 99% of cases are type 1 [7]. This type is also called "chronic non-neuropathic" or "adult Gaucher disease" and is, most common in Ashkenazic Jews, but it may be seen in non-Jewish families. In some cases, this form of Gaucher disease becomes apparent during childhood, and worsens as the patient gets older [14]. Clinically patients have skin pigmentation, bone lesion, splenomegaly, and hepatomegaly. Older patients develop a yellowish spot of proliferation on the bulbar conjunctiva near the sclerocorneal junction, usually on the nasal side (pingueculae). Aspiration biopsy of bone marrow or liver shows typical foam cells – histiocytes with cerebroside inclusions [7, 13].

Type 2: (MIM 230900): "Acute Neuropathic or infantile cerebral form." This type of Gaucher disease is rare, fatal, and has no particular ethnic predilection. Its clinical onset is shortly after birth or in the first few months of life, usually with pseudobulbar palsy. The average life span is about 1 year.

Another form of the disease, the "perinatal lethal form," has been reported, but has no MIM classification. This form, as the name indicates, is seen perinatally and is lethal [7, 15]. The perinatal period is variously defined as beginning with completion of the 20th to 28th week of gestation and ending 7–28 days after birth [16]. In the infant with Gaucher disease, visceral problems are more prominent than are osseous ones. These include hepatosplenomegaly and pulmonary infiltrates.

Type 3: (MIM231000): This type is the *subacute or juvenile form*. Patients develop hypertonicity, seizures, problems with gate, and mental retardation.

Radiological manifestations: The radiographic manifestations of Gaucher disease are variable, depending on the extent of osseous involvement, the speed with which the process progresses and the affected bone. The proliferation of Gaucher cells, the so-called "foam cells," may involve the marrow cavity of one or more bones either in a diffuse or localized manner. In either instance, the lesions are predominantly radiolucent. Any bone may be affected, but involvement of the calvarium and bones of the hands and feet is rare. Diffuse involvement of the marrow cavity results in a wide medullary canal, a thin cortex and sparse trabeculae. Diffuse femoral involvement causes failure of modeling of distal metaphysis resulting in an "Erlenmeyer flask deformity" (Fig. 13.29b). Failure of modeling is also observed in other major metaphyses where growth is active.

Focal lesions may cause localized radiolucencies in any portion of a bone (Fig. 13.29b). These may weaken bones enough to cause pathologic fracture, particularly in vertebrae and weight-bearing long bones (Fig. 13.29a). In severe or long-standing cases, patients may develop periosteal new bone and bone infarcts (Fig. 13.31). Epiphyseal osteonecrosis is common (Figs. 13.29a and 13.31b) and may cause growth disturbance in juvenile cases (Fig. 13.30).

CT, MRI, and bone scintigraphy may be used for further evaluation of these patients. MRI detects ischemic necrosis, medullary infarction, infection, and fracture in early phases of development. Scintigraphy is helpful in determining the extent and severity of marrow involvement.

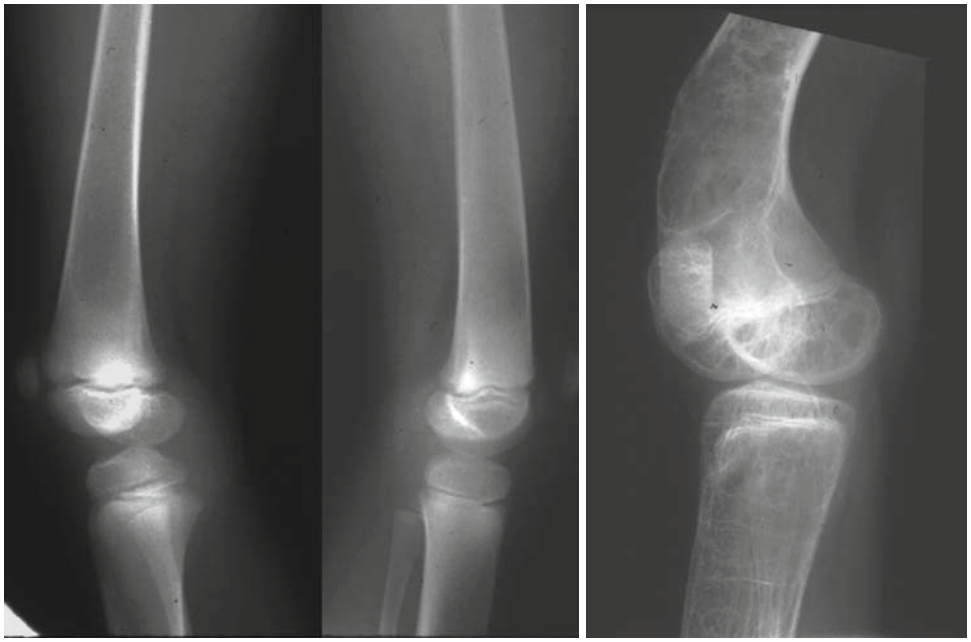

A-1970 B-1977

Fig. 13.30 Gaucher disease. **a** Shows lateral views of both knees in the same patient as in Fig. 13.29 in 1970. **b** is the lateral radiograph of the right knee in 1977 demonstrating significant progress of disease in 7 years. Note increased lucencies, thinning of the anterior cortex and bowing of the distal femur with minimal expansion. Courtesy of Dr Allen Cohen Temple University Hospital, Philadelphia, PA

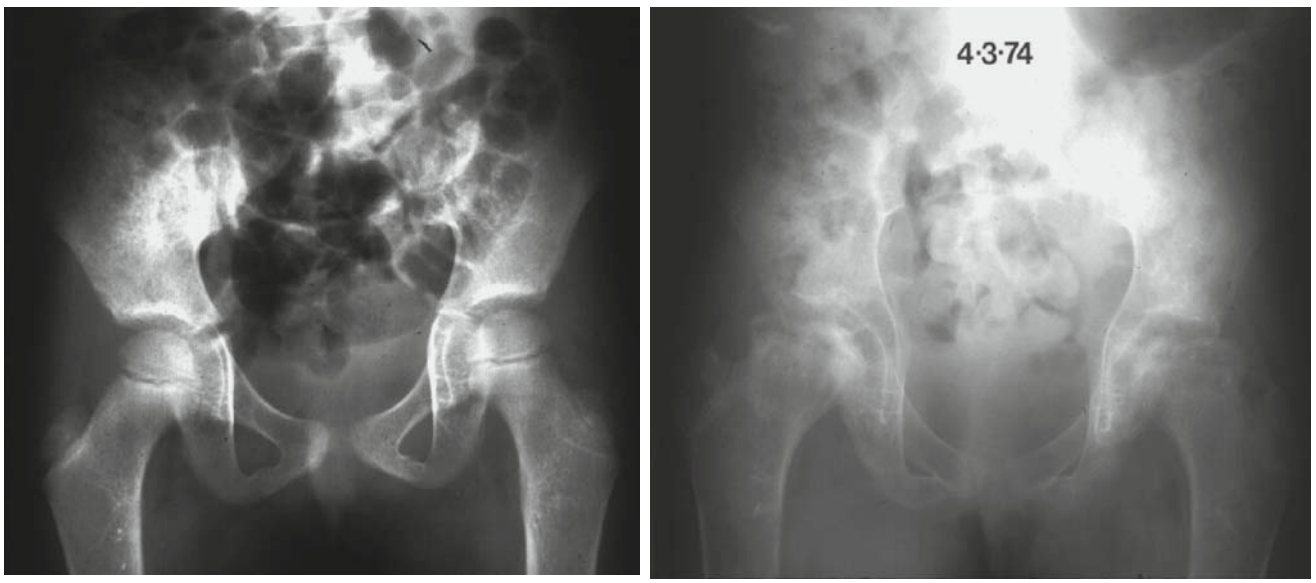

A B

Fig. 13.31 Gaucher disease. **a** AP pelvic radiograph of the cousin of patient in Figs. 13.29 and 13.30 who also had Gaucher disease. There is moderate medullary involvement causing cortical thinning. **b** Is a 4-year follow-up of the patient showing significant advancement of medullary disease and development of severe bilateral ischemic necrosis of proximal femoral epiphyses. Packing of the remaining bones by Gaucher cells is causing further cortical thinning and diminished density of bones. Courtesy of Dr Allen Cohen Temple University Hospital, Philadelphia, PA

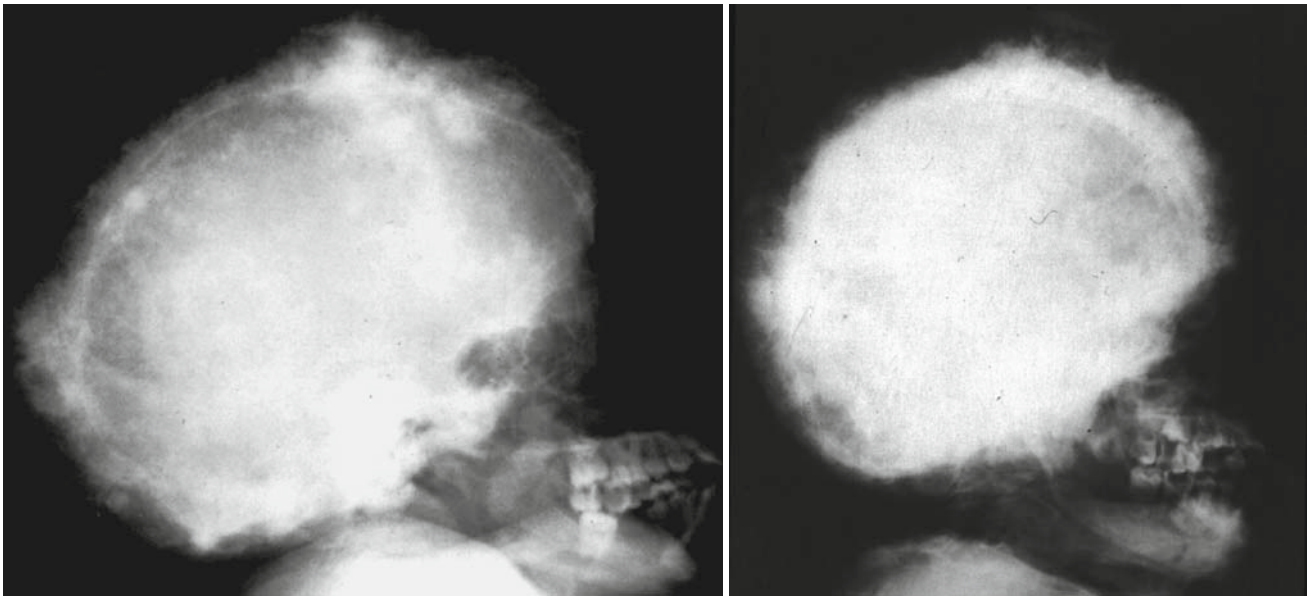

Fig. 13.32 Hyperphosphatasemia. **a** and **b** are skull radiographs of two siblings with hyperphosphatasemia: **a** is a 21-year-old sister and **b** is her 20-year-old brother. Lateral views of the skull reveal a great similarity to Paget disease (hence the name Juvenile Paget disease). Both skulls show thickening of the calvarium with non-uniform sclerotic densities (*Cotton wool appearance*). There is marked increased density of the bases as well

Hyperphosphatasemia (Juvenile Paget Disease), (MIM 239000) Group 23

Hyperphosphatasemia (osteoectasia with hyperphosphatasemia) is similar to Paget disease both radiographically and with respect to clinical biochemical markers, including markedly increased alkaline phosphatase and urinary hydroxyproline levels [17]. Typically, patients with this rare disease present in early childhood with skull deformity, refusal to bear weight, and bowing of the extremities. Notable radiographic features include bowing of the long bones, thickening of the cortex, osteopenia, coarsened trabecular pattern, expansion of the medullary cavity, and thickening of the calvarium.

Radiological manifestations: In all cases, the clinically observed enlargement of the head is related to thickening of the calvarium and widening of the diploic space with patchy regions of increased radio-density frequently described as "cotton wool appearance," resembling Paget disease (Fig. 13.32). A hair on end appearance has also been described in literature. The facial bones are variably affected. Osseous abnormalities in the spine include biconcave vertebral bodies with decreased height and scoliosis. The long bones develop a widened medullary space, (Fig. 13.33). There is progressive bowing of the long bones. The trabecular pattern is sparse and bone density in long bones is diminished [17]. Cortical thickness is variable and ranges from markedly thickened to paper thin. Transverse radiodense lines in the diaphysis are seen frequently, and are thought to represent healing infractions [17]. Subperiosteal new bone formation is frequently evident. Coxa vara and protrusio acetabulae are common. The tubular bones of the hand, ribs, scapulae, and clavicles show increased girth with areas of increased and decreased bone density.

Skeletal scintigraphy shows marked diffuse generalized radionuclide uptake. Excessive focal uptake is present in the calvaria, base of skull, spine, ribs, and pelvis. There is minimal uptake in the hands and feet, and the kidneys are barely visible, suggesting a superscan.

Hypophosphatasemia (MIM 241500, Infantile type) [1], (241510 childhood type) [7], (146300 Adult type) [1] and 171760 [3], Group 25

As the name indicates, patients with this disease are deficient in tissue non-specific alkaline phosphatase. The disease is rare with a frequency of about 1 per 100,000 births [7] and is thought to result from a mutation in the gene coding for tissue-non-specific alkaline phosphatase (ALPL).

At least six clinical forms of the disease have been described, but classification may be difficult. These forms include perinatal, infantile, juvenile, adult, and odontohypophosphatasia types as well as a related entity called

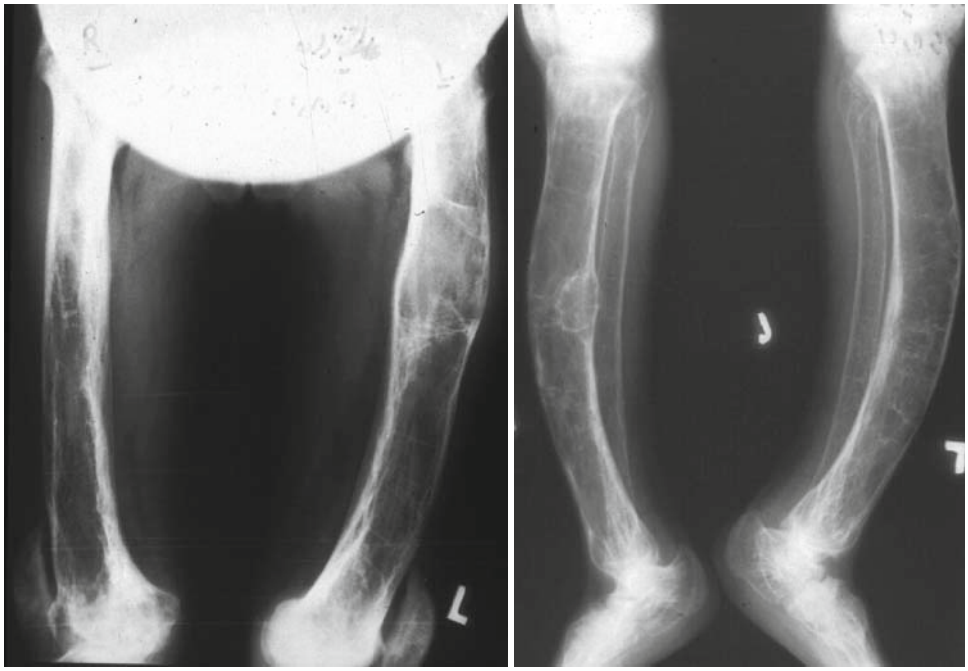

Fig. 13.33 Hyperphosphatasemia. **a** and **b** are radiographs of the femurs, tibias and fibulas of the 21-year-old sister (shown in Fig. 13.31a). They reveal increased girth of the bone (ectasia), bowing, thin cortices and areas of increased density. Increased density may be related to previously healed fractures. The patient's very young age differentiates this entity from Paget disease

pseudo-hypophosphatasia. The earlier the condition manifests itself the more severe its course is apt to be. In fact, the perinatal form is uniformly lethal. The older the patient is at the clinical onset of the disease, the better the life expectancy. The perinatal and infantile forms have autosomal recessive inheritance; the other forms are variable.

The cardinal laboratory feature of hypophosphatasia is a marked reduction in alkaline phosphatase levels in both serum and tissues. Serum calcium levels are apt to be high but fluctuate considerably. Serum phosphorus levels are elevated in about 50% of affected children and adults [3]. Another feature of this disease is excessive excretion of phosphorylethanolamine in the urine.

The perinatal form is lethal, mainly as the result of respiratory failure from poor formation of the thorax. In severe cases ultrasound studies after 14–16 weeks of gestation show failure of ossification of the fetal head and the legs that are bowed and short. At birth the cranium is globular, soft, and unossified. The skull base and facial bones also ossify poorly. The skeleton shows minimal irregular and non-uniform calcification. Some of the bones especially the short tubular bones are unossified. Numerous fractures are present and the long bones are markedly deformed.

In the infantile form, there are extensive skeletal lesions resembling the changes of classic rickets (Fig. 13.34) with severe widening of the metaphyses and fraying of their margins. Because of the inability to mineralize osteoid, there is failure of bone development in the calvarium so that in the most severe cases the brain appears to be ensheathed in a membrane (osteoid), with only small patches of ossification.

In the childhood form, surviving children have skulls similar in appearance to patients with osteogenesis imperfecta (Fig. 13.35a). The calvarium is very thin and the lambdoid suture contains multiple Wormian bones. Craniostenosis has been reported [3]. Death often results from suffocation or from respiratory infection because of a failure of ossification of the ribs.

In the juvenile form, the absence of alkaline phosphatase leads to osteomalacia and rickets. As a result these patients' radiographs resemble rickets (Fig. 13.35). The metaphyseal changes of rickets such as widening of the epiphyseal plate, paint brush appearance of the metaphysis, diminished bone density, thinning of the cortices, and bowing of the long bones are present (Fig. 13.34). In addition to these findings, radiographs tend to show a characteristic deep central triangular notch in the metaphysis projecting into the diaphysis. This notch is the easiest to see in the distal femurs and upper tibias (Fig. 13.35b).

In the adult form, bowing and pseudofractures of the long bones, calcifications of spinal ligaments and joint cartilage are present, but overall the changes are much milder and even may be overlooked entirely [3].

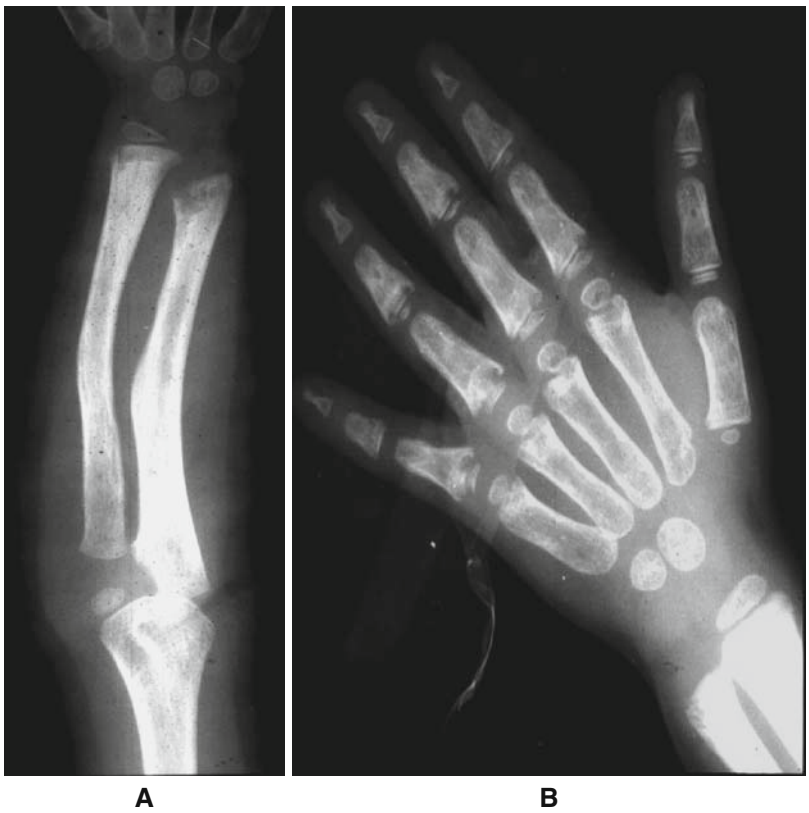

Fig. 13.34 Hypophosphatasia. This is a 3.5-year-old girl. Note indistinct zones of provisional calcification and metaphyseal lucencies. Changes are more marked in the fingers. Courtesy of Dr Parviz Eftekhari

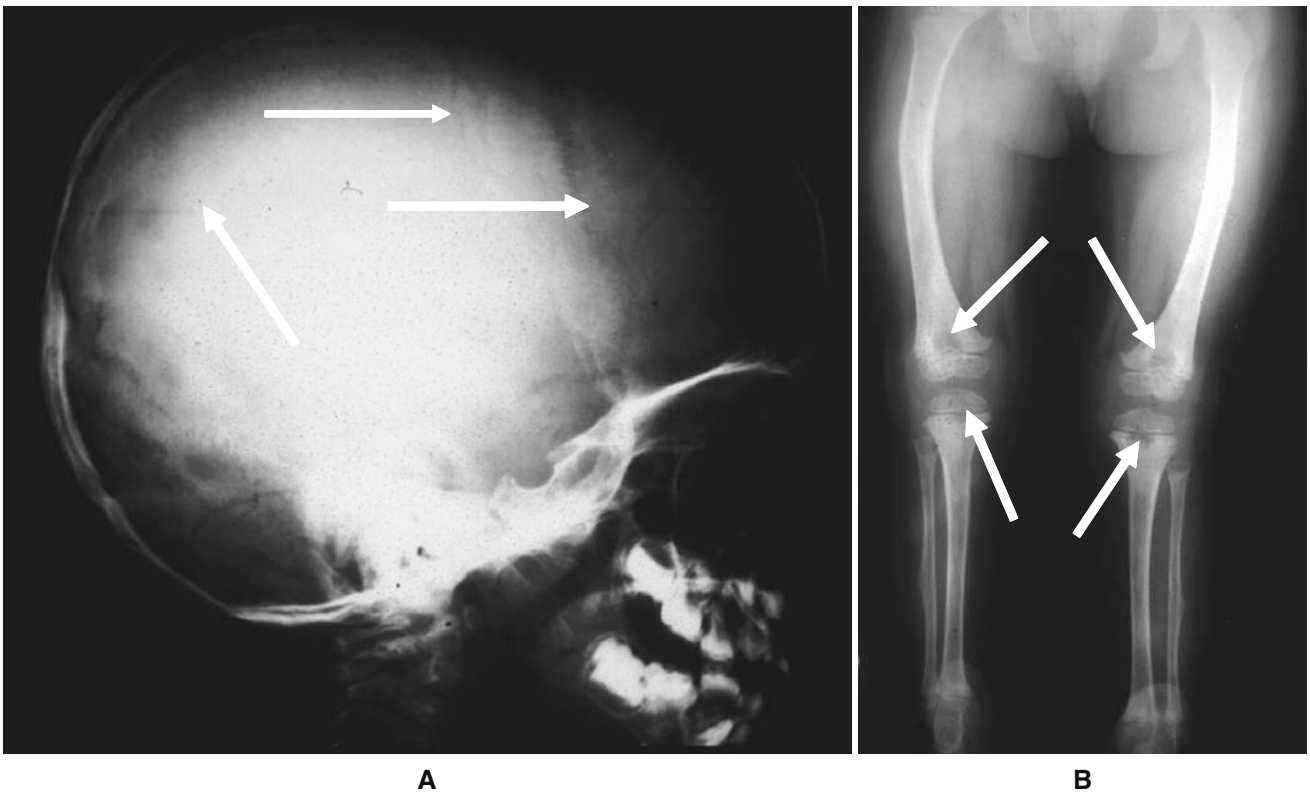

Fig. 13.35 Hypophosphatasia. This is a 3.5-year-old girl. **a** Lateral radiograph of the skull shows thinning of the calvarium and numerous wormian bones (*arrows*). **b** Shows indistinct zones of provisional calcification and radiolucent defects in the metaphyses that have a triangular appearance around the knee (*arrows*). The latter is frequently found in this disease. Laterally convex bowing of both femurs is present. Courtesy of Dr Parviz Eftekhari

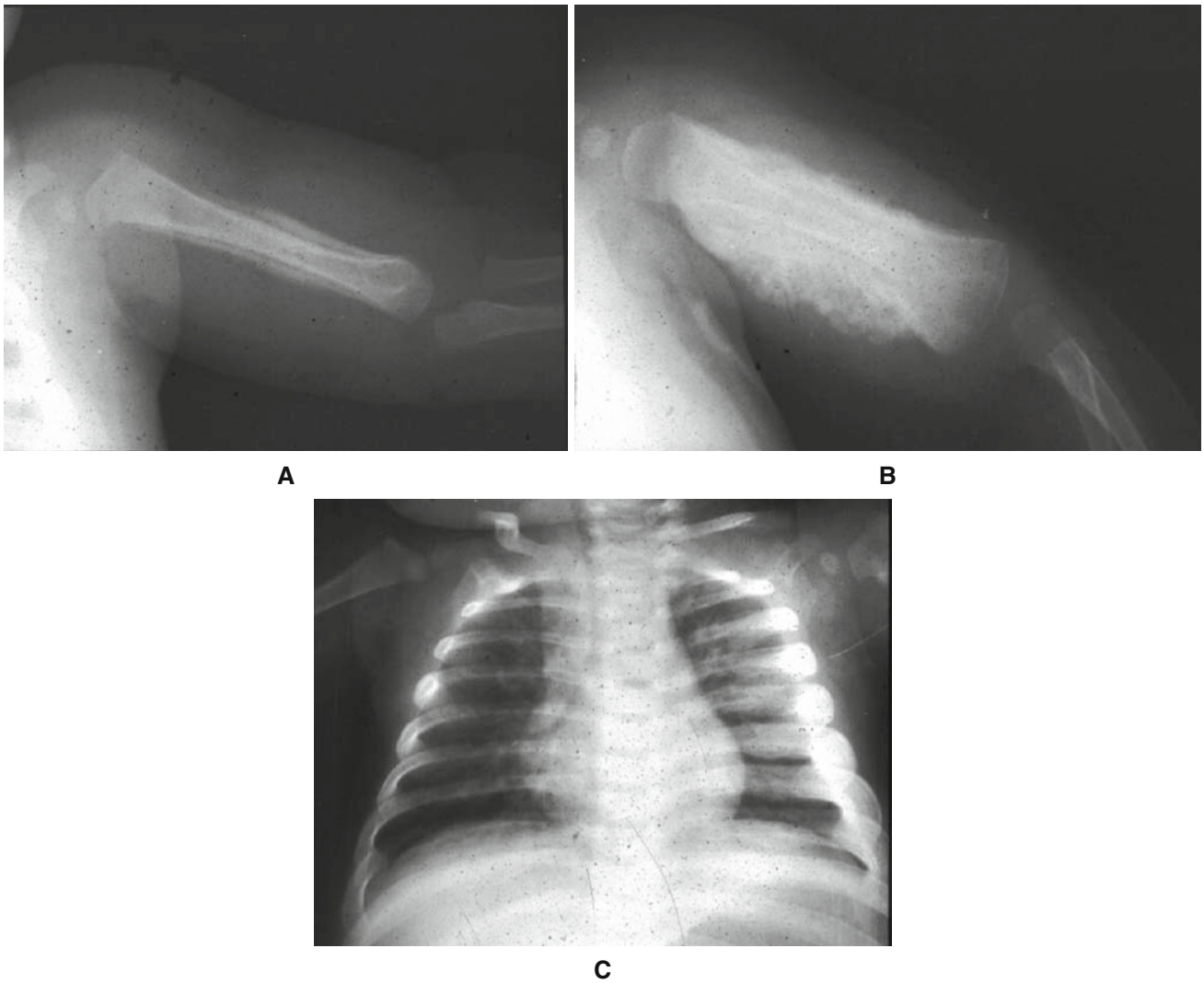

Fig. 13.36 Infantile cortical hyperostosis. *AP radiograph* **a** of the left humerus of an infant aged 11 weeks showing solid diaphyseal periosteal reaction. **b** shows the progress over 2 weeks. **c** is a chest radiograph from when **b** was made, showing marked left-sided costal periosteal reaction

Hypophosphatemic Rickets (Vitamin D Resistant Rickets, X-linked Hypophosphatemic Rickets) (MIM 307800, 193100) Group 25

X-linked hypophosphatemic rickets is discussed in detail in Chapter 2.

Infantile Cortical Hyperostosis (Caffey Disease) (MIM 114000) Group 21 (Neonatal Osteosclerotic Dysplasia)

Infantile cortical hyperostosis, at present, is extremely rare. In reported cases, the onset has been before the sixth month of life, but cases have been reported as late as 18 months. The symptoms at the onset usually resemble a systemic infection. Patients have fever, leukocytosis, and an increased erythrocyte sedimentation rate. The serum alkaline phosphatase level is elevated in most instances [2]. In a matter of days or weeks from onset of the disease, patients develop areas of soft tissue swelling over bones, particularly the mandible and clavicle, and the shafts of long bones. Ultimately, the disease is self-limited and benign.

Radiological manifestations: Radiographs of patients with infantile cortical hyperostosis show marked diaphyseal solid periosteal reaction (Fig. 13.36a). Early in the course of the process the underlying cortex is usually visible but later it blends with the surrounding newly formed bone. At this time, swelling of the surrounding soft tissues may be evident. As the process progresses, the new bone may become quite profound causing the surface of the bone to become

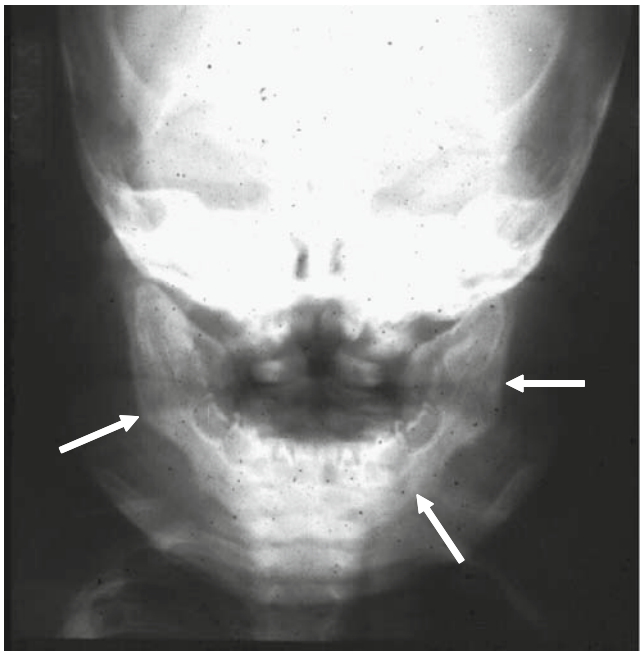

Fig. 13.37 Infantile cortical hyperostosis. This is the same patient as in Fig. 13.36. AP radiograph of the mandible at 13 weeks of age shows abundant new bone about the entire mandible (*arrows*). There is also marked swelling of the adjacent soft tissues

coarse and irregular in outline (Fig. 13.36b). The girth of the involved bones may become quite large (Fig. 13.37). Once healing commences, the involved bones show lamellation of the periosteal surface and over a period of months resume a normal contour. When involvement is severe, synostoses between the radius and ulna, tibia and fibula, and occasionally ribs may occur [2].

The differential diagnosis of Caffey disease includes hypervitaminosis A, syphilitic periostitis, trauma, and scurvy. Careful analysis of the radiographs and the history are usually adequate for differentiation. Progressive diaphyseal sclerosis (Camuratti–Engelmann), may be more difficult to exclude, but while Caffey disease usually remits the former is progressive [2].

Marfan Syndrome (MIM 154700)

Marfan syndrome is a congenital mesodermal growth disturbance that involves the musculoskeletal, cardiovascular, and ocular systems [2]. This syndrome is not included in the 2006 classification of skeletal dysplasias, but knowledge of the skeletal changes of Marfan syndrome is essential for radiologists. Patients are tall (Fig. 13.38), usually attaining a height of over 6 ft. The extremities are long and gracile.

All of the cylindrical bones are abnormally long and slender, thus producing the spider-like conformation of the hands and feet that gives rise to the name arachnodactyly. At the time of maturity hypotonicity of muscles, tendons, and ligaments may result in hypermobility of the joints with

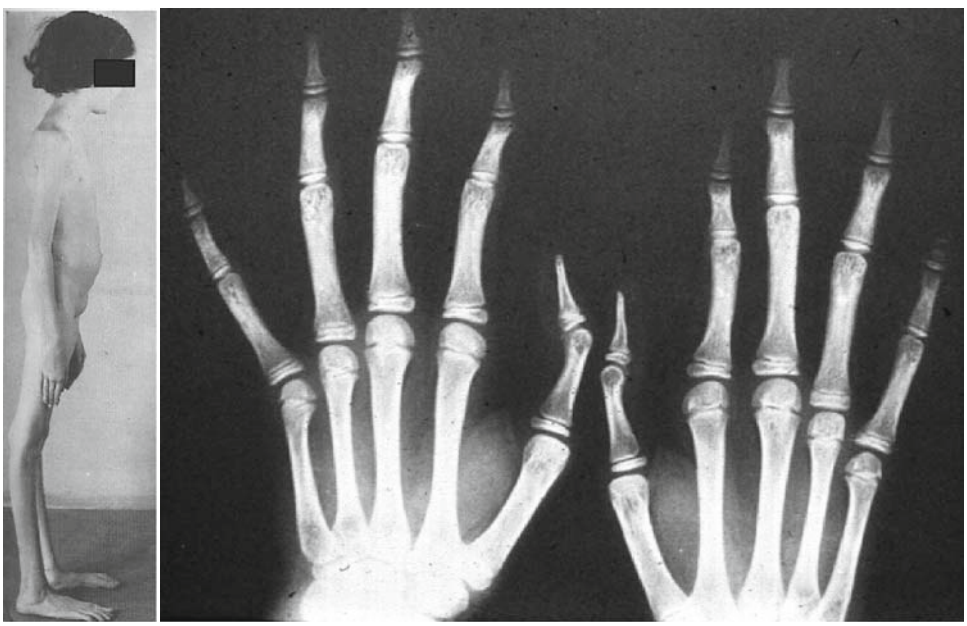

Fig. 13.38 Marfan syndrome. **a** Photograph of a patient with Marfan syndrome. Note thin and tall body habitus and the remarkably long extremities. The right hand shows long fingers. **b** PA radiographs of a patient with Marfan syndrome shows elongated metacarpals and phalanges (arachnodactyly)

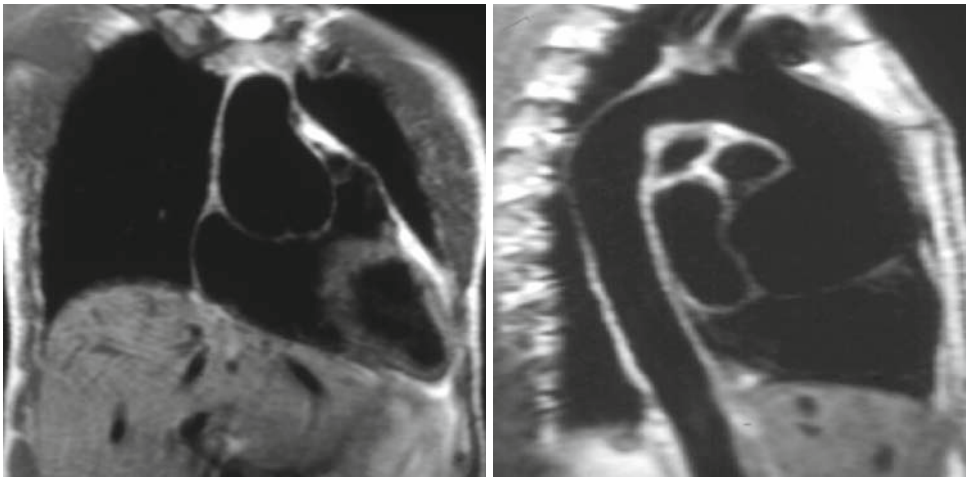

Fig. 13.39 Marfan syndrome. Sagittal and coronal T1 images from a chest MRI (**a** and **b**) show an aneurysm of the ascending aorta and coarctation of the arch. The coarctation is best seen in the sagittal image. Courtesy of Dr Richard Adams

dislocated hips, genu recurvatum, and dislocated patella and pes planes in some cases. Inguinal and diaphragmatic hernias are often present. Poor vision is a common accompaniment of this condition, usually a result of dislocation of the lens because of lax or torn suspensory ligaments.

Radiological manifestations: The bones are normal in density and architecture but are elongated, particularly the bones of the lower extremities and of the hands. The fingers and toes are slender and long giving "arachnodactyly" or spider fingers (Fig. 13.38b). Scoliosis and pectus excavatum are frequently present. Relative paucity of subcutaneous fat in the extremities is often evident. Numerous congenital anomalies have been reported in the heart, including dilatation of the ascending aorta, coarctation, aortic insufficiency and less frequently, mitral insufficiency and septal defects (Fig. 13.39).

Arachnodactyly, kyphoscoliosis, and deformities of the sternum are also present in patients with homocystinuria (Chapter 2). The clinical features differ, however, and the differential is easily made by checking for homocystine in the urine. Furthermore, patients with homocystinuria are osteoporotic and often mentally retarded while patients with Marfan Syndrome have neither osteoporosis nor mental retardation.

Melorheostosis (MIM 155950) Group 22

Incidence of melorheostosis is estimated to be 0.9 cases per million. It is often asymptomatic [7]. This disease affects both the soft tissues and the underlying bone [7]. Patients with melorheostosis most often present with chronic pain with or without swelling in adjacent joints. The pain may be difficult to localize because an entire bone or several bones may be involved simultaneously. More than three quarters of reported cases have been monomelic involving the bones of a single extremity. Occasionally, there is muscular atrophy and linear scleroderma (morphea) overlying the affected extremities. The correct diagnosis is usually made on the appearance of the radiographs.

Radiological manifestations: While the disease usually starts with focal soft tissue swelling and areas of calcification, eventually, the bones develop periosteal and/or endosteal longitudinally oriented areas of bone production. These areas appear to start proximally, progress distally along the entire length of the bone, involving bones of an extremity consecutively. The radiographs have a characteristic appearance reminiscent of melted wax flowing down the side of a candle [2, 7]. It is from this observation that the disease takes its name which translates literally to "candle bone" (Fig. 13.40).Usually the side of the pelvis or shoulder girdle corresponding to the involved limb is also affected. Involvement of one side of the mandible and maxilla has been reported. If the condition is marked and begins early, the epiphysis may close prematurely, causing shortening of the extremity. The hyperostosis may extend into the soft tissues or across a joint and interfere with motion. Circumferential bone production may compress the neurovascular bundle resulting in paresthesias or venous edema or both.

Prognosis: The abnormal bone production in this disease continues throughout the years of skeletal growth and ceases at skeletal maturation. The osseous lesions, once developed, neither progress nor regress.

Metaphyseal Dysplasia (Pyle Disease MIM 265900) (Braun–Tinschert 605946) Group 23

Metaphyseal dysplasia has two variants: Pyle disease is autosomal recessive; Braun–Tinschert is autosomal

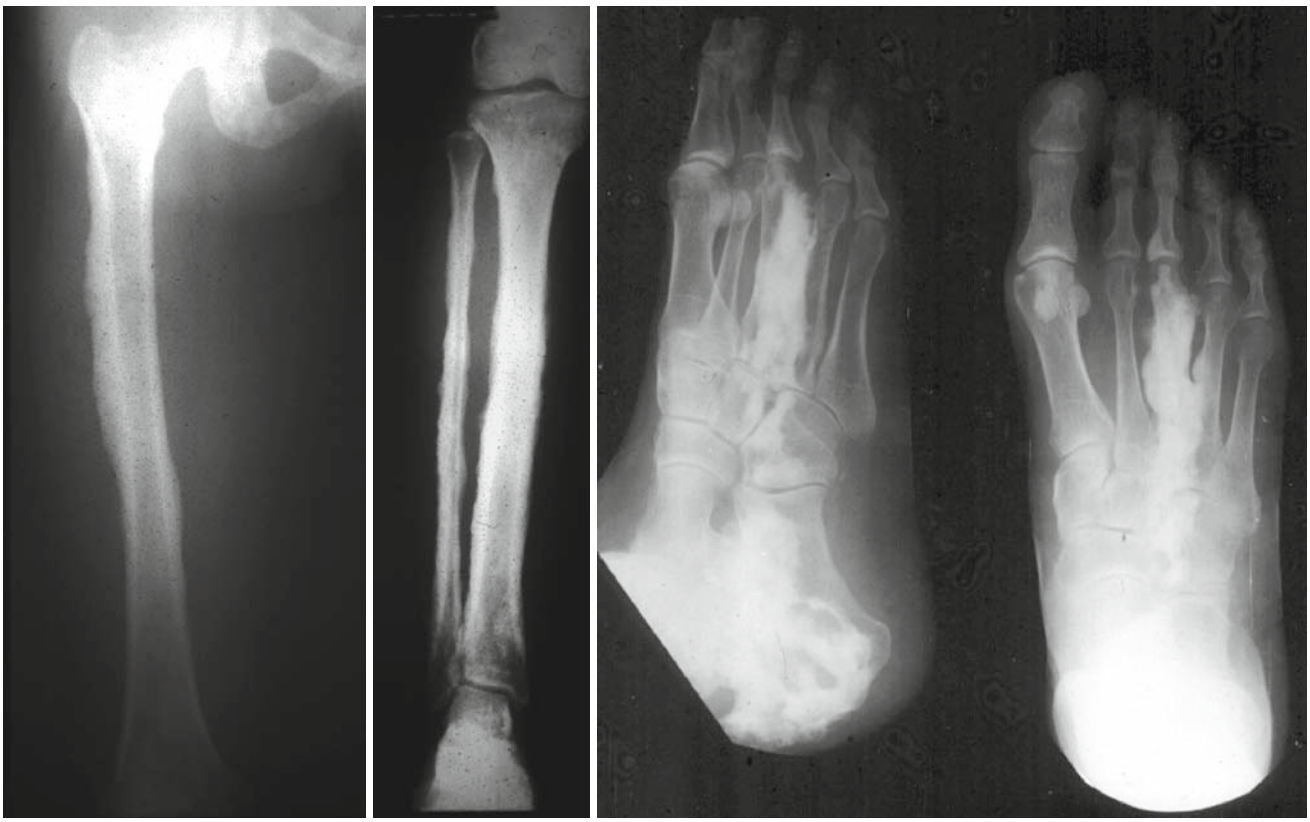

Fig. 13.40 Melorrheostosis. *AP* femur **a** and tibia **b** radiographs of a 24-year-old woman. The femur, tibia, and fibula show periosteal and to a lesser extent endosteal cortical thickening, similar to flowing candle wax. **c** Foot radiographs of a different patient showing marked increased density of the third metatarsal. Increased density is present along the outer and inner surfaces of the cortex. In this patient, the medullary canal is completely obliterated at the level of melorheostosis. Mild sclerosis is noted in distal fourth metatarsal as well as the proximal phalanx of the third toe

dominant. Metaphyseal dysplasia is a disturbance of enchondral bone growth in which there is failure of modeling of tubular bones so that the ends of the shafts remain larger than normal in circumference. As a result the distal femurs typically have Erlenmeyer flask deformities. The cortices of the bone ends are thinner than in normal patients and are, therefore, more subject to fracture. Other than a proclivity to pathologic fracture, general health is normal and life expectancy is not shortened. Patients attain normal height.

The distal femur and proximal tibia are involved most dramatically, but the metaphysis of any tubular bone may show abnormality (Fig. 13.41). The bones of the hands and feet often present the same changes as those seen in the long cylindrical bones. The epiphyses develop normally so that bone age is not altered.

Patients with Pyle disease also have mild to moderate hyperostosis of the cranial vault and mandibular prognathism, but no increased density of the mandible. The ribs, clavicles, pubis, and ischium are expanded. Mild platyspondyly and genu valgus are present.

Craniometaphyseal Dysplasia (MIM 123000 Autosomal Dominant) (MIM 218400 Autosomal Recessive) Group 23

These patients have overgrowth of the cranial bones and leontiasis ossea [2]. There is hyperostosis of the frontal and occipital bones, base of the skull, facial bones, and the mandible (Fig. 13.42a). Patients have hypertelorism and overgrowth of the bridge of the nose. Bone overgrowth at nerve foramina may lead to stenosis and neurologic symptoms, blindness, and hearing impairment [3, 7].

During infancy, the long bones show diaphyseal sclerosis (Fig. 13.42b) without metaphyseal abnormality. In children and adults, however, the long bones reveal failure of modeling in the areas of most active growth, such as distal femur, proximal humerus, and distal radius. Diaphyseal sclerosis becomes less prominent in older children and adults.

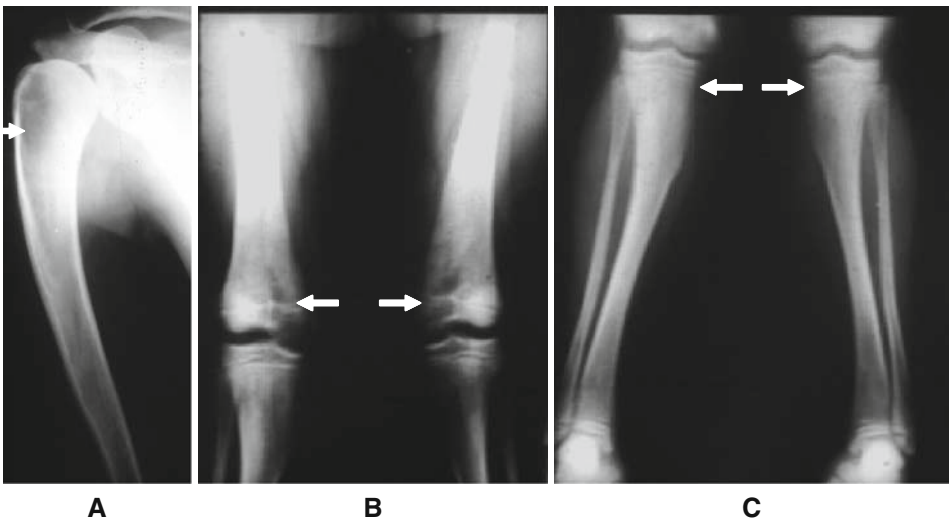

Fig. 13.41 Metaphyseal dysplasia (Pyle disease). **a R**adiographs of the humerus, **b** radiographs of the femurs, and **c** tibias and fibulas from two cases of metaphyseal dysplasia showing failure of metaphyseal modeling (*arrows*). As a result the metaphyses are wide, particularly where the bone growth is most rapid. The cortices in the metaphyses are thin. Please see Fig. 13.72a for a description of bone modeling. **a** is courtesy of Dr Robert Schneider, hospital for special surgery, New York, NY

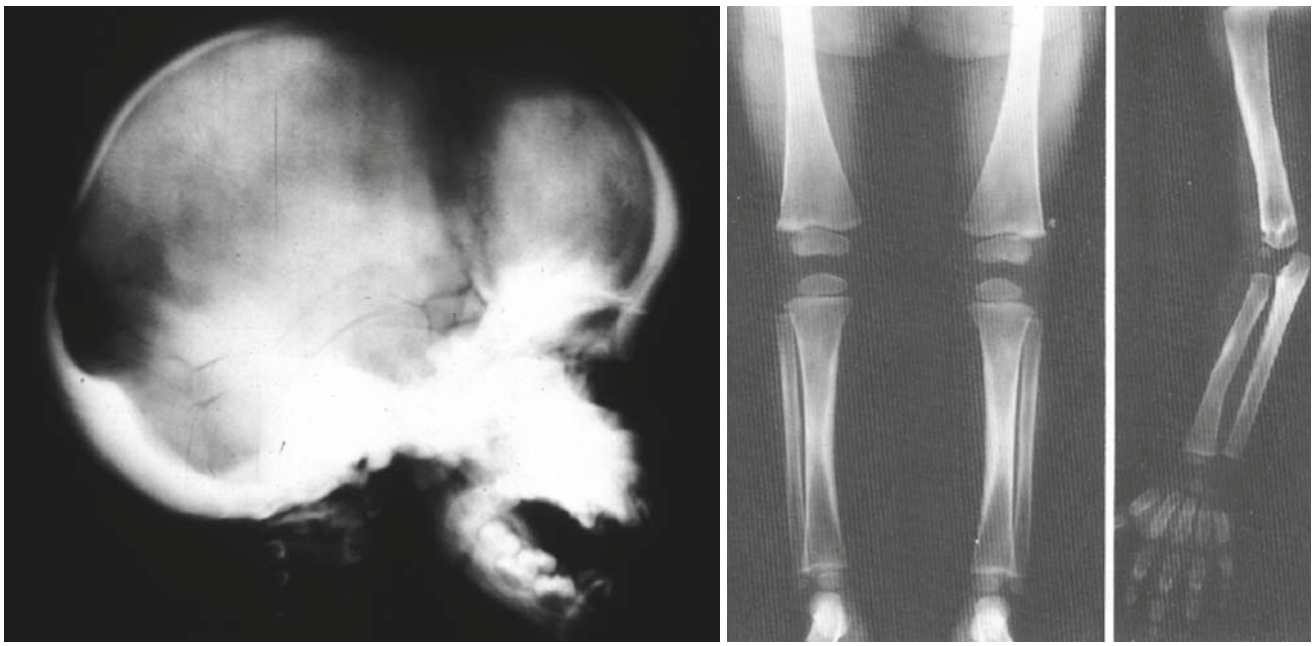

Fig. 13.42 Craniometaphyseal dysplasia**. a** Lateral radiograph of the skull shows increased density of the cranial bones, particularly of those of the base of the skull, and of the facial bones. AP radiographs of long bones of a boy, 18 months of age show broad metaphyses with mild increased density of the middle third of diaphyses. Courtesy of the late Dr J.W. Hope, of Children's Hospital of Philadelphia.

Metaphyseal Chondrodysplasia (Metaphyseal Dysostosis) (MIM 156500,250250, 156400, 309645, 250400) Group 9

In 2006 classification this group is named metaphyseal dysplasia, which may be confused with Pyle disease in group 23. Therefore, we prefer the term metaphyseal chondrodysplasia [3] or metaphyseal dysostosis [2].

In 1934, Jansen reported a case of skeletal dysplasia that he named metaphyseal dysostosis [2]. Metaphyseal chondrodysplasia (metaphyseal dysostosis) differs from metaphyseal dysplasia (Pyle disease and its Braun–Tinschert variant). Eight types of metaphyseal chondrodysplasia are identified in group 9 in the 2006 nosology. There is abnor-

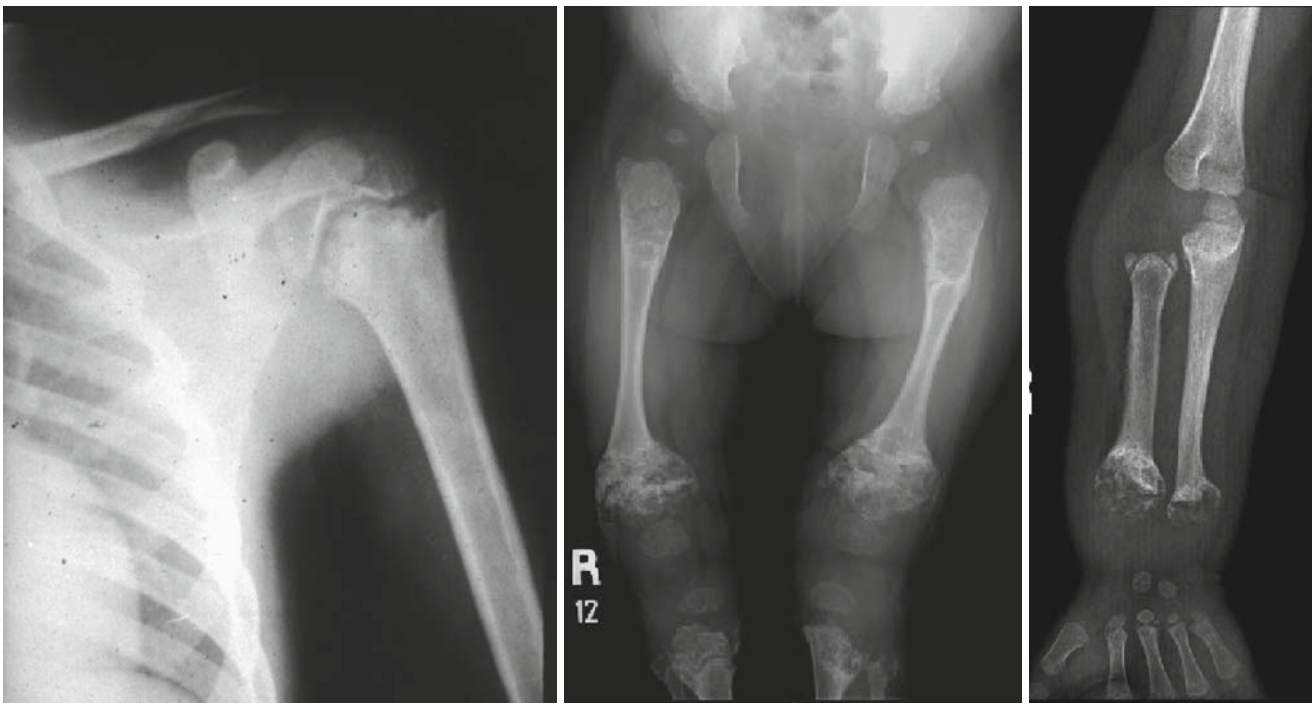

Fig. 13.43 Metaphyseal chondrodysplasia (metaphyseal dysostosis). AP shoulder radiograph (**a**) shows unclassified MCHD, with irregularity of the metaphysis of the proximal humerus similar to rickets. In contrast to rickets, however, there is no diminished bone density. The epiphyseal contour is very distinct and the provisional zone of calcification is normal. AP radiographs of the lower extremities (**b**) and AP radiograph of the upper extremity (**c**) of a patient with Jansen type of MCHD, the most severe form. Metaphyseal abnormalities are more severe than **a**. The epiphyses are normal. **b** and **c** are courtesy of Dr Ralph Lachman, Emeritus professor of Radiology, UCLA

mal maturation of growth plate chondroblasts in metaphyseal chondrodysplasia. In all forms of the disease, there are various degrees of dwarfism with alterations in the shape of the metaphyses.

The better known forms are as follows:

1. *Jansen type* (MIM 156400) is the most severe form, but it is rare. As of 2004, only 35 cases had been reported [7].
2. *Spahr type* (MIM 250400) is the least severe form [2].
3. *Schmid type* (MIM 156500) has moderate dwarfism, marked bowing and a waddling gait. About 125 cases were reported by 2004.
4. *McKusick type* (MIM 250250) is the second most common bone dysplasia among Amish, a religious sect with large populations in Pennsylvania, Illinois, Missouri, and Canada. Among the Amish its frequency is 1.5 per 1,000 births [7]. In Finland the frequency is also high 1 per 23,000 live births [7], but not as high as among the Amish.

   The McKusick type is also called cartilage-hair dysplasia. As the name implies, the patients' hair is abnormal being fine, sparse, short, and brittle. Intelligence is not impaired [2]. Dwarfing is marked with most patients attaining less than 4 ft at maturity. There may be costochondral beading along Harrison groove. This groove is a horizontal depression along the anterior lower border of the thorax corresponding to the costal insertion of the diaphragm [2, 16]. The ankles show characteristic deformities caused by relatively excessive length of the fibula compared with the tibia and accompanying loose jointed, flat foot. These patients are unable to fully extend their elbows and also have hyperextensibility of the wrist and fingers. Their digits are dramatically shortened. Dwarfism gives the appearance of the achondroplastic, but the skull in cartilage-hair dysplasia, unlike achondroplasia, is always normal.

Radiological manifestations: The radiographic manifestations of metaphyseal chondrodysplasia vary with the severity of the disease. The more severe the metaphyseal alterations and the more marked is the dwarfism. The radiology and pathology of metaphyseal chondrodysplasia are similar to rickets, but there is no diminished bone density in metaphyseal chondrodysplasia (Figs. 13.43, 13.44 and 13.45).

In McKusick cartilage-hair hypoplasia the zone of provisional calcification is irregular, and the metaphyses are broad and at times cup-shaped. Calcification may be present. The tubular bones of the hands and feet are similarly involved as are the areas of rapid growth in the pelvic bones. The skull

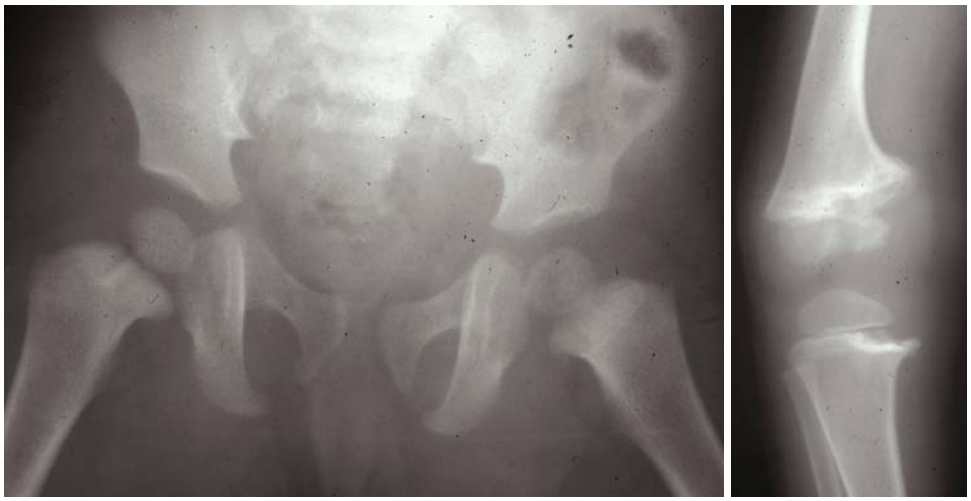

Fig. 13.44 Unclassified metaphyseal chondrodysplasia. This is an 18-month-old boy with mtaphyseal dysostosis. AP radiograph of pelvis (**a**) shows irregularity of proximal femoral metaphyses better seen on the right. Oblique radiographs of the right knee (**b**) show metaphyseal irregularity and widening of the medial aspects of the distal femoral and proximal tibial growth plates. This appearance is similar to rickets, but, in contrast to rickets there is no diminished bone density. The epiphyseal contours are very distinct, and the provisional zone of calcification is normal unlike in rickets

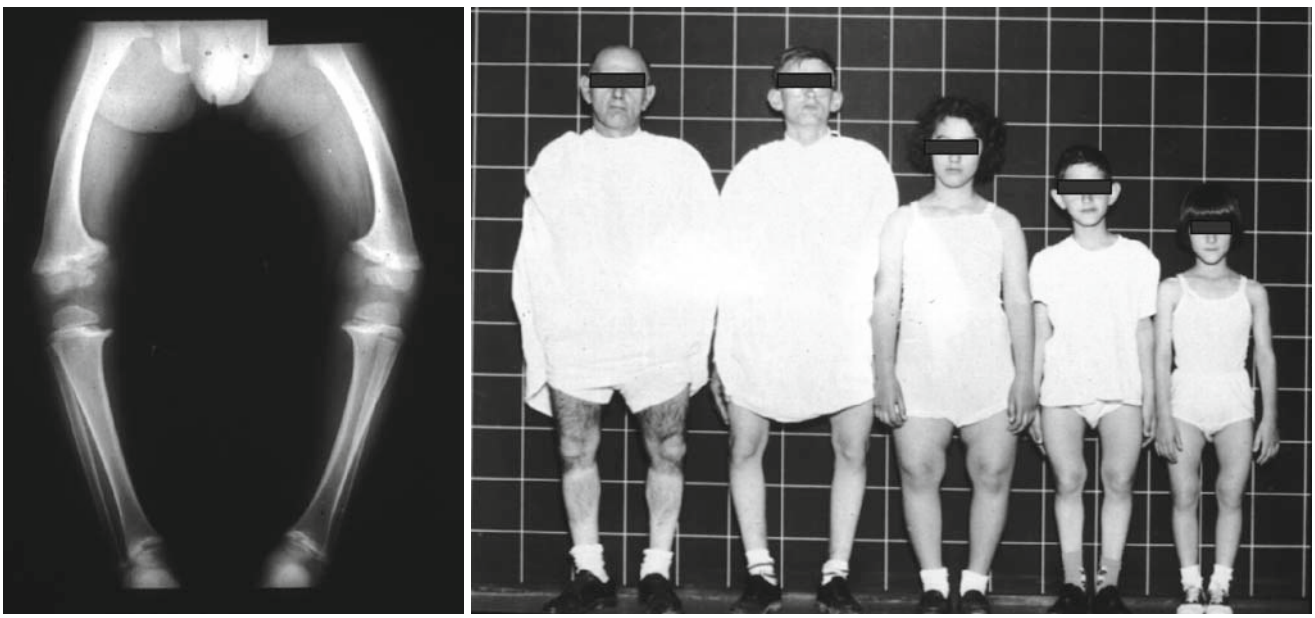

Fig. 13.45 Unclassified metaphyseal chondrodysplasia. AP radiograph (**a**) of the legs shows bowing. The epiphyses are normal in contour, and the provisional zone of calcification is normal in density. Photograph (**b**) of a father with four children all of whom have metaphyseal chondrodysplasia. (Courtesy of Dr G. Sticker) [8]

and spine are seldom affected, even in the most severe forms of the disease.

Some forms of metaphyseal dysostoses may show rachitic rosary, coxa vara, anterior bowing of femurs, and genu valgum with distortion of pelvis, clavicles, and small bones of the hand and feet.

Metatropic Dysplasia (MIM 156530, 250600) Group 11

Metatropic dysplasia is in the differential diagnosis of achondroplasia (Fig. 13.46). Genetic transmission may be

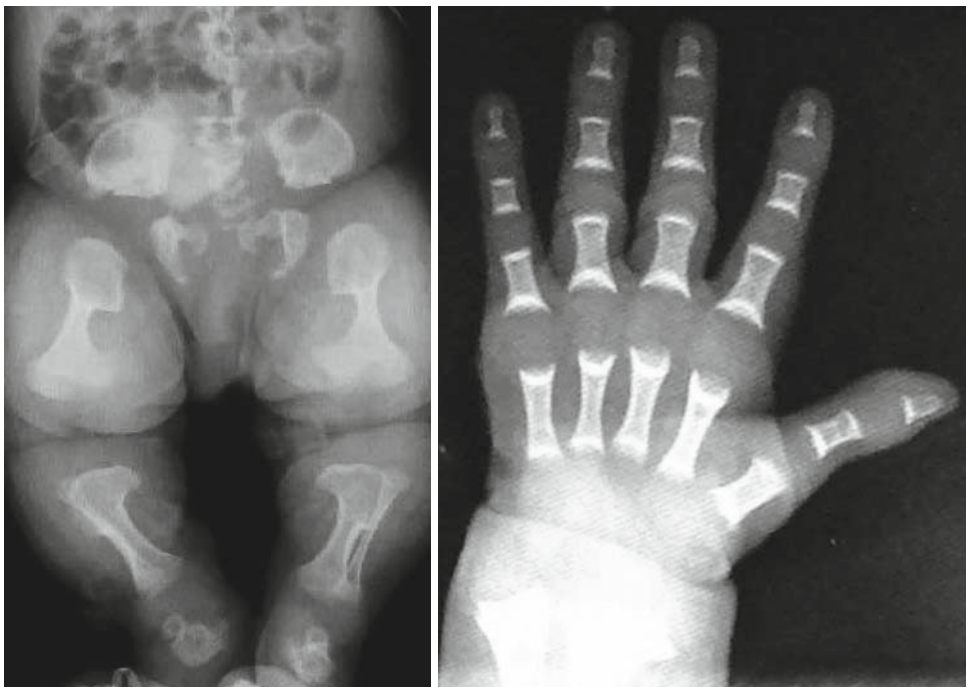

A B

Fig. 13.46 Metatrophic dysplasia**. a** AP lower body radiograph shows relatively flat vertebral bodies. The tubular bones are short with broad "battle axe shaped" metaphyses. The femurs are dumbbell shaped. The ilia are flared, and triangular in appearance, and pointed toward the triangular cartilage. No ossification of the epiphyseal centers is present. PA radiograph **(b**) of the hand reveals short and dumbbell-shaped tubular bones. Courtesy of Dr Ralph Lachman, Emeritus professor, UCLA

dominant or recessive [3]. At birth the metatropic and the achondroplastic dwarves may be indistinguishable. As the former matures, the limbs grow but the trunk develops kyphoscoliosis and so shortens. Thus, eventually the extremities appear to be disproportionately long for the trunk, just the opposite of achondroplasia. Maroteaux suggested the name "metatropic," precisely because the patients' appearance changes so greatly over the course of the disease.

Mucopolysaccharidoses (Dysostosis Multiplex) Group 26

Mucopolysaccharide is the old terminology, the new terminology being glycosaminoglycan. However, the common name of the group still is mucopolysaccharidoses (dysostosis multiplex). Mucopolysaccharidoses are lysosomal storage diseases with skeletal involvement. There are seven types and three subtypes of mucopolysaccharidoses that have been classified.

Mucopolysaccharidosis I H (MIM 252800 Hurler Disease) Group 26

Classically, Hurler disease (gargoylism) begins in early childhood, causing skeletal deformity, failure of mental development, clouding of the cornea, blindness, enlargement of the liver and spleen (Fig. 13.47a), and eventual mitral insufficiency with cardiac decompensation. The disease is uncommon but not rare. There were more than 200 cases reported up to 1975 [2]. The frequency is about 1 in 100,000 births [7]. The glycosaminoglycans at fault are dermatan sulfate and heparan sulfate.

The first symptoms may be noted soon after birth. Ellis, Sheldon, and Capon coined the term "gargoylism," because of the patients' strikingly repugnant appearance and their faces resemblance to the well-known architectural ornament. Although the condition progresses through early childhood, but the patient may live to middle age before cardiac decompensation occurs.

Radiological manifestations: Skeletal changes in Hurler disease vary from mild to severe. Lesions such as hepatosplenomegaly and umbilical hernia are sometimes evident radiographically and are easily identified by CT or MRI. Premature closure of the sagittal suture frequently occurs and is responsible for the shape of the head. The cranial vault is narrowed laterally and enlarged in its anteroposterior dimension. Typically, the calvarial bones are thick. In many instances, the sella turcica is shallow and elongated anteriorly beneath the anterior clinoids (J-shaped sella), a reflection of delayed growth of the sphenoid bone (Fig. 13.48a). The nasopharynx tends to be small and readily obstructed by lymphoid tissue. The development of the paranasal sinuses and mastoids is retarded. The mandible is short and broad.

These patients have broad ribs that narrow at their vertebral end and are blunt anteriorly (Fig. 13.47b, c). The

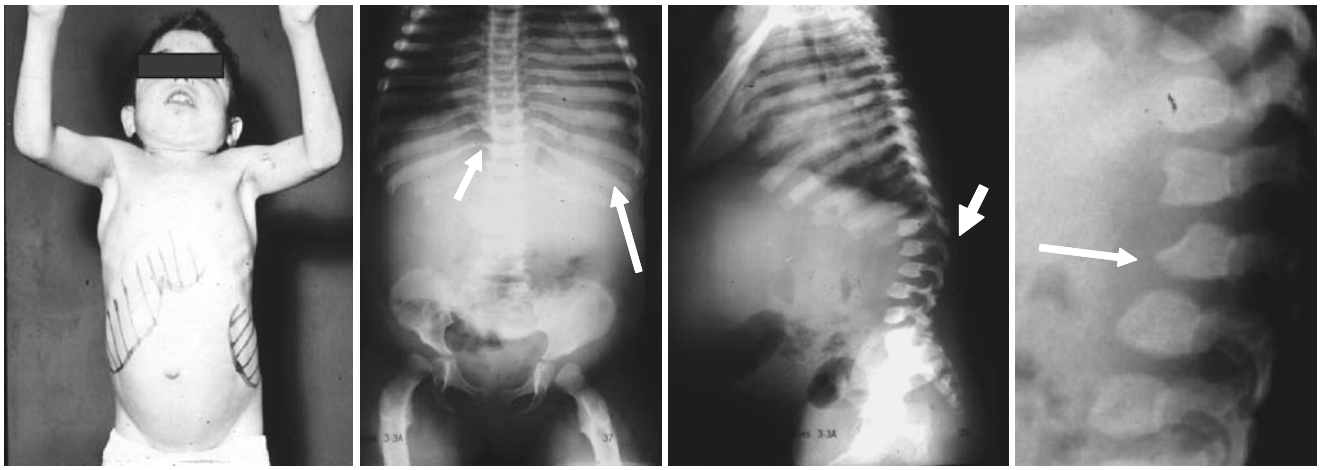

Fig. 13.47 Mucopolysaccharidosis I H, Hurler disease. **a** The liver and spleen margins have been outlined on the skin. There is a very small umbilical hernia. AP (**b**) and lateral (**c**) abdomen radiographs show hepatosplenomegaly, deformity of the pelvis, shallow acetabulum, deformity of proximal femoral epiphyses and coxa valga. The ribs are narrow posteriorly (*short arrow*) and wide anteriorly (*long arrow*). **c** also shows thoracolumbar kyphosis (*short arrow*). Coned down lateral lumbar radiograph (**d**) shows inferior beaking (*arrow*) of lumbar vertebral bodies. This deformity is characteristic of types I and II mucopolysaccharidoses

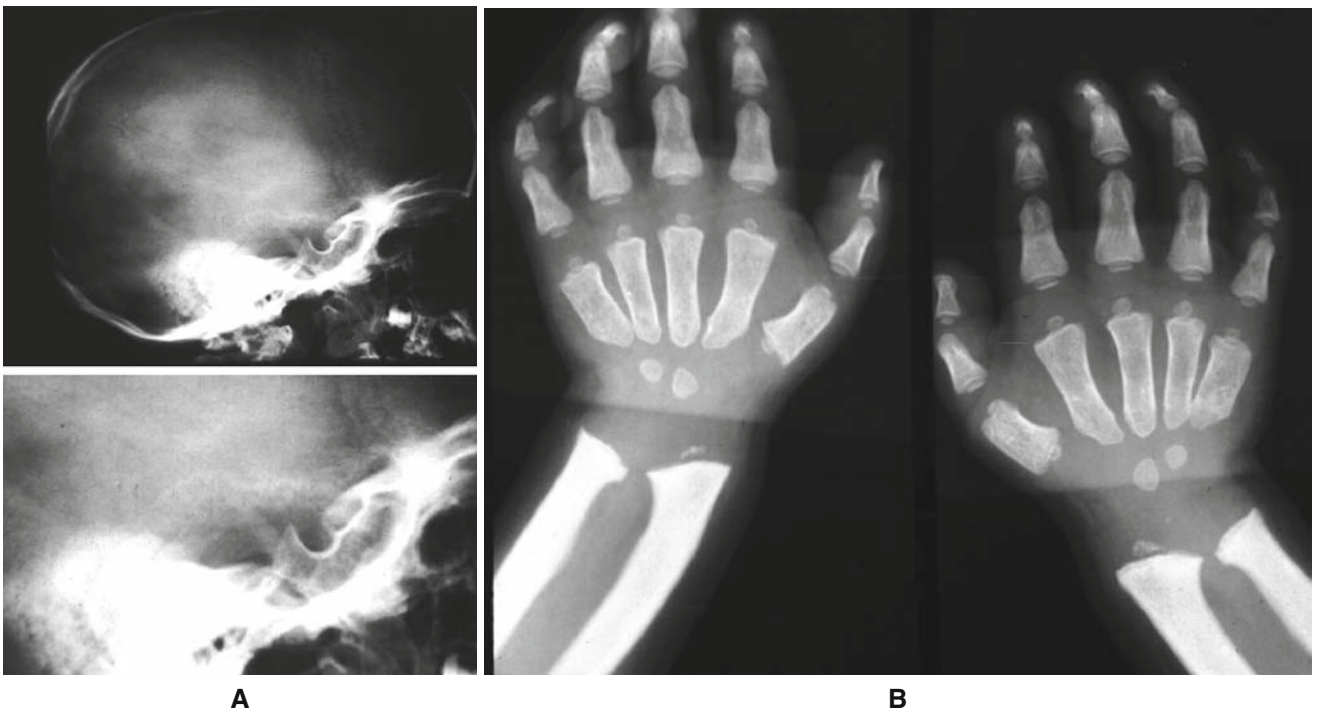

Fig. 13.48 Mucopolysaccharidosis I Hurler disease. Lateral skull and coned down lateral sellar magnification views (**a**) show elongation of the sella turcica, better visualized in magnification view (*left bottom*). PA radiograph (**b**) of the hands show that the wrists are V-shape formed by the distal radius and ulna. The hand shows narrowing of the proximal metacarpal bones. The phalanges are short and broad

clavicles are short and thick. There is a characteristic gibbus at the low dorsal or high lumbar region occasioned by deformity of one or more vertebrae (Fig. 13.47c). The affected vertebral bodies are hypoplastic, have an anterior inferior beak and are displaced posteriorly (Fig. 13.47c, d). The intervertebral disc spaces are maintained.

In general, ossification of secondary centers is delayed, and when it occurs, the centers are apt to be irregular and deformed. The bones of the upper extremity are more abnormal than are those of the lower extremity. The medullary canals are widened and the epiphyseal centers are flat and often irregular. The metacarpals tend to be narrow

proximally, and the phalanges are short and broad (Fig. 13.48b). The bones of the feet show changes similar to those of the hands. The bones of the lower extremity grow to normal length, but valgus deformity of the femurs and narrow femoral necks are common. The acetabula are shallow, the ilia flared, and the ischia thick. Subluxation of the hips may occur as a result of the shallow acetabula.

Prognosis: Victims of Hurler disease may die in childhood, but some live well into adulthood. The appalling skeletal deformity, mental deficiency, and blindness leave these patients severely disabled.

Mucopolysaccharidosis IS (MIM 607014 Scheie Disease) Group 26

Mucopolysaccharidoses IH/S and MPS IS (Scheie disease) are variations of Hurler disease [2]. Scheie disease is autosomal recessive. Clouding of the cornea is striking [2] and aortic insufficiency [14], stiff joints, retinitis pigmentosa, and excessive body hair occur [2]. Unlike Hurler disease, there is no impairment of the intellect. As with Hurler disease, the glycosaminoglycans at fault in this condition also are dermatan sulfate and heparan sulfate.

Mucopolysaccharidosis IH/S (MIM 607014), Group 26

This disorder is intermediate between Hurler and Scheie and is a moderate form.

Mucopolysaccharidosis II (MIM 309900 Hunter Disease), Group 26

Hunter disease is considerably less common than Hurler disease and is transmitted as a X-chromosomal recessive. In all respects, it is similar to Hurler disease, but milder. Clouding of the cornea does not occur; mental deterioration is later in onset and slower to progress. Spinal deformity is considerably less common than in Hurler disease, and a gibbus does not occur. Deafness and nodular skin lesions over the back and arms are common. The prognosis in Hunter disease is significantly better than in Hurler disease, with the majority of patients surviving to middle age. These patients excrete abnormal amounts of dermatan sulfate and heparan sulfate in the urine just as in Hurler disease. Two subtypes are recognized: Hunter A (severe) and Hunter B (moderate).

Mucopolysaccharidosis III (MIM 252900, 252920, 252930, 252940 Sanfilippo Disease), Group 26

Sanfilippo disease is similar to Hurler disease, but the intellectual decay is earlier in onset and more rapid in development while the somatic changes are much less severe. Clouding of the cornea apparently does not occur; hepatosplenomegaly is slight and dwarfing is moderate. Excessive heparan sulfate excretion in the urine is the major biochemical feature. Four subgroups of Sanfilippo disease have been described [3, 1].

Mucopolysaccharidosis IV (Morquio Disease, Universal Vertebra Plana) (MIM 253000, 253010) Group 26

Morquio disease is transmitted as an autosomal recessive and occurs equally in both genders. It causes dwarfism, kyphosis, and severe disability. These patients excrete increased amounts of keratan sulfate and chondroitin-6-sulfate in the urine. Two subtypes have been described: type A is more severe than type B [3].

Morquio disease is usually considered to be a disease of childhood, with signs typically appearing between 6 and 18 months, often when babies start bearing weight. The first sign is usually a thoracolumbar kyphosis, and as attempts at weight bearing continue, a galaxy of skeletal distortions appears. The neck is short so that the head appears to be thrust forward and jammed down into the thorax (Fig. 13.49a, b). The sternum is prominent with horizontal displacement (pigeon breast). The chest is increased in the anteroposterior dimension. The head is normal in size but it appears large because of the lag in growth of the rest of the body, this lag being progressively more evident in more caudal portions of the body (Fig. 13.49b). With age, patients develop a characteristic stance with a kyphosis and partially flexed hips, knees (knocked knees), and elbows. The hands are short and trident with thick fingers and ulnar deviation. The feet are short, wide, flat, and everted at the ankles.

Radiological manifestations: The radiologic manifestations of Morquio disease reflect abnormal conversion of cartilage to mature bone. Although the skull and facial bones are unaffected, the vertebral bodies manifest constant and distinctive alterations in their size and contour.

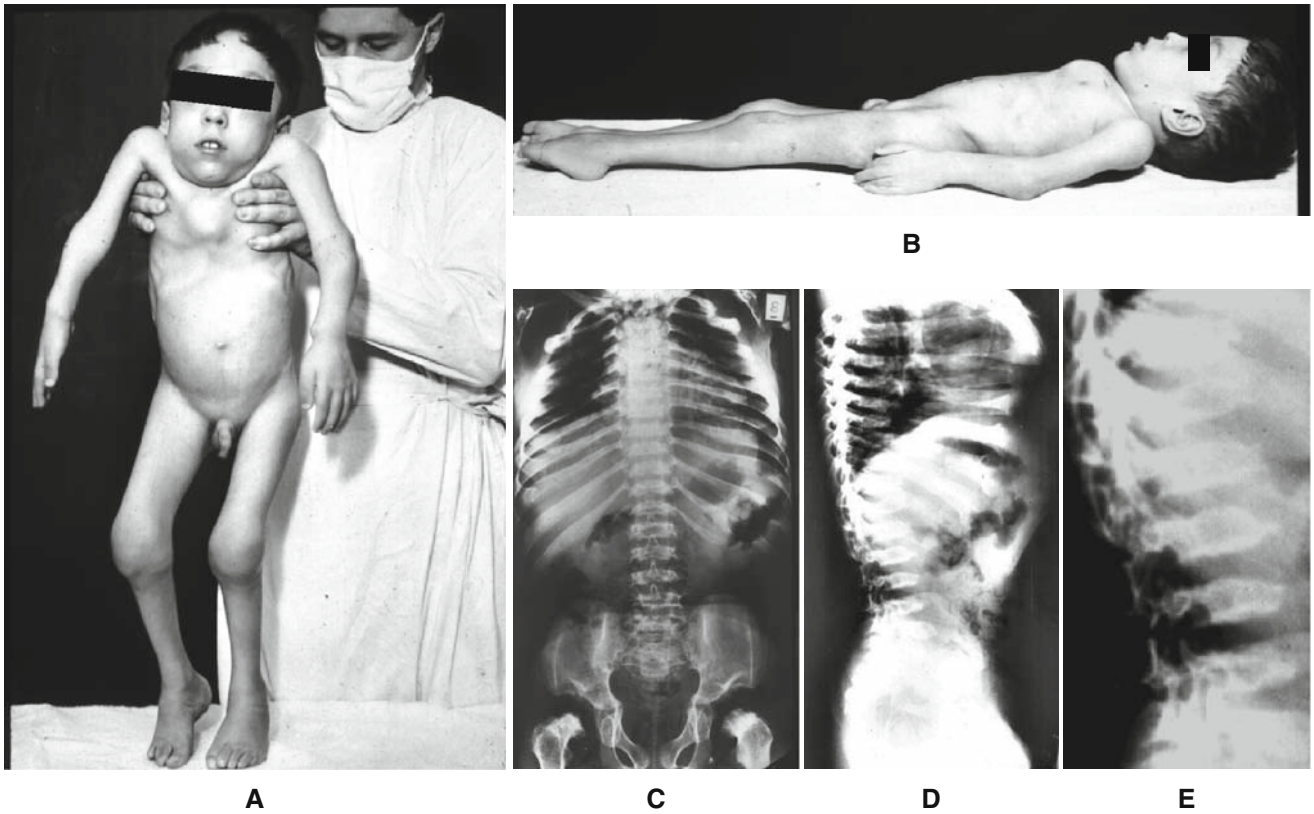

Fig. 13.49 Mucopolysaccharidosis IV Morquio disease. AP (**a**) and lateral (**b**) photographs of a patient showing dwarfism, disproportionately enlarged head, short neck, pectus carinatum (pigeon breast), short trunk and knock-knees (genu valgum). The lower extremities are underdeveloped. AP (**c**) and lateral radiographs of the chest (**d**) and the abdomen (**e**) show universal vertebra plana, prominent sternum and central beaking of lumbar vertebral bodies. The ribs are broad and deformed in their anterior ends and narrow posteriorly. The acetabulae are deep and irregular. The femoral epiphyses are underdeveloped, *Protrusio acetabulae* is noted. The pelvic bowl has a wine goblet type of appearance

The vertebral bodies are flat (universal vertebra plana) with rough, irregular contours, and an anterior central projection (Fig. 13.49c, d and e). The intervertebral discs are narrower than normal. Kyphosis is common and may be aggravated by posterior displacement or wedging of one or more vertebrae. Lumbar vertebral bodies tend to be smaller and more deformed than the dorsal ones. The posterior arch of C1 may lie within the foramen magnum; the odontoid may be absent or hypoplastic (Fig. 13.50d), and the body of C2 enlarges so that it encroaches on the neural canal [6]. Consistent with caudally delayed maturation, a small sacrum is common.

An increase in the anteroposterior diameter of the chest occurs as a result of kyphosis and a pectus carinatum deformity. The ribs tend to be broad and deformed at their anterior ends and the sternum may be short (Fig. 13.49c, and d).

The long bones are affected in most cases, but the degree of deformity varies. The growing ends of the long bones are broad with irregular zones of provisional calcification and irregularly ossified, with flattened ossification centers.

The long bones may be normal in length or short. Shortening is usually more apparent in the bones of the upper extremities while the lower extremities are less severely affected. On the other hand, the proximal femurs may show marked deformity and subluxations of the hip are not uncommon. The acetabula tend to be deep and their osseous roofs coarse in outline. The ilia flare laterally (Fig. 13.50a). The pelvic bowl takes on a "wine goblet" shape. The lower extremities often show a decrease in muscle mass. Knock-knee deformity is extremely common (Fig. 13.50b).

The carpal and tarsal bones are irregular in configuration and size. The tubular bones of the hands and feet tend to be short with irregular ossification of the epiphyseal centers.

Prognosis: Morquio disease usually slows its progression as patients' age. Some cases arrest at puberty though a few continue worsening through adolescence and even into adult life [2]. These patients have a variable life span [14].

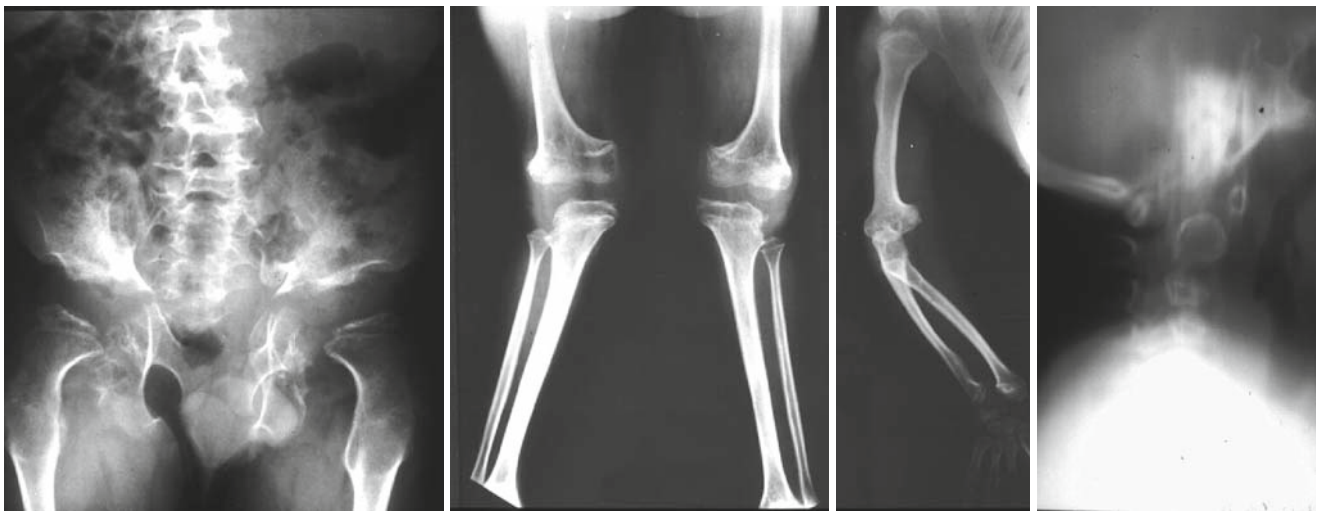

Fig. 13.50 Mucopolysaccharidosis IV Morquio disease. AP lumbar spine radiograph showing levoscoliosis. The pelvis is deformed, and the acetabulae are deep, irregular, and protruding into the pelvis. The proximal femoral epiphyses are underdeveloped and dense. AP radiographs of the knees (**b**) shows bilateral genu valgum and deformed epiphyses. AP radiograph of the upper extremity (**c**) shows varus deformity at the elbow. Lateral tomogram of the cervical spine (**d**) shows absence of the odontoid process and a large body of C2

Mucopolysaccharidosis VI, Maroteaux and Lamy Disease (MIM 253200) Group 26

Maroteaux and Lamy disease is autosomal recessive, and its somatic features are the same as those of Hurler disease, but mental deterioration does not occur. As in Scheie syndrome the chemical fault lies within the Dermatan sulfate. Again, there are two subtypes: type A (more severe) and type B (less severe) [3].

Mucopolysaccharidosis VII, Sly Disease, (MIM 253220) Group 26

This disease has a wide phenotypic spectrum. Patients have increased urinary secretion of glycosaminoglycans, mostly chondroitin-6-sulfate. There are three forms. The severe form shows broad ribs, hook-shaped vertebrae, and hypoplasia of the base of iliac bones. There are intermediate and mild forms of disease [3].

Mucolipidosis Type II, (I-Cell Disease), MIM 252500, Group 26

Mucolipidosis II, inclusion cell (I-cell) disease results from an enzyme deficiency in N-acetylglucosaminyl-phosphotransferase. Patients have facial dysmorphism, Hurler-like body configuration, corneal opacity (uncommon), thickened skin, psychomotor, and growth retardation [7].

Mucolipidosis III, Pseudo-Hurler polydystrophy, (MIM 252600), 252605, Group 26

Clinical manifestations are quite variable. Mild cases are recognized in late childhood. Growth may be normal, but patients have hip dysplasia [3].

Radiologic findings in the skeleton are similar to those of Hurler and Hunter disease [7]. The bodies of 12th thoracic and the first three lumbar vertebrae have an inferior beak. The long bones are of normal length, but their cortices are thin and there is failure of modeling of distal femurs, proximal tibias, and distal radius. The ribs and clavicles are broad. The cranial vault is enlarged, the sella turcica is elongated [2].

Multiple Epiphyseal Dysplasia (Fairbank [7] or Ribbing [7]) (MIM 132400) Other Forms [1] (600204, 600969,607078,120210, Group 8 and MIM 226900), Group 4

Dysplasia epiphysealis multiplex (Fairbank disease also called Ribbing disease), a genetic chondrodysplasia affecting enchondral ossification of the epiphyses, was first described

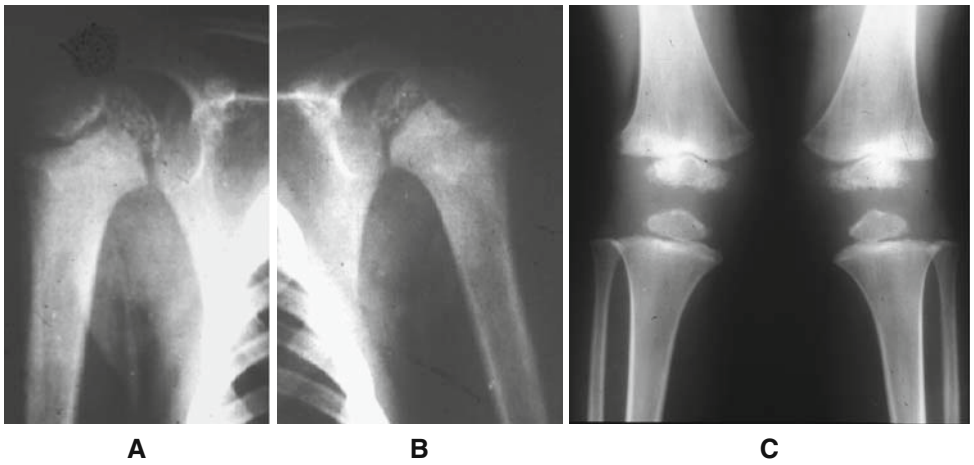

Fig. 13.51 Multiple epiphyseal dysplasia**.** AP radiographs of the shoulders bilaterally (**a** and **b**) show speckled non-uniform density and mild deformity of the proximal epiphysis of both humeri. AP radiograph **(c)** of the knees shows similar changes in the distal femoral and proximal tibial epiphyses

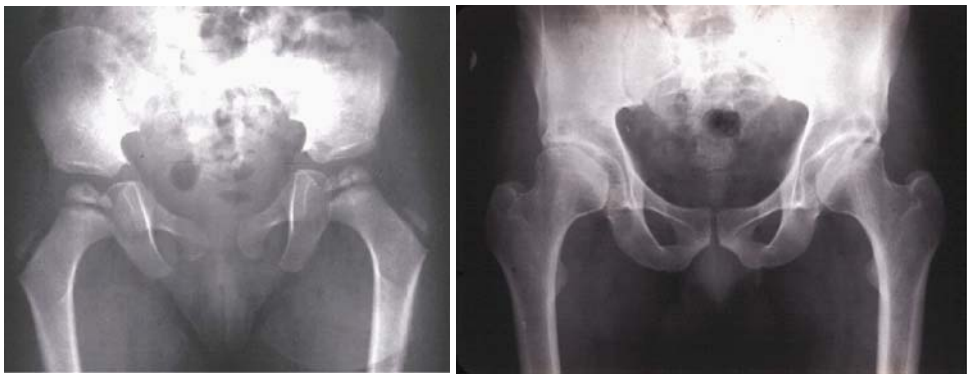

Fig. 13.52 Multiple epiphyseal dysplasias. AP pelvic radiographs from daughter (**a**) and father (**b**) with multiple epiphyseal dysplasia involving only the proximal femoral epiphyses. This is the Beuke type of MED. These images show the disease at different stages. Early on as is visible in the daughter's radiograph, the epiphyses appear irregular and non-uniform in density. At this stage multiple epiphyseal dysplasia should not be confused with bilateral ischemic necrosis. Later on in the disease (father), the epiphyses fuse with an abnormal contour that leads to premature secondary osteoarthritis

by Fairbank in 1935 [2] and by Ribbing in 1937 [2]. It is one of the most common non-lethal skeletal dysplasias (9 per 100,000 live births [7]). The illness rarely comes to the attention of the physician until the child begins to walk, when a waddling gait manifests itself.

Ribbing [5] divided this dysplasia into two types, the pseudoachondroplastic type, (MIM 177170) in group 8, which most closely resembles the cases Fairbank reported, and the tarda form, Ribbing disease. The latter is manifested principally by precocious osteoarthritis, particularly of the hips. One or all epiphyses may be involved, but in a large series the affliction was limited primarily to the lower extremities [2]. Nine autosomal dominant forms have been listed in group 8 and one autosomal recessive form (MIM226900) in group 4 in the 2006 classification [1].

The tibiae are usually curved with knock-knee or bowlegs. There is often some degree of flexion deformity. The appearance and fusion of ossification centers may be delayed, but usually not markedly so. Even so, as the child develops, a subnormal growth rate becomes clinically apparent. The vertebrae are usually not affected so that, similar to achondroplasia, dwarfing is confined to the extremities. Irregularities in the adult articular surfaces almost invariably lead to osteoarthritis by the time the patient reaches middle age. The digits of the hands and feet are noted to be short and stubby. Other than the difficulties in locomotion consequent to the deformities and secondary osteoarthritis, these patients may lead a fairly normal life of average duration [2].

Radiological manifestations: Poor enchondral epiphyseal ossification leads to multiple irregular and enlarged ossification centers with occasional flaring of the metadiaphyses. As noted, these centers will eventually fuse, but because of altered biomechanics, patients develop early secondary osteoarthritis (Figs. 13.51and 13.52). The ankles often show tibotalar slant.

The Beukes variety of MED [(MIM 142669) Group 8] involves only the epiphyses of the proximal femora (Fig. 13.52). This variant of the disease causes premature osteoarthritis of the hip secondary to the deformity of the proximal femoral epiphysis.

Blount Disease (MIM 259200 and 188700)

Some believe that osteochondrosis deformans tibiae, also known as tibia vara or Blount disease, is a clinical subvariety of multiple epiphyseal dysplasias [2]. Others [14] describe this entity as an osteochondrosis and not a dysplasia. Blount disease may be either unilateral or bilateral. There are two recognized forms of Blount disease, the common infantile form that appears during the first few years of life when toddlers begin to walk, and an uncommon adolescent form that presents between the ages of 8 and 15. In this disease, the medial epiphyses of the proximal tibiae form poorly and give rise to radiographically visible medial epiphyseal deformities along with consequent tibia vara (Fig. 13.53).

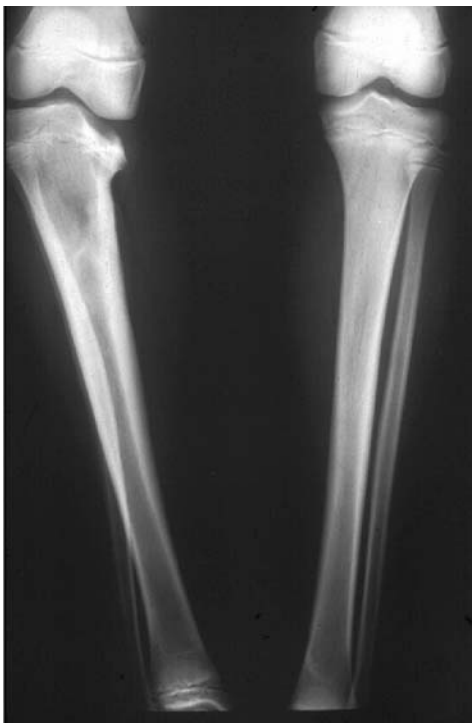

Fig. 13.53 Blount disease. AP radiograph of the knees and tibiae show hypoplasia of the right medial tibial epiphysis and compensatory hypertrophy of the medial femoral condyle, resulting in moderate genu valgum

Multiple Hereditary Cartilaginous Exostoses (MIM 133700, 133701, 600209) Group 28

Multiple hereditary cartilaginous exostoses (MHCE) is the best descriptive name to indicate this genetic disease (Fig. 13.54). It is also known as osteochondromatosis, but this name may be confused with synovial osteochondromatosis, a disease that is completely unrelated. The Term Metachondromatosis is used when both enchondromas and osteochondromas are present (Fig. 13.55). Osteochondromas are multiple bony excrescences that grow out from the cortical surfaces of the metaphyses and form extensions of the marrow space with cartilaginous caps.

Osteochondromas are usually discovered some time during childhood or adolescence. None has been reported present at birth. Osteochondromas, whether incidental or familial, are not true neoplasms but result from dysplastic growth of the physeal plate [2]. A small marginal portion of the growth plate separates from its main portion

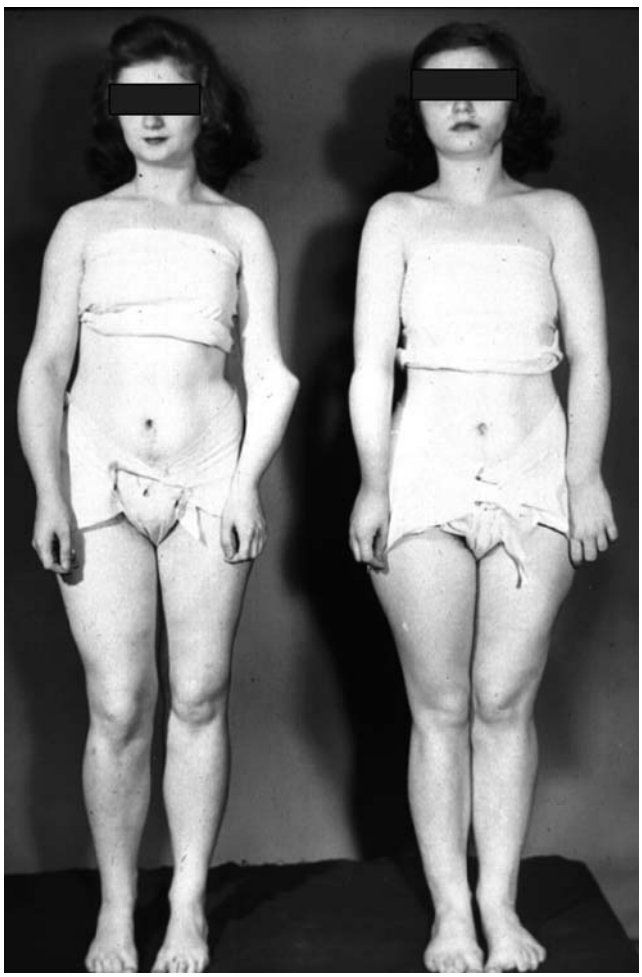

Fig. 13.54 Multiple hereditary cartilaginous exostoses**.** Two sisters show typical deformity of the elbows and knees. (From Shriner's Hospital, Philadelphia)

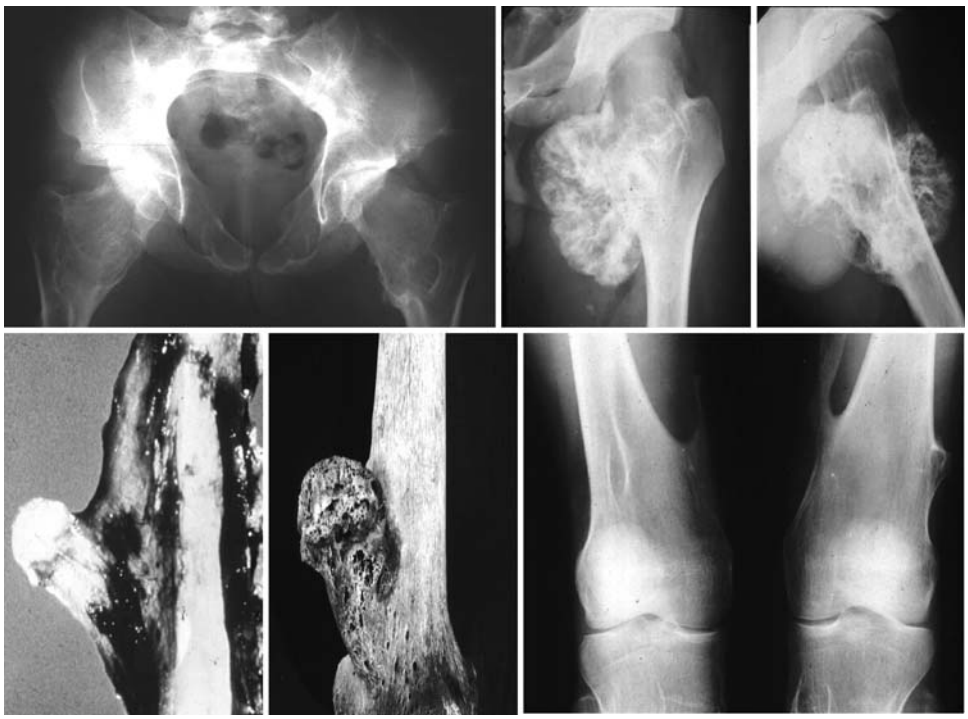

Fig. 13.55 Metachondromatosis and multiple hereditary cartilaginous exostoses. AP pelvis (top left) is metachondromatosis revealing combined enchondromas and osteochondromas of both femoral necks, AP and lateral views of the left hip (*top right*) show a large mushroom-like osteochondroma. The surface is lobulated, but smooth and has a non-aggressive appearance. Surgical and a dried specimens of an osteochondroma (*bottom left*). AP radiograph of the knees (*bottom right*) shows multiple osteochondromas of the femora and tibiae. The lesions are pediculated and pointed towards the diaphyses

and grows independently resulting in an osteochondroma, essentially a small "accessory diaphysis" with a cartilage cap. The cancellous (medullary) cavity extends from the native bone into the osteochondroma regardless of whether it is sessile or pedunculated. The osseous portion of osteochondromas is covered with an extension of periosteum from the normal cortex and the cap is covered with perichondrium [2]. As the bone grows, the osteochondromas "move" diaphyseally, away from the physeal plate. The growth of these lesions remains under normal hormonal control and ceases when bones mature and the growth plates fuse. Reactivation of growth and pain after puberty always must be regarded as possible malignant transformation to chondrosarcoma.

Exostoses are usually asymptomatic, but they may cause pressure upon adjacent structures. They may displace tendons. At times they may compress vessels, and interfere with blood supply or cause pain by pressure on nerves. Often in MHCE, if the wrist or ankle is affected, the ulna and fibula are shorter than their paired radius and tibia [2]. Multiple cartilaginous exostoses, in the areas of extensive growth, may interfere with metaphyseal modelling [2] (Fig. 13.55) and may interfere with joint mobility.

Radiological manifestations: Osteochondromas most frequently arise from the metaphyseal portion of long bones, but flat bones such as the pelvis (Fig. 13.55), scapula and the ribs, and the vertebrae too are sometimes involved. The small bones of the hands and feet are occasionally affected (Fig. 13.56). Since osteochondromas are disturbances of enchondral bone growth, they do not arise in areas of intramembranous bone formation, e.g., the calvarium.

In long bones, exostoses usually arise at the metaphyseal site of greatest enchondral growth (Figs. 13.55 and 13.56). They almost always grow in a direction away from the nearest epiphysis and point toward the mid-diaphysis (Fig. 13.55). They may have a small base (pedunculated) or a large base (sessile). Osteochondromas of the upper humerus are often broad based (Fig. 13.56).

The base of an osteochondroma, in one view, may appear as lucency with sclerotic borders, but in a perpendicular view, the exostosis is clearly profiled. Posttraumatic myositis ossificans at a site of tendinous attachment, especially around the knee may be similar to osteochondroma, but it does not show extension of medullary bone into the body of myositis ossificans.

On MRI, the thickness of an osteochondroma cartilage cap should be less than 1 cm in adults and less than 3 cm in children (Fig. 13.56). If it exceeds these measurements it is highly suspicious of malignancy. The cartilaginous surface of the cap usually has numerous lobular irregularities

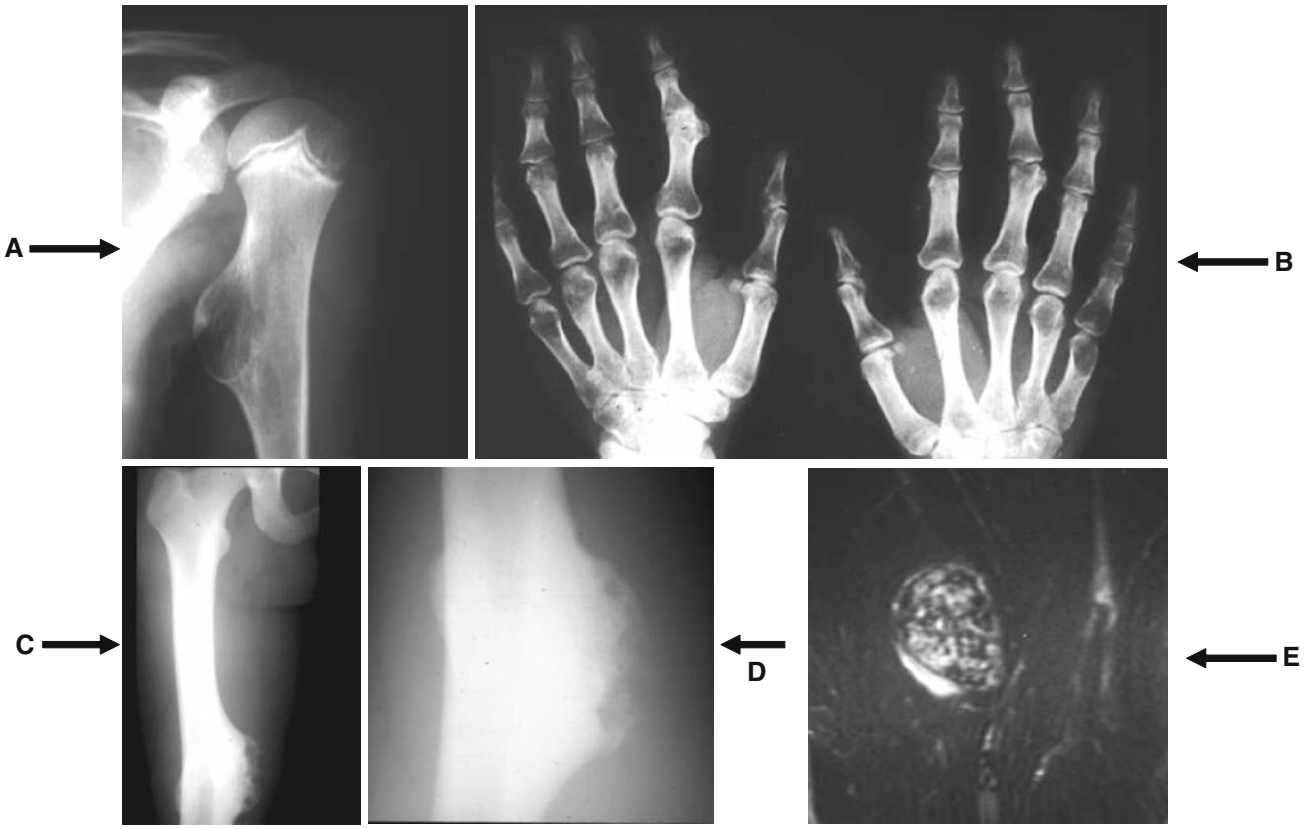

Fig. 13.56 Multiple hereditary cartilaginous exostoses.**a** AP radiograph of the left shoulder shows a sessile (broad based) osteochondroma of the humerus. **b** PA radiographs of the hands show bilateral osteochondromas. **c** AP radiograph and **d** magnified view of the right femur from the same patient show a sessile osteochondroma with an irregular surface arising from the femur. **e** T2 fat suppressed sagittal MRI reveals the cartilaginous cup is less than 1 cm thick, which is normal in an adult. The upper limit of normal in adult is 1 cm

(Fig. 13.55), but if the surface is markedly irregular, again one must be suspicious of malignant transformation and do an MRI to evaluate for chondrosarcoma (Fig. 13.56).

Prognosis: Malignant transformation to chondrosarcoma occurs infrequently. It is impossible to establish an accurate figure but most authors agree that this unfortunate complication occurs in about 1% of cases of MCHE.

Neurofibromatosis (MIM 162200, 101000, 162260, 162270, 601321,162220, 114030, 162210, 193520) [7]

Neurofibromatosis, falls into the class of phakomatoses along with Von Hippel–Lindau, tuberous sclerosis complex, Sturge–Weber, and Osler–Weber–Rendu syndromes. Neurofibromatosis is a disturbance in the supportive tissues of the nervous system, both central and peripheral. In addition to the nervous system, it also involves the skin, and it may involve the skeleton (secondarily), and even cause disturbances in other systems such as the endocrine and gastrointestinal tract [2]. Besides having associated benign and malignant neoplasms (Chapter 8), neurofibromatosis also has an associated secondary bone dysplasia.

Two main types of neurofibromatosis are recognized [7, 14]. Both types are autosomal dominant [7]. The first is Neurofibromatosis I or von Recklinghausen disease, which accounts for 97% of cases. Its estimated prevalence is 1 in 3,000 or 4,000 of population [7]. Type 1 is subdivided into several phenotypes [7]. Neurofibromatosis II (the central type), now also known as MISME (multiple inherited schwannomas, meningiomas, and ependymomas) syndrome, makes up the remaining 3% of patients [14]. Most patients with type II disease have bilateral acoustic neurinomas and frequently develop cystic astrocytomas. We discuss the cutaneous and osseous effects of type I neurofibromatosis (Von Recklinghausen disease) in this chapter. The peripheral soft tissue lesions are discussed in Chapter 8.

Cutaneous neurofibromas and café-au-lait spots are prevalent in neurofibromatosis. Café-au-lait spots may also be seen in fibrous dysplasia, but their borders have a different appearance. In neurofibromatosis the border of the spots is smooth, often likened to the coast of California, while in fibrous dysplasia the border is irregular like the coast of Maine. In neurofibromatosis large patches of skin may become

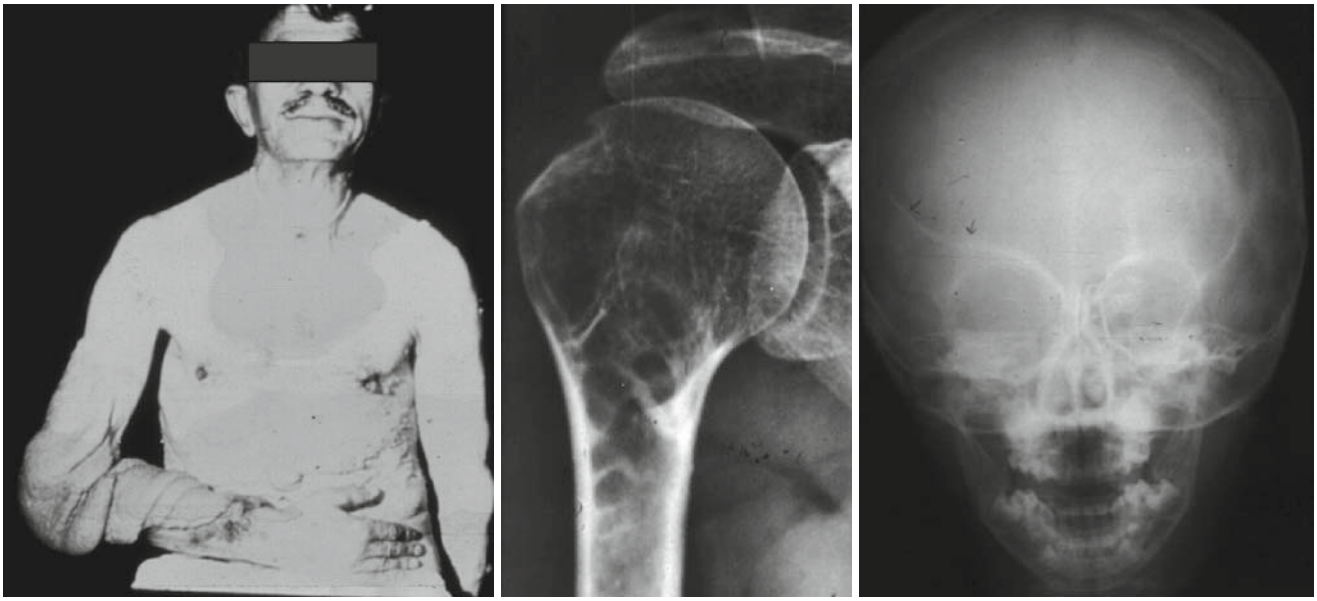

A B C

Fig. 13.57 Neurofibromatosis. **a** Photograph of a patient shows cutaneous neurofibromas and molluscum pendulum of the right upper extremity. **b** AP radiograph of the right shoulder reveals a radiolucent lesion of the upper humerus related to an intraosseous neurofibroma. **c** PA skull radiograph in a child demonstrates aplasia of the right greater sphenoid wing. The right orbit is larger than the left

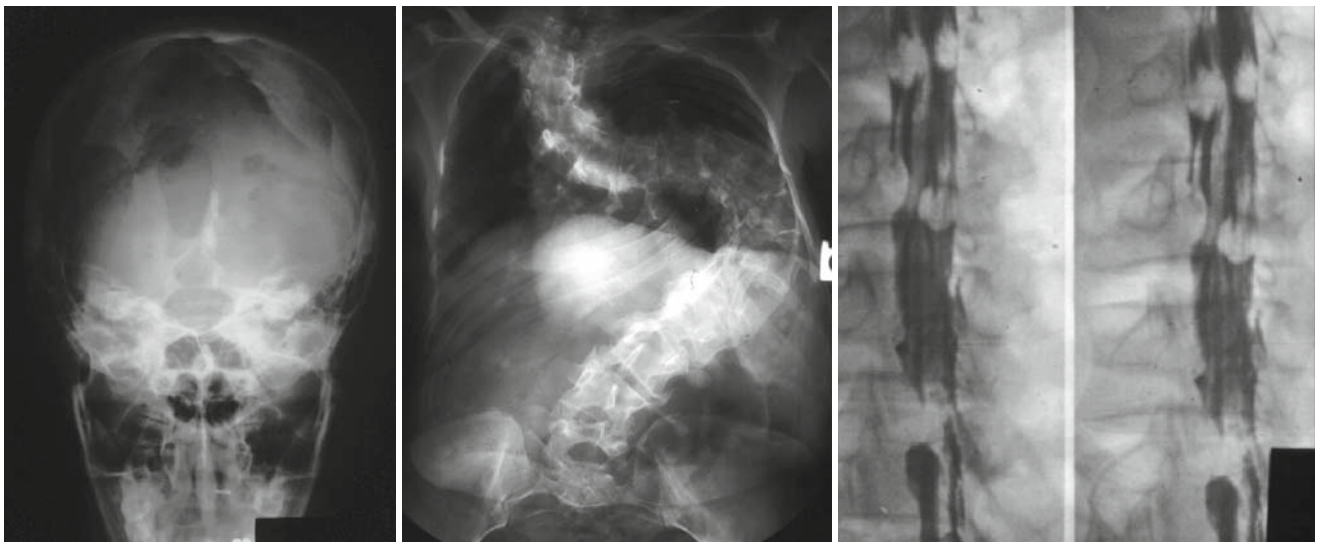

A B C

Fig. 13.58 Neurofibromatosis. AP radiograph of the skull (**a**) shows large defects (aplasia) of occipital and posterior portions of the parietal bones. AP thoracolumbar spine radiograph (**b**) shows severe levoscoliosis of the thoracolumbar spine. Note secondary deformity of the bony thorax and abnormal appearance of the ribs. (**c**) is a cervical myelogram demonstrating dumb-belle shaped neurofibromas of the intervertebral foramina. These findings may be demonstrated by MRI of the cervical spine which is a non-invasive procedure and without radiation exposure

diffusely thickened and redundant so that they hang in coarse, heavy folds, a condition called molluscum pendulum (Fig. 13.57).

The skull may show erosions and enlargement of neuroforamina secondary to pressure effects from slowly growing neurofibromas. Bone defects in the calvarium (Fig. 13.58a) or congenital absence of the greater wing(s) of the sphenoid [7] may be present (Fig. 13.57c). The spine may develop an acute angular scoliosis with or without kyphosis (Fig. 13.58b). Dumbbell-shaped neurofibromas cause enlargement of the intervertebral foramina (Fig. 13.58c). Dural ectasia and chronic CSF pulsation causes scalloping of the posterior

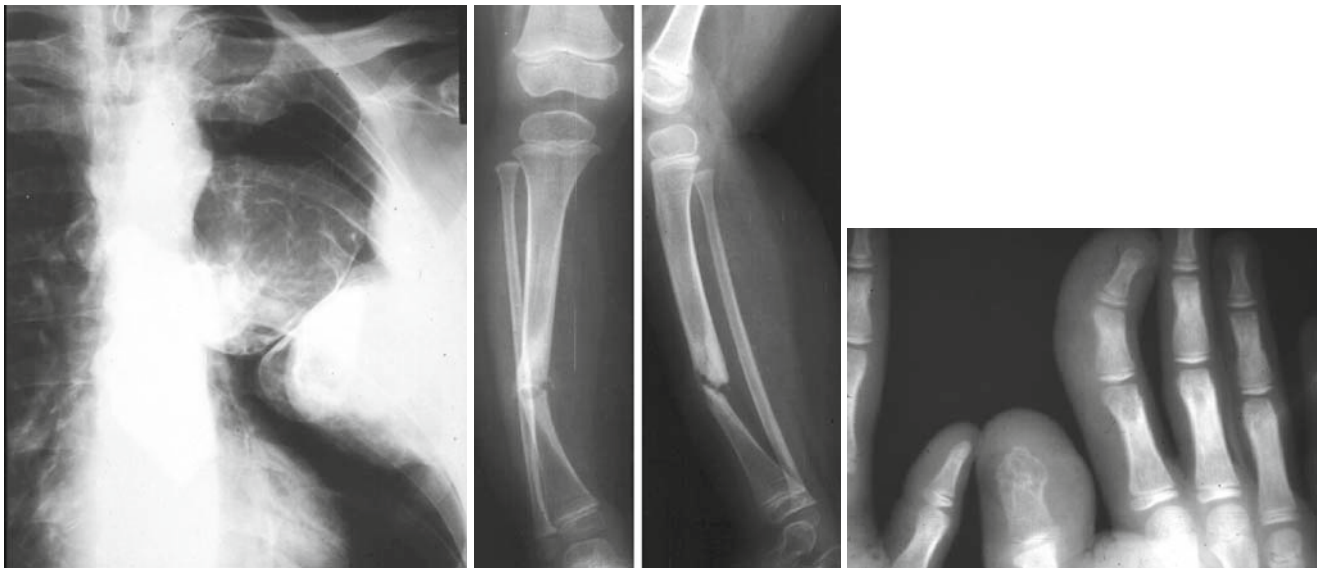

Fig. 13.59 Neurofibromatosis. **a** is an AP view of the left chest showing involvement of the ribs by intraosseous neurofibromas, causing marked focal enlargement of several left ribs. **b** includes AP and lateral radiographs of the right tibia demonstrating a pseudarthrosis of the right tibia in a case of neurofibromatosis. **c** is a PA coned down view of the right hand revealing focal giantism of the right thumb and index in a patient with neurofibromatosis. This should be differentiated from macrodystrophia lipomatosa of fingers (macrodactyly)

vertebral bodies. The spine may also show agenesis or hypoplasia of the pedicles, spondylolisthesis, and wedge-shaped vertebrae. Scoliosis in neurofibromatosis most commonly occurs in the thoracic and thoracolumbar portions of the spine, often showing sharp angulation. The scoliosis may progress to compress the spinal cord and cause paraplegia. Thinning and erosions of the ribs and transverse processes, attributed to a primary mesodermal dysplasia [14], may be present. Pseudarthrosis of the tibia is a common finding in patients with neurofibromatosis (Fig. 13.59b).

Focal gigantism (Fig. 13.59c) is perhaps the most bizarre and fascinating aspect of von Recklinghausen disease. The hypertrophy may involve a single bone, the bones of a part such as a single digit or an entire extremity [2]. The bones are usually normal in shape [2]. The associated muscles and joints are proportionately enlarged. The involved part is usually in the distribution or segment of an affected nerve. At times well-delineated neurofibromas occur within the bone (Figs. 13.57b and 13.59a). They cause focal lytic lesions within the bone and occasionally may enlarge the bone. They may progress slowly and can destroy a large segment of the host bone [2].

Prognosis: Cases of neurofibromatosis (von Recklinghausen) range along a spectrum from mild to severe. A patient may have only a few neurofibromas or café-au-lait spots, or the disease may involve almost every system with hideous skeletal deformity, fantastic skin lesions, and death from a glial tumor of the brain. In most cases, the disease progresses slowly, and sometimes may arrest altogether around the time of cessation of normal growth. The condition may then remain latent for the remainder of a normal life span or it may reactivate at any time and go on to death.

Pseudarthrosis

Pseudarthrosis, or false joint, in neurofibromatosis results from a hereditary pathologic deossification of a weight-bearing long bone, typically the tibia, leading to a non-healing pathologic fracture (Fig. 13.59b). At least half of the pseudarthrosis cases have some evidence of neurofibromatosis, most often café-au-lait spots [2]. The early stages of pseudarthrosis have been noted at birth. More attenuated cases develop during childhood or occasionally in adolescence. Pathologic fracture is the event that usually calls attention to the condition, though radiographic studies frequently reveal a more diffuse process than is represented by the fracture site. Pseudarthrosis most commonly occurs in the lower two thirds of the tibia, but frequently involves the fibula and rarely other long bones.

Prenatal tibial bowing should be differentiated from congenital pseudarthrosis because unlike pseudarthrosis, the former condition has a benign course. Prenatal bowing probably occurs as a result of fetal position in the uterus and regresses over the first years of life. The tibia shows cortical thickening that obliterates the medullary canal at the bowed

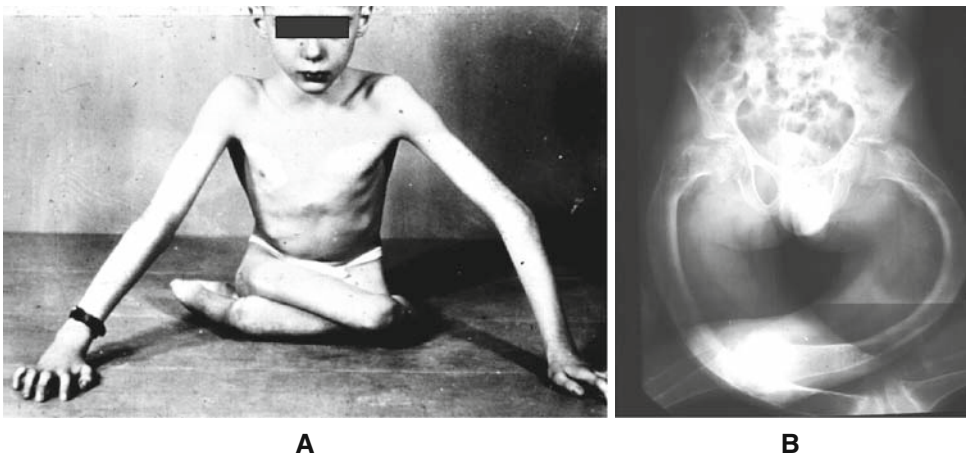

Fig. 13.60 Osteogenesis imperfecta. In osteogenesis imperfecta the bones are fragile and develop numerous fractures that heal with marked callus formation and bowing of the bones. Photograph of a child with OI (**a**) showing marked clinical bowing of the lower extremities. AP radiograph of the femurs (**b**) from the child shown in **a** reveals the bowing deformities

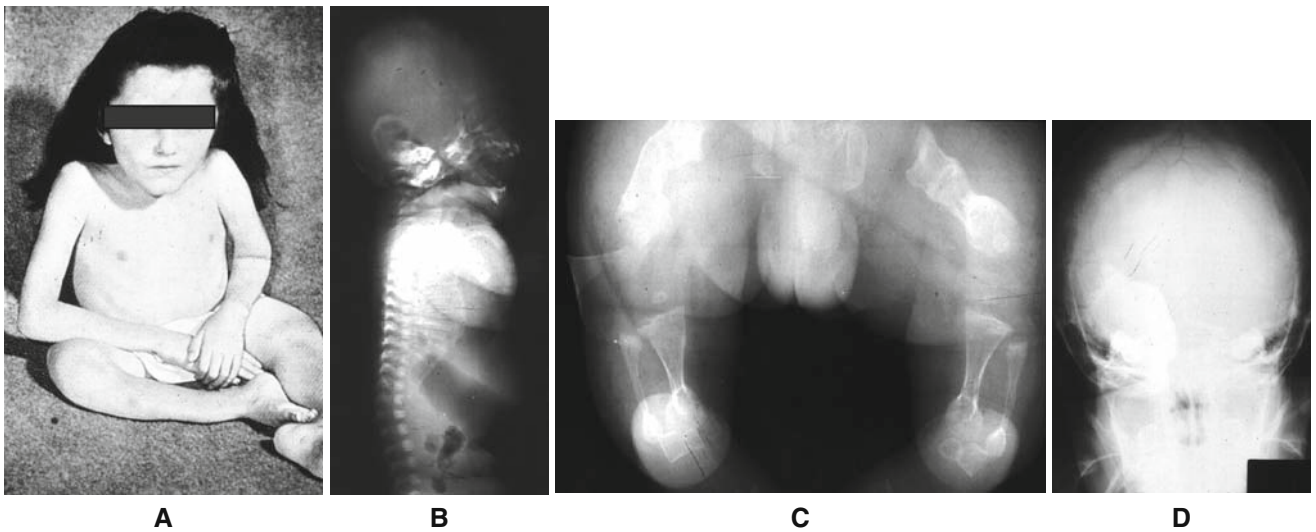

Fig. 13.61 Osteogenesis imperfecta**.** Photograph of a young girl (**a**) with osteogenesis imperfecta. (**b**) is a lateral infantogram of a still born type II, the lethal form OI, demonstrating generalized diminished bone density, cortical thining, fracture and deformed long bones. (**c**) is AP radiograph of the lower extremities of the same case revealing, several healing and fresh fractures of the long bones associated with shortening and severe deformity of the crumpled femurs. **d** is a fronto-occipital skull radiograph of a patient 2.5 years of age, showing calvarial thinning and wormian bones

concavity. As the tibia straightens, the medullary canal reestablishes through this area. Prenatal bowing typically shows medial convexity while in pseudarthrosis the convexity is seen laterally.

Osteogenesis Imperfecta (MIM 166200,166240, 166210, 259420,203760, 259440, 166220) Group 24

Osteogenesis imperfecta (OI) has been called osteitis fragilitans, fragilitas ossium congenita, osteopsathyrosis idiopathica, and brittle bones. OI occurs in 4 per 100,000 births [7]. It is the most common second-trimester ultrasound diagnosis with short bent limbs [7].

OI results from an inability to produce normal osteoid. This, in turn, is caused by a mutation in the genes that code for type1 procollagen alpha fibrils. Because of this mutation, the cartilage fibrils are unable to cross link at the normal copper binding sites. A number of genetic defects cause abnormal type1 collagen synthesis, but OI typically arises from mutations in one of two genes: the *COL1A1* gene on chromosome 17 and the *COL1A2* gene on chromosome 7. Mutations in these genes may cause varying combinations of production of abnormal collagen and/or decreased production of normal collagen, resulting in several OI phenotypes.

Type 1 collagen accounts for about 30% of normal body weight and occurs in multiple organs including the skin, tendons, organ capsules, meninges, fasciae, sclera of the eye, and bone. The result is a patient with a fragile skeleton (Figs. 13.60a and 13.61a), joint hypermobility, thin skin and blue sclera, poor dentition, and a tendency to macular

bleeding. Intramembranous bone formation is severely abnormal. Enchondral bone growth is also defective, but to a lesser extent.

When the teeth are involved, the condition is called "dentinogenesis imperfecta" or "hereditary opalescent dentin." Radiographs show short dental roots and sometimes obliterated pulp canals. Deafness in osteogenesis imperfecta patients who survive into adult life is a frequent complication. As a result of the poor type1 collagen in the sclera, the sclera may range from a barely detectable blue-white tint to a deep sky-blue color.

The 2006 nosology classifies seven types and two additional subtypes of OI. The first four types are true forms of OI while the last three are known as Syndromes Resembling OI (SRO) since the procollagen mutation is not present in these patients. The four clinically distinct types of true OI are [7] as follows:

- **Type I**: Autosomal dominant and blue sclera:
  Group A: Normal teeth;
  Group B: Dentinogenesis imperfecta (DI).
  These patients have little to moderately severe osseous fragility. Blue sclerae persist throughout their lives. Hearing loss develops in 50% of cases by age 40.
- **Type II:** Sporadic dominant mutations causes this disease in majority of cases [7]:
  Group A: have broad crumpled long bones (accordion-like) and beaded ribs. This form of the disease is associated with death in utero or shortly after birth (Fig. 13.61b and c).
  Group B: have broad crumpled long bones, usually without beading. Their ribs fracture easily. Survival is possible.
  Group C: is very rare with thin fractured long bones and thin, mildly beaded ribs.
- **Type III:** Autosomal recessive and non-lethal. Patients have severe limb deformities at birth, poor growth, fractures often at birth and suffer numerous fractures by 2 years of age. These patients have "triangular faces" with frontal bossing, and often have blue sclerae at birth and during infancy that later resolves. They develop kyphoscoliosis, pulmonary arterial hypertension and, diabetes insipidus (DI) may be present.
- **Type IV:** Autosomal dominant with normal sclerae:
  The patients have mild to moderate osseous fragility, similar to type 1, but no bleeding diathesis, a lower frequency of deafness, greater long bone deformities, and normal sclera (can be blue in infancy and childhood).
  Group A: with normal teeth
  Group B: DI.

Type I OI is the most common and least severe form of the disease. Type II is the most severe form with types III and IV have progressively milder clinical signs and symptoms compared with type II.

Patients have varying degrees of fragile, poorly formed bones that tend to have narrow diaphyses and wider epiphyses, creating a gracile appearance. These bones fracture easily, and heal with exuberant callus formation. Unfortunately, the quality of the new bone is the same as all of the bones in the disease. Furthermore, whether from muscle pull, multiple infractions from weight-bearing or simple remodeling under weight-bearing, patients tend to develop bowing of the long bones of their lower extremities.

Radiological manifestations: Osteogenesis imperfecta affects the entire skeleton (Figs. 13.60, 13.61, 13.62, 13.63, 13.64and 13.65). Radiographic manifestations vary according to the severity of the disease, but in general the bones show below normal bone mass (osteoporosis) and evidence of old or recent fractures (Fig. 13.63). The osseous changes may not be apparent during the first years of life, but when they appear, they progress rapidly.

The trabeculae are fine and sparse, and the cortex is thin. In the absence of fracture deformities, the cylindrical bones usually are close to normal in length. Their girth, however, tends to be smaller than normal, creating an appearance of long and gracile bones. The ends of cylindrical bones appear wide when compared to their shafts, and because the trabeculae are sparse the zone of provisional calcification may appear relatively more opaque than normal (Fig. 13.63a). Rarely metaphyseal popcorn calcifications may be observed (Fig. 13.63c).

In the severe neonatal form of the disease (Fig. 13.61b, c), the long bones have very thin cortices and appear wide and short secondary to telescoping multiple fractures, but the cortices are thin. Fractures are integral to the radiographic appearance, and may ultimately lead to marked osseous deformity and short stature. Fractures tend to heal with excessive callus formation. This should not be confused with tumor (Fig. 13.63b).

The skull is strikingly misshapen with protrusion of the frontal and parietal regions and a deeply overhanging occiput. Cranial bossing has been explained on the basis of a failure of ossification of the membranous skull. Multiple centers of ossification, less opaque than normal, arise along the lambdoid suture. As these centers enlarge, they exhibit a mosaic pattern. They are known as Wormian bones (Fig. 13.61d).

Dental radiographs show short roots and sometimes obliterated pulp canals. Chipping and crumbling of the teeth may result in radiographic findings resembling the appearance of caries.

Vertebral compression fractures are common. Biconcave deformities of the vertebrae are observed frequently (Figs. 13.62b and 13.65a).

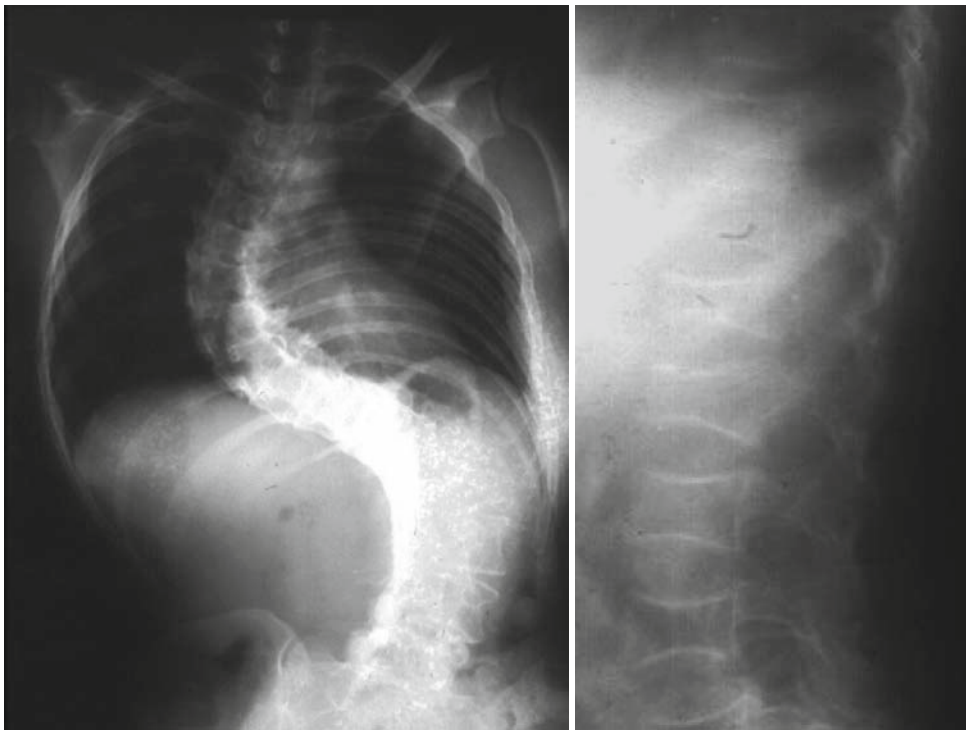

Fig. 13.62 Osteogenesis imperfecta**.** AP radiograph of the spine (**a**) shows S-shaped scoliosis of the spine. Lateral lumbar spine radiograph (**b**) in a different case shows osteoporosis with biconcave deformity of the lumbar vertebral bodies that simulate the appearance of senile osteoporosis

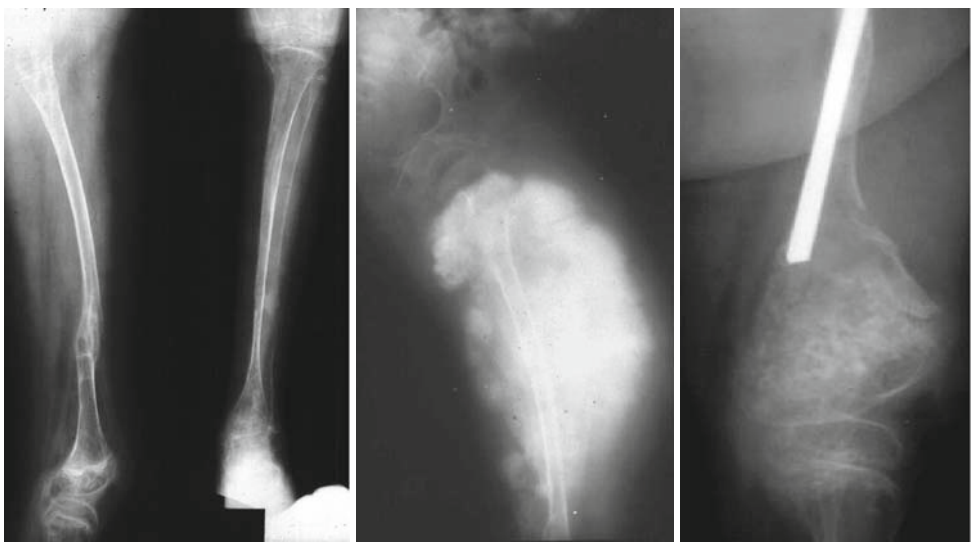

Fig. 13.63 Osteogenesis imperfecta**.** Lateral radiograph of the left femur and AP radiograph of the left tibia and fibula (**a**) showing osteogenesis imperfecta with gracile and osteopenic bones. Note the old healed fracture of the femur with mild residual deformity. Lateral femoral radiograph (**b**) from another patient shows a femoral fracture with excessive callus formation. The excessive callus during fracture healing in osteogenesis imperfecta should not be confused with osteosarcoma. AP radiograph of the left knee (**c**) shows metaphyseal pop corn calcification in another case. **c** is courtesy of Dr Robert Schneider, Hospital for Special Surgery, New York, NY

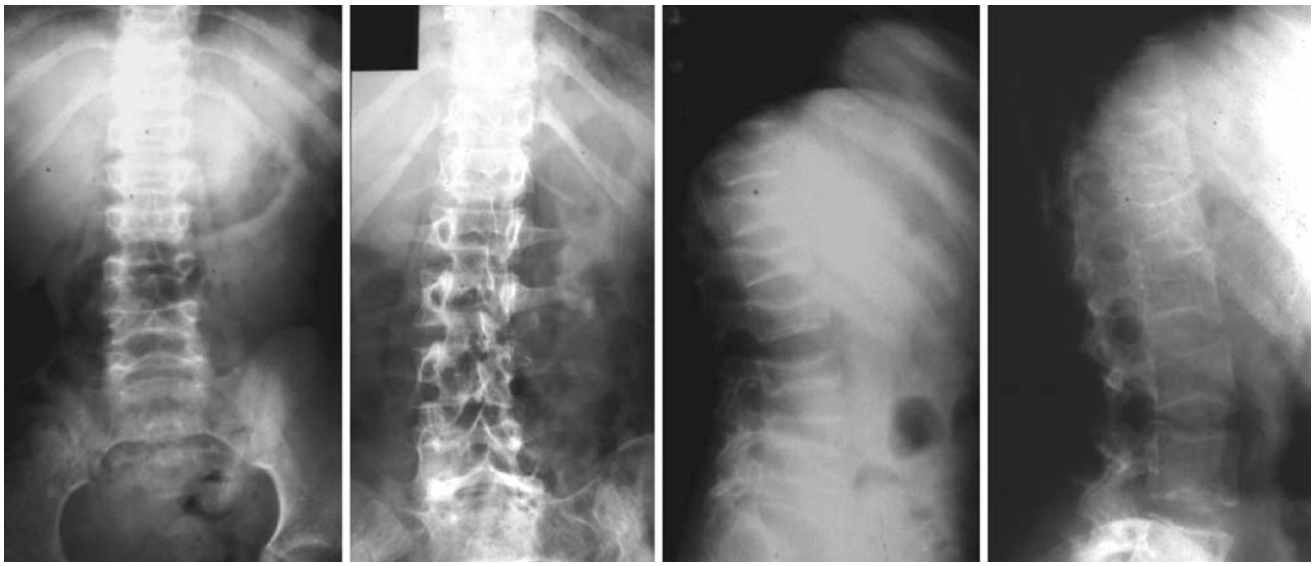

Fig. 13.64 Osteogenesis imperfecta**.** Comparison of AP and lateral views of lumbar spine from 11 years of age (1955) to 21 years of age (1965) shows improvement of biconcave vertebral body deformities. Residual mild biconcave deformity and osteoporosis are still present, but improved

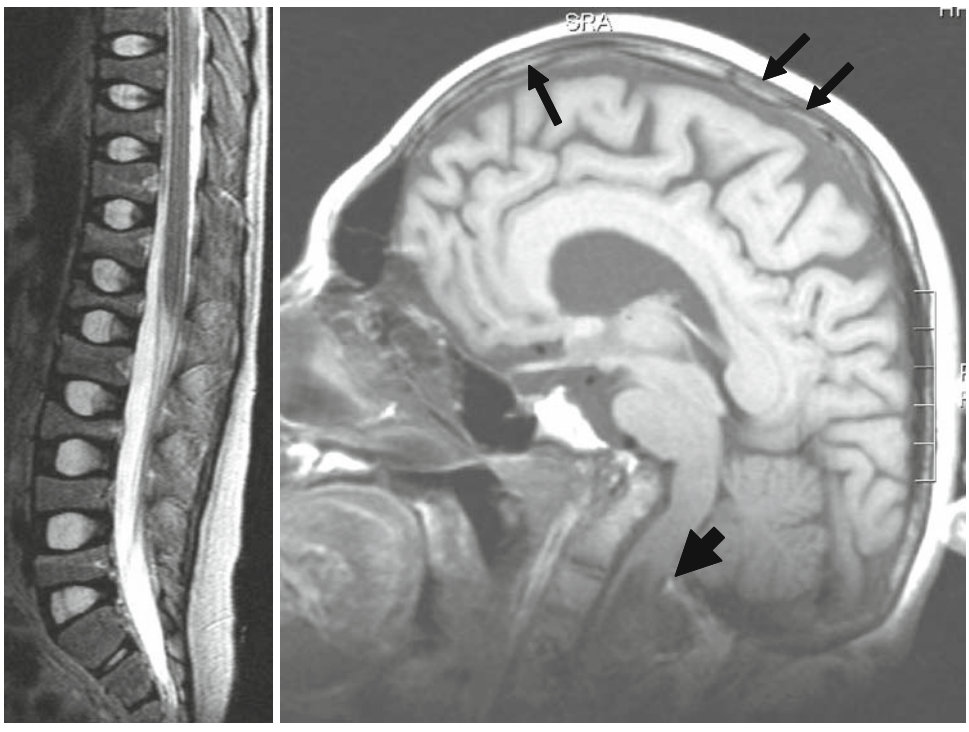

Fig. 13.65 Osteogenesis imperfecta**.** Sagittal T2 MRI of the thoracolumbar spine (**a**) in a 10-year-old girl with OI showing biconcave deformities of the vertebral bodies and large intervertebral disc spaces. T1 sagittal MRI of the head (**b**) of a 25-year-old man with OI showing basilar invagination and revealing that the tip of the odontoid process of C2 is markedly higher than foramen magnum, the posterior border of which is marked by a *short arrow*. This finding is most common in type IV OI. Note thinning of the calvarium and presence of wormian bones (*arrows*). Courtesy of Dr Ingrid B Kjellin, Loma Linda University Medical Center, California

In patients that survive to adulthood, the appearance of spine improves radiologically (Fig. 13.64). MRI shows osseous deformities better than radiographs and is particularly valuable for evaluation of serious changes such as basilar invagination as would be typical of type IV OI (Fig. 13.65b).

Osteolysis, Torg Syndrome (MIM 277950 and 259600) Group 27

Group 27 of the 2006 nosology [1] of genetic skeletal disorders includes diseases with osteolysis. Eight subgroups are reported in this classification. Spranger et al. [3] divide osteolysis syndromes into three categories: congenital forms that include 29 entities; acquired forms that include 28 entities; and syndromes with short distal phalanges that may mimic acroosteolysis that include 20 entities.

Multicentric osteolysis syndrome, also know as carpal–tarsal osteolysis syndrome and Torg (Torg–Winchester or Winchester–Torg) syndrome [18–20], is an excellent example of congenital osteolysis. In this autosomal recessive entity, patients have a deficiency of their MMP2 protein. They develop hand deformities associated with progressive decrease in size of hands, contractions, and swelling (Fig. 13.66a). In the Torg form of the disease, patients often develop subcutaneous nodules, frequently in plantar regions of the feet. In Winchester form, patients have cutaneous involvement including hyperpigmentation, erythema, and hypertrichosis. They also may have corneal opacities and enlarged tongue. These patients have acral bone loss, renal disease, hypertension, and they die in early childhood.

Radiographs show progressive and ultimately complete resorption of the carpus, tarsus, and partial resorption of adjacent tubular bones (Fig. 13.66b). The metacarpals have broad girth in the Winchester form of the disease.

Osteopathia Striata with Cranial Sclerosis (Voorhoeve Disease) (MIM 166500) Group 22

This disease is usually asymptomatic and is discovered serendipitously on radiographic examinations performed for another reason. Patients with osteopathia striata develop multiple linear condensations of cancellous bone tissue that begin at the epiphyseal plate and extend into the diaphysis (Fig. 13.67). In the ilium, the striations form a sunburst about the acetabulum and fan out toward the iliac crest. Any or all of the long bones may be involved. The disease tends to be more apparent in bone formed at the most active growth centers, e.g., the metaphyses around the knee. The base of the skull may show sclerosis and poor aeration of the mastoid cells and the sinuses [2]. Similar striations may be observed in enchondromatosis and types I–III of juvenile osteopetrosis [3].

Osteopetrosis (MIM 259 700, 259710, 259 730, 166600, 300301, 600329, 122900) Group 22

Osteopetrosis, also known as Albers–Schonberg disease, osteosclerosis fragilis, marble bones, and chalk bones, is a hereditary abnormality of bone growth [32]. More than 750 cases were reported by 1994. The frequency of osteopetrosis

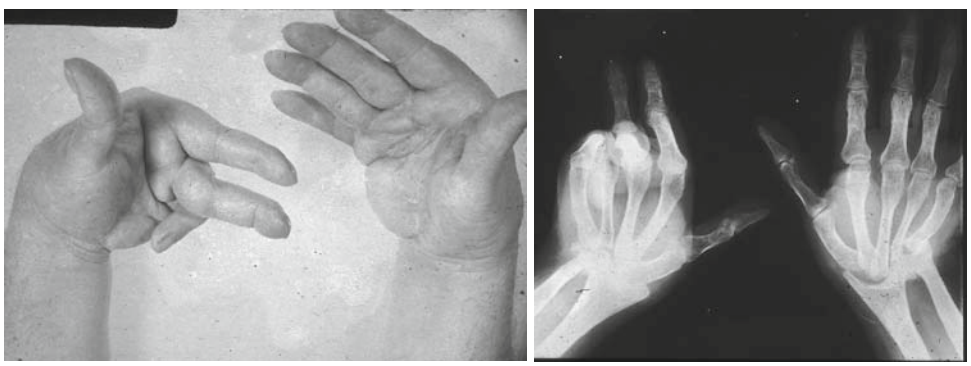

Fig. 13.66 Osteolysis**.** Photograph of hands (**a**) in a young woman with carpal–tarsal osteolysis (Torg type). PA radiograph of the same patient's hands (**b**) show bilateral carpal osteolysis. The radius and ulna are in contact with proximal first and fifth metacarpals on both sides. There is bilateral ulnar deviation of hands with flexion deformities of metacarpophalangeal joints, which is most advanced at the left fourth and fifth MP joints. (Courtesy of Dr Joseph Torg, Temple University Hospital, Philadelphia, PA)

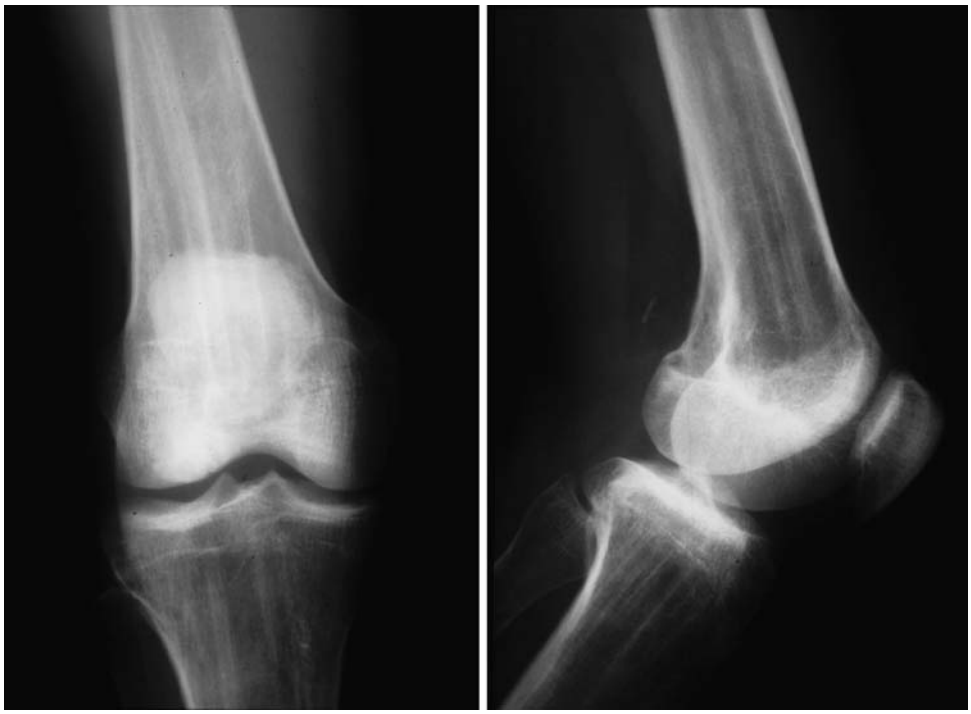

Fig. 13.67 Osteopathia striata. AP and lateral knee radiographs show multiple parallel linear dense streaks in the distal femur and in the proximal tibia. (Courtesy of Dr Murray K. Dalinka, Hospital of the University of Pennsylvania, Philadelphia, PA)

has been reported to range widely from 1 per 500,000 to 5.5 per 100,000 births [7 **].**

Six types of osteopetrosis have been included in group 22 of 2006 classification [1]. MIM 259700 includes three subtypes and MIM 166600 has two subtypes (166600, and 300301) [1]. Group 22 represents bone diseases of increased bone density without modification of bone shape. It is important to note, however, that osteopetrosis, the most important example of this group shows failure of modeling of the metaphyseal regions of long bones resulting in widening and deformity (Figs. 13.68a, b, 13.70b, 13.71a and 13.72b).

Springer et al. have divided osteopetrosis into two main groups [7]:

The infantile group has four subtypes [3]. Three of four infantile subtypes are associated with neonatal death. Patients with type 4, "malignant infantile type" die in first decade if untreated [3].

The Juvenile group has six subtypes. These patients survive to adulthood [3]. Type VI in their juvenile group is pyknodysostosis [3].

Osteopetrosis is caused by osteoclast failure. Bone is formed normally, but is not resorbed. The result is dense and thick bones with poor medullary canal formation. These findings vary greatly in severity depending upon the cause of the osteoclast failure. Over 100 different mutations along the pathway of osteoclast activation and function have been reported. This means that although osteopetrosis manifests as a certain phenotype, its causes are myriad.

Radiological manifestations: The infantile form of osteopetrosis shows striking uniform increased bone density of the entire skeleton without trabeculae and without differentiation between the cortex and medullary bone (Fig. 13.68).

In milder forms of the disease patients may survive into adulthood. Patients have generalized increased density of the calvarium, but the base of the skull shows the most marked thickening and sclerosis (Fig. 13.69a). The mastoid air cells and paranasal sinuses are underdeveloped. The cranial fossae may be distorted and the neural foramina may narrow causing cranial nerve deficits.

The spine shows a bone-within-the-bone appearance or a typical "sandwich" type [32] of increased density of vertebral bodies (Fig. 13.69c). The latter may be seen in other entities such as hypervitaminosis D. Increased spinal bone density similar to osteopetrosis also may be evident in craniometaphyseal dysplasia, osteomesopyknosis [3], and idiopathic hypercalcemia. The appearance of the remainder of the skeleton, however, is different in the latter cases. The pelvis shows uniform increased density and mild protrusio acetabulae (Fig. 13.70a). The ribs (Fig. 13.69b) and the long bones are very dense.

Distinct transverse alternating bands of density and lucency are seen in the long bones in milder cases [17]

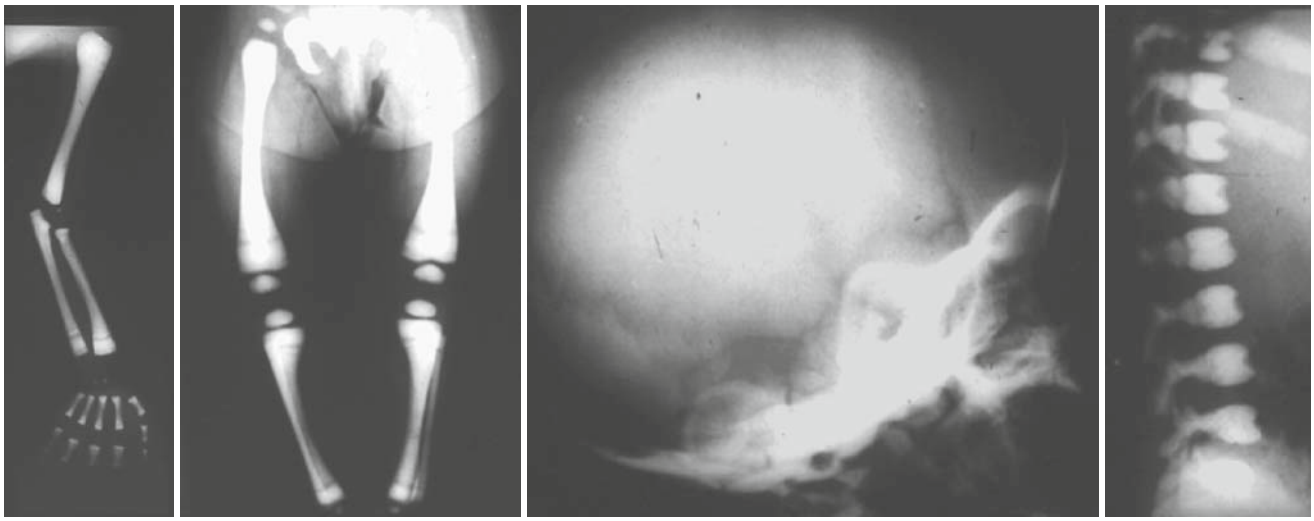

Fig. 13.68 Osteopetrosis. Radiographs of the upper (**a**) and lower (**b**) extremities, lateral skull **c** and lateral lumbar spine (**d**) of a patient with infantile osteopetrosis that show uniform increased bone density. No trabecular pattern can be identified in the bones, hence the name "marble bone disease." The medullary spaces are virtually non-existent. The base of the skull shows significantly more increased density compared with the calvarium **a** and **b** show metaphyseal transverse lucencies in the long bones and failure of metaphyseal modeling in the areas of most active growth (proximal humerus, distal radius, distal femur and proximal tibia). Please see Fig. 13.72a for description of bone modeling

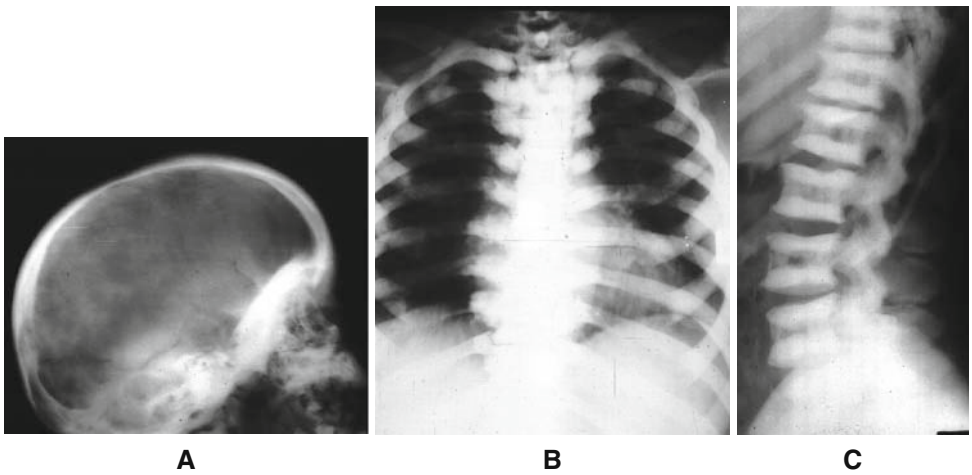

Fig. 13.69 Osteopetrosis in a 61-year-old man. Lateral skull (**a**), AP ribs (**b**), and lateral lumbar spine (**c**) radiographs show generalized increased density of bones. The base of the skull is uniformly thick and dense (**a**). The superior and inferior aspects of vertebral bodies have markedly increased density creating a so called (*sandwich appearance*) to the vertebral bodies (**c**)

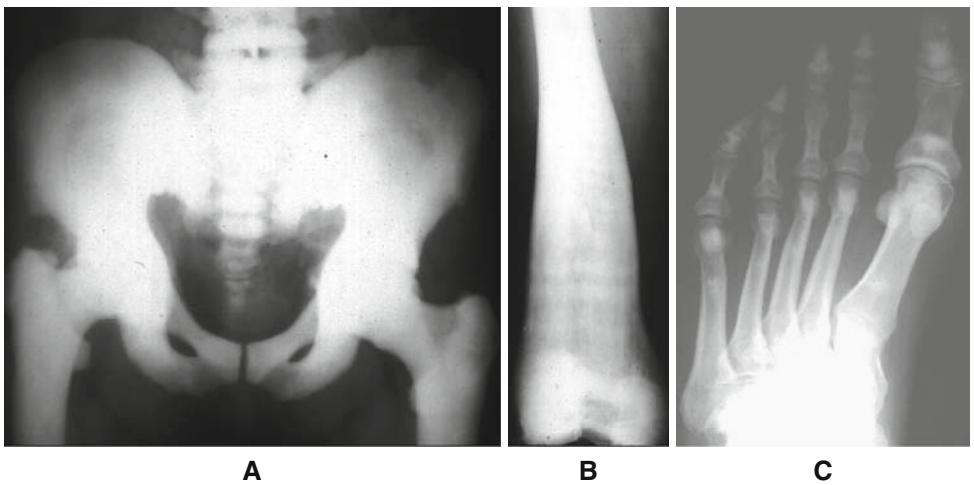

Fig. 13.70 Osteopetrosis. This is a 61-year-old man. AP pelvis radiograph (**a**) shows uniformly dense bones. Note mild protrusio acetabulae. AP radiograph of the distal femur (**b**) shows uniform increased density of the femur with distinct transverse radiolucencies and poor modeling. Radiograph of the forefoot (**c**) shows characteristic distinct transverse densities in the distal metatarsals and proximal phalanges

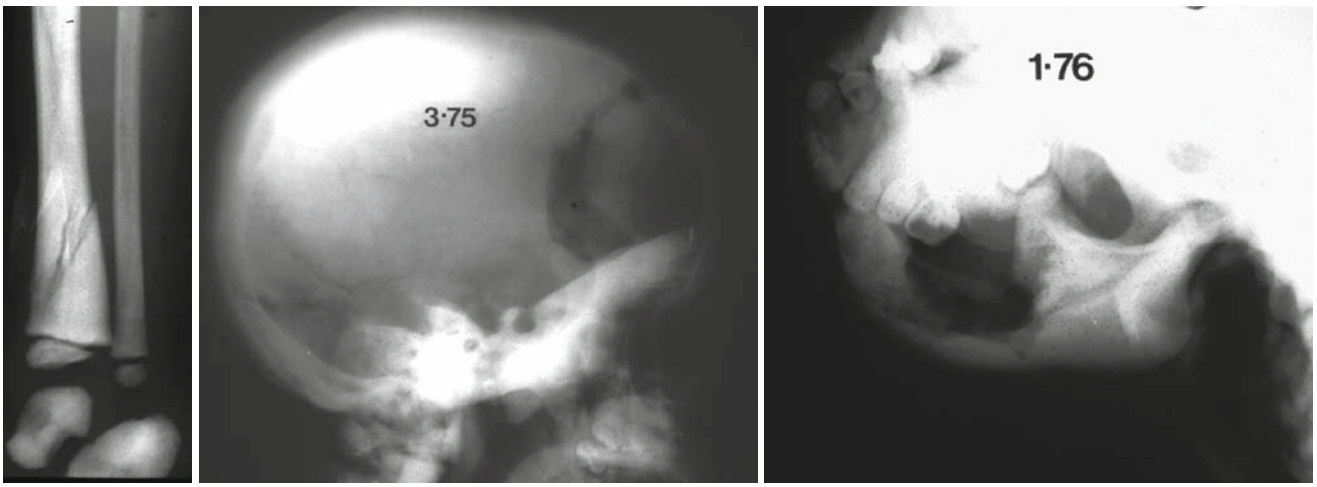

Fig. 13.71 Osteopetrosis**.** Oblique ankle radiograph (**a**) in a 4-year-old patient with osteopetrosis and a pathologic fracture of distal tibia. Lateral skull radiograph (**b**) in a 29-year-old man with osteopetrosis and a craniotomy for treatment of optic nerve compression. Oblique mandible radiograph (**c**) in the same patient as **b** showing a surgical defect of the right mandible that was performed for treatment of osteomyelitis

(Fig. 13.70b). The metaphyses of the long cylindrical bones are increased in girth as a manifestation of failure of metaphyseal modeling (Figs. 13.68a, b, 13.70b, and 13.72b). A schematic of the process of metaphyseal modeling is shown in Fig. 13.72a. As the long bone grows longitudinally, the old bone must be partially resorbed in its periphery, in order for the bone diaphysis to remain cylindrical and the metaphysis continue to have a funnel appearance (Fig. 13.1). Failure of metaphyseal modeling (funnelization) is most marked where bone growth is most rapid, and as a result it is particularly evident in the distal femurs, giving a characteristic appearance known as Erlenmeyer flask deformity (Figs. 13.68b, 13.70b, and 13.72b). This deformity persists to adult life after closure of the epiphyseal plate (Fig. 13.70b). A radiolucent outline may show a bone within a bone appearance in long bones, vertebral bodies, flat bones and ossification centers. The hands and feet of adults show distinctive transverse densities in the metacarpals, metatarsals, and phalanges (Fig. 13.70c).

Prognosis: The symptoms and ultimately the course of osteopetrosis depend largely upon the severity of marrow space involvement and the age at onset. The more severe the stenosis and loss of the marrow space, the more prone the patient is to infection and anemia. As a result, infection is the most common cause of death in these patients. If the patient survives early childhood, he has a fair chance of attaining adulthood and older age [32] (Figs. 13.69 and 13.70). The longer he lives, the less likely he is to die of this disease [2].

Fractures are common (Fig. 13.71a), and in the adults they are characteristically transverse. They heal rapidly with abundant callus. Two other adult complications that arise in osteopetrosis are osteomyelitis of the mandible and blindness from osseous narrowing of the optic foramen causing compression on the optic nerve (Fig. 13.71b, c).

Osteopoikilosis (MIM 155950) [1] (MIM 166700) [3, 7] Group 22

Osteopoikilosis literally translates to spotted bone. Typically patients with this condition, as with osteopathia striata, have no symptoms, but the former may have a dermatological condition known as dermatofibrosis lenticularis disseminata (disseminated areas of lenticular skin fibrosis).

Numerous spheroid or lenticular nodules of condensed bone (bone islands) occur in the spongiosa of the metaphysis or epiphysis of bones in patients with osteopoikilosis (Fig. 13.73). These well-delineated opacities have been described in almost every bone, but they most commonly occur in the small bones of the hands and feet, at the ends of the large bones of the extremities and in the pelvic bones about the acetabulum. They are rarely found in the skull. While this disease appears to be sporadic in humans, a genetic form of the disease has been described in sheep.

Melorheostosis may occur in conjunction with osteopoikilosis (IMM 155950, group 22). Whyte and Murphy described a series of patients with varying combinations of melorheostosis, osteopathia striata, and osteopoikilosis [2]. They coined the name mixed sclerosing bone dystrophy to describe these patients.

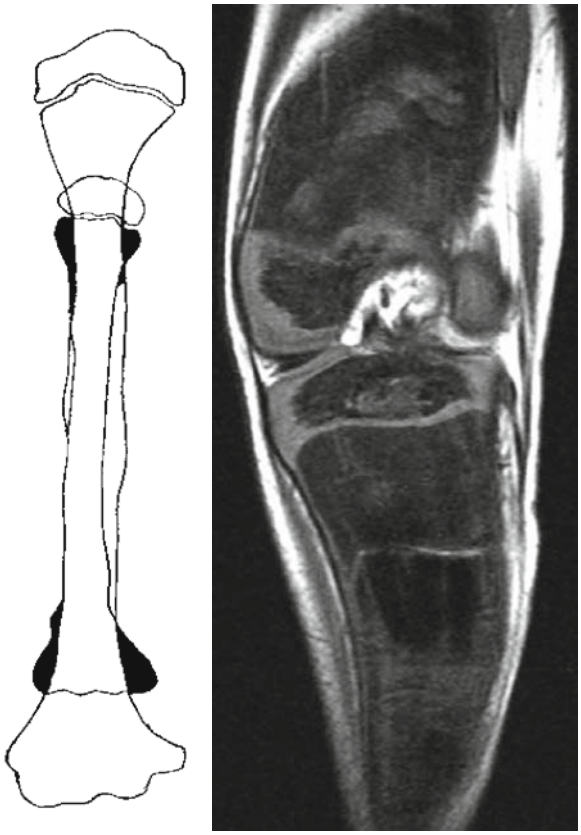

A B

Fig. 13.72 Bone modeling. **a** in this figure is a *line* drawing showing the silhouettes of a 5-year-old bone superimposed on a 12-year-old. Note portions of the younger bone that have undergone remodeling to form the shaft of the older bone. Several bone dysplasias such as osteopetrosis have failure of normal bone modeling as demonstrated in Figs. 13.70b and 13.72b. See Fig. 13.30 for an example of failure of modeling in Gaucher disease. **b** in this figure is T2 coronal MRI of the knee showing failure of modeling of the distal femur and proximal tibia in a seven year-old boy with osteopetrosis. (**b** is Courtesy of Dr Ingrid B Kjellin, Loma Linda University Medical Center, California)

Osteopoikilosis may be accompanied by hereditary multiple cartilaginous exostoses and by a tendency to form keloids [2]

Prognosis: Osteopoikilotic nodules may be present at birth or they may appear after birth and increase in number during growth. Periodically visualization of the lesions in some cases shows that they tend to grow larger during growth and may diminish in size or even fade away completely with bone remodeling.

Pseudoachondroplasia (MIM 177170) Group 8

This entity is also called the *achondroplastic form of spondyloepiphyseal dysplasia*. It is one of the most common forms of non-lethal skeletal dysplasias [7]. Patients have short limbs and disproportionately long trunk. The skull is normal. Kyphoscoliosis may be present. A constant finding is central beaking (togging) of vertebral bodies, but otherwise they do not have the same spinal abnormalities as achondroplasts. These patients have poor epiphyseal ossification, knock-knees, or bow legs and hypermobility of all joints except their elbows [3].

Pyknodysostosis (MIM 256800) Group 22

Pyknodysostosis results from mutations in the gene encoding cathepsin K (CTSK) [3]. As of 2004, 165 cases have been reported [7]. This dysplasia may be confused with osteopetrosis because the bones are denser than normal and also confused with cleidocranial dysplasia (Figs. 13.74, 13.75, and 13.76) because of skull and clavicular abnormalities. It is, in fact, classified in the Springer classification as type VI infantile osteopetrosis.

Many believe that Toulouse Lautrec, the famous French artist, suffered from this disease [3, 2]. Dwarfing occurs in

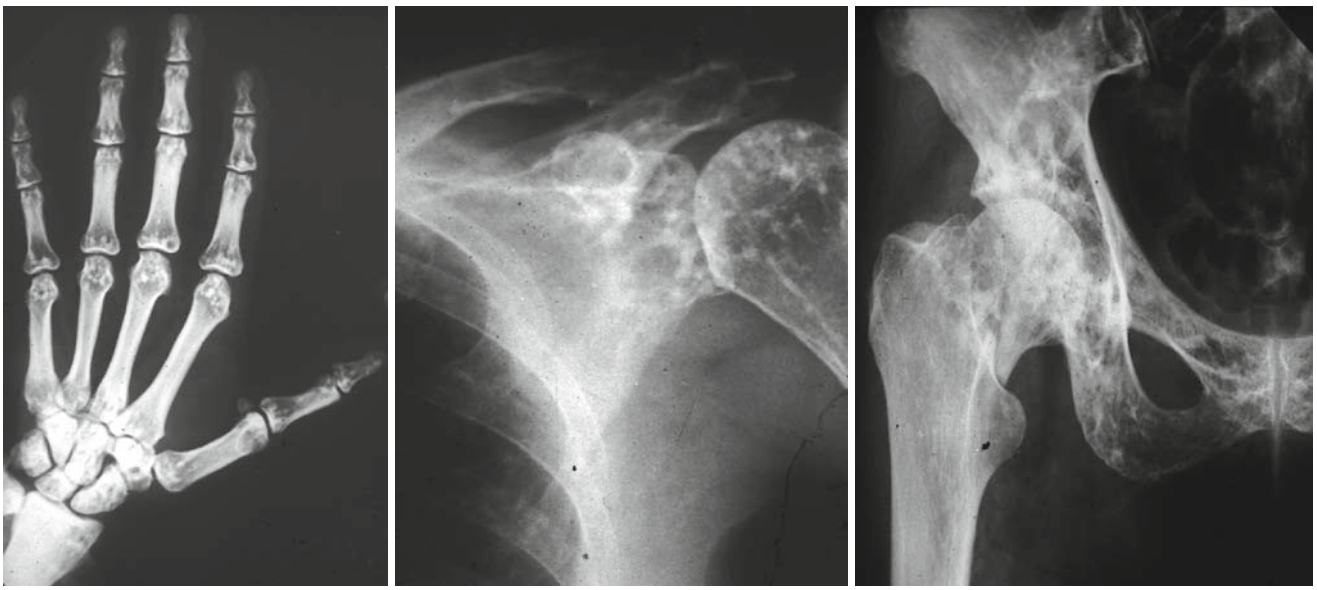

Fig. 13.73 Osteopoikilosis**.** PA hand (**a**), left shoulder (**b**) and right hip (**c**) radiographs show ovoid and spherical opacities bone islands in the bones clustered around the joints

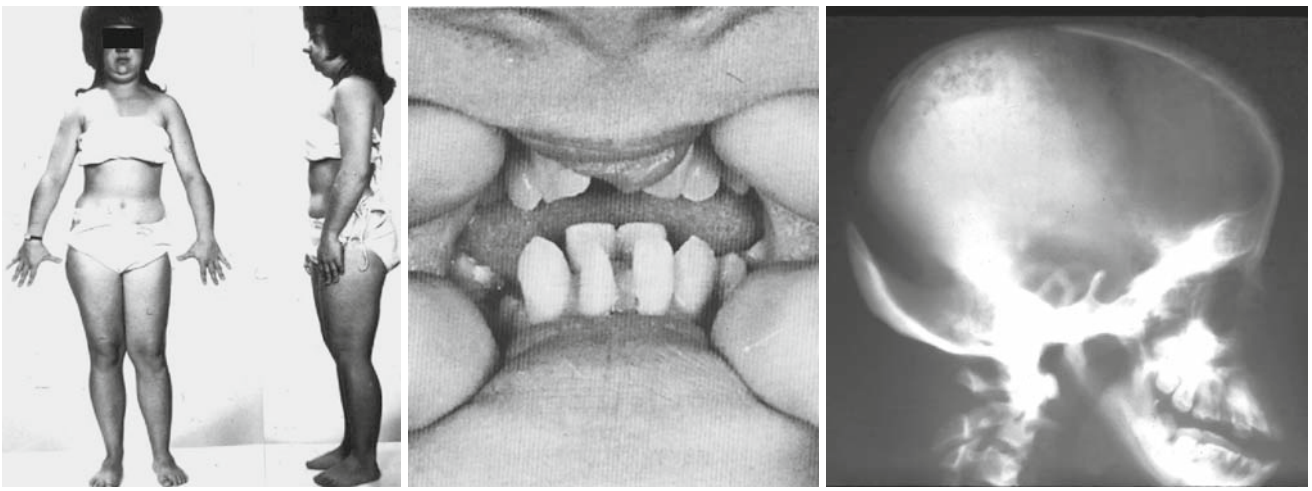

Fig. 13.74 Pyknodysostosis. AP and lateral photographs of a patient with pyknodysostosis (**a**) showing an enlarged head (related to open sutures), receding jaw and tapering of the ungual tufts due to osteolysis of the distal phalanges. Photograph of open mouth (**b**) shows a double set of teeth (Photo courtesy of Dr Eyering). Lateral skull radiograph (**c**) shows hypoplasia of the temporal bones and an open posterior fontanelle. (Radiograph **c** is courtesy of Dr Soroosh Mahboubi, Children's Hospital of Philadelphia, PA)

the more severe cases with patients growing to less than 5 ft in height [2]. Patients with this disorder suffer numerous fractures throughout their lives from poorly formed bone (Fig. 13.75b). These fractures may lead to progressive loss of height over the patient's lifetime. The hands are short and stubby (Fig. 13.74a) with acroosteolysis of the terminal phalanges [21] . The nails may show koilonychia (spoon nails). Deciduous teeth may persist with unerupted or malformed permanent teeth (Fig. 13.74b).

Radiologic manifestations: Radiographs of patients with pyknodysostosis have some similarity to those of osteopetrosis and cleidocranial dysplasia. The entire skeleton usually displays increased uniform bone density, without demonstrable trabecular markings (Fig. 13.75). The cranial sutures consistently fail to close and numerous Wormian bones develop. The mandibular angle is hypoplastic, resulting in a receding jaw (Fig. 13.74a). The hands are short and show acroosteolysis of terminal phalanges. Changes in the ungual tufts result

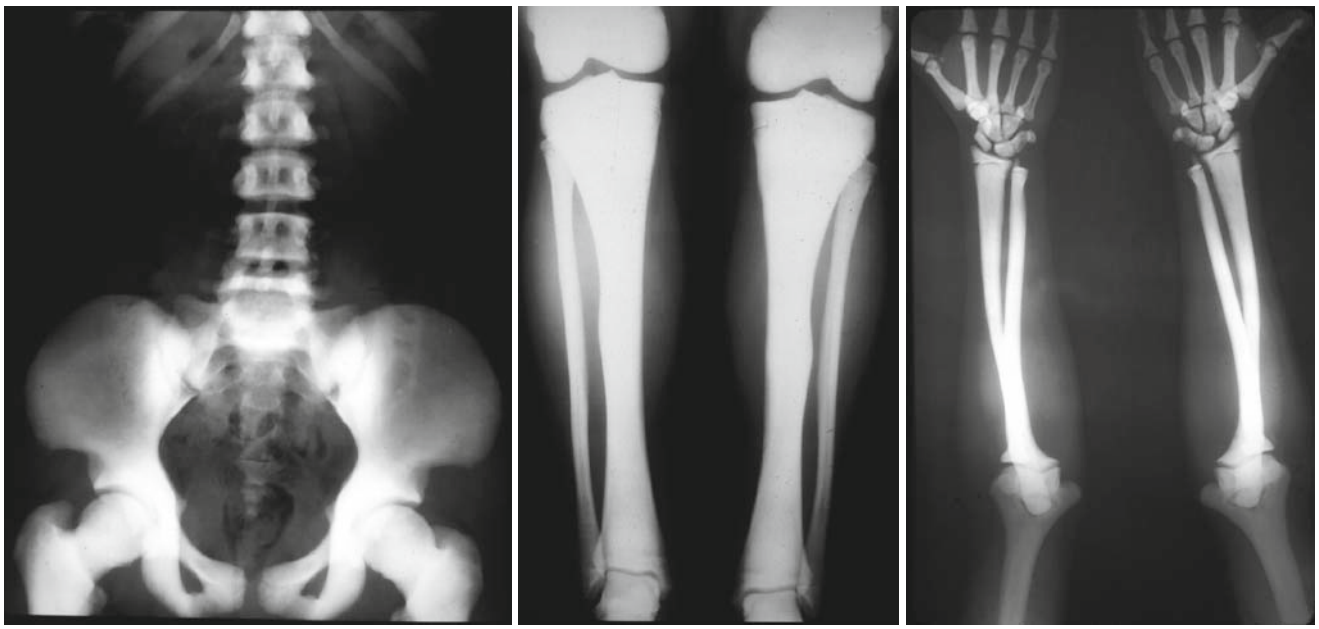

Fig. 13.75 Pyknodysostosis. AP abdomen radiograph (**a**) shows increased density of the lower ribs, lumbar spine, pelvis, and upper femurs. AP radiograph of the legs (**b**) shows increased density of the distal femurs, both tibiae and fibulae as well as the tali. Note old healed fractures of the tibias. AP radiograph of the forearms (**c**) also shows diffuse increased density of the bones. (Radiographs **a** and **b** are courtesy of Dr Murray K. Dalinka, Hospital of the University of Pennsylvania, Philadelphia, PA, Radiograph **c** is courtesy of Dr Soroosh Mahboubi, Children's hospital of Philadelphia, PA.)

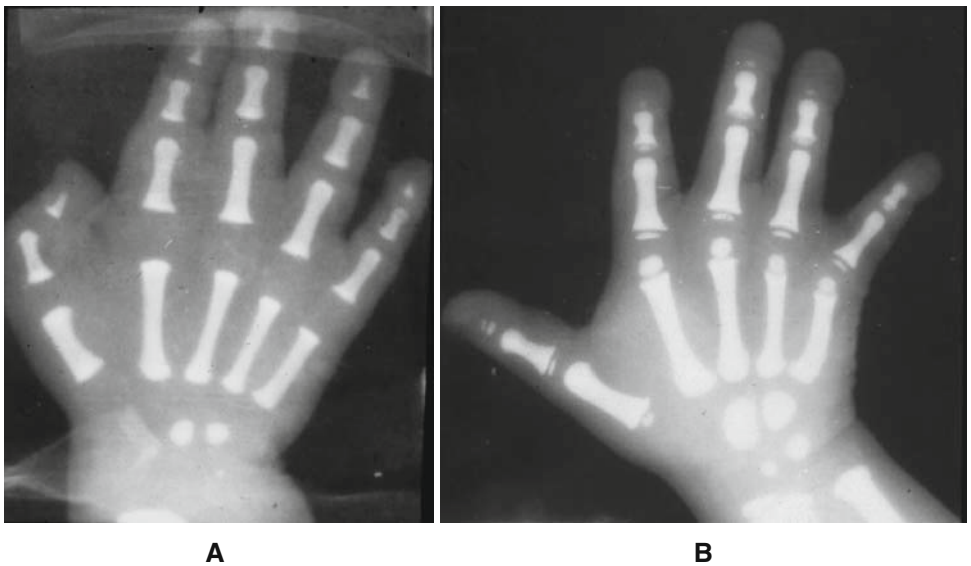

Fig. 13.76 Pyknodysostosis. PA radiograph of the right hand of a patient at 6 months of age (**a**) and at 4 years of age (**b**) showing diffuse increased osseous density and progressive acroosteolysis. This case shows that the changes of the tufts are from acroosteolysis and not hypoplasia. (Images are courtesy of Dr Murray K. Dalinka and Dr Edward Smith)

from Osteolysis, not hypoplasia. Thus, a child with pyknodysostosis with normal ungual tufts at the age of 6 months can develop acroosteolysis as they age (Fig. 13.76) [21].

As with cleidocranial dysostosis and Poland syndrome, the clavicles in pyknodysostosis are often hypoplastic. Unlike Poland syndrome and cleidocranial dysplasia, the clavicular abnormality in pyknodysostosis is usually confined to the distal ends of the clavicles.

Saddan: (MIM 134934) (Severe Achondroplasia, Developmental Delay, and Acanthosis Nigricans) Group 1

As the name indicates these patients suffer all of the skeletal abnormalities of severe achondroplasia and have developmental delay. They also have acanthosis nigricans, a diffuse hyperplasia and thickening of the prickle-cell layer of epidermis as occurs in psoriasis. This manifests itself clinically as diffuse velvety skin thickening with gray, brown, or black pigmentation, chiefly in the axillae and other body folds [16].

Spondyloepiphyseal Dysplasia

Patients with spondyloeopiphyseal dysplasia (SED) develop a dwarfism that arises from major abnormalities in the development of both the spine and epiphyses (Figs. 13.77, 13.78, 13.79, 13.80, 13.81, 13.82). Four types of SED have been catalogued in the 2006 nosology: spondyloepiphyseal dysplasia congenita in group 2, pseudoachondroplastic spondyloepiphyseal dysplasia in group 8 which has been described above. The third and fourth types are listed in group 11 (Kimberly and Wollcot–Rallison types) [1].

Spondyloepiphyseal Dysplasia Congenita (MIM 1839002) Group 2 (Collagen Group)

These patients show disproportionate dwarfism, with delay in development of ossification centers. As a result, the ossification centers of the pubic bones, knees, the sacrum, and the upper cervical spine are invisible on radiographs, and the patients have deformed vertebral bodies in their thoracic and lumbar spine (Figs. 13.77 and 13.79). At maturity, these patients have short spines, coxa vara, shortening of their long bones, and flattening of their epiphyses. Their hands and feet are normal in appearance in the majority of patients [3].

Spondyloepiphyseal Dysplasia Tarda, X-Linked (MIM 313400) (Spondyloepimetaphyseal Group) Group 11

These patients are micromelic and have a short trunk dwarfism. Clinically, they complain of back pain and develop premature osteoarthritis. Unlike achondroplasts, these patients do not have saddle nose. This is because membranous bones have no epiphyses, and so the skull is not affected. Typically the hips show the most severe changes (Fig. 13.81). The hands and feet appear short and pudgy [2].

Spranger et al.[3] describe two other types of spondyloepiphyseal dysplasia tarda (SEDT). One is progressive pseudorheumatoid chondrodysplasia in group 11 (MIM 208230) [1] and the other is the brachyolmia in group 13 (MIM 271530 and 271630) of 2006 classification [1].

Radiological manifestations: In the archetype of SEDT, the appearance of secondary ossification centers is delayed. Later, when they do appear, the epiphyseal centers of the long bones are fragmented and deformed (Figs. 13.79a, 13.80b and 13.81). Ossification is defective, with secondary alterations in the epiphyseal plate and, in some instances, in the metaphysis as well [2] (Fig. 13.79a).

In childhood the vertebral bodies are ovoid. During adolescence and adult life, the bodies show platyspondyly (Figs. 13.78 and 13.80) [7]. There are hump-like prominences posteriorly at the superior and inferior aspects of vertebral bodies [7] (Fig. 13.79d). Narrow disc spaces, scoliosis (Fig. 13.78a, b), and cone-shaped odontoid process are present [7]. During adulthood, the peripheral joints, particularly the knees and hips, develop premature osteoarthritis [2].

Thanatophoric Dysplasia (MIM 187600 and 187601) Group 1

Thanatophoric dysplasia is a severe rhizomelic dwarfism and is the most common lethal dysplasia. Thanatophoric dysplasia and achondrogenesis together account for 62% of lethal dysplasias [4]. (Other lethal skeletal dysplasias include achondroplasia and osteogenesis imperfecta (mostly type 2).) Thanatos is the Greek word for death. Patients with this dysplasia die at or soon after birth. It has two types (I and II), both of which are closely related to achondroplasia.

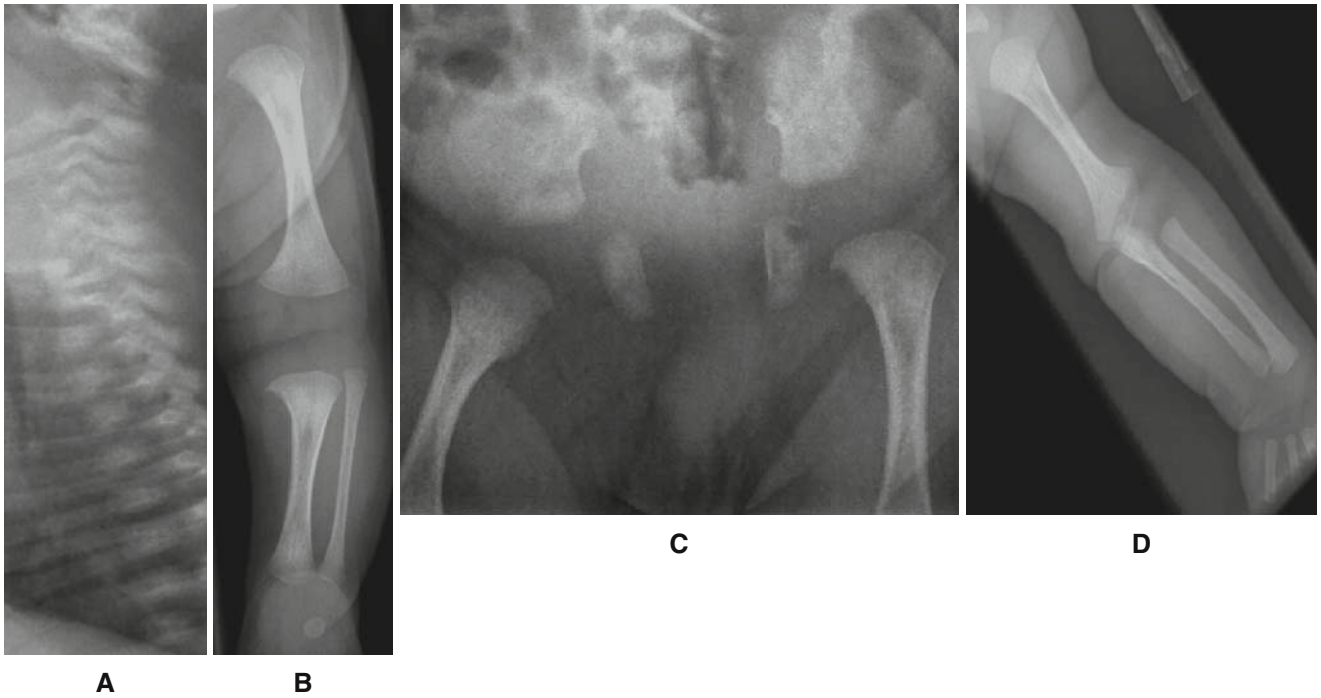

Fig. 13.77 Spondyloepiphyseal dysplasia. Lateral cervical and thoracic spine radiograph **(a)** shows vertebra plana deformity, mort marked in the cervical than the thoracic region. AP radiographs of the leg (**b**), pelvis (**c**) and left arm (**d**) show absence of epiphyseal ossification centers. (Images are courtesy of Dr Ralph Lachman, Emeritus professor of Radiology UCLA)

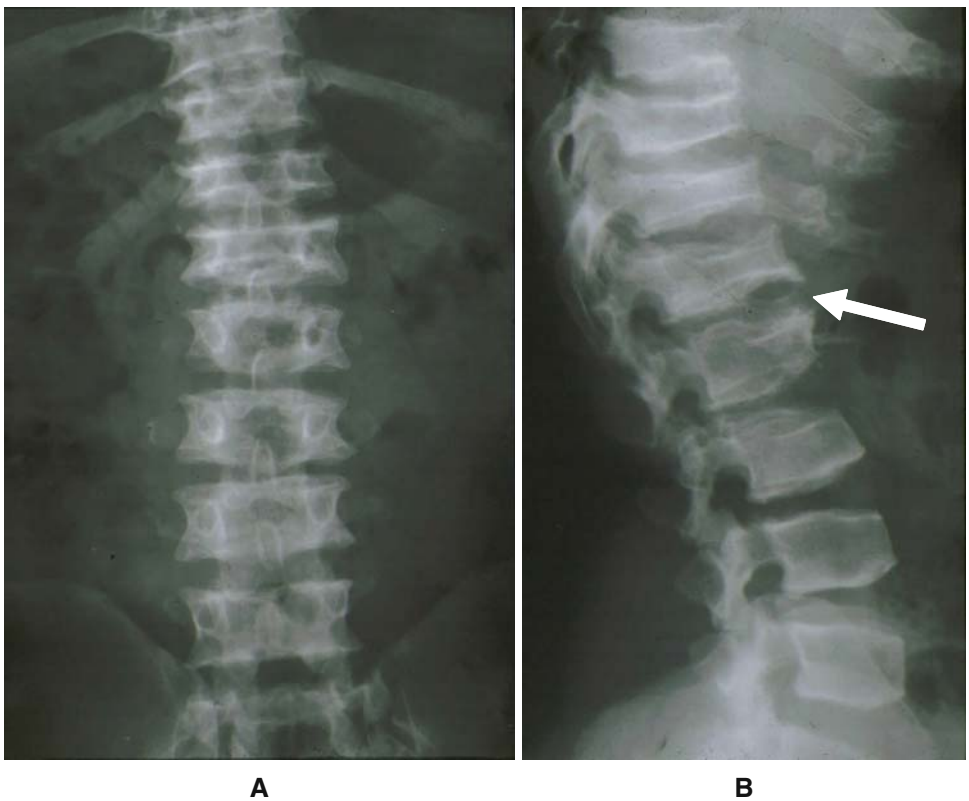

Fig. 13.78 Spondyloepiphyseal dysplasia**.** AP (**a**) and lateral (**b**) radiographs of the lumbar spine show decreased height of vertebral bodies, which diminishes in severity craniocaudally. There is over growth of anterior superior aspect of L2 vertebral body associated with a defect in the anterior inferior aspect of L1 (*arrow*). (Courtesy of Dr Robert Schneider, Hospital for Special Surgery, New York NY.)

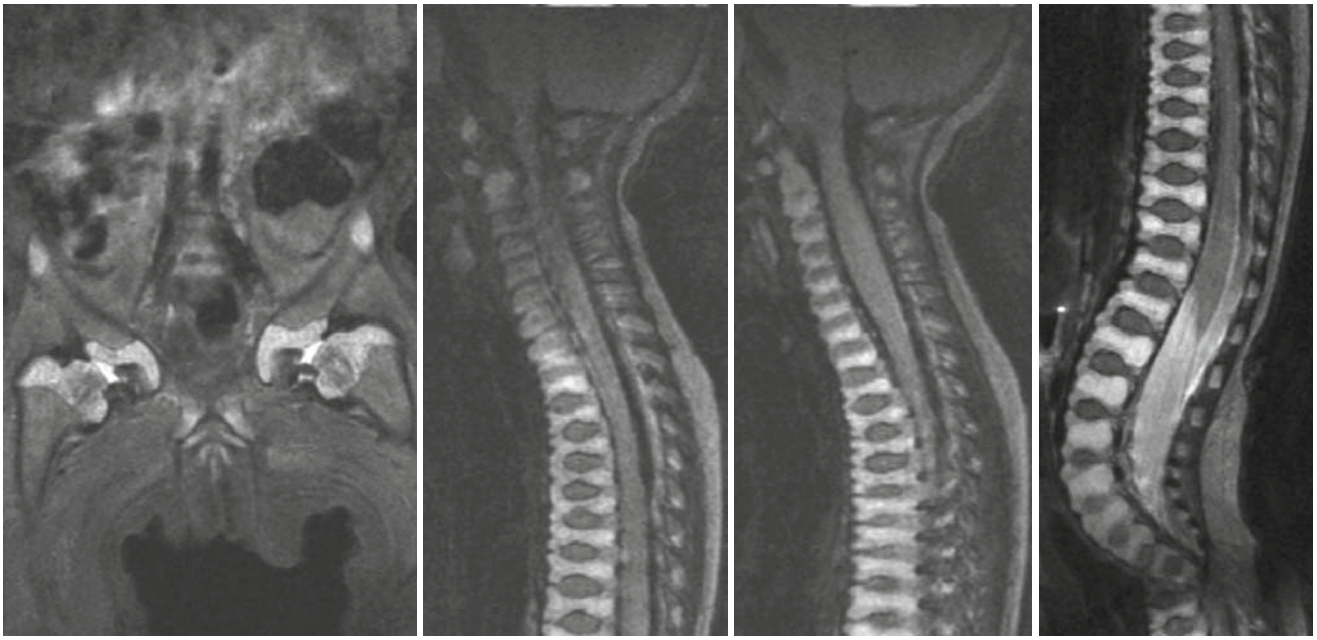

Fig. 13.79 Spondyloepiphyseal dysplasia: MR images from a one year-old patient. Coronal pelvic MRI STIR image (**a**) shows bilateral under development and deformity of the proximal femoral epiphyses and dislocated hips. Cervicothoracic spine T2 sagittal MR images (**b** and **c**) and thoracolumbar spine T2 sagittal MR image (**d**) show marked flattening and biconcavity of the vertebral bodies diffusely. The differential diagnosis is with Morquio disease. Unlike Morquio disease these vertebral bodies show no anterior central beaking, but instead they have posterior humping superiorty and inferiorly of the lower thoracic add upper lumbar vertebral bodies (Fig. 13.79d). (Courtesy of Dr Shenin, Loma Linda University, California)

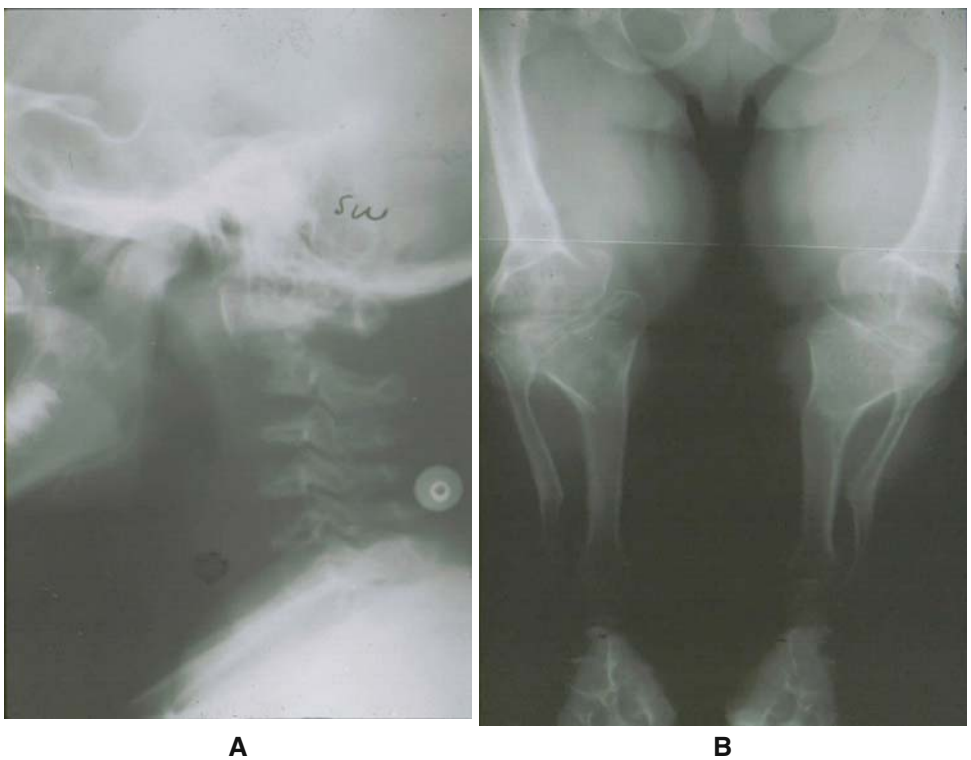

Fig. 13.80 Spondyloepimetaphyseal dysplasia: Lateral cervical spine radiographs (**a**) shows universal vertebra plana of the cervical spine. AP lower extremity (**b**) radiograph shows deformed and underdeveloped epiphyses of the knees as well as enlargement and deformity of the metaphyses. (Case courtesy of Dr Robert Schneider, Hospital for special surgery, New York NY.)

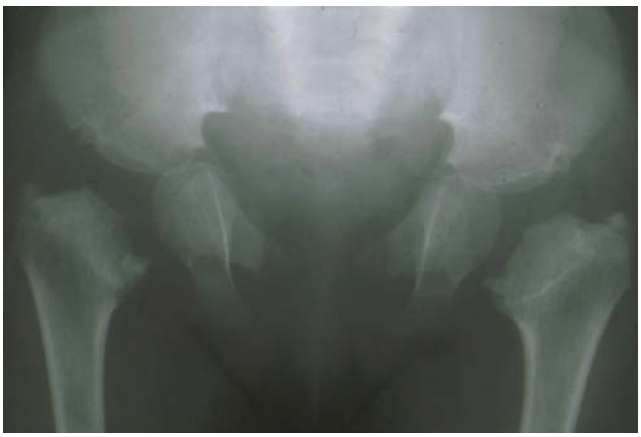

Fig. 13.81 Spondyloepimetaphyseal dysplasia. AP radiograph of the pelvis shows absence of calcification of the proximal femoral epiphyses. The ossification centers of the greater and lesser trochanters are poorly formed. The proximal femoral metaphyses are broad and irregular. The iliac bones have an open book appearance and are narrowed and pointed at the level of triangular cartilage of the acetabulum. (Case courtesy of Dr Robert Schneider, Hospital for special surgery, New York NY.)

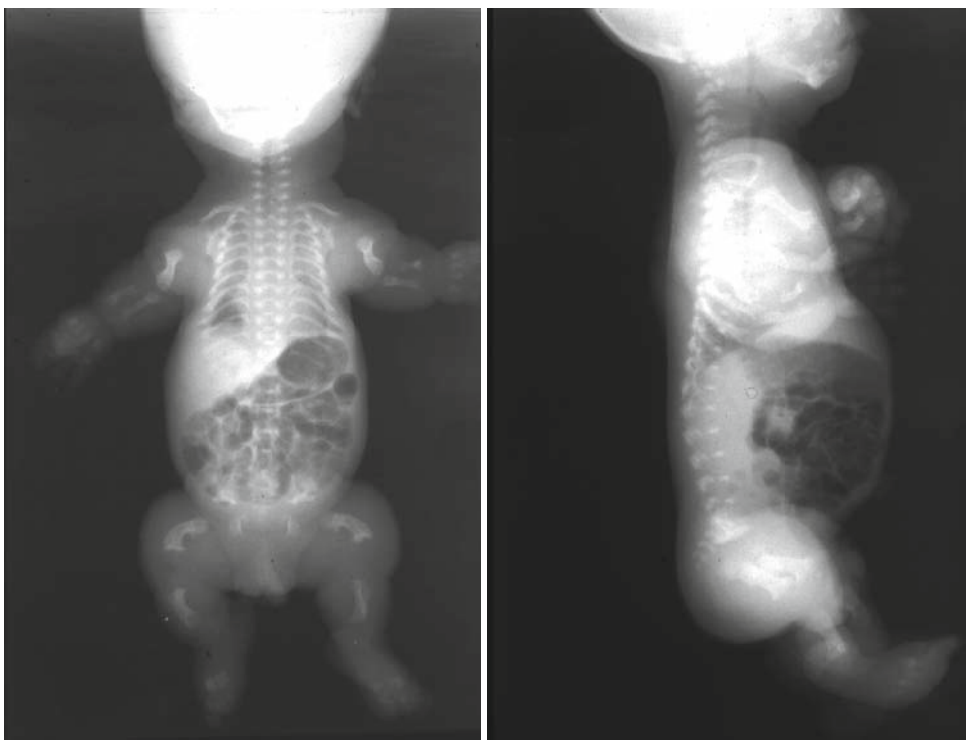

Fig. 13.82 Thanatophoric dysplasia. AP (**a**) and lateral (**b**) radiographs of a stillborn fetus show marked osseous deformities. Particularly there is shortening of the long bones and ribs. The alterations of the lumbar spine and pelvis are much more severe than achondroplasia. Note the "telephone receiver" shaped femurs

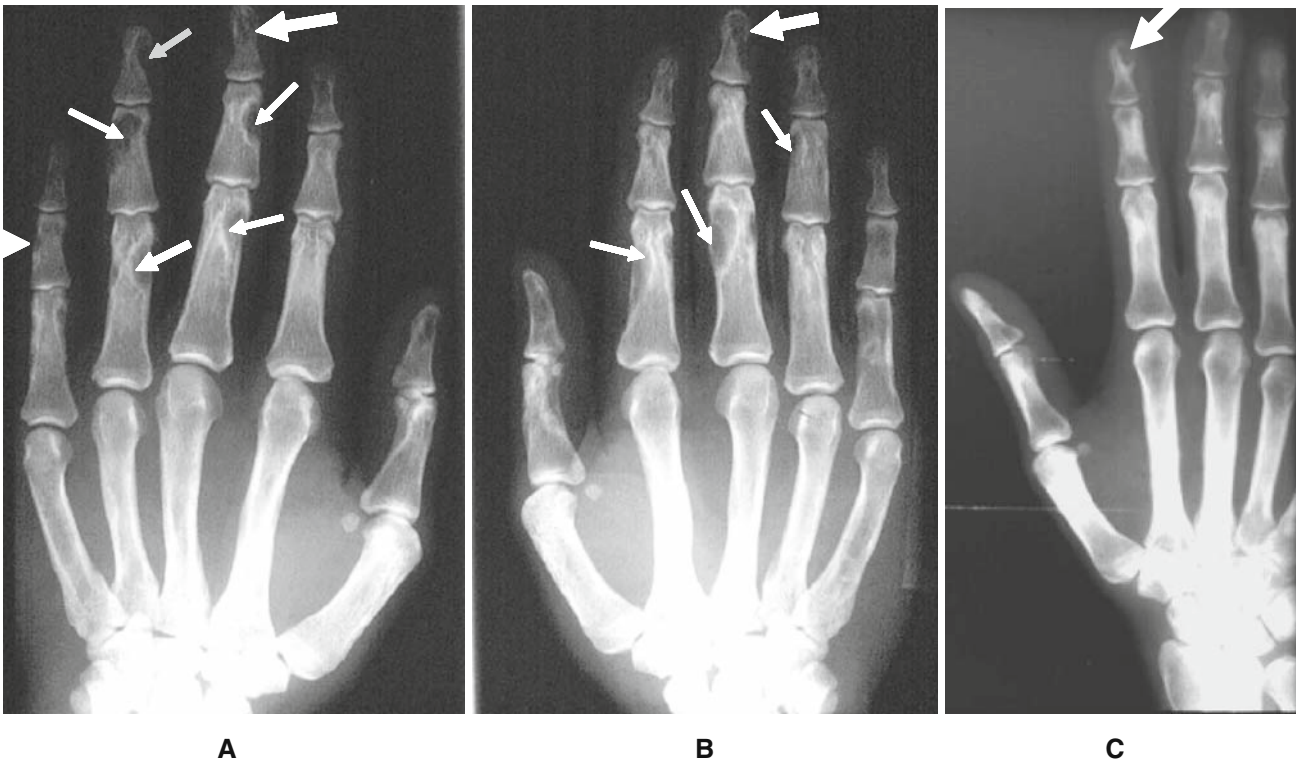

Fig. 13.83 Tuberous sclerosis (**a**) and (**b**) are PA radiograph of both hands of case 1 and **c** is PA of the R hand in case 2. *Thick arrows* show ungual fibromas in both cases (**a**, **b** and **c**). *Thin arrows* reveal lucencies with sclerotic borders and adjacent focal increased bone density in peripheral intramedullary fingers of case 1. Arrow head is pointing at the cortical pitting of the fifth finger of the left hand in **a**. In addition **c** reveals periarticular decreased bone density, probably related to disuse osteoporosis. **a** and **b** are courtesy of Dr William Reinus

The skull of the fetus with thantophoric dysplasia has a cloverleaf appearance. The fetus is short, has wide iliac bones, flattened vertebral ossification centers with end plate notching, short and bowed long bones, and flared metaphyses. The femurs have a "French telephone receiver" appearance (Fig. 13.82).

Platyspondylic chondrodysplasia patients show similar spine changes as patients with thanatophoric dysplasia, but their head is normal and they may survive to adulthood.

Tuberous Sclerosis Complex (MIM 191100)

Tuberous sclerosis complex (TSC) is an autosomal dominant disorder [22–24]. About 50% of cases are inherited and about 50% may be sporadic, but the number of sporadic cases may be higher than this figure [23].

Tuberous sclerosis may appear at any age, but most cases reveal clinical symptoms before the age of 10 years. This is a multisystemic disorder. The classic triad consists of seizures, mental retardation, and adenoma sebaceum (more accurately termed facial angiofibroma) [23]. In addition to skin lesions, TSC patients develop numerous brain lesions, angiomyolipomas (AMLs), Lymphangiomyomatosis, vascular abnormalities, and skeletal findings, all of which are demonstrable by diagnostic imaging [22].

The Diagnostic Committee of the National Tuberous sclerosis association has revised the comprehensive diagnostic criteria as a consensus statement with the following recommendations [23, 25]:

*Major features:*Facial angiofibromas or forehead plaque, non-traumatic ungual or periungual fibroma, hypomelanotic macules (three or more), Shagreen patch (connective tissue nevus), multiple retinal nodular hamartomas, Cerebral cortical tuber (cerebral cortical dysplasia), subependymal nodule, subependymal giant astrocytomas, cardiac rhabdomyoma (single or multiple), lymphangioleiomyomatosis and renal angiomyolipoma. When cerebral cortical dysplasia and cerebral white matter migration tracts occur, they should be counted as one rather than two features of TSC [25].

Minor features: Multiple randomly distributed pits in dental enamel, hamartomatous rectal polyp, bone cysts (radiographic confirmation is sufficient), cerebral white matter radial migration lines, gingival fibromas, non-renal hamar-

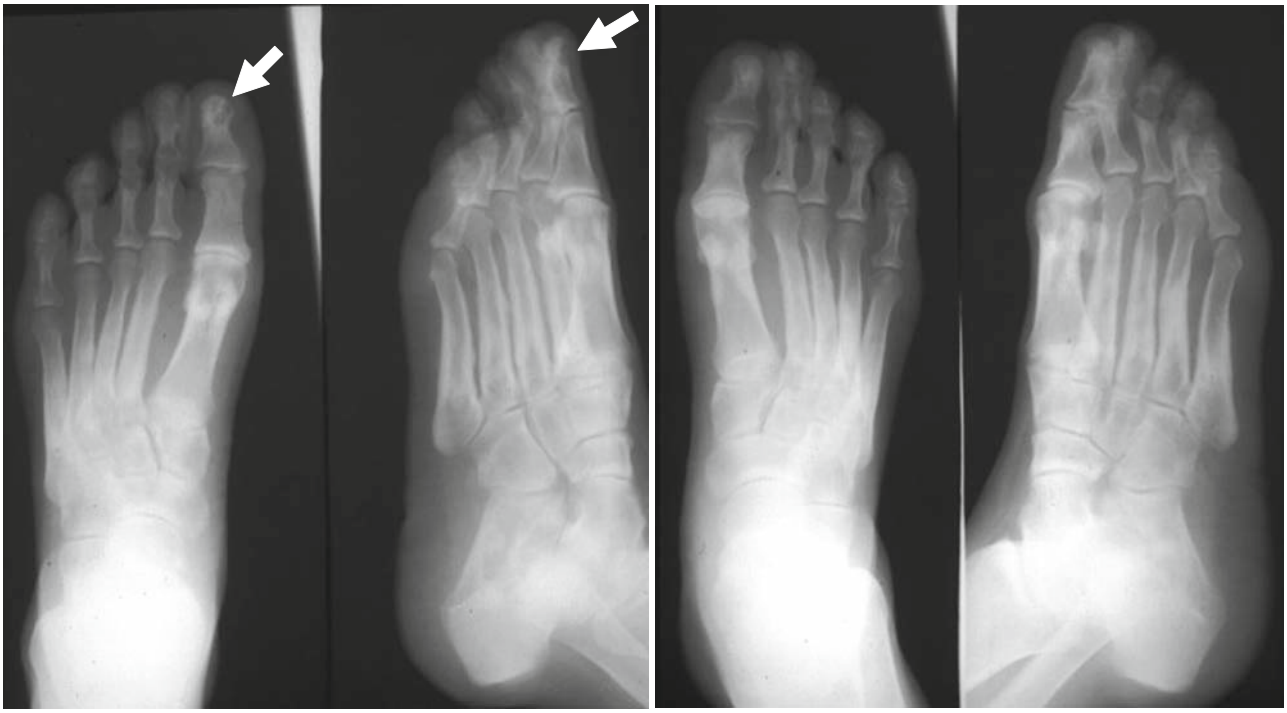

Fig. 13.84 Tuberous sclerosis case 2. **a** and **b** are the dorsoplantar and oblique views of the feet. *Thick arrows* reveal ungual fibroma of the distal phalanx of the left foot (**a**). Note the dorsal location of fibroma in (**a**). There is periarticular disuse osteoporosis. Note sclerosis of bones of both mid and hindfoot which is more noticeable in metatarsals

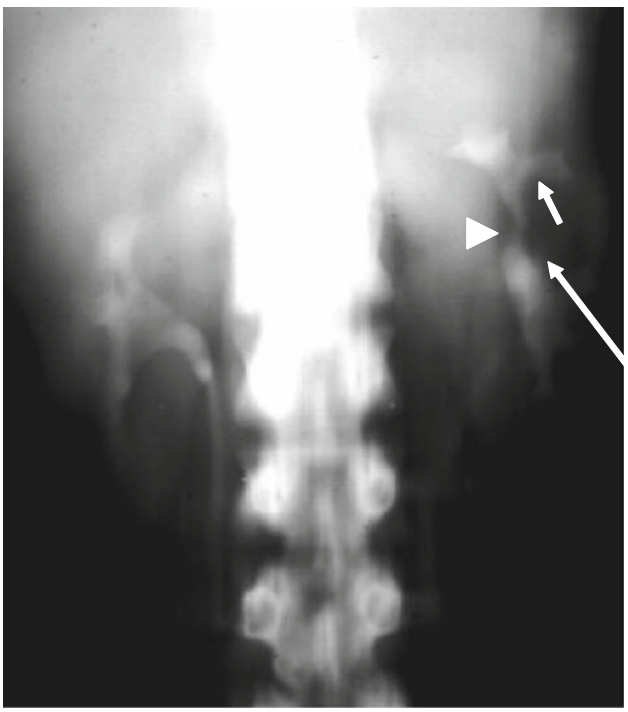

Fig. 13.85 Tuberous sclerosis case 2 Intravenous pyelotomogram shows a large radiolucent (fat containing) angiomyolipoma involving the cortical portion of the left mid and lower kidney displacing the middle and lower calices inferiorly and medially (*long arrow*). There is also mild narrowing (*arrow head*) and displacement of the superior calyx of the left kidney (*short arrow*)

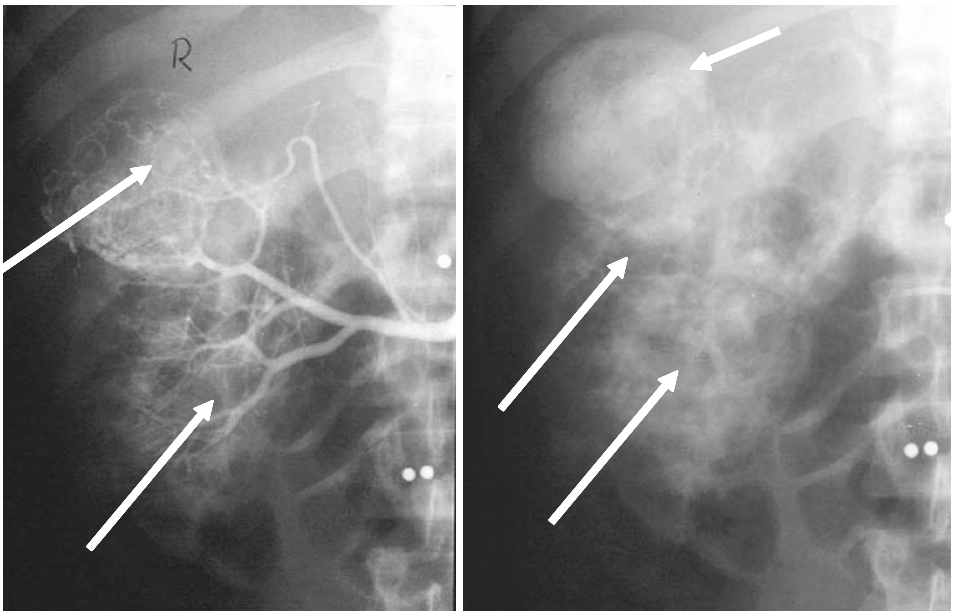

Fig. 13.86 Tuberous sclerosis case 1 **a** Anteroposterior selective renal angiography of the right renal artery, during late stage arterial combined with early capillary phase shows two vascular masses in the right kidney attributed to angiomyolipomas (*long arrows*). **b** The late capillary and early venous phase shows the previously seen angiomyolipomas. The opacified density in the upper right kidney should not be called a cyst (*short arrow*). Note there is residual gas in the transverse and the hepatic flexure of the colon. Courtesy of Dr William Reinus

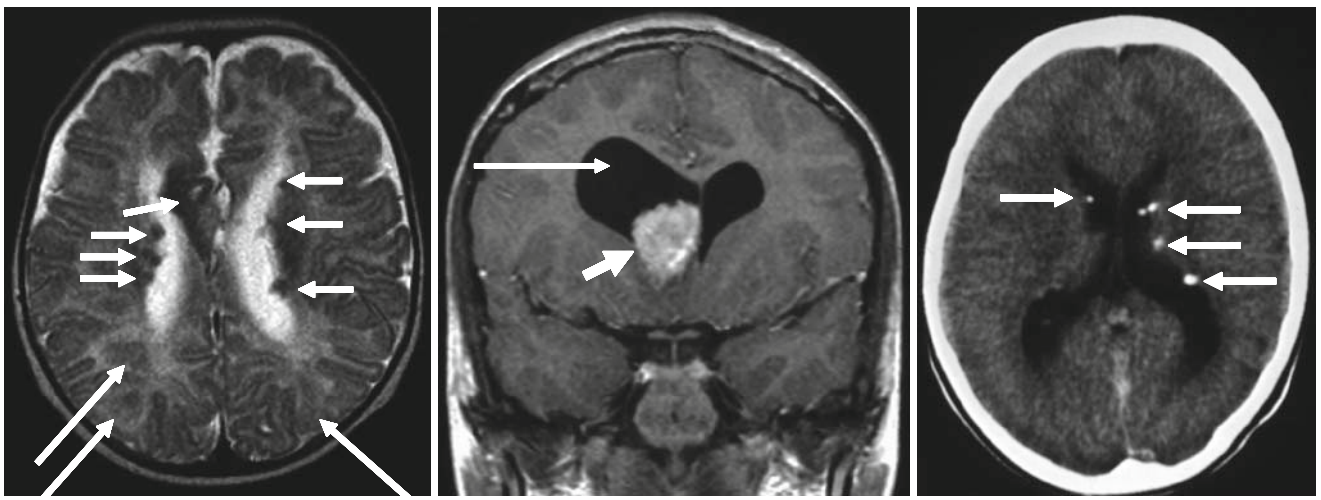

Fig. 13.87 Tuberous sclerosis comlex case 1 **a** Axial T2 MRI through the level of the lateral ventricles. *Short arrows* reveal calcified subependymal nodules (cortical dysplasias). *Long arrows* also demonstrate cortical dysplasias of the brain. **b** Is coronal T1 postcontrast image through the region of the frontal horns of the lateral ventricles. *Short arrow* shows a contrast enhancing benign giant cell astrocytoma that is associated with the septum pellucidum and is causing obstructive hydrocephalus (*long arrow*) at the level of the foramen of Monro. **c** Is **a**xial CT of the brain through the level of the lateral ventricles. *Arrows* point at calcified subependymal nodules (cortical dysplasias). Courtesy of Dr William Reinus, Department of Radiology, Temple university Hospital, Philadelphia, PA

tomas, retinal achromic patches, "confetti" skin lesions and multiple renal cysts.

Definite diagnosis of tuberous sclerosis complex can be made; if one major feature plus two minor features are present.

Probable diagnosis of tuberous sclerosis complex can be made; if one major feature and one minor feature are present.

Possible diagnosis of tuberous sclerosis complex can be made; if one major feature or two or more minor features are present.

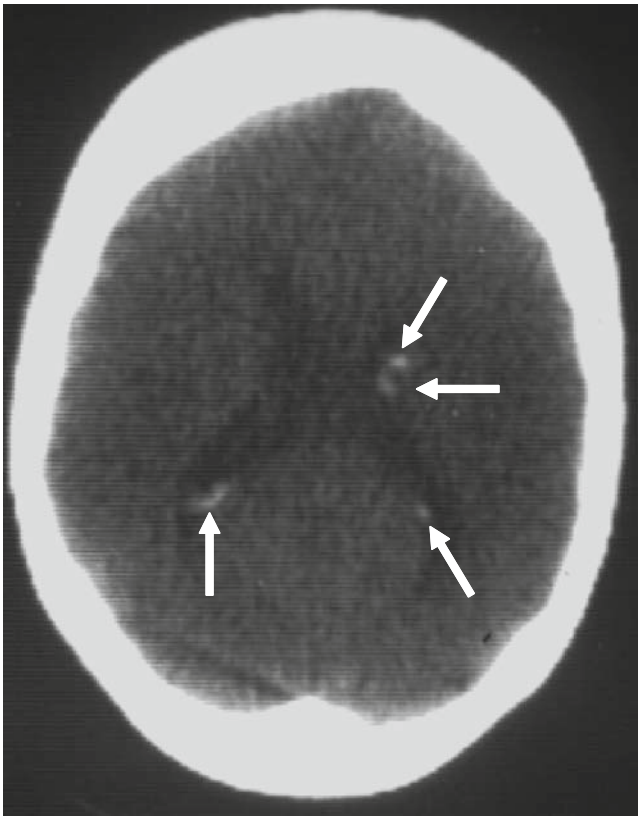

A

Fig. 13.88 Tuberous sclerosis case 2: An axial CT scan of the brain shows several calcified subependymal nodules or cortical dysplasias (*arrows*)

Diagnostic imaging – Diagnostic imaging modalities consist of radiographs, CT scans, MRI, ultrasound, nuclear medicine, PET scan, and angiography [22, 23, 26, 27, 28, 29, 30, 25, and 31].

Radiographic examination – Most findings detectable on radiographs are musculoskeletal or thoracic [23]. About one half of patients with multiple sclerosis have musculoskeletal lesions [23]. Osteoporosis and focal lucencies may be observed in metacarpals, metatarsals, and phalanges [26–29, 31] (Figs. 13.83 and 13.84). Ungual fibromas may be seen in 15–50% of patients [30]. These are small nodules located at the margin of or beneath the nails of the fingers and toes and often cause resorption of the ungual tufts [30] (Figs. 13.83 and 13.84). Sometimes periosteal reaction along the tubular bones develops, which is seen more often in metatarsals [30]. Osteosclerosis can affect the entire skeleton or multiple bone islands develop, which may be large (enostomas) with natural preponsity for the diploic space. Occasionally, macrodactyly may be observed. Expansile increased bone density of ribs has been described. Skull radiographs often reveal sclerosis or widening of the diploic space which is related to administration of phenytoin. Furthermore, skull roentgenograms may reveal intracranial calcifications, but the intracranial calcifications are more readily seen in CT scans of the brain (Figs. 13.87c and 13.88).

Chest radiographs rarely depict evidence of interstitial fibrosis or honeycombing [23]. Approximately one fourth of patients develop cardiac rhabdomyomas which places them at risk for congestive heart failure.

Between 50 and 90% of patients with tuberous sclerosis develop renal angiomyolipomas, most of which may be demonstrated by intravenous urography (Fig. 13.85), retrograde pyelography, or angiography (Fig. 13.86). The latter is no longer necessary for diagnosis of TBC after development of CT, MRI, and ultrasound.

Renal cysts are sometimes seen in association with angiomyolipomas.

Computed tomography – CT examination demonstrates about 85% of intracranial abnormalities. CT depicts calcified cortical dysplasias and calcified subependymal nodules (Figs. 13.87c and 13.88). CT scans after IV injection of contrast material may enhance subependymal nodules, but they are better demonstrated by MRI. Ten to fifteen percent of subependymal nodules may transform to giant cell astrocytomas which are benign and occur at or near foramen of Monro, sometimes causing ventricular dilatation

(Fig. 13.87b) and in advanced cases hydrocephaly. In IV contrast studies giant cell astrocytomas have an inhomogeneous density.

CT scans show renal angiomyolipomas that have a high fat content, but seldom develop calcification. After IV contrast injection CT clearly demonstrates both angiomyolipomas and renal cysts. However, differentiation with congenital multicystic kidneys as well as simple cysts may be difficult [22, 23].

Magnetic Resonance Imaging – MRI is the imaging of choice in evaluation of intracranial lesions of tuberous sclerosis complex [22, 23] (Figs. 13.87a, b). Cortical dysplasias are the most characteristic lesions of tuberous sclerosis and are detected in 95% of cases on MR imaging. Subependymal nodules are better demonstrated by MRI than CT (Fig. 13.87a and c). Subependymal giant cell astrocytomas are inhomogeneous with intense enhancement after the administration of gadolinium in MR images (Fig. 13.87b). However, MRI has no advantage in depiction of renal angiomyolipomas over CT [22, 23].

Other modalities – Ultrasound has been reported to be helpful in demonstration of renal angiomyolipomas [22]. Nuclear scans have a minor role in diagnosis of tuberous sclerosis complex, but positron emission tomography (PET scan) may be helpful in patients with seizure.

References

1. Superti-Furga A, Unger S, and the ISDS Nosology Group: International Nosology and Classification of Genetic Skeletal Disorders – 2006 Revision, AMJ Med Genet 2007; 143A: 1–18.
2. Aegerter E, Kirkpatrick JA: Orthopedic Diseases. London: WB Saunders; 1975.
3. Spranger JW, Brill PW, Poznanski A: Bone Dysplasias an Atlas of Genetic Disorders of Skeletal Development. Oxford: Oxford University Press; 2002.
4. Harold C: Skeletal Dysplasias, Emedicine from WebMD, 12-20–05.
5. Rubin P: Dynamic Classification of Bone Dysplasias. Chicago: Year Book Medical Publishers; 1964.
6. Ozonoff, MB: Pediatric Orthopedic Radiology. 2nd ed. Philadelphia: W.B. Saunders Company; 1992.
7. Taybi H, Lachman RS: Radiology of Syndromes, Metabolic Disorders, and Skeletal Dysplasias. 5th ed. by Lachman. Philadelphia: Mosby; 2007.
8. Lucas DR, Bridge JA: Chondromas: enchondroma, periosteal chondroma and enchondromatosis. In: Fletcher CDM, Unni KK and Mertens F, eds. World Health Organization Classification of Tumours, Pathology and Genetics: Tumours of Soft-Tissue and Bone. Lyon: IARC Press; 2002, 237–224.
9. Liu J, Hudkins PG, Swee RG, Unni KK: Bone sarcomas associated with Ollier's disease. Cancer 1987; 59: 1376–1385.
10. Schwartz HS, Zimmerman NB, Simon MA, et al.: The malignant potential of enchondromatosis. J. Bone Jt Surg Am 1987; 69: 269–274.
11. Thickman D, Bonakdarpour A, Clancy M, Steel H: Fibrodysplasia Ossificans Progressiva. Am J Roentgenol 1982; 139: 935–941.
12. Bonakdarpour A, Harwick R, Levy WM, Pickering J: Fibrous dysplasia and hyperparathyroidism. Skeletal Radiol 1977; 2: 52–55.
13. Beutler E: Gaucher's disease. N Engl J Med 1991; 325: 1354.
14. Resnick D, Kransdorf MJ: Bone and Joint Imaging. 3rd ed. Philadelphia: Elsevier-Saunders; 2005
15. Mignot C, et al.: Perinatal-lethal Gaucher disease. Am J Med Genet 2003; 120A: 338.
16. Dorland WAN: Dorland's Illustrated Medical Dictionary. 31st ed. Philadelphia: Saunders; 2007.
17. Bonakdarpour A, Maldjian C, Weiss, S, Roach N, Stein E: Hyperphosphatasemia: report of three cases. Eur J Radiol 2000; 35: 54–58.
18. Torg J, Steel H: Essential osteolysis with nephropathy. J Bone Joint Surg 1968; 50A: 1629–1638.
19. Torg J, Steel H: Sequential roentgenographic changes occurring in massive osteolysis. J. Bone Joint Surg 1969; 51A: 1649–1655
20. Torg JS, DiGeorge AM, Kirkpatrick JA, Trujillo MM: Hereditary multicentric osteolysis with recessive transmission. J Pediatr 1969; 75: 243–252.
21. Balthazar E, Smith EH, Moskovitz H: Pycnodysostosis: an unusual case. Br J Radiol 1972; 45(532): 304–307.
22. Baskin Jr.: The pathogenesis and imaging of the tuberous sclerosis complex. Pediatr Radiol 2008; 38: 936–952.
23. Greenspan B, Jordan LK, Glaiser CM. Tuberous sclerosis. eMedicine 2005; 1–19.
24. Kniffin LC updated Tuberous Sclerosis on 10-17-07 in Online Mendelian Inheritance in Man-Johns Hopkins University 2007; 1–26.
25. Feldman F: Tuberous sclerosis, neurofibromatosis, and fibrous dysplasia. In: Resnick D and Kransdorf MJ, eds. Bone and Joint Imaging. 3rd ed. Philadelphia: Elsevier-Saunders; 2002: 1407–1409.
26. Lonergan GJ, Smirniotopoulos JG: Case 64: tuberous sclerosis. Radiology 2003; 229: 385–388.
27. Altman NR, Purser RK, Post MJD: Tuberous sclerosis. Radiology 1988; 167: 527–532.
28. Jones J, Brenner C, Chinn R, Bunker CB: Radiological associations with dermatological disease. Br J Radiol 2005; 78: 662–677.
29. Kormar NN, Gabrielsen TO, Holt JF: Roentgenographic appearance of lumbar sine and pelvis in tuberous sclerosis. Radiology 1967; 89: 701–705.
30. Medley BE, McLeod RA, Houser OW: Tuberous sclerosis. Semin Roentgenol 1976; 11: 35–54.
31. Green GJ: The radiology of tuberous sclerosis. Clin Radiol 1968; 19: 135–147.
32. Green G, Bonakdarpour A, Levy W: Osteopetrosis (Tarda type) with hemorrhagic cyst. Skeletal Radiol 1984; 12: 59–62.

Chapter 14

Interventional Procedures in Musculoskeletal Radiology

Jamshid Tehranzadeh, Scott Seibert, and Afshin Gangi

Abstract Interventional radiological techniques are efficacious in diagnosing and treating certain types of musculoskeletal pathology. This chapter describes several of these techniques in three sections.

The first section describes the diagnosis and treatment of back pain. There is a detailed description of the relevant anatomy, including terminology, to describe pathology as it appears radiographically. Specific techniques are then described, including discography, nerve root injection, facet blocks, epidural injections, vertebroplasty, and kyphoplasty. Also included with each technique is a brief discussion regarding indications, potential complications, and figures to help elucidate the procedure.

In the second section of the chapter, arthrography and bursography are similarly described. Joint pathology is discussed and figures are included to depict techniques targeting the shoulder, wrist, elbow, hip, knee, and ankle. There is also a section that describes viscosupplementation vs. injection of corticosteroids. Again, indications and potential complications are included.

The third section describes percutaneous interventional techniques used to biopsy or treat lesions of the musculoskeletal system, both osseous and soft tissue. Both benign and potentially malignant lesions are discussed. Particular attention is paid to benign lesions such as osteoid osteomas, unicameral bone cysts, and aneurysmal bone cysts. The radiographic appearance of musculoskeletal lesions are described in great detail and demonstrated with figures as examples.

Finally, there is a list of further readings should the reader desire more information on a particular topic. Hopefully, the reader will find the chapter an informative guide to the aforementioned topics and procedures.

Keywords Interventional • MSK • Arthrography • Injection • Biopsy

Introduction

Interventional radiological techniques are efficacious in diagnosing and treating certain types of musculoskeletal pathology. Among these are diagnosis and treatment of back pain using discography, nerve root injection, facet blocks, epidural injections, vertebroplasty, and kyphoplasty. Similarly, arthrography may be used to diagnose joint pathology – often in conjunction with a post arthrogram MR or CT scan. Joints may be injected percutaneously with local anesthetic and corticosteroids to treat intra-articular conditions that may be causing pain, e.g., osteoarthritis. Percutaneous interventional techniques may also be used to biopsy lesions of the musculoskeletal system, both osseous and soft tissue.

Interventional Spinal Procedures

Approximately 80% of the population will suffer from back pain at some point during their lifetimes. Low back pain is the second leading reason for medical office visits in the United States, and it is the leading cause of work-related disability. "The total cost of low back pain in the United States exceeds $100 billion per year. Two-thirds of these costs are indirect, due to lost wages and reduced productivity" [12]. One-fourth of the working population will be affected each year, with 2–8% of these cases severe enough to be considered disabling.

Self-limiting soft tissue injury is most often the cause of pain, but many more serious and chronic conditions arising from the spine also cause pain. It is essential but often times

J. Tehranzadeh (✉)
VA Long Beach Health Care System, DMM Health Care Group
05/114, 5901 E. 7th Street Long Beach, CA 90822 USA
e-mail: jamshid.tehranzadeh@va.gov

A. Bonakdarpour et al. (eds.), *Diagnostic Imaging of Musculoskeletal Diseases: A Systematic Approach*,
DOI 10.1007/978-1-59745-355-4_14,

very difficult to differentiate among etiologies of chronic lower back pain. Known sites of pain-inducing spine pathology include the facet joints, the sacroiliac (SI) joint, the intervertebral disc, the vertebral body, the pars interarticularis, the spinal cord, and the spinal nerve root. Overlapping symptoms from these sources make clinical localization difficult. Furthermore, patients prone to degenerative changes in one part of the spine are likely to have concurrent pathology at other sites with radiographic evidence of multiple levels of disease. Interventional imaging techniques not only can elucidate the diagnosis when less-invasive modalities fail but in many cases can also treat the underlying disorder and alleviate the patient's pain.

We review current interventional spinal procedures that target different anatomical areas of the spine, including the intervertebral disc, the vertebra, and local neural structures.

Procedures Targeting the Intervertebral Disc

Percutaneous procedures targeting the intervertebral disc include discography, percutaneous lumbar discectomy, percutaneous laser disc decompression, nucleoplasty, and finally annuloplasty.

Anatomy of the Intervertebral Disc

The intervertebral disc is sandwiched between cartilaginous vertebral endplates above and below. Each disc consists of an external *annulus fibrosus* surrounding an internal gelatinous *nucleus pulposus*.

The annulus fibrosus consists of concentric lamellae of fibrocartilage and inserts circumferentially into the adjacent vertebral endplates. The lamellae of the annulus run obliquely with respect to one another. This morphology contributes strength to the vertebral column. The lamellae are thinner and less numerous posteriorly than they are anteriorly and laterally. As a result, the annulus fibrosus is weaker posteriorly, predisposing to more annular tears and herniated discs in this location.

The center of the intervertebral disc, the nucleus pulposus, consists of proteoglycans and collagen. The nucleus pulposus is avascular and receives nourishment by diffusion from adjacent structures. In healthy discs, the disc complex allows absorption and dispersal of compressive forces.

The posterior longitudinal ligament is a supporting structure running along the posterior aspect of the vertebral bodies. It forms the anterior border of the vertebral canal. This ligament is weaker than the anterior longitudinal ligament, which courses along the anterior border of the vertebral bodies. The posterior longitudinal ligament is broadest superiorly, where it is continuous with the tectorial membrane and attaches to the anterior aspect of the foramen magnum.

Imaging of the Intervertebral Disc

T2-weighted (T2W) magnetic resonance imaging (MRI) is often useful to distinguish different components of the intervertebral disc. The annulus fibrosus and the nucleus pulposus of a healthy disk have dark (low-signal intensity) and bright (high-signal intensity) appearance, respectively, on T2W MR imaging. The center of the nucleus pulposus contains the *intranuclear cleft* which has a high concentration of collagen and reticular fibers. It is denser than the surrounding nucleus pulposus and has low intensity on T2W MRI.

Pathophysiology of the Intervertebral Disc

A *degenerated disc* is an intervertebral disc that has lost water content (desiccated) and has fissuring of the annulus fibrosus. Loss of water causes loss of disc height and low-signal intensity on T2W MRI. These discs are prone to tears in the annulus fibrosis. Tears are described by their morphology: *radial*, *concentric*, or *transverse*. *Concentric tears,* believed to result from normal aging, are circular and are not considered clinically significant. *Transverse tears, or rim lesions,* signify avulsion of the fibers of the peripheral annulus fibrosus from their insertion onto the ring apophysis. These tears are present in all age groups after the first decade but are more prevalent after 30 years of age. *Radial tears* extend from the center outward and are present in all cases of disc herniation. These tears allow the central nucleus pulposus to herniate outward toward the periphery of the disc. Only those herniations that extend posteriorly into the vertebral canal or the neural foramina are likely to be clinically symptomatic. Depending upon the configuration of the tear, a number of abnormal disc configurations may result:

1. *Bulging disc.* A bulging disc is a circumferential, diffuse, and symmetric annular bulge. The annulus fibrosus and the posterior longitudinal ligament are intact. On MRI this appears as a broad-based bulge of the annulus fibrosus with dark signal extending beyond the vertebral endplate at a margin of the vertebral column. In general, the width of the lesion is greater than its depth.
2. *Disc protrusion* describes focal bulging of the annulus fibrosus in one direction without rupture through the posterior longitudinal ligament. There is no contact between the nucleus and the extradiscal space. On MRI this appears as a protrusion of the nuclear material at the

margin of the disc extending to anterior epidural space secondary to a tear in the annulus. This presents as a focal dark signal which may be associated with a small high-intensity zone (HIZ). In contrast to a bulge, a protrusion is typically focal in nature and is often deeper than it is wide.
3. With a *disc extrusion* the nucleus pulposus herniates through a rupture of the annulus fibrosus and the posterior longitudinal ligament, but the herniated material remains connected to the central nucleus through the tear, sometimes called a "rent." The distal tip of the extruded disc often extends above or below the disc level. Often extrusions will show a narrowed neck where they pass through the posterior longitudinal ligament.
4. The herniation may progress further into a *sequestered disc*. Here, the nuclear material that has been expelled from the disc separates from the disc and migrates in the spinal canal.

Discography

Discography has a history of controversy owing to a 1968 study by Holt who reported a 37% false-positive rate. Holt's article had flaws in design, however, and has been dismissed by other authors.

Discography can be used as a complementary test to MRI or CT myelogram prior to surgery. In this procedure, contrast material is injected into the nucleus pulposus under fluoroscopic guidance to evaluate possible degeneration of the intervertebral disc. The procedure not only allows the physician to visualize the disc morphology but also may recreate the patient's clinical pain when the correct disc is injected.

Indications and Contraindications

The following are indications for discography in patients who ultimately may be surgical candidates:

1. To determine which disc is responsible for pain when multiple levels of disc disease are present on imaging. If a discogram induces pain, cortisone or anesthetic may be injected into the disc to reduce the pain.
2. To evaluate recurrent or persistent pain after surgery for disc disease. After spinal surgery, it may be difficult to differentiate a recurrently herniated disc from scar tissue.
3. When planning a spinal fusion, to determine if the discs within the proposed fusion segment are symptomatic and to determine if discs adjacent to the segment are normal.
4. To evaluate patients with persistent, severe symptoms in whom other diagnostic tests (e.g. CT, MRI) have failed to reveal a suspected disc as the source of pain.
5. To confirm a contained disc herniation in candidates for minimally invasive procedures, such as percutaneous discectomy.
6. As a preliminary test if chemonucleolysis is being considered. This procedure involves injection of chymopapain into the nucleus pulposus. It is rarely used today and has been abandoned in the United States [18].
7. To diagnose painful vertebral column lesions such as an incompletely healed endplate fracture or a nonunion of a vertebral fracture.

Discography should not be performed in patients with an infection in the region to be examined (e.g. sepsis, cellulitis, osteomyelitis, discitis) and in patients with uncorrected bleeding diatheses, cauda equina syndrome, and vertebral fractures. Discography should not be performed when there is a high risk for contrast to escape beyond the intervertebral disc, e.g., segmental instability seen on flexion–extension films, severe degeneration associated with spondylolisthesis, intervertebral disk collapse, severe disk space narrowing, large disk protrusions, sequestered disk herniations.

Technique

The patient should be interviewed prior to the procedure with special attention paid to the type and nature of the patient's pain, the presence of referred pain, and the localization of pain. Any allergy to the contrast agent should be addressed. The patient should understand the purpose of pain provocation in this test. Additionally, the patient should be aware that they might experience a temporary worsening of symptoms for a short period of time after the procedure.

The physician should gauge the patient's state of anxiety and pain tolerance, something that differs widely among patients. Some physicians advocate avoiding sedation and local anesthesia, because the patient must be able to respond to a painful stimulus. Other physicians, however, will use 1 mg midazolam IV and 25 mg of IV meperidine hydrochloride 15 min before the procedure. During the procedure, the patient's blood pressure and pulse oximetry should be monitored.

Discography can be performed in all three disc-containing segments of the vertebral column, but most commonly is performed in the lumbar region. Lumbar discography can be performed with the patient in the prone, lateral, or oblique positions. The prone position offers improved stability and is often chosen by radiologists who are used to this view of myelography. In the prone position, the patient is positioned

with a pillow under the abdomen to straighten the lumbar curve.

After proper positioning, a line is drawn on the skin along the spinous processes. Next, under C-arm fluoroscopy the desired disc levels are marked (e.g., at L3–4, L4–5, L5–S1). A paramedian line is drawn 8 cm lateral and parallel to the midline. At the L3–4 or L4–5 levels, the intersection of the previously marked disc level with the paramedian line will be the point of needle entry (Fig. 14.1). The L5–S1 disc is approached from the paramedian line approximately halfway between the lines for L3–4 and L4–5.

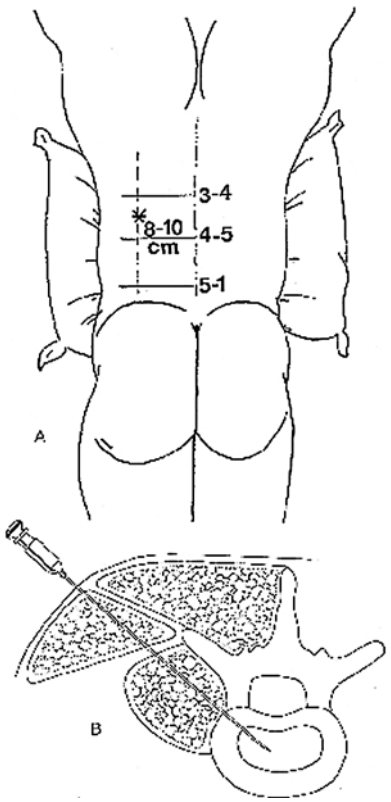

Fig. 14.1 Discography technique. (**a**) The patient is in a prone position. A paramedian line is 8–10 cm lateral to the midline. Note the site of needle insertion at L5–S1 (∗) is between L3–4 and L4–5 levels. (**b**) The needle is obliquely inserted and the needle tip is placed in the center of the disc (nucleus pulposus) (Reprinted with permission from J. Tehranzadeh Ref. 19)

After appropriate cleansing, draping, and administration of local anesthesia, the disc is injected using either single- or double-needle technique. The double-needle technique is preferred as it may reduce the chance of infection. Using the double-needle technique, first a 15-cm 18-gauge needle is inserted to within 1 cm of the disc. The stylet of this needle is removed and a 22-gauge 20-cm needle is inserted through the 18-gauge needle. For an L5–S1 discogram, the tip of the inner needle may need to be bent slightly to negotiate between the bony posterior elements and avoid the iliac wings.

To improve the accuracy of needle placement into the nucleus pulposus, the position of the needle is checked fluoroscopically in two orthogonal planes prior to entering the disc. Using C-arm fluoroscopy, the distance from the tip of the needle to the center of the disc should be equal when comparing the anteroposterior (AP) and lateral projections. This positioning technique permits the needle to be inserted into the center of the nucleus pulposus with greater accuracy.

After needle insertion, the disc is injected with a small volume of contrast and imaging is obtained either with fluoroscope or CT. There are several morphologic variations of a normal discogram (Fig. 14.2). One should record the volume of contrast injected, the pain response (with particular emphasis on its location and similarity to clinical symptoms), and the pattern of contrast distribution. Axial CT or MRI imaging following disc injection may be used to obtain more information about disc morphology.

Discussion

Discography of a healthy disc will show the contrast agent contained within the nucleus pulposus and will not recreate the patient's clinical pain (Fig. 14.3). On the other hand, an abnormal disc will permit extravasation of contrast out into the portions of the annulus fibrosus (Figs. 14.4, 14.5 and 14.6). Regardless of imaging findings, before a disc level is diagnosed as causative, the injection should replicate the patient's usual pain symptoms.

Disc disease seen on discography can be graded according to the "Dallas classification for disc morphology" (Fig. 14.7). This system grades on a scale of 0–7 and has been modified over the past several years. The original Dallas classification included only these first four (Grades 0–3). Grade 0 is defined as contrast entirely within a normal nucleus pulposus. In Grade 1, contrast extends radially along a fissure involving the inner third of the annulus fibrosus. In Grade 2, contrast extends into the middle third. In Grade 3, it extends into the outer third of the annulus, either focally or radially within the outer annulus filling no more than 30° of disc circumference.

The "modified Dallas scheme for annular tears" also includes four additional grades. Grade 4 represents a Grade 3 tear dissecting radially within the outer third of the annulus to involve more than 30° of the disc circumference. Grade 5 represents a full-thickness tear, either focal or circumferential, with extra-annular leakage of contrast (Figs. 14.8 and 14.9). Disc sequestration has been termed grade 6, and grade 7 is a diffuse annular tear in a degenerated disc

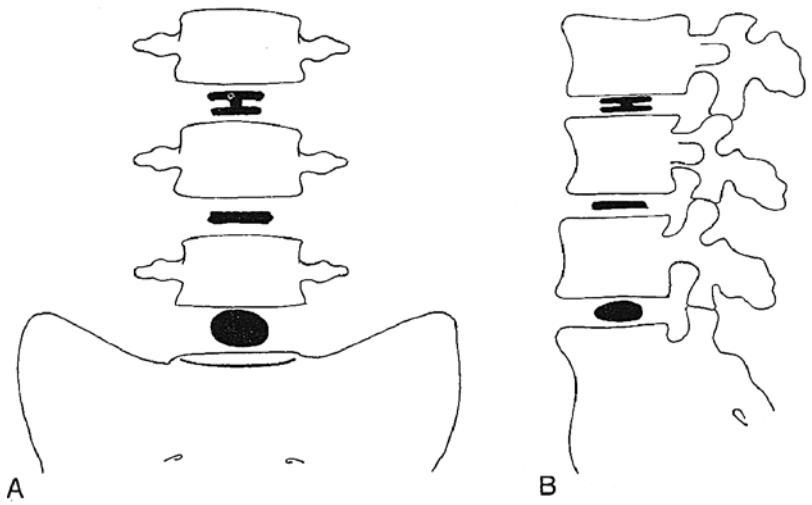

Fig. 14.2 Morphologic variation of normal discogram. From *top* to *bottom*: bilocular, unilocular, unilocular rectangular, and unilocular spherical are noted. (Reprinted with permission from J. Tehranzadeh Ref. 19)

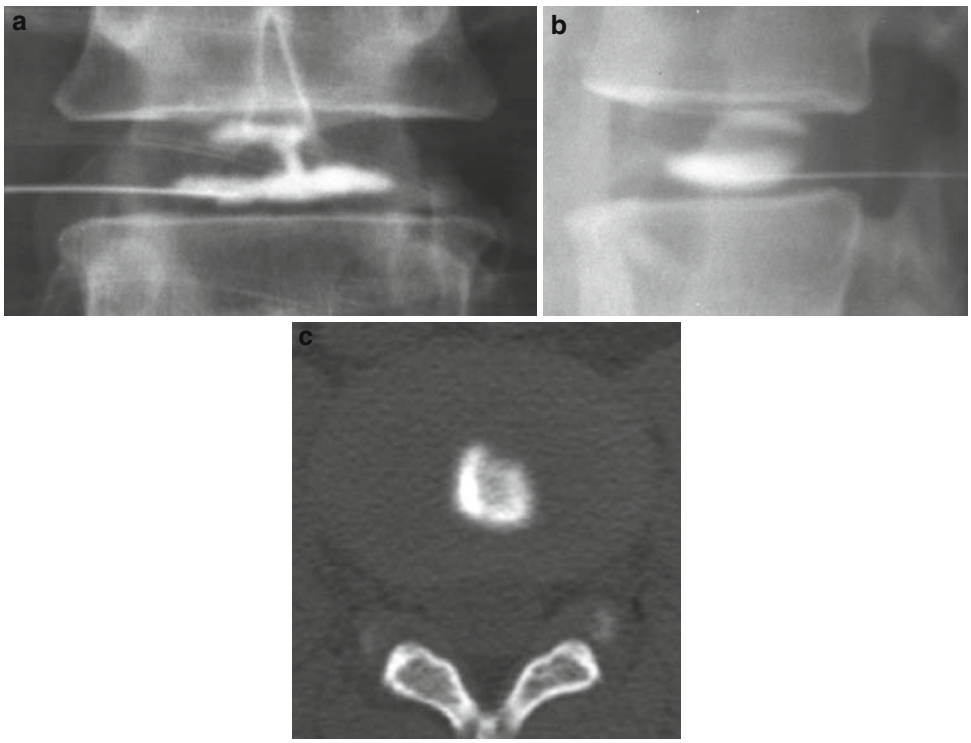

Fig. 14.3 Normal discogram at L3–4 level. AP (**a**) and lateral (**b**) views. Note normal bilocular or "hamburger" appearance of contrast agent in the disc. CT (**c**) shows accumulation of contrast agent inside nucleus pulposus and no annular tear. (Reprinted with permission from J. Tehranzadeh Ref. 19)

Recent research indicates that measuring injection pressure may improve diagnostic accuracy. A positive discography test produces significant pain (at least 6 on a scale of 10) at pressures above 15 psi but less than 50 psi, relative to the opening pressure within the disc. Significant pain with injection pressure greater than 50 psi above opening pressure is considered nondiagnostic. Similarly, patients who report pain with contact alone (0 psi) do not necessarily have a diseased disc at that level. It should be noted that if the needle inserts into the vertebral endplate, the patient may experience severe pain even in a healthy disc. Also, one is more certain to have found the symptomatic disc if at least one of two adjacent discs is shown to be asymptomatic upon injection.

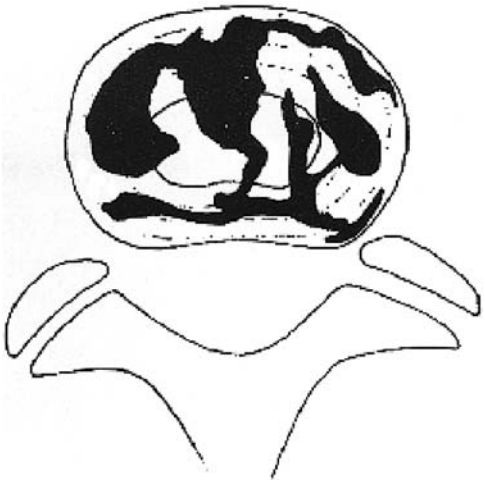

Fig. 14.4 Degenerative disc disease. Diffuse irregular pattern of tearing of disc substance suggests chronic and degenerative disc disease. (Reprinted with permission from J. Tehranzadeh Ref. 19)

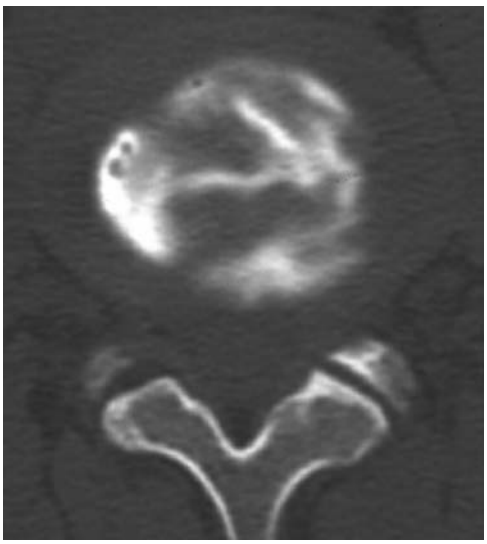

Fig. 14.5 Degenerated disc. Diffuse spread of contrast agent in the disc exhibits complex tear of annulus, typical for degenerated disc. (Reprinted with permission from J. Tehranzadeh Ref. 19)

Discography is an invasive procedure requiring attention to potential complications such as infection. To avoid discitis, some radiologists use periprocedural broad-spectrum antibiotics. Other reported complications include spinal headache and bleeding (including intrathecal hemorrhage).

Percutaneous Laser Disc Decompression

Percutaneous laser disc decompression (PLDD) uses laser light energy, transmitted through a thin optical fiber, to vaporize a portion of the nucleus pulposus. The goal is to reduce the intradiscal volume and pressure that contribute to disc herniation.

Indications and Contraindications

Percutaneous laser disc decompression (PLDD) aims to treat a contained disc herniation diagnosed by CT or MRI. PLDD is useful to treat a disc protrusion with positive neurological findings. It is not effective for extrusions or sequestrations. Clinically supporting symptoms include leg pain of greater intensity than back pain, a positive straight leg raise, and decreased sensation with normal motor function. Furthermore, the patient should have failed at least 6 weeks of conservative therapy.

Contraindications to this procedure include nerve paralysis, hemorrhagic diathesis, spondylolisthesis, spinal stenosis, previous surgery at the indicated level, significant narrowing of the disc space, and local infection.

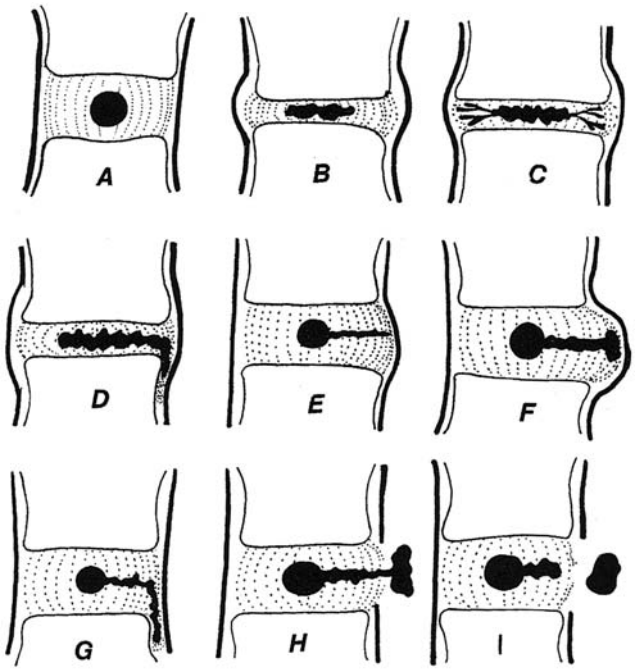

Fig. 14.6 Discogram morphology on lateral projection: *Solid black lines* represent anterior (*left*) and posterior (*right*) longitudinal ligament. **a**, Normal. **b**, Degenerative disc. **c**, Degenerative disc with annular tear. **d**, Degenerative disc with disc extrusion and extravasation of contrast agent. **e** and **f**, Radial annular tear (type III) in protruded disc. **g**, Extruded disc (candle drip). **h**, Extruded disc, tear of posterior longitudinal ligament. **i**, Sequestered disc, tear of posterior longitudinal ligament associated with separated fragment. (Modified from Fabris G, Lavaroni A, Leonardi M, et al.: Discography. Del Centauro Udine, Italy, European Society of Neuroradiology, Edizioni, 1991; with permission.) (Reprinted with permission from J. Tehranzadeh Ref. 19)

Technique

Percutaneous laser disc decompression (PLDD) is performed using both CT and fluoroscopy for guidance, allowing the operator to switch between the two at any time. CT is required to visualize vaporization of the nucleus pulposus during PLDD. The patient is placed in a prone, semiflexed position under local anesthesia. Using a posterolateral

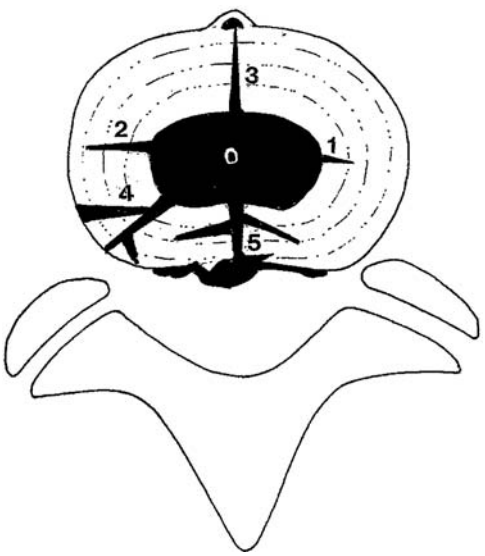

Fig. 14.7 Modified Dallas scheme for annular tear classification. Note epidural contrast agent extravasation in type V. (Reprinted with permission from J. Tehranzadeh Ref. 19)

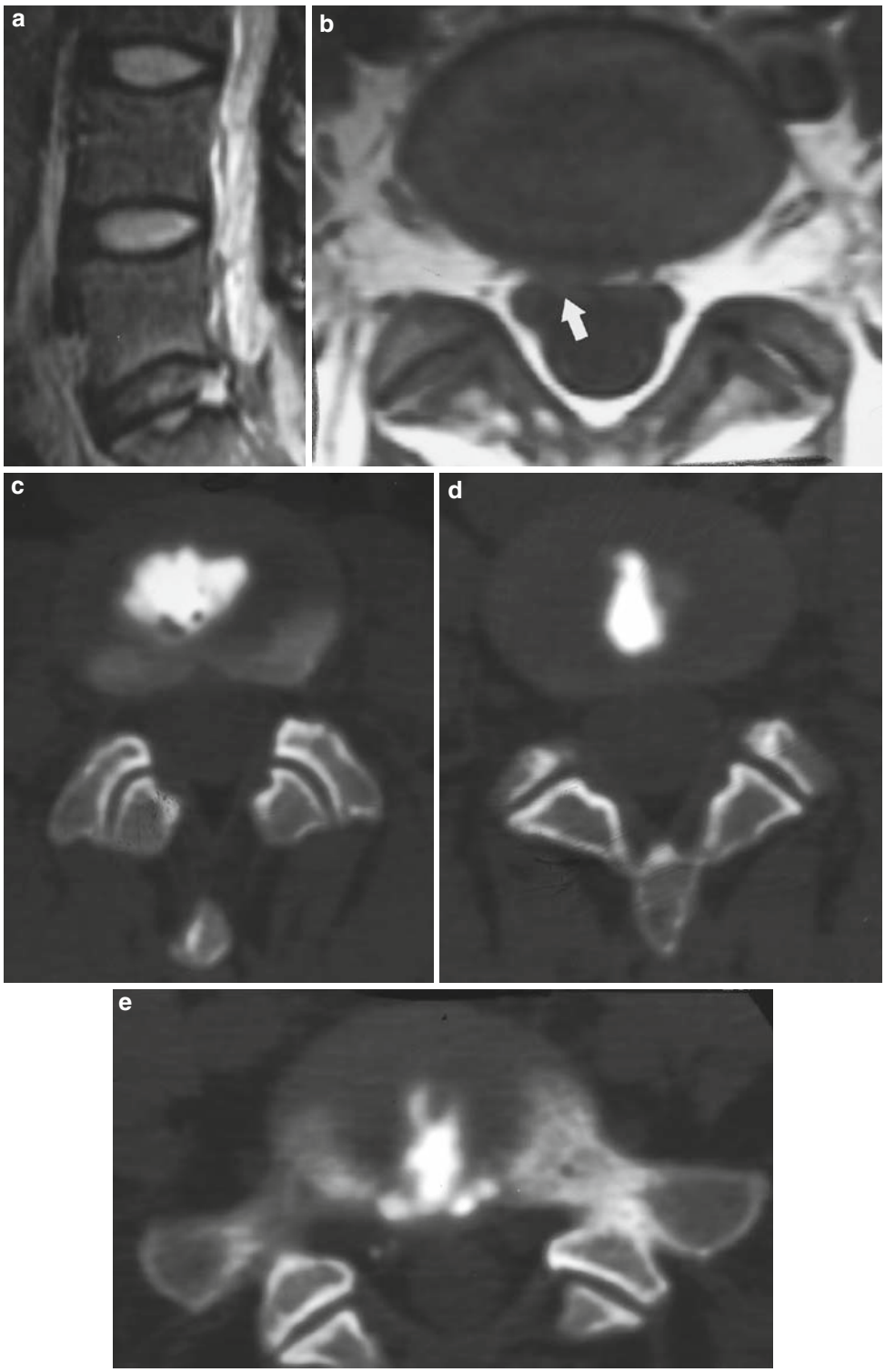

Fig. 14.8 HIZ (high-intensity zone) with disc protrusion. (**a**) T2-weighted (2500/80) parasagittal image shows low signal (desiccated) L5–S1 disc with focal HIZ. (**b**) Axial T1 MR image (800/20) shows right paracentral posterior disc protrusion (*arrow*). L3–4 (**c**) and L4–5 (**d**) were pain free and normal on CT discogram. Partial volume averaging of bony endplate is seen at L3–4 level. CT discogram at L5–S1 (**e**) shows type V posterior annular tear with extravasation. The patient experienced excruciating pain at L5–S1 during injection. (Reprinted with permission from J. Tehranzadeh Ref. 19)

approach, an 18-gauge trocar needle is inserted while monitoring the lateral view. The trocar should be parallel and midway between the vertebral body endplates. To ensure that the needle will enter the intervertebral disc behind the exiting spinal nerve root, one should overcorrect posteriorly and aim the needle to contact the facet joint. Then the needle is moved anteriorly until it just slides over the facet joint and is advanced until it contacts the annulus fibrosus.

At this point, one should determine appropriate positioning of the needle on anteroposterior and lateral fluoroscopic inspection. The tip of the needle should be radiographically at the "posterior vertebral body line," a line tangent to the most posterior aspect of the vertebral body on transverse view. The spinal nerve runs anterior to this line and is protected if the needle is posterior. On the AP view, if the needle is laterally positioned with respect to the line that joins the medial border of the pedicles, then it cannot be traversing the thecal sac. A 22-gauge 9-cm length needle is used to administer local anesthetic once the intervertebral disc has been reached. Care should be taken not to anesthetize the nerve root, because leg pain is monitored during the procedure (should such pain occur, the needle must be repositioned). An 18-gauge needle is then inserted parallel to the 22-gauge needle under fluoroscopic guidance, with the tip aimed toward the posterior aspect of the nucleus pulposus.

After needle positioning, the stylet of the 18-gauge needle is removed and an optical fiber is inserted into the disc with the tip 5 mm beyond the needle tip. After satisfactory positioning, laser therapy can begin. Infrared lasers such as neodymium–yttrium–aluminum-garnet (Nd: YAG) with a 1064-nm wavelength or diode lasers are used, pulsed "on" (15–20 W for 5–10 s) and "off" (4–10 s). The laser is pulsed in order to reduce heating of adjacent structures. One should monitor vaporization of the nucleus pulposus with intermittent CT scanning. If pain occurs, the physician can allow longer rest intervals between laser doses or aspirate the central nuclear contents to relieve pressure.

Discussion

Percutaneous laser disc decompression is an effective procedure. According to recent data, total resolution of leg pain occurs in 70% of patients treated with PLDD, with patient satisfaction after 6 months around 80%. The major potential complication is discitis.

Disc nucleoplasty is a similar procedure whereby a similar approach is used to introduce a "Spine Wand" into the nucleus pulposus (Fig. 14.10). The proposed advantage of this technique is that each electrode emits only a fraction of the total energy of a laser and therefore causes less damage to the surrounding tissue.

Intradiscal Electrothermal Therapy (IDET®) or Annuloplasty

Annuloplasty is a procedure developed by Joel and Jeff Saal in 1997, where RF energy is focused into the disc to treat discogenic pain. Discogenic pain manifests itself as pain confined to the lower back that does not radiate down the legs. The proposed etiology of such symptoms differs

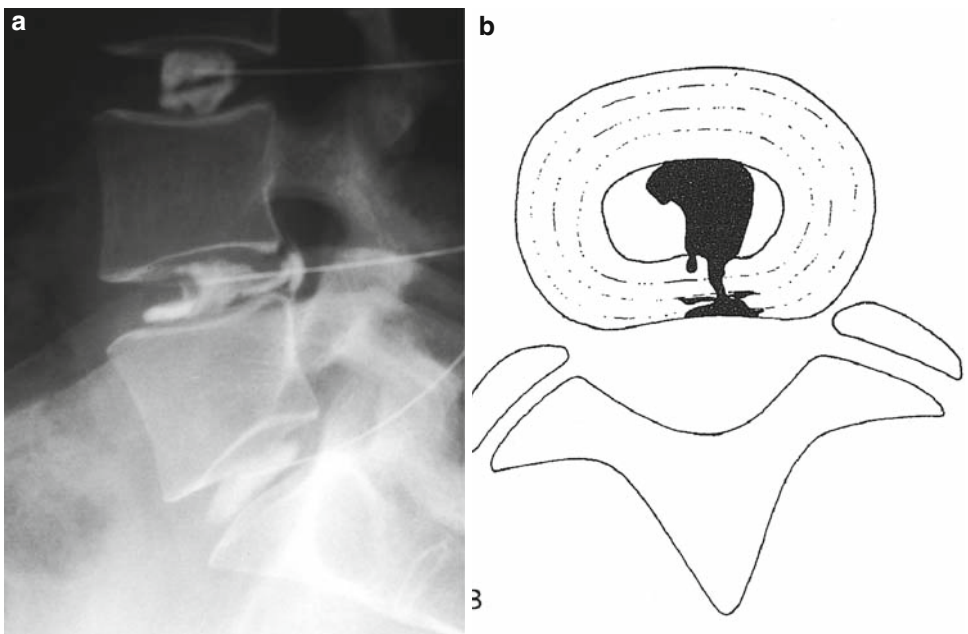

Fig. 14.9 Type V posterior annular tear with extravasation at L4–5 lateral discogram. (**a**) shows normal appearing discs at L3–4 and L5–S1 and a protruded disc with intact posterior longitudinal ligament at L4–L5. Line drawing from CT discogram (**b**) shows posterior annular tear. (Reprinted with permission from J. Tehranzadeh Ref. 19)

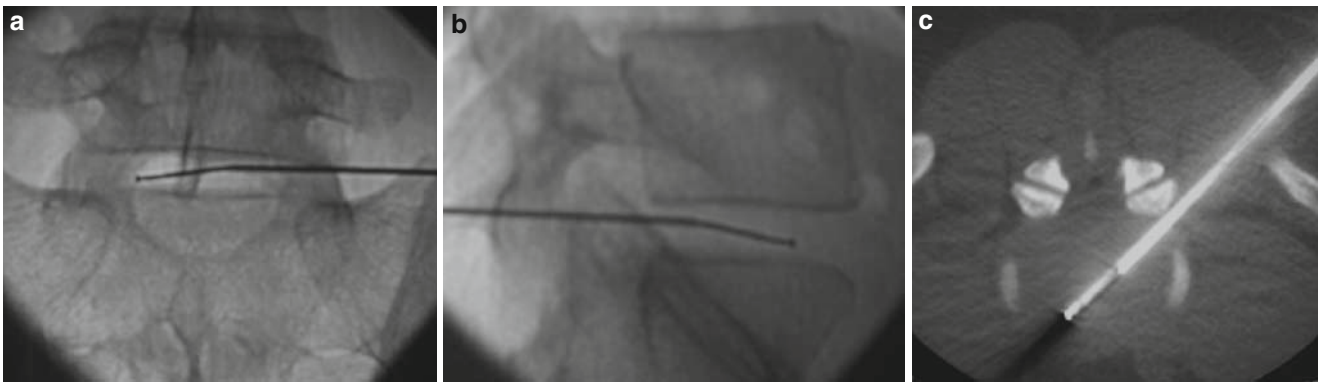

Fig. 14.10 Lumbar nucleoplasty. This is a 46-year-old male with a contained disc protrusion at L5–S1 who is complaining of sciatica. AP (**a**) and lateral (**b**) fluoroscopic images show the anteriormost positioning of the Spine Wand electrode in the nucleus pulposus. The access needle is at the posterior annular–nuclear junction. The electrode has a curve that allows for creation of multiple channels in the nucleus by rotation of the electrode. CT image (**c**) shows the access needle at the posterior annular–nuclear junction with the Spine Wand electrode deployed in the nucleus pulposus

from disc herniation or rupture. Discogenic pain arises from increased pressure within the disc stimulating surrounding nerves.

Annuloplasty focuses RF energy at a desired location within the disc. The energy is converted to heat in order to thermocoagulate intradiscal nerves. This procedure is used to treat painful lumbar degenerative disc disease in patients who would otherwise be candidates for spinal fusion.

Discussion

Radiofrequency and laser ablation are increasingly used to treat discogenic pain. Lasers can cut, coagulate, and vaporize tissue.

Besides the aforementioned uses for disc disease, lasers are also used arthroscopically for joint disorders (cartilage ablation and restoration), for photocoagulation of bone tumors (e.g., osteoid osteoma), and to remove polymethyl methacrylate (PMMA) cement.

Procedures Targeting the Vertebra

The following section describes three percutaneous procedures targeting the bony structures of the spine: percutaneous vertebroplasty, facet joint injection, and sacroiliac joint injection.

Percutaneous Vertebroplasty

Percutaneous vertebroplasty (PVP) was created by Galibert et al. in 1984 and first used to treat painful, aggressive vertebral angiomas. Later, its use broadened to include vertebral fractures secondary to malignancy or osteoporosis. In this procedure, polymethyl methacrylate (PMMA), a cement-like substance, is injected into a damaged vertebral body.

Indications and Contraindications

It is important to note that most vertebral compression fractures (about two-thirds) are asymptomatic, only diagnosed as an incidental finding on radiographs. Others become apparent because the patient loses height or becomes kyphotic. Vertebroplasty is not indicated for asymptomatic compression fractures.

The goal of PVP is pain relief. As such, vertebroplasty is performed when focal, intractable, midline back pain exists at the site of a vertebral fracture that has failed a trial of conservative management, lasting 6–12 weeks. The three most common etiologies of compression fracture requiring vertebroplasty are bone weakening from *osteoporosis, vertebral hemangioma*, and *malignancy*. Less common indications include spinal pseudoarthrosis, intravertebral vacuum phenomenon (Kümmell disease), Langerhans cell histiocytosis, osteogenesis imperfecta, and Paget disease. Features that are relative contraindications to vertebroplasty or make treatment difficult include burst fracture, severe compression fracture, spinal canal compromise, and malignant compression fracture with epidural involvement.

The following is a list of contraindications to PVP:

1. Uncontrollable bleeding disorder
2. Unstable fracture due to posterior element involvement
3. Infection
4. Nonpainful fracture

Relative contraindications include the inability to lay prone, the lack of surgical backup, and neurological signs and/or symptoms.

Technique

Preprocedural evaluation is important to assess the degree of vertebral compression and extent of destruction. Conventional radiographs alone are often insufficient to determine the stability of vertebral fractures. CT is used with particular attention to two areas: the posterior vertebral wall and the pedicles. If the posterior vertebral wall is damaged, there is a greater risk of spinal cord injury during cement injection. Second, a damaged pedicle may alter the approach to the vertebral body. Magnetic resonance imaging and bone scintigraphy may also be useful to evaluate patients with multiple levels of compression fractures.

Along with adequate imaging, percutaneous vertebroplasty requires spinal needles and PMMA cement. The length and gauge of the needles varies according to the vertebral level. The PMMA cement is packaged as two components: a liquid and a powder. Barium sulfate is present as a radiopaque substance in the powder; however, it is not strong enough for fluoroscopy and therefore radiopaque tantalum is often added.

PVP can be performed using local or general anesthesia. One may administer prophylactic antibiotics, but they are not mandatory. An anterolateral approach is used in the cervical spine. In the lumbar and thoracic regions, the physician uses a posterolateral approach to access the vertebral body through a pedicle. This transpedicular injection is done to prevent the leakage of cement along the needle into the surrounding structures.

The needle is inserted under C-arm or biplane fluoroscopic guidance through the center of the pedicle toward the midline of the anterior one-third of the vertebral body (Fig. 14.11). More recently, a bilateral approach to the pedicles has been favored, placing the needles into the lateral portions of the vertebral body. This method decreases the rate of cement extravasation because the midline has greater vascularity and supports a greater load than the lateral portions of the vertebral body. Some practitioners use a hammer to tap the needle into bone, claiming it allows for better control. Disadvantages of this technique include difficulty in removing the needle and a greater risk of penetrating the medial cortex of the pedicle. Should this cortex be violated, cement may extravasate into the intervertebral foramen. After the needle has been guided into the vertebral body, the radiologist may perform a biopsy when a metastatic lesion is suspected without a known primary source (spinal column biopsies are discussed further in section "Spinal Biopsy").

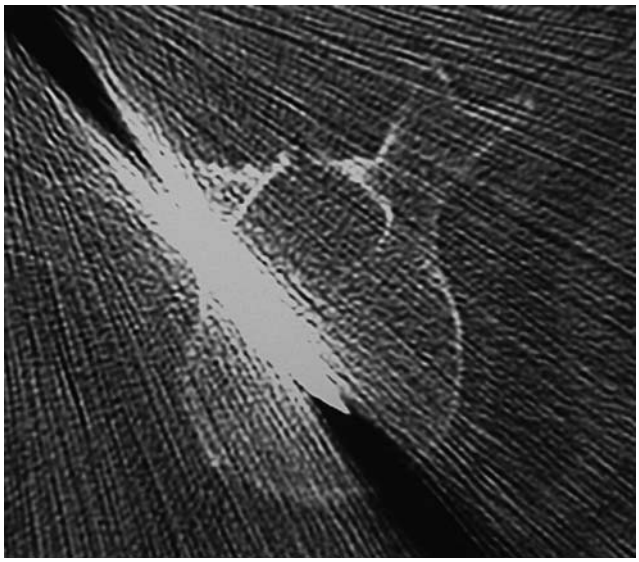

Fig. 14.11 CT image of the transpedicular placement of a 10-gauge vertebroplasty needle in the anterior median portion of the vertebra to achieve bilateral cement filling via a unipedicular approach

Local venous drainage is assessed using blush venography, the injection of a small amount of contrast. This contrast injection does not map the intended path of cement because the two have different viscosities. Occasionally, the injection may leave residual contrast in the vertebral body, interfering with accurate visualization of the subsequent cement injection. Therefore, only small amount of contrast (0.5–1 ml) is injected to ensure that the needle tip is not placed directly into a venous anastomosis with either central or epidural veins.

The powdered methacrylate and liquid are mixed and allowed to stand for 1 minute. The viscous material is injected into the vertebral body under lateral fluoroscopic guidance using a 3-ml Luer-Lok syringe. Adequate filling of cement should be demonstrated (Figs. 14.12 and 14.13). Should the injected cement reach the posterior wall or paravertebral veins, the procedure is immediately stopped to prevent spinal canal or neural foraminal extravasation. The injection often can be accomplished successfully through one pedicle but additional injection through the contralateral pedicle may be required if less than 50% of the vertebral body fills. The original needle is left in place to prevent leakage through the needle track until the second injection is complete. Evidence suggests that attempting to completely fill the vertebral lesion is inadvisable since it increases the risk of leakage of cement without added benefit.

Kyphoplasty is a variant of PVP that is used to treat vertebral compression fractures. When performing a kyphoplasty, inflatable balloons are inserted into the fractured vertebral body to elevate the vertebral endplates prior to cement fixation (Fig. 14.14)

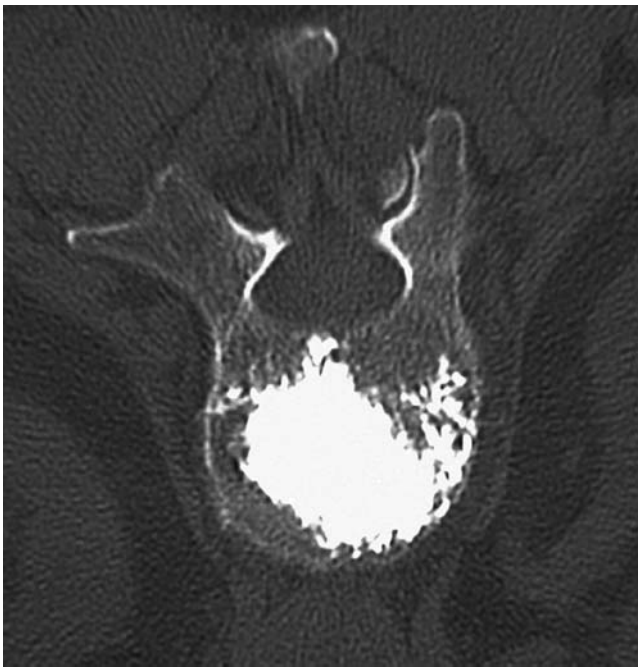

Fig. 14.12 CT scan showing satisfactory bilateral cement filling of the vertebral body following a unipedicular vertebroplasty

Complications

Leakage of cement into veins or surrounding tissues is common during PVP. The most frequent sites of cement leakage are into perivertebral veins, intravertebral discs, or surrounding soft tissues. Leaks into these structures are usually without negative consequences. If PMMA leaks into the local veins, there is a theoretical risk of pulmonary embolism.

More serious complications are possible when PMMA leaks into the intervertebral foramina, the spinal canal, or the epidural venous system. Leakage into the spinal canal is usually well tolerated if there is adequate space but may cause symptomatic spinal stenosis and even paraplegia. A leak into the intervertebral foramen may damage exiting spinal nerves, leading to radiculopathy. This complication is usually a result of technical error such as piercing the cortex of the pedicle. Though these complications may be serious, they are rare even when leaks do occur and can be minimized with careful fluoroscopic monitoring.

The underlying pathology contributing to vertebral body weakness may also increase the chances for cement extravasation. Extravasation is believed to occur more commonly when treating malignant than osteoporotic fractures. Furthermore, destruction of the vertebral cortex, posterior involvement of the vertebral body, highly vascular lesions,

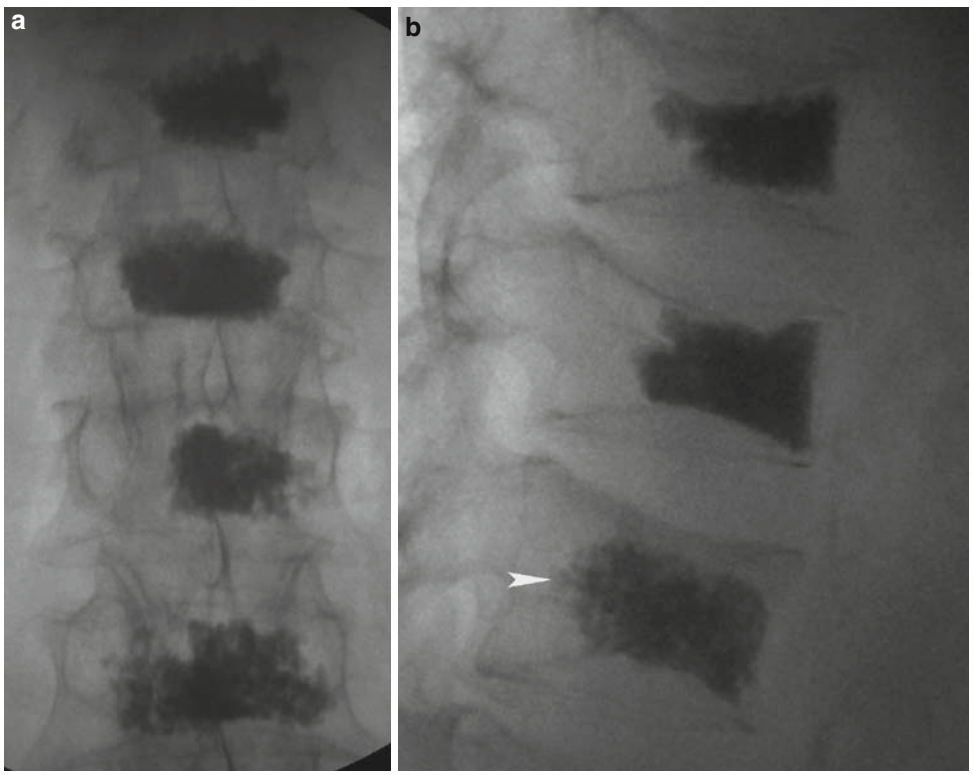

Fig. 14.13 AP (**a**) and lateral (**b**) radiographs showing satisfactory distribution of cement with good anterior consolidation of the four fractured osteoporotic vertebral bodies treated at a single session. Note the presence of cement in the basivertebral vein in the lowermost treated vertebra (*arrowhead*). There is absence of any cement leakage or complications. See also (Fig. 2.20) of Chapter 2

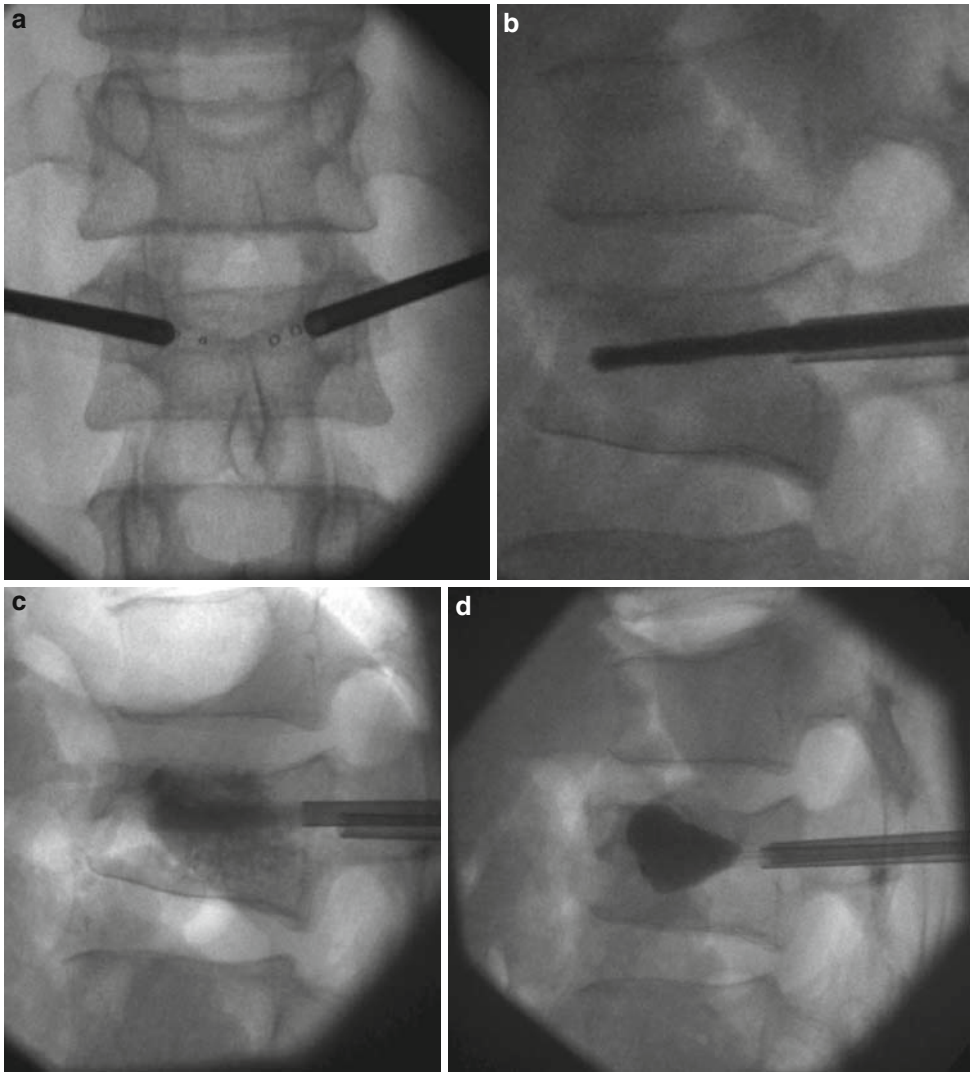

Fig. 14.14 Kyphoplasty. A 32-year-old male patient following an acute traumatic fracture of the superior endplate of the L1 vertebral body following a paragliding accident. AP radiograph (**a**) showing the precise positioning of the kyphoplasty balloons using a bipedicular approach. The round radio-opaque markers denote the ends of the balloon to facilitate accurate positioning within the midportion of the vertebral body. Lateral radiograph (**b**) showing creation of a channel within the normal dense bone using a bone reamer to allow for introduction of the kyphoplasty balloons. Lateral radiograph (**c**) showing gradual inflation of the kyphoplasty balloons to allow for compaction of the cancellous bone, resulting in reduction of the fracture with height gain and reduction of the kyphosis. Inflation of the balloons creates a cavity which is then filled with cement to achieve consolidation of the vertebral body. Lateral radiograph (**d**) showing injection of phosphocalcic cement (Jectos +) through bone fillers to achieve consolidation of the vertebral body

and severe vertebral collapse each may increase the risk of extravasation to such a degree as to preclude safe PVP.

In addition to cement extravasation, a theoretical risk of PVP is an increased risk of a fracture of an adjacent vertebra. Once a vertebra has been injected with PMMA, it stiffens, and adjacent vertebrae must absorb more force. Studies comparing PVP to conservative treatment for osteoporotic fractures have found no significant difference in the incidence of adjacent vertebral fractures. Furthermore, a person with an underlying disease such as osteoporosis is already at increased risk for future vertebral fractures. Needless to say, more evidence is required to investigate this issue.

Results

PVP is an effective treatment for severe back pain in some patients. Although a transient increase in pain may occur, pain relief and increase in mobility are expected within the first day after this procedure. Significant pain relief is most

common when PVP is used to treat osteoporotic fractures (90%) and least common when treating malignancy (70%). Furthermore, studies have shown that pain relief is sustained long term, even at 48 months following PVP. The age of the fracture before treatment does not seem to correlate with expected outcome. When treating a spinal metastasis, radiation therapy often follows PVP. It has been shown that radiation therapy does not interfere with the structural integrity of PMMA.

Facet Joint Injection

Facet joint injection is a therapeutic procedure to ameliorate pain arising from facet joints through injection of a mixture of corticosteroids and local anesthetic. It is most often used to treat or rule out "facet joint syndrome," which is a lower back pain originating from the facet joint. Though this procedure is usually performed on the lumbar facets, a facet joint injection can be performed at any level.

Anatomy

The facet joint is composed of a superior facet, from the vertebra below, and an inferior facet, from the vertebra above. The superior facets face anterolaterally and are concave, while the inferior facets face posteromedially and are convex. Therefore, the facet joint is curved with the posterior aspect farther away from midline than the anterior aspect of the joint.

The orientation of the lumbar facet joints becomes progressively coronal in orientation as one moves inferiorly. The more inferior facets have greater surface area and the pedicles increase in cross-sectional area, contributing to greater strength inferiorly. The facet joint has a unique structural role in the spine. The facets are better able to deal with shear forces than do the intervertebral discs, and they provide support while in extension by resisting compressive forces.

The facet joints contain nociceptors or pain nerve fibers that are thought to be a potential transmitter of back pain. Each facet joint has a dual innervation, one nerve from the dorsal rami above and one from the same level. This may account for the diffuse pattern of pain that accompanies facet joint syndrome.

Indications and Contraindications

Facet joint injection is used to treat lower back pain originating from the facet joint. Patients are selected by first eliminating other causes of lower back pain such as disc disease and spinal stenosis and by failing at least 6 weeks of conservative therapy. Patients with persistent pain after a spinal fusion may be appropriate candidates. Tenderness to palpation over the facet joint supports the diagnosis of facet joint syndrome. Radiographically abnormal facets (Fig. 14.15a, b) make entering the joint more challenging. The only major contraindication to this procedure is infection at the entry site.

Technique

Facet joint injection (Fig. 14.16) is performed on an outpatient basis under local anesthesia and does not require premedication. The patient is placed in the prone position and rotated slightly away from the joint to be injected. Fluoroscopy is used to access the joint space. Considering the facet joint is curved, with the posterior aspect closer to midline than the anterior aspect, rotating the patient too far may visualize the anterior portion of the joint. Additionally, the upper lumbar spine requires less obliquity than the lower lumbar spine because the upper facets are more sagittally oriented.

Once positioned correctly, a 22-gauge spinal needle is inserted vertically toward the joint, checking every 2 cm until the joint is reached. Contrast may irritate the tissues and does not need to be used to confirm intra-articular location. Approximately 2 ml of a mixture containing a long-acting anesthetic such as bupivacaine and corticosteroid is injected into the joint (Figs. 14.15c and 14.17). One should be mindful of patient allergies since some systemic uptake may occur. If resistance is encountered during injection, the procedure should be terminated to avoid disrupting the joint capsule.

Sacroiliac (SI) Joint Injection

An SI joint injection is a similar therapeutic procedure to facet joint injection. SI joint injection has shown to be of benefit in seronegative spondyloarthropathies as well as other locally destructive etiologies. This procedure is performed with either CT or fluoroscopic guidance, with the patient in prone position or slightly oblique. The same agents are used as in facet joint injection: a local anesthetic and corticosteroid mixture.

Technique

Joint injection is performed under fluoroscopic guidance. The SI joint has two components. The upper portion of the SI joint is amphiarthrodial or fibrous and has no joint space. The lower one-third is synovial, or diarthrodial, and is the

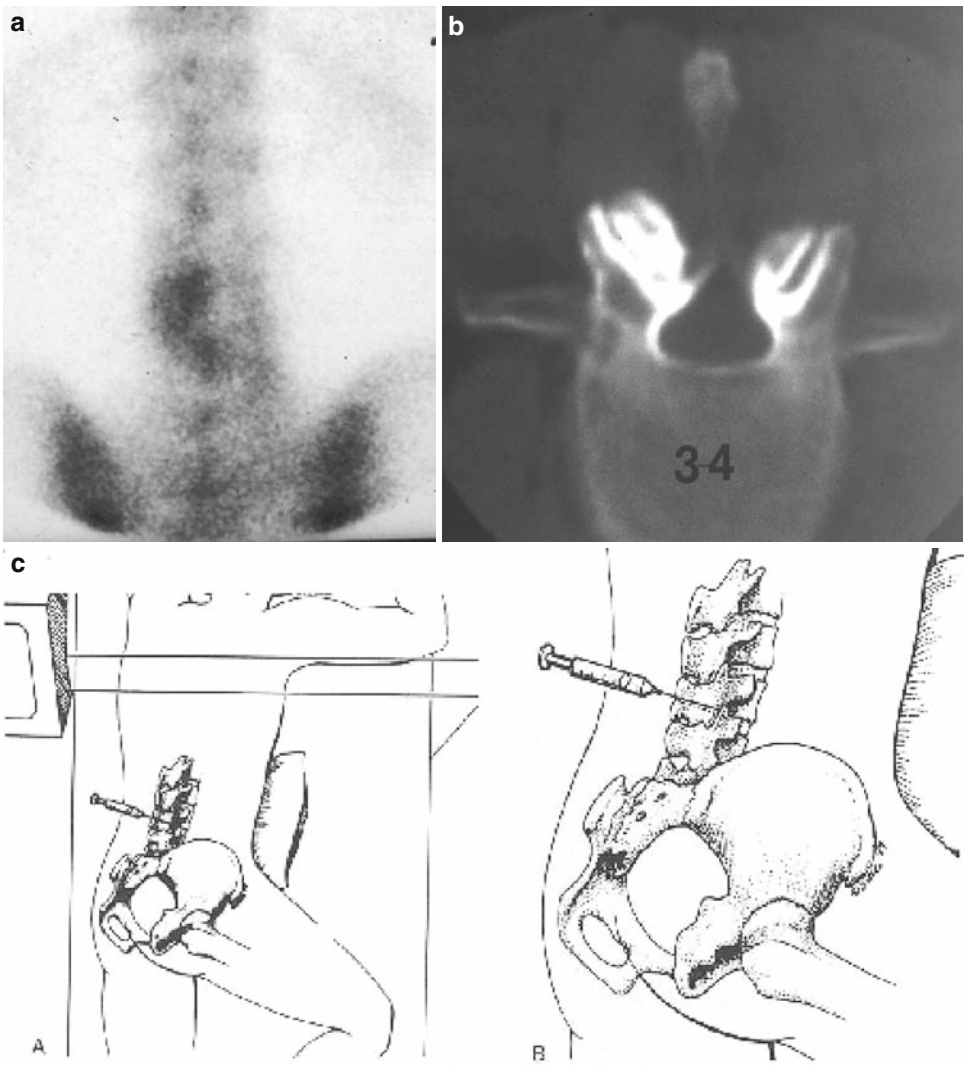

Fig. 14.15 Facet injection. Posterior view from a bone scan (**a**) showing increased uptake of radionuclide in the left facet joint due to facet arthritis. CT scan (**b**) showing narrowing and sclerosis at L3–4 level of the left facet joint. Fluoroscopic spot image (**c**) showing the patient is in the prone-oblique position. The needle has been inserted into the left L3–4 facet. About 0.5 cm^3 of contrast is injected prior to injection of methylprednisolone acetate and bupivacaine. Note the typical "s-shaped" outline of the joint by the contrast

desired site of injection. Under fluoroscopy, two joint planes are often visualized. The posterior edge of the superior SI joint is medial to its anterior edge. The most inferior portion of the joint is oriented nearly sagittally. Under fluoroscopy the anterior and posterior margins of the joint may overlap and create difficulty in differentiating the two. The anterior joint space is wider and can be distinguished from the posterior aspect by rotating the patient. Otherwise, to access the SI joint one can aim for a more lucent strip within the overlap, which will be the posterior aspect of the joint.

The needle is inserted into the joint from a superomedial position (Fig. 14.18a). It is angled laterally toward the medial border of the ilium where it articulates with the sacrum. Once the needle touches the medial aspect of the iliac bone, the needle can be redirected more medially to enter the joint space. A "pop" as the needle penetrates the ligaments indicates intra-articular needle placement. Nonionic contrast is used to confirm placement within the joint before applying the steroid/anesthetic mixture (around 4 ml per SI joint) (Fig. 14.18b).

Discussion of SI and Facet Joint Injections

The efficacy of facet joint injections and the most appropriate technique are debated. The debate more likely reflects the difficulty in identifying patients with facet joint syndrome, rather than the efficacy of treatment when patients are properly identified. Less controversy surrounds SI joint injection

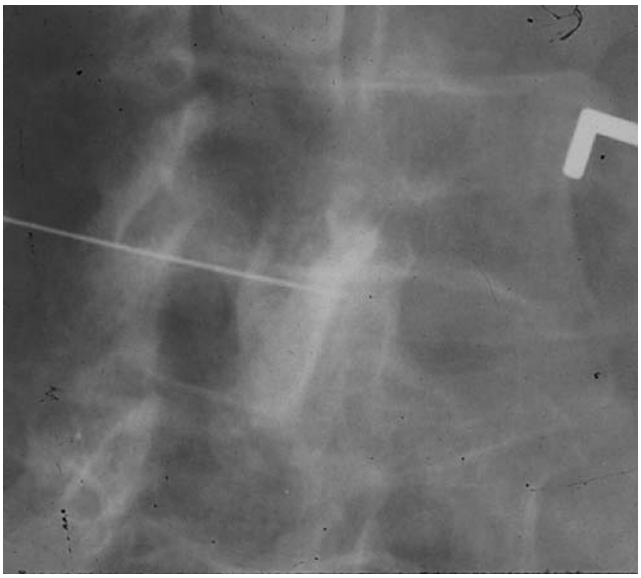

Fig. 14.16 Facet injection. Patient is in the prone position. The posterior aspect of the facet joint can be brought to tangent for needle placement by slowly raising the affected side often to a shallow anterior oblique position. The needle is inserted in the midportion of the facet joint and contrast is injected. (Reprinted with permission from J. Tehranzadeh Ref. 52)

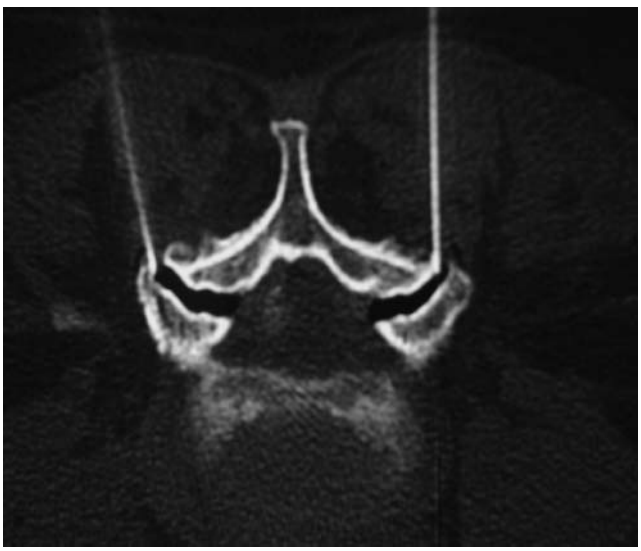

Fig. 14.17 CT Technique. This is a 55–year-old gentleman suffering from pure axial back pain. The lumbar CT scan showed degeneration of the facet joints. The image shows bilateral insertion of 22-gauge spinal needles into the facet joints. Injected air shows good distension of the joints prior to injection of a mixture of methylprednisolone acetate and bupivacaine

compared with facet joint injections since pain originating from this joint is usually clear-cut.

The therapeutic benefit of SI and facet joint injections is believed to result from a combination of the anesthetic inhibition of local nociceptors and the anti-inflammatory properties of the corticosteroid. Some researchers believe that the preservative that contains the corticosteroid contributes to local nerve damage. These researchers discount the role of anti-inflammatory properties in pain relief.

Patients may be concerned about corticosteroids contributing to bone destruction, especially when underlying osteoporosis is present. To date, there is no evidence to support this notion.

Procedures Targeting Neural Structures

The following is a description of two procedures targeting neural structures: the epidural block and the selective nerve root block.

Epidural Block

An epidural block is the percutaneous injection of steroid and long-acting local anesthetic into the epidural space of the spinal canal (Figs. 14.19 and 14.20). This procedure is performed to provide anesthesia before other invasive procedures or to provide longer term pain control in patients with local pathology that is causing back pain.

Anatomy of the Epidural Space

The epidural space extends from the foramen magnum superiorly to the sacral hiatus inferiorly. It is located superficial to the dura mater and deep to the periosteum of the vertebra. The epidural space contains Batson venous plexus and loose areolar tissue. It is occasionally divided by a midline septum known as the plica mediana dorsalis, seen as a thin linear lucency on epidurograms. Additionally, the epidural space is traversed by spinal nerve roots, which exit by passing beneath the pedicle of the same level (e.g., the L3 nerve root passes beneath the L3 pedicle).

Indications

Epidural blocks are used commonly to provide anesthesia during other procedures such as labor and delivery. Interventional radiologists perform epidural blocks to ameliorate pain in patients with mild to moderate spinal stenosis. Severe stenosis requires surgical laminectomy in most cases. An epidural block may help plan the type and extent of eventual surgical treatment.

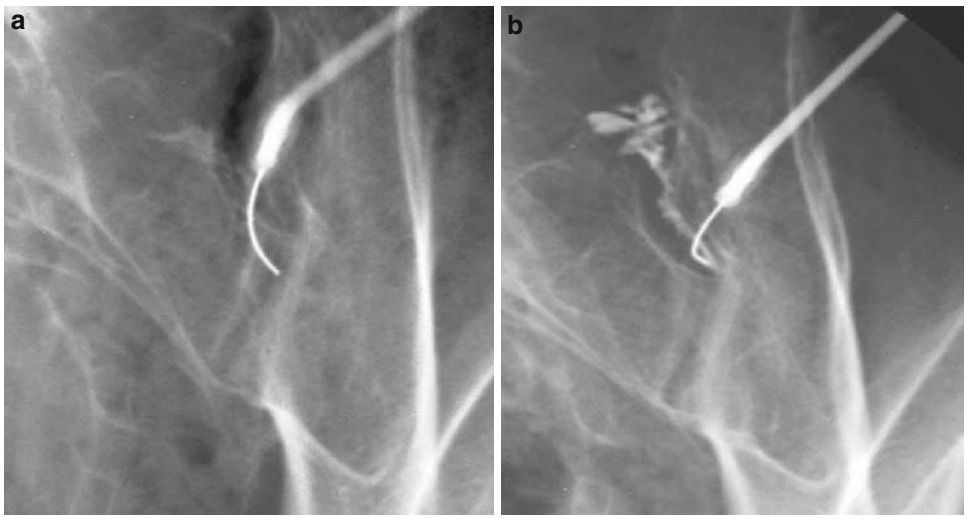

Fig. 14.18 SI joint injection under fluoroscopy control. The patient is in prone oblique position. (**a**) The needle is inserted in the lower aspect of the sacroiliac joint. (**b**) Injection of contrast confirms the accurate position of the needle inside the joint

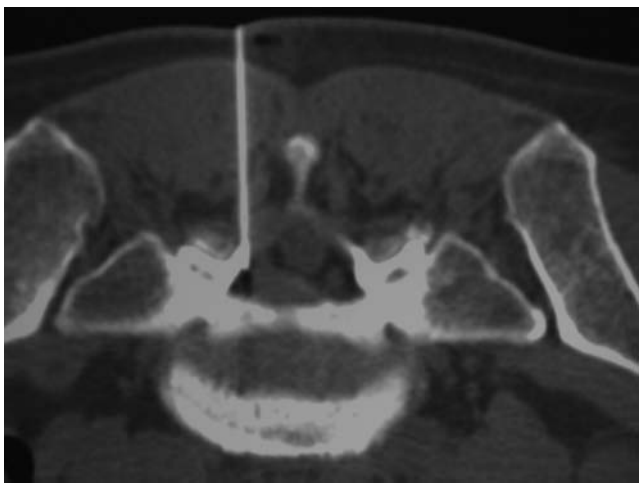

Fig. 14.19 A 35-year-old man suffering from left-sided sciatica. Axial CT with the patient in the prone position showing a symptom causing left posterolateral disc protrusion at L5/S1 compressing the S1 nerve root. CT image shows the tip of the 22-gauge spinal needle positioned in the epidural space at the level of the disco-radicular junction

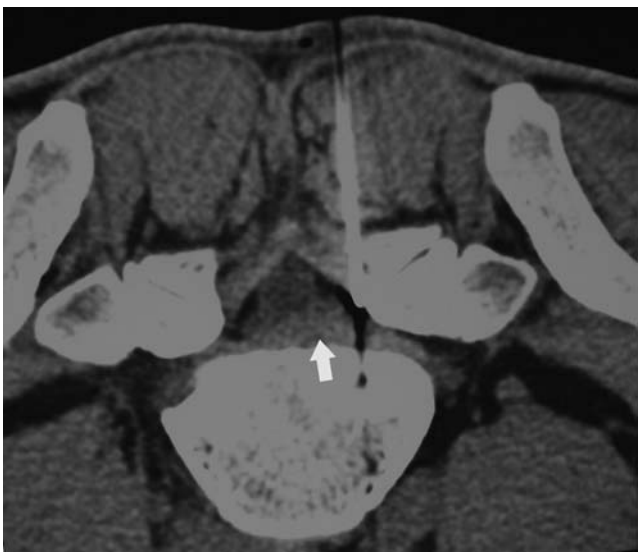

Fig. 14.20 A 42-year-old woman with a right-sided L5/S1 posterolateral disc protrusion (*arrow*) complaining of right-sided sciatica. CT scan showing the position of the tip of the 22-gauge spinal needle in the lateral epidural space close to the disco-radicular interface. Air epidurogram confirms the epidural position of the needle tip

Technique

Epidural blocks are performed using local anesthesia and C-arm fluoroscopy with the patient in the prone position. Preprocedure imaging is not mandatory but may be helpful. MRI can be used to demonstrate the inferior extent of the dural sac. Conventional radiographs allow the physician to visualize the shape of the sacrum.

Two common approaches are used to enter the epidural space. *The caudal approach* targets the sacral hiatus (a dorsal opening at the lowest portion of the sacrum) which is bordered by the palpable sacral cornua. After palpating the coccyx, the sacrum is palpated superiorly until the two sacral cornua are identified. Lateral fluoroscopy may be helpful in obese patients. The needle is passed into the sacral hiatus and advanced to the S3 vertebral level. Needle position should be midline on the AP view and between the laminae and the sacral vertebra on the lateral view.

The second method of accessing the epidural space is *the lumbar approach.* This method targets the interlaminar space

within a centimeter of midline. Lumbar lordosis should be accommodated by extra pillows under the abdomen to help increase the interspinous space. The needle is inserted toward the upper edge of the lower lamina of the desired space until one has contacted bone. Then, the needle is redirected rostrally and slightly medially until the ligamentum flavum is pierced. Penetration of the ligamentum flavum and entry into the epidural space is indicated by a "pop" and decreased resistance to saline injection.

The following steps are the same with either approach. Once the needle is placed, check for egress of CSF or blood by removing the stylet and having the patient perform the Valsalva maneuver. Confirmation of needle placement in the epidural space is obtained by performing a test injection with saline, which should meet little resistance. One can then inject nonionic contrast, which should flow away from the needle tip in the cephalad direction along the nerve roots. The plica mediana dorsalis, if present, may confine the injected solution to one side, leading to an ineffective epidural. If the needle is placed intravascularly, contrast will fill the epidural veins, necessitating redirection of the needle. The procedure should be discontinued if the thecal sac is entered.

The therapeutic injection consists of a solution containing 18 mg of betamethasone, 3–5 ml of 0.25% bupivacaine, and 4–5 ml of sterile saline. Greater volumes should be used when targeting a level above L4 from a sacral approach. Blood pressure and pulse should be monitored regularly because transient hypotension occurs in approximately 2.5% of patients.

Discussion

The affected vertebral level determines the appropriate approach. The caudal approach is performed if the L3–4 level or below is to be targeted or in a postsurgical patient with recurrent back pain. The lumbar approach is used for levels above L3–4. Most patients notice relief of pain shortly after the completion of injection. As described earlier, an uncommon side effect is transient hypotension. Steroid-induced side effects are minimal, but patients should not plan surgery within the following 3 weeks. If successful, injections can be performed up to three times a year.

The most common technical complication is a dural puncture, with a lower incidence using the caudal than the lumbar approach. If this is recognized and corrected prior to therapeutic injection, it usually results in only a spinal headache. If not recognized, anesthesia injection results in a spinal block (numbness, weakness, etc.). Intrathecal injection of steroids has unclear side effects but should be avoided nonetheless.

Selective Nerve Root Block

A selective nerve root block (SNRB) is the local administration of a solution containing anesthetic and steroid to a spinal nerve root as it exits the intervertebral foramen. SNRBs have both diagnostic and therapeutic applications.

Anatomy

The sinuvertebral nerve is a branch of the ventral nerve root and the sympathetic gray rami communicans. It contributes innervation to the outer portion of the annulus fibrosus, the posterior longitudinal ligament, the epidural membranes, and the dural sleeves of nerve roots. Each sinuvertebral nerve has multisegmental distribution and therefore pain stemming from this nerve is difficult to localize.

Indications

The most common etiology of sinuvertebral nerve pain is disruption of the annulus fibrosus, with leakage of substances such as phospholipase A_2 from the nucleus pulposus irritating local nerves. Physicians also use SNRB procedures to evaluate postoperative nerve root irritation, entrapment resulting from degenerative disc disease, spinal stenosis, foraminal stenosis, and spondylolisthesis.

Technique

For this procedure the patient is placed in the prone-oblique position with the targeted side off the table. The classic "Scotty dog" appearance of the vertebra is visualized, and using fluoroscopic guidance, the needle is aimed just beneath the pedicle from a posterolateral approach. The presence of bone hypertrophy from the adjacent facet joint may hinder access. As one approaches the targeted nerve, the needle travels lateral and anterior to the superior articular process of the facet below the level. The patient may jump reflexively if the needle touches the nerve root. The proper needle depth has been obtained when the needle touches the posterior aspect of the vertebral body. Proper needle placement should be confirmed with injection of 1–2 ml of contrast, which will outline the nerve root (Fig. 14.21). SNRB is likely to be effective if the pain from contrast injection recreates the patient's radicular symptoms. Subsequent to proper localization of the needle, the therapeutic block is performed. Corticosteroid and long-acting anesthetic are injected as the needle is slowly withdrawn.

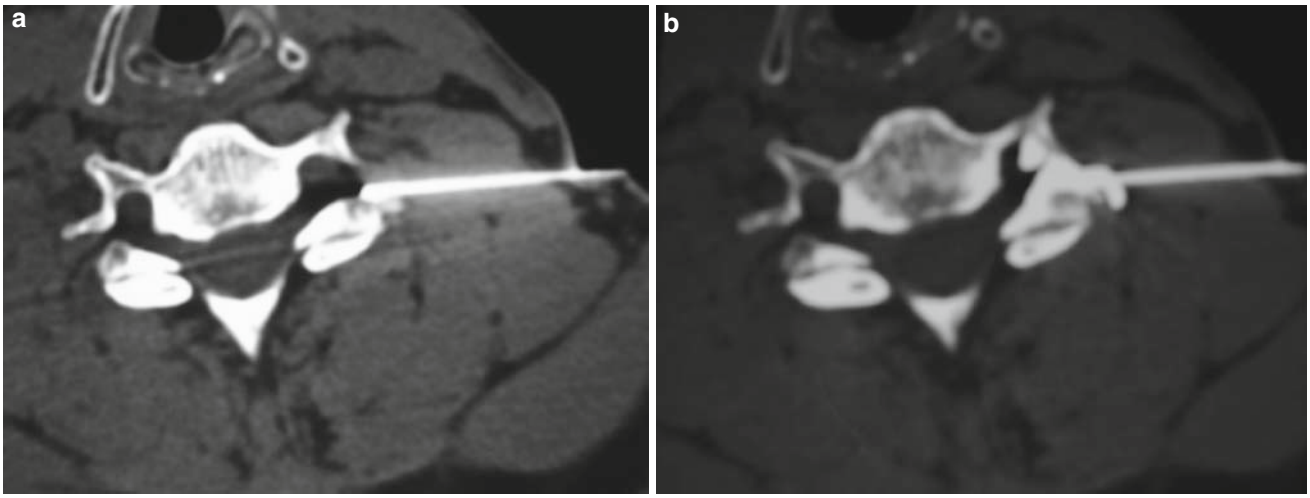

Fig. 14.21 A 46-year-old woman with left-sided C6 radicular symptoms due to a foraminal disc protrusion. CT image (**a**) shows a 22-gauge spinal needle positioned in the left C6/C7 foramina, posterior to the vertebral artery gliding along the anterior surface of the articular process. CT image (**b**) shows contrast injection diffusion around the nerve root in the foramen with some contrast entering the cervical canal. No vascular opacification is present

Discussion

When contrast elicits the patient's radicular pain and local anesthetic alleviates such pain, it is likely that the injected level is the source of the patient's pain. Partial pain relief suggests that the symptoms originate in part from a second nearby level or levels. Complete pain relief from injecting a second adjacent nerve root confirms its involvement. Considering that multiple structures may be contributing to the patient's pain, facet joint injection or discography may be indicated later if SNRB does not relieve the patient's pain completely. As a general rule, patients who do not respond to SNRB are unlikely to respond to surgery at that level.

Interventional Evaluation and Treatment of Joint Pathology

As imaging modalities such as CT and MRI have improved, many minimally invasive diagnostic procedures have been developed to evaluate joint pathology. CT and MR arthrography provide exceptional opportunities to evaluate structures that were invisible with conventional arthrography. Such structures include the glenoid labrum, glenohumeral ligaments in the shoulder, and acetabular labral pathology in the hip. MR imaging visualizes tendons, ligaments, and articular cartilages in detail. Therapeutic arthrography and bursography using corticosteroid, viscosupplementation, or anesthetic not only evaluate the origin of pain but can also provide as much as 6–9 months of pain relief in diseased joints. These procedures can also be done to gather information for the surgeon who is considering arthrodesis or other interventions.

Indications for Therapeutic Arthrography

The purposes of therapeutic arthrography are to define the origin of a patient's pain, alleviate the pain, and potentially decrease the rate of progression of osteoarthritis (OA). Nonpharmacologic therapies, including reduced activity, weight loss, supports and braces, and physiotherapy are important initial steps in managing patients who have joint disease. Joint injection should be considered after other therapeutic interventions such as oral nonsteroidal anti-inflammatory drugs (NSAIDS) have been tried.

Intra-articular corticosteroid injections are frequently used to treat symptomatic joint disease and soft tissue inflammatory disorders. Not only do these injections alleviate pain, but a positive response to intra-articular injection of anesthetics may also indicate which patients are likely to respond well to surgery.

Corticosteroids are used for the following:

1. Enthesitis (tennis elbow, golfer elbow, and rotator cuff tendonitis).
2. Joints: Various arthropathies including osteoarthritis, rheumatoid arthritis, and other inflammatory arthropathies.
3. Tendon sheath: De Quervain's tenosynovitis and trigger finger.

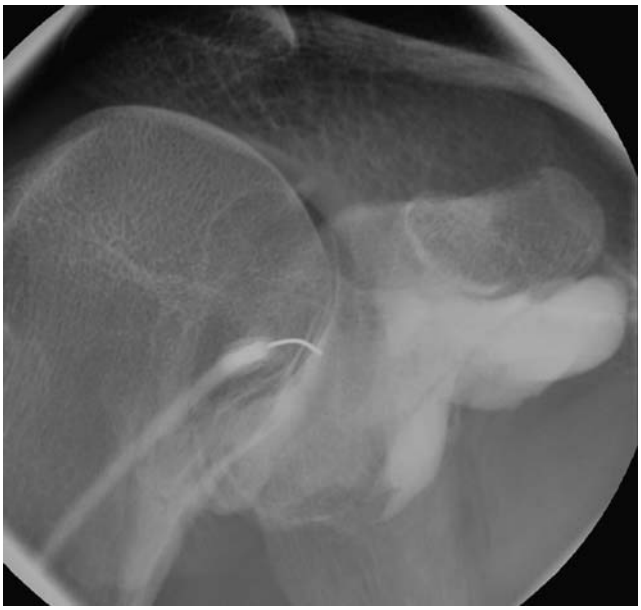

Fig. 14.22 Shoulder arthrogram. The patient is supine with the arm in neutral (thumb pointed anteriorly) position. The needle is positioned in the mid to lower third of the glenohumeral joint. The needle should be closer to the humeral cortex. (Reprinted with permission from J. Tehranzadeh Ref. 52)

4. Bursae: Trochanteric, subacromial, and olecranon bursitis.
5. Ligament and muscle: Strains, sprains, and other sports injuries.
6. Nerve compression: Carpal and tarsal tunnel syndrome.
7. Nodules and ganglia: Rheumatoid arthritis and trauma.
8. Trigger points: Cervical and lumbar.
9. Epidural: Nerve root compression.

Hyaluronic acid (HA) is an alternative to corticosteroids for the treatment of OA in the hip or the knee. It is used as a temporary replacement and supplement for synovial fluid to treat pain and decreased mobility associated with OA. Studies are inconclusive regarding the best responders with respect to age, severity of disease as depicted radiographically, and degree of symptoms. Intra-articular HA injections may be considered for patients who fail a trial of at least 3 months of conservative therapy or are unable to tolerate NSAIDs. HA is administered over a three to five injection course. Patients who are not candidates for total knee replacement or who have failed previous knee surgery for their arthritis, such as arthroscopic debridement, may also be candidates for viscosupplementation. Total knee replacement in younger patients may be delayed with the use of HA. Currently, HA is licensed only for the knee, but it used in hips as well.

HA preparations are contraindicated in patients who have severely inflamed joints, a history of joint infection, or patients who have skin diseases or infections around the injection site. Other contraindications include large intra-articular effusion, known hypersensitivity to hylan G-F 20, and hypersensitivity to avian proteins or poultry products.

General Technique for Arthrography

The general steps in fluoroscopically guided intra-articular injection of contrast, local anesthetic, corticosteroids, and HA are similar to other percutaneous procedures. One first places the patient in the appropriate position depending on the desired joint, followed by adequate preparation and draping. Depending upon the joint to be injected, a 20–25-gauge needle is used. The length of the needle is determined by the body part in question and the patient's body habitus. Prior to injection, the joint should be aspirated. If unable to draw back on the syringe, a small amount of contrast may be injected to verify intra-articular placement of the needle. With appropriate needle placement contrast will flow away instead of pooling around the needle tip.

The most commonly employed contrast agent is a non-ionic agent such as iohexol (Omnipaque 300) mixed with 0.25% bupivacaine hydrochloride in equal proportions to minimize discomfort from the injection. If indicated, a larger amount of contrast can be injected into the joint to evaluate the morphology of the synovium and other internal structures of the joint. The size of the joint and its recesses determine the amount of the mixture injected.

MR arthrography is performed with injection of a Gd mixture diluted to a 1:200 mixture with saline and iodinated contrast.

Therapeutic treatment of a joint with OA is accomplished with a mixture of 0.25% bupivacaine hydrochloride with methyl prednisone acetate. The bupivacaine or other long-acting local anesthetic is included to provide early relief of symptoms and helps confirm the diagnosis. Dosing is site dependent and summarized in Table 14.1. As a rule, larger joints require more corticosteroid. As discussed above, Hylan G-F 20 can be used in some cases instead of steroids.

Application of heat should be avoided for 24–48 h after intra-articular injection. Instead, ice should be used to minimize pain due to joint injection. Furthermore, intense activities or exercises should be avoided for about 2 weeks after intra-articular injection of corticosteroid.

It is generally recommended that the same joint be injected with corticosteroid no more than three or four times over a period of weeks to months, followed by a period of conservative treatment. Usually, one should allow 4–6 weeks between injections.

Table 14.1 Describing needle size and injection doses for therapeutic arthrography

Joint	Specific technique	Needle	Arthrographic dose: Omnipaque 300/bupivacaine hydrochloride 0.25% (1:1 ratio)	Therapeutic dose: bupivacaine hydrochloride 0.25%/methylprednisolone acetate (MA)
Shoulder	Therapeutic arthrography	20–22 gauge, 3.5 in.	3 ml	5 ml/1 ml
	Therapeutic acromioclavicular injection	22 gauge, 1.5 in.	0.5 ml	0.5 ml MA
	Subacromial–subdeltoid bursography	22 gauge, 1.5 in.	2 ml	3 ml/1 ml
Hip	Hip therapeutic arthrogram	20–22 gauge, 3.5 in.	2 ml	4 ml/1 ml
	Total hip replacement arthrogram	20–22 gauge, 3.5 in.	2 ml	4 ml/1 ml
	Greater trochanteric bursogram	22 gauge, 3.5 in.	2 ml	3 ml/1 ml
Knee	Therapeutic knee arthrogram	20–21 gauge, 1.5 in.	7 ml	5 ml/1 ml
	Therapeutic proximal tibiofibular arthrogram	22 gauge, 2.5 in.	1 ml	1 ml/1 ml
Elbow	Therapeutic elbow arthrography	22–25 gauge, 1.5 in.	2 ml	3 ml/1 ml
Wrist	Therapeutic wrist arthrography	25 gauge, 1.5 in.	1 ml	1 ml/1 ml
Ankle	Therapeutic ankle arthrogram	22 gauge, 1.5 in.	2–3 ml	3 ml/1 ml
	Therapeutic subtalar arthrogram	22 gauge, 2.5 in.	3 ml	2 ml/1 ml
	Therapeutic calcaneal spur injection	22 gauge, 2.5 in.	0 ml	1 ml/1 ml

Shoulder Arthrography

Injections into the shoulder may target the acromioclavicular joint, the subacromial–subdeltoid bursa, or the glenohumeral joint. Most radiologists prefer an anterior approach to the glenohumeral joint. It is approached with the patient in the supine position with arms in a neutral position (thumbs pointing anteriorly). The injection site is marked on the skin overlying the lower third of the glenohumeral joint. One should aim for the mid- to lower third of the glenohumeral joint. The needle tip is inserted closer to the humeral head articular surface than the glenoid margin to avoid piercing the overhanging labral cartilage (Fig. 14.22).

Injection into the glenohumeral joint is used to assess the rotator cuff and with MRI the labrum. Plain arthrography will show a full-thickness rotator cuff tear, through opacification of the subacromial subdeltoid bursa from the glenohumeral joint injection. Granulation tissue can delay visualization of a tear and lead to false-negative results. To minimize this problem, one can exercise the joint to lyse synechiae and then repeat imaging.

Glenohumeral injection is also useful to diagnose adhesive capsulitis (frozen shoulder). This diagnosis is made when there is decreased joint capacity (5 cm^3 or less) and moderate pressure is required to inject. One will see a contracted joint capsule and the axillary recess is absent. Therapeutic arthroscopy is the current treatment of choice for adhesive capsulitis.

Subacromial–subdeltoid bursography (Fig. 14.23) is another technique to evaluate pathology of the shoulder. The patient is placed in the supine position and a small gauge needle is directed into the bursa along the inferior cortex of the acromion. This procedure provides diagnostic information about the superior surface of the rotator cuff, as well as impingement and thickness of the cuff when used in combination with arthrography.

Contrast-enhanced magnetic resonance (MR) arthrography of the shoulder is also performed to investigate shoulder pathology and is most commonly indicated to evaluate labral pathology or recurrent rotator cuff tears. MR arthrography shows the labrum to good advantage and permits reliable diagnosis of labral tears and their variants.

MR imaging should be performed within 45 min of injection to avoid dissipation of contrast into the capsule and periarticular tissues. Imaging is performed in the axial, oblique coronal, and oblique sagittal planes using a T1-weighted spin-echo sequence with frequency-selective fat saturation (FS). Fat saturation sequence is needed to differentiate extravasation of the contrast agent through a cuff defect from the peribursal fat, which is normally bright on T1-weighted images. The fat saturation sequence

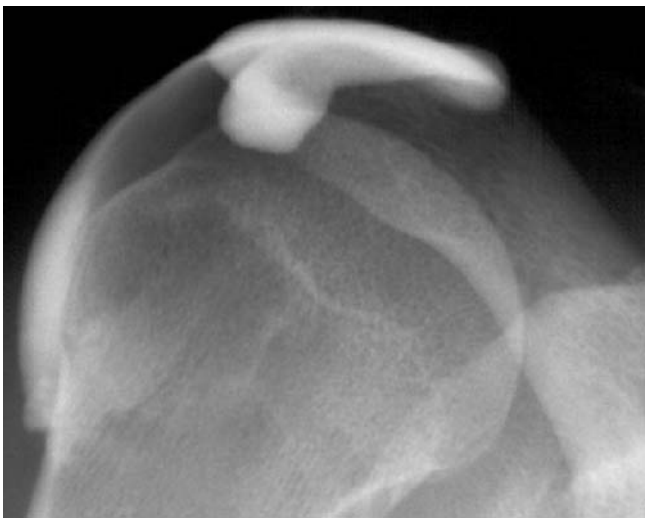

Fig. 14.23 Normal subacromial–subdeltoid bursa injection. (Reprinted with permission from J. Tehranzadeh Ref. 52)

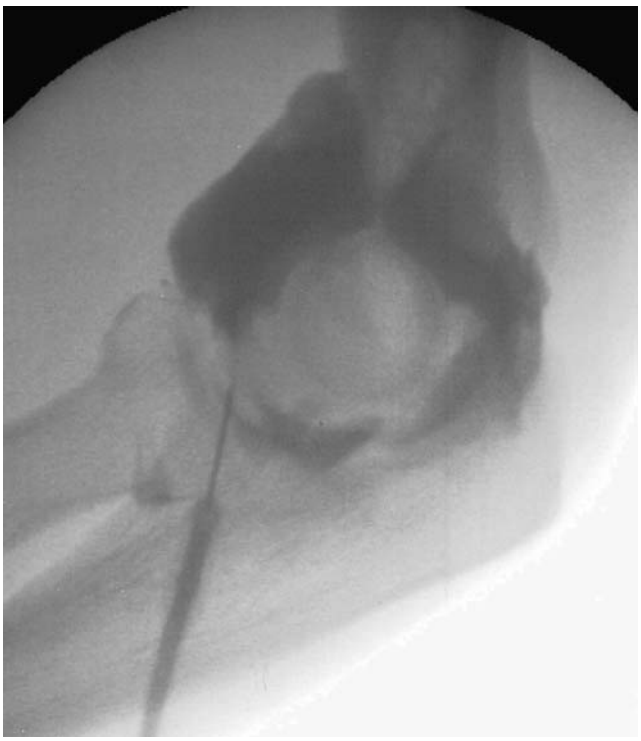

Fig. 14.24 Elbow arthrogram. The patient sits next to the fluoroscopy table; the elbow is raised with a few pillows to the level of the shoulder. The needle is inserted into the radiohumeral joint space. (Reprinted with permission from J. Tehranzadeh Ref. 52)

also improves visualization of small labrum tears by differentiating the contrast from pericapsular fat. T2W FS sequence in oblique coronal and axial planes should also be obtained to visualize preexisting periarticular fluid collections and further evaluate the labrum and the long head of the biceps tendon as it courses through the joint.

Elbow Arthrography

To perform a therapeutic elbow arthrography (Fig. 14.24), the patient either can sit next to the table or can lie prone with the arm parallel to the tabletop and the elbow flexed to 90° with the radial side facing upward. The elbow is raised to the level of the shoulder. The joint is entered through the radiohumeral joint space using 1.5-in. 22- or 23-gauge needle.

Wrist Arthrography

Therapeutic wrist arthrography (Fig. 14.25) is performed with the patient either sitting next to the examination table or prone on the table with the arm extended. The wrist is placed in flexion and ulnar deviation over padding. The injection site, typically the radioscaphoid joint at the level of the radial styloid process, is entered using a 0.75–1.5-in., 22–25-gauge needle. Depending on the reason for the arthrogram, other sites may be chosen to inject the midcarpal and radiocarpal joints.

The two primary interosseous ligaments of the wrist are the scapholunate (SL) and lunotriquetral (LT) ligaments. These ligaments extend along the proximal aspect of the respective carpal bones forming the SL and LT spaces along their distal surfaces. Contrast injected into a normal proximal carpal row should be prevented from extending into the midcarpal joint space by the intact SL and LT ligaments.

Midcarpal joint injection is most commonly performed into the space at the proximal tip of the hamate, the triquetrolunohamate space. In the normal setting, contrast flows into both the SL and the LT spaces and normally communicates with the carpometacarpal joints of the second through fifth digits, but not the first carpometacarpal joint.

MR wrist arthrography, using a Gd mixture, is supplanting standard wrist arthrography at many institutions.

Hip Arthrography

Fluoroscopically guided procedures targeting the hip can diagnose and treat hip pathology both in the native hip and following prosthesis placement. The greater trochanteric

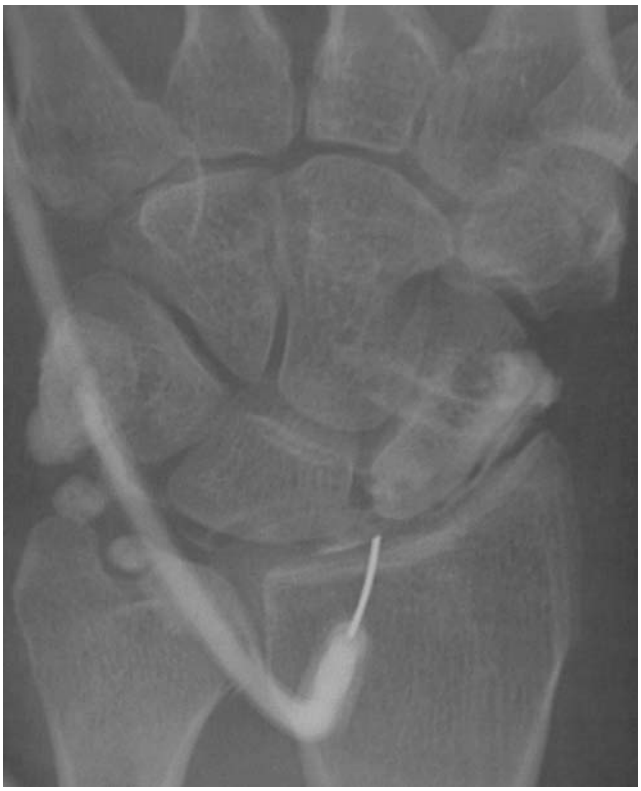

Fig. 14.25 Wrist arthrogram. The patient's wrist is positioned on a wedge sponge with the wrist in semiflexion and ulnar deviation. The needle is positioned between the scaphoid and the distal radius joint for a proximal carpal joint injection. (Reprinted with permission from J. Tehranzadeh Ref. 52)

bursa may also be injected for diagnostic and therapeutic purposes. For either procedure, the patient is laid supine with the hip internally rotated and the knee slightly flexed. The needle may be placed along either the medial or the lateral margins of the femoral neck. To perform the medial approach (Fig. 14.26), the needle is inserted toward the medial cortex of the femoral neck at the head and neck junction until it contacts bone. Then, the bevel is turned to place the needle tip in the joint capsule closely adjacent to the femoral neck. Therapeutic fluoroscopic arthrography is approached laterally at the head and neck junction (Fig. 14.27).

Arthrography also may be used to evaluate prosthetic loosening, particulate synovitis, and infection of a hip replacement (Fig. 14.28). For the last indication, a larger bore needle (18 gauge) should be used as pus can be viscous and difficult to aspirate. After correct needle placement, the joint should be aspirated for material for culture prior to contrast injection.

Greater trochanteric bursography (Fig. 14.29) is performed in a similar manner as arthrography, but the needle is directed toward the lateral cortex of the greater trochanter instead of along the femoral neck.

Knee Arthrography

The knee joint may be entered laterally with the patient in supine position or medially with the patient in the ipsilateral lateral decubitus position with the knee flexed and the contralateral leg flexed so that the opposite knee is posterior to the knee to be injected. A 1.5-in., 20–22-gauge needle is used. The tip of the needle should be adjacent to or just past the femoral condyle cortex when the injection is performed

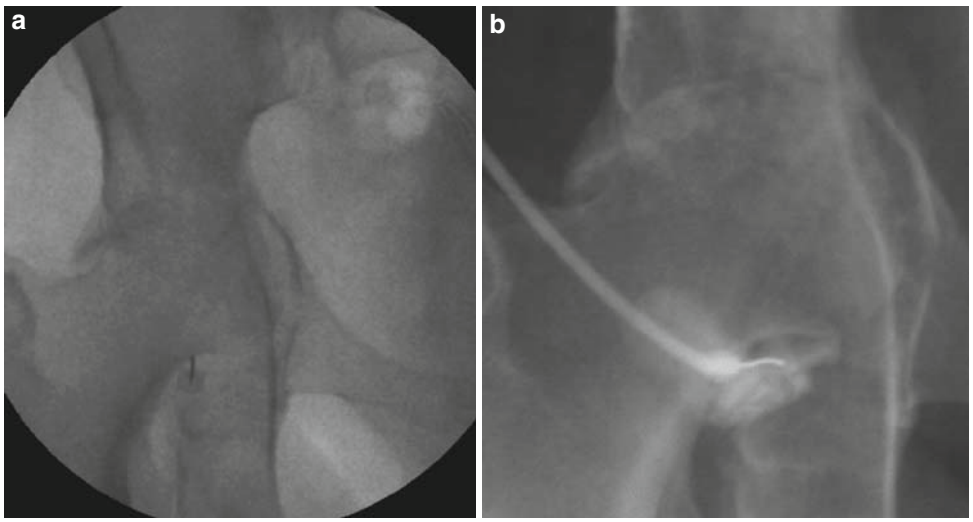

Fig. 14.26 Diagnostic hip arthrogram (medial approach). AP fluoroscopic spot film (**a**) showing the needle positioned in the medial aspect of the femoral head and neck junction. AP fluoroscopic spot film (**b**) showing injected contrast agent. (Reprinted with permission from J. Tehranzadeh Ref. 52)

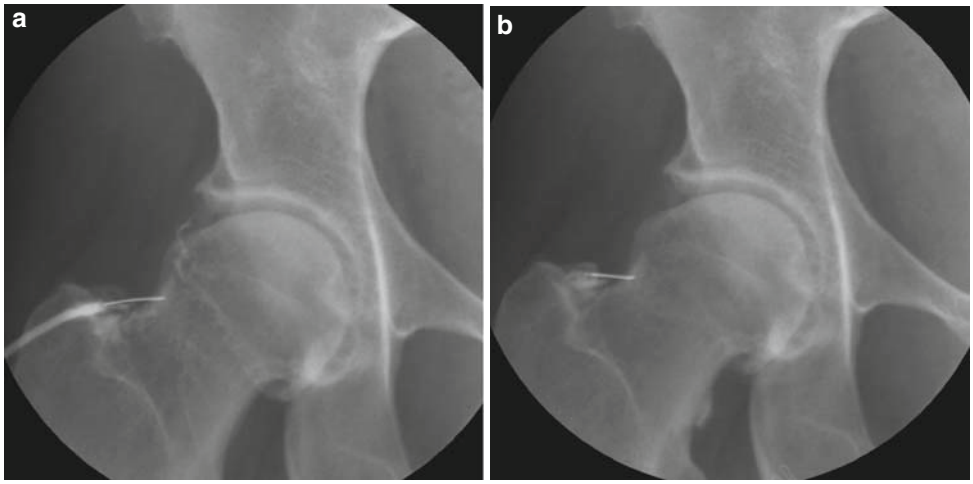

Fig. 14.27 Therapeutic hip arthrogram (lateral approach). AP fluoroscopic spot film (**a**) showing the needle inserted along the lateral aspect of the femoral head and neck junction. After the needle touches the cortex, the bevel of the needle is rotated and the contrast is injected (**b**). Note dilution of the contrast agent following methylprednisolone acetate and bupivacaine hydrochloride injection. (Reprinted with permission from J. Tehranzadeh Ref. 52)

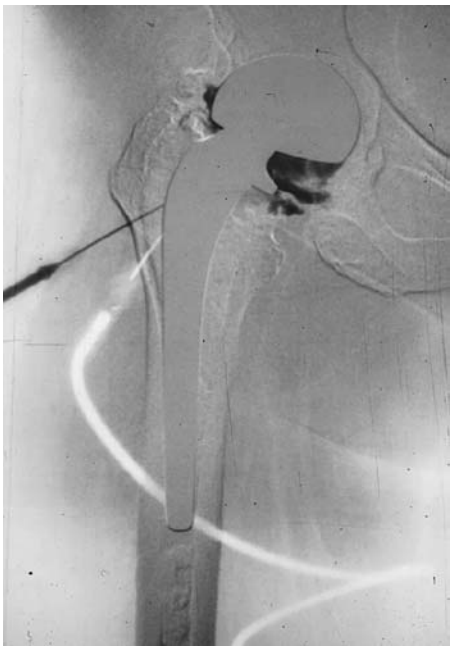

Fig. 14.28 Arthrogram in hip prosthesis. The needle tip is aimed toward the medial aspect of the head and neck junction of the prosthesis until contacting metal. The needle should then slide over the neck of the metal prosthesis. Contrast is injected after aspiration. (Reprinted with permission from J. Tehranzadeh Ref. 52)

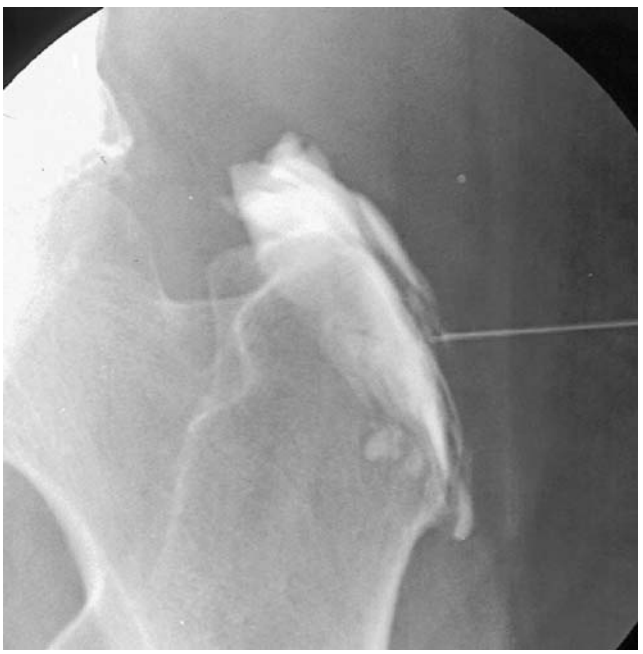

Fig. 14.29 Greater trochanteric bursogram. The patient is supine. The lateral aspect of the thigh at the point of maximum tenderness is marked at the level of the greater trochanteric region. The needle approaches from the lateral side to touch the greater trochanteric bone, then the needle is withdrawn slightly by 1–2 mm. First, the needle is aspirated for bursal contents and then the contrast is injected. (Reprinted with permission from J. Tehranzadeh Ref. 52)

(Figs. 14.30 and 14.31). Placement of the needle too deep into the joint may cause contrast extravasation into Hoffa fat pad.

To access the proximal tibiofibular joint, the patient is positioned in the contralateral lateral decubitus position. The midportion of the proximal tibiofibular joint is entered.

Ankle Arthrography

The patient is placed in the lateral decubitus position with the ankle relaxed (Fig. 14.32). The space between the anterior border of the tibia and the talus is marked under fluoroscopy.

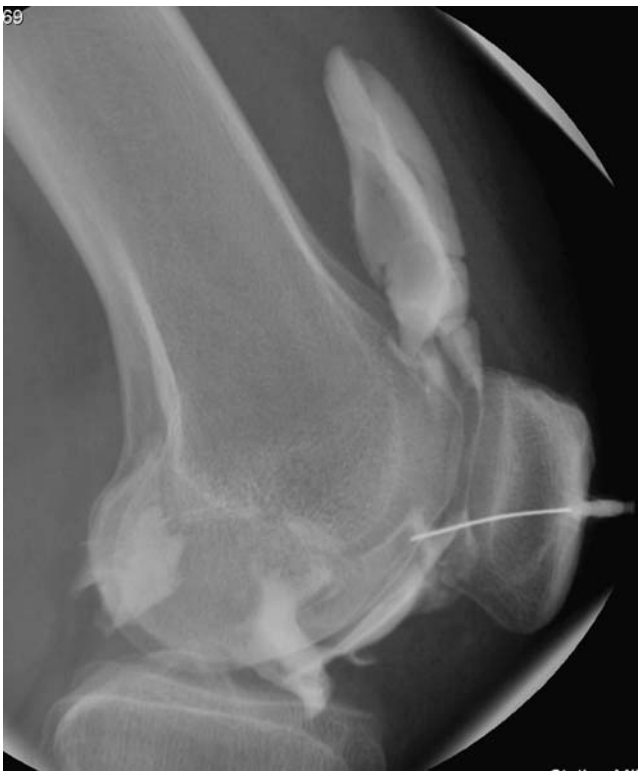

Fig. 14.30 Knee arthrogram. The patient is positioned in the contralateral decubitus position from the side to be injected with a small pillow under the ankle to elevate the tibia to the level of the femur and put the femur in perfect lateral position. The midportion of the femoropatellar joint is marked on the skin, and a 21-gauge, 1.5-in. needle is inserted between the dorsolateral patellar cortex and the anterior femoral condyle. The needle tip should be closer to the cortex of the femoral condyle. The joint is aspirated and contrast is injected. Contrast should flow freely from the needle tip. (Reprinted with permission from J. Tehranzadeh Ref. 52)

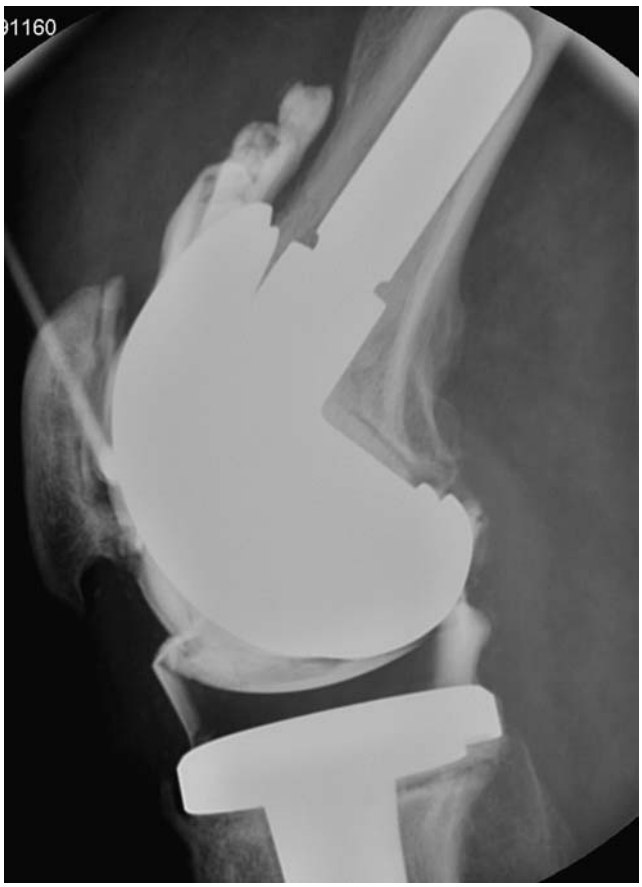

Fig. 14.31 Arthrogram in knee with a prosthesis. The patient is positioned in the contralateral decubitus position from the side to be injected with a small pillow under the ankle to elevate the tibia to the level of the femur and put the femur in perfect lateral position. The midportion of the femoropatellar joint is marked on the skin, and a 21-gauge, 1.5-in. needle is inserted between the dorsolateral patellar cortex and the anterior femoral condyle. The needle tip should be closer to the cortex of the femoral condyle. The joint is aspirated and contrast is injected. Contrast should flow freely from the needle tip. (Reprinted with permission from J. Tehranzadeh Ref. 52)

The needle is inserted in a cephalad direction to enter the joint followed by the therapeutic injection. The dorsalis pedis artery should be marked and avoided during needle insertion.

To access subtalar articulation (Fig. 14.33), the patient is placed in lateral decubitus position with the ankle relaxed. The medial subtalar joint is marked. The needle is angled in the cephalad direction to enter the subtalar joint. Injection is then performed after confirmation of intra-articular needle placement.

Side Effects and Complications of Arthrography

Complications from arthrography include postprocedure increase in pain, infection, vasovagal reactions, and chemical synovitis. Rare cases of allergic reactions, hypotension, seizures, air embolism, and laryngeal edema have been reported. While important to consider, none of these complications are common if the physician uses the appropriate technique with a precautionary approach.

Chondrolysis has been reported following intra-articular injections of corticosteroids. Corticosteroid injection of weight-bearing joints has led to multiple yellowish cystic lesions possibly due to direct mechanical damage to chondrocyte cells. Marked reduction in the elasticity of the articular cartilage is also found after intra-articular corticosteroid injections, resulting in possible end-range limitations of movement in the joints. "Charcot-like arthropathy" has been reported in the arthritic human knee and hip joints with the use of intra-articular corticosteroid injections. These changes are thought to be due to temporary suppression of pain, which encourages excessive and unguarded activities

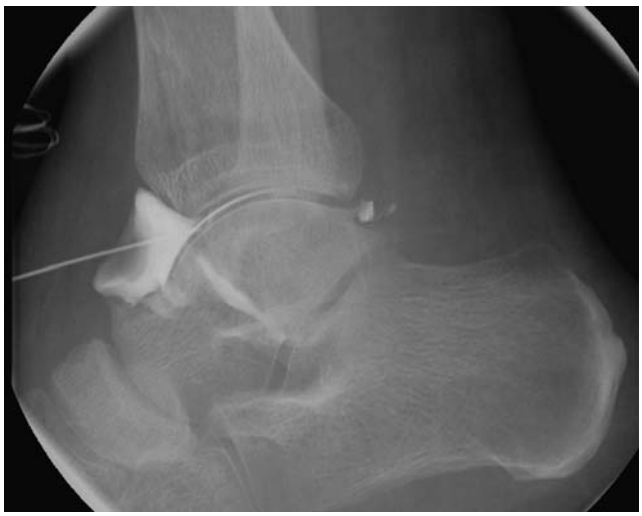

Fig. 14.32 Ankle arthrogram. The patient is positioned in the contralateral decubitus position from the side to be injected if necessary with a small towel under the foot to bring the ankle to perfect lateral position. The anterior margin of the ankle mortise is marked under fluoroscopy. The needle is positioned approximately 1 cm below the level of the ankle joint and is inserted obliquely in the cephalad direction to reach the joint. This is to avoid the anterior tip of the tibial plafond, which has a downward slope. After aspiration, the contrast is injected. Contrast should flow freely from the needle tip. Lateral radiograph of ankle arthrogram shows contrast in ankle joint. (Reprinted with permission from J. Tehranzadeh Ref. 52)

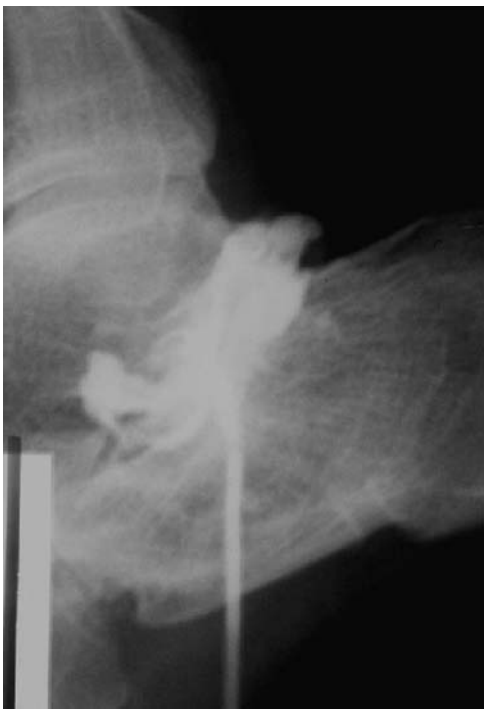

Fig. 14.33 Subtalar joint arthrogram. Patient is placed in the lateral decubitus position. The hind foot is positioned under fluoroscopy in a way to best profile the subtalar joint. The midportion of the posterior subtalar joint is marked. The needle is inserted between the talus and the calcaneus in the region of the posterior facet of the subtalar joint. Following aspiration, the contrast is injected. Contrast should flow freely from the needle tip. (Reprinted with permission from J. Tehranzadeh Ref. 52)

of diseased joints, resulting in rapid progression of joint destruction. Avascular necrosis of the hip and shoulder joints after intra-articular corticosteroid injections has been reported.

The side effects of viscosupplementation are relatively few. Systemic reactions to HA are rare and no long-term side effects have been reported.

Viscosupplementation vs. Corticosteroid Injection

HA, also known as hyaluronic acid, is a linear, unbranched glycosaminoglycan distributed throughout the body, especially as a component of synovial fluid and cartilage. The primary role of HA in synovial fluid is to maintain the viscoelastic structural and functional characteristics of the articular matrix. Hylans are cross-linked HAs, giving them a higher molecular weight and increased elastoviscous properties. The higher molecular weight of hylan may make it more efficacious than HA because of its enhanced elastoviscosity and its longer period of residence in the joint space. Nonanimal stabilized hyaluronic acid (NASHA) is a new-generation HA preparation, stabilized using a carefully controlled cross-linking process that increases the intra-articular residence time from hours to weeks. This facilitates single-injection treatment for OA without affecting the biocompatibility of HA. The preparations of HA that are used today require three (hylan G-F 20) to five injections.

The exact mechanism of viscosupplementation is uncertain. Restoration of elastoviscous properties of synovial fluid seems to be the most logical explanation. Articular cartilage has no blood supply, so all of its nourishment and lubrication comes from the fluid that ebbs and flows as pressure is applied to the joints and released.

The actual period of time that injected HA remains in the joint space is on the order of hours to days, but the time of clinical efficacy is on the order of months. It has been theorized that HA has anti-inflammatory or nociceptive effects or stimulates in vivo production of HA. A biopsy study of osteoarthritic knee injected with HA showed reconstruction of the superficial layer of cartilage and improvement in cartilage density. In addition, an anti-inflammatory effect of HA injection has been demonstrated, with a decrease in inflammatory cells and mediators of inflammation such as interleukins and leukotrienes.

Long-acting corticosteroids have been used to treat arthritis and other painful musculoskeletal conditions since the 1950s. Although the exact mechanism of action of intra-articular corticosteroids is unknown, there are several effects that have been documented. Prompt and effective reduction in local inflammation occurs after intra-articular injection of corticosteroid. Corticosteroids block the synthesis of the mediators of inflammation, reduce the number and efficacy of leukocytes at the site of inflammation, and stabilize lysosomes from rupturing. Therefore, most of the inflammatory substances are released in greatly decreased quantities. Corticosteroids also inhibit fibroblasts and collagen deposition, thus limiting the formation of scar tissue. They offer relief of pain and inflammation within a few hours of injection that lasts from a few days to weeks.

Although HA seems to produce significant symptomatic improvement, the relief has not been shown to be significantly better than with corticosteroid injections for OA of the hip or the knee. Maximum pain relief occurred in the first few weeks for intra-articular corticosteroids and at 8–12 weeks for HA.

There are a few points to consider when deciding between corticosteroid injection and viscosupplementation. Overall, corticosteroids are effective at treating OA short term, but long-term effects are inconclusive. HA seems to be as effective as corticosteroids with a delayed but prolonged response and a lower risk for adverse events. The effects of HA on joint stiffness may be superior to corticosteroids in some patients, with more durable and longer acting effects than corticosteroids. HA is considerably more expensive than corticosteroids, and the treatment regime is technically more difficult and inconvenient to the patient. Combination of HA and corticosteroid has been found to have a synergistic effect.

Therapeutic arthrography is an effective way to deliver corticosteroid, anesthetic, or HA accurately within a diseased joint. HA offers an alternative therapy for OA of the knee or the hip for people intolerant of NSAIDS or for patients when steroids are contraindicated. It should be noted that these therapies are only used to treat symptoms of OA and do not modify or cure the disease process.

Percutaneous Procedures Targeting Musculoskeletal Lesions

Minimally invasive methods of accessing musculoskeletal lesions have both diagnostic and therapeutic roles in medicine. While musculoskeletal lesions are common and relatively routine to diagnose and treat, they arise from myriad etiologies including trauma, infection, and neoplasia. The appropriate treatment depends on correct diagnosis of the underlying pathology. The following section describes percutaneous biopsy, treatment, and ultrasound-guided procedures targeting musculoskeletal lesions.

Biopsies of the Musculoskeletal System

Radiography may suggest the etiology of a musculoskeletal lesion, but most often is insufficient for definitive diagnosis. More information may also be required when a malignancy is certain but the best treatment is in question. For example, the radiologic appearance of a metastasis does not necessarily reveal the source of malignancy. In this situation a biopsy of the lesion may be warranted to reveal the tumor's cell type.

There are several advantages to percutaneous biopsy compared with open biopsy. Percutaneous biopsy is of lower cost and has lower postprocedure morbidity. Percutaneous biopsy is generally as accurate as open biopsy when properly performed. The following is a description of percutaneous biopsies of musculoskeletal lesions, specifically those arising in bone, cartilage, and soft tissue.

Indications and Contraindications

Percutaneous biopsy is indicated for the following:

1. To establish the definitive pathologic diagnosis when imaging is unclear.
2. To confirm the radiographic diagnosis of a metastasis to bone or soft tissue in a patient with a newly discovered primary neoplasm elsewhere.
3. To confirm cancer recurrence when the patient has a prior history of neoplasm.
4. To evaluate a pathologic fracture.

Not all musculoskeletal lesions require biopsy. A percutaneous biopsy is not warranted when the lesion has a classic definitive benign radiographic appearance. A history of trauma should be sought before performing interventional procedures in children where healing lesions can mislead the radiologist.

Contraindications to percutaneous biopsy include the following:

1. An inaccessible location that would endanger nearby vital structures
2. Surrounding infection
3. Uncorrectable bleeding diathesis

Technique

Preprocedural planning is of utmost importance before a biopsy. Biopsies, both open and percutaneous, can alter the later definitive surgery should a malignancy be discovered. Therefore biopsy should be planned in consultation with a tumor surgeon to choose an appropriate approach since when performed incorrectly the biopsy procedure may preclude limb-sparing surgery and instead make amputation mandatory. Particular attention should be paid to local anatomy. If the biopsied lesion is later diagnosed as a malignancy, the entire needle track must also be removed. Thus, one must not only avoid vital structures but also avoid contaminating uninvolved muscular compartments.

Certain characteristics of the lesion architecture further direct the biopsy. The following is a list of general considerations when choosing the biopsy target:

1. When biopsying a large lytic lesion, the periphery should be biopsied to avoid central areas of tissue necrosis.
2. It is preferable to biopsy a mixed blastic and lytic lesion in a lytic area as the sclerotic area often will show reactive bone formation.
3. When multiple lesions exist, it is prudent to biopsy the most accessible lesion.
4. When a soft tissue mass is adjacent to a bony lesion, sample both components of the lesion.

Imaging-guided biopsies may be performed with the aid of CT, fluoroscopy, or ultrasound. The patient position and the imaging modality depend on the site of the lesion. Fluoroscopy can be used alone for lesions that do not require careful negotiation of neurovascular structures. Otherwise, CT or a combination of CT guidance with fluoroscopy is commonly used. Ultrasound works well for superficial soft tissue lesions and requires minimal preparation. On occasion, open-configuration MR may also be used to guide percutaneous biopsy. MRI does not use iodinated contrast agents, lowering the possibility of allergic reactions, but is relatively inefficient and expensive.

The characteristics of the lesion to be biopsied direct the choice of needle used for biopsy. Fine needles are used for aspiration to provide cytology, while large-bore or "core" needles are used to obtain tissue sample for histology. Large-bore needles are also useful to penetrate bone but often require an initial skin incision before insertion. Jamshidi, Ackerman, and Craig needles are trochar instruments often required to penetrate sclerotic bone. They have thicker walls and are stronger than spinal needles. The Ackerman and Craig needles contain an inner and an outer cannula with the option of taking multiple tissue samples without needle replacement. The outer cannula can be left in place while the inner serrated cannula is withdrawn along with the biopsy. A Tru-cut needle is best for biopsy of soft tissue masses. At times, a combination of these needles is warranted.

General Technique for Skeletal Lesion Biopsy

The following are the general steps to biopsy a skeletal lesion under CT guidance:

1. Visualize using CT images with 3 mm thickness around the lesion.
2. Mark the skin with a metallic marker or metallic mesh and plan the approach.
3. Measure the distance from the skin to the target.
4. Under local anesthesia, iteratively insert the needle a few centimeters into the part; check its position and direction with a rescan; and adjust as necessary until the needle contacts the bone.
5. Anesthetize the periosteum with local anesthetic before bone penetration.
6. Advance the needle through the periosteum. This step is done with the stylet in place unless the lesion involves cortical bone, in which case the stylet is removed.
7. Confirm intralesional placement with a repeat scan before aspiration of the lesion contents. In general, specimens should always be sent for culture and sensitivity as well as histologic analysis. Purulence of the aspirated contents warrants a gram's stain.
8. Repeat the biopsy in different portions of the lesion.
9. Aftercare is specific to the location of the biopsy, with particular care for weight-bearing areas.

Spinal Biopsy

Spinal lesions are accessed using approaches that are similar to other procedures described in section "Interventional Spinal Procedures" (Fig. 14.34). Superficial paraspinal lesions are best accessed using a direct technique. Lesions in the intervertebral disc are biopsied in a technique comparable to that used for percutaneous discectomy.

Vertebral body lesions have many approaches depending on lesion location. Under fluoroscopic or CT guidance, the needle is placed in the vertebral body, rather than the intervertebral disc. A transpedicular approach with a Jamshidi needle often provides a safe approach if the pedicle is adjacent to the lesion.

The technique employed for biopsy of vertebral body lesions varies in different regions of the spine. Until recently, open procedures have been preferred to percutaneous ones for cervical spine lesions. Percutaneously, a posterolateral

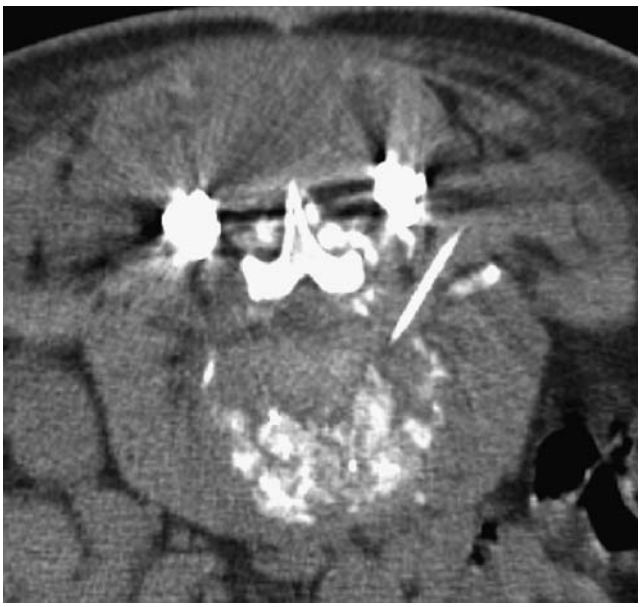

Fig. 14.34 Spinal biopsy. This patient has had a spinal fusion. The vertebral body was approached from the lateral paraspinal region to biopsy the disco-vertebral junction. Destruction of the endplate and a paravertebral soft tissue mass are also noted

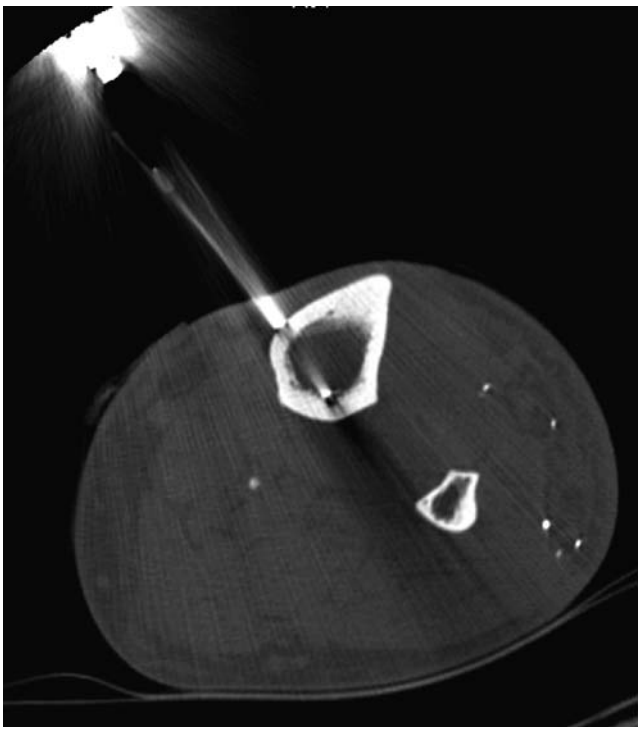

Fig. 14.35 Needle biopsy of the tibial shaft. The needle enters the tibia through the anterolateral tibial cortex. The distal tip is at the posterolateral cortex of the tibia

approach is used for lower cervical spine (below C4) lesions; an anterolateral approach is used for the mid-cervical spine and a transoral or transpharyngeal approach is used for C1–C3. Recent improvements in imaging have allowed safe and effective percutaneous biopsy of the cervical spine.

Varying approaches may be used in the thoracolumbar spine depending on the location of the lesion within the vertebral body. A transpedicular approach is similar to that used for percutaneous vertebroplasty. It is best for posteriorly or centrally located lesions. Using the intercostal approach, preferably on the right side to avoid the aorta, the needle is aimed posteromedially to avoid the pleural space. A costovertebral approach, between the tubercle of the rib and corresponding transverse process, is used for laterally located lesions.

In general, spinal biopsy complications are related to accidental damage to nearby structures. The risk to such structures depends on the region of the spine and specific technique employed.

Biopsy of Appendicular Bone

Biopsies of appendicular bone, such as the femur, are often straightforward but can be challenging. Curvature may cause the needle to slide along the bone's surface. This can be minimized with a diamond-tip needle. Anchor the tip into bone and use a mallet to avoid slippage. Compartmental anatomy should be considered when biopsying the long bones with a large bore needle. Skeletal biopsies vary in difficulty depending on the location and size of the lesion and the approach should be considered on a case-by-case basis (Figs. 14.35, 14.36, and 14.37).

Soft Tissue Lesion Biopsy

Ultrasound (US) guidance is especially useful for superficial soft tissue tumors. Before biopsy, Doppler US should be used to evaluate the vasculature along the intended needle tract and the vascularity of the lesion itself. Again, one must be mindful of compartmental anatomy when planning a musculoskeletal biopsy using larger bore needles. US-guided biopsies are best performed using 5- and 7-MHz linear array transducers. A 3.5-MHz transducer can visualize especially deep lesions and is helpful when the patient is overweight. Higher frequency transducers provide accurate visualization of superficial lesions.

Once local anatomy has been considered, a 20- or 22-gauge Chiba needle is advanced into the lesion using standard aseptic technique under US guidance. Negative pressure is then applied while moving the needle tip to different locations within the mass for biopsy. US-guided interventional

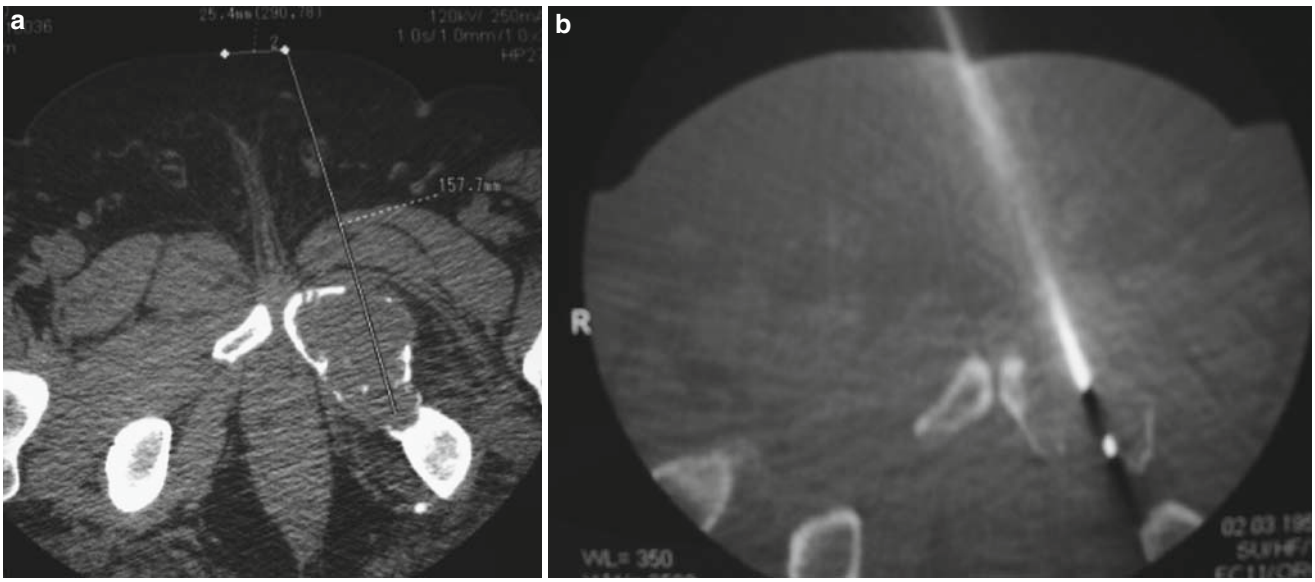

Fig. 14.36 CT through the left ischiopubic bone (**a**) shows an expansile osteolytic metastasis. CT (**b**) showing the biopsy needle placed from an anterior approach to biopsy this lesion

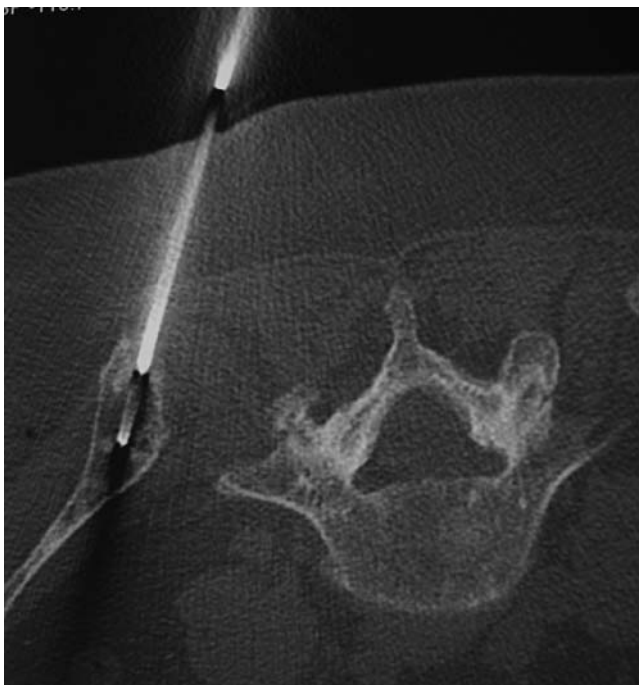

Fig. 14.37 CT image with the patient in the prone position shows a lytic lesion in the posterior iliac wing. The biopsy needle was inserted in this lesion parallel to the course of the iliac wing

procedures are not limited to soft tissue biopsies; other procedures using US are described at the end of this chapter.

Cartilaginous Lesion Biopsy

Cartilaginous lesions are particularly difficult to distinguish based on pathology. The benign enchondroma may appear similar in histologic appearance to the low-grade chondrosarcoma. To avoid nondiagnostic results, one should obtain both cartilaginous as well as noncartilaginous portions such as bone for comparison. Calcified areas of cartilage in the lesion are prone to sampling error since they are less likely to show the highest grade of cellularity within the lesion. Therefore, uncalcified areas are preferable for biopsy.

Discussion of Musculoskeletal Lesion Biopsies

Primary bone and soft tissue neoplasms are relatively uncommon. Perhaps, related to their low incidence, management of musculoskeletal tumors has a high complication rate. Bone and soft tissue sarcomas arising from mesenchymal tissue have characteristic patterns of spread. They tend to grow in centrifugal fashion until high resistance barriers such as bone, cartilage, tendon insertion, and major fibrous septa are reached. After a barrier is met, growth continues along the path of least resistance. Therefore, less aggressive tumors tend to remain within the muscular compartment from which they originate.

According to the musculoskeletal tumor staging system, classification of these tumors depends on extracompartmental spread. Tissue compartments are defined differently depending upon where the tumor arises. When it arises intra-

articularly, extracompartmental spread means that the tumor involves the soft tissue surrounding the joint. Paraosseous tumors spread extracompartmentally when they involve the bone or penetrate fascial planes. Bone tumors become extracompartmental when they involve structures surrounding the bone.

When a biopsy shows positive results it can be considered reliable, but negative results may be from sampling error. As such a negative biopsy requires clinical follow-up to confirm validity. The decision to repeat a biopsy depends on one's level of suspicion and the quality of the initial biopsy. The follow-up of a negative result should bear in mind the gravity of a missed diagnosis of malignancy.

Percutaneous Therapy of Benign lesions

Certain musculoskeletal lesions, specifically osteoid osteoma, unicameral bone cysts, and aneurysmal bone cysts, lend themselves to therapeutic percutaneous techniques.

Osteoid Osteoma

An osteoid osteoma (OO) is a benign osteogenic lesion. It occurs most commonly in the femur or the tibia, more often in men than in women, and is more likely to afflict people under age 25. Classically, patients with OO report local pain that gets worse at night and is relieved by aspirin. The majority of these lesions also have a characteristic radiographic appearance of a small radiolucent nidus surrounded by sclerosis (Fig. 14.38a).

Indications

Although osteoid osteomas will eventually resolve and can be palliated with chronic NSAIDS therapy, many patients choose intervention. Occasionally, the location of the lesion may predispose to joint damage and thereby necessitates definitive treatment – either removal or destruction of the nidus. Surgical en bloc excision is often successful, but the nidus may be difficult to localize intraoperatively, and excessive bone removal prolongs recovery time. In weight-bearing bones, in particular, percutaneous removal is an attractive alternative to surgery because it weakens bones to a far lesser degree than open resection.

Technique

Percutaneous removal of OO is performed under general anesthesia and after a course of prophylactic antibiotics. The nidus is approached using either fluoroscopic or CT guidance with a trocar and is drilled and a trephine is employed to remove the core lesion for pathologic analysis (Fig. 14.38b, c). To decrease recurrence, some radiologists recommend crossing the entire bone through both cortices and advocate postexcisional injection of alcohol to sclerose any remaining nidal remnants.

The lesion is approached using a slow-speed drill to limit the risk of heat damage to tissues. When the overlying skin contacts bone, such as the medial aspect of the tibia, there is risk of inducing skin necrosis at the drill point. To avoid this, one should make an incision in the skin large enough to allow the tissues to move away from the drill bit.

Laser photocoagulation and radiofrequency (RF) ablation are available as an alternative to percutaneous removal of OO. These procedures are nearly identical to percutaneous nidus removal, except optical fibers or RF electrodes are inserted into the incision and destroy the OO by direct heating. Lasers achieve a well-demarcated, predictable size of coagulated tissue. RF ablation can be used for cancer metastasis as well as OO ablation (Fig. 14.39).

Discussion

Benefits of laser or RF ablation include less risk of bone weakening, less chance of damage to nearby structures, faster return to normal activities, and a shorter hospital stay. In general, after percutaneous removal of the nidus, the patient should not bear weight for 6 weeks and should not play sports for 6 months. Percutaneous removal of the nidus allows tissue sampling for pathologic analysis and is more cost effective than laser therapy.

Intraosseous Cyst injection

Both unicameral bone cysts (UBCs) and aneurysmal bone cysts (ABCs) can be treated by percutaneous injection.

Indications

These cysts weaken bone and excision or percutaneous injection is justified to prevent pathologic fracture. Unlike UBCs, ABCs may arise from an underlying neoplasm and therefore the latter should be treated surgically whenever possible. On occasion, surgery may be difficult because of a problematic location or a large-sized cyst. Otherwise, if the lesion is proven to be a primary ABC, a UBC or the location makes surgery impossible, percutaneous injection may

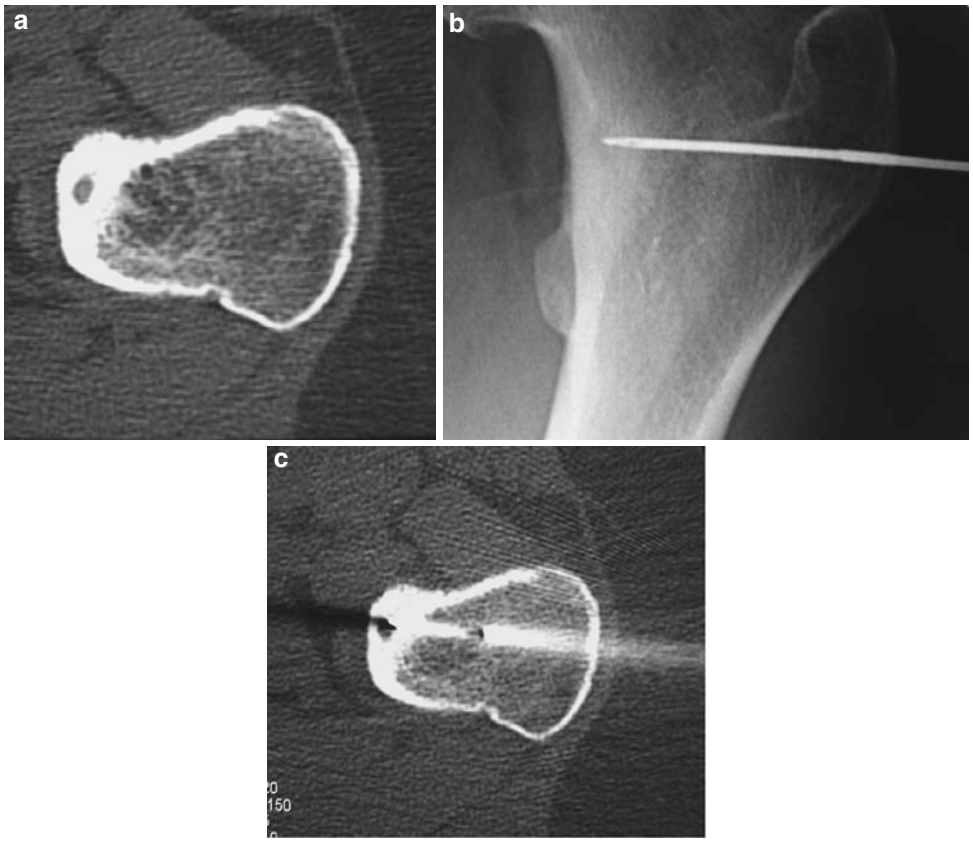

Fig. 14.38 Cortical osteoid osteoma in the femoral neck of an 18-year-old male patient. Axial CT image (**a**) beautifully shows the central lytic nidus and the surrounding laminated periosteal reaction. Fluoroscopic image (**b**) shows the tip of the drill of the 14-gauss Bonopty bone penetration set within the radiolucent nidus. The outer cannula is situated in the peripheral cortex. Another axial CT image (**c**) shows coaxial insertion of the 18-gauge spinal needle with laser fiber through the Bonopty needle into the radiolucent nidus. The nidus was ablated using 1000 J of energy

be considered. Drawbacks to surgical excision include frequent cyst recurrence in addition to the usual risks associated with general anesthesia and major surgery.

Technique

The technique for intraosseous cyst injection depends on the site. Since the most common location for these cysts is the metaphysis of long bones, percutaneous injection is usually straightforward. Two needles are used: one to inject the active agent and the second to allow fluid to escape. Contrast is injected after initial needle placement to ensure appropriate needle location; to look for any septa within the cyst that may prevent complete filling of the lesion, and to ensure no venous communication that would permit the injected medication to escape into the bloodstream. Generally, 120–160 mg of methylprednisolone acetate (MPA) is used to treat a de novo UBS. Ethibloc, a highly viscous ethanol agent, is used to treat primary ABCs or recurrent UBCs.

Discussion

Injection of MPA into a UBC induces slowly progressive cortical thickening and cyst shrinkage. There is no definitive explanation for why MPA induces healing in these lesions. Although UBCs usually heal completely after MPA injection, treatment may fail occasionally if the cyst is large or multiloculated.

Ethibloc induces tissue necrosis and secondary fibrosis. Biodegradation of Ethibloc by enzymatic cleavage occurs in a couple of weeks, at which point bone regrowth begins within the treated cyst. After 1 year, treated lesions should appear nearly healed on radiographs.

Ultrasound-Guided Interventional Procedures

In cases where a soft tissue lesion is superficial, ultrasound (US) provides a relatively fast, safe, and low-cost alterna-

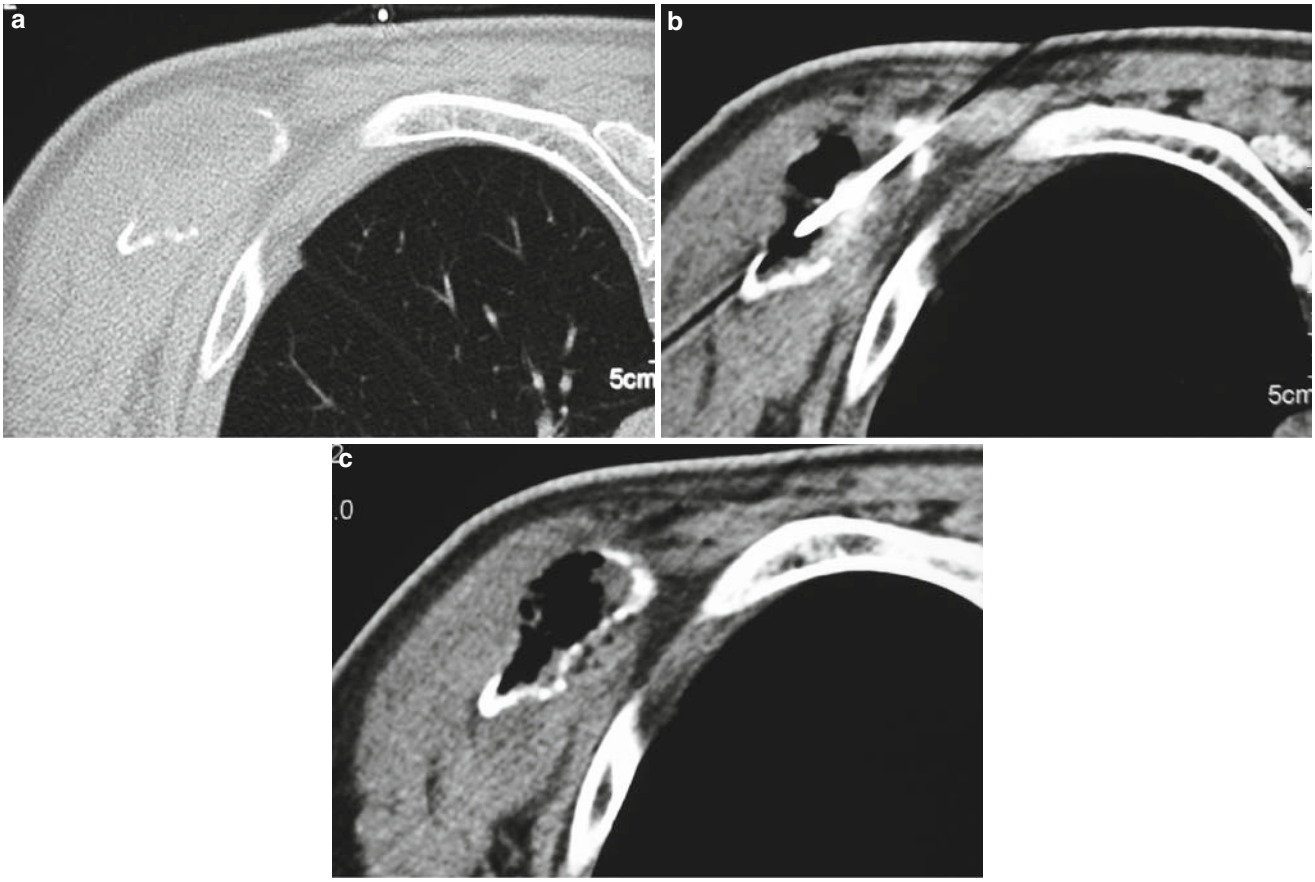

Fig. 14.39 Axial CT image (**a**) shows an expansile lytic metastasis of the inferior tip of the scapula in a patient with lung cancer. A second CT image (**b**) shows positioning of the electrode within the lesion to achieve complete ablation of the lesion. Gas within the lesion and around the electrode indicates a successful ablation. Post RF ablation control CT image (**c**) shows destruction of the tumor and gas replacing its substance

tive to fluoroscopic or CT-directed biopsy. This technique can be used for marrow aspiration or histologic examination of lesions involving bone destruction. US is also useful for arthrocentesis, treatment of calcific tendonitis, and steroid injection. In addition, US is used commonly for aspiration of fluid-containing lesions such as cysts, abscesses, and hematomas.

Technique

The approach to the target lesion should be planned by imaging the lesion in at least two planes with specific regard for important local anatomic structures. Color Doppler should be used to evaluate the vascularity of the lesion as well as identify adjacent arteries.

The technique for US-guided biopsy is similar to that of fluoroscopic biopsy, except that the needle is tracked using ultrasound instead of X-rays. Needles appear as bright echoic lines when the transducer is oriented longitudinally along the same plane as the needle track axis. If the needle is 90° to the ultrasound beam, its tip is seen as a bright echoic dot and may induce reverberation artifact or ring down on the image deep to the needle's location.

Aspiration of Fluid-Filled Lesions

Fluid-filled lesions, such as abscesses and cysts, require similar therapeutic approaches. A larger gauge needle or sheath needle is used since pus and the contents of ganglions cysts may be too viscous to withdraw with a small gauge needle. Larger abscesses may require placement of a drainage catheter.

After the needle is inserted under US guidance, some pus is aspirated to confirm location of the needle tip and obtain material for culture and sensitivity. If a sheath is to be placed, a guide wire is inserted through the needle using Seldinger

technique until it loops within the abscess. The needle is removed leaving the guide wire in position; the tract is dilated by placing serially larger dilators over the wire and finally an 8–10 F catheter is passed over the wire into the cavity. The guide wire is subsequently removed; the catheter is sutured in place and is placed either on suction or allowed to drain by gravity.

Discussion

These procedures are intended to alleviate pain and cure abscesses. Cysts produce pain because of chronic inflammation, increased internal pressure, compression of adjacent structures, or a combination of these etiologies. Percutaneous drainage relieves the pressure and removes inflamed fluid, thereby alleviating pain. Hematomas are usually aspirated to exclude infection and to improve patient comfort. If the lesion is within the muscle, aspiration may also promote muscle healing by reapproximating displaced muscle fibers. Whether treating a cyst, hematoma, or an abscess, US-guided aspiration has proven efficacious and more accessible than CT for some cases.

Further Readings

Interventional Spinal Procedures

Discography

1. Boswell MV, Shah RV, Everett CR, Sehgal N, Brown AM, Abdi S, Bowman RC, Deer TR, Datta S, Colson JD, Spillane WF, Smith HS, Lucas LF, Burton AW, Chopra P, Staats PS, Wasserman RA, Manchikanti L. Interventional techniques in the management of chronic spinal pain: evidence-based practice guidelines. Pain Physician 2005; 8(1): 1–47.
2. Carragee EJ, Alamin TF, Carragee JM. Low-pressure positive Discography in subjects asymptomatic of significant low back pain illness. Spine. 2006; 31(5): 505–509.
3. Carragee EJ, Chen Y, Tanner CM, Hayward C, Rossi M, Hagle C. Can discography cause long-term back symptoms in previously asymptomatic subjects? Spine. 2000; 25(14): 1803–1808.
4. Chou LH, Lew HL, Coelho PC, Slipman CW. Intradiscal electrothermal annuloplasty. Am J Phys Med Rehabil. 2005; 84: 538–549.
5. Derby R, Howard MW, Grant JM, Lettice JJ, Van Peteghem PK, Ryan DP. The ability of pressure-controlled discography to predict surgical and nonsurgical outcomes. Spine. 1999; 24(4): 364–371; discussion 371.
6. Derby R, Kim BJ, Lee SH, Chen Y, Seo KS, Aprill C. Comparison of discographic findings in asymptomatic subject discs and the negative discs of chronic LBP patients: can discography distinguish asymptomatic discs among morphologically abnormal discs? Spine J. 2005; 5(4): 389–394.
7. Derby R, Lee SH, Kim BJ, Chen Y, Aprill C, Bogduk N. Pressure-controlled lumbar discography in volunteers without low back symptoms. Pain Med. 2005; 6(3): 213–221; discussion 222.
8. Fraser RD, Osti OL, Vernon-Roberts B: Discitis after discography. J Bone Joint Surg Br.1987; 69: 31–35.
9. Goodman BS, Lincoln CE, Deshpande KK, Poczatek RB, Lander PH, Devivo MJ. Incidence of intravascular uptake during fluoroscopically guided lumbar disc injections: a prospective observational study. Pain Physician. 2005; 8(3): 263–266.
10. Guyer RD, Ohnmeiss DD. Lumbar discography. Spine J. 2003; 3(3): 11–27S.
11. Jenner JR. The application of chemonucleolysis (chymopapain injection) to lumbar disc protrusion has been pursued enthusiastically by some but deemed useless by others. Is there now a consensus? Br J Rheumatol. 1991; 30(2): 118.
12. Katz JN. Lumbar disc disorders and low-back pain: socioeconomic factors and consequences. J Bone Joint Surg Am. 2006 Apr; 88(2): 21–24.
13. Lander, PH. Lumbar discography: current concepts and controversies. Semin Ultrasound CT MR. 2005; 26(2): 81–88.
14. Laslett M, Öberg B, Aprill CN, McDonald B. Centralization as a predictor of provocation discography results in chronic low back pain, and the influence of disability and distress on diagnostic power. Spine J. 2005; 5: 370–380.
15. O'Neill C, Kurgansky, M. Subgroups of positive discs on discography. Spine. 2004; 29(19): 2134–2139.
16. Osti OL, Fraser RD, Vernon-Roberts B: Discitis after discography: The role of prophylactic antibiotics. J Bone Joint Surg Br.1990; 72: 271–274.
17. Pobiel RS, Schellhas KP, Pollei SR, Johnson BA, Golden MJ, Eklund JA. Diskography: infectious complications from a series of 12,634 cases. AJNR, Am J Neuroradiol. 2006; 27(9): 1930–1932.
18. Poynton AR, Hinman A, Lutz G, et al. Discography-induced acute lumbar disc herniation: a report of five cases. J Spinal Disord Tech. 2005; 18(2): 188–192.

19. Tehranzadeh J. Discography 2000. Radiol Clin North Am. 1998; 36(3), 463–495.
20. Tomecek FJ, Anthony CS, Boxell C, et al. Discography interpretation and techniques in the lumbar spine. Neurosurg Focus. 2002; 13(2), E13.

Percutaneous Discectomy

21. Onik GM, Helms C. Nuances in percutaneous discectomy. Radiol Clin North Am. 1998; 36(3), 523–532.
22. Singh V, Derby R. Percutaneous lumbar disc decompression. Pain Physician. 2006; 9(2), 139–146.
23. Singh K, Ledet E, Carl A. Intradiscal therapy: a review of current treatment modalities. Spine. 2005; 30(17): S20–S26.

Percutaneous Laser Disc Decompression

24. Gangi A, Basile A, Basille A, Buy X, Alizadeh H, Sauer B, Bierry G. Radiofrequency and laser ablation of spinal lesions. Semin Ultrasound CT MR 2005; 26(2): 89–97.
25. Gangi A, Dietemann JL, Gasser B, Guth S, de Unamuno S, Fogarrassi E, Fuchs C, Siffert P, Roy C. Interventional radiology with laser in bone and joint. Radiol Clin North Am. 1998; 36(3): 547–557.

Facet and SI Joint Injections

26. Falco FJ, Irwin L, Zhu J. Lumbar spine injection and interventional procedures in the management of low back pain. Clin Occup Environ Med. 2006; 5(3): 655–702, vii.
27. Hodge J. Facet, nerve root, and epidural block. Semin Ultrasound CT MR. 2005; 26(2), 98–102.
28. Maldjian C, Mesgarzadeh M, Tehranzadeh, J. Diagnostic and therapeutic features of facet and sacroiliac joint injection: anatomy, pathophysiology, and technique. Radiol Clin North Am. 1998; 36(3), 497–508.
29. Maugars Y, Mathis C, Berthelot JM, Charlier C, Prost A. Assessment of the efficacy of sacroiliac corticosteroid injections in spondylarthropathies: a double-blind study. Br J Rheumatol. 1996; 35(8): 767–770.
30. Tehranzadeh J. "Percutaneous facet injection for the treatment of lumbar facet syndrome". Current practice of Interventional Radiology, edited by Kadir, 750–753. B.C. Decker 1991.

Epidural Block

31. Link SC, el-Khoury GY, Guilford, WB. Percutaneous epidural and nerve root block and percutaneous lumbar sympatholysis. Radiol Clin North Am. 1998; 36(3), 509–521.

Percutaneous Vertebroplasty

32. Campbell SE, Phillips CD, Dubovsky E, Cail WS, Omary RA. The value of CT in determining potential instability of simple wedge-compression fractures of the lumbar spine. AJNR, Am J Neuroradiol. 1995; 16(7): 1385–1392.
33. Diamond TH, Bryant C, Browne L, Clark WA. Clinical outcomes after acute osteoporotic vertebral fractures: a 2-year non-randomised trial comparing percutaneous vertebroplasty with conservative therapy. Med J Aust. 2006; 184(3): 113–117.
34. Deramond H, Depriester C, Galibert P, Le Gars D. Percutaneous vertebroplasty with polymethylmethacrylate. Technique, indications, and results. Radiol Clin North Am. 1998; 36(3): 533–546.
35. Galibert P, Déramond H. [Percutaneous acrylic vertebroplasty as a treatment of vertebral angioma as well as painful and debilitating diseases]. Chirurgie. 1990; 116(3), 326–334; discussion 335.
36. Galibert P, Deramond H, Rosat P, Le Gars D. [Preliminary note on the treatment of vertebral angioma by percutaneous acrylic vertebroplasty]. Neurochirurgie. 1987; 33(2): 166–168.
37. Genant HK, Cooper C, Poor G, Reid I, Ehrlich G, Kanis J, Nordin BE, Barrett-Connor E, Black D, Bonjour JP, Dawson-Hughes B, Delmas PD, Dequeker J, Ragi Eis S, Gennari C, Johnell O, Johnston CC, Lau EM, Liberman UA, Lindsay R, Martin TJ, Masri B, Mautalen CA, Meunier PJ, Khaltaev N. Interim report and recommendations of the World Health Organization Task-Force for Osteoporosis. Osteoporos Int. 1999; 10(4):259–264.
38. Hide IG, Gangi A. Percutaneous vertebroplasty: history, technique and current perspectives. Clin Radiol. 2004; 59(6): 461–467.
39. Kaufmann TJ, Jensen ME, Schweickert PA, Marx WF, Kallmes DF. Age of fracture and clinical outcomes of percutaneous vertebroplasty. AJNR, Am J Neuroradiol. 2001; 22(10): 1860–1863.
40. Laredo JD, Hamze B. Complications of percutaneous vertebroplasty and their prevention. Semin Ultrasound CT MR. 2005; 26(2), 65–80.
41. Peh, WC, Gilula, LA. Percutaneous vertebroplasty: an update. Semin Ultrasound CT MR. 2005; 26(2):52–64.

42. Vogt TM, Ross PD, Palermo L, Musliner T, Genant HK, Black D, Thompson DE. Vertebral fracture prevalence among women screened for the Fracture Intervention Trial and a simple clinical tool to screen for undiagnosed vertebral fractures. Fracture Intervention Trial Research Group. Mayo Clin Proc 2000; 75(9): 888–896.

Interventional Evaluation and Treatment of Joint Pathology

43. Aliabadi P, Baker ND, Jaramillo D. Hip arthrography, aspiration, block, and bursography. Radiol Clin North Am. 1998; 36(4): 673–690.
44. Carrino JA, Blanco R. Magnetic resonance-guided musculoskeletal interventional radiology. Semin Musculoskeletal Radiol. 2006; 10(2): 159–174.
45. Coumas JM, Palmer W. Knee arthrography: evolution and current status. Radiol Clin North Am. 1998; 36(4): 703–728.
46. Haims A, Katz LD, Busconi B. MR arthrography of the Hip. Radiol Clin North Am. 1998; 36(4): 691–702.
47. Helgason WJ, Chandnani VP. MR arthrography of the Ankle. Radiol Clin North Am. 1998; 36(4): 729–738.
48. Linkous MD, Gilula LA. Wrist arthrography today. Radiol Clin North Am. 1998; 36(4): 651–672.
49. Parlier-Cuau C, Champsaur P, Nizard R, Wybier M, Bacque MC, Laredo JD. Percutaneous treatments of painful shoulder. Radiol Clin North Am. 1998; 36(3): 589–596.
50. Rafii M, Minkoff J. Advanced arthrography of the shoulder with CT and MR imaging. Radiol Clin North Am. 1998; 36(4): 609–633.
51. Schreibman KL, Gilula LA. Ankle Tenography: A therapeutic imaging modality. Radiol Clin North Am. 1998; 36(4): 739–756.
52. Steinbach LS, Schwartz, M. Elbow arthrography. Radiol Clin North Am. 1998; 36(4): 635–649.
53. Tehranzadeh J, Booya F, Root J. Cartilage metabolism in osteoarthritis and the influence of viscosupplementation and steroid: a review. Acta Radiol. 2005; 46(5): 288–296.
54. Tehranzadeh J, Mossop EP, Golshan-Momeni M. Therapeutic arthrography and bursography. Orthop Clin North Am. 2006; 37, 393–408.

Percutaneous Procedures Targeting Musculoskeletal Lesions

Biopsies of the musculoskeletal system

55. Choi JJ, Davis, KW, Blankenbaker, DG. Percutaneous musculoskeletal biopsy. Semin Roentgenol. 2004; 39(1): 114–128.
56. Ghelman B. Biopsies of the musculoskeletal system. Radiol Clin North Am. 1998; 36(3), 567–580.
57. Toomayan GA, Robertson F, Major NM, Brigman BE. Upper extremity compartmental anatomy: clinical relevance to radiologists. Skeletal Radiol. 2006; 35(4): 195–201.
58. Toomayan, GA, Robertson, F, Major, NM. Lower extremity compartmental anatomy: clinical relevance to radiologists. Skeletal Radiol. 2005; 34(6): 307–313.

Percutaneous Treatment of Benign Lesions

59. Gangi A, Dietemann JL, Gasser B, Guth S, de Unamuno S, Fogarrassi E, Fuchs C, Siffert P, Roy C. Interventional radiology with laser in bone and joint. Radiol Clin North Am. 1998; 36(3): 547–557.
60. Leclet H, Adamsbaum C. Intraosseous cyst injection. Radiol Clin North Am. 1998; 36(3): 581–587.
61. Parlier-Cuau C, Champsaur P, Nizard R, Hamze B, Laredo JD. Percutaneous removal of osteoid osteoma. Radiol Clin North Am. 1998; 36(3): 559–566.

Ultrasound Guided Interventional Procedures

62. Cardinal E, Chhem RK, Beauregard CG. Ultrasound-guided interventional procedures in the musculoskeletal system. Radiol Clin North Am. 1998; 36(3), 597–604.

Subject Index

The letters ‘f’ and ‘t’ following the locators refer to figures and tables respectively

A. Bonakdarpour et al. (eds.), *Diagnostic Imaging of Musculoskeletal Diseases: A Systematic Approach*,
DOI 10.1007/978-1-59745-355-4,

J